https://ntrs.nasa.gov/search.jsp?R=19670030808 2020-03-16T16:46:23+00:00Z

NASA SP-120

GPO PRICE $ ____________

CFSTI PRICE(S) $ ____________

Hard copy (HC) 3.00

Microfiche (MF) .65

ff 653 July 65

FUEL CELLS

A Review of Government-Sponsored Research, 1950-1964

FACILITY FORM 602

N67-40137 (ACCESSION NUMBER)	(THRU)
10 45 (PAGES)	1 (CODE)
✓ (NASA CR OR TMX OR AD NUMBER)	03 (CATEGORY)

National Aeronautics and Space Administration

NASA-SP-120

FUEL CELLS

A Review of Government-Sponsored Research, 1950-1964

L. G. Austin
Department of Chemical Engineering
North Carolina State University

Prepared under contract for the
National Aeronautics and Space Administration
by John I. Thompson & Co.

Scientific and Technical Information Division
OFFICE OF TECHNOLOGY UTILIZATION 1967
NATIONAL AERONAUTICS AND SPACE ADMINISTRATION
Washington, D.C.

For Sale by the Superintendent of Documents, U.S. Government Printing Office, Washington, D. C. 20402 • Price $2.75
Library of Congress Catalog Card Number 66-60090

Foreword

U.S. Government-sponsored research on fuel cells was started by the Navy in the early 1950's and expanded sharply about 1959. Primary Navy interest is in more buoyant submarines; Army interest concerns silent frontline power and more efficient use of fuel for motive power. Both services need silent, portable electric generators. The Air Force and NASA share the desire for minimum-weight spacepower systems. The Advanced Research Projects Agency of the Department of Defense considered direct energy conversion important enough to carry multimillion-dollar Project Lorraine for several years, which included sizable funds for fuel-cell work. In addition, the Atomic Energy Commission is looking into thermally regenerative fuel cells as possible adjuncts to nuclear power plants.

This variety of interests has led to a wide range of fuel-cell efforts. Hundreds of reports have resulted from that work, many of which are virtually unavailable today. A large part of the knowledge will not find its way into scientific journals. Because of the imminent danger of loss of information, it was decided to compile a summary book on the subject. Thanks to the excellent cooperation of the Government agencies involved and of many individuals in private organizations, a reasonably complete file of reports was assembled, summarized, and evaluated by Prof. L. G. Austin under contract NASw-1039 with John I. Thompson & Co.

It is hoped that this compilation will be useful as a guide to the past and future of fuel-cell research and development.

9

ERNST M. COHN,
Head, Electrochemical Systems
Office of Advanced Research and Technology

MARCH 7, 1966.

Acknowledgments

I should like to thank Harry Lerner, presently at Itek Corporation, Lexington, Mass., both for preparing the list of contract reports and for his help in reviewing the material discussed in Chapter 15.

L. *G.* **AUSTIN**
Professor of Chemical Engineering
North Carolina State University
Raleigh, N.C.

Formerly Professor of Fuel Science
Pennsylvania State University
University Park, Pa.

JANUARY 30, 1967

Contents

chapter *page*

1. SUMMARY AND RECOMMENDATIONS 1
   - 1.1 Introduction 1
   - 1.2 Principle of the Fuel Cell 1
   - 1.3 Application of Fuel Cells 3
   - 1.4 Electrodes, Catalysts. and Electrolytes 7
   - 1.5 Hydrogen-Oxygen Fuel Cells 10
   - 1.6 Hydrocarbon Fuels and Fuel Cells 13
   - 1.7 Other Types of Cells 16
     - 1.7.1 Amalgam Cells 16
     - 1.7.2 Thermally Regenerative Cells 16
     - 1.7.3 Thermogalvanic Cells 18
     - 1.7.4 Photochemically Regenerative and Redox Cells 19
     - 1.7.5 Dry-Tape Fuel Cells 20
     - 1.7.6 Hydrazine and Ammonia Fuel Cells 20
     - 1.7.7 Biochemical Fuel Cells 22
   - 1.8 Fundamental Kinetic Studies 23
   - 1.9 Mode of Operation of Diffusion Electrodes 26
   - 1.10 Recommendations 27
   - 1.11 References 29

2. PRINCIPLES. TYPES. AND USES OF FUEL CELLS 31
   - 2.1 The Fuel-Cell Principle 31
     - 2.1.1 The Basic Theory of the Fuel Cell 31
     - 2.1.2 Elementary Thermodynamics of the Fuel Cell 33
     - 2.1.3 Polarization, Power Density. and Efficiency 34
     - 2.1.4 Kinetics and Catalysis 36
     - 2.1.5 Concentration Polarization and Mass Transfer 38
     - 2.1.6 Gas Diffusion and Purging 39
     - 2.1.7 Improvement of Power Density 41
   - 2.2 Types of Fuel Cells 42
     - 2.2.1 General Classifications 42
     - 2.2.2 Low-Temperature Fuel Cells 42
     - 2.2.3 Medium-Temperature Fuel Cells 45
     - 2.2.4 High-Temperature Fuel Cells 46
     - 2.2.5 The Sodium Amalgam Cell 47
     - 2.2.6 Other Types of Cells 47

chapter *page*

2.3 Applications of Fuel Cells 50
2.3.1 Introduction 50
2.3.2 Space Applications 51
2.3.3 Small- and Moderate-Sized Military Power Generators . . 51
2.3.4 Military Vehicle Propulsion 52
2.3.5 Underwater Applications 55
2.3.6 Central Station Power 56
2.4 Guide to Fuel-Cell Literature 56
2.5 References 57
3. ELECTRODES. ELECTROLYTES. AND MATRICES 59
3.1 Introduction 59
3.2 Preparation of Electrodes 62
3.2.1 Porous Baked Carbon Electrodes 62
3.2.2 Sintered Metal Electrodes 65
3.2.2.1 Low-Temperature Cells 65
3.2.2.2 Medium-Temperature Cells 67
3.2.2.3 High-Temperature Cells: Molten Carbonate Electrolyte 67
3.2.2.4 High-Temperature Cells: Solid Electrolyte 70
3.2.3 Plastic-Bonded Electrodes 70
3.2.3.1 Introduction 70
3.2.3.2 General Electric Co., Niedrach-Alford Electrodes 71
3.2.3.3 American Cyanamid Co., Electrodes 71
3.2.3.4 Union Carbide Corp., Thin Fuel-Cell Electrodes 74
3.2.3.5 Miscellaneous Results on Electrodes 75
3.2.4 Solid-state Diffusion Membranes 75
3.3 Electrolytes 80
3.3.1 Aqueous Electrolytes 80
3.3.2 Ion-Exchange Membranes : Matrices 82
3.3.3 High-Temperature Electrolytes and Matrices 87
3.4 References 89
4. CELL AND STACK CONSTRUCTION: LOW-TEMPERATURE CELLS 91
4.1 General Features of Stack Construction 91
4.2 The Union Carbide Co. Hydrogen-Oxygen Cell 94
4.2.1 Carbon Electrode Fuel Cells, May 1960 to December 1962 94
4.2.2 Low-Temperature Fuel-Cell Battery, July 1960 to February 1961 95
4.2.3 H_2-O_2 Prototype Fuel Cell, 1960 to Present 95
4.3 General Electric Co. Ion-Exchange Membrane, Hydrogen-Oxygen Cell 97
4.3.1 Fuel-Cell Powerpack Development Program, June 1959 to May 1961 97

chapter *page*

4.3.2 Research on Compact Fuel-Cell Power Supplies, October 1960 to October 1961 98
4.3.3 HOPE Fuel-Cell Program; Flight Analysis of IEM Fuel Cell, April 1961 to October 1962 99
4.3.4 Ion-Exchange Fuel Cell, October 1961 to September 1962 100
4.3.5 Ion-Exchange Membrane Fuel Cell for Naval Propulsion, November 1961 to September 1963 101
4.3.6 Ion-Exchange Fuel Cell, October 1962 to September 1963 102
4.4 Allis-Chalmers Hydrogen-Oxygen Fuel Cell 103
4.4.1 Engineering Research Study of Fuel-Cell Powerpack, December 1961 to January 1963 103
4.4.2 Design of 400-Watt H_2-O_2 Capillary-Type Fuel Cell, May 1962 to October 1963 105
4.4.3 Research and Development of an Open-Cycle-Type, Fuel-Cell System, May 1962 to Present 106
4.4.4 Study of Energy Conversion Systems, May 1963 to June 1964 107
4.4.5 Design of H_2-O_2 Fuel Cells, November 1963 to January 1965 108
4.5 Ionics Double-Membrane Hydrogen-Oxygen Fuel Cell 109
4.5.1 Study of IEM Fuel-Cell Components, June 1960 to April 1962 109
4.5.2 Development of the Dual-Membrane Fuel Cell, July 1962 to June 1963 110
4.6 Conclusions 111
4.7 References 112

5. CELL AND STACK CONSTRUCTION: MEDIUM-TEMPERATURE CELLS 113
5.1 Patterson-Moos Research, Hydrox Cell, Continuous-Feed Fuel-Cell Systems, February 1957 to February 1962 113
5.2 Pratt & Whitney Aircraft, Modification of the Bacon Cell, Design and Development of a 250-Watt H_2-O_2 Fuel Cell, July 1961 to May 1962 113
5.3 Conclusions 116
5.4 References 116

6. CELL AND STACK CONSTRUCTION: HIGH-TEMPERATURE CELLS 118
6.1 Molten-Carbonate Fuel Cells 118
6.1.1 Pittsburgh Consolidation Coal Co., Conversion of Carbonaceous Fuels to Electrical Energy, May 1954 to August 1958 118
6.1.2 Central Technical Institute TNO in Holland, High-Temperature Galvanic Fuel Cells, January 1959 to 1962. 121

chapter *page*

6.1.3 Texas Instruments, Inc., Molten Carbonate Fuel Battery Program, February 1963 to February 1964 123

6.2 Solid-Electrolyte Fuel Cells 127

6.2.1 Westinghouse Electric Co., An Investigation of Solid Electrolyte Fuel Cells, February 1962 to April 1963.... 127

6.2.2 Westinghouse Electric Co., Contract With Office of Goal Research, December 1962 to Present. 129

6.3 Conclusions.. 131

6.4 References.. 133

7. CELL AND STACK CONSTRUCTION: SODIUM AMALGAM-OXYGEN CELLS.. 134

7.1 E. Yeager et al., Western Reserve University, The O_2 Electrode, 1951 to Present. 134

7.2 M. W. Kellogg Co., Sodium Amalgam-Oxygen Fuel Cell, May 1960 to December 1963... 135

7.3 Conclusions 138

8. SYSTEMS AND CONTROL 139

8.1 Introduction 139

8.2 Pratt & Whitney Aircraft, System Analysis of a Regenerative H_2-O_2 Fuel-Cell Powerplant, 1961. 140

8.3 Union Carbide Corp., Carbon Electrode Fuel Cell, H_2-O_2 Fuel-Cell 141

8.4 General Electric Co. (234 through 237, 244 through 248, 264 through 274, *276* through *290*) 142

8.5 Allis-Chalmers Manufacturing Co. (35 through 44, 47 through *57*, *59* through 61) 145

8.6 Conclusions 149

8.7 References 152

9. ELECTROLYTICALLY REGENERATIVE HYDROGEN-OXYGEN CELLS.. 153

9.1 Introduction 153

9.2 Research on 500-Watt Solar Regenerative Hydrogen-Oxygen Fuel-Cell Power Supply System, Pratt & Whitney Aircraft, October 1959 to October 1960 and September 1961 to December 1961 157

9.3 Ion-Exchange Membrane Regenerative Fuel-Cell Research and Development Program, General Electric Co., January 1960 to September 1960, October 1960 to October 1961, and October 1961 to November 1961. 159

9.4 Research on the Electrolysis of Water Under Weightless Conditions, Battelle Memorial Institute, June 1960 to November 1961, June 1961 to May 1962, and June 1962 to June 1963.. 160

chapter *page*

9.5 Evaluation of Electrolytically Regenerative Hydrogen-Oxygen Fuel Cell. Electro-Optical Systems. Inc., September 1960 to March 1962 (*160*), April 1962 to March 1963 *(183)*. June 1962 to July 1963 *(175)*. and October 1963 to Present **(186)** 162
9.6 Conclusions 165
9.7 References 166
10. THERMALLY REGENERATIVE FUEL CELLS 167
10.1 Introduction 167
10.2 Lithium Hydride Systems 167
10.2.1 Mine Safety Appliance Research Corp., Study of Energy Conversion Devices. July 1959 to May 1961 .. 167
10.2.2 TAPCO. Division of Thompson-Ramo-Wooldridge, Inc., Regenerative Fuel-Cell System Investigation. July 1959 to June 1961 168
10.2.3 Argonne National Laboratories. Thermally Regenerative Fuel Cells. 1961 to 1963 171
10.3 Other Molten Metal/Salt/Gas Cells 172
10.3.1 Lockheed Aircraft Corp., Solar Regenerative Chemical Systems. September 1959 to September 1962 172
10.3.2 Electro-Optical Systems. Inc., Investigation of New Solar Regenerative Fuel-Cell Systems. November 1959 to November 1960 and March 1961 to March 1962 .. 173
10.4 Regenerative Amalgam-Metal Cells 173
10.4.1 Allison Division of General Motors, Design and Development of a Liquid Metal Cell. January 1962 to April 1964 173
10.5 Other Thermally Regenerative Systems 175
10.5.1 Electro-Optical Systems, Inc., Solar Regenerative Fuel-Cell Systems. November 1959 to March 1962 175
10.5.2 Aerospace Corp., Energy Conversion Research Program, January 1961 to January 1962 176
10.5.3 Garrett Corp., SO_2-SO_3 Regenerative Fuel-Cell Research, March 1961 to April 1962 176
10.6 Conclusions 176
10.7 References 177
11. THERMOGALVANIC CELLS 179
11.1 Introduction 179
11.2 Simple Thermogalvanic Cells 180
11.2.1 General Electric Co., Solar Regenerative Fuel Cell, November 1960 180
11.2.2 Lockheed Aircraft Corp., Solar Regenerative Chemical Systems, September 1959 to September 1962 180
11.2.3 Aerojet-General *Corp.*, Investigation of an Energy Conversion Device, July 1961 to June 1962 181

chapter *page*

11.2.4 Electro-Optical Systems, Inc., Investigation of New Solar Regenerative Fuel Cell Systems, November 1959 to March 1962.................................. 182
11.3 Double Thermogalvanic Cells............................ 183
11.3.1 Lockheed Aircraft Corp., Solar Regenerative Chemical Systems, September 1959 to September 1962........ 183
11.3.2 Argonne National Laboratories, Thermally Regenerative Fuel Cells, April 1961 to 1963.................. 184
11.3.3 Delco-Remy Division, Feasibility Study of the Electrothermally Regenerative Transducer, May 1962 to June 1964.................................... 187
11.4 Conclusions.. 188
11.5 References... 188

12. PHOTOCHEMICALLY REGENERATIVE AND REDOX CELLS.. 189
12.1 Introduction... 189
12.2 Photochemical Regeneration of Reactants................. 190
12.2.1 Stanford Research Institute, Photochemistry in the Solar Furnace, April 1958 to December 1959 and March 1960 to June 1962.............................. 191
12.2.2 Sundstrand Machine Tool Co., Solar Regenerative Fuel Cell, April 1959 to May 1961..................... 194
12.2.3 P.E.C. Corp., Photochemical Decomposition of H_2O, October 1960.................................... 194
12.2.4 Lockheed Missiles & Space Div., Solar Regenerative Chemical Systems, September 1959 to September 1962. 196
12.2.5 Electro-Optical Systems, Inc., Solar Regenerative Fuel-Cell Systems, May 1960 to May 1961.............. 197
12.3 Nuclear Regenerative Fuel Cells, Union Carbide, June 1960 to September 1962....................................... 198
12.4 Redox Fuel Cells....................................... 200
12.5 Conclusions... 201
12.6 References... 203

13. HYBRID FUEL CELLS................................... 203
13.1 Introduction.. 203
13.2 Research on Electrochemical Fuel Cells, Aerojet-General Corp., November 1951 to August 1956.................... 203
13.3 Continuous Feed Battery, Armour Research Foundation of the Illinois Institute of Technology, April 1956 to July 1957.. 204
13.4 Organic Fuel-Cell Systems, Resin Research Laboratories, Inc., April 1959 to June 1960.............................. 204
13.5 Development and Feasibility Proof of the Dry-Tape Battery Concept, Monsanto Chemical Co., June 1963 to January 1964.. 204

3

chapter *page*

13.6 Graphite-Oxygen High-Temperature Fuel Cell. Iowa State University. 1963 206
13.7 Conclusions 207

14. BIOCHEMICAL FUEL CELLS 209
14.1 Introduction 209
14.2 Bioelectric Energy Sources. Ohio State University. December 1960 to December 1961 210
14.3 Biochemical Fuel Cells. Magna Corp., July 1962 to December 1964 212
14.4 Biochemical Fuel Cells. University of Pennsylvania. Institute for Direct Energy Conversion. June 1962 to 1963 215
14.5 Biochemical Fuel Cell. Melpar. Inc., July 1962 to 1964 216
14.6 Bioelectrogenic System. General Electric Co., MSVD. October 1962 217
14.7 Research on Applied Bioelectrochemistry. Magna Corp., March 1963 to 1964 217
14.8 Study of the Fundamental Principles of Bioelectrochemistry. Ford-Aeronutronic, March 1963 to March 1964 218
14.9 Biochemical Fuel Cells. Marquardt Corp., May 1963 to September 1964 219
14.10 Conclusions 219
14.11 References 221

15. DIRECT HYDROCARBON (ORGANIC) FUEL CELLS 223
15.1 Introduction 223
15.2 Screening Programs 224
  15.2.1 Activity of Fuels 224
  15.2.2 Catalyst Screening 228
15.3 General Electric Co., Hydrocarbon Fuel Cell *(294* through ***311).*** 237
15.4 Methanol Fuel Cells 238
  15.4.1 Esso Research & Engineering Co., Soluble Carbonaceous Fuel-Air Cells, January 1962 to December 1962 and January 1963 to December 1963 238
  15.4.2 Other Methanol Fuel Cells 239
15.5 Reaction Mechanisms 240
  15.5.1 Introduction 240
  15.5.2 Nonoxygenated Hydrocarbons 243
  15.5.3 Carbon Monoxide and Oxygenated Hydrocarbons 251
15.6 Conclusions 258
15.7 References 259

chapter *page*

16. MISCELLANEOUS FUELS (HYDRAZINE, AMMONIA, ETC.) AND OXIDANTS (HYDROGEN PEROXIDE, NITRIC ACID, ETC.) 261
- 16.1 Introduction 261
- 16.2 Basic Research in 'Fuel Cells: Ammonia, Ethylene Glycol, and Urea Systems: Lockheed Aircraft Corp., July 1960 to August 1961 and May 1961 to July 1963. 262
- 16.3 Compact Power Fuel Cell, Monsanto Chemical Co., December 1960 to December 1961. 264
- 16.4 Electrochemical Energy Conversion Systems Research, Monsanto Chemical Co., September 1960 to September 1961. 266
- 16.5 Study of Fuel Cells Using Storable Rocket Propellants, Monsanto Chemical Co., June 1963 to January 1964. 267
- 16.6 Direct Ammonia-Air Fuel Cell, Electrochimica Corp., July 1963 to August 1964. 270
- 16.7 Porous Flowthrough Electrodes of Platinum Black, Pennsylvania State University, March 1960 to April 1964. 273
- 16.8 Research on Materials, Processes, and Devices Related to Energy Conversion, MIT School of Engineering, June 1961 to January 1964. 273
- 16.9 Conclusions. 273

17. KINETICS OF HYDROGEN-OXYGEN FUEL-CELL REACTIONS 275
- 17.1 Introduction 275
- 17.2 Gas-Phase Chemisorption. 276
- 17.3 Catalysis: Hydrogen Electrode. 281
- 17.4 Catalysis: Oxygen Electrode. 284
  - 17.4.1 Introduction. 284
  - 17.4.2 Western Reserve University, the Oxygen Electrode, 1951 to Present. 284
  - 17.4.3 Engelhard Industries, Inc., Fuel-Cell Catalysts, July 1960 to June 1962 and July 1962 to June 1963. 288
  - 17.4.4 Esso Research & Engineering Co., Soluble Carbonaceous Fuel-Air Fuel Cell, January 1962 to December 1963.. 290
  - 17.4.5 Tyco Laboratories, Inc., Oxygen Electrode Studies, October 1961 to February 1963. 290
  - 17.4.6 University of Pennsylvania, Reversible Oxygen Electrodes, November 1961 to Present. 292
  - 17.4.7 Tracor, Inc., Study of the Oxygen Electrode Mechanism, January 1962 to December 1963. 295
  - 17.4.8 General Electric Co., Research on Low-Temperature Fuel Cells, February 1960 to November 1961. 296
  - 17.4.9 Conclusions From Oxygen Electrode Studies. 297

chapter *page*

17.5 Conclusions 301
17.6 References 302

18. THEORIES OF POROUS ELECTRODES 303
18.1 Introduction 303
18.2 Gas-Diffusion Electrodes: Thin-Film Model 303
18.3 Gas-Diffusion Electrodes: Simple-Pore Model 309
18.4 Gas-Diffusion Electrodes: Surface-Diffusion Model 311
18.5 Flooded Electrodes 312
18.6 Flowthrough Electrodes 315
18.7 Unsteady-State Measurements on Porous Electrodes 316
18.8 Effect of Pulsation on Gas Electrodes 318
18.9 Conclusions 320
18.10 References 321

Appendix A: FUEL-CELL GLOSSARY FROM REPORT **752** 323

Appendix B: TABULATED DATA 327

Appendix C: TECHNIQUES 341

Appendix D: MATERIALS. 355

Appendix E: HYDROGEN GENERATION AND GAS STORAGE ... 369

Appendix F: LIST OF CONTRACT REPORTS 373

SUBJECT INDEX 417

AUTHOR—CORPORATE SOURCE INDEX 435

CHAPTER 1

Summary and Recommendations

1.1 INTRODUCTION

The primary objective of this monograph is to review fuel-cell investigations funded by Government agencies of the United States of America. The magnitude of the U.S. effort to develop fuel cells can be judged by the contracts and reports within the scope of this book. Up to December 1963, nearly 200 contracts had been awarded to 90 contractors, and nearly 800 reports have been issued describing the work performed under the contracts. The reports contain so much detailed information that it is impossible to summarize them adequately even in a monograph of this size. The state of fuel-cell technology is still changing rapidly and it is not easy to decide which results are important enough to be reported in detail. Finally, development of practical fuel cells is a prime example of an interdisciplinary field of work requiring contributions from specialized chemical and engineering disciplines. The author has given due weight to all aspects of the field, but it is unavoidable that a review reflect the author's personal interests and abilities. For this reason, this work should be treated as a sourcebook for information existing in contract reports; it is definitely not intended as an authoritative survey of the complete field of fuel cells.

A comprehensive listing of the contractor reports used as the basis for the book is presented in Appendix F. The italicized numbers in the text refer to particular reports listed in that appendix.

1.2 PRINCIPLE OF THE FUEL CELL

A fuel cell is a device for converting the chemical energy of reaction between fuel and oxidant directly to electrical energy. The basic principle is similar to that of the flashlight battery or any other primary cell and *can* be illustrated using hydrogen and oxygen in alkaline electrolyte as an example:

$$\text{Anode} + H_2 + 2OH^- \rightarrow (\text{Anode} + 2e^-) + 2H_2O$$
$$(\text{Cathode} + 2e^-) + \tfrac{1}{2}O_2 + H_2O \rightarrow \text{Cathode} + 2OH^-$$
$$\overline{\qquad H_2 + \tfrac{1}{2}O_2 \rightarrow H_2O \qquad}$$

The cell has two electronically conducting electrodes immersed in an electrolyte of potassium hydroxide dissolved in water. Hydrogen is fed to one electrode (the anode), adsorbs upon it, and reacts with hydroxyl ion to form water in solution. Electrons left behind on the anode accumulate at the electrode-electrolyte interface and attract a corresponding quantity of positive ions in the electrolyte to this interface. A potential difference exists between the electrons and the positive ions in the same way as the potential difference between charges of opposite sign in a capacitor. Oxygen reacts at the other electrode (cathode) to give positive charge (deficiency of electrons) on the electrode and a layer of negative ions in the electrolyte. When the two electrodes are connected externally, electrons flow from the anode to the cathode. Hydroxyl ions flow from cathode to anode in the electrolyte and complete the circuit. As shown above, the net effect is the reaction of oxygen and hydrogen to water, but the reaction occurs via flow of electrons in the external circuit, which can be used to do useful work. The greater the energy (Gibbs free energy) of reaction per electron, the bigger is the theoretical potential between the electrodes.

Unlike electricity production by conventional heat cycles, the efficiency of energy production by primary cells is not limited by a Carnot-type relation, and (thermal) efficiencies of 60 percent have been obtained in practice at useful power levels. Unlike conventional primary cells or batteries, the fuel cell continues to supply current as long as reactants are fed in and products are removed. Recharging is accomplished by refilling the fuel and oxidant storage tanks while the cell is running, if necessary. These two features are major advantages of fuel cells; the cells can be more efficient when compared with conventional power production, or they can be used continuously when replacing conventional batteries. However, recent impetus to fuel-cell development for specialized requirements of the space program is due to a third characteristic of the cells. The total electrically available energy stored in hydrogen and oxygen is about 1650 W-hr/lb of reactants, much more than the 200 W-hr/lb of active materials in high-energy primary cells such as the zinc-silver oxide cell. Even with allowance for weight of fuel cells and storage tanks, fuel-cell systems using hydrogen and oxygen give more watt-hours per pound than the best available alternatives for certain space travel applications, as discussed in subsequent chapters of this book.

It is desirable for fuel cells to be efficient, compact, and capable of continuous, reliable operation. The voltage efficiency of a cell is the ratio of its working voltage to the ideal thermodynamic voltage, calculated from the Gibbs free energy of reaction (1.23 volts at room temperature for H_2 and O_2). Electrical (coulombic) efficiency can be close to 100 percent (about 83 percent thermal efficiency) at low currents, but in all cells there are power losses when current is drawn and the terminal voltage decreases with increased current. The power density in kilowatts per cubic foot (kW/cu ft) is a measure of compactness; since watts = amperes X volts, the power density increases as larger currents are drawn, until the decrease in voltage outweighs current increase. Thus, as current increases, the efficiency decreases; power density increases to a maximum and then falls. In any application, the requirement of efficiency has to be balanced against the requirement of power density. The ideal cell delivers high current with small internal voltage loss. It is clear that the causes of voltage loss (called polarization) are of paramount importance.

One of the three main causes of polarization (IR loss) is internal ohmic resistance occurring in electrode materials and the electrolyte. Electrodes have to be made with high conductivity, and the cell geometry must give a low electrolyte resistance between electrodes. A second cause of polarization, called concentration polarization, is due to slow supply of reactants to the electrodes. Voltage can be maintained only if reactant reaches an electrode without a large decrease in reactant concentration at the electrode. For example, the anode reaction of H_2 in alkali is $\frac{1}{2}H_2+OH^-=H_2O+e^-$; this reaction *can* proceed only as fast as H_2 and OH– are supplied. The rate of transfer to the reaction zone is often of the form

$$\text{Rate}=k\ (C_b-C_s)$$

where k is a mass transfer factor, C_b is the concentration of reactant as supplied, and C_s is the concentration at the reaction zone. $C_b—C_s$ is the driving force for mass transfer. When C_s becomes small, a limiting rate, equal to kC_b, is obtained. For good performance, these limiting rates should be as large as possible. In the above example, high concentration of OH– in the electrolyte *is* necessary to prevent low limiting currents due to limited mass transfer of OH–.

A third cause of polarization, called activation polarization, is due to slow electrokinetics. If an electrochemical reaction ($H_2+2OH^-\rightarrow 2H_2O+2e^-$, for example) is slow, some of the electrode voltage is used to drive the reaction to the rate required to match the current. Reactions are slow because molecules often have to be in a high-energy, “activated” state before chemical bonds are broken and formed. If the energy of the activated state is high, only a minute fraction of the available molecules are in the activated state, giving a slow rate. Activation polarization is decreased by increased cell temperature and therefore cell performance increases with increased temperature.

The application of these concepts can be illustrated by considering a typical fuel cell, as shown in figure 2.1. The cell consists of a sandwich of flat components; the electrolyte thickness between electrodes is small to reduce IR voltage loss. Concentrated electrolytes are used to give high conductivity and to supply ions for the reaction without mass-transfer limitations.

A thin chamber is used to supply fuel gas to the entire face of a porous anode and gas diffuses through the electrode to the electrode-electrolyte interface, where it reacts. A similar chamber supplies oxygen to a porous cathode. Porous, gas-diffusion electrodes are the heart of the normal fuel cell, since they provide a means of bringing reactant gas into intimate contact with electrode and electrolyte at high rates of mass transfer. With suitable electrode design, the rate of gas flow does not restrict performance even at current densities of 1000 amperes per square foot (A/sq ft) of electrode. In addition to acting as gas diffusers, the electrodes also supply active area for adsorption and ionization of gases to produce current. The internal area of porous electrodes is much greater than the area of solid electrode of the same size. For example, a porous electrode containing 10 grams of platinum black per square foot has an internal area of about 2000 square feet. The fraction of this area which is used in the electrochemical reaction has not been established with certainty (see below), but it produces much larger currents than a solid electrode of the same size.

Excessive activation polarization can occur, even with electrodes of high active area, if the electrode material is not catalytic to the desired electrochemical reaction. Considering hydrogen fuel in KOH electrolyte as an example, the reaction occurs by the steps: dissolved hydrogen approaches the electrode surface, adsorbs as H atom, and reacts with OH– at the surface, to form H_2O and an electron on the electrode. The electrode material is noncatalytic if it does not adsorb hydrogen, or if it adsorbs it to form stable surface compounds which cannot react further. Electrodes are, therefore, made of catalytic material, or made from a noncatalytic base material whose surface is covered with a thin film of catalyst. With good catalysts, hydrogen electrodes have small activation polarization, but oxygen or air electrodes always have some activation polarization. With the best available catalysts, hydrogen-oxygen cells give high currents with tolerable activation polarization even below 212" F (100° C). Hydrocarbon fuels, however, react slowly at the best anodes currently available and higher temperatures are necessary to give reasonable currents, so the performance of hydrocarbon fuel cells is not yet satisfactory. Catalytic properties are destroyed by adsorption of impurities which poison the surface.

A number of different types of fuel cells are described later, but the basic construction of most of them is similar to that of figure 2.1. If an electrode cracks, electrolyte leaks out into a gas chamber, and fuel and oxidant mix and may burn. Several types of cells use a porous matrix soaked in electrolyte between the electrodes, which retains the electrolyte and prevents gas from mixing even with a faulty electrode. In practice, cells are constructed *so* that they can be compactly stacked in series like slices in a precut loaf. The electrical performance of flat cells is characterized by ***(a)*** the current-voltage relation and *(b)* the thickness of the cell. To enable comparison between cells of different size, it is common practice to present curves of current density (A/sq ft) versus voltage, and to compare the watts per square foot of cell at a given efficiency.

1.3 APPLICATION OF FUEL CELLS

It is reasonable to expect that the first practical application of fuel cells will be for special purposes for which they have unique advantages. These applications are discussed first, and possible commercial applications discussed later.

The most promising immediate application is for electrical power supplies in space travel. It has already been pointed out that the energy storage density (kW-hr/lb) of hydrogen and oxygen is high compared to conventional batteries. It is well known that every extra pound of weight of a satellite or capsule put into a space flight requires many extra pounds of rocket fuel and motors and a considerable financial expenditure. Fuel cells are favored over other power supplies for certain types of missions because they give less weight for a given power and duration.

Conventional batteries or primary cells combine the functions of energy storage and energy conversion in one unit. The weight of a battery for a given duty is proportional to the product of power required (kilowatts) and the duration at this power (hours). For a given power, a doubling of mission time requires a doubling of battery weight. Fuel-cell systems have two parts: a fixed weight of energy converter (fuel cell and auxiliaries) and variable weight of energy storage (reactant and storage tanks). A fuel cell has to be big enough to supply the required power, but

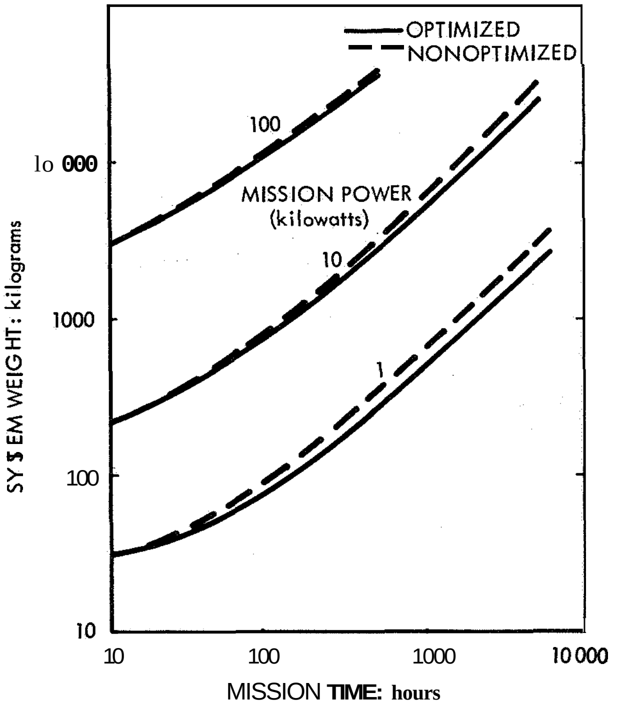

The weights are based on the Allis-Chalmers capillary fuel cell, with an expected future current density of 100 A/sq ft at 0.9 volt and 400 A/sq ft at 0.8 volt per cell. Values include the weights of hydrogen, oxygen, cryogenic storage tanks, insulation, controls and auxiliaries, etc.. and space radiators to reject the heat production of cells and electrical loads from the vehicle. Mathematical optimization was used to establish the conditions for minimum weight, and gave significant improvement over a nonoptimized system. At long-mission times, most of the total weight is weight of hydrogen and oxygen.

FIGURE 1.1.—Predicted total weight of hydrogen-oxygen fuel-cell system for space flight (Allis-Chalmers, 59, June 1964).

A combination of electrolytically regenerative hydrogen-oxygen fuel cells and solar cells looks promising for Earth satellites. Solar cells are used to supply power during the sunlight period of the orbit and also to charge a battery. The satellite power requirements during the dark period are obtained from discharge of the battery. Unfortunately, high-capacity batteries cannot be charged at high rates (A/lb) without drastically reducing the life of the battery. Extra battery weight has to be used, and for an orbit of *300* miles above the Earth's surface, the effective power density is only about **4** watts per pound of battery. Fuel cells can be used in place of batteries, with electrolysis of water to produce H_2 and O_2 in the light period and conversion of these back to water during the dark period. Research has indicated that the best system will use the fuel cells also as electrolyzer, with storage of generated H_2 and O_2 in high-pressure tanks integrated with the fuel-cell stack. Effective energy density may be 20 W/lb. Higher orbits reduce the advantage of fuel cells because the ratio of light to dark time is increased, and the required rate of battery charging is reduced to the point where the full capacity of the batteries can be used. Even so, when compared with batteries fuel cells have the promise of greatly increased lifetime, which is of great importance in a satellite designed to operate continuously for several years.

Fuel cells have also been considered for self-contained portable and semiportable power supplies for military applications, using hydrogen, methanol, or ammonia fuel and air oxidant. The advantage of the cells compared to batteries is their ease of recharging and the high specific energy (kW-hr/lb) of the fuels. The disadvantage is that a fuel-cell system is inevitably more complex than a conventional battery or primary cell, and it has not been possible to make small, reliable fuel cells for low powers (200 watts to be carried by a man, for example) which compare in weight or cost with batteries.

Above power levels of a few kilowatts, cheaper fuels with a high specific energy, such as gasoline, JP-4, or diesel fuel, must be used, either directly or indirectly (by re-forming to hydrogen). Compared with conventional generator sets, fuel cells have advantages of quieter operation and higher theoretical fuel efficiency. In practice, no present fuel cell can operate with the desired power density, efficiency, and reliability using hydrocarbons directly. When a re-former is used to generate hydrogen from the fuels, the overall fuel efficiency falls, since the re-forming process is about 50 to 70 percent efficient (depending on the process used). It is difficult to obtain high efficiency in small plants; large quantities of water are usually required, and noise level is increased. It has not been demonstrated that fuel cells will give higher efficiencies than other power supplies using these fuels, but work is continuing on systems for this application.

Another military application where the high fuel efficiency of fuel cells is a major advantage is in vehicle propulsion. The fuel efficiency of military vehicles is probably no greater than 15 to 25 percent and a fuel cell unit with an efficiency of 50 percent would have a great impact on the logistics of fuel supply. Again, only cheap fuels with a high specific energy (Btu/lb or Btu/gal) can be considered. There are other special requirements for a vehicle powerplant: it must be efficient and capable of widely varying load, have rapid start even at –65" F (–54" C), and have reasonable weight and size.

There is a disagreement about the required power density of the fuel cell and the size of the electric motors powered by the cell. It has been argued that a comparatively large gasoline engine (150 bhp, for example) is required because the engine has little overload capability for short periods of high power during acceleration. An electric motor has excellent overload capability and can be run at several times its continuous rated capacity for periods of minutes. Therefore, electric motors probably need only about one-fourth of the nominal rating of a gasoline engine; e.g., 28 kilowatts to replace 150 bhp. Counter to this, it has been argued that the rated capacity of a military engine is only about 40 percent greater than the required maximum continuous duty, and an equivalent electric motor must, therefore, be rated at about 70 percent of the gasoline engine, or 80 kilowatts to replace 150 bhp. The difference between a maximum continuous rating of 28 kilowatts and 80 kilowatts for fuel cell and electric motors makes a difference of several tons in the weight of the system. Power densities of 2 kW/cu ft and 22 W/lb for fuel cells have been quoted as requirements for vehicle propulsion (assuming 60 percent efficiency), but could be too low by a factor of **3.** These figures should include volumes and weights of cell auxiliaries. No present direct or indirect hydrocarbon fuel cells satisfy these requirements.

Fuel-cell systems for submarine propulsion, if mounted outside the hull, would improve buoyancy. Hydrogen-oxygen cells could be used, with hydrogen obtained from re-forming of methanol, ammonia, or JP–4, and oxygen stored cryogenically. An experimental fuel-cell system which uses sodium as fuel (see below) has been developed for submarine propulsion. Fuel-cell power seems feasible within the limits of space and weight involved in a submarine, but much development would be required to produce prototype units. The Allis-Chalmers Co. has developed a power supply for a one-man submarine, with hydrazine and oxygen as fuel and oxidant (ref. 1.1). The 750-watt unit measures 22 by 22 by 13 inches, including fuel for a 12-hour mission. It is mounted outside the internal shell of the submarine, so that the leakage of hydrazine vapor cannot produce a toxic atmosphere in the shell (hydrazine vapor is poisonous at 1 ppm).

Fuel cells have been considered for torpedo propulsion, but the requirement is for high power densities over 15 to 45 minutes, which is unfavorable for fuel cells in comparison with high-energy batteries. In addition, a solid rocket unit used in the Mark 46 torpedo produces about 4 horsepower per pound of engine weight, which is far beyond fuel-cell capability (ref. 1.2).

The discussion of possible space or military uses for fuel cells can be extended to many commercial applications, where the factors for and against their employment are similar. At present, fuel cells are expensive, perform well only on costly fuels such as hydrogen or hydrazine, and lifetime and ease of maintenance for extended operation have not been proved. Their use in the near future is likely to be limited to special applications where they offer particular advantages over other powerplants. Control systems which allow unattended operation for thousands of hours will probably be developed within the next few years. The cells may then find application as small powerplants for inaccessible locations where conventional generator sets cannot be used for some reason, or where the high efficiency of fuel cells allows longer times between refueling. The Institute of Physics in Bonn and the Brown Boveri Corp. are working on methanol-air cells for use in buoys (ref. 1.3); no controls appear to be needed for these units, nor do they use parasitic power.

A major difficulty in commercial application of advanced hydrogen-air cells is the cost and high storage volume of hydrogen. This disadvantage cannot be removed by development of better hydrogen cells. Either cells must be developed which operate efficiently on cheaper, more convenient fuels, or plants for producing cheap hydrogen must be integrated into a fuel-cell system. A number of industrial firms are developing hydrogen generators using liquid hydrocarbon fuels, but it is too early to predict the economics of an integrated fuel cell-hydrogen generator system. Present cells can be used where byproduct hydrogen is available, as demonstrated by Allis-Chalmers at Allied Chemical's chlorine-caustic soda plant (Solvay Process) in Syracuse, N.Y. (ref. 1.4). Control systems have to be developed and it is possible that some purification of H_2 will be necessary. The economics of the application may not be favorable even if cheap cells are produced.

Various demonstrations have been given of fuel-cell power for tractors, golfcarts, etc., but these must be considered as showing only that cells can be engineered into working units, since they would not be competitive with conventional power sources for these applications. The same remarks apply to demonstrations of cells lighting automobile headlights or working electric razors. An example of direct use of an organic fuel is the Esso methanol-air cell (ref. 1.5), operating at 140° F (60° C). The 100-watt unit has a volume of approximately 1 cubic foot, and an efficiency of 23 percent at maximum power and 40 percent at half power. Methanol is also used in the 5-kilowatt unit developed by Shell Research, England (ref. 1.6), but it is steam re-formed to H_2, which is then purified through a palladium-silver diffuser and used in a hydrogen-air cell, with caustic electrolyte at 140° F (60° C). The unit is mounted on a ¾-ton truck and has an overall efficiency of 20 to 25 percent. Again, the size, efficiency, reliability, and probable cost of such a unit offer no advantage over conventional generator sets.

Bottled gas (LPG) has been re-formed to hydrogen for use in a fuel-cell stack (ref. 1.7). The system could be used as a quiet generator for house-trailers already using bottled gas for heating and cooking. A wider application is the use of natural gas (mainly methane), either re-formed or directly in high-temperature fuel cells, in homes situated in areas where natural gas is cheap and electricity costly. Unfortunately, methane is a poor electrochemical fuel and is unsuitable for use in most cells. The economics of these home generators has been analyzed as a function of cell performance and load factor (ref. 1.8). Fuel-cell cost of $300 per kilowatt and life of 10 years would be competitive with commercial electricity, assuming delivered gas to cost 10 cents per therm (100 000 Btu). The assumptions involved, however, were somewhat optimistic.

Definite predictions of the feasibility of fuel cells for larger scale electricity production cannot be made this soon. Only cheap fuels such as coal, residual oil, natural gas, and vegetable fuels can be considered. At present, these fuels have to be converted to more active reactants for use in fuel cells; only natural gas offers any prospect of being directly usable in a cell. Gasification to a mixture containing hydrogen might be economically feasible on, a large scale, but purification and cooling for use in low-temperature cells would add capital cost and lower efficiency. High-temperature cells (see below) are less prone to poisoning by sulfur compounds in the gases and can use hot, dirty gases, but they have not yet been developed to satisfactory power densities, cost, and life.

Some of the problems of using fuel cells for large powerplants were discussed by Union Carbide (672,1960). This feasibility study of a 1000-megawatt plant operating at 500 volts for 30 minutes showed that more than 1 million cells and 45 tons of hydrogen would be needed for 30 minutes' operation. The sodium-amalgam cell (see below) was considered, but the inventory of mercury was equal to the annual world production, about six times the annual U.S. production, and would cost $52 per kilowatt for mercury alone. Fuel-cell electrodes with very large areas introduce problems of ohmic resistance in the electrode and current collector, current and temperature uniformity, gas distribution, and manufacture; maximum size is probably about 2 to 4 square feet. Cells are stacked to form modules containing up to 100 cells. Large amounts of power as low-voltage direct current require massive conductors and switch gear. It has been estimated (see sec. 2.3.6) that fuel-cell power will be competitive only when cost of the total system is not greater than $150 to $200 per kilowatt at fuel efficiencies of 55 to 60 percent.

Reid has discussed the use of fuel cells in automobiles (ref. 1.9). The units would be quieter than gasoline engines and would emit fewer air pollutants. He concluded that there might be a market for a small (15 hp) electric automobile with a range of 150 miles between refueling or recharging (electrolyzing to produce H_2 and O_2). A reasonable cost would be $50 per kilowatt, or $560 for the power unit. Hydrogen-oxygen fuels with a rating of 2 kW/cu ft and 25 W/lb would be suitable.

A principal difficulty with this concept is the storage space required for reactants. Such a unit would require about 60 kilowatt-hours of fuel, or more than 4 pounds of H_2. At 10 atmospheres pressure, this amount of hydrogen requires approximately 80 cubic feet of storage space. If hydrogen is produced by re-forming of hydrocarbons, the required overall power density probably cannot be obtained, and the system would probably emit some pollutants. There would undoubtedly be a large market for electric automobiles comparable in performance to conventional cars, since electric drive has many mechanical and safety advantages. However, conventional batteries have insufficient energy storage, and fuel cells do not look promising.

Various estimates have been made of the probable cost of fuel cells in standard production. Union Carbide (672, 1960) estimated about $83 per kilowatt for their hydrogen-oxygen cell, which is probably the lower limit for any cell. The raw materials for the Westinghouse high-temperature cell were given as $100 per kilowatt, mainly for platinum used in the electrodes. A catalyst loading of 1 gram of platinum per square foot ($\sim$1 mg/cm²) of electrode gives a platinum cost of approximately $40 per kilowatt when the cell produces 100 W/sq ft. Many electrodes contain about 5 grams Pt/ft². Jasinski states that nickel boride catalyst for hydrogen-alkaline anodes can be produced for $10 per kilowatt (ref. 1.10). There are indications that the amount of platinum for hydrogen anodes can be reduced considerably, certainly to less than $10 per kilowatt, by extending the platinum on boron carbide powder. It has not yet been possible to reduce the platinum loading for oxygen electrodes in acid electrolyte. The world production of platinum is about 10^6 troy ounces per year, and a large extra demand for platinum and palladium for fuel-cell units would undoubtedly lead to price increases, and possibly to inability to meet demand. Thus, no firm price can be estimated for future cells, since the factors affecting cost are changing with advancing technology.

1.4 ELECTRODES, CATALYSTS, AND ELECTROLYTES

Recent advances in single fuel-cell performance are due more to better electrode construction than any other single factor. The exact mode of operation of gas-diffusion electrodes is not understood, and electrodes cannot yet be designed from mathematical models. However, some qualitative facts are well established. First, examination of the mass-transfer equations for gas diffusing in the pores of electrodes indicates that pure H_2 and O_2 can diffuse at high rates even through relatively thick electrodes. However, when the gases contain impurities which are not reacted, these impurities build up during operation and reduce the mass-transfer rates. In particular, a baked carbon electrode of ¼-inch thickness and 30 percent porosity will transfer only enough O_2 from an air feed to support about 100 A/sq ft. Therefore, the trend has been toward thinner and more porous electrodes, and current electrodes are usually no thicker than 10 mils.

Second, it is known that electrodes which fill with electrolyte (flood) perform poorly as gas-diffusion electrodes. Flooded electrodes probably form a film of electrolyte over the gas face which is thick enough to prevent gas from reaching the electrode at sufficient rate, since diffusion of dissolved gas is slow. Therefore, electrodes are made nonwetting or they are made in two layers (double-layer electrodes), one of which contains fine pores while the other contains coarse pores. The fine-pore layer is next to the electrolyte and floods by capillary action. The coarser-pore layer is kept free of liquid by a small pressure differential between gas and electrolyte, which is not great enough to blow electrolyte out of the fine-pore layer. Electrolyte is stabilized at the junction of the two layers.

Third, electrodes are made with high internal surface area, catalytic to the reaction. The catalysts used are, in general, the same as those used a few years ago, but the effective area has been increased even though the weight of catalyst per electrode has decreased.

Electrodes of baked carbon, activated by impregnation with catalyst (usually platinum), give high initial performance on pure gases, but flood with time. They are wetproofed by immersing in a wax solution, removing and evaporating solvent to leave patches of wax in the interior. This prolongs life at low currents, but high current again produces slow flooding. Electrodes have to be thick to give long life; performance decreases with time and these electrodes are not competitive with other types.

Thin electrodes of porous nickel plaque are used in several advanced cells. They have double-layer structure, high porosity, and are impregnated with catalyst. Nickel cannot be used with acid electrolytes. The internal area of the plaque is relatively low and better performance is obtained at higher temperatures. Similar cathodes of porous silver perform well with oxygen and air at temperatures of 140" F (60" C) in alkaline electrolytes. The Justi type of electrode is similar to the nickel and silver electrodes, but is made with Raney nickel or silver particles. The Raney process involves dissolving one component of an alloy, which leaves the desired metal with very fine porosity and high internal area. The particles are formed into porous, double-layer electrodes, sintered to give strength. The electrodes have high performance in alkaline electrolytes but may be costly to make even in large quantities.

The most promising recent advance in electrode technology has been the development of plastic-bonded electrodes. A dispersion of small (0.2 to 0.5 μ) particles of inert plastic, usually Teflon, is mixed with small particles of catalyst, usually platinum black. The paste is spread on metal screen, pressed, and briefly heated to sinter the Teflon. These electrodes are thin, flexible but strong, very open and porous, and resist flooding to a high degree because the Teflon particles are hydrophobic. Performance on H_2 and O_2 is good in both alkaline and acid electrolytes, even at temperatures below 212" F (100° C), and the electrodes have been used up to 392" F (200° C). Platinum blacks prepared by reduction of platinum salt solutions with sodium borohydride are the most active blacks; they begin to sinter and lose activity at 302" F (150" C).

Thin membranes of Pd or Ag-Pd foil will absorb hydrogen and allow it to diffuse through at high rates. **A** suitably supported membrane can, therefore, be used as an H_2 electrode which retains electrolyte without any possibility of flooding. The electrode is activated on the electrolyte side by the deposition of a thin, porous, adherent film of high-area catalyst. The gas face adsorbs H_2 very rapidly when pure, but is easily poisoned, and it is also activated to increase gas-adsorption area. The main problem with this electrode when used at low temperatures appears to be short life due to poisoning.

Electrode life has been a problem in many cells. The general causes of decay of performance with time are: catalyst poisoning by impurities in electrolyte; poisoning by impurities from dissolution of other cell components; disintegration of an electrode due to slow attack; loss of contact between catalyst and current collector due to slow attack or poor initial bonding to the current collector; recrystallization of catalyst to less active area; and loss of wetproofing. Use of reasonably pure materials, inert cell components, and careful quality control of manufacture, plating, etc., have usually produced great improvement. Nonuniformity of current density and temperature across an electrode sometimes hastens attack of electrode components at certain areas of the electrode. Recrystallization of catalyst is more likely to be a problem as cell temperature increases, and probably involves either action of reactant gas on the catalyst (ref.1.11) or local corrosion cells. An extreme example is the high-temperature (1202" F (650" C)), molten carbonate cell where it has been found impossible to preserve high catalytic area in electrodes. The life of Teflon-bonded electrodes has been improved by a thin, porous film of Teflon particles on the gas face, which probably prevented flooding at this face. Problems of electrode life may not be an insuperable obstacle to long cell life, at least for low- and medium-temperature cells, since single-cell tests of many thousands of hours have been reported. Unlike batteries, fuel-cell reactions utilize only the surface layer of catalyst atoms and do not necessarily lead to massive rearrangement of electrode constituents. At present, units are more limited by occasional bad electrodes, or by other components.

It is impossible to summarize adequately all the work performed on catalysts. In many cases the comparison of true chemical activity cannot be made because of differences in effective area and electrode structure. Platinum or 50 Pt: 50 Pd weight-percent are the best catalysts for hydrogen electrodes, but Pd dissolves slowly in acid electrolytes. High-area nickel is good for H_2, especially at higher temperatures, but is improved by impregnation with platinum. Nickel boride is effective in KOH electrolytes, probably because it reacts to give high-area nickel. Polarization is small at good hydrogen electrodes and catalysis of the oxygen electrode is more important. Platinum appears to be the best catalyst for low-temperature oxygen electrodes, but silver of comparable area is also good (alkaline only), especially at somewhat higher temperatures. Nickel oxide, lithiated to provide semiconduction, is good for O_2 in medium-temperature, alkaline fuel cells.

The search for cheaper catalysts has not been successful, so attempts to use expensive catalysts more effectively by extending them on conductive carriers or by better electrode design are more likely to give immediate results. Oxygen electrodes and hydrocarbon electrodes usually have activation polarization and their performance increases with increase in the amount of catalyst used, expressed as mg Pt/cm^2 in Teflon-bonded platinum black electrodes, for example. Hydrogen electrodes have little activation polarization if a sufficient minimum of catalyst is present, and increased amounts of catalyst do not improve performance in the practical current region.

Concentrated aqueous electrolytes are used. Strong alkalis (KOH, for example) and acids (H_2SO_4) give best results; neutral electrolytes perform poorly in comparison. Potassium hydroxide is preferable to sulfuric acid for H_2-O_2 cells because it is less corrosive and because, under comparable conditions, the oxygen electrode gives about 0.1 volt more potential. However, for fuels containing carbon, or for air not purified from CO_2, KOH reacts with CO_2 to form carbonates and bicarbonates. Sulfuric acid is unsuitable for organic fuels in medium-temperature cells because it reacts with the fuels, and phosphoric acid or cesium fluoride-hydrogen fluoride have been used in direct hydrocarbon cells. Platinum electrodes are poisoned by adsorption of chloride ions and hydrochloric acid is not a good electrolyte.

Ion-exchange membranes (IEM) are used as electrolytes in the General Electric low-temperature hydrogen-air cell. An IEM consists of a lacy organic structure which contains firmly bonded, charged groups (sulfonate groups, for example). Ions of opposite charge are dissolved in water contained in the pores and are free to move. Thus, a cationic membrane will conduct by movement of H^+ through the water and an anionic membrane conducts via OH^-. In a fuel cell, H_2O is produced at the cathode (oxygen electrode) for a cationic membrane and at the anode for an anionic. Ohmic resistivity is high and the membranes must be thin to give low internal resistance of the cell.

Advantages of IEM's are that the electrolyte cannot flood an electrode and that they are easily assembled into thin cells. Intimate contact between electrodes and membrane must exist, since there is no free electrolyte to form a conducting bridge between electrodes and membrane. Cell performance is rather low, but the thinness of the cells compensates for this. Since water formed at one electrode by reaction cannot be taken up in the membrane, it tends to flood this electrode. On the other hand, the membranes are damaged by excessive drying, so careful water balance must be maintained.

Similar to the IEM is the use of a porous, nonconductive matrix to hold highly conductive electrolyte between electrodes. Porous asbestos is used in low-temperature cells and capillary forces retain electrolyte in the matrix, thus reducing electrode flooding. The matrix simplifies cell construction and improves reliability at the expense of only slightly higher internal resistance. A 30-mil asbestos membrane can tolerate an imbalance in the rate of water formation removal for a longer period of time than an IEM.

1.5 HYDROGEN-OXYGEN FUEL CELLS

Three low-temperature fuel systems are in an advanced state of development: the Union Carbide, General Electric, and Allis-Chalmers cells. They operate at less than 212" F (100° C) and near 1-atmosphere gas pressure; modules consist of a stack of flat cells in series with appropriate feed and control auxiliaries. When cells are stacked in series, the cathode of one cell is in contact with the anode of the next, and so on. This is usually accomplished by the sequence: cathode-0_2 space-barrier-H_2 space-anode (see ch. **4).** Electrical contact has to be made from cathode to anode across the gas spaces and barrier. The cell components are mounted in metal or plastic frames and bolted together to form the stack. Gas and electrolyte feeds are manifolded through connecting holes in the frames.

Union Carbide's cell has catalyzed, porous carbon electrodes and plastic frames. Electrolyte of 20 to 40 weight-percent KOH circulates through the cells and is used to remove product water and heat; the electrolyte space is packed with plastic mesh which spreads the electrolyte and prevents contact of anode and cathode. Silver-plated metal mesh is compressed in the gas space between electrode and metal barrier, to spread the gas and give electrical contact. The gas face of each electrode is coated with a thin, porous layer of nickel to reduce contact resistance between mesh and electrode.

The General Electric IEM cell also has plastic frames and electrodes of metal screen filled with Teflon-bonded platinum black. These are heat bonded into a sulfonated polystyrene cationic membrane which contains a strengthening mesh of inert plastic (Webril). A thin, ribbed sheet of titanium presses against the electrode and acts as current collector, gas barrier, and electrical contact between cathode and anode of consecutive cells. Oxygen electrodes are coated with a thin layer of porous Teflon, which aids the electrode in rejecting water to wicks pressed against it. These wicks are strips of absorbent material which take up and transport water by capillary action to an absorbent outside of the stack, or to a unit for water recovery.

The Allis-Chalmers capillary cell has anodes of porous nickel plaque catalyzed by impregnation with platinum and palladium, and cathodes of porous silver. Electrodes are pressed against a 30-mil-thick sheet of porous asbestos (soaked with 35 weight-percent KOH) which retains electrolyte by capillary action. The asbestos is contained in a gasket frame of neoprene. A grooved, nickel-plated magnesium plate acts as bipolar electrode holder, gas barrier, and electrical contact between anode and cathode of consecutive cells. Operating temperature is near 200" F (93.5" C) and product water is removed in circulating reactant gases or by transpiration through an auxiliary electrolyte-soaked membrane. In this last case (static water-vapor-control method), a chamber of water-vapor removal is present between anode and cathode of consecutive cells.

The Pratt & Whitney medium-temperature cell has been developed to a self-contained, automatic system for space use. Double-layer electrodes of porous nickel are fused to a grooved disk of nickel to form a barrier-gas space-electrode unit. Each cell has two of these units with facing electrodes, separated by a solid Teflon O-ring to form the electrolyte chamber. Cells are welded together to form a stack, with aqueous electrolyte of SO–85% KOH. This electrolyte is solid at room temperature but fluid at operating temperatures of 400" to 500" F (204" to 260" C). The low water content of the electrolyte enables the cell to operate at near-atmospheric pressure. Typical operating conditions are: temperature, 400" F (204" C); gas pressure, 50 psia; electrolyte and case pressure, 40 psia. (This cell evolved from the Bacon cell, which was similar in design but contained 40 weight-percent KOH electrolyte. At 400" F, gas pressures of approximately 50 atmospheres were required to prevent boiling of the electrolyte, with a consequent

TABLE ***1.1.–Performance of*** H_2-O_2 ***Fuel-Cell Units***[a]

Cell	Lpproximate electrod dimension, in.	Rated single-cell data		Unit power, watts	Weight, pounds	Life, hours
		A/sq ft	Volts			
Union Carbide:						
1961	6×6	40	0.8	560	...	150
1964	12×14	50	.8	[b] 320	...	>2600
General Electric IEM:						
Hope, 1962	7×10	15	.6	200	28	100
Gemini, 1965	7×8	40	.73	1000 (peak)	68	>400
Pratt & Whitney:						
1962	5 diam.	155	.87	280	...	>690
Apollo, 1965		...	.87	1400 2300 (peak)	220	>500
Allis-Chalmers:						
1962	11×6½	85	.8	1500	...	3000
1965	4×7½	150	.75	[b] 45	14.5	......

[a] The data are for complete units which were operated continuously with automatic or semiautomatic control. When no weight is quoted, the units were breadboard systems; weights given include all auxiliaries but exclude reactant and tankage weights. The number of cells in each unit depends on the desired power; the largest single units deliver between 1 and 2 kilowatts at normal rating. Higher power is obtained by connecting several units.

[b] These smaller units were built for specific purposes. Union Carbide and Allis-Chalmers have capability for larger units.

penalty of weight, cost, and difficulty of control.) Hydrogen and oxygen are fed to each cell via nickel tubes, and water is removed by condensation from circulated hydrogen.

Performance of the type of cell discussed above is shown in figure ***1.2,*** and table ***1.1*** gives some data on complete units. Single units range from approximately 50 watts to ***2*** kilowatts; **1** to ***2*** kilowatts appear to be a convenient maximum module size at present. The hydrogen and oxygen used are relatively pure (better than 99 percent) and the gas feeds are dead-ended into the cells. As gas is consumed, inert gas impurities build up in the cell chambers and cause decreased performance, so the cells are purged with a preset purge cycle. Purge consists of flushing the gas chamber with reactant gas, allowing the flushed gases to be wasted in the atmosphere. Purge was necessary on all of the units and represented **1** to **3** percent loss of efficiency. The flow of reactant gases to cells is automatically regulated by the pressure of gas in the cells. Removal of the waste heat developed in a cell stack has been accomplished by a number of different techniques during development of units, but the general pattern for the units in table ***1.1*** is as follows. Union Carbide cells have circulating electrolyte, which emerges hot from the cells and is cooled before readmission. General Electric cells are cooled by natural conduction along metal parts for small units, and by cooling fluid circulated through auxiliary chambers between cells for larger units. Allis-Chalmers cells are composed mainly of metal parts and operate at somewhat higher temperatures, giving good conduction to the external surface of a cell stack. The stack is encased and coolant gas blown through the case. Alternatively, the stack is surrounded by a jacket of adjustable vanes which allow heat loss when open but reduce heat loss when closed. Pratt & Whitney stacks have heaters to bring the cells to operating temperatures and heat removal is controlled by circulating hydrogen.

Before comparing the relative advantages and

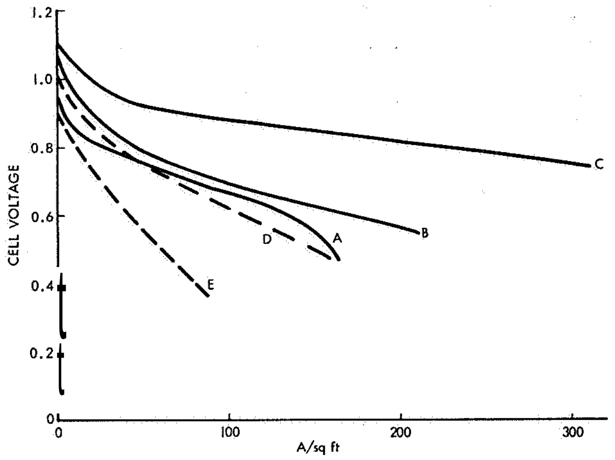

Key:
- A. General Electric IEM: 100° F (38° C) *(287)*
- B. Union Carbide: 12 *N* KOH, 113° F (45° C) *(652)*
- C. Allis-Chalmers: 35% KOH, 210° F (99° C) (37)
- D. Ionics double-membrane: concentrated H_2SO_4, 77° F (25° C) *(604)*
- E. Texas Instruments molten carbonate: 1112° F (600° C). Feed of $\frac{1}{3}H_2:\frac{1}{3}CO_2:\frac{1}{3}H_2O$
- F. Pratt & Whitney: 85% KOH, 392° F (200" C). Recent data not available, but curve is probably above curve C.

FIGURE 1.2.—Single-cell performance of various fuel cells.

disadvantages of the systems, it must be pointed out that the data given in figure 1.2 and table 1.1 are already out of date and by no means represent the ultimate capabilities of the systems. Performances in table 1.1 are those of currently available units, which were designed 2 to 3 years ago. The system experience gained with these units is being combined with advances in single-cell design to give improved power density and life, and this second generation of fuel-cell systems will be available within a year or two. Many of the research results on which future designs will be based are not readily available, and it is necessary, therefore, to accept reasonable estimates of future capabilities made by the industrial organizations developing the cells.

The single-cell performance of the Union Carbide cell has been greatly improved over that shown in figure 1.2, but the problem of short life at high performance has not been solved. Common electrolyte manifolds give internal shorting of the cell and parasitic current of self-discharge. This can be kept to small values by suitable design. A self-contained, automatic system has not been developed to the point where a firm figure for kilowatts per pound can be quoted. It is claimed that a new ion-exchange membrane has been developed for General Electric cells which will increase the life to thousands of hours at power densities of 20 W/lb. (Oxidative destruction of membranes, accelerated at higher temperatures, has been the major cause of short life.) Advantages of this cell are the lightweight components and simplicity of water removal. Disadvantages are the relatively low basic performance of the cell in W/ft^2, lack of flexibility of the water removal system using wicking, and the low upper limit of cell temperature. If water is not removed rapidly enough from the cathode, it fills the electrode pores and reduces performance by preventing oxygen from reaching the reaction area. Greatly improved power density has been obtained in research cells of Pratt & Whitney design (better than curve C of fig. 1.2) and considerable improvement in unit performance is expected in the future (35 W/lb at 60 percent efficiency). Advantages are the high basic power density plus flexibility of water control by circulated hydrogen. When a unit gives low performance, the temperature and water removal can be adjusted to improve performance. The all-metal construction gives a proportionately-high weight, and the circulating-hydrogen system introduces reliability problems of the auxiliaries involved. The cell cannot start from cold under its own power, since the electrolyte is solid at room temperature. The Allis-Chalmers system combines several advantageous features: it has a fairly high basic power, more temperature flexibility than the General Electric cell, and its static method of water removal is simple, yet capable of control to accelerate or retard water vapor removal.

The power densities and efficiencies of the three advanced systems (General Electric, Pratt & Whitney, and Allis-Chalmers) are similar for identical duties, even though single-cell performance is widely different, due to compensation of the factors involved. They have been shock, vibration, and acceleration tested and all can produce potable water for space missions.

The combination of high-performance, Teflon-bonded electrodes with the porous-matrix principle looks promising and may displace some of the cells used above. This type of cell, using electrolyte in porous asbestos as in the Allis-

Chalmers cell, is being actively developed by American Cyanamid, without, however, the systems experience of the other firms.

Another cell which has been investigated is the Ionics double-membrane cell. To avoid the problem of water removal from cells using ion-exchange membranes, two membranes are used with liquid electrolyte between them. Product water goes into solution and electrolyte is circulated, as in the Union Carbide system. Since concentrated electrolyte can be diluted to a considerable extent before performance falls, the external electrolyte loop acts as a reservoir for product water. In space missions it is desirable to recover the water, which can be done by osmosis of water through a vapor-permeable membrane. However, the cell performance is low (see fig. 1.2) and the complexity of the water-removal system is a major disadvantage.

An ideal space system would feature good single-cell performance, low operating temperatures (but ability to withstand higher temperatures), lifetime better than the mission requirements, and least complexity and number of moving parts compatible with flexibility of operation. The higher the power density of a given type of cell, then the the higher is fuel efficiency and unit power density. Eventually, however, a limit is reached where the removal of waste heat from the cell requires extra volume and weight which counteract the advantage of greater power density. The second generation of fuel cells may approach the limit where increased cell performance produces little extra advantage for space missions.

At present, control systems are based on conventional mechanical devices such as flow regulators, pressure controllers, temperature controllers, etc. Future systems will probably utilize digital computer control on a real-time, time-sharing basis on a computer in the spacecraft. Sensors and valves will still be required, but digital logic will be interposed between the sensed parameters and the control components. Such a system should be capable of automatic control over a wide range of load and environment fluctuations, and should be able to correct for certain expected malfunctions of the system.

As discussed in section **1.3,** solar cell-electrolysis-fuel cell combinations can be used for orbiting satellites. General Electric IEM cells were not satisfactory on electrolysis, due to rapid oxidative destruction of the membrane at an electrode evolving oxygen. The Pratt & Whitney system became excessively complex when used with a separate electrolyzer and circulating electrolyte. In this cell, the electrolyte must be maintained within a narrow range of water content, and a close balance of gas pressure across a cell is required to prevent electrolyte from being blown through the porous electrodes. The electrolytically regenerative cell being developed by Electro-Optical Systems is basically the same as the Allis-Chalmers fuel cell; it has catalyzed porous-nickel electrodes with electrolyte retained in a matrix of porous asbestos. Hydrogen and oxygen generated at the electrodes during electrolysis are stored in high-pressure containers built around the fuel-cell stack. The cells are thus surrounded by gas at the same pressure as gas within the cells, and do not have to be strong or heavy. Electrolyte in the matrix serves as a reservoir of water, and up to 50 percent of its water can be converted to H_2 and O_2. The matrix forces evolved gas to pass through the electrodes to the storage chambers, it retards diffusion of H_2 across the electrolyte space to the oxygen electrode (self-discharge of the cell), and it can withstand appreciable pressure differential without the electrolyte blowing out. Pressure increases during electrolysis and falls when the gases are converted to water in the fuel cell part of the cycle, but the cell operates satisfactorily with these varying pressures. When developed, this system will probably give considerable weight savings and increased life over conventional solar cell-battery units. Replacement of porous nickel electrodes with higher performance, Teflon-bonded electrodes may be feasible.

1.6 HYDROCARBON FUELS AND FUEL CELLS

Use of high-purity hydrogen and oxygen is clearly feasible only for special purpose such as spacecraft power supplies; general applications will require air and cheaper, more convenient fuels, such as natural gas, bottled gas, petroleum hydrocarbons, and coal. Methanol and ethanol are more costly, but would be feasible for some applications. All of these fuels contain carbon, and complete reaction produces carbon dioxide and water. The electrochemical reaction is different in principle from those of H_2, NH_3, N_2H_4, etc., because oxygen has to be supplied from the electrolyte at the anode. For example, adsorbed hydrogen reacts in acid or alkali as follows:

$$[H] \rightarrow H^+ + e^-$$
$$[H] + OH^- \rightarrow H_2O + e^-$$

Methane, however, requires decomposition of water:

$$CH_4 + 2H_2O \rightarrow CO_2 + 8H^+ + 8e^-$$

The steps involved in the formation of CO_2 are not known with certainty, but the formation is much slower than hydrogen ionization and large activation polarizations occur.

Two techniques are available for utilization of fossil fuels in fuel cells. The indirect method is to re-form them into H_2 and CO_2, take out CO_2, and use H_2 in the fuel cell:

$$CH_4 + H_2O \xrightarrow{\text{heat}} CO + 3H_2$$
$$CO + H_2O \longrightarrow H_2 + CO_2$$

Re-forming or partial oxidation processes are well known, and large-scale industrial equipment is available for generation of impure hydrogen. There is some loss of thermal efficiency and one estimate is that the cost is not likely to be lower than $1 per million Btu's produced for large plants using cheap fuel such as low-grade coal (ref. 1.12). Assuming an overall thermal efficiency of 70 percent in the fuel cell, fuel cost would be approximately 5 mils/kW-hr.

A more recent estimate is that impure hydrogen can be made from coal or natural gas at a cost of 50 cents per million Btu. Cost goes up as the size of the re-former goes down. Therefore, large-scale electricity production with re-formers and gas purification will not normally be competitive with conventional power production. On a smaller scale, the re-former/fuel-cell process might be competitive with diesel generator sets if cheap, efficient, small-scale re-formers can be developed.

Another approach is to develop fuel cells which use hydrocarbon fuels directly or semidirectly. In direct cells the fuel is electrochemically consumed to produce CO_2 and H_2O. Semidirect cells use hot, dirty fuel gases from a re-former integrated with the cell to reduce heat losses and capital cost. Re-forming may be carried out in the cell or in auxiliary chambers in the cell stack. Usually H_2 reacts much more quickly in a fuel cell than CO, so enough steam should be added to shift CO to H_2 and CO_2.

Rates of electrochemical reaction can be increased by increasing cell temperature. Two principal. types of high-temperature cell have been developed specifically for use with organic fuels. The molten-carbonate cell has an electrolyte of molten K, Na, and Li carbonates, and cell temperatures of 932" to 1292"F (500" to 700" C). Reactions are:

Anode: $CH_4 + 4CO_3^{=} \rightarrow 5CO_2 + 2H_2O + 8e^-$
Cathode: $2O_2 + 4CO_2 + 8e^- \rightarrow 4CO_3^{=}$

Note that the cathode must be supplied with carbon dioxide in addition to air. Molten carbonates have a tendency to creep over surfaces and it has not been possible to construct a cell with free electrolyte contained between porous electrodes. Electrolyte is, therefore, retained in a porous matrix of MgO refractory which has pore size less than electrode pore size. Capillary action prevents flooding of the electrodes. Alternatively, a paste of electrolyte and fine ($0.1\,\mu$) MgO has been used since it gives better conductivity, yet does not flow. Electrodes of porous metal are pressed against or bonded to the electrolyte matrix. Nickel anodes and silver cathodes, sometimes with double-layer structure, have normally been used.

Figure 1.2 shows a typical performance curve of this type of cell with a mixture of H_2, CO_2, and H_2O as fuel. Activation polarization is low with H_2 and air, but CO gives poor performance. Much better performance can be obtained with high flow rates of hydrogen, but a semidirect fuel cell must operate on fuel gases containing CO_2, H_2O, and CO. The cell cannot be run with dead-ended fuel feed, since CO_2 has to be removed; it must run with once-through fuel feed, and efficiency is high only if fuel is largely consumed before the gas exits. In practice, the cell does not appear to react methane or hydrocarbon fuels directly; steam has to be added to form hydrogen from the fuels.

The technical problems are as follows: molten carbonate cannot be expanded or contracted in volume by adjusting the rate of removal of water from the cell, as can an aqueous electrolyte.

Any change in volume of electrolyte in a matrix due to loss of carbonate by creep, reaction with components, or loss of volatile lithium compounds causes contraction of electrolyte away from the desired electrolyte-electrode interface. Electrolyte may have to be replenished from time to time. Because of the higher temperature, the loss of potential due to concentration polarization is three times that of room-temperature cells, for the same concentration change. A major cause of low performance is the depletion of hydrogen and buildup of carbon monoxide and carbon dioxide as the gas goes through the cell. Excess quantities of water for re-forming aggravate this effect. Direct electrochemical use of CO or hydrocarbons would have the same effect as an increase in mean partial pressure of H_2. However, high-area catalytic electrodes lose area by sintering and the extra performance is lost. Electrodes should also be thin to avoid concentration polarization of gas transferred through them. The lack of satisfactory electrodes is a major problem, although material, mechanical, and cost problems must also be solved.

The second principal type of high-temperature cell uses a solid electrolyte of zirconia-thoria or zirconia-calcia at 1652" to 1832" F (900° to 1000" C). These materials contain oxygen ions which become mobile at high temperatures and pass through the lattice, thus behaving similarly to ion-exchange membranes. Porous metal electrodes are intimately bonded to the solid electrolyte and fuel reacts with $O^{=}$ at the anode, while $O^{=}$ is formed from oxygen at the cathode. The only known suitable solid electrode at present is a thin film of platinum. Some of the same problems exist with this type of cell as with the molten-carbonate cell. Performance is good with H_2, but the cell does not use CO or hydrocarbons directly. As H_2 is consumed within the cell, performance decreases noticeably. The cell does not have the problem of stabilizing fluid electrolyte at the electrodes, which is an advantage over the molten-carbonate cell The major requirement is for cheaper electrodes which can utilize CO and hydrocarbons, although more feasible construction techniques are also required.

It is interesting that a great deal of unsuccessful work in the 19th century was aimed at reacting carbon anodes to produce power, carbon being in the form of coke or coal.

Investigation of true direct cells was spurred by the demonstration of complete conversion of ethylene to CO_2 and H_2O at a platinized anode at 176" F (80° C) in sulfuric acid (M. J. Schlatter, California Research *Corp.,* 1960). Even the most active hydrogen electrodes perform poorly with hydrocarbons, and higher cell temperatures are needed. General Electric has obtained promising results with propane fuel in a cell with Teflon-bonded, platinum black electrodes and electrolyte of concentrated phosphoric acid or cesium fluoride-hydrofluoric acid solutions at 300" F (149" C).

Direct hydrocarbon fuel cells have not reached a useful stage of development, primarily due to slow rates of electrochemical reaction of organic fuels. Platinum is the best simple catalyst for the reactions, and although binary and ternary alloys have shown improvement over platinum in certain circumstances,the improvementhas not been sufficient to make high power density practical anodes. Methane and hydrocarbons with more than 5 carbon atoms are more difficult to react than ethylene, ethane, propane, and butane. Straight chain hydrocarbons react faster than branched or cyclic analogs. Complete conversion of reactive hydrocarbons to CO_2 and H_2O has been obtained at platinum electrodes, but incomplete conversion occurs with fuels of more practical interest such as gasoline or JP–4. Concentrated acid is better than concentrated alkali for saturated hydrocarbons and the two electrolytes are comparable for unsaturated hydrocarbons such as ethylene.

Because activation polarization is a principal cause of polarization at hydrocarbon electrodes, performance is improved by higher operating temperature. Increase in temperature of the General Electric propane cell mentioned above gave doubled performance from 230" F (110° C) to 350" F (177" C); the factor of increase was low probably because other factors such as decreased fuel solubility were also involved.

The performance of methanol cells (reported in the contracts considered here) is poor. Again, the electrochemical reaction of the fuel is slow in acid solutions even though it can be used in high concentrations in the electrolyte. In addition, diffusion of dissolved methanol to the cathode seriously affects the cathode performance (this problem is not present with sparingly soluble reactants at gas diffusion electrodes). Complete conversion to CO_2 and H_2O was obtained. Porous electrodes pressed against an ion-exchange membrane have been used, with methanol dissolved in electrolyte flowing over the anode face. Carbon dioxide produced in the reaction became trapped between the electrode and IEM, and performance was improved by providing escape channels. Performance of methanol anodes and oxygen cathodes is better in concentrated potassium hydroxide, but the CO_2 produced combines with the electrolyte to form potassium carbonate. A system using dissolved methanol, KOH, and air cathodes is being developed for use as remote power source to operate for a year without refueling or supervision (ref. 1.13).In this case, potassium hydroxide is one of the fuel-cell reactants and is consumed with time.

Prognostications of long-term prospects for direct hydrocarbon fuel cells cannot yet be made with any degree of certainty. Some factors which have to be considered are as follows. Hydrogen-oxygen cells have been increased in useful current densities by two orders of magnitude by the extensive program of research dating from World War II. However, there is no guarantee that similar improvement will be obtained with direct hydrocarbon cells, because the present advanced technology of hydrogen-oxygen electrodes has already been applied to hydrocarbon fuel cells. The performance values for the General Electric propane cell were obtained with flow rates of fuel greater than stoichiometric. It is known from work on high-temperature cells that use of cells with near-stoichiometric feed (once-through operation) leads to lower performance or to excessive fuel loss in the exit CO_2-H_2O stream. It has also been found that hydrocarbons of high chain length, or methane, perform poorly compared with propane. A significant activation polarization of the cathode can be tolerated with hydrogen-oxygen cells, provided that the hydrogen electrode has low polarization. The large activation polarization occurring at both fuel electrode and cathode of hydrocarbon-air cells cannot be tolerated. A major breakthrough in catalysis and electrode construction is needed if the advantages of the simplicity and long life of low-temperature fuel cells are to be retained for hydrocarbon-air utilization.

1.7 OTHER TYPES OF CELLS

1.7.1 Amalgam Cells

The amalgam cell was first investigated by E. Yeager's group at Western Reserve University, which generated much of the basic information necessary for development of the cells. The M. W. Kellogg Co. has taken the cell to prototype development, with semiautomatic control (although the unit has not run for long periods of time). The anode consists of a vertical steel plate down which flows a thin film of sodium amalgam on the electrolyte side, containing approximately 0.4 weight-percent of sodium. A porous silver cathode (Electric Storage Battery proprietary electrode) is used with oxygen or air and electrolyte is sodium hydroxide at 150" F (65.5" C). Mercury is collected and cycled to an amalgamator where fresh sodium is added. The cell reaction is

Anode: $2Na \rightarrow 2Na^+ + 2e^-$

Cathode: $\frac{1}{2}O_2 + H_2O + 2e^- \rightarrow 2OH^-$

Thus sodium, water, and air are reactants and sodium hydroxide is the product. Unlike the cells described previously, the open-circuit voltage of the cell is near 2 volts; current density of 300 A/sq ft at 1.4 volts is readily attained with a good cathode.

This fuel-cell system has a high power density (12 kW/cu ft), but it is obviously limited in the applications for which it can be used. Sodium is expensive, and the amalgamator and mercury feed-collection components add complexity to the system. Much waste heat is generated in the amalgamator and the cell, and large volumes of cooling water are required. A feasible application is for submarine propulsion, but the fuel cost is still a disadvantage.

1.7.2 Thermally Regenerative Cells

A fuel-cell system with thermal regeneration of reactants is a means for converting heat into electricity which does not use the conventional heat cycle-electromagnetic generator principle. Thermally regenerative cells were investigated to determine whether they could produce electricity more efficiently and cheaply than conventional plants. The principle can be illustrated by means of the lithium hydride system. The anode is molten lithium in contact with an electrolyte of molten salts (LiCl-LiF, for example). The cathode is a high-temperature, gas-diffusion electrode of porous metal, supplied with hydrogen as oxidant. The cell reactions are:

$$\begin{array}{ll} \text{Anode:} & 2Li \rightarrow 2Li^{+} + 2e^{-} \\ \text{Cathode:} & \underline{H_2 + 2e^{-} \rightarrow 2H^{-}} \\ & 2Li + H_2 \rightarrow 2LiH \end{array}$$

The lithium hydride produced is removed from the cell and passed through a regenerator at a higher temperature to decompose it into liquid Li and gaseous H_2, which are cooled and reused in the cell.

A thermodynamic treatment shows that a simple cycle of this kind has a maximum theoretical efficiency of

$$\xi = \frac{\text{Electrical work}}{\text{Heat input}} = (T_2 - T_1)/T_2$$

where T_1 and T_2 are cell and regenerator temperatures. Several requirements must be fulfilled if such a cycle is to be feasible. The product must decompose rapidly at a reasonable temperature, since cell materials will deteriorate rapidly at excessive temperatures. The vapor pressure of lithium must be low at this temperature; otherwise, it is difficult to separate Li and H_2. The components must be in forms which are easy to recycle. The electrolyte must not undergo secondary reactions with the components (obviously, water must be excluded). Finally, the solubility of Li in the electrolyte must be low or the electrolyte becomes electronically conducting and shorts the cell.

Thermodynamic limitations also exist because a high cell voltage is obtained when the heat of reaction is high, but a high heat of reaction means that it is difficult to decompose the product. For a simple cycle, assuming the heat of reaction AH is approximately constant between T_1 and T_2, it can be shown that

$$\xi = (T_2 - T_1)/T_2 = \Delta F^0/\Delta H$$

where ΔF^0 is the standard-state, Gibbs free energy of reaction at T_1. If $\Delta F^0/\Delta H$ is low the efficiency is low, but if it is too near 1, the ratio T_2/T_1 is high and T_2 may be too high to be feasible, especially if it is above the boiling point of a liquid component. Applying these criteria, there are only a few reactions which are likely to be feasible.

Best cell results were obtained with a 5-mil niobium foil cathode in a cell made from niobium alloys, with special precautions to insure purity of all reactants and components. A steady OCV of 0.45 volt was found at 1020" F (549" C) and limiting current density was over 1500 A/sq ft. However, the cell had low electrode area per unit volume and was not a practical design. In addition, it was not possible to overcome the problems of moving molten components, regeneration of Li and H_2 was difficult, and a successful regenerator-cell cycle was never accomplished. Similar problems were found with other reactants; construction of practical cells was particularly hampered by problems of sealing the cells.

Another thermally regenerative cell is the potassium amalgam cell investigated by the Allison Division of General Motors. The cell is

$$KHg(l)/\text{molten } KOH\text{-}KBr = KI/KHg(l).$$

The amalgams acted as their own electrodes and, being liquid, made good contact with molten salt electrolyte contained in a porous refractory matrix. Cell reactions were

$$\begin{array}{ll} \text{Anode:} & K \text{ (high conc. in Hg)} \rightarrow K^{+} + e^{-} \\ \text{Cathode:} & K^{+} + e^{-} \rightarrow K \text{ (low conc. in Hg).} \end{array}$$

A reasonable concentration potential is obtained because the activity of K in Hg changes by orders of magnitude for relatively small changes of K concentration. Mercury was flowed through the cathode chamber at fast rates so that it never reached high concentrations of K, and pure K was used at the anode, with cell temperatures of 550" to 600" F (282.5° to 316" C). Regeneration would be accomplished by distilling mercury from the cathode stream to form potassium-rich mercury for return to the anode. Principal problems were rupture of the refractory matrix, leakage of seals under the pressure of mercury, electronic conduction due to potassium dissolved in electrolyte, and handling of the fluid streams. **A** mercury boiler was designed, but it was used only to regenerate some of the mercury required since it did not operate at a sufficiently high temperature to 'produce liquid potassium or even a suitable K-enriched Hg for the anode. A complete regenerative cycle was not achieved.

Regenerative cycles have low potentials and, therefore, ohmic resistance must be kept small or cell efficiency becomes small (0.2-volt polarization is not excessive for a normal fuel cell with an OCV of 1 volt, but it is a 50-percent loss of efficiency for an OCV of 0.4 volt). The construction and materials problems of these systems are formidable and cost is likely to be high. Complete regenerative operation was not achieved in any of the systems investigated and in several cases the thermodynamic limitations on regeneration were not fully appreciated. Since thermally regenerative cells have no special advantage over conventional heat-electricity cycles, they must compete directly in efficiency, cost, weight (for spacecraft), reliability, and life. Enough work has been done to show that they are not likely to be competitive and that high development costs would be necessary.

1.7.3 Thermogalvanic Cells

This type of cell is similar to thermally regenerative cells and is again used to convert heat to electricity. Instead of heat being absorbed in an external regenerator, thermogalvanic cells have one hot and one cold electrode. Alternatively, two cells at different temperatures are connected in parallel. Several different mechanisms may produce potential in thermogalvanic cells, but the basic principle is that electrode potential changes with temperature according to the well-known thermodynamic equation

$$nF\ (\partial E/\partial T)_P \simeq \Delta\phi,$$

where n is the number of electrons in the reaction, F is Faraday's constant; E electrode potential; T absolute temperature; P pressure; and $\Delta\phi$ is defined by $\Delta F^0 = \Delta H_0^0 = T\Delta\phi$; ΔF^0 is the standard-state free energy of the electrode reaction and ΔH_0^0 the ground-state (absolute zero) enthalphy of reaction. It is assumed that $\Delta\phi$ does not change much with temperature. Thus the OCV between two electrodes identical except for their temperatures is

$$\begin{aligned} E &= (\Delta\phi/nF)\ (T_2 - T_1) \\ &= K(T_2 - T_1) \end{aligned}$$

If two cells at different temperatures are connected, the same relation holds but $\Delta\phi$ is for the overall cell reaction. K has units of volts per degree.

In a simple thermogalvanic cell, heat flows from the hot electrode to the cold, and since the temperature differential must be maintained to give voltage, heat is continually lost from the cell. Assuming only IR polarization in the cell, the maximum electrical output compared to the loss of heat is

$$\frac{\text{Maximum power}}{\text{Thermal flux}} = (K/4\rho c)\,V$$

K is the temperature coefficient, ρ is the specific electrical resistance of the electrolyte, c the specific thermal conductance, and V is the OCV. Using representative values, the efficiency of thermal conversion is less than 2 percent.

Typical examples of such cells are: $Cl_2(g)$/molten $AgCl/Cl_2(g)$ using porous carbon electrodes; $Pb(l)$/molten $PbBr_2/Pb(l)$; BiI_3/molten salt/BiI_3 with porous carbon electrodes. Potentials are low unless high-temperature difference is used and thermal efficiencies and power outputs were small. Mass transfer from one electrode to the other is necessary to maintain operation. Cl_2 must transfer from the cold cathode to the hot anode, for example. Considerable trouble was experienced in attempts to build self-contained cells to operate at wide temperature differentials, especially with sealing problems due to differential thermal expansion. Work was discontinued when it was realized that efficiencies could be only a few percent.

An example of a double thermogalvanic cell is the Na/molten $NaCl/Cl_2$ cell proposed by Delco-Remy. In this system, calculations showed that if one cell was kept at 2732" F (1500° C) and the other at 1517" F (825° C), the theoretical potential of the cells connected in opposition would be 1.0 volt, at an efficiency of **34** percent (ignoring heat conduction from cell to cell). Sodium and chlorine would be ionized and combined to NaCl in the low-temperature cell and the NaCl pumped to the high-temperature cell. About 2 volts of the 3.2-volt output of the first cell would be used to electrolyze NaCl in the hot cell, regenerating Na and Cl_2 for return to the cold cell.

Laboratory cells were built of alumina, with liquid sodium anodes and porous carbon, chlorine diffusion cathodes. At 1517° F (825° C), OCV of a single cell was 3.2 volts and only IR polarization was observed even at current densities of 3000 A/sq ft. However, sodium dissolved in the melt and caused electronic conduction; faradaic efficiency of sodium consumption was less than 40 percent. Attempts to build practical cells failed due to materials problems. The higher temperature cell and the double-cell unit were not built.

The double thermogalvanic cell is basically unattractive because of complexity and the necessity for flowing molten metals or salts from one cell to another. High thermal efficiencies can only be obtained with large temperature differences, and high temperatures lead to severe materials problems. High temperatures favor intersolubility of liquid metals and molten electrolyte, so that the requirement of clear-cut phase separation is not obtained. There is also electronic conduction through the electrolyte due to dissolved metal, which leads to lower thermal efficiencies.

1.7.4 Photochemically Regenerative and Redox Cells

One possible means for converting radiant energy (sunlight, for example) to electrical energy is by means of photochemical decomposition of a compound to form reactants for a fuel cell

$$\mathrm{A} \xrightarrow{h\nu} \mathrm{B} + \mathrm{C}$$

$$\mathrm{B} + \mathrm{C} \xrightarrow{\text{fuel cell}} \mathrm{A}.$$

Photochemical decomposition occurs when a molecule absorbs radiant energy and converts it to intramolecular energy. The excited state produced may then decompose, it may revert to the original stable form by emission of radiation, or it may share the energy with other molecules by collision, giving rise to heat increase without decomposition. There are only a few reactions which convert most of the absorbed energy into decomposition products suitable for use in fuel cells. Examples are:

$$\mathrm{Ce^{4+}} + \tfrac{1}{2}\mathrm{H_2O} \xrightarrow[\mathrm{HClO_4}]{h\nu} \mathrm{Ce^{3+}} + \mathrm{H^+} + \tfrac{1}{4}\mathrm{O_2}$$

$$2\mathrm{NOCl} \xrightarrow{h\nu} 2\mathrm{NO} + \mathrm{Cl_2}$$

Early estimates of the possible efficiencies of photochemical decomposition were in error. When correct estimates were made, theoretical efficiencies fell to 5 to 10 percent. Unwarranted extrapolation from limited data suggested feasible power densities, but work since has shown the rates of formation of photolytic products to be small and experimental efficiencies are less than theoretical.

Nuclear radiation from fission products was used to produce a redox reactant and hydrogen, which were then used in a fuel cell:

Anode: $\tfrac{1}{2}\mathrm{H_2} \rightarrow \mathrm{H^+} + e^-$

Cathode: $\mathrm{Fe^{3+}} + e^- \rightarrow \mathrm{Fe^{2+}}$

Regenerator: $\mathrm{H^+} + \mathrm{Fe^{2+}} \xrightarrow{h\nu} \tfrac{1}{2}\mathrm{H_2} + \mathrm{Fe^{3+}}$

$$\overline{\text{radiation} \rightarrow \text{electrical energy}}$$

The system was partially developed for application as a long-life, low-power (5 watts) underwater power source, with a maximum efficiency of about 4 percent, but cost and unreliability made the system nonfeasible.

Redox cells employ aqueous redox couples which have high rates of electrochemical reaction; thus, in principle, avoiding activation polarization. An example is

Anode: $\mathrm{Ti^{3+}} + \mathrm{H_2O} \rightarrow \mathrm{TiO^{2+}} + 2\mathrm{H^+} + e^-$

Cathode: $\tfrac{1}{2}\mathrm{Br_2} + e^- \rightarrow \mathrm{Br^-}$

Anode and cathode are separated by an ion exchange membrane which allows $\mathrm{H^+}$ to pass but prevents mixing of anolyte and catholyte. To obtain continuous performance, products are removed and regenerated by chemical reaction:

Anode regeneration:

$$\mathrm{TiO^2} + \mathrm{H^+} + \tfrac{1}{2}\mathrm{H_2} \rightarrow \mathrm{Ti^{3+}} + \mathrm{H_2O}$$

Cathode regeneration:

$$\mathrm{Br^-} + \tfrac{1}{4}\mathrm{O_2} + \mathrm{H^+} \rightarrow \tfrac{1}{2}\mathrm{Br_2} + \tfrac{1}{2}\mathrm{H_2O}$$

For this example the cell potential corresponds to the overall reaction $\mathrm{H_2} + \tfrac{1}{2}\mathrm{O_2} \rightarrow \mathrm{H_2O}$. Under ideal, reversible conditions it was hoped that regeneration could be accomplished with cheap fuels, at low capital cost.

Thermodynamics imposes restrictions on the couples which are suitable. When the standard-state free energy of fuel corresponds to approximately zero volts in acid electrolyte, the couple must also have a standard potential close to zero volts. The fuel does not have enough energy to reverse the reaction and give regeneration if the standard couple potential is much more negative. On the other hand, when the standard potential is much more positive, then a reasonable fractional conversion of $Ti^{3+} \rightarrow TiO_2^+$, for example, occurs only near this electrode potential, which is a direct loss of energy from the fuel potential. Similar arguments apply to cathode couple and oxidant.

Anode couples which can be used in acid solution and regenerated with hydrocarbon fuels are titanous/titanyl or stannous/stannic. Unfortunately, regeneration is slow at ordinary temperatures, and at higher temperatures the couples form insoluble oxides which cannot be readily returned to the desired state. Similarly, regeneration of bromine with air is slow even in the presence of catalyst, and scrubbing towers are required to prevent loss of bromine in effluent nitrogen. The size and cost of regeneration units are prohibitive.

A redox cathode to increase the performance of air electrodes was investigated by Esso. Five weight-percent nitric acid in concentrated sulfuric acid gave reasonable cathode performance and the NO produced was reoxidized to nitric acid with air bubbled through the electrode or contacted with circulated electrolyte in an external regenerator. Regeneration was not complete, nitric acid was consumed, and the nitrogen oxides dissolved in the electrolyte diffused to the anode and adversely affected performance. The concept was abandoned.

1.7.5 Dry-Tape Fuel Cells

The Monsanto dry-tape fuel cell is an interesting attempt to combine the high-power density of conventional primary cells with the high-energy density of fuel cells. The cell consisted of a consumable zinc anode, a porous tape containing aqueous KOH electrolyte, and a cathode tape containing powdered AgO. On pressing the tapes together between the fixed zinc anode and fixed gold-plated cathode current collector, the cell $Zn/electrolyte/Ag_2O$ was obtained. A motor pulled tapes through the Zn/current collector jaws (spring loaded) at a rate to match the desired current density. Recharging is accomplished by putting in fresh reels of tape.

The energy density of the tapes was no better than that of a conventional Zn/AgO cell. The removal of spent reels and addition of new reels is a simple operation, but so would be removal of a discharged Zn/AgO cell and replacement with a new cell. The main advantage of the tape concept is that only the combined tapes are reactive; therefore, the tapes can be stopped and the remaining reactants will have only a slow rate of self-discharge. The concept is being applied to reactants with high-energy density, with an aim of a 200-W-hr/lb energy density. For reactants which do not self-discharge at open circuit, the conventional rectangular plate cell is preferable. For reactants which do self-discharge, it may be possible to employ conventional cell geometry with electrolyte tape pulled through the cell at the desired rate.

1.7.6 Hydrazine and Ammonia Fuel Cells

Fuel cells using inorganic fuels such as hydrazine or ammonia, and oxidants such as hydrogen peroxide or nitric acid, have progressed beyond the exploratory stage, but have not been developed into complete systems under Government contracts falling within the scope of this monograph. The energy density per unit volume is usually good for these liquid reactants, and the weights of storage tanks are low compared with high-pressure gas storage.

Hydrazine and ammonia *can* be considered as hydrogen carriers and nitrogen is produced in the half-cell reactions:

$$N_2H_4 + 4OH^- \xrightarrow{\text{Alk.}} N_2 + 4H_2O + 4e^-$$

$$N_2H_4 \xrightarrow{\text{Acid}} N_2 + 4H^+ + 4e-$$

$$NH_3 + 3OH^- \xrightarrow{\text{Alk.}} \tfrac{1}{2}N_2 + 3H_2O + 3e^-$$

or

$$NH_4^+ + 4OH^- \xrightarrow{\text{Alk.}} \tfrac{1}{2}N_2 + 4H_2O + 3e^-$$

Similarly, hydrogen peroxide can be considered as an oxygen carrier. It is not usually possible to obtain theoretical electrode potentials of these reactants when they are more negative than hydrogen evolution or more positive than oxygen evolution, even at very active electrodes. For example, the reversible hydrazine potential is over 0.2 volt more negative than the reversible hydrogen electrode, and hydrazine will ionize and hydrogen will be evolved at an active electrode. The OCV will lie somewhere between the two reversible potentials. A somewhat similar situation applies to hydrogen peroxide, which *can* react in two ways

	E_0, *volts*
$H_2O_2+2H^++2e^-\rightarrow 2H_2O$	1.77
$H_2O_2\rightarrow O_2+2H^++2e^-$	*0.68*

OCV will usually lie between these two potentials, and oxygen will be evolved.

Highly soluble reactants, such as hydrazine, ammonia, or nitric acid, are used in dissolved form, although some of them can obviously also be used as gases fed to a gas-diffusion electrode. A flooded diffusion electrode for dissolved fuels must have sufficient catalytic area to give low activation polarization and it must be open enough to allow reactant to diffuse into the area. A useful technique is to force dissolved fuel through an electrode at a rate corresponding to the current required (flowthrough electrode), since this reduces concentration polarization. There is evidence that N_2 evolved from N_2H_4 or NH_3 holds up in flooded diffusion electrodes and reduces performance, whereas it is forced out in a flowthrough electrode. A major problem with highly soluble reactants, which does not exist with H_2, O_2, or sparingly soluble hydrocarbons, is that fuel *can* diffuse through electrolyte and reach the oxidant electrode in high concentration, and vice versa. Normally, this drastically reduces cell performance and faradaic efficiency, and has to be prevented by ion-exchange membranes between the electrodes.

Most of the work on these reactants reviewed here was of an exploratory nature. Primary conclusions are:

(1) Hydrazine in solution is an effective fuel and can be reacted at high current density, even at relatively low-area electrodes and low temperatures; catalysts for the reaction are similar to those for hydrogen ionization, but rhodium is especially active. At active electrodes the reaction has an OCV more negative than hydrogen and the electrode will evolve hydrogen, especially at high hydrazine concentrations. As current is drawn, the electrode ceases to evolve hydrogen and hydrazine is used at close to 100 percent faradaic efficiency.

(2) Evolution of gases in flowthrough electrodes has no deleterious effect on performance of the electrode.

(3) Ammonia is relatively inert as **an** electrochemical reactant and requires very active electrodes or high temperatures. It ***can*** be used only with basic electrolytes since NH_4^+ formed in acid solutions is stable and not readily oxidized. It is perhaps best used by first cracking it to N_2 and H_2 followed by H_2 reaction in a gas-diffusion electrode.

(4) Hydrogen peroxide normally gives a **po**tential less than the reversible oxygen potential; oxygen evolution **occurs** and faradaic efficiency is low. Under comparable conditions the polarization in sulfuric acid electrolyte was about 0.2 volt higher than in potassium hydroxide electrolyte.

(5) The cathodic nitric acid reaction is complex and produces mainly NO; no conversion to N_2 was found. It is necessary to use high concentrations of nitric acid to obtain potentials near 1 volt, and it is difficult to consume appreciable fractions in one pass through a flowthrough electrode.

(6) The ion-exchange membranes used were not satisfactory as separators between the anode and the cathode chambers, since they passed other ions or dissolved reactants in addition to hydrogen ion (cationic) or hydroxyl ion (anionic). This allowed depolarization of one electrode by the other electrode reactant.

(7) Best performance was obtained with concentrated acid or alkali electrolytes; neutral electrolytes were not satisfactory. Results in this area have sometimes been contradictory. For example, faradaic efficiency of hydrazine in acids was low due to the formation of NH_4^+ by a side reaction, but some investigators reported 100 percent faradaic efficiency in sulfuric acid solution. Similarly, one report stated that ammonia used with molten hydroxide electrolytes gave large fractions of nitrates and nitrites, but another reported only slight formation of these compounds.

Hydrazine derivatives such as dimethyl hydrazine were less active, and electrochemical conversion at good potentials was incomplete, giving organic products such as methanol. Thus, the complete energy content of the compounds was not obtained.

Fuel cells using hydrazine and oxygen (or some other oxidant) could undoubtedly be developed as high-power-density cells for special applications. The cell would have no advantage over hydrogen-oxygen cells unless the hydrazine were stored and used in liquid form to make storage tanks light weight and allow nitrogen to be easily separated from the circulated electrolyte. For long-term operation, water must be removed from the electrolyte, but it is still possible that control of the cell would be simpler, with fewer auxiliaries, than for hydrogen-oxygen cells. A disadvantage for manned-flight applications is the high toxicity of hydrazine, **1** part per million. For short-term operation, the cell could be competitive with high-energy-density primary cells. Low-resistance membranes able to prevent the intermixing of the anodic and cathodic reactants must be developed, as well as an electrochemically reactive, high-energy-density oxidant which can be easily added to circulating electrolyte, and whose reaction product can be easily removed from the electrolyte.

1.7.7 Biochemical Fuel Cells

A biochemical fuel cell usually consists of a normal cathode (oxygen or air) and an anode immersed in electrolyte containing organic material and micro-organisms. Alternatively, an enzyme or organism may be attached to the bioelectrode. Electrolyte with organic matter is usually separated from electrolyte near the other electrode by a permeable membrane which allows ions to pass through but retains the relatively large bacterial cells and enzymes. Cell performance is low until active bacteria or cell extracts containing enzymes are added. Two distinct modes of operation of bioelectrodes have been proposed. First, it is possible that bacterial or enzymatic action on the primary reactant produces compounds which can react in the normal way at the electrode. For example, production of alcohol from fermentation of a sugar gives an electrode performance comparable to that of the same concentration of alcohol added to the anolyte. Such systems are called "indirect" biochemical fuel cells. Second, direct biochemical-fuel-cell action has been proposed where the biological agent transfers electrons directly to or from the electrode.

There are three major uses for biochemical fuel cells. In underdeveloped countries without indigenous fossil fuels, a biochemical fuel cell could be used to generate electricity from vegetable or animal matter. A cell suitable for this application would have to be cheap, long lived, and not require skilled supervision. Use of biochemical fuel cells for military purposes is somewhat similar; the advantage of the system is that it could use natural products as fuels and sulfate-containing sea water as electrolyte as well as a source for cathodic oxygen. A third application is in space travel, where the biochemical fuel cell might form part of a closed ecological cycle involving human food and waste products.

The first two applications share the feature that it might not be possible to have the invariant electrolyte which is required in most other fuel-cell systems. The ideal system would, of course, degenerate organic material completely to evolved gases such as carbon dioxide, water vapor, nitrogen, etc., but it is improbable that this can occur with fuels of practical importance. Another desirable alternative would be decomposition to gases and a sludge or ash which could be readily separated from the electrolyte, leaving it invariant with time. Again, this is not likely to occur in practice. The third alternative is to have a cheap, readily available electrolyte which can be discarded with the products and unconsumed material. On the other hand, the closed ecological system for space travel will require virtually complete recovery of the electrolyte from unconsumed (in the fuel cell) material.

There is little evidence to support the concept of the "direct" bioelectrode. A "direct" action would be expected only where enzymes are liberated from the cells, since the wall of a bacterial cell separates enclosed reactants (enzymes) from an electrode surface by a distance which is too great for the reactants to affect the potential energy path of electron transfer across the electrical double layer. The contents of the reports reviewed suggest that cell suspensions and cell-free suspensions of enzymes give similar results at bioanodes. Results *can* always be explained on the basis of electroactive chemicals, such as H_2, HN_3, or HCOOH released in the bioelectrolyte by bacterial or enzymatic reaction, followed by diffusion of the chemicals to the electrode surface.

If it is accepted that bioelectrodes have an "indirect" mode of operation, then two performance parameters are significant: rate of chemical production in W/cu ft or W/lb, and electrode performance in watts per square foot. No estimates have been given for the upper limit of the first-performance criterion, but the maximum value achieved was approximately 30 W/cu ft. It would be helpful to have a listing of the rates of other biochemical reactions to see what order of magnitude is to be expected. This would give an indication of upper limits which might be obtained by selective breeding of bacterial strains. Performance of electrodes in watts per square foot was low, but the values could probably be increased considerably by normal techniques of electrocatalysis and improvement in mass transfer. In all cases, electrochemical tests were made at the temperatures at which bioaction was optimum; these temperatures were about 86" to 104" F (30" to 40" C). If chemical production is separated from use at an electrode, then the electrode performance can be improved by using higher temperatures.

Bacterial cells were grown in nutrient solutions containing raw fuel, and produced electrochemically active fuel in the process. If the growth solutions were not buffered, pH changes caused by the reactions decreased the rate. Rates of cell growth and enzymatic production of chemicals were strongly affected by pH and temperature, and small increases or decreases of these parameters about optimum values rapidly decreased the rates. The rate of production of chemicals was higher in growing conditions than in resting conditions, which is hard to explain on the basis of enzymatic breakdown of fuels. Optimum pH was usually in the region of 6 to 7 pH units. Unfortunately, the performance of oxygen electrodes is poor in this pH range.

Bacillus pasteurii produced ammonia from urea and human urine at significant rates. However, the ammonia formed NH_4^+ in the neutral buffered solutions used and ammonium ion was unreactive as an electrochemical fuel. Power density from platinized platinum electrodes in urine-feces mixtures containing indigenous microorganisms was only 0.03 W/sq ft. ***Aeromonas formicam*** was active in producing formic acid from sugars and coconut juice in phosphate-buffered electrolyte. However, it was thought that 1 mole of formic acid was formed per mole of glucose, giving a low rate of conversion of energy to a usable form. In addition, the other products of the enzymatic and biological reactions poisoned the system, and the electrolyte must either be discarded or regenerated from the side products.

Hydrogen was produced from several systems, including ***Escherichia coli*** plus formate and ***Clostridium welchii*** plus glucose. This latter system gave a production rate of approximately 30 W/cu ft, at 35" C and pH 6.8 to 7.0, with 1 to 2 weight-percent glucose, plus nutrients. The practical conversion of glucose to H_2 was not determined. It was not found possible to generate sugars from bacterial or fungal attack on cellulose.

In summary, it can be concluded that there is little immediate prospect for the application of biochemical fuel cells in industrialized societies. However, with the advent of solid-state electronic devices (e.g., the transistor radio) which have long life and low-power requirements, it is possible that a low-power biochemical fuel cell will find application in underdeveloped countries. A principal requirement for this application is a cheap, foalproof, air electrode with a lifetime of at least 10 years.

1.8 FUNDAMENTAL KINETIC STUDIES

The usefulness for fuel-cell work of the basic information on hydrogen-oxygen kinetic mechanisms discussed in chapter 17, and hydrocarbon reaction mechanisms discussed in section 15.5, has been probably rather small. Practical electrodes have been developed by trial and error, using the general concepts that an electrode must have *(a)* high catalytic area, *(b)* good mass-transfer properties, and (c) low ohmic resistance.

The term "fundamental" research is used here to mean research aimed at providing a precise causal description of phenomena. Basic or fundamental research used in the titles of contracts or reports sometimes means preliminary or laboratory scale experimentation. Information from "basic" research, using the wide definition, is obviously of great value, since development of practical devices is dependent on this information. The difference in definition is largely a matter of degree: a quick empirical survey of the relative activities of different fuels at an electrode is of considerable value, but the reasons why the fuels behave as they do are more fundamental and require orders-of-magnitude more effort to elucidate. Accepting that fundamental research, in the narrow definition, is more time consuming, it is not surprising that practical results are often achieved empirically before details of the basic chemistry are completely understood. This does not mean that fundamental research is of no practical importance. The three general concepts used in the development of practical electrodes which were quoted above can be considered as products of forms of fundamental research, and present research on kinetics and catalysis will eventually lead to similar general concepts of great importance.

Experience shows that platinum and platinum-palladium alloys are the best catalysts for hydrogen; nickel is suitable in alkali, especially at high temperatures. Similarly, platinum is best for oxygen electrodes, with silver suitable in alkali, and lithiated nickel oxide at higher temperatures in alkali.

A satisfactory theory of catalysis, including electrocatalysis, is urgently needed. Elucidation of the chemical mechanisms of gas adsorption, surface rearrangement, and electrochemical reaction is a laborious process. Few surface reactions are satisfactorily described and understood in spite of many years of effort expended in this study. Unlike normal chemical compounds, the properties of surface compounds vary with the amount of surface covered. No satisfactory theory of surface bonding exists, and even if the mechanisms were known, the slow rates of reaction would have to be improved before practical application would be profitable. Unfortunately there is at present no way of predicting which catalyst would best accelerate the process, although a general theory of surface reactions might possibly aid in such a choice. Such a theory will be developed when the mechanisms of enough reactions at different materials are elucidated to form a basis for theoretical models. Fundamental chemical theory must advance to the state at which precise models can be proposed for the bonding states of surface compounds.

A major breakthrough in catalysis theory probably will not occur in the immediate future unless novel methods and concepts are introduced. Empirical exploratory research usually produces immediate benefits, but research on reaction mechanisms and catalysis should be considered a long-term investment. Empirical testing should be carefully controlled and use fundamental techniques; otherwise, results may be meaningful only for the particular arbitrary conditions used. Whatever type of research is performed will eventually be productive if it is done well and does not follow paths that have already been shown to be sterile.

The work on oxygen adsorption on metals discussed in section 17.2 is an example. It was stated that adsorption was slow on platinum until 302" F (150" C). Yet this metal is the best known catalyst for oxygen in low-temperature fuel cells. Oxygen formed surface compounds on silver at 900° F (482.5" C); it was several layers thick, but it could be readily desorbed. This explains why silver is a good oxygen electrode for high-temperature cells, but raises the question of the nature of this compound, which is unlike any known oxide of silver. Similar contradictions and lack of knowledge appear in many places in chapter 17 and section 15.5.

Oxygen ionization is basically a much slower reaction than hydrogen ionization. Thus a hydrogen-oxygen fuel cell with anode and cathode of comparable structure will experience more activation polarization at the cathode.

In acid solution, hydrogen probably ionizes in the following steps, which may each consist of several steps:

$$H_2(aq)+2Pt\,[H_2O]\rightarrow 2Pt\,[H]+2H_2O$$

or

$$H_2(aq)+Pt\,[H_2O]\rightarrow Pt\,[H]+H^+\cdot H_2O+e^-$$

and

$$Pt[H]+2H_2O\rightarrow Pt\,[H_2O]+H^+\cdot H_2O+e^-$$

The brackets denote a surface compound.

In alkaline solution

$$H_2(aq)+2Pt\,[H_2O]\rightarrow 2Pt\,[H]+2H_2O$$

or

$$H_2(aq)+Pt\,[H_2O]+OH^-\rightarrow Pt\,[H]+2H_2O+e^-$$

and

$$Pt[H]+OH^-+H_2O\rightarrow Pt\,[H_2O]+H_2O+e^-$$

All surface complexes probably have some bonding with further water molecules.

At open circuit, platinum hydrogen electrodes have large amounts of hydrogen adsorbed on the surface. Five percent carbon monoxide poisons platinum hydrogen electrodes at 176" F (80° C), but the effect is less for lower concentrations of carbon monoxide and higher temperatures. Presumably, the CO adsorbs on the platinum and prevents surface [H] from being formed.

It seems probable that a platinum cathode in contact with oxygen tries to reach 1.23 volts, but at potentials greater than about 0.8 volt, oxide layers start to form on the electrode. At about 1.0 volt, the oxide film, formed over a long time, is thick enough to slow the rate of oxygen ionization considerably compared to that of bare platinum, and the rate becomes so slow that secondary reactions interfere to give an OCV of about 1.0 to 1.1 volts. Gold does not form a low-reactivity film until about 1.25 volts, but the rate of oxygen ionization on gold is much slower than on platinum.

Oxygen ionizes, in alkaline solution, by the steps

$$O_2(aq)+Pt[H_2O]\rightarrow Pt[O_2\cdot H_2O]$$

$$Pt[O_2\cdot H_2O]+e^-\rightarrow Pt[HO_2]+OH^-$$

$$Pt[HO_2]+H_2O+e^-\rightarrow Pt[H_2O]+HO_2^-$$

and

$$Pt[HO_2]+2H_2O+2e^-\rightarrow Pt[H_2O]+2OH^-$$

or

$$Pt[HO_2]+H_2O+e^-\rightarrow Pt[H_2O]+OH^-+\tfrac{1}{2}O_2$$

This is called the peroxide mechanism. Activation polarization can be due to the slow breakdown of peroxide. Practical hydrogen-oxygen fuel cells give close to 100 percent conversion of hydrogen and oxygen consumed to current (100 percent faradaic efficiency) showing that any hydrogen peroxide produced is eventually utilized. The mechanism in acid solution is not understood, but may involve dissociative adsorption of oxygen.

Carbon dioxide poisons the platinum oxygen electrode at room temperatures, but the poisoning is eliminated at 176" F (80" C). Platinum is the best catalyst for hydrocarbons and oxygenated hydrocarbons although there is some evidence (see sec. 15.2.2) that alloys of Pt-Ru, Pt-Ru-Au, and Ru-Rh are better than platinum alone for methanol.

Ethylene is electrochemically oxidized completely to CO_2 and H_2O in sulfuric acid at 176" F (80" C) on platinum, iridium, and rhodium electrodes, but goes to aldehydes and ketones at gold and palladium electrodes.

An interesting attempt to study the effect of catalyst structure was made by Monsanto (sec. 15.2.2), using planar metal chelates as catalysts. The catalysts were impregnated on porous carbon electrodes. With dissolved hydrazine, formic acid, and methanol as fuels, the impregnated electrodes were more active in many cases than noncatalyzed electrodes; electrolytes were KOH at 194" F (90° C) and cesium carbonate at 302" F (150" C). No pattern was present in the results, but chelates containing platinum were consistently superior to other chelates, with effects varying between one platinum chelate and another.

Oxygen adsorbs on platinum and poisons it as a hydrocarbon electrode; the electrode has an open-circuit potential between that expected from the fuel and that expected from oxygen. Slow reaction of the fuel removes oxygen from the electrode and the rate of fuel ionization increases. The electrode potential then comes nearer to the expected value for the fuel and the electrode becomes active. Adsorbed oxygen, therefore, leads to an induction period of low electrode activity.

A mechanism suggested for hydrocarbon reaction is:

$$Pt+H_2O\rightleftharpoons Pt[H_2O]$$

$$Pt[H_2O]\xrightarrow{\text{slow}}Pt[OH]+H^++e^-,\ \text{low coverage}$$

$$Pt+\text{fuel}\rightleftharpoons Pt[\text{fuel}]$$

$$Pt[\text{fuel}]+Pt[OH]\rightleftharpoons Pt+CO_2+H^++e^-.$$

The slow step is the decomposition of adsorbed water molecule and rates of reaction of all hydrocarbon fuels should be almost the same. Another possibility is the formation of a fuel-water complex on the surface, followed by slow decomposition of the complex

$$Pt[\text{fuel}]+H_2O\rightleftharpoons Pt[\text{fuel}\cdot H_2O]$$

$$Pt[\text{fuel}\cdot H_2O]\xrightarrow{\text{slow}}Pt+CO_2+H^++e^-.$$

This mechanism predicts rates dependent on the bonding energy of fuel-electrode water and hence dependent on the type of fuel. Theoretical predictions of behavior based on these mechanisms do not agree with experiment and it seems probable that complex mechanisms and surface compounds are often involved. Rates of adsorption of fuels may also be rate controlling; rates of adsorption increase in the order: acetylene > ethylene > ethane, but rates at low polarization are in the reverse order (see table 15.13). Thus, at low power output and high efficiency, saturated hydrocarbons are preferred, but at high output and low efficiency, unsaturated hydrocarbons may be better. A more detailed discussion of the various mechanisms proposed for organic fuels is given in chapter 15.

1.9 MODE OF OPERATION OF DIFFUSION ELECTRODES

As stated previously, gas-diffusion electrodes are the heart of many types of fuel cells. Three major theories exist for the mode of operation of porous, gas-diffusion electrodes of sparingly soluble gases (see ch. 18). One theory postulates that reactant gas chemisorbs on metal surface in the electrode which is not covered by electrolyte. The adsorbed gas travels over the surface by surface diffusion, jumping from one site of adsorption to the next, and diffuses to a site covered by electrolyte. It is then in a position to ionize or react with the electrolyte.

A second theory postulates that the interior surface of an electrode is entirely covered by a thin film of electrolyte, of 0.1- to 1-micron thickness. The exact cause of the film is not known, but it is presumed to be due to capillary forces which can form the film without completely flooding the pores of the electrode. Gas diffuses along the axis of a pore, dissolves in the thin film of electrolyte on the pore walls, and diffuses in the liquid to submerged metal surface. Here it chemisorbs and reacts with the electrolyte. High rates of mass transfer occur because the electrolyte film has a high area and is very thin. There is evidence that this thin-film model applies to wetted, porous, metal electrodes.

A third theory postulates that gas diffuses along a pore until it reaches the electrolyte surface, where it dissolves and diffuses in the liquid till it reaches submerged metal. This model was proposed to explain the high current densities of nonwetting electrodes, where it seems improbable that an extended thin film exists within the electrode. This simple-pore model can only give high rates of mass transfer to submerged surface if the mean diffusion path for a dissolved gas molecule is short. This occurs only when the pore size in contact with electrolyte is small (less than 0.5 micron).

Gases such as H_2, O_2, and hydrocarbons dissolve rapidly in aqueous electrolytes, but their solubility and diffusivity are low. High rates of mass transfer of dissolved gas are obtained only if the length of liquid between the point of dissolution and the point of reaction on the catalytic electrode is short. An electrode can be visualized as having a spongy structure containing interconnected pores, some of which are large (several microns in diameter) and others of which are small (less than 1 micron). When the large pores are kept free of electrolyte, gas diffuses in and dissolves in the electrolyte contained in the small pores. The effective internal area of gas-electrolyte interface at which gas solution occurs can be very large for a wetted electrode; i.e., several hundred square feet per square foot of plane area.

However, the second model states that the interior tends to be covered with a continuous film of liquid which hinders diffusion of dissolved gas. Then the electrolyte in the micropores is not saturated with dissolved gas when current is drawn. When an electrode is made nonwetting by incorporation of a wetproofing agent, the interior of the electrode is not completely covered by electrolyte. Double-layer capacity measurements have shown that a 5-mil-thick Teflon-bonded platinum black (9 mg Pt/cm^2) electrode, used as an H_2 diffusion electrode in $1N$ H_2SO_4 at 77° F (25° C), has only 3 percent of its internal area in contact with electrolyte (unpublished results of S. Almaula and L. G. Austin). The internal area of gas-electrolyte interface is undoubtedly greater than the plane area, but not several hundred times greater. The third model states that dissolution and diffusion of gas to wetted platinum black can still be rapid, provided the micropore diameter is small.

The ideal gas-diffusion electrode would have the internal area of fine-pore catalyst completely wetted, yet not have films of liquid covering this area, or liquid filling the larger pores which act as gas feeders. This ideal electrode has not yet been achieved.

A flooded diffusion electrode consists of a porous electrode completely immersed in electrolyte containing a dissolved fuel, such as methanol, dissolved in aqueous potassium hydroxide. Theoretical treatments predict that the interior area of the electrode is completely utilized at low currents, but mass-transfer and ohmic effects come into play at higher currents. Under useful current conditions, diffusional mass transfer of dissolved fuel into the electrode can lead to depletion of reactant concentration to zero in the electrode interior. In these circumstances, only part of the electrode is being used. Theoretical calculations are useful in predicting the optimum thickness of electrode for a given set of conditions; the use of thicker electrodes will not improve performance, since the extra thickness will not be utilized.

In flowthrough electrodes, fuel dissolved in electrolyte is forced through a porous electrode to insure reactant supply to the interior area of the electrode. Again, theoretical treatments indicate the variation of polarization with current, rate of flow, thickness of electrode, etc., but the treatments are not yet sophisticated enough to be used as design equations.

1.10 RECOMMENDATIONS

This monograph does not propose to prepare a complete set of recommendations to guide future Government-sponsored development of fuel cells. The progress that has been made in the United States toward practical fuel cells is ample evidence of the capable guidance of development programs. The combination of industrial organizations looking for commercial uses and Government agencies looking for well-defined special uses has been very fruitful. Although much of the original fundamental research was performed in England or Europe, fuel-cell development in these countries is minor compared with progress in the United States. There was little prospect 10 years ago of short-term returns from money spent on fuel-cell research for commercial applications, but Government support for military and space applications led to continued development in this country. Even now fuel-cell systems are not insured of eventual wide use, but prospects are much better than they were. The potential market for applications in the space program over the next 10 years is large enough to justify continued company interest; at the end of that time, the wider market potential should be clearly defined. Fuel cells will probably continue to receive the attention of competent scientists, engineers, and policymakers in many industrial firms and Government agencies.

The recommendations here are not inclusive, and many of them are already being implemented. They are a personal selection of factors which the author believes should receive more attention than they are getting at present.

The information in this book on materials of construction and techniques of cell manufacture is not adequate, and a more complete report should be prepared. In many reports the descriptions of techniques are too brief to enable them to be readily duplicated; this is probably often due to a desire to keep important process steps proprietary. However, it is remarkable how often the same mistakes in cell construction are made, and reported, in different systems. (An example is the spread of gaskets over manifold holes when the cell is assembled; this is mentioned frequently and is, of course, prevented by cutting the holes in the gaskets greater than required.) Most of the cells described here are the end product of a long line of cells, each somewhat better than the one before it. There is probably sufficient information available, in contract reports and elsewhere, to prepare a manual of cell materials and construction procedures.

The search for cheaper and more effective catalysts must be pressed on the grounds of both cost and availability. There seems no reason why Teflon-bonded electrodes should not be made with other catalysts with the same ease as with platinum black. Teflon has no chemical effect and the electrode is good primarily because of its geometrical structure. Therefore, other catalysts should be prepared in sizes comparable to those of platinum black and tested in this electrode form. Empirical testing of catalysts is probably the best technique to follow at present, provided the catalysts are compared under identical geometric and true area conditions (which is rarely done at present).

Another area of catalytic investigation which should be continued is that of using existing, expensive catalysts more efficiently. This has three facets. First, work on the theory of porous electrodes must progress to the state at which it is known what fraction of the catalyst area is truly effective in the electrode. Second, it must be determined how thinly a layer of catalyst can be spread on a supporting particle and still behave as a solid particle of pore catalyst. Is this 1, 10, or 100 monolayers? The answer could make the difference between feasibility or nonfeasibility of the use of platinum. Third, investigations should be made of how to apply these thin layers, of contact resistance between the resulting particles, of the stability of these thin films under operating conditions, etc. Perhaps it is theoretically feasible to use a monolayer but impractical to prepare or preserve the layer.

Theories of porous electrode behavior should be experimentally tested and expanded to give a precise description of the mode of operation of electrodes. These are fundamental electrochemical-engineering problems involving solubility, mass transfer, conduction, kinetics, and heat transfer. When the behavior of simple experimental electrodes under isothermal conditions has been defined, the treatment must be extended to larger electrodes with nonuniform current density and nonisothermal operation. This type of investigation should be of considerable use in showing how electrodes can be improved in practice, and will lead to design equations for optimization of electrodes for a specified purpose. All three types of porous electrode need further investigation, although most attention has been given to gas-diffusion electrodes.

Once the theory of electrode behavior and catalytic effectiveness has been developed, it will be possible to forecast the expected ultimate limit of electrode and cell performance. At present, it might be guessed that cells will ultimately deliver 1000 A/sq ft at 0.5 volt with a cell thickness of % inch. Power densities of 20 kW/cu ft are then possible. The ultimate limit is an important factor in deciding how much research effort should be expended.

Allied with the question of ultimate capability discussed above is that of optimum power density as a function of mass and heat transfer to and from a cell stack. From a priori reasoning, it can be argued that there is an optimum electrode performance beyond which the weight and volume of a cell stack must be increased (to provide heat and/or mass transfer) to such an extent that power density falls. To my knowledge, this problem has not yet been set up mathematically and computed to predict ultimate capability.

More generally, the chemical engineering of fuel cells, fuel-cell stacks, and fuel-cell systems needs more detailed and systematic investigation than it has received. A number of important principles of cell design have been developed (see ch. 4), and quantitative treatments of some aspects such as pressure drop through cell stacks, heat and mass balance, water balance, etc., have been given for specific hydrogen-oxygen cells. There are, however, many gaps in quantitative design information. For example, the problem of three-component, gas-phase mass transfer in a porous cathode using air, with transpiration of water vapor from the electrolyte through the electrode, has not been rigorously solved for ranges of electrolyte composition and temperature. A major drawback in attempts at mathematical modeling and quantitative design is lack of basic data. Data on solubilities and diffusion coefficient of dissolved gases as a function of electrolyte pressure, concentration, and temperature are sparse. Diffusion coefficients through porous electrodes have not been measured, and mass-transfer relations in electrolyte-filled matrices have not been quantitatively expressed. There are gaps in conductivity and partial pressure relations for concentrated electrolytes of interest.

As shown in appendix B, such data are being generated and assembled from literature reviews. The preparation of a text on design principles should be possible in the next few years, provided that the determined efforts to establish basic chemical principles and data are continued and expanded. .

There is every reason to expect that the integration and optimization of a fuel-cell system with the other contents of a spacecraft will lead to significant improvement in capability for this application. It is difficult to judge how far this has been carried out at present, but fuel-cell units described have been designed as modules rather than as an integral part of the spacecraft. The module concept has the advantages of simplicity and ready replacement; integrated systems may be less reliable. Systems engineering of a spacecraft or submarine falls outside of the scope of this report, but digital-computer control of the fuel-cell system would seem an obvious future objective requiring principally software development rather than hardware.

Hydrogen-oxygen fuel cells have the advantages that gas feed is easily controlled and that the low solubility of the gases prevents excessive diffusion of oxygen through the electrolyte to the hydrogen electrode, and vice versa. The use of fuels of high-energy density in liquid form, such as hydrazine, has not been fully explored for special purposes. Such fuels would have the advantage of smaller volume and tankage weights without cryogenic storage. The major drawbacks appear to be difficulty of feed control and product removal, and the cross-diffusion effect. There is need for low-resistance, ion-exchange membranes which will pass H^+ or OH^-, but not pass dissolved fuel or other ions, to prevent the diffusion effect.

The necessary power density required for vehicle propulsion is in a state of dispute. Since it is likely that fuel cells will be developed to the power density originally suggested (2 kW/cu ft and 22 W/lb) within the next few years, the described electrical performance for vehicle duty should be settled by direct experiment.

More work should be performed on the factors limiting high-temperature, direct hydrocarbon fuel cells. If performance is limited by thermodynamic factors, then an estimate of ultimate capability could be made. If they are limited by ohmic, kinetic, and mass-transfer factors, it may be possible to develop the equivalent of high-performance, Teflon-bonded electrodes for use in the cells. At the moment, it is not known whether electrode development can give improved performance.

1.11 REFERENCES

1.1. Venture-Tech, Inc.: Fuel Cell Progress, vol. 2, no. 11, June 1964.
1.2. American Chemical Society: Chem. Eng. News, Jan. 4, 1965, p. 86.
1.3. Venture-Tech, Inc.: Fuel Cell Progress, vol. 2, no. 10, May 1964.
1.4. American Chemical Society: Chem. Eng. News, Mar. 25, 1963.
1.5. Venture-Tech, Inc.: Fuel Cell Progress, vol. 3, no. 2, Feb. 1965.
1.6. American Chemical Society: Chem. Eng. News, Dec. 28, 1964, p. 31.
1.7. Fuel Cell Corp., St. Louis, Mo.; and Venture-Tech, Inc.: Fuel Cell Progress, vol. 2, no. 10, May 1964.
1.8. VON FREDERSDORFF, C. G.: Fuel Cells. Vol. 11, G. J. Young, ed., Reinhold Pub. Corp., 1963, pp. 50–67.
1.9. REID, W. T.: Battelle Tech. Rev., Apr. 1965.
1.10. JASINSKI, R.: Proceedings 18th Annual Power Sources Conference. PSC Publications Committee, Red Bank, N.J., May 1964.
1.11. NORRIS, L. F.: Chem. Eng. News, Dec. 7, 1964, p. 39.
1.12. Battelle Memorial Institute: Economics of Fuel Gas from Coal. McGraw-Hill Book Co., Inc., 1950.
1.13. VIELSTICH, W.: Brennstoffelemente. Verlag Chemie, G.m.b.H., Weinheim/Bergstr., 1965.

CHAPTER 2

Principles, Types, and Uses of Fuel Cells

In this chapter the electrochemical basis of the fuel cell is explained. This explanation is then extended into the several existing and experimental types of fuel cells where additional discussion defines the specifications of the various fuel cells in terms of potential applications. Also within this chapter, definitions have been provided for many of the terms peculiar to the fuel-cell development efforts, and general references have been cited for the reader's use in obtaining fuller information on electrochemical theory and on fuel-cell design and operation.

2.1 THE FUEL-CELL PRINCIPLE

2.1.1 The Basic Theory of the Fuel Cell

A fuel cell is an electrochemical device which

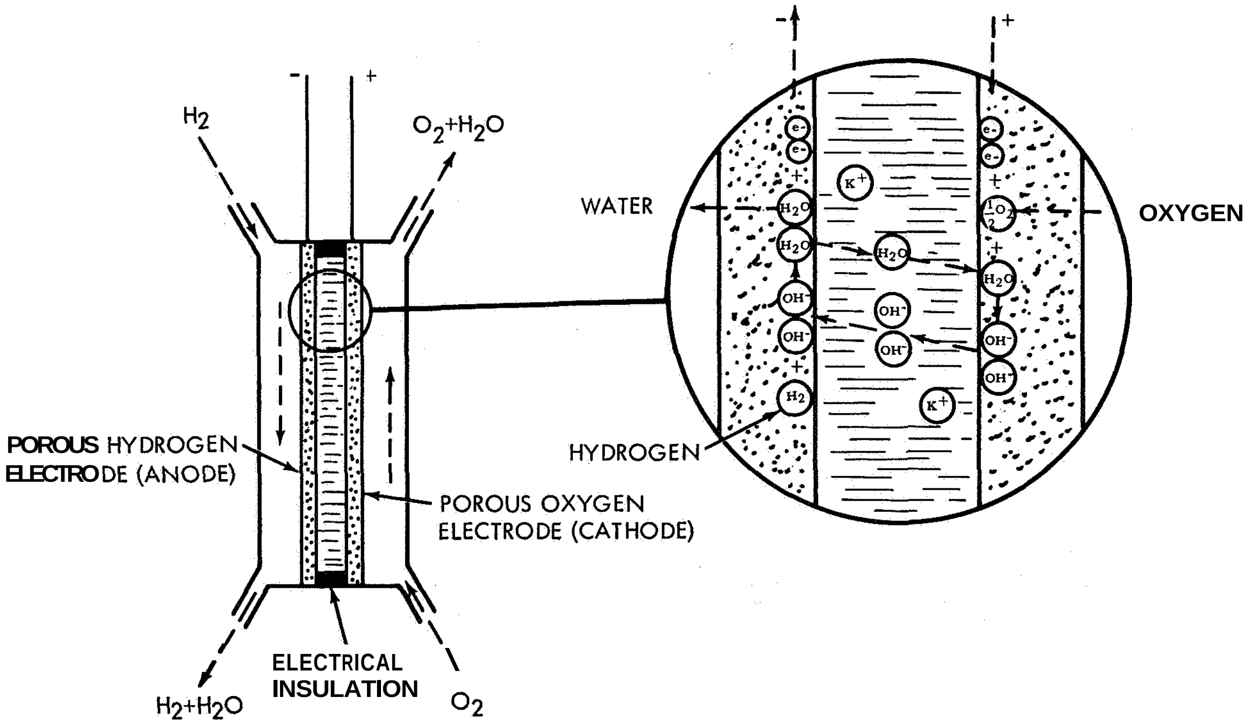

The basic features of the cell from left to right are: a hydrogen gas chamber; a porous conducting electrode (anode); an electrolyte chamber filled with electrolyte; a porous conducting electrode (cathode); and an oxygen gas chamber. Direct flow of electrons from the anode to the cathode through the case of the cell must be prevented by electrical insulation separating the two electrodes.

The gases and electrolyte react to produce a flow of electrons. Hydrogen adsorbs on catalyst embedded in the anode and reacts with hydroxyl ions from the electrolyte to form water. The reaction produces electrons on the electrode. The electrons flow through the external circuit to the cathode, where they combine with oxygen adsorbed on catalyst and water to form hydroxyl ions. The ions complete the circuit by migrating from the cathode through the electrolyte to the anode.

Important secondary features not shown include means of introducing reactants and insuring proper feed to each part of the cell, gaskets between parts of the cell to prevent gas or electrolyte leakage, and current collectors.

FIGURE 2.1.—Cross section of simple hydrogen-oxygen fuel cell.

PRECEDING PAGE BLANK NOT FILMED.

converts some of the chemical energy of reaction of chemical species directly into electrical energy. Most are primary electrochemical cells and produce electrical power in the same way as conventional primary cells, such as the zinc/manganese dioxide flashlight battery. They differ from conventional primary cells principally because their construction permits continuous feed of reactants and continuous removal of products, the remainder of the cell being as invariant with time as possible. This continuing operation requires radically different design and engineering from that found in conventional cell technology. Reactants used in fuel cells differ from those of conventional primary cells, and fuel-cell reactions involve chemisorption and catalytic processes.

The general mode of operation of a fuel cell is illustrated in figure 2.1; hydrogen and oxygen are the reactants, and aqueous potassium hydroxide is the electrolyte. Hydrogen gas diffuses through the porous electrode, adsorbs on a catalyst at the surface of the electrode and reacts according to

$$H_2+2OH^- \xrightarrow{\text{catalyst}} 2H_2O+2e^-.$$

At the same time, oxygen diffuses through the other porous electrode, adsorbs on a catalyst, and reacts with the water of the electrolyte according to

$$\tfrac{1}{2}O_2+H_2O+2e^- \xrightarrow{\text{catalyst}} 2OH^-.$$

The sum reaction is

$$H_2+\tfrac{1}{2}O_2 \rightarrow H_2O$$

but the electrochemical reaction can be sustained only by a steady flow of electrons from anode to cathode via an external circuit, plus a steady flow of OH- ion through the electrolyte from cathode to anode. Flow of electrons in the external circuit is the useful electric current from the cell. Water produced by the reaction can be evaporated by flow of dry gas, which picks up water as it passes through the cell. The porous electrode structure must allow gas to diffuse freely through it, but the pores must also be sufficiently small in diameter to prevent flow of electrolyte through them. If electrolyte fills the pores, it blocks gas transfer and the electrode does not function properly; this is referred to as "electrode flooding." Gas pressures must be balanced to prevent a pressure differential from one gas chamber to another from driving the electrolyte through the electrodes. A knowledge of how a single electrode reaction can develop the potential to drive the electrons into the external circuit and give useful work will help in understanding complete fuel-cell reactions. Since the overall process occurring in a porous electrode system is complex, a smooth, solid electrode surface will be considered.

Hydrogen dissolved in an acid electrolyte at a catalytic metal electrode (e.g., platinum) adsorbs on the metal as atoms

$$H_2+2M=2M[H]. \tag{2.1}$$

When the pressure of hydrogen over the electrolyte is 1 atmosphere and when dissolved

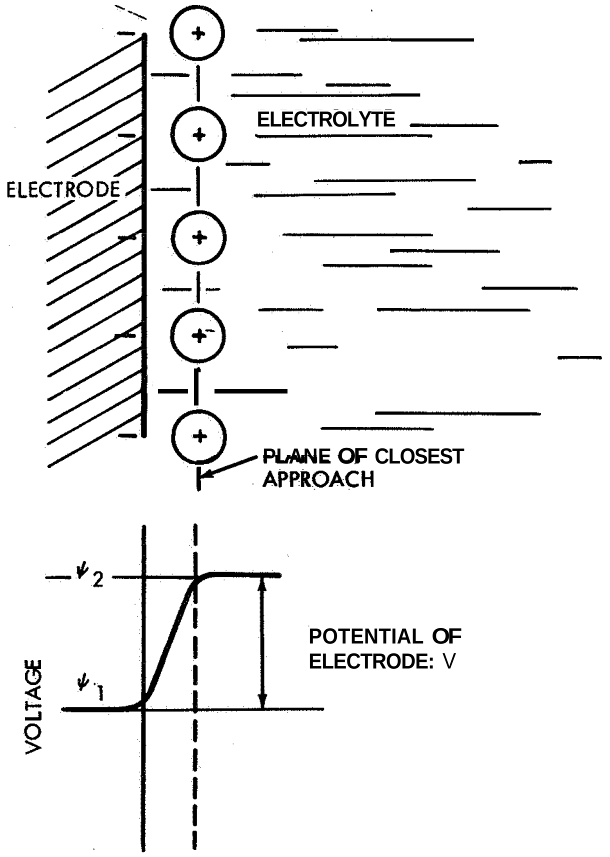

The layer of electrons (negative charge) on the electrode attracts positive ions from the electrolyte. Thus a double layer of charge is formed at the electrode surface, which behaves like a plane capacitor. The lower figure shows the voltage developed across this double layer. ψ_1 is the absolute potential of the electrode and ψ_2 is the absolute potential of the electrolyte; it is common practice to call $\psi_1-\psi_2$ the potential of the electrode.

FIGURE 2.2.—Illustration of the double layer at the surface of a smooth electrode.

hydrogen is in equilibrium with this pressure, the chemical free energy of dissolved hydrogen is the same as that of gaseous hydrogen at 1 atmosphere (since $\Delta F = 0$ for an isothermal equilibrium process). Similarly, when reaction (2.1) is in equilibrium, the chemical free energy of adsorbed hydrogen, M[H], is also that of 1 atmosphere of hydrogen gas. However, this adsorbed hydrogen can ionize

$$M[H] \rightarrow M + H^+ + e^-. \qquad (2.2)$$

The chemical free energy of hydrogen ion in the electrolyte is less than that of adsorbed hydrogen, so the reaction is favored from left to right. Electrons released in the reaction will accumulate at the smooth face of the electrode and attract a corresponding layer of positive charge from the electrolyte, forming a double layer as shown in figure 2.2. This double layer of charge sets up a potential difference between electrolyte and electrode.

2.1.2 Elementary Thermodynamics of the Fuel Cell

If no electrons are removed from the electrode (i.e., the electrode is at open circuit), the progress of reaction (2.2) builds up a larger layer of charge and develops a greater potential difference across the double layer. The potential gradient opposes the reaction, since the net effect is that the positive charge must be moved from low to high potential. This opposition slows down reaction (2.2) while aiding the reverse reaction until a dynamic equilibrium is reached

$$H_2 + 2M \rightleftharpoons 2M[H] \rightleftharpoons 2M + 2H^+ + 2e^-. \qquad (2.3)$$

Let ΔF_c be the chemical free-energy change of $2H^+ + 2e^- \rightarrow H_2$, when no voltage gradient is present. When a double-layer voltage difference is present, the hydrogen ion is at a different potential than that of the electron on the metal, and the free energy of the reaction is therefore changed. If the potential of the electrode, V, is defined as the absolute potential of the electrode minus the absolute potential of the electrolyte, then the electrochemical free energy of the reaction is

$$AF = \Delta F_c + 2FV. \qquad (2.4)$$

Here, AF refers to a fixed amount of reactants (kcals/g-mole or Btu/lb-mole, for example), and F is Faraday's constant in appropriate units. At equilibrium, the electrochemical free energy change is zero and

$$nFE = -AF,. \qquad (2.5)$$

(*n* is the number of electrons in the reaction and is 2 for the example given, since AF, refers to a unit quantity of H_2). The voltage E is the theoretical open-circuit potential. When reactants and products are at standard-state concentrations (1 g-mole/liter and 1 atmosphere, for example), E becomes E_0, the standard-state, open-circuit potential of the electrode reaction.

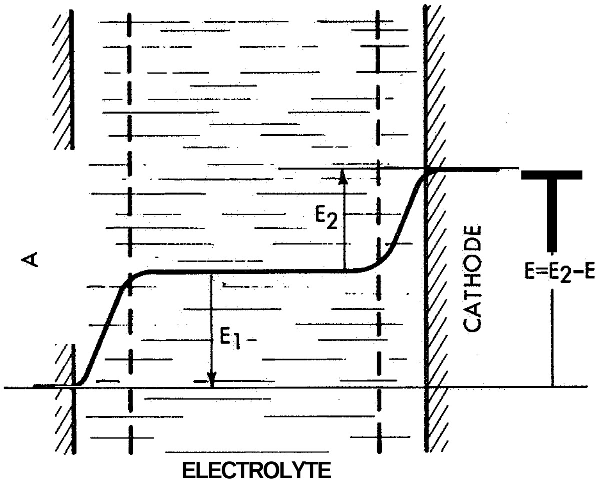

FIGURE 2.3.—Illustration of the potential of a cell as the sum of two half-cells.

The above reasoning can be applied to any electrode reaction; for example, at the oxygen electrode in acid solution the ionization of oxygen gives positive charge on the electrode, which attracts a layer of negative ions from the electrolyte. Reaction proceeds until a potential is established which brings the reaction into equilibrium,

$$\tfrac{1}{2}O_2 + 2H^+ + 2e^- \rightleftharpoons H_2O.$$

The potential relations of a complete cell are shown in figure **2.3.** The ideal open-circuit voltage (OCV) of the cell is the sum effect of the two half cells. Half-cell potentials are usually given as reduction potentials, which correspond to the potential difference: electrode-minus-electrolyte. Using this convention, the cell potential is

$$E = E_{\text{cathode}} - E_{\text{anode}}. \qquad (2.6)$$

For example, the standard reduction potentials of hydrogen and oxygen in alkaline media are -0.83 and 0.4, respectively, giving a cell potential of 1.23 volts. (Remember that standard reduction potentials are actually the potential of the half-cell versus a standard hydrogen electrode.)

Writing the alkaline hydrogen-oxygen fuel-cell reactions in the reduction direction

$$2H^{+}+e^{-}=H_2+E_a+\Delta F_a$$

$$\tfrac{1}{2}O_2+2H^{+}+2e^{-}=H_2O+E,+\Delta F_c$$

we see from equations *(2.6)* and *(2.5)* that the cell potential is

$$E=E,-E_a=-(\Delta F_c-\Delta F_a)/nF=-\Delta F/nF \quad (2.7)$$

Here ΔF is the Gibbs chemical free energy of the overall reaction $\tfrac{1}{2}O_2+H_2=H_2O$. A number of tables of standard potentials, taken from the contract reports covered by this book, are given in appendix **B.**

For a general reaction

$$aA+bB+\ldots\rightleftharpoons xX+yY+\ldots$$

the chemical free-energy change ***AF*** in equation *(2.5)* or *(2.7)* can be replaced using the Van't Hoff isotherm to give

$$nFE=-\Delta F_0-RT\ln[(X)^x(Y)'\ldots/(A)^a(B)^b\ldots].$$

$(X),(Y)$,etc., and $(A),(B)$,etc., stand for the activities of the products and reactants, respectively, and ΔF_0 is the standard-state chemical free energy. This is generally used in the form

$$E=E_0-(2.3RT/nF)\log[(X)^x(Y)^y\ldots/(A)^a(B)^b\ldots] \quad (2.8)$$

the Nernst equation, where E_0 is the standard potential. When applied to a complete cell reaction, it shows that the potential of the cell increases as the concentrations of reactants are increased and the concentrations of products decreased. $2.3RT/F$ is approximately 0.06 volt at room temperature.

Figure *2.3* shows the relationship between the double layers in a simple plane geometry. The geometry of the electrode-electrolyte boundary is considerably more complex in most fuel cells, particularly those with gas-diffusion electrodes. This obviously does not affect the equilibrium thermodynamic relations, although the geometry of the double layer may considerably influence the rates of reaction when current is drawn. The double layer (fig. *2.2)* is composed of a layer of charge in the electrode surface and a corresponding layer of charge in the electrolyte. When ions are removed from the electrolyte layer, they experience electrostatic attractive forces tending to pull them back; conversely, when they are forced close to the surface, they experience the usual repulsive forces which exist when a molecule is brought close to a surface. Therefore, they tend to occupy a stable position called the plane of closest approach. Since repulsive forces operate only over distances of a few angstroms, it follows that the thickness of the double layer is a few angstroms. Thus the double layer will follow the contours of a rough or porous electrode filled with electrolyte.

2.1.3 Polarization, Power Density, and Efficiency

The ideal open-circuit potential of a fuel cell (or an electrode) can be estimated for a given set of circumstances from the reversible thermodynamics given above. Useful work is obtained from the cell only when a reasonably large current is drawn, but the potential will fall due to irreversibilities in the cell. The most compact fuel-cell configuration is that of rectangular plate or disk electrodes stacked facing one another, as shown in figure *2.1.* Under these circumstances a good guide to the power output of the cell is the watts per square foot (W/sq ft) of flat electrode area. Watts per square foot are the product of current density in amperes per square foot (A/sq ft) and cell voltage at this current density. An ideal electrode would produce high A/sq ft at as high a potential as possible (providing other factors such as lifetime, cost, fuel efficiency, heat generation in the cell, etc., are taken into account). Therefore the loss of reversible potential upon drawing current is the critical factor in improving the voltage efficiency of the cell; the location and exact causes of this loss must be pinpointed. Loss of potential from ideal (or sometimes from open circuit) potential is called polarization, overvoltage, or overpotential. The three principal types of polarization are ohmic or IR polarization, activation polarization, and concentration polarization.

An obvious cause of voltage inefficiency is the IR polarization. This ohmic loss occurs within

!

the electrolyte and electrodes of a cell, since a voltage gradient is needed to drive the charged ions through the electrolyte and to drive electrons through the electrode material. Internal resistance losses in experimental electrode materials can be reduced to a negligible level, but this is not always possible for practical electrodes. Since electrolytes behave according to Ohm's law, ohmic voltage loss can be easily calculated for simple geometries.

Activation polarization is due to the irreversibility of the electrochemical reactions under current drain. When current is being taken from the cell, the reactions cannot be at equilibrium. A physical model for the voltage change can be extracted from figure **2.3.** In order for the anode to produce electrons, the reaction $[H] \rightleftharpoons H^+ + e^-$ must proceed faster from left to right than from right to left and positive charge crosses the double layer into the electrolyte. This occurs when the voltage of the double layer is changed from its equilibrium value to make the voltage from the electrolyte to the electrode (E_1) more positive. The potential gradient retarding $[H] \rightarrow H^+ + e^-$ then becomes less or even aids the reaction; the same gradient retards $H^+ + e^- \rightarrow [H]$. The total effect is to give a net anodic current. Similarly, E_2 must decrease at the cathode to give cathodic current. Thus, as soon as the equilibrium cell is connected to an external load, current will flow and the voltage gradients will change until a steady state is reached, with $V<E$ for the complete cell. The voltage change, when an electrode is taken from zero current to current i, depends on the rate of the electrochemical reactions at equilibrium. For example, if the current of $[H] \rightarrow H^+ + e^-$ at equilibrium were 1000 A/sq ft, then the current of $H^+ + e^- \rightarrow [H]$ would also be 1000 A/sq ft. If the rate of $[H] \rightarrow H^+ + e^-$ is increased by 10 A/sq ft and the reverse reaction decreased by 10 A/sq ft, the net current of 20 A/sq ft represents only a small departure from equilibrium of each of the basic reactions, and the voltage change would be small. On the other hand, if equilibrium current (called exchange current) were 1 A/sq ft, an increase of $[H] \rightarrow H^+ + e^-$ by 10 A/sq ft would represent a tenfold increase in rate, which obviously throws the reaction to the right and away from equilibrium, and a large voltage change would be obtained. The rate of the reverse reaction would be decreased to negligible values in this case, and the net current would be 11 A/sq ft. Section 2.1.4 treats activation polarization in more detail.

Concentration polarization, the third cause of voltage loss on current drain, is the resistance to mass transport of the reacting species. Ohmic resistance is resistance to mass transport of ions which are being driven by a potential gradient. However, if a reactant is removed rapidly by the electrochemical reaction, concentration gradients will be set up. Hydrogen dissolved in an electrolyte near an anode, for example, will be removed by reaction, and more hydrogen has to diffuse to the electrode from the bulk of the electrolyte in order to maintain reaction. A concentration gradient is set up and is greater for more resistance to mass transfer. The Nernst equation shows that even if the rest of the system were behaving reversibly, a lower hydrogen concentration at the electrode surface would lower the cell potential from the expected for the hydrogen concentration in the bulk. Thus mass-transfer effects appear as a change in double-layer voltage, whereas electrolyte ohmic effects appear as a voltage gradient in the electrolyte between electrodes. At steady state, the mass transfer of dissolved H_2 equals the current (assuming complete faradaic efficiency). The free energy of hydrogen is lower at the electrode surface than it is in the more concentrated bulk of the electrolyte (since energy has been lost in overcoming the resistance to mass transfer) and it appears as heat in the cell electrolyte near the electrode; this heat can be considered to be frictional heat. For all types of polarization, the magnitude of the voltage loss depends on the current being drawn, and is greater for larger currents; cell voltage decreases for higher current densities.

Power density per square foot is a first indication of the performance of a fuel cell. The most useful power densities are kilowatts per cubic foot or watts per pound. Therefore, the volume and weight of a single cell are important magnitudes. Power density obviously depends on the current density at which a given cell is operated. At low currents, the cell will have a low-power density. At high currents, when the cell is shorted across its terminals, the power density is again low, since the terminal voltage is small and the energy of the cell reaction is used only to generate heat within the cell. A current at which the power density is maximum lies between these two extremes. (If only IR polarization is present, the maximum-power density exists when the external load resistance equals the internal cell resistance.) A fuel cell, however, is usually required to operate at a high efficiency as well as a high-power density. The work output of a cell is iV, where i is the current and V the terminal voltage. The ideal maximum work obtainable from the cell at this current is iE, where E is the ideal reversible potential of the cell. The electrochemical or voltage efficiency is, therefore, V/E, and is directly proportional to the operating cell voltage. Power densities are usually quoted at voltages corresponding to about 55 to 65 percent electrochemical efficiency, or approximately 0.7 to 0.8 volt for a standard low-temperature, hydrogen-oxygen cell. Cell life may be shortened if excessively high currents are used, so power density should be calculated at a current density not exceeding that which gives the required life.

Faradaic or coulombic efficiency is the amount of charge produced compared to the theoretical amount for a given quantity of reactant. Leakage of fuel (or oxidant) from the cell, or direct chemical reaction of fuel with oxidant, causes loss of coulombic efficiency. This efficiency does not depend directly on polarization, but on the mechanical design and mode of operation of the cell.

2.1.4 Kinetics and Catalysis

Activation polarization is directly related to the speed of electrochemical reactions. The topic of electrochemical kinetics is a broad one and only the very briefest outline is given here. (See sec. 2.4 and ch. 17 for references to more detailed studies.) When the rate of an electrochemical reaction at an electrode surface is not limited by a chemical kinetic restriction, the only limitation to current is that of mass transfer; i.e., the speed with which the reactants can be supplied to the electrode and the products removed. Polarization is then concentration polarization. However, the transfer of an electron across the double layer is often an activated process. A reactant on the surface, a metal atom (M) on a metal electrode, or adsorbed H atom, for example, is bonded to the surface. To escape as an ion, leaving an electron behind, the atom has to vibrate along the bond joining it to the surface, and this vibration must be long enough to take it to a region where the net attractive force becomes weak. In this region the chemical bonding force of M to H is canceled by the repulsive force between M^- and H^+. Similarly, when an ion is brought up to the surface it must have sufficient translational energy to carry it close to the surface against the repulsive forces, so that the attractive bond forces pull it onto the surface. The region where forces balance is called the transition state (or activated state) and it is a region of high potential energy. Only a few of the vibrations, or collisions, have sufficient energy to reach the transition state.

By applying transition-state theory to an electrode reaction, it can be shown (see references in sec. 2.4) that—

$$\nu_{\text{anode}} = K(A)^a(B)^b \exp(-\Delta F^\ddagger/RT) \exp(\alpha nF\psi/RT) \quad (2.9a)$$

$$\nu_{\text{cathode}} = K(X)^x(Y)^y \exp[-(\Delta F^\ddagger - \Delta F^0)/RT] \exp[-(1-\alpha)nF\psi/RT]. \quad (2.9b)$$

ν is the rate in g-moles/cm²-sec; K is a constant which contains the units of rate, g-moles/cm²-sec; (A) and (B) are activities of anodic reactants, (X) and (Y) are activities of anodic products (i.e., cathodic reactants); $\Delta F^\ddagger$ is the standard-state free energy of activation, ΔF^0 is the standard-state free energy of reaction in the anodic direction, α is a constant called the transfer coefficient (usually close to one-half), n is the number of electrons transferred in the rate controlling step (usually 1), and ψ is the absolute potential difference electrode-minus-electrolyte. The equations are rarely used in this form, but they are given here because they demonstrate the important parameters more clearly than do other forms. Equations (2.9) should be applied to each electron (charge) transfer step in the reaction, and other kinetic equations should be used for noncharge transfer steps in the reaction. Thus, complex reactions require the combination of a number of rate equations, giving relations between current and voltage which are considerably more involved than equations (2.9). This fact is frequently overlooked in fuel-cell investigations, where researchers try to apply the simple equation under conditions where it obviously is not valid.

Assuming that the reaction under study is a simple one to which equation (2.9) can be applied without complicating factors, the general features of the rate equation are as follows. In general, large changes in rate v are desired with only small change in ψ; that is, we want large currents at small polarizations. First, the value of rate refers to the true reaction area, which is the contact between solid and electrolyte (area of the double layer). When rough or porous electrodes are used, the actual double-layer area may be much greater than the geometric apparent area. The rates per unit of geometric area are then those of equation (2.9) multiplied by a roughness factor, which is the ratio of true to geometric area. It is advantageous to have as great a roughness factor as possible. Second, the equation shows that the rates are greatest for high concentrations of reactants. Hence a proposed mechanism of a reaction should not contain steps in which a stable reactant is present in minute amounts, For example, in the evolution of hydrogen from a strongly alkaline solution, the proton is unlikely to discharge; the generally accepted mechanism is discharge from water, $H_2O+e^- \rightarrow [H]+OH^-$.

In addition, since electrode reactions are surface reactions, one of the activity terms will always be a surface activity. Therefore, rate is proportional to the number of active sites per square centimeter of true area. An active site is a position on the electrode surface at which reaction is favored. The number of active sites per square centimeter depends principally on the nature of the electrode material (mercury, carbon, platinum, alloy, and silver oxide, for example), but crystal defects, such as grain boundaries, vacancy clusters, dislocations, and relatively amorphous material, may sometimes provide more active regions than a smooth crystal plane.

Equations (2.9) show that the rate depends on the free energy of activation, $\Delta F^{\ddagger}$. It is in this term that the effect of catalysis occurs. The principal component of the free energy of activation is the potential energy barrier of the transition state. It depends on the chemical nature of the electrode material and the reactant. An activated (high internal area) carbon electrode permits only slow hydrogen usage, but catalytic activation by a thin film of platinum on the internal surface increases the rate at a given potential by several orders of magnitude. The principal effect of temperature is also contained in the free energy of activation. A thermodynamic function $\Delta\phi$ can be defined by the relation

$$\Delta F^0 = \Delta H_0^0 - T\Delta\phi, \tag{2.10}$$

where ΔH_0^0 is the ground state (zero temperature) standard-state enthalpy change of a reaction. Applying this to the activation energy gives

$$\Delta F^{\ddagger} = \Delta H_0^{0\ddagger} - T\Delta\phi^{\ddagger}.$$

ΔH_0^0 is identified with the activation energy of the reaction and, if $\Delta\phi^{\ddagger}$ does not change much with temperature

$$\log \text{rate} \propto -\Delta H_0^{0\ddagger}/2.3RT. \tag{2.11}$$

Thus increase of temperature increases the rate of reaction, with the biggest effect being observed in highly activated reactions which have large values of $\Delta H_0^{0\ddagger}$.

The basic rate equation (2.9) can be expressed as current density using $i = n_1 F v$, where n_1 is the total number of electrons transferred for one occurrence of the rate-controlling step. The voltage of an electrode is compared with that of a standard hydrogen electrode (SHE); when the SHE has a true reduction potential of E_H, the measured electrode potential is $V = \psi - E_H$. Several variations of the rate equation are used, but the most widely used form employs rate constants in the form of exchange currents. When the reversible potential of the cell is E, (versus SHE), polarization is

$$\eta = \pm(E_r - V). \tag{2.12}$$

The sign is chosen arbitrarily so that, as the reaction of interest becomes faster, η becomes more positive. Thus if the primary interest is in an anodic current, $\eta = V - E$, and

$$i_a = n_1 F k (A)^a (B)^b \exp[-(\Delta F^{\ddagger} - \alpha n F E_H - \alpha n F E_r)/RT] \exp(\alpha n F \eta/RT).$$

For simple reactions the Nernst equation can be substituted for E, and, on rearrangement

$$i_a = n_1 F K_1 [(A)^a (B)^b]^{1-\alpha} [(X)^x (Y)^y]^{\alpha} \exp(\alpha n F \eta/RT),$$

where K_1 contains free energy of activation and standard-state free energy of reaction terms. Similarly

$$i_c = n_1 F K_1 [(A)^a (B)^b]^{1-\alpha} [(X)^x (Y)^y]^\alpha \exp[-(1-\alpha) nF\eta/RT].$$

At ideal open-circuit conditions, $\eta = \mathbf{0}$ and $i_a = i_c = i_0$; i_0 is called the "exchange current density." The net current density is

$$i_{\text{anodic}} = i_0 \{\exp(\alpha nF\eta/RT) - \exp[-(1-\alpha)nF\eta/RT]\}. \quad \textbf{(2.13)}$$

When η is large (usually greater than 50 to 100 millivolts at room temperature), $\alpha nF\eta/RT < \mathbf{1}$ and the second exponential term become negligible. For this irreversible condition

$$\eta = (2.3RT/\alpha nF) \log i - (2.3RT/\alpha nF) \log i_0 \quad \textbf{(2.14)}$$

A plot of η as a function of log i is a straight line. In the form

$$\eta = a + b \log i \quad \textbf{(2.15)}$$

the equation is called the Tafel equation and b is the Tafel slope.

2.1.5 Concentration Polarization and Mass Transfer

The simple rate equations (2.13) and (2.14) are derived on the assumption that the concentrations (activities) of reactants and products remain constant at known values, which determine the reversible potential, as current is drawn. This is often not true, because the reactants cannot reach the electrode surface rapidly enough to maintain constant concentration. When R_b is the known concentration of a reactant in the bulk, R is actual surface concentration, and P_b and P are corresponding product values, then equation (2.13) becomes

$$i = i_0 \{(R/R_b)^r \exp(\alpha nF\eta/RT) - (P/P_b)^p \exp[-(1-\alpha)nF/RT]\}. \quad \textbf{(2.16)}$$

Thus the effect of mass transfer can be incorporated if the relation between i, R, and R_b can be found,

Precise treatment of the effect of mass transfer is often difficult, but a number of adequate approximations and simplifications exist. Diffusional mass transport can be approximately described by Fick's first law of diffusion

$$\text{Rate of mass transfer} = -AD\partial R/\partial x. \quad \textbf{(2.17)}$$

A is the area through which diffusion occurs perpendicular to the x-axis along which the concentration gradient is measured. D is a diffusion coefficient and, with concentration R and the rate in consistent units, D has the dimensions of (L^2/T). Consider an electrode which is being supplied with a reactant dissolved in electrolyte. The reactant may be charged; it can be brought to the surface by three methods: diffusion under the influence of a concentration gradient; migration under the influence of a potential gradient; and bulk movement of the fluid. Solving the fluid dynamic equations describing bulk flow is not usually easy for the types of electrode-electrolyte systems used in fuel cells. As a crude approximation, the Nernst stagnant-film concept can be applied. This assumes that the surface is covered by a boundary layer behaving as though it were a uniform stagnant film. No transfer by convective bulk movement occurs within the film; outside of the film, convection suffices for uniform concentration. For a noncharged reactant (dissolved H_2 or O_2, for example), the mass-transport equation at steady state is

$$i = nF \text{ (rate of transfer per unit area)} = nFD(R_b - R_s)/\delta \quad \textbf{(2.18)}$$

where D is the diffusion coefficient of the dissolved reactant in the electrolyte, R_b is the concentration in the bulk of the electrolyte; R_s is the concentration at the surface of the electrode (the surface here being taken as a position near the plane of closest approach); and n is the number of electrons transferred per molecule of R and is not necessarily the same as the n in the kinetic equations (2.9) to (2.16).

The effective thickness of the stagnant film is 6. As a first approximation it is assumed to be constant under a given set of conditions, irrespective of the values of R_s. This is not necessarily valid, since depletion of reactant at the surface may cause density gradients and thus convective mass transfer, lowering the value of δ at low R_s values.

When the discharging species is an ion, the steady rate of mass transfer per unit area toward the electrode is

$$\text{Rate} = DdR/dx + Ru\, dV/dx \quad \textbf{(2.19)}$$

where u is the mobility of the ion, D is its diffusion coefficient through the electrolyte, and

x is measured in the direction electrode to electrolyte. The term dV/dx is the potential gradient in the electrolyte. Similar equations have to be written for all other ionic species present. With the law of electroneutrality, the equations are solved simultaneously, for appropriate boundary conditions, to eliminate dV/dx. The solutions are usually complex and can be approximated by

$$\text{Rate} = D_{\text{eff}} dR/dx \qquad \textbf{(2.20)}$$

and

$$i = nFD_{\text{eff}}(R_b - R_s)/\delta.$$

D_{eff} is the effective diffusion coefficient, including the effect of migration; it is fairly close to the true diffusion coefficient.

It is clear that when R_s approaches zero at the surface, the current cannot increase further even with increased polarization (until some other reaction occurs, oxygen or hydrogen evolution, for example). This current is the "limiting current density"

$$i_L = nFDR_b/\delta \qquad (2.21)$$

or

$$R_s/R_b = 1 - i/i_L \qquad (2.22)$$

This approximate relation can be substituted in equation (2.16) to give the effect of mass transfer. A fuel cell should be designed to eliminate limiting currents, if possible.

For many molecules and ions dissolved in aqueous electrolytes, the diffusion coefficient is approximately 10^{-5} cm^2/sec (it varies with electrolyte concentration and temperature), and in stagnant electrolyte δ is about 0.5 mm. For $1N$ concentration of diffusing component, nR_b is 10^{-3} g-equivalents/cm^3 and $i_L \sim$ 20 mA/cm^2 at room temperature (1 mA/cm$^2 = 0.93$ A/sq ft). For example, 1-mole concentration of methanol ($n = 6$) dissolved in electrolyte would have a limiting rate of diffusion to the electrode of approximately 110 A/sq ft. The limiting current is increased by higher concentrations and by flowing the electrolyte past the electrode to reduce δ. The effective diffusion coefficients of H^+ and OH^- are abnormally high (roughly 7 and 4 times normal values, respectively). One N acid and alkali concentrations would, therefore, give limiting currents of roughly 140 A/sq ft and 80 A/sq ft for H^+ or OH^- transport to the electrode at room temperature. To avoid concentration polarization of these ions, it is necessary to use concentrated electrolytes; for example, KOH concentrations of 20 to 40 weight-percent (30 weight-percent is almost 7 N). Diffusion coefficient and conductivity decrease in concentrated solutions and increase with temperature, and an optimum concentration exists for a particular set of conditions.

2.1.6 Gas Diffusion and Purging

The slow transport of reactant gas through a porous diffusion electrode also gives rise to concentration polarization and limiting currents. Figure 2.4 shows the process for air. Two mechanisms of mass transport are possible: First, there may be a total pressure gradient across the electrode so that forced flow (permeability) occurs. Most porous electrodes would require only a small pressure gradient to support practical current. Second, if another component (water vapor or nitrogen, for example) is present, it builds up within the electrode to give an almost constant total pressure. Mass transfer is then by diffusion of oxygen through the gas in the pores. This process is much slower than forced flow and can lead to large partial pressure gradients and hence concentration polarization. It is this mechanism of mass transfer which normally occurs.

Figure 2.4 shows that there is a partial pressure gradient of nitrogen in the electrode which leads to diffusion out of nitrogen. Since nitrogen is not produced or consumed within the electrode,

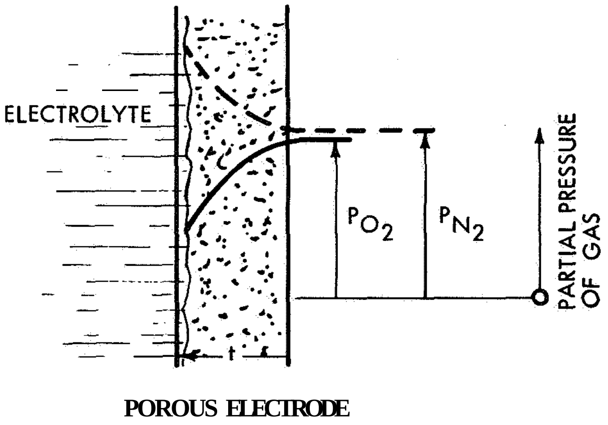

Oxygen is consumed at the oxygen-electrolyte interface and a concentration gradient is set up which causes more oxygen to diffuse in. The total pressure through the electrode remains about constant and inert gas (nitrogen, for example) builds up in the electrode.

FIGURE 2.4.—Gas pressure gradients through a porous diffusion electrode.

this diffusion gradient is matched by a bulk forced flow into the electrode. The mass transfer equation is (ref. *2.1*)

$$J_1 = -D_{12}(dc_1/dx) + (c_1/C)J \qquad (2.23)$$

J_1 is the molar flux (g-moles/cm^2, for example) of component 1 of concentration c_1 (moles/cm^3); J is the total molar flux; C is the net molar concentration present; and D_{12} is the binary diffusion coefficient of component *1* in component *2.* If J_2 is the molar flux of component *2* of concentration c_2, then $J = J_1 + J_2$. Consider component *1* to be reactant gas and component *2* to be inert gas, with the gas in the electrode gas chamber composed of c_{10} and c_{20}. Since component *2* is inert, J_2 is zero. As the total pressure remains almost constant, $c_1 + c_2 = c_{10} + c_{20} = C$. Integration of equation *(2.23)* over a thickness t for these conditions gives

$$J_1 = (D_{12}/t)C \ln\,[(C-c_1)/c_{20}], \qquad (2.24)$$

where c_1 is the concentration of reactant at the reaction interface. This can be put into the limiting current form

$$i_L = (nFD_{12}/t)c_{10}f \qquad (2.25)$$

where $f = (C/c_{10})\ 2.3 \log\,(C/c_{20})$.

Values of f are given in table *2.1.*

TABLE 2.1.—*Correction to Fick's Simple Law When Inert Gas Is Present*

[Ref. 2.21

Molar fraction of inerts in bulk gas stream. c_{20}/C	Correction factor, f
1.0	1
0.9	1.04
0.8	1.11
0.6	1.28
0.4	1.52
0.2	1.93
0.1	2.55
0.01	4.6
0.001	6.91

As the percentage of inerts in the gas compartment increases, the limiting current goes down because *(a)* c_{10} is less, and *(b)* f is less. For example, if the limiting current for 99.9 percent O_2 were *2000* A/sq ft, the limiting currents for other concentrations of oxygen would be as shown in table *2.2.*

TABLE 2.2.—*Calculated Limiting Current Densities as a Function of Percent Oxygen in Oxygen-Nitrogen Mixtures, Using (Arbitrarily) a Limiting Current of 2000 A/sq ft* for *99.9 Percent* O_2

Volume, percent O_2	i_L, A/sq ft
99.9	2000
99.0	1320
80	455
60	265
40	150
20	70

The limiting current for air would be about 70 A/sq ft. Figure *2.5* shows experimental results obtained with the Union Carbide fuel cell cathode of ¼-inch-thick porous carbon. There is a strong similarity between the results of table *2.2* and the experimental results of figure *2.3.* The value of D_{12} for O_2 and N_2 at cell temperature is about *0.2* cm^2/sec in free gas, and is probably reduced by about *10* for diffusion through porous baked carbons. The limiting current for air at a ¼-inch electrode would, therefore, be predicted to be approximately *120* A/sq ft, which is in reasonable agreement with the experimental value.

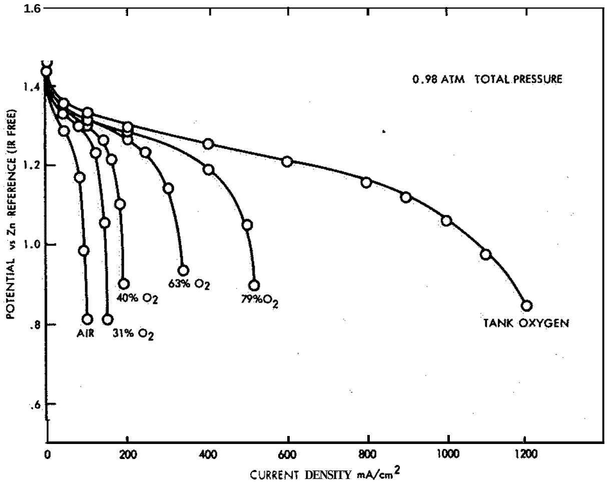

FIGURE 2.5.—Cathode currents for the ¼-inch-thick carbon electrodes (Union Carbide cell) as a function of oxygen partial pressure.

The equations above were developed using the normal binary diffusion coefficient, which is inversely proportional to total pressure. Under these conditions an increase in total pressure will not increase the mass transfer since $D \propto 1/p$. When the diameter of pores in the electrode is less than about 0.1 micron, mass transfer is by Knudsen diffusion. Knudsen diffusion is not affected by the presence of inerts, and the diffusion coefficient is independent of pressure. In this case, mass transfer is directly proportional to the partial pressure of reactant gas. Since many electrodes contain fine pores, mass transfer is probably a mixture of the two cases, and the effect of inerts is not quite as drastic as that shown in table 2.2.

This striking decrease in limiting current density with increasing percentage of inerts in the gas chamber leads to two important conclusions. First, a cell which operates satisfactorily on a flow of pure oxygen might not operate well on air. Second, small amounts of inert gas impurity build up in the system with time, leading to decrease in performance. The accumulated inerts have to be flushed either steadily or preferably by completely purging the system with reactant gas. Purge has been found necessary in all cells described in chapters 4 and 5. It leads to faradaic inefficiency, and the amount of purge must be adjusted to give optimum conditions.

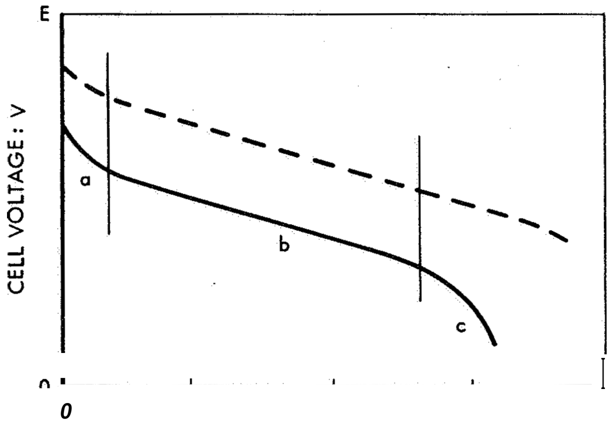

The total cell polarization is a complex interaction of activation, mass transfer, and IR polarizations at each electrode and in the electrolyte. As a first approximation, region *a* can be assigned primarily to activation polarization. *b* to IR losses in the electrolyte and electrodes, and c to mass transfer polarization. The broken line shows the effect of increasing temperature and concentration of the mass-transfer-limited component. *E* is the ideal reversible-cell potential.

FIGURE 2.6.—Fuel-cell voltage as a function of current density.

2.1.7 Improvement of Power Density

Knowing the causes of polarization and consequent loss of power density, we can give general methods for decreasing polarization and increasing power density or efficiency. Separation of the various types of polarization in **a** cell is not always possible, since they interact. As a first approximation, polarizations can be assigned as shown in figure 2.6. The loss of potential in region *a* is due primarily to activation polarization, and that in *b* to IR polarization (with possibly some concentration polarization as well); region *c* is the concentration polarization region.

Frequently the open-circuit voltage **(OCV)** does not correspond to the expected ideal reversible potential. Equation (2.14) shows that; for small exchange currents of one or both electrodes, considerable polarization, η, is needed to reach practical reaction rates. In theory, a sensitive potential measuring device with a high impedance (such as a vacuum tube voltmeter) can be used to measure potentials at very low cell currents, to give the ideal potential. In practice, as the cell current is decreased to very low values, small currents from minor side reactions become of the same magnitude as the current from the main-cell reaction. A balance is reached when the net current is zero (within the limits of the measuring device), but several reactions may be proceeding at the electrode. The **OCV** is then a mixed potential due to the mixture of reactions at the electrode. Diffusion of reactants from one electrode to another at open circuit is often sufficient to give a mixed potential. The faster the basic reaction, then the closer the potential is to the ideal value. A high degree of purification of the system also sometimes yields the ideal **OCV** by eliminating minor impurity currents, but this will not necessarily improve performance at practical current densities.

If the current-voltage curve has an *a* region suggesting activation polarization, each electrode should be checked against a reference electrode to see which electrode is polarized. Activation polarization is decreased by: (1) operating at higher temperature, (2) using more active catalyst, **(3)** using the same catalyst but changing the electrode structure to give more area, and (4) increasing the concentration of reactant by orders of magnitude. If other factors are unaffected, these improvements will shift the curve to the broken line shown in figure 2.6. The OCV may be near the ideal value, but, more important, the polarization at a practical current density is reduced.

If the slope of the *b* region of the curve is too steep, the IR polarization may be excessive. This should be tested by measuring the cell resistance with a Kordesch-Marko bridge, a current interruption technique, or an ac bridge (see app. C). Simple IR polarization disappears almost instantaneously when the current is interrupted. A resistance higher than expected from the conductivity of the electrolyte and from cell geometry may be due to : (1) contact resistance between the particles of the porous electrode or a high-resistance film on the electrode material; (2) contact resistance of a current collector on the electrode; (3) a pulling away of the electrolyte from the electrode, giving only a few small points of contact for current flow ; and (4) a high-resistance path of ions in electrolyte in the pores of the electrode (remember that a porous electrode filled with electrolyte may have one-tenth the conductivity of the equivalent free electrolyte). These difficulties are solved by correct mechanical design, including adequate current collectors and contact pressures between parts, and by suitable design of electrodes.

Finally, when mass-transfer limitation is suspected, each electrode should be tested to see which electrode is limiting. The species taking part in the reaction are then considered, to see which might be limiting. If it is a dissolved species, its concentration might be increased, or mass transfer might be improved by changes in cell design. If it is a gaseous reactant, the rate can be increased by raising its partial pressure, adequate purging, or redesign of the electrode for better mass transfer through the pores.

The above description is oversimplified; it often takes a great deal of investigation to pin down the causes of polarization. For example, a region *a* can result from accumulation of reaction products from an essentially reversible reaction, due to mass-transfer limitations. Again, ohmic resistance in electrolyte within the pores of an electrode may be combined with mass and activation effects, so that on current interruption a relatively slow readjustment is obtained. In this case, the polarization is not a “simple” IR effect.

2.2 TYPES OF FUEL CELLS

2.2.1 General Classifications

Although numerous methods of classifying fuel cells have been proposed, no single classification has been generally accepted. In this book, cells are grouped as follows:

1. Cells in advanced stage of development:
   - *a.* Low temperature
   - *b.* Medium temperature
   - *c.* High temperature
   - *d.* Amalgam
2. Cells which have not reached an advanced stage of development:
   - *a.* Electrolytically regenerative
   - *b.* Thermally regenerative
   - *c.* Thermogalvanic
   - *d.* Redox and photochemically regenerative
   - *e.* Hybrid
   - *f.* Biochemical

The advanced cells are most important at present, having been taken to the stage of systems engineering. Cells in the second group are either not very promising or have not yet received sufficient attention to show their capabilities. Grouping the advanced cells by temperature rather than fuel is advantageous, because the design of cells and their advantages and disadvantages are largely governed by temperature of operation. Amalgam cells have been separated from the others because of their special design characteristics. This order of treatment is a reasonable compromise between classification by type and classification by present importance.

The different types of cell are briefly described here to illustrate the general mode of operation. Later chapters contain specific points of design taken from the contract reports. Possible applications for advanced cells are discussed in section **2.3.**

2.2.2 Low-Temperature Fuel Cells

Low-temperature cells are defined as those operating below the normal boiling point of aqueous electrolytes. General advantages of low-temperature operation are better materials stability and life than for high-temperature cells, cheap lightweight case materials, operation at elevated pressures without excessive sealing problems, and quick startup. The major disadvantage is that the rates of reaction tend to be low at low temperatures (see discussion in previous sections). Thus electrode structure and catalysis become of overriding importance. Generally, noble-metal catalysts have to be used and porous electrodes have to contain a highly developed internal area, as well as the relatively large pores through which mass transfer occurs.

One of the earliest fuel cells to show promising power outputs was the hydrogen-oxygen cell developed by Union Carbide (see sec. 4.2). It consisted of the basic structure shown in figure 2.1, with the additional feature that electrolyte could be circulated through the cell. The carbon electrodes were specially developed for high reactivity when catalyzed and for good gas transfer. At the same time, they had a sufficiently small pore structure to prevent electrolyte from flowing through the pores. Noble-metal catalyst was impregnated into the carbon. The electrolyte was 25 to 40 weight-percent aqueous potassium hydroxide, and gas pressure ranged from 1 to 5 atmospheres. Very high currents could be drawn, but they caused electrolyte to creep through the electrodes and flood them. Electrodes were wetproofed by depositing thin films or patches of hydrophobic materials on them, but slow creep of electrolyte still occurred. For long life, the electrodes had to be thick (¼ inch) and current densities were restricted to about 50 A/sq ft. Both of these features kept the power output of the cell to about 0.4 kW/cu ft and 5.5 W/lb (excluding auxiliaries).

The hydrogen-oxygen cell developed by the General Electric Co. shares some structural features with that shown in figure 2.1, but the electrolyte is a synthetic, organic, ion-exchange membrane. Ion-exchange membranes have a lacy network of interlinked molecules which have anionic and cationic groups attached. The membrane retains water during its preparation and the ionic groups tend to split off and go into solution. A cationic membrane will readily split off the cation groups into solution, but the anion groups are more firmly bonded to the base structure and are retained (and vice versa for an anionic membrane). The dissolved ions can be exchanged with other suitable ions (of the same charge sign) by putting the membrane into a concentrated solution of the ion to be added. The amount of ions taken up must balance the electrical charge of the firmly bonded ionic groups. When current is passed, only the dissolved ion is transported through the membrane, *so* that the mechanism for a cationic membrane is

$$H_2+2M\rightleftharpoons 2M[H]$$

$$2M[H]\rightarrow 2H^+ +2M+2e^-$$

$$2H^+ \text{ anode}\rightarrow 2H^+ \text{ cathode}$$

$$2H^+ +M[(\tfrac{1}{2})O_2]+2e^-\rightarrow H_2O.$$

Thus water is formed at the cathode. The fixed ions are uniformly distributed through the membrane and, because a balance of electrical charge is maintained (law of electroneutrality), the concentration of free ions also remains constant through the membrane. This means that concentration gradients of the free ion cannot occur and no limiting current (see sec. 2.1.6) will arise.

Although no ionic limiting currents should be obtained, the driving force for mass transfer through the membrane is voltage gradient and the ohmic resistance tends to be high (giving IR polarization). This is counteracted by employing as thin an electrolyte membrane as possible. It is also clear that H^+ ions cannot jump large distances from the electrode to the water in the membrane; therefore, the electrode catalyst has to be bonded into the membrane. This led to considerable trouble with contact resistance and it is sometimes advantageous to saturate the membrane with concentrated electrolyte. In this case, the cationic membrane has a charge balance of: fixed anions+dissolved anions = free cations, and the membrane has something of the character and purpose of an asbestos matrix; cf. the Allis-Chalmers cell below. The free electrolyte serves the purpose of forming a bridge of high ionic conductivity between the electrode catalyst and the membrane.

The electrodes consist of metal screens (tantalum, for example) with platinum black catalyst packed into the screen and bonded into the membrane surface with heat and pressure. Strength and bonding are improved by incorporating about 10 weight-percent of Teflon particles (less than 1 micron in diameter) into the platinum black and heating to just sinter the Teflon. Because of the rather low water capacity of the thin membrane, close water balance has to be maintained to prevent drying out of the membrane. Drying out leads to high ohmic resistance, membrane embrittlement and cracking, and passage of gas through the membrane. Platinum black is sufficiently catalytic to combust hydrogen and oxygen at ambient temperatures, so that gas passage burns holes in the membrane. The necessary water balance is obtained by a capillary wicking system (see sec. 4.3). Power densities of 1 to 2 kW/cu ft and 20 W/lb are possible; the cell current is low, but the small thickness of the cell partially compensates for this, and the cell components are lightweight.

The Allis-Chalmers hydrogen-oxygen cell is again similar in construction to the basic cell of figure 2.1. However, it uses a mat of asbestos between the electrodes as an electrolyte matrix. The capillary forces of the fine asbestos fibers retain the electrolyte (concentrated aqueous KOH) and prevent it from flooding the electrodes. Cell temperature is close to 200° F. The electrodes are of porous sintered nickel about 28 mil thick, catalyzed by impregnation with platinum or platinum-palladium mixtures. Porous silver cathodes are also used. The cell is rated at 3kW/cu ft and 30 W/lb.

A double-layer electrode structure has been used in the alkaline hydrogen-oxygen cell developed by Prof. E. Justi and by Brown Boveri Corp. The two layers consist of a noncatalyzed fine-pore layer next to the electrolyte and a coarse-pore catalyzed layer on the gas side. The fine-pore layer fills with electrolyte by capillary attraction; but a pressure differential is maintained to prevent liquid from flooding the coarse-pore layer. The catalytic hydrogen electrode is made from fine particles of Raney nickel sintered into a matrix of larger size nickel particles. Raney nickel contains holes of molecular dimensions and thus has a large area for adsorption of reactants. The oxygen electrode has Raney silver in a nickel matrix.

A number of cells have used fuels which are electrochemically reactive and highly soluble in alkaline or acid electrolytes. The fuels most investigated are hydrazine (N_2H_4), ammonia (NH_3), and methanol (CH_3OH). The first two have the advantage that nitrogen and water are the only products of reaction; hydrazine is the more active electrochemical fuel. Methanol produces carbon dioxide, which reacts with alkaline electrolyte to give carbonates. Unfortunately, carbonate solutions are not good electrolytes and give considerable polarization. In a strongly acid electrolyte, sulfuric acid, for example, the oxygen electrode is more polarized than in alkaline electrolytes and, of course, corrosion problems limit the materials which can be used. When the temperature is raised to decrease activation polarization, concentrated sulfuric acid and fuel react directly.

Cells for highly soluble fuels may have a somewhat different structure from those for hydrogen and oxygen. A highly soluble reactant will pass through the porous anode shown in figure 2.1 and its concentration will build up in the electrolyte, even while current is being drawn. When the oxygen electrode is also active to the fuel, dissolved fuel will react at the oxygen electrode, thus decreasing performance considerably. For example, at the cathode

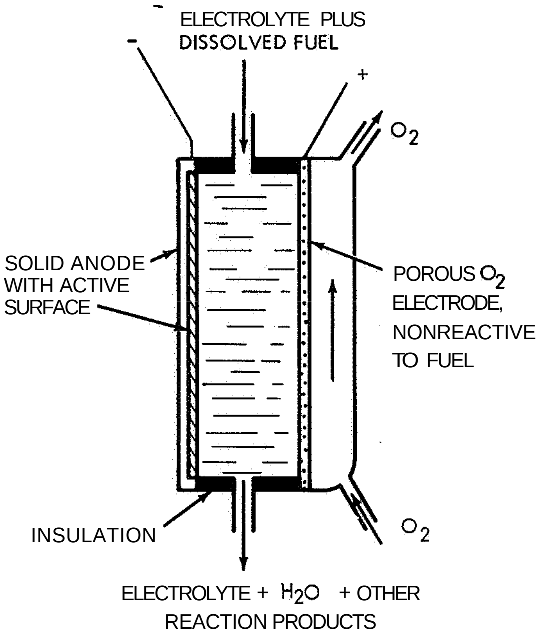
ELECTROLYTE PLUS DISSOLVED FUEL
-
+
O_2
SOLID ANODE WITH ACTIVE SURFACE
POROUS O_2 ELECTRODE, NONREACTIVE TO FUEL
INSULATION
O_2
ELECTROLYTE + H_2O + OTHER REACTION PRODUCTS

The essential feature of the cell is that the dissolved fuel (hydrazine. for example) must not be electrochemically active at the oxygen electrode.

FIGURE 2.7.—Schematic of a dissolved fuel-oxygen fuel cell.

$$\begin{array}{r} O_2+2H_2O+4e^- \rightarrow 4OH^- \\ N_2H_4+4OH^- \rightarrow 4H_2O+N_2+4e^- \\ \hline O_2+N_2H_4 \rightarrow 2H_2O+N_2 \end{array}$$

At zero net current, the voltage is such as to make both reactions proceed at the same rate, giving a net effect comparable to direct (nonuseful) reaction between fuel and oxidant. The mixed potential lies between the ideal oxygen and hydrazine potentials. This effect is reduced by an ion-exchange membrane between the electrodes which will not pass fuel; by adding fuel, dissolved in electrolyte, to the anode chamber at a rate such that it is electrochemically consumed before it passes through the electrode; or by having selective catalysts, which ionize oxygen but not fuel, at the oxygen electrode. The last alternative is the simplest and leads to the design shown in figure 2.7.

These cells are capable of relatively high power density (at least 2 kW/cu ft with hydrazine). Electrolyte is circulated, products of reaction are removed, and fresh fuel is added.

2.2.3 Medium-Temperature Fuel Cells

One of the earliest high-power fuel cells was the hydrogen-oxygen cell developed by F. T. Bacon. This cell overcame activation polarization by operation at about 390° to 465° F (200° to 240° C) with 45 percent aqueous potassium hydroxide. The high temperature required a high pressure, 600 to 800 psi, to prevent boiling of the electrolyte. The sintered nickel electrodes were of double-layer structure, a fine-pore layer next to the electrolyte acting as an electrolyte stabilizer; total electrode thickness was about 1/16 inch. At these temperatures nickel tends to oxidize and form a high-resistance coating, so electrodes were lithiated to provide semiconducting properties. The major disadvantage of the Bacon cell was the high pressure, which led to heavy and expensive construction, and to problems in balancing the pressure of the hydrogen chamber against that of the oxygen chamber.

The basic principle of the Bacon cell has been further developed in the Pratt & Whitney cell, which uses an electrolyte of about 85 percent potassium hydroxide. The electrolyte is thus a

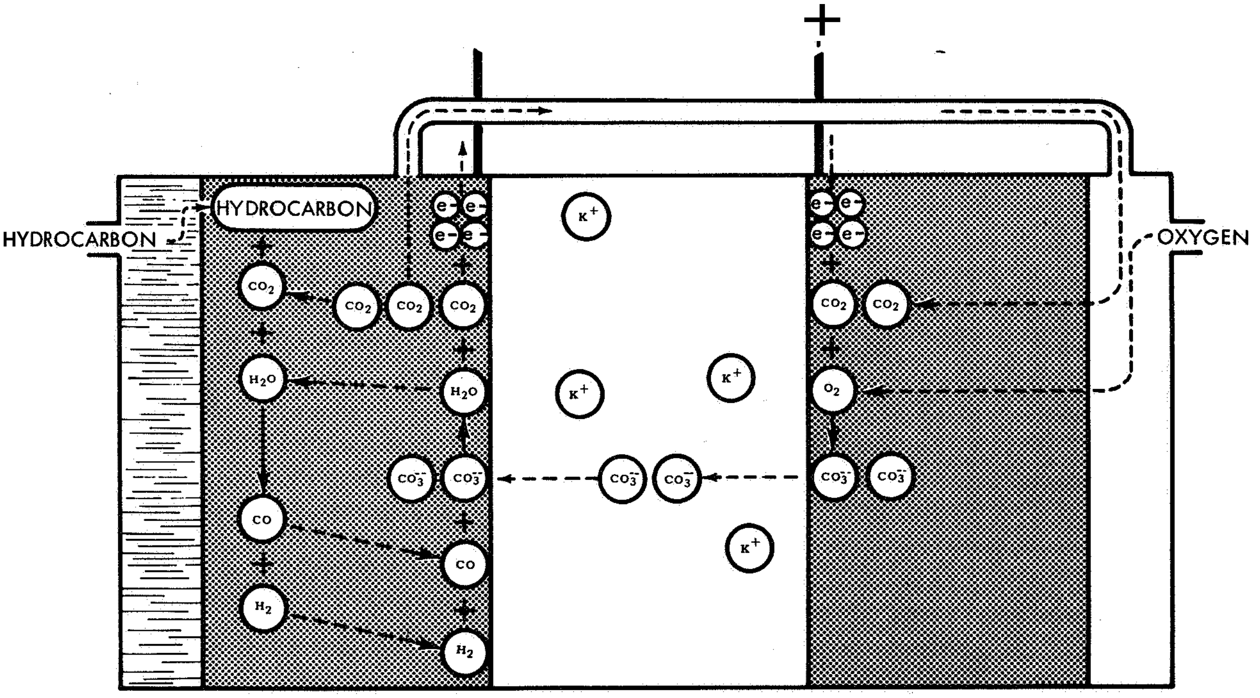

The cell operates at temperatures above 500° C and the hydrocarbon fuel is re-formed with water to give hydrogen and carbon monoxide. These are oxidized by carbonate ions (probably via oxide ion from $CO_3^{=} \rightarrow CO_2+O^{=}$) to produce H_2O, CO_2, and electrons. The supply of carbonate ion is replenished at the cathode by the reaction of CO_2, O_2, and electrons.

FIGURE 2.8.—Principle of operation of the molten-carbonate fuel cell.

molten base with some dissolved water, and the partial pressure of water over the melt is less than 1 atmosphere. As the cell need not be highly pressurized to prevent boiling, its major disadvantage is removed. But the electrolyte is solid at room temperature; therefore, the cell is not rapid starting and requires special procedures for filling with electrolyte.

Alkaline electrolyte is not suitable for hydrocarbon fuels because of carbonate formation and because nickel anodes become poisoned. Concentrated sulfuric acid oxidizes the fuels directly when temperatures are raised. General Electric and Allis-Chalmers have described laboratory cells which operate at 350" to 400" F (177° to 204" C) using 85 weight-percent phosphoric acid as the electrolyte. The General Electric cell uses 10-mil electrodes containing Teflon-bonded powdered platinum on screens. Fuels such as propane, methanol, butane, and isobutane have been used. Power densities of up to 25 W/sq ft have been obtained.

2.2.4 High-Temperature Fuel Cells

Hydrocarbons can be oxidized electrochemically to water plus carbon dioxide and some carbon monoxide at 932" to 1292" F (500" to 700" C) with molten carbonate electrolytes. The basic configuration is again similar to that of figure 2.1, but the electrolyte, usually a eutectic of potassium-sodium-lithium carbonates, is retained in a porous ceramic matrix (MgO), and the electrodes are bonded to the matrix. Alternatively, pastes of carbonate and ceramic have been used. Porous electrodes of sintered metal particles consist of nickel on the fuel side and silver, silver-plated nickel, or iron on the oxygen side. The exact mechanism of the reaction is not known, but it can be represented as shown in figure 2.8. Even at these elevated temperatures, direct oxidation of hydrocarbons and carbon monoxide does not give high currents, probably because the primary fuel is hydrogen, produced from the hydrocarbons by thermal cracking. Output is improved by supplying water with the fuel, since steam re-forming aids in producing hydrogen. Carbon dioxide is supplied with the oxygen (or air) to maintain the electrolyte as carbonate.

These cells have suffered from a variety of materials problems, and longevity has not been good. Current density and power output are small, and the cell is not suited for applications where a compact, rapid-starting, high-power-density source is required. Rather, it is primarily suitable as a steady power generator, using cheap and readily available fuels. The reasons for the low current densities are not fully understood, but are apparently combinations of activation, mass, and ohmic polarization. Attempts to use high-area active electrodes fail because the metallic materials sinter slowly and lose active area. If the cell is to supply cheap electrical power, it must have low capital cost and long life (several years), and neither of these requirements has yet been met.

The Westinghouse cell and similar ones operate at about 1832" F (1000" C) and can be of the basic form of figure 2.1. The solid electrolyte is, e.g., zirconia-thoria. In these stable ceramic oxides, some of the oxygen ions become mobile at high temperatures; the metal ions do not, and the structure remains strong and refractory. The mobility of the oxide ion leads to ionic conductivity, while the electronic conductivity remains low. The obvious advantages of a solid electrolyte with these properties were realized long ago and several efforts were made to develop such material. However, the conductivity of the solid electrolyte was usually due to a molten salt phase, with consequent slow loss of electrolyte and structural strength. The alternative, material which would allow sufficient mobility of oxide ion, would probably be highly permeable to the small hydrogen molecule. The Westinghouse electrolyte appears to be a true solid electrolyte, nonpermeable to gases.

In addition to the properties mentioned above, the electrolyte must be able to accept oxygen ions from a cathode placed in contact with it and discharge oxygen ions to an anode,

$$O_2+2M\rightleftharpoons 2M[O]$$

$$2M[O]+4e^-\rightleftharpoons 2M+2O^= \quad \text{(in solid electrolyte).}$$

Since there is no liquid electrolyte to form a bridge between the metal electrode and the electrolyte, the metal must be in intimate contact with the electrolyte. Platinum has been sprayed onto the solid electrolyte to form an adherent but highly porous layer. Hydrocarbons and carbon monoxide do not give good performance and it is again advantageous to admit steam to form hydrogen at the fuel electrode.

This type cell is under intensive development, but no firm values for power density are available. Major problems have been stability of electrode materials and seals and the cost of platinum electrodes. Like the molten carbonate cell, the Westinghouse cell is not yet suitable for many fuel-cell applications and must be developed into a cheap cell with long lifetime.

A variation of the solid electrolyte cell described above has been patented by the General Electric Co. It uses the same type of electrolyte at 1832" to 2192" F (1000" to 1200" C), but the electrodes are in liquid form. Molten silver is used for the cathode, and iron or cobalt-tin saturated with carbon for the anode. Hydrocarbon fuels crack to dissolved carbon at the anode, which is then oxidized to carbon monoxide, presumably by the steps:

$O^{=}+Fe \rightarrow FeO+2e^{-}$, $FeO+C \rightarrow Fe+CO$,

or

$O^{=}+C$ (dissolved)$+CO+2e^{-}$.

The use of liquid electrodes insures good contact between the electrode and electrolyte, but makes the system more difficult to engineer as a practical cell.

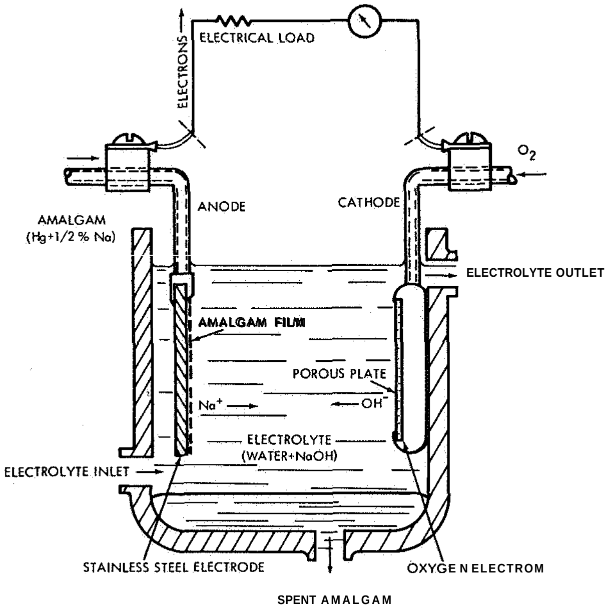

FIGURE 2.9.—The sodium amalgam cell.

2.2.5 The Sodium Amalgam Cell

This low-temperature cell was invented by Prof. E. Yeager; its development has been due principally to the M. W. Kellogg Co. The principle of the cell is shown in figure 2.9. The electrolyte is aqueous sodium hydroxide, and the fuel is sodium dissolved in mercury. The amalgam wets a stainless-steel plate anode and runs down, forming a thin film on the plate. Dissolving the sodium in mercury retards hydrogen evolution because of catalytic action of the mercury surface. The overall reaction

$$\begin{array}{c} 2Na \rightarrow 2Na^{+}+2e^{-} \\ \underline{2H_2O+2e^{-} \rightarrow H_2+2OH^{-}} \\ 2Na+2H_2O \rightarrow 2NaOH+H_2 \end{array}$$

does not occur, even though the electrode voltage is greater than the reversible hydrogen evolution potential. Sodium ionizes with little polarization, and the combination of this anode with an oxygen cathode gives

$$\begin{array}{c} 2Na \rightarrow 2Na^{+}+2e^{-} \\ \underline{\tfrac{1}{2}O_2+H_2O+2e^{-} \rightarrow 2OH^{-}} \\ 2Na+\tfrac{1}{2}O_2+H_2O \rightarrow 2NaOH \end{array}$$

Thus the reactants are sodium, oxygen, and water, and the product is sodium hydroxide. Removal of concentrated electrolyte and feed of water are continuous. Amalgam depleted in sodium runs out of the bottom of the cell and is circulated to an amalgamator where the sodium content is renewed.

The cathode used in the Kellogg cell is a porous sintered silver electrode (developed by the Electric Storage Battery Co.), in the form of a number of tubes sintered along their sides to form a plate. These electrodes are very efficient (but also expensive). The cell has a high power density and is capable of at least 5 kW/cu ft (excluding auxiliaries). It requires special auxiliaries and configurations to prevent the mercury stream from forming a high-conductivity short circuit between the anodes.

2.2.6 Other Types of Cells

A specialized but important possible use for fuel cells is as an auxiliary power supply for small orbiting satellites. For long-mission durations, the best source of power at present is sunlight acting on solar cells carried by the satellite. However, the solar cells obviously cannot produce power in the dark period of the orbit, during which an auxiliary battery is used.

Batteries are charged by solar cells during the light period; the combined battery-solar cell system should have minimum weight for a given power duty. A hydrogen-oxygen fuel cell system *can* be used as the battery, with H_2 and O_2 regenerated from electrolyte by electrolysis in the light period. In the dark period, the gases are converted back to water in the electrolyte, thus producing power. At first sight, a fuel-cell system seems unlikely to compete with the simplicity and capability for energy storage of a conventional battery. However, conventional batteries with high capacity in watt-hours per lb, such as zinc-silver oxide or cadmium-silver oxide, suffer from a major disadvantage. To give long life the batteries must be charged at low rates, even though they can be discharged at high rates. It can be shown that the full capacity of the batteries cannot be obtained for the charge-discharge cycles of an orbiting satellite, which leads to excessive weight. **A** H_2-O_2 fuel cell can be charged at high rates by electrolytic production of H_2 and O_2 and can offer some savings in weight. Nearly all of the H_2-O_2 cells have been considered for this application, but the most advanced unit is that developed by Electro-Optical Systems. It uses a basic cell similar to that of Allis-Chalmers, with electrolyte retained in a porous matrix of asbestos and porous electrodes of platinized nickel plaque. The cell is used both as electrolyzer and fuel cell, with sufficent volume of high-pressure tanks to store the amount of H_2 and O_2 required for the dark period. The unit is completely enclosed so that gases or water cannot escape and the reactants are used and regenerated for many cycles.

Thermally regenerative cells have been proposed for converting heat into electricity. The basic principle is that reactants are combined in a fuel cell to give power, the product of reaction is removed from the cell and thermally decomposed to re-form the reactants, which are separated for return to the cell. For example, lithium and hydrogen can be combined to form molten lithium hydride:

$$\begin{array}{ll} \text{Anode:} & 2Li \rightarrow 2Li^+ + 2e^- \\ \text{Cathode:} & \underline{H_2 + 2e^- \rightarrow 2H^-} \\ & 2Li^+ + 2H^- \rightarrow 2LiH \end{array}$$

Lithium hydride is then decomposed to liquid Li and gaseous H_2 in a hot regenerator, for reuse in the cell. Problems of low thermodynamic efficiency and voltage, separation of components, and corrosion of materials have prevented successful development of this type of cell.

Thermogalvanic cells are somewhat similar in application and principle. The potential of an electrode depends on temperature; if two electrodes in a cell are held at different temperatures, a potential is established between them. For example, in a Pb (hot)/PbI_2 (molten)/Pb (cold) cell, Pb ionizes at the anode, Pb ions discharge to Pb at the cathode, and molten Pb circulates from cathode to anode. The maximum efficiency is low due to a high flux of waste heat by conduction from cold to hot electrodes. Two complete cells can be used (one hot, the other cold), and the products from one cell electrolyzed in the other cell to regenerate reactants. Since the cells are at different temperatures, a net potential exists between them. Again, problems of handling and containing molten salts have prevented successful development of thennogalvanic cells.

The regenerative principle is also used in two other variants of fuel cell: the photochemically regenerative cell and the redox cell. In photochemical regeneration, the fuel-cell product is decomposed to reactants by a photochemical process, for example

$$2NOCl \xrightarrow{\text{radiation}} 2NO + Cl_2.$$

The reactants are separated and fed to the fuel cell, NO at the anode, Cl_2 at the cathode. The size and cost of the system depend on the speed and efficiency of the regeneration. Unfortunately, photochemical reactions have shown little promise of providing an economic means of converting the energy of sunlight into electricity. The photolytic decomposition of water into H_2 and O_2 by sunlight proceeds too slowly and inefficiently to be useful.

The principle of the redox cell is shown in figure 2.10. Instead of using fuel directly in the fuel cell, it is used to produce a reduced ion, which then oxidizes at the anode, giving up electrons. The ionic product is cycled to the regener-

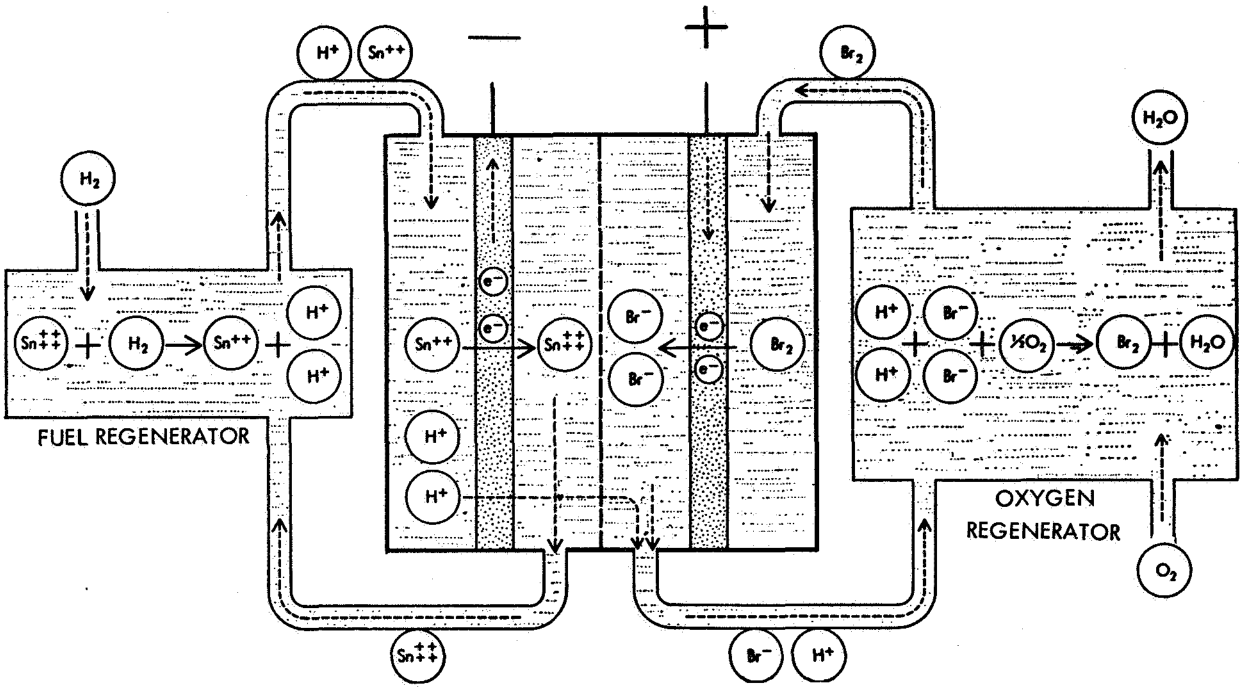

The electrode reactions are redox reactions involving ions dissolved in electrolyte in high concentration. The rates of these reactions can be high but the anodic and cathodic products, Sn^{4+} and Br^- in the figure, have to be chemically regenerated to anodic and cathodic reactions, Sn^{2+} and Br_2.

FIGURE 2.10.—Principle of redox cell.

ator for conversion to the reduced form, and so on. Similarly, oxidant is used to produce an oxidized reactant from a reduced product at the cathode. There are three basic requirements for the intermediate reactants which take part in the electrode reactions: they must be soluble in high concentration, they must react at the electrodes to give high current density, and they must be readily regenerated from product to reactant by available fuels and oxidants. The reactants used are "redox couples," which readily convert between oxidized-reduced forms at an electrode, without side reactions which remove intermediates.

The standard-state free energy of conversion of the redox couple must be close to that of the chemical regeneration. (In the case shown *(480)*, the reversible anode potential is for $H_2 \rightleftharpoons H^+ + e^-$, since Sn^{2+}, Sn^{4+} are only intermediates in the reaction. Thus the ideal open-circuit concentrations of Sn^{2+}, Sn^{4+} correspond to this potential. If the equilibrium value of Sn^{2+} were low, it would be necessary to circulate electrolyte at high rate to transfer enough Sn^{2+} to support current. If the equilibrium value of Sn^{4+} were very low, then production of Sn^{4+} during cell operation would lead to large values of P/P_b in equation (2.16) and, hence, concentration polarization due to buildup of product. A redox couple must be selected which avoids either of these extremes.) Combined with the requirement of stability under cell and regenerator conditions, this limits the feasible couples to a few. It has not been possible to regenerate suitable redox couples at sufficient rate to make, the system feasible (see ch. 12).

Hybrid fuel cells consist of one fuel-cell electrode combined with a conventional battery electrode. One example is a zinc anode combined with an air cathode, which is more properly a modified primary cell than a fuel cell. The term "hybrid" can also be used for fuel cells in which a conventional battery reactant (solid) is fed into a cell as a layer on a tape. It has not yet been demonstrated that tape systems have any advantage over conventional batteries or fuel cells.

Biochemical fuel cells normally have an air cathode, but the anode is immersed in a mixture of organic matter and bacteria or enzymes. Bacterial or enzymatic action on the organic matter produces electrochemically active fuels such as H_2 or CH_3OH, which react to give current at the anode. Alternatively, H_2 is generated in a biochemical reactor and fed to the fuel cell. One possible use for a biochemical fuel cell is power production during treatment of waste matter in a closed ecological cycle in a space vehicle. Another is as a source of power using indigenous organic fuels where there are logistic or cost problems with conventional power sources. The power density of biochemical fuel cells has, so far, been so low as to make them unattractive in comparison with other systems.

2.3 APPLICATIONS OF FUEL CELLS

2.3.1 Introduction

When considered only as a source of electric power, the fuel cell has possible use in a myriad of applications. Considered in terms of the present and near-future capabilities and limitations, the fuel cell has probable use in a rather restricted number of applications. At present, the best case for fuel-cell development requires consideration of those uses for which the fuel cell has unique advantages; if the fuel cell cannot prove itself in these applications, then it is quite unlikely that fuel cells would be suitable for more general applications where they would be competing with other power systems.

One dampening feature in the development of fuel cells is the initial extravagance of claims made by their sponsors, particularly in the area of immediate applications. This is forgivable in an industrial milieu where a development must be oversold generously to attract management support and research moneys. This generosity of claim has extended to a number of the Government contracts reviewed here, wherein the hardware contracted was never delivered or, if it was, fell far short of contract requirements in performance. In many of these cases, contract requirements were supplied by the developer on the basis of inadequate extrapolation of research data and inept examination of the theoretical system limitations.

The danger of this extravagance arises from the inevitable failure to secure the initial claims, followed by disenchantment with, and neglect of, the fuel cell even in those applications where it possesses unique qualifications.

The direct fuel cell has several advantages over other sources of electrical power. First, it does not have the thermodynamic limitations of conventional heat cycles (referred to here as Carnot-type limitations), so it is theoretically possible to obtain high thermal efficiencies from the fuel cell, thus substantially reducing the amount of fuel required for a given duty. This is especially desirable for applications involving the logistics of fuel storage and transport. Second, its storage tanks can be filled very quickly, which represents a rapid charging of the system when compared to the electrical charging of secondary batteries. Third, the energy conversion part (the fuel cell) is distinct from the energy storage part (the storage tanks), so the energy storage per pound of reactants can be very high in comparison with the best conventional primary or secondary batteries available (the zinc-silver oxide alkaline battery, for example).

On the other hand, fuel cells cannot generally be used at the very high power density obtainable from batteries. For a given power P in kilowatts, the fuel cell relation is, crudely

$$W = (P/\alpha) + (Pt/\xi\beta) \qquad \textbf{(2.26)}$$

where W is the system weight in pounds, α is the cell power density in kW/lb (including auxiliaries), β is the energy density of the reactants in kW-hr/lb (including tankage), ξ is the efficiency of fuel conversion, and t is the duration of steady operation between recharging in hours. Thus the system weight per kilowatt is

$$(W/P) = (1/\alpha) + (t/\xi\beta). \qquad \textbf{(2.27)}$$

The weight per kilowatt for a conventional battery, however, is almost directly proportional to time (i.e., kW-hr/lb is almost constant), so that

$$(W/P) = t/\xi\beta' \qquad \textbf{(2.28)}$$

where p' is much less than β'. It can be seen, therefore, that a battery is favored by short durations (t small), while beyond a certain mission time a fuel-cell system becomes favorable in terms of lb/kW. A solar cell system has principally the α term and is favored by long-mission times.

Since a general discussion of the possible applications of fuel cells is readily available (ref. 2.1), the following sections stress the military and space applications of fuel cells. Most of the work within the scope of this book has been done with these applications in mind, and the feasibility of any wide applications of fuel cells beyond these purposes has not been demonstrated.

2.3.2 Space Applications

Much of the fuel-cell research and development discussed in this book has been sponsored by the Air Force and NASA, and fuel cells are being used as capsule electrical power sources in the Gemini and Apollo programs. A brief report on spacecraft secondary-power requirements from 1960 through 1970 was issued by the Jet Propulsion Laboratory in April 1960 (*377*), specifying a required load of 3 to 5 kW. The major disadvantage of fuel cells was the lack of ruggedness. In May 1962, a report from the U.S. Signal Missile Support Agency (798) showed that fuel cells had advantages over silver-zinc batteries (rated at 40 W-hr/lb) at mission times greater than about 3 to 10 hours, but were not favorable compared to a gas turbine-ac aircraft generator (allowing for fuel weight but not oxygen weight). Solar cells were quoted as having a power density of 2.3 W/lb (irrespective of mission time). It was also claimed that fuel cells had the advantage over conventional cells of simplicity of design, but this is not true. A more general comparison of energy conversion systems was presented by Fisher and Menetrey at the 14th Annual Power Sources Conference (ref. 2.2, May 1960). Revised versions of their conclusions have been given by Starkey (ref. 2.3) and Szego and Cohn (ref. 2.4). Figure 2.11 shows the basic correlation (from ref. 2.4). There is, of course, overlap of the favorable regimes of the different power sources, which has not been shown for the sake of clarity. Fuel cells are most favorable for the power levels and durations of the current Gemini and Apollo programs. The advantage of fuel cells for these mission requirements is shown in figure 2.12 (ref. 2.5); the fuel cell and chemical engine have the weight/duration relation of equation (2.27). The specific chemical consumption for hydrogen-oxygen fuel cells was estimated at 1 lb/kW-hr compared to 1.5 lb/kW-hr for the engine.

2.3.3 Small- and Moderate-Sized Military Power Generators

Use of fuel cells for self-contained portable and semiportable military power supplies has been

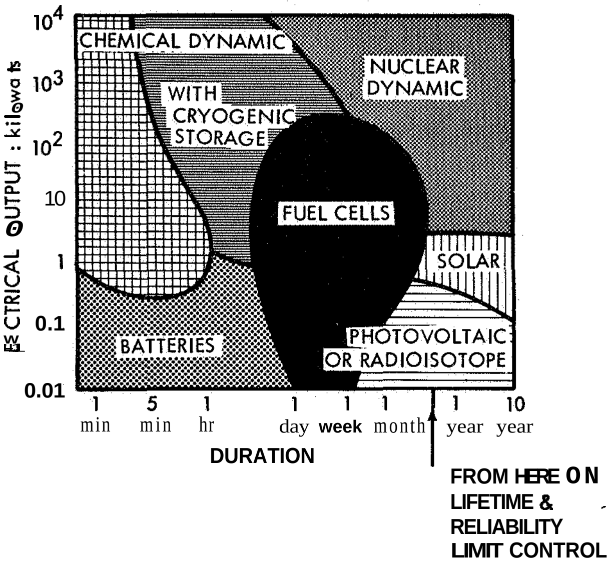

It can be seen that fuel cells are favorable power sources for the relatively low loads (1 to 10 kilowatts) and short flight times (1 to 30 days) which are presently the secondary-power requirements of manned space flight. Primary power for thrust (at high loads over short output times) is best obtained at present from direct chemical fuels. Large secondary-power requirements (greater than 100 kilowatts) are best satisfied by chemical fuels in a turbine generator (or similar) system for short durations; for long times, nuclear reactors are most promising. Solar cells and photovoltaic devices are best suited for low power and long life.

FIGURE 2.11.—Comparison of space power sources (after ref. 2.4).

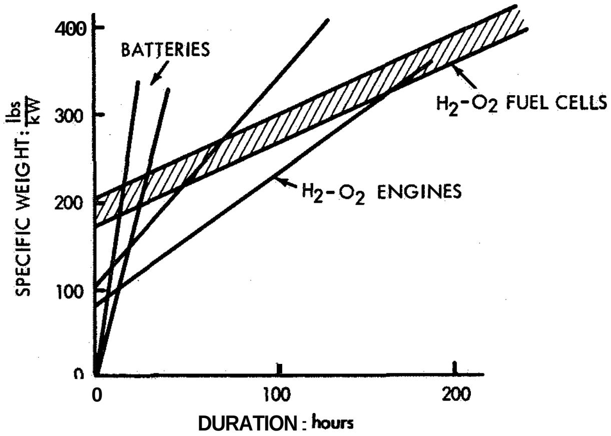

FIGURE 2.12.—Comparison of specific weights of batteries, fuel cells, and chemical engines.

discussed by Hunger (ref. *2.6)* and Alamaula (ref. ***2.7).*** Fuel cells using hydrogen or ammonia, plus air, would be competitive both in weight and cost with batteries and engine generators for powers between ***200*** watts and ***1.5*** kW, and durations of *2* to *24* hours. At these power levels, the low weight and rapid rechargeability of the fuel-cell system give it advantages over batteries. At higher power levels it is necessary to use combat gasoline, ***JP–4,*** or diesel fuels in the fuel cell, either directly or indirectly (by re-forming to hydrogen). Other fuels are unattractive because of high cost, restricted availability, and low-energy density (kW-hr/lb). For these higher power levels, the primary advantage of the fuel cell is the promise of higher fuel efficiency with consequent improvement in fuel logistics problems. Technical feasibility has not yet been demonstrated. Table *2.3* (from ref. *2.7)* gives some typical performances of the self-contained power generators with which fuel cells must compete.

Another proposal advanced for military uses is the energy-depot concept wherein a nuclear reactor supplies heat to regenerate electrochemical reactants from the products of a fuel cell. Thus the logistics would consist of ***(a)*** taking reactants to the fuel cells and returning products to the regenerator, and ***(b)*** transporting the nuclear reactor with the moving army. The problem is to develop a fuel-cell system whose product can be easily regenerated to fresh reactants with the minimum of material losses. The potassium-mercury cell investigated by the Allison Division of General Motors (see ch. 10) was proposed as the thermally regenerative cell. It is shown in section ***10.4*** that this system, at least as currently proposed, would have a low efficiency of utilization of thermal energy.

2.3.4 Military Vehicle Propulsion

The major energy consumption of an army on the move is fuel for the various internal combustion and diesel engines of the army's vehicles. Since these engines operate at about ***15*** to ***25*** percent efficiency, a fuel-cell system of ***50*** percent fuel-utilization efficiency would have a great impact on the problems of fuel supply. Fuel efficiency alone is not an accurate guide; the useful Btu per pound or gallon is the true criterion. Fuels with high efficiencies but low-energy densities per pound must be ruled out.

Cather (ref. ***2.8)*** set the requirements for a useful fuel-cell system for vehicular power at a net power density of *2* kW/cu ft and ***0.022*** kW/lb; 60 percent conversion efficiency on standard petroleum fuels; air oxidant; capability of repeated cycling and extended stand at open circuit; and quick start at ambient temperatures in the range ***–65"*** to ***120"*** F ***(–54"***C to ***49" C).*** Cather estimated that the weight of a fuel-cell

TABLE 2.3.—***Self-Contained Power Generators***

[Ref. 2.71

Type	Size, kW	Fuel	Weight				Fuel use	
			Total lb	lbs/kW	Total cu ft	cu ft/kW	lbs/kW-hr	Efficiency[a]
General purpose..	0.150	Gasoline	43	286	3.2	21.4	....	....
Military design.	.50	Gasoline	80	160	6.0	12.0	3.0	6.3
Military design.	1.5	Gasoline	185	123	8.5	5.7	1.57	12.3
Military design..	3.0	Gasoline	285	95	12.2	4.1	1.57	12.3
Military design..	5.0	Gasoline	500	100	25.2	5.0	1.5	12.6
Military design..	10.0	Gasoline	850	85	36.1	3.6	1.5	12.6
Turbine..	10	JP4	325	32.5	12.0	1.2	....	....
Turbine..	45	JP4	975	21.6	44.5	1.0	2.22	7.8
Turbine..	60	JP4	....	....	53.6	.9	2.0	8.6
Turbine..	100	JP4	1300	13.0	68.0	.7	1.80	9.5
Diesel.	45	Diesel	4200	93.5	107	2.4	.78	23.7
Projected high-speed diesel.	45	Diesel	2200	49	51	1.1	.71	26.0

[a] Efficiency = electrical output as Btu divided by 18 000 Btu per lb of fuel. All values are correct within ±10 percent.

system plus fuel becomes favorable compared to spark-ignition engines after 10 continuous days of normal battlefield duty. Szego (ref. *2.9)* repeats the data and argues that a gasoline engine, because of parasitic and transmission losses (available bhp to wheels about 60 percent of original bhp) and unfavorable torque characteristics, is equivalent in output to an electric motor of about one-fourth to one-sixth of the rated bhp of the engine.

Schlatter et al. (ref. *2.10)* recalculated Cather's data, as shown in table *2.4,* and disagreed with his conclusions. For a 150-bhp gasoline engine compared with the same output fuel cell, the fuel cell has over 7000 pounds greater weight but consumes nearly 400 pounds of fuel a day less than the engine. Thus the fuel cell becomes favorable at mission lengths greater than about 17 days, not 10. Such lengthy periods of operation without refueling are not realistic, since this 17-day mission represents a total initial powerplant and fuel weight of over 7 tons. Thus

TABLE 2.4.—*Comparison of Ignition Engines for Military Vehicles With Their Fuel Cell-Electric Motor*

					330 bhp			
	Gasoline engine		Fuel cell					
	lb	cu ft	lb	cu ft	lb	cu ft	lb	cu ft
Powerplant:[a]								
Engine..	[d]750	18.8	....	....	[e]1600	31.4	....	....
Fuel cell..	....	......	5040	56	......	....	11100	123
Transmission...	512	7.5	....	....	2300	25.2	....	....
Electric motor.	....	......	3600	16	......	....	7 400	33
Total powerplant..	1262	26.3	8640	72	3900	56.6	18500	156
Fuel consumed per combat day:[b]								
Average bhp under load[a].	118		118		326		326	
Efficiency (under load), percent.	23.5		42		32.7		[c]42	
Fuel consumed in 10.8 hr under load, lb..	688		386		1370		1067	
Fuel consumed at idle (7.2 hr), lb	92		0		37		0	
Total fuel:								
lb	780		386		1407		1067	
cu ft..	17.1		7.9		28.9		21.9	
Powerplant and fuel for 1 combat-day:								
lb	2042		9026		5307		19 576	
cu ft.	43.4		79.9		85.5		177.9	

[a] Data from Cather.

[b] Calculations by method of Cather; the results of calculations by Schlatter et al. do not agree with those by Cather. A combat-day is defined as a continuous 18-hour period, of which 40 percent is at idle, 40 percent is overland on secondary roads, and 20 percent is overland on cross-country terrain. Fuel calculated on Cather basis: 20 000 Btu/hr; sp. gr. gasoline 0.73, diesel fuel 0.78

[c] Fuel-cell efficiency, 60 percent; electric motor efficiency, 70 percent.

[d] This figure is higher than for current engines, for which an average of 590 pounds is quoted in a later report (ref, 2.13).

[e] This figure is lower by half than for industrial diesel engines and applies to a highly developed military engine (ref. 2.13).

the fuel cell has no ability to increase mission times of a vehicle. The diesel engine in table 2.4 would be favored over the fuel cell at mission durations of up to 36 days. In order to obtain a net power density of 2 kW/cu ft and a corresponding weight performance, it would probably be necessary to obtain 3 to 4 kW/cu ft from the actual cell to allow for the weight and volume of auxiliaries and parasitic power. Assuming a current density of 200 A/sq ft at 0.5 volt and a platinum catalyst loading of 3 g/ft^2 (about 3 mg/cm^2), a 100-kilowatt unit would require about 6 pounds of platinum. The world production of platinum group metals has been given (*11*) as about 10^6 troy ounces per year; this total annual production therefore would be capable of supplying catalyst for about 8500 units of 100 kilowatts each. Platinum metal catalysts are in too short supply to provide an appreciable number of military vehicles, even if the cost were not prohibitive. This conclusion would not be significantly changed if catalyst loadings were reduced to 1 g/ft^2 (1 mg/cm^2) or if power densities in W/sq ft were increased by a factor of 3.

A recent report by Schlatter (ref. 2.11) gives an extensive treatment of the feasibility of fuel cells for military vehicle propulsion. The argument that a fuel cell-electric motor system need only be one-fourth to one-sixth of the horsepower rating of a gasoline engine to perform a given duty is fallacious for the following reasons. First, the ratio of the maximum short-duration power to steady rated power depends a great deal on the application. A lawnmower requires a high ratio to prevent stalling when a sudden change in load is applied, without benefit of gears, to a gasoline engine. Since a gasoline engine does not have much overload capacity (about 35 percent), the normal rating of the engine has to be large enough to take the maximum demand, even though the engine then runs much below its rated capacity when used for normal duty. An electric motor can tolerate overloads of 100 percent for 15 minutes and even higher overloads for shorter durations; a sudden increase of load on the blades tends to reduce the speed of the motor, which brings higher current and higher power into operation. In this particular application, the normal continuous rated capacity of the electric motor can be much lower than the maximum demand, and hence lower than the equivalent gasoline engine. However, this wide mismatch of normal to maximum power does not apply to heavy vehicles using a geared transmission system. The rated intermittent bhp of the engine is about 30 to 40 percent greater than the bhp for continuous operation, and thus only that much greater than an equivalent electric motor. The advertised output of passenger automobiles is over double the required continuous rating. Second, the transmission losses of 60 percent quoted by Szego (ref. 2.4) were considered too great and, based on California Research tests, a figure of 75 percent was taken as a good average. Third, it is implied in Szego's treatment that the fuel-cell output matches the electric motor rating. This is not true, because the fuel cell must supply the actual load power being used irrespective of the rating of the motor. In addition, the motor and controls are likely to have an efficiency of about 70 percent, not 100 percent (this just about matches the 75-percent transmission loss of the gasoline engine system).

Schlatter concludes that a fuel cell-dc electric motor system for a given duty cycle of a military vehicle must have a continuous rating close to that of a spark ignition engine-transmission system, and not one-fourth to one-sixth of the rating. Table 2.5 compares fuel consumptions of fuel cells and heat engine power systems. These show, as did table 2.4, that an assumed fuel-cell thermal efficiency of 60 percent leads to considerably greater hp-hr/gal output from the fuel-cell system; but more important, it *can* be seen that improved logistics over a diesel engine of 34 percent engine efficiency can only be expected with the use of hydrocarbon fuels in the fuel cell. Therefore, fuel cells are unlikely to replace most of the internal combustion engines used by the military, principally because it is unlikely that the volume of the fuel-cell system can be reduced to feasible levels.

Another way of looking at the figures in table 2.4 is to consider a definite mission duration between refuelings (1 day, for example). The 150-bhp gasoline engine consumes 780 pounds of fuel compared to 386 pounds for the fuel cell, and at first sight it appears that the fuel supply for a vehicle fleet *can* be halved by using fuel cells. However, a 150-bhp system is not necessarily

TABLE 2.5.—*Available and Recoverable Energy per Gallon for Some Fuels in Fuel Cell and Heat Engine Power Systems*

[Ref. 2.111

		Vehicle power systems		
Fuel	Heat of combustion,[a] 77" F (25" *C*), H_2O vapor, Btu/gal	Engine[b] only, hp-hr/gal	Engine[b] +power train, hp-hr/gal	Fuel cell system,[c] hp-hr/gal
Hydrogen[d]	30 600	...	...	5.1
Methanol	[e]56 100	4.4	3.3	9.3
Ammonia	[e]36 400	...	...	6.0
Hydrazine	[e]58 500	...	...	9.7
Methane[f]	75 800	6.0	4.5	12.5
Propane	82 100	6.5	4.8	13.5
n-octane	111 000	[g](8.7)	[g](6.6)	18.3
Motor gasoline (30% aromatics)	115 000	9.0	6.8	[h]19.0
Diesel fuel	120 000	16.0	[i]12.0	[h]19.8
Assumed efficiencies:				
Overall fuel cell, %	...	...	60	60
Electric motor and controls, %	...	...	70	...
Spark ignition engine, %	20	20	...	...
Diesel engine, %	34	34	...	...
...	...	75	...	...

[a] Energy available from fuel in the form oxidized (gaseous except as noted). Temperature corrections amount to only 1 to 2 percent in the range 25" to 200° C and were not made.

[b] Spark ignition engine unless otherwise indicated.

[c] Fuel-cell system includes motor and controls.

[d] At 431" F (257" C).

[e] Heats of combustion for methanol, ammonia, and hydrazine are for aqueous solutions as they would be used in a low-temperature fuel cell.

[f] At 256" F (160" C).

[g] Isooctane fuel in spark ignition engine.

[h] Complete combustion of these materials in low-temperature fuel cells has not been positively established.

[i] Diesel engine.

sufficient when the powerplant is increased from *1260* to *8640* pounds; to get equivalent vehicle performance (in pulling the vehicle up a long grade, for example), the fuel-cell powerplant probably has to be increased in size, bhp, and fuel consumption. Some of the extra efficiency of the fuel-cell system is inevitably used in dragging along its own weight. The high volume of the fuel-cell powerplant might also lead to a higher power requirement by increasing air drag on the vehicle. The requirement of *0.022* kW/lb (about 50 lbs/kW) is probably not stringent enough, and the electric motors must be reduced in weight to realize the potential fuel savings of the fuel-cell system.

2.3.5 Underwater Applications

There has been considerable interest in the use of fuel cells as propulsion units for submarines (see ch. 7 and app. E). The primary advantage of the fuel cell over other powerplants is the possibility of locating it outside the hull, thus increasing buoyancy. If oxygen is to be used as oxidant in the fuel-cell reaction, it would be stored cryogenically or at high pressures.

The sodium-amalgam cell discussed in chapter 7 is especially suited for this application, since it is a high-power-density system with a large energy density per pound of fuel. The cell system requires large volumes of cooling water to remove the heat of amalgamation. In fact, the high cost of sodium makes it unlikely that this cell will have any application other than special uses of this kind. The system is quite advanced and is apparently technically feasible, but even for military uses the cost and handling of the fuel is preventing further development.

Use of fuel cells for torpedo propulsion has been considered, but torpedo duty calls for a very high power density over short periods (15 to 45 minutes), which is unfavorable to fuel cells in comparison with high-energy batteries (see eqs. (2.27) and (2.28).

2.3.6 Central Station Power

Use of fuel cells for large-scale generation of electricity has been discussed by Hart (ref. 2.12) and Cochran (ref. 2.13). The principal requirements are that the systems cost no more than $150 to $200 per kilowatt and have fuel efficiencies of 55 to 60 percent (with maintenance expense no higher than those for conventional plants), using cheap, available fossil fuels. No present fuel-cell system even approaches this cost requirement. Higher costs can be tolerated for nonpolluting power stations in heavily populated areas, since the high cost of underground electrical supply from conventional plants or a grid tap on the edge of the city can be eliminated.

Very-high-voltage dc transmission has special advantages for electrical supply over national or regional power grids. However, the feasibility of connecting many fuel cells in series to obtain high voltages has not been demonstrated. Even moderate amounts of low voltage, direct current require massive conductors, so for the heavy electrochemical industries (production of aluminum, magnesium, specialty steels, chlorine, etc.) this supply would have to come from small localized fuel-cell units rather than from a large central unit.

The costs of electrical power from large nuclear plants have been decreasing steadily and it seems almost certain that they will be well enough developed to provide severe competition for the fuel cell by the time the fuel cell is well developed.

24 GUIDE TO FUEL-CELL LITERATURE

References to fuel-cell work or to electrochemical studies of relevance to fuel-cell work are quite numerous. There are many reviews, books, and collections of articles which are good starting points for more detailed literature searches. In particular, several reviews and bibliographies have been generated under sponsorship included within the scope of this book.

A valuable review of early work on fuel cells is that of Howard (2.14, 1945), which gives nearly 100 references. A bibliography produced by the British Electricity Authority (2.15, 1947) gave over 500 references, divided into subject classifications. This bibliography may not now be available but the references are included, alphabetically by author, in the bibliography (2.16, 1962) prepared at Alfred University. This bibliography contains over 1000 references, but it does not include much coverage of sponsored contract reports. Fragmentary fuel-cell bibliographies are contained in reports *507*, *508*, April and September 1959. Other bibliographies are those prepared by Lockheed (2.17) and North American Aviation (2.18). Three sponsored status reports on fuel cells were issued in 1959, by Stein (2.19), Yeager (2.20), and the Hoffman Electronics Corp. (2.21). One of a number of popular articles on fuel cells produced about this time is that of Austin (2.22).

A short chapter on fuel cells, with particular reference to aerospace use, is contained in the ***Energy Conversion Systems Reference Handbook*** (2.23, 1960). A brief review of fuel-cell systems was given by McCormick (2.24, 1960). The ***Status Report on Fuel Cells,*** mentioned above (2.19), has been followed by ***Second*** (2.27, 1960), ***Third*** (2.26, 1962), ***Fourth*** (2.27, 1963), and ***Fifth*** (2.28, 1965) ***Status Reports.***

Collections of short papers on fuel-cell work sponsored by Federal sources are contained in the ***Proceedings of the 12th through 18th Annual Power Sources Conferences*** (2.29, May 1958, to 2.35, May 1964). Widely available collections of articles are the three volumes of the ***American Chemical Society Symposium on Fuel Cells*** (2.36, 1960; 2.37, 1963; 2.38, 1965). A German-language book which describes the fuel-cell work of Justi et al. (2.39, 1962) also contains short contributions from English, French, and American sources (in English language). Fairly complete coverage of the fuel-cell field is given in ***Fuel Cells,*** edited by Mitchell (2.40, 1963), and ***Fuel Cells,*** edited by ***Chemical Engineering Progress*** (2.41, 1963).

More recent review articles include those of Fox and Roberts (2.42, 1962), those in a special issue of the ***Proceedings of the IEEE*** (2.43, 1963), and a state-of-the-art report (2.44, 1964) by Jasinski and Kirkland.

A report on Communist-bloc work is available (2.45, 1962). A bibliography of translations of Communist-bloc plus some French, Italian, and Japanese articles is available (2.46, 1963) but is incomplete and random.

Electrochemical theory has been developed by electrochemists, whose main concern was not with fuel cells. Therefore, there are few general references dealing with electrokinetics from the point of view of fuel cells. A good introductory text is ***Electrochemistry*** by Potter (2.47, 1956). **A** more detailed text is that of Kortum and Bockris (2.48, 1951). An excellent book on electrochemical kinetics (in German language) is that of Vetter (2.49, 1961). Other books which contain valuable chapters at an advanced level are ***Modern Aspects of Electrochemistry*** (2.50, 1954; 2.51, 1959) and ***Advances in Electrochemistry and Electrochemical Engineering*** (2.52, 1961; 2.53, 1962; 2.54, 1963).

Useful information is contained in ***The Theory of Electrochemical Cell Reactions,*** Foster D. Snell, Inc. (2.55, 1954 to 1958), although its main concern is with conventional primary and secondary cells. A brief treatment of electrode kinetics from the fuel-cell point of view is that of Austin (2.43, 1963). **A** lengthy chapter on the electrochemical theory of fuel cells is due to appear shortly (2.56), and Prof. J. O'M. Bockris of the University of Pennsylvania is also preparing a book on this subject.

A recent complete text on the theory and applications of fuel cells is that of W. Vielstich, ***Brennstoffelemente*** (2.57).

2.5 REFERENCES

2.1. ADAMS, D. R.; et al.: Fuel Cells: Power for the Future. Fuel Cell Research Associates, P.O. **Box** 157, Cambridge 38, Mass., 1960.

2.2. FISHER, J. H.; AND MENETREY, W. R.: Proceedings 14th Power Sources Conference. U.S. Army Signal Research and Development Laboratory, Fort Monmouth, N.J., May 1960, pp. 94–96.

2.3. STARKEY, G. E.: Proceedings 17th Power Sources Conference. PSC Publications Committee, P.O. Box 891, Red Bank, N.J., May 1963, pp. 84–85.

2.4. SZEGO, G. C.; AND COHN, E. M.: Astronautics and Aerospace Engineering, May 1963, pp. 107–111.

2.5, COHN, E. M.: Proceedings 17th Power Sources Conference. PSC Publications Committee, P.O. Box 891, Red Bank, N.J., May 1963, p. 86.

2.6. HUNGER, H. F.: Proceedings 17th Power Sources Conference. PSC Publications Committee, P.O. Box 891, Red Bank, N.J., May 1963, pp. 80–82.

2.7. ALAMAULA, B. C.: Proceedings 17th Power Sources Conference. PSC Publications Committee, P.O. Box 891, Red Bank, N.J., May 1963, pp. 82-84.

2.8. CATHER, H. D.: Diamond Ordnance Fuze Laboratories Report TR–777. Sept. 1960.

2.9. SZEGO, G. C.: Proceedings 17th Power Sources Conference. PSC Publications Committee, P.O. Box 891, Red Bank, N.J., May 1963, pp. 88–92.

2.10. SCHLATTER, M. J.; et al.: Special Report No. 1, Sept. 1963 ***(141,*** appendix F).

2.11. SCHLATTER, M. J.: Special Report No. 2, Feb. 1965 ***(145, 146,*** appendix F).

2.12. HART. A. B.: Times Sci. Rev., autumn 1962, pp. 15–17.

2.13. COCHRAN, N. P.: Proceedings 17th Power Sources Conference. PSC Publications Committee, P.O. Box 891, Red Bank, N.J., May 1963, pp. 87–88.

2.14. HOWARD, H. C.: Direct Generation of Electricity from Coal and Gas (Fuel Cells). Chemistry of Coal Utilization, Vol. 11, H. H. Lowry, ed., John Wiley, Inc., N.Y., 1945, pp. 1568–1585.

2.15. British Electricity Authority (now Central Electricity Generating Board, United Kingdom): Bibliography on Fuel Cells. 1947.

2.16. State University of New York, College of Ceramics: Fuel Cell Bibliography. Alfred University, Alfred, N.Y.

2.17. Lockheed Missiles and Space Division: Electrochemical Fuel Cells: An Annotated Bibliography. AD 251660, Nov. 1960; AD 253809, Feb. 1961; AD 459609, Mar. 1962; NASA N63-17331, Dec. 1962.

2.18. North American Aviation: Fuel Cells: A Bibliography. Space and Information Systems Division, NASA; N63–86115 (undated—references to early 1962).

2.19. STEIN, B. R.: Status Report on Fuel Cells. ARO Report No. 1, Office of the Chief of R&D, Department of the Army, Washington 25, D.C., June 1959.

2.20. YEAGER, E.: A Review of the State of the Art and Future Trends in Fuel Cell Systems. Technical Rep. No. 10, NOnr 2391(00), Western Reserve University, Cleveland, Ohio, Dec. 1959.

2.21. SMATKO, J. S.; CHRISNEY, J. B.; AND COOK, ***C.*** C.: Survey of State-of-the-Art Fuel Cell Development. Final Report, Part A (Unclassified), Hoffman Electronics Corp., Dec. 1959.

2.22. AUSTIN, **L.** G.: Fuel Cells. Sci. Am., Vol. 201, Oct. 1959, pp. 72–78.

2.23. MENETREY, W. R.; AND CHRISNEY, J.: Energy Conversion Systems Reference Handbook. Vol. VI, Chemical Systems, Electro-Optical Systems, Inc.. Sept. 1960. WADD Technical Rep. 60-699, Vol. VI.

2.24. MCCORMICK, J. E.: Technical Note—Fuel Cell Systems. Rome Air Development Center, Griffiss Air Force Base, N.Y., RADC–TN-60–118, July 1960.

2.25. STEIN, B. R.; AND COHN, E. M.: Second Status Report on Fuel Cells. ARO Rep. No. 2, Office of the Chief of R&D, Dept. of the Army, Washington 25, D.C., Dec. 1960.

2.26. HUNGER, H. F.; FRANKE, F. R.; AND MURPHY, J. J.: Third Status Report on Fuel Cells. U.S. Army Signal Research and Development Laboratory, Fort Monmouth, N.J., June 1962.

2.27. FRANKE, F. R.; AND HUNGER, H. F.: Fourth Status Report on Fuel Cells. U.S. Army Electronics Research and Development Laboratory, Fort Monmouth, N.J., July 1963.

2.28. BARTOSH, S. J.; MCDONAGH, J. M.; AND TASCHEK, W. G.: Fifth Status Report on Fuel Cells. U.S. Army Electronics Command, Fort Monmouth, N.J., June 1965.

2.29. U.S. Army Signal R&D Laboratory: Proceedings 12th Annual Power Sources Conference. Fort Monmouth, N.J., May 1958.

2.30. U.S. Army Signal R&D Laboratory: Proceedings 13th Annual Power Sources Conference. Fort Monmouth, N.J., May 1959.

2.31. US. Army Signal R&D Laboratory: Proceedings 14th Annual Power Sources Conference. Fort Monmouth, N.J., May 1960.

2.32. PSC Publications Committee: Proceedings 15th Annual Power Sources Conference. P.O. Box 891, Red Bank, N.J., May 1961.

2.33. PSC Publications Committee: Proceedings 16th Annual Power Sources Conference. P.O. Box 891, Red Bank, N.J., May 1962.

2.34. PSC Publications Committee: Proceedings 17th Annual Power Sources Conference. P.O. Box 891, Red Bank, N.J., May 1963.

2.35. PSC Publications Committee: Proceedings 18th Annual Power Sources Conference. P.O. Box 891, Red Bank, N.J., May 1964.

2.36. YOUNG, G. J., ed.: Fuel Cells. Reinhold Pub. Corp., N.Y., 1960.

2.37. YOUNG, G. Y., ed.: Fuel Cells. Vol. 11, Reinhold Pub. *Corp.*, N.Y., 1963.

2.38. American Chemical Society, Fuel Cell Systems. Advances in Chemistry Series, no. 47, Washington, D.C., 1965.

2.39. JUSTI, E. W.; AND WINSEL, A. W.: Kalte Verbrennung—Fuel Cells. Franz Steiner Verlag G.m.b.H., Wiesbaden, 1962.

2.40. MITCHELL, W., ed.: Fuel Cells. Academic Press, New York, 1963.

2.41. Editors of Chemical Engineering Progress: Fuel Cells. Am. Inst. Chem. Eng., N.Y., 1963.

2.42. FOX, H. W.; AND ROBERTS, R.: Fuel Cells. IRE Trans. on Military Electronics, Jan. 1962, pp. 46–57.

2.43. Proceedings of the Institute of Electrical and Electronics Engineers: New Energy Sources, Vol. 51, May 1963.

JUSTI, E. W.: Fuel Cell Research in Europe. p. 784.

PEATTIE, C. 'GORDON: A Summary of Practical Fuel Cell Technology to 1963. p. 795.

KORDESCH, K. V.: Low Temperature Fuel Cells. **p.** 806.

COLICHMAN, E. L.: Preliminary Biochemical Fuel Cell Investigations. p. 812.

AUSTIN, L. G.: Electrode Kinetics and Fuel Cells. p. 820.

2.44. JASINSKI, R. J.; AND KIRKLAND, T. G.: A State-of-the-Art Report. Mechanical Engineering, Mar. and Apr. 1964, pp. 51–57, 121–126.

2.45. Von STACKELBERG, M.; AND VIELSTICH, W.: Russian Research in Fuel Cells and Alkaline Type Batteries. University of Bonn, 1961.

2.46. DDC: Power Generation. June 1963.

2.47. POTTER, E. C.: Electrochemistry. Cleaver-Hulme Press, Ltd., London, 1956.

2.48. KORTUM, G.; AND BOCKRIS, J. O'M.: Textbook of Electrochemistry. Elsevier Pub. Corp., N.Y., 1951.

2.49. VETTER, K. J.: Elektrochemische Kinetik. Springer-Verlag, Berlin, 1961.

2.50. BOCKRIS, J. O'M, ed.: Modern Aspects of Electrochemistry. Butterworth's Scientific Publications, London, 1954.

2.51. BOCKRIS, J. O'M., ed.: Modern Aspects of Electrochemistry: No. 2, Butterworth's Scientific Publications, London, 1959.

2.52. TOBIAS, C.; AND DELAHAY, P., eds.: Advances in Electrochemistry and Electrochemical Engineering. Vol. 1, Interscience Pub., N.Y., 1961.

2.53. TOBIAS, C.; AND DELAHAY, P., eds.: Advances in Electrochemistry and Electrochemical Engineering. Vol. 2, Interscience Pub., N.Y., 1962.

2.54. TOBIAS, C.; AND DELAHAY, P., eds.: Advances in Electrochemistry and Electrochemical Engineering. Vol. 3, Interscience Pub., N.Y., 1963.

2.55. Foster D. Snell, Inc., Theory of Electrochemical Cell Reactions. Vols. 1, 2, 1954; Vol. 3, 1955; Vol. 4, 1956; Vol. 5, 1957; Vol. 6, 1958.

2.56. AUSTIN, L. G.: Electrochemical Theory of Fuel Cells. Handbook of Fuel Cell Technology. C. Berger, ed., Prentice-Hall, N.J. (in press).

2.57. VIELSTICH, W.: Brennstoffelemente. Verlag Chemie, G.m.b.H., Weinheim/Bergstr., 1965.

CHAPTER 3

Electrodes, Electrolytes, and Matrices

3.1 INTRODUCTION

The most important primary components of a fuel cell are the anode and cathode, whose performance and life characteristics affect the design of the whole fuel-cell system. At present, several electrodes—the result of many years of development—give power densities (in W/sq ft) unheard of a few years ago. The development of electrodes has involved extensive trial and error and there is as yet no established "theory of porous electrodes" enabling derivation of equations from which electrodes may be designed (see ch. 18). However, a number of general rules have been followed in the development of gas-diffusion electrodes:

(a) The electrode material and structure must have high electronic conductivity.—Thick electrodes (of porous electrode carbon, for example) must have sufficient conductivity to be the sole means of transferring electrons to and from the cell. Recent trends in electrode manufacture are toward thin electrodes, with current collectors in contact at many points with the face of an electrode. Current collectors are made of high-conductivity metals which do not form insulating surface films and have low contact resistance when they are pressed against the electrode. Alternatively, thin electrodes are formed on a base of metal grid, which collects current from the particles of the electrode.

(b) Electrode material must be inert to the gases and electrolytes in the cell.—"Inert" is used here in the sense that the main body of the material does not corrode or dissolve, although the surface of the material adsorbs gas and is an essential intermediate in the electrochemical reactions.

(c) The electrode material must be either catalytic to the electrochemical reaction involved *or* coated with a stable, conductive catalytic agent.—Methods of depositing catalyst on a preformed base, such as porous carbon or porous nickel, include electroplating or impregnation with a salt of the catalyst followed by decomposition of the salt to metal. The electrodes can be made from powders of the catalyst or catalyst mixed with other conductive materials. Various techniques for incorporating catalyst are described in detail in later sections.

Catalysis is discussed in chapters 15, 16, and 17. The most widely used catalysts for low-temperature fuel electrodes are platinum or platinum-palladium alloys. Platinum is generally used for low-temperature oxygen electrodes; silver is also used in alkali at temperatures near 200° F (93.5' C). For medium-temperature alkaline fuel cells, nickel is an active fuel catalyst, while silver and nickel oxide (lithiated to give conduction) are active cathode catalysts. Nickel, silver, and nickel oxide are stable in alkali but not in strong acid.

(d) Electrode construction has to provide a pore system through which gas can be readily trans-*ferred*, but which does not leak electrolyte into the gas chamber *or flood* the electrode.—Leakage occurs by flow through larger pores or pinholes under the hydrostatic head of the electrolyte or differential gas pressure across the cell. Pores should be small enough to give strong capillary forces which resist free flow of electrolyte through the electrode. (Pore sizes are usually in the range of 1 to 100 microns.)

When pores completely fill with electrolyte, as a sponge fills with liquid, the electrode is said to be flooded. A flooded electrode is a proven poor performer. If the electrode material is wetted by electrolyte, the smaller diameter macropores tend to fill with electrolyte by capillary action. This *can* be prevented by maintaining a pressure difference between gas and electrolyte, thus keeping capillary forces balanced. Hence, a narrow range of macropore size is desired; otherwise, at a given differential pressure, some small-diameter pores will be flooded, while larger diameter pores will bubble gas into the electrolyte. Pores of most porous electrodes cannot be considered as a collection of parallel tube bundles, since they are highly interconnected and of irregular shape. Thus, it is possible that no large pores traverse thick electrodes without containing a length of small diameter. For thin electrodes, however, the possibility of large pores right through the electrode increases, and control of flooding becomes more difficult. This can be achieved either with double-layer electrodes or a matrix, or by making the electrode nonwetting and, hence, resistant to flooding. These possibilities are discussed later.

Another aspect of flooding is the electrochemical production of water in hydrogen-oxygen and other types of cells. In alkaline electrolytes, water is produced at the hydrogen electrode (anode), while in acid electrolytes it is produced at the oxygen electrode (cathode). The higher the current density and the lower the amount of electrolyte per unit area of electrode, the more rapidly the electrolyte becomes diluted. At high current densities (100 to 1000 A/sq ft, for example) diffusion of product water into the bulk of electrolyte may be too slow to maintain uniform electrolyte concentration across the cell, and the electrolyte will become dilute at the water-forming electrode. When alkali is the solute, the dilute electrolyte at the anode becomes low in OH^-, leading to polarization. This situation is aggravated by the use of a double-layer electrode or electrolyte matrix, because of the reduced mass-transfer coefficient of product water into electrolyte (and ions from electrolyte to electrode). The problem becomes less severe upon cycling electrolyte through the cell and with control of water-vapor removal from the electrode to balance the rate of water formation. Long-term water balance is necessary even when electrolyte is of uniform composition across the cell.

(e) Active electrodes require a high internal *catalytic* area.—The manner in which this area is utilized is not clearly understood, but the amount of activation polarization is decreased by the higher electrode area. For example, an electrode of smooth platinum spheres sintered together has an internal area of about 1000 cm^2/cm^3 if the spheres have diameters of about 50 microns. An electrode 1 mm thick, therefore, has 100 cm^2 of internal area for 1 cm^2 of plane area. Platinum black has areas of about 20 m_2/g and the incorporation of 10 milligrams of platinum black into each cm^2 of plane area gives an internal area of 2000 cm^2. Probably only a fraction of the area takes part in reaction, and the other requirements given above also have to be satisfied, but, as a general rule, an electrode which has activation polarization is improved by reconstruction with a higher active area.

The three principal gas-diffusion electrodes at present are carbon electrodes, sintered-metal electrodes, and plastic-bonded metal electrodes. Porous electrode carbons of high conductivity are readily available from commercial suppliers; they have high internal areas and can be machined. Carbon is inert in most electrolytes used for low-temperature fuel cells. Carbons are not catalytically active to fuels, but can be easily plated or impregnated with metal catalyst.

Sintered-metal electrodes are made from fine metal powder compressed into sheets and sintered by heat. These may be plated or impregnated with catalyst. Nickel plaque supplied by battery manufacturers is now widely used. The internal area of normal sintered electrodes is relatively small, but it can be increased greatly by using metal particles which have microporosity. Metals are usually wetted by electrolyte and tend to flood; therefore, sintered metal electrodes are often used in double-layer form. The double-layer electrode consists of two layers of different-pore diameters sintered together. The smaller diameter layer is in contact with electrolyte, which fills the small pores by capillary action. The larger diameter pores in the second layer are kept from flooding by maintaining a feed-gas pressure that is higher than the electrolyte pressure by a few inches of water gage. This pressure difference sets up a force which counteracts the capillary force trying to flood the large pores, but is not sufficient to cause bubbling through the small-pore layer.

Plastic-bonded electrodes are made by mixing high-area, catalytic metal blacks with *a* suspension of small plastic particles. The paste is spread on a support of metal grid, dried, and heated to sinter the plastic. Admixture of plastic (Teflon is widely used) makes the electrode non-flooding, while sintering bonds the particles together without covering the surface of the active metal or preventing conductivity. The methods for preparing these electrodes are given in detail in section 3.2.

A fourth electrode is the membrane or solid-state diffusion electrode. These are distinguished from gas-diffusion electrodes by not having large pores through which gas diffuses as free molecules. Mass transfer occurs by atoms or ions traveling through the interstitial spaces of a crystal lattice. Such electrodes are completely immune to flooding or leakage, since they behave as solid metal membranes, except to the diffusing species. As might be expected, the effective diffusion coefficient is low and the electrodes have to be very thin to give suitable rates of mass transfer. The notable example of this is hydrogen at thin foils of Pd or Pd-Ag alloy (see sec. 3.2.4).

Electrolytes are classified into three groupings: aqueous solutions, nonaqueous (organic) solutions, and molten salts. Molten salt electrolytes are used in high-temperature fuel cells (see ch. 6) and aqueous solvents are generally used in low- and medium-temperature cells. The choice of aqueous electrolyte is quite limited, as becomes apparent from considering the hydrogen and oxygen reactions, as follows. The hydrogen reactions are

$$H_2+2M\rightarrow 2M[H] \qquad (3.1)$$

$$M[H]\rightarrow M+H^++e^- \qquad (3.2)$$

$$M[H]+OH^-\rightarrow M+H_2O+e^- \qquad (3.3)$$

The theory of electrode reactions shows that kinetics of charge transfer is most favorable for high OH– or H^+ concentrations. The general physical reasoning is as follows. Reactions (3.2) and (3.3) are accelerated by positive potentials. Reaction (3.2) has a theoretical OCV which is most positive for high activity (concentration) of H^+. Neutral electrolyte has a more negative potential, by about –0.41 volt, than standard state of reaction (3.2) and the exchange current (proportional to $a_{H^+}{}^{1/2}$, where a_{H^+} is the activity of H^+) is consequently about 1/3000 of the standard-state value. On the other hand, reaction (3.3) is aided, through the law of mass action, by high concentrations of OH–. A neutral electrolyte has a concentration of 10^{-7} **of** the standard-state value of reaction (3.3). Although the more positive potential in the neutral electrolyte partially counteracts this large difference, the effect of concentration outweighs the potential effect. The theoretical exchange current (proportional to $a_{OH^-}{}^{1/2}$) of reaction (3.3) in neutral electrolyte is, therefore, about 1/3000 of that in standard alkali. In practice, suitably catalyzed hydrogen electrodes work well in strong acid or strong base, but less well in intermediate solutions. Similarly, the overall oxygen reactions are

$$\tfrac{1}{2}O_2+2H^++2e^-\rightarrow H_2O \qquad (3.4)$$

$$\tfrac{1}{2}O_2+H_2O+2e^-\rightarrow 2OH^- \qquad (3.5)$$

The reactions are favored by negative potentials, so that reaction (3.5) is expected to have the highest exchange current in electrolytes with high activities of OH–. Reaction (3.4) is less favored because of its positive potential, but higher concentrations of H^+ are expected to give better rate, and-reaction (3.4) may take over at low pH.

Other factors are of importance as well as the kinetic factors discussed above. Electrolytes must have as high ionic conductivites as possible and be stable under the conditions used. Components which take part in the reactions must be present in high concentrations to avoid concentration polarization. For example, reactions (3.3) and (3.4) require H^+ or OH–. In an unbuffered neutral electrolyte the concentrations of these components are small. Reactions (3.2) and (3.5) produce H^+ and OH–, respectively, and these have to be carried away from the electrode by diffusion and migration. Therefore, concentration at the electrode builds up to provide a concentration gradient for mass transfer. In neutral electrolyte, a buildup to **1** *N* concentrations at the electrode gives a change in reversible potential of (2.3 RT/F) log (10^7), or about 0.41-volt polarization from OCV. Use of buffered electrolytes reduces this effect, since buffer molecules take up H^+ or OH– produced at the electrode and prevent rise in concentration. However, kinetic effects are still present, and strong acids and bases are the best electrolytes.

Potassium hydroxide is the most widely used basic electrolyte and has high solubility and conductivity. It can be used over a wide temperature range because concentrated solutions do not freeze even at −65" F (−54" C), and KOH-H_2O can be heated (with decreasing equilibrium amounts of H_2O at a given water vapor pressure) to the melting point of KOH. A number of materials can withstand the corrosive effects of KOH (see app. D). A major disadvantage is that it forms bicarbonate and carbonate with CO_2, leading to loss of desirable electrolyte properties and eventual bicarbonate precipitation in low-temperature cells. Thus, unless this electrolyte is regenerated, it cannot be used for organic fuels and CO_2 has to be removed from air supplied to a cathode.

Sulfuric acid has high conductivity and can be used over a wide range of temperatures. It reacts with organic fuels at temperatures over 212" F (100° C). Concentrated hydrochloric acid is unsuitable because it poisons noble-metal catalysts by adsorption of chloride ion on the metal and loses HCl at higher temperatures. Perchloric acid, $HClO_4$, is widely used for mechanism studies but is not practical for actual use in a cell; although ClO^-_4 adsorbs to the least extent of the strong acid anions, its conductivity and temperature stability properties are not good. Phosphoric acid can be used over a wide temperature range even in the presence of organic fuels, but its conductivity is not as high as H_2SO_4.

Hydrogen-oxygen fuel cells can be typed by the two methods used for containing electrolyte. In a free electrolyte type, the electrolyte of a single cell is contained between a porous anode and a porous cathode. The electrode-current collector assembly must be rigid to provide a fixed-electrolyte chamber between electrodes. Union Carbide carbon electrodes and Pratt & Whitney double-layer nickel electrodes are examples of this type.

In a matrix type, electrolyte is contained by capillary action in a porous matrix, with electrodes pressed against the matrix. This arrangement has the advantage that the matrix can be made with finer pores than the electrode, which is effective in preventing flooding of electrodes. In addition, electrodes can be flexible since the matrix prevents buckling. The IR loss across an electrolyte-filled matrix is greater than for a corresponding thickness of free electrolyte. The ratio of effective resistivity to resistivity of free electrolyte is called the labyrinth or formation factor, λ. It tends to infinity when the porosity of the matrix tends to zero, because at zero porosity there is no electrolyte to provide conduction. The Allis-Chalmers hydrogen-oxygen cell uses an asbestos matrix. An ion-exchange membrane behaves in somewhat the same way as an electrolyte-filled matrix; the electrodes are pressed against, or bonded into, the surface of the membrane. The General Electric hydrogen-oxygen IEM cell is an example of this type. In high-temperature, molten-carbonate fuel cells, electrolyte is usually contained in a matrix of porous refractory.

3.2 PREPARATION OF ELECTRODES

3.2.1 Porous Baked Carbon Electrodes

Porous carbon electrodes have been used in many of the contracts. They are readily available from commercial suppliers. Excellent power densities have been reported for carbon electrodes developed by Union Carbide. The electrodes are made by mixing filler (petroleum coke flour) with binder (coal-tar pitch), baking to carbonize the pitch, and firing at high temperatures, 1800° to 3000" F (982" to 1649" C). Pore structure is determined by the size of filler particles and the holes produced by gas escaping during carbonization. It is usually spongelike with very irregular holes. Conductivity depends on physical structure and on degree of graphitization produced by prolonged firing at high temperatures. The electrodes are usually activated by burning out with air, steam, or CO_2. Activation produces a sharp rise of internal area over a few percent of burnoff, probably due to unblocking of fine pores by preferential burning of carbonized binder (ref. **3.1**).

The electrodes have some catalytic activity as oxygen cathodes, but are usually catalyzed by plating or impregnation with metal or metal oxide catalyst to increase their effectiveness.

They have little activity for hydrogen without catalysts. Hydrogen and oxygen electrodes prepared by Union Carbide have given current densities over 1000 A/sq ft for short-term operation (see fig. 4.7). The electrodes have two serious disadvantages. First, they flood slowly with time, and at increasing rates at high current densities. Flooding cannot be prevented by a differential gas pressure and appears to be irreversible; i.e., expulsion of electrolyte by gas bubbling does not restore performance. Possibly the mode of operation involves gas transport through micropores which cannot be freed of electrolyte by gas bubbling. Electrodes are often wetproofed with hydrocarbon to retard flooding. Second, the electrodes are brittle and have to be relatively thick (⅛ inch) to be sufficiently strong and give long life as slow flooding occurs. This leads to gas-transport polarization at air electrodes (see sec. 2.1.5).

Carbon electrodes will support small currents with inert gas, caused by attack of the carbon, in N H_2SO_4 at 176" F (80° C) ***(139).*** There is also evidence of small currents in concentrated KOH at 194" F (90° C) *(587)*, presumably due to carbonate formation. Since many carbons contain inorganic impurities which can be slowly removed (by chlorination at high temperatures, for example), there is also the possibility of small impurity currents from these constituents. In spite of these slow reactions, baked carbon electrodes retain their strength and structure for many years in low-temperature cells.

Methods of activating and catalyzing carbon electrodes are described in table 3.1. The most successful porous carbon electrodes are those manufactured by Union Carbide, whose procedures for preparation, catalysis, and wetproofing are proprietary. Some requirements for carbon electrodes for use in concentrated alkali solutions have been given ***(329)*** as: ***(a)*** high internal surface for electrochemical activity, ***(b)*** ability to decompose hydrogen peroxide, (c) formation of interconnecting capillaries for rapid distribution of gas to the electrode-electrolyte interface, and *(d)* resistance to wetting. Slow penetration of electrolyte into the electrodes, leading to IR loss in electrolyte contained in the pores and eventual flooding of the electrodes, has been reported ***(329, 772,*** and ***774).*** For long life, electrodes must be thick to allow for this penetration. Penetration rate increases with increased current density and polarization.

Wetproofing is performed by immersing the electrode in a solution (about 2 weight-percent) of paraffin wax in petroleum ether, draining and drying, or by painting with the solution and drying. Stackpole 219X or 219XG (graphitized) porous carbon electrodes were wetproofed with paraffin wax, ceresin wax, or other agents ***(252).*** The paraffin-treated electrodes were wetted by 30 weight-percent KOH over several hours, but ceresin was 20 times better. Other agents were inferior to paraffin. Performance depended crucially on wetproofing and was poorly reproducible. National Carbon AUC and Speer Carbon 552 porous graphite resisted wetting in 30 weight-percent KOH ***(23).*** However, when the electrodes were catalyzed with 1 to 5 weight-percent Pt by immersion in chloroplatinic acid, dried, and reduced at 842" F (450" C) in H_2, they wetted rapidly. Paraffin wetproofing reduced BET areas of Pt-catalyzed carbon electrodes from 70 to 170 m^2/g to 0.2 to 2 m^2/g ***(571).*** It also considerably reduced the electrochemical performance (short term) of the electrodes. U.S. Patent 3 160 530 to Union Carbide describes use of 0.5 to 5 weight-percent aliphatic monohydroxy alcohols containing 8 to 18 carbon atoms for wetproofing.

An extensive program of electrode construction was performed ***(569*** to ***576)*** in which materials, methods, baking cycles, etc., were varied. Physical parameters and electrochemical performance were measured for hundreds of electrodes. Results of the work were not compiled, but a number of conclusions can be reported. Because molding produced a narrow-size range of macropore diameters while extrusion always gave a wide range, only molded samples were extensively investigated. The contact angle (nonwetting surfaces have angles greater than 90") depended on materials and fabrication. Mixes containing 1 weight-percent silicone resulted in electrodes with contact angles greater than 100" when baked at 572" F (300" C), but wetproofing was destroyed upon normal baking to 1652" F (900° C). Petroleum pitches and resins were used as binders in place of

TABLE 3.1.—*Activation and Catalysis of Carbon Electrodes*

Reference	Preparation	Remarks
4	Mix 300 g Halo C activated carbon, 300 g neoprene putty (Binney & Smith Co., N.Y.) with 1500 cc toluene. Evaporate till crumbly. Press onto carbon electrode and heat-press cure.	Flooded slowly.
9	Stackpole graphite Y–21. Heat to 10% wt loss at 1562° F (850° C), N_2. Put on hot plate 392" F (200" C), spray both sides with 5 wt-% chloroplatinic acid, 15 mg Pt/in². Spray Teflon on one face (Du Pont 852-201 clear enamel), 12 mg/in². Bake 752" F (400" C), ½ hour.	Used as Cl_2 cathode.
19	Vacuum impregnate carbon with 3 to 10 wt-% salt solution, reduce in H_2 752" F (400" C), 3 to 6 hours. For W reduce at 1832" F (1000° C); for alloys anneal in He 1472" F (800" C); keep in H_2 at 752" F (400" C) before use.	
22	Ag electroplated from AgCN or saturated Ag_2O. Impregnate with Ag_2O suspension, heat to produce Ag.	
30	Chloroplatinic acid solution, 1 wt-% Pt, 10 ml conc. HCl per liter. Force plating electrolyte in and out of electrode, plate 20 minutes at 40 mA/cm².	
140	Pure Carbon Go. FC–14: *(a)* Plated as above. *(b)* Triethyl aluminum in dry liquid n-pentane added to carbon containing chloroplatinic acid, 10 wt-% Pt. *(c)* Carbon in chloroplatinic acid solution, pass H_2 with ultrasonic stirring. *(d)* Vacuum impregnate, draw off solution, dry, heat in He to 752° F (400" C), reduce in H_2, 752" F (400" C) for 3 hours.	Method *(d)* gave best results.
142	Catalyst powder placed on polypropylene film on face of horizontal carbon electrode. Heated to 482" F (250" C) to melt and carbonize film and thus bond powder to C surface.	
167	Carbon dipped in 50% nitric acid, heated in air at 392" F (200° C), 6 hours. Brush on chloroplatinic acid and fire in air; 40 mg Pt/in².	
456	National Carbon grade 20, nominal pore diameter 150 μ ½ cm thick. Heat in furnace 1292" F (700" C), quench in distilled H_2O. Or soak in 15 *M* HNO_3, 24 hours, heat 752" F (400° C), quench. Catalyze: *(a)* Immerse in 3% chloroplatinic acid, heat 1292" F (700" C), quench in H_2O. *(b)* Immerse in 3% alkaline Na chloroplatinate, dry. Add 36% HCHO. Dry, wash, dry. *(c)* As in *(b)*, but reduce with 20% N_2H_4. *(d)* Electroplate with Pt at 20 to 80 mA/cm².	Used as anodes for N_2H_4 dissolved in electrolyte. Procedure *(c)* best. Better for increased Pt from 0.5 to 25 mg Pt/cm².
460	Pure Carbon Go. FC–14. Impregnate with salt solution, drop into 1% $NaBH_4$. Drain, wash, and dry at 80" C under vacuum.	
588	Porous carbon: 5 m²/g BET area, porosity 0.56 cc/g; pore diameter 3 μ. Impregnated catalyst.	Suffered from flooding.
601	Stackpole Carbon Co. PC–57, porosity 1.07 cc/g, BET 300 m²/g, pores 3 to 7 microns. Soak in solution of 2 g paraffin/100 ml pet. ether. Dry, heat 392" F (200" C) for 2 hours. While hot, paint with 10% H_2PtCl_4, 2 mg Pt/cm². Dry at 212" F (100" C) for several hours, heat in vacuum at 302" F (150° C) for 5 hours.	Used on H_2-O_2 double IEM cell (H_2SO_4), performance was poorer than Pt black electrodes.
764	Disperse active carbon (Nuchar) in polystyrene, gum rubber, or polyethylene. Sprayed on porous C support at 104" to 122" F (40" to 50" C).	
767	Porous carbons as Cl_2 cathodes in 2.5 N HCl.	About 0.5-volt polarization at 50 mA/cm²; much poorer than platinized platinum electrode.

coal-tar pitch, but gave disperse pore sizes and low BET areas.

Although it was possible to make carbons with a wide variety of physical parameters and electrodes consisting of two or three layers of different pore size, no conclusive correlations of physical properties with electrochemical performance (H_2, O_2, KOH, and H_2SO_4) were obtained from this work. Electrodes were usually wetproofed with paraffin, followed by Pt impregnation according to the methods of Hunger or Taschek and Wynn (see table 3.1, **167, 601**). The method of electrochemical testing was crude, so that random variations in wetproofing and catalysis probably obscured the effects of electrode structure. Permeability coefficients of forced-gas transfer through the electrodes were measured; but for steady fuel-cell conditions the effective diffusion coefficient is the important variable to investigate (see **483**, for example).

Other fragmentary results on baked carbon electrodes include the following: Two carbons impregnated with various catalysts were tested with **30** weight-percent KOH contained in an asbestos matrix (**167**). The first had 40 percent porosity and a mean pore size of about 65 μ; the second had 36 percent porosity with most of the porosity in pores of diameter within the range 1 to 10 μ. The second carbon was consistently superior.

Performance of small, thin, catalyzed-carbon electrodes on air, 30 percent H_2SO_4, 176" F (80° C), was 0.45-volt polarization at 100 A/sq ft (Esso, **217**). Larger electrodes (4-inch square) flooded due to hydrostatic pressure, giving 0.2 volt more polarization at 100 A/sq ft. Reduction of hydrostatic head did not remove the electrolyte. A series of carbons with macropore sizes 40 to 350 μ gave maximum performance for 150 μ pore size. From the takeup of electrolyte, it was concluded that the pores were almost completely flooded. Double-layer electrodes were prepared with one layer catalyzed and the other uncatalyzed. Performance was best with catalyst next to the electrolyte, because of greater hydrophobicity and less flooding of uncatalyzed carbon. On small electrodes, performance was constant for thickness greater than 11 mils.

Suitably activated and catalyzed carbon electrodes give high initial performance with H_2 and O_2 in alkaline electrolytes. However, only thick, wetproofed electrodes used at relatively low current densities give long life. The success of plastic-bonded platinum-black electrodes in resisting flooding has led to the study of plastic-bonded carbon electrodes, which are considered in section 3.2.3.

3.2.2 Sintered Metal Electrodes

3.2.2.1 *Low-Temperature Cells*

As does the porous carbon electrode, the porous metal electrode that is completely flooded with electrolyte performs poorly. However, if the electrode is made in double-layer form, with the fine pores next to the electrolyte, electrolyte can be stabilized in the fine pores by a gas-pressure differential. It is possible to allow a porous metal electrode to flood, since its performance can be recovered by forcing out the fluid with increased gas pressure. Since the electrodes are hydrophilic, fine pores will hold fluid more tenaciously than coarse pores. (Possibly the modes of operation of porous carbon and porous metal electrodes are different, since a carbon electrode which has been flooded does not recover its activity.) Another method of stabilizing a porous metal electrode is to retain the electrolyte in a porous matrix which has a stronger capillary retention than the electrode. Sintered metal electrodes have the advantage, therefore, of resistance to slow flooding and they can be made much thinner than baked carbon electrodes.

Laboratory development of satisfactory electrodes has required continuous and diligent development of techniques and skills. The Allis-Chalmers and Electro-Optical Systems low-temperature, alkaline fuel cells use commercially available nickel plaque, which is then catalyzed with platinum or palladium-platinum. Some characteristics of the plaque have been determined: porous Ni battery plate from Gould National Batteries was 80 percent porous (**185**); Clevite No. 3, porous nickel on nickel screen, has a nitrogen BET area of 0.2 m^2/g, with most of the porosity (0.32 cm^3/g) in pore sizes between 2 and 12 μ, as measured by a mercury porosimeter (**28**). A 30-mil-thick plaque had an uncatalyzed BET area of 200 cm^2/cm^2. The method

TABLE 3.2.—*Catalysis* of ***Porous Metal Electrodes***

Reference	Preparation	Remarks
24	Clevite **3** porous Ni, impregnate chloroplatinic acid, dry, reduce in H_2 at 482" to 842" F (250" to 450° C).	
19	Impregnate with ultrasonic stirring, 5 minutes, plate at 45 mA/cm² for 1 minute.	
182	Clevite porous Ni electroless plated by sucking through 0.4 g H_2PtCl_2 $6H_2O$/100 ml, 158° F (70" C). Similarly with 0.14 g $PdCl_2$/100 ml. Repass solution until all catalyst deposited (test with neutral KI).	Plating throughout much improved performance. 20 mg Pt/cm² for O_2. 5 mg Pd: 5 mg Pt/cm² for H_2.
186	As above	10 mg Pt/cm².
408	Clevite porous Ni electroless plated in Pt solution. Rinse, dry, heat at 572" F (300° C) in H_2 for 1 hour.	Pt did not penetrate very far into plate, 50 mg Pt/cm². Used for N_2H_4 anode.
456	Micrometallic (Ball Corp., Glen Cove, N.Y.) stainless-steel filters, retain 2-μ particles. Immersed in Na chloroplatinate, dried, reduced with N_2H_4 solution.	As anode for dissolved N_2H_4 or cathode for HNO_3, H_2O_2, Pt > Au > raw stainless steel.

of catalysis was not given for the Allis-Chalmers electrode but was probably similar to the methods given in table 3.2.

Justi DSK ("Double Skeleton Katalyst") electrodes have not been extensively used in any of the contracts reported here. A brief description of the preparation of a DSK anode is as follows ***(329):*** Equal quantities of nickel and aluminum are first alloyed to form Raney nickel. After crushing in a ball mill, the powdered alloy is separated into fractions according to particle size. A definite fraction is selected and mixed thoroughly with nickel powder (prepared from nickel carbonyl) in some definite proportion as, for example, one part of Raney alloy to two parts of nickel. The powdered mixture is poured into a mold and compressed into a disk 4 cm in diameter and 2 to **4** mm thick with a pressure of about 4000 kg/cm². The disk is then sintered in an atmosphere of hydrogen for 30 minutes at 1202" to 1292" F (650 to 700" C). Aluminum is removed electrolytically from the Raney alloy by applying a positive potential to the electrode contained in a strong caustic solution. Electrodes are made in double-layer form, with a layer of smaller diameter nickel particles sintered on the electrolyte side. A Raney silver cathode is made similarly, using special techniques to prepare brittle Ag/Al alloy, which is reduced to Raney Ag before hot pressing into an electrode. Detailed descriptions are given in references 3.2 and 3.3.

Similar techniques have been used by Lockheed *(408).* Raney Ag or Ni powders were made into double-layer electrodes, with the fine side facing the electrolyte. Electrode disks of 2½-inch diameter were pressed at 100 tons and sintered at 1472" F (800" C) for 30 minutes with a 2-kilogram weight on top to prevent buckling. The alloying component was then leached out.

The principal disadvantage of the electrodes is the cost and difficulty of manufacture, compared with catalyzed commercial nickel plaque used for essentially the same purpose.

For use near 200" F (93" C) in alkaline cells, silver has been substituted for platinum on porous Ni cathodes ***(56).*** Proprietary porous silver cathodes for these conditions are also available ***(167*** and ***385,*** German patent 1 174 080 to Electric Storage Battery Co.). In sodium amalgam cells (*383*), the performance of a porous silver cathode was improved by coating its electrolyte face with a slurry of Teflon 30 (17 weight-percent), MgO (6) and polyethylene oxide, Polyox WSR 35 (2) in water. Two or three coats were applied with drying at 212" F (100° C) between coats, and the coated electrode was sintered at 1455" F (734" C) for 4 minutes. The coat was permeable to electrolyte, but prevented mercury from reaching the surface.

3.2.2.2 *Medium-Temperature Cells*

The Bacon-type cell also used sintered nickel electrodes with KOH electrolyte, at temperatures between 300° and 500" F (149" and 260" C). At these higher temperatures one usually does not need so highly active catalysts and high-area (internal) electrodes as for low-temperature cells. In addition, the high areas of platinum-black or Raney-type electrodes tend to disappear due to gradual sintering. The preparation of anodes of porous nickel and cathodes of lithiated, oxidized, porous nickel is described in reference 3.4. Details of the preparation of electrodes for the Pratt & Whitney fuel cell are not available, although they are based on the above work and are probably similar to those given next.

Of several methods of electrode manufacture, the following was judged the most satisfactory *(478)*. A backup plate of commercial porous nickel was degreased in CCl_4 and roughened by shotblasting or wire brushing to improve the adherence of the sintered electrode. A liner consisting of Ni powder in Lucite solution was brushed onto the backup plate. After evaporation of the solvent, the plates were kept in a furnace for one-half hour at 1830" F (999° C). For the anode, a mixture of "B" nickel powder and NH_4HCO_3 was tamped onto the backup plate and compacted under small pressures with a resilient pad. For the cathode, "D" nickel powder was used. This coarse-pore layer was sintered for 45 minutes in a reducing atmosphere, the anode at 1560" F (849" C) and the cathode at 1830" F (999" C). The electrodes were then inspected for defects (cracks, fissures, etc.), which resulted when the preheat and cooldown times were not sufficiently long. A fine-pore layer was then applied by rubbing a suspension of "A" Ni powder in CH_3OH on the surface of the coarse-pore layer.

Rubbing resulted in a better bond between the two layers. The anode was sintered for three-fourths hour at 1470" F (799" C); the cathode for three-fourths hour at 1830" F (999" C). Another fine-pore application was made on the anode and at least two more on the cathode, with sintering temperature lowered to 1740" F (949" C). Electrodes were acceptable if they showed a bubble pressure greater than 4 psig. Local low-bubble areas were repaired by the adding of Ni suspension and sintering. Cathodes were lithiated and oxidized by vacuum impregnation with a solution of Li and Ni nitrate, removal of excess solution, followed by heating at 1290" F (699" C) for 45 minutes in the presence of air. X-ray analysis showed this method to result in the inclusion of Li in the Ni oxide lattice. Anodes were chemically activated by vacuum impregnation with $Ni(NO_3)_2$ solution, with decomposition of the nitrate at 850" F (454" C) for three-fourths hour. These were then reduced at 850" F in a forming gas atmosphere. Both electrodes were pressure tested and considered acceptable for use if no bubbles appeared at a 5-psig differential.

3.2.2.3 *High-Temperatme Cells: Molten Carbonate Electrolyte*

Sintered metal electrodes are also used in high-temperature cells with molten-salt electrolytes (see ch. 6), operating typically at 932" to 1292" F (500" to 700" C). As it has not been possible to make satisfactory practical cells with free electrolytes of molten salts, which have strong tendencies to wet and creep over materials of construction, the electrolyte is retained in a porous matrix of refractory. Alternatively, a thick paste electrolyte of molten salt and fine (less than 1 μ) refractory powder is used. Electrodes cannot be made with high internal areas because they flood, and the usual methods of wetproofing, i.e., impregnation with wax or admixture of nonwetting halogenated hydrocarbons such as Teflon, obviously cannot be applied at these temperatures. In addition, the high area rapidly disappears by sintering and growth of crystal size. However, catalytic areas do not appear to be a basic problem with H_2 and O_2 as reactants (oxidation of CO is much slower than that of H_2). It is more important to establish a stable electrode-electrolyte interface, with good mass transfer of reactants through the electrode. It is also important to avoid high-resistance oxide films on the electrodes.

Table 3.3 shows that iron may be oxidized at the anode, while nickel anodes will oxidize if too much polarization occurs at the electrode. Nickel cathodes will oxidize and must be made

TABLE 3.3.—*Standard Potentials for Oxidation at High Temperatures (151)*

Reaction	E_0: mV, for—			
	932" F (500" C)	1112" F (600° C)	1292" F (700" C)	1472" F (800° C)
$H_2+\frac{1}{2}O_2 \rightarrow H_2O$	1062	1034	1005	976
$CO+\frac{1}{2}O_2 \rightarrow CO_2$	1114	1068	1024	980
$Ni+\frac{1}{2}O_2 \rightarrow NiO$	899	853	810	766
$Fe+\frac{1}{2}O_2 \rightarrow FeO$	1082	1044	1004	966

conductive by lithiation. A final problem is that nickel catalyzes the thermal decomposition of hydrocarbons and carbon is deposited on nickel anodes using these fuels.

In early work on molten carbonate cells (*491* and *502*), several metals or oxides were spread in thin layers over porous stainless steel (average pore size 65 μ), with the powder side pressed against the electrolyte matrix. At 1112" F (600" C), stainless steel alone was a satisfactory cathode, but required fine iron oxide or sodium ferrite as activator for anodes (with H_2). Porous nickel cathodes oxidized and gave low electrode conductivity (*498*), but could be used as anodes without activator powder. Table **3.4** gives later techniques; lithiated NiO cathodes were used with porous nickel anodes.

TABLE 3.4.—*Electrodes for Molten Carbonate Cells*

Reference	*Preparation*
502. . .	Lithiated NiO cathode. NiO and $LiNO_3$ (aq) slurried, dried in vacuo, heated on Pt to 2012° to 2192° F (1100" to 1200° C), several hours. Mill < 60 mesh. Impregnate with 2% ceresin wax, press, fire 2732° F (1500" C). Regrind, take < 60 mesh, 5% wax, press, fire 2732° F, 8 hours. Grind to shape. Good conductivity.
503. . .	Macropore of above electrode ≈ 25-p diameter (air permeability technique).
	Silver screen satisfactory as cathode. Pt corroded. Porous Ni anode.
506. . .	Dual porosity NiO (lithiated) made as above with layers of −100 mesh and 48 by 100 mesh.
498. . .	Porous stainless-steel cathode.
497. . .	Porous Ni anode for hydrogen.
492. . .	Cu or CuO unsatisfactory for cathode.
147. . .	Ni powder anode, **Ag** powder cathode. Most of polarization at anode. Fine powders slowly sintered.
607. . .	Anode: 60 wt-% carbonyl nickel, 30% **Ag** (−325 mesh), 10% Zn (−325 mesh) blended with 20% of fired carbonate (50 to 150 mesh). Sintered at 1472" F (800" C). Cathode: equal-size double layers of **Ag** powder, 80 to 100 mesh, 100 to 150 mesh, sintered at 1562" F (850" C).

Sintered nickel anodes were also used in the work described in reports *147* to *151*, where it was considered necessary to keep anode polarization below the point of nickel oxide formation *(151)*. Porous silver cathodes gave low polarization with O_2, but polarization had to be high enough to prevent silver ionization; otherwise, Ag dendrites formed at the electrode.

In the Texas Instruments cell, the electrodes were mounted on the electrolyte matrix *(609)*. The matrices were sintered MgO disks (Norton LM ***833***, 4¾-inch diameter, ⅛ inch thick, **31** percent porosity, 18-p average pore size). They were processed as follows:

1. Wash disks with water, using brush to remove loose MgO powder.
2. Dry at low temperature.
3. Candle disks for imperfections (cracks, pinholes, severe pockmarks, chips, etc.).
4. Degrease in trichloroethylene vapor bath.
5. Flame spray with fine Ag, using 10 to 11 grams per disk. Make sure spray coating is continuous.
6. The flame-sprayed area must not be handled with fingers, and the disks should be kept in desiccators when not in use.
7. Inspect disks under low-power microscope for any cracks that may occur during flame-spray operation.

The cathodes were prepared on the disk with the procedure:

1. Place flame-sprayed disk in a stainless-steel mold suitable to give a 4.2-inch-diameter electrode with cathode side (grounded) up.
2. Spread 12.5 grams, 100 to 150 mesh Ag

(Engelhard type J-6) evenly across the flame-sprayed area inside the mold.

3. Follow with 12.5 grams, 80 to 100 mesh Ag (Engelhard type J–6), also spread evenly with a brush.
4. Place ceramic plug (lava, 275 grams) lightly on Ag powder, leaving brush marks.
5. Place in sintering furnace with argon atmosphere.
6. Bring furnace to 1562" F (850" C) over a 5-hour period, then hold for 1 hour. Allow furnace to cool normally with power off.
7. Inspect disks for cracks.

The technique of anode preparation was—

1. Place disk with attached air electrode into mold and insert 20-mesh fine Ag screen with the four attached 16-gage fine Ag leads onto the anode flame-spray area. This is shown in figure 3.1. Slots on mold for wire leads will hold the assembly in place.
2. Spread 12.5 grams, 120 to 150 mesh Ag (Engelhard type J-6) over screen. Brush for even distribution. Place ceramic plug on Ag.
3. Place in sintering furnace with argon atmosphere.
4. Bring furnace up to 1562" F (850° C) over a 5-hour period, then hold for 1 hour. Allow furnace to cool normally with power Off.
5. Inspect disk for cracks.
6. Spread 17.5 grams, 100 to 120 mesh Ag (Engelhard type J-6) evenly over the sintered 120- to 150-mesh Ag. Use brush for even distribution.
7. Place the ceramic plug lightly on the Ag powder, leaving brush marks.
8. Repeat steps 3, 4, and 5.

The anode was catalyzed with nickel as follows:

1. Place MgO disk with attached electrodes in bottom half of stainless-steel mold and heat on hot plate to 250" F (121° C).
2. Add 7 grams Ni resinate (No. 58–A, Han-

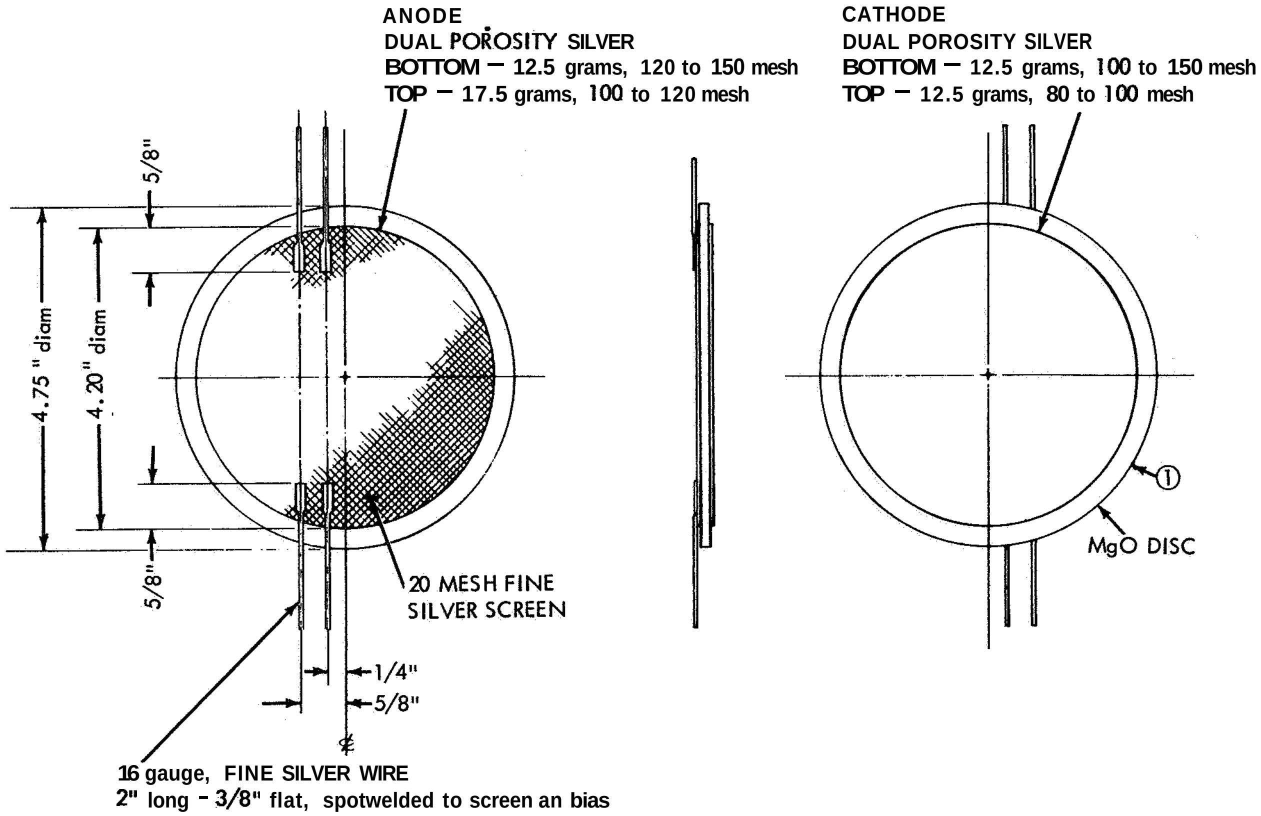
ANODE
DUAL POROSITY SILVER
BOTTOM — 12.5 grams, 120 to 150 mesh
TOP — 17.5 grams, 100 to 120 mesh
CATHODE
DUAL POROSITY SILVER
BOTTOM — 12.5 grams, 100 to 150 mesh
TOP — 12.5 grams, 80 to 100 mesh
5/8"
4.75" diam
4.20" diam
5/8"
20 MESH FINE SILVER SCREEN
1/4"
5/8"
℄
①
MgO DISC
16 gauge, FINE SILVER WIRE
2" long - 3/8" flat, spotwelded to screen an bias

FIGURE 3.1.—Construction of electrodes mounted on ceramic matrix; Texas Instruments molten carbonate cell.

ovia Liquid Gold Division, Engelhard Industries, Inc.) to 30-ml beaker and partially evaporate organic vehicle.

3. Use brush to paint anode. A relatively dry brush should be used to paint area within one-fourth inch of electrode periphery.
4. Place in oven with argon atmosphere and heat to 338" F (170" C). Raise temperature in 10" increments to 572" F (300" C) over a 3-hour period. When smoke has subsided, heat to 752" F (400" C) and leave for 1 hour. Allow furnace to cool normally with power off.
5. Repeat steps 1, 2, 3, and 4.
6. Again repeat steps 1, 2, 3, and 4, but make final temperature in step 4, 1292" F (700" C) instead of 752" F (400" C).

The nickel-coated Ag had the catalytic properties of nickel combined with the electrical conductivity of Ag.

The final step was to impregnate the matrix with electrolyte:

1. Paint the exposed Ag flame-spray area with liquid Ag (No. 2228, Hanovia Liquid Gold Division, Engelhard Industries, Inc.). Allow to dry in air.
2. Record weight of disk with attached electrodes.
3. Place disk on rack in furnace above bath of electrolyte sufficient to cover one-third of disk when submerged in CO_2 atmosphere.
4. Raise furnace temperature to 1112" F (600" C). Oils of paint will burn off in the process.
5. When electrolyte is thoroughly melted, lower disk into melt and leave for 1 hour.
6. Lift rack out of melt so excess electrolyte will drip out.
7. Allow furnace to cool to ambient temperature.
8. Scrape off any excess electrolyte on electrodes, and sand and scrape disk to bare metal on Ag flame-spray area.
9. Weigh and record amount of electrolyte adsorbed. This is usually around 36 grams.

3.2.2.4 *High-Temperature Cells: Solid Electrolyte*

The solid electrolytes used in the Westinghouse high-temperature cell have been produced in several forms (see ch. 6). This type of electrolyte requires close contact between electrode and electrolyte surface, since no liquid is present to form a bridge between the two. The only electrode material found suitable in the work reported here (***790*** through ***793***) was platinum. The procedure for preparing the electrode-electrolyte bond was given (***790***) as follows. Electrolyte was washed in acetone, baked in air at 1832" F (1000" C) and cooled. It was then sandblasted and etched in aqua regia, followed by a water wash and rebaking. Platinum powder (−300 mesh) dispersed in organic solvent (Hanovia No. 6926) was sprayed onto the required parts of the electrolyte surface. This was airdried, dried further at 158° F (70" C), and sintered at 2012" to 2552" F (1100" to 1400" C) for 1 hour.

Platinum evaporated onto the electrolyte was not satisfactory due to low porosity (***792***) Nickel powder plus a Hastelloy grid current collector was investigated as a fuel electrode (Office of Coal Research reports), but suffered from oxidation which destroyed adhesion to the surface. A number of doped oxide electrodes were prepared for obtaining electronic semiconductors which would bond to the solid electrolyte (ionic conducting). Details are given in chapter 6, but the oxide electrodes were not satisfactory for several reasons, although work was continuing on these materials.

3.2.3 Plastic-Bonded Electrodes

3.2.3.1 *Introduction*

Electrodes prepared from catalyst powder mixed with an organic binder and pressed onto a screen or porous backing plate were described in several early reports (8 and ***764,*** for example). However, development of excellent electrodes of this type seems to have occurred via the following steps. A simple method of testing the activity of metal blacks is to form a paste of the black with electrolyte, spread it on a noncorroding metal screen, and press against an electrolyte-filled matrix. The matrix can be porous asbestos, glass filter paper, an ion-exchange membrane (IEM), etc. This structure then forms an electrode-electrolyte interface for test as a gas-diffusion electrode. It is not suitable for practical electrodes because of low durability, and if the blacks are sintered to the screen by high temperatures they lose area and catalytic activity. Durability is improved by including an organic binder of small particles in a suitable dispersion (usually Teflon-30, Du Pont) and pressing.

One method of making electrodes for IEM fuel cells is the addition of a layer of catalyst powder to the cast membrane before it is completely dry, thus giving a bond between the particles and the membrane. It is more convenient to prepare the membrane, cover it with catalyst powder and a screen and hot-press to bond the particles to the membrane. Forming a paste of catalyst black with Teflon dispersion and hot pressing the paste (plus screen) against an IEM in one step improved the durability of the bond between the electrode and the membrane. Also, a paste of catalyst-black and Teflon dispersion could be hot pressed onto a screen to give a durable electrode which resisted flooding and which could be used with electrolyte in a matrix, or with free electrolyte if the hydrostatic head on the electrode was not too great.

The advantages of this type of electrode for low-temperature cells as compared with porous sintered metal are: *(a)* they can be made very thin and lightweight; *(b)* they do not need a double-layer structure to prevent flooding; (c) manufacture is relatively simple, quick, and reproducible; and *(d)* the amount of catalyst can be small.

3.2.3.2 *General Electric Co., Niedrach-Alford Electrodes*

This electrode consists of a metallic substrate (typically a Pt screen of ~45 mesh and 5- to 8-mil wire) embedded in a mixture of Teflon and catalyst with a thin porous film of Teflon (~1 mg/cm²) on the gas side. Its method of preparation may vary as to amount of catalyst and ratio of catalyst to Teflon, type of metallic substrate, the thickness and method of application of Teflon film, pressing temperatures and pressures used in sintering and bonding the electrode, etc. The use of the porous Teflon layer on the gas side was reported in 286.

The following description of the method of preparing large electrodes of this type was given before the use of the Teflon film was developed *(285)*. The electrodes were 20 by 11 inches by 4 mils thick, total weight 80 grams, with catalyst loading about 30 mg/cm².

1. Blend catalyst mixture and reduce agglomerated particles in size.
2. Line mold with aluminum-foil release material, and smooth free of wrinkles.
3. Shim mold cavity ring to approximately 0.020-inch height and lock with holddown screws.
4. Fill mold cavity with an excess of sieved catalyst and remove excess by carefully stroking special screenlike blade over cavity ring in such a manner as to avoid excessive catalyst compaction.
5. Accurately position tared, precut, chemically cleaned electrode reinforcement screen with tape and clamp within screen-support frame.
6. Invert and lower screen-support frame over cavity ring and mold assembly. Cubes of a soft puttylike material inserted between the support frame and external mold base corners provide an effective method of slowly lowering the frame, thus eliminating possible blowout of catalyst mixture resulting from sudden escape of entrapped air within the mold and screen.
7. Remove shim strips from under cavity ring and apply slight but firm pressure to top of mold assembly to seat cavity ring, and slowly remove any remaining entrapped air.
8. Transfer mold assembly to 1000-ton press, avoiding jarring, and insert ⅛-inch-thick Teflon sheet stock between mold and top press platen to equalize pressure distribution in the pressing operation.
9. Adjust platen speed to minimum rate to avoid catalyst blowout upon platen closure, and apply 1000 tons (4.5 tons/sq in) to mold assembly.
10. Relieve pressure, rotate mold 90° on bottom platen, and again apply 1000 tons. Repeat this operation twice more to minimize any dimensional runout existing between the mold and press platen.
11. Remove mold from press, disassemble, and strip catalyst electrode from support frame.
12. Place electrode, with aluminum foil still

firmly adhered, between two ¾-inch-thick stainless-steel plates and again subject to 1000 tons' force.

13. Remove package from press and carefully strip aluminum foil from electrode.
14. Weigh electrode, subtract weight of tared screen, and compute weight of catalyst.
15. Store flat in clean polyethylene bag.

When used with ion-exchange membranes, the electrodes were bonded to each side of the membrane as follows:

1. Place a 24-inch (approx.) piece of moist, prepared membrane (AMF sulfonated polystyrene) between two 20- by 11-inch catalyst area electrodes and aline catalyst areas.
2. Insert cell assembly between two 1/8-inch-thick stainless-steel press plates with 0.001-inch-thick Teflon film backed up with 0.001-inch-thick Mylar film which serves as an effective release agent between the cell press plates.
3. Transfer package to a hydraulic press, apply and hold 440 tons' pressure and 265°±5° F (130°±3° C) temperature for approximately 15 minutes. Teflon sheet stock, 1/8 inch thick, placed between the package and top and bottom press platens, is used to distribute pressure equally.
4. Cool to approximately 80" F (27° C), release platen pressure, and remove assembly from press.
5. Trim excess membrane from cell perimeter, moisten cell with distilled water, and store flat in sealed, clean polyethylene bag.

Since development of the above-described method, approximately 17 scaled-up cells of good quality have been fabricated. Total weight and thickness of these were in the order of 210 grams and 0.012 inch, respectively. Weight and thickness variation between different cells was approximately ±5 percent. The total cell resistance was 0.0008 ohm for 1.5 square feet, or (1.2) (10^{-3}) ohm-ft^2; this would give an IR loss of 0.12 volt at 100A/sq ft. Cell output was 100/A sq ft at 0.73 volt, 200 A/sq ft at 0.57 volt. The optimum weight of Teflon in the catalyst mixture was 10 to 15 weight-percent (287).

Small disk electrodes with high performance are prepared as follows (397; also ref. 3.5) :

1. A Teflon-30 suspension (Du Pont) diluted with seven volumes of water is sprayed onto a piece of Al foil to obtain the desired film thickness of Teflon (0.79 to 2.9 mg/cm^2). During this application, in which care is exercised to obtain as uniform a film as possible, the foil is on a hot plate maintained at 248° to 302" F (120° to 105° C) so as to evaporate off the water and prevent the formation of wet areas and running of the suspension on the foil. Following this, the foil is heated to 662" F (350" C) for about 1 minute. This results in the removal of the wetting agent from the Teflon and the sintering of the Teflon particles (—0.2 to 0.5 μ in diameter) to form a film.
2. A slurry of platinum black (or other catalyst) in Teflon-30 with the ratio of 1 gram of Pt to 0.09 gram of Teflon (1 gram Pt to 0.1 cc of Teflon-30) is then spread on a circular piece of Al foil containing the Teflon film and on another piece of Al foil alone. The total amount of platinum used is such as to give —34 mg/cm^2 of electrode. The wetting agents in the Teflon-catalyst slurry on the two pieces of Al foil are then removed by heating, initially very slowly, up to —572" F (~300° C). A circular Pt screen containing a wide tab for maintaining good electrical contact to the electrode is sandwiched between the two catalyst layers, and the whole assembly is pressed between two ferrotype plates at 1800 to 3000 psi of electrode, 662" F (350" C) for 2 minutes.
3. The Al foils are removed from the electrode with warm 20 percent NaOH and the electrode is washed and air dried. The resultant electrode is hydrophobic on the Teflon-film side and permeable to water on the other side.

The performance of electrodes prepared as described above is given in figure 3.2. Studies to reduce the amount of platinum led to the following conclusions *(310)*. For hydrogen, the catalyst loading could be reduced from 34 to 1.1 mg/cm^2 without significant decrease in performance. For oxygen and hydrocarbons, there was a direct relation between platinum loading and performance. Tungsten or tantalum powder was used as a diluent to maintain electrical conductivity to the embedded screen. When used in concen-

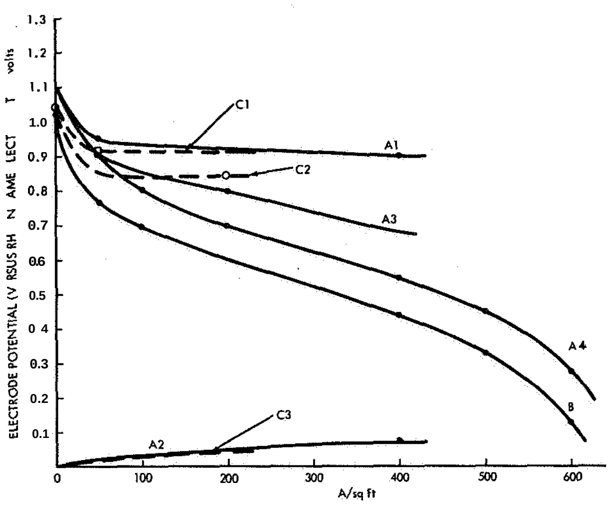

General Electric Niedrach-Alford electrodes:

A. Ambient temperature, 6 *N* KOH, 35 mg Pt/cm², 3.2 mg Te/cm², Teflon film 1 to 4 mg/cm²

A1 O, cathode

A2 H_2 anode

A3 H_2-O_2 cell including IR

A4 H_2-air cell including IR

B. 5 *N* H_2SO_4, 35 mg Pt/cm², 3.2 mg Te/cm², Teflon film 2 mg/cm². H_2-air cell including IR

Internal heating at high current densities produced temperatures up to 158° F (70° C). Platinum black catalyst had particle size of about 0.01-μ diameter, Teflon particles 0.2 to 0.5 μ. Electrolyte was circulated between electrodes.

American Cyanamid electrodes:

C1. 86° F (30° C) ambient, 5 *N* KOH, 9.5 mg Pt/cm², O, cathode

C2. 86° F (30° C) ambient, 5 *N* H_2SO_4, 8.5 mg Pt/cm², O, cathode

C3. C1 or C2 used as H_2 anode

Electrolyte in Johns-Manville asbestos matrix.

FIGURE 3.2.—Performance of Teflon-bonded electrodes with H_2, O_2, and H_2-air.

trated H_3PO_4 at 302" F (150° C), electrodes containing platinum cracked due to recrystallization of platinum. Mechanical stress, thermal cycling, or deterioration of the binder were not causes of electrode cracking. More stable electrodes were obtained by pressing platinum black and Teflon onto a porous tantalum substrate, with 30 percent Teflon better than 10 percent.

Boron carbide, B_4C, was also used as a diluent; 32 mg B_4C and 0.16 mg Pt/cm² gave about 50 mV more polarization with H_2 than 45 mg Pt/cm², at 400 mA/cm², in 6 *N* H_2SO_4. The B4C used was an impure commercial material with a N_2 BET area of **14** m²/g, and a probable particle size of about 0.1 to 0.2 μ. Mechanical admixture of platinum black and B_4C did not give a satisfactory electrode. B_4C activated by H_2PTCl_6 solution, followed by reduction to Pt in H_2 at 752° F (400° C) for *24* hours, was also not satisfactory and it was believed that chloride ion was retained and poisoned the Pt. The activation procedure which gave the result quoted above was: boron carbide powder was wetted with a solution of diaminodinitro platinum, Pt $(HN_3)_2(NO_2)_2$, dried, and reduced in flowing H_2 at 752" F (400" C) for 20 hours. Boron carbide alone was a reasonable catalyst for O_2 in 5 *N* KOH, but poor in H_2SO_4 or H_3PO_4. Activated with 0.16 mg Pt/cm², it gave 275 mA/cm² at 0.8 volt (versus reversible H_2 in same electrolyte) in 5 *N* KOH.

3.2.3.3 *American Cyanamid Co., Electrodes*

The method of preparing these electrodes is proprietary but is probably similar to that of the General Electric electrodes discussed above. Contract reports 86 through 88 describe a laboratory hydrogen-oxygen cell using these electrodes pressed against an asbestos matrix, saturated with concentrated KOH electrolyte. The best electrodes contained 40 mg Pt/cm² and **14** to 25 weight-percent Teflon in the Pt-Teflon mixture. Engelhard platinum black was as effective as high-area blacks formed from $NaBH_4$ reduction of platinum salts (see app. C). The screen base was 40-mesh Ni of 10-mil wire. However, there was a slow deterioration with time (loss of about 3mV/100 hours at 100 mA/cm²) which was attributed to oxidation of the screen. Zirconium, low-carbon nickel, and Inconel were being investigated as substitutes.

In specification literature supplied by American Cyanamid, electrodes for alkaline electrolyte have been described as containing 9.5 g Pt/ft², on 70-mesh Ni or gold-plated Ni screen of 4½-mil wire, with a thickness of 8 to 9 mils and a weight of 60 g/ft². Operating life, at 158° F (70° C) and 100 A/sq ft, has been better than 1500 hours. For sulfuric acid electrolyte the specifications are similar, but 50-mesh Ta screen of 3-mil wire is used, giving a thickness of 6 to 7 mils and a weight of 40 g/ft². Performance with an asbestos matrix is given in figure 3.2. Comparing the General Electric and American Cyanamid electrode performances, we see that the H_2 electrodes behave identically. Cathode performance is also similar, except that the lower catalyst loading of the Cyanamid electrodes gives greater polarization at low currents. However, the matrix in the Cyanamid cell probably allows the electrodes to heat up more at higher currents than does the General Electric test cell, leading to identical performance at 200 to 300 mA/cm².

The effect of temperature on cell performance is shown in figure 3.3. Increased temperature improves performance due to lower activation polarization at the cathode and higher conductivity of the electrolyte. The increased temperature, however, produces larger equilibrium vapor pressures of water vapor over the electrolyte, which lowers the partial pressure of reactants and causes concentration polarization due to gas transfer at higher current densities. When the electrolyte loses water the conductivity goes down. The effects balance at higher temperatures, so that for a given reactant pressure a region of optimum temperature is obtained.

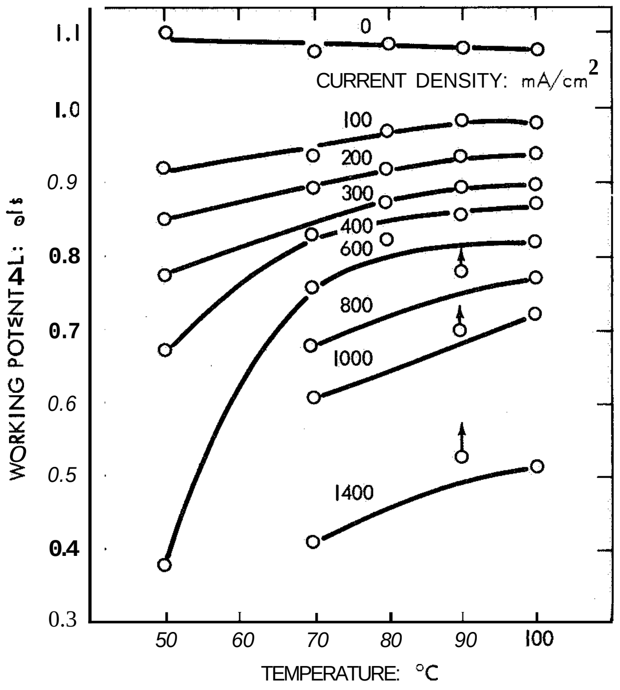

Electrodes: High-loading (40 mg Pt/cm²)
Matrix: 20-mil ACCO asbestos
Pressure: 0 psig
KOH concentration: 13 N

FIGURE 3.3.—Effect of temperature on performance of American Cyanamid Teflon-bonded electrodes.

3.2.3.4 Union Carbide Corp., Thin Fuel-Cell Electrodes, June 1963 to May 1964

As discussed previously, the major disadvantage of baked carbon electrodes is that they have to be thick to give strength and long life; although they can give high current densities when suitably catalyzed, they have long life only at relatively low current densities. It is obviously desirable to combine the catalytic properties of activated carbon with the advantages of Teflon-bonded electrodes to give active, thin wetproofed electrodes. Electrodes were constructed with a layer of catalyzed carbon powder on a layer of inactive carbon powder with plastic bonding on a layer of porous nickel containing an embedded Ni screen *(663)*. Total thickness was 35 mils. The process is shown in figure 3.4. The carbon powders used were pitch-bonded or sugar-bonded carbon flour ground to less than 20-μ diameter. At 158° F (70° C), the initial cell performance on H_2 and O_2 with 12 *M* KOH was 0.8 volt at 400 mA/cm² (IR free), with most of the polarization occurring at the cathode. However, the anode deteriorated in 200 hours due to separation of the wetted active layer from the wetproofed carbon layer. The nickel backing had no effect on per-

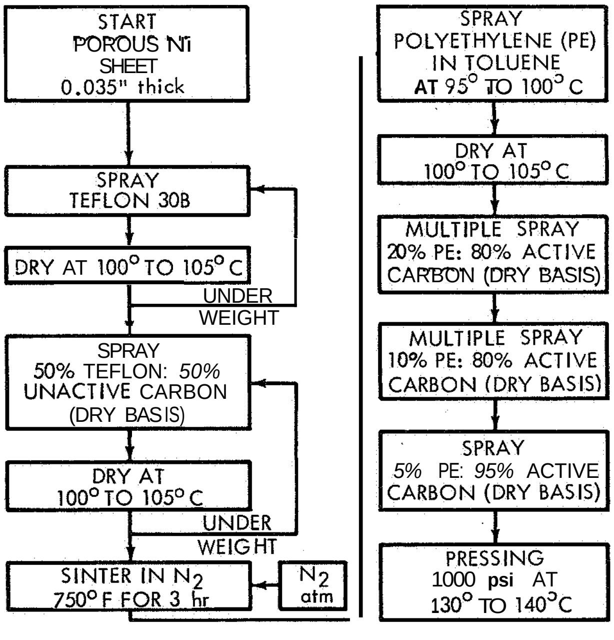
START
POROUS Ni
SHEET
0.035" thick
SPRAY
TEFLON 30B
DRY AT 100° TO 105° C
UNDER
WEIGHT
SPRAY
50% TEFLON: 50%
UNACTIVE CARBON
(DRY BASIS)
DRY AT
100° TO 105° C
UNDER
WEIGHT
SINTER IN N2
750° F FOR 3 hr
N2
atm
SPRAY
POLYETHYLENE (PE)
IN TOLUENE
AT 95° TO 100° C
DRY AT
100° TO 105° C
MULTIPLE SPRAY
20% PE: 80% ACTIVE
CARBON (DRY BASIS)
MULTIPLE SPRAY
10% PE: 80% ACTIVE
CARBON (DRY BASIS)
SPRAY
5% PE: 95% ACTIVE
CARBON (DRY BASIS)
PRESSING
1000 psi AT
130° TO 140° C

FIGURE 3.4.—Processing flow sheet for Union Carbide thin electrodes (663).

formance, providing it was strong, thin, and permeable to gas.

The sugar-bonded flour gave electrodes more resistance to failure *(664)*. The performance of a cell improved over the first 2 weeks of use. Changing from 158° F *(70"* C) to room temperature greatly decreased the performance of the cathode and also decreased the anode performance at higher current densities. Both air and H_2 electrodes showed an increased rate of polarization at current densities between **100** and 200 mA/cm^2, indicating concentration polarization effects (electrolyte was not circulated).

TABLE 3.5.—*Miscellaneous* ***Plastic-Bonded Electrodes for Low-Temperature Fuel Cells***

Reference	*Preparation*
213...	Teflon sponge made by sintering mixture of acrylic acid and Teflon in air. Mixture of metal black and 15 to 50% Teflon pressed with 80-mesh Pt screen onto sponge, 20 mg Pt/cm^2.
238...	Platinum black slurried with distilled water and Teflon 30 emulsion (Du Pont). Spread on Al foil, dried, baked in press, Al dissolved in dilute caustic, ½ mil thick.
240...	Platinum black bonded into IEM led to breakdown of membrane. Went to Pt-Teflon electrode pressed against an IEM saturated with electrolyte.
252...	Acetylene black activated with 10% Pt used in place of platinum black (20% Teflon binder). Poor for H_2 and O_2 in 30% KOH.
605...	1 gram Bishop platinum black with water to thick paste. Spread on 4-inch square of 80-mesh Pt screen. Dry 5 minutes at 230" F (110° C). Spray both sides with Teflon (Oil-Es-Oil, American Durafilm Co., Newton Lower Falls, Mass.). Press 500 psi, 1 minute. Side with Pt used against cationic membrane.
	2 grams platinum black + 0.14 gram Teflon dispersion (No. 852–201, American Durafilm Co.) + 0.2 gram reagent grade MgO + water to thick paste. Spread on 4-inch square screen, dry. Place between Al foil dusted with MgO, press at 4000 psi, 600° F (316° C), 5 minutes. Leach MgO by boiling in 6 *N* H_2SO_4, 15 minutes. Rinse and dry. Stronger than electrode above.
408...	Lockheed proprietary electrode. Coarse and fine metal screens sandblasted and welded together and into Ni rim. High area activated carbon, catalyst, and Teflon binder ball milled together. Product dried and crushed. Powder put into the rim with the fine screen down and hot pressed from the top. The fine-screen side sprayed with Teflon. Coarse screen with embedded powder faces the electrolyte, Teflon-sprayed side is O_2 side. In 7 *N* KOH, OCV of 0.1 volt versus SHE on O_2; little polarization at 20 A/**sq** ft, but 0.2-volt polarization with air.

3.2.3.5 Miscellaneous Results on Electrodes

Some other results on plastic-bonded electrodes are summarized in table ***3.5.*** Thompson-Ramo-Wooldridge reported that Kel-F binder, sintered at ***475"*** F (246° ***C)*** and ***700*** psi, did not give so strong an electrode as Teflon ***(605).*** **A** proprietary cathode made by Esso, containing platinum and Teflon in 95:5 weight-percent ratio, gave an open-circuit polarization of ***0.25*** volt, and ***0.45*** volt at ***100*** mA/cm^2, ***140" F (60" C), 3.7*** *M* H_2SO_4 ***(217).*** Shawinigan carbon black, platinum black, and Teflon powder were mixed to a paste with quinoline (Monsanto, ***466).*** This was spread on a metal screen, covered with a porous Teflon sheet (gas side), and the assembly sintered. The relation between sintering temperature and performance is shown in figure ***3.5.***

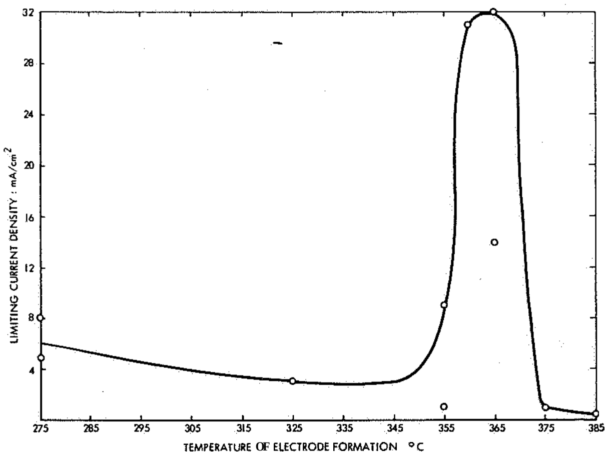

FIGURE 3.5.—Dependence of catalytic activity of platinum for electrochemical oxidation of propane in 85% H_3PO_4 at 302° F (150° C) on temperature of electrode formation ***(466).***

Table ***3.6*** gives a summary of results of oxygen electrode investigations from a number of sources.

3.2.4 Solid-state **Diffusion Membranes**

A solid-state diffusion membrane is a thin sheet of metal that absorbs gas and allows it to

TABLE 3.6.—*Miscellaneous Oxygen Electrodes*

Reference	Electrolyte	Temperature	Pressure	Electrode and catalyst	Remarks
7.	Sea water.	Ambient.	1 atm. .	Porous Ni-plated Pd, Pt, Ag; carbon.	Pt, Pd/Ni>Ag/Ni, C.
57	KOH in porous asbestos	195° F (91° C)	1 atm. .	Catalyzed porous Ni.	Ag used instead of Pt to improve life.
67.	KOH in porous asbestos	200° F (93° C)	50 psig.	a. Porous C, activated and platinized by method of Hunger; 40 mg Pt/cm².	Platinized C and platinized Ni best of a, b, c, d, e.
				b. Also impregnated with metal nitrates and fired in air, 392° F (200° C), 6 hours, to give Cu, Co, Cr, Fe, and Ni oxides.	Considerable improvement of lithiated NiO with higher temperature.
				c. Also impregnated with Kordesch spinel.	
				d. 22-mil porous Ni (Gould National Batteries, raw unimpregnated plate) immersed in 3% chloroplatinic acid to deposit 40 mg Pt/cm².	
				e. Nickel powder 44 to 74 μ, sintered in alumina mold, H_2, 2462° F (1350° C), 1 hour. Soak in 10% LiOH solution, fire in air 1382° F (750° C), 5 minutes.	
				f. Radioactive electrode supplied by Yardney (presumably a porous Ag electrode).	Better than a, b, c, d, e.
182	KOH in porous asbestos	. . . .	. . . . . .	Ag powder, 100 to 200 mesh, sintered on Ag screen. Doped with Po^{210} α emitter or Pm^{147} emitter.	No conclusive effect of radioactive doping.
156.	Molten KOH-NaOH in paste with MgO	572° F (300° C)	1 atm. .	Porous Ni catalyzed with Pt. Porous Ag.	Ag slowly dissolved in presence O_2.
215	H_2SO_4.	Ambient.	1 atm. .	Teflon-bonded metal blacks, produced by $NaBH_4$ reduction of metal salt. Codeposits of a number of metals.	See sec. 17.4.4.
28.	Phenolsulfonic formaldehyde cationic IEM	Ambient.	1 atm. .	Various powder catalysts pressed into IEM.	Pt>Pt-C, Pd-C, tungsten carbide-Pt, titanium carbide-Pt. Contact resistance higher, catalysis poorer.
250.	3 *N* NaOH.	Ambient.	1 atm. . . .	Plastic-bonded Ag powder (325 mesh).	Poor performance compared to plastic-bonded platinum black.
251.	. . . .	. . . .	. . . .	Plastic-bonded AgO reduced to Ag.	

404.	Various...........	....		Powdered C pressed on screen at 4000 psi with Teflon binder.	Polystyrene, polyethylene, Kel-F also used. 7 wt-% binder best.
408.	KOH-NaOH-LiOH-12 wt-% H_2O	302° F (150° C).	1 atm.	Raney Ag silver flake on sintered Ni backing. 3 8 Ni. Pressed carbon.	Silver flake on Ni backing best.
433.	Buffered Na phosphate pH 7.	Ambient.......	1 atm.	Sandwich of porous Teflon sheet/Teflon-platinum black mixture (25:75 parts by weight)/platinum black-Pt screen. Pressed at 60 000 psi.	Surface of platinum black next to electrolyte wetted, rest did not.
762.	KOH...............	Ambient..	1 atm	Suspension of activated carbon (Nuchar C, West Virginia Pulp & Paper Co.) in polyethylene sprayed onto porous C to 1 mm thick. Heated to soften plastic.	Gives O_2-H_2O_2 potential.
329.	KOH..............	Ambient.......	1 atm.	Union Carbide porous carbon electrodes impregnated with $AgNO_3$, decomposed to Ag or Ag oxides.	Ag effective in decomposing peroxide. Amount Ag used was up to 15% by weight of the carbon.
300.	....	....	1 atm....	Teflon-bonded Niedrach-Alford electrodes.	
	KOH..............	Ambient..........	....	B_4C catalyst, 35 mg/cm^2........................	0.7 volt (vs rev. H_2) at 120 mA/cm^2.
	85% H_3PO_4	302° F (150° C).....	....	B_4C catalyst, 35 mg/cm^2........................	Poor.
	KOH..............	Ambient..........	....	B_4C catalyst activated with 0.16 mg Pt/cm^2.........	0.8 volt at 275 mA/cm^2.
	H_2SO_4..............	Ambient..........	....	B_4C catalyst activated with 0.16 mg Pt/cm^2.......	0.6 volt at 140 mA/cm^2.

diffuse through the solid structure. An example is Pd foil, through which H_2 diffusesatomically or ionically. This type of electrode cannot flood, since it is not porous; it is, therefore, ideal for containing electrolyte. It has these disadvantages: rates of diffusion are low unless the membrane is thin; diffusion depends strongly on temperature, so the cell cannot be started cold; and electrodes are poisoned by any impurity which adsorbs strongly on the surface and prevents adsorption of hydrogen. This type of electrode does not pass H_2O or CO_2, so that product gases cannot be removed by transpiration through it.

Palladium-silver alloy membranes have been used for some years to purify H_2. Differential pressure of H_2 is maintained across a membrane, and pure, dry H_2 diffuses from the high-pressure side to the low-pressure side. Palladium is also known to be one of the best catalysts for hydrogen ionization in acid or alkali (see table 17.6). Two phases (α, β) of H/Pd exist, and the diffusion rate is different in each phase. Chemisorption of H_2 on clean Pd is rapid, but the surface is readily poisoned, leading to lower rates of adsorption.

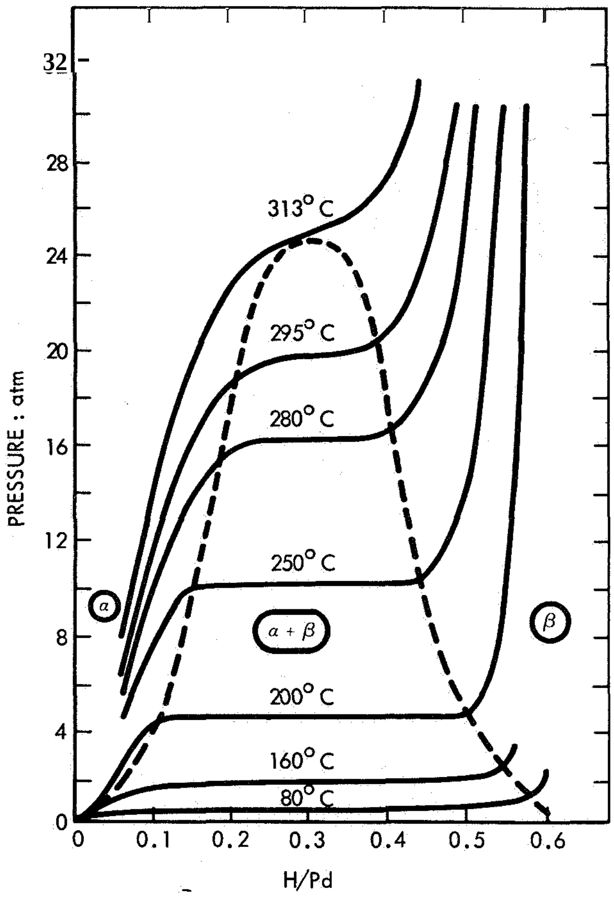

The curves are based on the results in the following references:
Gillespie, L. J.; and Hall, F. P.: J. Am. Chem. Soc., Vol. 48, 1207, 1926; Gillespie, L. J.; and Galstaum, L. S.: J. Am. Chem. Soc., Vol. 58, 2565, 1936.
Sieverts, A.: Z. physik. Chem., Vol. 88, 451, 1914; Sieverts, A.; and Hagen, H.: Z. physik. Chem., A174, 247, 1935; Sieverts. A.; and Zapf, G.: Z. physik. Chem., A174, 359, 1935; Bruning, H.; and Sieverts, A.: Z. physik. Chem., A163, 409, 1932.
These references also give more detail in the room-temperature, I-atmosphere region.

FIGURE 3.6.—Phase diagram of hydrogen adsorbed in palladium *(618)*.

A review of the theory of transfer of H through Pd and Pd-Ag was given in *124* (Battelle) based largely on reference **3.6.** It was calculated that a concentration difference of 0.1 atom H/Pd across a 1-mil membrane would give a limiting mass-transfer rate corresponding to 4380 A/sq ft at **392"** F **(200"** C), using diffusion coefficient for α phase. The experimental rate (see table 9.4) at **392"** F **(200"** *C)* was 150 A/sq ft, determined by cathodic discharge at the membrane, in KOH pressurized to **20** psig. The H_2 transmitted through the membrane was 100 percent of that predicted from the electrolysis current, showing that H_2 was not evolved on the electrolyte side of the membrane. The discrepancy between experimental and predicted result had three contributing causes. First, the phase diagram in figure **3.6** shows that the pressures used could not possibly give 0.1 atom H/Pd concentration difference. Second, there was evidence of slow surface reactions which were an additional rate limitation; the Pd surface had to be activated by oxygen evolution at 150 A/sq ft and the limiting current decayed after this activation. Third, no allowance was made for the presence of mixed phases, although this error was recognized. It was suggested that the plane of α- to β-phase transition in the membrane slowed down the diffusion and that alloying with Ag changed the lattice constants until the cy and β phases fused at 25 to 45 atom-percent of Ag.

A tube of Pd of 10-mil wall thickness was immersed in electrolyte and used as an anode with H_2 in the center (Tyco, *650*). The OCV was 0.05 volt versus reversible H_2 in the same electrolyte and an anodic limiting current was found.

The electrode potential was allowed to go to over *1.4* volt at the limiting current, and on decreasing the current, the polarization remained high even for low current densities. The electrode had to be taken to H_2 evolution to restore the initial performance. This effect was due to the formation of Pd-oxide on the electrolyte face of the Pd, which was removed by H_2 evolution.

A similar technique was used in report *558* (Rensselaer Polytechnic). However, it was found necessary to activate Pd by heating in air at *1112"* F *(600"* C) to *1382"* F *(750" C)*. Heating in argon did not activate Pd; a blue-surface film of oxide was observed after heating in air, which was determined by X-ray diffraction to be PdO. Abrasion of the film on the electrolyte side of the Pd produced no effect, but it did on the gas side. The limiting current was higher for thinner membranes, but not in the expected linear manner *(559)*. It was concluded that a film of PdO was necessary on the gas side to give rapid chemisorption of H_2. It was also advantageous to deposit Pd black on the electrolyte side. The formula of Ash and Barrer

$$\frac{J=D_\beta(C_0-C_1)+D_\alpha(C_2-C_3)}{L} \qquad \textbf{(3.6)}$$

was used to calculate D_β from the experimental values of J, where J=rate of transport per unit area; D_β =diffusion coefficient of H in the p-phase of H/Pd; C_0=concentration of H at the gas face, determined from the pressure of H_2 and the phase diagram; C_1 =concentration of H in the p-phase at the phase boundary; C_2 =a-phase concentration at the boundary; C_3 =H concentration at the electrolyte face, assumed zero at the limiting current; L =membrane thickness. This equation is readily derived by writing the equations for diffusional flux through a thickness 11of α-phase, l_2 of p-phase and putting $l_1+l_2=L$. The result is given in table *3.7;* the value of *D,* was calculated from *(4.3)*(10^{-3}) exp [$-5600/RT$]. The value of i_L at *86"* F *(30" C)*, *1* atmosphere H_2, was *140* mA/cm² for the 10-mil membrane, but polarization was about *0.5* volt at *100* mA/cm².

A review of H_2 diffusion in Pd (University of Florida, *686)* should be disregarded, since a later report *(688)* concluded that the data used could not be extrapolated to fuel cell temperatures.

TABLE 3.7.—*Diffusion of Hydrogen Through* Palladium

Reference	**Diffusion** *coefficient, cm²/sec*
3.6. . . .	$D_\alpha=(4.3)(10^{-3})\exp(-5620/RT)$
625. .	$D_\alpha=(4.3)(10^{-3})\exp(-5600/RT)$
558. . . .	$D_\beta=(3.8)(10^{-4})\exp(-2930/RT)$

An excellent discussion of Pd and Pd-Ag membrane electrodes was given in a report by (Tyco Laboratories, Inc., *625)*. Evidence from the literature suggested that absorbed H donated electrons to the d-band of Pd (saturation about *0.6* H/Pd), and that the diffusing component was H^+ screened by electrons; a reasonably accurate theoretical description of the phase diagram was also reported. Above *392"* F (200° *C)*, diffusion at *1* atmosphere was due to diffusion in the α phase (see fig. *3.6)*. A limiting current of *78* mA/cm² at *176"* F *(80" C)* was predicted for a membrane thickness of 10^{-3} cm. (The calculation seems too low by a factor of *10,* even assuming diffusion only in the α phase). The main disadvantage of Pd membranes was folding and cracking in use due to dimensional changes in going between cy, *p* phases; therefore, Pd-Ag was preferred.

The lattice parameters of Pd-Ag electrodes were determined from X-ray diffraction patterns, after holding at various potentials in $HClO_4$ electrolyte bubbled with H_2; on removal the electrodes were coated with Apiezon to prevent absorbed H_2 from escaping during the X-ray measurement. At potentials near the reversible H_2 potential, the alloys absorbed H_2 and formed the p-phase (high H content), with lattice spacing of about *4.03* angstroms from Pd to *30* atom-percent Ag-Pd. At more positive potentials *(0.1* volt, giving a low equilibrium pressure of H_2), the a-phase was formed with a spacing of *3.89* to *3.94,* depending on the amount of Ag present in the alloy.

When an electrode was immersed in H_2-saturated electrolyte, the surface took up H_2 and rapidly came to a potential corresponding to the pressure of the cy, *p* transition pressure. It held this potential until sufficient hydrogen was absorbed to form p-phase completely, and the potential then changed rapidly to the equilibrium value of *1* atmosphere of H_2; i.e., 0 volt. Thus the measurement of the pseudo-steady voltage during hydrogen absorption enabled the α and β transition pressure, p_t, to be determined as a function of Ag content and temperature. A plot of log p_t versus $1/T$ gave the standard state (e= ½) heat of absorption of H_2 in the alloy. This increased from 9.3 kcal/mole H_2 for Pd to 12 kcal/mole for 20 atom-percent Ag-Pd. At the same time, the saturation quantity of H_2 absorbed, determined by anodic discharge at 0.6 volt, decreased linearly from 0.7 H/Pd to 0.4 H per metal atom at 40 atom-percent Ag. The α, p-phase transition disappeared above 30 atom-percent Ag.

Ag-Pd alloy was cleaned by ion bombardment and the surface oxidized at 1292" to 1382" F (700" to 750" C). The rate of diffusion through an alloy membrane was then determined with H_2 on one side and vacuum on the other. The rate of diffusion was the same for the oxidized surface as for a surface reduced by H_2 at 1292" F (700" C) for a few seconds, although results were not very reproducible. Reproducibility was improved by plating with Pd black, although the surface became poisoned after 10 minutes of permeation. It was concluded that oxidation cleaned the surface, but an oxide film was not necessary for rapid H_2 absorption. Cleaning in chromic-sulfuric acid gave 10^5 lower diffusion rates. Rates were somewhat lower with Ag-Pd alloys than with pure Pd and were inversely proportional to membrane thickness, showing that they were diffusion controlled. An H_2 anode was constructed using a 2-mil, 20 atom-percent Ag-Pd membrane, palladized on both sides. In 2 *N* $HClO_4$ at 81" F (27" C), the limiting current was 30 mA/cm², although the rate predicted from the diffusion measurements was 300 mA/cm². The limiting current decreased with time, indicating poisoning or deactivation of the surface. Since anodization followed by H_2 evolution reactivated the surface to some extent, poisoning occurred on the electrolyte side. In 85 weight-percent KOH at 392" F (200" C), the limiting current was about 800 mA/cm²; polarization was about 0.15 volt at 100 mA/cm², 0.27 volt at 300 mA/cm², and 0.3 volt at 500 mA/cm². The polarization increased steadily over periods of hours.

A 25 atom-percent Ag-Pd membrane (thickness not given) was used as a hydrogen electrode in 5 *M* KOH at 194" F (90" C) (Monsanto, ***466***). The membrane was heated in air at 1562" F (850° C) for 2 hours, plated with Rh on the electrolyte side and heated in air at 1202" F (650" C) for 2 hours. The limiting current was about 400 mA/cm² at 0.2-volt polarization, and a current density of 150 mA/cm² produced 0.1-volt polarization. A 30-micron Pd-Ag membrane gave a limiting current with H_2 of 600 mA/cm² at 25" C (77" F), but was strongly poisoned by CO (Siemens-Schuckertwerke, A-G Erlangen, ref. 3.7). A 100-micron foil in electrolyte of molten KOH-NaOH at 250" C (482° F) gave 400 mA/cm² at 0.1-volt polarization and was not poisoned by CO. A 3-mil Pd-Ag foil catalyzed on both sides with Pd or Pt black was a satisfactory H_2 anode in molten hydroxide paste electrolyte, but current with NH_3 was less than 5 mA/cm² (Electrochimica *Corp.*, ***159***).

For the values of diffusion coefficient in table 3.7 and for concentrations taken from the phase diagram, the values of limiting current for a 10-mil Pd membrane at 1 atmosphere H_2 are: 86" F (30" C), $i_L = 140$ mA/cm², almost entirely in p-phase; 176" F (80° C), $i_L = 424$ mA/cm², mainly in p-phase; 392" F (200" C), $i_L = 120$ mA/cm², entirely in α-phase. The lower values at higher temperatures are due to the lower solubility of H_2, which counteracts the increased diffusion coefficient. (The problem of low solubility can be overcome by increased pressure.) Theoretically, a 1-mil membrane should give high current densities, but poisoning leads to slow surface reactions on the electrolyte side which decrease performance considerably.

Other metals have been used as H_2 electrodes in high-temperature systems. The activation energy for diffusion of H_2 through pure iron was 10.4 kcal per gram atom H (Argonne, *105*). Even at high temperatures, poisoning of the gas or electrolyte sides of the membranes occurred.

3.3 ELECTROLYTES

3.3.1 Aqueous Electrolytes

As discussed in section 3.1, the most widely used electrolytes for low-temperature cells are strong acids and bases of high conductivity. Figure 3.2 shows that H_2-O_2 cells with platinum catalysts have about 0.1 volt more polarization with H_2SO_4 than with KOH. This extra polarization occurs at the oxygen electrode. KOH is also less corrosive and can be taken to higher temperatures than H_2SO_4. For these reasons, low-temperature H_2-O_2 cells usually employ concentrated KOH solutions as electrolyte. Concentrated solutions are necessary to eliminate concentration polarization due to limiting mass transfer of OH− and to give high ionic conductivity. As cell temperature is increased, electrolyte concentration is also increased to keep the partial pressure of water vapor down to a reasonable level. This technique is used in the Pratt & Whitney medium-temperature H_2-O_2 cell.

Acid and neutral electrolytes have been investigated with the primary aim of developing CO_2-rejecting electrolytes for use with fuels contain-

TABLE 3.8.—*Results of Aqueous Electrolyte Studies*

Reference	Electrode	Reactant	Temperature	Result
19	Pt catalyzed porous C	H_2	...	0.15 volt polarization more with K_2CO_3 than KOH
	Ag on C	o 2	147" F (64" *C)*	0.2 to 0.3 more polarization with 40% K_2CO_3 than 8 *N* KOH (200 A/sq ft)
182	Pt-Pd on porous nickel 30 wt-% KOH in asbestos	Hz	77" F (25" C)	Polarization increased by presence of carbonate in KOH
		O_2 (75 psig)	77" F (25" C)	Polarization increased somewhat by carbonate in KOH
Ref. 3.4	Teflon-bonded Pt black	H_2-O_2 cell	Ambient	At 200 mA/cm²: *IR-free cell voltage* 6 *M* KOH ... 0.92 3 *M* KOH/1.5 *M* K_2CO_3 ... .75 1.5 *M* KOH/2.25 *M* K_2CO_3 .45 3 *M* K_2CO_3 ... .38
88	Teflon-bonded Pt black	H_2-O_2 cell	158" F (70" C)	20% KOH/15% K_2CO_3 gave same performance as KOH alone
256	Teflon-bonded Pt black	H_2, O_2	Ambient	IEM saturated with aqueous K_2CO_3. Large concentration polarization due to buildup of H^+ at anode and OH^- at cathode
664	Plastic-bonded catalyzed C	H_2-O_2 cell	Ambient to 158" F (70" C	KOH: 12 *N*>9 N>6 *N* for O_2. 6 *N*, 9 *N*> 12 *N* for H_2
423	Teflon-bonded Pt black	o 2	77' F (25" C)	Sodium hydrogen phosphate buffer, pH 7. About 0.5 volt polarization at 1 A/sq ft, 0.75 at 100 A/sq ft
434	Pt screen	Dissolved O_2	Ambient	Polarization decreased with increasing pH from pH 1 to 15
252	Impregnated porous C	o 2	...	Poor performance in sodium acetate-acetic acid, pH 4
213	Teflon-bonded Pt black, 20 mg Pt/cm².	Dissolved CH_3OH	Up to 392° F (200° C)	2 *N* H_2SO_4 better than 2 *M* NaH_2PO_4>2 *M* Na_2SO_4; 2 *M* KHCO, better at low temperatures, same as H_2SO_4 at 302" F (150" C)
		o 2	302" F (150° *C)*	H_2SO_4 much better than $KHCO_3$> NaH_2PO_4> >Na_2SO_4

TABLE 3.8.—*Results of* Aqueous Electrolyte Studies—Continued

Reference	Electrode	Reactant	Temperature	Result
309.	Various..	Hydrocarbons.. .	194" to 365" F (90"to 185° C)	Cs_2CO_3; $i<5$ mA/cm². Optimum at 302° F (150" C)
	Teflon-bonded Pt black. .	CH_3OH_2, O_2. . . .	266° F (130"C).	Aqueous Cs_2CO_3; 500-hour run showed invariant electrolyte.
		Hydrocarbons. . .	248° F (120° C). .	Aqueous CsF-HF; great improvement over Cs_2CO_3. Presence of CsF decreases performance at given temperature but increases boiling point. More concentrated electrolytes better
	Pt.	H_2.	. . . .	Chloride dissolved in $HClO_4$ poisoned electrode
407.	Platinized Pt screen.	N_2H_4 (dissolved)	77° F (25° C). . .	4 *M* K_2CO_3 gave 0.2 volt more polarization than 7 *N* KOH. Addition of 0.5 *M* K_2CO_3 to KOH gave 0.1 volt more polarization
460.	Various. . .	in electrolyte	194° F (90° C)	KOH > H_3PO_4 > > KNO_3, Na_2HPO_4
466.	Pt, Rh, Ir, Pd, Ag, Au..	CH_3OH. .	Ambient	Strong acid or base much superior to Na_2SO_4
457.	Various; platinized Pt foil	H_2O_2	Ambient	3 *M* NH_4Cl poor **3** *M* $KHCO_3$ better 5 *M* KOH, 5 *M* H_2SO_4 much better 14 *M* H_2SO_4 best

ing carbon. The effect of carbonate in KQH is shown in table 3.8. Although there is some disagreement as to whether the presence of small amounts of CO_3 in KOH decreases the performance of H_2-O_2 cells, it is generally agreed that KHCO, and K_2CO_3 are not satisfactory electrolytes. Cs_2CO_3 at **194**" to 266" F (90° to 130" C) does not form bicarbonate in the presence of CO_2, but the current densities with hydrocarbon fuels are low (table 3.8). Neutral electrolytes perform poorly even when buffered. Figure 3.7 shows the low performance of NaH_2PO_4 and KHCO, compared to H_2SO_4 with O_2 cathodes, even at 302° F (150" C). The use of H_3PO_4, Cs_2CO_3, and CsF-HF solutions for hydrocarbon fuel cells is discussed in chapter 15.

3.3.2 Ion-Exchange Membranes: Matrices

An ion-exchange membrane electrolyte consists of ions of one sign chemically bound to part of the membrane and ions of the other sign weakly associated with the bound ions. The weakly bound ions are free to move, under a potential gradient, in the gel-like structure of water in the membrane. Concentration polarization in the membrane is not possible because the membrane allows only ions of one sign to transport. Thus ion transport occurs via migration in the potential gradient, and Ohm's law is obeyed. Close contact between the membrane and the electrode surface is required, since the distance between ions bound in the membrane and electrode surface must be only a few angstroms to allow mobile ions to reach the electrode surface. There is evidence of contact resistance between electrode particles pressed into the membrane and the membrane: performance is better if the membrane is equilibrated with strong electrolyte to give electrolyte bridges between the membrane and the electrode. The

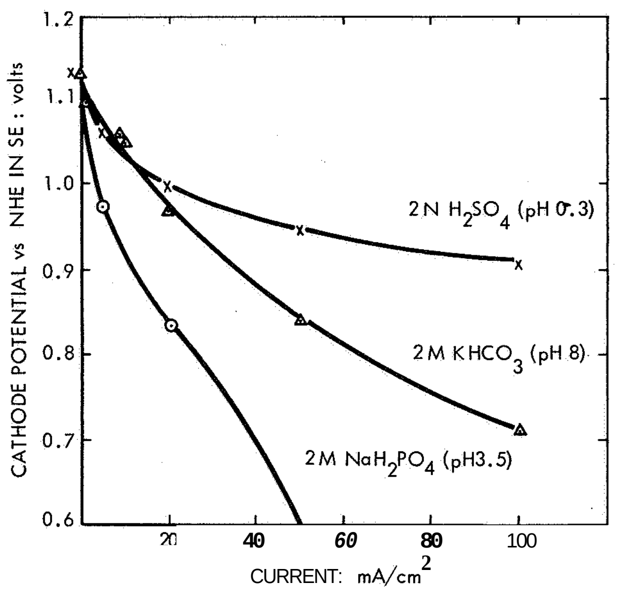

Electrodes were of platinum black and the cell was pressurized at 200 psi.

FIGURE 3.7.—Performance of O_2 electrode in various electrolytes at 302” F (150° C) *(213)*.

membrane then behaves partially as a porous matrix and concentration gradients can occur. The concentration of mobile ions cannot fall below the concentration of bond ions and, therefore, ionic-limiting currents do not occur.

Ion-exchange membranes have been applied to fuel cells most extensively by General Electric Co. Membranes were made by the usual techniques, with a supporting mesh of various materials (see app. D) to give added strength and prevent pinholes. Early cationic membranes, the polymerized phenolic resins, were replaced with sulfonated polystyrene membranes *(234)*. Commercial membranes (AMF, supported sulfonated polystyrene) had better life and were more convenient to use *(316* through *321)*. Table *3.9* gives some data on membranes prepared by General Electric. Table 3.10 describes performance of various membranes.

The requirements for IEM’s and methods of preparation were discussed in reports *316*

TABLE 3.9.—*Properties of Cation Exchange Polymers in Acid Form (248)*

Polymer form used			Measured “pK_a” value [a]	Ionic conductance at 92.5% relative humidity,[b] milliohm^{-1} cm^{-1} [c]
	Theoretical	Experimental		
Linear polyvinyl phosphoric acid. (1 proton off only)...........	9.26	7.22	2.43	0.84
Linear polystyrene sulfonic acid....	5.45	2.99	.50	140.
Crosslinked polyacrylic acid.......	....	....	6.00	.07
Linear polyacrylic acid............	13.9	12.5	5.70	.10
1.15 moles HCHO per mole p-phenolsulfonic acid...........	[d] 3.75	3.13	2.14	[e] 68.
1.25 moles HCHO per mole p-phenolsulfonic acid...........	[d] 3.55	2.90	2.22	[e] 44.
1.40 moles HCHO per mole p-phenolsulfonic acid............	3.08	2.40	2.29	[e] 35.
1.55 moles HCHO per mole p-phenolsulfonic acid............	[d] 2.77	2.10	2.40	[e] 29.
Polyvinyl toluene sulfonic acid 13.5% crosslinked....................	5.04	4.60	.90	187.
Polyvinyl sulfonic acid............	9.26	8.42	.45	480.
Polystyrene sulfonic acid...........	6.45	1.93	1.20	80.
Polystyrene-DVB PO_3H_2...........	5.00	4.31	2.25	.40

[a] −log (free H ion concentration).

[b] Conductivity drops as membranes dry out.

[c] Higher values are better.

[d] Assumed mol. wt. or “mer” unit based on ion exchange capacity, signifying amount of crosslinking caused by some excess formaldehyde bridging at sites of hydrolyzed-off SO_3H groups. Linear value = meq /g.

[e] Measured at 100% relative humidity.

TABLE 3.10.—*Experience With Ion-Exchange Membranes in Various Systems*

Reference	System	Result
216.........	$CH_3OH/H_2SO_4/O_2$..........	Ionics CR-61 best; Nalfilm D–30 too porous and allowed CH_3OH to diffuse to cathode. AMF C–313, IR too high
217.........	....	Permion 1010 (Radiation Applications, Inc.) best. IR loss, 0.01 volt at 50 mA/cm^2
		Nalfilm D–30 treated with decane allowed CH_3OH to diffuse through but not water
234.........	General Electric H_2-O_2 cell. . .	Sulfonated polystyrene resins preferred over phenolic resins (phenol-sulfonic-formaldehyde)
238,239,240.	H_2-O_2 electrolytically regenerative	Acid membranes had short life. Best anionic membrane Zerolit Type A–20, hydroxide form (United Water Softeners, Ltd., Gunnersbury Avenue, London, England)
285.........	General Electric H_2-O_2 cell. . .	Sulfonated polystyrene from AMF (American Machine & Foundry, Inc.) preferred over previous membranes
456.........	Dissolved N_2H_4/membrane/ HNO_3	AMF–A104 (anionic) allowed NO_3^- to pass. AMF–C103 (cationic) allowed N_2H_4 to pass, possibly as $N_2H_5^+$. AMF–C103 stable when separating acid solutions, but blistered with acid on one side and base on the other; Ionics AR–111–A, stable
460.........	....	Cationic membrane passed N_2H_4 at rate of 130 mA/cm^2 at open circuit
605.........	H_2-O_2, H_2SO_4, 140° F (60° C).	Ionics 61–A2G best of several tested. With Teflon-bonded Pt black electrodes, gave 130 mhos/ft^2 (about 7 ohm-cm^2)

through *321.* In addition to high ionic conductivity, other requirements are: good temperature, chemical, and dimensional stability; no pinholes; and slow diffusion of H_2 and O_2 through the membrane. The electrical resistance of a membrane depends on how firmly ions of opposite sign are associated. Weak association allows the mobile ion to move, while strong association gives high ohmic resistance. Loss of water from the membrane increases the concentration of ions in the remaining gelled water, thereby increasing association and ohmic resistance.

Liquid organic fuels diffuse into membranes and decrease the dielectric constant of the gel system. This increases the degree of association, and ohmic resistance increases. Transport of water by electroendosmosis is also important. The voltage acting on mobile ions tends to move fluid through the membrane. This force is not counteracted by a force due to other ions moving in the opposite direction, because those ions are fixed. Consequently, water moves with the transporting ion, tending to dry out one face of the membrane and flood the other. (In general, drying of a membrane, which typically consists of 50 to 80 percent by weight of water, cannot be tolerated since it leads to dimensional change and irreversible loss of performance.) It was suggested *(321)* that mosaic cationic-anionic membranes could be made consisting of cationic membrane with low-pore size and a small amount of anionic membrane with large-pore size. The small fraction of current carried by the anions would provide a reverse osmotic flow sufficient to balance the cationic flow.

Table *3.11* gives compositions and properties of relatively low-resistance membranes made during this contract. Epoxy crosslinking gave dimensional stability in water and DMF was considered the best solvent. Epon **828** could not be used as the sole matrix, since the membranes were then brittle and of high resistance. Attempts to use the membranes in H_2-O_2 fuel cells with platinized carbon or impressed platinum black electrodes were not successful. For example, membranes used in a small General Electric

TABLE 3.11.—*Properties* of *IEM's Prepared in Reports 316 through 327*

Matrix	grams	Polyelectrolyte	grams	Solvent	ml	Thickness, microns	Resistance, ohm-cm²	Remarks
Dynel		MPVI	1	PCO_3	8	128	2.1	Strong
Dynel		BPVI	1.25	DMF	8	62	.7	Hydrophobic
Dynel		BPVI	1.25	Eth CO_3	8	150	.3	
Dynel		MPVI	1.25	Eth CO_3	8	150	.5	
Dynel	1.5	BPVI	2	PCO_3	14	120	1.2	Strong
Dynel	1.0	BPVI	2	Eth CO_3	12	160	1.0	
Dynel 828 TET	10 1.0 .1	BPVI	2	DMF	12	28 58	1.2 1.8	Strong Strong
Kynar	0.88	BPVI	0.75	DMF	9	78 22	6.4 2.6	Saran-like, very strong Saran-like, very strong
Kynar	0.88	MPVI	0.75	DMF	9	....	....	Weak
Kynar Dynel	0.8 1	PSA 0.6 BRL	0.33	DMF	16	....	4 5	Strong
Kynar 828	0.75 .12	PSA	0.5	DMF	7			Strong, homogeneous
Kynar	0.5	PSA 0.5 Epon	0.05	DMF	4	....	1.2	Strong

See app. D, table D.8, for materials code.

H_2-O_2 cell gave *1* mA/cm² at 0.5 volt. No explanation was provided *(325).* Mosaic membranes were prepared *(324, 325).* Performances of some of the Gregor membranes in the General Electric H_2-O_2 cell are given in report *229,* but since no cross-reference was given, it is not possible to match performance against composition. The best short-term performance quoted was 0.8 volt at *100* A/sq ft.

The resistance of anionic membranes equilibrated with KOH solution was measured as a function of KOH concentration (Ionics, *343).* For concentrations less than *1 N,* conductivity was proportional to concentration, but between **1** and *12 N,* the resistance was 0.9 to *1.1* ohm-cm² for a membrane *0.041* cm thick. This was 10 times the resistance of the same thickness of KOH. Similar results were found with cationic membranes in HCl. A H_2-O_2 fuel cell was built with the electrolyte contained between two membranes. The saturated membranes prevented electrode flooding, but behaved similarly to porous matrices, since concentration polarization resulted from mass-transfer restriction in the membrane; the membranes had to have high diffusivity to give high limiting currents.

Table *3.12* gives gas permeabilities of some IEM's and table *3.13* gives rates of electroosmotic water flux. Table *3.14* gives some information on porous matrices used for low-temper-

TABLE 3.12.—*Gas Permeabilities* of *IEM (General Electric, 263)*[a]

Membrane	Gas	Permeability, cm³/sec-atm-cm²
Polyphenolsulfonic acid-formaldehyde	H_2 O_2	$(2.5)(10^{-8})$ $(5.2)(10^{-8})$
Sulfonated polystyrene	H_2 O_2	$(5.4)(10^{-8})$ $(3.7)(10^{-8})$
Sulfonated polystyrene plus polytrifluorochloroethylene	H_2, O_2	(1 to 4) (10^{-9}) Long induction period of 1 to 12 minutes before steady state reached

[a] Ref. 3.8.

ature fuel cells. When ion-exchange membranes are saturated with concentrated electrolyte before use, they can be considered as porous matrices, which retain electrolyte and retard electrode flooding. Porous asbestos is used for the same purpose in Allis-Chalmers, American Cyanamid, and Electro-Optical Systems cells.

TABLE 3.13.—*Electro-Osmotic* Water *Flux* Through Ion-Exchange Membranes

Reference	Current density, mA/cm^2	Electro-osmotic water flux, g H_2O/cm^2-sec
290 (General Electric)	1	$(7)(10^{-7})$
323 (Gregor)...	20	$(1)(10^{-4})$
	10	$(0.6)(10^{-4})$ (almost linear with current density)
	25	AMF–C103: $(1.3)(10^{-5})$ AMF–A104: $(2)(10^{-5})$

TABLE 3.14.—*Porous Matrices for* *Low*-Temperature Cells

Reference	Preparation
25.......	Add Methocel 90 H.G. (Dow) slowly to hot 15% KOH with ultrasonic stirring. Formed gel stable for at least 2 months
30.......	Johns-Manville carbonate-free asbestos, 50 mil thick
59.......	Asbestos membrane requires 100 psi to blow out all liquid
167......	Asbestos membrane absorbs 0.7 part by wt. 35 wt-% KOH per 1 part of dry asbestos. Could stand up to 10-psi pressure differential across 1/16-inch electrolyte-filled membrane before gas passage
185......	Compression of porous asbestos (Johns-Manville, 32 mil), 2 layers, from 66 mils to 25 to 35 mils, eliminated variation of performance in H_2-O_2-KOH cell
87.......	Membranes for 35 wt-% KOH. Johns-Manville fuel cell asbestos, 10 to 20 mil thick, assembled at 120 to 180 psi; 0.5 to 1.0 g KOH/g asbestos, gave minimum resistance; ACCO asbestos, 20 to 40 mil, 60 to 100 psi; 1.5 to 3.0 g KOH/g asbestos, gave minimum resistance
217......	12-mil porous carbon filled with 30% H_2SO_4 used to replace IEM. Pore size in range 100 to 350 μ. No details of preparation given. 6-inch hydrostatic head gave no flow through the membrane
126......	Microporous rubber matrix, 32 mil thick, 45% porosity, satisfactory in 85% H_3PO_4 at 120° F (49" C) (American Hard Rubber, Amerace Corp., Butler, N.J.)

Inorganic membranes have been constructed of zeolitic materials (Astropower, *121*). These materials are in the form of small crystals (1 to 5 p) and have crystal structures containing small cavities interlinked with holes. For example, Linde 3A and 5A synthetic zeolites have cavities of about 12 angstroms diameter joined by holes of effective diameter about 3 and 5 angstroms, respectively. The effective diameter is determined by the sizes of molecules which will or will not readily diffuse through the materials. The cavities absorb water very strongly, and Na^+, K^+, Ca^{++} are displaced from the structures, giving ion-exchange properties. Teflon, PVC, phenolics, and silicone rubbers were used as binders, but the powder-binder mix has insufficient strength even up to 30 weight-percent binder. Epoxy resins had to be used at 20 to 30 weight-percent to give strength; at this level the ion-exchange capacity was low. Sodium silicate and proprietary silicate mixtures were not effective.

Membranes were formed by cold pressing or casting mixtures of zirconia, zeolite, and phosphoric acid solution, followed by sintering to form oxide-phosphate bonding. ZrO_2 was stabilized by precalcining; otherwise low strength was obtained. Fibers were used to strengthen the membrane; acid-washed asbestos and aluminosilicate fibers were not satisfactory but zirconia and calcia-stabilized zirconia (H. I. Thompson Fiber Glass Co., Tech. Bul. Nos. 1 to lb) fibers were. Hot pressing or flame spraying of the mix was not satisfactory.

Mixtures of Zeolon (Norton Co., synthetic mordenite), ZrO_2, and H_3PO_4 were pressed at 10 to 15 tons/in^2, dried at 302" F (150° C), and sintered between 662" to 1292" F (350" to 700" C) for 15 to 24 hours. Final thickness was about 1 mm. The resistance was measured by ac with Pt electrodes pressed against the membrane. It was concluded that a conductive zirconium phosphate polymer was formed. However, performance as an H_2-O_2 fuel-cell membrane with American Cyanamid electrodes was poor unless the membrane was immersed in water for 10 seconds before use. Even with this wetted membrane and with a layer of platinum black between electrode and membrane, the cell produced only 50 mA/cm^2 at 0.5 volt. The effective cell resistance was 8 ohm-cm^2, while the ac resistance of the membrane alone was 2 ohm-cm^2.

Mineral ion-exchange membranes were also studied by SERAI *(568).* Solutions of salts of Sn, Ti, Ni, or Ge were treated with a stoichiometric excess of H_3PO_4 and deionized water. A gel formed on stirring for some hours. This was rinsed and dried at less than 86" F *(30"* C), giving white crystals of metal phosphate ion-exchange polymers. The crystals were made into membranes by fine grinding, adding a binder in water, mixing in a high-speed mixer, forming the membrane on a clean glass surface, drying slowly, and peeling off the membrane. Collodion and ethyl cellulose were too resistive, but a suitable starting mixture was 10 grams carboxy methyl cellulose and 10 grams ion exchange polymer in 700 cc H_2O. The membrane was soaked in 5 weight-percent H_2SO_4 solution for some hours. Ionic resistance was about 2 to 5 ohm-cm^2 for thicknesses of 0.1 to 0.2 mm. It was used as a membrane in an H_2-O_2 fuel cell, with electrodes of porous carbon electroplated with platinum black. Open-circuit voltage was 0.9 volt, the maximum current was 50 mA/cm^2, and the effective cell resistance was 10 to 20 ohm-cm^2. The report contains a large measure of theoretical discussion of dubious value; the electrochemical testing was performed using relatively crude techniques.

3.3.3 High-Temperature Electrolytes and Matrices

The most important high-temperature electrolytes at present are eutectics of molten Li/Na/K carbonates and the Westinghouse solid electrolytes (see ch. *6*). The molten carbonates are usually retained in porous ceramic matrices of MgO, but they can also be used as a paste with fine powder MgO. The preparation of paste electrolytes is summarized in table *3.15.* Contract reports *147* and **148** contain a great deal of information of the various methods of shaping these paste electrolytes.

Table *3.16* gives details of ceramic matrices for molten-salt electrolytes.

Preparation of solid electrolyte of calcia-zirconia was described as follows (Westinghouse,

TABLE 3.15.—*Preparation of Paste Electrolytes*

Reference	Electrolyte	Preparation
81........	Molten: KOH, 70; KBr, 15; KI, 15 (mole-%)	Fused 0.08 μ MgO (Fisher Scientific, Morton Chemical Co., Electronic grade, M–300) was better than 0.05 μ light calcined MgO or 5 μ MgO. Electrolyte mixed, melted at 10^{-3} torr for 2 hours, 650" F (343" C), in Ni can. Solidified quickly under dry argon. Ball-milled to <60 mesh. Repeat with admixture including MgO. Pressed in hardened steel die, dry argon atmosphere, 30 000 psi, to form disk. Disk packed in bed of 5 μ MgO, baked 1 hour 650" F (343" C) under vacuum, cooled in dry argon at 10" F/hour. The baked disk was only 80 to 95% of theoretical density but was impermeable to gas even at 30-inch water gage. The 0.08 μ fused MgO could retain 65% weight electrolyte; 4-inch diameter, ⅛-inch-thick disk had strength of 4 psi. Formation factor was 2 to 3.
147, 148..	Molten Li/Na/K carbonates...	MgO of mean size 0.05 to 0.10 μ. Best mixture was 50:50 wt-%. Mixture heated at 1292" to 1472" F (700" to 800" C), cooled, ground to fine powder, reheated to 1292" to 1472" F, reground. Powder placed in graphite-coated mold, cold-pressed at >800 kg/cm^2. Heated to about 72" **F** or 40" ***C*** above melting point and hot-pressed at 2000 kg/cm^2. Final density was 96% of theoretical. Hot paste could also be extruded into a mold through a 2-cm hole, and gave good density forms.

TABLE 3.16.—*Matrices* for ***Molten-Salt Electrolytes***

Reference	Electrolyte	Preparation
489......	Na_2CO_3, 43; precalcined monazite sand, 27; WO_3, 20; Na_2SiO_3, 10(wt-%)	Mix, melt, cool, crush to fine powder under infrared lamp to prevent caking by moisture, press 10 to 20 tons/in.^{2} in graphite-lubricated mold. Sinter 1382" F (750°C), 1 to 2 hours, cool slowly. Porous and weak. Conductivity due to liquid phase.
490......	Same as above..............	Heat to 2282" F (1250" C) and pour. 2 phases observed.
491......	Na_2CO_3, Na_2SiO_3, small amount ceria (nominal Na_4SiO_4)	As above. Fused stronger, but became porous with time at 1382° F (750° C). Liquid phase at 1382" F.
494......	Above plus more Na_2CO_3....	Na_2SiO_4 dissolves in Na_2CO_3, recrystallizes as large crystals. Porosity develops and grows weak.
496......	Na_2CO_3, Li_2CO_3 in refractory matrix	Harbison-Walker periclase ground through 65 mesh, make paste with 2% aq. methylcellulose, press 4200 psi. Fire 2642" F (1450° C), 14 hours.
499......	....	MgO (Baker) calcined 2732° F (1500° *C)* to form periclase. Grind to <65 mesh. Mix with 5 to 10% caruba wax in CCl_4, warm to drive off CCl_4. Press 2500 psi, 10 minutes. Fire. Matrix disks still breaking in use.
500..	....	Calcined MgO of 100 x 270 mesh used in above. Press at 4000 psi.
506.....	....	As ahove. Fire 1 hour, 2732" F (1500" C), cool, turn over and fire 5 hours 2732° F (1500° C). Gave flatter and more strain-free matrix. Labyrinth factor approximately 3.
607......	Equimolar Li_2CO_3, Na_2CO_3.	Norton LM 833: MgO disks, 31% porosity, 18μ pores. LM 833A: 40% porosity, 24μ pores.
	Ni, Ag, Zn fuel electrode, Ag cathode	Addition of Na_2MoO_4, Na_2CrO_4, Na_2WO_4, or Na_2ZnO_2 to electrolyte gave no improvement. Addition of Na_2S gave improvement, attributed to production of higher Ag area by sulfide ion.
68......	KOH-KBr-KI...........	LM 833 MgO (Morganite, Inc., Long Island City, N.Y.). Porosity 40 to 45%, pore size 20μ. Formation factors 4.2 to 11.8. LA 831 MgO. Formation factor 4.2.

790). $CaCO_3$ (99.87 percent) and ZrO_2 (99.8 percent) powders were blended in the proportions desired to give $(CaO)_{0.15}(ZrO_2)_{0.85}$. The mixture was calcined at *2462"* F (1350° *C)* for 5 hours, cooled, and ground for 80 hours in a ball mill with SiO_2 balls. The powder was mixed with an organic binder (see app. D) and pressed to the required shape. This was presintered to decompose the binder and fired at *3002"* F *(1650"* C) for *4* hours. The electrolyte should have a density at least 95 percent of theoretical. $(ZrO_2)_{0.9}(Y_2O_3)_{0.1}$ solid electrolyte was prepared similarly (the relation of conductivity to temperature for these materials is given in app. B). The electrolyte powder after the ball-milling step could also be slip-cast into shape, using a paste with HCl of carefully controlled pH **(793).**

3.4 REFERENCES

3.1. WALKER, P. L., JR.; RUSINKO, F., JR.; AND AUSTIN, L. G.: Advances in Catalysis, Vol. II, 1959, pp. 133–221.

3.2. JUSTI, E.; PILKUHN, M.; SCHEIBE, W.; AND WINSEL, A.: Akad. der Wissenschaften und der Literatur, no. 8, Mainz, 1959.

3.3. DITTMAN, **H.** M.; JUSTI, E. N.; AND WINSEL, A. W.: Fuel Cells. Vol. II, ch. 10. G. J. Young, ed., Reinhold Pub. Corp., N.Y., 1963, p. 133.

3.4. BACON, F. T.: Fuel Cells. G. J. Young, ed., Reinhold Pub. Corp., 1960, Chap. 5, p. 51. Brit. Patent 950 096, U.S. Patent 3 167 457.

3.5. NIEDRACH, L. W.; AND ALFORD, H. R.: Electrochem. Soc. Vol. 112, 1965, p. 117.

3.6. ANDRUS, D. E.: Hydrogenation With Pd Diaphragms. Ph. D. thesis, Univ. of Wisconsin, 1960, 340 pp.

3.7. Venture-Tech, Inc.: Fuel Cell Progress. Vol. 3, no. 8, Mar. 1965.

3.8. BROWN, W. E.; AND Sauber, W. J.: Dow Gas Transmission Cell for Low Permeability of Gases Through Membranes. Modern Plastics, Aug. 1959.

CHAPTER 4

Cell and Stack[1] Construction: Low-Temperature Cells

4.1 GENERAL FEATURES OF STACK CONSTRUCTION

Many types of small laboratory cells are used for initial testing, but certain features are common to almost all designs of practical cell stacks. For instance, flat disk or plate (rectangular) electrodes are normally used to obtain high-power density per unit volume and low electrolyte resistance. These electrodes are placed face to face, with minimum electrolyte spacing between them. Such cells are readily stacked in series to form a module, with the cathode of one cell connected, usually internally, to the anode of the next. The module resulting from stacked plate cells can, in theory, be combined with other modules in a minimum of space. However, the corner areas of rectangular electrodes may become starved of reactant, and fragile ones are hard to produce without breakage. Disk electrodes are somewhat easier to construct, since they have no weak corners and can be removed from molds without excessive breakage.

Weight, volume, and cost of fuel-cell stacks are reduced by channeling the reactants through passages in the cell frame, rather than supplying them from external feeds to each electrode. The feed can be either in series or in parallel, as illustrated in figure 4.1, and a number of possible combinations of feed systems exists. For example, one system uses series flow of hydrogen from an inlet at one end of the stack, countercurrent to oxygen with its inlet at the other end. (Countercurrent or parallel in this context refers to flow of fuel and oxidant from one end of the stack to the other.) In addition, the fuel and oxidant can be run countercurrent or in parallel from top to bottom (or side to side) of the cell's chambers. Generally, parallel flow from common manifolds (fig. 4.1) is used because it insures good reactant feed to each cell. Hydrogen and/or oxygen either can be recirculated from the outlet back to the

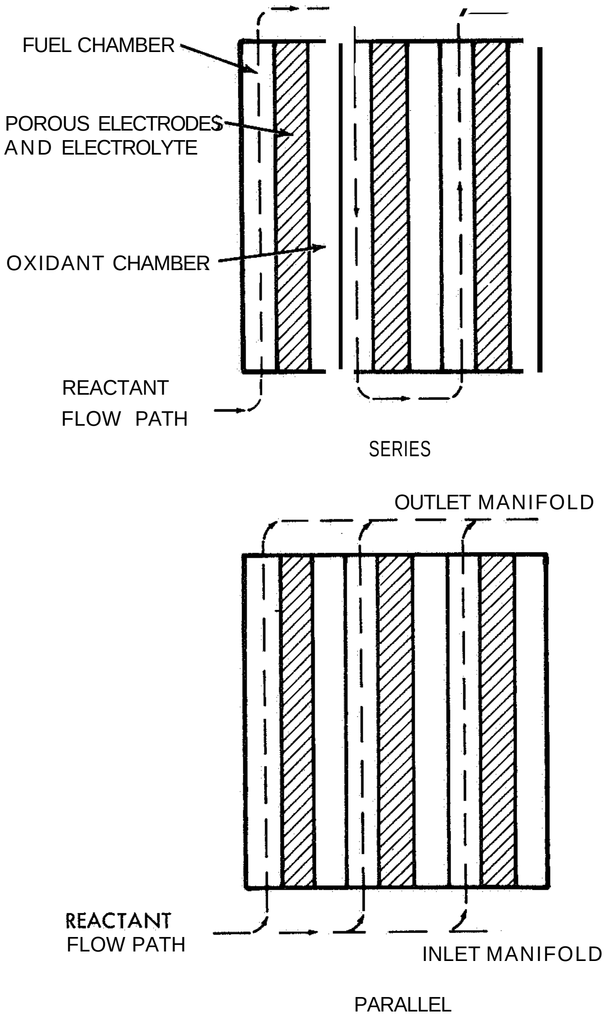

FIGURE 4.1.—Series and parallel feed of a reactant (hydrogen, for example) through a fuel-cell stack.

---

[1] The term "fuel battery" has not been used here (even though it is literally correct) because it carries connotations of conventional batteries.

PRECEDING PAGE BLANK NOT FILMED.

inlet or can be dead ended. A dead-ended cell has gas input but no outlet, so that the gas feed is entirely consumed in the cell. Nonetheless, outlet manifolds are usually necessary in a dead-ended cell to permit purging of the gas chambers (see sec. 2.1.5). Typical case manifolding can be seen in figures 4.5 and 4.17.

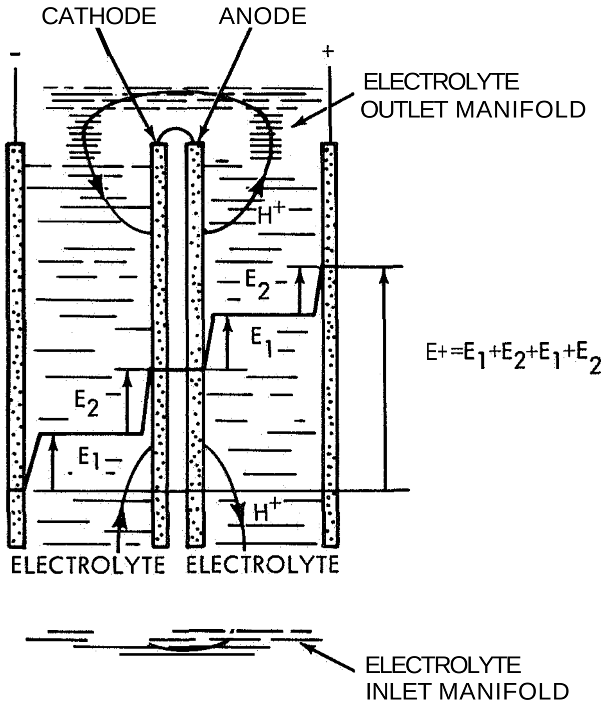

Connection of electrolyte *A* to electrolyte *B* by the electrolyte manifold allows self-discharge of the two cells, giving parasitic current and loss of potential.

FIGURE 4.2.—Effect of electrolyte manifold.

For cells in which free liquid electrolyte is used or where moisture is removed by circulating the electrolyte, electrolyte is added to the chambers through inlet and outlet manifolds. An electrolyte manifold joins all the electrolyte of the individual cells by an ionic bridge; figure 4.2 illustrates what happens when two cells are connected in series. Each half cell tends to come to its equilibrium voltage (E_1 and E_2), and the ideal OCV is $2E_1+2E_2$. However, when the electrolytes are joined by an ionic bridge, positive charge flows from high potential to low and tends to equalize the electrolyte potentials. Positive ions are produced at the central anode and taken up at the central cathode, and fuel and oxidant are consumed. Thus the two cells self-discharge and the OCV is less than ideal. This parasitic current may be kept at a reasonable level by dimensioning the manifold to give a high-resistance path between electrolyte chambers (see fig. 4.3). Obviously, series manifolding gives a higher resistance than the parallel arrangement. Manifolds must also be designed for suitable pressure balance among the fuel, electrolyte, and oxidant chambers, to prevent flow of electrolyte through a porous electrode or bubbling of gas into the electrolyte chamber.

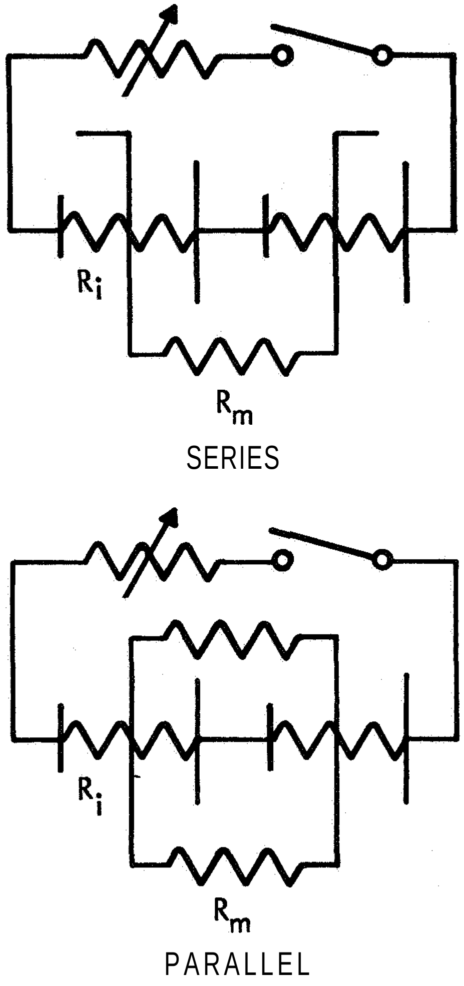

Ri is the internal (ionic) ohmic resistance between electrodes, while Rm is the (ionic) ohmic resistance of the electrolyte path through the manifold. Internal parasitic current under load is small when Ri/Rm is small. Series connection of the electrolytes gives a larger total resistance to parasitic current.

FIGURE 4.3.—Equivalent circuits for common electrolyte manifolding in parallel or in series.

Since gas spaces are necessary to distribute fuel or oxidant over the face of a porous electrode, and since the electrodes and electrolyte matrices used may be thin, the interior of the cell is not necessarily rigid. This leads to two major construction and assembly problems. First, use of a free electrolyte can cause buckling of the electrodes, allowing them to touch each other across the electrolyte space and thus short-circuit the cell. An insulating electrolyte matrix prevents this problem. Second, if the components are fragile, buckling can lead to breakage or tearing. Fracture of an electrode, an electrolyte matrix, or a gas separation barrier leads to mixing of fuel or oxidant. Not only will the cell involved malfunction but fuel and oxidant might react nonelectrochemically at catalyst surfaces, burning large portions of the stack. In addition, when reactant manifolding is used, a fracture leads to mixing of fuel and oxidant, which may extend into the manifolds causing feed of a mixture of reactants to other electrodes, which is very deleterious to performance.

Usually, frames of cell components are bolted together to form a continuous, rigid, leaktight case. As an alternative, the cell stack may be placed between end plates joined by a number of spring-backed tie rods. There are three principal methods of mounting cell components. When the electrodes are strong (able to withstand unequal forces on each side), the bipolar electrode assembly shown in figure 4.4(*a*) can be used. It consists of the cathode of one cell, the anode of the next cell, a thin gas barrier between them, and an electronic connection between cathode and anode, all mounted in a frame or frames. The electrodes can be strengthened by rigid connections between electrodes and gas barrier, providing the connections allow good gas distribution over the electrode. When the electrodes are fragile, the metal barrier can be made thick enough to provide rigidity, with channels for gas distribution cut in the faces. An electrode is then supported flat against the metal barrier face on one side (see fig. 4.18, for example). The other side has to be supported by an electrolyte matrix. With a rigid electrolyte matrix, both electrodes of one cell can be mounted on it as shown in figure 4.4(*b*). Finally, when none of the components is rigid, permeable packing in the fluid chambers can give reasonable strength to the assembled stack. If rigid frames are used in this case, close size tolerance and careful assembly are required to prevent the components from shifting with respect to the frames, which may rupture the components. With flexible frames, the pressure necessary to seal the stack is applied by bolting the assembly between heavy end plates, which spread the pressure over the whole cross section of the stack rather than over the frames alone.

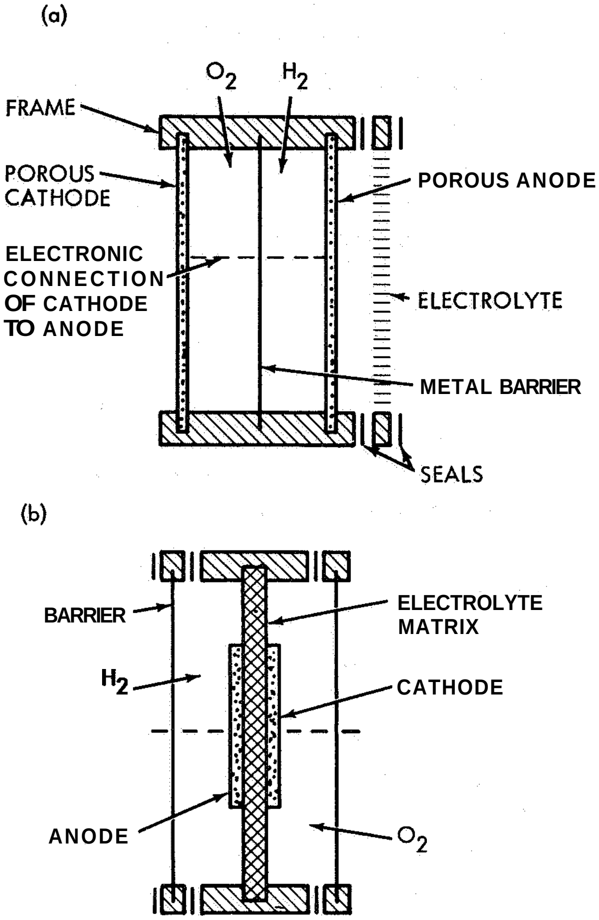

FIGURE 4.4.—Mounting of electrodes. (*a*) Bipolar mounting for rigid electrodes. (*b*) Electrodes mounted on electrolyte matrix.

Cell and stack construction of the most advanced cell systems are discussed below. The different techniques are best illustrated by reference to actual cell designs that have been developed.

4.2 THE UNION CARBIDE CO. HYDROGEN-OXYGEN CELL

4.2.1 Carbon Electrode Fuel Cells, May *1960* to December *1962*

The purpose of this contract was to package a 560-watt system and test it for feasibility, without consideration of size or weight optimization (*651*). The basic cell has been described in section 2.2.2. It is a low-temperature, hydrogen-oxygen cell using concentrated potassium hydroxide electrolyte (13 to 14 *N*). The electrodes were ¼- by 6- by 6-inch porous-carbon electrodes (activated and catalyzed according to proprietary procedures) encased in injection-molded, rubber-modified polystyrene frames. Figure 4.5 shows the cell components. Manifolding of the electrolyte by holes through the frames can be seen clearly. Not visible, however, is the channel in the frame just above the inlet holes, although the feeder slots in the frame which spread the electrolyte over the face of the electrode can be seen. Similar slots are present at the electrolyte outlet. The carbon electrodes were sprayed with a thin porous layer of nickel on the gas-entry face, which made good electrical contact with the mesh packing in the gas chambers. This was a flat, wire-woven mesh of silver-plated copper, which acted as a gas spreader and as electrical contact between the electrode and the metal gas barrier (2-mil stainless steel, silver plated). Thus the assembly is bipolar. A rubber button fixed in the center of the electrolyte face of the carbon prevented contact of the electrodes in case of buckling of the assembly. The electrolyte chamber was also filled with a 3-mil felted-fiber mat of Dynel. Oxygen and hydrogen were manifolded through the case.

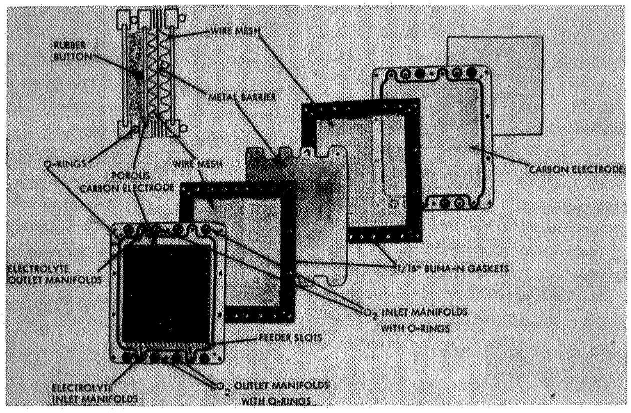
RUBBER BUTTON
WIRE MESH
METAL BARRIER
O-RINGS
POROUS CARBON ELECTRODE
WIRE MESH
CARBON ELECTRODE
ELECTROLYTE OUTLET MANIFOLDS
1/16" BUNA-N GASKETS
O_2 INLET MANIFOLDS WITH O-RINGS
FEEDER SLOTS
ELECTROLYTE INLET MANIFOLDS
O_2 OUTLET MANIFOLDS WITH O-RINGS

FIGURE 4.5.—Unit cell construction of Union Carbide H_2-O_2-KOH cell *(651)*.

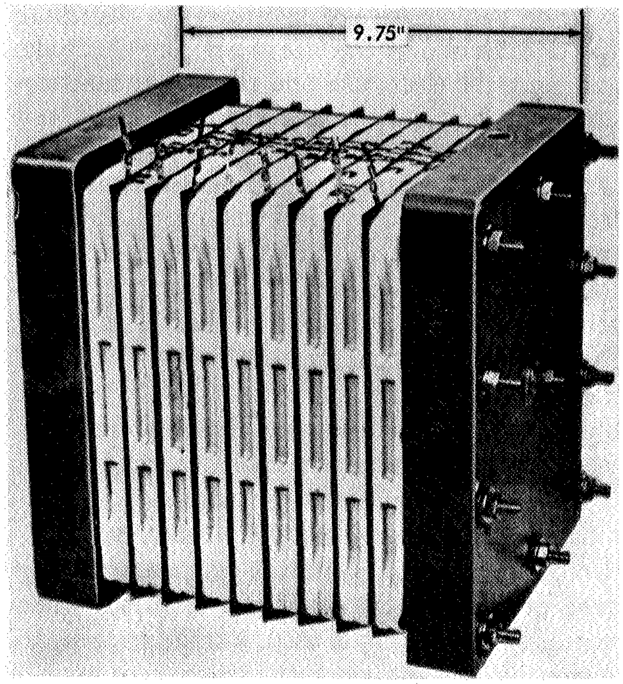

FIGURE 4.6.—Module of Union Carbide cell *(651)*.

A nine-cell stack was constructed (see fig. 4.6) with tie bolts and followup springs at 15 in-lb torque. This module had a nominal rating of 70 watts at 7 volts (volume about ¼ cubic foot). A 560-watt unit consisted of eight modules connected as four parallel pairs in series. The output of each cell was about 40 A/sq ft at 0.8 volt, giving 20 amperes at 28 volts. When oxygen of 99.5 percent purity and hydrogen of 99.98 percent purity were used, a purge (see sec. 2.1.5) of 3 minutes once every hour was satisfactory (giving about 3 percent loss of reactants). A laboratory test of this unit showed some control problem, and over a period of 50 hours the voltage fell from 29.5 to 24.0 volts as the current was increased to maintain the output at 560 watts. Voltage efficiency was 65 percent and thermal efficiency 45 percent. When switched on at 50 A/sq ft, the unit took about 2 seconds to reach almost steady voltage, with another few seconds to reach complete steady state; similarly, switching off gave the major voltage change in 4 seconds. Temperature had little effect on the system at low currents, but at 50 A/sq ft a change from 95" to 135" F (35" to 57.2" C) gave almost 0.1 volt more per cell. Cell temperature was limited to 158"F (70"C) by the plastic frame.

Later work *(652)* showed occasional failure of cells due to carbon dust, which prevented bonding of the plastic frame to the electrode and led to leakage. Preheating the electrode, covering the edges with polystyrene cement, and then molding the frame to the electrode was tried. When thinner electrodes were used (1/8 inch), shrinkage of the plastic frame caused hoop-stress buckling of the electrode. Also, short lifetimes were caused by irreversible wetting of the electrodes where cold hydrogen entered the anode. Hydrogen was subsequently preheated about 20" F above battery temperature (using 10 watts of the 560-watt output).

Parallel electrolyte manifolding gave the least pressure loss but led to higher parasitic current (1.2 to 2 A/sq ft). A satisfactory flow rate of ½ to 1 milliliter per second per cell gave 114" F (45.6° C) at the inlet and exit of the stack and 126" F (52.2" C) in the middle. It was not sufficient to allow for the pressure drop of fluids through the modules; the electrolyte head had to be considered. At gas pressures of 10 inches (water gage) below the electrolyte pressure, electrolyte leaked through the electrodes.

The unit was shock, vibration, and acceleration tested without deleterious effects.

4.2.2 Low-Temperature Fuel-Cell Battery, July 1960 to February 1961

The object of this contract was to build a 28-volt, 200-watt unit with a total weight of 35 pounds or less for 24 hours of use, with a life of 1000 hours *(653)*. The contract was terminated because the cell would not give satisfactory power with air so the weight restriction could not be met. The basic cell design was that described above. It was estimated that the fuel system and fuel would weigh 14 pounds, accessories 12 pounds, and the fuel cell 60 to 30 pounds (depending on current density). Thus, electrode thickness and cell weight had to be reduced and the A/sq ft rating improved.

Modifications made to the cell design in figure 4.5 were *(a)* ⅛-inch electrodes and *(b)* replacement of O-rings by neoprene frames, which were elastic enough to give tight seals at the edges and at the manifold holes. Use of transparent plates and dye injection showed that the slotted-electrolyte arrangement indicated in figure 4.5 was necessary for good electrolyte distribution. Simpler entry ports caused streaming from inlet to outlet, leaving much of the electrode area immersed in relatively stagnant electrolyte. It was also shown that ohmic loss in the electrolyte (0.067 to 0.082 volt at 50 A/sq ft) was about 90 percent of the total ohmic resistance.

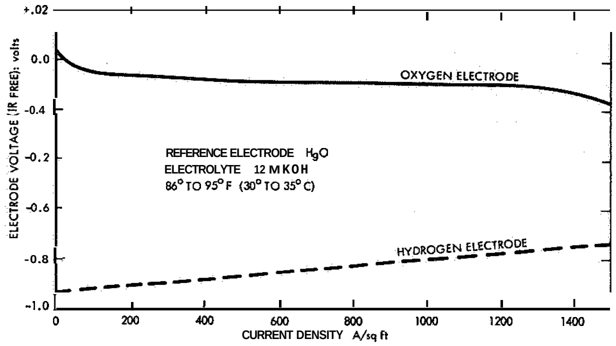

FIGURE 4.7.—Polarization as a function of current density for half-cell tests on Union Carbide carbon electrodes (652).

Figure 4.7 graphically depicts the results of improvements in electrode fabrication. Also, the lifetimes of cells were improved so that at 50 A/sq ft, 80 percent lasted to 2000 hours, and 95 percent to 500 hours. However, limiting currents of 35 to 50 A/sq ft were obtained with air instead of oxygen and were not improved by rapid air flow (see sec. 2.1.7).

4.2.3 H_2-O_2 Prototype Fuel Cell, 1960 to Present

The earlier reports for this contract were not available, but it appears that the objective was to consider the feasibility of using the cell for submarine or marine propulsion. The basic cell was the same as that considered in section 4.2.1, but the reports show steady development. For example, in February 1962 *(654)* the molded frame was replaced by a snap-on frame of neoprene sealed to the electrode with epoxy. This construction gave less loss of electrodes by breakage. Extruded polyethylene or polypropylene (Exmet pattern) mesh was used on both sides of the Dynel felt in the electrolyte chamber. This packing was necessary to provide good electrolyte flow and prevent loose carbon particles from bridging the electrolyte *(655).* Electrodes were scaled up to *12* to *14* inches with no loss of performance; these were also satisfactorily shock and vibration tested. Life was improved by eliminating stainless steel from the electrolyte circulation system, since a buildup of poison was discovered in the electrolyte (fresh electrolyte improved performance). Loss of power with time was also reduced by precompressing the nickel-mesh bipolar packing to *16* to *20* psi. This material had been weakening with time and as a result not pressing firmly against the electrode, thus giving high contact resistances (see table *4.1).*

TABLE 4.1.—*Resistance of Nickel Flat Wire Mesh Compressed Between Ag-Plated Stainless Steel and Ni-Coated Carbon*

Compression, psig[a]	Thick., in.	Contact resistance, mohms-cm^2
None	0.1	15
2	.1	4
16	.015	2

[a] Precompression to 16 to 20 psi was chosen.

A module of **13** cells leaked initially due to high spots on the frames and surge pressures from the electrolyte circulation pump. Spreading of elastic materials over the manifold holes caused some cells to be starved. Also, gas bubbles, trapped in the electrolyte chambers on filling, led to poor electrolyte distribution. High-rate intermittent purging resulted in better flushing of inerts than steady purging *(656).* Figure 4.8 shows improved porting for electrolyte and gases.

To further improve fluid distribution *(657),* an orifice was added, feeding from the manifold to the distribution ports (see fig. *4.9)* to insure a fixed pressure loss and thereby prevent the cell starvation and accompanying high temperature that can easily attend casual and variable pressure losses. The extra parasitic power for pumping electrolyte through orifices was compensated for by the lower parasitic current through the electrolyte manifolds (the orifices gave a higher resistance path). Use of ammonia gas and filter paper soaked in phenolphthalein showed that, contrary to expectations, gas distribution across the face of an electrode by diffusion was *not* rapid and that gas entry and exit ports had to be designed for proper coverage by flow.

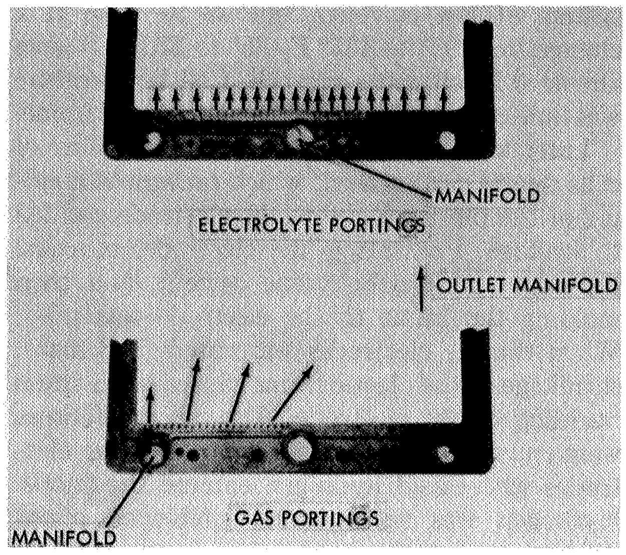

The larger size of slots at the end of the electrolyte channel gave lower pressure drop and hence compensated for the pressure drop along the channel, giving even flow over the face of the electrode. Ports to the outlet manifolds were identical with those for the gas flow, but set at the other side to the inlet ports.

FIGURE 4.8.—Improved electrolyte and gas porting of Union Carbide cell *(656).*

At 200 A/sq ft, cell polarizations from an OCV of about *1.0* were: *0.12* volt IR in the ⅛-inch-thick electrolyte, *0.2* volt at the oxygen electrode, *0.1* volt at the hydrogen electrode, and less than *25* millivolts in contact resistances.

Eight-cell and sixteen-cell modules were constructed, with water transpiration through the electrodes *(658,659,660).* Gas recirculation rates were about *10* times the use rate. Electrolyte was recirculated to remove heat. **A** cell temperature of *185"* F (85" **C)** sufficed to remove all water

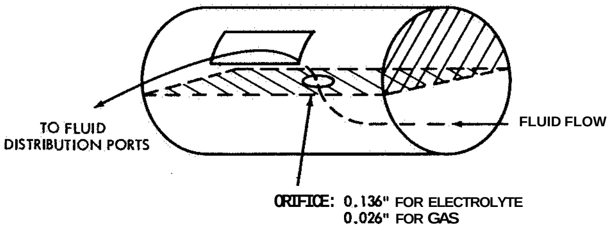

The capsule was inserted in the manifold **(see** fig. **4.8)** or a tube containing orifices was used as the manifold.

FIGURE 4.9.—Capsule containing orifice to give **a** controlled pressure drop from manifold to distribution ports.

produced at 90 A/sq ft, which transpired almost equally through anode and cathode (although somewhat more through the anode, at which water is produced). Life tests, at 50 A/sq ft and occasional overloads, were progressing.

4.3 GENERAL ELECTRIC CO. ION-EXCHANGE MEMBRANE, HYDROGEN-OXYGEN CELL

4.3.1 Fuel-Cell Powerpack Development Program, June 1959 to May 1961

The contract aim was development of a 200-watt, 24-volt powerpack to operate continuously 14 hours a day for 7 days on hydrogen and air **(273).** The weight, including 1 day's fuel supply, was to be about 35 pounds. Cell construction is shown in figure 4.10. The electrodes were catalytic metal powder (palladium-platinum black) bonded into a cationic **IEM** electrolyte, giving a basic structure corresponding to figure 4.4(*b*). Ribbed titanium sheets were used as current collectors. The ribs pressed tightly against the bonded electrode, while the spaces between the ribs formed gas-distribution channels. Current collectors were mounted in plastic frames, and the reinforced IEM was also mounted in a plastic frame. The life of the **IEM** was short if the membrane dried out; therefore, water was retained by wicks on the oxygen side. Thus, the ribbed cathode current collector provided wick

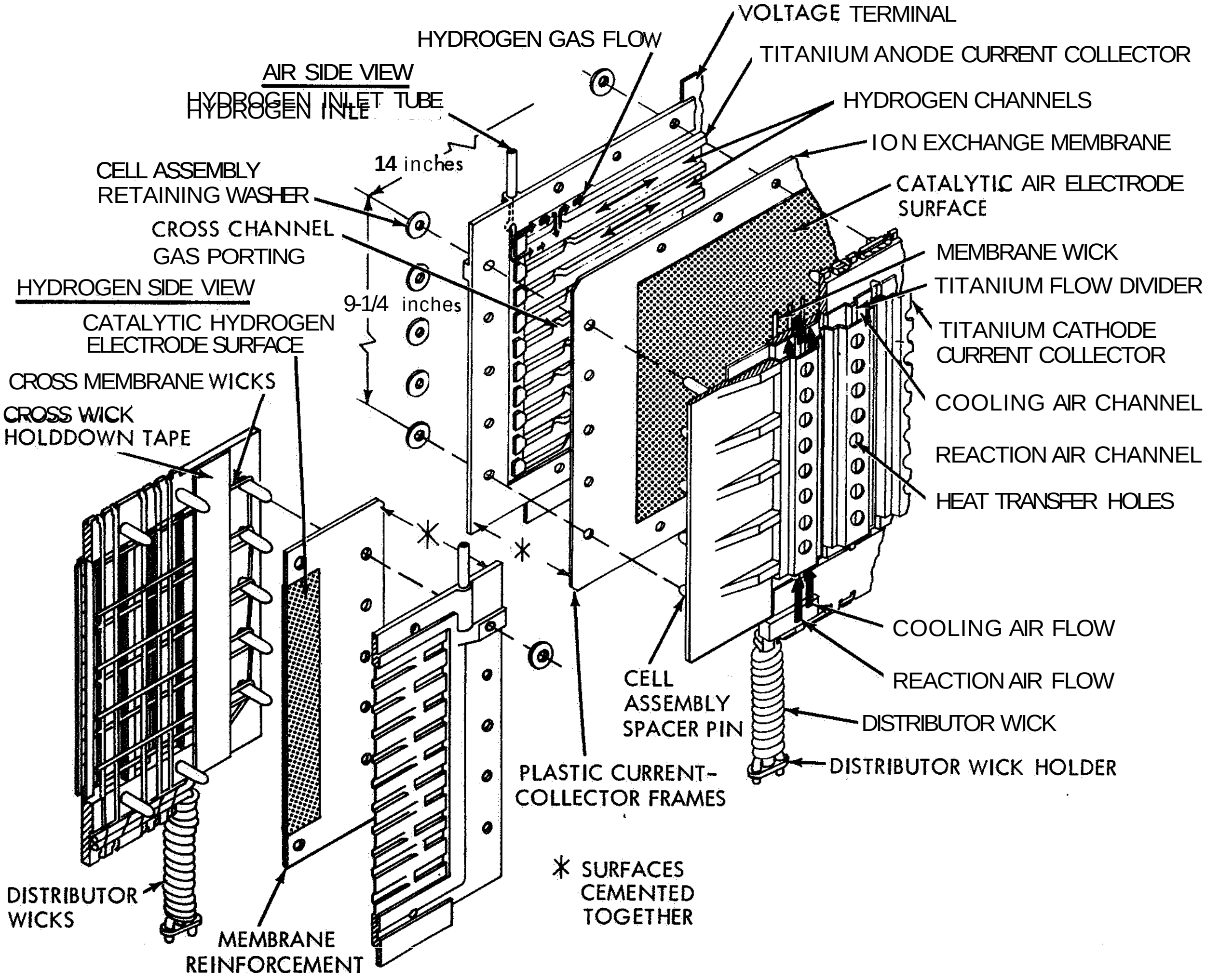
VOLTAGE TERMINAL
HYDROGEN GAS FLOW
AIR SIDE VIEW
TITANIUM ANODE CURRENT COLLECTOR
HYDROGEN INLET TUBE
HYDROGEN CHANNELS
ION EXCHANGE MEMBRANE
CELL ASSEMBLY RETAINING WASHER
14 inches
CATALYTIC AIR ELECTRODE SURFACE
CROSS CHANNEL GAS PORTING
MEMBRANE WICK
HYDROGEN SIDE VIEW
TITANIUM FLOW DIVIDER
9-1/4 inches
CATALYTIC HYDROGEN ELECTRODE SURFACE
TITANIUM CATHODE CURRENT COLLECTOR
CROSS MEMBRANE WICKS
COOLING AIR CHANNEL
CROSS WICK HOLDDOWN TAPE
REACTION AIR CHANNEL
HEAT TRANSFER HOLES
COOLING AIR FLOW
REACTION AIR FLOW
CELL ASSEMBLY SPACER PIN
DISTRIBUTOR WICK
PLASTIC CURRENT-COLLECTOR FRAMES
DISTRIBUTOR WICK HOLDER
* SURFACES CEMENTED TOGETHER
DISTRIBUTOR WICKS
MEMBRANE REINFORCEMENT

SINGLE-CELL ASSEMBLY CONFIGURATION

FIGURE 4.10.—General **Electric ion-exchange membrane cell** (273).

space as well as air distribution over the face of the electrode. Without wicks, the air which was blown through the cathode channels dried out the membrane unless the humidity was carefully controlled. A titanium sheet with wide ribs and holes punched through was placed between the cathode current collector of one cell and the anode current collector of the next. This provided the necessary electrical contact between the current collectors and formed channels through which cooling air was passed.

A stack of 42 cells was made, with a mean weight of 0.65 pound per cell, or about 28 pounds total. The stack operated about 30° F above ambient temperature and had a nominal rating of 15 A/sq ft at 0.6 volt. At 15 A/sq ft the cell voltage fell from 0.7 to 0.4 volt over 500 hours, and rated capacity was obtained for only 100 hours. One reason for the short life was flaking away of the palladium-platinum black electrode deposit from the IEM and, therefore, platinum black alone was used. Also, the water wicks joined to a common carrier wick acted as a common electrolyte manifold (see sec. 4.1), giving parasitic current (showing that water was leaching ions from the membrane).

Although the cell stack was under the 35-pound limit, the total weight including the hydrogen generation system (see app. E) was 70.6 pounds, with a fuel canister (sodium borohydride and sulfuric acid) of 7 hours' capacity. A high-pressure hydrogen storage bottle was a far simpler fuel supply, but still weighed 16 pounds for an 8-hour supply.

4.3.2 Research on Compact Fuel-Cell Power Supplies, October 1960 to October 1961

No power unit was called for under this contract. The aim was to improve the power density of the IEM cell (248). A number of experimental techniques were developed (see app. C) to measure polarization. For example, a Kordesch-Marko bridge was used, and the results were compared with steady dc measurements. The ammeter and voltmeter of the bridge gave average values over the on-off cycle, but the results agreed with dc measurements, showing that the rate of change of activation polarization was slow (frequencies of 60, 180, and 240 cycles per second gave identical results). The bridge was then used to measure IR-free polarization. A driven cell was used with hydrogen at each electrode. No hydrogen activation polarization was seen up to 25 A/sq ft.

Membrane resistances were measured with screens pressed into IEM polymers of different thicknesses. Upon extrapolation to zero thickness, the contact resistance of metal to membrane was found to be small. Contact resistances (ohm-cm^2) between various current collectors and platinum-palladium black-coated membranes were measured. They varied with pressure and material, as shown in figure 4.11. The resistivities of powders under compression also were measured, and from the resistance of platinum black at a given pressure and the measured resistance of the catalytic film on the electrode, the film was estimated to be 1 to 2 mils thick at a loading of 15 g/sq ft (16 mg/cm^2). Combinations of catalytic powders were tried as oxygen electrodes, but

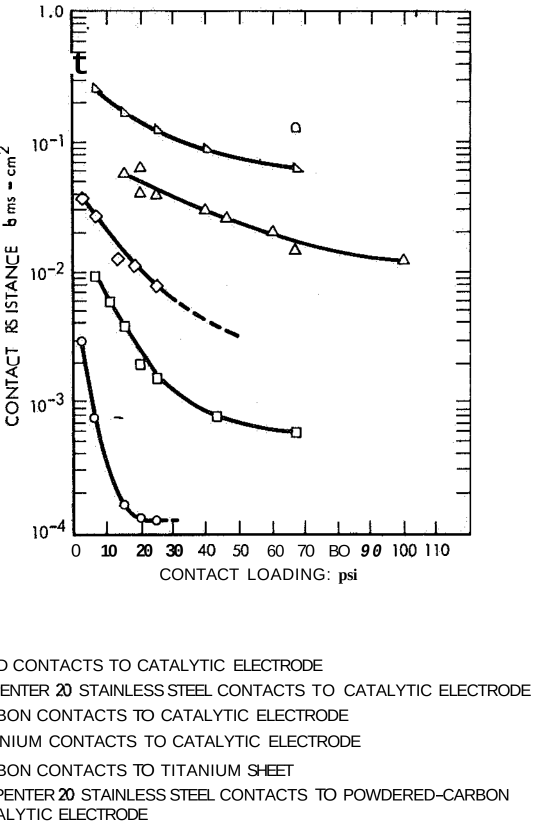

FIGURE 4.11.—Contact resistance of various materials (*248*).

Pt-C, Pd-C, tungsten carbide-Pt, and titanium carbide-Pt all gave higher contact resistances and poorer catalytic activity than the standard 54 g/sq ft of platinum-palladium black.

A contact pressure of 200 psi was chosen for cell construction; the components of total cell resistances are shown in table 4.2. A total cell resistance of 3.3 ohm-cm^2 would give about 0.30-volt IR polarization at 100 A/sq ft. (Other work under this contract is reported in other chapters.)

TABLE 4.2.—*Approximate Contributions* of Various Resistive Components *to* Overall Cell Resistance

Resistive component	Approximate cell assembly resistance, percent
A. Phenolsulfonic IEM cells with platinun and palladium:	
1. Current collectors:	
a. ⅛ inch thick or larger	Negligible
b. 0 *005* inch thick—Carpenter *20* stainless steel or titanium	5
2. Catalytic electrode: *0.0376* g Pt+ *0.0375* g Pd per square inch	10
3. Contact resistance (contact area is 5% of cell area; pressure is 200 psi):	
a. Au versus Pt or Pd	Negligible
b. Carpenter 20 stainless steel versus Pt or Pd	1
c. Ti versus Pt or Pd	*5*
4. Membrane resistance: Overall cell resistance is *3.3* ohm-cm^2......	85
B. Phenolsulfonic IEM cells with carbon electrodes:	
1. Catalytic electrode	*30*
2. Contact resistance	*30*
3. Membrane resistance........	40
Overall cell resistance is 5 to 10 ohm-cm^2	

4.3.3. HOPE Fuel-Cell Program; Flight Analysis of IEM Fuel Cell, April 1961 to October 1962

The contract aim (modified during contract progress) was to study the performance of the IEM cell under orbital space-flight conditions (*234*). A self-sufficient 50-watt satellite system for a 7-day mission, including telemetry and despin compartment, was to be designed, constructed, and orbited. The fuel-cell system contained two 25-watt modules of 28 volts, regulated to within ±2 volts. The basic cell was rated at 12 A/sq ft and 0.8 volt, with 35 cells of 6- by 2-inch electrodes making up each module. Reactant weight for the mission was calculated as 0.8 pound hydrogen and 6.4 pounds oxygen. (The weight of zinc-silver oxide batteries at 80 W-hrs/lb would be over 100 pounds.) The total system is discussed in chapter 9, while work specifically related to the fuel cell is given here.

Use of the fuel cell for this particular application led to some modifications of the cell design discussed above. Removal of heat from the cell was accomplished by replacing the bipolar, air-cooled electrical connection (with holes punched in, fig. 4.10) with a stainless-steel-coated copper sheet (three-ply, tin-soldered, 3.5-mil s.s./5-mil Cu/3.5-mil s.s.) which was attached to a space radiator. Product water formed at the oxygen electrode condensed at this cooler plate and was wicked (15 mil, cleaned, glass-fabric wicks) to a storage tank containing water absorbent (Solka-Floc). Since direct contact of the bipolar heat conductor to a metal radiator would short-circuit the cells, contact was made through 1-mil-thick Mylar coated with silicone grease to give reasonable thermal conductivity, as illustrated in figure 4.12, Other materials of cell construction were injection-molded Cycloloc T-frames and epoxy-glass honeycomb end plates. End covers for; the

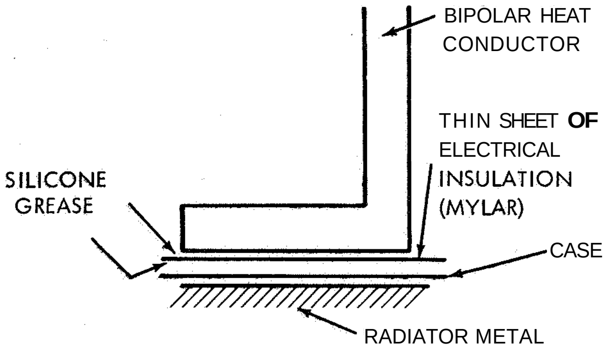

FIGURE 4.12.—Bipolar heat-conductor plate, with a "foot" contacting a space radiator through an electrically insulating coat.

case (see below) were machined from 1-inch-thick epoxy-glass laminate.

At this stage, work on membranes led to development of "polymer A" membranes (a sulfonated polystyrene resin) which gave the single-cell performance shown in figure 1.2, curve A (see ch. 1). The dead-ended hydrogen feed arrangement shown in figure 4.10 was unsatisfactory because the hydrogen chambers could not be purged; therefore, an external hydrogen manifold (of epoxy laminate tube) was fitted. The oxygen chambers of the cells were left open as shown in figure 4.10, and the cell stack was enclosed in a case (15-mil Carpenter 20 Cb stainless steel) filled with oxygen (see fig. 4.13). Best cell operation occurred when hydrogen pressure was slightly higher (about 2 psi) than oxygen pressure.

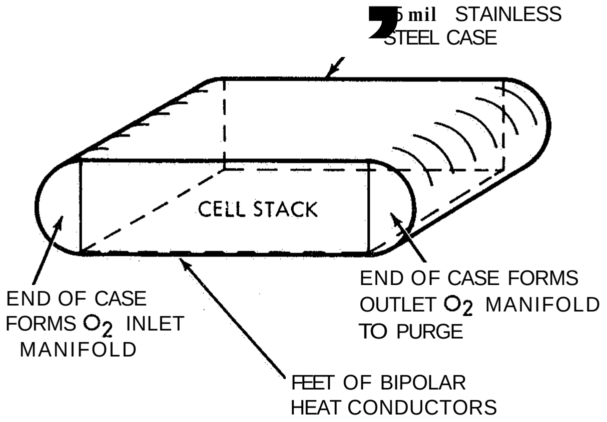
5 mil STAINLESS
STEEL CASE
CELL STACK
END OF CASE FORMS O_2 INLET MANIFOLD
END OF CASE FORMS OUTLET O_2 MANIFOLD TO PURGE
FEET OF BIPOLAR HEAT CONDUCTORS

FIGURE 4.13.—Oxygen manifolding by means of a thin case, for the General Electric IEM module.

Tests in a simulated thermal-vacuum chamber, and other life tests, showed deficiencies in the cell and system. First, freezing of water vapor in gaslines led to ice blockage, and since the cells consumed the gas remaining between the cell and the blockage, vacuum developed in the cell. The IEM's punctured due to pressure imbalance (a pressure imbalance of 5 psi could not be tolerated). Second, sulfuric acid leaching from the IEM decomposed the silicone grease and decomposition products crept up the wicks and poisoned the electrodes. Third, when dry hydrogen was used, the IEM tended to dry out at the hydrogen inlet point, giving a weak spot which would leak gas and burn out. This was cured by placing small Orlon felt pads at these points, on the oxygen side of the membrane. The wicking action of the felt in the humid oxygen atmosphere kept the IEM wet. Controls were developed which purged the stack when the voltage among any group of three cells fell below 2.1 volts, with a 2.2-second hydrogen purge and 15-second oxygen purge.

Shock, acceleration, vibration, and zero-gravity tests gave satisfactory results, with the cell both off and on load. Storage of cells connected to the hydrogen and oxygen supplies gave a high rate of failure due to slow leakage of hydrogen through pinholes in the IEM, and consequent burning. Longer shelf life was obtained by replacing hydrogen with nitrogen during storage and by insuring 100 percent relative humidity in the stack to prevent drying of membranes. Under these high-humidity conditions, the IEM developed by the General Electric Co. suffered from electrode delamination. A sulfonated-polystyrene IEM from American Machine & Foundry, more resistant to delamination under these conditions, was used in life tests. Under load the performance fell 12 percent in 2000 hours **(237)**; the failure rate was estimated as about 8 percent per 1000 hours of operation for a 35-cell stack.

The project was terminated in October 1962, and the satellite was not launched. Increase in cell performance and development of the Gemini and Apollo programs of NASA made the overall system design obsolete.

4.3.4 **Ion-Exchange Fuel Cell, October** 1961 **to September** 1962

The scope of this contract included the study of catalysis, membranes, electrode structure, and heat and mass transfer ***(263)***. (Some of the work is reported in other places; see ch. 3.) The cell investigated was the IEM cell described above, with modifications to allow for easier testing. For example, cells were constructed with a small separate electrode on the membrane. This secondary electrode was fed with its own hydrogen supply and current was not drawn from it, so that it acted as a reference electrode. Alternatively, a fine Luggin capillary was placed against the membrane, and contact between the capillary fluid and the membrane was established with a drop of sulfuric acid. The capillary was connected to a standard calomel electrode in the normal way.

By operating an IEM cell dead ended and measuring the rate of gas consumption as a function of current, it was shown that the faradaic efficiency was close to 100 percent up to at least 25 A/sq ft. The very rapid drop of cell voltage when the current was switched on was used to measure ohmic resistance galvanostatically. Potential drop was proportional to current, as required, and the values of resistance agreed with those obtained by other methods (see sec. 4.3.2). The ohmic polarizations of anode, membrane, and cathode were found from the potential drop between working electrode and hydrogen-reference electrode. The response of the hydrogen electrode was very rapid, but the oxygen electrode took about 5 seconds to develop most of its polarization.

Three methods were used to get double-layer capacities of the electrodes. A transient current pulse gave 14 to 40μf/cm^2; a high frequency (1000 to 3000 cps) ac bridge gave 6μf/cm^2; and current interruption gave 14μf/cm^2. The first two techniques were used without gas reactant present, in the range (0.4 to 0.9 volt versus SHE in the same electrolyte) where pseudocapacity is small. These double-layer values were about one-thousandth those expected from the area of the platinum black on the electrode. This suggests that either the measurement of double-layer capacity is not valid for porous electrodes on an IEM, or that only a small percentage of the electrode is in direct contact with the ions of the membrane.

Steady polarization was measured with a Wenking potentiostat (see app. C) and corrected for IR polarization. The lowest and most reproducible values were obtained when the IEM (sulfonated polystyrene) was equilibrated with 30 weight-percent sulfuric acid. The hydrogen electrode showed a linear voltage-current relationship to over 150 A/sq ft, both anodic and cathodic (the polarization at 150 mA/cm^2 was 20 millivolts, giving an exchange current density of about 0.45 A/cm^2 or about 400 A/sq ft). The oxygen electrode showed a typical activation polarization curve with almost 0.4-volt polarization from the ideal OCV (1.23 volts) at 50 A/sq ft.

Best results were obtained when the oxygen flow rate was at least three times stoichiometric. Lower flow rates were not sufficient to remove product water from the membrane surface; presumably the cathode was flooded, resulting in hindered mass transfer of oxygen through a thin film of water, or increased contact resistance. Temperature differences from anode to cathode were small (2.3" F at 60 A/sq ft, for example), but temperature differences of up to 10" F were found between points on the same electrode.

4.3.5 Ion-Exchange Membrane Fuel Cell for Naval Propulsion, November 1961 *to* September 1963

The contract aim was to investigate the feasibility of using an IEM cell with improved membranes for submarine propulsion *(283)*. Analysis of the requirements led to an electrode area of 20 by 11 inches, with a module size of about 26 by 13 by 21 inches. The method of preparing electrodes of this size was described (285) and is given in chapter 3. American Machine & Foundry membranes were used; table 4.3 gives the characteristics of the cell components.

TABLE 4.3.—*Characteristics* of General Electric Cationic *IEM*, Series ***D***, Sulfonated Polystyrene (285, 1962)

Ion exchange capacity, millieq/g	0.64
Membrane thickness, mils	5 to 6
Membrane resistivity, ohm-cm	30 to 60
H_2O pickup at 160° F (71.1" C), percent	12
Electrode catalyst loading, g/ft^2	38
Electrode thickness, mils	4
Cell[a] resistance, ohm-cm^2	0.08 to 1.3
Cell[a] weight, (g/ft^2 of active cell)	90 to 100
Maximum W/ft^2 on laboratory hardware	150

[a] "Cell" here means the electrode-membrane-electrode plate, and not a complete single cell.

These large cells had an output comparable to that of smaller laboratory cells, but their life was not so good as expected. It was proposed to evaporate water as fast as it was formed by keeping the cell hotter than the bipolar, cooled condenser plate situated between the cathode of one cell and the anode of the next. This could be done by putting a thermal impedance between the bipolar plate and the hydrogen electrode (anode). However, improved wetproofing—a thin coat of Teflon on the cathode (*286*)—produced an electrode which did not suffer from flooding (water rolled off the electrode under gravity), so that careful water control was not so important. Incorporation of more bonding Teflon in the electrode (increased from 10 to 15 weight-percent) did not have the same effect and actually gave reduced performance.

The cell design shown in figure 4.10 was modified to allow for manifolding of oxygen, hydrogen, and coolant water through the cell frame (287). The ribbed bipolar connection with channels for cooling air (shown in fig. 4.10) was replaced with a flat sheet, which gave a set of coolant passages along the outer ribs of the oxygen current collector. The ribbed titanium current collector-gas distributor at the anode was replaced by two crossed, pressed-tantalum screens. These modifications are shown in figure 4.14. Titanium was a suitable structural material ;gold-plated copper or brass poisoned the electrodes. Also proposed was a plastic coolant chamber between the anode and cathode, with the bipolar connections made by running conducting studs through the chamber.

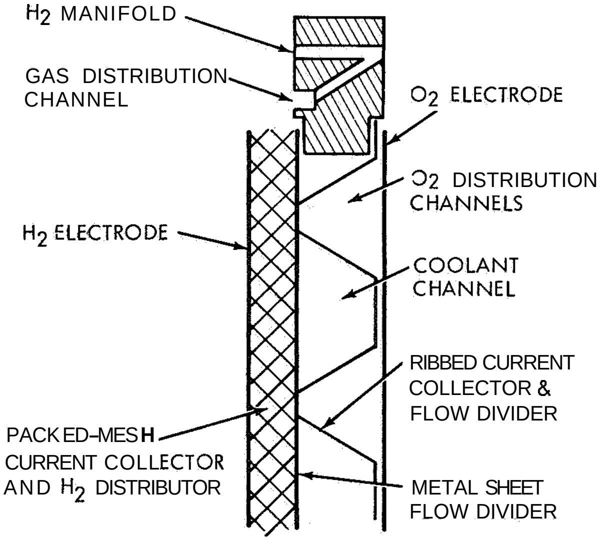
H_2 MANIFOLD
GAS DISTRIBUTION CHANNEL
O_2 ELECTRODE
O_2 DISTRIBUTION CHANNELS
H_2 ELECTRODE
COOLANT CHANNEL
RIBBED CURRENT COLLECTOR & FLOW DIVIDER
PACKED-MESH CURRENT COLLECTOR AND H_2 DISTRIBUTOR
METAL SHEET FLOW DIVIDER

FIGURE 4.14.—Method of forming coolant distribution channels in a bipolar assembly.

Tests on **3-** by 3-inch cells gave less than 1000 hours of life due to pinholes in the membranes. The large-cell designs discussed above were not fabricated, and effort was concentrated on solving the problem of life of the small cells. When a cell with a bare patch (no catalytic electrode) on the membrane was used, the pinholes occurred in the active (covered by electrode) part of the membrane. Other tests failed to give a positive cause for failure. Thicker membranes or two membranes bonded together gave better life. Ion-exchange material was lost from the membrane, and the polymer degraded; when it had lost 25 to 30 percent of its ion-exchange capacity, it was likely to fail. Temperature and voltage were crucial factors; an increase in temperature decreased life rapidly (20° F increase halved life), while operation at open circuit instead of 0.75 volt also markedly decreased life. Although some cells put out reasonable power up to 4000 hours, the lifetimes of others were much less.

4.3.6 Ion-Exchange Fuel Cell, October 1962 to September 1963

This work involved improvement of cathodes and cathode current collectors operated on forced-flow air instead of oxygen (289). Smaller limiting currents, similar to those shown in figure 2.5, resulted from replacement of oxygen with air. Dead-ended or convective (self-breathing) air cathodes had even smaller limiting current densities in some cases.

Sufficiently fast air flow made current density independent of further changes in flow rate (except for small effects due to temperature variation at different flow rates). With air, there was only a small dependence of limiting current density on total pressure. However, at 1 atmosphere total pressure and varying partial pressures of oxygen in nitrogen, the limiting currents were directly proportional to oxygen pressure

$$i_L \simeq 500\,(p_{O_2},\ \text{atmospheres}),\ \text{A/sq ft} \quad (4.1)$$

The limiting currents were much lower than those predicted from the diffusion coefficients of gas through the porous electrode. Knudsen diffusion in small pores was proposed as the limiting mass-transfer process. (General Electric appears to have relied upon the concept that the diffusion coefficient is inversely proportional to total pressure, so that increasing total pressure at a fixed proportion of oxygen would give little overall effect. However, Knudsen diffusion coefficients are independent of pressure, so this interpretation is not valid.)

Experiments on self-breathing cathodes (ref. 4.1) indicated that the center of an electrode with two edges open to the air (see fig. 4.15) had lower limiting current density than its edges.

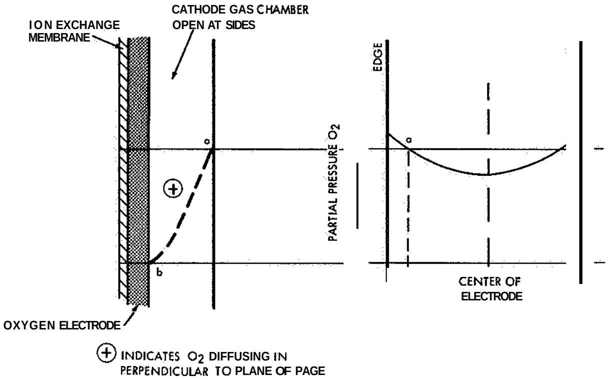
CATHODE GAS CHAMBER OPEN AT SIDES
ION EXCHANGE MEMBRANE
a
b
EDGE
PARTIAL PRESSURE O2
a
CENTER OF ELECTRODE
OXYGEN ELECTRODE
⊕ INDICATES O2 DIFFUSING IN PERPENDICULAR TO PLANE OF PAGE

At limiting current conditions. the partial pressure of oxygen at the back of the cathode gas chamber *a* varies across the width of the electrode, while the partial pressure at the electrode face ***b*** is small Thus diffusion occurs to the face and across the width as shown by the arrows Limiting current densities are smallest in the center of the electrode.

FIGURE 4.15.—Concentration gradients of oxygen diffusing into a self-breathing air electrode.

The oxygen concentrations at the electrode face were taken as zero at limiting-current conditions, and the concentrations at the rear of the cathode chamber fell to give the necessary diffusion gradient. Thus the partial pressure gradient for diffusion from *a* to *b* was smallest at the center of the electrode. The two-dimensional diffusion problem was solved (infinite-series solution), but the solution assumed independent diffusion of each component rather than an integrated three-component (O_2, H_2, and H_2O) diffusion. It was concluded that air-breathing cathode chambers will not support sufficient overall current when the channel thickness (face *a* to back *b)* is less than about 0.15 inch. The restricting factor was diffusion of water, and not oxygen supply, since the equilibrium partial pressure of water vapor over the IEM did not provide sufficient driving force for diffusion. Presumably this means that the produced water must both flow away and diffuse away in order to maintain a mass balance, setting up a barrier to oxygen diffusion.

Statements by the different groups of workers reporting under this contract are contradictory, presumably because there were different opinions between the groups. The primary disagreement is whether diffusion in the gas phase or diffusion through a liquid film is rate controlling. The best overall conclusion is that if water vapor is not rapidly diffused away from the cathode, the water balance is maintained by formation of liquid water in the pores which flows out of the nonwetting cathode. Either the water blocks many of the pores so that they cannot diffuse gas, giving a much lower gas transfer than expected, or it partially blocks all of the pores so that dissolved O_2 has to diffuse through a layer of water. Variation of water-vapor removal obviously affects the state of flooding of the pores. A higher operating temperature and resultant higher water-vapor pressures would reduce this effect.

A newly designed cathode-current collector and air distributor improved the cell performance on air. A perforated sheet was made from Carpenter 20 Cb stainless steel or molybdenum, using a photoetching process. The thickness and hole diameter extended from 3 to 10 mils, while open areas ranged from 10 to 50 percent. The holes were smooth and streamlined with convergent-divergent, convergent, or divergent nozzle shapes. Inlet-to-throat-diameter ratios of 2.5 to 3.5 were used. The written description of the collector suggests that it was as shown in figure 4.16. Use of these collectors in place of solid punched-hole sheets or screens increased limiting currents (using air) from 155 to 290 A/sq ft.

4.4 ALLIS-CHALMERS HYDROGEN-OXYGEN FUEL CELL

4.4.1 Engineering Research Study of Fuel-Cell Powerpack, December 1961 to January 1963

The contract called for design and construction of a 1.5-kilowatt "capillary" fuel-cell system *(35).* Life and operational characteristics of the system were studied. The basic cell, described in chapter 2 (sec. 2.2.2), consisted of catalyzed, porous, sintered-nickel plaque electrodes mounted in a bipolar assembly (see fig. 4.4(a)). The electrolyte was concentrated potassium hydroxide, absorbed by capillary action in a sheet of porous asbestos. The 1.5-kilowatt (net) unit was made

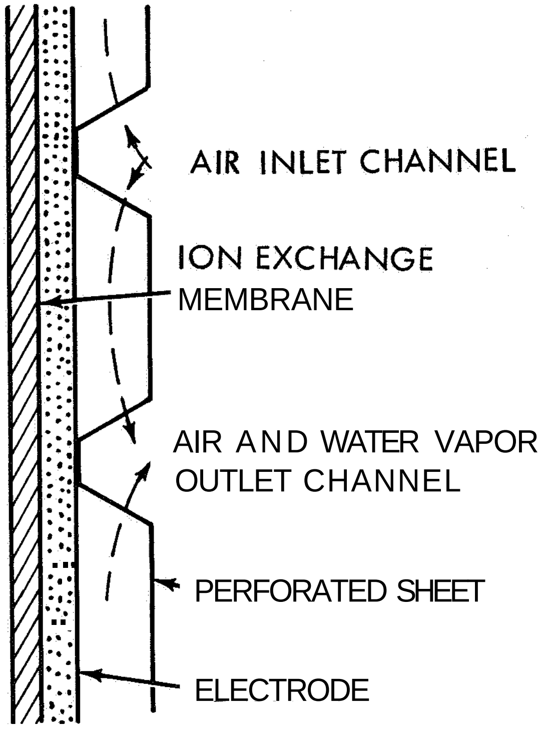

FIGURE 4.16.—Perforated sheet current collector and gas distributor.

up of four 500-watt modules, each module of 15 series-connected cells delivering 12 volts.

Reports from this contract did not give much detail about design, but the plate cell had an electrode area of almost 0.5 square foot. (Thus each cell was rated at about 85 A/sq ft at 0.8 volt.) Nickel-plated magnesium formed a frame and divider for the bipolar assembly. The electrodes fitted into shoulders in the frame, and the divider had gas distribution channels across its faces. Electrodes were $10\frac{11}{16}$ inches wide by $6\frac{19}{32}$ inches high by 28 mils thick. The plaque was 80 percent porous, and both anode and cathode had platinum-palladium catalyst deposited on the nickel surfaces. (Figs. 4.17 and 4.18 represent a design similar to that used in this contract.) The edges of the electrolyte-filled asbestos were sealed with wax. Oxygen was channeled in parallel through the frame, using a common inlet manifold and a common outlet manifold. Hydrogen was also admitted through a common inlet manifold, but separate exit manifolds were used to control the flow of hydrogen through each cell independently. Water was removed by circulation of hydrogen with a water condenser in the stream; heat was removed by conduction along the bipolar assembly, with forced air cooling of the edges to keep temperatures between 125" and 150° F (51.7" to 65.6" C). The gas pressures were 5 psig, balanced to less than ±0.2 psi from anode to cathode gas chambers.

The feature which distinguishes this cell from the Union Carbide cell (sec. 4.2) is that electrolyte is not circulated, nor is the cell filled from a common electrolyte manifold. The electrolyte-soaked asbestos was placed in the cell during assembly, and thus resembled the IEM of the General Electric cell. It was proposed to maintain the electrolyte at a suitable concentration by monitoring the voltage of each cell. At a given current density the cell voltage varied with electrolyte concentration; therefore, the voltage of each could be tied to the hydrogen circulation through each cell to vaporize more or less water.

Problems encountered during preliminary testing included variability of electrodes, failure of wax seals at the edge of the asbestos, and pressure pulses from the diaphragm pump used for hydrogen circulation.

The four-module unit was tested in the second phase of the contract *(36)*. Pumping capacity of the hydrogen circulation system was not sufficient for water removal at full power, so the unit was run at a net output of 750 watts instead of the designated 1500 watts. When the pump was used on one module alone, rated capacity and control were obtained. Tests at ambient temperatures of 14" to 125" F (–10" to 51.7" C) demonstrated satisfactory thermal balance. However, considerable trouble was experienced with pressure controls and valves (see ch. 8). Part of this trouble was due to wax from the asbestos-edge seal which reached the solenoid valves and caused them to stick. Potassium hydroxide was found in the condensed water (up to about 8 grams per liter). The voltage sensors and differential-pressure regulators varied with time. A big disadvantage of the voltage-sensor method of water control was that it was preset for a given current density, voltage, and temperature, and therefore had little flexibility. It was concluded that the major problem was the complexity of the hydrogen circulation-water removal subsystem.

Faradaic efficiency was close to 100 percent. Gross thermal efficiency was 53.5 percent, but the auxiliaries reduced this to a net efficiency of 33 percent. A cell loaded to 42 amperes (about 85 A/sq ft) gave a spike current of 50 amperes, but reached steady current and voltage within 50 milliseconds. A load of 82 amperes gave a spike of 110 amperes. The voltage returned to open circuit in about 1 second when the current was cut off. The cells were stored for 6 months with no loss of performance. Operation of four modules for 8 months gave about 2.5 percent decrease in voltage at rated current density for three modules, but one module deteriorated 10 percent over 5 months.

4.4.2 Design of 400-Watt H_2-O_2 Capillary-Type Fuel Cell, May *1962 to* October *1963*

The objective was to adapt the Allis-Chalmers hydrogen-oxygen cell to space use, as a 400-watt (600-watt gross) unit of 28±1.5 volts (49). The cell was basically similar to that described above. Additional design features reported were: 35 weight-percent potassium hydroxide, 200" F (93.3" C) operating temperature, and 2-mil-thick nickel plating on magnesium or magnesium alloy for the bipolar electrode holder and gas divider. Figure 4.17 shows the stack with a case to contain the coolant flow over the cooling fins shown in figure 4.18. The grooves in the bipolar plate for distributing gas over the face of the electrode can be clearly seen in figure 4.17. The module was to contain 36 cells of 0.27-square-foot area, rated 80 A/sq ft at 0.85 volt, falling to 0.77 volt after about 700 hours of operation.

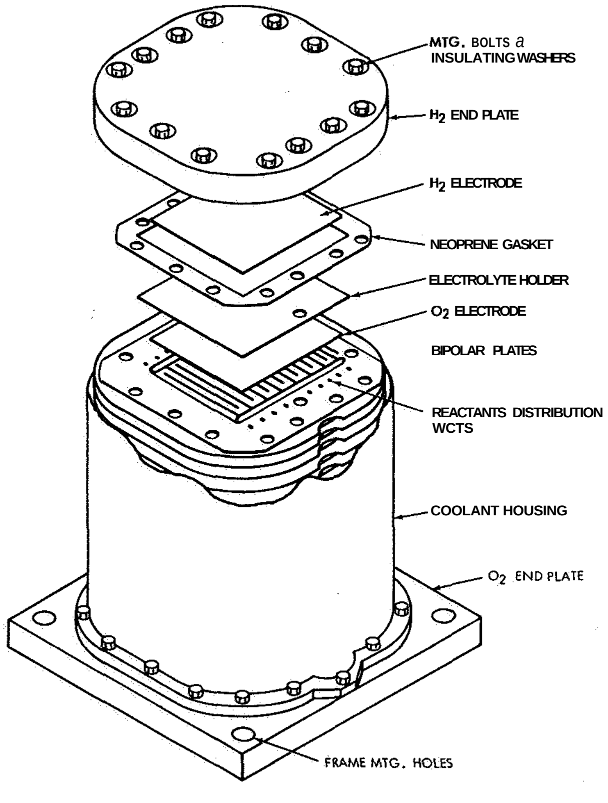
MTG. BOLTS a INSULATING WASHERS
H_2 END PLATE
H_2 ELECTRODE
NEOPRENE GASKET
ELECTROLYTE HOLDER
O_2 ELECTRODE
BIPOLAR PLATES
REACTANTS DISTRIBUTION WCTS
COOLANT HOUSING
O_2 END PLATE
FRAME MTG. HOLES

FIGURE 4.17.—Allis-Chalmers fuel-cell module *(49).*

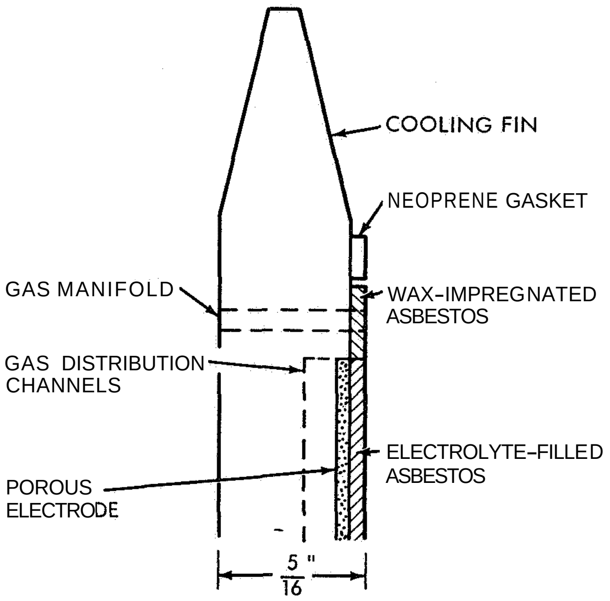
COOLING FIN
NEOPRENE GASKET
GAS MANIFOLD
WAX-IMPREGNATED ASBESTOS
GAS DISTRIBUTION CHANNELS
ELECTROLYTE-FILLED ASBESTOS
POROUS ELECTRODE
5/16 "

FIGURE 4.18.—Bipolar electrode assembly of Allis-Chalmers fuel cell (not to scale).

A modification to the contract *(50)* called for orbiting a 50-watt unit, which had to be less than 35 pounds in weight and 0.75 cubic foot in volume, exclusive of fuel supply, tankage, and plumbing (to be supplied by sponsors). Total weight was to be less than 95 pounds for a mission of 2 to 5 days.

To obtain satisfactory water control by voltage sensing, module temperature had to be held within 195°±5° F. This was done by heaters and evaporative cooling of water- (see below). Water was removed by purging hydrogen; the purge was actuated by voltage sensing of each cell. Oxygen purge was also based on cell voltage. The 50-watt unit was designed with two plate cells in series at a total voltage of 1.62 to 1.56 volts. A water tank was mounted on the fuel cell; the cell was cooled by water that passed through the case of the cell and was evaporated to vacuum. Several forms of water tank and mounting were tried *(52)*, including a horizontal cylindrical tank fixed to the fuel cell with C-clamps, a vertical cylindrical tank with one end bolted to the flat fuel cell, and a semicylindrical D-shaped tank, with the flat of the D bolted to the fuel cell (the form finally adopted). Although all models were satisfactory in shock, acceleration, and vibration tests, resonance and failure of some attached auxiliaries was found ***(53)***. In addition, trouble was again experienced with pressure sensors, regulators, and solenoid valves.

The hydrogen flow pressure regulating valve *(51)*, having an aneroid bellows as a diaphragm, drifted to higher pressures with time. Hydrogen at 200° F (93.3° C) slowly permeated the nickel of the bellows, thus changing the reference pressure setting. This problem was solved by gold-plating the bellows. Repeats of the vibration tests ***(54)*** showed that all components were satisfactory. The unit was flight tested at zero-gravity (on a jet aircraft) for 11 periods of about 20 seconds each. Automatic control was not used because the modified pressure regulators were not obtained and tested in time for the flight. Required electrical performance was obtained before, during, and after the zero-gravity tests.

A 50-watt unit designed for 100 hours' duration weighed 33.5 pounds, excluding fuel tanks and supply lines but including 5 pounds of cooling water, voltage sensor and controller, pressure regulators-flow valves, and solenoid valves.

4.4.3 Research and Development of an Open-Cycle-Type, Fuel-Cell System, May 1962 to Present

The purpose was to develop materials and processes for adapting the Allis-Chalmers cell to space vehicle use ***(37)***. In particular, water removal had to be simplified. The voltage-sensor method used in the two previous contracts had obvious disadvantages, and a method of dynamic vapor-pressure control was proposed. Basically this consisted of circulating hydrogen with a fixed partial pressure of water vapor at the inlet to the cell. The partial pressure equaled the equilibrium partial pressure of water vapor over the desired electrolyte concentration, 35 weight-percent KOH, at the cell temperature; therefore, the cell could not dry out beyond this concentration. Product water diluted the electrolyte and raised the equilibrium pressure of water vapor, leading to water evaporating into the hydrogen stream. Hydrogen was circulated through a condenser whose temperature maintained the desired vapor pressure, at a rate sufficient to remove all product water.

A four-cell module was operated at 85 A/sq ft for over 100 hours with about 0.03-volt variation in cell potential. Both hydrogen and oxygen were circulated through water-bath condensers. The partial pressures of water vapor entering and leaving the stack were measured (by a gas chromatograph with helium carrier) at various cell temperatures; experimental values agreed well with theoretical predictions from flow rates, current density, and the KOH concentration-water vapor pressure-temperature relations in the International Critical Tables. The optimum electrolyte conditions were 0.07 $\mathrm{ml/cm^2}$ (30-mil-thick membrane) of 35 weight-percent potassium hydroxide; the current-voltage curves of the cell are shown in figure 1.2. Increasing the reactant gas pressures gave larger current densities (at 0.8 volt) up to about 5 atmospheres, where the effect leveled off. When the cells were operated dead ended, the faradaic efficiency was 100±2.7 percent.

Additional tests with flowing hydrogen only ***(38)*** showed that when a cell operating at steady water balance at 100 A/sq ft was loaded to 250 A/sq ft, it took about 20 minutes to exceed the wet limit of the cell. Therefore, a control system need not have rapid response to change in conditions. Hydrogen flow rates were about 12 to 24 times the usage rate. A variety of tests showed reasonable agreement between theory and experiment, although the potassium hydroxide concentration in the electrolyte could vary across the asbestos retainer from the anode to the cathode. Contrary to previous experience, the water removed was neutral, contained no iron, chromium, or nickel, and was potable. Investigation ***(39)*** of differences between theory and experiment in the water balance showed that it was not correct to assume equal KOH concentrations at the anode and cathode sides of the electrolyte. The concentration was lower at the hydrogen side where water was produced and higher at the oxygen side, by about ±7 percent of the mean (depending on the conditions). It was decided, therefore, to circulate both hydrogen and oxygen in order to maintain uniform electrolyte concentrations across the cell.

A slow loss in cell potential with time, due to loss of potassium hydroxide, was noted. Since no KOH was found in the water or catalyst, it was thought to be reacting with the high-temperature (300° F (149° C)) wax employed as the edge seal for the asbestos. The wax was replaced by gaskets on each side of the edge of the asbestos. An eight-cell module was run for 450 hours and the voltage fell from 6.75 to 6.15 volts in this time. The oxygen-circulation rate was 4 times that of consumption, and the hydrogen rate was 24 times that of consumption. Current density at 0.8 volt was improved from 209 A/sq ft to 465 A/sq ft by decreasing the membrane thickness from 30 mil to 10 mil *(42)*. The effect was due to lower IR loss and more even electrolyte concentration.

Work performed under another contract (see sec. 4.4.4) had indicated that a "static vapor pressure" method of controlling water removal had a number of advantages over the "dynamic" method. A 28-volt, 1500-watt stack was built, using the static water-removal method (see below), which contained 35 units in series, each consisting of 2 cells in parallel ***(45)***.Butyl rubber (65 mil) gaskets were used and insulating spacers were made of melamine (grade G–5, 65 mil). The stack was cased in a cylindrical magnesium case (40-mil/wall thickness) with ½-inch magnesium flanges and end plates. Coolant gas (hydrogen or helium) was blown around the stack by fans mounted in the case and the gases cooled by a water-cooled heat exchanger also mounted in the case (see ch. 8). It was not possible to maintain completely automatic control, but water removal, heat balance, and cell performance were satisfactory with manual control. The gradient in cell temperature between the center of a cell and the cooling fins were kept below 7° F. The mean cell performance is shown in figure 1.2; performance fell at rates of 0.2 millivolt/hour at 100 A/sq ft and 0.4 at 200 A/sq ft. The stack output was 2 kilowatts at 25 volts after 160 hours, at a voltage efficiency of nearly 60 percent.

4.4.4 Study of Energy Conversion Systems, May 1963 to June 1964

Most of this contract was concerned with optimum design calculations for a space mission, but some work was done on cell construction and life ***(59)***. Instead of the "dynamic water vapor pressure method'' of removing water (see sec. 4.4.3), a "static water vapor pressure method" was investigated. The principle is shown in figure 4.19. Except for occasional purge, the hydrogen and oxygen chambers were dead ended, thus simplifying the auxiliary control and pumping system. Large potassium hydroxide gradients were found across the face of the electrolyte (top to bottom in fig. 4.19). These appeared to be due to removal of water from the electrolyte by the entering dry gases; therefore, the cell was

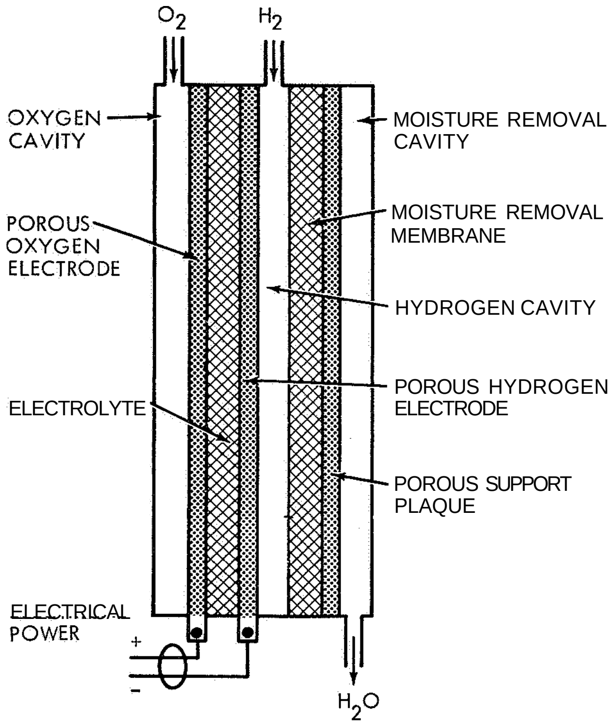

Cell construction employed an asbestos membrane and a water-removal-chamber next to the hydrogen chamber. The membrane is soaked in concentrated potassium hydroxide, which dissolves or evaporates water depending on conditions. It thus acts as a water-diffusion membrane. The water-removal chamber is maintained at the desired water-vapor pressure. Water produced in the cell causes the vapor pressure in the hydrogen chamber to go up, and water thus diffuses through the membrane into the water-removal chamber.

FIGURE 4.19.—Principle of Allis-Chalmers static water-vapor control method for removing water *(59)*.

designed for countercurrent flow (still dead ended) of hydrogen and oxygen.

The membranes required a pressure differential of about 100 psi to blow out all of the absorbed liquid; and the water-removal chamber could, therefore, be kept at a much lower pressure than the rest of the cell (the required equilibrium pressure of water vapor over 35 weight-percent KOH at 200" F (93.3" C) is about 0.33 atmosphere). Hydrogen at 2.5 atmospheres with cell temperatures of 199.4" F (93° C) gave a loss of hydrogen through the water-removal membrane of about 0.08 g/hr/m², or less than one-fourth percent of the hydrogen consumption. The required water-vapor pressure was maintained by connecting the chambers to a condenser (set at the temperature necessary to give this pressure), but the slow buildup of inert gases as hydrogen was consumed made an occasional purge of the condenser system necessary. The membrane system supported at least 200 A/sq ft. A four-cell stack with a central manifold to the water-removal chambers ran for several hundred hours.

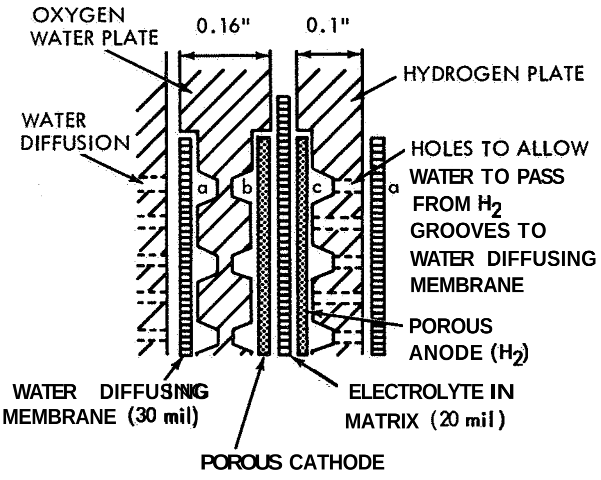
OXYGEN WATER PLATE
0.16"
0.1"
HYDROGEN PLATE
WATER DIFFUSION
a
b
c
a
HOLES TO ALLOW WATER TO PASS FROM H_2 GROOVES TO WATER DIFFUSING MEMBRANE
POROUS ANODE (H_2)
WATER DIFFUSING MEMBRANE (30 mil)
ELECTROLYTE IN MATRIX (20 mil)
POROUS CATHODE

The grooves designated *b* contain oxygen and those designated *c* contain hydrogen. These gases react electrochemically to give water in the electrolyte (contained in asbestos matrix). The water-vapor pressure tends to build up in grooves *c* and water diffuses through the holes in the metal hydrogen plate, across the asbestos-KOH solution water-diffusion membrane to grooves *a*. These grooves are kept at a low pressure of water vapor (⅓ atmosphere) by removal of the water vapor.

FIGURE 4.20. —Illustration of assembly of plates, membranes, and electrodes in Allis-Chalmers fuel cell with "static water-vapor pressure control."

4.4.5 Design of H_2-O_2 **Fuel Cells,** November 1963 **to** January 1965

One of the objectives was to deliver two 45-watt packages of Allis-Chalmers capillary cells, using the static water-vapor pressure for moisture removal **(57).** A system was to operate at least 48 hours in space orbit with maximum weight of 35 pounds and maximum size of 0.75 cubic foot. The basic cell design was similar to that described above, but porous, sintered-silver cathodes, which gave better life, replaced the platinum-catalyzed nickel cathodes. Each 45-watt unit contained two cells in series, with 0.2-square-foot electrode area, operating at 150 A/sq ft and 0.75 volt per cell. The two-cell stack was contained between end plates of magnesium, which gave sufficient structural support to withstand vibration of launch and orbit. The grooves for gas distribution shown in figures 4.17 and 4.18 (cut in the bipolar plate) were crosscut with other grooves to give a checkered pattern of channels. The bipolar plate, containing a recess for the oxygen electrode on one side and one for the water diffusion membrane on the other, was 0.16 inch thick, while the hydrogen plate was 0.1 inch thick (see fig. 4.20). The flat gasket shown in figure 4.18 was replaced with one of circular cross section, which fitted into a square recess cut in the plate.

Heat balance was provided by auxiliary heaters before launch and by a thermal shield over the unit during operation. The shield was designed to radiate heat to the space vehicle at a rate which would maintain cell temperature at 195° F (91° C). The purge rates of 0.005 pound per hour for hydrogen and 0.04 pound per hour for oxygen were too low to be handled reliably by needle valves or orifices, since the small holes might clog. Therefore, a new valve consisting of a porous resilient plastic under pressure was developed. The final unit is shown in figure 4.21; it weighed 14.5 pounds including valves and pressure regulators.

The contract also required delivery of a 400-watt unit with an operational life of 400 hours. One-hundred-watt modules of 28 cells in series were built, with dimensions of 7 by 7 by 16 inches and a weight of 30.5 pounds. Cells were similar to that described above, with electroless nickel-plated-magnesium anode plates and gold- or silver-plated-magnesium cathode plates. The average cell voltage declined from 0.9 to 0.86 volt

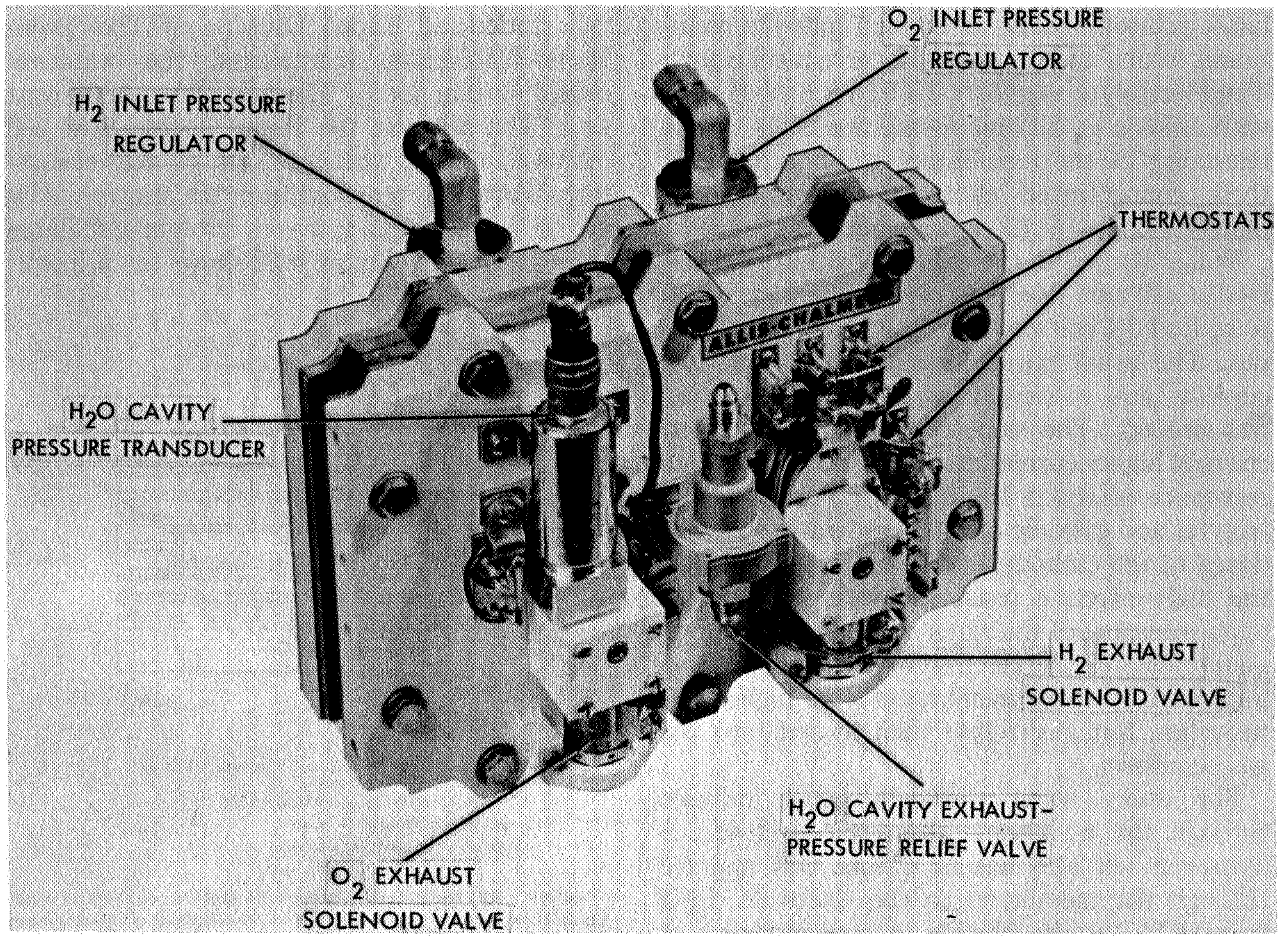
O_2 INLET PRESSURE REGULATOR
H_2 INLET PRESSURE REGULATOR
THERMOSTATS
H_2O CAVITY PRESSURE TRANSDUCER
H_2 EXHAUST SOLENOID VALVE
H_2O CAVITY EXHAUST-PRESSURE RELIEF VALVE
O_2 EXHAUST SOLENOID VALVE
ALLIS-CHALMERS

This 45-watt unit consisted of two cells in series, between magnesium end plates. Water removal was by static-pressure control (see fig. 4.20). with the pressure in the water-vapor cavities controlled electronically via the water-cavity pressure transducer and pressure-relief valve (this could be connected to a condenser to recover the water for drinking purposes). The oxygen and hydrogen solenoid exhaust valves were controlled electronically to purge the oxygen and hydrogen cavities of inert gases which build up as the cell is used. The package shown here weighed 14.5 pounds.

FIGURE 4.21.—Allis-Chalmers hydrogen-oxygen fuel cell for space use (57).

at a constant load of 80 A/sq ft over 400 hours of test. This was attributed to corrosion products from poor-quality control of plating. Microscopic burs in the grooves proved to be weak points in the coating so the plates were polished with a plastic pellet polisher before electroplating. Ethylene-propylene rubber was used as gasketing material. A new method of filling the matrices with electrolyte was to flood the cell with dilute electrolyte, drain, and evaporate water until the desired electrolyte concentration was reached.

4.5 IONICS DOUBLE-MEMBRANE HYDROGEN-OXYGEN FUEL CELL

4.5.1 Study of IEM Fuel-Cell Components, June 1960 to April 1962

One of the major early problems with ion-exchange-membrane (IEM) cells was water balance in the membrane (see sec. **4.3.1).** Thin ion-exchange membranes had little water capacity and dried out rapidly when the humidity of circulated gases was low; this resulted in high ohmic resistance and short life. In this contract *(343)* it was suggested that some of the advantages of the IEM cell could be retained by employing two membranes with electrolyte between them, thus eliminating the disadvantage of the membrane's drying. A laboratory cell was constructed and operated, demonstrating feasibility. Life was good with varying rates of water removal or water accumulation, so that drying of the membranes was not a problem. The electrodes were not described, but presumably were similar to those of the single IEM cell (platinum black pressed against or bonded into the membrane, with a metal screen as a current collector). The electrolyte was 6 *N* KOH or 6 *N* H_2SO_4, with anionic or cationic membranes. The ohmic resistance of the membranes equilibrated with these concentrated electrolytes was approximately 1 ohm-cm² (20-mil membranes).

Water formed in the electrolyte, and the electrodes did not flood. A current density of 50 A/sq ft at 0.4 volt was near-maximum power output. The usual initial loss of potential at low currents due to oxygen activation polarization was present. The slope of the voltage-current curve at higher current densities gave an effective resistance of about 10 ohm-cm². For acid electrolytes and cationic membranes, water was produced at the cathode, and it was suggested that the high effective resistance was due to slow mass transport of the water through the cathode membrane into the electrolyte. Performance was improved by using membranes with higher diffusivities, but electrolyte then leaked into the gas chambers.

For every water molecule which diffuses through the membrane from the electrode, a hydrogen ion also has to diffuse and migrate through the membrane to the electrode. In a true IEM system, change in concentration of hydrogen ion through the membrane is not possible, but when the membrane is equilibrated with strong acid it acts more like a porous matrix, containing free anions and cations in the water in the membrane. Therefore, a buildup of water is probably accompanied by a concentration decrease of hydrogen ion (and anion) through the membrane to the electrode, leading to concentration polarization. If the IEM passed current purely by migration of H^+ (Ohm's law), the countercurrent diffusion of water would not affect the cell resistance very much, since each water molecule would carry with it an amount of hydrogen ion corresponding to the ratio of concentration of H^+ to H_2O, which is low. Possibly an electrolyte bridge is necessary between membrane and electrode, so that concentration polarization would occur in this bridge.

4.5.2 Development of the Dual-Membrane Fuel Cell, July 1962 and June 1963

In this contract, Ionics, Inc., supplied the fuel-cell stack, and Tapco Division of Thompson-Ramo-Wooldridge constructed the water-removal system (*605*). The aim was a 1500-watt unit. The cell was the Ionics double-IEM cell discussed above, with 6 *N* sulfuric acid electrolyte. Water was removed from the electrolyte by an osmotic still and the electrolyte circulated through the cell. Figure 4.22 shows the principle of the osmotic still.

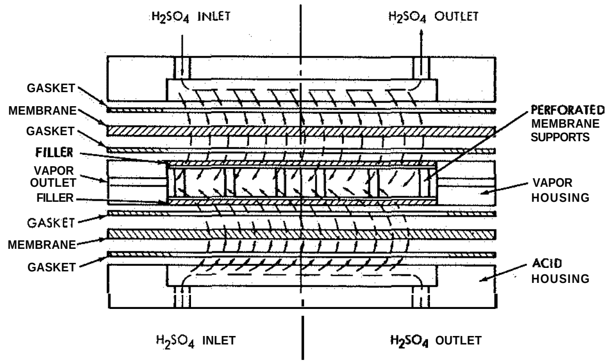

MATERIALS

ACID HOUSING, VAPOR HOUSING, & PERFORATED MEMBRANE SUPPORTS POLYVINYL DICHLORIDE

GASKETS POLYETHYLENE AND POLYPROPYLENE

HOUSING OUTSIDE DIAMETER 9 inches

HOUSING INSIDE DIAMETER 6-3/4 inches

Sulfuric acid solution is passed through a disk-shaped chamber which has an IEM as one face. The chamber on the other side of the membrane is maintained at a low pressure of water vapor, so that water diffuses from the acid through the membrane. The low vapor pressure of sulfuric acid (H_2O+SO_3, in the vapor phase) prevents objectionable amounts of acid from being evaporated from the membrane. The membrane must not be so permeable that it will allow droplets of liquid to fall into the water-vapor chamber. Not shown is a flow spreader at the inlet, to insure good acid distribution over the membrane face.

FIGURE 4.22.—Principle of Tapco osmotic still *(5.94)*.

After materials evaluation, polyvinyl dichloride was used in the osmotic still. A number of IEM's and porous plastics were tested as water-diffusion membranes. Some did not pass water rapidly enough, some leaked acid, and some were not strong enough or had pinholes. An American Machine & Foundry membrane (AMF A–60) was best; at 200° F (93° *C)* and a water-vapor compartment pressure of 436 psia, it passed 136 liquid cm³/hr-ft² of water. At this temperature the water-vapor pressure over the 25 weight-percent sulfuric acid was 9 psia, so the differential diffusion pressure was 4.64 psi. The membrane was supported on Monel metal screens coated with Kel-F as follows. The screens were dipped in full strength Kel-F dispersion (KX-633), the excess Kel-F was blown off with argon, and the screens were air dried; then the coated screens were heated at 500° F (260"C) for 20 minutes. The process was repeated three times. When acid was first admitted to the still, drops of strong acid appeared as sweat on the water-vapor side of the membrane and contaminated the effluent water. When the still had operated for a while, the drops dried out and satisfactory water was obtained. A still for 2-kilowatt duty consisted of 14 membranes of 9.6-inch diameter, with a flow rate of 0.69 gallon per minute of acid.

As in the previous contract, the fuel cell was not described in detail. Electrode dimensions were changed from 6 by 6 inches to 2 by 18 inches. Gas and electrolyte fluid flowed along the long axis of the cell, and the new configuration eliminated dead areas at the corners of square electrodes. A 10-cell stack was constructed with parts as detailed in table 4.4. The performance of the cell is given in figure 1.2.

TABLE 4.4.—*Components of* Ionics Double-Membrane Hydrogen-Oxygen 10-Cell Stack *(604)*

[Electrode area is 0.25 square foot]

Numbe:	Component	Material	Weight, lb
2	End plates	⅜-inch stainless steel	29.2
12	Fittings	Swagelock Hale connectors, No. 400-1-4 Gas inlets: Stainless steel Other inlets and outlets: PVC Plugs ¼-inch NPT, PVC plugs	
12	Studs	⅜-inch National Coarse, stainless steel	1.74
24	Washers	⅜-inch National Coarse, stainless steel	.16
24	Nuts	⅜-inch National Coarse, stainless steel	.46
2	Insulators	60-mil butyl rubber	.44
20	Pusher plates	10-mil niobium	2.58
11	Collector plates	10-mil niobium	2.93
20	Electrodes	Standard sintered Pt-Teflon	1.68
20	Membranes	Ionics CR61AZG	2.35
20	Gas compartments	64-65-mil Teflon	4.11
10	Electrolyte compartment	118-135-mil Teflon	4.80
20	Trilok filler	US. Rubber No. 6027-1-1	.32
60	Gaskets	8-mil Dacron-backed Viton **A**	1.27
44	Grommets	8-mil Dacron-backed Viton **A**	.01
	Electrolyte	$6NH_2SO_4$	2.98
Total			55.03

4.6 CONCLUSIONS

Although the pioneering work of Union Carbide led to notable advances in cell design, the low current density of the cell and its thickness make it uncompetitive with other cells. (The cell has long life only with low currents and thick electrodes, due to gradual creep of electrolyte into the electrode.) The General Electric IEM cell also has low watts/sq ft, but its small thickness and light weight compensate to a considerable degree. Units developed under the Gemini program (classified) have the power density given in table 1.1 (15 W/lb), and are competitive with other H_2-O_2 cells. It is claimed that future cells (using newly developed polymers that withstand higher temperatures without degradation) will yield units with power density of 20 lbs/kW (50 W/lb) and life of 2000 to 5000 hours. Water is now recovered from the wick system by applying a pressure differential across a wick supported on a permeable plate, which forces water out through the plate. The simplicity of water removal from the electrodes by wicking is on one hand an advantage in terms of weight and absence of mechanisms, but on the other hand it is relatively inflexible. If a cathode drowns, it is not possible to revive it by increasing the water removal rate, although suitable auxiliary water removal in circulated gas could probably be installed at the cost of added weight.

The Allis-Chalmers cell has a higher power density in watts/sq ft, but it is heavier and thicker. The combination of flexibility and simplicity of water removal by static water vapor control is an advantage which may weigh heavily for manned spacecraft applications.

The double-membrane fuel cell offers little advantage over the later developments of the General Electric and Allis-Chalmers systems and its overall complexity and low power density are unattractive.

The most promising line of future development is likely to be combination of high-performance, light-weight, Teflon-bonded electrodes (see Ch. 2) with the design principles of the alkaline cells described above, employing light-weight plastic and magnesium frames and holders. Low-temperature H_2-O_2 cells will undoubtedly play a significant role in the space program, but any commercial application remains to be demonstrated.

4.7 REFERENCES

4.1. MAGET, H. J. R.; AND OSTER, E. A.: Diffusion Polarization in Air Channels. Fuel Cell Systems, Advances in Chemistry Series, no. **47,** Am. Chem. Soc., 1965, pp. 83–94.

CHAPTER *5*

Cell and Stack Construction: Medium Temperature Cells

5.1 PATTERSON-MOOS RESEARCH, HYDROX CELL, Continuous-Feed Fuel-Cell Systems, February 1957 to February 1962

The contract called for construction and testing of a 1.5-kilowatt Bacon cell (see sec. 2.2.3). The design temperature was 392" to 464" F (200° to 240" C) at a pressure of 400 to 800 psi, with concentrated aqueous potassium hydroxide electrolyte (478). The bipolar electrode holder was made of nickel (see fig. 5.1). Dual-porosity electrodes were formed by applying and sintering two layers of nickel powder to a thin porous backup plate of nickel (see ch. 3 for detailed method), the outer layer being of finer powder than the inner. The cathodes were lithiated and oxidized by heating in air. (Bacon had shown that lithiated nickel oxide was a good semiconductor, while nickel oxide was passive and did not corrode at the positive potential of the cathode.) The electrodes were welded into the bipolar holder, and the holders stacked as shown in figure 5.2, using gaskets between the holders. Gaskets of Klingerit (a rubber-base asbestos) were satisfactory ; Teflon or Teflon-filled gaskets were not.

An Inconel-X case contained the stack, and an external gas supply maintained a flowing nitrogen atmosphere in the shell. The nitrogen pressure was kept slightly above the hydrogen and oxygen pressures so that any gasket leaks would allow nitrogen to flow into the cells, but not hydrogen or oxygen out (to prevent explosions due to mixing of high-pressure oxygen and hydrogen). Oxygen, hydrogen, and electrolyte were manifolded through the frames of the bipolar holders and the gaskets. Water was condensed from circulating hydrogen, and the electrolyte was also circulated. A 25-cell stack, including piping, gas-pressure regulator, etc., was assembled in a frame 3 by 3 by 3 feet.

The performance of the stack, shown in figure 5.3, declined over some hours. The unit failed due to gas breakthrough, but single cells lasted up to 2000 hours at 150 A/sq ft. It was concluded that electrodes had to be made of very homogeneous powder, both in size and shape.

5.2 PRATT & WHITNEY AIRCRAFT MODIFICATION OF THE BACON CELL, Design and Development of a 250-Watt H_2-O_2 Fuel Cell, July 1961 to May 1962

The modification of the Bacon cell (see sec. 2.2.3) developed by Pratt & Whitney Aircraft is one of the most advanced fuel cells at present. A complete system is being developed for the Apollo project. Since the main development of this cell was funded and sponsored by Pratt & Whitney, little detailed design information is available; even the contract reports (532–535) are short and do not disclose any proprietary details. The aim was to design and construct a 250-watt hydrogen-oxygen fuel-cell system to demonstrate feasibility for spacepower. The unit was rated at 12±1 volt, with an efficiency of 50 percent at maximum load.

The 12-volt module was made from 15 cells stacked in series. It operated at 500" F (260" C) with 85 weight-percent aqueous potassium hydroxide at atmospheric pressure, and hydrogen and oxygen at 23 psia. Water was removed by hydrogen circulation through a condenser, with prior heat exchange between hot exit gas and cold inlet gas. The basic cell construction is shown in figure 5.4. It was a disk cell made from dual-porosity, sintered-nickel electrodes welded to disk backing plates of nickel. These plates were stamped or spun to give suitable support ribs. Since all the parts were made of nickel, any

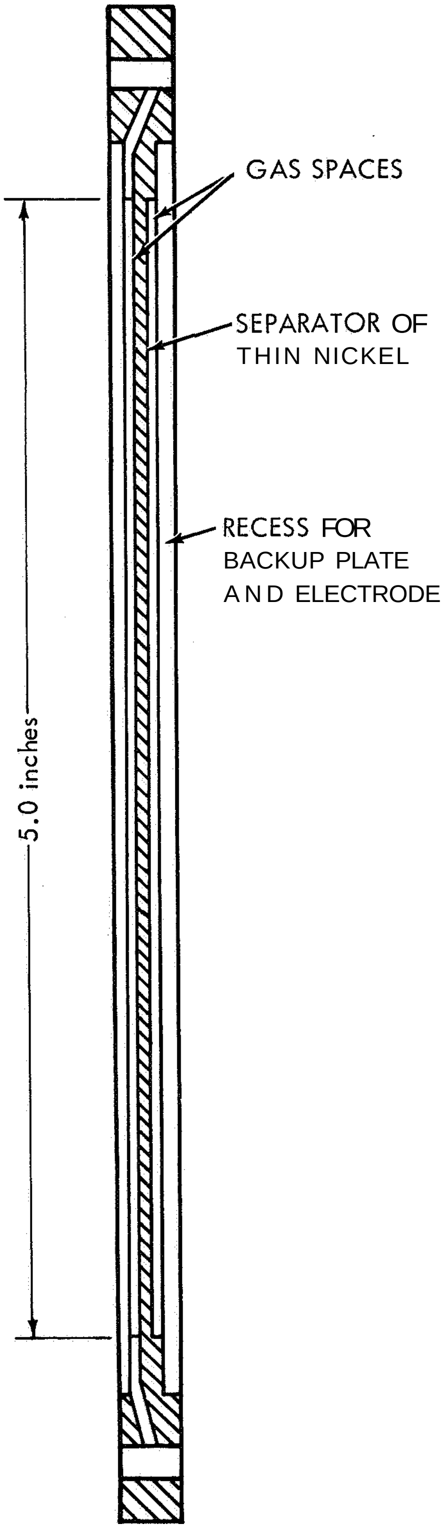
GAS SPACES
SEPARATOR OF THIN NICKEL
RECESS FOR BACKUP PLATE AND ELECTRODE
5.0 inches

The holders were machined from disks of nickel. A dual-porosity nickel anode fits into one recess and a dual-porosity lithiated and oxidized nickel cathode fits into the other recess.

FIGURE 5.1.—Bipolar electrode holder, Patterson-Moos Bacon cell (478).

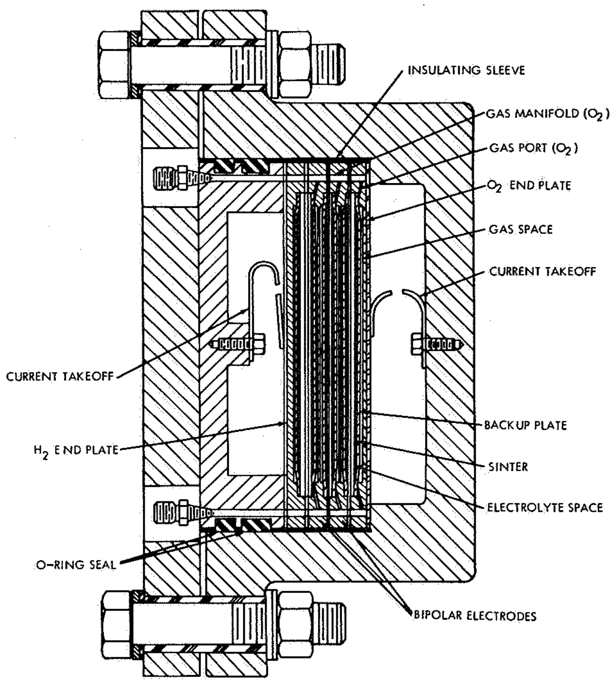
INSULATING SLEEVE
GAS MANIFOLD (O_2)
GAS PORT (O_2)
O_2 END PLATE
GAS SPACE
CURRENT TAKEOFF
CURRENT TAKEOFF
BACKUP PLATE
H_2 END PLATE
SINTER
ELECTROLYTE SPACE
O-RING SEAL
BIPOLAR ELECTRODES

FIGURE 5.2.—Patterson-Moos hydrox cell *(478)*

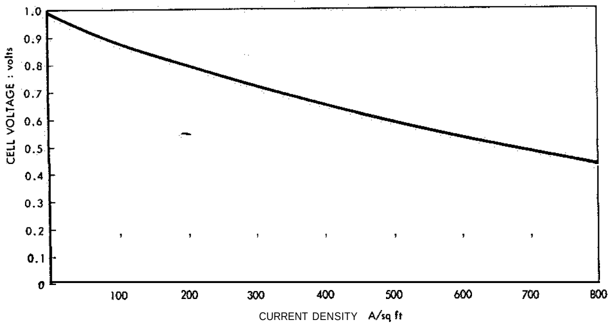

The electrodes were 5 inches in diameter, and 25 cells were stacked in series. The figures shown here are the average values per cell. The unit had a maximum power output of about 1300 watts at 0.43 volt per cell.

FIGURE 5.3.—Short-time performance of Patterson-Moos hydrogen cell *(478)*.

manifolding through the edges of the cells and spacers would have short circuited the cells. Therefore, individual gas inlet and outlet tubes (nickel, 0.074-inch diameter) were welded to each electrode gas chamber, and a Teflon or aluminum oxide insulating connection was placed between the tubes and an external gas manifold. The correct flow of gas from the manifold to the tubes was obtained by orifices in the mouths of the tubes at the manifold. Several sealing-insulating

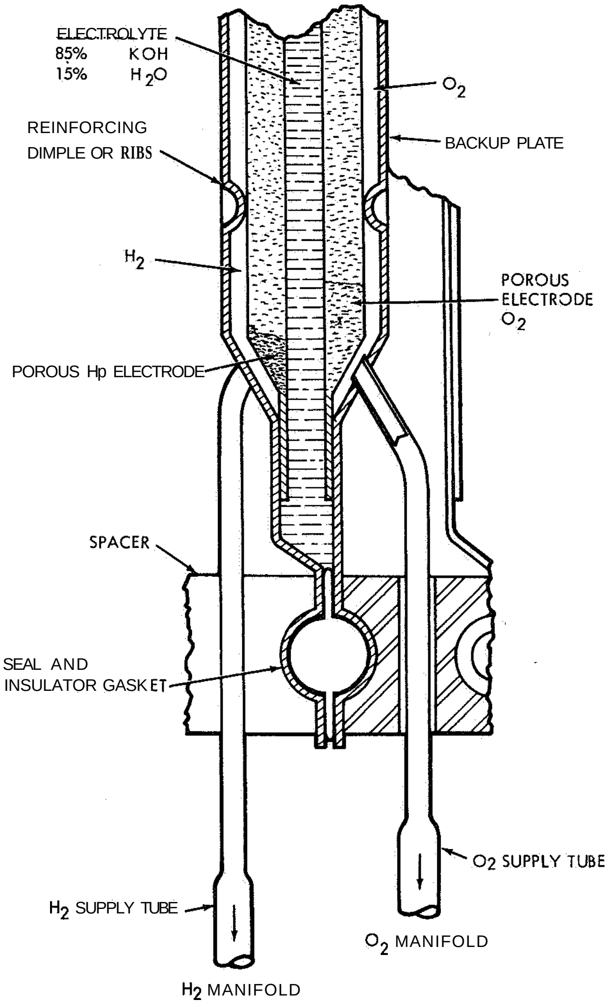

The cell contains disks of dual-porosity sintered nickel welded at ribs or dimples to backing support plates of nickel, thus leaving a gas-distribution space. Each cell has reactant inlet and outlet tubes on opposite sides of the disks.

FIGURE 5.4.—Cell configuration for Pratt & Whitney cell (after *532).*

gasket configurations were tried, and the best was found to be a machined, solid-Teflon O-ring with ears, as shown in figure 5.4.

The electrode backing plate construction shown in figure 5.4 was modified in later designs. Figure 5.5 shows the types of plates and electrodes used. Gas distribution over the electrode face was accomplished by offset ribs in the backing plate or by similar ribs in the electrode disks. These ribs prevented streaming of gas from the inlet to the outlet. The oxygen electrodes were lithiated and oxidized on the surface, using the techniques developed by Bacon (see sec. 3.2.2.2).

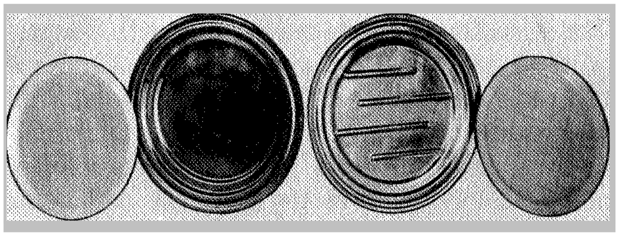

A disk of dual-porosity sintered nickel was welded to a backing plate of nickel, with ribs insuring flow of gas over the whole face of the electrode. The ribs were stamped in the backing plate (right hand of figure), or were on the porous disk (left hand of figure).

FIGURE 5.5.—Components of the hydrogen electrodes of the Pratt & Whitney cell.

Electrode disks were initially brazed to dimples in the backing plates, but the braze did not have sufficient strength and the electrodes broke away, buckled, and shorted out across the electrolyte chamber. This problem was solved by using the structures shown in figure 5.5 and by line welding to the ribs. Electron-beam welding was used for the hydrogen electrode and resistance welding for the oxygen electrode.

The electrolyte was solid at ambient temperature, so the cell was assembled with a cast disk of electrolyte. The disk melted at operating temperature but did not completely fill the electrolyte compartment, and additional molten 80 percent KOH was added through a filling cap. Internal heaters of Teflon-coated nickel chrome wire were assembled in the stack, and the stack was bolted between end plates with 12 steel tie rods, using followup springs between the nuts and the end plate. The stack was enclosed in a twin-walled case (thin steel walls) with thermal insulation between the walls. When the cell operated at 495° to 500" F (257" to 260" C), most of the heat generated in the stack was lost through the insulating case and external connections; the internal heaters and heat exchange from circulated hydrogen were used to control the stack temperature (see ch. 8).

This unit gave 280 watts gross power and 250 watts net, at a thermal efficiency of 54.2 percent. The hydrogen pump and the internal heaters were run from the fuel cell. The current density was about 155A/sq ft at 0.87 volt per cell; therefore, the diameter of the electrodes was about 5 inches, although the actual cell diameter, thickness, and weight are not given in the reports.

The variation of single-cell voltage with temperature at 150 A/sq ft is given in table 5.1. Some fuel cells were operated for over 4000 hours, and the module operated for 690 hours without failure. Several cell tests showed indications of nickel dissolving from the cell case and going into solution.

TABLE 5.1.—*Variation of Performance With Temperature for Pratt & Whitney Hydrogen-Oxygen Cell*

[85 KOH: 15 H_2O, wt-%]

Current density, A/sq ft	Temperature, °F	Voltage
150	500 (260° C)	0.87
	475 (247° C)	.85
	450 (232° C)	.825
	425 (219° C)	.77
	400 (204° C)	.71
	375 (191° C)	.645

TABLE 5.2.—*Apollo Fuel Cell System, Pratt & Whitney PC3A-2 Powerplant*

Number of cells	**31**
Cell pressure	50 psia
Nominal temperature	400° F (204° C)
Reactant gas pressure	10 psi above cell pressure
Heat and water removal	By hydrogen circulation
Voltage	27–31 volts
Power	563–1420 watts
Duration	400 hours
Maximum power	2295 watts at 20.5 volts
Watt-hours/lb reactants	1220 (at 1420 watts)
Weight	220 lbs

5.3 CONCLUSIONS

Table 5.2 summarizes the latest release on performance of the Pratt & Whitney fuel-cell system for the Apollo project (ref. 5.1). Three of these powerplants, which are fully automatic, supply all the electricity for life support, guidance, and communications, and provide drinking water for a 2-week lunar mission. The systems have performed satisfactorily in vacuum, acceleration, and vibration tests, and they have been stored without deterioration for over 2 years. Figure 5.6 shows photographs of the powerplant and auxiliary controls.

Advances in electrode fabrication, quality control, and cell construction have produced cells of considerably higher output than those used in the PC3A-2 powerplant. Pratt & Whitney assert the possibility, in the next 2 or 3 years, of *(a)* quadrupling power densities at the same efficiency, *(b)* reducing weight and volume by 50 percent, and (c) obtaining a service life of 2500 hours (limited incidentally by the mechanical components [such as pumps] rather than by the fuel cell).

The Pratt & Whitney hydrogen-oxygen cell has considerable potential as a space-vehicle power source. If future development leads to the power levels predicted above (sixfold improvement), the system will give power densities of over 35 watts per pound (28 lbs/kW) at a thermal efficiency of 60 percent.

The cell cannot use hydrocarbon fuels directly, and the above performance figures are based on oxygen, not air. If hydrogen were generated from an associated re-former, or if a re-forming catalyst were incorporated in the fuel-cell stack, a considerable drop in power density would occur. The use of air may lead to further loss. Assuming a twofold increase in weight, the future capability could be about 18 W/lb. This is fairly close to the 22 W/lb considered feasible by Cather (ref. 2.8) for vehicle units competing with internal combustion engines (see sec. 2.3.4). Even this future high-power-density system may not be satisfactory for this application, for the reasons given in section 2.3.4. However, the re-former fuel-cell system has distinct possibilities for the self-contained generator sets discussed in section 2.3.3.

5.4 REFERENCES

5.1. MORILL, C. C.: 19th Power Sources Conference, May 1965.

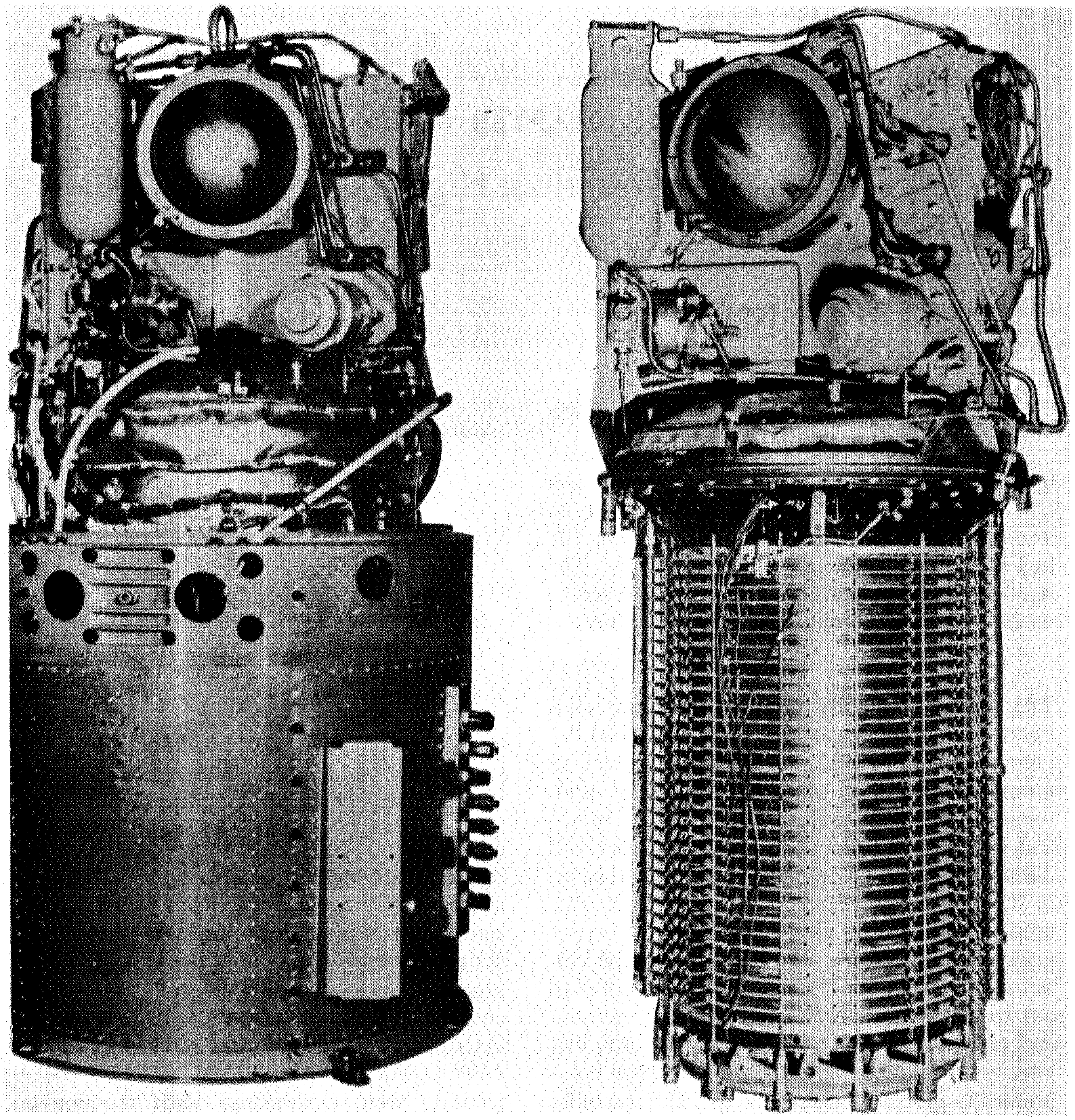

At left, shown completely assembled. At right, mounting structure and power section pressure cylinder are removed to reveal the 31-cell stack.

FIGURE 5.6.—Apollo fuel-cell powerplant by Pratt & Whitney Aircraft; Model PC3A-2 (ref. 5-1).

CHAPTER 6

Cell and Stack Construction: High Temperature Cells

6.1 MOLTEN-CARBONATE FUEL CELLS

6.1.1 Pittsburgh Consolidation Coal Co., Conversion of Carbonaceous Fuels to Electrical Energy, May 1954 to August 1958

The contract purpose was to develop a high-temperature fuel cell for use with water gas (H_2, CO, H_2O, and CO_2) as fuel and air as oxidant, with the eventual aim of integrating the fuel cell with a water-gas generator *(489)*. The waste heat generated in the cell would be used to supply the endothermic heat of the reaction

$$C+H_2O \xrightarrow{\text{heat}} H_2+CO.$$

The system originally proposed was the solid electrolyte high-temperature cell described by Davtyan (ref. 6.1). The electrolyte consisted of a mixture of sodium carbonate, monazite sand, tungsten trioxide, and sodium silicate melted and cast into a solid disk. The laboratory cell using this electrolyte was of the basic form shown in figure 4.4(b), with porous metal electrodes pressed against the electrolyte disk by screw-loaded spiders, which also acted as current collectors (see fig. 6.1). The area of contact between cell case and electrolyte was originally ground and polished to give a tight seal, but this was later found to be unnecessary. The cell was compressed to give a gastight seal, and the assembly was heated in a fluidized sand furnace. The contact between the electrolyte disk and the metal case establishes a half cell between the electrolyte and the case. Since the electrodes are connected to the two halves of the case, the case-electrolyte-anode forms a corrosion cell, as does the case-electrolyte-cathode. The case-electrolyte half cell must therefore be highly polarized; otherwise it will pass current by case corrosion.

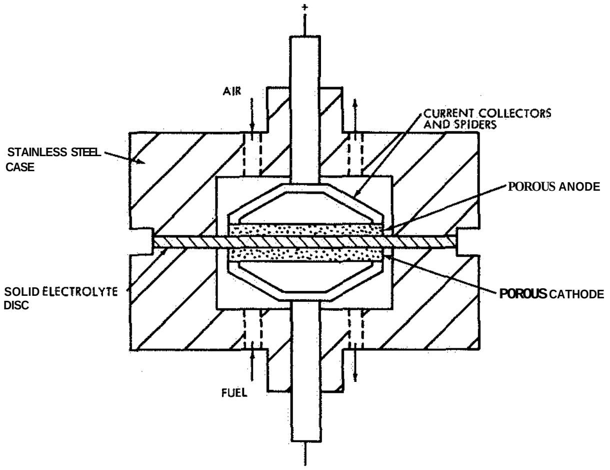

The cell was operated in a furnace containing fluidized sand to give even temperature.

FIGURE 6.1.—Original fuel cell for high-temperature solid electrolyte (after *489)*.

The electrodes were ⅛-inch-thick by 13/16-inch-diameter porous stainless-steel disks with an average pore size of 65 microns (*490*), which were welded into stainless-steel rings. Casting of the electrolyte by Davtyan's method led to phase separation; therefore, the mix was melted, cooled, ground, pressed at 10 to **20** tons per square inch, and the compact sintered at **1382**" F (750" **C)** for some hours. Even with slow cooling, troubles were experienced with warping and cracking. **A** layer **of** fine powder (a mixture of iron and iron oxides) had to be placed between electrolyte and electrodes; otherwise, the cell would produce only a small voltage at **1202°** to **1382" F** (650" to 750° C) with hydrogen and air as reactants. Impregnation of ferric nitrate into the porous disk was not as advantageous as the coat of fine powder *(491)*. Between *896"* and **1112**" F (480° and 600" **C),** the log of electric-cell resistance was proportional to reciprocal absolute temperature, the relationship expected for a true solid electrolyte. However, at 1112" F (600" C) the ohmic resistance fell suddenly, showing the presence of a liquid phase in the electrolyte disk. Cell performance decreased rapidly with time.

Copper-copper oxide on the air side gave poorer life ***(492).*** Switching hydrogen and air supplies increased performance, and the decay of performance with time was ascribed to concentration polarization due to buildup of oxide ion, $O^{=}$, at the cathode. High initial OCV was obtained (1.4 volts) since little product water was formed, but in use the water led to an OCV of about 1.1 (from the Nernst equation, a high reversible potential is obtained when the reaction product is present in minute amounts).

Since the electrolyte contained a fluid phase, the advantages of a true solid electrolyte were not present in the Davtyan or other carbonate-silicate electrolytes used. Therefore electrolyte disks were made from porous MgO refractory (about $\frac{1}{8}$ inch thick) and soaked in molten sodium carbonate ***(493).*** Measurement of ohmic resistance as a function of temperature showed a fluid phase at 1427" F (775" C). The IR loss in the cell was two to three times that expected from free carbonate electrolyte, and cell performance was improved over that with the previous electrolyte matrices. Heating and weighing of sodium carbonate in an airstream at 1562" F (850" C) showed no loss of carbon dioxide.

All the electrolyte matrices used cracked in the cell; and the cell design (see fig. 6.1) was such that the molten phase could be slowly lost to fluidized sand, leading to porosity of the electrolyte ***(494).*** A manometer was installed across the air and hydrogen feed streams to allow the differential gas pressure across the disks to be kept small in order to reduce cross-mixing of fuel and air through flaws in the electrolyte disk. Electrolytes of Na_2CO_3 in a matrix of Na_2SiO_4 were tried (not in a refractory disk), but solubility of silicate in molten carbonate led to the growth of large crystals of silicate and devitrification of the matrix.

Use of carbon dioxide in the airstream improved life. CO_2 must be supplied in the airstream in order to maintain cell operation, if oxygen is transferred across the electrolyte by carbonate ions, with release of CO_2 at the anode. A theory based on concentration polarization of oxide ion was proposed, in which diffusion of $O^{=}$ through the melt was the controlling factor. The Nernst equation for the system was given as

$$E=E^0+(2{\cdot}3RT/nF)\log\left[\frac{(H_2)(O_2)^{\frac{1}{2}}(O^{=})_{\text{anode}}}{(H_2O)(O^{=})_{\text{cathode}}}\right] \tag{6.1}$$

It was assumed that the anode reactions were

$$H_2+CO_3^{=}=H_2O+CO_2+2e^-$$
$$H_2+O^{=}=H_2O+2e^-$$

and that the concentration of oxide ion at the anode remained constant at a very low value. On the other hand, the concentration of $O^{=}$ at the cathode was assumed to build up to enable it to diffuse, thus leading to concentration polarization at the cathode. An attempt to fit experimental results to a mathematical prediction based on diffusion of $O^{=}$ was not succesful. (The principal error was probably the assumption that all current was carried by sodium ion. **A** molten salt obviously cannot behave like a salt dissolved in a large volume of supporting water; if sodium ion migrates to the cathode and is not discharged as sodium, it must be balanced by a corresponding amount of carbonate ion to maintain electrical neutrality. Since the molten sodium carbonate already occupies all the volume present, it cannot increase in concentration without causing pressure. This pressure at the cathode will cause bulk flow of the electrolyte toward the anode until the migration (due to the voltage gradient) of sodium ion is balanced by the reverse bulk flow of sodium ion. Then oxide ion and carbonate ion migrate and flow toward the anode. The treatment of this situation requires more than mere diffusion of oxide ion. When carbonate ion is discharged at the anode, some of the current is carried by carbonate, and when no CO_2 is supplied at the cathode, the electrolyte gradually changes to sodium oxide, with a higher ohmic resistance.)

The cell was redesigned to allow an inverted-cup electrolyte matrix to be used, with the sides of the cup contained in a trough containing molten salt ***(495).*** An asbestos gasket was used around the edge of the matrix, between the cell halves, to reduce loss of electrolyte. Fabricating the cups involved an excessive loss rate due to cracking. A high-purity periclase (95 percent MgO) was ground below 65 mesh, mixed with 2 percent aqueous methyl cellulose, pressed into the cup shape, dried, and fired for 15 hours ***(496)***.

Equimolar sodium lithium carbonate was used as electrolyte and gave a fluid phase at about 932" F (500" C). The stainless-steel electrodes were replaced with nickel electrodes in the form of sintered disks or mesh. At these lower cell temperatures, carbon monoxide fuel was found to deposit carbon, so the fuel was restricted to hydrogen. The layer of activator powder used previously was unnecessary with nickel electrodes. The nickel cathodes oxidized above 1292" F (700" C) and gave high resistance. Cell power failed within an hour, and the electrodes were flooded. Cell and furnace were modified by *(a)* eliminating the asbestos gaskets, which absorbed molten carbonate; and *(b)* insulating the furnace so that even temperatures were obtained without fluidized sand ***(497)***. Stainless-steel electrodes were again used with a layer of iron oxide activator powder; these worked satisfactorily down to 932" F (500° C), but were variable in performance due to variations in the electrode-electrolyte contact. The experiment showing the stability of sodium carbonate was not repeated with the new electrolyte.

At temperatures of 1112" F (600" C), a blank test with direct contact of electrodes showed that resistance of the leads, spiders, etc., was low ***(498)***. The air side, with CO_2, operated satisfactorily with stainless-steel electrodes, while the fuel side operated best with nickel electrodes, both without activator powder. (The use of reference electrodes would have considerably reduced the amount of experimental work at this stage.) Other methods of matrix preparation were tried ***(499)***, but the cups or disks were still breaking in use, partly due to reaction of carbonate with impurities in MgO. The stainless-steel cathodes corroded and were not suitable for extended use (500 and *501*). It was concluded that, apart from life factors, any metal gave a satisfactory electrode above 1112" F (600" C) on the air side, but that the fuel side needed nickel or stainless steel, plus iron activator powder at 1472" F (800" C).

In a later contract (*502*), porous air electrodes were made by applying a paste of silver to the MgO disk, drying, and firing at 1292° F (700" C). However, the silver film did not have satisfactory conductivity. Lithiated nickel oxide electrode disks were prepared, and gave good conductivity with no formation of lithium carbonate in contact with the melt. Calcining at 2732" F (1500" C) removed the fine pores and gave good strength. Air permeability tests indicated a mean pore size of 25 microns. These disks were welded in a ring, and the cell was redesigned as shown in figure 6.2 ***(503)***. Silver gaskets were used between the stainless-steel flanges and the electrodes, but problems of gas leakage and contact resistance were found.

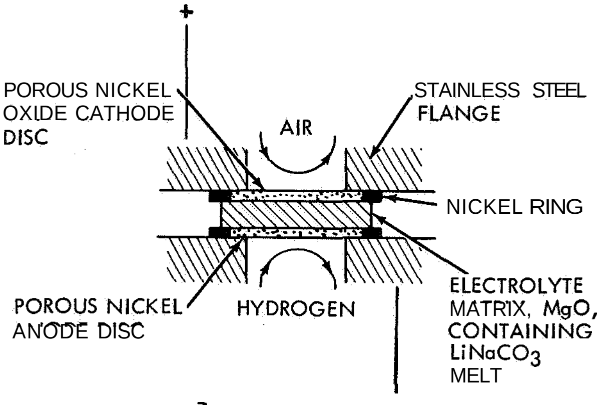
+
POROUS NICKEL OXIDE CATHODE DISC
AIR
STAINLESS STEEL FLANGE
NICKEL RING
ELECTROLYTE MATRIX, MgO, CONTAINING $LiNaCO_3$ MELT
POROUS NICKEL ANODE DISC
HYDROGEN
-

The stainless-steel flanges were used as current collectors, with silver gaskets between the flange and electrode contact areas.

FIGURE 6.2.—Modification of cell shown in figure 6.1.

Molten carbonate tended to flood the nickel oxide electrode; therefore, dual-porosity electrodes were used with the fine-pore layer next to the electrolyte disk. Stainless-steel corrosion products destroyed the conductivity of the lithiated nickel oxide. The OCV was between 1.0 and 1.1, and a current density of about 60 A/sq ft at 0.5 volt was obtained at 1292" F (700" C). Performance was fairly steady over some days of operation.

Another cathode system tested was silver screen backed by a porous stainless-steel disk ***(504)***. This gave good electrochemical performance, but was difficult to seal. With these electrodes, temperature variation from 932" to

1472" F (500" to 800" C) gave little change in performance with hydrogen and air (plus CO_2); but with carbon monoxide-carbon dioxide as fuel at lower temperatures, the performance was poor.

The final report on this contract (506) gave additional information on the methods of preparing electrodes and electrolytes (see ch. 3). The principal mechanical problems were cracking of the electrolyte matrix and electrolyte balance in the matrix: too much electrolyte led to flooding, while too little led to poor contact between electrolyte and electrode. Corrosion was severe at higher temperatures. Figure 6.3 gives current-voltage curves obtained under varying conditions for the first few days of operation. The effect of gas diffusion in the electrodes was calculated and the results suggested that the concentration drop across the electrode was small. The mean value of water in the fuel chamber was calculated for known flow rates of hydrogen at a specified current density, and the Nernst equation was used to get the theoretical reversible potential at this current density. The results are shown as the top curve in figure *6.3.*

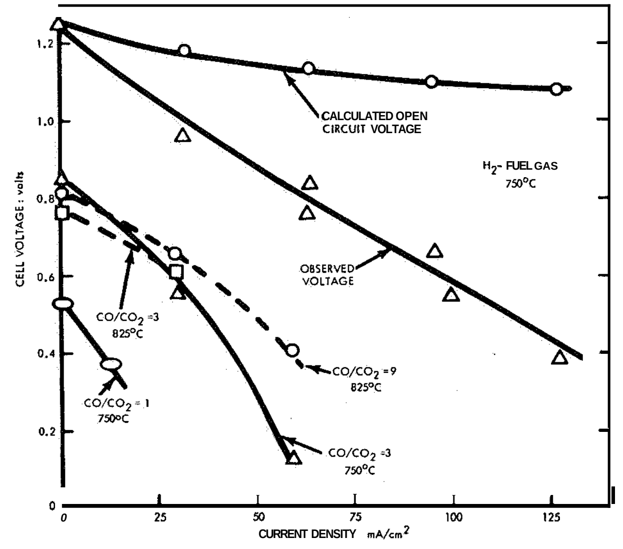

The cell used porous nickel anodes and 80-mesh silver-screen cathodes. **Air** (plus CO_2) was used at the cathode and hydrogen or CO-CO_2 mixtures at the anode.

FIGURE 6.3.—Current-voltage curves for the Consolidation Coal high-temperature fuel cell.

Since temperature did not affect performance with hydrogen at the temperature used, it was concluded that there was no activation polarization. The large difference between actual and predicted performances, shown in figure 6.3, was ascribed to ohmic polarization. The slope of the current-voltage curve gave a value of specific resistance of 5 ohms-cm², whereas direct measurement on the electrolyte with an ac bridge gave 0.7 ohm-cm². The extra resistance (ref. 6.2) was explained as being due to restriction of electronic conduction at the small points of contact of the electrode with the melt. The theory would explain the results if the contact area of the electrode with the electrolyte was about $(3)(10^{-4})$ cm²/cm². It is difficult to see why a fine-pore or mesh electrode pressed against an electrolyte-filled disk should make such poor contact. It was also shown that permeation of gas through the solid metal would be much too slow to support the currents found.

6.1.2 Central Technical Institute TNO in Holland, High-Temperature Galvanic Fuel Cells, January 1959 to 1962

Work at the Central Technical Institute TNO in Holland paralleled, in many respects, the work reported above.-Work prior to this contract was fully reported '(refs. 6.3 and 6.4). In this prior work a disk cell similar to that described above incorporated molten carbonates contained in an MgO matrix. Electrodes were made of thin layers (0.2 to 0.4 millimeter) of metal powder. The use of very fine powder led to slow sintering at cell temperatures. Silver made a satisfactory cathode above 932" F (500° C). A platinum anode showed no activation polarization at 932" F (500° C) with hydrogen as fuel. Activation polarization was observed for all anode materials with carbon monoxide as fuel at 1292° F (700° C); the order of activity was platinum and platinized metal powders > iron > nickel > cobalt > copper > chromium > manganese.

Carbon dioxide had to be added to the airstream. For good cells, with hydrogen at platinum anodes and oxygen-carbon dioxide at silver cathodes and after correction using the Nernst equation for the amounts of CO_2 and H_2O present, only IR polarization was observed, and the cell resistance obtained from the polarization agreed with that measured by ac techniques. Problems were experienced with leakage of gases from one electrode to the other and loss of electrolyte from the cell. The cathode was not much affected by hydrogen leakage (since water was rapidly formed) and was insensitive to inert gases. It operated well even at low partial pressures of oxygen. Similarly, the anode was relatively insensitive to the partial pressure of hydrogen except at low percentages (2 percent). When carbon monoxide was the fuel, oxygen leakage formed carbon dioxide, and the anode was sensitive to the partial pressure of CO. At partial pressures of CO lower than about 0.25 atmosphere, a limiting current was observed that decreased with decreasing CO pressure.

The principal aim of the contract was to further the studies by using a cell with lower ohmic resistance of the matrix melt (147). This cell was fabricated from a porous metal tube coated with metal powder on the outside. A paste of one-to-one ratio by weight of MgO-$LiNaCO_3$ was spread about 1 millimeter thick on the outside of the tube to form the electrolyte; the MgO was in the form of very fine powder (about 0.01-micron particle size). A layer of metal powder was coated on the outside of this, and the whole wrapped with wire gauze. Thus the inside of the tube was one gas chamber, and the other gas was on the outside of the tube. The cell was heated in a tube furnace, its ends projecting from the furnace and therefore relatively cold. This construction was used to avoid the gas leakage and electrolyte loss found with disk cells. The paste electrolyte was sufficiently conductive (about two-thirds of free electrolyte), gastight, and rigid over the temperature range 932" to 1292" F (500" to 700" C). However, contact between the various cell parts was not good (due to differential thermal expansion), and measured cell resistance was much higher than that of electrolyte alone.

Hydrogen performed better than carbon monoxide, which was in turn better than methane. Addition of steam to carbon monoxide or methane improved performance when nickel catalyst was present, due to formation of hydrogen. Hydrocarbons dissociated at cell temperatures to give hydrogen (see app. B). The major problems were the difficulty of making cells and the high IR losses in the cells. Reference electrodes were not used. Two similar electrodes of different sizes were assembled into a cell and fuel and oxygen passed alternately over the small and large electrodes. Fuel at the large electrode and oxygen at the small gave much better results than vice versa, showing that the fuel electrode was limiting. This technique obviously cannot give as precise information on the behavior of each working electrode as can reference electrodes.

Much of the work performed in 1960 (148) was concerned with methods for making paste forms and cells suitable for commercial production. Lifetimes of at least several weeks were obtained when silver or nickel was the central anode and silver or silver-zinc oxide was the cathode. Preliminary data were obtained on a "canal" cell in which a block of paste electrolyte was formed around porous tubes, some of which were anodes and others cathodes. The electrodes were connected in parallel.

Later work (151) led to the following conclusions: power output from the tube cells was limited by the fuel electrode to about 15A/sq ft at 0.6 volt with 1 H_2:1 CO_2 percent by volume, at flow rates allowing over 50 percent utilization of hydrogen and oxygen (from air). Faster flow rates gave better performance, but less utilization of reactants. This is in direct contradiction to previous conclusions that cell performance was not greatly dependent on the partial pressures of hydrogen or oxygen, unless the increased performance at higher flow rates is due to some effect other than the mean partial pressure of reactants present. Methane was an inferior fuel unless catalytically re-formed to hydrogen with steam, either outside the cell or with catalyst in the cell gas chamber. When a cell had been run on hydrogen, enough hydrogen was adsorbed on the catalyst to maintain performance for many hours after switching to methane or even nitrogen. It was concluded that methane was only slightly electrochemically active at 1292" F (700° C). Higher hydrocarbons were reactive at this temperature due to hydrogen produced from thermal cracking, with carbon deposition.

Performance was improved by mixing the anode powder with electrolyte powder. At operating temperature this formed an electrolyte bridge between electrode and paste. The electrode powder was nickel made from nickel oxide reduced in hydrogen at 1472" F (800° C), and 10 weight-percent of lithium-sodium-potassium carbonate was added. The eutectic melting point of this mixture was 752" F (400" C), while that of the $LiNaCO_3$ used in the paste was 950" F (510" C). When more than 30 weight-percent was added to the nickel powder, electrode flooding occurred. The electrode was formed from a layer about 1 millimeter thick, but a backing-screen current collector was needed for satisfactory long-term operation.

Corrosion of materials, which limited cell life, was particularly noticeable at junctions of dissimilar metals. Leads should therefore be made of the same material as electrodes. Corrosion was caused by creep of electrolyte over nickel or iron surfaces, but creep was less pronounced with silver. Silver dissolved in the electrolyte at the cathode, possibly to the extent of 10^{-3} mole-fraction at open circuit. On current drain, the ohmic gradient in the electrolyte and any polarization at the cathode favors the deposition of silver, and growth of dendrites on the cathode was observed. Lifetime of cells extended to some months, but they could not be cooled below the melting point of the electrolyte since the paste cracked, giving gas mixing across the electrolyte.

It was suggested that the principal cause of polarization at the anode was formation of bubbles of water and carbon dioxide between melt and electrode, which lowered the electrode-electrolyte contact area. Bubbles would come off sporadically, comparable to gentle boiling. The reasons why this process would give high polarization were not discussed clearly. If activation polarization were negligible, as claimed, a variation of true current density by as much as tenfold should produce little activation polarization. If electrolyte bridges existed between the electrode and electrolyte, then reduction of the number of these bridges should not give much constrictive ohmic resistance until the contact area was reduced to less than a percent of the total area (see sec. 6.1.1). It is possible that the presence of entrapped bubbles would lead to mass-transfer restrictions of hydrogen dissolved in electrolyte, and that this could be the major factor involved.

Many of the above results have been reported (ref. 6.5); the work is being continued, but not under sponsorship within the scope of this book.

6.1.3 Texas Instruments, Inc., Molten Carbonate Fuel Battery Program, February 1963 to February 1964

The purpose of the contract was to produce a 400-watt unit operating on gas from re-formed liquid hydrocarbons (see app. E), using the molten-carbonate fuel cell developed by Texas Instruments (607). The basic cell structure is shown in figure 6.4, in an experimental form which included a reference electrode on the cathode side. The porous metal electrodes (of silver, for example) were bonded to the electrolyte disk, which was thick enough ($\frac{1}{8}$ inch) to give adequate strength: The method of sealing disk to case to prevent gas leakage was not given. Methods of bonding the electrodes to the disk and constructing electrodes were given in a later report and are described in chapter **3.** The electrolyte was $LiNaCO_3$ in a refractory MgO disk (Norton LM833) of 30 percent porosity and 18 microns mean pore size. The cell was operated at 1112" F (600" C). The cell was thus similar to that investigated previously (secs.

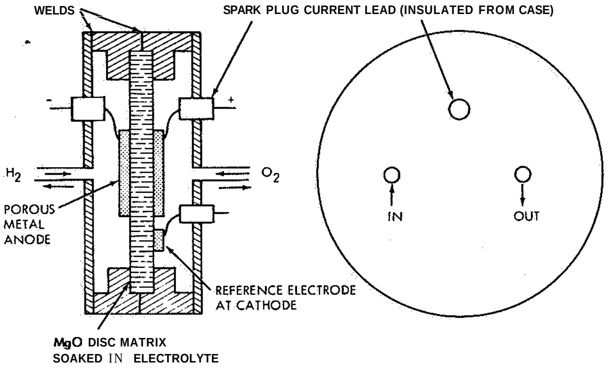
WELDS
SPARK PLUG CURRENT LEAD (INSULATED FROM CASE)
-
+
H_2
O_2
POROUS METAL ANODE
IN
OUT
REFERENCE ELECTRODE AT CATHODE
MgO DISC MATRIX SOAKED IN ELECTROLYTE

The porous metal electrodes were bonded onto the electrolyte matrix, which was supported in a steel case welded around the matrix. Since the two halves of the metal case were in contact, the leads from the electrodes were isolated from the case by taking them out through a modified spark-plug mounting. The area of an electrode was about one-sixtieth of a square foot.

FIGURE 6.4.—Texas Instruments' experimental high-temperature, molten-carbonate disk cell.

6.1.1 and 6.1.2) but without the problems of gas leakage, electrode-to-matrix contact, and fragility of electrodes. Results of this previous work suggest that 1112° F (600" C) would not suffice for electrochemical oxidation of carbon monoxide or hydrocarbons, but the life of the electrodes is increased by the lower temperature. Insulation of electrodes from the case eliminated the case-electrolyte-electrode corrosion cell of previous models.

The IR drops of anode versus reference and cathode versus reference were measured by interrupting the current through the cell and measuring the rapid change in voltage with an oscilloscope (see app. C for the circuit). Polarizations were directly proportional to preinterruption current, as expected, and the values of resistance (R_A and R_C) corresponding to these polarizations were therefore constant. The sum of R_A and R_C was less than the total cell resistance, R_T, measured in the same way, using the full cell potential; the difference was ascribed to the resistance of the electrolyte. (This is not correct. The difference is probably due to the reference electrode's being so far away from the working electrodes.) With hydrogen and 4:1 air plus carbon dioxide, the OCV was over **1.4.** Adding CO_2 to the hydrogen stream gave no change in the values of R_A, R_C, and R_T, but reduced the OCV and the voltage at low current density. The high OCV was explained as due to the small amounts of carbon dioxide and water present at high flow rates of pure H_2 (see below). The ohmic resistance of the anode had the same temperature coefficient that the electrolyte did; therefore, R_A was ascribed to constricted electrolyte current paths at the electrode-electrolyte interface. The ohmic resistance of the free electrolyte would have been 0.011 ohm for the one-sixtieth of a square foot of electrode area present. Since R_A was 0.05 ohm, and assuming that R_A consisted principally of the resistance of the electrolyte in the disk, the labyrinth factor of the disk would be 0.05/0.011, or about 4.5. This value is reasonable, and there is therefore no reason to believe that an ohmic constriction effect was present. The temperature coefficient of the cathode resistance was higher than that of electrolyte, and this resistance was ascribed to poor conductivity of silver oxide on the cathode. But both forms of silver oxide are very unstable at these temperatures, and even at low temperatures there is sufficient conductivity in silver oxide battery plates to give very high current densities.

A theory of cell operation was proposed, with the following anodic reactions:

(a) $M+O^{=}\rightarrow MO+2e^{-}$

(b) $MO+H_2\rightarrow M+H_2O$

(c) $CO_3^{=}\rightleftharpoons CO_2+O^{=}.$

In addition, equilibrium of the water gas shift was assumed:

(d) $H_2+CO_2\rightleftharpoons H_2O+CO.$

The Nernst equation for the anode was then taken as

$$E=E_0-(2{\cdot}3RT/nF)\log\left[\frac{(H_2O)(CO_2)}{(H_2)}\right] \qquad (6.2)$$

where E values are reduction potentials (more negative values give greater cell potential). Thus the high initial OCV with pure hydrogen was due to the small amounts of H_2O and CO_2 present; during current drain the buildup of these products reduced the potential. No activation polarization was present, although different catalysts could affect the performance by establishing the water-gas shift. This theory explained why faster flow rates of hydrogen or hydrogen-nitrogen mixtures caused increased performance, since the increased flow at a given current density would maintain lower mean pressures of H_2O and CO_2. Figure 6.5 shows typical results of current interruption. The rapid rate of fall of

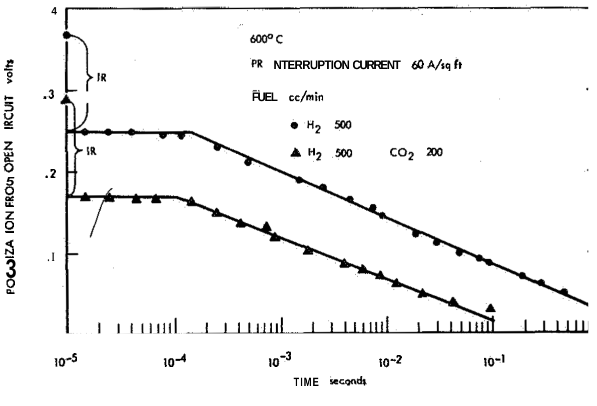

FIGURE 6.5.—Change of anode polarization after current interruption; Texas Instruments' cell.

polarization is anomalous, since there does not appear to be time for the flow to sweep out the anode gas chamber. The rapid fall also shows that the double-layer capacity was small.

Analysis of the electrolyte showed that lithium was lost, perhaps as Li_2O. The Li-Na carbonate phase diagram indicated that at 1112° F (600° C), solid Na_2CO_3 would precipitate when the lithium/sodium mole-ratio became less than 0.67. This was observed after 100 days of operation and caused higher IR losses in the electrolyte. Power densities were within the region of 50 to 100 W/sq ft and lifetimes of up to 1000 hours were possible.

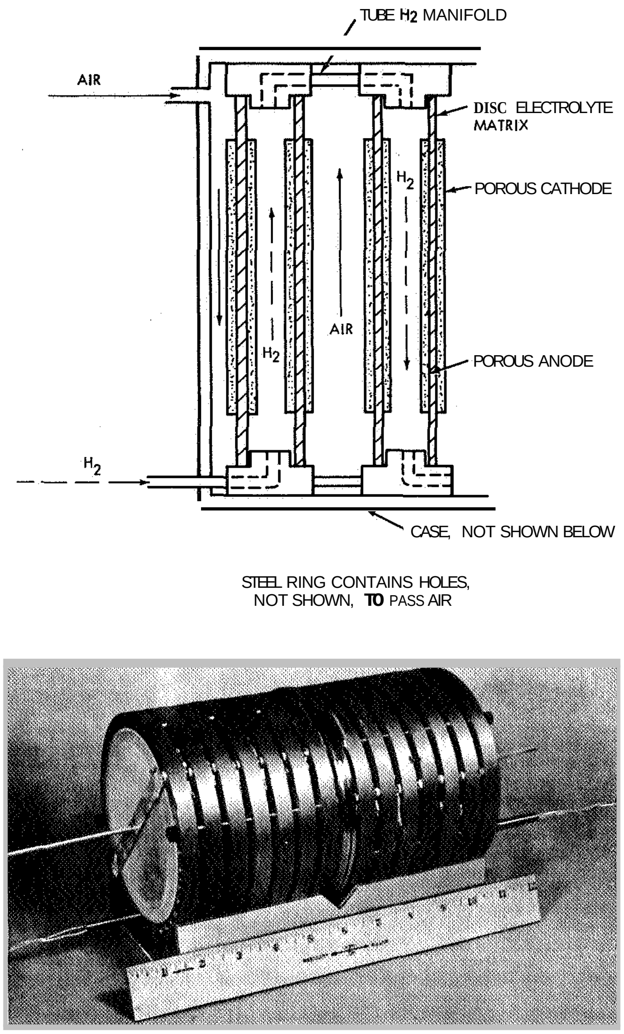

Each steel ring had two electrolyte disks sealed to it, with the space between acting as the fuel-gas chamber. Fuel gas was fed in series through the cells, using metal tubes to connect the manifold passages in the rings. Air was contained (by a case) in the spaces between the rings and was passed from one space to the next through holes in the rings. In the lower figure, the current collector on the end cathode is visible. This was a strip of silver screen embedded in the electrode. The strips on all cathodes in the left-hand 14 cells were connected to a common bus, insulated from the case. The anodes were connected to the rings and hence to the case. The opposite, arrangement was used on the right-hand side, *so* that the module was 2 stacks in series, each of 14 cells in parallel.

FIGURE 6.6.—Module of Texas Instruments' high-temperature cell.

A cell stack was built of 14 cells with electrodes of about 4½-inch diameter. Two cell stacks were joined together as shown in figure 6.6; the cells in one stack were connected in parallel, while the two stacks were connected in series. Parallel connection does not require a gas barrier between cells, as does the bipolar series arrangement, and it is particularly suitable where the electrode-electrolyte assembly is rigid, as in this cell. The case was used as one current connection between the cells in parallel, which reintroduces the possibility of a case-electrolyte-electrode corrosion cell. The other current connection was by means of a metal rod (silver) insulated from the rings by ceramic bushings. Because the cell products are hot water and carbon dioxide, it is not feasible to recirculate unconsumed hydrogen as is normally done in the cells discussed in chapters 4 and 5; therefore, series flow of fuel was employed to get complete fuel utilization in one pass through the stack.

As is nearly always the case with new cell designs, mechanical problems of machining tolerances and problems with minor points of design were found. When these were eliminated, it was found that silver dendrites were growing from the anode near the point at the edge of the electrode where the anode was grounded to the case. These dendrites grew right through the electrolyte matrix and shorted the cell (see later). It was also found that bringing the cell up to temperature with a simulated re-formed hydrocarbon gas (CO, H_2, H_2O, and CO_2) led to flooding of the anode by electrolyte. The use of this fuel mixture also gave lower performance than hydrogen alone. Single cell tests showed that 0.2 mole-percent of hydrogen sulfide did not affect cell performance.

To eliminate dendritic formation at the grounded anodes, later modules were built with only the cathodes grounded (622). The ohmic resistance of the parallel cathode connection was reduced by making taps through the case of each ring and connecting the taps to an external silver bus bar; the anodes were connected as before through an internal bus. The cells were brought up to temperature and activated with hydrogen (plus 5 percent CO_2) instead of the re-formed gas mixture. The hydrogen appeared to keep the nickel of the anodes in the reduced form, which prevented electrolyte flooding of the anode. The air side was fed with carbon dioxide during activation; the cell reached steady performance in about 12 hours, at 1112° F (600" C). Appreciable loss of carbon dioxide from the electrolyte was found unless small percentages of carbon dioxide were maintained in both reactant streams. Modules were made from mild steel, 304 stainless steel, and mild steel plated with 1 mil of silver. Lifetime was about 50 days, with power densities of about 40 W/sq ft. The output of single cells tested separately was 100 W/sq ft.

Shorts due to dendritic growth of silver were a common cause of failure. The dendrites grew out from the cathode at points distant from the strip of screen used as current collector. The dendrite problem was analyzed as follows. As Broers had shown (see sec. 6.1.2), the solubility of Ag+ in molten carbonates in the presence of carbon dioxide and oxygen is quite high (10^{-3} ion fraction). The rate of dissolution of silver as Ag^+ is increased by positive electrode potentials, and the cathode will dissolve silver, especially at open circuit. The ion can diffuse through the melt and deposit on the anode (as observed previously), but when current is drawn from the cell the potential gradient opposes diffusion and silver ion migrates back to the cathode. Thus silver ion continues to dissolve but is not completely diffused, and it is therefore redeposited in a dynamic equilibrium. The deposit occurs as dendrites, which grow out from the cathode. Any unevenness in current distribution and voltage across the face of an electrode leads to more favorable dissolution-deposit conditions at certain spots and hence to more rapid growth of dendrites at these spots. In a more detailed form, it can be reasoned that the potential gradients in the vicinity of an electrode are made up of ohmic gradient in the electrolyte, the double-layer voltage, and ohmic gradients across the face of the electrode (since current is removed at the edge of the electrode), as illustrated in figure 6.7. The bigger IR potential gradient in the electrolyte at side *b* leads to less movement of silver ion away from the silver cathode at *b*. Dendrites will be found toward side ***a***, where silver dissolves at ***a*** and is redeposited by the steeper IR gradient at a point between ***a*** and *b*. Screen current collectors over the entire face of the electrode were used to reduce IR gradients in the electrode (20-mesh silver screen). Bus bars were made of ⅛-inch-diameter silver.

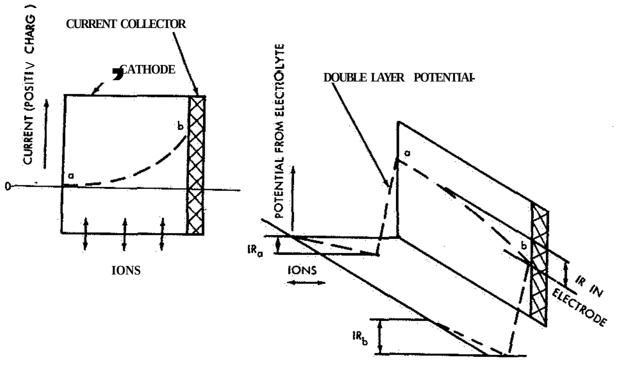

If the double-layer potential is the same on both sides of the electrode, *a* and *b*. IR_a must be greater than IR_b. This means that a bigger ionic current density is flowing at side *b*.

FIGURE 6.7.—Illustration of potentials in vicinity of cathode, with IR polarization in metal of electrode.

Four modules of 18 cells each were used to make a 100-watt demonstration unit using re-formed JP 4 as fuel. Silver-plated mild steel was used, and connections of the cathodes to the plated rings were made by silver flame sprayed on the electrolyte disk. The exit gases from the anode sides of the modules contained about 14 percent of uncombusted gas and 27 percent carbon dioxide. This was cycled to the air inlet to provide the carbon dioxide needed at the cathodes; combustion of unconsumed fuel also provided heat for the cell. The air-CO_2 mixture was passed through the stack in parallel flow to reduce pressure drop. At 100 watts and 2.8 volts, the power density was 15 W/sq ft. Mean cell voltage was 0.7 volt at 20 A/sq ft. This was considerably less than that found with single cells (100 W/sq ft at 0.7 volt with hydrogen and 60 W/sq ft at 0.5 volt with 50–50 hydrogen-carbon dioxide). The reasons for this reduced performance were not given. Sixty watts of power were required for air circulation.

6.2 SOLID-ELECTROLYTE FUEL CELLS

6.2.1 Westinghouse Electric Co., an Investigation of Solid Electrolyte Fuel Cells, February 1962 to April 1963

The contract called for demonstration of technical feasibility of the Westinghouse solid-electrolyte fuel cell for space applications (790). This fuel cell (see sec. 2.2.4) used a solid electrolyte with the nominal composition $(ZrO_2)_{0.85}$ $(CaO)_{0.15}$. Oxygen-ion mobility in this material is about 10^6 times the mobility of the other ions; and stabilized zirconia behaves as a true solid electrolyte, passing oxygen ions while maintaining its solid structure. The solid electrolyte was prepared by blending the zirconia and calcia, calcining, milling, pressing with an organic binder, and sintering. The final sintering-densification process was carried out at 3002° F (1650° C) to give a density at least 95 percent that of theoretical.

Densifying the material from about 50 percent to less than 5 percent porosity halved the specific resistance to oxygen-ion transport (see app. C for resistivity as a function of temperature). In the absence of oxygen (with argon passed over a niobium getter), the membrane could no longer transfer oxide ions, and conductivity was due to the electronic current through the solid. Under these conditions, electronic conduction was found to be less than 1 percent of ionic conduction during cell operation. A survey of compatible electrode materials was made (see app. C). Electrodes were made by spraying a suspension of platinum onto the solid electrolyte, followed by drying and sintering. The resistance of this porous platinum, 2 to 3 g/ft², was about twice that of the resistance of bulk platinum.

Cells were made from disks about 2 inches in diameter and 0.05 inch thick. Because they cracked on heating, during operation, and because of leakage of seals, the design shown in figure 6.8 was proposed. The segments shown were made from pressed and fired electrolyte, ground to tolerance. They were 1.26 centimeters long and 2.37 centimeters in diameter, with a wall thickness of 0.03 centimeter. A gold-platinum alloy was used for the bond between the porous platinum electrodes and the seal between segments (see detail in fig. 6.8). The cell gave less than 10 A/sq ft at 0.7 volt.

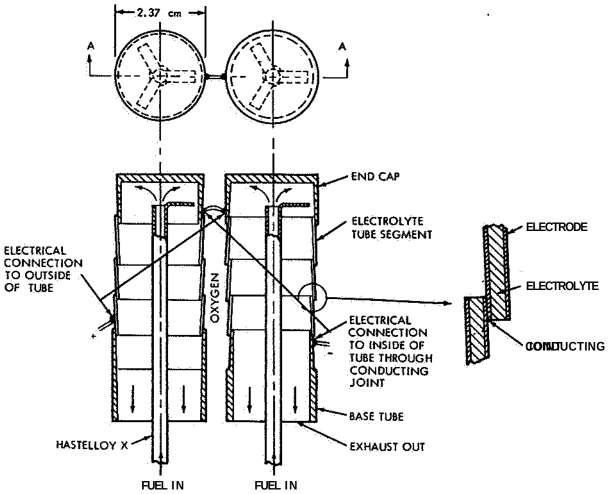

Electrodes of thin porous films of platinum were sprayed on the outside and inside of the segments. The detail on the right-hand side shows that the outer cathode of one segment was connected to the inner anode of the next, so that the segments were electrically in series.

FIGURE 6.8.—Segmented tube-cell design of Westinghouse solid electrolyte fuel cell (*790*).

Since it was believed that the cell operated as a concentration cell, the possibility of using the vacuum of space as fuel was investigated. The cell would be limited by mass transfer of oxygen away from the anode. At high vacuum, molecules leaving a layer close to the surface should not return to the surface, therefore the rate of loss of gas should be:

rate per unit area = concentration at surface × mean molecular velocity away

or

$$\frac{\text{Moles}}{\text{Area second}} = (P/RT)(8RT/\pi M)^{\frac{1}{2}}. \qquad (6.3)$$

At 1832" F (1000" C), a current density of 0.1 A/cm² (93 A/sq ft) would require a mass transfer of oxygen from the anode of about (2.5) (10^{-7}) g-mole/cm²-sec. A mean molecular velocity of 10^5 cm/sec thus gives a value of P close to the anode of about 10^{-7} atmospheres. The Nernst equation predicts a maximum (no polarization) cell potential of

$$E = (2 \cdot 3RT/4F) \log (10^7/1)$$

when the cathode oxygen pressure is 1 atmosphere. Therefore, at 1273"K (1832"C), E would be about **0.4** volt. With this type of cell, heat would have to be supplied to maintain the operating temperature (especially since the anode would radiate large amounts of heat); it was concluded that the vacuum system would have little or no advantage over the direct use of hydrogen fuel.

A new electrolyte, $(ZrO_2)_{0.90}(Y_2O_3)_{0.10}$, was investigated and found to have less than one-fifth of the resistance of the zirconia-calcia electrolyte *(791)*. Again, the electronic conductivity was less than **1** percent of the ionic conductivity. The electrolyte was sandblasted and etched in aqua regia before being sprayed with platinum paint (Hanovia 6926), followed by drying and sintering to form a porous platinum electrode. This treatment gave more stable resistance of the platinum with time. Seals were made with platinum paint-platinum gasket-platinum paint fired for **4** hours at 2552° F **(1400" C)**; they were strong, but not gastight. Other seals were tried, including metal oxides, a vitreous enamel, and gold-plated platinum. At low flow rates of hydrogen, sufficient oxygen leaked through the seals into the fuel to reduce cell performance to very poor values. Also, above **1940° F (1060° C)**, platinum was volatilized; the electrodes were blistered, and hydrogen appeared to loosen the anode. However, cell performance was considerably better with yttria-stabilized than with calcia-stabilized zirconia, giving about **100** A/sq ft at **0.7** volt for a disk cell.

Tests with hydrogen *(792)* showed that there was no activation or concentration polarization, but the ohmic resistance of the cell changed with time due to sintering of the electrodes, changes in the electrode-electrolyte bond, and loss of volatile platinum oxides at the oxygen electrode. It was felt that this last problem could be solved by alloying the platinum (with gold, for example). The resistance of a flat-cell sandwich was measured in a dry hydrogen atmosphere and with an applied potential. Without current flow the electrodes were adherent, but anodes loosened when oxygen ions were discharged. It was not explained how the cell would continue to support current when no oxygen was supplied to renew the ions. Leads were fastened on an electrode and current passed along the electrode from an external source, with no cell current being drawn. Electrode adherence was good, showing that it was not current flow in the electrode which caused separation.

Disk cells were made with lava end plates. Platinum-foil gaskets were used between the end plates and the electrode-electrolyte-electrode sandwich, and vitreous enamel was the sealant between lava and gasket. The cell was not completely tight; its performance decreased with time, dropping to about half the initial value after **900** hours. Assembly of cell stacks led to cracking of the solid electrolyte. **A** bell-and-spigot design was constructed, as shown in figure **6.9.** A mathematical optimization was used to arrive at the cell dimensions, which were **0.472-**

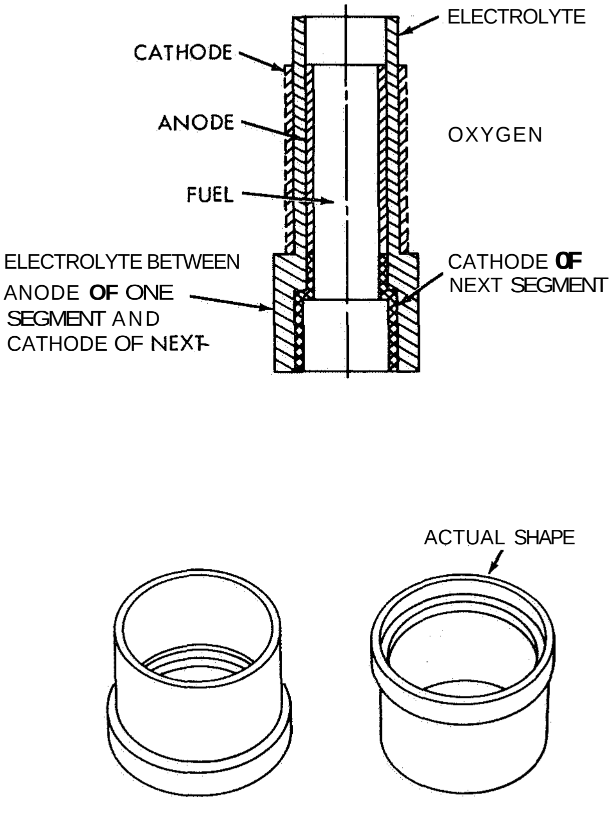

To give better sealing between the tube segments shown in figure 6.8, the design shown here was adopted. The electrode layer is very thin (the drawing is not to scale) and the top of a cell fits into the bottom of the next cell, giving series connection of the cells. It can be seen that there is an electrolyte connection between the anode of one segment and the cathode of the next, which leads to an internal partial short circuit. Ions flow from the cathode to the anode of the upper segment and electrons from the anode to the cathode, giving a current loop in the region shown. This parasitic current must be kept small.

FIGURE 6.9.—Bell-and-spigot design of the Westinghouse solid electrolyte fuel cell.

inch (1.2 cm) diameter and 0.354 inch (0.9 cm) long, with 0.078-inch (0.2 cm) overlap, giving an effective cell length of about half a centimeter. Electrolyte thickness was 0.015 inch (0.037 cm), and the segment weighed 1.92 grams. This type of design has a current flow pattern as shown in figure 6.10. An optimum size exists for a given set of conditions, maximizing the power output per pound or cubic foot at a set efficiency. The measured cell resistances were 0.18 ohm for the electrolyte, 0.06 ohm for the electrodes, and about 0.1 ohm for the contact.

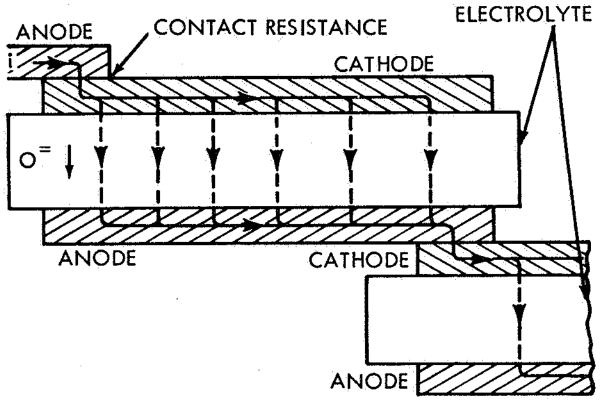

Optimum design is when maximum power output is obtained for a given length of tube of a given diameter. Because the electrodes are very thin, they have a relatively high ohmic drop along them. It is readily visualized that the mean current path is: entry point to halfway along the anode, across the electrolyte, along cathode to exit point. Thus the mean electrode resistance per cell goes down as the length of the cell decreases. However, the mean electrolyte resistance goes up. In addition, the fraction of dead area due to the contacts between cells goes up (keeping a fixed contact resistance per cell) as the cells are made smaller. There is, therefore, an optimum size of cell for any given set of conditions.

FIGURE 6.10.—Flow pattern of current in segmented-tube construction.

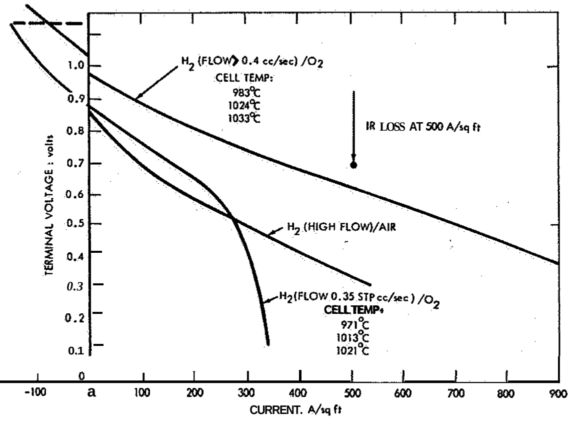

The figures are the mean values per cell taken from a three-cell stack ($1.95 cm^2$ per cell). The fuel was hydrogen saturated with water at 36° F (2° C). The solid electrolyte was $(Zr_2O)_{0.9}$ $(Y_2O_3)_{0.1}$.

FIGURE 6.11.—Performance of the Westinghouse solid electrolyte tube cell.

The final report *(793)* briefly summarizes the previous work and estimates the power output possible from tube cells. For cells alone, it was estimated that a 500-watt unit would weigh 25 to 47 pounds. Figure 6.11 gives the power output of the cell. The platinum coat was electroplated with **3** mils of platinum at the seal portion, followed by 7 mils of gold. **A** brazing shim of 18 percent nickel and 82 percent gold (by weight) was positioned between the surfaces, and the parts were heated at 2057" F (1125" **C)** for 20 minutes in hydrogen. This procedure was developed from a study of the phase diagram of nickel-gold-platinum. The nickel-gold shim melted at 1742° F (950° C) and as the temperature was raised, first gold and then platinum went into solution. Solidification of the joint metal then took place, leaving a well-filled joint of Pt-Au-Ni attached to solid platinum firmly bonded to the electrolyte.

6.2.2 Westinghouse Electric Co., Contract With Office of Coal Research, December 1962 to Present

The first phase of the contract had the purpose of developing a 100-watt unit, using the cell described above, to burn pulverized or gasified coal (ref. 6.6). The second phase was the construction of a 100-kilowatt unit, to provide design data for a full-scale plant. Progress reports issued under this contract are now available, and the final report will be made available (ref. 6.7). The general concept has been discussed briefly (ref. 6.8).

A brief outline of progress will be given here, without reference to each progress report.

The cell design was similar to that shown in figure 6.9, although search was made for less expensive materials of construction. Electrolytes of zirconia-calcia-magnesia were investigated in the hope that the expensive yttria in the formulation $(ZrO_2)_{0.9}(Y_2O_3)_{0.1}$ could be replaced. However, resistance of the new electrolytes was too high. Materials other than platinum were investigated as electrodes but most were not satisfactory due to failure of adherence to the electrolyte with time. Nickel was the most promising electrode material, although oxidation at the electrode-electrolyte interface led to high contact resistance.

Semiconducting electrodes with mixed electronic and oxygen-ion conductivity were investigated, with the objectives of obtaining (1) high electronic conductivity, (2) high oxygen-ion conductivity and hence good oxygen transfer, and **(3)** good adherence to the solid electrolyte. Semiconducting electrodes were made from zirconia or doped with oxides which have two valence states; the following were tried: Ce^{3+}-Ce^{4+}, Pr^{3+}-Pr^{4+}, Nd^{3+}-Nd^{4+}, Sm^{2+}-Sm^{3+}, Eu^{2+}-Eu^{3+}, Yb^{2+}-Yb^{3+}. Materials were reacted at 1400" C, pressed, presintered at 1400" C for 2 hours, and fired at 2000" C for 2 hours. Conductivities and the activation energy for conduction were measured, in addition to X-ray crystallographic properties. It was concluded that ZrO_2-Ce_2O_3 was a mixed conductor but the others were probably almost entirely ionic conductors and thus not useful as electrodes; conductivities were low. Praseodymium oxide stabilized with calcia showed electronic conduction, but conductivity was too low and the material lost oxygen at 1000" C. Spinel structures were investigated but gave multiphases instead of the required solid solutions. Promising results were obtained with perovskite systems such as $LaCoO_3$-$SrCoO_3$, $LaFeO_3$-$SrFeO_3$, and $LaFeO_3$-$ThFeO_3$.

A 100-watt unit was built from 20 tubes containing 20 cells each, the active area of each cell being about 2 cm². Series electrical connection was used, and the OCV was about 200 volts. Performance with hydrogen and air was close to that predicted from previous single-cell studies, although about 5 percent of the joints leaked, even after repeated repairing. Carbon monoxide was *not* a satisfactory fuel and, therefore, it was necessary to provide a shift reactor to give the reaction

$$CO + H_2O \xrightarrow{\textit{catalyst}} CO_2 + H_2.$$

This reaction is not favored at the high temperatures of the cell. It was suggested that Cr_2O_3 catalyst be used as sintered bars in the tubes, or that fuel be supplied to the outside of the tubes, with catalyst then contained between stacks of tubes.

A general design of a 100-kW unit was given, assuming that the fuel cells would be similar to the experimental tube cells. To avoid introducing diluent nitrogen in the fuel gases, coal was gasified by hot, partially-reacted, fuel gas coming from one stack of fuel cells. The exit gas from the gasifier went to fuel cell stacks in series, with as complete oxidation as possible being obtained in the later stacks. The fraction of partially-oxidized fuel gas which was circulated back to the gasifier was adjusted to supply endothermic heat of gasification and heat losses:

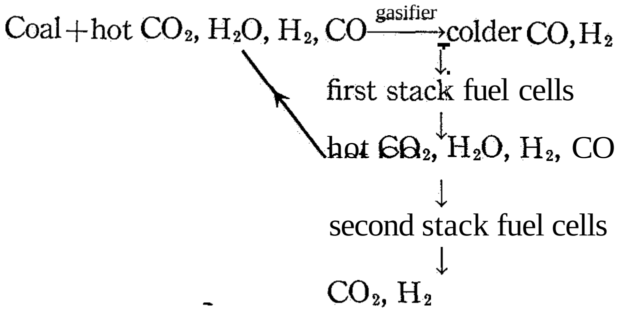

The exit flue-gases (separate streams of combusted fuel and nitrogen) from the last fuel cell stack exchanged heat with the incoming air to the fuel cells. The fuel gas from the gasifier was cooled to 750" F, and hydrogen sulfide removed with iron oxide. The gas was then reheated by heat exchange before entering the fuel cell stacks.

This design consisted principally of material and heat-flow sheets and gave no mechanical details. Several features of the system can be criticized and any final process which evolves is unlikely to be like that proposed. For example, heat for gasification is supplied by gas entering at 1850" F and leaving at 1750" F. The small temperature difference means that a great deal of heat is being circulated for every Btu used for gasification, which will surely lead to excessive heat losses. Economic analysis showed that platinum was too expensive to be used as electrode material and that electrolyte fabrication procedures were too expensive. It was concluded that a power density about 360 W/sq ft and a 5-year life would be necessary to make the process economic. The 100-watt unit performed at 150 W/sq ft on hydrogen and air, and it apparently could not utilize carbon monoxide or gases containing sulfur impurities. The objectives of the contract were unreasonably ambitious, considering the basic knowledge of cell behavior available at the time. Certainly there is little point in preparing large-scale units and designs if basic cell problems have not been overcome.

6.3 CONCLUSIONS

The molten-carbonate cell has not been taken to the advanced stage of development of the lower temperature hydrogen-oxygen cells. The power outputs, e.g., Texas Instruments modules, can possibly be improved by further research and development, but the molten-carbonate cell is rather low powered compared with the others available and not suitable for applications in which hydrogen and oxygen are the reactants. The great potential advantage of high-temperature cells is that they can use cheap, dirty fuel gas from hydrocarbons or coal. For applications of this kind the cells must have long life, low maintenance, high efficiency, and low construction cost. None of these requirements are met at the moment.

The technical problems of molten-carbonate cells are as follows: molten-carbonate electrolyte is not like an aqueous electrolyte, which can be expanded or contracted in volume by adjusting the rate of removal of water from the cell. Any change in volume of salt electrolyte in a matrix (due to loss of carbonate by creep, reaction with components, or loss of lithium in volatile products) causes contraction of electrolyte away from the desired electrolyte-electrode interface. Thus electrolyte may have to be replenished from time to time. Again, because fuel cannot be recycled to any appreciable extent, a cell stack must consume a reasonable amount of fuel in one pass. Faradaic efficiency is lower than with systems which can return unused fuel to the cells. Because of the higher temperature, the loss of Nernst potential due to decrease in concentration of reactants and buildup of products is about 0.09 volt per concentration-decade of hydrogen instead of the 0.03 volt of low-temperature cells. To avoid buildup of oxide ion at the cathode, carbon dioxide is added to the air stream; current is carried by carbonate ions, with carbon dioxide being evolved at the anode. This is unfavorable to the Nernst potential, which becomes, at 1112" F (600" C),

$$E = E_0 + (0.09)\log\left[\frac{(H_2)(O_2)^{\frac{1}{2}}(CO_2)_{\text{cathode}}}{(H_2O)(CO_2)_{\text{anode}}}\right] \qquad (6.4)$$

At the electrolyte-electrode interface, $(CO_2)_{\text{anode}}$ tends to increase with higher current, while $(CO_2)_{\text{cathode}}$ goes down.

The cells do not utilize carbon monoxide, methane, or higher saturated hydrocarbons directly at temperatures of 1112" to 1292° F (600" to 700" C), and water has to be added to re-form them to hydrogen. This addition of water is also unfavorable to the Nernst potential. For example, adding stoichiometric water to re-form methane to CO_2 and H_2 leads to a final product (assuming $CO_3^{=}$ discharges) of $4H_2O + 4CO_2$, while direct electrochemical oxidation gives $2H_2O + 4CO_2$. Theoretically, the water produced electrochemically should re-form the hydrocarbon without the need for additional water, but this does not appear to work in practice.

Undoubtedly, a major cause of the low-power output of cell stacks-is depletion of hydrogen and buildup of carbon monoxide in the gases passing through the cells. Direct electrochemical reaction of carbon monoxide would have the same effect on potential and power as increasing the pressure of hydrogen. But high-area catalytic electrodes, for direct reaction of carbon monoxide or hydrocarbons, would probably sinter at cell temperatures, leading to decrease in performance with time.

Massive silver is too expensive as electrode material. Dendrite formation also weighs against its use. At the fuel electrode, nickel leads to carbon deposition from carbon monoxide (by the reaction $2CO \xrightarrow{Ni} CO_2 + C$), although it can be silverplated to avoid this problem. At the air electrode, nickel or silver-plated nickel oxidizes to give a high resistance (nickel oxide is stable at these temperatures in the absence of a strong reducing agent). The high temperatures make metal conductivities low, so that ohmic resistance of electrodes, current collectors, and cell connections are a problem.

To summarize, the major problem (apart from mechanical problems which *can* probably be solved) seems to be lack of cheap, stable electrodes which *can* directly utilize carbon monoxide and hydrocarbons.

The significance of the calculation quoted in the Westinghouse work must not be overlooked. If fuel reacts with O_2 discharged from the anode, the behavior is identical to that of a high vacuum in the anode chamber. The calculation shows that a current density of 100 A/sq ft produces a cell potential of approximately 0.4 volt, due to the relatively high pressure of O_2 required at the electrode to transfer O_2 to the anode chamber. Good cell voltage will only be obtained if fuel reacts with oxygen within a distance of 1 mean-free-path from the electrode surface. The results of Central Technical Institute and Texas Instruments suggest that H_2 adsorbs and reacts on the surface, thus keeping the effective partial pressure of O_2 very low at the electrode. It can be presumed that hydrocarbons and CO do not react in this way.

Some of the same problems appear in the Westinghouse cell discussed above. The power outputs shown in figure 6.11 look impressive, but in the region of acceptable voltage efficiency, about 0.7 volt, the current densities with hydrogen/air are similar to those obtained with the molten-carbonate cell at high flow rates of hydrogen. When the flow rate is restricted, performance falls off rapidly as hydrogen is used **up.** For the space application investigated, one might have removed water and returned unused hydrogen, thus maintaining the partial pressure of fuel. This is not possible when the cell is run on gas from hydrocarbons or coal. However, if this were a true concentration cell, as originally claimed, it could use carbon monoxide or hydrocarbon vapor directly, since the function of the fuel is to keep the partial pressure of oxygen low near the electrode surface. It is amazing that this claim was made and later had to be retracted, since the identical error was made years before with the molten-carbonate cell. The inability to use carbon monoxide, without first performing the water-gas shift reaction, removes one of the major advantages claimed for the cell. If hydrogen sulfide has to be removed as well, the system has little advantage over a medium-temperature cell using purified hydrogen from a re-former or gasifier.

Because the electrolyte is solid, there are no problems of electrolyte flow in the electrode, and this is a big advantage over the molten-salt cell. It means that the electrodes can be made very thin, since they do not have to stabilize a fluid; consequently, gas-diffusion problems are reduced. The segmented-tube design is, in my opinion, not likely to be useful for larger scale units and the mechanical problems of making plate cells and stacks will have to be solved.

The major drawbacks, in comparison with the molten-salt cell, are *(a)* platinum is used in the construction, and *(b)* it has not been demonstrated that solid electrolyte cells will have long lives at the high temperatures required to give suitable conductivity of the electrolyte. The cost of platinum will make the cell uneconomic for most uses and an alternative material must be found.

Use of the cell for the type of space application suggested in section 6.2.1 is unlikely. Even if the cell had zero weight, the associated insulation and starting heaters would be heavy. If fuel were circulated through a condenser, the heat exchangers and condenser would have to be large to remove heat from the exit gases at over **1832**" F (1000° C). Similar power densities can be obtained from lower temperature cells, with less complexity of associated equipment.

Investigation of this cell should continue, but the emphasis should be on the basic problems of electrode materials, electrochemical catalysis of carbon monoxide and hydrocarbon oxidation, lower operating temperatures, and more feasible construction techniques. Unless the cell is developed to the stage where it is cheap, has long life, and can use dirty fuels, it is not likely to compete with other fuel cells or other methods of generating electricity.

6.4 REFERENCES

6.1. **Davtyan, O. K.: Bull.** Acad. Sci. USSR, no. 2, 1946, pp. 215–218.

6.2. **Gorin, E.; and Recht,** H. L.: Fuel Cells. Ch. 8. G. J. Young, ed., Reinhold Pub. Corp., 1960.

6.3. **Broers,** G. H. J.: **and Ketelaar,** J. A. A.: Fuel Cells. Ch. 6. G. J. Young, ed., Reinhold Pub. Corp., 1960.

6.4. **Broers,** G. H. J.: High Temperature Galvanic Fuel Cells. Ph. D. thesis, University of Amsterdam, 1958.

6.5. **Broers,** G. **H.** J.; **and Schenke, M.**: Fuel Cells. Vol. **11,** ch. 3, G. J. Young, ed., Reinhold Pub. *Corp.*, 1963.

6.6. **Office of Coal Research, Deft. of Interior:** Publicity Release. Dec. 9, 1962.

6.7. **Office of** Coal **Research, Dept.** of **Interior.**

6.8. **Zahradnik,** R. L.; **Elikan,** L.; **and Archer, D.** H.: Fuel Cell Systems. Advances in Chemistry Series no. 47, Am. Chem. Soc., 1965, pp. 343–355.

CHAPTER 7

Cell and Stack Construction: Sodium Amalgam-Oxygen Cells

7.1 E. YEAGER ET AL., WESTERN RESERVE UNIVERSITY, The O_2 Electrode, 1951 to Present

The amalgam cell was first investigated by a group headed by Prof. E. Yeager, who generated much of the basic information necessary for the development of the cells. The half cell NaHg/NaOH/H_2(Pt) was tested in a simple u-tube containing amalgam, with electrolyte floating on the amalgam in one arm of the u *(761,* December 1951). A platinized-platinum electrode in the electrolyte acted as a low-polarization hydrogen-evolution electrode. The sodium concentration was 0.1 to 0.8 weight-percent (the upper limit being the concentration at which a solid phase appeared). The cell reaction was

$$\begin{array}{c} 2Na \rightarrow 2Na^+ + 2e^- \\ \underline{2H_2O + 2e^- \rightarrow 2OH^- + H_2} \\ 2Na + 2H_2O \rightarrow 2NaOH + H_2. \end{array}$$

Open-circuit voltage was about 1.0, and current densities of 1000 A/sq ft were obtained; the straight-line relationship between voltage and current indicated that most of the polarization was IR polarization in the electrolyte. Activity coefficients of dissolved sodium were derived from the open-circuit potentials of the sodium-amalgam half cells and agreed with literature values (*763*), as shown in figure 7.1. The OCV values were, therefore, theoretical reversible potentials. Only IR polarization was present out to 1000 A/sq ft. The self-discharge rate due to hydrogen evolution at the amalgam was low.

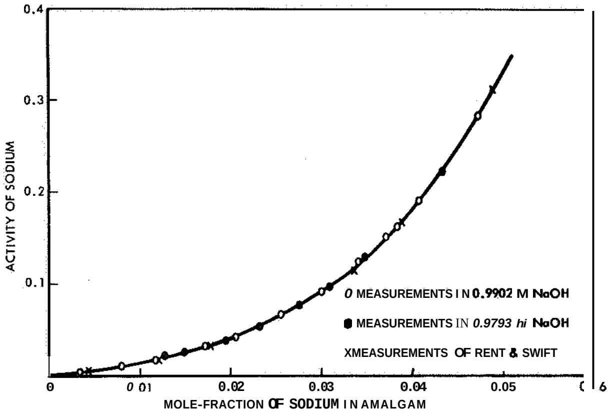

The reference state was taken as

$$\lim_{\substack{x \to 1 \\ Hg}} \frac{\alpha_{Na}}{x_{Na}} = 1$$

where α_{Na} is the activity of sodium in amalgam, x_{Na} the mole-fraction of sodium in amalgam, x_{Hg} the mole-fraction of mercury. (The standard state is therefore 1 mole-fraction of sodium; i.e., pure sodium.)

FIGURE 7.1.—Activities of sodium in dilute sodium amalgam 77" F (25" *C*) (763).

An extensive review of the properties of alkali metal amalgams (766) gave densities, viscosities, thermal and electrical conductivities, transference numbers, phase diagrams, activities, etc. (see also 778 for additional chemical properties). The diffusion coefficients of alkali metals in mercury were about (0.5)(10^{-5}) to (1)(10^{-5}) cm^2/sec. In addition, work was carried out on oxygen electrodes (see sec. 17.4.2) in alkaline solutions.

The proposed sodium amalgam-oxygen continuous-feed cell *(774)* gave an anode potential at 77° F (25° C) of

$$E = -1.957 + 0.0591 \log [\alpha_{Na^+}/\alpha_{Na}]. \qquad (7.1)$$

The activities of sodium were related by $\alpha_{Na} = \gamma x_{Na}$ to the concentration of sodium in the amalgam in mole-fraction units where the activity coefficient γ could be approximated by

$$\log \gamma - 16.4 x_{Na}. \qquad (7.2)$$

(For example, a sodium concentration of 0.5 weight-percent is 0.045 mole-fraction of sodium.

The activity coefficient is then 5.47, and the sodium activity is about 0.25.)

The amalgam electrode consisted of a vertical steel plate with amalgam fed to the top. The amalgam wetted the plate and formed a thin, flowing film on the steel. The cathode was a vertical plate of porous carbon, drilled to receive an oxygen feed tube (copper, force fitted into the hole) which also acted as the electrical lead. One face of the carbon was sprayed at 122° F (50° C) with a suspension of active carbon powder and gum rubber in benzene (90 weight-percent carbon to 10 of rubber). The active carbon was Nuchar C (West Virginia Pulp & Paper Co.) which had been impregnated with 15 weight-percent of silver. A polymethacrylate coat was applied to seal the pores on the back and sides of the porous carbon, and was also applied to the back of the steel anode. The electrodes were placed in 5 *M* sodium hydroxide solution, and the flowing amalgam which dripped off the bottom of the anode was collected and recirculated to the top (see fig. 7.2 for cell performance). Polarization was due to IR losses and activation polarization at the oxygen electrode.

Air was excluded from the amalgam to prevent impurities from causing flow restriction in the amalgam-distribution nozzles, and sodium concentration was kept below 0.55 weight-percent to prevent slush formation. Iron oxide particles from unclean steel led to the formation of amalgam "butter."

The work reported had been carried out prior to 1955 and no further work had been done, since Union Carbide and the M. W. Kellogg Co. had started work on the cell at that time. One problem with the cell was high heat release, about 0.7 watt per watt of electrical energy, at 150 A/sq ft and approximately 1.5 volts.

7.2 M. W. KELLOGG CO., Sodium Amalgam-Oxygen Fuel Cell, May 1960 to December 1963

The purpose of this contract was to investigate the feasibility of the sodium-amalgam cell for submarine applications (*385*). The proposed design was based on prior investigations (dating from 1956) by the Kellogg Co., under contracts whose reports are not generally available. The criteria to be met by the cell were: 1000 kilowatts at 300 volts for 1 hour, 100 kilowatts at 480 volts for 5 hours; maximum roll and pitch angle of 45 degrees; weight 10 000 pounds; volume 200 cubic feet; and flooded operation to 6000-foot depth of sea water.

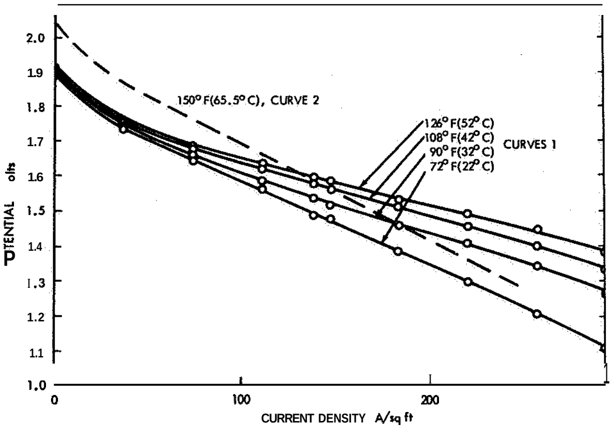

Curves 1 (774): Western Reserve University

Amalgam concentration: 0.44 weight-percent Na; 5 M NaOH+sea water; oxygen pressure, 1 atm; electrode areas, about 1/40 ft² each; electrode spacing, 0.12 inch. IR polarization was about 0.1 volt at 100 A/sq ft.

Increase in performance with temperature was due to lower activation polarization at oxygen electrode and to higher conductivity of electrolyte.

Curve 2 (384): M. W. Kellogg Co.

Amalgam concentration: 0.4 weight-percent; 4 M NaOH+sea water; oxygen pressure, 8 psig; electrode areas, about 1/10 ft² each; electrode spacing, 0.11 inch; 12-mil microporous PVC between electrodes.

This cell obviously has less activation polarization (at the oxygen electrode) but higher IR.

FIGURE 7.2.—Performance of small sodium amalgam-oxygen fuel cells.

The basic cell design was similar to that described in section 7.1, except that the oxygen electrode was a proprietary porous-silver cathode supplied by the Electric Storage Battery Co. A five-cell, continuous-feed stack was constructed to obtain operating and design experience ***(384)***. The inlet concentration of mercury was set at 0.4 weight-percent sodium, since this was not too near the slush point; the exit was set at 0.2 percent, since lower concentrations gave poorer cell performance. The optimum hydroxide concentration was 14 weight-percent (highest conductivity). The cells consisted of concentric tubes, the inner steel tube being the anode and the outer the cathode, with electrolyte in the annulus. A microporous plastic roll between anode and cathode prevented mercury from reaching the porous silver cathode, which was 14 inches long by 1.2 inches in diameter, with a wall thickness of about 60 mils. Thirty-seven of these tubes were fastened into a bundle and connected in parallel by joining the cathodes to an end plate of silver-plated copper. The end plate formed the top of a cylindrical case (which acted as a common oxygen chamber) around the electrodes. Five of these bundles made up the cell stack.

Considerable trouble was experienced with cathode-end-plate joins. Conducting epoxy had too high an ohmic resistance, and brazing alloys containing cadmium were not satisfactory because electrolyte attacked the cadmium and the flux wicked into the cathodes and poisoned the electrodes. Handy-Harman Silflake No. 855, a silver-powder paste, was applied and air dried at 180" F (82" C) for 30 minutes, then sintered in an oxygen-free atmosphere at 1000" F (538" C) for 20 minutes. A highly conductive bond was formed, but it had to be filled with epoxy (Epoxolite No. 807) to make it sufficiently strong and nonporous for use.

Another design problem was that pressure imbalances caused the microporous plastic barrier to stick to one electrode or the other, resulting in low flow of electrolyte between the electrode and the plastic. Therefore, electrolyte flow outlets were redesigned to prevent pressure imbalance across the barrier. Amalgam was admitted to the central tube of a cell through an orifice at the top, filling the tube and running over to give the required thin film of amalgam on the outside of the tube. The diameter of these orifices was set at one-sixteenth inch or greater in order to achieve the desired flow rate, since smaller diameters throttled the flow of amalgam (ascribed to wetting of the tube by the amalgam).

The difficulty of keeping the plastic barrier centered in the electrolyte space led to investigations of other techniques for preventing amalgam from contacting the cathode material. The Electric Storage Battery Co. developed a coating for the oxygen electrode which allowed good electrolytic penetration and conduction, but prevented mercury penetration. A dispersion of 17.5 weight-percent Teflon 30, 6 percent magnesium oxide, and 2 percent polyethylene oxide in water was painted on and dried at 212" F (100° C). Two or three coats were applied with drying between coats, and the electrode sintered at 734" F (390" C) for 4 minutes ***(383).***

The anodes in the tube bundle were connected in parallel by the mercury feed, which was insulated from the cathodic end plates and case ***(384).*** When the five bundles were assembled into a series-connected stack, however, the common mercury feed shorted the cells, so various amalgam interrupters which would disconnect the mercury manifold from the anodes were investigated. Figure 7.3 shows the positions at which amalgam interruption is required for a single cell. A pinched elastomer tube did not work, since the amalgam wetted the tube and gave electrical conduction through the pinch. A nonmetallic rotary feeder became plated with amalgam and shorted the cell; it also had excessive wear. The most satisfactory solution proved to be breaking the stream into droplets (as in fig. 7.3). A "shower-head" design allowed a reasonable amalgam flow with no electrical path between the inlet to the head and the stream of droplets collected below the head. Higher flow rates were obtained with an "umbrella" interrupter in which the amalgam was sprayed up into the umbrella, spread, and dripped off the edge. An extruder for feeding sodium into the amalgamator was also developed.

Results from small tube cells showed that 2-psig oxygen performed poorly, presumably due to flooding of the cathode. An increase to 4 psig gave much better performance, and a further increase to 8 psig gave slightly more improvement. Performance was best at 150" F (66" C), falling off rapidly at higher and lower temperatures, especially at currents greater than 100 A/sq ft. Faradaic efficiency for sodium and oxygen utilization was 100 percent within experimental error. Tilt of 30" from vertical decreased performance up to 35 percent with a plastic barrier and up to 15 percent with the porous anode coat. A typical current-voltage curve is given in figure 7.2.

The unit of 5 tube cells in series, each containing 37 electrode pairs connected in parallel, was run for periods up to 5 hours. The OCV was about 10 volts and the power output 8.35 kilowatts at 2000 amperes. (This was a current density of about 200 A/sq ft; the extrapolation of

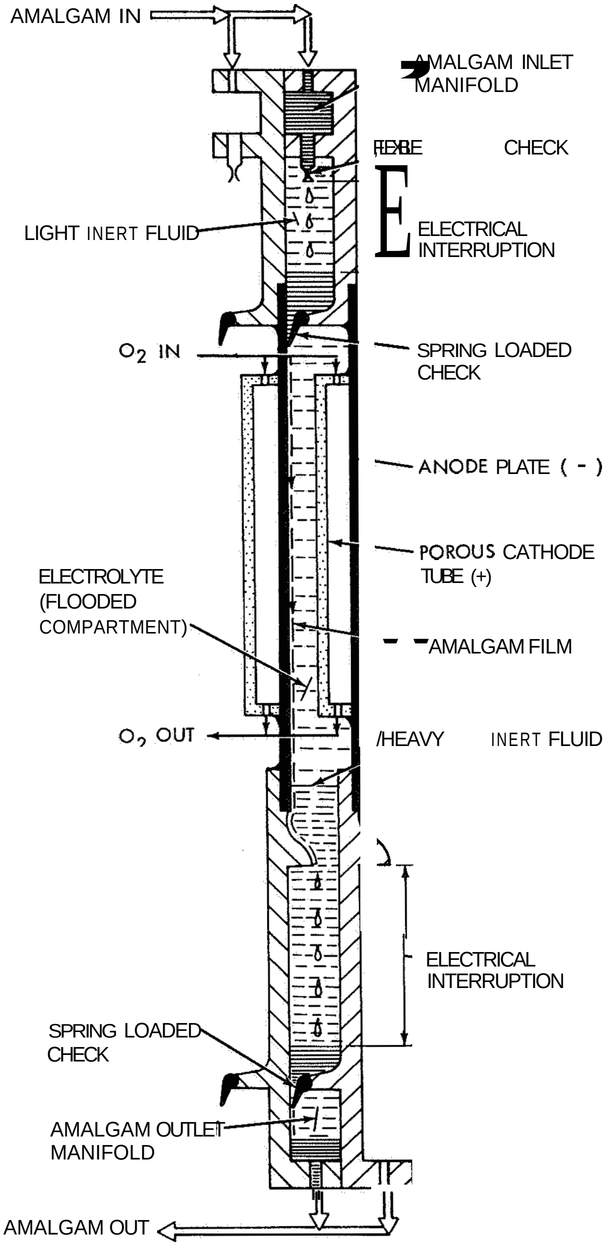

The anodes consisted of steel plates over which the sodium amalgam flowed in a thin film. The cathodes were of porous, sintered silver (supplied by Electric Storage Battery Co.) .The rate of flow of amalgam must be accurately controlled and electrical breaks between the cells and the mercury feed and exit streams are necessary to prevent short circuit of the cells.

FIGURE 7.3.—Schematic of the M. W. Kellogg Co. sodium amalgam-oxygen cell *(385).*

single-cell tests predicts a power of almost 14 kilowatts at this current density; therefore, there was considerable power loss somewhere in the unit.)

A design was prepared for the 1000-kilowatt unit specified in the contract ***(385).*** The unit contained 243 plate cells in series, with a single-cell OCV of about 2 (see fig. 7.2). Sodium was stored in liquid form, being kept hot by electrical heating. The amalgam feed was maintained at 0.4 weight-percent sodium; the exit from the cells had 0.2 weight-percent sodium. Cell temperature was 140" to 165" F (60" to 74" C). The amalgam temperature rose to about 260" F (127" C) in the amalgamator where sodium was added (dissolution of sodium in mercury is highly exothermic), and temperatures of the cell feed and the cell were controlled by heat exchange with cooling sea water. Since the cell reaction produces sodium hydroxide in the electrolyte, some electrolyte was bled out and makeup water (not sea water) added to keep it at 14 weight-percent sodium hydroxide. The electrolyte pressure in the cell was 35 psi above ambient sea pressure, and oxygen pressure in the cathodes was 10 psi above this. Oxygen was put in the storage tank as liquid at 2740 psia, with a relief valve set at 2940 psia. As the storage tank warmed up, the pressure rose, and if oxygen were not used in the cell, the relief valve would operate after about 2 to **3** hours; this time could be controlled by varying the tank insulation.

Suggested storage tanks for sodium and makeup water consisted of concentric inner and outer walls of double neoprene, with the 2-inch space between the walls packed with quilting agent and mineral oil. These tanks were soft and collapsible, with a pressure equal to that of the sea water surrounding them. At a load of 100 kilowatts, the heat releases were calculated as (3.71) (10^6) Btu/hr from the cell stack and (2.56) (10^6) Btu/hr from the amalgamator. About (0.7) (10^6) Btu/hr were removed from the cell by the exit amalgam stream, which passed through the amalgamator to a cooling heat exchanger. The rest of the cell heat was removed by circulating electrolyte through a heat exchanger cooled by sea water. Parasitic power was estimated at 6 percent of the stack output.

Figure 7.3 is a schematic of the bipolar cell design, with the frames made of laminated plastic. Figure 7.4 shows a detail of the cathode-anode assembly. The electrodes were about 11 square feet in plane area, operated at 325 A/sq ft and 1.24 volts to give 1060 kilowatts. **At** the 100-kilowatt level the current density was 22 A/sq ft. Overall dimensions were **3** by 4 by 8 feet.

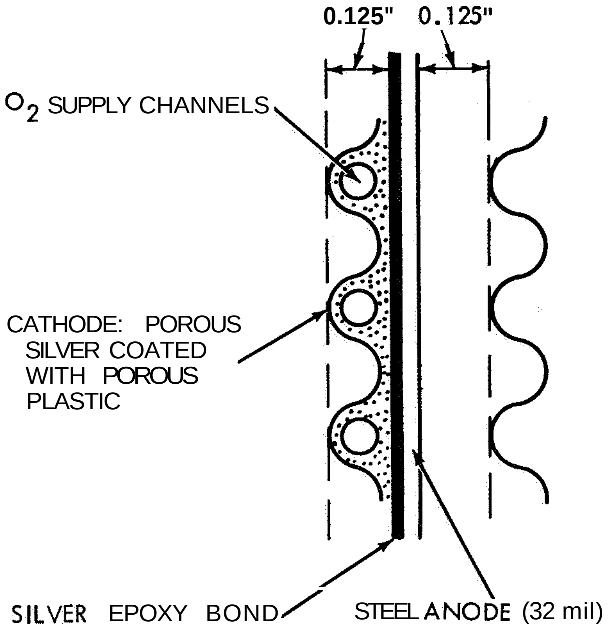
0.125"
0.125"
O_2 SUPPLY CHANNELS
CATHODE: POROUS SILVER COATED WITH POROUS PLASTIC
SILVER EPOXY BOND
STEEL ANODE (32 mil)

FIGURE 7.4.—Detail of bipolar electrode assembly of M. W. Kellogg amalgam cell.

Figure 7.5 shows the proposed system *in situ.* The volumes of the components were: fuel-cell stack, 85.5 cubic feet; oxygen tank, 23.2 cubic feet; sodium tank, 57.3 cubic feet; and water makeup, 13.9 cubic feet. Total component volume was 204 cubic feet, with an assembled volume of 340 cubic feet. Dry weight was nearly 10 000 pounds, and filled weight 17 500 pounds. The problems envisaged in system construction were cathode extrusion and cell construction, check valves for amalgam distribution, a sodium-concentration sensor to control the inlet and outlet concentrations via change in amalgam rate, the amalgamator, and assembly and life of the multifluid cell design.

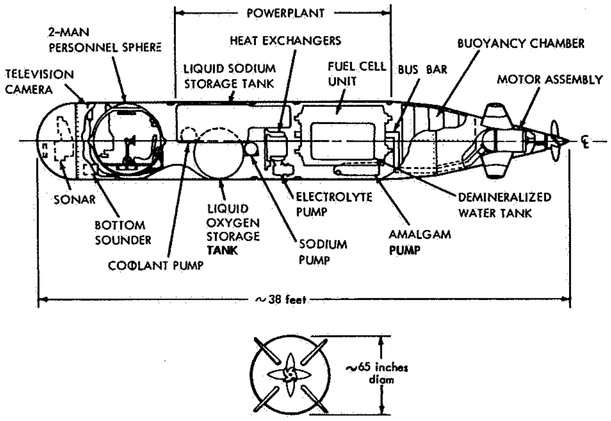
POWERPLANT
2-MAN PERSONNEL SPHERE
HEAT EXCHANGERS
TELEVISION CAMERA
LIQUID SODIUM STORAGE TANK
FUEL CELL UNIT
BUS BAR
BUOYANCY CHAMBER
MOTOR ASSEMBLY
℄
SONAR
BOTTOM SOUNDER
LIQUID OXYGEN STORAGE TANK
ELECTROLYTE PUMP
DEMINERALIZED WATER TANK
SODIUM PUMP
AMALGAM PUMP
COOLANT PUMP
~38 feet
~65 inches diam

FIGURE 7.5.—Pictorial configuration of two-man submarine with fuel-cell powerplant *(385).*

7.3 CONCLUSIONS

The sodium amalgam-oxygen fuel cell is a high-power-output cell. The design proposed by the M. W. Kellogg Co. was detailed and probably realistic. It gave outputs of nearly 12 kW/cu ft for the fuel cell, and about 13.5 kW/lb for the system, excluding reactants but including mercury. However, the short operating periods of the 8-kilowatt units which were actually constructed indicate that a number of engineering problems have yet to be solved.

As discussed in section 2.2.5, the cell is suitable only for special applications, since sodium is an expensive fuel. Furthermore, the system is more complex than most other fuel cells and probably would require constant supervision. The steel-plate anode can operate only under gravity forces and it must be nearly vertical, which imposes a considerable restriction on application and design. As far as I know, this type of cell is not being investigated further at present.

CHAPTER 8

Systems and Control

8.1 INTRODUCTION

Fuel-cell reactants are stored separately from the energy converter, which is a major difference from conventional batteries. Near-theoretical watt-hours per pound of hydrogen and oxygen cannot be obtained in practice because the weights of storage tanks have to be included, but the energy-storage density for fuel cells is still very favorable. An advantage of the fuel cell is that the reactants combine with electrode material in a surface reaction involving at most the top few molecular layers of material. Unlike a conventional battery, therefore, fuel-cell electrodes are basically stable; that is, the fuel-cell reactions need not cause major chemical changes in the electrodes. If secondary effects can be eliminated, fuel-cell electrodes should have long life. These advantages, however, are obtained only by introducing concomitant disadvantages. A fuel-cell stack must have a feed and control system to regulate the supply of reactants and remove products in a controlled manner and temperature control is often necessary. Conventional batteries have the advantage of simplicity and absence of moving parts; some of them also maintain an almost constant voltage over a wide range of current density. On the other hand, batteries used at high-power densities often suffer from short life due to overheating; their performance varies with temperature and it is often necessary to store them dry and activate them by filling with electrolyte. Under these conditions, auxiliaries must be used to give temperature control and voltage control (power conditioning), and to supply electrolyte. The battery system and fuel-cell system then become more comparable in complexity.

High-temperature cells using cheap organic fuels have relatively few control problems because the fuel cannot be circulated and the electrolyte is invariant; therefore, cell products are immediately exhausted. In the other systems considered in chapters 4 through 7, fuel is cycled to obtain high fuel utilization and the products of reaction dilute the electrolyte. For these systems, the first requirement is that a cell produce a reasonable power density; the second is that the cell have a reasonable life. Once these two conditions have been met, a complete, self-contained system must be constructed to provide control of a practical cell stack. The system must be highly reliable, reasonably priced (considering the application in mind), and as light weight and compact as possible. The future choice among hydrogen-oxygen systems for space applications will probably depend on auxiliary control features of such systems, rather than on watts per square foot of electrode. For example, a small high-temperature cell has unfavorable heat-loss characteristics and it must have heavy and bulky insulation to be self-sustaining. A large heat exchanger is required to cool exit gas to the point of water condensation. Again, as low-temperature cells are made larger, the heat release in the cell raises the internal temperature to undesirable levels unless gas is circulated at high rates or unless auxiliary cooling is used.

Most electrodes give higher current density at higher temperature. If a system design relies mainly on natural conduction to transfer heat from the interior to the exterior, the middle of the cell will be at the highest temperature and more of the current will be produced at this central hot spot. The larger current density leads to higher heat release and higher temperatures. If, at some temperature, the rate of heat release increases faster with temperature than the rate of heat conduction, the cell will be inherently unstable and will burn out at the hot spot. No obvious cases of thermal instability were reported in the contracts under review, since stacks were redesigned with provision for adequate cooling as soon as it was discovered that temperatures were widely uneven through the stack.

A major objective of many of the system designs discussed in this chapter has been to reduce the weight and volume for a given power density and mission duration. Optimum designs have been obtained using mathematical system optimization. This technique consists of expressing the required parameter as a function of all the other independent parameters of the system. Each of the parameters is varied, usually stepwise, through a practical range and the overall weight calculated. There will be one particular set of parameters, or perhaps a set of short ranges of parameters, which give optimum weight. This is equivalent to determining the minimum in an n-dimensional surface, where n is the number of independent variables. Weight is usually expressed as an algebraic function of all the other parameters. Various mathematical techniques can be applied, and a digital computer is used to perform the many calculations involved. Possibly a generalized equation for all fuel-cell systems, using general functions, can be derived and applied to any particular system by substituting known functional relations for the general functions. However, once the value of the technique is realized, it is easy to set up an equation from first principles for a particular system and program it for a computer. All other required dependent dimensions, temperatures, flow rates, etc., can then be calculated. The technique is used in conjunction with commonsense. For example, it might predict an optimum current density which is not suitable because of poor life or insufficient overload capacity, etc.; thus, bounds are placed on some dependent variables, which result in bounds on the parameters in the equation.

Van Winkle and Carson (ref. 8.1) presented a general scheme, applicable to all kinds of primary fuel cell systems, for minimizing volume, weight, or cost. They assumed a linear dependence of voltage on current density; of weight (or volume or cost) on geometric area of electrode; and of chemical storage (fuel, oxidant, tanks, and associated equipment) on the number of chemical equivalents of fuel corresponding to the required total energy output. The minimum can then be found in terms of the operating voltage, of a single cell, which was chosen as the independent variable.

Eisen (ref. 8.2) described an optimization technique that is also based on single-cell voltage and, though applicable to any primary fuel-cell system, was developed specifically for the IEM system. He presented an alinement chart for voltage, current density, mission time, and weights of heat exchanger, fuel subsystem, and fuel battery. His results confirm the fact that current density, which determines operating voltage, is a strong function of mission length. In his specific case, minimum system weight resulted at 100 A/ft^2 for 2-day, 55 A/ft^2 for 4-day, and 50 A/ft^2 for 6-day use.

This chapter gives only a general outline of the control systems reported in the contracts surveyed and no attempt is made to describe the calculations for system optimization. In many cases the contract reports themselves do not give detailed information on the sizes and types of values used, etc. The cells involved normally use hydrogen and oxygen and water has to be removed. This is often done by circulation of reactant gases through the cell and a condenser. This technique is somewhat self-regulating, since a high cell output causes an increase in cell temperature and dilution of the electrolyte, both of which increase the partial pressure of water vapor in the gas leaving the cell.

8.2 PRATT & WHITNEY AIRCRAFT, System Analysis of a Regenerative H_2-O_2 Fuel-Cell Powerplant, 1961

Virtually no information is available on control systems for the Pratt & Whitney modification of the Bacon cell (see ch. 4). Figure 9.1 shows an early system (*531*) for the cell used as part of an electrolytically regenerative orbiting system. Water and heat removal were accomplished by circulation of the hydrogen stream, with cooling and condensation of water. The electrolyte was pressurized by nitrogen contained in the case of the module; the electrolyte reached nitrogen pressure by gas leakage through the gasket shown in figure 5.4. The figure also shows that hydrogen and oxygen were supplied to each cell by individual gastight connections. The pressure of these gases was adjusted to about 10 psi over that of the nitrogen blanket by using the nitrogen pressure as the reference pressure for the oxygen and hydrogen pressure regulator (diaphragm flow valves), as in figure 9.1. The connection from the nitrogen pressure regulator to the module case is not shown in the figure. Vacuum was used as reference pressure for the nitrogen pressure regulator. In the event of an electrode failure allowing hydrogen or oxygen to pressurize the module case, the nitrogen valve also had a relief outlet on the case side. System optimization showed that an operating pressure of 60 psia gave lower weights than 20, 200, or 500 psia. For a pressure of 60 psia, the weight-current density relation is shown in figure 8.1. Water was removed at a rate of 0.45 pound per pound of hydrogen circulated; this was a partial pressure of 2.86 psia at the fuel cell exit and was, therefore, condensed at temperatures below 138" F (59° C).

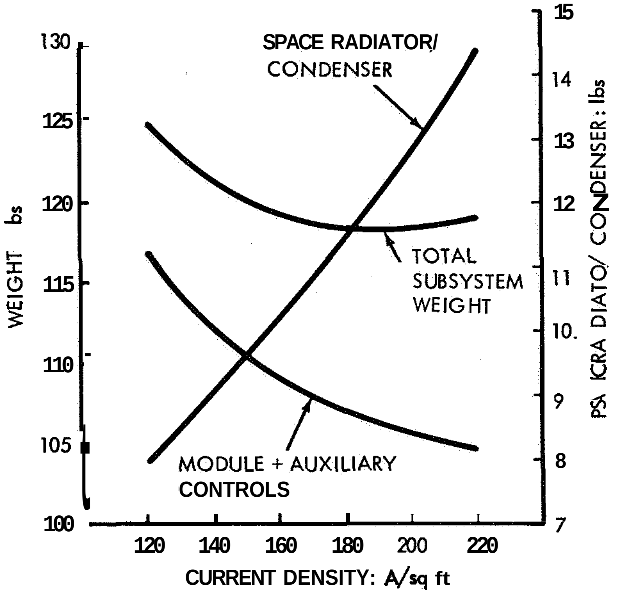

At lower current densities, the weight of the fuel cell was larger but the more efficient fuel utilization (less waste-heat release) made the weight **of** space radiator smaller. A value of **1** lb/sq ft was used to calculate space-radiator weight.

FIGURE 8.1.—System weight for Pratt & Whitney 500-watt fuel-cell module and auxiliaries; operating pressure 60 psia *(531).*

In a later contract (*535*), some further details of auxiliaries were given for a 250-watt module. The hydrogen pump used was a sliding-vane pump powered by a 12- to 18-volt dc motor with less than 25-watt power consumption. The hydrogen and oxygen supply valves were flat-face (cones were unsatisfactory) valves with rubber seals and neoprene (Teflon was unsatisfactory) diaphragms, with fine surface finishes on all sliding parts. Pressure control was 7.5±0.5 psi over the nitrogen reference, at flow rates up to twofold that of design flow and with supply pressure varying from 30 to 100 psig. No leakage was found over a test of 1400 hours.

Temperature control of the module was obtained by a combination of heaters in the module and cooling by hydrogen circulation. The control pattern was as follows. If the module temperature as sensed by a mercury thermostat fell below 480" F (249" C), an electrical relay switched in the heaters. These turned off as temperature reached 490" F (254" C). If module temperature rose above 500" F (260" C), the circulating hydrogen returning to the cell was manifolded around the regenerator and therefore entered the cell cold. At 495" F (257" C), the regenerator was switched in, giving heat exchange from hot exit hydrogen to the return hydrogen. When the temperature was above 485" F (252" C), hydrogen was circulated through the cell and condenser at a fixed rate. This rate of circulation evaporated water from the electrolyte and caused cooling. Below 485" F, a bypass valve from the pump exit to the pump entry was opened, so that the hydrogen circulated to the cell dropped and the cell temperature rose. Normal operation was between about 481" and 499" F (249" and 260" C), since overshoot in cell temperature around the 485" F control level was about ±4° F. Bypass valves were similar to the regulators described above, with flat-faced rubber-coated valves, flat seats, and polished, stainless-steel sliding parts. Even though the metal hydrogen and oxygen feed tubes to each cell from external manifolds led to excessive heat loss, the unit operated at 54 percent thermal efficiency for a 691-hour test.

8.3 UNION CARBIDE CORP., Carbon Electrode Fuel Cell, H_2-O_2 Fuel Cell

Early tests on the Union Carbide low-temperature cell used low hydrogen circulation, one-tenth of use rate, plus electrolyte circulation for water removal and temperature control *(651)*. Heat transfer was from exit electrolyte to inlet gases. A laboratory system showed several problems: gas rates through needle valves changed with time, float rotameters gave excessive pressure drops, and pressure transducers were unstable and hunted. The electrolyte pump gave pressure surges. Better control of hydrogen flow to the cell stack was obtained by replacing the spring loading of a diaphragm valve (positioned after the gas pump) with a pressure connection to the stack inlet. In effect, this damped the valve action, so that high hydrogen pressure in the cell would throttle the valve but not close it entirely. The pumping power for a 500-watt system was 25 watts. An electrolyte pump which was developed had a plastic case, a ceramic internal magnet supported on nickel and carbon ball and cup bearings, and an external magnetic coupler driven by a 28-volt dc motor. This pump circulated concentrated potassium hydroxide solution for 3000 hours without wear, but was only 25 percent efficient.

A high circulation rate of hydrogen (10 times the use rate) could be used to remove water by transpiration through the electrodes, without electrolyte circulation. The evaporation of water through thin membranes was studied with electrolyte on one side of the membrane and vacuum on the other. Porous Teflon sheet was an unsatisfactory membrane, since it allowed weep-through of electrolyte. Ethocel film at 140° F (60° C) gave water permeation rates of about 1 kilowatt per **36** square feet.

A Vanton all-plastic positive displacement pump used for electrolyte circulation required a large surge tank to prevent pressure pulses *(655)*. Water was removed *(657)* by circulating hydrogen and oxygen at the rate of 90 A/sq ft at 185° F (85° C); standard ¼-inch-thick carbon electrodes were used. A fixed recirculation rate of 10 times the use rate was satisfactory *(660)* for water removal; heat removal was by electrolyte circulation.

8.4 GENERAL ELECTRIC CO. *(234* through *237,244* through *248,264* through *274,276* through 290)

A two-stage, pressure-regulating valve is mentioned in two contracts *(273* and *348)*, but no details of design or supplier are given. The valve maintained a constant inlet pressure to a cell stack from a supply pressure ranging from 5 to 5000 psig. Its weight was 0.7 pound and dimensions were 1.75-inch diameter by 1-inch height. The inlet pressure could be maintained at 1 psig ± 10 percent for both hydrogen and oxygen. **A** system analysis was performed for a submarine powerpack *(283)* using the General Electric IEM fuel cell, and gave optimum cell dimensions (active area) of 20 by 11 inches; deionized water (used as liquid coolant) passed through coolant channels within a bipolar assembly (see sec. 4.3.5 and fig. 4.14). Water formed by the cell reaction was removed by wicks as described in section 4.3. General Electric did not build the system, since life of the IEM-electrode assemblies was quite poor.

TABLE 8.1.—*HOPE Spacecraft Weight Breakdown (234)*

Component	*Weight, lb*
Oxygen tank compartment	24.4
Hydrogen tank compartment	37.3
Experiment compartment (including fuel cells)	76.2
Electrical compartment	50.5
Despin compartment	11.7
Total	200.00
Experiment compartment:	
Fuel-cell modules (2)	25.2
Radiators and pressure plates (2)	15.0
Structure	14.3
Water tank	4.4
Valves, regulators, controls, etc.	17.3
Total	76.2

A complete 50-watt system for orbital space flight was constructed using IEM fuel cells *(234)*. Table 8.1 presents some of the data that were involved. Spherical storage tanks were used at maximum pressures of 2500 psia. Heat production was 50 watts of waste heat from fuel-cell stacks plus 50 watts of useful energy in the electronics compartment. The surface of the satellite was insulated with multilayers of aluminized Mylar-Fiberglas (absorptivity/emissivity = 0.4) to give a total mean heat loss of 50 watts. The waste heat from two fuel-cell stacks (25 watts each) was conducted out of the stacks by bipolar heat conductors (see figs. 4.12 and 4.13) to space radiators mounted in the surface of the satellite. The area and emissivity of the radiators were designed to maintain the cell temperature at 120" F (49" C). However, a detailed analysis of the heat fluxes on a spherical satellite during orbit showed that they could vary from 20 to 200 Btu/ft^2/hr during the orbit, with the upper limit dependent on the position of the orbit. A "hot case" was defined by averaging the mean fluxes during orbits which had maximum heat flux onto the surface, and a "cold case" was similarly defined for orbits with minimum flux. The mean equilibrium temperatures were calculated from

$$[(S+a)\alpha+(E)\epsilon]A+Q_g=\sigma\epsilon AT^4. \qquad (8.1)$$

S is the mean solar flux, a the albedo flux (sunlight reflected from the Earth's surface), α the absorptivity, E the flux from the Earth, ϵ the emissivity, A the radiator area, Q_g the desired rate of heat-loss from the radiator, and σ the Stefan-Boltzmann constant. The lowest temperature is obtained for the cold case plus Q_g zero, and the highest for the hot case plus Q_g a maximum. Calculations showed that on-off operation of the fuel-cell system would lead to temperature limits outside of those necessary for correct operation. For example, an absorptivity of 1.0 and an emissivity of 0.5 gave an upper temperature (hot case plus fuel cells "on") of 177" F (81° C), and a lower temperature (cold case and fuel cells "off") of -10" F (-23" C). No combination of $\boldsymbol{A}$, α, and ϵ produced temperatures within an acceptable range of 40" to 120" F (4" to 49" C). An analysis was made of melting-solidifying methods of damping temperature fluctuations, but it was decided to use a steady fuel-cell output, with $\alpha=0.33$, $\epsilon=0.91$, and $A=0.9$ ft^2; temperatures were then in the region of 66" to 107" F (19° to 42" C).

Removal of product water was by a wicking arrangement, as shown in figure 8.2 (see also sec. 4.3). Wicks were of 15-mil-thick glass fabric (Glass Web No. 1 (T), Style 2275, Atlas Asbestos Co.) and the water absorber was Solka-Floc BW20 (Brown Paper **Co.)**. This material had a density **of 3.8** g/in^3 and gave water storage of 80 to 95 percent of the volume. Water transport from cell wicks to the container was through 0.25-inch-thick Orlon felt (Troy Blanket Mills, No. 2B–9–250).

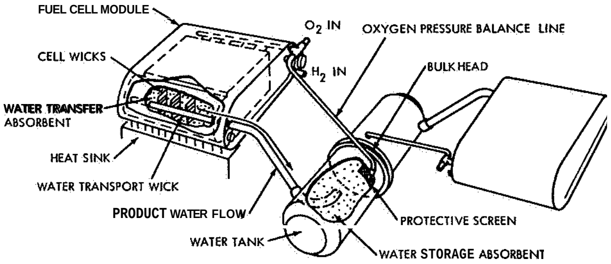
FUEL CELL MODULE
O$_2$ IN
OXYGEN PRESSURE BALANCE LINE
CELL WICKS
H$_2$ IN
BULKHEAD
WATER TRANSFER ABSORBENT
HEAT SINK
WATER TRANSPORT WICK
PRODUCT WATER FLOW
PROTECTIVE SCREEN
WATER TANK
WATER STORAGE ABSORBENT

FIGURE 8.2.—Water-removal system for General Electric IEM fuel cell *(234)*.

The control and monitoring system is shown in figure 8.3; table 8.2 gives some details of the control valves. A newly developed electronic fuel-cell controller monitored the voltage of the cells. When the voltage among any three cells fell below 2.1 volts, the controller operated the hydrogen and oxygen purge valves. Hydrogen purge was 2.2 seconds to vacuum, giving a pressure drop from 15 psia to 13 psia; oxygen purge was a flush for 15 seconds. Apart from these purge conditions, hydrogen and oxygen were dead ended to the cells and flow control was simply by pressure control.

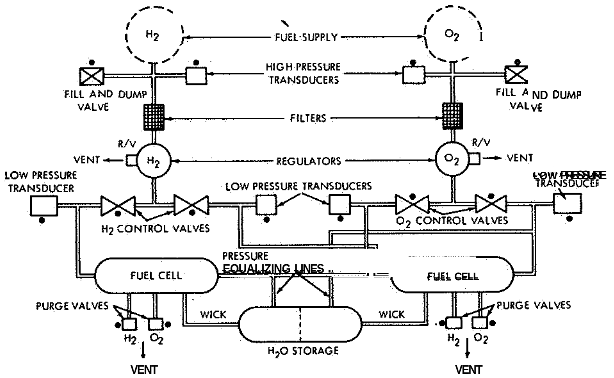
H$_2$
FUEL SUPPLY
O$_2$
HIGH PRESSURE TRANSDUCERS
FILL AND DUMP VALVE
FILL AND DUMP VALVE
FILTERS
R/V
R/V
VENT
H$_2$
REGULATORS
O$_2$
VENT
LOW PRESSURE TRANSDUCER
LOW PRESSURE TRANSDUCERS
LOW PRESSURE TRANSDUCER
H$_2$ CONTROL VALVES
O$_2$ CONTROL VALVES
PRESSURE EQUALIZING LINES
FUEL CELL
FUEL CELL
PURGE VALVES
WICK
WICK
PURGE VALVES
H$_2$
O$_2$
H$_2$O STORAGE
H$_2$
O$_2$
VENT
VENT

NOTE.
• INDICATES ELECTRICAL CONNECTIONS

FIGURE 8.3.—Monitoring and control system for HOPE fuel cell *(234)*.

The complete system was tested in a simulated thermal-vacuum environment. Freezing of water vapor in the gas lines, followed by membrane failure, prevented a complete test, but simulated fuel-cell operation showed that thermal balance was satisfactory. It should be noted that the control system was relatively simple because (*a*)

TABLE 8.2.—*Auxiliaries for* HOPE Fuel *Cell System*

Component	Vendor	Specifications		
		Response time	Life cycles	Range
Fill/dump solenoid valves. . . .	Marotta Corp..	35 msec. . .	10 000	200 SCFM at 2500 psi
Regulators.	Sterer Corp..	Regulation within 1 sec	10 000	Inlet 100 to 3900 psig; outlet 16±0.25 psig; 0 to 0.04 SCFM H_2
Pressure transducers.	Trans-Sonics, Inc..	50 msec. . .	200	0 to 3500 psia or 0 to 40 psia
Stainless steel filters.	Aircraft Porous Media, Inc.. .	. . . .	500	5 micron; 25 SCFM at 100 psig
Latch control solenoid valves.	Valcor.	. . . .	1000	
Purge solenoid valves.	Eckel.	. . . .	. . . .	

there was no recirculation of reactants, so no pumps were required and the control valves were not subject to pressure pulses; *(b)* the stack was run at constant load and, therefore, the required rate of heat removal was almost constant; and (c) the constant load enabled voltage to be used to trigger the purge cycle. If the module had been required to operate under a range of voltage-current conditions, the system might have been considerably more complex.

For applications which utilize air in an open cycle rather than pure oxygen in a dead ended or closed cycle, it is possible to remove product water and heat from the cell by the flow of air (*290*). The rate of evaporation of water into air under the flow conditions within the cell was

$$\text{Rate} = k_{H_2O} \Delta p_{H_2O}$$

$$k_{H_2O} = (3)(10^{-6}) v^{0.76} \qquad (8.2)$$

where k_{H_2O} is in g-moles/cm² sec atm, v is velocity of flow in cm/sec, and Δp_{H_2O} is the difference in partial pressure of water vapor between the surface and the airstream. The relation was derived from tests at 70" to 105"F (21° to 41" C), relative air humidities of zero to 68 percent, and flow rates of 1 to 10 cm/sec. Empirical equations were also given for heat removal as a function of inlet air temperature, humidity and flow rate, and the thermal conductivity of the current collector. An electronic device controlled the flow rate by the voltage of the cell at a given current (see sec. 8.5 for a similar control method).

As part of a general study of "voltage regulation and power stability in unconventional electrical generators systems," attempts were made to control cell voltage at varying loads internally (instead of using an external voltage regulator). The electrical characteristics of the cell fitted (*265*) an empirical equation,

$$E = E_i - rI + (E_0 - E_i) \exp[-0.575\, I] - C \exp[10.5\, rI] \qquad \textbf{(8.3)}$$

E is cell voltage; I current density, A/sq ft; E_i the intercept at zero current of the linear portion of the current-voltage curve, and r the slope of this portion, ohm-ft². C is a constant which depends on mass transfer within the cell. Values were: $E_0 = 1.05$, $E_i = 0.95$, and $C = (1.5 \text{ to } 6)\, 10^{-4}$; r is a function of temperature having a minimum of about 0.01 ohm-ft² at 122° F (50° C). The first exponential term in the equation is important at low currents and the second at high currents. Alternatively, an equivalent circuit as shown in figure 8.4(a) was proposed.

A membrane containing a metal grid was placed between the anode and cathode and a potential applied between the grid and an electrode to slow the migration of ions through the electrolyte (*267*). The effect was that the fuel-cell output voltage was low and the grid power was excessively high. (From an electrochemical point of view, this technique is patently absurd. A

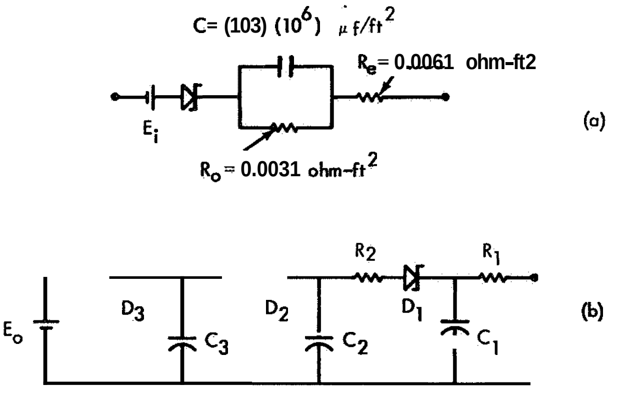

FIGURE 8.4.—Equivalent circuits of General Electric IEM fuel cell: *(a)* Simple (266); *(b)* Triple lag (280).

metal grid placed in an electrolyte between an anode and cathode does not “impart potential” to the electrolyte and it could only affect the current-voltage relation of the cell by acting as an auxiliary current-passing electrode which evolved oxygen or hydrogen.) Another method used to control cell voltage at a given current density was by variation of the amount and velocity of cathodic oxygen supply (269). This method was inherently inefficient, since it amounted to voltage control by starving the cell of oxygen.

In later work *(280)*, the simple equivalent circuit of figure 8.4(a) was replaced by the “triple-lag” circuit shown in figure 8.4(b). This equivalent circuit predicted the transient behavior of the cell quite closely.

8.5 ALLIS-CHALMERS MANUFACTURING CO. (35 through *44, 47* through *57, 59* through 61)

Early Allis-Chalmers’ hydrogen-oxygen cells (described in ch. 4) featured water removal by circulation of hydrogen through a condenser and heat removal by coolant flow in the case surrounding the fuel-cell stack *(35)*, as in figure 4.18. As with several of the contracts reported above, pressure pulses from the hydrogen circulation pump (a diaphragm pump, in this case) caused trouble. The first method used for control of the rate of water removal was monitoring the voltage of each cell and adjusting the rate of circulation of hydrogen to maintain an optimum voltage. This method, which is illustrated in figure 8.5, had three major disadvantages. First, it could be applied only at a preset current density and temperature, which limited the module to a set power output. Second, variation between cells in a cell stack meant that the total stack voltage could not be used to control all cells simultaneously. Each cell voltage was sensed and used to regulate a separate hydrogen outlet valve on that cell. Third, the electronic control device was large and drifted with variation in temperature.

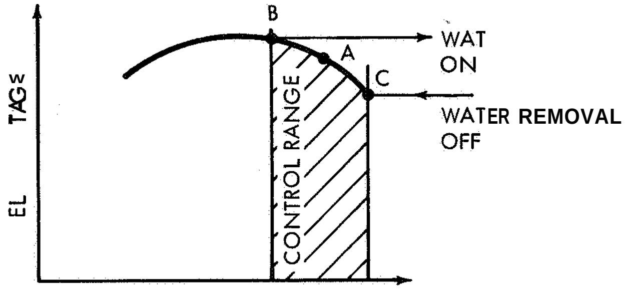

At a given current density, the relation between cell voltage and water content of electrolyte is as shown. The resistance of the electrolyte is high at both low and high water contents; in addition, a high-water content expands the electrolyte volume and floods the electrode, while a low water content shrinks the volume and pulls electrolyte away from the electrode. These effects give rise to a maximum voltage at an optimum water content. The cell is maintained within a specified range of water content by using the voltage at *B* to turn off water removal (by stopping circulation of hydrogen, for example). The water produced in the cell reaction then dilutes the electrolyte until voltage C is sensed, at which point water removal is turned on. The cell potential thus hunts about a mean voltage at *A*.

FIGURE 8.5.—Control of water content of electrolyte by voltage sensing.

Thermal balance with circulated gas coolant in the external case was good when the environmental temperature was from 14° to 125° F (−10° to 52° C). Failures and faulty operation occurred with pressure regulators and valves, heaters, and cooling fans *(36)*. The original system had a differential pressure regulator through which both oxygen and hydrogen were admitted to the module at 5 psig, with the pressure difference between the gases maintained at less than 0.2 psi. During operation, the cell inlet pressure supplied by the regulator drifted with time, and insufficient flow was obtained at higher currents. It was replaced with separate standard gas regulators, Fisher-Governor Type 67–R for oxygen and Type 95–L for hydrogen. These maintained stack pressures at 9 psig±0.5 psi. Solenoid valves on the hydrogen exits (for on-off control of the surplus hydrogen flow used for water removal) failed with time because faulty threads on the inlet collars and poor fits between ball and gasket allowed excessive leakage. They also deformed in use and stuck in the OPEN position. They were replaced with air-actuated solenoid valves (Humphrey Products Division, General Gas Light Co., Series 250 AE–2) which enclosed the gas passage with leaktight diaphragms.

Similar control systems used in a third contract *(49* through *55)* used cooling by evaporation of water and heaters in the stack for temperature control over a short-mission duration (see sec. 4.4.2). Temperature was regulated between 192" and 198" F (89" and 92" C) by heating or cooling. Such close temperature control was necessary for satisfactory operation of the voltage-sensing method of product water removal. A pressure-relief valve which was set at the water-vapor pressure corresponding to 195" F blew when the fuel cell and water jacket became too hot, thus permitting evaporative cooling. A thermostatic solenoid valve was also satisfactory for the water-cooling system. Regulators with nylon and silicone did not withstand temperatures of 200" F (93" C) in the presence of potassium hydroxide. Miniature solenoid valves (Electric Auto-Lite Co., Toledo, Ohio) had excessive leak rates, and closure and seating varied with temperature: The hydrogen pressure-flow regulator was unstable with time at 200" F (93" C) because hot hydrogen leaked through the nickel aneroid bellows used as a diaphragm *(53)*. This leakage was cured by goldplating the bellows. Satisfactory final equipment included pressure transducers from Servionics Instruments, Inc., gold-plated pressure regulators from Firewel Co., and solenoid valves from Weatherhead Co. and Whittaker Controls and Guidance *(54)*.

Since the major problem seemed to be control of product-water removal, a "dynamic vapor pressure control" method was investigated *(37)*. This consisted of circulating hydrogen with a fixed water-vapor pressure at the cell inlet, at sufficient rates to remove product water from the cell and maintain an almost constant partial pressure of water throughout the cell. The acceptable range of electrolyte concentration was 27 to 45 weight-percent of potassium hydroxide, with an optimum at 200" F (93" C) of 35 percent. Thus, the minimum partial pressure of water vapor permitted in the cell ($p_{\min}$) corresponds to the equilibrium pressure over 45 percent KOH at the upper allowed limit of cell temperature. When the cell temperature is controlled below this limit and the entering hydrogen contains this minimum partial pressure (or more), then the cell cannot possibly dry out beyond 45 percent KOH, even under no-load conditions and high hydrogen flow rates. Similarly, maximum partial pressure of water vapor ($p_{\max}$) corresponds to the equilibrium pressure of water over 27 percent KOH at the lower limit of cell temperature. A decrease in partial pressure of water vapor or an increase in cell temperature results in removal of water from the electrolyte, which cannot then fall below 27 percent KOH.

Test of this method was accomplished by maintaining temperature of the condensers within a range whose lowest temperature ($t_{\min}$) corresponded to $p_{\min}$ (the saturated vapor pressure of water at $t_{\min}$), and whose highest temperature ($t_{\max}$) corresponded to $p_{\max}$. The test then measured quantities and pressures of water removed from the cell at various temperatures to determine if the values agreed with those predicted in International Critical Tables for equilibrium water-vapor pressure over potassium hydroxide, and found that they did agree. This showed that the rate of evaporation of water was not rate restricting, so equilibrium pressures could be used to establish condenser temperatures. A water-mass balance was set up in mathematical form *(38)* with the empirical relation

$$p=An_k+B \qquad (8.4)$$

where p is the equilibrium partial pressure of water over potassium hydroxide of mass fraction n_k; A and B are constants for a given temperature. From this balance it was predicted that raising current density from 100 A/sq ft to 250 A/sq ft at otherwise fixed conditions (and **30** percent KOH) would lead to electrolyte concentrations exceeding the wet limit after 30 minutes. Experimental results using hydrogen circulation (12 to 24 times usage rate) agreed with theoretical predictions, provided that allowance was made for a concentration gradient of potassium hydroxide across the electrolyte matrix (lower KOH concentration at hydrogen side, where water was formed). Further investigation of concentration gradients across the electrolyte (contained in a porous-asbestos matrix) showed that the electrolyte concentration varied by as much as ±7 percent of the mean when only hydrogen was circulated *(39).* This made it difficult to control cells within the required concentration range unless oxygen circulation was also used.

Several types of gas circulation pump were compared. Ejector pumps and diaphragm pumps were inefficient. A vane pump leaked around the shaft seal and became worn prematurely. The bore of this pump was chromium plated and ground smooth to reduce wear. Graphite vanes were best, although they occasionally broke; synthetic polymer vanes (Du Pont Type A Polymer SPI) showed excessive wear. A shaft seal of carbon was satisfactory for hydrogen and shields of Viton were necessary for the ball bearing of the oxygen pump, since Buna-N rubber deteriorated rapidly. Several models of gas-water separators were built; figure 8.6 shows a combined condenser-separator which was satisfactory. A centrifugal liquid pump became vapor-bound and a positive-displacement gear pump was preferable.

A breadboard system was tested using a fixed gas circulation rate which could cope with the largest load *(40).* The hydrogen rate was 24 times consumption and the oxygen 4 times; most of the water was removed in the hydrogen stream. The oxygen pump leaked after 170 hours and the graphite vanes for both pumps had a life of about 700 to 800 hours.

Mathematical optimization of electrode-assembly dimensions determined minimum weight for specific limitations (41). In figure 4.18, for example, the width of the seal area was invariant, since it had to be big enough to give a correct seal; the length of the cooling fin was set by the required heat transfer to coolant circulated around the fins. The heat generated in the cell also had to be conducted along the assembly to these fins, at the top and bottom, without excessive temperature difference between the middle of the electrode and the top and bottom edges. Assuming a uniform current density, the relation between heat generated per unit area, *q*, and the assembly dimensions was

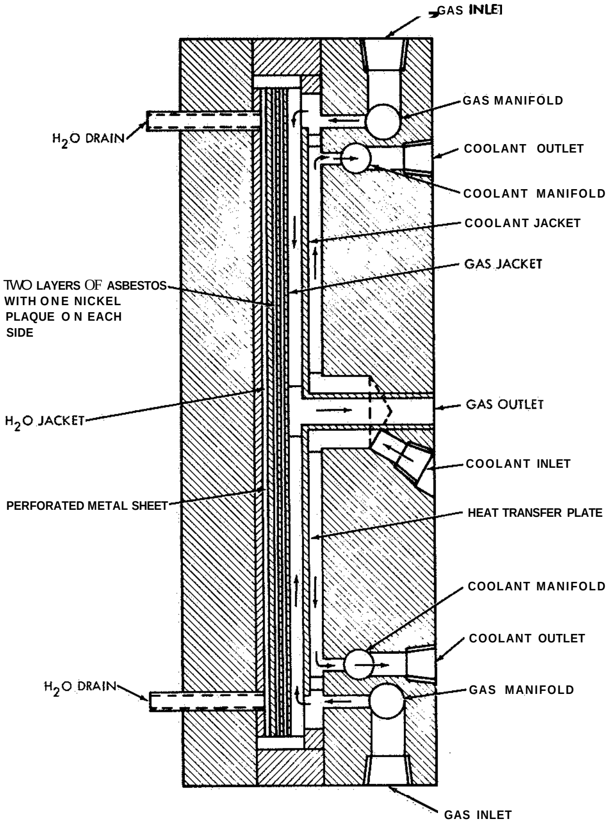

Hydrogen was circulated through the cell stack to remove product water from the cells, then passed through the condenser shown, cooled by water, and water condensed from the gas. The condensed water was absorbed in the layers of nickel plaque and asbestos by capillary action and forced to the drains by the gas pressure.

FIGURE 8.6.—Condenser and separator assembly (Allis-Chalmers, *39).*

$$q=(l/2)^2 2k\Delta T/\delta \qquad (8.5)$$

where l is the electrode height, k the thermal conductivity of the assembly, 6 its thickness, and *AT* the allowable temperature difference. The area of the electrode was fixed for a given power output per cell; therefore, an algebraic expression was obtained relating height of the cell, I, and thickness, 6, as a function of current density, *AT*, power output, etc. This could be optimized to give minimum weight.

The breadboard system was modified to eliminate oxygen circulation, but give oxygen purge corresponding to about 3 percent of the oxygen consumed. The hydrogen condenser temperature was kept constant by two coolant streams, one hot and the other cold, with the flow of each determined by a mixing valve. The mixing valve was set by the hydrogen temperature at the condenser exit. This system controlled the hydrogen temperature *(42)* to within ±5° F when coolant temperatures ranged from 63" to 158° F (17" to 70" C).

To eliminate the circulation of hydrogen through the cells, a static water-vapor control method was used. The principle is illustrated in figure 4.19, and cell assembly is shown in figure 4.20. The water-removal compartments were kept at the required equilibrium pressure of water vapor (equilibrium with 35 percent KOH at 200" F (93" C), for example) by connecting them to a water-cooled condenser *(45)*. The system is shown in figure 8.7. A 1500-watt stack containing 70 cells was built and cased in the magnesium cylinder. Hydrogen or helium was circulated within the case, over the cooling fins of the cells, as shown in figure 8.8. The gas in turn was cooled by passing through a water-cooled heat exchanger in the case. The flow of coolant water into the heat exchanger was controlled by a solenoid valve operated by a temperature regulator receiving temperature data from a thermocouple located in a cooling fin of a fuel cell. Purging for 15-second periods every 15 minutes was controlled by a timer. A test of the unit over a period of 160 hours showed the following problems. At low loads, the stack did not maintain temperature and required insulation. At higher loads, the coolant system (using coolant water at a fixed temperature) performed well at steady load, but when the load was changed the temperature control had to be reset to keep a constant cell temperature. It was thought that resetting was required because the control thermocouple, mounted on a cooling fin, did not follow cell temperature at varying loads. The vacuum cavity controller also had to be manually manipulated to allow for temperature changes within the stack. Finally, a fan bearing failed after 100 hours of operation and a replacement fan was not satisfactory.

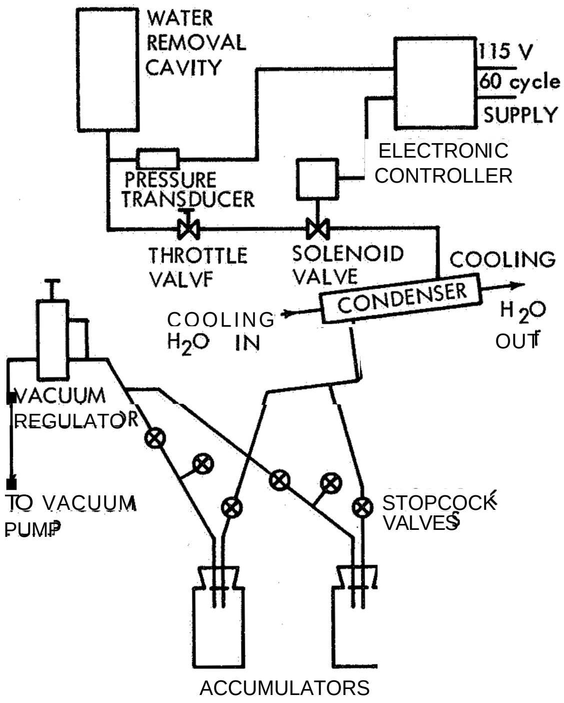

The water-removal cavities of the cell stack were connected to a condenser via a solenoid valve. The condenser was kept at a lower pressure than that desired in the cavities by water cooling and by the vacuum pump. When the pressure in the cavities rose beyond a preset value, the pressure-transducer reading activated the electronic controller to open the solenoid valve, thus reducing the cavity pressure by removing water vapor. The vacuum regulator was used as a "backup" control in the event of failure of the main control. It was necessary to purge the water cavities occasionally to prevent buildup of hydrogen in the cavities.

FIGURE 8.7.—Water removal by static vapor pressure control (Allis-Chalmers, *45*).

A temperature-compensating electronic pressure controller was designed *(56)* to maintain the electrolyte at a desired water concentration over a temperature range of 180° to 210° F (82° to 99° C). Figure 8.9 shows the circuit, whose output was to a solenoid valve connected to the water cavity; input was from a 500-ohm pressure transducer connected to the water cavities (see fig. 8.7). The operation of the controller was described as follows:

> The controller (fig. 8.9) consists of an amplifier T_1 and trigger circuit T_3 and T_4. T_2 sets the operating pressure and is part of the temperature-compensation network. T_5 and D_2 regulate the voltage to the controller.
>
> T_1 acts as a voltage and current amplifier. This limits the amount of current taken from the transducer, thereby keeping a linear pressure voltage curve. T_2 sets the point at which T_1 will begin to conduct. This point is quite stable with temperature because of the differential amplifier-type connection. Note that the base drive of T_2 is connected to the same power as the transducer. In case the power to the transducer changes, this type of connection will change

the set point in the same proportion, keeping the calibration of R_5 reasonably constant despite changes in transducer power supply. R_7 is a thermistor which will change the set point with temperature in such a way as to follow the vapor pressure of the electrolyte. The trigger circuit consists of T_3 and T_4 and D_1. When T_1 turns on enough to make the voltage across R_1 equal to V_{be} of T_3 plus V_z of D_1, T will turn on. This turns on T_4 which, due to the positive feedback loop (R_{14} and D_4), will cause T_3 and T_4 to saturate. When voltage across R_1 drops below $V_{be}+V_z$, due to reduced current through T_1, T_3 will shut off. This differential is set by R_{14}. Diode D_4 prevents T_3 from turning on with power-supply changes and allows the differential to be set without changing the trigger point. T_5 is optional. T_5 and D_2 make up the controller's regulated power supply. T_5 was added to reduce pcwer needed and also to reduce the heat, which would otherwise have to be dissipated in Zener D_2. Optional resistor R_{15} reduces the dissipation of T_5, making possible use of a smaller size transistor.

A test of the controller on a two-cell stack showed that electrolyte concentration was held between 36 and 42 weight-percent KOH between 180" and 220° F (82" and 104" C), and between 39.5 and 40 percent KOH from 190" to 217" F (88° to 103" C).

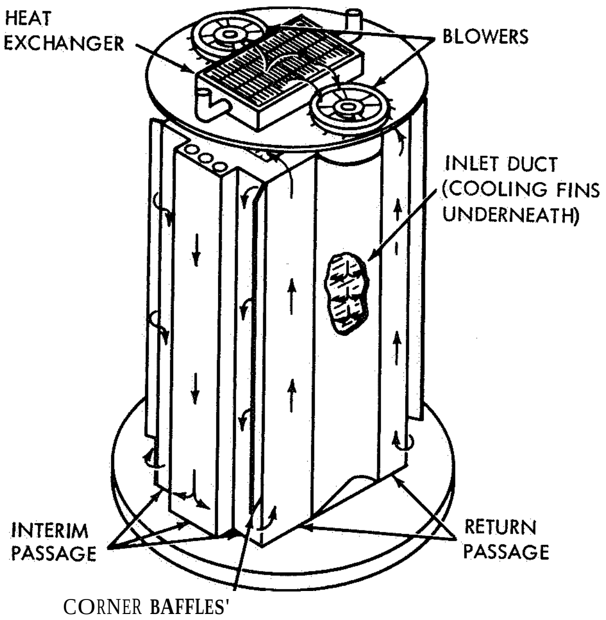

The cell **stack had inlet ducts over the cooling** fins **of the cells. A cylindrical ease (not shown) surrounded the stack, touching the comer baffles. The coolant gas exits from the fan through an inlet manifolding duct from which it enters the respective cell-fin passages. After traversing the fuel-cell plate** fins **and cooling the fuel-cell module, the gas Row turns and continues down an interim passage formed by the canister walls and baffles attached to the reactor. At the lower portion of the interim passage, the accumulated gas flow enters a return passageway defined by the canister walls and baffling. It then travels the length of the reactor before entering the heat exchanger and continuing into the blower inlet. The heat exchanger is supplied with cooling water,** *so* **that heat removal from the stack is by means of this water** (see **fig. 8.7).**

FIGURE 8.8.—Circulation pattern of gaseous coolant in Allis-Chalmers 1.5-kW fuel-cell stack ***(45).***

A new thermal-control subsystem which did not use any external liquid coolant system included heat elements with heat rejection accomplished by thermally actuated shutters instead of a case around the module (see fig. 8.8). Extra heat loss by radiation was sufficient when the shutters were open to give satisfactory control at 200° F (93" C), eliminating the blowers and heat exchanger shown in figure 8.8. Thus, thermal control of the system is maintained by radiation coupling with the space vehicle. Tests on a laboratory prototype showed satisfactory control of 400-watt modules with environment temperatures below 100° F (**38**" C).

Mathematical optimization was also used to determine the best system for Advanced Station Vehicle Missions (59). It was assumed that the fuel cell would operate at 93 A/sq ft at 0.93 volt, 186 A/sq ft at 0.88 volt, and 372 A/sq ft at 0.82 volt, based on extrapolation to 1968 performance from present experience. The general results of the analysis are given in chapter 1, but it is interesting to see that mathematical optimization generally produced weight savings of 15 to 20 percent of the unoptimized weight.

8.6 CONCLUSIONS

The devices discussed above have been primarily for hydrogen and oxygen cells for space applications, which require simple, reliable, lightweight control systems. Union Carbide Co. control system used hydrogen circulation for water removal and electrolyte circulation for heat removal and must, therefore, be considered as more complex and unreliable than other systems. The principal advantage of this method is that the circulated electrolyte acts as a reservoir of heat and water, so that control need not respond rapidly to fluctuations in conditions. The other principal types of cell (Pratt & Whitney, General Electric IEM, Allis-Chalmers asbestos membrane) cannot tolerate much dilution or drying of the relatively small volumes of electrolyte contained in the cells and control response must be fairly rapid.

It is difficult to compare the three most de-

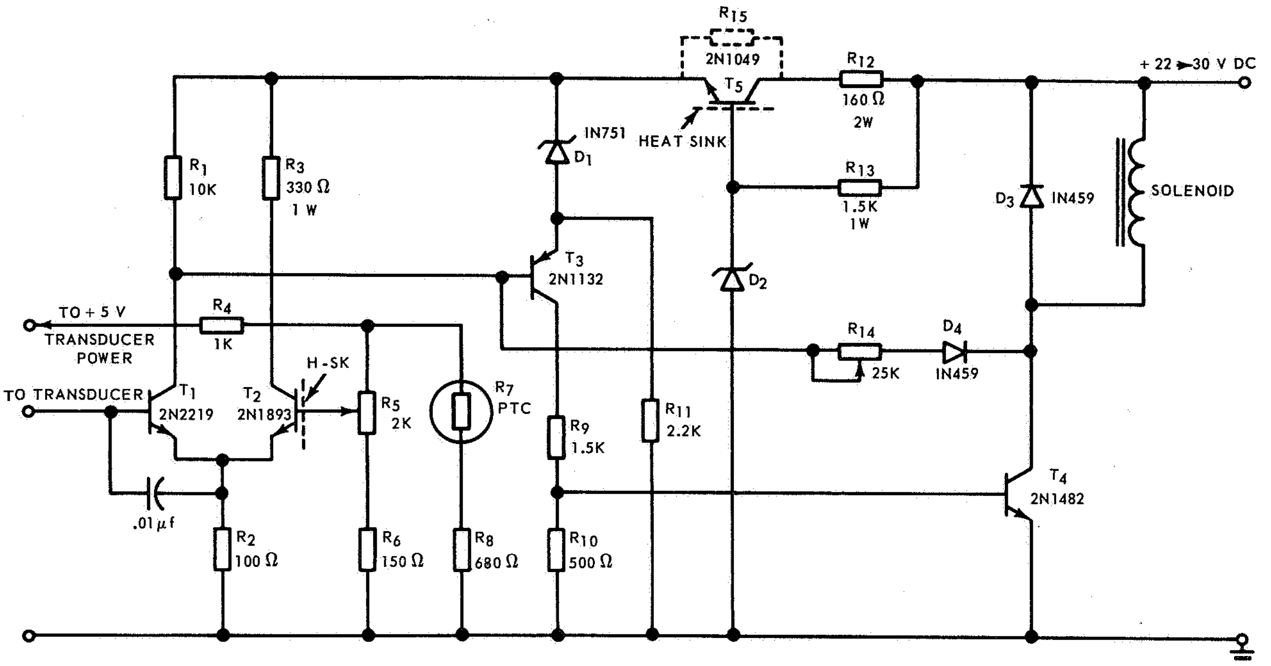

To maintain concentration of electrolyte within a desired level, the pressure of the water-removal cavities is adjusted as temperature varies. The solenoid valve which controls pressure (measured by the pressure transducer) operates at different pressures at different stack temperatures. This is done by a thermistor, R_7, which changes the pressure to follow the variation of required electrolyte vapor pressure with temperature.

FIGURE 8.9.—Allis-Chalmers' temperature-compensating electronic pressure-controller (56).

veloped systems because information is not available for the latest Pratt & Whitney and General Electric space systems. In the Pratt & Whitney cell, water removal and heat removal are controlled by one stream (circulated hydrogen), which is a definite advantage. This is possible because of the higher operating temperature (400" F (204" C)) of the cell and the concomitant high heat content of the hydrogen stream. The large change in equilibrium water vapor pressure over concentrated KOH at 400° F (204" C) as the electrolyte becomes diluted also makes the water removal system self-regulating to a considerable extent. However, auxiliary heaters are required to bring the cell to temperature, and pumps, valves, condensers, and water separators are required in the circulation system, which are disadvantages. The General Electric ion-exchange-membrane cell is simpler because (except for purge) the reactant gases can be dead ended to the cells. However, heat removal by thermal conduction at low temperatures is not very flexible and is inadequate for larger units which operate at varying load. Auxiliary cooling by passing fluid through the stack is necessary. The water-wicking method of water removal is also very simple but it has some disadvantages. It seems likely that the low current density of the cell may be partly due to mass-transfer limitations of gases through films of water on the electrodes. This is particularly important for applications where air is used instead of oxygen. In addition, the wicking method will probably be unsatisfactory at temperatures close to, or above, the boiling point of water, so that cell performance cannot be improved by higher temperature even if higher temperature membranes are developed. Also, if a cell drowns, the wicking system is relatively inflexible and there is no means of adjusting conditions to dry out the cathode. If water removal is carried out by hydrogen or oxygen circulation, or by air flow, the low electrolyte capacity of the membrane requires rapid response of control to change in conditions.

Of the three methods of water removal employed by Allis-Chalmers (voltage sensing, dynamic vapor pressure control, and static vapor pressure control), the static method is simplest. **As** discussed above, voltage sensing and dynamic vapor pressure control required circulating hydrogen and careful control of cell temperature. Voltage sensing was satisfactory only at fixed load, and required an invariant cell performance. The static method used dead-ended reactant feed, but needed a condenser control system to maintain vacuum in the water-removal cavities. The extra compartment leads to thicker cells and fewer watts per cubic foot yield.

The simplest purge system is a steady leak of cell gases to waste, but this was not, in general, satisfactory. It was better to have a flushing purge lasting for a few seconds, once or several times per hour. The simplest control method was to purge for preset periods of time at regular intervals, using a timing control; however, this wasted reactants at lower loads, since the purge rate is determined by the maximum steady load. The purge rate was usually about **3** percent of reactant and is a direct loss of efficiency.

Several of the designs given in the contracts used space radiators to dispose of waste fuel-cell heat from the spacecraft, and system optimization was strongly dependent on the space radiators required. For larger spacecraft, however, it may not be necessary for a low-temperature fuel cell to have individual heat rejection; the fuel-cell unit can lose heat to the interior of the vehicle, and the heat balance of the spacecraft determined for all components present, using much of the vehicle surface for heat rejection.

One surprising feature of the control systems reported here is that they are all based on mechanical automatic control. Since spacecraft contain digital computers, it would seem logical to control the fuel-cell subsystems by computer control, using time sharing with existing computer equipment. Presumably this will become possible with larger spacecraft, in which case control can be made sophisticated by interposing programed digital logic and memory between parameter sensors (e.g., temperature, pressure, voltage, current, time, etc.) and regulation equipment such as solenoid valves and relays. It is also surprising that little attempt has been made to develop novel, lightweight flow regulators, valves, etc., and their corresponding fittings.

When military or commercial applications are considered, the control problems are somewhat different from those of space and have not received much attention in the contracts within the scope of this book. Assuming that these applications will necessitate the use of air and cheap fuel, a major change may be required in the purge control. For example, dead ending or circulation of oxidant cannot be used for air; it would be used in a once-through manner. Similarly, when hydrocarbon fuels are used, the buildup of CO_2 and CO during reaction prevents circulation or dead ending and again leads to a once-through fuel supply. For this case, the fuel supply must be adjusted to the load in a different manner from that described above. If cheap hydrogen is obtained by re-forming hydrocarbons or other carbonaceous fuels, it is likely to contain appreciable fractions of inert gases. These may lead to excessive loss of hydrogen by purging unless the fuel is used in a once-through manner (through cells in series) so that the exit gas is highly enriched in inerts. .

Because few full-size fuel-cell plants had been operated for extended times during the period with which this book is concerned, many operating and system problems had either not become apparent or acute. subjects that had hardly been touched include quality control, starting with raw materials and ending with packaging of the product; effects of storage; starting, stopping, standby, and sudden load changes; degradation and catastrophic failure of fuel cells and auxiliary components; simple yet adequate controls of heat and mass transfer; minimization of parasitic power; optimum use of modular construction; and experimental determination of the reliability of complete fuel-cell plants.

Two examples of studies of this type are papers published by Evans and Evans et al. on the importance of cell and circuit design. The former (ref. 8.4) shows that nonuniformity of temperature, concentration, or current can seriously reduce performance. Such simple devices as repositioning the cell connectors contribute to marked improvements in performance and hence in life as well. In the latter (ref. 8.3), Evans made reasonable (but arbitrary) assumptions for module reliability and showed that ***8*** modules can be arranged in 10 circuits *so* that calculated circuit reliability varies from 0.66 to 0.9978 for two-thirds of the parallel strings being operable; and from 0 to 0.9999999 for one-third of the strings.

Other system considerations in need of further evaluation are use of oxygen instead of air for terrestrial purposes, and choice of acid or basic electrolyte for low-temperature or medium-temperature systems supplied with carbonaceous fuels. Use of air means passing 80 percent inert diluent through the system and thus imposing penalties of heat and moisture control; for use with alkaline electrolyte, a further requirement is scrubbing of carbon dioxide from air to avoid carbonation. Enrichment of oxygen in air, for example by permselective membranes, entails an expenditure of parasitic power, some of which might be needed anyway for removing carbon dioxide. Since the performance of a fuel cell is quite sensitive to the partial pressure of oxygen, there must be a "break-even" point up to which the parasitic power is more than compensated for by enhanced performance. The location of this point is not known.

Basic electrolyte permits use of cheaper materials of construction, cheaper catalysts, and better cathode performance than does acid electrolyte. But carbon dioxide from the air and from carbonaceous fuels reacts with and neutralizes the base, causing a drop in ionic conductivity and hence in performance. Alkali bicarbonate and carbonate products can either be regenerated or replaced by fresh caustic solution. Thus, either the power for regeneration must be subtracted from the gross power output or the replacement caustic becomes part of the "fuel" cost and the logistics problem. The European methanol-air fuel cell with caustic electrolyte—developed by Professor Vielstich at the University of Bonn, Germany, and being produced by Brown Boveri & *Corp.* in Baden, Switzerland—indicates the practicability of this last approach. But again, no data exist on which to base a rational choice of approach for various possible applications; i.e., when to use consumable or regenerable caustic and when to choose acid electrolyte.

Finally, the form of electricity available from a fuel-cell system is often not suitable for the user. Hence the power is "conditioned," or the using device must be modified. Thus far, emphasis has been on power conditioning rather than modification of the using device. Conceivably, however, the reverse approach may not only result in better systems for some purposes but it may actually make fuel cells attractive for uses for which they do not appear particularly suited now. Historically, much electric equipment has been tailored to fit available forms of electricity. If the fuel cell is to be taken seriously as a new power source, some thought must be given to adapting electric equipment to make the best use of its low-voltage, high-amperage, direct-current output.

8.7 REFERENCES

8.1. VAN WINKLE, J.; AND CARSON, W. N., JR.: Electrochem. Technol., vol. 1, no. 1–2, Jan.–Feb. 1963.

8.2. EISEN, M. P.: Fuel Cell System Analysis for Space Power Applications. General Electric Co., Direct Energy Conversion Operation, Lynn, Mass., Aug. 1963.

8.3. EVANS, G. E.: Reliability Engineering of Fuel Cells for Space Power. AIAA, Third Biennial Aerospace Power Systems Conference, Sept. 1964, paper 64–746.

8.4. EVANS, G. E.; HILVETY, N.; WINTERS, C. E.; AND BAILEY, R. V.: Mass Transport and Heat Transfer in Fuel Cell Systems. AIChe, 58th Annual Meeting, Dec. 1965.

CHAPTER 9

Electrolytically Regenerative Hydrogen-Oxygen Cells

9.1 INTRODUCTION

When the product of a self-contained fuel-cell system is regenerated to reactants by electrolysis, the cell becomes a secondary battery. Regeneration can take place *in situ* (fuel cell acts also as electrolyzer) or in an independent electrolysis cell. The *in situ* method has the obvious advantage that one unit fulfills two functions, thereby reducing weight, cost, and complexity. The "separate" method has the advantage of greater flexibility; the fuel cell and the electrolyzer can each be designed uncompromisingly for optimum performance. In addition, a separate fuel cell can be charged rapidly by refilling the reactant tanks and emptying the product tank, while the product can be electrolyzed to reactant at leisure in the separate electrolyzer.

A secondary fuel-cell system for industrial use must combine high-power density (kW/lb), large capacity (A-hr/lb), reliability, cheap regeneration, and low overall cost. Hydrogen-oxygen cells are unlikely candidates because it would probably be cheaper to use externally generated hydrogen, plus air, and discard product (direct fuel cell) rather than regenerate hydrogen and oxygen by electrolysis of product water. However, the convenience of electrolytic generation versus chemical generation might be an important factor in favor of an electrolytically regenerated fuel cell, especially if the cost and efficiency were comparable to normal batteries. Alkali amalgam-halogen cells have been recommended *(334)* for their high-power density and easy electrolytic regeneration. Also, use of two sodium/molten salt/chlorine cells of different temperatures was proposed (see sec. **11.3.3)** as a vehicle battery; the lower temperature cell has a higher potential than the higher temperature cell, so it electrolyzes the hot cell. The product of reaction from the cooler cell is fed into the hot and is there regenerated to reactants for the cooler cell by the electrolysis. Electrolytic regeneration of a single battery by a separate generator, as in conventional vehicle battery-generator sets, is also feasible.

For the most part, development of fuel cells as secondary batteries has been directed toward use in orbiting Earth satellites. Systems developed for orbiting Earth satellites have been based on hydrogen-oxygen fuel cells, which are charged by solar cells in the sunlight interval of the orbit and discharged during the shade interval.

Direct hydrogen-oxygen fuel cells for space travel require either high pressure or cryogenic storage of reactant gases. The gases are reduced in pressure or heated before entering the cells. In a fuel-cell-electrolpsis cycle for orbital applications, it is theoretically possible to reverse these processes by electrolytically generating gases at low pressures, and either pressurizing them for storage or cooling them for cryogenic storage. However, reversing the process presents additional difficulties. While pressures can be reduced by use of a simple reduction or regulator valve, increasing the pressure requires a compressor unit which would carry a heavy weight penalty. This problem occasioned development of a closed system to generate high-pressure gas, wherein the electrolyzer acts as a compressor: gas pressure builds up and the electrolyzer acts as a pump (sec. 9.5). In the separate method, the electrolyzer is designed to operate up to the maximum storage pressure desired, and the fuel cell can be operated at a constant, lower, optinium pressure. The electrolyzer, an extra piece of equipment, must be as small and efficient as possible. Water formed during the fuel-cell cycle must be stored and fed to the electrolyzer, which again requires auxiliary equipment. An example of the complexity of a separate system is shown in figure 9.1. For the *in situ* method, the fuel-cell electrolyzer is designed to take the maximum pressure; the unit should preferably operate as a fuel cell over the range of pressures involved.

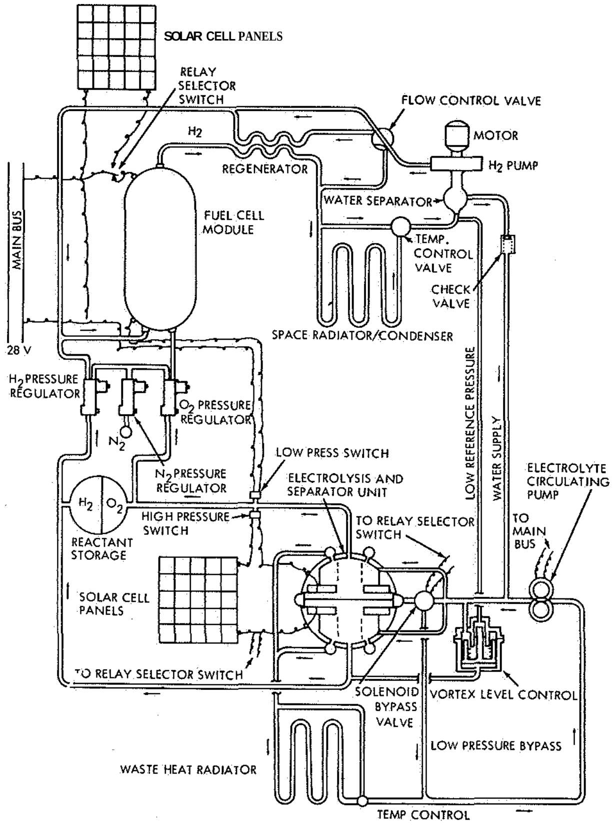
SOLAR CELL PANELS
RELAY SELECTOR SWITCH
FLOW CONTROL VALVE
H_2
MOTOR
H_2 PUMP
REGENERATOR
WATER SEPARATOR
MAIN BUS
FUEL CELL MODULE
TEMP. CONTROL VALVE
CHECK VALVE
SPACE RADIATOR/CONDENSER
28 V
H_2 PRESSURE REGULATOR
O_2 PRESSURE REGULATOR
N_2
LOW REFERENCE PRESSURE
WATER SUPPLY
LOW PRESS SWITCH
N_2 PRESSURE REGULATOR
ELECTROLYSIS AND SEPARATOR UNIT
ELECTROLYTE CIRCULATING PUMP
H_2
O_2
HIGH PRESSURE SWITCH
REACTANT STORAGE
TO RELAY SELECTOR SWITCH
TO MAIN BUS
SOLAR CELL PANELS
TO RELAY SELECTOR SWITCH
SOLENOID BYPASS VALVE
VORTEX LEVEL CONTROL
LOW PRESSURE BYPASS
WASTE HEAT RADIATOR
TEMP CONTROL

The proposed system used a Pratt & Whitney modified Bacon fuel-cell module. Water was removed from the fuel-cell electrolyte by condensation from the circulated hydrogen stream. During the light interval of the orbit when power was supplied by solar cells, the water was electrolyzed to hydrogen and oxygen in the electrolysis unit and the gases separated from the electrolyte. The high fuel-cell temperature (about 450° F (232° C)) meant that dilution of the electrolyte in the cell could not be allowed (otherwise excessive pressure developed). Therefore, the product water could not be stored in the fuel-cell electrolyte.

FIGURE 9.1.—500-watt regenerative hydrogen-oxygen fuel-cell system for orbital applications; Pratt & Whitney *(531)*.

When water *can* be stored in the fuel-cell electrolyte, the system is much simpler than that shown in figure 9.1.

One approach to eliminating the weight of high-pressure storage tanks, i.e., storing reactants in solid form, is unfortunately limited by the poor storage capacity of fuel-cell electrodes as compared with conventional batteries. An extreme example would be storage of chemisorbed hydrogen on a palladium- or platinum-catalyzed active carbon surface. Assuming one hydrogen atom per atom of palladium or platinum, the theoretical maximum capacity is about 70 A-hrs/lb of catalyst, without allowance for catalyst support, current collectors, etc. This can be compared with a theoretical 385 A-hrs/lb of zinc. The theoretical capacity of zinc cannot be obtained in practice, but the recoverable energy per pound of fuel-cell electrode would probably be less than theoretical by a similar factor.

The performance of a fuel-cell-electrolyzer-battery for orbital applications has to be compared with that of conventional batteries. Complete systems use solar cells as the power supply during the light interval, with some of the power used for charging the battery subsystem. For a given power level and orbit, the weight of solar cells and heat-control equipment can be taken as approximately the same for the use of either the fuel-cell or conventional battery subsystem. For a specified power level, the power density for the fuel-cell subsystem depends principally on the weight of the fuel cell (W/lb almost constant) and the weight of gas storage (W/lb increases with length of the shade interval). A circular orbit of 300 miles gives a shade period of 0.6 hour and a light interval of 1.00 hour, while an orbit of 22 400 miles (escape distance) gives 1.2 hours shade and 22.8 hours light. Over such short dark times, the power density of the fuel-cell subsystem does not depend very markedly on the orbital radius, because the fixed weight of components overrides the additional weights for extra gas storage as the dark time changes (from 0.6 to 1.20 hours, for example). However, the power density of a conventional battery does depend strongly on the orbital radius, as discussed next.

As a rough guide, the power density of the best existing direct fuel cells can be taken as approximately 10 W/lb, exclusive of reactants and tankage. The energy density of conventional high-capacity batteries is shown in table 9.1 (ref. 9.1; see also ref. 9.2 and *192)*. The silver-zinc battery has a rating of 40 W-hrs/lb, which is almost independent of the rate of discharge;

TABLE 9.1.—*Data for High-Capacity Batteries*

[Ref. 9.1]

Characteristics	Lead-acid	Nickel-cadmium (pocket-plate)	Nickel-cadmium (sintered plate)	Edison (nickel-iron)	Silver-zinc	Silver-cadmium
Open-circuit voltage of fully charged cell	2.1	a	1.3	1.4	1.86	1.4
Nominal voltage	2.0	r	1.2	1.2	1.5	1.1
Average discharge voltage at 1-hr rate:[a]						
at 80° F (27° C)	1.86	1.05	1.18	0.85	1.43	0.99
at 0° F (−18° C)	1.84	1.00	1.15	....	1.27	0.95
at −40° F (−40° C)	1.72	0.75	1.08	....	....	0.77
Voltage range for constant current charge	2 to 2.6	1.3 to 1.7	1.3 to 1.7	1.5 to 1.8	1.6 to 2.1	1.2 to 1.7
Constant current charging at 80° F	10-hr rate to constant voltage	5-hr rate for 7 hr	5-hr rate for 7 hr	5-hr rate for 7 hr	20-hr rate to 2.1 volts	20-hr rate to 1.7 volts
Time to 50 percent capacity retention:						
80° F	55 days	300 days	300 days	25 days	Estimated over 2 years	Over 2 years
125° F (52° C)	7 days	17 days	17 days	....	115 days	115 days (est)
160° F (71.5° C)	¾ day	4 days	4 days	....	58 days	58 days
Cycle life	200 to 2000	Over 2000	Over 2000	Over 2000	10 to 400	300 to 1000
W-hr/lb[b]	7 to 26	6 to 10	10 to 15	11 to 14	25 to 56	11 to 38
W-hr/cu in.[b]	0.45 to 2.75	0.4 to 0.7	1.08	0.98 to 1.16	1.3 to 3.8	0.67 to 2.9
W-hr/dollar[b]	45	9.6 (est)	8.5 (est)	9.5	2.8	2.8
A-hr/lb[b]	4 to 13	4 to 8	8 to 12	9 to 12	16 to 37	10 to 35
Major advantages	Low cost, general availability, good cycle life, high voltage per cell, good capacity, life and charge retention	Excellent cycle life, reliable with care, rugged	Excellent cycle life, reliable with care, good low-temperature charge/discharge performance, rugged, can be hermetically sealed	Excellent cycle life, reliable, extremely rugged, not damaged by overcharge or overdischarge	Excellent energy output per unit weight and volume, excellent performance at high discharge rates	Good energy output per unit weight and volume, good cycle life
Major disadvantages	Sulfates on discharged stand, cannot be charged at subzero temperatures, cannot be hermetically sealed	High cost, poor high-rate and low-temperature performance	High cost	High cost, poor charge retention, poor low-temperature performance	High cost, poor cycle life, poor low-temperature performance	High cost

[a] Based on 20 percent drop in voltage during the discharge period.

[b] Figures dependent upon capacity. Figures based on large capacity at 80° F operation.

for discharge time of 1 hour it has, therefore, a power density of 40 W/lb. At first sight, fuel cells do not appear to be competitive. However, the electrochemical reactions in conventional batteries involve massive rearrangement of electrode materials on charge and discharge. This leads to short life if they are cycled at high charge-discharge rates because electrode materials fall away from the battery plates. In particular, many cycles of use can only be obtained if the cells are charged relatively slowly. The relation between the minimum allowable time of charging, battery weight, and orbit radius is as follows. Let

P =required power output in shade, watts
t_d =shade time; i.e., discharge time
t, =light time; i.e., charge time
R =maximum permissible mean rate of charging during t,, A/lb
V =effective discharge potential, volts per cell
e =fractional current efficiency of charging (coulombs out per coulomb in)
W=weight of battery, pounds

The permissible rate of charging a battery is usually expressed in terms of the maximum recoverable capacity, C, W-hrs/lb, and the minimum time of charge to full charge, t_f hours

$$VRt_f=C. \tag{9.1}$$

If t_f is greater than t,, the battery cannot be charged from low to full capacity during the light time without loss of life. Equating A-hrs discharged to A-hrs charged

$$(P/V)t_d=\epsilon t_c RW, \quad t_f \geq t_c$$

or

$$P/W=(e)(t_c/t_d)(C/t_f), \text{ W/lb, when } t_f \geq t_c. \tag{9.2}$$

For a given C and t_f, the power density goes up as t_c/t_d increases; that is, the orbit radius increases. If the radius is such that $t_f=t_c$, the equation reduces to

$$P/W=\epsilon C/t_d, \quad t_f \leq t_c. \tag{9.3}$$

In this case, the maximum capacity of the battery is obtained, longer light times will give a lower rate of charging than the maximum permitted, and equation (9.3) also holds for $t_f<t_c$.

This analysis is oversimplified because it ignores change of E and C with rate of charge-discharge, but it serves to demonstrate the principle. For example, to obtain a life of several thousand cycles, the charging time should be no less than 10 hours (192). The maximum capacity of a silver-cadmium battery was given as 30 W-hrs/lb and E as greater than 0.9. Therefore, a 300-mile orbit gives, from equation (9.2), a power density of $P/W=(0.9)(1/0.6)(30/10)=4.5$ W/lb. Thus, a fuel-cell system must give as good a power density as this (including reactants and tankage) or be capable of a greatly extended lifetime.

Other factors enter into the complete system, since the weight of auxiliary solar cells for charging the secondary batteries depends on the power efficiency of battery charge-discharge, K. Solar cells have to be provided to produce total power

$$P_T=P\,(1+t_d/Kt_c). \tag{9.4}$$

Space radiator weight may vary depending on the waste heat produced. A more detailed discussion of complete systems is given in reference 9.3. Table 9.2 gives data for a solar-cell nickel-cadmium battery system, based on 7 W/lb for solar cells and a maximum battery capacity of 13 W-hrs/lb; an overcharge factor of 0.18 ($\epsilon=1/1.18$) and an allowable time of charge of 10 hours.

TABLE 9.2.—*Power Densities for Solar cells Plus Nicad Batteries*

[Ref. 9.31

Power, kW	W/lb				
	Orbit altitude: miles				
	100	*300*	1000	22 400	Lunar surface
21..........	1.1	1.3	2.2	2.5	0.04
0.5..........	1.1	1.3	2.2		
0.1..........	1.1	1.3	2.2		

A study was made of a system using direct fuel cells, with reactant storage for the whole mission, to supply power during the dark interval (ref. 9.4). Obviously this system is suitable only for short-mission durations. The fuel-cell subsystem was assumed to have a power density of 12.5 W/lb, exclusive of reactants and tankage weights. The silver-zinc battery was not considered feasible due to short life, and silver-cadmium cells of 30 W-hr/lb energy density and minimum charging time of 10 hours were chosen. Power density of 11 W/lb was assumed for solar cells. For a 170-mile orbit, the silver-cadmium battery gave an energy density of 3.3 W/lb, whereas the direct fuel-cell system gave energy densities ranging from 9.9 W/lb for a 1-day mission to 3.3 W/lb for a 10-day mission. It was concluded that the direct fuel-cell system was favored at low orbits and low mission times. The rechargeable fuel-cell system was not considered in the comparison.

9.2 RESEARCH ON 500-WATT SOLAR REGENERATIVE HYDROGEN-OXYGEN FUEL-CELL POWER SUPPLY SYSTEM,

Pratt & Whitney Aircraft, October 1959 to October 1960 and September 1961 to December 1961

The research objective was to generate design data for a 500-watt, 28-volt, fuel cell-electrolysis system, for Earth satellite applications *(538)*. The fuel cell considered was the modified Bacon cell developed by Pratt & Whitney, and a separate electrolyzer-gas separator was used. Hydrogen and oxygen were generated by electrolysis at storage pressure to avoid compression, and the electrolysis cell had to withstand high pressures (500 psi). The first electrolyzer consisted of two flat, polished nickel-plate electrodes mounted in the expanding section of a venturi. The electrodes were separated by a 28-mil nickel screen of 3½ percent open area, that kept hydrogen-electrolyte froth generated at the cathode from contacting oxygen-electrolyte froth generated at the anode. The screen had to be thin and permeable to allow ionic current flow without too much IR loss. The venturi converted pressure into high electrolyte velocity between the plate electrodes, insuring good mass transfer of hydroxyl ion and a thin boundary layer at the plate containing the froth. At 700 A/sq ft, nickel electrodes gave a lower electrolysis polarization than platinum-clad nickel, so nickel was used for all subsequent tests. The formation of froth led to a higher IR drop than expected, but at velocities greater than 1 ft/sec, the correction for the presence of gas bubbles was negligible even at 700 A/sq ft. Tafel plots of cell voltage as a function of log i gave design values of $\alpha = 0.44$, $i_0 = (1.3)(10^{-3})$ A/sq ft, for i less than 13 A/sq ft; $\alpha = 0.25$, $i_0 = (1.2)(10^{-2})$ A/sq ft, for i greater than 16 A/sq ft. Pressure up to 500 psi did not affect the current polarization relations. Above 135" F (57° **C),** the effect of temperature on current density at a given potential was small. Figure 9.2 gives typical performance.

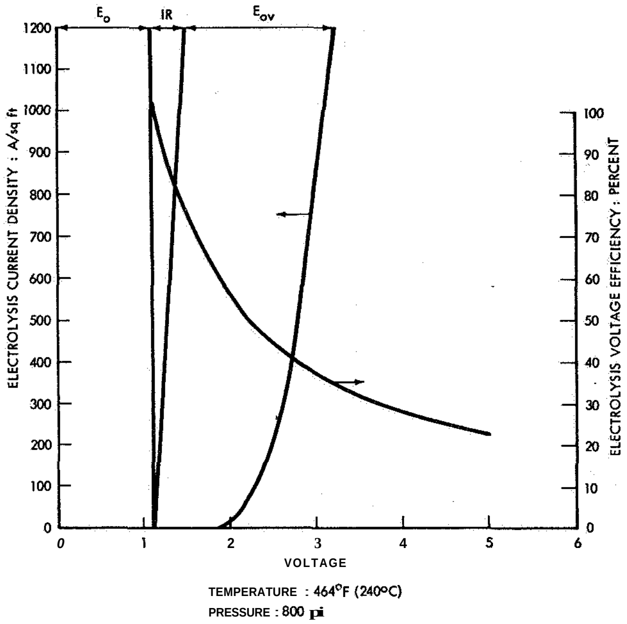

E_0 is the theoretical electrolysis potential, IR is ohmic polarization, and E_{ov} is activation over potential.

FIGURE **9.2.—Electrolysis of aqueous potassium hydroxide (27 weight-percent) on nickel electrodes at high flow rates (537); predicted performance extrapolated from experimental data.**

Figure 9.3 shows a vortex separator which combines the functions of electrolyzer and gas-electrolyte separation. An extensive theoretical analysis was performed to give the dimensions of the separator, but experimentally the drag of the screen on the vortex (ignored in the theory) interfered with the formation of the core. Best results were obtained with tangential electrolyte admission into the cylindrical vortex chamber instead of into the annulus between electrodes, but the unit was not fully tested.

A later contract *(531)* gave a more coherent system analysis (see fig. 9.1), based on the presumption that the electrolyzer-separator would work. Design was for a 500-watt unit, and the weight of the fuel cell and its auxiliary controls was

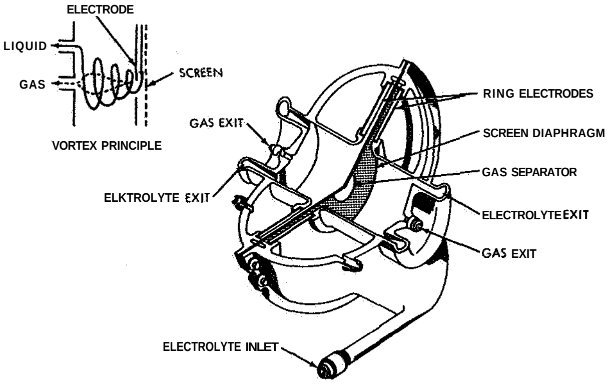

The electrolyte entered tangentially and flowed across the ring electrodes where it was electrolyzed to electrolyte-hydrogen froth at the cathode and electrolyte-oxygen froth at the anode. It swirled into the vortex chamber where centrifugal force threw the electrolyte to the walls and formed an inner hollow of gas (see insert). Separation was improved by a smaller vortex-chamber radius and higher electrolyte velocities, while larger currents were obtained by increasing the outer diameter of the ring electrode to increase electrode area.

FIGURE **9.3.—Combined electrolysis cell and separator; Pratt & Whitney Aircraft (531).**

virtually independent of working time spent by the cell in each orbit. Similarly, a fixed weight of solar cells was used to supply the mission power during the sunlight interval. Separate solar cells supplied the electrolyzer, and since

$$K \text{ (time in sun) (solar cell rate)} = \text{(time in shade) (fuel cell rate)}, \quad (9.5)$$

the weight of the extra cells depended on the particular orbit. K is the efficiency of conversion of solar-cell output to fuel-cell output, via electrolysis, gas separation, gas storage, and gas utilization in the fuel cell; a small "K" has to be balanced by a large solar-cell rate; i.e., more area and weight of solar cells. The system was optimized for a complete heat balance, pressure of gas storage, current density and efficiency of the fuel cell, space radiators for condensation of water from the fuel cell and overall heat rejection, and solar-cell current density and efficiency. Another variable was the circulation rate of hydrogen through the fuel-cell stack, since this determined the partial pressure of water vapor and hence the condenser temperature (chosen to be about 140° F (60° C)).

The results are shown in table 9.3. A relatively low fuel-cell current density of 160 A/sq ft was used, since the higher efficiency permitted a smaller space radiator. Similarly, a current density of 500 A/sq ft at 2.5 volts was chosen for the electrolyzer; the main effect of a more efficient electrolyzer was to reduce radiator area and weight. Since the electrolyzer and its radiator have a weight-time-efficiency relation similar to equation (9.5), the electrolyzer output and space-radiator size decreased for longer sunlight intervals. The power density of the fuel-cell subsystem was estimated at 4.2 W/lb.

It was recommended that the system be developed for orbital applications. However, the design compares unfavorably with an equivalent solar cell-conventional battery system because of its complexity. The battery charge and discharge cycle would be at least as efficient as the electrolyzer-fuel-cell cycle and would therefore require no additional radiator weight. While the fuel-cell system has been claimed to be highly reliable for long periods of time (batteries are definitely limited as to the number of times they can be cycled), the system is sufficiently complex that is is unlikely to give hundreds of hours of unattended service without considerable development of 'valves, pumps, controls, etc. Unlike a solar cell-battery system, it does not adapt to subdivision into self-contained power modules which can be individually switched out on failure, leaving the rest of the modules operative.

The system weight could have been reduced significantly at low orbits by using a more efficient electrolyzer, but no attempt was made to reduce activation polarization by the usual techniques of catalysis and high area electrodes. The values of α and i_0 indicate that both electrodes were irreversible above 16 A/sq ft, although no reference electrode was used to check this. (It is also surprising that the current had no temperature dependence.) The electrolyzer current density of 500 A/sq ft at 2.5 volts used in the design does not correspond to extrapolated experimental electrolyzer performance (see fig. 9.2), so perhaps some allowance was made for possible catalytic improvement in the electrolyzer.

TABLE 9.3.—500-*Watt System Characteristics for Various Orbits* (531)

Orbit, miles	*300*	*2000*	*5000*	*10 000*	*22 400*
Orbit interval, hrs.	1.6	2.645	4.72	9	24
Shade interval, hrs.	0.60	0.645	0.82	1	1.2
Sunlight interval, hrs.	1.00	2.00	3.90	8	22.8
System wt-lbs*	536	420	345	315	275
System vol-ft^3	1.59	1.58	1.565	1.56	1.562
Solar power total, watts	1770	1220	935	790	687
Fuel cell heat rejection, Btu/hr:					
a. Module and controls	250	250	250	250	250
b. Space radiator	1290	1290	1290	1290	1290
Electrolysis cell-gas separator, Btu/hr:					
a. Space radiator	1100	523	450	262	175
Total heat rejection, Btu/orbit	2025	2041	3070	3640	5850
Subsystem efficiency, percent:					
a. Fuel-cell module	71	71	71	71	71
b. Fuel-cell subsystem	65	65	65	65	65
c. Electrolysis cell-gas separator	52	53	55	57	60
d. Solar cells	10	10	10	10	10
Electrolyte concentration:					
a. Fuel cell	79	79	79	79	79
b. Electrolysis cell	25–35	25–35	25–35	25–35	25–35
Water formed, lbs/orbit	0.370	0.400	0.510	0.620	0.745
Reactant storage pressure, psia	80–240	80–240	80–240	80–240	80–240
Temperature, °F:					
a. Fuel-cell module	500	500	500	500	500
b. Electrolysis cell-gas separator	250	250	250	250	250
c. Space-radiator sink	80	80	80	80	80
Radiator area, ft^2:					
a. Fuel cell	10.2	10.2	10.2	10.2	10.2
b. Electrolysis	4.75	2.24	1.925	1.11	0.755
Flow rates:					
a. Fuel cell H_2 recirculation rate, lbs/hr	0.5	0.5	0.5	0.5	0.5
b. Electrolysis electrolyte circulation rate, lbs/min	61.5	61.5	61.5	61.5	61.5

*Fuel cell, 85 lbs; fuel-cell subsystem, 118 lbs.

9.3 ION-EXCHANGE MEMBRANE REGENERATIVE FUEL-CELL RESEARCH AND DEVELOPMENT PROGRAM, General Electric Co., January 1960 to September 1960, October 1960 to October 1961, and October 1961 to November 1961

The scope of the first contract was to generate ideas for a 500-watt hydrogen-oxygen system for space applications (240). The cell used was the General Electric IEM cell, with 80-mesh platinum screens embedded in a reinforced (sulfonated phenolformaldehyde resin) IEM, plus platinum black packed onto the screen and bonded to the membrane. The cell was tested as an electrolyzer by filling the hydrogen and oxygen compartments with water. The current densities initially obtained were 100 A/sq ft at 2.5 volts and 420 A/sq ft at 3.5 volts, but after 140 hours the anode (the oxygen electrode of the fuel cell) had peeled away from the membrane, resulting in poor performance of the fuel cell. Peeling occurred much more rapidly when acidified electrolyte was used in place of water. With hydrogen on both sides, the ohmic resistance of the cell did not increase and the peeled electrode was a satisfactory hydrogen electrode. It was concluded that the sulfonic acid groups in the membrane were degrading at the oxygen electrode, and that a liquid electrolyte bridge was necessary between the cathode and the membrane. Concentration polarization of the hydrogen ion occurred in this bridge.

The sulfonic acid groups were stabilized by etherification or esterification, but the resultant membranes had too high an ohmic resistance. To overcome the problem, Teflon-platinum electrodes were used without bonding to the membrane (see ch. **3)** and the membranes soaked in strong sulfuric acid (Zerolit C–20 membrane) or potassium hydroxide (Zerolit A–20). Thus the membrane behaved partly as a permeable electrolyte matrix and strong acid or alkali was electrolyzed. A cell was cycled for **44** days at current densities of 15 A/sq ft on discharge (for about 70 minutes) and 4 A/sq ft on charge, but deterioration occurred with time.

The use of the electrodes in a separate electrolyzer was investigated *(248).* To keep the gases separated, a Monel diaphragm was placed between the electrodes; the bottom of the diaphragm had holes for ion transport. Not surprisingly, the diaphragm acted as a bipolar electrode, evolving hydrogen at one side and oxygen at the other. Porous polyethylene worked satisfactorily as a separator up to 1000 A/sq ft (no voltages were given).

A 50-watt dual-purpose unit was built from a fuel cell similar to that described in section **4.3.3,** with a bipolar heat conductor ***(238).*** A number of the oxygen and hydrogen gas-distribution channels in the cell were filled with neoprene sponge. The water formed during fuel-cell operation was absorbed in the sponge and was then available for electrolysis. The bipolar plates were 4-inch-diameter stainless-steel disks, with ribs pressing against the screen current collectors. A Lucite case was used, with steel end plates to bolt the stack together. Electrodes were Teflon-bonded platinum black on nickel screen (stainless-steel screen corroded), and membranes were Zerolit A–20 soaked in potassium hydroxide. Hydrogen and oxygen passed between the cell and storage tank through manifolds. The storage tank contained twice the volume of hydrogen as oxygen, and separated the two gases by a thin rubber membrane which insured equal pressure to the two gases on electrolysis. System weight was 44½ pounds for 50 watts.

The unit was charged to 100 psig by electrolysis (using low current densities and voltages less than 1.8). The hydrogen chambers had to be thoroughly purged of oxygen with inert gas to prevent catalytic hydrogen-oxygen combustion and burnout of the membranes. The electrolysis-fuel-cell cycle (90 minutes charge, **30** minutes discharge) gave 80 to 100 percent current efficiency and **30** to 50 percent power efficiency. Lifetime was poor, with most of the trouble occurring at the oxygen electrode. Half of the water at the hydrogen electrode was electrolyzed to hydrogen and oxygen and the other half was transported to the oxygen electrode,

$$2OH^- \rightarrow H_2O + \tfrac{1}{2}O_2 + 2e^- \quad \text{(oxygen electrode)}$$

$$2H_2O + 2e^- \rightarrow 2OH^- + H_2 \quad \text{(hydrogen electrode)}$$

$$\overline{}$$

$$2H_2O \text{ (hydrogen electrode)} + \\ H_2 + \tfrac{1}{2}O_2 + H_2O \text{ (oxygen electrode).}$$

On current drain, the process was reversed, giving all of the water on the hydrogen side.

The unit was aircraft tested at 0 to 2½ gravity (for periods **up** to 20 seconds) and performed satisfactorily. A rocket launch test did not give information, since a bad launch led to destruction of the rocket after **35** seconds.

It can be concluded that the low power density (just over 1 W/lb) and the short life were unfavorable in comparison with conventional batteries.

9.4 RESEARCH ON THE ELECTROLYSIS OF WATER UNDER WEIGHTLESS CONDITIONS, Battelle Memorial Institute, June 1960 to November 1961, June 1961 to May 1962, and June 1962 to June 1963

In this program, electrolysis was studied as a source of oxygen for life support. While the work was not directed toward fuel cells, efforts on hydrogen-oxygen electrolysis merit reporting here. Two initial parameters were determined: one man requires the oxygen content of 2.25 pounds of water per day; and the theoretical minimum energy needed for electrolysis of this water is about 155 watts.

The initial design (fig. 9.4) consisted of a stack of disk cells spun on a vertical axis of 500 rpm by an electric motor **(125).** The rotation threw the electrolyte to the perimeter, creating by this action a satisfactory gas vortex in the center. Operating at 1.9 to 2.0 volts and using 250 amperes, the system separated about 4.5 pounds of water per day into hydrogen and oxygen and supplied enough oxygen for the needs of two men. An unanticipated loss of about 50 watts of power occurred and was traced to contact IR at the silver-plated graphite brushes used in transferring current to the rotating assembly; this loss could be reduced to negligible proportions through bipolar series connection of the cells to obtain a tenfold reduction of current density at the brush. Parasitic power of the motor was much too high (90 watts), but designers felt this could be reduced to **30** watts.

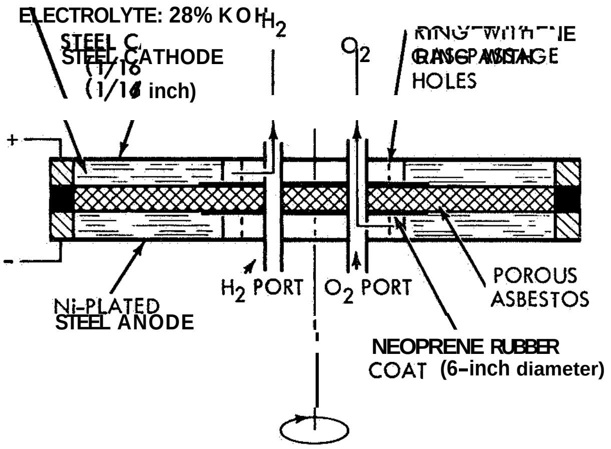

When the disk-shaped cell was spun around its axis, the electrolyte was thrown **to** the outside, and gas formed a vortex at the center. The gases evolved by electrolysis were separated by a porous asbestos membrane which retained electrolyte by capillary action. Hydrogen evolved at the cathode was taken off through central ports, as was the oxygen evolved at the anode. **A** stack of the cells was built, with electrolyte pumped through manifolds in the outer rim (not shown). The cells were connected in parallel.

FIGURE 9.4.—Schematic of Battelle electrolyzer (125).

The total weight was 284 pounds, including **30** pounds of electrolyte, and the volume was 4.4 cubic feet. It was estimated that optimization would reduce the weight by 50 percent. The design obviously is not feasible because of its excessive size. The useful power density of 300 watts (used to electrolyze 2.5 pounds of water) per 284 pounds is low in comparison with electrolyzers developed for fuel-cell use. No attempt was made to obtain higher current densities (at the same electrolysis potential) by catalysis, improved mass transfer, or lighter cell configurations. The unit was built without adequate knowledge of the electrochemical process or use of relevant literature which could have led to considerable improvement in design.

A more imaginative approach was the use of a spinning system to form an oxygen vortex at the center of a cell, with hydrogen removal at the rim using a palladium-silver diffusion cathode (124). The hydrogen ion discharges at palladium or palladium-silver to form absorbed H atom. If a thin membrane cathode is used, with one face next to electrolyte and the other face next to a gas-removal chamber, the proton diffuses through the membrane and is evolved at the gas-chamber face.

The rates of diffusion were tested in a stationary cell employing a 1-mil Pd-Ag alloy cathode as the bottom of the cell and platinum gauze immersed in electrolyte as the anode. The cell was heated and pressurized; evolved oxygen was removed from the top through a condenser which returned steam to the electrolyte. A Teflon liner or a sprayed Teflon lining was used to isolate electrodes and electrolyte from the cell body. The results obtained are given in table 9.4.

TABLE 9.4.—*Hydrogen Transmission Through a 1-Mil Pd-Ag Cathode Membrane (124); 50 to 65 Weight-Percent KOH Aqueous Electrolyte*

Pressure, psig:			
Electrolyte.	122	20	13–25
H_2 chamber..	0	0	0
Temperature, °F. . . .	392 (200° C)	392 (200"C)	446 (230° C)
Current, **A**/sq ft..	15	150	265
Voltage.	1.34	2.0	1.76
Hydrogen transmission, percent. .	93	100	100

At the conditions of electrolysis, the reversible cell potential was about 1.0 volt, so that at 50 percent voltage efficiency the membrane would pass over 200 A/sq ft of hydrogen, depending on the temperature. However, it was necessary to activate the membrane by oxygen evolution at 150 A/sq ft, and performance declined over periods of ½ to 1 hour, requiring reactivation. The current densities were less than those predicted from the equilibrium-phase diagram and were not reproducible. Since high-purity conditions were not used, it is likely that the membrane was being poisoned by absorption of a material which could be removed by anodic oxidation.

A more direct method of removing water from air and replacing it with oxygen involved an electrolysis cell of design similar to low-temperature hydrogen-oxygen fuel cells *(126)*. The electrodes were expanded metal mesh (Exmet)—stainless steel for cathodes and platinum for anodes. The electrolyte was concentrated (85 weight-percent) phosphoric acid contained in a 32-mil-thick matrix of microporous rubber. The cells were contained in polyvinylchloride end plates having grooves cut through for gas distribution; neoprene gaskets were used and the cell components were secured with stainless-steel bolts, nuts, and washers. Nitrogen was circulated through the cathode chamber and moist air (30 to 50 percent relative humidity at 80" F (27" C)) was passed through the anode chamber. The equilibrium vapor pressure of water over concentrated phosphoric acid is low; therefore, water was absorbed by the electrolyte and electrolyzed to oxygen in the airstream, and hydrogen in the nitrogen stream. Phosphoric acid provided an advantage over potassium hydroxide in that it does not absorb carbon dioxide.

A two-cell stack operated for nearly 200 hours at about 35 A/sq ft. The air was enriched in oxygen but contained considerable hydrogen (and ozone). Similarly, the generated hydrogen contained some oxygen. The electrolysis voltage was over 4 volts per cell. Useful power density was 450 watts (used to electrolyze water) per 159 pounds (about **3** W/lb), which is still low: a unit capable of supplying enough oxygen for three men was estimated to weigh 159 pounds, have a volume of 1.1 cubic feet, and require 1560 watts for electrolysis. Again, little attempt was made to analyze the causes of the high overpotential and low-current density. Apparently, it was assumed that the polarization obtained on the smooth metals was the minimum obtainable.

9.5 EVALUATION OF ELECTROLYTICALLY REGENERATIVE HYDROGEN-OXYGEN FUEL CELL, Electro-Optical Systems, Inc., September 1960 to March 1962 (*160*), April 1962 to March 1963 (*183*), June 1962 to July 1963 (*175*), and October 1963 to Present (*186*)

The original aim of this work was to develop a fuel cell in which hydrogen was stored as chemisorbed gas, and oxygen stored as compressed gas (167). The electrodes used were 22-mil-thick porous nickel plates (Gould National Batteries, raw unimpregnated plates, 80 percent porous). The electrolyte was 35 weight-percent aqueous potassium hydroxide. A single cell which contained two nickel-plaque electrodes in a bed of electrolyte-soaked asbestos (in a high-pressure case) was electrolyzed to give hydrogen chemisorbed on the nickel cathode (fuel-cell anode) and oxygen dissolved in the electrolyte. It was necessary to raise the cell temperature above 200° F (93" C) to get high-current densities, and both charge (electrolysis) and discharge (fuel cell) polarization was less for higher temperatures. The cell self-discharged rapidly, presumably from reaction of oxygen with chemisorbed hydrogen, or of both gases at both electrodes. Using a 65-minute charge and a 35-minute discharge, the maximum current efficiency was 65 percent at 278" F (137" C).

A cell similar to the Allis-Chalmers cell (see fig. 4.18) was constructed with platinized-nickel electrodes. The nickel plaque was immersed in **3** weight-percent chloroplatinic acid solution to deposit 40 milligrams of platinum per square inch. The electrolyte was contained in an asbestos matrix between two electrodes, and taps to the hydrogen and oxygen electrodes showed that during electrolysis, sufficient gas was evolved on both electrodes to give 80 psig in the storage compartments; the amount of chemisorbed hydrogen was small compared to that evolved. The pressure was held for 30 days at open circuit at 70" F (21" C); discharge then gave 91 percent current efficiency. Charge retention was apparently a function of temperature: at 180" F

(82" C) the self-discharge of the cell was fairly small, but the loss rapidly went up, and was 15 percent per hour at 300" F (149" C). The rate of loss was only a weak function of pressure even up to 500 psig. Polarization on discharge was about 0.1 volt less at 200 psig than at 50 psig. Use of platinum catalyst improved cell performance from 0.4 to 0.77 volt at 100 A/sq ft, 200" F (93" C).

Bipolar electrode holders were made from Plexiglas or Lucite plated with 2 mils of nickel, with the shape shown in figure 9.5. Cell stacks were made from platinized-nickel electrodes and two layers of 1/32-inch asbestos as the electrolyte matrix. The unit described in figure 9.5 was shock, acceleration, and vibration tested with satisfactory performance. It was also cycled for over 1000 cycles (1800 hours' operation). The theoretical capacity of the cell based on the water in the electrolyte was 3.9 A-hrs/in^2, but as electrolysis proceeded, the loss of volume of electrolyte caused diffusion of hydrogen and oxygen across the membrane to give excessive self-discharge (plus higher electrolysis voltage). A practical capacity of 2 A-hrs/in^2 was claimed. The pressure difference which could be tolerated between the oxygen and hydrogen sides without blowing out the electrolyte was 10 psig, but even at 200" F (93" C) blowing out did not lead to explosion.

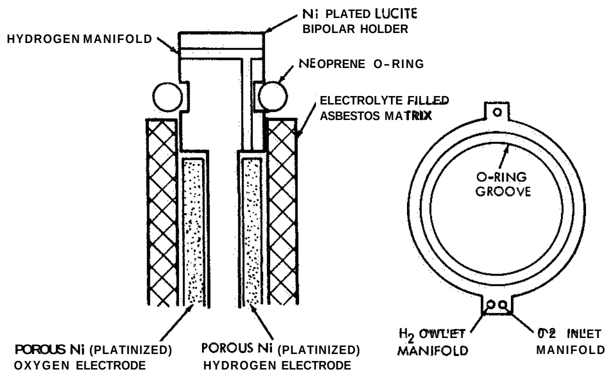
Ni PLATED LUCITE BIPOLAR HOLDER
HYDROGEN MANIFOLD
NEOPRENE O-RING
ELECTROLYTE FILLED ASBESTOS MATRIX
O-RING GROOVE
POROUS Ni (PLATINIZED) OXYGEN ELECTRODE
POROUS Ni (PLATINIZED) HYDROGEN ELECTRODE
H_2 OUTLET MANIFOLD
O_2 INLET MANIFOLD

The cells were disk cells of 4-inch diameter, stacked with a common hydrogen inlet manifold, a common hydrogen outlet manifold, and a single oxygen manifold. End plates of stainless steel were used and the manifolds led to 4-inch-diameter stainless-steel caps welded to the end plates. Electrolysis of electrolyte in the porous matrix gave hydrogen and oxygen at high pressures in the storage caps; the gases were used to form water in the matrix during the fuel-cell cycle.

FIGURE 9.5.—Detail of EOS electrolytically regenerative cell.

A nine-cell unit weighing 10.5 pounds, of which 2 pounds were fuel-cell weight, gave almost the performance predicted from single cells. The unit produced 25 watts at 6.2 volts when the temperature was 150" F (66" C), and 7 watts at 6.9 volts when the temperature was 70" F (21° C). The maximum capacity was not given, although the test cycle was 1 A-hr. (The fuel cell used as an electrolyzer produced 25 watts of hydrogen and oxygen corresponding to a theoretical power of 25 watts per pound of cell. This can be compared with 3 W/lb obtained by workers at Battelle. See sec. 9.4.)

The second contract required the delivery of regenerative cell stacks to the Jet Propulsion Laboratory ***(185).*** The general design was based on that given above, but more sophisticated engineering was used in stack construction ***(183).*** The hydrogen manifold location was changed from a tab at the disk edge (see fig. 9.5) to a central hole running through the stack. Two oxygen manifolds in tabs were employed. Gas-distribution channels were cut in the bipolar holder (cross and circle pattern); the channels were connected to the oxygen manifolds on the oxygen side, with an O-ring around the central hydrogen manifold on each side of the oxygen electrode, and to the hydrogen manifold on the hydrogen side. Holes in the edge of the bipolar holders took positioning pins to prevent rotation leading to nonalinement of the oxygen manifolds. Electrodes were 6 inches in diameter, with a 2-inch i.d. hole for the hydrogen manifold. The electrolyte matrix was four disks of sheet asbestos, 6¼ inches o.d. and 1½ inches i.d. The 1/32-inch sheets were compressed to about 30 mils, since this gave reproducible voltage-current relations for the cell. The capacity of the matrix was 31.6 grams of 26 weight-percent aqueous KOH.

The electrodes were catalyzed by forcing catalyst solution through the plaque ***(184);*** in addition to platinum, palladium was a suitable oxygen catalyst and platinum-palladium a superior hydrogen catalyst. Heat sterilization (required by the contract) of plated Plexiglas 55 caused separation of the plate, and other plastics were tried (see app. D). Melamine "NEMA

Grade G–5" was selected. Another problem encountered was that occasionally a "bad" cell would reverse and generate oxygen and hydrogen during the fuel-cell cycle.

Thirty-eight cells were connected in series, as shown in figure 9.6. The unit was tested on electrolysis by following the pressure increase with time ***(185).*** The volumes of the storage cylinders had been designed to give a pressure increase of 10 psi/A-hr, and this theoretical value was obtained up to nearly 300 psig. At greater periods of charge, the pressure increase was less, showing that self-discharge was occurring. (Based on the water contained in each cell, the theoretical capacity is about 70 A-hrs per cell. Since the cells are in series, a charge of 30 A-hrs is 30/70 or 43 percent of the theoretical maximum.) The self-discharge at 300 psig was about 10 A/sq ft. After 25 cycles, gas from the hydrogen chamber was 100 percent hydrogen, but the oxygen contained 4.7 percent hydrogen. Temperature rose from ambient to 122° F (50° C) during the complete cycle (no provision was made for cooling of the unit). Typical charge conditions were 30 A/sq ft at 1.7 volts per cell; typical discharge was 25 A/sq ft at 0.8 volt per cell. The maximum discharge capacity was about 20 A-hrs, because charging up to 30 A-hrs gave self-discharge rates comparable to the useful discharge rate. The unit weighed 85 pounds, and thus the power density was about **1.3 W/lb.**

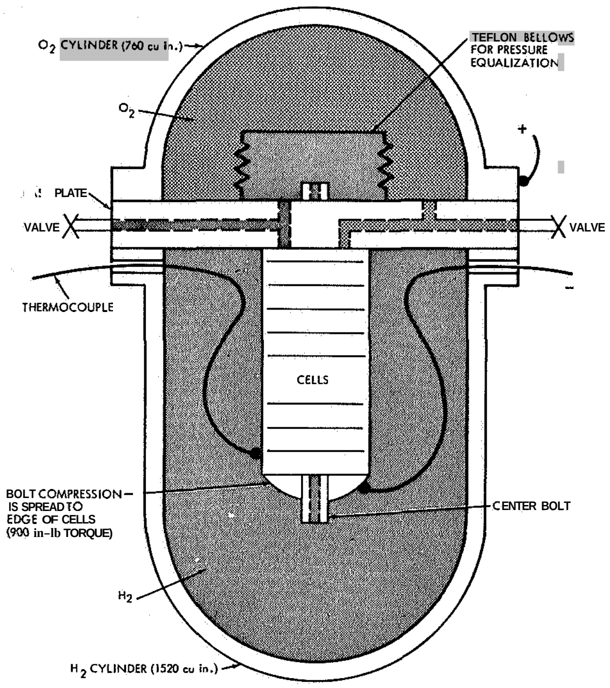
O_2 CYLINDER (760 cu in.)
TEFLON BELLOWS FOR PRESSURE EQUALIZATION
O_2
+
PLATE
VALVE
VALVE
THERMOCOUPLE
−
CELLS
BOLT COMPRESSION IS SPREAD TO EDGE OF CELLS (900 in-lb TORQUE)
CENTER BOLT
H_2
H_2 CYLINDER (1520 cu in.)

Hydrogen evolved from the cathodes during electrolysis passed into the bottom cylinder via a central hydrogen manifold. The hollow bolt used as manifold also bolted the cell stack together. Oxygen was taken to the upper cylinder via manifolds at the edge of the disk cells. The storage cylinders were of ¼-inch-thick aluminum alloy (6061–TS) with 5 mils of nickel plating, and had base flanges 1 inch thick. The cylinders and base plate (on which the stack was mounted) were bolted together with twelve ½-inch bolts.

FIGURE 9.6.—Schematic of EOS electrolytically regenerative hydrogen-oxygen fuel-cell module *(185)*.

Concurrent with the above work, basic studies carried out on another contract *(182)* led to the palladium-platinum catalyst used above. The rates of diffusion of hydrogen and oxygen across electrolyte-filled asbestos matrices were measured, but results were too variable to give a relation between pressure and diffusion coefficient, although there was a pronounced trend toward higher diffusion rates at higher pressures. Better diffusion values were obtained in later work (187). When the total pressure across the membrane was kept constant, the rate of diffusion was only weakly dependent upon the partial pressure of diffusing gas. The corresponding self-discharge rate due to hydrogen diffusion was less than 1 A/sq ft, provided the asbestos was filled with electrolyte. Diffusion was high when 50 percent of the water was removed by electrolysis. Oxygen diffusion rates were less than one-tenth those of hydrogen.

The combination of a conventional silver oxide electrode with a hydrogen chemisorption electrode was investigated (182). Palladium black was sintered onto a platinum screen, the pores filled with palladium chloride, and the chloride decomposed at 932° F (500° C). Charge of the Pd/KOH/Ag_2O silver cell showed little pressure buildup. The current efficiency on discharge was 95 percent at 40 A/sq ft and 70 percent at 140 A/sq ft. However, it was concluded that the capacity of the system would be low compared to a zinc-silver oxide battery, since complete utilization of palladium to $PdH_{0.6}$ gives only 42 A-hrs/lb of palladium,

A 75-watt unit similar to that above was built under another contract. Electrodes were 20-mil porous nickel catalyzed with (5 mg Pt+5 mg Pd)/cm^2 for hydrogen and 10 mg Pt/cm^2 for oxygen **(186)** Magnesium end plates were coated with epoxy or were nickel plated. Bipolar holders were of Teflon, and the cell case was of thin aluminum alloy. The stack contained six cells of 6-inch diameter, with a storage pressure of 400 psig at full state of charge.

To estimate the possible performance of the system, mathematical optimization was used for various orbits, assuming 95 percent current efficiency, a power conditioner (developed by EOS) of 75 percent power efficiency, and 90 percent utilization of stored gases in the cycle. To use precise weight-pressure-size equations, three equally sized spherical gas storage tanks, two for hydrogen and one for oxygen, of 195000-psi tensile strength titanium alloy were assumed (with a safety factor of 2 in the equation: wall thickness $=rP/\sigma$, r being radius, P pressure, and σ tensile strength). A power density of 5 W/lb was used for silicon solar cells. The various simultaneous linear equations relating orbit duration, current density, storage pressure and weight of tanks, number and radius of cells, etc., were solved on a digital computer for a given voltage (28 volts) and power. The fuel-cell design equation used was: volts $=1-0.00143i$, i being current density in mA/cm^2. Optimum current densities varied from 80 mA/cm^2 (74 A/sq ft) for the lowest orbit to 120 mA/cm^2 (110 A/sq ft) for the highest, with the total system weight being only a weak function of current density. (This is true for a given cell, but would not be true with a system comparing various cells with different voltage-current relations.) Typical results are shown in figure 9.7. The optimum performance of a 100-watt unit was calculated to be 11.5 W-hr/lb of fuel-cell subsystem for a 300-mile orbit and 25.3 for 22400 miles, with slightly higher values for a 500-watt unit. (As an electrolyzer, the fuel-cell subsystem gives about 150 watts of water electrolysis per 5 pounds, or 30 W/lb.) A case containing stearic acid surrounded the fuel-cell stack and was used as a means of smoothing out the cell temperature during the charge-discharge cycle. Stearic acid melts at the required operating temperature, acting as a heat sink at high heat release rates, and a heat source at lower rates.

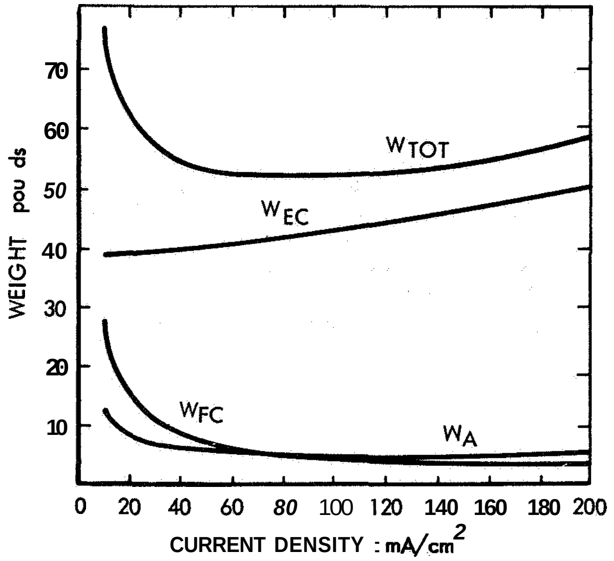

W_{FC} is the weight of the fuel cell including storage tanks; W_A, weight of auxiliaries (a thermal storage material and 2 pounds of voltage controller); W_{EC} is weight of silicon solar cells for charging the fuel cell; W_{TOT} is total weight (but note that temperature control is not included).

A 300-mile orbit has a shade interval of 0.6 hour; therefore, a 100-watt unit needs a net energy storage of 60 watt-hours. A fuel-cell subsystem weight of 5 pounds gives an energy storage density of 12 watt-hours per pound of subsystem and a power density of 20 W/lb.

FIGURE 9.7.—Optimization calculations for idealized 100-watt EOS regenerative fuel-cell system **(186)**.

9.6 CONCLUSIONS

The major short-term prospect for electrolytically regenerative fuel cells is for orbiting satellites. For this application they may give significantly reduced weight and increased life over conventional batteries. By building gas storage tanks around the cell stack, the pressure difference between the inside and outside of the stack is small and lightweight cell components can be used. Lighter electrodes of higher performance than those described can probably be used in the cell-electrolyzer unit. Improvements in conventional secondary batteries, or development of new batteries **(410** through **415,** for example) could eliminate the advantage of fuel cells for this application, although there does not appear to have been much progress in this area over the last few years.

As far as wider commercial application is concerned, it is unlikely that electrolytically regenerative H_2-O_2 fuel cells will be used as replacements for conventional secondary batteries in the near future, due to the high pressure or volume of gas storage and high present cost of fuel cells. High cost also rules out their use as peakload power capacity in large generation systems.

9.7 REFERENCES

9.1. GARNER, R. V.: Investigation of Electrical Power Sources for Missile-Borne Applications. U.S. Army Missile Command, Redstone Arsenal, RE–TR-64–29, AD459406, Dec. 1964.

9.2. FRANCIS, HOWARD T.: Space Batteries. NASA SP–5004, 1964.

9.3. THIELMAN, J. H.: Discussion and Weight Prediction of Regenerative Fuel Cell Systems. Boeing Go., Nov. 1964.

9.4. STAFFORD, G. B.; AND MAHEFKEY, E. T., JR.: Hybrid Fuel Cell-Solar Cell Space Power Subsystem Capability. Tech. Doc. Rept. APL–TDR-64–11, Air Force Aero Propulsion Lab., Air Force Systems Command.

CHAPTER 10

Thermally Regenerative Fuel Cells

10.1 INTRODUCTION

In a thermally regenerative fuel cell, reactants A and B are electrochemically combined at temperature T_1, and the product C is removed from the cell and passed through a "regenerator" at T_2, where it is thermally decomposed to A and B. A and B are separated, cooled, and passed back to the anode and cathode of the fuel cell. Liebhafsky (ref. **10.1, 1959)** showed that a simple ideal system has a maximum theoretical efficiency given by

$$\xi=\frac{\text{Electrical work}}{\text{Heat input}}=(T_2-T_1)/T_2 \quad (10.1)$$

The open-circuit cell voltage is

$$E=(\Delta H^0/nF)(T_2-T_1)/T_2 \qquad (10.2)$$

where ΔH^0 is the heat absorbed per mole of C in the dissociation $C \rightarrow A+B$. Obviously, C must decompose at a reasonable temperature, A and B must be easy to separate, and **A,** B, and C must be in physical states which can readily be moved around the system.

Lithium hydride was chosen in two early studies (dating from **1959)** because it decomposes at a reasonable temperature. The melting point of lithium is low **(367**" F **(186**" C)) and hydrogen and lithium are readily separated since the vapor pressure of lithium is low (boiling point **2437**" F **(1336**" **C)).** A molten-salt electrolyte was used, requiring low solubility of lithium metal in the salt to prevent electronic conduction. Laboratory cells using molten-salt electrolytes are mounted in furnaces to obtain the required temperature.

10.2 LITHIUM HYDRIDE SYSTEMS

10.2.1 Mine Safety Appliance Research Corp., Study of Energy Conversion Devices, July 1959 to May 1961

The objective of the contract *(470)* was to develop a LiH system which would operate at **100** A/sq ft and more than **0.3** volt per cell, with an output of 10 W/lb. Previous work at Mine Safety Appliance Research Corporation on company funds had shown that the cell

$$Li(l)/\text{molten LiCl-LiF}/H_2(g)$$

would produce a reasonable output with electrodes of stainless steel or nickel in the form of mesh or microporous filter sinters. Calcium and sodium had also been used. The cell reactions are

$$\begin{array}{c} 2Li \rightarrow 2Li^+ + e^- \\ \underline{H_2 + 2e^- \rightarrow 2H^-} \\ 2Li + H_2 \rightarrow 2LiH \end{array}$$

The product lithium hydride is dissolved in the melt, which is recycled between cell and regenerator. Decomposition of lithium hydride in the regenerator produces gaseous hydrogen and a layer of molten lithium floating on top of the melt.

The salts used as electrolytes had to be vacuum dried to prevent hydrolysis to insoluble oxides *(474).* A number of cell/regenerator configurations were built (see figs. **10.1** and 10.2 for examples). Considerable difficulties were experienced with pumping and flow of molten electrolyte, and with plugging of lines. Lithium hydride with the eutectic **20** LiF: **80** LiCl mole-percent (melting point **896**" F **(480**" C)) in a cell/regenerator system operating at **1022°/1634°** F **(550°/890° C)** gave poor results (OCV only 5 mV). There was some doubt as to whether the hydride was decomposing to give sufficient hydrogen (see fig. 10.3); therefore, an external supply of hydrogen was attached. Potassium and hydrogen supplied externally gave better than 0.7 OCV initially, with a melt of Cs-Rb-Li-Na chlorides. The potassium hydride which was produced dissolved in the molten electrolyte and the voltage dropped to 0.25 OCV. A closed cycle was attempted, with argon pumped up through the molten salt-LiH-Li in the regenerator to blow hydrogen out (see fig. 10.1), but the system did not operate satisfactorily. Materials and leakage problems were present; and satisfactory seals and electrical insulation were obtained only by using the flange shown in figure 10.2, which formed the seal with solidified electrolyte. Porous nickel, platinum, palladium, and carbon electrodes and Pd-Ag diffusion membranes corroded rapidly. A number of other results were obtained (summarized in table 10.1) in the search for lower melting electrolytes and suitable cell systems. Current densities were less than 60 A/sq ft in all cases.

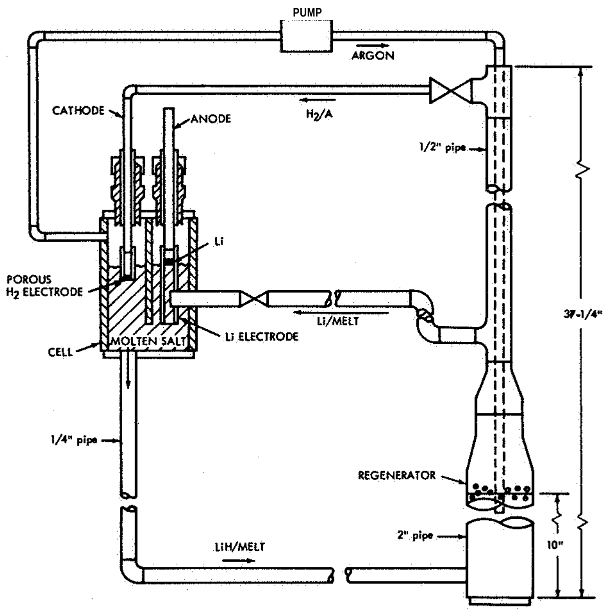
PUMP
ARGON
CATHODE
ANODE
H_2/A
1/2" pipe
Li
POROUS
H_2 ELECTRODE
Li/MELT
37-1/4"
MOLTEN SALT
Li ELECTRODE
CELL
1/4" pipe
REGENERATOR
2" pipe
10"
LiH/MELT

This cell had a porous-metal hydrogen electrode which dipped into the molten-salt electrolyte. A porous-metal disk was also used in the lithium electrode, but in other types the molten lithium floats on top of the electrolyte, in the tube shown. In theory, the molten salt containing lithium hydride is decomposed to give lithium; the melt and lithium are returned to the cell as shown and the lithium floats up to renew the anode fuel. Hydrogen from the decomposition is circulated by pumping argon as shown.

FIGURE **10.1.—Lithium hydride regenerative fuel cell.**

Because of low outputs from cells without an external supply of hydrogen, tests were performed in a bomb to determine the equilibrium pressure of hydrogen over lithium hydride dissolved in LiCl-LiF melts (table 10.2). Since reasonable operation can only be expected with a hydrogen pressure near 1 atmosphere, the regenerator temperatures were obviously too low. Slow mass transfer of dissolved lithium hydride away from the anode was suggested as the principal cause of polarization, as well as flooding of the porous hydrogen electrode.

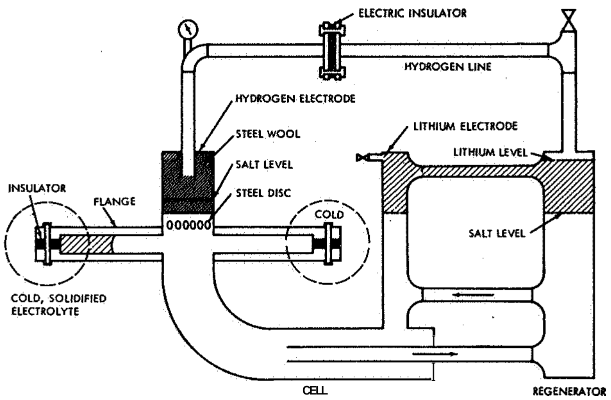
ELECTRIC INSULATOR
HYDROGEN LINE
HYDROGEN ELECTRODE
STEEL WOOL
SALT LEVEL
STEEL DISC
LITHIUM ELECTRODE
LITHIUM LEVEL
INSULATOR
FLANGE
COLD
SALT LEVEL
COLD, SOLIDIFIED
ELECTROLYTE
CELL
REGENERATOR

FIGURE 10.2.—Lithium **hydride regenerative fuel cell with cold-salt seal flange.**

The above work was an unsuccessful attempt to operate a regeneration system. The original company-sponsored work had been done with externally supplied liquid metal and hydrogen reactants, and with an electrolyte which had not been stabilized with the product of the reaction. This system may have given promisingly high voltages, but the work reported below shows that these values were probably spurious, arising from utilization of impurities in the system.

10.2.2 TAPCO, Division of Thompson-Ramo-Wooldridge, Inc., Regenerative Fuel-Cell System Investigation, July 1959 to June 1961

The objective was to develop a thermally regenerative lithium hydride fuel cell, suitable

TABLE 10.1.—*Lithium Hydride Regenerative Fuel-Cell Results From (474)*

Electrolyte	Eutectic melting point,[a] "F	Comments
LiClFI	743 to 806 (395" to 430° C)	Melting point high
KBrFI	1050 (566" C)	Melting point high
LiNaRuCsCl	543 to 550 (284" to 288° C)	Best; wt-% analysis of eutectic 28•5 LiCl, 3•1 NaCl, 30.5 RbCl, 38•9 CsCl
LiKBH$_4$		Low-power densities
LiKCl	675 (357° C)	
LiKIBr	626 to 662 (330° to 350° C)	When used in Li/H$_2$ cell, indicated I$_2$ release

[a] By differential thermal analysis.

Melt	Weight-percent LiH	Temperature, "F	Partial pressure of hydrogen, torr
LiCl-LiF eutectic	0.35	1472 (800" C)	LOW
		1652 (900° C)	20
		1832 (1000" C)	50
		2012 (1100" C)	200
	4.2	1652 (900° C)	60
		1796 (980" C)	150
		1868 (1020" C)	300

for use under zero-gravity conditions with a nuclear heat source (*590*). (Again, it is questionable whether the state of the art in 1959 warranted such a precisely defined objective.) Figure 10.3 shows that the pressure of hydrogen over Li-LiH is not high at feasible regenerator temperatures; therefore, it was proposed to use a pump to raise the pressure of hydrogen from the regenerator to the cell. The work was performed in a dry box under an argon atmosphere (using titanium sponge as a getter for O_2, N_2, and H_2O) with vacuum drying of molten LiCl-LiF eutectic. The lithium anode was similar to that shown in figure 10.1, and the hydrogen electrode consisted of an iron (2 mil) or niobium (5 mil) diffusion membrane, Heliarc welded to the hydrogen inlet tube. Stainless steel 316 was used in the construction of the cell. Without lithium and hydrogen present, small voltages were obtained, with lithium alone, a large voltage (≈ 2 volts) was obtained, which decayed to almost zero over about an hour. Lithium was observed to dissolve in the melt, and hydrogen bubbled into the melt reacted chemically with dissolved lithium. Twenty mole-percent lithium hydride was added to the melt; the cell Li/LiH-LiClF melt/H_2 gave a steady OCV of about 0.5 volt. With large amounts of dissolved lithium hydride, the lithium anode extracted lithium hydride from the melt, while for smaller amounts lithium dissolved in the melt; about 11 percent lithium hydride appeared to be optimum.

A LiCl-LiF eutectic containing 5 or 10 mole-percent of dissolved LiH was heated in an iron (Armco) regenerator at 1630" F (880° C) and gave an initial equilibrium pressure of hydrogen of about *200* torr. However, as LiH decomposed, the equilibrium pressure fell rapidly to about 80 torr and then moved slowly to low values. Figure 10.3 shows that the plateau pressure of hydrogen over pure lithium-lithium hydride at 1600" F (871° C) should be much greater than 80 torr. Obviously, when the lithium hydride dissolves in the melt, the equilibrium dissociation pressures are lowered considerably. Equilibrium pressures over 10LiH :90 LiCl mole-percent were generally about one-third to one-tenth those of lithium hydride, depending on temperature and degree of decomposition. Between 1560" and 1750" F (849" and 954° C), LiH was soluble in the melt in all proportions, but as it decomposed a separate lithium phase was seen.

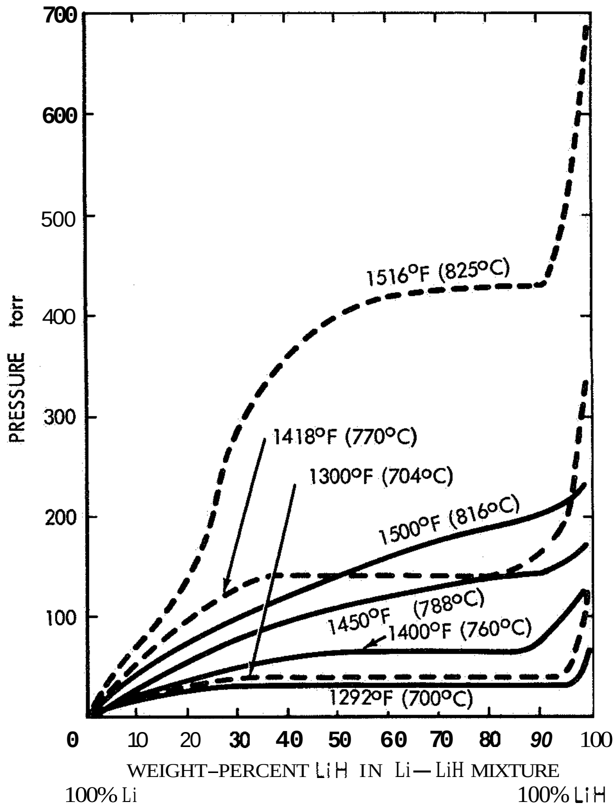

- _ - data cited in reference 10.2
—— data from *590*

The explanation for the shape of this curve can be found in Hansen (ref. 10.3).

FIGURE 10.3.—Equilibrium pressures of hydrogen over lithium-lithium hydride melts.

(The equilibrium being studied is $\mathrm{H_2+2Li \rightleftharpoons 2LiH}$. When distinct phases of Li and LiH are present, they have unit activities. Decrease in equilibrium hydrogen pressures could be caused by a change in the standard-state free energy of the reaction when it is carried out in molten salt due to compound formation of LiH with the melt. Decreased pressures could also be due to lowered activity of lithium hydride. This occurs when the hydride is dissolved at low concentrations, since its activity cannot then correspond to that of a separate phase of LiH. The lithium hydride was soluble and the decrease in pressure was roughly that expected from the lowered concentration, indicating no compound formation.) Qualitatively, the rates of decomposition were slow. Also, the appreciable vapor pressure (12 torr) of lithium at 1630° F (880° *C)* led to recombination of evolved hydrogen and lithium as the gases were pumped off and cooled, forming liquid lithium hydride in the hydrogen exit line.

Later studies *(591)* were performed with the batch cell shown in figure 10.4. Use of high-purity iron instead of stainless steel to contain the melt eliminated some of the spurious high initial voltage, and steady OCV was 0.38 to 0.58. A 4-mil iron membrane, used as a nonporous hydrogen diffusion electrode, gave a diffusion-limited (see ch. 2) current of 21 A/sq ft at 1000° F (538° C) and 1 atmosphere of hydrogen. As expected, lower pressures of hydrogen in the cathode chamber gave lower currents. Arsenic added to the chamber also decreased performance, presumably by adsorptive poisoning of the membrane. A survey of permeabilities (see app.

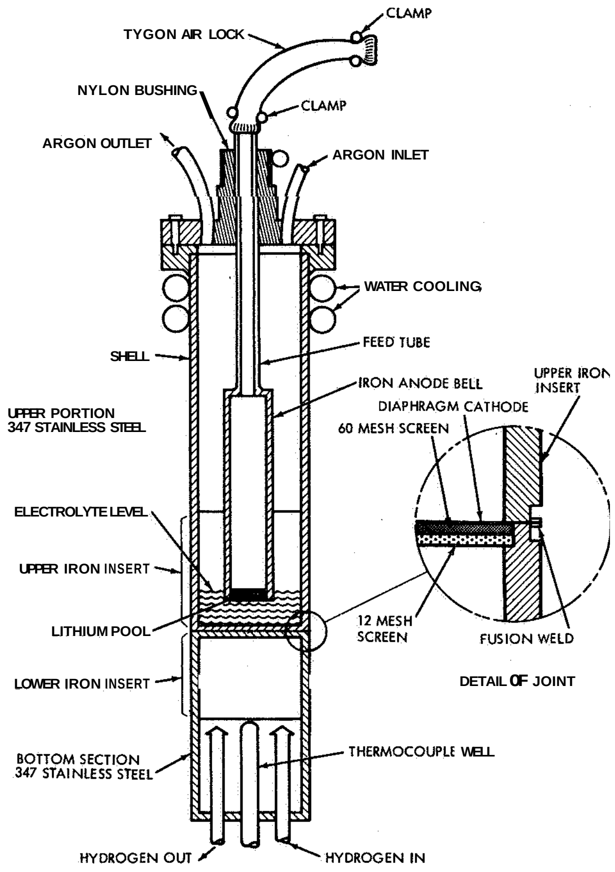
CLAMP
TYGON AIR LOCK
NYLON BUSHING
CLAMP
ARGON OUTLET
ARGON INLET
WATER COOLING
FEED TUBE
SHELL
IRON ANODE BELL
UPPER IRON INSERT
UPPER PORTION 347 STAINLESS STEEL
DIAPHRAGM CATHODE
60 MESH SCREEN
ELECTROLYTE LEVEL
UPPER IRON INSERT
LITHIUM POOL
12 MESH SCREEN
FUSION WELD
DETAIL OF JOINT
LOWER IRON INSERT
BOTTOM SECTION 347 STAINLESS STEEL
THERMOCOUPLE WELL
HYDROGEN OUT
HYDROGEN IN

A supported diaphragm of iron or niobium was welded between two iron inserts, which were then welded to the rest of the cell. This diaphragm formed a hydrogen solid-diffusion electrode. The anode was lithium floating on the molten electrolyte. This type of cell is very convenient for mounting in a vertical furnace.

FIGURE 10.4.—Batch lithium-hydrogen cell.

B) combined with corrosion measurements indicated that niobium and tantalum might give much higher limiting currents. However, they both developed stable oxide films under cell conditions.

It was also found that lithium wetted steel wool strongly and was retained, while lithium chloride ran out. Therefore, a cell was built as illustrated in figure 10.5. This cell was never tested because of lack of a suitable pump for the melt; electromagnetic pumps were unsatisfactory due to the high resistance of the melt, a bellows pump did not work, and a Belleville spring pump leaked badly due to corrosion and mechanical failure of the parts.

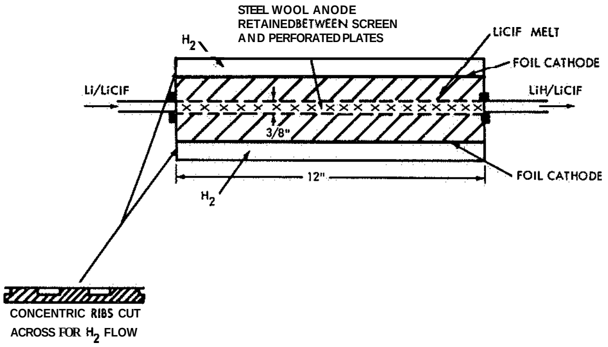
STEEL WOOL ANODE RETAINED BETWEEN SCREEN AND PERFORATED PLATES
H_2
LiClF MELT
FOIL CATHODE
Li/LiClF
LiH/LiClF
3/8"
12"
FOIL CATHODE
H_2
CONCENTRIC RIBS CUT ACROSS FOR H_2 FLOW

The cell was disk shaped. The central anode of steel wool acted as a capillary matrix to retain molten lithium, while the lithium chloride/fluoride eutectic would not penetrate this matrix. The foil cathodes (solid-state diffusion electrodes) were supported on the top and bottom disks, which had concentric grooves cut in them to give supporting ribs. These ribs were cut across to feed hydrogen to the grooves. The lithium-entry tube was the anode connection; cold-salt seals and electrical insulation separated the anode from the case, which was cathodic.

FIGURE 10.5.—A **more practical design for a lithium hydride regenerative fuel cell** *(591)*.

A second contract *(593)* to study the niobium-foil cathode showed that niobium turnings added to the LiClF melt gettered oxygen very effectively, preventing the formation of scum on the melt observed previously (niobium was not soluble in the salt). In addition, ultra-high-purity tank hydrogen was further purified from oxygen by passing it over coarse titanium sponge at 1550"F *(843"* C). An experimental cell similar to that shown in figure 10.4 was constructed from niobium and niobium alloys, which allowed niobium turnings to be kept in the melt. With these precautions to remove oxygen, no spurious initial voltage was found, a steady OCV of 0.45 was obtained in a few minutes, and limiting-current densities using a 5-mil niobium-foil cathode and a porous-niobium anode filled with lithium were as high as 1600 A/sq ft.

10.2.3 Argonne National Laboratories, Thermally Regenerative Fuel Cells, 1961 to 1963

The work done at Argonne was at a more basic level than that discussed above, and no attempt was made to build complete cell/regenerator systems. The techniques were similar, and a dry box was used with circulation of purified helium to reduce oxygen and water contamination to low levels. The iron cell, somewhat similar in design to that shown in figure 10.1, had an iron-foil diffusion cathode, and the electrolyte was the eutectic 41 KCl:59 LiCl mole-percent (melting point 675" F (357° C)). Spurious initial currents and voltages were found, and iron foils would not support much current. A lithium reference electrode showed that polarization at the lithium working electrode was fairly small.

Considerable effort, expended in measuring diffusion rates of hydrogen through iron, confirmed the fact that the rate was too low to be useful. Platinum and palladium-silver foils corroded rapidly, and a vacuum-deposited 1-mil coat of iron on palladium-silver did not prevent corrosion, since the iron was porous. When a source of alpha-particle radiation was used to ionize hydrogen, diffusion through iron increased somewhat but not enough to be useful. Diffusion through vanadium, tantalum, and niobium was good when they were clean, but oxide films formed and could not be reduced by hydrogen; therefore, the rate fell with time *(110)*. Molybdenum-iron-alloy diaphragms (prepared by Battelle) had good hydrogen solubility, but permeation rates were near those for pure iron.

A phase diagram of the system LiH/LiCl showed a eutectic (melting point 924.1" F (495.6" C)) at about 35 mole-percent of LiH. On the basis of 1 molal lithium hydride as standard state, activity coefficients of LiH and LiCl were determined from the phase diagram and found to be close to 1. Thus the system is close to ideal and there is no compound formation. This is in agreement with the concept that the lower equilibrium pressures of hydrogen found when lithium hydride is dissolved in a melt are due to lower concentrations of lithium hydride.

Later reports ***(114)*** state that vanadium was found to be suitable as a hydrogen solid-state diffusion electrode, with a permeation rate of 200 to 400 A/sq ft at 932" F (500" C) for a 10-mil membrane. OCV for the Li/melt/(V)H_2 cell followed the Nernst equation; that is, a plot of ln ($\sqrt{p_{H_2}}$) as a function of OCV was a straight line with a slope corresponding to $n=1$.

10.3 OTHER MOLTEN METAL/SALT/GAS CELLS

10.3.1 Lockheed Aircraft Corp., Solar Regenerative Chemical Systems, September 1959 ***to*** September 1962

The object of this contract was to produce systems capable of utilizing solar energy. Three simple regenerative systems, Sn/SnI_2 melt/I_2, Pb/PbI_2 melt/I_2, and Cd/CdI_2 melt/I_2, were investigated (*403*). Experimental techniques were similar to those discussed above. Because stainless steel was corroded by iodine, a porcelain beaker was used as the cell container. Molten salt floated on the molten metal anode. A %-inch-thick porous carbon cathode (National Carbon C–40) was the iodine vapor electrode. An iodine pressure of 20 inches Hg above atmospheric was needed to avoid limiting currents and to get a stable OCV. The results are summarized in table 10.3. A larger cell was built but was abandoned because of seal problems.

SnI_2 was added to molten tin at 1814" F (990" C). No iodine vapor was observed. Similarly, no iodine was seen when CdI_2 was passed over a hot wire filament, passed through a hot tube, or heated under vacuum in a hot tube and rapidly quenched. Thermodynamic data for the materials showed that decomposition of SnI_2 and PbI_2 at their boiling points is small. Also, the reaction

$$SnI_2(g) \rightleftharpoons Sn(l) + I_2(g)$$

has a small temperature coefficient; therefore, significant decomposition could not be expected at reasonable regenerator temperatures. Similarly, the partial pressures (estimated from thermodynamic data) of I (10 torr) and I_2 (2 torr) at 1701" F (1200" K) and a total pressure of 600 torr showed that the amounts of decomposed iodine in the CdI_2 vapor would be small. It was also claimed, via a fallacious kinetic argument, that a sufficiently rapid rate of $A+B \rightarrow C$ in the cell meant that $A+B \rightarrow C$ in the regenerator would be too fast to separate the components. (The correct argument (ref. 10.4) is that the thermodynamic equilibrium constants at the cell and regenerator temperatures must be such as to give a reasonable potential for the cell and a reasonable degree of decomposition in the regenerator. In addition, the regenerator temperature must be low enough for iodine to be gaseous and metal iodide to be liquid, since

TABLE 10.3.—*Summary* of Regenerative Cell Performances ***From (403)***

System	Cell temperature, °F	Theory	Actual	A/sq ft	Volts	Remarks
Sn/I_2	Not given	0.8	0.4	......	......	Electrolyte solidified
Pb/I_2	842 (450° C)	....	.63	50	0.3	IR polarization only
Cd/I_2	698 (370" C)	....	.87	50	.35	IR polarization only
	878 (470° C)	....	.83	50	.65	
Hg/$HgBr_2$-KBr/Br_2 electrolyte 50 : 50 mole-%	500 (260° C)	.61	....	....	....	$Hg+HgBr_2 \rightarrow Hg_2Br_2 \downarrow \therefore$ would not melt at 572" F (300° C). Higher temperatures gave sublimation of Hg_2Br_2

iodine can then be readily removed from the other phases, allowing decomposition to proceed.) The thermodynamic proof that iodides are unlikely to be thermally decomposed came after considerable experimental work attempting to decompose them.

10.3.2 Electro-Optical Systems, Inc., Investigation of New Solar Regenerative Fuel-Cell Systems, November 1959 to November 1960 and March 1961 to March 1962

In a general analysis (*191*), the efficiency of a simple regenerative system was given as

$$\xi=\frac{T_2-T_1}{T_2}=\Delta F/\Delta H \qquad \textbf{(10.3)}$$

where ΔF and AH are at cell temperature T_1, and AH is assumed constant between T_1 and T_2. Thus if $\Delta F/\Delta H$ is too low, the efficiency is low; if it is too high (close to 1), the ratio T_2/T_1 is high, meaning that regenerator temperatures will be too high to be feasible. Table B.15 gives some systems which were considered feasible. Exception can be taken to these values since they do not allow for phase change before T_2 is reached. For example, the CdI_2 system has melting points of Cd 610" F (594" K) and CdI_2 729" F (660" K), which are reasonable, and a $\Delta F^0/\Delta H^0$ at 801" F (700" K) of 0.63. Thus, the regenerator temperature at which I_2 vapor is at 1 atmosphere is, from equation (10.3)

$$T_2=\mathbf{700}\text{" K}/(1\text{–}0.63)=1890\text{" K (2943" F)}.$$

However, at this temperature CdI_2 would be vaporized, the assumption of constant AH is no longer applicable, and the new AH is much lower, so that it is unlikely that the CdI_2 system would be feasible.

An attempt was also made **(*191*)** to calculate the theoretical rate of decomposition in the regenerator, but the units were mixed up, giving erroneous conclusions. Later work **(*174*)** corrected the error and derived the rate as

$$\text{A/cm}^3=(2\cdot 1)n10^{15}CTe^{-E^{\ddagger}/RT} \qquad \textbf{(10.4)}$$

where C is the concentration of AB in g-moles/cm³ and $E^{\ddagger}$ is the activation energy for decomposition. (This assumes, however, that molten **AB** decomposes at a rate corresponding to that of gaseous **AB,** without any mass transfer restriction, which is doubtful.) Assuming that $E^{\ddagger}$ is the bond energy of the weakest bond in AB, a value of 80 kcal/g-mole gives a rate at 1341" F (1000" K) of the order of 1 A/cm³, or roughly 100 W/lb of decomposing AB. It was concluded that thermodynamic feasibility is a more restrictive factor than kinetic feasibility (although work above (sec. 10.2.2) indicated slow decomposition rates).

10.4 REGENERATIVE AMALGAM-METAL CELLS

10.4.1 Allison Division of General Motors, Design and Development of a Liquid Metal Cell, January 1962 to April 1964

The original scope of this contract was to produce a spacepower system of 310 watts at 3.5 volts. However, this was modified to a demonstration of electrochemical and regenerative feasibility (*68*). The cell investigated was

$$\text{KHg}(l)/\text{KOH-KBr-KI melt}/\text{KHg}(l).$$

The potential difference is obtained by having high concentrations of potassium in the amalgam at the anode (actually pure potassium was used) and low concentrations at the cathode. Figure 10.6 shows how the OCV varies for different concentrations of potassium in amalgam (ref. 10.5). Clearly, compound formation occurs between potassium and mercury. Regeneration is accomplished by heating the cathode fluid to decompose it into (1) a potassium-enriched amalgam which is returned to the anode, and (2) mercury vapor which is condensed and returned to the cathode. The phase diagram showed KHg to be liquid for all compositions above 513" F (540" K).

Of a number of cell materials investigated (see app. D), 410 stainless steel was chosen; the electrolyte was retained within a porous MgO disk (LM–833, Morganite, Inc.) of 40 to 45 percent porosity and 20-μ pore size. The 70 KOH : 15 KBr : 15 KI mole-percent eutectic (dry melting point 410" F (210" C)) had to be dried under vacuum and gave a resistance of 1.35 ohm-cm at 572" F (300" C) (see app. C for methods). A disk cell was built, and then a number of other configurations were tried, but considerable difficulty was experienced with matrix breakage

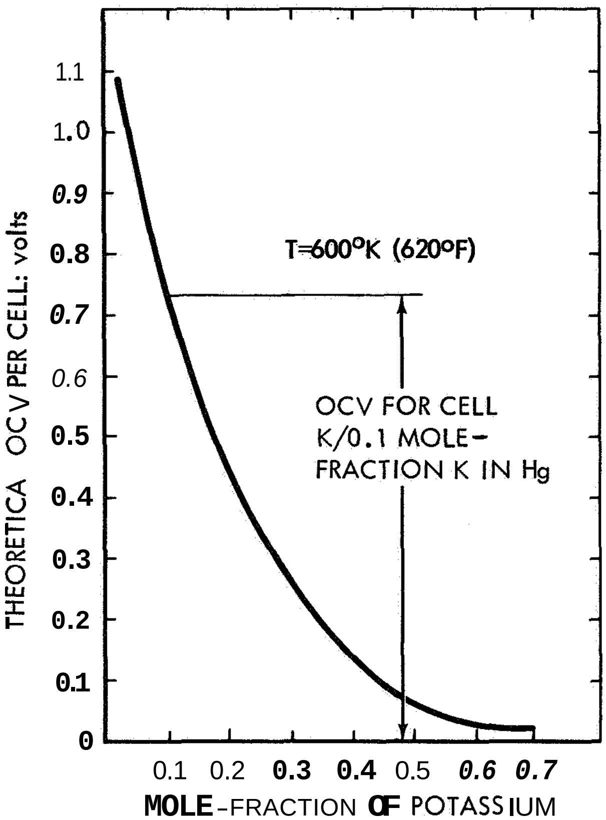

(The OCV of a cell employing amalgams with different potassium contents at the anode and cathode can obviously be found from this figure.) Experimental values obtained by the Allison group confirmed these calculated values.

FIGURE 10.6.—Calculated open-circuit voltage for the cell potassium versus potassium amalgam as a function of the mole fraction of potassium present in the amalgam.

and seal leakage. A simple cell was built which employed molten potassium floating on molten electrolyte floating on mercury, held within a ceramic crucible. Leads were taken into the mercury and potassium by wires passing through ceramic tubes which had their ends dipping into the potassium or mercury layers. A flowing system of this type was also made by suitable inlets and outlets, using a stainless-steel body.

Initial OCV values of 0.9 to 1.0 volt were observed and current was a direct function of voltage on short-time discharge, indicating that only IR polarization was present; 100 A/sq ft at 0.5 volt was obtained. During longer times of operation, potassium was transferred to the mercury and, since the cell was batch operated, the OCV fell accordingly. Also, about 5 mole-percent potassium dissolved in the electrolyte, giving rise to self-discharge and coulombic inefficiency. The principal problems were thought to be matrix strength and resistivity, and seals to withstand the pressures of mercury. Any crack in the matrix allowed mercury to connect the anode and cathode compartments, leading to an internal short.

The labyrinth factors of the LM–833 ceramic matrices were between 4.2 and 11.8. Another material, LA–831, was more uniform in characteristics and gave a value of 4.24. A threefold increase in conductivity was found upon raising the temperature from 482° to 662" F (250" to 350" C). Paste electrolytes gave a resistance of 7.25 ohm-cm. Thus, the electrolyte resistance of 1.35 ohm-cm at 572° F (300° C) gave effective resistances of 5 to 15 ohm-cm for the matrix-electrolyte combinations; and since the matrix thickness was about 0.195 inch (5 mm), the effective resistance was a minimum of 2.5 ohm-cm^2. Clearly, this resistance was too high to give high-current density. A separate contract had the objective of reducing the resistance to 0.5 ohm-cm^2. Methods of preparation are discussed in chapter 3; a paste electrolyte was developed with a labyrinth factor of 2, which gave a specific resistance of 2.7 ohm-cm (81). The minimum thickness for suitable strength was one-eighth inch; therefore, the resistance was 0.86 ohm-cm^2. A test of this matrix in a disk-cell configuration gave an apparent value of 1 ohm-cm^2, calculated from the slope of i versus V near-open circuit.

Further work was performed under another contract with the long-range goal of producing a system suitable for space applications, with specifications of 5 kilowatts at 28 volts, to last 1 year (85). Leakage under the heads of mercury in the system was overcome by having (a) very smooth surface-to-surface contact (requiring expensive and troublesome finishing operations) or, preferably, (b) ribbed contacts. Based on the seal-contact area, pressures greater than 14220 psi (1000 kg/cm^2) were required to squeeze the points of the ribbing tightly against another surface. The concentric ribs can be seen in a picture of the cell (fig. 10.7). Kovar alloy was used for the metal parts of the cell. Cells were tested horizontally, and pressure was applied from a

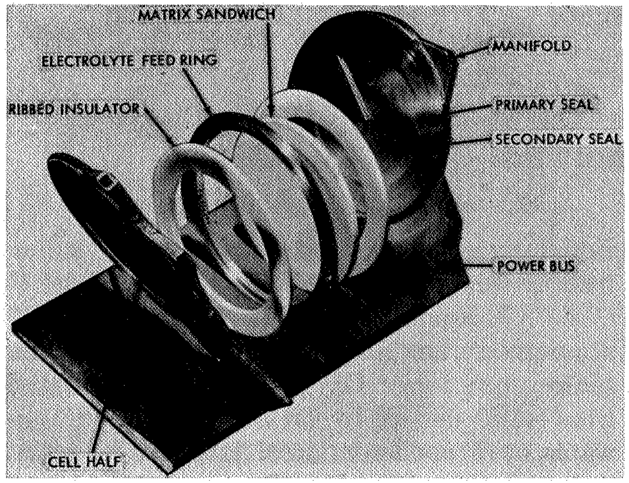

FIGURE 10.7.—Exploded view of regenerative potassium-amalgam cell.

hydraulic press through a large steel ball between platen and cell. Figure 10.7 also shows that a matrix "sandwich" was used to contain the electrolyte. Porous ceramic disks were hollowed out from one face, and a sandwich contained free electrolyte in the central hollow, as shown in the insert of the figure. Once again, the main problem was rupture of these diaphragms. The ceramic LM–833 weakened in use (crushing strength decreased from 17064 to 9954 psi (1200 to 700 kg/cm^2) after 400 hours' immersion), but LM–833A appeared to be better from limited tests.

A three-cell unit was built and performed at about 50 W/sq ft initially, with performance decreasing with time (70 hours' running time). Troubles were experienced with hot-mercury circulation and with the potassium-level control. When the potassium anode compartment was starved of feed, the pressure of mercury in the cathode forced electrolyte out of the matrix or cracked the matrix, leading to internal shorts. The system was not run in a fully regenerative manner, since liquid potassium was fed from a tank. The potassium-enriched mercury from a mercury boiler was stored (rather than being returned to the cell), and the mercury vapor from the boiler, which was condensed and fed to the cathode, had to be replenished from time to time. The mercury condenser was operated to 0.04 torr (equivalent to a mercury temperature of 446" F (230" C)).

The anode feed into the cell was potassium and the cathode feed was mercury; therefore, true regeneration of these reactants would require complete separation of potassium from amalgam. Since the cell gave a considerable voltage at 572" F (300" C), an exothermic reaction occurred between potassium and mercury, which would have to be reversed at a higher regenerator temperature. Thus, when product amalgam is distilled to high concentrations of potassium, the partial pressure of mercury over the remaining amalgam would fall, requiring higher and higher temperatures for further distillation. The condensing system used, however, did not correspond to such a cycle. The potassium amalgam received heat at the temperature of the mercury boiler, and heat was discarded in the mercury condenser. Cold mercury was then heated as it entered the cell. The complete thermodynamic cycle including the cell is thus complex, and there are inefficiencies in the mercury regenerative section, as follows.

Heat taken in at the mercury boiler supplies the heat of decomposition of the KHg compound and latent heat of vaporization of mercury. The mercury was condensed at 446" F (230" C), so the latent heat of vaporization and specific heat content of the mercury were rejected. Additional heat was then supplied to bring liquid mercury up to cell temperature; clearly the latent and specific heats were wasted. The cycle was operated over a small temperature differential, with irreversible rejection of the latent heat of mercury; therefore, it was a very inefficient cycle in terms of heat utilization.

10.5 OTHER THERMALLY REGENERATIVE SYSTEMS

10.5.1 Electro-Optical Systems, Inc., Solar Regenerative Fuel-Cell Systems, November 1959 to March 1962

Among other regenerative systems considered (see secs. 10.3.2 and 11.4) was the possibility that hydrogen molecules could be dissociated at high temperatures, and hydrogen atoms used as fuel at a low-temperature electrode. Since the standard reduction potential for hydrogen atoms is considerably greater than that for hydrogen molecules, a cell could be set up in which hydrogen atoms were used at the anode and hydrogen molecules evolved at the cathode. It was claimed that electrochemical ionization of hydrogen atoms would occur in preference to atom recombination, but no valid reason was given to expect that a significant fraction of hydrogen atoms would remain in the cold gas fed to an electrode.

Another thermally regenerative material considered was iodine monobromide, with a melting point of 107.6" F (42" C) and a boiling point of 240.8" F (116" C). The conductivity is low, but it can be increased by dissolving potassium bromide in the melt. The dissociation at room temperature and 572" F (300" C) was quoted as 8 percent and 20 percent, respectively. No work was done on this material.

10.5.2 **Aerospace Corp., Energy Conversion Research Program, January** 1961 **to January** 1962

The following reaction was proposed (9) as a regenerative cycle

$$PCl_5 \rightarrow PCl_3 + Cl_2$$

$$PCl_3/\text{electrolyte}/Cl_2$$

with an E_0 value of 0.28 volt at 59" F (15° C). Organic solvents of high dielectric constant were used for the electrolytes, with dissolved PCl_5 giving conductivity, presumably via PCl_4^+, PCl_6^-. Nitromethane (which deteriorated with time), methylthiocyanate, dimethyl sulfoxide (which produced a violent reaction), acetonitrile, and dimethylformamide (DMF) supported with $LiNO_3$ were tried. A cell was built, but no significant results were reported.

Phosphorus pentachloride in methyl thiocyanate was passed through a heated reflux column; no chlorine was found, since it reacted with the solvent at reflux temperatures to form a colored solid product *(17)*. The reduction of various chlorides ($SbCl_5$, $SbCl_3$, PCl_5, PCl_3, $POCl_3$, $SiCl_4$, $SeCl_4$, $SnCl_4$, and WCl_6) was carried out at a platinum electrode in dimethylformamide supported by $1.5M$ $LiNO_3$, using a gold counter-electrode. It was claimed that values of i_0 were determined, with WCl_6 being reduced (possibly to $WCl_5 + Cl^-$) by a 1-electron reversible reduction ($D = 0.3 \times 10^{-5}$ cm²/sec). The significance of the results with respect to a regenerative fuel cell was not made clear ***(16)***.

10.5.3 **Garrett Corp., SO,-SO, Regenerative Fuel-Cell Research, March** 1961 **to April** 1962

This was a feasibility study of the system

$$SO_3(g) \rightarrow SO_2(g) + \tfrac{1}{2}O_2(g)$$

$$SO_2/\text{electrolyte}/O_2 \qquad E_0 = \mathbf{0.36} \text{ volt.}$$

Equilibrium constants show ***(222)*** that sulfur trioxide would be largely decomposed at 1940" F (1060" C); equilibrium mole-fractions at 0 to 100 atmospheres are given in the report for a wide temperature range. Oxygen was to be separated from sulfur dioxide by *(a)* absorption of SO_2 in water, or ***(b)*** condensation of liquid SO_3 to act as a scrubber for SO_2. However, method *(a)* was not feasible due to the high water-vapor pressures at temperatures at which sulfur dioxide could be distilled from water. Two electrolytes were tested, the $LiHSO_4$-$KHSO_4$ eutectic (melting point approximately 300" F (149" C)) and dimethyl sulfate saturated with $LiHSO_4$-$KHSO_4$. The expected reactions were

$$SO_2 + 2SO_4^{=} + H_2O \rightarrow 2HSO_4^- + SO_3 + 2e^-$$

$$\tfrac{1}{2}O_2 + 2HSO_4^- + 2e^- \rightarrow H_2O + 2SO_4^{=}.$$

Platinized mesh electrodes were supported on a glass frit, with oxygen and sulfur dioxide supplied through'the frit. An OCV of about 0.1 volt at 350" F (177" C) was found for the melt, and 0.17 at 200" F (93.3" C) for the dimethyl sulfate. Currents were low and the project was abandoned.

10.6 CONCLUSIONS

The thermally regenerative fuel cell has considerable theoretical appeal as a means for converting heat directly into electricity. It must compete, however, with more conventional power cycles, and since it is limited by a Carnot type of efficiency (with a reasonable maximum of about 50 percent), it would have to demonstrate compactness and reliability to be useful. The theoretical open-circuit voltages available from completely regenerative cycles are rather low; therefore, ohmic resistance and mass-transfer polarization must be low to get suitable power densities and efficiencies. The work discussed above demonstrated that laboratory electrochemical cells of suitable current density can be built. However, the cells had small electrode areas per unit cell volume, and a practical design would require compact electrode stacking to get high-power densities. In addition, in no case was the feasibility of complete thermal regeneration shown. No system was developed which came close enough to a practical scale to enable a satisfactory estimate to be made of watts per pounds or overall cycle efficiencies.

The lithium hydride or molten metal/salt/gas type of cell, with gravity feed and differential density separation of reactants, products, and electrolyte, does not appear to be suited to redesign as a compact, reliable system. Pumps and porous matrices introduce considerable materials problems due to the corrosive nature of the melts and the high temperatures necessary for good cycle efficiency. Laboratory cells can be sealed reasonably easily by having the top of the cell water cooled (see fig. 10.4), but this technique could not be used for practical cells which have to remain leakproof at cell temperature. The potassium-amalgam cell has the advantages that molten salt need not be recirculated and a compact cell can be employed, with the electrolyte retained in a matrix. The matrix introduces a penalty of ohmic resistance, which might be severe for a completely regenerative cycle, with a lower voltage than that obtained with pure potassium as fuel. In addition, high-temperature distillation of potassium-mercury mixtures would require an exceptionally reliable system in the confined spaces of manned vehicles.

10.7 REFERENCES

10.1. LIEBHAFSKY, H. A.: A Fuel Cell and the Carnot Cycle. J. Electrochem. Soc., vol. 106, 1959, pp. 1068–1071.

10.2. GIBB, T. R. P., JR.; AND MESSER, C. E.: A Survey Report on Lithium Hydride. AEC Rept. no. NYO–3957, May 1954, and NYO–8022, Aug. 1957.

10.3. HANSEN, M.: Constitution of Binary Alloys. McGraw-Hill Book Co., Inc., 1958.

10.4. AUSTIN, L. G.: Electrochemical Theory of Fuel Cells. Handbook of Fuel Cell Technology, C. Berger, ed., Prentice-Hall (in press).

10.5. KUIBASCHEWSKI, O.; AND EVANS, E. L.: Metallurgical Thermo-Chemistry. Pergamon Press, 1958.

CHAPTER 11

Thermogalvanic Cells

11.1 INTRODUCTION

Several of the contracts discussed in chapter 10 involved work on thermogalvanic as well as thermally regenerative cells. Certain cells are mixtures of the two types, and the name "thermally regenerative'' has sometimes been used to include thermogalvanic cells, since the two types are similar in many respects. By definition, a thermogalvanic cell is one in which two or more electrodes are at different temperatures. There are several mechanisms by which such cells generate voltage.

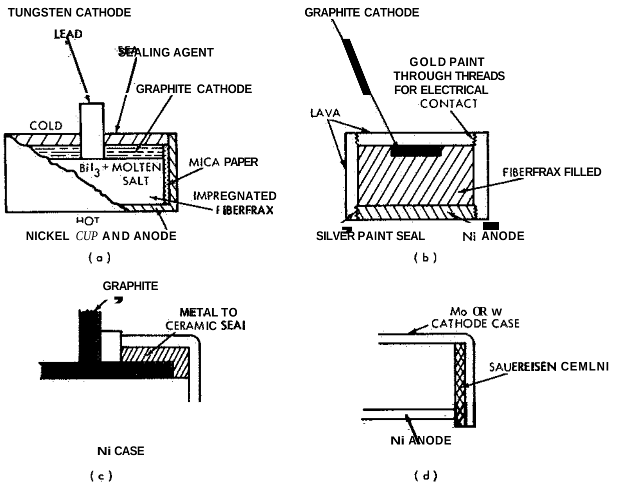

TUNGSTEN CATHODE
LEAD
SEALING AGENT
GRAPHITE CATHODE
COLD
BiI3 + MOLTEN SALT
MICA PAPER
IMPREGNATED FIBERFRAX
HOT
NICKEL CUP AND ANODE
(a)
GRAPHITE CATHODE
GOLD PAINT THROUGH THREADS FOR ELECTRICAL CONTACT
LAVA
FIBERFRAX FILLED
SILVER PAINT SEAL
Ni ANODE
(b)
GRAPHITE
METAL TO CERAMIC SEAl
Ni CASE
(c)
Mo OR W CATHODE CASE
SAUEREISEN CEMLNI
Ni ANODE
(d)

FIGURE 11.1.—Sketch of disk-type thermogalvanic **cell** (*4*), and variations.

The simplest thermogalvanic cell is a completely encased one, with one electrode hot and the other cold (see fig. 11.1).As an example, consider the cell $I_2(Pt)/AgI/(Pt)I_2$. When the electrodes are at the same temperature, and if the same activity of iodine is maintained at each, the theoretical QCV is zero. However, the potential of each half cell depends on its temperature. When the two electrodes are kept at different temperatures, the sum of the potentials of the two half cells is not zero, and an equilibrium QCV is obtained. When the cell is placed on load, iodine is evolved at one electrode and consumed at the other, and internal mass transfer of iodine must take place to support the current.

If the chemical free energy change, ΔF_T, of the half-cell reaction at temperature T is expressed (see ch. 2) as

$$\Delta F_T = \Delta H_0^0 - T\Delta\phi_T \tag{11.1}$$

and if $\Delta\phi_T$ is approximately constant with temperature, then

$$nF\left(\frac{\partial E}{\partial T}\right)_P = \Delta\phi. \tag{11.2}$$

Thus the OCV between two electrodes, identical except for their temperatures, will be

$$E = (\Delta\phi/nF)(T_2 - T_1) \tag{11.3}$$

where $\Delta\phi/nF$ is in units of volts per degree. In practice, this relation rarely holds ideally for thermogalvanic cells because ***(a)*** the temperature difference gives rise to different concentrations (of the iodine, for example) at the anode and cathode, and *(b)* $\Delta\phi$ may not be constant, especially if phase change occurs between reactant at the anode and cathode. The theoretical potentials can be calculated more accurately by substituting exact values for $A+$ as a function of temperature. However, the usual procedure is to give the mean millivolts per degree as an index of the QCV expected for any temperature differential. For the iodine cell given above, the hot electrode is the anode, and the cold electrode is the cathode. Iodine is ionized to iodide at the cathode, iodide ion is discharged to iodine at the anode, and a mass transfer of iodine from one electrode to the other must be maintained.

A more complex cell is the double thermo-

PRECEDING PAGE BLANK NOT FILMED.

galvanic cell in which two cells are connected, one being hot and the other cold. This cell is discussed in section 11.3. Equation (11.3) still yields the simple theoretical OCV, where $\Delta\phi$ is the value for the cell reaction (and not for a half-cell reaction, as before). Later sections of this chapter will cover the thermodynamic principles of other types of thermogalvanic and thermal-concentration cells.

11.2 SIMPLE THERMOGALVANIC CELLS

11.2.1 General Electric *Co.*, Solar Regenerative Fuel Cell, November 1960

Most of the experiments in this early work involved the cell Ag(hot)/AgI/Ag(cold). Solid silver iodide was the ionic conductor (between 293" F (145" C) and its melting point of 1031" F (555" C)). The theoretical potential is 0.56 mV/°K; therefore, the expected OCV was a maximum of 0.22 volt. Disks of silver/silver iodide/silver were compressed in a bolted stainless-steel case with one face placed on a hot plate. The temperature differential between the hot and cold silver face was 662" F (350" C), and up to 70 percent of the hot silver electrode could be transferred to the cold electrode. The disks tended to separate upon expansion and contraction, so an Inconel spring was incorporated to maintain contact. Growth of silver dendrites through the silver iodide caused shorts, but amalgamation of the electrodes retarded this growth considerably. Voltage-current relations were linear, giving short-circuit current of about 50 A/sq ft. (This cell is, of course, not a true fuel cell, but a consumable-electrode primary cell.)

The cell I_2(Pt)/AgI/I_2(Pt) was also investigated, using a U-tube containing the electrolyte in the bottom and a platinum electrode in each arm. A horizontal tube connected the upper arms of the U, providing a path for the return of iodine from the hot to the cold arm. The theoretical potential is 1.5 mV/°K, but the cell did not give theoretical potential and yielded only small currents.

11.2.2 Lockheed Aircraft Corp., Solar Regenerative Chemical Systems, September 1959 to September 1962

This contract evolved from an earlier, unproductive study on thermally regenerative cells (see ch. 10). The aim of the new study, which was on thermogalvanic cells, was to develop systems suitable for use of solar energy (*403*).

These experiments utilized the simple cell A(T_1) /AB melt/A(T_2). In some cases a metal ion was discharged at the colder electrode as liquid metal and run back to the anode by gravity flow. Cells Pb(l)/$PbBr_2$ melt/Pb(l) and Pb(l)/PbI_2 melt/ Pb(l) were tested in this way, but gave only about 0.03 to 0.04 mV/°K. Thallium-thallous oxide-thallium was very corrosive. The cell Cl_2(g)/AgCl(l)/Cl_2(g) was studied, using external feed of chlorine to porous carbon electrodes dipping into the melt, and gave about 0.66 mV/°K. The voltage curve showed only IR polarization to at least 300 A/sq ft. Similar results were found with the cells I_2(g)/PbI_2(l)/ I_2(g) and I_2(g)/LiI_2(l)/I_2(g), although PbI_2 had too high a vapor pressure to be useful. Table 11.1 gives calculated theoretical OCV, with a minus sign showing that the hot electrode is negative (anodic).

TABLE 11.1.—*OCV Calculated for Thermocells With Molten Salt Electrolytes and Arbitrarily Assigned Value* of *Entropy* of *Transport (403)*

[*A T*=2240.4" to 440.4° F; 1500° to 500° K]

Thermocell	*Voltage*
Li/LiX/Li	—0.1
Na/NaX/Na	+.2
K/KX/K	(+.2)
Rb/RbX/Rb	(+.2)
Ag/AgCl/Ag	—.4
Tl/TlX/Tl	—.2
Mn/$MnCl_2$/Mn	—.5
Al/$AlCl_3$/Al	(.6)
F_2/MF/F_2	[a]—.7
Cl_2/MCl/Cl_2	—.7
Br_2/MBr/Br_2	—.7
I_2/MI/I_2	[a]—.7
O_2/Tl_2O/O_2	—.3

[a] Might be increased as much as twofold because atoms are present at high temperatures.

Some reactants were used in disk-type cells having porous carbon electrodes, with the molten salt contained in a porous MgO matrix. Power densities were low due to high internal resistance of the melt in the MgO disk. Simple thermogalvanic cells of this type have the same limitation as conventional thermoelectric devices: the electrical conductivity of the melt cannot be

TABLE 11.2.—*Examination of Potential Thermally Regenerative Reagents in Molten Electrolyte (4)*

	Voltage obtained at 1652"F (900° C)		Voltage obtained at 752° F (400° C)	
	OCV	*i* mA	OCV	*i* mA
Electrolyte No. 12 (Aerojet proprietary).....	0.50	1.5	0.16	1
BiI_3 alone..........................	.25	12	....	....
BiI_3 in electrolyte........................	.49	22	.14	2
ZnI_2 in electrolyte........................	.55	15	.12	1
AuCl in electrolyte........................	.44	16	.33	7
$PtCl_2$ in electrolyte........................	.67	20	.44	14
$PdCl_2$ in electrolyte........................	.55	38	.32	5
ZnI_2 in electrolyte........................	.59	3	....	....
CdI_2 in electrolyte........................	.57	4	....	....
CuI in electrolyte........................	.66	4	....	....
HgI in electrolyte........................	.64	2	....	....
KI in electrolyte........................	.56	Small	....	....

made higher without also increasing the thermal conductivity. Assuming only IR polarization, the ratio of maximum electrical output to thermal flux through the cell is given by

$$\frac{\text{Maximum power}}{\text{Thermal flux}} = (K/4\rho c)\,(\text{OCV}) \qquad (11.4)$$

where K is the half-cell temperature coefficient in volts per degree; ρ, specific electrical resistance of the electrolyte; c, specific thermal conductance of the electrolyte; and OCV, open-circuit voltage. With consistent units, the ratio is the maximum thermal efficiency obtainable. Using a thermal conductance of *1.5* Btu/hr-ft-°F (ref. *11.1)* as a representative value for molten-alkali metal salts, K as 0.66 millivolt/°C, and an OCV of 0.7 volt, efficiencies of thermal conversion are about *2* percent.

11.2.3 Aerojet-General Corp., Investigation of an Energy Conversion Device, July 1961 to June 1962

The thermocell investigated *(I)* was

BiI_3(hot)/molten salt electrolyte/BiI_3(cold).

Since bismuth triiodide decomposes at 932° F (500° *C),* iodine is evolved at the hot electrode and ionizes at the cold electrode, with mass transfer occurring within the cell. Preliminary company work using unsealed simple disk cells and a proprietary electrolyte had shown about 0.5 OCV (hot face *1652"* F *(900"* **C))** and *100* A/sq ft at *0.1* to *0.2* volt. (Table *11.2* summarizes comparative results on other reactants.) Graphite electrodes were used, and electrolyte was retained in Fiberfrax. Free iodine was present, and air in-leakage burnt out the electrodes.

Aerojet constructed a number of sealed cells similar to those shown in figure *11.1 (4).* The major problems were sealing and maintaining sufficient electrical contact. Much of the work on materials is contained in appendix D. Differential thermal expansion led to cracking and loss of electrolyte in all cells. *Also,* absorption of electrolyte in cell materials led to electrical breaks. Ceramic-to-metal seals were destroyed by the process of welding the cells together. Cells were also made with a sandwich of electrolyte absorbed in Fiberfrax or porous ceramic between graphite disk electrodes (United Carbon Spectroscope Grade U120). These were coated with Sauereisen cement and fired at *1742"* F (950° **C)** in nitrogen. None of the surface coatings tested as sealing agents for the cement was satisfactory.

Cells of this type were delivered; they had a life of only *230* hours (instead of the desired 1000 hours) at a hot-face temperature of *932"* F *(500"* C). In addition, performance failed to equal that obtained for the preliminary unsealed cells. (This could be due either to lower hot-face temperatures necessary to give reasonable life to the *sealed* cells, or, possibly, a secondary current reaction resulting from the presence of oxygen in the unsealed cells.) The average thermal conductivity of the cells was 8.2×10^{-4} Btu/hr-in-°F, and the maximum thermal efficiency (see eq. (11.5)) was calculated to be only 0.4 percent, even when the current-voltage relations of the original, unsealed higher power cells were used.

While the theory of the cell was investigated, the thermodynamics used was that of a thermally regenerative cell (in which the cell operates at one temperature and is regenerated at another) and obviously does not apply to the actual reactions, probably a mixture of the cell reaction given above and the reaction $I_2(g)(T_2)/BiI_3\text{-melt}/I_2(g)(T_1)$.

11.2.4 Electro-Optical Systems, Inc., Investigation of New Solar Regenerative Fuel Cell Systems, November 1959 to March 1962

The general objective was to investigate, analytically and experimentally, possible systems for solar regenerative fuel cells **(191)**. Much of the theoretical and thermodynamic analysis was similar to that discussed in section 10.3.1.

One thermocell proposed was the cobaltous-cobaltic redox couple in the presence of cyanide. At low temperatures the cyanide complex is formed, giving

$$\phi Co^{3+}+e^{-}\rightleftharpoons \phi Co^{2+}, \qquad E_0=0.8 \text{ volt}$$

(where ϕ stands for the cyanide complex). At high temperatures, the uncomplexed couple would give the reaction

$$Co^{3+}+e^{-}\rightleftharpoons Co^{2+}, \qquad E_0=-1.84 \text{ volts.}$$

In this cell, Co^{3+} diffuses from the hot electrode to the cold, forming ϕCo^{3+} and being reduced to ϕCo^{2+}; ϕCo^{2+} diffuses to the hot electrode, decomposes to Co^{2+}, and is oxidized to Co^{3+}. No stability constants for the cobalt cyanide complexes could be found, so the concept was not investigated further. It can be argued, however, that such a cycle cannot escape Carnot limitations and, since the range of possible temperature differential is small, thermal efficiency would be small.

Experimental work done on a sulfuric acid thermal concentration cell followed the principle that an enclosed cell with aqueous electrolyte has a uniform pressure of water vapor; but the respective concentrations of $H_2O\text{-}H_2SO_4$ in equilibrium with this pressure vary with temperature. Thus, the cold electrode will have dilute acid due to condensation of water, while the hot electrode will have concentrated acid due to evaporation of water. Since the activity of the hydrogen ion varies considerably from weak to strong sulfuric acid (due to the formation of $H_2SO_4^-$ in strong acid), a difference in potential between the electrodes results. Hydrogen is evolved at the hot electrode and is consumed at the cold electrode. Hydrochloric acid did not work, due to the small change in activity between the dilute and concentrated acid.

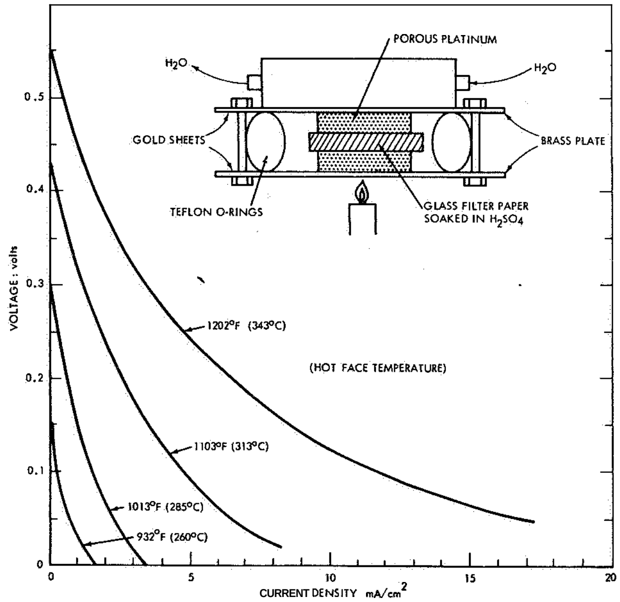

The temperature difference establishes a concentration gradient across the electrolyte, with concentrated acid at **the** hot face and dilute acid at the cold. Thus, hydrogen is evolved at the hot face (cathode) and is utilized at the cold face (anode),

FIGURE 11.2.—Diagram of thermal concentration cell using concentrated sulfuric acid electrolyte; voltage-current relations for the cell.

Figure 11.2 shows the experimental cell and the type of result obtained. Hydrogen was taken out of the cycle by the reaction $(\frac{1}{2})H_2+H_2SO_4\rightarrow H_2O+HSO_3$ at the hot face; therefore, oxygen was admitted to be consumed at the hot electrode and evolved at the cold. In this case water produced at the hot electrode was distilled to the cold electrode. Power outputs were not so good as with hydrogen, presumably due to oxygen activation polarization (overpotential) at the cold electrode.

Since the thermal efficiency of such a cell would be very low (for reasons discussed in sec. 11.2.2 (see eq. (11.4)), the temperature difference could be applied across a vertical refractionator packed with glass wool, with a hot bottom and a cold top. The concentrated sulfuric acid from the bottom of the refractionator would run into an electrode at the bottom of a cell, while the dilute acid from the top would run into an electrode at the top of the cell. The thermal gradient is then not applied directly across the cell, except via a long heat conduction path. In a later report (*174*), a T-shaped cell was designed in which the leg of the T was the refractionator, and the cross was the cell electrodes, but a workable model of the cell was never constructed.

11.3 DOUBLE THERMOGALVANIC CELLS

11.3.1 Lockheed Aircraft Corp., Solar Regenerative Chemical Systems, September 1959 to September 1962

As mentioned in section 11.2.2, this contract originally involved thermally regenerative cells, which led to work on thermogalvanic cells. Much of the work concerned the feasibility of the double thermogalvanic cell, as illustrated in figure 11.3. If both cells were at the same temperature and activities, the net OCV would be zero. However, the cell at T_1 has a higher potential than that at T_2; therefore, it reverses the T_2 cell to make it an electrolysis cell. Thus, the reactants in cell T_1 are electrolytically regenerated in cell T_2. The expression for the theoretical OCV is identical with that of the simple thermogalvanic cell (eq. (11.3)), but $\Delta\phi$ now is the value for the cell reaction instead of the half-cell reaction.

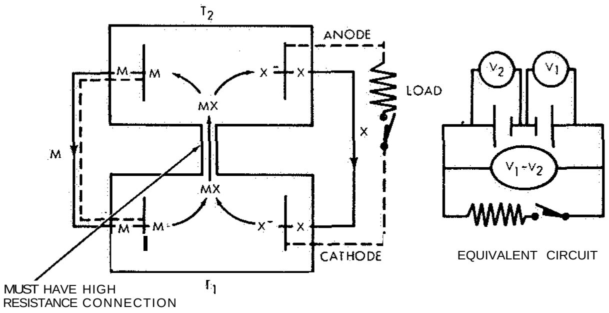

In this system the two cells are operated at two different temperatures, T_1 and T_2, with mass transfer as shown. The electrical connections are shown by the broken lines; since M stands for molten metal (lithium, for example), the mass-transfer path is also the electronic path. X stands for a nonconducting cathodic reactant such as iodine gas.

FIGURE 11.3.—Principle of the double thennogalvanic cell.

A primary requirement for this type of cell is that the reactions $M \rightleftharpoons M^+ + e^-$ and $X + e^- \rightleftharpoons X^-$ be capable of high current densities. Therefore, the voltage-current curve of the single cell Li/LiI/(porous C)I_2 was investigated in a simple cell similar to that described in section 10.3.1. At 932" F (500° C) the cell gave close to theoretical OCV (2.5 volts), a limiting current of about 350 A/sq ft and a current of 300 A/sq ft at 1.5 volts. At least 2 mole-percent lithium dissolved in the melt, but the effect on coulombic efficiency could not be obtained. Electrolysis of CdI_2 and PbI_2 at temperatures from 860° to 1499" F (460" to 815° C) showed only IR polarization. Comparative resistance measurements showed that much cadmium would dissolve in molten-cadmium iodide, giving rise to conductivities up to four times that of the cadmium iodide alone. This implied some electronic conduction of the mixture, with consequent reduced coulombic efficiency. Lead/lead iodide did not give this effect, and electrolysis of PbI_2 with a molten lead anode gave 100 percent coulombic efficiency.

The efficiency of the system as a heat cycle (the electrical work done per mole of reaction) is nFE, where E is given by equation (11.3). If electrolysis occurs reversibly at T_2, the heat taken up is $T_2\Delta S$. Neglecting specific heat effects, A+ is approximately equal to AS. Therefore

$$\xi = nFE/T_2\Delta\phi = (T_2 - T_1)/T_2. \qquad (11.5)$$

Allowance for the specific heat terms makes the theoretical efficiency somewhat less than the Carnot efficiency. Using T_1 as the melting point and T_2 as the boiling point of the melts, the values calculated were: PbI_2, $\xi = 35.5$ percent, OCV = 0.21; LiI, $\xi = 48.4$, OCV = 0.41. However, these efficiencies assume perfect heat exchange between hot M and X (leaving the hot cell and cooled to enter the cold) and cold MX (leaving the cold cell and heated to enter the hot). Even more important, they assume that no heat is (irreversibly) conducted from the hot cell to the cold. Since *M* forms an electronic path, it also forms a heat path. Thermal efficiencies of such systems are likely to be considerably below simple Carnot efficiencies, especially with the reduction of potential due to ohmic polarization at practical current densities.

Another proposed variation, shown in figure **11.4,** is a thermal concentration cell, in which two different concentrations are maintained at the two X_2 (for example, I_2) electrodes by the different temperatures in chambers T_1 and T_2. Iodine would be at a low equilibrium partial pressure in the cold trap T_1; therefore, the left cell would discharge iodine vapor. The condensed iodine is transferred (via a nonreturn valve) to the hot trap, where it picks up heat at T_2, vaporizes, and is ionized at the right electrode. The system might be run in cycles, with the T_1 trap being first cold and thus condensing I_2, and then made hot and the cell reversed. Electrolysis of cadmium iodide at 1022” F **(550”** C) into a liquid-nitrogen trap for the iodine gave currents up to **2000** A/sq ft with a coarse-pore carbon electrode. However, the coulombic efficiency was low **(30** to **40** percent) due to dissolution of cadmium and consequent internal electronic conduction.

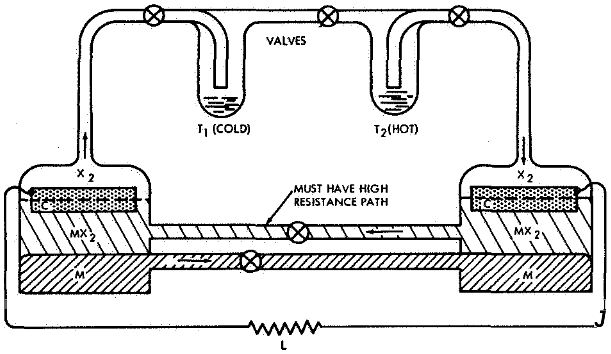

In this system, the two cells have different potentials due to different concentrations of reactant X_2. As in figure 11.1, one cell (the right one) is a fuel cell which drives the other cell as an electrolysis cell, thus regenerating the reactants. The difference in concentration of X_2 is obtained by having condensing chambers at different temperatures. T_1 and T_2.

FIGURE 11.4.—Thermal **concentration cell.**

Such a system would be impractical by its very complexity. To obtain high thermodynamic efficiencies, T_2 should be high; but the equilibrium pressure of X_2 must not be too high (much above **1** atmosphere) at T_2, or problems of sealing and strength arise. T_1 must be sufficiently low for X_P to be liquid; otherwise, it could not be transferred to T_2 without excessive pumping power. An inert gas would have to be used to equalize total pressures on each side, or the cell as shown would "blow round." Whether or not high currents could be obtained with inert gas present was not demonstrated. It might be argued that outer space would be a suitable cold sink, but the T^4 relation of radiant heat loss would probably lead to an excessive radiator size, The major advantage of this cell over that of a simple thermogalvanic cell is that irreversible heat conduction from T_2 to T_1 can be minimized.

11.3.2 Argonne National Laboratories, Thermally Regenerative Fuel Cells, April 1961 to 1963

This work concerned tests on liquid bimetallic cells, starting about December 1961 (*104*). The cells were of the type

$$M_1(l)/\text{KCl-LiCl melt}/M_1M_2(l)$$

where M_1 is an alkali metal and M_2 a heavy metal such as tin, lead, bismuth, etc. They can be considered to be concentration cells with a low activity of dissolved or compound M_1 in M_2 (see sec. **10.4** for a similar cell using mercury). The brief descriptions do not show whether the work was aimed at purely thermal regeneration, or whether the double thermogalvanic method was envisaged. Purely thermal regeneration is probably not feasible, due to the difficulty of getting suitable phase changes at usable temperatures; phase change is required for easy physical separation of M_1 and M_2. Therefore, the work is discussed in this section (rather than in sec. **10.2.3).**

Reactants were selected for differences between melting and boiling points, these being taken as the limiting temperatures for Carnot efficiency (eq. **(11.5)).** In addition, strong compound formation between M_1 and M_P (as evidenced by melting points of the intermetallic compounds higher than the melting points of M_1

TABLE 11.3.—*Properties of Cells With Lithium Anodes and Various Cathodes (104)*

Cathode	Minimum cell operating temperature,[a] "F	Maximum cell operating temperature,[b] "F	Maximum Carnot efficiency	Metallic compound (ref. 11.2)	OCV
Ga	366.8 (186" C)	2436.8 (1336" C)	0.71	....	....
In	366.8 (186" C)	2436.8 (1336° C)	.71	....	....
Sn	449.6 (232" C)	2436.8 (1336" C)	.69	Li_7Sn_2	0.73
Bi	519.8 (271" C)	2436.8 (1336" C)	.66	Li_3B	.93
Tl	575.6 (302" C)	2436.8 (1336° C)	.64	....	....
Pb	620.6 (327" C)	2436.8 (1336" C)	.63	$Li_{10}Pb_3$	.69
Te	845.6 (452° C)	2436.8 (1336" C)	.56	Li_2Te	1.93
Se	429.8 (221° C)	1265 (685°C)	.48	....	....
Cd	609.8 (321" C)	1412.6 (767" C)	.43	LiCd	.66
Zn	788 (420" C)	1664.6 (907" C)	.41	Li_2Zn_3	.67
Hg	366.8 (186" C)	678.6 (357" C)	.27	....	....

or M_2) was claimed as desirable for a high voltage per cell. (In a complete regenerative system, however, the effective entropy change $\Delta\phi$ is the important thermodynamic parameter, not *AH* (see eq. *(11.3)).*A high cell voltage is not useful unless it changes rapidly with temperatures.) Table *11.3* gives properties of some reactants considered.

The experimental conditions were similar to those described in section *10.2.3,* but a differential density cell was used (see fig. *11.5).* With a lithium anode, the results shown in figure *11.6* were obtained. The OCV values were somewhat indefinite, since they depended on the amount of lithium built up in the heavy metal. Separation of solid phases from the heavy metal was noted. The lithium-tellurium system cor-

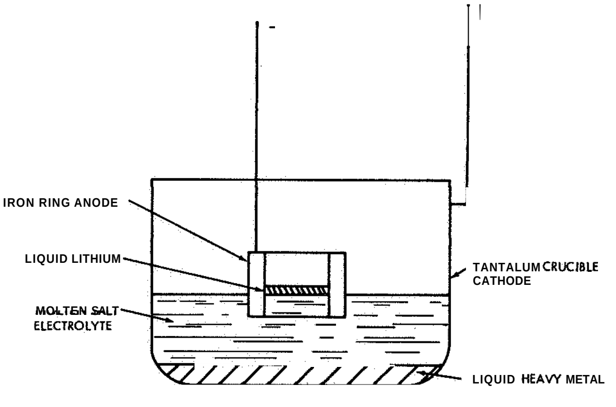

The cell was contained in a furnace under highly purified helium.

FIGURE 11.5.—Illustration of differential density, liquid bimetallic cell.

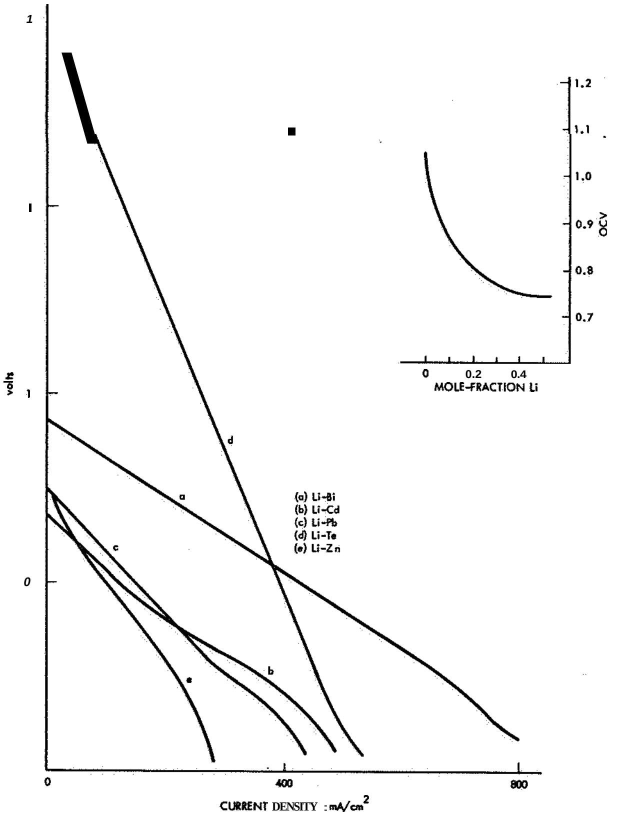

FIGURE 11.6.—Polarization curves for lithium-metal cells (892.4" to 919.4" F; 468" to 493° *C).*

roded the tantalum crucible (beryllium oxide crucibles were unsatisfactory due to attack by the molten chlorides); therefore, attention was directed to the lithium-bismuth cell. The OCV temperature variation of the cell was unstable and depended on the mole-fraction of lithium in bismuth. Above 932" F (500" C), lithium reduced some potassium ions, resulting in volatilization of potassium. Therefore, the eutectic 30 LiF: 70 LiCl (mole-percent) was used as the molten electrolyte in subsequent work.

Voltage instability due to variation of lithium activity was overcome with time by saturating bismuth with solid Li_3Bi. Since discharge of lithium into this material gave further deposition of Li_3Bi, the variation of lithium activity was small. The OCV as a function of temperature was obtained for the two cells

$$Li(l)/LiCl\text{-}LiF/Li_3Bi(s)\text{-}Bi(l)$$
$$Li_3Bi(s)\text{-}Bi(l)/LiCl\text{-}LiF/Bi(Li)(l).$$

In the second cell the potential depended on the activity of lithium at the right electrode, but this activity did not vary rapidly with time (as with a pure lithium anode), since the low activity of free lithium in the $Li_3Bi(s)$-Bi(*l*) electrode retarded dissolution and transfer of lithium through the melt. Thus, the second was also stable, and could be investigated at known mole-fractions of lithium. The sum of the two cell measurements gave values for the cell Li(l)/LiCl-LiF/Bi (Li)(l). The results are shown in figure 11.7. The temperature coefficient of the cell is low, except for high mole-fractions of lithium in bismuth. In the hotter cell of a double thermogalvanic system, lithium would ionize from the Bi(Li) electrode and Bi(Li) would have to be supplied from the cold cell fast enough to keep the concentration of lithium high. For example, if the mole-fraction of lithium in the hot cell went down to 0.3 from a value of 0.6 in the cold cell, the potential difference between the cells would disappear (see fig. 11.7).

Purely thermal regeneration of lithium from lithium-bismuth might be difficult because of the low vapor pressure of lithium, and because the vapor pressures of lithium and bismuth are comparable at 1832" F (1000° C). Therefore, attention was given to the Li/Sn cell, since the vapor pressure of tin is low at these temperatures. Results are shown in figure 11.7 **(112)**. In addition, solubilities of lithium in lithium chloride (approximately 2 atom-percent in the range 1112" to 1472° F (600" to 800" C)) and of lithium and bismuth (from bismuth saturated with Li_3Bi) in LiCl-LiF eutectic were measured (see app. B). The ratio of lithium to bismuth in the second case indicated that Li_3Bi was the principal soluble component, and a deep red color was found **(114)**.

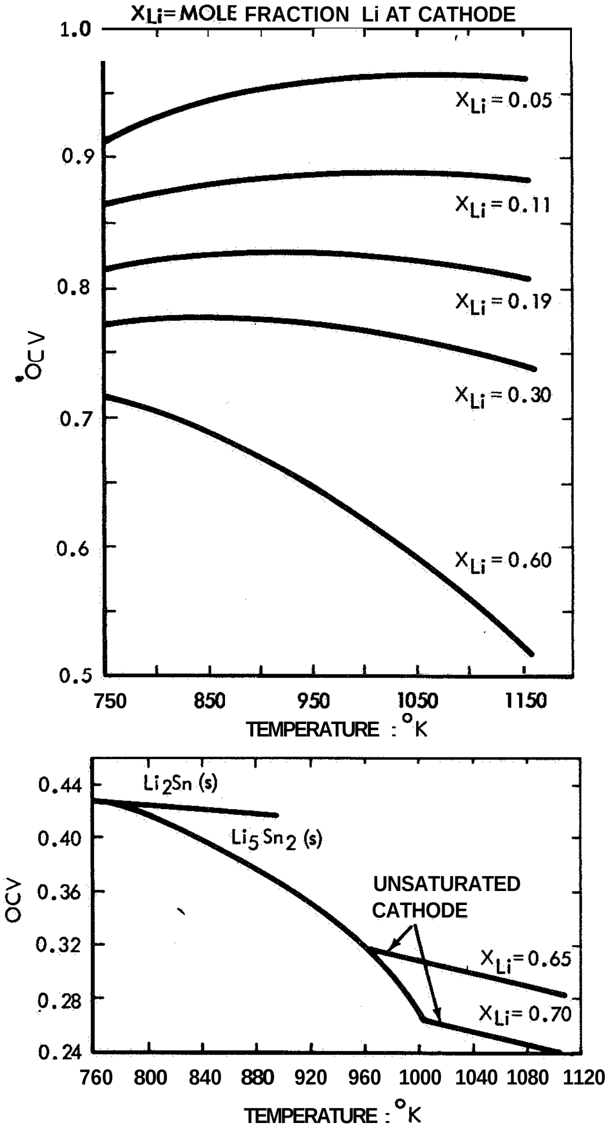

FIGURE 11.7—Variation of OCV with temperature and mole fraction of lithium at the cathode for the cells Li(*l*)/LiCl-LiF melt/Bi(Li)(*l*) (after **116**) and Li(*l*)/LiCl-LiF melt/Sn(*l*) (after *112*).

From a mass spectrometric study of vapor pressures of lithium and bismuth over Li_3Bi, the thermodynamic data were found to be

$Li_3Bi\,(s) = 3Li(g) + Bi\,(g)$:
$T = 2606°$ F (1050" K)
$\Delta H^0 = 192$ kcal/mole
$\Delta F^0 = 94$ kcal/mole
$Li_3Bi\,(s) = 3Li\,(l) + Bi\,(l)$:
$T = 3092°$ F (1200" K)
$\Delta F^0 = 46$ kcal/mole.

The value of ΔF^0 for the second reaction agreed well with the value estimated from the OCV of the cell $Li(l)/LiCl\text{-}LiF/Bi(l)\text{-}Li_3Bi(s)$. The high positive free energy for the first reaction shows that thermal regeneration is not feasible. Studies were continued on rubidium-bismuth and sodium-bismuth cells.

The work reported in this section was carefully performed using modern analytical techniques and instrumentation, with considerable attention to detail and accuracy. It is, however, difficult to justify solely on the grounds of regenerative fuel-cell development. Little attempt was made to explore the thermodynamic or practical feasibility of regeneration of the cells studied.

11.3.3 Delco-Remy Division, Feasibility Study of the Electrothermally Regenerative Transducer, May 1962 to June 1964

The "electrothermally regenerative transducer" turned out to be the double thermogalvanic cell illustrated in figure 11.3, and described some years previously by Lockheed and Electro-Optical Systems. (Adequate acknowledgments were not made to the earlier work, so perhaps some breakdown in scientific communication was involved.) The cell was proposed *(154)* as a possible means of filling the duty cycle for an armored vehicle; that is, 500 amperes continuously, 1000 amperes for 5-minute periods, and 5000 amperes over 10-second periods, at voltages from 30 to 18 volts. This is a maximum power of 90 kilowatts.

The general requirements for the double cell were given as *(a)* large voltage difference with temperature, *(b)* high ionic conductivity, *(c)* good separation of the phases present, *(d)* a wide difference between melting and boiling points (to give a large $T_2 - T_1$ value), and *(e)* good materials stability. For these reasons, halogen compounds of lithium, sodium, and potassium were proposed, with fluorine excepted because of likely materials problems. The OCV for sodium chloride, with the hot cell at 2732" F (1500" C) and the cold at 1517" F (825° C), was estimated at 1 volt, with a thermal efficiency of 34 percent. (The $\Delta\phi$ value (see eq. (11.3)) used in the calculation was for $2NaCl(l) \rightleftharpoons 2Na(g) + Cl_2(g)$, but the cold cell would operate with liquid sodium, which implies an irreversible loss of the heat of condensation.) A paper study based on a cell thickness of 1 inch indicated that the system would give about 1 kW/ft^3 and about 40 lb/kW. This was not favorable when compared with a conventional diesel engine, which gave 7 lb/hp or 9.4 lb/kW. However, it was said that the sodium-chlorine cell might have advantages for short periods of high power required for acceleration, in place of the conventional generator-battery system.

A porous carbon cup immersed in sodium chloride at 1472" F (800° C) was used as the chlorine cathode. This produced IR-free polarization of only a few millivolts for current densities up to 2000 A/sq ft, and there was no sign of a limiting current even at 3000 A/sq ft. A pore-size range of 2 to 4 microns was found to be best, with graphitized carbon better than electrode carbon. Evacuated carbon of pore size less than about 3 microns was not wetted by molten sodium chloride at 1472" F (800° C). However, sodium that was dissolved in the salt rapidly attacked the carbon. The equilibrium solubility of sodium in sodium chloride at a fixed pressure of sodium (obtained by connecting sodium boiling at a lower temperature with the solubility cell at a higher temperature) was found to be about 1 weight-percent at 1517" F (825" C) and 0.03 at 2192" F (1200° C).

Later work *(155)* was aimed at constructing cells of more practical configuration. Of a number of metals and alloys tested with chlorine at 1562" F (850" C), only gold and platinum were satisfactory (see app. D). Borosilicate glass coated on a small tungsten specimen in the laboratory was satisfactory, but no industrial glaze or suitable larger scale firing method was found. Designs of plate-to-plate cells were not satisfactory, due to leaks, breakage, corrosion, etc.

The basic cell parameters were further investigated in a laboratory-scale cell. A commercial alumina U-tube was used as a cell body, with a hollow carbon cathode in one arm. The sodium electrode was made from an iron or nickel tube flared at the end, with a porous metal-disk Heliarc welded on the flare. This was immersed in electrolyte in the other arm. The simple U-cell was not sealed, but kept under argon. Sodium chloride was purified by bubbling *dry* HCl through the melt, evacuating and solidifying. At 1517" F (825" C) an OCV of 3.2 volts was obtained, with only IR polarization at more than 3000 A/sq ft at the anode. High current densities were obtained from all types of metal-disk anodes, but the coarse-pore disks allowed more sodium to dissolve in the melt. Faradaic efficiencies of sodium usage were only 30 to 40 percent.

Measurement of the variation of OCV with temperature gave a decrease in potential with temperature of 1.37 mV/°K for the reaction

$$Na(g)+\tfrac{1}{2}Cl_2(g)\rightleftharpoons NaCl(l).$$

The value was, of course, lower for temperatures below the boiling point of sodium, since the effective entropy for $Na(l)+\tfrac{1}{2}Cl_2(g)\rightleftharpoons NaCl(l)$ is a less-negative quantity.

11.4 CONCLUSIONS

Many of the conclusions drawn in section 10.6 can be applied to thermogalvanic cells. The simple thermogalvanic cell could perhaps be developed into a compact, reliable single cell, although there would obviously be problems in making cell stacks. However, the thermodynamic argument leading to equation (11.4) shows that thermal efficiencies are not likely to exceed a few percent.

The double thermogalvanic cell is basically unattractive because of its complexity and the necessity for flowing molten metals or salts from one cell to another. As with the thermally regenerative cell, high thermal efficiencies can only be obtained with large temperature differences. High temperatures lead to severe materials problems and favor intersolubility of liquid metals and molten electrolyte, so that clear-cut phase separation cannot be obtained. Also, electronic conduction through the electrolyte, due to dissolved metal, leads to lower thermal efficiencies.

11.5 REFERENCES

11.1. GAMBILL, W. R.: Chem. Eng., vol. 129, Aug. 1959.
11.2. HANSEN, M.: Constitution of Binary Alloys. Second ed., McGraw-Hill Book Co., Inc., 1958.

CHAPTER 12

Photochemically Regenerative and Redox Cells

12.1 INTRODUCTION

Conversion of radiant energy to electrical energy can occur through photochemical decomposition of a compound to form reactants for a fuel cell.

$$A \xrightarrow{h\nu} B + C$$

$$B + C \xrightarrow{\text{fuel cell}} A.$$

Photochemical decomposition occurs when a molecule absorbs radiant energy and converts it to intramolecular energy. The excited state produced may then decompose, or revert to the original stable form by emission of radiation, or share the energy with other molecules by collision, giving rise to heat increase without decomposition. Only a few reactions convert most of the absorbed energy into decomposition products suitable for use in fuel cells.

The basic principle of the redox cell has been discussed in chapter 2. The redox ion produced by the fuel-cell reaction must be regenerated to the reactant form by chemical fuels or photochemical processes. Redox cells and photochemically regenerative cells are considered in one chapter because of this overlap between the two types—a redox cell is not necessarily photochemically regenerative and a photochemically regenerative cell does not necessarily use redox couples, but several of the systems described below are photochemically regenerative redox cells.

A photochemical decomposition is useful for fuel-cell applications only if the products of decomposition, B and **C**, have a higher free energy than the decomposed molecule, **A.** The absorption of radiation produces a high-energy excited state, but on decomposition this energy may be released as heat, so that the overall reaction is not necessarily endothermic. Therefore, the decomposition should have a reasonably large positive free energy, which means that it should be endothermic. The products of reaction must be separated to be fed to the cathode and anode; therefore, they must not recombine rapidly. In addition, the quantum yield of the decomposition must be high; i.e., the conversion of quanta of absorbed radiation to decomposition products capable of producing current should be close to theoretical (theoretical quantum yields are usually 1 or 2). Only radiation of sufficiently high energy (short wavelength) to supply the energy of decomposition will be effective (ref. 12.1). If the reaction enthalpy is ΔH, the longest wavelength which will cause photodecomposition is given by

$$AH\text{, kcals/mole} = (2.86)(10^5)/\lambda \text{ (angstroms).} \tag{12.1}$$

In practice, photodecomposition has an activation energy greater than the enthalpy of reaction (see fig. 12.1). The threshold wavelength is defined by

$$\Delta H^{\ddagger} = (2.86)(10^5)/\lambda_0, \tag{12.2}$$

and is smaller than the theoretical wavelength of equation (12.1). The efficiency of conversion of absorbed energy to available electrochemical free energy (ref. 12.2) is

$$Q = 100 \Delta F^0 \phi / E_\lambda, \tag{12.3}$$

where Q is the percent efficiency, ΔF^0 is the standard-state free energy of the reaction, ϕ is the quantum yield, and E_λ is the enthalpy of light of wavelength λ. (This assumes that the products of decomposition give a standard-state potential in a cell.) E_λ must be greater than or equal to the threshold energy, and equation (12.3) holds only for a single wavelength. For a

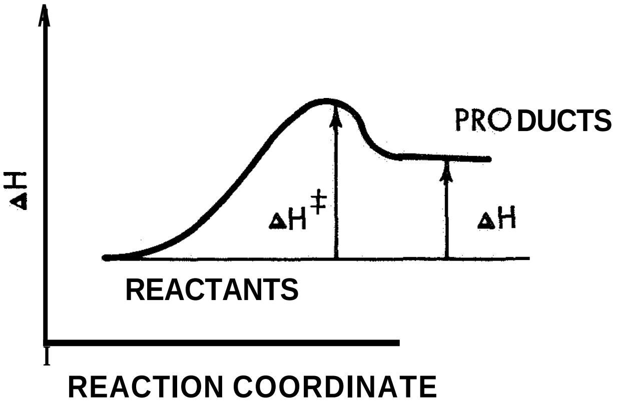

Only light of sufficient energy to supply the activation energy $\Delta H\ddagger$ will cause photodecomposition.

FIGURE 12.1.—Enthalpy for an endothermic photochemical reaction.

spectral range of light, the efficiency is

$$Q=100\frac{\Delta F^0\phi k}{E_{\lambda_0}} \qquad (12.4)$$

where k is a dimensionless factor less than 1. Out of the total radiation absorbed, only wavelengths shorter than λ_0 cause decomposition, and for each of these wavelengths, the fraction of the energy which is used in causing decomposition is E_{λ_0}/E_λ. The energy contained in a spectral band is

$$E=\int_{\nu_1}^{\nu_2} h\nu n(\nu)d\nu$$

where ν is frequency and $n(\nu)$ is the spectral distribution; therefore, if ν_0 is the threshold frequency, then

$$k=h\nu_0\int_{\nu_0}^{\infty} n(\nu)d\nu\Big/\int_0^{\infty} h\nu\, n(\nu)d\nu \qquad (12.5)$$

Figure 12.2 shows values of k for sunlight entering the Earth's atmosphere *(174)*. At higher threshold wavelengths, $\int_{\nu_0}^{\infty} n(\nu)d\nu$ is large but ν_0 is small, while at lower threshold wavelengths, the opposite is true. Thus a maximum exists in figure 12.2. Equations (12.4) and (12.5) give an efficiency of conversion of absorbed radiation to free energy. In practice, not all of the incident light will be absorbed, so the true efficiency will be less than Q.

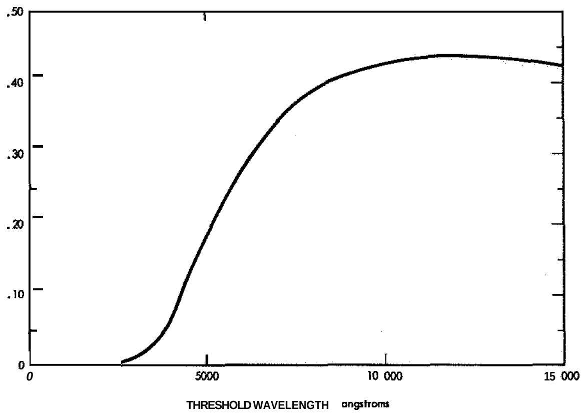

FIGURE 12.2.–Fraction solar enthalpy used in photochemical decomposition, as a function of threshold wavelength *(170, 174)*.

12.2 PHOTOCHEMICAL REGENERATION OF REACTANTS

12.2.1 Stanford Research Institute, Photochemistry in the Solar Furnace, April 1958 to December 1959 and March 1960 to June 1962

The early work at Stanford (578) showed that oxygen could be produced from water containing stannous ion by a photochemical process according to

$$Ce^{4+}+\tfrac{1}{2}H_2O\xrightarrow[HClO_4]{h\nu}Ce^{3+}+H^++\tfrac{1}{4}O_2.$$

This effort, already described in the literature (ref. 12.3), used a solar furnace as a cool, intense light source with a radiation **flux** of 49 watts over an image of 0.039 cm². Another possible and desirable reaction would have been

$$Ce^{3+}+H_2O\xrightarrow[HClO_4]{h\nu}Ce^{4+}+OH^-+\tfrac{1}{2}H_2,$$

except that no hydrogen was found. If the H radical was produced, it could have been removed by reduction of perchloric acid to chlorate

$$2H+ClO_4^-=ClO_3^-+H_2O$$

but no chlorate ion was detected, and the nonappearance of hydrogen was unexplained. A more detailed study of the possibility of producing hydrogen was made (*579*), using the general reaction

$$M^{2+}(aq)+H^+\xrightarrow{h\nu}M^{3+}(aq)+\tfrac{1}{2}H_2.$$

The reduced ion could be Co^{2+}, Ni^{2+}, Mn^{2+}, Fe^{2+}, V^{2+}, or Cr^{2+}. The minimum light energy had to be enough to supply the energy of reaction, plus any extra activation energy for photo-oxidation, given as 34 to 42 kcal/mole. Since the reaction $H^{+}+e^{-}\rightarrow\frac{1}{2}H_2$ has an energy of 48 kcal/mole (the source of this figure was not given), the total energy for a couple with zero volts ionization potential is about 86 kcal/mole; i.e., 3300 angstroms. It was concluded that little hydrogen would be produced on Earth due to the small fraction of light with sufficient energy for reaction.

Another reaction suggested as suitable for photochemical regeneration and fuel cell use was

$$2NOCl\xrightarrow{h\nu}2NO+Cl_2.$$

The solvent was carbon tetrachloride and the principal problem was to prevent back reaction to nitrosyl chloride, known to occur rapidly in solution. Some NOCl disappeared when the solution (0.1 *M* in NOCl) was passed through the solar furnace beam, but no chlorine was observed. Analysis was difficult due to heating of the solution in the beam. The average quantum yield for disappearance of NOCl was 0.22. In unconcentrated light (*581*), an absorption cell long enough to absorb most of the light gave a rate of about 10^{-5} mole/liter-min (equivalent to 1/60 A/liter), and the quantum yield was less than one-tenth that observed with the concentrated solar furnace beam.

12.2.2 Sundstrand Machine Tool Co., Solar Regenerative Fuel Cell, April 1959to May 1961

The objective was to develop a nitrosyl chloride solar-regenerative fuel-cell system with output of 10 watts at 1.5 volts ***(583).*** Nitrosyl chloride was selected for its wide spectral absorption range and the ease of separating the products by solution of chlorine in suitable solvents. The threshold wavelength for decomposition was about 6300 angstroms. About 43 percent of solar energy is composed of light of shorter wavelengths and therefore sufficiently energetic for decomposition. Table 12.1 gives a review of photochemical data for other systems.

Assuming complete absorption of sunlight (intensity about 1.4 kW/m^2 at edge of Earth) and a quantum yield of 2 for wavelengths below the threshold wavelength, equations (12.1) and (12.5) give an efficiency of 9.3 percent and an energy density of 95 W/m^2.

Considerable effort was expended in building an elaborate system for liquid-phase photolysis and in preparing and purifying NOCl. Liquid nitrosyl chloride was radiated at 3 atmospheres' pressure and ambient temperature, but the rapid back reaction of $NO+Cl_2$ in solution prevented separation. The rate constant for recombination was $(1.14)(10^7)(mole/cm^3)^{-2}$ sec^{-1} at 63" F (17" C). Recombination rates in the gas phase were also studied and used to correct the observed photolysis rates for the back reaction. In the gas phase, decompositions of 6 to 10 percent were obtained and quantum yields were about 1.7.

After testing material compatibility, Sundstrand constructed disk fuel cells with porous carbon electrodes (Stackpole RB66 or National Carbon No. 60). Tantalum and Teflon were used with Scotchcast No. 808 epoxy seals; Teflon was pretreated with sodium in liquid ammonia to give a surface which bonded to the epoxy. The electrolyte was liquid NOCl containing 50 weight-percent $AlCl_3$, which had high conductivity and less than 2-psig vapor pressure at room temperature. The cell $NO/NOCl\text{-}AlCl_3/Cl_2$ gave OCV of about 0.2 volt (the standard potential of $NO+\frac{1}{2}Cl_2\rightarrow NOCl[g]$ is 0.21 volt), but the electrodes flooded and gave poor performance under load. **A** coat of Viton dissolved in 2-butanone was brushed on, dried, and the Viton polymerized at 250" F (121" C) and 400" F (204" C), but the coat did not prevent wetting.

The photolysis products were to be separated by solution of chlorine and nitrosyl chloride, followed by distillation to remove them from the solvent. Carbon tetrachloride, tetrachloroethane, and Arochlor 1221 (Monsanto) dissolved NOCl and Cl_2 without taking up NO, and a packed bed scrubber was built. A 500-watt flight design was considered feasible if given further development (3 to 5 years).

A test fuel cell was built with glass backplates *so* that flooding could be observed ***(584).*** Viton putty (PR1730, Products Research Co., Los Angeles, Calif.) sealed the glass into the cell. National Carbon C–13 electrodes cured the

TABLE 12.1.—*Ultraviolet Endothermic Photochemical Reactions*

[Ref. 12.2]

	Overall chemical reaction	Effective wavelengths, Å	Quantum yield, ϕ (product)	ΔF^0_{298}, kcal/mole	Q,[a] percent efficiency at threshold wavelength	Reference[b]
(1)	$3/2O_2 \to O_3$	<1751 (weak	2.0 (O_3)	32.4	40.5	1, 2
		absorption) 2070	2.0	...	47.0	...
(2)	$CO_2 \to CO + \frac{1}{2}O_2$	<1692	1.0 (CO)	61.4	36.4	3
(3)	$H_2O \to H_2 + \frac{1}{2}O_2$	<1800	Small	54.4	Small	4, 5
(4)	$CO + H_2 \to CH_2O$	<1470	0.5 (CH_2O)	6.6	1.7	3
(5)	$NH_3 \to \frac{1}{2}N_2H_4 + \frac{1}{2}H_2$	<2138	0.5 (H_2)	17.1	12.8	6
				(ΔH^0_{298})		
(6)	$CH_4 \to \frac{1}{2}H_2 + \frac{1}{2}C_2H_6$ or $CH_4 \to H_2 + \frac{1}{2}C_2H_4$	<1450	...	6.9	...	7
		1295	0.5 (H_2)	...	3.1	...
				18.4	4.2	8
(7)	$HBr \to \frac{1}{2}Br_2 + \frac{1}{2}H_2$	<2537	1.0 (Br_2)	12.5	22.2	9
		2090	1.0	...	18.3	...
(8)	$SO_3 \to \frac{1}{2}O_2 + SO_2$	<2760	Small	16.2	Small	10
(9)	$COCl_2 \to CO + Cl_2$	2750	0.9 (CO)	16.3	14.0	11
		2537	...	...	13.1	...
(10)	(a) $Fe^{+2} + H_2O \to \frac{1}{2}H_2 + Fe^{+3} + HO^-$ (water solution)	<2900	0.05 (H_2)	36.2	3.7	12
	(b) $Fe^{+2} + H^+ \to Fe^{+3} + \frac{1}{2}H_2$ (acid solution)	2537	0.1 (H_2)	17.1	3.0	13
(11)	$NO_2 \to NO + \frac{1}{2}O_2$	<4350	0.046 (NO)	9.0	9.0	15
		4050	0.36	...	4.6	...
		3660	0.77	...	8.8	...
(12)	$NOCl \to NO + \frac{1}{2}Cl_2$	<6370	2.0 (NO)	4.9	21.8	16
		3650	2.0	...	12.5	17
(13)	$NO_3^- \to NO_2^- + \frac{1}{2}O_2$ (water solution)	<3350	0.014 (NO_2)	18.0	.20	18
		2304	0.024	...	.42	19
		2700	0.07	...	1.2	...
		2540	0.30	...	4.8	...
(14)	$2Fe^{+2} + I_3^- \to 2Fe^{+3} + 3I^-$ (water solution)	<5460	2.0 (Fe^{+3})	9.4	9.0	20
		3660	...	...	6.0	...
(15)	$I_2 + NO_2^- + H_2O \to NO_3^- + 2HI$	<5790				
		4360	0.1 (NO_3^-)	13.8	2.1	2
(16)	$Fe^{+2} + \frac{1}{2}$ thionine $\to Fe^{+3} + \frac{1}{2}$ leucothionine (acid solution, pH=2)	Visible	...	9.5	...	2
		~6000	0.5 (Fe^{+3})	...	9.9	...
(17)	$H_2O \to H_2 + \frac{1}{2}O_2$ (Ce^{+3}, Ce^{+4}, $HClO_2$ solution)	<3500	...	56.7	...	23
		2537	0.0007 (H_2)	...	.035	...
(18)	2 Anthracene→dianthracene (organic solution)	<3800	...	15.6	...	24
		3660	0.25 (Dian)	(ΔH^0_{298})	5.0	...
		3130	0.23	...	3.9	...

[a] Assumes that $k=1$ (see eq. (12.5)); values would be decreased by over 2 for the sunlight spectrum (see fig. 12.2).

[b] See list below.

TABLE 12.1.—*Ultraviolet Endothermic Photochemical Reactions*—Continued

[Ref. 12.2]

Overall chemical reaction	Effective wavelengths, Å	Quantum yield, ϕ (product)	ΔF^0_{298}, kcal/mole	Q,[a] percent efficiency at threshold wavelength	Reference[b]
(19) (a) $AgCl(s) \rightarrow Ag(s) + \frac{1}{2}Cl_2$	<4050	1.0 (Ag)	26.2	37.1	25
(b) $AgBr(s) \rightarrow Ag(s) + \frac{1}{2}Br_2$	<4600	1.0 (Ag)	22.9	37.0	26
(c) $AgI(s) \rightarrow Ag(s) + \frac{1}{2}I_2$	<4400	1.0 (Ag)	15.8	24.3	27
(d) $AgCl(s) + \frac{1}{2}H_2O \rightarrow Ag(s) + HC$ $\frac{1}{4}O_2$ (water suspension)	<4050	(1.0)?	23.2	(32.9)	28
(20) (a) $H_2O + \frac{1}{2}O_2 \rightarrow H_2O_2$ (water sus sion f ZnO)	<4000	....	25	....	29
	3660	0.09 (H_2O_2)	....	2.9	30
	3130	0.13	....	3.6	....
(b) $H_2O + \frac{1}{2}O_2 \rightarrow H_2O_2$ (water suspension of CdS)	<5460	(0.02)	25	(1.0)	31
	4360	(0.09)	....	(3.4)	....
	3650	(0.11)	....	(3.5)	....
(c) $H_2O + \frac{1}{2}O_2 \rightarrow H_2O_2$ (water suspension of CdSe)	<5780	(0.007)	25	(.4)	32
	5460	(0.024)	....	(1.1)	....
	3650	(0.024)	....	(.8)	....

1. Warburg, E.: Sitzber. kgl. preuss. Akad. Wiss., 872, 1914.
2. Vaughan, W. E.; and Noyes, W. A., Jr.: J. Am. Chem. Soc., vol. 52, 559, 1930.
3. Groth, W.: Z. physik. Chem., vol. B37, 307, 315, 1937; vol. B38, 366, 1937.
4. Terenin, A.; and Neuimin, H.: Nature, vol. 134, 255, 1934.
5. Groth, W.; and Suess, H.: Naturwiss., vol. 26, 77, 1938.
6. Noyes, W. A., Jr.; and Leighton, P. A.: The Photochemistry of Gases. Reinhold Pub. Corp., New York, 1941, pp. 370–382; review of the research on this reaction up to 1940.
7. Groth, W.: Z. physik. Chem., vol. B38, 366, 1937; Groth, W.; and Laudenkloe, H.: Naturwiss, vol. 24, 796, 1936.
8. Leighton, P. A.; and Steiner, A. B.: J. Am. Chem. Soc., vol. 58, 1823, 1936.
9. Warburg, E.: Sitzber. kgl. preuss. Akad. Wiss., 314, 1916.
10. Kornfeld, G.: Trans. Faraday Soc., vol. 33, 614, 1937.
11. Montgomery, C. W.; and Rollefson, G. K.: J. Am. Chem. Soc., vol. 56, 1689, 1934.
12. Poterill, R. H.; Walker, O. J.; and Weiss, J.: Proc. Roy. Soc. (London), vol. A156, 561, 1936.
13. Weiss, J.: Nature, vol. 136, 794, 1935.
14. Uri, N.: J. Chem. Phys., vol. 20, 348, 1952.
15. Dickenson, R. G.; and Baxter, W. P.: J. Am. Chem. Soc., vol. 50, 774, 1928.
16. Bowen, E. J.; and Sharp, J. F.: J. Chem. Soc., vol. 127, 1026, 1925.
17. Kistiakowsky, G. B.: J. Am. Chem. Soc., vol. 52, 102, 1930.
18. Warburg, E.: Sitzber. preuss. Akad. Math.-Phys. Klasse, 1228, 1918.
19. Villars, D. S.: J. Am. Chem. Soc., vol. 49, 326, 1927.
20. Kistiakowsky, G. B.: J. Am. Chem. Soc., vol. 49, 976, 1927.
21. Durrant, G. G.; Griffith, R. O.; and McKeown, A.: Trans. Faraday Soc., vol. 34, 389, 1938.
22. Rabinowitch, E.: J. Chem. Phys., vol. 8, 551, 560, 1940.
23. Heidt, L. J., ref.; Trivich, D.; and Flinn, P. A.: Solar Energy Research. F. Daniels and J. A. Duffie, eds. Univ. Wis. Press, Madison, 1955, pp. 203–219; review of Heidt's previous work on this reaction.
24. Weigert, F.: Naturwiss, vol. 15, 124, 1927.
25. Luther, R.: Z. physik. Chem., vol. 30, 628, 1899.
26. Hartung, E. J.: J. Chem. Soc., vol. 121, 682, 1922; vol. 123, 2198, 1924.
27. Hartung, E. J.: J. Chem. Soc., vol. 1349, 1926.
28. Baur, E.: Z. physik. Chem., vol. 63, 683, 1903; and Baur, E.; and Rebmann, A.: Helv. Chim. Acta, vol. 4, 256, 1921.
29. Baur, E.; and Neuweiler, C.: Helv. Chim. Acta, vol. 10, 901, 1927.
30. Veselouskii, I.; and Shub, O. M.: Zhur. Fiz. Khim., 26509, 1952; Markham, M. C.; and Laidler, K. J.: J. Phys. Chem., vol. 57, 363, 1953; Rubin, T. R.; Calvert, J. G.; Rakin, G. T.; and Mac Nevin, W. M.: J. Am. Chem. Soc., vol. 75, 2850, 1953; Vail, C. B.; Holmquist, J. P.; and White, L., Jr.: J. Am. Chem. Soc., vol. 76, 624, 1954; Calvert, J. G.; Theurer, K.; Rankin, G. T.; and Mac Nevin, W. M.: J. Am. Chem. Soc., vol. 76, 2575, 1954.
31. Stephens, R. E.; Ke, B.; and Trivich, D.: J. Phys. Chem., vol. 59, 966, 1955.

flooding problem. Impregnation of the electrodes with cobalt, nickel, or silver, and activation in carbon dioxide did not change cell performance. The cell had NO/NOCl bubbling through the anode and gave an OCV of about 0.23 volt and about 10 A/sq ft at 0.14 volt.

The completed system featured photolysis chambers made from television picture tubes exposed to light through the face and silvered at the back. Nitrosyl chloride gas in these tubes at 4 psig decomposed about 35 percent in 15 minutes of irradiation. The products were pumped into an absorber, NO was taken off, and the solvent (Kel-F–1 oil) from the absorber was fed to a heated desorber which gave off NOCl and Cl_2. A 10-cell stack using the photolysis products gave virtually zero current, while the auxiliaries used 300 watts of power.

While the development program was elaborate and led to the creation of special equipment (stills, scrubbers, pumps, and valves, as well as development of materials), the system is extremely complex and has no advantage over solar cells. It probably would not have been built if a preliminary investigation of photolysis and some simple and inexpensive tests had been made.

12.2.3 P.E.C. Corp., Photochemical Decomposition of H_2O, October 1960

Aqueous solutions of ceric, cerous, cupric, ferric, ferrous, manganous, thallic, and uranyl cations were irradiated by means of five different lamp systems ***(479).*** Results varied with the different lamps; efficiency of production of oxygen and hydrogen was low. This was ascribed to low absorption of the incident radiation (even with sensitizers present) and low quantum yields (less than 0.02) due to competing processes. Chromic and cobaltous ions, 0.05 *M* in 1 *M* perchloric acid, gave no gas. Ferrous ion gave some hydrogen.

12.2.4 Lockheed Missiles & Space Div., Solar Regenerative Chemical Systems, September 1959 to September 1962

The photochemically regenerative cell studied here featured an electrode of platinum foil and 1/32-inch-thick Lucite windows ***(403).*** The potential of this electrode versus a reference electrode was measured in darkness and under light irradiation of intensity comparable to sunlight. A number of dye-plus-reducing-agent systems were investigated (see tables 12.2 and 12.3), as well as water-insoluble dyes deposited on the

TABLE 12.2.—*Photoinduced* Potentials of Some Dye Reducing-Agent Systems ***(403)***

Dye	Reducing agent	Dark potential,[a] (V)	Photoinduced potential,[a] (V)	Photo potential,[a] (V)	pH	Remarks
Thionine	Ferrous ion	+0.338	+0.243	-0.095	2	Very reversible
	Ferrous-EDTA complex	−.104	−.150	−.046	6.8	Irreversible
	Chromic ion	+.325	+.340	+.015	4.0	
	EDTA	−.015	−.147	−.132	6.8	Irreversible
Proflavine sulfate	Ascorbic acid	−.091	−.435	−.344	6.8	Fairly reversible
	Cuprous amino ion	−.112	−.112	.00	8.0	
	EDTA	+.004	−.480	−.476	8.0	Irreversible
	Cobaltous hexamino ion	+.400	+.400	.00	8.0	
Phenosafranine	Ascorbic acid	+.014	−.278	−.292	6.8	Fairly reversible
	EDTA	−.012	−.420	−.408	6.8	Irreversible
	EDTA+ascorbic acid	−.135	−.500	−.365	6.8	Fairly reversible
	Ethylenediamine	−.110	−.238	−.128	6.8	Irreversible
	TMPD[b]	−.027	−.035	−.008	6.8	Irreversible
	Citric acid	−.018	−.104	−.086	6.8	Irreversible
	Oxalic acid	−.056	−.400	−.344	6.8	Irreversible
	Hydroquinone	−.115	−.123	−.008	6.8	Irreversible
Euflavin	Ascorbic acid	−.190	−.545	−.355	6.8	Fairly reversible
Riboflavin	Riboflavin[c]	+.046	−.418	−.464	6.8	Irreversible

[a] All potentials are measured versus Ag-AgCl reference electrode.

[b] TMPD is *N,N,N′,N′*-tetramethylphenylenediamine.

[c] For riboflavin, dye and reducing agent are combined in 1 molecule.

TABLE 12.3.—*Photopotentials of Complex Ion Reducing Agent Systems (403)*

Complex[a]	Reducing agent[b]	Dark potential,[c] E_{dark} (V)	Photoinduced potential: E (V)	Photo-potential: $E-E_{dark}$ (V)	pH	Remarks
cis-$Cr(en)_2Cl_2$ Cl	Ascorbic acid	-0.054	-0.100	-0.052	4	Very reversible
$Cr(NH_3)_5Cl$ Cl_2	Ascorbic acid	-.198	-.243	-.045	4	Precipitate
	Disodium ethylenediamini tetra-acetate	-.032	-.075	-.043	7	Irreversible
	Ascorbic acid-Fe^{++}	-.013	-.053	-.038	7	Irreversible
	Ascorbic acid	-.060	-.122	-.062	7	Slightly reversible
	Fe^{++}	-.144	-.256	-.112	6	Precipitate
	Hydroquinone	+.165	-.035	-.200	7	Slightly reversible
	Fe^{++} hydroquinone	+.212	+.011	-.201	7	Slightly reversible
	Fe^{++}	-.140	-.068	-.208	7	Irreversible
	Fe^{++} and trace ascorbic acid	-.036	-.290	-.254	7	Irreversible
$Co(NH_3)_6(NO_3)_3$	EDTA	+.263	+.263	.0	4	
	Fe^{++}	+.165	+.165	.0	4	
	Ascorbic acid	-.040	-.040	.0	4	
	Fe^{++}	+.244	+.260	+.016	2	Irreversible
	Fe^{++}	-.017	-.054	-.037	6	Irreversible
	EDTA	+.205	+.209	+.004	6	Irreversible

[a] Concentrations were 0.014*M*.

[b] Concentrations were 0.01*M*.

[c] Potentials are measured versus Ag-AgCl reference electrode.

platinum electrode by precipitation from saturated methanol solutions (table *12.4).*

A cell was made with the quinone-hydroquinone redox couple as one half-cell and the test electrode as the other. The test half-cell electrolyte contained. proflavine hydrochloride

TABLE 12.4.—*Miscellaneous Dye-Coated Electrode Systems (403)*

Dye[a]	E_{dark},[b] (V)	E^*,[b] (V)	ΔE, (V)	Current,[c, d] (μA)
Pinacyanol	+0.023	-0.330	0.353	7
Pinacyanol	+.012	-.290	.302	1
Aniline Blue	+.115	-.290	.405	45
Aniline Blue	+.080	-.340	.420	52
Coralline Red	+.095	-.145	.240	2
Coralline Red	+.105	-.150	.255	2
Rose Bengal	+.048	-.160	.208	0
Rose Bengal	+.015	-.180	.195	0
Victoria Blue R	+.070	-.325	.395	13
Victoria Blue R	+.065	-.325	.390	14
Ethyl Eosin	+.114	-.195	.309	0
Ethyl Eosin	+.133	-.215	.348	0
Sulfon Cyanine Blue G	+.090	+.078	.012	....
Sulfon Cyanine Blue G	+.083	+.071	.012	....
Victoria Blue B	+.120	-.360	.480	59
Victoria Blue B	+.098	-.355	.453	75

[a] Reducing agent is 0.1*M*/l ascorbic acid with pH 4.

[b] Potential vs. a silver-silver chloride electrode.

[c] Electrode area: 2 cm^2.

[d] The cell resistance in all cases, except as noted, was between 800 and 1200.

as sensitizer (2×10^{-4} *M*) and ascorbic acid as reducing agent. The half-cell reactions were hypothesized to be

$$RH+D\xrightarrow{h\nu}R+DH$$
$$DH\rightarrow D+H^{+}+e^{-}$$

where RH is ascorbic acid, R the oxidized form, D the dye, and DH the reduced dye. The Nernst potential is

$$E=E_0+0.059(\mathrm{pH})-0.059\log[\mathrm{D/DH}]. \quad (12.6)$$

This relation was tested by measuring D colorimetrically; the relative concentration of reduced dye was $DH=D_T-D$, where D_T is the initial dye concentration and D the concentration at a stationary OCV. Log $[D/(D_T-D)]$ as a function of E was a straight line of slope 0.059 volt. Figure 12.3 shows the electrochemical performance of the cell. The quantum efficiency was measured from the current and the amount of light absorbed, and was about 1 percent at the maximum. The rate of photobleaching was best at pH 4 and was improved by the addition of 1*M* potassium bromide.

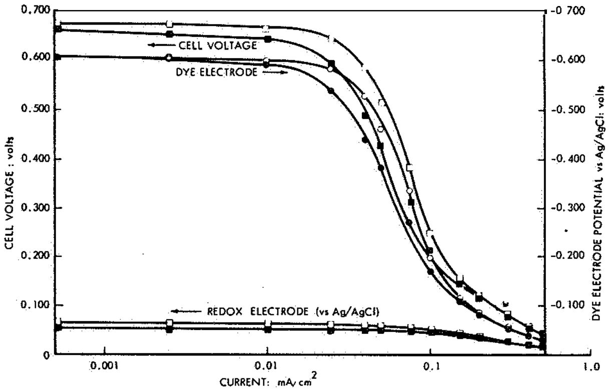

Pt/pro HCl-ascorbic acid//quinone-hydroquinone/Pt:
Light intensity: 120 mW/cm²
Temperature: 10° to 15° C
Dye flow rate: 10 cc/min
Redox flow rate: 44 cc/min

Current increasing: □ ○
decreasing: ■ ●

FIGURE 12.3.—Electrode potentials and cell voltage as a function of current: Light intensity of 120 mW/cm².

An electrode with a solid coat of Victoria Blue B was tested with inorganic redox couples under irradiation and failed. Ascorbic acid was used at pH near 4; pH 1 gave no current, and pH 5 caused hydrolysis of the acid. Open-circuit voltage was −0.45 versus a dark electrode, but maximum current density was only 0.2 mA/cm². This was not significantly improved by increasing the concentration of ascorbic acid from 0.1 to 2 moles. Concentration polarization of the reduced form of the dye was not expected, since it was present as a thin coat on the electrode. The potential was independent of wavelength of incident radiation below 7000 angstroms (the dye was known to absorb in the region 5000 to 7000 angstroms), but the amount of light absorbed depended on wavelength, and power output was maximum for 6000-angstrom light. Limiting current was proportional to radiation intensity, I, up to 100 mW/cm², then leveled off. Similarly, OCV was proportional to log I up to this level, with a slope of 0.055 volt. The amount of light absorbed increased as the dye coat was made thicker, but conversion efficiency decreased. An optimum value of 0.2 percent was obtained at $(5)(10^{-6})$ gram dye per cm². The thicker layer probably led to IR polarization of the electron transfer through the coat to the electrode.

A double cell was made using the stannous-stannic couple,

$$\text{Light}\begin{cases}2RH+\text{sensitizer}\rightarrow 2R\pm 2H+2e^{-}\\ Sn^{4+}+2e^{-}\rightarrow Sn^{2+}\end{cases}$$
$$\text{Dark}\begin{cases}Sn^{2+}\rightarrow Sn^{4+}+2e^{-}\\ 2R+2H^{+}+2e^{-}\rightarrow 2RH\end{cases}$$
$$\overline{\qquad\text{light}\rightarrow\text{potential}\qquad}$$

Again, maximum current density was about 2 A/sq ft. Why a double cell was used rather than a single cell with one side light and the other dark is not clear. It was concluded that no feasible photochemical system was known.

12.2.5 Electro-Optical Systems, Inc., Solar Regenerative Fuel-Cell Systems, May 1960 to May 1961

Water photolysis was studied, with the purpose of separating hydrogen and oxygen (*169, 170*). Separation was accomplished by passing oxygen and hydrogen through a palladium tube (10-mil wall thickness) at 1832° F (1000° *C*), while the outside of the tube was maintained under vacuum. Hydrogen diffused through and oxygen was retained. A quartz window was fitted to the end of the tube, through which water vapor was irradiated by means of a hydrogen discharge lamp. A decomposition chamber was built around a mercury lamp. The threshold wavelength was known to be 1875 angstroms, but mercury was added (6×10^{-3} torr) to cause decomposition by excited mercury atoms (mercury absorbs at 2537 angstroms).

No significant decomposition of water was found at radiation levels of about 10^{15} quanta per second (less than 10^{-5} quantum yields), with the presence of mercury or palladium making no difference, presumably due to rapid back reaction. A good review of water photolysis was given and some theoretical work was done (see fig. 12.2).

Calculations of theoretical efficiencies are given in *(191)* and (170). It was demonstrated that a high-temperature solar collector has low absorption efficiencies.

12.3 NUCLEAR REGENERATIVE FUEL CELL, Union Carbide, June 1960 to September 1962

This fuel cell used nuclear fuel and was aimed at long-life, low-power (5 watts) underwater applications (*662*). The reactions were

Anode: $\frac{1}{2}H_2 \rightarrow H^+ + e^-$ $(E_0 = 0)$
Cathode: $Fe^{3+} + e^- \rightarrow Fe^{2+}$ $(E_0 = 0.771)$
Regenerator:

$$\frac{H^+ + Fe^{2+} + \text{radiation} \rightarrow \frac{1}{2}H_2 + Fe^{3+}}{\text{radiation} \rightarrow \text{electrical energy}}$$

The literature specifies ferric ion and hydrogen yields of 8.2 ions and 4.1 molecules, respectively, per 100 eV of gamma radiation, giving an efficiency of (0.771)(8)/(102), or 6.2 percent. Other systems considered (ref. 12.4) had efficiencies less than 2 percent.

In 0.4 M H_2SO_4, the reaction scheme is

$$4.5H_2O \xrightarrow{\text{rad}} 3.7H + 2.9OH + 0.4H_2 + 0.8H_2O_2$$

followed by

$$Fe^{2+} + OH + H^+ \rightarrow Fe^{3+} + H_2O$$
$$Fe^{2+} + \frac{1}{2}H_2O_2 + H^+ \rightarrow Fe^{3+} + H_2O$$
$$Fe^{2+} + H + H^+ \rightarrow Fe^{3+} + H_2.$$

An undesirable competing reaction occurs in concentrated Fe^{3+} solutions

$$Fe^{3+} + H \rightarrow Fe^{2+} + H^+,$$

and efficiency is less when ferrous ion builds up in the system. Although over 100 references to the radiation-induced reaction of ferrous ion and sulfuric acid were found, none were in the high-concentration range. Therefore, 3500 curies of cobalt 60 (1.17 and 1.33 MeV gamma rays) were placed in a water well 1 foot in diameter by 12 feet deep. The gamma radiation was 45 watts, and about 10 watts were absorbed. Ferric ion was determined spectrophotometrically (0.8 N H_2SO_4, 2750 angstroms). The maximum efficiency obtained was 4.2 percent at ferric concentration of 0.01 M, but this low concentration led to large polarization at the fuel-cell electrode, and lower efficiencies had to be tolerated. Increase of temperature gave somewhat higher yields due to an increase of H and OH with a decrease in H_2 and H_2O_2. Pressure had little effect up to 100 atmospheres. Dosages greater than 10^5 rads/sec decreased the yield, but this was a thousand times the rates to be used in the regenerator.

A cell designed to operate directly in the irradiation field was constructed with hollow-rod electrodes of porous carbon (surface area 200 m^2/g; small-diameter pores made up most of pore volume) as shown in figure 12.4. The anode

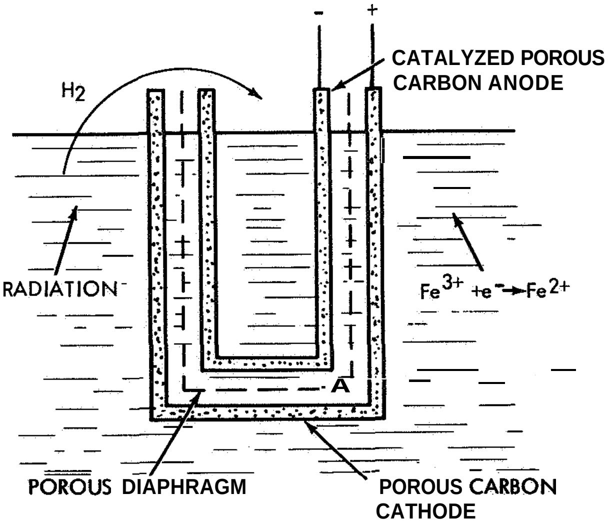
-
+
CATALYZED POROUS CARBON ANODE
H2
RADIATION
$Fe^{3+} + e^- \rightarrow Fe^{2+}$
A
POROUS DIAPHRAGM
POROUS CARBON CATHODE

$$Fe^{2+} + H \xrightarrow{+\text{rad}} Fe^{3+} + \frac{1}{2}H_2.$$

Hydrogen is evolved from solution and reacts at the platinum-catalyzed anode. while Fe^{3+} is reacted at the anode. The electrolyte space between the electrodes is small, to give low IR loss.

FIGURE 12.4.—Irradiated fuel cell (Union Carbide (662)).

was catalyzed with platinum and wetproofed with paraffinic material. The wetproofing failed under irradiation, as did other organic materials. A layer of pyrolytic carbon laid down from carbon monoxide was tested; it improved wetproofing but made catalyst distribution difficult. Small cracks in moisture-resistant Sauereisen 31 cement allowed leakage, so it did not wetproof or seal well. Eventually Apiezon-W was used, even though it was affected by irradiation. Performance of this cell was poor; other electrodes tested also flooded while being operated under irradiated conditions. A cell was run at 50 atmospheres so that the concentration of hydrogen produced by irradiation built up to 0.05 *M*. The steady state Fe^{3+}/Fe^{2+} ratio in 0.4 *M* H_2SO_4 was 50:1. The potential of a completely immersed platinum screen anode was determined by the Fe^{3+} and not hydrogen, thus giving small anode-to-cathode potential. The anode was then floated on the electrolyte surface, on top of an asbestos mat, but this also gave poor performance.

Figure 12.5 shows the design of a cell used external to the radiation chamber. Hydrogen generated in the chamber was used as a bubble pump to raise electrolyte for circulation, and the top of the pump tube had a free volume where hydrogen separated. The cathode was 2-inch i.d. by 12 inches long, with a wall thickness of one-fourth inch. Union Carbide Graphicell Grade 60 was used (33-micron pores, porosity 48 percent). The anode was 1½ inch o.d. and ¼ inch thick, catalyzed with platinum, and wetproofed. This cell gave satisfactory output (6 to 15 A/sq ft, 0.35 V) for 40 days, during which time the electrolyte had penetrated halfway into the electrodes.

Design calculations showed that about 60 pounds of unseparated fission products would be required to give 5 watts after 2 years, assuming a 3-percent fuel-cell yield from irradiation (the isotopes decay in the 2-year use period). Cobalt 60 and cesium 137 were too expensive (about $20 000 for the required charge). The irradiation vessel was 5 feet in diameter by 6 feet high, containing 680 gallons of solution. The project terminated at this stage, presumably due to the high cost and probable unreliability of the system.

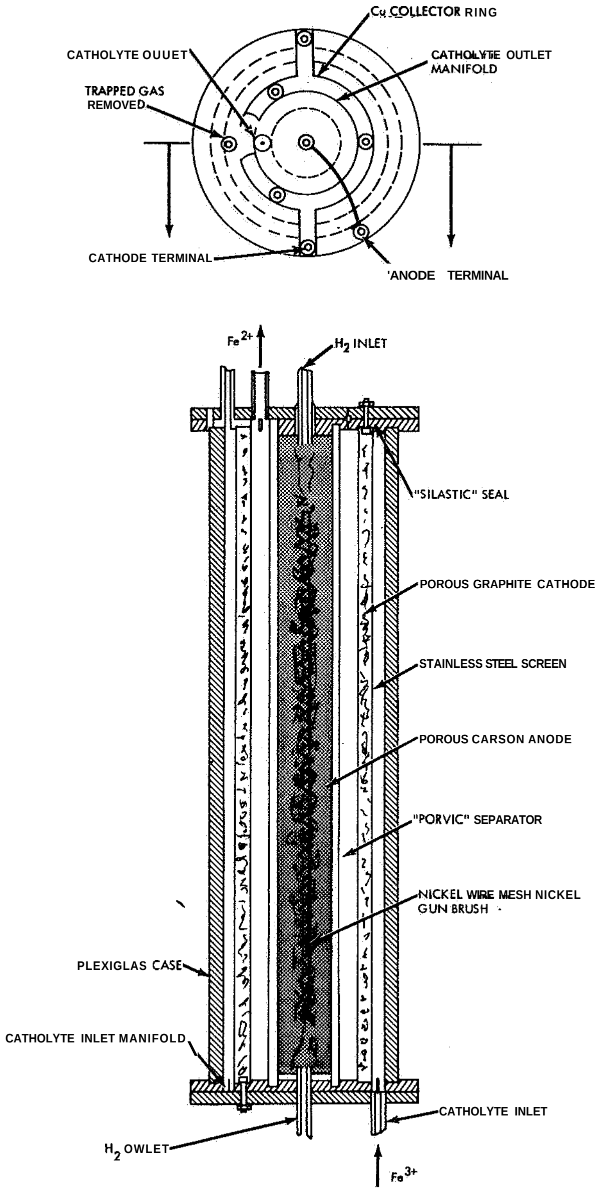
Cu COLLECTOR RING
CATHOLYTE OUTLET
CATHOLYTE OUTLET MANIFOLD
TRAPPED GAS REMOVED
CATHODE TERMINAL
ANODE TERMINAL
Fe^{2+}
H_2 INLET
"SILASTIC" SEAL
POROUS GRAPHITE CATHODE
STAINLESS STEEL SCREEN
POROUS CARBON ANODE
"PORVIC" SEPARATOR
NICKEL WIRE MESH NICKEL GUN BRUSH
PLEXIGLAS CASE
CATHOLYTE INLET MANIFOLD
CATHOLYTE INLET
H_2 OUTLET
Fe^{3+}

Hydrogen generated by gamma radiation was used as fuel. The oxidant Fe^{3+}, also generated by irradiation, was fed to the outer annulus and flowed through the porous carbon cathode, being converted to Fe^{2+} which was returned to the irradiation chamber.

FIGURE 12.5.—Union Carbide hydrogen-Fe^{3+} cell.

12.4 REDOX FUEL CELLS

An extensive investigation of low-temperature, acid-electrolyte, redox fuel cells was carried out by General Electric Co. *(249,* October 1958 to April 1960). The titanous-titanyl couple in sulfuric acid or hydrochloric acid was used at the anode:

$$Ti^{3}+H_2O \rightarrow TiO^{2+}+2H^{+}+e^{-} \qquad (E_0=0.1)$$

Regeneration was by hydrogen:

$$TiO^{2+}+H^{+}+\tfrac{1}{2}H_2\rightarrow Ti^{3+}+H_2O.$$

The regenerator was a packed column of platinum-palladium catalyst, with gas and electrolyte flowing through the column. Rates of regeneration corresponded to 2 to *3* cubic feet of regenerator volume per kilowatt. Carbon monoxide and hydrogen sulfide poisoned the regeneration. Many organic and inorganic cathode couples with potentials close to 1.23 volts were investigated but none were satisfactory, since they were unstable or could not be regenerated with air. It was proposed, therefore, to use the bromine-bromide couple with nitric oxide catalyst

$$Br_2+2e^{-}\rightarrow 2Br^{-}$$

$$\tfrac{1}{2}O_2+2Br^{-}+2H^{+}\xrightarrow{NO}Br_2+H_2O.$$

Electrochemical performance was tested in simple cells with plate carbon electrodes separated by a membrane. Titanous-titanyl solution flowed through the cell space between one electrode and the membrane, and bromine-bromide through the other space. Current densities up to 100 A/sq ft were obtained, with better results at higher flow rates.

Design calculations showed that a 1500-watt system, based on re-formed hydrocarbons to supply hydrogen, would have a power density of 0.04 kW/cu ft at 25 percent efficiency. A diesel-electric unit has similar efficiency, but a power density at least tenfold higher. The effort on this contract was redirected to investigate direct oxidation of hydrocarbons in membrane cells.

The anodic couples Sn^{2+}/Sn^{4+} and Ti^{3+}/TiO^{2+} and cathodic couples Br_2/Br^{-}, Ce^{3+}/Ce^{4+}, and $Cr^{3+}/Cr_2O_7^{2-}$ were studied at solid, porous, and flowthrough electrodes (Diamond Ordnance Fuze Laboratories, ***333,*** April 1960). Steady current-voltage curves were obtained for each half cell. Ti^{3+}/TiO^{2+} and Br_2/Br^{-} gave the best results. Considerable activation polarization was present with the tin couple.

The feasibility of regeneration of redox couples by hydrocarbons was studied by calculation of the free energies of conversion to alcohol (University of Florida, 679, March 1960, and ***682,*** April 1962). For example, the free energy of the reaction

$$Sn^{4+}+H_2O+CH_4(aq)\rightarrow$$
$$Sn^{2+}+CH_3OH(aq)+2H^{+}$$

was estimated as

$$\Delta F=27\,600+2.3RT\log\left[\frac{(H^{+})^{2}(Sn^{2+})(x_1)}{(Sn^{4+})(x/x_s)}\right] \quad (12.7)$$

where x_1 is the mole-fraction of methanol in solution, x the mole-fraction of methane in solution, and X, the mole-fraction of methane in equilibrium with 1 atmosphere of methane (2.35 10^{-5}). Taking all activities except that of methanol as close to 1.0, the equilibrium concentration of methanol at 77" F (25" C) is 10^{-20} mole-fraction. Thus, for the regeneration reaction to proceed via an alcohol intermediate, the alcohol in turn must react so rapidly as to maintain its concentration less than 10^{-20} mole-fraction. Similar conclusions were reached for the titanium redox couple and for ethane and hexane.

The regeneration of stannous ion from stannic, or titanous ion from titanyl, using soluble oxygenated hydrocarbons, was investigated by heating the reactants in heavy-walled, sealed glass tubes (Pennsylvania State University, *480,* August 1962). The concentrations were about 0.1*N* redox ion, 0.2 to 1*N* organic, and 1 to 5*N* acid (hydrochloric or sulfuric). No significant reduction of stannous or titanous ion occurred in 24 hours at temperatures up to 392" F (200° C) with formic acid, formaldehyde, or methanol. Titanium ions demonstrated best stability in **4** *N* acid, but under all conditions they slowly and irreversibly hydrolyzed to rutile (TiO_2). **A** slight reduction of titanyl to titanous occurred in 24 hours with oxalic acid and glyoxal at 212" F (100° C), and the resulting complexes prevented hydrolysis to rutile. High-area (1000 m^2/g) active carbon impregnated with platinum was added to several of the systems, but again no significant regeneration was observed. Similar results were obtained with the tin couple; it hydrolyzed rapidly and decomposed the organics at 200" C ($2HCHO\rightarrow CH_4+CO$, for example), but was not regenerated. Hence, direct reduction by oxygenated hydrocarbons was not feasible. Since hydrocarbons are less soluble in and less reactive than alcohols and acids, practical use of direct reduction by hydrocarbons is extremely unlikely.

The bromine-bromide cathode couple was also investigated (University of Florida, 680, June 1960). A 10-kilowatt unit designed according to the calculations of Posner (ref. 12.5) would require a regeneration tower 40 feet high by 1.5 feet in diameter, in which HBr in electrolyte flowing downward would be oxidized by a countercurrent stream of oxygen. The reaction is

$$2Br^{-}+2H^{+}+\tfrac{1}{2}O_2(+N_2)\xrightarrow{NO}Br_2+H_2O(+N_2).$$

Therefore, with air as the oxidant, exit nitrogen from the packed tower would have to be scrubbed to recover bromine and catalytic nitrogen oxide. The scrubber would have to be about 20 feet by 1 foot diameter. The analytical technique used by Posner ***(692,*** 1961) to determine bromine regeneration proved to be inaccurate in the presence of nitric oxide. Redetermination of the rates of bromine regeneration reaffirmed that nitrogen oxide was necessary, but gave lower rates than those found by Posner. The size of the regeneration tower and scrubber were prohibitive.

Esso Research & Engineering Co. investigated a nitric acid-oxygen redox electrode for use with acid electrolytes ***(214).*** Nitric acid was the cathodic reactant and the reduction products of nitric acid were oxidized with oxygen. Several cathodes of platinum or carbon were used with 1 weight-percent HNO_3 in **30** weight-percent H_2SO_4 electrolyte. On taking current from the anode the potential fell, but then increased slowly with time (autocatalytic effect). The limiting current decreased with stirring, indicating that a reactive intermediate was removed from the electrode. Saturation of electrolyte with NO removed the autocatalytic effect, and the limiting current was proportional to the concentration of HNO_3 (500 A/sq ft for 5 percent HNO_3, 179.6" F (82" C)). The mechanism was proposed as

$$HNO_3\xrightarrow{heat}HNO_2(\text{trace})+\tfrac{1}{2}O_2$$

$$HNO_2+H^{+}+e^{-}\longrightarrow NO+H_2O$$

$$2NO+HNO_3+H_2O\xrightarrow{slow}3HNO_2.$$

Regeneration was by

$$NO+O_2\rightarrow NO_2$$

$$NO_2+H_2O\rightarrow HNO_3.$$

Platinum and tungsten were active electrodes, but lead coated with PbO_2 was not. Performance improved with higher temperatures and acid concentration.

The regeneration of nitric acid was not complete and nitric acid was consumed as NO diffused away from the electrode into the electrolyte or into the O_2 stream at the cathode. Most efficient regeneration was obtained with a wetproofed porous carbon electrode, which gave 18 coulombs per coulomb of HNO_3 consumed. Reaction products reaching the fuel electrode adversely affected its performance. Regeneration was improved by bubbling oxygen through electrolyte with a surfactant (1 percent sodium nonyloxydibenzene disulfonate) to form foam ***(215).*** This gave 40 coulombs per coulomb HNO_3 with O_2 and 12 with air. Sodium nitrate could be used in place of HNO_3 ($H_2SO_4+2NaNO_3\rightarrow Na_2SO_4+2HNO_3$). One percent of fine silica powder (Cab-0-Sil) stabilized the foam; dense foams were most effective. A cell was constructed of thin, porous electrodes separated by an IEM. Sulfuric acid containing dissolved fuel (CH_3OH) was passed through the anode chamber and air-HNO_3-H_2SO_4 was passed through the cathode chamber, over the face of the cathode (80-mesh Pt screen). At 82" C, the cathode gave about 100 A/sq ft at 0.2-volt polarization.

External regenerators were constructed in which air-NO-electrolyte foam reacted and broke down, to give HNO_3-electrolyte draining back to the cell and N_2-O_2 exhausting to the atmosphere. This gave an efficiency of about 6 coulombs per coulomb HNO_3 consumed, with air. Although good electrochemical performance was obtained from the nitric acid electrode, the adverse effect of intermediates diffusing to the anode led to the abandonment of the redox electrode. The added complexity of a system with external regenerators and foaming electrolyte, plus the inevitable loss of nitric acid, also make the nitric acid redox electrode unattractive.

12.5 CONCLUSIONS

The early and exciting prospects surrounding photo- or heliochemical decomposition of water to provide hydrogen and oxygen for fuel cells have, in general, dwindled to disappointing conclusions. Part of the original hope *can* be attributed to overpublicized inaccurate or ill-considered results; more was based on the following errors in early assumptions: (1) Wrong theoretical efficiencies of photochemical decomposition, based on total energy of radiation; only the free energy of the products is recoverable. (2) Use of efficiency at the threshold frequency in lieu of total efficiency; theoretical analyses (contract reports 403 and 174) showed this figure to be too high by a factor of at least 2.3, usually much more. Theoretical efficiencies fell to 5 to 10 percent. (3) Low experimental net rates of formation of photolytic products.

The low maximum efficiencies (which will probably be halved by losses in the fuel cell and by parasitic power), the low rates of formation, and the complexity of the systems make them unattractive in comparison with solar cells or solar boilers.

No determined effort was made to develop highly active electrodes for redox couples. Electrochemical cells of suitable power output could probably be developed, since redox reactions have high rates even at low-area electrodes. However, even if cell volume and cost were zero, a redox system would be hampered by the size, cost, and doubtful feasibility of regenerators. Economical regeneration of electrode reactants does not seem possible due to the slow rates of regeneration; in addition, use of air at the cathode leads to problems of carryover in the effluent nitrogen.

12.6 REFERENCES

12.1. TRIVICH, D.; AND FLINN, P. A.: Maximum Efficiency of Solar Energy Conversion by Quantum Processes. Solar Energy Research. Univ. of Wisconsin Press, Madison, Wis., 1955, p. 143.

12.2. CALVERT, J. G.: Introduction to the Utilization of Solar Energy. A. M. Zarem, ed.. McGraw-Hill Book Co., Inc., 1961.

12.3. MARCUS, R. J.; AND WOHLERS, H. C.: Photochemistry in the Solar Furnace. Ind. Eng. Chem., vol. 51, 1959, pp. 1335–1338.

12.4. FRICKE, H.; AND HART, E.: J. Chem. Phys., vol. 3, p. 596, 1935.

12.5. POSNER, A. M.: J.A.C.S., vol. 77, 1955, p. 2634.

CHAPTER 13

Hybrid Fuel Cells

13.1 INTRODUCTION

The term "hybrid fuel cell" as used here refers to the combination of a conventional primary-cell electrode with a fuel-cell electrode. (A cell using a reacting metal anode and a fuel-cell oxygen cathode is an example.) The term also covers cells using conventional battery electrodes which are continuously replaced, as in the dry-tape battery.

13.2 RESEARCH ON ELECTROCHEMICAL FUEL CELLS, Aerojet-General Corp., November 1951 to August 1956

The aim of this research program (8) was the production of a high-energy density battery for submarine applications. The engineering problems of continuously feeding solid electrodes were too difficult to overcome, so fixed consumable anodes were used. The cell featured thick zinc anodes and chlorine oxidant at porous-carbon cathodes. It operated at about 140° F (60° C). Electrolyte was sea water containing up to **30** weight-percent zinc chloride. Bipolar electrodes were made by bonding zinc (flame sprayed with zinc to give a rough surface) and carbon electrodes together with resin, with sufficient resin in the surface pores of the carbon to prevent chlorine gas from reaching the zinc yet still give electrical conduction (resistance of **0.33** ohm-cm^2). The electrolyte surface of the carbon electrode was covered with a mixcake of finely powdered activated carbon and neoprene binder (to prevent flooding of the electrode by electrolyte), and the base carbon was wetproofed with **350** cm^3/sq ft of **15** percent Fluorolube (Hooker Chemical Co.) in petroleum ether. Holes were drilled across the top and bottom of the carbon electrode (1-foot by 1-foot by ½-inch electrode dimensions) and chlorine was manifolded (through the electrodes and gaskets) in and out of these holes so as to flow through the porous carbon from top to bottom.

Similarly, the electrolyte side of the zinc electrode was grooved across the top and bottom to take plastic tubes with open ends. Electrolyte was channeled into these tubes and flowed across the faces of the electrodes from bottom to top. High-flow-resistance orifices regulated the electrolyte flow and gave high ohmic resistances, thus checking internal short circuiting (due to common electrolyte manifolding) by reducing parasitic current. Small variations in other resistances did not greatly affect the flow rate. Purging **5** to 10 percent of the chlorine also helped maintain performance.

The principal problem was that electrolyte flooded the carbon cathode; dissolved zinc ions then plated on the carbon, leading to dendritic shorting. Chlorine dissolved in the electrolyte and diffused to the zinc; therefore, faradaic efficiency was never better than **85** percent. Empirical operating equations were

$$R = 0.40 + 2.2L, \text{ ohm-in}^2 \qquad \textbf{(13.1)}$$

$$V = 1.9 + RI, \text{ volts} \qquad \textbf{(13.2)}$$

where R is the effective ohmic resistance and L is electrolyte thickness. A 2-kilowatt unit of 120 cells was built with sufficient thickness of zinc to last 10 days. Current density reached **45** A/sq ft, but the unit performed poorly due to flooding of the cathode. (When high currents were drawn, loss of chlorine from the cathode pores caused suction of electrolyte into the electrode.) The cells were about **1** inch thick, and current density of **45** A/sq ft gave a power density of about ½ kW/cu ft. Since these were not true fuel cells, the size, number, and current density of cells were dictated by the need to

PRECEDING PAGE BLANK NOT FILMED.

store zinc required for the mission rather than by possible power density.

This work predates most other fuel-cell developments discussed in this book; it must have been one of the first attempts to build a complete unit with manifolding through the electrodes, control of feed to each cell, etc. The principal cause of failure was probably the design of the chlorine electrode, which must have given pressure drop and uneven current distribution from top to bottom of the electrode (leading to flooding), as well as severe mass-transfer limitations at higher currents. Equation **(13.1)** contains a rather large constant resistance of **0.4** ohm-in^2 (2.6 ohm-cm^2) which was not explained, and the general electrochemical properties of the system were not elucidated.

Other anode metals investigated were magnesium and aluminum. Magnesium gave excessive hydrogen evolution and potentials considerably lower than theoretical; in addition, magnesium hydroxide precipitation occurred except in strong acid solution. Aluminum formed a high-resistance surface film, probably oxide, which passivated the electrode. Amalgamation of the surface prevented passivation, but hydrogen evolution was then excessive. Hydrogen at thin, porous, carbon anodes was tested, but results were poor since no catalysts were used. Oxygen test electrodes showed that platinum or palladium black or sintered nickel was better than carbon or silver-plated nickel.

13.3 CONTINUOUS FEED BATTERY, Armour Research Foundation of the Illinois Institute of Technology, April 1956 to July 1957

The cell proposed *(335)* was aluminum-hydrogen peroxide with sea-water electrolyte **(3.5** weight-percent sodium chloride). An aluminum alloy (Alclad 7075) containing 90 weight-percent aluminum (plus Cu, Mg, Cr, and Zn) gave only a low voltage; therefore, a magnesium anode was substituted. The cathode was fiber copper, porous graphite, or porous asbestos containing deposited manganese, silver, or nickel; peroxide was run through the cathode. A simple plate cell gave OCV much less than theoretical, combined with anodic hydrogen evolution, and performance was 10 A/sq ft at less than **1** volt.

Another cell investigated was

$$\begin{array}{ll}\text{Anode:} & Mg \rightarrow Mg^{2+} + 2e^- \\ \text{Cathode:} & \underline{2H_2O + 2e^- \rightarrow 2OH^- + H_2(g)} \\ & Mg + 2H_2O \rightarrow Mg(OH)_2 + H_2\end{array}$$

Cathodes tried were silver, smooth platinum, rough nickel, and platinized copper screen. Both electrodes evolved hydrogen on open circuit, and the cell gave 15 A/sq ft at 0.5 volt. Precipitated magnesium hydroxide did not appear to interfere with cell performance. (The investigators apparently had very little knowledge of electrochemistry.)

13.4 ORGANIC FUEL-CELL SYSTEMS, Resin Research Laboratories, Inc., April 1959 to June 1960

The purpose was to investigate the feasibility of the hybrid cell using organic cathode reactants for Air Force applications *(561).* The cell reaction was

$$\begin{array}{c} 3Mg \rightarrow 3Mg^{2+} + 6e^- \\ \underline{\phi NO_2 + 4H_2O + 6e^- \rightarrow \phi NH_2 + 6OH^-} \\ 3Mg + \phi NO_2 + 4H_2O \rightarrow 3Mg(OH)_2 + \phi NH_2 \end{array}$$

where ϕNO_2 was nitrobenzene (or a similar nitro aromatic). The theoretical energy storage density was **643** W-hr/lb. The electrolyte was aqueous magnesium bromide; a paper separator was used between magnesium anode and cathode. The liquid organic was fed into a porous carbon cathode which had been coated with an activated carbon (Darco G-60) and Teflon suspension sintered onto the surface to prevent flooding. Power output was low, and hydroxide precipitate blocked the cathode pores. As in the previous contract, the report unintentionally reveals that the investigators had virtually no knowledge of electrochemistry or electrochemical techniques: the experiments as designed did not yield useful electrochemical information. The only conclusion was that the cell did not work, but no reasons could be assigned for this failure.

13.5 DEVELOPMENT AND FEASIBILITY PROOF OF THE DRY-TAPE BATTERY CONCEPT, Monsanto Chemical Co., June 1963 to January 1964

The cell employed conventional primary-cell materials, but was in reality a fuel cell since the reactants were continuously supplied to the electrodes ***(462).*** The principle of the device is illustrated in figure 13.1. The unit built had a consumable zinc anode-current collector instead of an anode tape; therefore, it was a hybrid system. The cathode reactant was silver oxide (AgO) and electrolyte was 30 to 40 weight-percent aqueous potassium hydroxide.

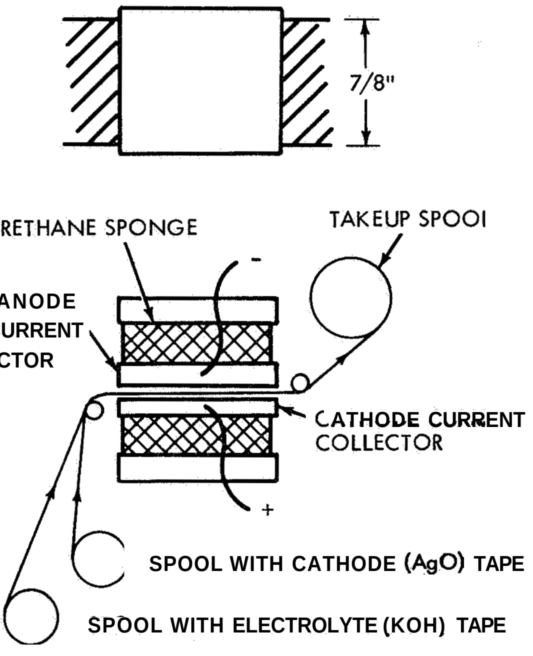
7/8"
1/4" URETHANE SPONGE
TAKEUP SPOOl
ZINC ANODE AND CURRENT COLLECTOR
-
CATHODE CURRENT COLLECTOR
+
SPOOL WITH CATHODE (AgO) TAPE
SPOOL WITH ELECTROLYTE (KOH) TAPE

Two porous tapes are used, one containing electrolyte and the other cathodic reactant. These are joined just before the current collectors and are passed through at the required rate to give the desired power output. The metal current collectors, backed by springy urethane foam, press the tapes tightly together without giving too much resistance to tape movement. The foam is glued to the current collector and the backing plate with epoxy resin, and separation of the backing plates is set to give the required pressure (6 oz/in^2).

FIGURE 13.1.—Illustration of Monsanto dry-tape battery (spools not to scale).

The cathode tape was made by soaking the fabric with distilled water, drawing off excess water with a Gardner knife, and clamping the wet fabric in slight tension. Silver oxide slurry was spread on the fabric with the knife, and the sheet dried by warm air in darkness (to prevent photochemical loss of AgO) at room temperature. The slurry was made by ultrasonically dispersing 31 weight-percent AgO (Ames Chemical Works) and **a** binder of 6 percent Gelvatol (a polyvinyl alcohol made by Shawinigan Resins) in ***63*** percent water, giving about 85 percent AgO on a dry basis. Electron micrographs of the silver oxide indicated a size range of 0.3 to 4.0 microns, which showed it could penetrate porous fabrics. The thickness of the coat was controlled between 2 and 8 mils, and had an effective density of 1.5 g/cm^3. The thickest coats had an energy density of 0.08 $W\text{-}hr/in^2$. The tape could be stored at room temperature and 88 percent relative humidity with a loss of about 1 to 2 percent capacity per month. However, at 85° F (29° C), the loss rate went up to 30 percent per month with polypropylene tape and even higher with nylon tape (nylon was oxidized by AgO). Storage life was improved by using Methocel (Dow Chemical Co.) as binder, but the tape was then less readily wetted by electrolyte, requiring a longer tape-to-tape contact before passing between the current collectors.

A reel of the 10-mil-thick electrolyte storage tape in a plastic case was stored for 3 months with no deterioration when the tape exit slit was closed. This was accomplished by having nonpermeable leaders of polyvinylchloride (PVC) attached to the tape; the leaders went through the exit slit, which was then closed with a cylinder of soft neoprene rubber. The cathode tape was similarly stored. The unit was activated by removing the cylinder and starting the drive motor, which pulled the tapes through the current collectors.

Theoretical capacities for the combined weights of zinc, AgO, and electrolyte were between 65 W-hr/lb for zincate (K_2ZnO_2) as the product, and 169 W-hr/lb for zinc hydroxide as the product. The actual capacities of the zinc plus cathode and electrolyte tapes were between 20 and 40 W-hr/lb. Open-circuit voltage varied from 1.65 to 1.86, depending on whether the cathode-current collector was plain silver or gold-plated silver, since the use of plain silver tended to give OCV corresponding to Ag_2O and not **AgO.** For appreciable current drain the voltage-current relation was linear, with an extrapolated OCV of 1.5 volts. Voltage was 1.3 at a current density of 300 A/sq ft (providing, of course, that the tape was run fast enough to oversupply the required capacity). The best recovery of cathode capacity, about 85 percent, was obtained by having cathode tapes with smooth surfaces and a minimum (compatible with adherence of oxide) amount of binder, and by matching the tape speed to the current. Higher tape speeds (up to 2 inches per minute) and current gave less recovery of theoretical current. No analysis of speed-size relations was given but, presumably, a larger current collector area would improve recovery at higher speeds. If the tape has velocity v, width W, capacity per unit area C, and if the current collector is L long, the theoretical limiting current density is

$$I_L = vWC/WL$$
$$= (v/L)C. \qquad (13.3)$$

It is possible that the best fractional recovery of capacity is obtained when the current density and I_L are reasonably low. Then, for a given velocity, increasing L will lower current densities and improve recovery. This could be tested by measuring fractional recoveries as a function of v/L for different v and L combinations.

It was concluded that the feasibility of the system had been demonstrated. Higher capacities could be obtained by storing free electrolyte and wetting the cathode tape with electrolyte before it reached the current collectors, to eliminate the weight of electrolyte tape. It was suggested that the concept be applied to high-capacity reactions such as Mg/metadinitrobenzene, which has a theoretical capacity of 766 W-hr/lb, including 8 moles of water per mole of organic.

13.6 GRAPHITE-OXYGEN HIGH-TEMPERATURE FUEL CELL, Iowa State University, 1963

Much of the early work on fuel cells (see ref. 2.14, for example) attempted, without significant success, to utilize carbon as a fuel. The hybrid cell investigated in these contracts also used solid carbon as fuel plus oxygen as oxidant. The high-temperature cell proposed was

$$C/Na_2MoO_4;\ MoO_3/O_2(Pt)$$

where the carbon was in the form of a graphite rod *(345)*. The actual cell consisted of a Vycor U-tube containing the molten-salt mixture in a furnace. The graphite anode was partially immersed in electrolyte in one arm of the U, and an atmosphere of carbon dioxide was maintained over the exposed portion. Similarly, a partially immersed platinum wire in an atmosphere of oxygen was used at the cathode in the other arm of the U. Graphite reduced the salt to molybdenum, so this system was not feasible.

Other salts proposed were sodium tungstate and sodium tetraborate. The cell reactions were envisaged as

$$\begin{array}{r} C + 2WO_4^{-} \rightarrow CO_2(g) + 2WO_3 + 4e^{-} \\ 2WO_3 + O_2(g) + 4e^{-} \rightarrow 2WO_4^{-} \\ \hline C + O_2(g) \rightarrow CO_2(g) \end{array}$$

Extrapolation of lower temperature values of the standard-state free energy of carbon dioxide formation predicted an OCV of 1.025 at 1472" F (800" C), but experimental values were in the range of 0.869 to 0.876 volt. The difference was ascribed to supersaturation of dissolved carbon dioxide at the graphite surface. The variation of OCV with partial pressure of carbon dioxide depended on whether pressure was being increased or decreased, and it did not agree with the value predicted by the Nernst equation. The variation of OCV with temperature was about $(3.1)(10^{-4})$ volt/°K, giving an apparent entropy of 28.5 eu. (The theoretical prediction was 0.12 eu.) The glassware failed over a period of weeks. Surely at these temperatures the favored reaction product would be carbon monoxide, and not carbon dioxide? At 1472" F (1073° K) the equilibrium ratio CO/CO_2 is about 10.

A somewhat similar cell was used to investigate polarization-current relations for the sodium tungstate-tungstic salt in proportions 60 Na_2WO_4 : 40 WO_3 weight-percent *(346)*. Polarization was measured versus reference electrodes of the same form as the working electrodes. At the platinum-oxygen electrode, the anodic reaction (oxygen evolution) gave 3 mA at 0.07-volt polarization with no sign of a limiting current, and it could be taken to 300 mA. The cathodic reaction gave 0.5-volt polarization at 3 mA; most of the potential change occurred over one order of current (0.3 to 3 mA), with obvious mass-transfer limitations. At the CO_2-graphite electrode the anodic-cathodic curves were similar, with a polarization of 0.10 volt at 3 mA, again with apparent mass-transfer effects.

The results were analyzed by fitting to the relation

$$\eta\zeta = (2 \cdot 3RT/nF) \log (\pm i/i_L).$$

The value of n was concluded to be 1, and it was referred to as the "number of electrons transferred in the rate controlling step.'' However, this equation only applies for simple, one-dimensional concentration polarization, and n must be the charge on the transporting ion, which is 2 for the proposed mechanism. The experimental results did not give sharp limiting currents, and it is difficult to see how the equation could possibly be applied to the results. The mass-transfer equations of oxygen at the partly immersed platinum-O_2 electrode must have been complex. The current at the graphite electrode might well have been due to other reactions, since metallic crystals were observed at high currents. It must be concluded that the work did not demonstrate the feasibility of the cell.

13.7 CONCLUSIONS

Considering applications for space travel or submarines (both require high power outputs and energy-storage densities), the principal advantage of conventional primary cells is their capability of high power outputs (kW/cu ft); however, the energy storage density (W-hr/lb) is low, so they are best suited for short-time uses (see sec. 2.3.1). The advantage of fuel-cell systems is that they can have high energy-storage density, but they have relatively low power outputs; therefore, they are best suited for longer term applications (see fig. 2–12, for example). Hybrid cells will be useful only if they combine the advantages of primary cells and fuel cells to give better watts per pound in some time region between these limits (a few hours to several days). Unfortunately, hybrid cells also may have the ***disadvantages*** of primary cells and fuel cells. For example, if a fuel-cell cathode using oxygen is combined with a zinc anode built into the cell, the power density is restricted by the cathode, while the energy density is restricted by the zinc and associated cell structure. The Monsanto dry-tape cell used reactant tapes which had less energy-storage capability than the corresponding primary cell, and the power was limited by the size of the current collectors; therefore, it gave lower output on both accounts than a conventional cell. Other reactants proposed for the dry-tape concept can also be used in conventional cells activated by electrolyte, and use of tape feed gives no unique advantage in terms of watt-hours per pound. The sole advantage of the system is that only the combined tapes are reactive, so the reels can be stopped and the remaining reactants will not suffer self-discharge. If the components self-discharge after activation, it should be possible to use the tape concept to supply electrolyte to a conventional, compact, rectangular plate cell.

The hybrid cell may have specific advantages, under special circumstances, for other applications. For example, if a fuel-cell cathode using air is combined with a zinc anode, the cost of power from the cell might be considerably less than if manganese dioxide were used as oxidant, and the energy density may be improved. This type of cell (which has, of course, been investigated) falls, by reason of possible applications, into the category of a conventional primary cell, and lies outside the scope of this book. A low-temperature cell using solid carbon as fuel would be an ideal primary cell, but carbon is a relatively inert material and can probably only be reacted in high-temperature cells.

CHAPTER *14*

Biochemical Fuel Cells

14.1 INTRODUCTION

The concept of obtaining electrochemical energy from a bacterial reaction was first demonstrated by Potter (ref. **14.1**) in an experiment wherein he combined a half cell containing glucose solution with a similar half cell containing glucose-solution-plus-yeast. The assembled cell gave potential and current. After a long period of inactivity, a flurry of events in biochemical fuel cells occurred in the early **1960's** and a symposium was held in **1962** (ref. **14.2**). To define generally from the articles of this symposium, a biochemical fuel cell consists of a normal oxygen or air cathode, plus an anode immersed in an anolyte containing organic material. The anolyte is usually separated from the catholyte by a permeable membrane which allows ions to pass through but retains the relatively large bacterial cells and enzymes. The cell performance is low until active bacteria or cell extracts containing enzymes are added to the anolyte.

Two distinct modes of operation of bioanodes have been proposed (for example, see ref. **14.3**). The first entails possible bacterial or enzymatic action on the organic material to produce compounds which react normally at the electrode. For example, fermentation of a sugar to alcohol would give an electrode performance comparable to that of the same concentration of alcohol added to the anolyte. Such systems are called indirect biochemical fuel cells. In the second proposed mode the biological agent reacts upon the organic material to form a compound that is more electrochemically active than the original material. This direct biochemical fuel-cell action has been described (ref. **14.3**) as

$$\mathrm{Ez}+\mathrm{A}\rightleftharpoons\mathrm{EzA}$$
$$\mathrm{EzA}+\mathrm{M}\rightleftharpoons\mathrm{M[EzA]}$$
$$\mathrm{M[EzA]}\rightleftharpoons\mathrm{M}+\mathrm{Ez}+\mathrm{B}+\mathrm{H}^{+}+e^{-},$$

where Ez represents an enzyme, A the reactant, B the product, and M the electrode surface. In this case, the enzyme acts as a true electrochemical catalyst, affecting the electrochemical properties of the fuel.

There are three major uses for biochemical fuel cells. In underdeveloped countries without indigenous fossil fuels, a biochemical fuel cell could be used to generate electricity from vegetable or animal matter. A cell suitable for this application should be cheap, long lived, and need no skilled supervision. Use of biochemical fuel cells for military purposes is somewhat similar; the advantage of the system is that it could use natural products as fuels (and electrolyte, if possible). A third application is in space travel, where the biochemical fuel cell might be considered to be part of a closed ecological cycle involving human food and waste products.

The first two applications have the common feature of not requiring the invariant electrolyte needed in most other fuel-cell systems. The ideal bioanode should be able to decompose organic material completely to evolved gases such as carbon dioxide, water vapor, nitrogen, etc., but this is improbable with fuels of practical importance. A less ideal, but still desirable, condition would be decomposition to gases and a readily separable sludge or ash, leaving the electrolyte invariant with time. This again is not likely to occur in practice. The third possibility is to have a cheap, readily available electrolyte which *can* be discarded with the products and unconsumed material. However, in space travel, the closed ecological system would require virtually com-

PRECEDING PAGE BLANK NOT FILMED

plete recovery of electrolyte from unconsumed organic fuel-cell material. Another potential application for biofuel cells (ref. **14.3**) is that of lightweight batteries for military purposes, using pure organic fuels of high-energy density carried with the battery. However, the current densities obtained with bioanodes are low and it is unlikely that such a biochemical fuel cell could compete with a battery using electrochemically reactive fuels.

In the contracts reported in the following sections, much effort was devoted to determining whether the fuel cells had direct or indirect biochemical action, since the limitations of the two types of cell differ importantly. With direct action, cell power density would be a direct function of activity and area of the electrodes, as in a conventional fuel cell. The important variable is power density per unit electrode surface; and the electrode will operate as long as fuel is supplied and product (or unconsumed material) removed. **A** qualification to this concept is that it may be necessary to have auxiliary volume to support a continuous growth of bacteria, although cell conditions might be such that growth of bacteria in the cell matches removal in effluent from the cell. In a direct bioanode, the important reactions occur at the surface of the electrode, and good mass transfer to the electrode of components present in small concentrations is not necessary. The indirect bioanode uses fuels developed by a volume reaction, and the volume has to be large enough to provide a sufficient rate. Thus an extra parameter of importance is power density per cubic foot of biochemical reactor. If the electrochemical reactant is produced in low concentrations, it must be brought to the electrode in adequate quantities, since diffusional mass transfer alone may not suffice. The rate of reaction at the electrode and the volume rate of biochemical reaction must be matched to provide efficient operation.

In much of the work discussed below, the production of reactants and power are reported for two distinct systems. First, active bacteria were used to seed a growth medium containing nutrients as well as the fuel under study. Second, when the bacterial growth reached a steady resting concentration, the bacteria were removed by centrifuging, washed, and used to inoculate an anolyte containing fuel but no nutrients. Under these conditions, it can be presumed that no further cell multiplication occurred, although metabolic processes liberating an electrochemically active component did. In the following discussions of reported research, it may not always be clear which system is being considered, although an attempt has been made to separate and identify the results from the two systems. No attempt has been made to describe the techniques used in growing, identifying, separating, and analyzing the bacteriological agents (ref. **14.4**).

14.2 BIOELECTRIC ENERGY SOURCES, Ohio State University, December 1960 to December 1961

This report was a survey of bioelectricity, with the principal emphasis directed toward electric organs and membrane potentials. No information of direct relevance to biochemical fuel cells is included, but a brief review is given here to indicate the contents of the report. The unit electric cells (electroplaques) of fishes were described as being **4** to **10** millimeters in diameter and 7 to **40** microns thick, with one face being smooth and innervated and the other face being covered with papillae. They are found in combinations of series and parallel connection, and the electric cell banks can deliver **3** to 800 volts (800 volts for the electric eel, *Electrophorus electricus*); potential of each cell is about 0.06 to **0.15** volt. Figure **14.1** shows the mean current and voltages for an electric eel discharged across different loads with discharge times of **2** to **10** milliseconds.

The mode of operation of the electroplaque was described *(530)* as—

1. **An** action potential sweeps down the nerve endings which terminate like the small branches of a tree in the apposition to the innervated faces of the electroplaques.
2. At each terminal a chemical substance is released.
3. This chemical substance moves across the tiny gap between nerve terminal and electroplaque.
4. The region of the electroplaque involved is depolarized, and the chemical is rapidly inactivated. In some electroplaques (***Torpedo,*** *Astroscopus, Raia*), this depolarization con-

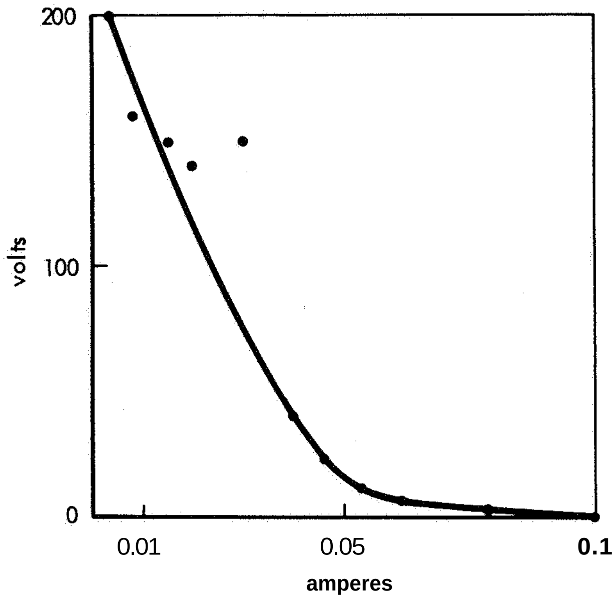

FIGURE 14.1.—Mean current and voltage of an electric eel discharged across various loads (after *477).*

stitutes the entire discharge of the electroplaque. In others, such as *Electrophorus* and *Gymnotus carapo,* an additional event occurs.

5. This event is a propagated action potential similar to that observed in nerve and muscle.
6. In most organs, only the innervated face discharges. In some, however, e.g., *Gymnotus carapo* and *Malapterurus electricus,* the noninnervated face also discharges a short time after the discharge of the innervated face.
7. The depolarized membranes rapidly repolarize.

This report also served to underscore the existing language barrier between the electrochemist and the biochemist or biologist. Presuming a basic understanding of the closed dc circuit, it is difficult to understand what the reporters mean when "only the innervated face discharges." If an electric charge flows from the innervated face, it must return to the cell by some path to complete the circuit; if this is not the case, the report fails to explain otherwise. Similarly, the use of "depolarized" in this report needs clarification; does it mean that the equivalent anode and cathode of the electroplaque are at the same potential at rest and depolarization of one of them gives rise to potential difference between the electrodes? Or does it mean that a rest potential exists between electrodes which does not discharge through an external circuit because of high internal resistance, and that "depolarization" gives a suddenly reduced internal resistance which allows discharge to occur?

The biopotentials were accepted as membrane potentials resulting from different concentrations of potassium, sodium, and chloride ions between the fluid within a biological cell and in the extracellular fluid. A review was given of the theory of membrane potentials. At rest, extracellular fluid contained mainly Na^+ and Cl^-, while fluid within the cell was mainly K^+ and Cl^-, with concentrations outside being about 15 times that inside. This gave rise to a resting potential between microelectrodes positioned in the two fluids. When the electroplaque was excited by applying a small counterpotential between the microelectrodes, a small current was observed initially, followed by a buildup in reverse potential (the action potential) from the biological cell and a large reverse current, which decayed within a few milliseconds to the original conditions. The resistance between the electrodes went from 1000 ohm-cm^2 at rest to 40 ohm-cm^2 at the peak discharge current. The change in conductance was due to a large increase in conductance of Na^+ through the cell membrane.

At rest conditions the relative permeabilities of ions through the membrane were calculated to be $K^+ : Na^+ : Cl^- :: 1 : 0.04 : 0.45$, while during the action potential they were $K^+ : Na^+ : Cl^- :: 1 : 20 : 0.45$. At rest conditions the potential was determined principally by the potassium ion; since this is at higher concentration in the cell, the steady-state potential is positive on the outer wall and negative at the inner wall, opposing the diffusion of K^+ through the membrane. When the cell is activated, the potential is controlled by the much higher sodium permeability. Since sodium diffuses into the cell, the potential which builds up is in the opposite direction. The decay of the rest potential and the flow of sodium ion constitute discharge of the cell. The capacity was estimated as about $1\,\mu F/cm^2$. Described in this way (which is hopefully an accurate interpretation of the report) the process seems comparable to the internal discharge of a capacitor whose dielectric fails; it is not clear how this produces an external electric current. The electroplaque is recharged by a biological pumping process in which the sodium ion passed into the cell was pumped out until the original conditions were restored. The mechanism of this process was not known.

A model was proposed for the production of electricity by concentration differences and semipermeable membranes, as shown in figure 14.2.

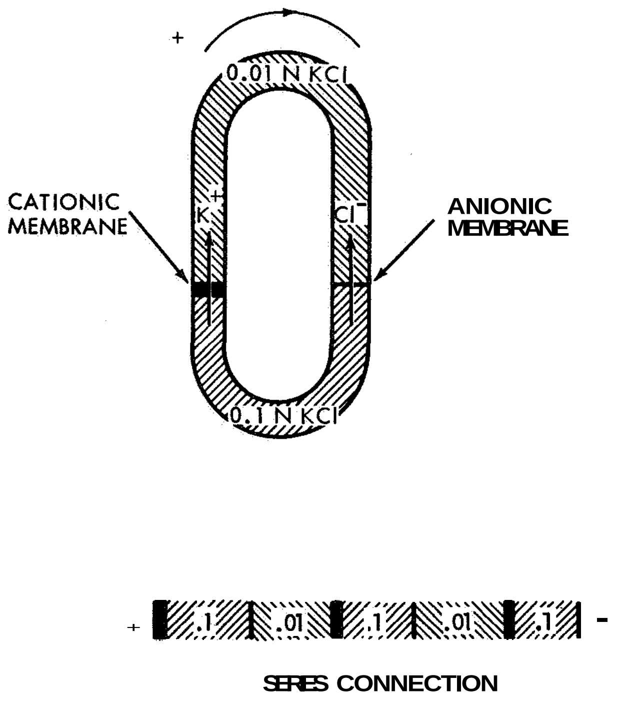

Diffusion of potassium ion through the selective cationic membrane produces a positive potential at the upper face. Similarly, negative potential is produced at the upper face of the amionic membrane. Positive charge then flows from left to right in the upper compartment and from right to left in the lower. The current density, and consequently the rate of mixing of the electrolytes, depends on the electrolyte resistance and on the membrane permeability.

FIGURE 14.2.—Production of current by concentration differences between electrolytes separated by semipermeable membranes *(477)*.

Two membranes are required, but the correspondence between this model and the electroplaque discussed above was not discussed.

14.3 BIOCHEMICAL FUEL CELLS, Magna Gorp., July *1962* to December *1964*

The aim of the contract was to investigate biosystems which could convert natural vegetable products to electricity via fuel cell anodes *(417)*.

One early objective of this work was to determine whether bioanodes produced electricity by the bacterial production of a conventional fuel (indirect bioanode) or whether the bacterial metabolism directly influenced the electrochemistry of the anode (direct bioanode). There was some evidence in the literature that enzymes were true catalysts and affected the activation polarization and activation energy of electrodes. Table B.18 gives systems which were considered; *Clostridium butyricum*/glucose, L-amino oxidase/leucine, Bacterium *pasteurii*/urea, urease/urea, and *Escherichia coli*/formate were selected for study. Relatively pure materials were used in the experiments described below.

The growth rate of cells in a nutrient solution (phosphate plus nutrients), and the production of hydrogen in the same solution, was as shown in figure 14.3. The fall in rate of hydrogen production as the resting-cell concentration was reached was attributed to pH changes in the system. The cells were harvested by centrifuging and washing, and used to inoculate fuel-electrolyte solutions. Under most conditions, the rate of hydrogen release in resting-cell (nongrowth) electrolyte solutions was constant and increased with higher bacterial concentrations *(421)*. Other results are summarized in table 14.1.

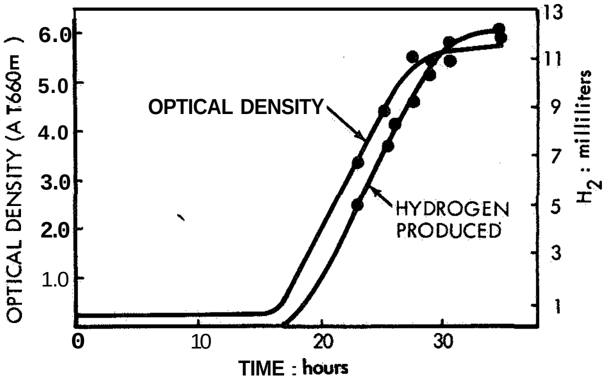

The number of bacteria present was measured by the optical density of the suspension; hydrogen evolved during growth was collected and measured. After seeding, rapid growth occurred after a timelag of 10 to 20 hours; the period of rapid growth lasted about 10 hours until a steady concentration of "resting cells" was obtained.

FIGURE 14.3.—Growth rate and hydrogen production of ***Clostridium butyricum*** in glucose+nutrient +phosphate solution *(423)*.

TABLE 14.1.—*Summary of Some of the Results of (417) Through (426)*

System		Results	Report
Bacterial agent	Fuel		
Clostridium butyricum	Glucose+yeast or neopeptone in phosphate electrolytes	3.7 to 22.5% KCl inhibited growth. Best H_2 production rate at pH 6.5 to 6.9, 91.4" F (33" C), with rapid fall-off on either side. 0.1 *M* glucose inhibits H_2 rate.	*417*
		At pH of 6.8, 0.01 *M* glucose+nutrients gave OCV of –0.4 volt versus SHE at platinized-platinum anode. $i_L \simeq 0.1$ A/sq ft.	*418*
	Glucose..........	Paste with Pt-black, carbon, on screen, gave $i_L \leq 0.1$ A/sq ft.	*419*
	Glucose thioglycolat	More consistent growth observed with thioglycolate medium.. .	*421*
Escherichia coli (cell-free extract)	Formate..........	Best H_2 production at 91.4" F (33" C), pH 6. Direct reaction of formate at platinized-platinum electrode obscured any bioeffect.	*418*
***Escherichia coli*..**	Glucose..........	1% glucose, pH 6 (0.1 *M* phosphate), 0.2 milligram protein/ml gave mainly H_2; 24 ml/liter-hour (about 1 W/cu ft). Acid produced lowered pH.	*421*
		At higher pH, formic acid was formed. Aerobically grown cells were more effective than anaerobic. Rate$\simeq$1 millimole/liter-hour (about 1 W/cu ft).	*422*
		H_2+CO_2 formed at pH 5.7 and less. Nitrate and nitrite gave little effect. Best pH was 6.7 to 7.5, giving $i_L \simeq 5$ A/sq ft. Palladium electrode poisoned at high bacterial cell concentrations.	*423*
Bacterium pasteurii	Urea.............	Best NH_3 production at pH 7; 0.5 mg NH_3 per minute/ml of suspension. $i_L \simeq 0.1$ A/sq ft at platinized-platinum.	*418*
		Paste with Pt-black, carbon, on screen, gave $i_L \simeq 3$ A/sq ft.. . .	*419*
		Best NH_3 production at 120.2° F (49° C). Best electrochemical performance at 116.6"F (47" C); therefore, it appears that rate of NH_3 production is limiting. Poisoning of platinized-platinum electrode with time.	*420*
Urease,........	Urea.............	Best NH_3 at pH 8, 0.2 *M* urea, 113° F (45"C).........	*418*
L-amino acid oxidase	1-leucine..........	At pH 7, 0.1 *M* 1-leucine plus 0.01 *M* methylene blue gave limiting current of ≤ 0.1 A/sq ft at platinized-platinum electrode.	*418*

To test the catalytic activity of enzymes, urease and platinized carbon black (Engelhard 5 percent platinum-on-carbon) were mixed in proportions of 50 milligrams to 30 grams and pressed (2.45 tons/cm²) onto 80-mesh Monel screen. The back was covered with paraffin wax and the exposed electrode face immersed in 3 *M* KCl containing 0.25 *M* urea (pH 9.5). Open circuit was about 0.1 volt versus SHE, and current densities of 1 A/sq ft were obtained. Using Nessler reagent, it was shown that ammonia concentrations produced by enzymatic decomposition of urea were in excess of 0.2 *M* in the vicinity of the electrode. Pastes of carbon black-platinum black-urea-urease (or ***Bacterium pasteurii***) were used to prepare electrodes (*418*), but gave low current (limiting current about 1.4 A/sq ft). The tests summarized in table 14.1 had shown the urea was hydrolyzed to produce ammonia

$$CO(NH_2)_2+H_2O \xrightarrow[\text{or } B.\ past.]{\text{urease}} 2NH_3+CO_2$$

$$2NH_3+CO_2+H_2O \longrightarrow 2NH_4^{+}+CO_3^{=}.$$

Therefore, the rate of electrochemical oxidation of ammonium carbonate was determined, to test whether the low current was due to slow oxidation. A platinized-platinum electrode in sodium sulfate electrolyte (pH 9.5) gave limiting current densities of about 1 A/sq ft at ammonium carbonate concentrations of 0.25 to 1 molar; even smaller values were found at a palladium-black electrode. The low currents were attributed to the small amounts of free NH_3 present, since equilibrium of the reaction $NH_4^+ + OH^- \rightleftharpoons NH_3 + H_2O$ is not favorable to NH_3 at the low pH used.

The nonbiological anodic reaction of dissolved hydrogen was studied at a palladized-palladium electrode *(419)*. A steady current of about 1 A/sq ft was attributed to a limiting rate of adsorption of hydrogen, whereas it was obviously a mass-transfer-limited current; other results with palladium can be assigned to the presence of adsorbed H in palladium. Formic acid (formate) was also studied without bioagents *(422)*; palladium black was better than platinum black, and both better than nickel, rhodium, or gold. Glucose inhibited the reaction somewhat, but acetic acid, lactic acid, and ethanol did not (these are produced in the decomposition of glucose, in addition to formic acid).

At this stage, the results can be summarized as follows. No evidence for direct biocatalysis by enzymes had been found; the results could all be interpreted on the basis of electrochemical reaction of H_2, NH_3, or formic acid produced by biological action (indirect bioanode). Biological action was rapid only over a narrow range of pH and temperature. In a system which produced hydrogen, e.g., *C. butyricum* and glucose, the low solubility of hydrogen gave mass-transfer-limited currents of about 1 A/sq ft in unstirred solution, even when the rate of production of hydrogen was greater than this current. In systems which produced ammonia, the stability of ammonium ion at the pH values suitable for bioaction led to low concentrations of NH_3 and low limiting currents. In addition, ammonia is a relatively inert fuel (see ch. 16), and requires high polarization. On the other hand, formic acid or formate ion is readily soluble and is reasonably electrochemically active at pH values near 7. At pH values above 7, glucose and ***E. coli*** produced formic acid, but hydrogen was also produced when the acid production lowered the pH.

The emphasis of the work was shifted to a search for bioagents which would produce formic acid from glucose without concomitant hydrogen production *(423)*. *Pseudomonas formicans* (later called *Aeromonas formicans*, stock culture from Hopkins Marine Station, Pacific Grove, Calif.) produced formic acid, under anaerobic conditions, from glucose, sucrose, fructose, coconut juice, and water extract of coconut meat. It hydrolyzed starch under aerobic conditions. Hydrogen was not produced because of the absence of hydrogenlyase enzymes, allowing formic acid to accumulate. Used with a palladized-palladium electrode, *A. formicans* and glucose gave better results when separated from the electrode by a dialysis membrane, showing that the bacteria poisoned the electrode.

An oxygen electrode was constructed from a 1-millimeter sandwich of porous Teflon sheet (25 percent Teflon and 75 percent platinum black) platinum screen packed with platinum black, pressed at 60000 psi. Electrolyte wetted the platinum-black screen but did not penetrate the Teflon-platinum mixture. At pH 7, the electrode gave an OCV of 0.68 versus SHE (theoretical is 0.81 volt) with oxygen and 10 to 100 A/sq ft at 0.4- to 0.6-volt polarization from OCV. Performance was about 80 millivolts more polarized with air.

Further studies *(424)* on *A. formicans* showed that it grew best in 0.2 to 0.3 M phosphate buffer, with a rapid fall in growth rate at higher phosphate concentrations. Growth rate was best as pH approached 7 and was zero below pH 5.8. Coconut milk containing equivalent amounts of glucose performed as well in a fuel cell as pure glucose (with the anode separated from the bacteria by a dialysis membrane, cellophane sheet, or parchment paper). A banana-water extract containing equivalent quantities of sugars did not perform well. Lyophilized *A. formicans* was as satisfactory for producing fuel as freshly prepared resting cells.

A three-cell demonstration stack was built, using perforated, palladized-palladium-foil anodes (25 square centimeters) and platinum-black gas-diffusion cathodes. The electrolyte and growth medium was 0.2 M phosphate buffer, the fuel was coconut milk, and the oxidant was air. The basic cell was a disk cell with an anode chamber separated from a bacteria chamber by a dialysis membrane, the bacteria chamber in turn being separated from a cathode chamber by an ion exchange membrane. Figure 14.4 shows the mean performance of the cells. It can be seen that maximum power density was low, and the maximum current was an order of magnitude less than the value of 5 A/sq ft obtained with laboratory single cells.

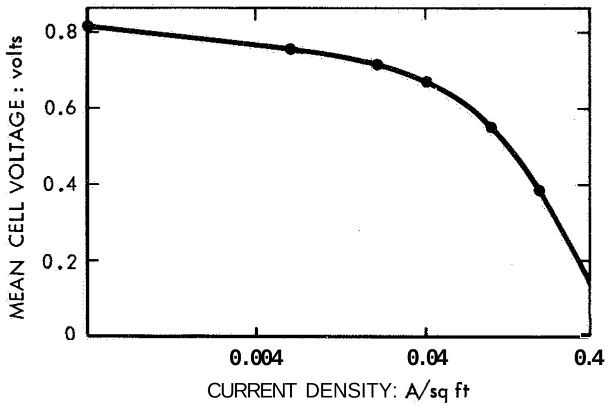

FIGURE 14.4.—Voltage-current curve of a demonstration biochemical fuel cell (Magna Corp., *424).*

There are several deficiencies in this work which make it difficult to judge the potentialities of the biochemical fuel cell using ***A.** formicam.* First, no mass balance was made (presumably because it was not possible to measure the concentrations of formic acid in the growth media). The results are in a form such that it is not possible to calculate the important value of watts per cubic foot of anolyte. One figure only is given, for *E. coli* and glucose (see table 14.1), which leads to a value of about 1 W/cu ft. The efficiency of glucose conversion to formic acid is not known from this work, although other sources (refs. 14.5 and 14.6) give it as about 1 mole of formic acid per mole of glucose. Since the bacterial decomposition proceeds only in near-neutral solution, other acids produced must be neutralized, even if all of the formic acid is electrochemically oxidized. These other acids appear to be electrochemically inert, and the system is not likely to be economically or logistically attractive if large quantities of electrolyte have to be discarded for every watt-hour of power produced. The research did not establish the limitation to the current density of the anode, since the bacterial and electrode processes were considered together. If the limitation consists of a mass-transport-limited current due to low steady-state concentrations of formic acid, then other electrode systems (high flow rate or flow-through electrodes, for example) may well give much higher current densities. The research consisted principally of making a suitable medium for bacterial production of fuel, adding the bacteria and putting in solid, immersed electrodes to see what current could be obtained after some hours. Such a technique produces somewhat arbitrary data, which are applicable only for the particular experimental conditions used and for the short time in which steady conditions apply.

14.4 BIOCHEMICAL FUEL CELLS, University of Pennsylvania, Institute for Direct Energy Conversion, June 1962 to 1963

As part of a research grant for the study of direct energy conversion processes, some work was done on fundameptal aspects of biochemical fuel cell reactions. Hydrogen release from formic acid, due to the action of formic dehydrogenase enzyme, was studied in sodium phosphate buffer. The enzyme was prepared *(741)* by growing *E. coli* anaerobically; the resting-cell preparations were stored under nitrogen at 39.2" F (4" C). Results were expressed as specific activities; i.e., the rate of hydrogen production per milligram of dry bacteria weight. Sodium formate concentrations of 10^{-4} *M* gave the largest hydrogen production over a 6-hour period, with the rate decreasing with time. The specific activity was highest at bacteria concentrations of 1.5 to 3 mg/cm^3, but total activity was best at 10 mg/cm^3. For example (*742*), a bacteria concentration of 1.5 mg/cm^3, at 98.6" F (37" C) and 6.1 pH, gave an optimum rate of (250)(10^{-6}) liters/mg-hr at formic concentrations between 50 and 100 micromoles/cm^3. (This corresponds to approximately 20 A/cu ft.) The value fell to (40)(10^{-6}) liters/mg-hr after 6 hours, then leveled out at this figure. This fall in activity was not due to depletion of formic acid.

A blank run with a platinized-platinum anode in a solution of formic acid and electrolyte showed that formic acid gave low currents and high polarization. When the solution was bubbled with hydrogen, polarization was low until current densities approached the mass-transfer-limited current of dissolved hydrogen, about 1 A/sq ft. When, instead of bubbling hydrogen, bacteria were added to the solution, the current-voltage curve was almost identical to the bubbled hydrogen case. This demonstrated that bacterial action on formic acid produced a solution saturated with hydrogen and that there was no direct bioelectrochemical action. Also, the hydrogenlyase enzymes are contained within a bacterial cell which has a wall thickness of about 200 angstroms. Thus, the active agents are separated from the electrical double layer at the electrode surface by a distance of 200 angstroms, and direct bioelectrochemical action could hardly occur under these circumstances. The optimum power density, based on the best total rate of hydrogen production, was estimated to be about 30 W/cu ft. The work was not continued.

14.5 BIOCHEMICAL FUEL CELL, Melpar, Inc., July *1962 to 1964*

The aim of the contract was generation of hydrogen by micro-organisms from suitable fuels ***(448)***. A brief review of biochemical mechanisms was given, taken mainly from Gest (ref. 14.7). Cells were grown in suitable media, filtered, washed, and transferred to the fermentation (not growth) substrate under test; the amounts of gas evolution were measured and the gases analyzed by gas chromatograph. The hydrogen-producing capacities of suspensions of *E. coli, A. aerogenes, A. cloacae, Pseudomonas* sp. (strain G4A), *Serratia kielensis,* and *C. butylicum* with various sugars and formate were measured and indicated *E. coli* as the most promising ***(449)***. The amount of oxygen present during the growth period affected the production of hydrogenlyase enzymes, and thus affected the hydrogen production during fermentation. Once the enzymes had been formed, addition of oxygen did not affect the enzymatic production of hydrogen. Similarly, the growth medium affected hydrogen-production capabilities and little hydrogen was produced from *Clostridium* cells grown in thioglycolate medium. The system *E. coli*-glucose had an induction period ***(450)*** and maximum rates of hydrogen production were obtained after 6 to 10 hours (this is in contradiction to the results quoted in section 14.3, and was probably due to different growth conditions). Hydrogen production was best from cells which were grown anaerobically at 91.4" F (33"C) using a glucose-supplemented growth media.

Aeromonas hydrophila produced no gas, but *Clostridium welchii* (NC1B 6785) was very promising (*451*). The Pseudomonas-formate system was shown to have an induction period. Other strains of *C. welchii* produced much less hydrogen ***(452)***. A 10-liter fermenter was used to study hydrogen production under nutrient conditions where cells were both growing and present at high concentrations from an initial addition of resting cells. *C. welchii* (6785)-glucose under anaerobic conditions (about 2×10^{10} cells per milliliter) gave 8.2 liters H_2 per liter-hour, or about 35 W/cu ft. It was argued that it might be possible to increase this by a factor of 10^4 by increasing the bacteria cell concentration, optimizing conditions, and selectively breeding more active strains of bacteria. Table 14.2 gives the reducible sugar content of some commonly available vegetable materials.

In later reports ***(453*** and ***454)*** the best conditions for hydrogen formation from glucose were: growing *C. welchii;* 0.1 *M* buffer K_2HPO_4 at 6.8 to 7.0 pH; 1 to 2 percent by weight glucose, 98.6" F (37" C); and a nutrient addition of 100 grams tryptone, 100 grams yeast extract, 1000 milliliters liver extract, and 50 milliliter salts per 10 liters. Initial cell concentrations were about 10^8 cells per milliliter and increased by 10^2 in 16 hours to a steady concentration. Hydrogen production as a function of time was similar to that shown in figure 14.3, but the lag was only 2 hours and a steady rate of production was reached in 10 hours. This steady rate was considerably lower than the rate of hydrogen production during the rapid growth period.

Work was also started on breeding new strains. Existing strains were exposed to ultraviolet irradiation at wavelengths near the absorption peak wavelength of DNA (2600 angstroms), and the hardy, nonkilled cells were grown and spot tested for active mutants. The production of

TABLE 14.2.—*Approximate Sugar Composition of Selected Grains and Grasses (452)*

Grains	Starch, % range	Total, % range	Reducing sugars			Acid iydrolyzable sucrose
			Total	Glucose	Fructose	
Barley	60.1–67.1	2.5	....	....	....	....
Corn	22.6–73.7	1.5–9.1	....	....	....	....
Oats	38.7–62.3	1.2–1.6	....	....	....	....
Rice	63.8–66.1	0.34.5	....	....	....	....
Sorghum	65.9–73.3	0.8–3.1	....	....	....	....
Wheat	6.17–69.3	2.74.5	....	....	....	....
Dry roughage:						
Alfalfa, all forms	1.6–4.1	3.2–10.8	....	....	....	....
Brome hay, smooth	....	3.7	....	....	....	....
Clover, all forms	....	2.4–8.6	....	....	....	....
Orchard grass	1.1	5.1–5.7	....	....	....	....
Sorghum, all forms	2.8	0.6–34.8	....	....	....	....
Timothy	....	4.4	....	....	....	....
Green roughages:						
Alfalfa forage	....	4.7–10.5	....	....	....	....
Bluegrass forage	....	5.0-16.3	3.22–3.32	....	....	4.11–5.15
Blue stem forage	....	1.3–5.4	....	....	....	....
Brome forage	....	2.8–13.6	2.51–2.58	....	....	8.17–8.25
Canarygrass forage	....	5.1–10.3	2.84–3.15	....	....	4.43–5.65
Clover, forage	....	3.1	....	....	....	....
Fescue, forage	....	3.2–14.9	3.744.17	....	....	4.51–7.36
Oatgrass, forage	....	5.6–16.9	3.00-3.13	....	....	7.81–9.65
Redtop, forage	....	4.6–15.6	1.85–2.63	....	....	4.44–9.25
Sorghum, fodder	....	3.2–9.1	....	....	....	....
Timothy forage	....	2.4–9.7	2.44–2.88	1.05	1.02	4.22–12.14
Orchard grass forage	....	....	4.11–4.51	....	....	4.32–4.54
Ryegrass	....	....	....	2.00	1.81	6.62–9.69

hydrogen from glucose by *C. welchii* was very sensitive to the growth temperature (*455*), being good at 95" F (*35"C*) but almost absent at *104"* F (40° *C*). Several different bacteria and fungi were used to break down cellulose, but little free glucose was found, since apparently the microbes used the sugar for growth. Cellulase failed to produce glucose from cellulose at a useful rate.

14.6 BIOELECTROGENIC SYSTEM, General Electric Co., MSVD, October *1962*

Yeast and glucose solution was used in the anode compartment of a General Electric IEM cell with platinum-black electrodes **(242).** Air was used at the cathode; OCV was 0.9 and current density was about *10* A/sq ft at 0.5 volt. The action was shown to be due to ethyl alcohol produced from the glucose, and the same potential and current were obtained with cell-free supernatant liquor from the fermentation. Ethyl alcohol was determined, and the rate of its disappearance agreed with that predicted from current density.

14.7 RESEARCH ON APPLIED BIOELECTROCHEMISTRY, Magna Corp., March *1963* to *1964*

This contract studied the use of human urine and feces as fuels for fuel cells (*427*), for space-travel applications. The normal production of urine is *1200* grams per day, containing *22* grams of urea. Daily feces production is 80 to *150* grams, with a calorific value of 70 to *140* kcals. Use of ammonia developed from urea would give **68** watt-hours per man-day, nearly **3** watts per man. Use of polysaccharides in feces would give only about 8 watt-hours per man-day; therefore, experimental work was started on the use of urine. *Sarcina ureae* and *Micrococcus ureae* produced ammonia, but only under aerobic conditions. *Brevibacterium ammoniagenes* produced ammonia at slow rates. *Bacillus pasteurii* gave ammonia under aerobic and anaerobic conditions, decomposing 99 percent of the urea in urine in 1 day.

B. pasteurii was further studied and gave optimum breakdown at 86° to 95" F (30" to 35" C) and pH 9.0. The ammonium carbonate produced buffered the solution between pH 9.2 and 9.5. Optimum urea concentration was 1.9 weight-percent. Addition of feces inhibited the reaction and attempts to grow active, adopted subcultures on urine containing 5 percent feces were not successful. Continuous culture of *B. pasteurii* in urine systems showed that 80 percent of the urea in urine could be utilized with a retention time of 12 hours in the reactor. The precipitation of salts (calcium phosphates and carbonates) was prevented by the addition of 0.2 percent EDTA, but this inhibited the growth of the bacteria.

Platinized-platinum anodes in urine gave better voltage and current in the presence of *B. pasteurii,* but current was still low. Once again, the main problem was that ammonia could not be electrochemically utilized at the temperatures and pH values suitable for bacterial ammonia production.

14.8 STUDY OF THE FUNDAMENTAL PRINCIPLES OF BIOELECTRO-CHEMISTRY, Ford-Aeronutronic, March 1963 to March 1964

A number of enzymes-substrate mixtures were tested at a bright platinum anode. Results are summarized in table 14.3. Because of the activity of D-amino acid oxidase (DAO) with tryptophan, it was investigated further. The main intermediate appeared to be Indole3 pyruvic acid (IPA), since when oxygen was admitted, the absorption-spectra peak of IPA in the solution rose proportionally to the current. IPA went to a less electrochemically active form in solution in a buffer, which was believed to be the keto form; the enol form was stable and active at pH 3. The electrode became poisoned with time with tryptophan and the potential was independent of the rate of stirring. This was attributed to control by the rate of adsorption of the molecule (but the potential was sufficient to form oxide on the platinum). Current density was not dependent on the enzyme concentration.

TABLE 14.3.—*Summary of Some Results From (218) through* **(220)**; *Activity at Bright Platinum Anode*

System	*Comments*
Arginine: arginase	No activity
Amino acids: glutamic decarboxylase from ***E. coli***	No activity
Urea: urease	Slight activity due to impurities in enzyme
Sugars: glucose oxidase, lactic dehydrogenase, alcohol dehydrogenase, diaphorase, mitochondria	Inactive unless redox couple present (e.g., $K_3Fe(CN)_6$). Hydrogen peroxide produced aerobically
Amino acids (serine, histidine, alanine, tyrosine, tryptophan): D-amino acid oxidase	Some activity aerobically. Tryptophan best.
Nitrite or sulfite: reductase from ***E. coli***	No activity

Thin films of agar-plus-enzyme were deposited on the electrode which was then placed in the tryptophan-enzyme solution. Results were about the same as with the tryptophan-enzyme solution, although enzyme concentrations were much higher in the layer. Incorporation of platinum filings into the film did not improve performance. Attempts to attach a redox dye to the amino acid were not successful.

A theoretical discussion was given using a mechanism in which the enzyme is oxidized at the electrode and reduced by amino acid in the bulk volume of the electrolyte. There is no evidence in the results of such a mechanism and a number of dubious or incorrect assumptions were made in the theoretical treatment. However, one general concept is probably of wide application; since the enzyme molecular weight is high ($\sim 10^5$), the maximum possible concentration is small. Thus, any mechanism in which current is dependent on the transport of enzyme over appreciable distances is likely to give low currents due to the small concentrations available for diffusional driving force.

The choice of bright platinum as the anode material was probably unfortunate, since it is a difficult material to work with even in very pure systems. The strong absorptive capacity of platinum for many compounds and the low area of bright platinum mean that it is readily poisoned by trace impurities. Platinized platinum would have been preferable; the actual area can be determined by techniques such as double-layer capacity or the galvanostatic discharge of absorbed hydrogen atom. Oxide layers and films form on the electrode above 0.8 volt (versus hydrogen in the same electrolyte), which changes the properties of the electrode.

14.9 BIOCHEMICAL FUEL CELLS, Marquardt Corp., May *1963* to September *1964*

The contract objective was an empirical study of biochemical fuel cells using human waste ***(428).*** An "H" cell was used, with electrodes of 1-inch-square platinized-platinum. The bridge of the H contained a cellulose acetate membrane (Sargent S–14825, 1 mil thick) to separate the anode and cathode compartments. A mixture of urine and feces was put in the anode compartment and 5 weight-percent NaCl-KCl solution in the cathode compartment; oxygen was bubbled through the catholyte. Work by Rosenwalt et al. (ref. 14.8) had shown that copper, zinc, brass, and butyl rubber were toxic to the indigenous micro-organisms of human waste; while tin, lead, aluminum, stainless steel, epoxy resins, polyethylene, silicone rubber, and polyvinyls were not. With 30 grams of feces and 100 milliliters of urine, the cell OCV was about 0.5 and the short-circuit current density 0.02 A/sq ft; results were irreproducible. Anolyte pH increased from 6.1 to 8.8 during the tests; cell power reached a maximum after 24 hours and then fell slowly. Controlling the pH below 7 was detrimental.

The specific resistance of urine was determined with 400-cps alternating current; raw urine had a value of 60 ohm-cm and frozen-and-thawed urine, 90 ohm-cm ***(429).*** To duplicate conditions likely to apply in space travel, feces were obtained from personnel on a low cellulose diet. Variation of the concentration of feces between 10 to 40 grams per 100 milliliters of urine did not change performance. The use of a saturated calomel reference electrode showed that the OCV of the anode increased from 0.1 volt to between –0.5 and –0.6 volt after 10 hours (OCV of reversible hydrogen electrode is about –0.65 for the pH of the solution).

A three-legged cell was built, consisting of a biochemical chamber/separator/anode chamber/separator/cathode chamber (*430*). The anode chamber contained heat-sterilized biological anolyte. The performance was compared with a two-legged cell containing sterilized anolyte. Initially, the performance was similar, showing that some power could be immediately obtained from chemical reactants in the anolyte. However, biologically produced reactants diffused, after many hours, from the biochemical chamber to the sterile anode chamber and increased power output. Similar results were also obtained with electrolyte circulated across screen electrodes of 10 percent Rh: 90 percent Pt.

Higher performance was obtained in natural feces-urine mixtures than with urine, supernatant liquor, or diluted mixtures ***(431).*** In the natural mixtures, frothing was a problem. Waste from an omnivorous diet gave higher power than that from a vegetarian diet. Frozen urine or feces was satisfactory, but lyophilization of feces reduced its activity considerably. The addition of nutrients and other organisms (than those naturally present) had no effect. A total charge of 5.3 coulombs per 100 milliliters of waste was obtained; at a mean cell potential of 0.6 volt, this was about 0.032 watt-second per gram of waste.

Several cell power densities were given, but they have little meaning because the cathode performance was very poor, as might be expected from a cathode utilizing bubbled oxygen. The short-circuit currents and maximum power densities were principally limited by the cathode; since an external power source was not used with the anode half cell, it was not possible to increase the current density beyond that set by the cathode. Anodic current densities of about 0.04 A/sq ft were obtained at about 0.5-volt polarization from a reversible hydrogen electrode in the same electrolyte. The power density of the anode versus an ideal oxygen electrode is about 0.03 W/sq ft at this current density.

14.10 CONCLUSIONS

It is a problem to evaluate the quality and importance of the research reported above; the somewhat lax use of terminology makes review difficult and evaluation doubly so. In terms of electrochemistry, the overall quality of the work (save that at the University of Pennsylvania, sec. 14.4) has been poor, and the best reported performance of solid, immersed electrodes was most unpromising, as the current densities usually were below 1 A/sq ft. Abandonment of biochemical efforts most certainly cannot be suggested on the basis of low current-density figures; the early experiments with hydrogen/oxygen cells gave figures no more promising than were obtained in the biochemical efforts.

However, the figures do suggest that research should be directed first to the basic problem of understanding why the current densities are low. If improvements are possible, they will come most readily when the basic problem is studied and clarified.

It was frequently noted that researchers in biochemical techniques were ill informed or were ignoring the knowledge already available to them. In one report (ref. 14.9) the authors observed that "another complication in the study of biological fuel cells is the fact that electrochemistry has been a somewhat backward science and still uses a complicated nomenclature." But on closer examination of that report, it seems that only the biochemist's understanding of electrochemistry is backward, and that much good would be served by having a sound grounding in both the principles and the language of electrochemistry.

No evidence was found to support the concept of the direct bioanode. As pointed out in section 14.4, a direct action would be expected only where enzymes are liberated from the cells. The wall of a bacterial cell separates enclosed reactants (enzymes) from an electrode surface by a distance which is too great for the reactants to affect the potential energy path of electron transfer across the electrical double layer. What information is available from the reports suggests that cell suspensions and cell-free suspensions (enzymes liberated by crushing the cells) give similar results at bioanodes. Results can always be explained on the basis of electroactive chemicals released in the bioelectrolyte by bacterial or enzymatic reaction, followed by diffusion of the chemicals to the electrode surface. In one case (sec. 14.4) the activity of a freshly prepared bacterial suspension (nongrowing) decreased with time, while in other cases an induction period was observed, so that the rate of production of chemical fuel increased with time until a steady state was reached. A commonly observed feature which was not explained was that growing cells gave a higher rate of chemical production than resting cells.

For bioanodes with an indirect mode of operation, two performance parameters are significant. The maximum rate of chemical production was about 30 W/cu ft. No estimates were given for the upper limits of this performance criterion. It would be helpful to have a listing of the rates of other biochemical reactions to see what order of magnitude is to be expected. This would give an indication of upper limits which might be obtained by selective breeding of bacterial strains. Performance of electrodes in watts per square foot was low, but the values could probably be increased considerably by normal techniques of electrocatalysis and improvement in mass transfer. In all cases, electrochemical tests were made at the temperatures at which bioaction was optimum; these temperatures were about 86° to 104" F (30° to 40" C). If biochemical production is separated from use at an electrode, theh electrode performance can be improved by increasing temperatures.

In summary, the interesting and potentially useful phenomena of bioelectricity and biochemical production of chemicals should be investigated further. Investigations should be carried out by teams consisting of biochemists, electrochemists, and chemical engineers, so that all facets of the problem can be adequately explored. There is little immediate prospect for application of biochemical fuel cells in industrialized societies. However, with the advent of solid-state electronic devices (e.g., the transistor radio) which have long life and low-power requirements, a low-power biochemical fuel cell might find wide application in underdeveloped countries. A principal requirement for this application is a cheap, foolproof, ambient temperature air electrode, with a lifetime of at least 10 years; in short, a minimum improvement in current density of one to two orders of magnitude is required before biochemical fuel cells would be useful for any commercial or Government application.

14.11 REFERENCES

14.1. Potter, M. C.: Proc. Royal Soc., **B84,** London, **1912,** pp. **260–276.**

14.2. American Institute of Biological Sciences: Developments in Industrial Microbiology. Vol. **4,** Washington, D.C., **1963.**

14.3. Del Duca, M. **G.;** Fuscoe, J. M.; and Zurilla, R. W.: Developments in Industrial Microbiology. Vol. **4,** Am. Inst. Biol. Sci., **1963,** pp. **81–91.**

14.4. Neish, A. ***C.:*** Analytical Methods for Bacterial Fermentations. Rept. No. **46–8–3,** Second rev., National Research Council, Saskatoon, Saskatchewan, Canada, Nov. **1952.**

14.5. Crawford, I. P.: J. Bacteriol., vol. **68, 734, 1954·**

14.6. Pivnick, H.; and L. R. Sabina: J. Bacteriol., vol. **73, 249, 1957.**

14.7. Gest, H.: Bacteriol. Rev., vol. **18, 43, 1954.**

14.8. Rosenwalt, **A.** J.; et al.: App. Microbiol., vol. **10, 345–347, 1962.**

14.9. Alexander, N. E.: Proceedings of the Biochemical Fuel Cell Session. Held under the auspices of the Electrochemical Working Group, Interagency Advanced Power Group, Sept. **1962,** pp. **7–12.** (No. **OTS)**

CHAPTER 15

Direct Hydrocarbon (Organic) Fuel Cells

15.1 INTRODUCTION

General commercial or military use of fuel cells will probably be realized only when systems which can utilize cheap, high-energy density, hydrocarbon fuels are developed. Unfortunately, such fuels are relatively inactive at an anode in comparison with hydrogen or hydrazine. For example, fuel cells using methane or other types of natural gas might find wide application where piped gas is cheap and readily available. However, methane is a stable molecule which cannot be reacted electrochemically at rates comparable to hydrogen and does not give high current densities, even in high-temperature fuel cells. Liquid hydrocarbons are also relatively inactive and usually have low solubilities in aqueous electrolytes, which leads to mass-transfer limitations.

Hydrocarbon derivatives, particularly oxygenated hydrocarbons such as methanol or ethanol, are usually not cheap enough for commercial power production but would be advantageous where low weight is of importance, as in space travel. The energy density for complete oxidation of ethanol is 3600 W-hr/lb, compared with 14800 W-hr/lb for hydrogen, but the weight of the storage tank for ethanol would be much less than that for high-pressure hydrogen gas storage.

There are two main techniques for the use of hydrocarbons. The hydrocarbon or carbon-containing fuel can be re-formed to hydrogen and carbon monoxide and the carbon monoxide combined with steam to give further hydrogen (water-gas shift reaction, $CO+H_2O \rightarrow H_2+CO_2$). The major advantage of this method is technical feasibility (see app. E), since it *can* be used with existing hydrogen-air fuel cells. The disadvantages include additional cost and weight of the hydrogen generation unit, loss of energy in the unit, greater system complexity and unreliability, and increased cost of the electricity produced. The other technique is to develop direct hydrocarbon fuel cells which *can* oxidize specific organic fuels at useful rates. High-temperature cells utilizing hydrocarbons, with steam added to prevent carbon deposition, are discussed in chapter 6. Since high-temperature cells have a number of problems, use of direct, low-temperature, hydrocarbon fuel cells is preferable. Research on these cells was given considerable impetus by the demonstration, in 1960 (*130*, or ref. 15.1), that propane and ethylene could be electrochemically reacted almost completely to CO_2 and H_2O at a platinized carbon electrode, in 5 *N* sulfuric acid, 176" F (80° C).

Low-temperature organic fuel cells have some specific features which distinguish them from hydrogen-oxygen cells. First, an alkaline electrolyte will absorb CO_2 produced at the anode and change to carbonate. Performance of electrodes, especially cathodes, is usually poor in carbonate solution, and CO_2 must be removed to regenerate hydroxyl ion. Most research has, therefore, concentrated on acid electrolytes which are CO_2-rejecting. Strongly oxidizing acids cannot be used at higher temperatures because they react with the fuel; for example, sulfuric acid cannot be used at temperatures much above 212° F (100° C). Second, organic fuels can undergo partial reaction, yielding soluble products in the electrolyte, which leads to inefficiency. The products may poison the electrodes, and, in addition, the dissolved material can diffuse to the cathode where it may react and reduce the effective cathode current. Third, since CO_2 is produced at the anode, it is not possible to cycle a gaseous fuel; fuel must either be used in **a**

PRECEDING PAGE BLANK NOT FILMED.

once-through manner, or unconsumed fuel must be separated from the exhaust gases. Thus, the degree of oxidation is very important, since conversion to CO_2 and H_2O must be nearly complete for once-through operation. Condensed fuel vapor can be removed with water from the exhaust stream, but condensation, separation, and revaporization adds to the complexity and cost of the system.

Electrochemical oxidation of hydrocarbons and hydrocarbon derivatives is receiving much attention, including an American Chemical Society symposium in September 1965. Because of the volume of research being conducted, present work on direct, low-temperature, hydrocarbon fuel cells is likely to become out of date rapidly. Therefore, this chapter will present a general survey instead of a detailed contract-by-contract summary. No detailed system descriptions will be given because systems have not yet been developed to a useful stage.

Most of the work falls into three categories: electrode construction from different catalysts and testing in simple cells under varying conditions to determine power densities; detailed investigations to determine degree of utilization of fuel, production of byproducts, and cell life; and programs concerned with mechanisms and rate studies in idealized systems, considered mainly in section 15.5.

Much of the material in this chapter is taken from a recent review (*397*), but the original sources are given.

15.2 SCREENING PROGRAMS

15.2.1 Activity of Fuels

The activity of a fuel or its ease of oxidation at a fuel-cell anode is usually indicated by the current it will support at a given voltage or by the maximum power density it will support, versus a half-cell system. Many factors in addition to intrinsic electrochemical activity of the fuel can affect the measured activity and slow time-dependent effects may significantly affect the results. However, screening studies are of value in guiding more detailed types of studies.

The oxidation was studied (Monsanto Research Corp., 469,1960; 458,1962) of 148 organic fuels dissolved in basic (1 *M* KOH, pH≅14), acidic (1 *M* H_3PO_4, pH = 1), and neutral (KOH-H_3PO_4 buffer, pH≅7) electrolytes at *86"* F (30"C) and 194" F (90° C), with electrodes of platinized Pt and platinized porous carbon (Pure Carbon Co., Fuel Cell Grade No. 14, 3.5 percent Pt content). Concentration of fuel was usually half-molar and insoluble compounds were stirred into electrolyte with surfactant (0.001 weight-percent Santomerse) or absorbed in the porous carbon electrode before immersion in electrolyte. Current-voltage curves were obtained by scanning from 0 to 100 mA/cm^2 in about 18 minutes. The voltages were measured against a SCE (Luggin capillary) and converted to values versus a reversible hydrogen electrode in the same solution via calculation from the Nernst equation, with no correction for liquid junction potentials. To compare the activity of the various fuels, maximum power densities for the fuel half cells were calculated by assuming they were coupled with an ideal (nonpolarizable) O_2 electrode with a voltage of 1.2. The reproducibility of the results in terms of mean deviation was determined to be about 16 percent. Lack of reproducibility in preparing the electrode was believed to be largely responsible for this deviation. Table 15.1 presents the maximum power densities. Table 15.2 classifies the fuels in groups according to the currents they could support at 0.5 volt (versus SHE).

Some general conclusions were drawn from this work:

(1) A large number of organic compounds can be anodically oxidized at a significant rate.
(2) Organic acids (especially HCOOH) oxidize best in neutral solution.
(3) Several sulfur-containing compounds are easily oxidized in acid.
(4) Epoxides (e.g., ethylene and propylene oxides in base); hydrazides (e.g., semicarbazide); benzoquinone; formamide; and certain esters (e.g., ethyl formate, methyl lactate, and diethyl oxalate) are readily oxidized electrochemically.
(5) The relative reactivity of alcohols in base is $CH_3OH > C_2H_5OH >$ i-propanol >> *t*-butanol.
(6) At increased temperatures of 248" to 392" F (120" to 200°C) in concentrated H_3PO_4,

TABLE 15.1.—*Average Power Densities for Fuels Tested (458)*

	References*	Maximum power, m /cm^2		
		pH 14	pH 7	pH 1
Hydroxy compounds:				
Methanol	1, 2, 3, 4	250	24	15
Ethanol	1, 2, 4, 5	38	4.8	13
Isopropanol	1, 2, 4	16	10	10
t-Butyl alcohol	2	1.4	1.0	1.8
Cyclohexanol	....	3.4	1.4	....
Benzyl alcohol	2	5.6	....	1.7
Diphenylcarbinol	....	....	....	....
α-Naphthol	....	6.1	....	1.7
Phenol	2, 6	1.2	1.6	2.2
Allyl alcohol	2	12	2.8	3.4
Propargyl alcohol	....	4.3	4.8	5.0
Furfuryl alcohol	....	5.4	2.6	1.6
Ethylene glycol	1, 2, 4	98	10	6.9
1,2-Propanediol	5	68	7.4	1.2
1,3-Butanediol	....	4.5	3.2	5.2
Pinacol	....	1.6	1.2	1.1
Catechol	6	23	8.8	15
Resorcinol	6	6.4	3.3	2.4
Hydroquinone	6	40	27	34
Phloroglucinol	6	3.8	3.1	3.6
Pyrogallol	6	60	22	36
Glycerol	1, 2, 3, 4	180	15	7.8
Pentaerythritol	....	5.9	5.6	3.6
Inositol	....	36	6.0	....
Ethers:				
n-Butyl ether	....	1.4	....	....
Methyl benzyl ether	....	....	....	....
Tetrahydrofuran	....	....	....	12
Furan	....	x	x	x
Dihydropyran	....	1.4	1.2	1.2
Tetrahydropyran	....	2.0	1.9	5.3
Trimethylene oxide	....	4.0	3.8	2.4
1,2-Dimethoxyethane	....	1.8	2.5	2.1
p-Dioxane	2	....	....	....
2-Ethoxyethanol	....	21	4.0	1.6
Diethylene glycol	....	15	5.8	1.1
Triethylene glycol	....	7.7	3.7	3.5
Aldehydes:				
Formaldehyde	1, 2, 3, 4, 5	152	93	22
Acetaldehyde	5	1.2	2.9	4.0
Benzaldehyde	2	....	....	....
Glyoxal	....	20	14	2.0
Acrolein	....	1.8	1.8	1.6
5-Hydroxypentanal	....	15	2.4	4.2
Dextrose	2	23	6.7	1.2
Ketones:				
Acetone	1, 2	1.2	1.1	....
Methyl isopropyl ketone	....	2.1	1.3	1.4
Cyclohexanone	....	2.6	....	2.0
Acetophenone	....	....	....	....
2,4-Pentanedione	....	1.2	....	2.2

*See list at end of table.

TABLE 15.1.—*Average Power Densities for Fuels Tested* (*458*)—Continued

	References*			
		pH 14	pH 7	pH 1
Ketones—Continued				
2,3-Butanedione		20	2.6	
Methyl vinyl ketone		1.2	1.9	2.5
Mesityl oxide		1.9	1.7	
Furfurylacetone		1.3		
p-Benzoquinone		76	7.3	9.2
Acetoin		16	2.4	1.6
Methylglyoxal		7.4	5.9	5.3
Carboxylic acids:				
Formic	1, 2, 3, 4	16	350	16
Acetic	2, 3		1.6	
Butyric		1.0	1.2	
Pivalic				
Benzoic				
Phenylacetic				
β-Phenylpropionic				
Oxalic	2		8.1	9.5
Malonic			1.0	
Acrylic	2	2.7	1.8	1.5
Maleic			1.1	
Glycolic	2, 4	12	3.6	
Mandelic		1.5	1.0	
Glyoxylic		55	12	7.2
Pyruvic		1.5	1.2	1.2
Esters:				
Ethyl formate		18	60	54
Diethyl oxalate		32	7.5	50
Methyl acrylate		10	1.1	
Methyl lactate		88	6.1	
Amides:				
Formamide		21	8.2	53
Dimethylformamide		1.6		9.4
2-Pyrrolidone		5.3	12	
Imide: Succinimide		3.0		
Urea	1, 7	2.6		
Amines:				
Butylamine		6.6	2.1	
Aniline	1, 6		1.3	3.1
Diethylamine		5.1	2.0	
Piperidine		1.4		
Pyrrolidine		2.5		
Pyrrole			2.3	14
Triethylamine		3.2	5.1	
Hexamethylenetetramine	1	1.2	2.4	5.6
Dimethylaniline			2.1	40
Ethylenediamine		1.3		
1,2-Diaminopropane		1.2		
o-Phenylenediamine	6	5.9	10	17
p-Phenylenediamine	6	110	13	7.4
Allylamine		1.0		
1-Amino-2-propanol		13	1.0	
1-Amino-3-propanol		4.3	1.8	10
o-Aminophenol	6	21	5.4	7.4

*See list at end of table.

TABLE 15.1.—*Average Power Densities for Fuels Tested* (*458*)—Continued

	References*	Maximum power, mW/cm^2		
		pH 14	pH 7	pH 1
Amines—Continued				
p-Aminophenol	2, 6	37	10	20
p-Dimethylaminobenzaldehyde	...	...	...	1.7
Glycine	...	1.1	...	...
Alanine	...	2.0	...	...
Hydrazine	1, 2, 6, 7	1600	1000	700
Methylhydrazine	6	5.6	4.1	10
1,1-Dimethylhydrazine	6	8.0	36	6.2
Phenylhydrazine	6	12	23	9.1
Formohydrazide	...	630	240	210
Semicarbazide hydrochloride	6	530	305	275
Hydrocarbons:				
Hexane	...	1.1	1.4	...
Decalin	8	1.0	...	...
2-Methylbutene-1	...	...	...	1.1
2-Methylbutene-2	...	1.0	...	1.3
4-Methylpentene-2	...	1.0	...	1.1
Hexene-1	...	...	1.2	...
Hexene-2	...	...	...	...
Heptene-3	...	1.0	...	...
2,4,4-Trimethylpentene-1	...	...	...	...
Cyclopentene	...	...	1.1	...
Cyclohexene	...	1.0	...	...
Styrene	...	...	...	...
Iso-allylbenzene	...	...	...	...
1,5-Hexadiene	...	...	1.4	...
Fluorene	...	...	...	...
Pentyne-2	...	1.0	...	...
Hexyne-1	...	1.0	...	...
Alkyl halides:				
n-Propyl chloride	...	...	...	...
n-Propyl bromide	...	...	...	...
n-Propyl iodide	...	...	...	...
Epoxides:				
Ethylene oxide	5	100	10	9.7
Propylene oxide	...	120	3.	13
Styrene oxide	...	16	...	...
Cyclohexene oxide	...	2.7	...	1.5
2,3-Epoxy-1-propanol	...	98	9.	4.3
Acetals:				
Glycolformal	...	1.7	3.	58
Acetaldehyde dimethylacetal	...	12	9.	5.6
Malonaldehyde tetraethylacetal	...	3.2	1.	2.8
Ketal: 2,2-Dimethoxypropane	...	13	20	46
Ortho ester: Triethylorthoformate	...	6.9	5.	8.2
Ketene: Ketene dimer	...	...	1.	1.2
Cyano compounds:				
Acetonitrile	...	1.5	...	...
β-Methoxypropionitrile	...	2.2	...	...
Cyanoacetic acid	...	1.8	...	...
Iminodiacetonitrile	...	1.4	...	...
Oxime: Acetaldoxime	...	1.9	2.	2.6
Nitroso compound: 2,4-Dinitrosoresorcinol	...	2.5	1.	3.8

*See list at end of table.

TABLE 15.1.—*Average Power* Densities *for* Fuels Tested (*458*)—Continued

	References	Maximum power, mW/cm²		
		pH 14	pH 7	pH 1
Sulfur compounds:				
1,2-Ethanedithiol		4.2	3.8	2.2
Thioglycolic acid		13	18	110
Ethyl sulfide				
Thioacetic acid		32	12	4.3
Thiourea		78	16	310
Ethylenethiourea		5.8	12	132

1. Monsanto: Report *458.*
2. Moos, **A.** M.; von Fredersdorff, C. G.; and Schlatter, M. J.: Ind. Eng. Chem., vol. 54, 1962, p. 65.
3. Report ***195.***
4. Esso: Report *214.*
5. Report *253.*
6. Glicksman, R.: J. Electrochem. Soc., vol. 108, no. 1, 1961, **p.** 922.
7. Lockheed: Reports *404* and 408.
8. California Research Co. : Report *130.*

there was a large increase in the oxidation rate of many fuels.

(7) Insoluble compounds gave low performance.

Oxidation of vapors of gasoline, 2,2,4-trimethylpentane, and cyclohexane at platinum-impregnated porous-carbon caps was investigated (Surface Processes, 587, 1962) in H_2SO_4 and KOH. Fuel vapor and inert gas were bubbled through the carbon electrode immersed in electrolyte. Open-circuit potentials were about 0.5 volt anodic to the reversible hydrogen electrode (in the same solution) and current densities of 1 to 5 A/sq ft were obtained at 0.7 to 0.8 volt anodic, in 6 *M* KOH or 6 *N* H_2SO_4 at 194" F (90° C). Open-circuit voltage was reached more quickly in KOH and performance increased with temperature. Cyclohexane gave a lower performance than the other hydrocarbons.

The relative reactivity of straight-chain saturated hydrocarbons (C_1 through C_{16}) at Pt electrodes (Teflon-bonded type) and in several different electrolytes was studied by the General Electric Co. (***294*** through ***311,*** January 1960 to present). Results are summarized in table 15.3. For all of the electrolytes (conc. H_3PO_4, 35 percent HF, CsF·HF, and Cs_2CO_3), activity went through a maximum at C_2H_6, C_3H_8, or C_4H_{10} (usually C_3H_8), depending on the electrolyte, voltage, and temperature. The activities of C_2 through C_4 hydrocarbons were generally considerably higher than other hydrocarbons tested. Tests in H_3PO_4 with i-butane, i-pentane, cyclopentane, cyclohexane, and iso-octane showed these fuels to be less reactive than their straight-chain analogs. The relative activity of some straight-chain saturated hydrocarbons (C_1 through C_7) in **3** ***N*** H_2SO_4 at 212" F (100° C) at Raney platinum electrodes containing 180 mg Pt/cm² (ref. 15.2) gives conclusions similar to those above (see table 15.4).

15.2.2 Catalyst Screening

The following metals, as well as some mixtures and alloys of these metals, were tested (General Electric, ***249*** through *260,* 1960 to 1962) for catalytic activity in the anodic oxidation of hydrocarbons: B, Ti, Zr, Ta, Cr, Mo, W, Mn, Fe, Ru, Os, Co, Rh, Ir, Ni, Pd, Pt, Cu, Ag, C Si, Sn, Pb, Sb, and Bi. Polarization curves at room temperature were obtained with the catalyst either incorporated into a Teflon binder (at times mixed with activated carbons), or mixed with carbon and pasted onto an Ni or Pt screen. Both acidic and basic electrolytes were used with a variety of fuels including H_2, CO, C_2H_4, C_3H_6, and C_3H_8. About 500 systems were tested. Platinum was found to be the most active simple catalyst for anodic oxidation of hydrocarbons. Teflon electrodes containing the catalyst on activated carbon gave the poorest performance ($i_L < 1$ mA/cm²) ; performance improved for Teflon electrodes containing the catalyst alone ($i_L \sim 5$ mA/cm²). In general,

TABLE 15.2.—*Fuel Current Density at 0.5 Volt Versus Hydrogen Electrode; Platinized Platinum Electrodes (458)*

Current density, m/Acm^2	Tempertture, °C	1M KOH	Tempertture, °C	1M buffer	Tempertture, °C	1 *M* H_3PO_4
>100	90	Hydrazine	90	Formic acid (pH 6.1)		
	30	Hydrazine				
	90	Formohydrazide				
	90	Semicarbazide HCl				
50 to 100	30	Formaldehyde	90	Hydrazine (pH 9)	90	Formamide
	30	Formohydrazide	90	Semicarbazide HCl	90	Hydrazine (pH 2.2)
	30	Semicarbazide HCl				
10 to 50	90	Methanol	90	Formaldehyde	90	Formic acid
	90	Ethanol	30	Formic acid (pH 6.1)	90	Ethyl formate
	30	Ethanol	90	Ethyl formate	30	Hydrazine (pH 2.2)
	90	Benzyl alcohol	90	Formamide	90	Formohydrazide (pH 1.6)
	90	Ethylene glycol	30	Hydrazine (pH 9)	90	Semicarbazide HCl
	90	1,2-Propanediol	30	Semicarbazide HCl	30	Semicarbazide HCl
	90	Glycerol	90	Thioglycolic acid (pH 5.9)	90	Thioglycolic acid
	90	Inositol			90	Thiourea
	30	Inositol				
	90	Formaldehyde				
	90	5-Hydroxypentanal				
	30	Glyoxylic acid (pH 13.2)				
	90	Diethyl oxalate				
	90	Formamide				
	90	Ethylene oxide				
	90	Thioacetic acid (pH 13.2)				
5 to 10	90	Isopropanol	90	Methanol	90	Ethanol
	30	Isopropanol	90	Isopropanol	30	Ethanol
	30	Glycerol	90	Glyoxal	90	Isopropanol
	90	2-Ethoxyethanol	90	Formohydrazide	30	Hydroquinone
	90	Diethylene glycol	90	Ethylene oxide	30	Formic acid
	90	Glyoxal (pH 13)	90	Thioacetic acid (pH 5.8)	90	Glyoxylic acid
	30	Dextrose	30	Thioacetic acid	30	Ethyl formate
	90	Acetoin			90	Hexamethylene tetramine
	90	Methyl glyoxal			90	Glycol formal
	90	Ethyl formate				
	30	Diethyl oxalate				
	30	Ethylene oxide				

group 8 metals were best for hydrocarbons, and Cu and Ag showed some activity for CO. Performance was better in acid than in base for saturated hydrocarbons, while for C_2H_4, performance was about the same in acid and in base. No surface areas were reported for these catalysts.

Teflon-bonded platinum black (*20* mg Pt/cm^2),

TABLE 15.3.—*Relative Reactivity of Straight-Chain Saturated Hydrocarbons (294 through 311)*

System	arbon No.	i(mA/cm^2) at 0.2 V (cell voltage, IR included)				
		150" *C*	175" *C*	200" C		
Hydrocarbon (Pt)/H$_3$PO$_4$($\sim$90%)/(Pt)O$_2$.	2	75	103	....		
	3	100	131	164		
	4	101	131	....		
	5	89	....	....		
	6	68	....	....		
	7	56	....	....		
	8	46	81	103		
	10	36	....	85		
		i(mA/cm^2) at 0.5 V (anode versus RHE, IR free)				
Hydrocarbon (Pt)/Cs$_2$CO$_3$/(Pt)O$_2$, $t = 130$" *C*......	1	....	0.27	....		
	2	....	3.00	....		
	3	....	3.00	....		
	4	....	.88	....		
	5	....	.99	....		
	6	....	.51	....		
		i(mA/cm^2) at indicated voltage (anode versus RHE, IR free)				
		0.3 V	0.4 V	0.5 V	0.6 V	0.7 V
Hydrocarbon (Pt)/CsF ·HF/(Pt)O$_2$, t = 150"C. ...	1	12	30	55	90	130
	3	40	130	300	400	500
	4	6	20	58	140	200
	6	6	18	35	68	100
	8	7	18	35	68	90
		i(mA/cm^2) at indicated voltage (anode versus RHE, IR free)				
		0.4 V	0.5 V	0.6 V	0.7 V	
Hydrocarbon (Pt)/HF(35%)/(Pt)O$_2$, $t = 110$" C.. ..	1	11	22	28	29	
	2	8	45	....	60	
	3	18	54	74	88	
	4	13	50	71	90	
	5	10	24	45	55	
	6	5	12	29	42	
	8	.7	2.2	4.3	7.0	
	10	.5	2.2	4.0	5.5	
	16	.7	2.1	3.5	4.0	

pressed onto platinum screen, was used as a methanol electrode (Engelhard, ***213,*** *1963)* at *212"* F (100° *C),* *2 N* H$_2$SO$_4$, *2* weight-percent methanol. The electrolyte was pressurized so that higher temperatures could be used (see app. *C).* Raney-type blacks (made from alloy with aluminum, pulverized, and leached with NaOH at less than *176"* F (80"C)) were compared to conventional platinum blacks. Platinum, **Ru,** and Rh were stable in air, but Ir and Rh were pyrophoric; they gave good OCV with methanol, but were not as good as normal platinum black under load. Increased temperature gave better performance, leveling off at 212° to *257"* F *(100"* to *125" C),* possibly due to recrystallization of the Raney structure. **A** number of noble-

TABLE 15.4.—*Anodic Oxidation of Hydrocarbons on Raney Platinum Electrodes:* 3 *N* H_2SO_4, *212" F (100" C)*[a]

Fuel	Percent oxidation to CO_2 and H_2O	OCV		
			50 mA/cm²	200 mA/cm²
H_2	...	0	0.07	0.24
CO	...	0	.10	.42
CH_4	100	.14	.35	>.66
C_2H_4	100	.21	.35	.68
C_2H_6	100	.12	.30	.60
C_3H_8	100	.13	.30	.60
C_4H_{10}	< 100	.15	.41	.78
C_5H_{12}	< 100	.15	.45	>.79
C_6H_{14}	< 100	.15	.55	...
C_7H_{16}	...	.15	.66	...

[a] Ref. 15.2.

metal alloy blacks were found to be more active for the anodic oxidation of CH_3OH (in 2 *N* H_2SO_4 at 212" F (100° C)) than platinum black alone (table *15.5*). The greater activity of alloys

TABLE 15.5.—*Comparison of Catalytic Activity of Platinum Black and Some Noble-Metal Alloys in* CH_3OH *Oxidation (213)*

Catalyst	Polarization at 50 mA/cm², volts	Remarks (wt-% used)
Pt black	0.49	Better than Ir>Rh>Ru.
Binary alloys:		
(1) Pt+base metals:		
(a) Ti, Zr, V, Nb. Ta	0.40–0.45	Best: Pt 67:Mo33; Pt 80:Re20 (Improvement gone at 302° F (150" C) except for Pt-Nb).
Mo, W, Mn, Re	0.37–0.51	
(b) Fe, Ni, Co, Be, Pb, Cu, Bi and Sb	Worse than Pt black alone	
(2) Pt+noble metals:		
Os	Better	
Ru	0.29	Best for 20% Ru (RuPt) and 33% Ru(Ru_2Pt). More stable with time.
Rh	Same	
Ir	Better	
(3) Ru or Os+Zr, W, Re..	Worse	
Ru+:		
Pd	Same	
Ir	Worse	
Rh	0.37 to 0.42	Best for Ru 90:Rh 10.
Os+: Rh, Pd	Same	
Ternary alloys of Pt and Ru with—		
Au	0.29-0.33	Best for Pt 60:Ru 20:Au 20. Not so readily poisoned by HNO_3.
Re.	0.28–0.34	
W	0.30–0.45	
Ta, Zr, Pd, Mo..	0.30–0.36	

than of platinum black alone could not be correlated with electronic factors. Possibly an increased concentration of surface defects was responsible for the increase in activity. X-ray crystallography of the blacks showed true alloys between Pt, Ru, and Os.

The gas-phase exchange reaction between methane and deuterium was used as a means of screening metals and alloys for catalytic activity (General Electric, **294** through **311).** The catalysts were equilibrated with D_2, and the rates of formation of each deuterated methane, HD, and H_2 and the rates of disappearance of CH_4 and D_2 were measured after admitting CH_4 to the system. Catalysts were prepared by reduction of aqueous chloride solutions of the appropriate metal salts with a 5 weight-percent solution of $NaBH_4$. Surface areas, which ranged from 3 to 10 m^2/g, were determined by the BET method. X-ray measurements revealed that the Rh-Pd, Pt-Pd, and Pt-Ru systems form true solid solutions over their entire composition ranges, but Ru-Rh does not. All of the catalysts tested showed considerable activity for the exchange reaction above 212" F (100° C). The order of activity at 302" F (150" C), as rate of CH_4 disappearance per square centimeter of catalyst, was $Pt > Rh > Ir > Ru > Pd$ for pure metals. Increased activity was found for binary alloys of Pt-Ru, Pt-Rh, and Ru-Rh. Rate of propane cracking was also measured on the same catalysts. The volume of CH_4 produced (major product of the cracking reaction) in 1 hour at 302" F (150" C) was used as a measure of the rate of cracking. Results obtained from these measurements were in qualitative agreement with those of the CH_4-D_2 exchange reaction.

This test was used to investigate the effects of the method of preparing a catalyst on its catalytic activity. Platinum black was prepared by each of the following methods:

(1) A boiling neutral solution of H_2PtCl_6 was reduced with sodium formate. The product was colloidal but coagulated upon addition of $Al_2(SO_4)_3$. Electron micrographs of washed and dried black showed it consisted of uniform particles of about 100 angstroms in diameter.

(2) An alkaline solution of H_2PtCl_6 was reduced with 85 percent hydrazine hydrate. The washed and dried black consisted mainly of regular spherical particles about 0.3 to 0.5 micron in diameter.

(3) A boiling neutral solution of H_2PtCl_6 was reduced with a 40 percent formaldehyde solution. The washed and dried product consisted of large regular particles about 1 micron in diameter.

(4) A warm solution of H_2PtCl_6 was reduced with an excess of 5 percent $NaBH_4$ solution. The black was further reduced for 3 hours in flowing H_2 at 572" F (300° C). The resultant black was composed of irregular amorphous agglomerates.

(5) A solution was prepared in same manner as (4), with the final reduction in H_2 at 572" F omitted. The black was composed of fine uniform particles of about 100 angstroms in diameter.

(6) This black was obtained from Fisher. It consisted of very small particles similar to those of sample (5) with a diameter of about 100 angstroms.

These six samples were reduced with H_2 at room temperature, and after evacuation at 302" F (150" C) their BET areas were determined. This treatment sintered samples (5) and *(6)* from areas of 15 m^2/g and 19.5 m^2/g to 10.5 m^2/g and 10 m^2/g, respectively. Table 15.6 shows the rate of CH_4 formation at 302" F (150° C) for each of the samples. These results indicate that reduction with $NaBH_4$ solution gives the most active platinum black. No tests were made on the electrocatalytic activity of the blacks.

Relative electrocatalytic activity of some noble metals for ethylene oxidation (186" F (80" C), 1 *N* H_2SO_4) was determined under ultrapure conditions (University of Pennsylvania, **740** through **743;** also ref. 15.3). Smooth, solid electrodes were degassed and cooled in an inert atmosphere in a furnace mounted directly to the electrolytic cell, so that electrodes were immersed without being exposed to contamination. Complete oxidation of C_2H_4 to CO_2 was observed on Pt, Ir, and Rh. On Au and Pd, practically no CO_2 could be detected and the

TABLE 15.6.—*Comparison of Catalytic Activity of Platinum Blacks Prepared by Various Methods via the Rate of* CH, *Formation from* C_3H_8 *Cracking at 302" F (150" C) (294 Through 311)*

Sample	Reducing agent	Surface area, $M^2/8$	Specific rate of CH_4 formation, molecules CH_4/sec-cm²
1	HCOONa	6.6	7.7×10^{10}
2	$N_2H_4 \cdot H_2O$	1.3	$<6\times10^8$
3	HCHO	1.8	0.17×10^{10}
4	$NaBH_4$	1.9	1.0×10''
5	$NaBH_4$	10.5	3.6×10^{10}
6	Fisher Pt black	10.0	1.5×10^{10}

main products of the reaction were aldehydes and acetone. The Tafel slopes as well as pH and pressure effects were different for the two groups of metals. The order of chemical reactivity in the two groups of metal catalysts was Pt> Rh>Ir and Pd>Au.

Table *17.4* gives some results on relative activity of catalysts deposited in porous carbon electrodes, using OCV as an index of relative activity. Platinum, Ir, or Rh was electroplated onto platinum screen, which was immersed in ethane-saturated *6 M* H_2SO_4 (see sec. *17.5).* Galvanostatic techniques indicated that platinum adsorbs fuel and can support current at *194" F (90" C)*, whereas Rh and Ir do not.

Solid electrodes were electroplated at different current densities to give relatively smooth or rough deposits of catalyst (Monsanto Chemical Co., *469, 1960).* Half-cell studies were made with electrolyte stirred ultrasonically (Branson Ultrasonic, No. L.G., *150)* at 30 *000* cps. Polarization at a constant current density varied with time, and values after *1* minute were used as an index of activity. Catalytic results are shown in table *15.7;* current densities were not affected by rate of stirring at concentrations greater than about 0.5 molar. Although higher area, rough electrodes gave better performance than smooth electrodes, the order of catalytic effect was not always the same for the two types. This is difficult to explain and results must be considered inconsistent.

TABLE 15.7.—*Catalyst Results From 467 Through 469 (Monsanto)*

Fuel	Electrolyte	Electrode	Result
N_2H_4	5 MKOH	Smooth	Rh>Ir, Pt, Pd>Ag, **Au**
		Rough	Rh>Au>Pt, Pd, Ir
NH_4OH	5 M KOH	Smooth	Ir> >rest
		Rough	Pd>Ir>rest
CH_3OH	KOH	Smooth and rough	Pt>Pd>Ir>Au, Rh
	H_2SO_4	Smooth and rough	Pt, Ir>Pd>Au, Rh
	Na_2SO_4		Rough Au best, but all results poor compared to strong acid or base

Catalysts were tested (Esso, *214* through *217)* for anodic oxidation of *1 M* methanol in 30 weight-percent H_2SO_4 at *140"* F (60" **C).** Electrodes were prepared by coelectrodeposition of platinum and metal onto platinum sheet *(214).* Results are shown in table *15.8.* The Tafel slopes and exchange currents were taken over short current ranges and probably have little theoretical significance. The results showed a compensation effect; catalyst with high exchange current also had a steeper Tafel slope, so that polarization at 50 mA/cm² was not greatly different for any of the catalysts. The second group of catalysts was prepared by coprecipitation

TABLE 15.8.—*Tafel Slopes and Exchange Currents of Platinum and Cocatalysts, 1 M* CH_3OH, *30 Percent* H_2SO_4, *140" F (60" C), Esso (214)*

Catalyst composition	Polarization at indicated mA/cm²			−Log exchange, current (I_0)	Tafel slope (b)
	1	10	50		
Pt-Fe				4.0	0.103
Pt-Ni				4.3	.109
Pt-Rh-Fe				5.4	.081
Pt-co				5.5	.084
Pt-Pb				6.0	.085
Pt				7.3	.066
Pt-Rh				7.9	.063
Pt-Cu				8.4	.059
Pt-Au				8.8	.058
Pt-Pd				21.0	.033
Pt	0.48	0.57	0.61	11.2	.047
Pt-Co	.55	.59	.65	9.4	.058
Pt-Ni	.55	.61	.68	9.1	.060
Pt-Fe	.41	.55	.60	6.5	.073
Pt-Mo	.22–.37	.52	.57		
Ir	0.52	.58	.62	9.9	.053
Ru		.60			

using $NaBH_4$, followed by evaporation of the aqueous suspensions on a platinum sheet to form the electrode. The compensation effect is clearly seen from polarizations reported for this group. Nickel and nickel boride dissolved in the acid, but Pt+Fe was stable; X-ray data showed the Pt-Fe codeposit to be a true alloy.

Later work *(217)* using coprecipitated catalysts showed that Pt-W, Pt-V, Pt-Ni, Pt-Co, Pt-Pb, Pt-Mn, Pt-Au, and Pt-Ir gave results similar to those in table *15.8.* Addition of Fe, Cu, Au, or Re to Rh poisoned the rhodium, but Rh-Ir was active. Au and Re were inactive. X-ray lattice spacing showed that alloys were formed in most cases. Molybdenum cocatalysts (Pt-Mo-Co, Pt-Mo-Fe, Pt-Mo, and Rh-Mo) were more active at low current densities than single or binary catalysts, but Au-Mo, Ir-Mo, and Pd-Mo were inactive. The effect was attributed to a surface redox couple

$$Pt[Mo^{6+}]+\text{fuel}\rightarrow Pt[Mo^{5+}]+CO_2+H_2O$$
$$Pt[Mo^{5+}]+e^-\rightarrow Pt[Mo^{6+}].$$

Dissolved Na_2MoO_4 (0.025 *M*) caused chemical decomposition of CH_3OH and HCHO to CO_2 at *176"* F (80° C) in the presence of platinum black, with the production of Mo^{5+}, which could be electrochemically oxidized to Mo^{6+} at **0.3** to 0.5 volt (versus SHE). At higher current densities the molybdenum cocatalysts were not better than platinum and the improved performance at low current densities was irreversibly lost. This initial activity could not be restored.

Electrodes were also prepared by pressing catalyst powder at 2000 psi into a platinum screen welded onto platinum foil. Pt-Ag, Au-Fe, Au-Re, and combinations of Re with Ru, Sn, and Zn were inactive *(216).* Pt with U, Cr, Zn, Sn, or Ir-Ni, was as active as platinum alone; in all cases performance was better than platinum at low currents, but polarization increased more rapidly with increased current. Pt-Ru, Pt-Ru-Fe, and Pt-Au-Fe were better than platinum black. Current density at a given polarization *(217)* was directly proportional to the amount of catalyst. Amounts up to 35 mg/cm² were used.

Titanium nitride, niobium carbide, tantalum boride, molybdenum carbide, zirconium boride, titanium carbide, and titanium boride were found to be noncatalytic in H_2SO_4 (California Research, ***139).*** Impregnated porous-carbon electrodes with H_2SO_4 electrolyte at *176"* F (80° C) gave catalytic activity for ethylene in the order Pt>Pd and Ru>Rh>Ir *(140* and *142).* For propane the order was Pt>Rh>Ru and Pd>Ir. A *10* mole-percent addition of Ir to Pt produced little effect with hydrogen or ethylene fuels, but showed increased activity to propane oxidation. A mixed metal oxide was made by alternate melting and freezing of $LiCO_3$, MoO_3, and V_2O_5. A powder of this material was mixed with platinum black or carbon black and pressed into pellets. Only those pellets with platinum showed activity to anodic oxidation of hydrogen or hydrocarbons. Nickel phosphide and cobalt phosphide had conductivities comparable to those of metals and were active for hydrazine fuel dissolved in acid or alkali electrolytes, but not active for methanol, propane, or ammonia.

Chelates of different metals have been proposed as catalysts for hydrocarbon fuels (Monsanto, ***463*** through ***466,*** 1964). Table 15.9 gives

TABLE 15.9.—*Chelates Prepared for Catalyst Testing* ***466)***

No.	Ligand name	Metal (M)	Decomposition or melting point. °C	Chelate structure
1	Hexafluoroacetylacetone	Ni (II)	194	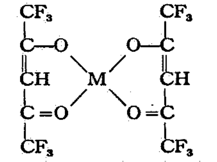
2		Mn (II)	140	
3		Co (II)	155–176	
4	Acetylacetone	Co (II)	140-210	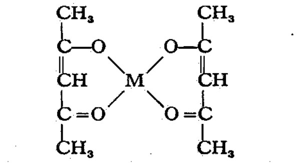
5		Pd (II)	230	
6		Cu (II)	230	
7		Ni (II)	220	
8		Zn (II)	> 300	
9		Pt (II)	> 300	
10	Acetylacetoneethylenediimine	Ni (II)	200	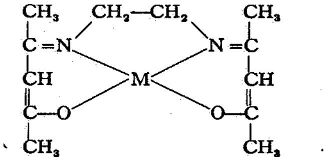
11		Cu (II)	141	
12	8-Hydroxyquinoline	Co (II)	250	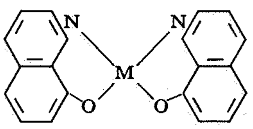
13		Ni (II)	> 300	
14		Cu (II)	290	
15		Pd (II)	200	
16		Pt (II)	> 250	
17	dii (Sal-en)	Ni (II)	283	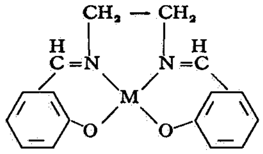
18		Cu (II)	280	
19		Pt (II)	> 300	
20		Pd (II)	> 300	
21		Co (II)	> 273	
22		Zn (II)	> 300	
23	Tetraphenylporphine	Pd (II)	> 360	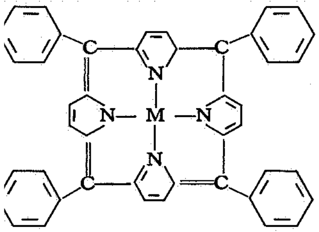
24		Ni (II)	320	
25		Zn (II)	> 360	
26		Pt (II)	> 360	
27		Co (II)	> 360	
28	Tetrabenzodiazoporphine	Cu (II)	> 360	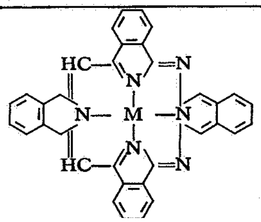

TABLE 15.9.—*Chelates Prepared for* Catalyst Testing (*466*)—Continued

No.	Ligand name	Metal (M)	Decomposition or melting point, °C	Chelate structure
29	Phthalocyanine.	Co (II)	> 360	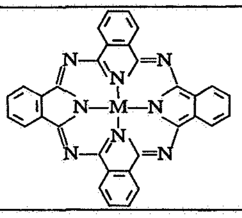
30		Ni (II)	> 360	
31		Cu (II)	> 360	
32		Pd (II)	> 360	
33		Pt (II)	> 360	
34	Octachlorophthalocyanine	CU (II)	>360	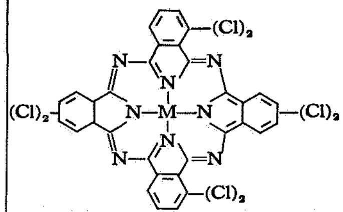
35	Polychlorophthalocyanine	Cu (II)	> 360	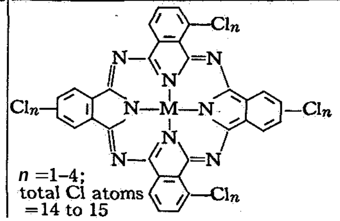 n =1-4; total Cl atoms =14 to 15

the chelates tested and the temperature at which visible physical change occurred on heating. Anodic stability of chelates was determined by polarograms of 0.01 *M* solutions in pyridine (0.1 *M* Li_2CO_3); they were all stable. Stability to reduction by fuel was tested using 1 *M* N_2H_4 in **KOH** at 194" F (90° C); palladium-acetylacetone was not stable. Stability to electrolytes was measured in 35 weight-percent **KOH** at 194" **F** (90° C), saturated cesium carbonate solution at 302° F (150" **C**), and phosphoric acid at 302" F (150° **C**); only the phthalocyanines were expected to be stable in strong phosphoric acid. Hexafluoroacetones, acetylacetones, and acetylacetoneethylenediimines hydrolyzed in days or weeks in **KOH** and $CsCO_3$; the others were insoluble and stable. Copper octachlorophthalocyanine was stable in phosphoric acid.

Solutions of chelate in dimethylformamide (DMF) were sprayed onto porous carbon cubes (pure carbon FC–14) in a vacuum chamber. The solvent was evacuated and the process repeated until 1 to 5 weight-percent of chelate was impregnated into the carbon, which was then dried under vacuum at 212" F (100° C) for several hours. The carbon cube was immersed in electrolyte containing dissolved fuel (N_2H_4, **HCOOH**, and CH_3COOH), and the current-voltage curve of a linear current increase to 150 milliamperes over 30 minutes was compared to that of a carbon cube containing no catalyst. Thirty-three of the chelates were found to be active for hydrazine (in **KOH**), 19 for formic acid, and 12 for acetic acid. No pattern was apparent with respect to ligand field strength. polarization in creased within several hours.

Porous electrodes were made from acetylene black (Shawinigan), chelate catalyst, and Teflon mixtures sandwiched between porous Teflon sheet and metal screen, sintered at 482° F (250" C). These were used as gas diffusion electrodes in Cs_2CO_3 or H_3PO_4, with hydrogen or propane fuel. Results were erratic, potential oscillations occurred, and activity was low except for hydrogen at platinum-black catalyzed electrodes. Copper phthalocyanine was formed in situ on the substrate before sintering, but results were inconclusive. Physical effects of electrode structure and wetting were found to be obscuring catalytic effects. To overcome this problem, Ag-Pd membranes were used as diffusion electrodes (see ch. 3), with chelate deposited on the electrolyte side by evaporation of solvent or sublimation. It was necessary to rhodium-plate the gas side to get good performance; limiting currents with hydrogen were 300 to 400 mA/cm². Deposition of chelates (about 0.3 mg/cm²) decreased performance.

Chelate catalysts impregnated into carbon cubes gave significant current densities for dissolved fuels, indicating that the catalysts have sufficient semiconductivity to pass current to the carbon substrate, but the arbitrary nature of the test makes it difficult to draw positive conclusions concerning catalyst activity. Results were reported as "polarization from open circuit," but the open circuit values varied considerably for **a** given fuel so that polarizations are not directly comparable. Table *15.10* gives the best results from carbon cube experiments, with potentials referred to hydrogen electrode in the same solution.

TABLE 15.10.—*Comparative Activity of Chelate Catalysts (466)*

Fuel/electrolyte/temperature	Ligand	Metal	OCV versus H_2	Potential at 100 mA/cm²	10 mA/cm²
N_2H_4/KOH/194° F (90° C)		Pt	−0.15	0.08	....
	Sal-en	Pt	.16	.21	....
	HFAc	Ni	.025	.05	....
	Sal-en	Ni	−.07	....	....
	8-HQ	Pt	.18	.32	....
	8-HQ	Ni	.02	.15	....
	8-HQ	Co	.02	.20	....
	TPP	Pt	.17	.23	....
HCOOH/K_2HPO_4-KH_2PO_4, pH 6/194° F (90"C)		Pt	.16	.5	....
	Ac	Pd	−.02	.35	....
	Sal-en	Pt	.00	.47	....
CH_3COOH/pH 6/194° F (90° C)		Blank	.56	....	1.66
		Pt	.94	....	1.25
	Ac-en	Cu	.47	....	.65
	TBP	Cu	27	....	.76
	Ac	Pt	.13	....	.32
CH_3COOH/Cs_2CO_3/302° F (150"C)	No proven activity.				
CH_3COOH/5*N* H_2SO_4/194° F (90° C)					

15.3 GENERAL ELECTRIC CO., HYDROCARBON FUEL CELLS, (*294* through *311*)

At present, the most advanced saturated hydrocarbon fuel cell is the medium-temperature propane cell developed by General Electric with proprietary Teflon-bonded platinum electrodes and concentrated phosphoric acid electrolyte. Cell construction is still in the development stage. The results reported here are for cells with electrolyte circulation and small fractional utilization of fuel passing through the anode chamber. Propane was shown to be one of the most active saturated hydrocarbons. Use of *85* percent phosphoric acid enables cell temperature to reach 302° F (150° C) without boiling of electrolyte or direct reaction with fuel. Figure *15.1* shows performance of laboratory cells *(309* and *310).*

Most results have been obtained with electrolytes of aqueous phosphoric acid or cesium carbonate solutions. The latter gave poor performance with saturated hydrocarbons, with limiting currents of about *5* A/sq ft. This was attributed to low solubility of hydrocarbons in carbonate solutions. Unstable operation was also observed in the Cs_2CO_3 system, with voltage cycling at higher current densities. Phosphoric acid concentration had to be high to prevent water loss to the fuel stream, and performance was considerably improved by using water in the propane feed. The faradaic efficiency of conversion of propane to CO_2 and H_2O was 100 per-

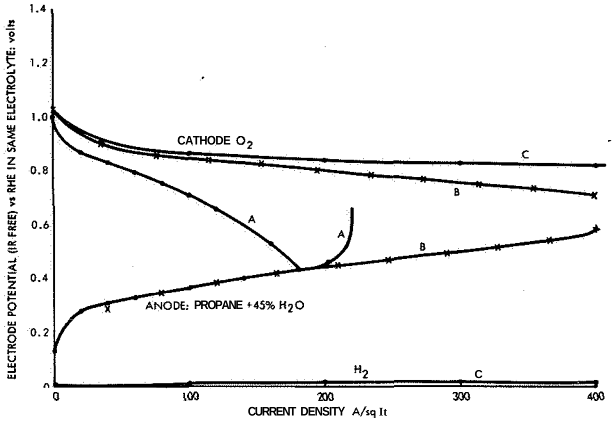

All cells use the Teflon-bonded platinum-black electrodes developed by General Electric. Hydrocarbon vapor flows at high rates through the anode gas-chamber and electrolyte is circulated.

A. 85 weight-percent H_3PO_4 aqueous electrolyte; 35 mg Pt/cm^2; 302° F (150° C); life test of over 800 hours; **IR** loss at 200 A/sq ft=0.22 volt for ⅛-inch-thick electrolyte.

B. 60 HF:29 CsF:11 H_2O mole-percent; 37 mg Pt/cm^2; 302° F (150° C); no life data.

C. Hydrogen-oxygen fuel cell, 6 ***N*** H_2SO_4; 77° F (25"C); **45** mg Pt/cm^2.

FIGURE 15.1.—Performance of GE propane cell *(310)*.

cent. Adding HF, KH_2PO_4, $HClO_4$, or H_2SO_4 to phosphoric acid did not improve performance. Temperature increase from 230° to 356" F (110° to 180" C) improved performance by a factor of nearly 2.

Platinum, iridium, rhodium, and palladium blacks were tested, and only platinum was satisfactory; an alloy of Pt-Ru (28 weight-percent Ru) was better than Pt alone. Mixtures of platinum black with WO_2, MoO_2, WC, W_2C, Mo_2C, NbN, TaN, TiN, and VN gave poorer performance than platinum black alone. For oxygen cathodes and propane anodes, performance was directly related to amount of platinum black used (mg/cm^2). It was not possible to dilute the platinum with tungsten or tantalum. The anodes cracked during prolonged use at 302" F (150° C) in 85 percent H_3PO_4, due to shrinkage of the catalyst caused by recrystallization of the platinum and not by thermal cycling or deterioration of the Teflon binder. Tendency to crack was reduced when sintered metal substrates W and Ta were used in place of platinum screen.

Performance was greatly improved by using HF-CsF-H_2O electrolytes (see fig. 15.1). The function of CsF was to lower vapor pressure and allow higher temperatures to be used. The anode improved as HF concentration was increased. Again, faradaic efficiency of propane use was 100 percent. Corrosion tests showed Rh, Pd, Ir, Pt, and Au to be stable under cell conditions.

15.4 METHANOL FUEL CELLS

15.4.1 Esso Research and Engineering Co., Soluble Carbonaceous Fuel-Air Cells, January 1962 to December 1962 and January 1963 *to* December 1963

Table 15.8 gives preliminary results of methanol oxidation at solid electrodes immersed in methanol-sulfuric acid solution. **A** platinum electrode having 8 mg/cm^2 of platinum black deposited on the surface had minimum polarization for acid concentrations between 0.15 and 3 *M;* complete conversion to CO_2 and H_2O was obtained *(214)*. The electrode was used in conjunction with the Esso air-nitric acid cathode and reaction products from the cathode poisoned the anode and caused voltage cycling. Similarly, methanol decreased performance of the cathode at concentrations greater than 0.1 *M*. Therefore, it was necessary to separate the anode and cathode by membranes which allowed ionic conduction but reduced diffusion from one electrode to another.

Laboratory,cells were constructed *(217)* with platinized-platinum screen anodes and proprietary cathodes. Electrodes were pressed against each side of an Ionics CR–61, sulfonated polystyrene cationic membrane (IEM) which separated anode and cathode compartments. Fuel (1 volume-percent CH_3OH) dissolved in electrolyte (30 weight-percent H_2SO_4) was flowed through the anode Compartment, with CO_2 removal from gas ports at the top of the cell. Similarly, air, nitric acid, and sulfuric acid flowed through the cathode compartment, with excess air removed at the top of the cell. At 176" F (80" C), a maximum power density of 15 W/sq ft (current density 50 A/sq ft) was obtained, with IR loss less than 50 millivolts. Loss of methanol in the CO_2 exhaust was about 3 percent of methanol consumed.

Anodes of catalyst black pressed into screen (P-type) operated for 1000 hours at 50 mA/cm^2 with little loss in activity *(203)*. Performance was insensitive to methanol concentration above 0.4 *M*. Improvement of power density was obtained by providing escape channels for CO_2 between the electrode and membrane. Direct O_2 diffusion electrodes (platinum black, Teflon) gave as good performance as O_2-nitric acid cathodes. American Cyanamid cathodes were used but leaked, even with a membrane, in the presence of methanol-H_2SO_4 at the anode. At 140" F (60° C), cell performance was 50 A/sq ft at 0.3 volt. Poor cathode operation was attributed to CO_2 production at the cathode, since some methanol diffused to the electrode and was oxidized.

A 10-cell stack was built, with single-cell dimensions of 9 by 5⅝ by 5/16 inch. Stack power was as expected from single-cell studies. The study demonstrated need for considerable improvement in both the methanol anode and the direct oxygen cathode. Some systems work was done, but was obviously premature in the light of low basic power density and efficiency of the cell. Figure 15.2 gives the best performance quoted; at 20 A/sq ft, power density was 10 W/sq ft at a voltage efficiency of about 40 percent.

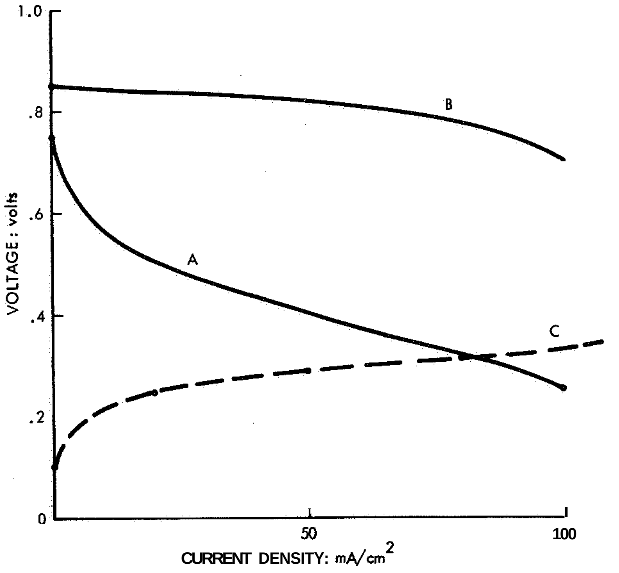

A. Potential of Esso methanol-air fuel cell *(217)*.

4 volume-percent CH_3OH in 30 weight-percent H_2SO_4 at 181° F (83° C); proprietary Teflon-bonded anode; American Cyanamid air electrode.

B. Potential (versus hydrogen in same electrolyte) of American Cyanamid air electrode.

30 percent H_2SO_4; 181° F (83° C).

C. Potential (versus SHE) of Engelhard methanol electrode (*213*).

2 volume-percent CH_3OH in $2N_2$ H_2SO_4 at 194° F (90° C); Teflon-bonded 60 Pt:20 Ru:20 Ta catalyst, 20 mg/cm².

FIGURE 15.2.—Performance of methanol cells.

15.4.2 Other Methanol Fuel Cells

Carbon powder impregnated with catalyst, or catalyst powder, was painted as a fluid suspension with 5*N* sulfuric acid onto one side of Fiberfrax (aluminum silicate) paper % inch thick (Engelhard, *193).* Two pads were placed on either side of a cation-exchange membrane, forming the system :powder/acid-wet-pad/membrane /acid-wet-pad/powder. Inactive screens were used as current collectors and the system was tested as a hydrogen-oxygen fuel cell or as a methanol vapor-oxygen fuel cell. When methanol or formic acid vapor was used as fuel at room temperature, CO_2 was produced at the cathode and poisoned it *(195).* Addition of CO_2 to the O_2 feed had the same effect. Poisoning occurred for platinum or palladium blacks and Pt or Pd on carbon. CO_2 did not affect the fuel electrode, but 30 percent of CO in the fuel feed strongly inhibited the reaction, even with hydrogen as fuel. CO also poisoned the cathode, but at 179° F (82" C) the poisoning effect of CO_2 or CO at the cathode was virtually eliminated *(196).* Concentrations of 5 percent CO poisoned a hydrogen anode even at 176° F (80° C), with rapid disappearance of inhibition when the supply of CO was stopped.

Addition to the electrolyte of Rh, Cu, Fe, Mn, or Ag ions produced no improvement in anode performance. Sb, As, and Bi rapidly poisoned the electrodes *(198).* O_2 inhibited the methanol anode if potential was less than about 0.6 volt, versus hydrogen in same electrolyte, but at more anodic potentials the presence of O_2 had no effect. Electrodes of sintered platinum black-Teflon at catalyst loading of 35 mg/cm² were used with methanol dissolved in electrolyte, and gave better performance as the temperature was raised to 194" F (90° C) *(199).* Gold and lead on platinum were better than platinum alone for a cathode used in conjunction with a methanol anode, because these metals inhibited methanol oxidation at the cathode *(200).*

Table 15.5 gives results of catalyst studies *(213).* By using a pressurized cell (see app. C), temperatures up to 392° F (200° C) were obtained. Electrolytes tried were 2 *M* Na_2SO_4, NaH_2PO_4, and KHCO,. The first two gave poorer anode performance than sulfuric acid, while potassium bicarbonate was better at lower temperatures and the same at 302" F (150° C). Cathode performance was much worse than sulfuric acid for all three electrolytes. Reacted methanol was virtually completely converted to CO_2 and only small traces of HCHO were detected; HCOOH was not detected. Anodes gave increased polarization with time; 0.13-volt increase at 20 mA/cm^2 over 600 hours. Pt-Ru-W anodes gave less deterioration than any other catalysts tested.

Cathodes of Teflon-bonded platinum black gave improved performance as pressure and temperature were increased, but at 1 atmosphere the electrodes were more readily inhibited by methanol at higher temperatures. For example, at 77" F (25" C) the electrode could tolerate 0.5 volume-percent of CH_3OH in the electrolyte, but at 167" F (75" C) only 0.1 percent could be tolerated. Increase of oxygen pressure increased the amount of CH_3OH which could be allowed. **A** methanol-oxygen fuel cell gave about 25 W/sq ft at 40 percent voltage efficiency, with methanol feed rate adjusted to current density to prevent buildup of methanol in electrolyte near the cathode. Figure 15.2 shows anode performance.

The General Electric cell described in section 15.3 was also used with methanol vapor as fuel. Operation at 20 mA/cm^2 for over 500 hours showed no deterioration in power and no accumulation of CH_3OH or products in circulated electrolyte. With Cs_2CO_3 electrolyte at 266" F (130" C), power output was about 10 W/sq ft at a voltage efficiency of 40 percent.

15.5 REACTION MECHANISMS

15.5.1 Introduction

Heterogeneous reaction mechanisms and kinetics form one of the most difficult branches of chemistry to discuss adequately, since very few reactions have been satisfactorily described and the fundamental theory of surface reactions is not well advanced. It is not possible, at present, to predict from *a priori* reasoning how fast a given reaction will proceed under specified conditions. The electrochemical kinetics of hydrocarbon oxidations are particularly difficult to describe because of several effects which interfere with simple interpretations. It is not possible to review here the mass of recent literature or describe in detail all of the data generated in contract reports. Much of the data is contradictory or based on incorrect experimental procedures, and might be explained by several alternative hypotheses. For these reasons, this section will deal mainly with general facts which have been reasonably well established and avoid detailed discussion of specific mechanisms.

Most of the work discussed here has been performed on noble-metal electrodes in aqueous electrolytes. Noble metals are relatively invariant compared to other catalytic electrode materials but, even so, reproducible results can only be obtained by carefully reproducing the surface conditions. For example, the true area of the electrode must be known to obtain basic rate constants. True area corresponds reasonably well to geometric area for a smooth, bright surface, but smooth electrodes often give results which drift with time, due to adsorption of trace impurities which cover the surface. Smooth electrodes are generally activated by alternate anodic and cathodic current pulses, thus stripping off adsorbed impurity, but this may roughen the surface and give nonreduced oxide coatings on the metal. Stable results are more easily obtained with electrodes coated with electrodeposited catalyst such as platinized platinum, which have much greater true surface areas and are not so susceptible to poisoning by trace impurities. The increased area gives order-of-magnitude increase in current density at a prescribed potential, so that currents due to impurity or secondary reactions become negligible compared to current from the main reaction.

In aqueous electrolytes, anodic hydrocarbon oxidation may be studied only over the potential range from hydrogen evolution to oxygen evolution. Electrodes which are active for hydrocarbons are also active for hydrogen, so the lower limit of potential is close to zero volts versus hydrogen in the same electrolyte. If the electrode is set at lower, more negative, potential, vigorous hydrogen evolution will obviously interfere with the reaction under study (electrode potential is actually change in potential in going from the electrolyte to the interior of the electrode, versus reference electrode potential). In practice, the potential range over which no interference occurs is much shorter than hydrogen evolution to oxygen evolution; this can be illustrated as follows.

Consider a platinum electrode which has been reduced in hydrogen and lowered into the electrolyte without contact with air. Chemisorbed hydrogen on the surface reacts according to

$$\mathrm{Pt[H]} \rightleftharpoons \mathrm{Pt} + \mathrm{H}^+ + e^-$$

or

$$\mathrm{Pt[H]} + \mathrm{OH}^- \rightleftharpoons \mathrm{Pt} + \mathrm{H_2O} + e^- \qquad (15.1)$$

These reactions supply electrons to the metal, which set up the electrical double layer and produce a potential close to that of the normal hydrogen electrode in the same electrolyte (thereafter symbolized as NHE in SE). The reaction is fast on platinum and is close to equilibrium. At a given potential versus NHE in SE, there is a set fractional coverage of the surface with [H]. A simple Nernst-Langmuir treatment applied to the equilibrium gives

$$\psi = -\Delta F^0 + (RT/F) \ln [(\mathrm{H}^+)(1-\theta)/\theta] \qquad (15.2)$$

where e is fractional coverage of surface by chemisorbed hydrogen, ΔF^0 is standard-state free energy of reaction (standard state is 1 gram-equivalent per liter of H^+ and $\theta = \frac{1}{2}$) and + is true, rational electrode potential. Potential of a normal hydrogen electrode in the same electrolyte is

$$\psi_{\mathrm{NHE}} = -\Delta F^0_{\mathrm{NHE}} + (RT/F) \ln [(\mathrm{H}^+)],$$

and

$$V = \psi - \psi_{\mathrm{NHE}} = -(\Delta F^0 - \Delta F^0_{\mathrm{NHE}}) + (RT/F) \ln [(1-\theta)/\theta]. \qquad (15.3)$$

V is potential versus NHE in SE. Clearly, at a given V, e is fixed; it tends to 1 at low potentials and becomes less as V increases. Equation (15.3) predicts that for a constant value of ΔF^0, θ should range from near 1 to near 0 over about 0.2-volt change in potential. Apparently, e changes less rapidly with potential than this prediction, either because there are different types of surface sites which have different ΔF^0 values or because ΔF^0 changes with coverage. The coverage by chemisorbed hydrogen is low at about 0.4 volt (versus NHE in SE); at lower potentials [H] exists even if no gaseous hydrogen is admitted to the system, since reaction (15.1) is reversible.

As potential is increased from 0.4 volt to about 0.6 volt, the current is mainly capacitative, without reactant present, and faradaic current is small. (A useful technique in transient measurements is to hold the electrode at 0.4 volt before beginning the test to insure that surface hydrogen is eliminated.) At higher potentials, oxygen is put on the surface (see ch. 16) from

$$\mathrm{Pt} + \mathrm{H_2O} \rightarrow \mathrm{Pt[OH]} + \mathrm{H}^+ + e^- \qquad (15.4)$$

and/or

$$\mathrm{Pt} + \mathrm{H_2O} \rightarrow \mathrm{Pt[O^*]} + 2\mathrm{H}^+ + 2e^-. \qquad (15.5)$$

The exact state of the oxygen on the surface is not known. Therefore, [O*] is used to indicate adsorbed oxygen without implying a 1:1 stoichiometry of Pt and O. At potentials greater than about 0.95 volt (versus NHE in SE), adsorbed oxygen is incorporated into the platinum lattice (739) and the higher the potential, the thicker the oxide film formed after holding the electrode at the potential for some hours. Thick oxide films have a profound influence on rates of reactions on the surface, usually inhibiting reaction. Oxidations are not rapid and reversible, and to remove oxide films it is necessary to hold the electrode at 0.6 volt for long periods of time or to go to hydrogen evolution potentials. It is not certain whether a surface can be completely stripped of adsorbed oxygen, even at hydrogen evolution potentials.

The presence of adsorbed hydrogen and oxygen and oxide films must certainly be taken into account in the study of anodic hydrocarbon oxidations, especially in transient-state methods. For example, if an electrode which has been anodized or chemically oxidized is placed in electrolyte, it attains an OCV which is toward the oxygen potential. If inert gas is bubbled through the electrolyte, the electrode slowly loses $\mathrm{O_2}$ by

$$2\mathrm{Pt[O^*]} \rightarrow 2\mathrm{Pt} + \mathrm{O_2} \qquad (15.6)$$

Partial replacement of lost oxygen by reaction (15.5) gives lower OCV due to the production of electrons, which retards the reaction. At some point, the rate of loss of oxygen becomes very small and a stable potential is obtained. If fuel is admitted to the system, the positive potential produces anodic oxidation such as $\mathrm{H_2} \rightarrow 2\mathrm{H}^+ + 2e^-$, and the electrons produced drive the electrode potential to lower, more cathodic, values until a new equilibrium is established. A fuel which cannot react on the oxided surface will produce no change in OCV, while one which reacts to remove surface oxygen will rapidly drive the OCV toward the balance given by

$$\begin{aligned} &\text{Fuel}+H_2O\rightarrow CO_2+2H^++2e^- \\ &2H^++2e^-\rightarrow H_2 \end{aligned} \qquad (15.7)$$

occurring at equal currents. Since the hydrogen reaction is relatively fast compared to the oxidation reaction, the "mixed potential" obtained at open circuit will usually be more positive (anodic) than the NHE in SE. If the fuel reacts slowly on the oxided surface, the OCV may stay at the original positive value with a current balance between

$$\begin{aligned} &Pt[O^*]+2H^++2e^-\rightarrow Pt+H_2O \\ &\text{Fuel}+H_2O\rightarrow CO_2+2H^++2e^-. \end{aligned}$$

This proceeds until Pt[O*] is used up. Then the rate of the fuel reaction accelerates due to greater activity of the bare surface, and OCV rapidly changes to more negative values. Thus, an induction period is observed before the OCV changes.

Rate-limiting factors for hydrocarbon fuels can be generally discussed as follows. First, if the fuel is sparingly soluble the mass-transfer-limited current is small. Limitations of this kind can be discovered by determining dependence of limiting current on rate of stirring of electrolyte and concentration of reactant. Second, the rate of chemisorption of fuel onto the electrode may be slow. This can sometimes be determined by allowing the electrode to stand in contact at open circuit with dissolved fuel for a given period of time and then anodically stripping the fuel. If the quantity of charge passed during stripping depends on time of immersion, a slow chemisorption is indicated, if mass transfer is not limiting. A slow chemisorption can give rise to a "chemisorption limited'' current, because when surface coverages tend to zero, the steady current cannot be more than the maximum rate of chemisorption. Third, charge-transfer processes can be the major rate limitation. Oxidation of carbon-containing fuels is basically different to that of hydrogen because, even in acid solution, oxygen must be added to the carbon to form CO_2 at the anode. The overall reaction must involve decomposition of water in acid solution and/or hydroxyl ion in alkali; for example

$$M[CH_4]+2H_2O\rightarrow M+CO_2+8H^++8e^-$$

or

$$M[CH_4]+8OH^-\rightarrow M+CO_2+6H_2O+8e^-.$$

Rate of charge-transfer limited reactions is strongly dependent on potential, with a tenfold increase of rate produced by potential changes of 60 to 150 millivolts, near room temperature and at solid electrodes.

If hydroxyl ion were the only efficient source of oxygen, the rates of oxidation at a given polarization in strong alkali would be much greater than in strong acid. Since this is not generally true, it is necessary to postulate oxidation via water in acid electrolyte. Possibly hydrocarbons are only anodically oxidized at high rates when the electrode is at a sufficient potential to produce metal oxides on the surface. In this case, the fuels would act as depolarizers of an oxide electrode by chemically reducing the oxide. However, rates of formation of Pt[O*] are rather slow until about 0.8 volt (versus NHE in SE) and equilibrium coverage is low at 0.6 volt. Some organic fuels give good current density at much lower potentials than those for appreciable oxide formation on the same electrode. Oxide films formed at potentials greater than 0.95 volt strongly inhibit the fuel reaction. Another hypothesis is that surface complexes are formed consisting of Pt-organic-water, which give increasing anodic current at higher potentials

$$\begin{aligned} &Pt[CH_4]\rightarrow Pt[CH_2]+2H^++2e^- \\ &Pt[CH_2][H_2O]\rightarrow Pt[CH_2O]+2H^++2e^- \\ &Pt[CH_2O][H_2O]\rightarrow Pt+CO_2+4H^++4e^-. \end{aligned} \qquad (15.8)$$

Each of these reactions would proceed in several steps. If one particular charge transfer were rate controlling, a Tafel equation could result, with exchange current dependent on bonding between fuel, catalyst and water, and hence dependent on fuel. Third, some evidence suggests that exchange currents are almost identical for a number of different fuels, leading to a requirement of a common rate-determining step which is independent of the fuel. The step proposed is

$$Pt[H_2O]\rightarrow Pt[OH]+H^++e^-$$

where Pt[OH] is available for oxidation of adsorbed organic molecules in further rapid reactions. To overcome the same objections as those for formation of Pt[O*] as the slow step, reaction (15.4) must proceed at appreciable rates at low potentials. Since there is little evidence for large equilibrium surface concentrations of [OH] at 0.6 volt, organic +[OH] reactions are postulated to be fast even at small concentrations of [OH]. This implies that [OH]+[H] reactions are also fast, since [H] is at least as active as hydrocarbons. Therefore, negligible [OH] probably exists in the potential region where appreciable [H] is present. Again, it would follow that competition exists between

$$\begin{array}{rcl}
H^+ & \overset{\text{very fast}}{\rightleftharpoons} & [H]+e^- \\
H_2O & \overset{\text{slow}}{\rightarrow} & [OH]+H^++e^- \\
\underline{[H]+[OH]} & \overset{\text{fast}}{\rightarrow} & \underline{H20\qquad\qquad} \\
H_2O & \rightarrow & H_2O
\end{array}$$

and

$$\begin{array}{rcl}
H_2O & \overset{\text{slow}}{\rightarrow} & [OH]+H^++e^- \\
\underline{\text{fuel}+[OH]} & \overset{\text{fast}}{\rightarrow} & \underline{CO_2+H_2O+H^+\qquad} \\
\text{fuel}+H_2O & \rightarrow & CO_2+H_2O+H^++e^-.
\end{array} \qquad (15.9)$$

The second-reaction sequence produces current and is expected to be the preferred reaction only at potentials greater than 0.3 or 0.4 volt, versus NHE in SE.

The influence of pH and reactant concentration on anodic reaction is, crudely, as follows. An increase of unit pH decreases reversible potential by about 60 millivolts, at room temperature. If rate of reaction is independent of hydrogen ion or hydroxyl ion concentration, as in reaction (15.9), the potential, versus SHE, at a given current density is independent of pH. Therefore, in the irreversible Tafel region, the polarization, η, from theoretical open circuit is increased by 60 millivolts per unit pH increase and the exchange current, i_0, is less. If rate is proportional to pH, assuming a Tafel slope of 0.12 volt/current decade, the potential versus SHE at a given current density decreases by 120 millivolts, η is 60 millivolts less, and i_0 is greater. If rate is proportional to $\sqrt{pH}$, a given current density gives the same η and 60 millivolts less potential versus SHE. These relations are summarized in table 15.11, where R stands for pH. R can also stand for concentration of a reactant raised to the $1/m$ power, where m is total number of electrons in reaction per molecule of reactant. For example, for hydrogen fuel $R=p^{1/2}$, p being partial pressure of hydrogen in equilibrium with the electrode. The η must be measured from a theoretical OCV defined in the same way for acidic and basic reactions. For example, $HCHO+H_2O \rightleftharpoons CO_2+4H^++4e^-$, and $HCHO+4OH^- \rightleftharpoons CO_2+3H_2O+4e^-$ are the same reaction, with theoretical potential defined by 1 atmosphere of CO_2. However, $HCHO+6OH^- \rightleftharpoons CO_3^{=}+4H_2O+4e^-$ is not the same reaction, since theoretical OCV is defined by $1N$ $CO_3^{=}$. The value of η in the relations in table 15.11 can be replaced with electrode voltage versus NHE in SE, since the same relations apply.

TABLE 15.11.—Variation of Polarization and Exchange Current With Concentration (Activity) of Species in Reaction

	$\left(\frac{\partial V}{\partial\, pH}\right)_i$, millivolts	$\left(\frac{\partial \eta}{\partial R}\right)_i$, millivolts	$\frac{\partial \log i_0}{\partial R}$	Assumed $\left(\frac{\partial \eta}{\partial \log i}\right)_R$, volts
Rate ∝ R	−120	−60	0.5	0.12
Rate not dependent on R	0	60	−.5	.12
Rate ∝ $R^{\frac{1}{2}}$	−60	0	0	.12

15.5.2 Nonoxygenated Hydrocarbons

Anodic oxidation of ethane, propane, and isobutane dissolved in $6M$ H_2SO_4 was studied on an electrode of platinized-platinum screen (Surface Processes, ***588,*** November 1962). The electrode was initially brought to 0.6 volt and gas bubbled into the electrolyte until it was saturated at 1 atmosphere; open-circuit potentials of about 0.25 volt were obtained. A constant anodic current (galvanostatic technique) was passed and potential followed to the point of oxygen evolution. The result depended on time from start of bubbling to current pulse, and 20 minutes' equilibration time was used. This could indicate slow mass transfer to the surface or a slow rate of adsorption. Hydrogen equilibrated rapidly, which suggests a slow adsorption rate for saturated hydrocarbons. At 77" F (25" C), there was no clear transition time due to hydrocarbon oxidation before surface oxiding and oxygen evolution, but at higher temperatures an oxidation wave could be seen. Amount of charge supported by fuel oxidation increased with temperature and potential of start of wave decreased to about 0.5 volt at 158" F (70" C). Results were not reported as current density, but the stripping current was 2 milliamperes for an electrode of 0.8 M^2 BET area, and transition times were of the order of 1 to 10 minutes. The charge supported by ethane was several times that for propane or isobutane.

After anodization of the electrode, ethane could restore OCV to unanodized values at temperatures greater than 167" F (75" C), but propane and isobutane could not. Electrodes plated with Ir or Rh gave smaller transition times, and when anodized could only be brought up to normal OCV by ethane at temperatures greater than 212" F (100° C). Ir and Rh were concluded to be inferior catalysts to Pt. Unfortunately, blanks were not run at all temperatures to show temperature variation of oxygen discharge on the surface. However, at higher temperatures, oxidation of the fuel probably always occurred at much lower potentials than required for comparable rates of oxidation of the surface. There is no way of knowing, however, whether this fuel oxidation was complete, including that preadsorbed plus that diffusing to and adsorbing on the surface, or was only an unsteady-state partial oxidation. Increase of transition time with temperature could be due to more complete oxidation, larger amounts preadsorbed in the 20 minutes, or faster rates of fuel chemisorption during anodic oxidation.

Saturated and unsaturated hydrocarbons were oxidized on electrodes of platinum black pasted or bonded with Teflon on screen in a General Electric IEM cell ***(250,*** April 1960). The anode chamber was filled with electrolyte and the electrode held at 0.5 volt versus NHE in SE. The electrolyte was then drained from the anode chamber, and gas was admitted and allowed to absorb up to 30 minutes, until a steady OCV was obtained. The anode chamber was reflooded with electrolyte and a galvanostatic discharge performed. Transition times were not clearly defined, but an estimate was made of charge supported by adsorbed fuel before oxygen discharge onto the surface, compared to that from hydrogen under the same conditions. In 5 *N* H_2SO_4, the ratios were: methane, small; ethane, 1; propane, 2; isobutane, 2; and ethylene, **4** (258, September 1961). Excepting ethylene, only labile hydrogen atoms were utilized in the potential range before oxygen discharge onto the surface. In 6 *M* KOH the current supported by fuel was small except for ethylene, which gave a value of 4 as in acid. Fuel adsorption did not occur at electrodes in alkaline electrolyte. Poor performance in alkali agreed with normal cell tests, which showed low currents for saturated hydrocarbons at 149" F (65" C), whereas acid electrolytes gave currents of 1 to 5 A/sq ft at 0.5 cell volt. The **3** *M* $KHCO_3$ was polarized even for hydrogen and gave significant transition times only for ethylene and cyclopropane.

Temperature increase from ambient to 149" F (65" C) gave sharper transition times but did not increase total quantity of charge. When ethane was left in the anode chamber for many hours, increased current could be supported; ethylene gave about 20 percent more charge for an increase in equilibration time from 30 minutes to 2 hours. Ethylene was found to use two sites for adsorption and to be oxidized completely, thus giving four times the charge from hydrogen adsorption on the sites.

Gas-phase decomposition of propane over platinum black or nickel at 212" to 392" F (100° to 200" C) gave mainly methane, some ethane, no hydrogen, and a carbonaceous residue (General Electric, ***291,*** November 1962). Rate of cracking on platinum under comparable conditions was in the order propane>ethane>ethylene. Preadsorbed oxygen inhibited reaction, but water was reversibly adsorbed and did not affect the rate. Ethylene dissolved in 1*N* $HClO_4$ did not give appreciable transition times for galvanostatic discharge at a bright platinum electrode below 185" F (85" C).

General Electric diffusion anodes of platinum black were used in 6 *N* H_2SO_4 at 149" F (65" C) with propane fuel (*302,* June 1962). At open circuit, methane appeared in the anode gas, but under load only CO_2 was seen. Similar current densities were obtained from H_2SO_4, H_3PO_4, and $HClO_4$, except for H_3PO_4 containing less than 15 weight-percent of water. In this case, acetic acid and aldehydes were produced in the electrolyte. At 194" F (90° C), a direct reaction took place between propane and 4 *M* H_2SO_4, leading to H_2S. In cells under normal conditions the CO_2 in the anode gas corresponded to 70 to 85 percent of propane used, but no intermediates were detected in the electrolyte. Intermediates apparently were reacted and removed at the cathode and thus prevented from building up to high concentrations. This is in direct contradiction to the results of California Research, section 15.1.

The previously described method of alternately filling the anode chamber with electrolyte (5*N* H_2SO_4) and gas was extended by measuring rate of uptake of gas during equilibration. This rate was initially much faster for unsaturated hydrocarbons than for saturated, which cannot be explained by solution followed by slow mass transfer in electrolyte. Volumes of gas taken up in 30 minutes compared to volume of hydrogen were: ethylene, 75 percent; cyclopropane, 70 percent; propylene, 60 percent; propane, 20 percent; ethane, 20 percent; methane< 10 percent. At open circuit, large amounts of ethane were produced from ethylene. Methane was produced from ethane, but at much lower rates. Hydrogen was evolved to strip off adsorbed hydrocarbon. Ethylene equilibrated for 10 minutes gave mainly ethane, about 5 percent by volume of butane, about 1 percent methane, and about 0.1 percent propane. These results were independent of current density when the current density (hydrogen discharge) was large enough to strip the material rapidly from the surface. Slightly larger volumes were found at low current densities. Ethane gave back ethane and about 2 percent methane, with somewhat lower volumes for long equilibration times (attributed to CO or HCOOH formation). Ethylene gave severalfold increases in evolved volumes of butane, methane, propane (and a concomitant lower value of ethane) as equilibration times were increased to several hours. Thus surface conversions for ethylene can be written

1.	$C_2H_4+\text{surface}\rightarrow[C_2H_4]$	Initially rapid, and almost complete after **30** minutes.
2.	$2[C_2H_4]\rightarrow[C_2H_6]+[C_2H_2]$ $[C_2H_6]\rightarrow C_2H_6$ $([C_2]+\text{cathodic H}\rightarrow C_2H_6)$	Ethane builds up in gas stream, at open circuit, over several hours, evolution being almost complete in **4** hours.
3.	$[C_2]\rightarrow[C_1+C_3+C_4]$ $([C_1]+\text{cathodic H}\rightarrow CH_4)$ $([C_3]+\text{cathodic H}\rightarrow C_3H_8)$ $([C_4]+\text{cathodic H}\rightarrow C_4H_{10})$	Increasing (at decreasing rate of increase) with time. C_1 and C_4 mainly complete in 4 hours. C_1 about 5 percent of ethane volume, C_4 about 10 percent. C_3 still increasing after 16 hours, being about 1.5 percent.
4.	$[C_1]\rightarrow CH_4$	Mainly complete in 8 hours. About 2.5 percent of ethane volume.

A number of molecular rearrangements occur on the surface, involving loss and gain of hydrogen atoms and breaking and forming of carbon-carbon bonds. When current is drawn from the cell, surface intermediates are converted to CO_2 and do not desorb as methane or ethane. The fast reaction $[H] \rightleftharpoons H^+ + e^-$ allows rapid transfer of chemisorbed H from one place on the surface to another at open circuit. It is not necessary to postulate mobile H atom. This equilibrium also explains how the entire surface of the catalyst can be rapidly covered with [H], even if the reaction $H_2 \rightarrow 2[H]$ is occurring only near the gas-electrolyte-electrode interface.

Reference has already been made to demonstration of complete oxidation of propane to CO_2 (see sec. 15.1). This result was confirmed in ***135.*** Ethane, propane, n-butane and butane, and butene were used (California Research, ***134,*** August 1961) as fuels at diffusion electrodes of porous, platinized carbon (electrode of hollow rod immersed in electrolyte, with gas feed to interior). Current densities in 5 *N* H_2SO_4 at 176" F (80° C) were low and similar for all fuels, and the electrodes were readily poisoned by oxygen in the gas feed or the electrolyte. When oxygen was removed, the electrodes recovered activity and their normal OCV after an induction period (see sec. 15.5.1). The linear voltage-sweep method was applied to solid, spherical, platinum electrodes in 5 *N* H_2SO_4 containing dissolved hydrocarbon ***(135).*** Well-defined peak currents were obtained, but currents depended on time between scans, requiring about 4 minutes for butane and propane. In addition, peak currents were much greater for platinized electrodes and were independent of stirring rate. Therefore, peak currents could not be due to **mass** transfer, as in the conventional treatment of the voltage-sweep method. Peak currents were attributed to oxidation of preadsorbed fuel, with slow rate of chemisorption limiting further adsorption during the sweep. Faster oxidation was found for ethylene and butene ***(136)*** and there was no dependence of peak current on time between sweeps. However, peak currents were still independent of stirring rate. Similarly, galvanostatic tests on a solid-platinum-foil electrode showed that ethylene, propylene, and butene oxidized at lower polarizations than ethane, propane, and butane, but the transition times were not mass-transfer transition times.

TABLE 15.12.—*Solubilities* of Hydrocarbons at ***1*** Atmosphere Total Pressure ***(138)***

Hydrocarbon	Electrolyte	Temperature, "F	Solubility, moles/cm³
Methane	H_2O	77 (25" *C*)	$(1.5)(10^{-6})$
Ethane	......	......	$(1.8)(10^{-6})$
Propane	......	......	$(1.5)(10^{-6})$
Butane	......	......	$(1.2)(10^{-6})$
			$(4.8)(10^{-6})$
Ethylene	H_2O	158 (70" *C*)	$(2.5)(10^{-6})$
Ethylene	5 *M* H_2SO_4	77 (25" *C*)	$(1.2)(10^{-6})$
Ethylene	......	104 (40° *C*)	$(0.8)(10^{-6})$

Recovery from poisoning by oxygen had shorter induction times at 176" F (80° C) than at **104**" F (40° C), and no inhibition due to CO_2 was observed ***(137).*** Carbon monoxide alone gave bigger currents than propane. Therefore, any inhibition of CO on the propane reaction was masked. The solubilities of hydrocarbons were investigated (see table 15.12 and app. B) and mass-transfer transition times were calculated ***(138).*** Even for ethylene, experimental transition time was greater than mass-transfer transition time. The quantity of charge, ***Q,*** passed during an experimental voltage sweep was plotted as a function of time taken to perform the sweep; time from 0 to 1.0 volt was up to 2 seconds. The relation was nearly linear and the intercept at zero time, very fast sweeps, was taken as amount of preadsorbed fuel. This was 1.8 mC/cm² for a platinized electrode and 0.23 mC/cm² for a smooth electrode. Corresponding values to form chemisorbed oxygen on the electrodes were 7.8 and 0.5. Q was 10 times larger for a 2-second sweep. The wave normally obtained due to adsorbed hydrogen, starting from *0.25* volt versus NHE in SE, was almost eliminated by ethylene, indicating that adsorption of ethylene prevented hydrogen adsorption from $H^+ + e^- \rightleftharpoons [H]$.

At potentials near zero, some [H] replaces adsorbed ethylene and a hydrogen wave is observed. At potentials greater than 0.4, no [H] is expected from the equilibrium $H^+ + e^- \rightleftharpoons [H]$. Conflicting statements on presence of hydrogen current in galvanostatic or voltage-sweep tests on hydrocarbons probably depend on starting potential and whether this potential is deliberately controlled by a potentiostat or is attained by natural faradaic charging of the double layer on admission of fuel. Presence of a hydrogen wave does not prove that adsorbed fuel is dissociating to give [H], but absence of a wave at potentials between 0 and 0.4 volt does prove that it is not dissociating.

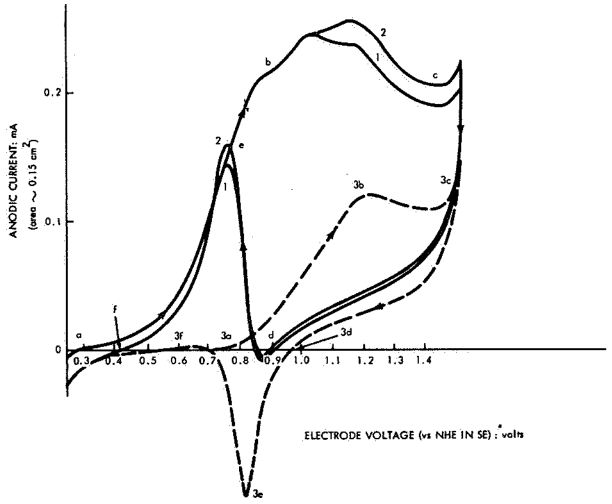

Ethylene-saturated, 1 *M* H_2SO_4 solution at 176° F (80° C): dv/dt =28 mV/sec.

1 0 rpm
2 6000 rpm
3 Blank

FIGURE 15.3.—Oxidation **of** ethylene at a rotating platinum disk electrode.

The voltage-sweep method was used on a rotating disk electrode to eliminate mass-transfer effects. Figure *15.3* shows the results. The interpretation of the curves is as follows. Considering first the blank, at *3a* the equilibrium $[H] \rightleftharpoons H^+ + e^-$ is weighted to the right-hand side, so no anodic discharge of hydrogen is present. At about 0.7 volt, water is discharged to form surface [O*]. This discharge is irreversible. As coverage by [O*] increases, rate is not increased as much by more positive potentials as expected from a simple Tafel equation. At *3b* the surface is covered by Pt[O*], and further potential increase to *3c* produces growth of oxide film several monolayers thick and oxygen evolution by discharge of water at an oxided surface. When the voltage sweep is reversed at *3c*, water continues to discharge, but at a lower rate at a given potential because the oxide film is a less active surface than bare metal. Eventually, the reaction reverses at *3d* and cathodic discharge of [O*] to H_2O occurs. The area within the wave *3d, 3e,* and *3f* is the discharge of loosely bound [O*], which is completely discharged by 0.6 volt. There is disagreement whether a more strongly bound surface oxygen exists after the electrode has been taken to hydrogen evolution.

The ethylene curve, starting at *a,* shows increased current with increased potential, but the relation from *a* to *b* is not a simple Tafel form. Because this portion is not changed when speed of electrode rotation is increased from 0 to 6000, there are no mass-transfer limitations. At the low sweep rate, *28* mV/sec, the charge due to preadsorbed fuel is fairly small compared to the charge from utilization of fuel taken up during the sweep. The blank run indicates that discharge of water onto bare metal is negligible at potentials in the *a* and *b* region, so the non-Tafel form is not due to oxide poisoning of the surface. Previous results indicate that rate of adsorption of ethylene is not sufficient to maintain a constant surface coverage at higher currents; therefore, departure from the Tafel form may be due to a slow chemisorption process. Alternatively, there may be potential-dependent adsorption of anion ($SO_4^=$), which reduces the number of active sites on the surface and/or changes the structure of the double layer to reduce the effect of voltage. Since no current wave is noted in the blank, this adsorption involves no charge transfer to the electrode metal. At point *b* oxygen is placed on the surface and the poisoning effect with increased potential balances the acceleration of fuel reaction due to more positive potentials, giving almost constant current from *b* to *c*. At point *c* the anodic current is the sum of fuel oxidation and oxygen evolution. A slight mass-transfer effect is noted from *b* to *c*, which may be due to the fuel or to more rapid removal of evolved oxygen, leading to less rapid incorporation of oxygen into the platinum lattice.

The oxide film reduces activity of the electrode to fuel oxidation, so that the reverse sweep gives only slightly greater anodic current in region *c* to *d* than in the blank run. As potential is reduced, however, discharge of oxide film at 3d causes rapid reactivation of the surface, so that anodic current from the fuel balances the cathodic current of [O*] at d. Thereafter, the rate rises to near its previous value at *e*, and somewhat lower values at f. The lower values at f may be due to slow chemisorption of fuel so that coverage by ethylene is less on the reverse sweep than on the forward, or it may be due to strongly retained oxygen which still poisons the surface to a certain extent. The larger cathodic current due to $H^+ + e^- \rightleftharpoons [H]$ indicates that more sites are available for [H] and, therefore, the surface coverage by ethylene is smaller.

No desorbable intermediates were concluded to form during the sweep, since higher rotation speeds would have produced faster intermediate removal and lower total charge if intermediates were formed. A maximum in current with increased potential was also found with propane on platinized-carbon diffusion anodes. By using very fast sweep rates, values of total charge for hydrocarbon oxidation were obtained which were independent of sweep rate and corresponded only to oxidation of preadsorbed fuel *(139)*. Assuming complete oxidation, molecules of hydrocarbon per surface atom of platinum were 0.06 for ethylene, 0.04 for ethane, and 0.03 for propane. A solid electrode had to be immersed for 7 minutes to obtain equilibrium coverage of ethane or propane. The approximate mean rate of chemisorption up to 2 minutes was about $(1.7)(10^{-4})$ mA/cm^2 for ethane and $(2.3)(10^{-4})$ mA/cm^2 for propane. These values were much less than peak currents obtained during fast voltage sweeps (oxidation of preadsorbed fuel), indicating that chemisorption rate limitations were present in slow sweeps or steady current runs.

The steady current-voltage relations for a platinized-carbon diffusion electrode (Pure Carbon FC 14, reduced in hydrogen at 752" F (400" C)) in *N* H_2SO_4 at 176" F (80° C) showed that the current increased to a maximum current and then decreased as potential was increased. The values of maximum current and potentials at which they occurred were: propane, 4 A/sq ft at 0.5 volt; ethane, 4 A/sq ft at 0.9 volt; ethylene 30 A/sq ft at 1.0 volt; propylene, no decrease in current up to oxygen evolution. Peak currents decreased over periods of days but could be restored by washing electrodes in hot water.

Voltage-sweep measurements were made on acetylene, *N* H_2SO_4, 176" F (80° C), at a solid rotating-wire electrode *(140)*. The buildup of surface oxygen at positive potentials strongly inhibited rate of oxidation of acetylene. However, the surface coverage by acetylene could not be obtained because the quantity of charge did not come to a constant value at high sweep rates. Adsorption appeared to be fast but to a small coverage. The quantity of charge passed in a voltage sweep decreased when the electrode was left for some minutes after immersion and before the sweep, due to deactivation by rearrangement of adsorbed acetylene to a stable form. Because of fast adsorption, the initial portion of the anodic sweep, before oxygen appeared on the electrode, gave a good Tafel plot with a value of αn of about 0.57, a Tafel slope of 0.13 volt per decade, and an exchange current, based on a theoretical potential of –0.024 volt versus NHE in SE, of $(5)(10^{-12})$ A/cm^2. Low current densities correlated with fuel-cell performance in acid at useful potentials, where the order was propane >ethylene >acetylene. General conclusions are summarized in table 15.13.

Ultrapure conditions were used in the investigation of reactivity of unsaturated hydrocarbons (University of Pennsylvania, *737* through *739*, October 1962 to present; see sec. 15.2.2 at ref. 15.3). The results are summarized in table 15.14 (refs. 15.4 through 15.7).

Steady-state galvanostatic or potentiostatic methods were used and gave identical results. Electrodes were activated in 20 percent H_2SO_4 by 10 anodic-cathodic cycles at 0.1 A/cm^2 for 1 second, followed by 100 seconds cathodic at 0.1 A/cm^2. Other methods of pretreatment did

TABLE 15.13.—Comparison of Ethane, Ethylene, and Acetylene (*130* through *146*, California Research *Corp.*)

Property	Order
Current density at low polarization	Ethane>ethylene >acetylene
Maximum current	Acetylene>ethylene>ethane
Rate of adsorption	Acetylene>ethylene>ethane
Ability to remove adsorbed oxygen	Acetylene>ethylene >ethane
Resistance to poisoning at OCV	Ethane>ethylene>acetylene

not affect results, but slow deactivation with time was attributed to buildup of organic material on the electrode. Contrary to California Research Corp. results, good Tafel curves were obtained with ethylene and the Tafel slopes did not indicate a slow chemisorption step. As in the California Research *Corp.* work, poisoning by surface oxygen led to a maximum current followed by a considerable decrease in current at more positive potentials. The maximum current occurred at potentials corresponding to a surface coverage by [O*] of about 10 percent. Differences in results can be partly explained by high purity of the system in the University of Pennsylvania study, which enabled steady low currents to be obtained at currents too low for the rate of chemisorption to affect the rate. It is not possible to tell whether rate of adsorption was affecting current density near current maximum in this work, but transition from Tafel line to maximum current peak was quite sharp.

Similarity of electrochemical parameters for all of reactions except acetylene indicated that a common rate-controlling step was present. This was claimed to be

$$H_2O+Pt\rightarrow Pt[OH]+H^++e^-, \qquad \textbf{(15.4)}$$

for the following reasons. Since current at a fixed potential decreased with increased reactant concentration ($[\partial i/\partial P]_{V,\,pH}<0$), apparently rate was proportional to amount of surface not covered by adsorbed fuel. Tafel slopes of near 140 mV indicate that the rate-controlling step is a charge transfer, with rapid subsequent reaction steps. If the rate-controlling step became

$$Pt+OH^-\rightarrow Pt\,[OH]+e-$$

at high pH, exchange currents should be highest in strong alkali. This was not observed since $\partial\ (\log i_0)/\partial(\text{pH})$ was constant.

If reaction **(15.4)** is the slow step, there are several conditions which must also be satisfied to explain the California Research results, and similar results of other studies, which show that surface oxygen concentrations, including Pt[OH], are small at the potentials over which Tafel parameters were obtained, in the absence of fuel. Transient current in the presence of fuel is much higher than surface oxygen current without fuel in this region. The rate of equation (15.4), therefore, must be as high as the fuel oxidation current, but equilibrium at these potentials must be satisfied by small surface coverage of [OH]. Since more positive potential drives equilibrium surface coverage and rate to higher values, formation of Pt[OH] or Pt[O*] should be faster at higher potentials. Equilibrium coverage is certainly higher at 0.8 to 1.0 volt, but the rate is not fast. Reaction (15.4) must therefore be assumed to rapidly poison itself as surface coverage increases. California Research *Corp.* results indicate that equilibrium coverage by ethylene is about 12 percent, assuming two platinum sites per molecule. If this is adsorption on active sites, which compose 12 percent of the surface, possibly surface [O*] will go on these sites at positive potentials and hence considerably retard ethylene oxidation even at 10 percent coverage of the surface. On the other hand, self-poisoning of reaction (15.4) at these potentials in the presence of fuel means that rates of $Pt[H_2O]\rightarrow Pt[OH]+H^++e-$ and $Pt[OH]+\text{fuel}\rightarrow Pt$ are high at low potentials and low values of [OH], but fall as potential is increased beyond a given point to give lower rates. There is no apparent reason for this. If poisoning is by another species of adsorbed oxygen such as [O*], coverage by [OH] must be small because [O*] is formed at potentials before appreciable coverage by [OH] occurs. This implies that $Pt[OH]\rightarrow Pt[O^*]+H^++e^-$ is faster at more positive potentials than $Pt[OH]+\text{fuel}\rightarrow Pt+CO_2+H^++e^-$. Poisoning is, therefore, dependent on reactions following formation of Pt[OH] and would be expected to vary with type of fuel.

The preceding lines of argument can be summarized as (*a*) $$\mathrm{Pt}+\mathrm{H_2O}\rightleftharpoons\mathrm{Pt[H_2O]}$$

(*b*) $$\mathrm{Pt[H_2O]}\xrightarrow{\text{slow}}\mathrm{Pt[OH]}+\mathrm{H^+}+e^-,\ \text{low coverage}$$

(*c*) $$\mathrm{Pt}+\text{fuel}\rightleftharpoons\mathrm{Pt[fuel]}$$

(*d*) $$\mathrm{Pt[fuel]}+\mathrm{Pt[OH]}\rightarrow\mathrm{Pt}+\mathrm{CO_2}+\mathrm{H^+}+e^-$$

(*e*) $$\mathrm{Pt[OH]}\xrightarrow[\text{high positive potentials}]{\text{slow until}}\mathrm{Pt[O^*]}+\mathrm{H^+}+e^-$$

Pt [O*] is stable and removes active sites; extent of coverage at high positive potentials and consequent poisoning depend on the relative rates of reactions (*d*) and (*e*).

Although the explanation of the results by reaction (15.4) is very attractive, there are some major objections. Table 15.11 shows that pH dependences should be $(\partial\eta/\partial\ \mathrm{pH})_i=60$ millivolts and $\partial\log i_0/\partial\ \mathrm{pH}=-0.5$, whereas they are actually zero. Also, it is frequently postulated (see ch. 17) that hydrogen ionization in strong alkali occurs via

$$\mathrm{Pt[H]}+\mathrm{OH^-}\rightarrow\mathrm{Pt}+\mathrm{H_2O}+e^-.$$

There seems to be no reason why a comparable reaction should not occur in hydrocarbon oxidation. This lack of dependence of polarization on pH for the unsaturated hydrocarbons is very hard to explain.

Similar pH and pressure dependencies were found for Pt, Rh, and Ir, with exchange current in $1N\ \mathrm{H_2SO_4}$ in the order Pt > > Rh > Ir. For Au and Pd, the products of reaction were acetaldehyde, acetone, and propionaldehyde (ref. 15.6), and $(\partial V/\partial\ \mathrm{pH})_i$ was approximately zero. Thus, exchange current decreased as pH increased. Current increased with increased concentration of fuel, and Tafel slopes were about 70 millivolts for Au and 80 to 110 for Pd. Potentials of maximum current were Rh, 0.6 volt; Ir, 0.65 volt; Pd, 0.8 volt; Pt, 0.85 volt; and Au, 1.2 volts.

No organics were detected after oxidation of acetylene (ref. 15.7) and a diffusion-limited current was not obtained until pressure of acetylene was less than about 0.04 atmosphere. The rate-determining step (see table 15.14) was postulated as

$$\mathrm{Pt[C_2H_2]}+\mathrm{Pt[OH]}\xrightarrow{\text{slow}}\mathrm{[C_2H_2OH]}\ \text{or}\ \mathrm{[C_2H]}+\mathrm{H_2O}.$$

This rate is slower than the water discharge reaction (15.4) because of strong bonding of acetylene to the surface (high exothermic heat of adsorption). Passivation occurred at 1.0 volt

TABLE 15.14.—*Summary of Results for the Anodic Oxidation of a Number of Hydrocarbons: 1 Atmosphere Gas,* 1 *N* $\mathrm{H_2SO_4}$, *80° C* [Ref. 15.4]

Hydrocarbon	E^0 versus NHE, V	i_0, mA/cm²	$\left(\frac{\partial V}{\partial \log i}\right)_{V,\mathrm{pH}}$, V	$\left(\frac{\partial \log i}{\partial\ \mathrm{pH}}\right)_V$	$\left(\frac{\partial \eta}{\partial\ \mathrm{pH}}\right)_i$, mV	$\left(\frac{\partial \log i_0}{\partial\ \mathrm{pH}}\right)$	$\left(\frac{\partial V}{\partial\ \mathrm{pH}}\right)_i$, mV	$\left(\frac{\partial i}{\partial P}\right)_{V,\mathrm{pH}}$	Faradaic efficiency, percent	Activation energy of i_0, kcals/mole
Ethylene........	0.03	10^{-5}	0.14 to 0.16	0.45	~0	~0	−65	<0	100	17
Allene..........	.00	2.5×10^{-5}	0.14 to 0.16	.41	~0	~0	−68	<0	93	....
Propylene.......	.08	2.9×10^{-5}	0.14 to 0.16	.35	~0	~0	−52	<0	97	....
1,3-Butadiene...	.06	0.7×10^{-5}	0.14 to 0.16	.39	~0	~0	−65	<0	58–62	....
1-Butene........	.09	1.8×10^{-5}	0.14 to 0.16	.47	~0	~0	−67	<0	71	....
2-Butene........	.09	1.8×10^{-5}	0.14 to 0.16	.45	~0	~0	−66	<0	83	....
Benzene.........	.10	0.3×10^{-5}	0.14 to 0.16	.40	~0	~0	−51	<0	90–60	....
Acetylene.......	−.11	4.5×10^{-15}	0.07 to 0.08	.8	~0	~0	−50	<0	100	42 acid 48 base

Effects of pH were studied with sodium sulfate and sodium hydroxide over the range 0.5 to 12.5 pH.

versus NHE in §E, which indicates that acetylene was more effective in keeping the surface reduced. The lack of dependence of η on pH at a **fixed** i is understandable, since rate is proportional to equilibrium value of [OH], which is affected by pH in the same way as open circuit potential, so that [OH], is constant at a fixed η.

15.5.3 Carbon Monoxide and Oxygenated Hydrocarbons

Using a galvanostatic stripping technique, the mean rate of adsorption of CO on bright platinum in $HClO_4$ or NaOH was estimated (ref. 15.9) to be 0.08 cm/sec at 77" F (25° C). This corresponds to a steady current density at 1 atmosphere CO, 10^{-6} moles/cm^3 dissolved CO, of 16 mA/cm^2. In transient measurements this rate was fast enough to give transition times dependent on the rate of diffusion. An electrode at 0.4 volt versus NHE in SE rapidly adsorbed CO to a coverage about 30 percent greater than the H coverage at zero volts. CO oxidation occurred over 50 millivolts (see app. C) at about 1.0 volt. Using similar techniques and voltage-sweep methods, rate of adsorption of CO on platinum (1*N* $HClO_4$, 77" F (25" C)) was estimated to be 0.07 cm/sec at fractional coverage near 0.95 and greater at lower coverages (ref. 15.10).

High rates of stripping were used to measure CO adsorbed on smooth platinum at 77" F (25° C) in 1*N* H_2SO_4 (ref. 15.11). The electrode had an oxygen area, determined by the charge required to saturate the surface with [O], of **0.43** mC/cm^2. The theoretical value for 1 oxygen atom per Pt atom is 0.46 mC/cm^2 of smooth surface, and for one OH per Pt atom it is 0.23. The coverage by CO was 0.45 mC/cm^2 at 1 atmosphere, **0.44** at 0.1 atmosphere, and only slightly less when the solution was bubbled with He, showing the irreversible nature of the adsorption. CO oxidation occurred over a short potential range at about 1.0 to 1.2 volts, depending on CO pressure. The mechanism was proposed as

$$Pt+CO\rightarrow Pt[CO]$$
$$Pt+H_2O\xrightarrow{slow}Pt[O]+2H^++e^-$$
$$Pt[O]+Pt[CO]\rightarrow Pt_2[CO_2]\rightarrow 2Pt+CO_2.$$

The anodic reaction of carbon monoxide appears to be similar to that of acetylene. It adsorbs relatively rapidly, is very stable and does not react rapidly with [OH] at low potentials, but is not readily poisoned by [O*] formation. The slow step given above is unlikely to be a single process, since the reverse reaction is termolecular and therefore improbable. The principle of microreversibility requires that true reaction steps be feasible from either side. It could just as well be written

$$Pt[H_2O]\rightarrow Pt[OH]+H^++e^-$$
$$Pt[OH]\rightarrow Pt[O]+H^++e^-.$$

By analogy with the acetylene reaction, reaction between adsorbed CO and adsorbed O or OH might be the slow step rather than the charge transfer. The rapid increase in oxidation rate over 50 millivolts' potential charge indicates that it is not a single-electron charge-transfer process which is rate controlling.

An alternative hypothesis similar to that proposed for hydrocarbons (see sec. 15.5.1) is (ref. 15.12)

$$Pt[CO]+Pt[H_2O]\rightarrow Pt_2[CO][H_2O]$$
$$Pt_2[CO][H_2O]\xrightarrow{slow}Pt_2[CO\text{-}OH]+H^++e^-$$
$$Pt_2[CO\text{-}OH]\xrightarrow{fast}2Pt+CO_2+H^++e^-$$

in several steps.

The result of such a mechanism would be similar to that of the mechanism

$$Pt+H_2O\xrightarrow{slow}Pt[OH]+H^++e^-,$$

except that rate of fuel-water decomposition would be expected to depend on the nature of fuel-metal-water bonding and, therefore, to depend on the fuel under investigation.

Some mechanisms which have been proposed for the anodic oxidation of formic acid are:

(1) Surface decomposition of HCOOH followed by a slow H_2 discharge step (Tyco, *633)*

$$HCOOH+Pt\rightarrow Pt[HCOOH]$$
$$Pt[HCOOH]\rightarrow Pt+H_2+CO_2$$
$$H_2\xrightarrow{slow}2H^++2e^-.$$

(2) Slow decomposition of adsorbed HCOOH followed by fast H_2 discharge (Tyco, *633)*

$$Pt+HCOOH\rightarrow Pt[HCOOH]$$
$$Pt[HCOOH]\xrightarrow{slow}Pt+H_2+CO_2$$
$$H_2\rightarrow 2H^++2e^-.$$

(3) Slow dissociative adsorption of HCOOH followed by fast discharge of adsorbed radicals (ref. 15.13)

$$HCOOH + 2Pt \xrightarrow{\text{slow}} Pt[H] + Pt[COOH]$$
$$Pt[COOH] \rightarrow Pt + CO_2 + H^+ + e^-$$
$$Pt[H] \rightleftharpoons Pt + H^+ + e^-.$$

(4) Slow discharge step of adsorbed COOH radical (ref. 15.14)

$$Pt + HCOOH \rightleftharpoons Pt[HCOOH]$$
$$Pt[HCOOH] + Pt \rightarrow Pt[H] + Pt[COOH]$$
$$Pt[COOH] \xrightarrow{\text{slow}} Pt + CO_2 + H^+ + e^-$$
$$Pt[H] \rightleftharpoons Pt + H^+ + e^-.$$

The variety of mechanisms proposed for this reaction is in part due to conflicting experimental results obtained in these studies. Time-dependent effects, effects of electrode pretreatment, and poor reproducibility of measurements have been noted in many studies.

Measurements of surface coverage (θ) of HCOOH as a function of time (ref. 15.13) showed that θ increased slowly with time, with most change occurring within about 2 minutes. Rate of adsorption fitted Langmuir kinetics in this time period. Beyond this time, deviations from Langmuir kinetics were observed. Adsorption of impurities from the system may be responsible. Measurements of θ versus V showed that current was directly proportional to $(1-\theta)$. Thus, the adsorbed species acted as a blocking agent and poisoned the reaction. The identity of this adsorbed species was not established but, for a number of reasons, it was not believed to be CO, HCOOH, HCOO', or $HCOO^-$. Presence of a poisoning species, or incomplete reaction leading to a stable complex on the surface, has been indicated by a number of studies (refs. 15.15 through 15.19). The poisoning species has been variously given as CO, CHOO', or a product of a side reaction, such as

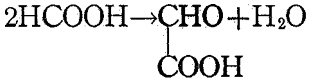

$$2HCOOH \rightarrow \underset{\displaystyle COOH}{\underset{|}{CHO}} + H_2O$$

There is considerable evidence that rate of adsorption or rearrangement is slow compared to normal mass-transfer rates, giving a constant current at sufficiently positive potentials. A limiting current was found (Pt wire, N $HClO_4$, 104" F (40" C)) at 0.45 volt, which was independent of the speed of rotation of the wire (ref. 15.14). Rate was first order from 0.01 to 1 M HCOOH and $(\partial \log i/\partial \text{ pH})_V \simeq 1$. The accelerating influence of potential below the limiting current was ascribed to lower values of [H] in the equilibrium $[H] \rightleftharpoons H^+ + e^-$ leaving more sites open for adsorption. Mechanism (3) was also proposed (ref. 15.20) from galvanostatic studies in a variety of electrolytes (Pt, 77" F (25" C)). For 0.01 M HCOOH in NaOH, adsorption was slow and currents at transition times up to 10 seconds were entirely from oxidation of preadsorbed fuel, that is, $i\tau$ was constant. Rate of adsorption was higher for less-alkaline electrolytes, with a maximum at pH of 5. This does not agree with the result given above, $(\partial \log i/\partial \text{ pH})_V \simeq 1$, which is the same as $(\partial \eta/\partial \text{ pH})_i \simeq -0.06$ volt at room temperature. At porous flowthrough electrodes of platinum black, polarization under comparable, steady-current conditions was about 0.4 volt more for HCOOH in 30 percent H_2SO_4 than in 4 N KOH at 77" F (25" C) (see ***485***). This is in agreement with

$$(\partial \eta/\partial \text{ pH})_i \simeq -0.06 \text{ volt.}$$

In addition, $i\tau^{1/2}$ for 0.1 M HCOOH in KOH was found to be constant (ref. 15.21), which implies a fast adsorption. In this case, however, transition times were from about 100 to 1000 seconds, on a platinized electrode.

Steady-state measurements gave limiting currents at about 0.5 volt (ref. 15.14), which were not affected by stirring, with an activation energy from 77" to 194" F (25" to 90" C) of 12 kcals/mole. Hydrogen charging (H++e–+[HI) was used to determine uncovered surface and hence coverage by HCOOH, assuming that HCOOH did not desorb during the charge. Coverage started to decrease at anodic potentials: 0.7 volt, 77" F (25" C); 0.6 volt, 113" F (45" C); 0.4 volt, 158" F (70" C); and 0.1 volt, 194" F (90" C). It can be concluded that the net rate of electrochemical discharge of HCOOH is increased more by temperature than rate of adsorption. At 113" F (45" C), a Tafel relation of 0.11-volt slope was found at currents and potentials below the limiting current, indicating a slow-charge transfer as the rate-controlling step, mechanism (4). At 194" F (90° C), the Tafel slope was about

0.07 volt, which is more consistent with mechanism (3).

Bright and platinized platinum electrodes (*N* H_2SO_4, 73" F (23" C)) were anodized to 1.35 volts and allowed to return to a steady OCV in 0.01 to 1*M* HCOOH solutions, which took a few seconds (ref. 15.22). Constant current was applied, potential measured after 5 seconds, current switched off, and the electrode allowed to return to OCV in a few seconds, after which another current step was applied. Tafel lines were found between about 0.2 volt and 0.3 volt, with an approximate slope of 0.10 volt per decade. Current density at 0.2 volt was about 10^{-6} A/cm² of true area determined by oxygen coverage or double-layer capacity. These results, however, are not true steady-state values. There was indication of an approach to a limiting current density of 10^{-4} A/cm² at 0.5 volt.

During linear voltage sweep to >1.4 volt versus NHE in SE, three current maxima were obtained (*N* $HClO_4$, Pt, 86" F (30" C)); see ref. 15.15). These were discussed as follows: for the first region, at approximately 0.4 to 0.6 volt, dissociation of adsorbed HCOOM [step *(b)* below] is slow; for the region at 0.8-volt adsorption of HCOOH and discharge of [COOH], steps *(a)* and (c) are slow; above 1.4 volts direct oxidation of HCOOH without prior adsorption, step *(e)*, is rate limiting.

(a) $Pt + HCOOH \rightarrow Pt[HCOOH]$

(b) $Pt[HCOOH] + Pt \rightarrow Pt[COOH] + Pt[H]$

@) $Pt[COOH] \rightarrow Pt + CO_2 + H^+ + e-$

(d) $Pt[H] \rightleftharpoons Pt + H^+ + e^-$

(e) $HCOOH \rightarrow CO_2 + 2H^+ + 2e-.$

Step *(e)* occurs by some sequence of events not indicated, possibly by collision of HCOOH with a surface evolving oxygen.

A picture of formic acid oxidation during voltage sweep was also suggested by California Research *(239)*. A rotating platinum-disk electrode (*N* H_2SO_4, 86° F (30" C)) was held at 0.24 volt while equilibrating with 0.085 *M* HCOOH for 4 minutes. Adsorption occurred, and transient anodic current was required to maintain the potential:

(a)(b) $2Pt + HCOOH \rightarrow Pt[COOH] + Pt[H]$

(d) $Pt[H] \xrightarrow{\text{fast}} Pt + H^+ + e-.$

The surface became saturated with [COOH], and adsorption and current stopped. On applying a linear anodic voltage sweep, a current wave (wave 11) was obtained with a **peak** at 0.95 volt, due to reaction *(c)*. Oxygen evolution and direct oxidation of HCOOH occurred at about 1.5 volts, reaction *(e)*, current being greater for higher rates of rotation, which give higher rates of mass transfer. The electrode was returned to zero volts, held for a set period of time, and the anodic sweep repeated. A flat wave was found with a peak at about 0.55 volt (wave I). Peak current ***decreased*** for longer wait times. At 1 second it was almost twice the value for 20 seconds. This wave was attributed to reactions *(a)*, *(b)*, and *(d)* occurring on a surface which was not presaturated with [COOH]; the longer the wait time, the smaller was the amount of bare surface available for fresh adsorption during the sweep and the lower the charge within the wave. The current passed through a maximum, which was not increased by faster rotation, because surface coverage increased during the sweep, but the maximum was not pronounced for fast sweep times, showing that the increase in fractional coverage was small. The approach to the maximum was also not sharp, because of discharge of preadsorbed [H] on surface not covered by [COOH].

At fast sweep rates, height of wave II ***increased*** with wait time because it consisted of oxidation of a large amount of preadsorbed [COOH], by reaction (c). The data do not indicate whether reaction *(a)* or *(b)* is slow. At 0.24 volt a slow rearrangement leads to fresh sites and hence further adsorption by ionization of [H]. If adsorption were fast, the amount of [COOH] on the surface at short times would be about half that at long times, which corresponds fairly well to the ratio of peak currents of wave II at short and long wait periods. At a fixed wait time, **total** amount of charge during sweep, Q_t, was given by

$$Q_{\text{total}} = Q_{\text{preadsorbed}} + nFkC_{\text{HCOOH}}(1-\theta)t \qquad (15.10)$$

where C_{HCOOH} is concentration of formic acid, $1-\theta$ fractional surface coverage, and t time of the sweep. Assuming the mean value of $1-\theta$ to be constant with sweep rate, a plot of Q_t as a function of t should be a straight line with positive slope and intercept; this was found to be so for sweep rates from 10 V/sec to 0.25 V/sec. Mean rate of charge was about 10^{-4} C/cm^2 sec for an electrode with a roughness factor of about 2. Results from dissolved CO under comparable conditions were similar to the second wave of HCOOH, suggesting that oxidation occurred via the same transition state for both fuels.

Transient galvanostatic and potential-sweep methods are sometimes difficult to translate into terms useful for practical fuel cells. The practical problem is whether formic acid can be oxidized to CO_2 at potentials up to 0.5 volt versus NHE in SE, at useful current densities. If CO_2 cannot be evolved at appreciable rates until about 0.8 volt, then it is immaterial whether other steps are also slow at lower potentials, since 0.8 volt is not practical for a fuel-cell electrode. Any transient currents observed at lower potentials in voltage-sweep tests represent incomplete reactions which cannot be maintained and are of no interest for steady current supply (providing that the transients are not due to mass-transfer effects). For steady currrents, either charge transfer controls rate at low currents and polarization, with control by adsorption or rearrangement at higher potentials, or adsorption or rearrangement controls rate at all potentials up to direct oxidation. The principal contradiction in the results discussed above is in the potential at which a chemical limiting current is observed.

The term "oxidation starts at X volts" is misleading, since "appreciable current" is relative. A transient sweep on a, bright electrode may show that current is small at 0.5 volt and much less than at 0.8 volt, but this does not necessarily mean that the system is of no use for a fuel cell. Higher temperatures and porous electrodes of high internal area may result in satisfactory current densities at 0.5 volt. In 1 *N* H_2SO_4 at bright Pt electrodes, limiting rate of formic acid oxidation appears to be in the range 0.1 to 1.0 mA/cm^2.

Contradictory results exist for the effect of pH. It was claimed (ref. 15.20) that rates of adsorption in base were much slower than in acid, leading to a lower limiting current than in acid. Peak currents from voltage-sweep measurements were lowest at pH 12 to 14, and higher at pH 1 to 10 (ref. 15.21). The position of potential of peak current varied linearly, with considerable scatter, from about 0.65 volt versus SHE at pH 0 to -0.2 volt at pH **14,** suggesting that $(\partial\mu/\partial\,\text{pH})_{ip}$ -0, which is not the same as $(\partial\eta/\partial\,\text{pH})_i \sim 0$. It was claimed that potassium formate did not oxidize at all ***(127).*** However, a porous flow-through electrode of high-area platinum black gave much better results with potassium formate in KOH than with HCOOH in H_2SO_4 ***(485).*** The effect of pH was given (ref. 15.13) as $(\partial\eta/\partial\,\text{pH})_i \sim -0.06$, which means greater rate in alkali at a given polarization. In table 15.1, a number of results are reported which give performance as comparable in acid and alkali but much higher in neutral solution.

Production of intermediates in the anodic oxidation of methanol was investigated by California Research, ***130*** through ***133*** (see also ref. 15.1). In 20 percent KOH, methanol fluid fed to a platinum-catalyzed, porous carbon electrode produced formate stoichiometrically at 73° F (23° C). Concentrations of HCHO built up with time to steady-state values of less than 10^{-4} *M.* Specific rates of reaction were in the order: HCHO > CH_3OH > HCOOH. In sulfuric acid with 1.5 *M* CH_3OH, steady-state concentrations of about 10^{-2} *M* were obtained for HCOOH and HCHO. Anodic voltage sweep on platinized-platinum in acid showed two current peaks, the second of which was ascribed to oxidation of HCHO or HCOOH produced in the prior wave. After reaching the potential for oxygen evolution, the electrode was poisoned and did not react with methanol on the reverse sweep until about 0.8 volt. (See fig. 15.3 for a somewhat similar situation.) HCHO gave similar results but was more reactive; HCOOH was less reactive.

A slow voltage sweep (0.025 to 0.2 *M* CH_3OH and 1 *M* H_2SO_4) in acid, at a rotating disk electrode, led to the following conclusions ***(136*** through ***138).*** A peak current proportional to methanol concentration was obtained at about 0.8 to 1.0 volt, versus NHE in SE, depending on conditions. Decrease in current after the peak was due to oxidative poisoning of the platinum and not to mass-transfer limitations of methanol to the electrode. Peak current went down with increased speed of rotation, showing that a desorbed intermediate could diffuse away from the electrode before it reacted. Extrapolation of current versus speed to zero or infinite speeds gave values in the ratio of 3:2. This was interpreted as:

No stirring: $CH_3OH \rightarrow HCOOH \rightarrow CO_2 + 6e^-$

Stirring: $CH_3OH \rightarrow HCOOH \xrightarrow[\text{away}]{\text{diffuse}} 4e^-$.

The order of reaction rates was found to be: $HCHO > CH_3OH > HCOOH$. However, rate of HCOOH oxidation is not so much slower than that of CH_3OH that a pronounced break in the current-voltage curve is observed; only a short shoulder was seen.

Adsorption of methanol on platinum and other noble metal electrodes has been discussed in a series of papers (refs. 15.23 through 15.26). Amount adsorbed at a given set of conditions was determined by anodic stripping or by double-layer capacity. In this second technique, 8 was assumed related to capacity by Frumkin's equation

$$C_\theta = C_{\theta=0}(1-e) + C_{\theta=1} \qquad (15.11)$$

where C is double-layer capacity, 8 is coverage, and capacities at 1 and 0 are determined before and after anodic stripping. At open circuit, Temkin isotherms were found ($8 \propto \log C_{\text{methanol}}$). Using superimposed ac (amplitude 5 mV, frequency 300 cps) values of double-layer capacity were determined during voltage-sweep tests when current was passing (ref. 15.23). At relatively low sweep rates (30 mV/sec, for example, with N $HClO_4$, Pt, 86" F (30" C)), the coverage by methanol was constant from 0.1 to 0.6 volt and fell rapidly to zero at 0.8 volt.

Figure 15.4 shows a typical voltage-sweep result. The first wave up to the shoulder corresponded to large coverage by methanol, with coverage falling rapidly at the shoulder. In this wave, between coverages of $0.3 < \theta_{\text{MeOH}} < 0.9$, current due to oxidation of adsorbed methanol followed the rate law (N $HClO_4$, Pt, 86° F (30" C)).

$$i = k\theta_{\text{MeOH}} e^{\alpha nFV/RT} \qquad (15.12)$$

where αn was 0.6 and $k = 10^{-8.1}$ mA/cm^2 (ref. 15.27). Peak currents predicted from mass transfer of CH_3OH to the surface were much greater than those observed experimentally, indicating that an adsorption step became rate-limiting at high currents, leading to fall in θ. Values of k were higher on the reverse sweep, which was attributed to a higher activity of freshly anodized and reduced surface.

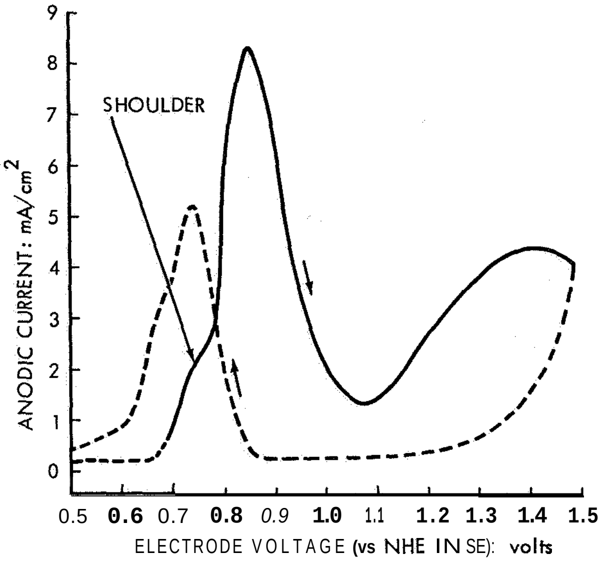

The sweep rate was 30 mV/sec, so that time-to-peak current was about 10 seconds.

FIGURE 15.4.—Linear voltage sweep of 1 M CH_3OH on smooth platinum, in N $HClO_4$.

The rate of adsorption, i_a, was determined (ref. 15.25) by

$$i_a \simeq i - dQ/dt$$

where i is current of equation (15.12) and dQ/dt current from fall of e on the surface. Adsorption up to the shoulder followed the rate law:

$$i_a = f(v)\theta_f^{1.85} C_{\text{methanol}} \qquad (15.13)$$

where $f(v)$ was a slight function of potential and e, was the free surface. The value of 1.85 was considered indicative of a two-site adsorption of CH_3OH. During anodic oxidation, $f(v)$ was about 2 A cm/mole, which gives an adsorption-limited current of 2 mA/cm^2 for 1M CH_3OH and $\theta \rightarrow 0$. Equation (15.12) gives a current density of about 5 mA/cm^2 at 0.6 volt; therefore, rate of adsorption becomes a factor between about 0.5 and 0.6 volt. However, when 8 fell toward zero, the current did not fall as predicted by equation (15.12) and it increased beyond the limiting current of equation (15.13). Figure 15.4 shows that the current increased considerably beyond the shoulder and reached a peak at the point where oxidative poisoning of the surface started. This increase in rate was attributed to much faster adsorption on active sites at θ values of less than **0.3.** There is some evidence that the rate of adsorption on bare surface is very rapid and falls off logarithmically as θ increases. This is an Elovitch rate law, which leads to Temkin equilibrium isotherms.

The effect of chloride ion was determined (ref. 15.28) at various concentrations of HCl (CH_3OH, Pt *N* $HClO_4$, 86" F (30" C)). Oxidation was inhibited with 10^{-6} *M* HCI, and at concentrations greater than 10^{-2} *M*, no methanol oxidation occurred. Capacity measurements revealed that chloride ion adsorption predominated over CH_3OH adsorption at potentials in the oxidation region, thus preventing reaction.

The effeet of pH was to shift potential of peak current by roughly –0.06 volt per unit increase pH or $(\partial\eta/\partial\,\text{pH})_{i_p}\sim 0$ (ref. 15.21). Different electrolytes were used in oxidation of a number of alcohols and carboxylic acids as well as HCHO on Pt at 77" F (25° C) (ref. 15.29). Contrary to results quoted above, current at a given voltage was found to be proportional to (concentration)'. Potentials of peak currents were shifted by approximately –0.06 volt per unit pH increase and $(\partial \log i/\partial\,\text{pH})_V$ was about 0.5. The rate law was expressed as

$$i = kF(V_r)f(V_r)C^{\alpha}(a_{OH^-})^{\beta}e^{\gamma FV/RT}, \quad (15.14)$$

where F(V,) accounts for changes in [O], $f(V,)$ changes in θ_{organic}, and $\alpha,\beta,\gamma\cong\frac{1}{2}$. V_r is reversible potential. The half-order dependence of i on activity of hydroxyl leads to the observed pH dependency, $(\partial\eta/\partial\,\text{pH})$,—0, as in table 15.10. It is difficult, however, to determine a feasible mechanism leading to this order of reaction. Inhibition of rate was in the order $I^- > Br^- > Cl^- > PO_4^{\equiv} > SO_4^{=} > ClO_4^-$.

The double-layer capacity method was used (American Oil Co., *93* through *101*) to study rate of adsorption of methanol on bright platinum (*M* H_2SO_4 at 77" F (25° C)). Results were variable throughout the reports, but adsorption of methanol appeared to follow an Elovitch rate law

$$d\theta/dt = k_1 C_{\text{MeOH}}(1-\theta)^2 e^{-k_2\theta/RT}. \quad (15.15)$$

Rate of adsorption at $\theta\to 0$, $C_{\text{MeOH}} = 0.1$ *M*, was $d\theta/dt\sim 10^{-2}$ fraction per second. Assuming that e = l corresponds to a maximum of 1.4 mC/cm², the adsorption-limited rate is (1.4) (10^{-2}) mA/cm². It would be tenfold higher for 1 *M* CH_3OH; that is, $i_L = 0.14$ mA/cm². This is less than one-tenth the 2 mA/cm² obtained from equation (15.13), which in turn was believed to be much lower than the true rate at $\theta\to 0$. Rate of adsorption of CH_3OH, HCHO, and HCOOH on platinum (H_2SO_4, 77" F (25" C)) was studied by holding the electrode in H_2SO_4 at a potential to remove [H], removing and putting in fuel and electrolyte for a given time, removing, washing, and anodically stripping in H_2SO_4 (Esso, *214).* HCHO and HCOOH were adsorbed to equilibrium in less than 1 second, while CH_3OH took 15 to 30 seconds. The coulombs of adsorbed material were 2:1 for HCHO or HCOOH to CH_3OH. Transient galvanostatic tests showed that reaction of HCHO was diffusioncontrolled ($i\tau^{\frac{1}{2}}$ constant), but HCOOH and CH_3OH were not; this indicated a rapid adsorption of HCHO.

Platinum was doped with 0.1 to 1 weight-percent of other metals by heating metal chloride with platinum in a sealed tube (Leland Stanford Junior University, *394).* Fe, Ni, Mn, Cu, Zn, and Co doping did not change performance of Pt as a catalyst for anodic oxidation of methanol. Chloride ion completely poisoned oxidation below 1.15 volts, versus NHE in SE. Linear voltage sweep gave oxidation starting at about 0.55 volt, with poisoning beyond 0.85 volt (see fig. 15.4 for similar results). It was concluded that oxidation occurred only when $Pt + H_2O \to Pt[OH] + H^+ + e^-$ becomes appreciable.

Repetitive voltage-sweep methods were used to study CH_3OH, HCOOH, and HCHO oxidations at a rotating platinum wire (Baylor University, *127).* Results were similar to those described above. Peak currents occurred at the same polarization for 2 *N* H_2SO_4 and 2 *N* NaOH, so that $(\partial\eta/\partial\,\text{pH})_{i_p}\sim 0$. No wave was obtained for potassium formate and formate (HCOOH in KOH) did not react. The linear relation between total charge and sweep time of equation (15.10) was obtained with CH_3OH, and the main product of reaction was CO_2, with some HCHO and HCOOH. Because potential of oxidation changed with pH in the same way as theoretical open circiit $(\partial\eta/\partial\,\text{pH}\sim 0)$, the rate of oxidation was concluded to be a chemical rate and controlled by an equilibrium process, that of the "redox couple," $Pt + H_2O \rightleftharpoons Pt[OH] + H^+ + e^-$.

The conclusion that oxidation occurs only at the potential of the "redox couple," $Pt+H_2O \rightleftharpoons Pt[OH]+H^+ +e^-$ is unclear. Such a reaction does not have a single equilibrium potential because the activity of Pt[OH], represented by θ, and of Pt, represented by $1-\theta$, can vary from 0 to 1 at equilibrium, giving any number of equilibrium potentials. If the statement is taken to mean that reaction is only appreciable when the surface approaches a coverage of about $\theta_{OH}=0.5$, then the reason for slow rate at smaller coverages must be determined. At these potentials the overall oxidation of the organic is far removed from equilibrium and, from a free energy standpoint, the organic should reduce Pt[OH] to disturb the equilibrium $Pt+H_2O \rightleftharpoons Pt[OH]+H^+ + e^-$. The problem is one of kinetics and not equilibrium. The equilibrium can be introduced by postulating a mechanism

$$Pt+H_2O \rightleftharpoons Pt[OH]+H^+ +e^-$$

$$Pt[fuel]+Pt[OH] \xrightarrow{slow} Pt+CO_2+H^+ +e^-$$

with rate equations

$$i=k(\theta_{fuel})(\theta_{OH}) \qquad (15.16)$$

$$\theta_{OH}=f(\eta).$$

The last equation represents the equilibrium and θ_{OH} is the same function of potential versus a NHE in SE at all pH values. Variation in current with polarization then depends on variation of θ_{OH} with potential and will be of the same form for electrolytes of different pH, which does not appear to be the case for steady-state measurements (see table 15.1). Predictions of this mechanism are that *(a)* k would vary with the type of fuel, *(b)* saturation of the surface with adsorbed fuel would reduce the rate of reaction unless OH could readily replace adsorbed fuel, and (c) dependence of i on η in a given electrolyte would not be a simple Tafel form with slope corresponding to $\alpha n \sim \frac{1}{2}$.

Ethanol at platinized platinum in N H_2SO_4 gave the following results (ref. 15.30) in linear voltage sweep. Both ethanol and acetaldehyde showed two current peaks (—0.9 and 1.3 volts) on the forward potentiostatic scan and one current peak (—0.65 volt) on the reverse potentiostatic scan. Ethanol (1 percent and 5 percent) gave a flat minimum of capacitance as a function of voltage from —0.3 to 0.9 volt on forward scan. For reverse scan, capacitance began decreasing at —0.7 volt and showed a minimum from —0.6 to 0.3 volt. From 0.55 to 0.75 volt of the reverse scan, a Tafel plot was obtained of —0.11 volt slope. The mechanism was proposed as

$$CH_3CH_2OH \xrightarrow{fast} [CH_3 \cdot CHOH]+H^+ +e^-$$

$$[CH_3 \cdot CHOH] \xrightarrow{slow} CH_3CHO+H^+ +e^-.$$

For the second peak,

$$Pt+nEtOH \xrightarrow{slow} Pt(OEt)_n+nH^+ +ne^-$$

$$Pt(OEt)_n+H_2O \rightarrow Pt(O)_n+n\ EtOH+nH^+ +ne^-$$

$$Pt(OEt)_n \rightarrow Pt+nCH_3CHO+nH^+ +ne^-.$$

Product analysis showed that the primary product formed was acetaldehyde with some acetic acid formed after longer times.

In my opinion much of the confusion in these results on the oxidation of methanol arises from use of unsteady-state measurements, especially triangular voltage sweep. These methods are excellent for simple reactions which are mass-transfer controlled, but they are difficult to interpret for complex reactions involving rates of adsorption, poisoning, and preadsorbed material. For example, many of the investigators quoted above use repetitive scan techniques in which the electrode is cycled and recycled from one potential to another without a waiting period. Wait time between sweeps is an important variable and by making this zero, the surface has a coverage by adsorbed fuel which depends on rate of adsorption and rate of oxidation during the reverse scan, decreasing with time and potential. This is a complex situation to analyze quantitatively over the whole cycle. There has been a tendency to lay stress on the potential of peak current, non-mass-transfer controlled, occurring at about 0.9 volt. If decrease of current at more positive potentials is due to oxidative poisoning of the surface, then it is not surprising that many fuels have a current peak at this potential, or that the peak potential from NHE in SE is the same for different pH values. More important is the current density at lower potentials on a true area basis, especially for comparing acidic and basic electrolytes, or different electrodes. Steady-state measurements, such as those performed by Bockris et al., for unsaturated hydrocarbons (see table 15.13) require more experimental care and effort, but they are an excellent guide to fuel-cell performance. Such steady-state methods should always be used in addition to voltage sweep methods to obtain a convincing picture of the electrochemical process.

The fact that HCHO will oxidize at least partially at lower potentials than methanol is fairly well established. Thus, if a surface intermediate is formed during oxidation of methanol which could desorb and diffuse away as HCHO, then steady-state concentration of the intermediate is low and/or rate of desorption slow, so that HCHO is not formed in large quantities in the electrolyte. Surface intermediates which can form HCOOH must exist in fairly high concentrations and be fairly readily desorbed, since HCOOH can be removed from an electrode by rapid rotation, i.e., good mass transfer. Usually, however, these surface intermediates are oxidized sufficiently rapidly to lead to CO_2, or $CO_3^=$ in strong alkali. As with HCOOH, there is disagreement on the effect of pH on reaction rate. Equation (15.14) gives $(\partial\eta/\partial \text{pH})_i \sim 0$, which states that rates are comparable at a given potential versus NHE in SE for all pH values. Table 15.1 gives power output of methanol in alkali as over tenfold that in acid. With porous flowthrough electrodes of platinum (*485*), potential versus NHE in SE was about 0.7 volt at 100 mA/cm² for CH_3OH in **32** percent H_2SO_4 and about 0.2 volt in **4** *N* KOH, showing much less polarization in alkali. All these rates are measured at irreversible conditions, so the formation of CO_2 in acid versus $CO_3^=$ in alkali should not affect the results. More work has been done on acid systems than on alkaline because alkaline cells require regeneration of OH– from $CO_3^=$ for continuous operation.

There are few precise data on the rates of adsorption of methanol. The general consensus is that rate of adsorption affects but does not limit currents obtained at potentials below that of oxidative poisoning.

15.6 CONCLUSIONS

Direct hydrocarbon fuel cells have not reached a useful stage of development, primarily due to slow rates of electrochemical reaction of organic fuels. Platinum is the best simple catalyst for the reactions, and although binary and ternary alloys have shown improvement over platinum in certain circumstances, the improvement has not been sufficient to make practical high-power-density anodes. Methane and hydrocarbons with more than five carbon atoms are more difficult to react than ethylene, ethane, propane, and butane. Complete conversion of reactive hydrocarbons to CO_2 and H_2O has been obtained at platinum electrodes. Electrolytes of sulfuric acid, phosphoric acid, and perchloric acid give similar results under comparable conditions, but phosphoric acid *can* be used at higher temperatures without pressurization or reaction with the fuel. High-boiling-point electrolytes of $CsF\text{-}HF\text{-}H_2O$ show considerable promise.

The performance of methanol cells reported in the contracts considered here is poor. Again, electrochemical reaction of the fuel is slow in acid solutions, even though it can be used in high concentrations in the electrolyte. In addition, diffusion of methanol to the cathode seriously affects the cathode performance. Complete conversion to CO_2 and H_2O was obtained.

Scientific investigation of reaction mechanisms has provided much data, but no satisfactory general theory of reaction has emerged. Results from different techniques are often contradictory and extrapolation of results to practical fuel cells in some cases leads to conclusions which are not borne out by experience with practical electrodes.

Prognostications of long-term prospects for direct hydrocarbon fuel cells cannot yet be made with any degree of certainty. Some factors which have to be considered are as follows. Hydrogen-oxygen cells have been increased in useful current densities by two orders of magnitude through the extensive program of research dating from World War 11. However, there is no guarantee that similar improvement will be obtained with direct hydrocarbon cells, because the present advanced technology of hydrogen-oxygen electrodes has already been applied to hydrocarbon fuel cells. The performance values for the General Electric propane cell were obtained with flow rates of fuel greater than stoichiometric. Work on high-temperature cells has revealed that use of cells with near-stoichiometric feed (once-through operation) leads to lower performance or to excessive fuel loss in the exit $CO_2\text{-}H_2O$ stream, and hydrocarbons of high chain length, or methane, have been found to perform poorly compared with propane. A significant activation polarization of the cathode can be tolerated with hydrogen-oxygen cells when the hydrogen electrode has low polarization. But the large activation polarization occurring at both fuel electrode and cathode of hydrocarbon-air cells cannot be tolerated. Thus, a major breakthrough in catalysis and electrode construction is needed for the advantages of the simplicity and long life of low-temperature fuel cells to be retained for hydrocarbon-air utilization.

15.7 REFERENCES

15.1. Schlatter, M. J.: Fuel Cells. Vol. 11, G. H. Young, ed., Reinhold Pub. Corp., 1963, p. 190.

15.2. Binder, H.; Köhling, A.; et al.: Electrochemical Oxidation of Certain Hydrocarbons and Carbon Monoxide in Dilute Sulfuric Acid. J. Electrochem. Soc., vol. 112, no. 3, 1965, pp. 355–362.

15.3. Dahms, Harold; and Bockris, John O'M.: The Relative Electrocatalytic Activity of Noble Metals in the Oxidation of Ethylene. J. Electrochem. Soc., vol. 111, no. 6, 1964, p. 728.

15.4. Wroblowa, H.; Piersma, B. J.; and Bockris, J. O'M.: The Mechanism of the Anodic Oxidation of Ethylene in Acid and Alkaline Media. J. Electroanal. Chem., vol. 6, no. 5, 1963, pp. 401416.

15.5. Green, Mina; Weber, Jan; and Drazic, Vera: The Electrochemical Oxidation of Ethylene: An Experimental Study. J. Electrochem. Soc., vol. 111, no. 6, 1964, pp. 721–728.

15.6. Dahms, Harold; and Bockris, John O'M.: The Relative Electrocatalytic Activity of Noble Metals in the Oxidation of Ethylene. J. Electrochem. Soc., vol. 111, no. 6, 1964, pp. 728–736.

15.7. Johnson, James W.; Wroblowa, Halina; and Bockris, John O'M.: Mechanisms of the Electro-Oxidation of Acetylene on Platinum. J. Electrochem. Soc., vol. 111, no. 7, 1964, pp. 863-870.

15.8. Bockris, J. O'M.; Piersma, B. J.; and Gileadi, E.: Extended Abstracts of Papers Presented at Fall 1964 Meeting of the Electrochemical Society, Battery Division. Vol. 9, p. 29.

15.9. Munson, R. A.: Carbon Monoxide Adsorption on Platinum Electrodes. Constant Current Transition Time Study. J. Electroanal. Chem., vol. 5, 1963, pp. 292–294.

15.10. Gilman, S.: Study of the Mechanism of Carbon Monoxide Adsorption on Platinum by a New Electrochemical Process. J. Phys. Chem., vol. 67, 1963, pp. 78–84.

15.11. Warner, T. B.; and Schuldiner, S.: A Study of Adsorption and Oxidation of Carbon Monoxide on Platinum Using Constant Current Pulses. J. Electrochem. Soc., vol. 111, no. 8, 1964, pp. 992–997.

15.12. Gilman, S.: Anion Adsorption on Platinum by the Multipulse Potentiodynamic Method. J. Phys. Chem., vol. 68, no. 8, 1964, pp. 2098–2119.

15.13. Brummer, S. B.; and Makrides, A. C.: Adsorption and Oxidation of Formic Acid on Smooth Platinum Electrodes in Perchloric Acid Solutions. J. Phys. Chem., vol. 68, no. 6, 1964, pp. 1448–1459.

15.14, Fleischmann, C. W.; Johnson, G. K.; and Kuhn, A. T.: The Electrochemical Oxidation of Formic Acid on Platinum, J. Electrochem. Soc., vol. 111, no. 5, 1964, pp. 602–605.

15.15. Breiter, M. W.: Anodic Oxidation of Formic Acid on Platinum. Electrochem. Acta., vol. 8, 1963, pp. 447456, 457470.

15.16. Giner, J.: The Anodic Oxidation of Methanol and Formic Acid. Electrochim. Acta, vol. 9, 1964, p. 63.

15.17. Juliard, Andre L.; and Shalit, Harold: Application of Cyclic Voltammetry to the Kinetic Study of Electro-Oxidation of Organic Compounds. J. Electrochem. Soc., vol. 110, no. 9, 1963, pp. 1002–1006.

15.18. Rhodes, D. R.; and Steigelmann, E. F.: Catalytic Decomposition of Aqueous Formic Acid on Electrodes. J. Electrochem. Soc., vol. 112, no. 1, 1965, pp. 16–21.

15.19. Steigelmann, E. F.; and Rhodes, D. R.: The Effect of Ultraviolet Light on the Anodic Oxidation of Formic Acid. J. Electrochem. Soc., vol. 112, no. 1, 1965, pp. 21–24.

15.20. Munson, Ronald A.: Constant Current Transition Time Investigations of the Electrochemical Oxidation of Formate-Formic Acid at a Smooth Platinum Electrode. J. Electrochem. Soc., vol. 111, no. 3, 1964, pp. 372–376.

15.21. Buck, R. P.; and Griffith, L. R.: Voltammetric and Chronopotentiometric Study of the Anodic Oxidation of Methanol, Formaldehyde, and Formic Acid. J. Electrochem. Soc., vol. 109, no. 11, 1962, pp. 1005–1013.

15.22. Gottlieb, M. H.: Anodic Oxidation of Formic Acid at Platinum Electrodes. J. Electrochem. Soc., vol. 111, no. 4, 1964, pp. 465–472.

15.23. Breiter, M. W.; and Gilman, S.: Anodic Oxidation of Methanol on Platinum. I. Adsorption of Methanol, Oxygen, and Hydrogen in Acidic Solution. J. Electrochem. Soc., vol. 109, no. 7, 1962, pp. 622–634.

15.24. Breiter, M. W.: Double-layer Capacity and Methanol Coverage of Platinum in Perchloric Acid Solution. Electrochim. Acta, vol. 7, 1962, pp. 533–542.

15.25. Breiter, M. W.: Comparative Voltametric Study of Methanol Oxidation and Adsorption. Electrochim. Acta, vol. 8, 1963, p. 973.

15.26. Breiter, M. W.: Anodic Oxidation of Methanol on

Platinum. III. Adsorption Kinetics in Acid Solution. J. Electrochem. Soc., vol. 110, no. 5, 1963, pp. 444-452.

15.27. Gilman, S.; and Breiter, M. W.: Anodic Oxidation of Methanol on Platinum. II. Interpretation of Potentiostatic Current-Potential Curves in Acidic Acid. J. Electrochem. Soc., vol. 109, no. 11, 1962, pp. 1099–1104.

15.28. Breiter, M. W.: Voltametric Study of Inhibition of Methanol Oxidation on Platinum. Electrochim. Acta, vol. 9, 1964, p. 827.

15.29. Bagotsky, V. S.; and Vasilyev, Y. B.: Some Characteristics of Oxidation Reactions of Organic Compounds on Platinum Electrodes. Electrochim. Acta, vol. 9, 1964, p. 869.

15.30. Rightmire, R. A.; Rowland, R. L.; Boos, D. L.; and Beals, D. L.: Ethyl Alcohol Oxidation at Platinum Electrodes. J. Electrochem. Soc., vol. 111, no. 2, 1964, pp. 242–247.

CHAPTER 16

Miscellaneous Fuels (Hydrazine, Ammonia, etc.) and Oxidants (Hydrogen Peroxide, Nitric Acid, etc.)

16.1 INTRODUCTION

Fuel cells already developed for use in complete systems were discussed in chapters 4, 5, 6, and 7; these cells for the most part use hydrogen and oxygen reactants. A great deal of work is also being done to fuel cells that use hydrocarbons or oxygenated hydrocarbons directly as fuel, and do not require conversion into hydrogen (see ch. 15). Most of the work on hydrocarbon fuel cells is still in the exploratory stage. Fuel cells using inorganic fuels such as hydrazine or ammonia, and oxidants such as hydrogen peroxide or nitric acid, have progressed beyond the exploratory stage, but have not been developed into complete systems under Government contracts falling within the scope of this monograph. These reactants are not likely to compete with hydrocarbons and air in the production of cheap electricity, but they may have application in space or military uses. The energy density per unit volume is usually good for the liquid reactants under discussion in this chapter (see app. B), and the weights of storage tanks are low compared with high-pressure gas storage. As will be seen below, other factors enter into the usefulness of the reactants for space travel or military power generators.

Hydrazine and ammonia can be considered as hydrogen carriers and nitrogen is produced in the half-cell reactions:

$$N_2H_4 + 4OH^- \xrightarrow{\text{alkali}} N_2 + 4H_2O + 4e^-$$

$$N_2H_4 \xrightarrow{\text{acid}} N_2 + 4H^+ + 4e^-$$

$$NH_3 + 3OH^- \xrightarrow{\text{alkali}} \tfrac{1}{2}N_2 + 3H_2O + 3e^-$$

or

$$NH_4^+ + 4OH^- \xrightarrow{\text{alkali}} \tfrac{1}{2}N_2 + 4H_2O + 3e^-.$$

Similarly, hydrogen peroxide can be considered as an oxygen carrier. Table 16.1 gives some thermodynamic data for these reactants. It is not usually possible to obtain theoretical elec-

TABLE 16.1.—Thermodynamic Data for Ammonia, Hydrazine, Nitric Acid, Borohydrides, and Hydrogen Peroxide

Reaction	E^0, volts[a]	Theoretical, W-hr/lb	Report
$2NH_4OH(aq) + 6OH^- \leftrightharpoons N_2(g) + 8H_2O(l) + 6e^-$	–0.74	....	408
$N_2H_4 + 4OH^- \leftrightharpoons N_2 + 4H_2O + 4e^-$	–1.16	....	456
$N_2H_4 \cdot H^+ \leftrightharpoons N_2 + 5H^+ + 4e^-$	–.23	....	456
$HNO_3 + 5H^+ + 5e^- \leftrightharpoons \tfrac{1}{2}N_2(g) + 3H_2O$	1.24	....	456
$5N_2H_4 + 4HNO_3 \leftrightharpoons 7N_2 + 12H_2O$	1.58	929	456
$3N_2H_4 + 4HNO_3 \leftrightharpoons 3N_2 + 4NO + 8H_2O$	1.29	539	456
$H_2O_2 + 2H^+ + 2e^- \leftrightharpoons 2H_2O$	1.77	....	456
$HO_2^- + H_2O + 2e^- \leftrightharpoons 3OH^-$	.88	....	456
$N_2H_4 + 2H_2O_2 \leftrightharpoons N_2 + 4H_2O$	2.2	1608	456
$B_5H_9 + 15H_2O \leftrightharpoons 5H_3BO_3 + 24H^+ + 24e^-$	–.61	....	456
$B_5H_9 + 29OH^- \leftrightharpoons 5BO_2^- + 19H_2O + 24e^-$	–1.57	....	456
$BH_4^- + 8OH^- \leftrightharpoons BO_2^- + 6H_2O + 8e^-$	–1.26	....	456

[a] Half-cell potentials are measured versus standard (pH 0) hydrogen electrodes.

trode potentials of these reactants when these are more negative than hydrogen evolution or more positive than oxygen evolution, even at very active electrodes. For example, the reversible hydrazine potential is over 0.2 volt more negative than the reversible hydrogen electrode, and hydrazine will ionize and hydrogen will be evolved at an active electrode. The OCV will lie somewhere between the two reversible potentials. A somewhat similar situation applies to hydrogen peroxide, which can react in two ways

$$H_2O_2+2H^++2e^-\rightleftharpoons 2H_2O, \qquad 1.77 \text{ volts}$$

$$H_2O_2\rightleftharpoons O_2+2H^++2e^-, \qquad 0.68 \text{ Volt.}$$

The OCV will usually lie between these two potentials, and oxygen will be evolved.

16.2 BASIC RESEARCH IN FUEL CELLS: AMMONIA, ETHYLENE GLYCOL, AND UREA SYSTEMS, Lockheed Aircraft Corp., July 1960 to August 1961 and May 1961 to July 1963

Fuels were tested (*404*) in a laboratory cell which had an oxygen diffusion cathode and a flowthrough anode, as in figure 16.1. The flowthrough electrode consisted of two plates of porous-nickel plaque (32 mils thick) with a thin sandwich of platinum black between them. Alternatively, nickel plaque was electroplated with platinum, with 10 to 15 mg/cm² being required for good performance. The cathodes were Lockheed proprietary cathodes, made from carbon and plastic binder pressed onto metal screen. In most runs, the electrolyte was **30** weight-percent potassium hydroxide, and the fuel-electrolyte stream was passed through the anode at a velocity of 1 cm/sec. Urea and glycol performed poorly. A 3 *M* ammonia solution gave a half-cell OCV near that of the reversible hydrogen electrode, but on current drain the polarization increased sharply (by about 0.15 volt) at 10 A/sq ft and then fell more gradually with increased current density. On reducing current density below 10 A/sq ft, the half cell remained polarized. The initial current and OCV were undoubtedly caused by adsorbed hydrogen on the electrodes, produced during the preparation of the electrode. Once this hydrogen had been discharged, the potential changed to more anodic potentials at which ammonia was reacted. Nitrogen bubbles were noted at the point where the sharp change of potential occurred.

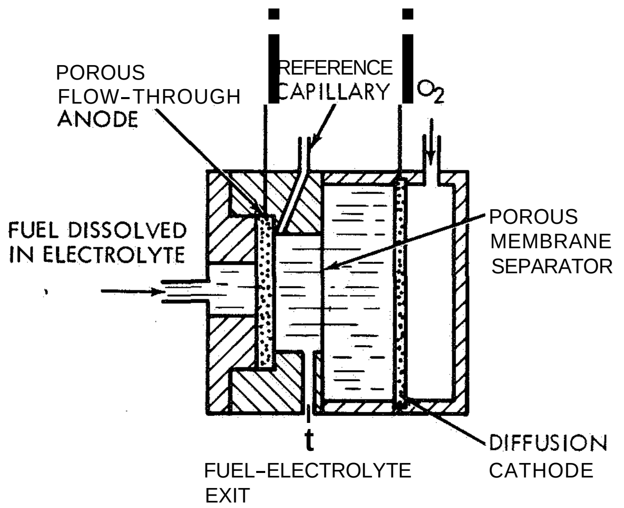

Fuel (hydrazine, for example) is dissolved in the electrolyte and is forced through a porous anode, where it reacts. The electrolyte plus spent reactant passes *out* from the anode chamber and is usually replenished with fuel and circulated back to the anode entrance. A flowthrough cathode (using hydrogen peroxide dissolved in electrolyte, for example) can also be used. A porous separator is placed between anode and cathode to allow ions to pass, but prevent unconsumed fuel from flowing into the cathode.

FIGURE 16.1.—Illustration of a flowthrough anode combined with a diffusion cathode.

The solubilities of ammonia in 30 percent KOH were determined (see app. B). It was proposed that potassium carbonate be used as electrolyte for carbon-containing fuels and the conductance and pH of K_2CO_3-ethylene glycol solutions were determined (see app. B). Potassium bicarbonate can be formed by

$$H_2O+CO_2+CO_3^{=}\rightarrow 2HCO_3^-,$$

and will precipitate at rather low concentrations. It was suggested that temperatures of 176" to 230° F (80° to 110° C) would decompose the bicarbonate to more soluble carbonate. The solubility and pH of bicarbonate in **3** *M* and 4 *M* K_2CO_3 were determined at temperatures up to 212" F (100° C) (see ch. **3),** and demonstrated a range of 0.5 mole/liter at 77° F (25° C) to 2.44 mole/liter at 212° F. Presumably, at the higher temperatures it is potassium carbonate which precipitates at the sum of the molar concentration of the original solution and added bicarbonate. The hydroxyl concentration in potassium carbonate solution is about 0.001

molar, and if hydroxyl takes part in the fuel cell reaction, the performance is likely to be low in carbonate solution.

A 10-cell stack was built, using ammonia as fuel, oxygen as oxidant, and 30 percent KOH as electrolyte. At 122" F (50° C), the average cell performance was about 0.4 volt at 10 A/sq ft, although no separator was used between the anode and cathode (this probably led to reaction of fuel at the oxygen electrode).

Ammonia in potassium hydroxide solution at 122" F (50° C) was investigated also, in a second contract *(408)*. Flowthrough electrodes of platinized-platinum screen were used. The standard state potential of the reaction

$$2NH_4OH\,(ag)+6OH^- \rightleftharpoons N_2(g)+8H_2O(l)+6e^-$$

was calculated to be –0.74 volt versus SHE (standard hydrogen electrodes). The OCV was experimentally determined to be –0.4, and it can be concluded that considerable activation polarization was present, since performance was poor and grew worse with time. To overcome the problem of activation polarization, a higher temperature cell was built using molten hydroxide electrolytes. A molten paste of 42 NaOH: 37 KOH: 9 LiOH: 12 H_2O percent by weight (softening point 266" F (130" C)); see app. B) was poured into a Teflon ring and allowed to solidify. Porous electrodes were placed on each side and the assembly mounted in Teflon end plates. The anode chamber was supplied with ammonia vapor and the cathode chamber with oxygen or air. A similar design using silver-plated Inconel was used for higher temperatures, with calcium hydroxide added to the electrolyte to increase its viscosity. At 284" F (140" C), current densities of 20 A/sq ft were obtained, but lifetime was poor due to the formation of nitrates and nitrites in the electrolyte. An electrolyte of KOH-NaOH-LiOH contained in a porous ceramic matrix was used at temperatures of 518" to 752" F (270" to 400" C). As before, anodes were platinized-nickel plaque, but the cathodes were porous, sintered silver. A current density of 20 A/sq ft at 0.35 volt was obtained, with most of the voltage loss from open circuit being due to cathode polarization and IR loss. Similar results were found with $KNaLiCO_3$ eutectics at 896° F (480" C).

An eight-cell stack was constructed, using aqueous KOH electrolyte. Various flowthrough anodes were used, including titanium or nickel screen, bright plated with platinum and then platinized, and platinized nickel plaque. Proprietary carbon cathodes were used. Power densities and life were poor.

Hydrazine was investigated, using techniques similar to those described above. Platinized-nickel-plaque anodes were used in alkaline solutions, while platinized-platinum sheet or screen was used in acid. At 77" to 104" F (25" to 40" C), 1 *M* nitric acid electrolyte was better than sulfuric acid, giving an OCV of 0.18 volt and 140 A/sq ft at 0.38 volt, versus SHE. The low solubility of hydrazine in sulfuric acid appeared to be the principal reason for its poor performance. Current density at a given potential was independent of hydrazine concentration above 0.1 molar. The flow rates used corresponded to about 20 000 A/sq ft, so the fractional utilization of hydrazine in one pass was very low. In 6.9 *M* potassium hydroxide, the OCV was –0.9 volt versus SHE, and increased concentration of hydrazine gave better performance. Three-molar hydrazine decomposed spontaneously and very rapidly, evolving hydrogen. Under comparable conditions, the addition of 0.5 *M* potassium carbonate increased polarization by about 0.1 volt, while performance in 4 *M* carbonate electrolyte was about 0.2 volt more polarized than in potassium hydroxide. Similarly, performance decreased as the KOH concentration was decreased from 7 *M* to 0.001 *M*.

Faradaic efficiencies were determined by comparing the product of current and time with the amount of nitrogen collected from the anode chamber (note that this is not the fraction of fuel used in one pass through the electrode, which was always very small). Nitric acid gave values of 60 to 95 percent and sulfuric acid 30 to 55 percent. The amounts of hydrogen collected, arising from spontaneous decomposition, were not sufficient to explain the low faradaic efficiencies, which were ascribed to formation of ammonium ion by

$$3N_2H_4\cdot N^+ + H^+\cdot H_2O \rightarrow N_2 + 4NH_4^+ + H_2O.$$

Oxygen was also found in the anode gas. With freshly platinized nickel plaque, the rate of spontaneous decomposition in potassium hydroxide was about 1.2 percent per second. It was necessary to heat the electrode in hydrogen at 572° F (300° C) for 1 hour to decrease the decomposition rate by a factor of 10. Heating caused sintering and hence loss of active area of the platinum; the electrochemical performance was also considerably reduced (0.25 volt more polarization at useful current densities). Faradaic efficiency with sintered electrodes was 92 to 94 percent, with some hydrogen occurring in the exit nitrogen.

A number of cell stacks were built with 4.5-inch-diameter disk electrodes, spot welded into nickel rims. Hydrazine in potassium hydroxide was circulated through the stack, using flow-through anodes of platinized-nickel plaque and the Lockheed proprietary oxygen electrodes. A 10-cell stack gave a net output of 36 watts at 6 volts, with the circulating pump being powered by the stack. Complete dimensions were not given, but the electrodes were 32 to 64 mils thick and the total cell thickness was probably 0.5 inch; this amounts to a power density of 1 kW/cu ft for the cell stack. Cell performance fell in the first 2 days, then remained fairly stable for several weeks of operation. The faradaic efficiency of hydrazine use was 40 to 70 percent, since there was direct reaction of hydrazine with the oxygen electrode; this occurred because no separator was used. Figure 16.2 gives typical performance data. Typical lifetime was 1000 hours, at which time cathode disintegration caused cell failure.

There was no attempt in the project at Lockheed to examine the theory of flowthrough electrodes or to obtain any fundamental data. Since no model was given for the electrode, it is not possible to analyze the data in terms of expected effects of flow rate, concentration, thickness of electrode, catalytic area of electrode, temperature, etc. The results are, therefore, entirely empirical. They are, of course, perfectly valid and of considerable practical interest, but it seems probable that a more systematic and scientific program would have led to better understanding of the electrode processes, and that a better cell design would have resulted.

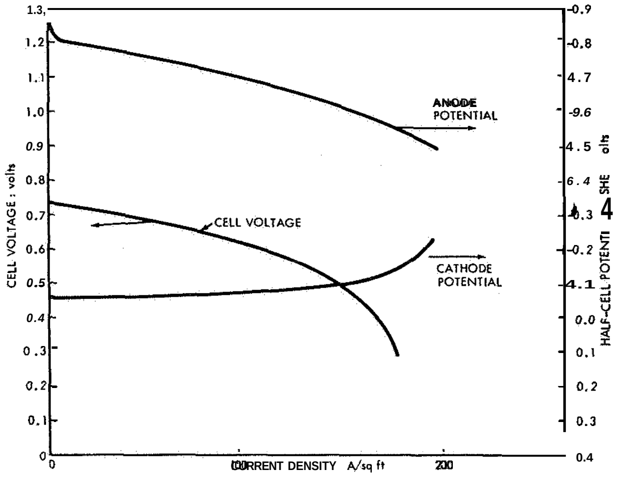

Hydrazine dissolved in **30** weight-percent **aqueous** potassium hydroxide was flowed through porous anodes. Oxygen-diffusion cathodes were used. Since no separating membrane was present between the electrodes, hydrazine reacted at the oxygen electrode and the cathode had an initial polarization of over 0.45 volt.

The results shown were obtained with an electrode area of 100 cm², after continuous operation for 2 weeks at 65 A/sq ft or greater. Maximum power density was about 70 W/sq ft.

FIGURE 16.2.—Performance of Lockheed hydrazine-oxygen fuel cell *(408)*.

16.3 COMPACT POWER FUEL CELL, Monsanto Chemical Co., December 1960 to December 1961

The aim of the contract was to develop a hydrazine-nitric acid fuel cell which would produce 15 watts at 5 amperes for 8 hours ***(456).*** Initial tests were made using a half-cell technique with the test and reference electrodes contained in one compartment and a counterelectrode in another, with an electrolyte bridge between the compartments; hydrogen or oxygen was evolved at the counterelectrode. The potential of a solid, platinized-platinum electrode immersed in the electrolyte-fuel solution was measured against a saturated calomel reference electrode, and the results corrected to potential versus SHE. The OCV and current density of nitric acid in a number of electrolytes were measured, allowing a few minutes to reach steady state between each change of current density. The results are summarized in table 16.2. Although sulfuric acid gave the best performance, it was rejected because of the rather low solubility of hydrazine in sulfuric acid. Voltage-current curves were measured for various concentrations of nitric acid,

TABLE 16.2.—*Nitric Acid at a Solid, Platinized-Platinum Cathode (1 M* HNO_3, *Ambient Temperature)* *From 456*

Electrolyte	Concentration, molar	OCV[a]	Current density at 0.3-volt polarization from OCV: mA/cm^2
NH_4HSO_4	5.0	1.17	10
H_2SO_4	5.0	1.14	50
$NaNO_3$	5.0	1.09	10
$NaHSO_4$	3.0	0.9 to 1.1	Less than 1.0 and often less than 0.1
Li_2SO_4	2.0		
$KHSO_4$	2.3		
NH_4NO_3	5.0		
$(NH_4)_2SO_4$	**3.2**		
Na_2SO_4	3.0		
NaH_2PO_4	3.6		
CH_3COONa	2.5		
$(NH_4)HPO_4$	2.7	0.6	
KOH	5.0		

[a] Versus reversible hydrogen electrode in the same solution.

plus 0.8 *M* sodium nitrate. Polarization was high for 0.025 and 0.25 *M* HNO_3. Good voltage at low currents was obtained with 2.5 *M* HNO_3, but polarization increased sharply at about 30 A/sq ft (apparently the electrolyte was not stirred to improve mass transfer to the electrode). Ten-molar nitric acid was satisfactory to over 100 A/sq ft. The gas evolved was mainly NO, with some NO_2 and N_2O, but no nitrogen. Hydrazine concentrations of 0.001 to 0.01 *M* had little effect on the nitric acid (10 *M*) cathodic-current curve, but 0.1 *M* hydrazine reduced the current density considerably, and 0.5 *M* hydrazine destroyed the performance of the cathode.

Hydrazine was similarly tested at a platinized-platinum electrode. Best results were obtained with concentrated potassium hydroxide electrolyte; 5 *M* sodium nitrate gave somewhat poorer results. Hydrochloric, phosphoric, oxalic, benzene sulfonic, and fluoroboric acids gave poor results. Open-circuit voltage was between −0.86 and −0.89 in 10 *M* KOH with 1 to 5 *M* hydrazine. At current densities of 100 A/sq ft, the polarization from open circuit was less than 0.1 volt (but after 80 days at 25 A/sq ft the electrode potential was only −0.4 volt), and the product nitrogen corresponded to 100 percent faradaic efficiency. Addition of 1 *M* nitric acid or hydrogen peroxide increased polarization by about 0.1 volt at 100 A/sq ft.

Pentaborane, B_5H_9, was investigated as fuel, but its low solubility in acid or alkali gave mass-transfer limitations to current density. The addition of dioxane to dissolve water and pentaborane led to vigorous hydrogen evolution.

Fuel cells were constructed using flowthrough anodes and cathodes of platinized, noble-metal screen (10 Pt : 90 Rh, 80-mesh), polystyrene end plates, and Viton (Du Pont) gaskets. Both ion-exchange membranes and porous separators were tried as barriers between anode and cathode. Membranes were better than porous separators because small pressure differentials did not cause bulk flow from anode to cathode (or vice versa), although anionic membranes allowed nitric acid to reach the anode chamber and cationic membranes passed hydrazine into the cathode chamber. Higher watt-hours per pound were obtained with hydrazine-KOH/membrane/nitric acid than with the hydrazine-sodium nitrate-nitric acid originally proposed. Cell voltage was 1.6 to 1.0 volt (decreasing with time) at 30 A/sq ft, with reactants circulated at much higher rates than theoretical consumption. A three-cell stack of approximately ⅙-square-foot electrodes gave 20 watts at 5 amperes for 8 hours, with an energy density of 35.5 W-hr/lb.

Fragmentary tests were performed on porous electrodes of catalyzed porous carbon (National Carbon 20, nominal pore diameter 150 microns) and catalyzed porous 316 stainless steel (Micro-metallic H, retain 2-micron particles). Catalytic activity for hydrazine, nitric acid, and hydrogen peroxide was in the order: platinum>gold> stainless steel.

The combination of two half cells, one alkaline and one acid, will not necessarily give an equilibrium cell with the sum of the two half-cell potentials, because a "junction potential" will build up at the junction of the acid and alkaline electrolytes. For example, the theoretical OCV of an alkaline hydrogen half cell and an acidic oxygen half cell is

$$\begin{array}{rcll} & & & E^0 \text{ volts} \\ \tfrac{1}{4}O_2+H^++e^- & \rightleftharpoons & \tfrac{1}{2}H_2O & 1.23 \\ \tfrac{1}{2}H_2+OH^- & \leftarrow & H_2O+e^- & .83 \\ H_2O & \overset{\text{reversible junction potential}}{\rightleftharpoons} & OH^-+H^+ & -.83 \\ \hline \tfrac{1}{2}H_2+\tfrac{1}{4}O_2 & \rightleftharpoons & \tfrac{1}{2}H_2O & 1.23 \end{array}$$

However, when the junction occurs across an ion-exchange membrane or separator which allows nonequilibrium chemical reaction to proceed, the theoretical reversible junction potential will not be attained, and a high cell voltage will result. In this case the reactants include acid and alkali as well as hydrogen and oxygen.

This situation applies to the hydrazine-KOH/ nitric acid cell. At open circuit the acid and alkali react, so that the OCV may be up to about 0.83 volt higher than equilibrium potential (varying somewhat, depending on the activity of OH–, H^+, and H_2O). The cell can be used only while hydrazine, nitric acid, and potassium hydroxide are supplied to maintain the electrode and nonelectrode reactions. Even though the potential is higher, this situation is not usually desirable for fuel-cell purposes, since the faradaic efficiency of nitric acid consumption is reduced and extra reactant weight (nitric acid and potassium hydroxide) is required. The energy density obtained, 35.5 W-hr/lb, was far less than theoretical. As in the previous contract, it is likely that more active electrodes, lower reactant flow rates (nearer theoretical consumption), and the elimination of nonfaradaic reaction would have improved performance considerably.

16.4 ELECTROCHEMICAL ENERGY CONVERSION SYSTEMS RESEARCH, Monsanto Chemical Co., September 1960 to September 1961

The principal objective was to determine the suitability of hydrogen peroxide as a cathodic oxidant for fuel cells *(457)*. Techniques used were similar to those described in section 16.3; peroxide was dissolved in electrolyte and tested in a nonstirred half cell with a solid electrode. The results are summarized in table 16.3. Strong acids and bases gave best results.

Electrolyte	Electrode	OCV[a]	Voltage[a] at mA/cm² of— 1	10	100	Remarks
3 *M* NH_4Cl	Various	0.82 to 0.65	....	....	....	Pd > Ir > Pt > Rh > Au > Ag
3 *M* NH_4Cl	Pt	0.65	0.62	0.53	0.31	
2.3 *M* $KHCO_3$	Pt and various	.87	.86	.85	.72	Ag > Ir > Au > Pt > Pd > Rh
5 *M* KOH	Various	.89	....	....	....	All gave about the same OCV
5 *M* KOH	Pt	.92	.92	.91	.87	
5 *M* H_2SO_4	Pt	.89	.88	.85	.80	
14 *M* H_2SO_4+2 *M* H_2O_2	Bright Pt	1.09	1.06	0.99	....	Increased catalyst area gave increased performance
	Platinized Pt	1.23	1.23	1.19	....	
	Etched and platinized Pt	1.47	1.47	1.45	....	
1*M* Peracetic acid and 0.1 *M* H_2SO_4	Pt	0.98	0.98	0.96	0.78	

[a] Versus reversible hydrogen electrode in same solution. More positive better.

In an attempt to form reactive peroxy compounds, molar quantities of CrO_3, Na_2MoO_4, and Na_2WO_4 were added to *5 M* KOH and *1 M* H_2O_2. No significant improvement in potential or current density was found. Similarly Na_2Mo_4, TiO_2, and Na_2WO_4 were added to *5 M* H_2SO_4 plus peroxide, with no improvement. Peroxide decomposition inhibitors (8-hydroxy quinoline, $Na_4P_2O_7$, Na_3PO_4, Na_2SnO_3, $NaAlO_2$, and pyrogallol) were added with little effect.

The tests were not run under pure conditions, nor was the mass transfer to the electrode well defined. Reproducibility was poor and the comparison of different catalysts is not accurate. The information is very incomplete, since faradaic efficiencies of peroxide reduction were not determined.

16.5 STUDY OF FUEL CELLS USING STORABLE ROCKET PROPELLANTS, Monsanto Chemical Co., June 1963 to January 1964

The objective was to demonstrate the feasibility of hydrazine-type fuels and nitrogen tetroxide or chlorine trifluoride oxidants for fuel cells *(460)*. Table *16.4* gives thermodynamic data for reactions of interest. The entropy of the reaction

TABLE 16.4.—*Energy Yield and Cell Potentials* **for** *Reversible Reactions at 77" F (25° C) and 1 Atmosphere (460)*

Reaction	W-hr/lb	Fuel cell, volts
$3N_2H_4+4HNO_3\rightarrow8H_2O+4NO+3N_2$	610	1.45
$5N_2H_4+4HNO_3\rightarrow7N_2+12H_2O$	1000	1.7
$N_2H_4+N_2O_4\rightarrow N_2+2NO+2H_2O$	557	1.42
$2N_2H_4+N_2O_4\rightarrow3N_2+4H_2O$	1080	1.74
$N_2H_4+ClF_3\rightarrow N_2+HCl+3HF$	950	2.42
$3CH_3NHNH_2+4HNO_3\rightarrow3CH_3OH+3N_2+4NO+5H_2O$	495	1.33
$CH_3NHNH_2+2HNO_3\rightarrow CO_2+2N_2+4H_2O$	1000	1.41
$3CH_3NHNH_2+10HNO_3\rightarrow3CO_2+3N_2+10NO+14H_2O$	550	1.16
$CH_3NHNH_2+N_2O_4\rightarrow CH_3OH+2NO+N_2+H_2O$	460	1.30
$3(CH_3)_2NNH_2+16HNO_3\rightarrow6CO_2+3N_2+16NO+20H_2O$	535	1.09
$5(CH_3)_2NNH_2+16HNO_3\rightarrow10CO_2+13N_2+28H_2O$	1000	1.34
$(CH_3)_2NNH_2+4N_2O_4\rightarrow2CO_2+N_2+8NO+4H_2O$	480	1.06

Basis:

Liquid phase:	Gas phase:
All fuels	N_2O_4
HNO_3	NO
CH_3OH	HCl
H_2O	HF

$$N_2O_4(l)+N_2H_4(g)\rightleftharpoons N_2(g)+2NO(g)+2H_2O(g)$$

was calculated to be *134* cal/mole °K, or a heat absorption of *10* kcal/g equivalent at *77"* F *(25" C)*. Thus, heat absorption in a fuel cell using this reaction could be used to convert waste heat in a space vehicle to useful electrical energy. Experimental techniques were similar to those used in sections *16.3* and *16.4*, except that catalyzed porous carbon electrodes were used in some instances. Electrodes were ⅛-inch-diameter cylinders of carbon, nickel, or stainless steel wrapped with Teflon tape to leave the bottom exposed. The exposed face was electroplated with platinum, gold, or rhodium. Alternatively, carbon *(FC–14)* cubes of ½-centimeter edge were impregnated with the required salt solution, dropped into *1* percent sodium borohydride to reduce the salt to metal, and dried at 176° F (80° *C)* in vacuum.

Results for anodic hydrazine consumption are summarized in table *16.5*. No clear picture emerges, except in the case of rhodium, which consistently appears as a good catalyst. Mono-

TABLE 16.5.—*Electrochemical Oxidation of Hydrazine at Various Electrodes* (1*M* N_2H_4, 80"-90" C) (*460*)

Electrolyte	pH	Electrode	Versus hydrogen[a]	Versus oxygen[b]
M H_3PO_4	4.8	Rh/Ni	0.11	1.12
		Rh/C	.08	1.15
		Pt/stainless steel	.23	1.0
		Pt/Ni	.26	.97
		Pt/C	.4	.83
		Au/C	.85	.38
M KOH	14.0	Pt/Ni	.09	1.14
		Pt/stainless steel	.24	.99
		Au/Ni	.11	1.12
		Rh/Ni	.05	1.18
Buffer	8.8	Pt/C	.32	.91
5 *M* HNO_3	0	...	0.4–0.55	0.83–0.68
M KNO_3	11.1			
M H_3PO_4	4.8			
			At 100mA/cm^2	
			Versus hydrogen[a]	Versus oxygen[b]
M KOH	14	Carbon cube plus precipitated—		
		Pt	0.38	0.85
		Rh	.06	1.17
		Ru	.02	1.21
		Au	.55	.68
		Ir	.36	.87
		Ni	.15	1.08
		Pt 80 : Ru 20	.06	1.17
		Pt 60 : Ru 20 : Au 20	.13	1.10
		Ir 32 : Ru 68	.06	1.17
		Pt 80 : Ni 20	.2	1.03
		Rh 80 : Ni 20	.07	1.16
		Pt 40 : Rh 40 : Au 20	.11	1.12
5 *M* H_3PO_4	.7	Pt	.34	.89
		Rh	.30	.93
		Ru	.18	1.05
		Au. Ir	([c])	...
		Ni	([d])	...
		Pt 80 : Ru 20	.33	.90
		Pt 60 : Ru 20 : Au 20	.31	.92
		Ir 32 : Ru 68	.22	1.01
		Rh 80 : Ni 20	.28	.95
		Pt 40 : Rh 40 : Au 20	.25	.98

[a] Versus reversible hydrogen electrode in same solution.

[b] Versus reversible oxygen electrode in same solution.

[c] Poor.

[d] Dissolves.

methyl hydrazine and unsymmetrical dimethylhydrazine were also tested, and under comparable conditions gave 0.2 to **0.3** volt more polarization than hydrazine. Gold was the best catalyst for the cylindrical electrodes, but was not good for the carbon-cube electrodes containing precipitated catalysts. Ruthenium and Rh80:Ni20 were best for the latter. Experimental conditions were so arbitrary that the comparative value of the results appears doubtful. No measurements were made of true electrode surface area (using double-layer-capacity techniques, for example), and differences between catalysts may have been due to variations in surface roughness. Experimental reproducibility was not given, but was probably poor. The effects of mass transfer were ignored; it is likely that in the case of porous electrodes the results were influenced by the amount of fuel stored within the pores, and thus by the time taken to perform the measurements.

Gas-diffusion electrodes were made by pressing, at 5000 psi, a 25 mg/cm^2 layer of platinum-black plus 10 percent Teflon onto a porous, 316 stainless-steel disk (65 percent porosity, 4 mils thick) and sintering at 437" F (225" C) for 15 minutes. Tantalum holders and current collectors were used. Hydrazine vapor was fed to the electrode and gave 60 mA/cm^2 at 140" F (60" C) in 5 M H_3PO_4, and 300 mA/cm^2 at 86" F (30" C) in 1 M H_2SO_4.

The cathodic reaction of nitric acid was studied with the same technique as before. It was concluded that catalysts had little effect and that high concentrations of nitric acid were needed for good performance (5 M at 86" F (30" C), and 2.5 M at 194" F (90" C)). One-molar nitric acid H_3PO_4 showed little current at 86" F (30" C), but gold was a good catalyst at 194" F (90° C). Better performance was obtained with stronger nitric acid and with stronger sulfuric acid; at 194" F, 5 M H_2SO_4 required nitric acid concentrations greater than 0.2 M for good performance. The voltage remained close to 1 volt (versus hydrogen) over a wide range of current. Aqueous N_2O_4 was tested with gold or stainless steel. The solution was blue colored and acidic ($N_2O_4+H_2O \rightarrow HNO_3+HNO_2$). In strong acids ($6N$ H^+), the voltage remained near 1 volt at current densities out to 100 mA/cm^2. Similar results were obtained with N_2O_4 gas at a carbon-diffusion electrode in acid electrolyte, but in basic or buffered electrolytes the nitrogen tetroxide reacted with the electrolyte, giving local acid formation and unstable high voltages and currents.

Stability studies showed that hydrazine reacted with 5 M HNO_3, whereas it was stable in phosphoric acid or potassium hydroxide. However, hydrazine electrodes showed rapid time increase of polarization in acid and base electrolytes, while nitric acid cathodes showed no change in performance after 40 days. Contrary to the results quoted in section 16.2, the faradaic efficiency of hydrazine ionization in H_2SO_4 (and KOH) was found to be 100 percent at current densities of 50 and 100 mA/cm^2. With monomethyl hydrazine, the main reaction was

$$H_2O+CH_3NHNH_2 \rightarrow CH_3OH+N_2+4H^++4e^-.$$

A fuel cell was built with perforated stainless-steel-sheet electrodes (14-mil holes, Perforated Products, Inc.) pressed against a cation-exchange membrane. Water and hydrazine vapor were fed to the anode and nitric acid solution to the cathode. Cell potentials were high, and for short-term operation, current densities of 50 to 100 A/sq ft at 1 volt were obtained. Hydrazine disappeared at the rate of 110 A/sq ft at open circuit, showing that the membrane was allowing direct reaction of hydrazine and nitric acid.

The electrochemical oxidation of hydrazine in nonaqueous solvents was studied at immersed, solid-platinum electrodes of 1-square-centimeter area, electroplated with catalyst, in a cell made from Teflon and Kel-F. The results are summarized in table 16.6. The reduction of chlorine trifluoride bubbled over the electrode was also investigated, with a possible overall cell reaction

$$N_2H_4+ClF_3 \overset{HF}{\rightleftharpoons} N_2+HCl+3HF, \quad 2.42 \text{ volts.}$$

This has an energy density of 950 W-hr/lb. Chlorine trifluoride and hydrazine reacted vigorously in the electrolyte when the concentration of hydrazine was greater than 1 molar; explosive reaction occurred at high concentrations, although this may have been due to traces of water in the electrolyte. Table 16.6 shows that the sum of two half cells using N_2H_4 and ClF_3 would yield voltage much lower than the theo-

TABLE 16.6.—*Summary of Results in Nonaqueous Electrolytes From (460)*

Electrolyte	Reactant	Electrode	Temperature, “C	Performance, mA/cm² at volts[a]	Remarks[b]
Anhydrous HF·NaF	1*M* $N_2H_4 \cdot 2HF$	Carbon or Pt/Pt	3	20 at 0.5	Electrodes of Pt, Rh/Pt, Pd/Pt, Au/Pt, Ru/Pt, and Ir/Pt not as good
	ClF_3 bubbled around electrode	Pt/Pt; Au-Pt	5	20 at 1.0	Electrodes attacked
KF·3HF (melts about 80”C)	1*M* N_2H_4	Rh-Pt; Ru-Pt	85	100 at 0.5	Carbon, Pt, Au, poor
	ClF_3 bubbled around electrode	C	85	Limiting current develops beyond 2 mA/cm²	C >Rh/Pt >Ir/Pt > Pt/Pt>Ru/Pt>Pt
Acetonitrile[c] or DMF	1*M* N_2H_4	Pt/stainless steel	20	20 at 0[d]	
Pyridine.	1 *M* N_2O_4	Pt/stainless steel	20	10 at 0.2	
Propylene carbonate	1 *M* N_2O_4	Pt/stainless steel	20	OCV=0.3	
Acetonitrile.	1 *M* N_2O_4	Pt/stainless steel	20	10 at 0.9; 50 at 0.4	OCV 1.02 to 1.16
DMF.	1*M* N_2O_4	Pt/stainless steel	20	10 at 0.9; 50 at −0.3	OCV 1.07 to 1.24

[a] Versus reversible hydrogen electrode in same solution.

[b] “Rh/Pt” stands for rhodinized platinum. “Pt” stands for “bright” platinum.

[c] Solvents contained $Mg(ClO_4)_2$.

[d] Versus Ag/AgCl electrode.

retical value of about 2.4 volts; although this conclusion necessarily applies only to the immersed, solid electrodes used in the study. The direct reaction of dissolved hydrazine and chlorine trifluoride in the electrolyte is also disadvantageous.

Other solvents considered were acetonitrile, dimethylformamide (DMF), propylene carbonate, and pyridine containing dissolved salts. Hydrazine was compatible with all four, but N_2O_4 reacted violently with pyridine and with KSCN in solution. Magnesium perchlorate, $Mg(ClO_4)_2$, was selected as a suitable dissolved salt. One-molar hydrazine was tested in a half cell containing a platinized stainless-steel test electrode, using a Luggin capillary connected to a silver-silver chloride reference electrode. Results are given in table *16.6.* Again the sum of the two half cells to make a complete cell, $2N_2H_4+N_2O_4 \rightleftharpoons 3N_2+4H_2O$, gives a low cell potential. Since water is produced in the overall cell reaction, it was added to the N_2O_4 half cell; for acetonitrile the presence of water had little effectup to **3** *M* concentrations, but it increased polarization considerably for DMF solutions.

16.6 DIRECT AMMONIA-AIR FUEL CELL, Electrochimica Corp., July 1963 to August *1964*

The aim of the contract was to explore the feasibility of direct ammonia fuel cells *(156).* Arguing from gas-phase kinetic studies on iron catalysts for ammonia decomposition, the mechanism was proposed as

$$NH_3 \rightarrow [NH_2]+[H]$$
$$[NH_2] \rightarrow [NH]+[H]$$
$$[NH] \xrightarrow{\text{slow}} [N]+[H].$$

Since decomposition rate increases with temperature, the cell chosen had molten alkali-hydroxide electrolyte, with a temperature range of 338° to 752" F (170° to 400" C). Possible reactions were

	ΔF^0, *kcals/mole*
$2NH_3(g)+3/2O_2 \rightleftharpoons N_2+3H_2O,$	−156
$NH_3(g)+2O_2^-+KOH(aq) \rightleftharpoons KNO_3(aq)+2H_2O(l),$	−98
$NH_3(g)+3/2O_2+KOH(aq) \rightleftharpoons KNO_2(aq)+2H_2O(l),$	−80

It was concluded that the formation of nitrates and nitrites was not favored. (In sec. 16.2, the poor life of ammonia-molten hydroxide cells was ascribed to nitrate and nitrite formation. The thermodynamic reasoning given above is not strictly valid, since it considers the total cell reaction, whereas it is the electrode reactions at the ammonia anode which will determine whether nitrates and nitrites will be formed.)

A simple cell was constructed with diffusion electrodes immersed in molten KOH-NaOH contained in an oxidized nickel vessel. The melt contained up to 40 weight-percent MgO powder to increase the viscosity and prevent flooding of the electrodes, and a porous barrier was placed between the anode and cathode. The electrode design is shown in figure 16.3. Silver was discarded as a cathode material because it slowly dissolved in the melt when oxygen was present. Double-porosity nickel plaque, catalyzed with platinum, was used for the anode and cathode. Reference electrodes of Hg-HgO, Ag, and Pt were not satisfactory; Au or Ni were better, but not completely stable with time. Nickel battery plaque covered with a paste of precipitated nickel hydroxide was finally chosen as the reference electrode (*159*), and this was used to obtain a current-voltage curve for ammonia at a 52-mesh platinum electrode at 572" F (300" C). A considerable increase in polarization from open circuit (to 0.4 volt) occurred at about 1 A/sq ft, and the slope of the Tafel line at higher voltages was 74 millivolts. It was concluded that the slope was $(2/3)RT/nF$ and that the rate-controlling step was, therefore

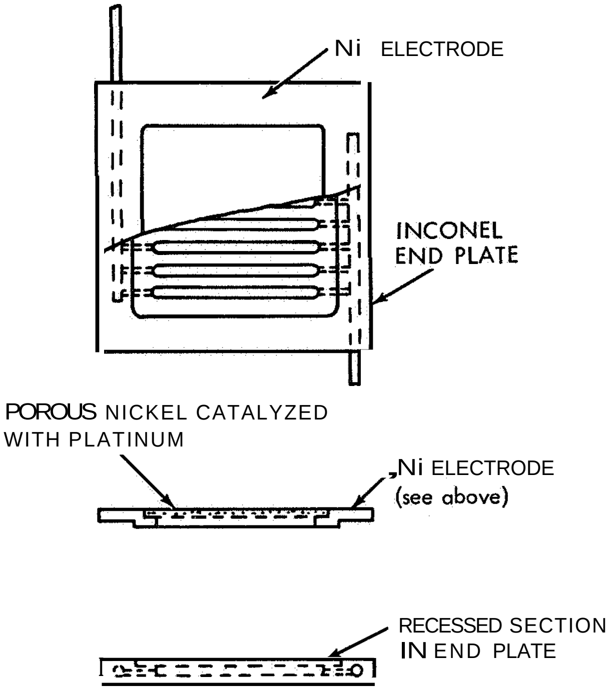
Ni ELECTRODE
INCONEL END PLATE
POROUS NICKEL CATALYZED WITH PLATINUM
Ni ELECTRODE (see above)
RECESSED SECTION IN END PLATE

FIGURE 16.3.—Ammonia or air diffusion electrode for use with molten sodium-potassium hydroxides (*156*).

$$M[NH_2]+OH^- \rightarrow M[NH]+H_2O+e^-,$$

with surface coverage, following a Langmuir isotherm. The Tafel slope extended over only a very short current range and was followed by a section of rapidly increasing polarization. Few valid conclusions can be drawn from such limited data.

A sample of electrolyte was weighed, leached with hydrochloric acid, and filtered. The filtrate was tested colorimetrically for nitrite, or treated with sulfamic acid to convert nitrite to nitrate and colorimetrically tested for nitrate. Slight traces were found and ascribed to direct reaction between leaking oxygen and ammonia.

Fuel cells with the electrodes shown in figure 16.3 performed as shown in figure 16.4. High flow rates of anode gas improved cell performance (presumably by better removal of water from anode pores). It was assumed that all of the water was formed and removed at the anode

$$2NH_3+6OH^- \rightarrow 6H_2O+N_2+6e^-.$$

The equilibrium partial pressure of water over the melt was estimated at 150 torr at 572" F (300" C); therefore, the rate of ammonia flow

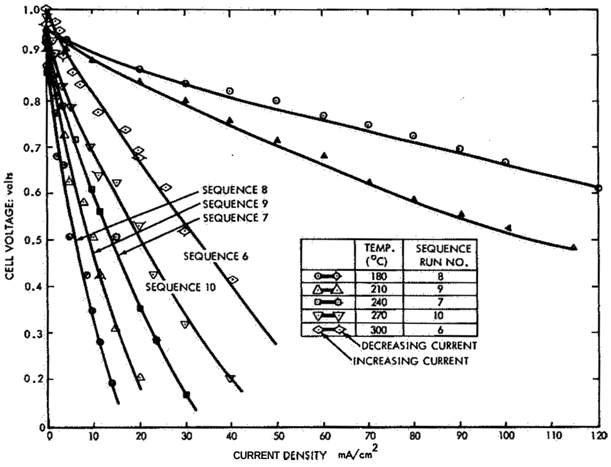

FIGURE 16.4.—Performance of ammonia-oxygen fuel cell ***(159)***.

at 1 atmosphere should be 13.2 moles per mole oxidized. However, this mechanism lacks any means of getting water to the cathode reaction

$$3/2O_2+3H_2O+6e^- \rightarrow 6OH^-.$$

Measurements of water content of the anode exit gas showed that 55.5 percent of the water formed at the anode was carried out in the gas. (It is questionable whether the cell would continue to run without admission of water to the oxygen feed, since this figure is greater than 50 percent.)

Three-mil-thick palladium-silver membrane cathodes were tried. Both sides of the membrane were catalyzed with palladium or platinum black. The membranes worked with hydrogen fuel, but with ammonia the current density was less than 5 A/sq ft. Nickelized-nickel anodes and lithiated nickelized-nickel cathodes performed almost as well as platinized-nickel electrodes.

The variable performance of the cell was probably due to lack of control of the water balance in the cell. At low flow rates and high current densities, water accumulates in the electrolyte and in the exit gas until a higher equilibrium partial pressure and a steady mass balance is obtained. If gas-diffusion limitations are present in the pores of the anode, the higher partial pressure of water vapor in the pores will lead to lower current densities. The answer to this problem lies in making electrodes which do not have gas-diffusion limitations. Unlike hydrogen electrodes, it is not possible to circulate ammonia at high rates and remove water, since circulation would lead to nitrogen buildup and nitrogen is not easily separated from gaseous ammonia. A gaseous ammonia cell must operate satisfactorily with one pass of fuel through the cell, and it must, therefore, be able to tolerate low ammonia concentrations and high water-nitrogen concentrations. It is also possible that the cathode was starved of water, especially when large fractions of MgO were used.

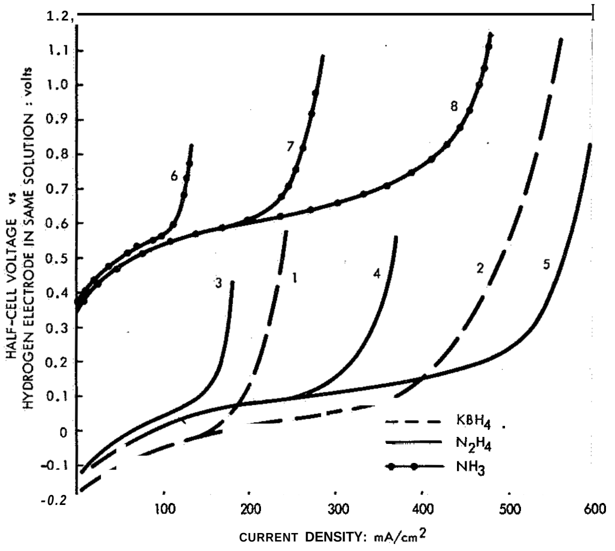

The fuels, dissolved in 4 *M* **KOH**, were passed through an electrode consisting of 80 mg/cm² of platinum-black powder sandwiched between platinum screens. The conditions were:

Curve	Fuel	Molar concentration	Flow rate, cm/min	Theoretical limiting current, mA/cm²
1..........	KBH_4	0.1	0.2	258
2..........			.47	600
3..........	N_2H_4	0.1	0.3	192
4..........			.6	385
5..........			1.0	640
6..........		0.1	0.23	113
7..........		.1	.60	290
8..........		.5	.17	400

FIGURE 16.5—Anodic currrents for various fuels dissolved in aqueous KOH, at flowthrough electrodes of platinum black; ambient temperature.

16.7 POROUS FLOWTHROUGH ELECTRODES OF PLATINUM BLACK, Pennsylvania State University, March 1960 *to* April 1964

As part of an investigation of the theory of flowthrough electrodes, hydrazine, ammonia, potassium borohydride, nitric acid, and hydrogen peroxide were ionized at flowthrough electrodes consisting of a sandwich of platinum-black powder between platinum screens ***(484*** and ***485).*** Low flow rates were used, so that almost complete utilization of reactant could be obtained in one pass through the electrode. Results for anodic reactants are shown in figure 16.5. The electrode was less than 1 millimeter thick, and although the weight of platinum black was high (80 mg/cm^2), similar catalytic area could probably be obtained using high area substrates catalyzed with small amounts of platinum. The effect of increased reactant concentration and flow rate is principally to increase the limiting current ($i_L = nFvC$, where n is the number of electrons in the reaction, F the faraday, v the velocity, and C the concentration of reactant). Hydrazine and potassium borohydride were active fuels, giving open-circuit voltages more negative than the reversible hydrogen electrode. Hydrogen evolution was observed at open circuit for high concentrations of hydrazine or borohydride, but was not observed under current drain. Polarization became high near the limiting current, and only about 70 percent of the fuel could be consumed in one pass through the electrode (at reasonable potentials). Ammonia was relatively inert, requiring 0.3- to 0.4-volt polarization from its theoretical OCV of 0.09 (versus NHE in SE) to produce reasonable current.

Figure 16.6 shows results obtained with nitric acid and hydrogen peroxide. Unlike the other reactants, the concentration of nitric acid had to be at least 1M to give good performance. Therefore, it was not possible to consume large fractions of the nitric acid in one pass through the electrode. Hydrogen peroxide gave low faradaic efficiencies and oxygen evolution was observed. Polarization in 7 M H_2SO_4 was almost 0.2 volt more than in **4**M KOH.

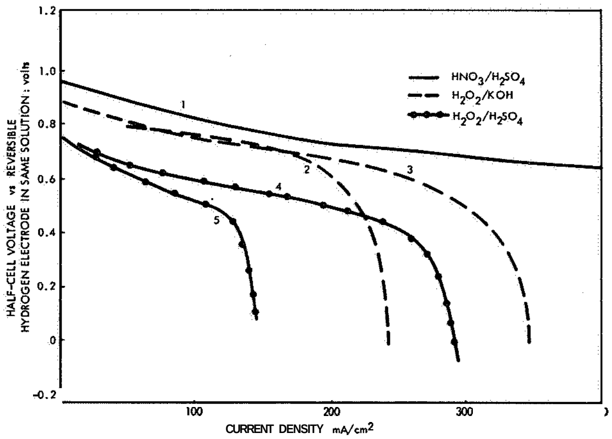

Conditions were similar to those of figure 16.5.

Curve	Fuel	Molar concentration	Flow rate, cm/min	Theoretical limiting current, mA/cm^2
1.......	HNO_3	2 *(7M* H_2SO_4*)*	**0.33**	**Large**
2.......	H_2O_2	0.2 (4 M KOH)	0.67	426
3.......			1.07	682
4.......	H_2O_2	0.2 (7 M H_2SO_4)	0.23	150
5.......			.67	426

FIGURE 16.6 —Cathodic currents for nitric acid and hydrogen peroxide at flowthrough electrode of platinum black; ambient temperature.

16.8 RESEARCH ON MATERIALS, PROCESSES, AND DEVICES RELATED TO ENERGY CONVERSION, MIT School of Engineering, June 1961 to January 1964

A brief report of studies of hydrazine electro-oxidation was given as part of a summary report ***(436).***One-molar hydrazine in 20 weight-percent KOH was reacted at anodes of 80-mesh platinum screen, plated with platinum, iridium, or rhodium, or combinations of these three. Initially, current-voltage curves were best in the order Rh > Ir > Pt, but performance deteriorated with time, especially for iridium. Activity could be regenerated by immersing the electrodes in 98 percent sulfuric acid at 77° F (25° C). Combinations of Ir and Rh with Pt gave essentially the same results as platinum.

16.9 CONCLUSIONS

Most of the work reported in this chapter was of an exploratory nature, and much of it was performed under arbitrary conditions which cannot be extrapolated to other circumstances. The conclusions can be enumerated as follows:

(1) Hydrazine in solution is an effective fuel and can be reacted at high current density, even at relatively low-area electrodes and low temperatures; catalysts for the reaction are similar to those for hydrogen ionization, but rhodium is especially active. At active electrodes the reaction has an OCV more negative than hydrogen and the electrode will evolve hydrogen, especially at high hydrazine concentrations. As current is drawn, the electrode ceases to evolve hydrogen, and hydrazine is used at almost 100 percent faradaic efficiency.

(2) Evolution of gases in flowthrough electrodes has no deleterious effect on performance of the electrode.

(3) Ammonia is relatively inert and requires very active electrodes or high temperatures.

(4) Hydrogen peroxide normally gives a potential less than the reversible oxygen potential; oxygen evolution occurs and faradaic efficiency is low.

(5) The cathodic nitric acid reaction is complex and produces mainly NO. It is necessary to use high concentrations of nitric acid to obtain potentials near 1 volt, and it is, therefore, difficult to consume appreciable fractions in one pass through a flowthrough electrode.

(6) The ion-exchange membranes used in the work described above were not satisfactory as separators between the anode and cathode chambers, since they passed other ions in addition to hydrogen ion (cationic) or hydroxyl ion (anionic). This allowed deactivation of one electrode by the other electrode reactant.

(7) Best performance was obtained with concentrated acid or alkali electrolytes; neutral electrolytes were not satisfactory.

Fuel cells using hydrazine and oxygen (or some other oxidant) could undoubtedly be developed as high-power-density cells for special applications. The cell would have no advantage over hydrogen-oxygen cells unless the hydrazine were stored and used in liquid form in order to make storage tanks light weight and allow nitrogen to be easily separated from the circulated electrolyte. For long-term operation, water must be removed from the electrolyte, but it is still possible that control of the cell would be simple, with fewer auxiliaries, than for hydrogen-oxygen cells. A disadvantage for manned-flight applications is the high toxicity of hydrazine (1 part per million, *456*). For short-term operation, the cell could be competitive with high-energy-density primary cells. Low-resistance membranes able to prevent the intermixing of the anodic and cathodic reactants must be developed, as well as an electrochemically reactive, high-energy-density oxidant which can be easily added to the circulating electrolyte, and whose reaction product can be easily removed from the electrolyte.

CHAPTER 17

Kinetics of Hydrogen-Oxygen Fuel-Cell Reactions

17.1 INTRODUCTION

This chapter describes some of the more fundamental research on fuel-cell reactions performed under Government contracts (see ch. 15 for hydrocarbon reactions). No attempt has been made to discuss the relevant work not conducted under Government contract because of the tremendous volume of material which would have to be covered.

Although extensive empirical testing of catalysts for hydrogen and oxygen electrodes has been conducted by the major companies producing fuel cells, the results of the tests are not readily available. However, the catalysts most acceptable for practical development are known. For example, low-temperature fuel cells generally employ platinum or platinum-palladium as catalysts for hydrogen anodes and oxygen cathodes; silver cathodes are used also in alkaline electrolytes. Many metals which might be catalytic dissolve at excessive rates in aqueous acid or alkali solutions, or form thick nonconductive oxide films at potentials between hydrogen evolution and oxygen evolution. The platinum metals, gold, and possibly copper and silver, are suitable for strong acids and the same metals plus nickel are suitable for strong alkalis. Stable oxides which can be made semiconductive are not good catalysts for hydrogen ionization but have been used for oxygen ionization in alkaline solutions. Nickel or silver oxygen cathodes in alkali, for example, probably have thick oxide films in most cases, and require higher temperatures to give performance comparable to platinum catalysts.

Section 2.1.5 gives a brief outline of the concepts leading to electrochemical rate equations. Simple rate equations are not likely to apply to the reactions of interest in fuel-cell work. Hydrogen ionization is a relatively simple reaction compared to organic fuels, but the hydrogen evolution-ionization reaction has been investigated for many years and is still not fully understood. A description of the cathodic rate equations for hydrogen ionization, based on current theories (ref. 17.1) of hydrogen evolution, is given in 481 (see also ref. 17.2). Consideration of the various rate equations leads to an important general conclusion for reactions in which a reactant is adsorbed on an electrode before reaction. The equations indicate that the standard-state free energy (based on a standard state of fractional coverage $=\frac{1}{2}$) of chemisorption at the temperature of reaction should be close to zero. Physically, this means that reactant should adsorb to give a good coverage of the surface, but should not be so strongly adsorbed that it cannot be detached from the surface. Strong bonding to the surface will give a stable adsorbed molecule which is difficult to ionize. On the other hand, when the reactant is very weakly adsorbed there is little adsorbed component to react and reaction can be rapid only if all activation energies in the reaction mechanism are low.

This theory is not fundamental, since it replaces the question, “Why are certain materials catalytic?” with the question, “Why do certain materials adsorb certain reactants with the bond strengths suitable for further reaction?” However, if the phenomenology of material-reactant adsorptions can be classified, predictions of catalytic behavior *can* be made. For example, the heats of chemisorption of oxygen from the gas phase onto metals is proportional to (but not equal to) the heat of formation of the bulk oxide (ref. 17.3). The lowest heats of formation are for Ag, Pt, Pd, Ir, and Ni oxides, *so* these metals are considered the best candidates for oxygen electrode catalysts. This approach is obviously extremely crude, since it extrapolates electrochemical results from gas-phase results. At potentials near the reversible oxygen electrode, the metals have oxide films, and it is the energy of chemisorption onto oxided surface which is significant; as potential changes the surface changes, and probably the energy of interaction of reactant with the surface also changes. In addition, adsorption on an electrode surface in aqueous electrolytes undoubtedly involves rearrangement of water-surface bonding. The reaction is probably

$$R+M—H_2O\rightarrow M—R\text{--}H_2O$$

where $M—H_2O$ represents a fairly strong interaction of water with metal and $M—R\text{--}H_2O$ represents a weak interaction of water with the adsorbed reactant.

17.2 GAS-PHASE CHEMISORPTION

The mathematical derivation of the relation between rates of electrochemical reaction and free energies of chemisorption (refs. 17.1 and 17.2) assumes that the potential energy curves of an ion being removed from a surface varies from metal to metal only because of variation of the strength of chemisorption of the atom on the surface. This is only likely to be true as a first approximation, but an electrode probably must adsorb reactant readily if it is to be active.

There is at present no general theory of surface bonding and catalysis which enables the calculation of energies of chemisorption and corresponding activation energies. In spite of the great amount of effort put into the study of chemisorption, there are few surface reactions which are completely described and understood. For example, data on the heats of chemisorption of simple gases on solids are very variable from one group of workers to another; a review of data is given in 725. The first selection of catalysts for fuel-cell electrodes was, therefore, based primarily on prior experience, either of electrochemical studies of hydrogen evolution or of gas-phase catalytic reactions. Electrochemical catalysis is probably not identical to gas-phase catalysis, but there is certainly a close tie between the two.

Because of the connection between chemisorption from the gas phase and electrocatalysis, investigations have been made on gas-phase chemisorption, with the intention of applying the results to fuel cell catalysis. In work by Atomics International *(122* and ***123,*** September 1961 to September 1962), gases were adsorbed on metals supported on high-area carriers and the solids studied by infrared spectroscopy using the techniques described by Eischens and Pliskin (ref. 17.4). Dissolved metal salts were added to support powder (Cab-0-Si10.02 micron or Linde B alumina 0.1-micron polishing powder) and the paste spread on a nickel support screen. This was pumped out, dried, reduced with hydrogen at 1292" F (700" C) and the cell pumped out to 10^{-6} torr at 1292" F. After cooling to ambient temperature, gas was admitted at pressures of 10 to 150 torr and pumped out to 10^{-1} torr. When strong adsorption was indicated, the system was pumped out to 10^{-6} torr and infrared absorption measured to see if material was still adsorbed. The results are summarized in table 17.1. The normal band of carbon monoxide gas is 2100 cm^{-1}, but it is known (ref. 17.5) that the nature of the support affects the infrared peak positions and values near 2075 cm^{-1} were taken as due to linear CO with the oxygen atom sticking out from the surface. The values 2962 and 2872 were assigned to modes in the CH_3 structure, and the values 2926 and 2853 to modes in CH_2. These wavelengths correspond to stretching modes between the hydrogen and carbon bonds. Thus the results in table 17.1 (those which are not immediately obvious) were interpreted as follows: Carbon monoxide adsorbs on NiO with a bridge adsorption, since the infrared band of 1650 is much less than that expected for linear CO. When H_2 was adsorbed, followed by C_2H_4, the bands corresponded to CH_2 on the surface. In the presence of platinum, OD bands were observed on Cab-O-Sil, indicating exchange of deuterium with OH in the Cab-0-Sil.

The Pt-Cab-0-Si1 system was treated with deuterium, pumped out to 10^{-2} torr, and C_2H_4 admitted. It was then briefly pumped, followed by equilibration into a mass spectrograph. The approximate analysis of the carbon gases pumped

TABLE 17.1.—*Summary of the Results of (122 and 123)*

support	Catalyst	Gas	Infrared absorption spectra bands, cm^{-1}	Remarks
Alumina (transparent in 1000 to 2000 cm^{-1} region, little spectra)	NiO	CO	1650	Strong adsorption (10^{-6} torr), removable by heating
	Ni	CO	2175 1995 1915	Strong adsorption (10^{-6} torr), removable by heating
	Pt	CO	2075	Attributed to linear CO
	RuO_x	None	None	RuO_x gives no spectra
		CO	2080 2035 2150	Much gas adsorbed but could be pumped off
		CH_4	None	No adsorption
		C_2H_4	None	No adsorption
		C_2H_6	None	No adsorption
		CO_2	[a] 2020	Weak adsorption
	Ru (0.8 wt-%).	CO	2060 2125	Strong adsorption
		CO_2	None	No adsorption
		C_2H_6	None	No adsorption
		H_2	None	
		H_2 followed by C_2H_4	Many 1280	The 1280 band was left after pumping at 1292" F (700° C)
	Ir(l-83 wt-%).	CO	[a] 2070	Weak adsorption
		C_2H_4 followed by H_2	....	
Cab-0-Si1 (transparent in 2000 to 5000 cm^{-1} region, but produces spectra)	Ru (0.8 wt-%).	CO	2151 2083	Strong adsorption (10^{-6} torr), removable at 1292" F (700"C)
		H_2	None	Pumping was slow, indicating much adsorption
		C_2H_4	2938 2867 2997	Strong adsorption
	Ir (4.5 wt-%). .	CO	2074 to 2044	As pumped out, peak slid to 2044 cm^{-1}
		H_2 followed by C_2H_4	None	
	Pt (7.8 wt-%). .	D_2 followed by C_2H_4	2929 2856	OD band seen at 30 torr
		H_2 followed by C_2H_4	2928 2854 2992	OH band seen at 30 torr
	None	C_2H_4	....	No C_2H_4 adsorption on Cab-0-Sil with or without hydrogen treatment

[a] Weak.

into the mass spectrograph is shown in table 17.2. Heating to 572" F (300" C) gave more gas evolution, mainly of dideuterated pentanes and butanes. Because no HD or H_2 was observed, it was concluded that chemisorption of ethylene does not produce adsorbed H atoms and that the collision of ethylene with the deuterated surface produces deuterated hydrocarbon radicals.

Reflectance of light from metal films was also investigated, since the light has to pass through adsorbed gas on the metal and should give absorption spectra. This method would extend the range of spectra down to less than 500 cm^{-1}, where metal-carbon bond frequencies are located, and give direct information on the bonding of the hydrocarbon to the metal. However, it proved impossible with gaseous adsorbates (see app. C). The infrared technique gave some evidence of the structure of adsorbed compounds, but since peak wavelengths changed with the support material and with the degree of surface coverage, the wavelengths cannot be used to distinguish between structures which have only small differences in wavelength (CH_2 and CH_3, for example).

TABLE 17.2.—*Gases* Pumped *Off* Platinum Treated With Deuterium Followed by Ethylene *(122* and *123)*

Hydrocarbon gas	*Percent by volume*
Toluene	0.5
Hexanes	6.0
Hexenes	
Pentanes	18.0
Pentenes	
Butanes	35.0
Butenes	
C_2H_6 or $C_2H_2D_2$	6.0
C_2H_4	26.0
CH_4	None
D_2	
HD	
H_2	

It was also proposed (Polytechnic Institute of Brooklyn, *509* to *525,* June 1960 to April 1962) to measure infrared spectra of gas adsorbed on a thin film of metal used as an electrochemical electrode, and to follow the change in amount of adsorbed material by measuring the magnetic susceptibility of a thin-film electrode. The Hall effect was also suggested as a method of following the amount of adsorbed gas on an electrode. Not surprisingly, all these projects were abandoned due to experimental difficulties. In addition, the investigators seem to have had only the vaguest idea of the complexity of the quantitative relations between the amount of material adsorbed and infrared spectra, magnetic susceptibility, and Hall coefficient, or of the effect on these relations of the presence of an electrolyte.

Oxygen adsorption was studied (Westinghouse Electric Corp., 787 through 789, July 1961 to January 1962) at the surface of materials that could be incorporated into oxygen electrodes for aqueous or other electrolytes at moderate temperatures (789). A prime objective was to determine whether dissociative or molecular adsorption occurred. The technique used was to admit oxygen at −319" F (−195"C) at pressure below 0.3 torr, and raise the temperature in a controlled manner (ref. 17.6). The 18 and 16 isotopes of oxygen were used, since if dissociative chemisorption occurred, heating would lead to desorption of $O^{16}O^{18}$ molecules. The rate of ortho-para hydrogen conversion was used to determine whether the surface was paramagnetic (ref. 17.7). The analysis system, a mass spectrometer connected to the adsorption vessel with a flexible stainless-steel tube, gave no interchange of oxygen between O_2^{16} and O_2^{18} at 572" F (300" C) in 18 hours, even with water present. Silver powder (sintered into a pellet) of 99.999 percent purity (Handy & Harman) was degassed for several days in oxygen and hydrogen in a quartz vessel at temperatures up to 1292° F (700" C). Evolution of carbon-containing gases was observed. Adsorption of oxygen on the degassed material occurred at −319° F, and as the sample was heated, the pressure rose rapidly due to desorption. At −112"F (−80° C), slow readsorption occurred, and at about 392" F (200" C), desorption started to occur. The sintered powder had krypton BET areas of 350 cm^2/g. Physically adsorbed oxygen at low temperatures increased the ortho-para hydrogen conversion rate, but the chemisorbed gas at 32" F did not, showing that oxygen ions were not present.

The general picture of the chemisorption of oxygen on the silver, derived from the results in the contract reports, is as follows. The reaction is activated and the adsorption is not rapid until about 212" F (100° C). Even then, the rate of adsorption falls rapidly as chemisorption proceeds, giving a very slow rate even though coverages are much less than equilibrium. At

392" F, slow desorption is seen; if O_2^{18} is admitted after O_2^{16}, then O_2^{16} and $O^{16}O^{18}$ desorb, which is expected if O^{16} and O^{18} exist on the surface. The isotopic balance was confused by the presence of oxygen from the pretreatment dissolved in the surface layers of the metal. At 437" F (225" C), $O^{16}O^{18}$ was formed when the powder was exposed to equal pressures of O_2^{16} and O_2^{18}. The formation rate was approximately half order with respect to oxygen (16 or 18) pressure between 2- and 20-torr pressure (no mechanism was proposed to explain this result).

Higher temperatures favor desorption and less equilibrium surface coverage. When chemisorption is not observed, it may be due either to a slow rate of adsorption, or to weak chemisorption in which the equilibrium coverage is too small to be seen. In the second case, the surface gives isotopic exchange when dissociative chemisorption occurs, whereas the first case does not.

Gold powder of 99.999 percent purity (Handy & Harman) was also used. As with silver, anomalous results were obtained unless the gold was degassed at high temperatures for several days in oxygen, with CO and CO_2 being emitted from the material. Alloy wires (75 Au: 25 Ag weight-percent) were prepared by melting in vacuum, cooling in a copper mold, swaging to 50 mil in a stainless-steel tube, and annealing in a silica tube for 50 hours at 1382" F (750" C) in purified oxygen. The wires were used to form colloidal particles by spark erosion in triple-distilled water bubbled with oxygen. The powder formed was heated at 392" F (200" C) for 3 days and then had an area of about 1 m²/g. Results are given in table 17.3.

In a continuation of the work (797, September 1962 to March 1964), the equilibrium coverage of silver at 3.3-torr pressure of oxygen and 392" F was 0.7 monolayer, using $(6)(10^{14})$ molecules of oxygen per square centimeter as the total coverage. However, silver pretreated at 932" F (500" C) contained sufficient oxygen (0.5 to 2.5 monolayers) to throw off oxygen mass balances. The expected bulk solubility of oxygen at this temperature was only 2 percent of a monolayer; therefore, the oxygen was present in surface layers. At 932" F, O_2^{16}, O_2^{18}, and $O^{16}O^{18}$ exchange was complete in about 5 minutes; $k=(O^{16}O^{18})/(O_2^{16})^{\frac{1}{2}}(O_2^{18})^{\frac{1}{2}}=4$ was found to apply, where $(O^{16}O^{18})$ is the partial pressure of the mixed isotope, (O_2^{16}) that of oxygen 16, etc. Thus the rates of adsorption-desorption were fast, so the retained oxygen was present due to a high heat of adsorption and not due to slow desorption. There were two adsorptions, the first being reversible with a surface coverage near 1 at about 392" F (200" C), the second occurring only at higher temperatures and being much more strongly held, so that the surface coverage (actually several monolayers deep) was near 1 even at 932" F.

Further experiments at 392" F showed that O_2^{16} and O_2^{18} admitted to the silver adsorbed to almost steady state within an hour, but $O^{16}O^{18}$ release was slow. The gaseous oxygen was removed by admitting some argon and pumping out until no argon was present. The release of O_2^{16}, O_2^{18}, and $O^{16}O^{18}$ from the surface then followed. This gave ratios of 1:1:2, which are the equilibrium ratios, and demonstrated that isotopic equilibrium was obtained on the surface and was independent of the external gas composition. The slow release of $O^{16}O^{18}$ must then be due to slow desorption and not a slow surface reaction of adsorbed O^{16} and O^{18}. The rate of release followed the equation

$$\log[(p_\infty-p_0)/(p_\infty-p_t)]=kt \qquad (17.1)$$

where p was the pressure of $O^{16}O^{18}$. The rate constant for desorption, k, had an apparent activation energy of 33 kcals/mole. Similarly, O_2^{16} was put on the surface and the system pumped out. The release of O_2^{16} followed the same rate. The equation implies that the rate of release is first order with respect to the amount on the surface as expected from a Langmuir rate law $d\theta/dt=k\theta$. However, the rate of adsorption did not appear to follow a Langmuir law. Table 17.3 also gives results for palladium and platinum (Engelhard), which were purified from carbon by heating in oxygen as described above.

Some electrochemical measurements were made with pure silver foil in 15 percent KOH with oxygen bubbled through the electrolyte (high-purity system). The electrode took several hours to reach an OCV of about 1 volt (versus SHE in the same electrolyte). The cathodic

TABLE 17.3.—*Results of Adsorption of Oxygen on Pure Metals (787 Through 789, 797)*

Material	Temperature, °C	Amount of adsorption	Rate of adsorption	Desorption (isotopic exchange)	Remarks or conclusions
Ag..........	200	Large	Rapid, then slow	Slow (hours)	$O^{16}O^{18}$ off, $E‡\approx 37$ kcals/mole
	Ambient	Small	Slow	Slow, decreasing with time	Addition of 10 torr H_2O prevented chemisorption of O_2
Au..........	Up to 400	None	Zero	Zero	No chemisorption
75 Au:25 Ag .	200 to 250	Some	Rapid, then slow	Slow	$O^{16}O^{18}$ off, $E‡\approx 30$ kcals/mole
Pd..........	Ambient	Large	Rapid	Very slow	No $O^{16}O^{18}$ seen in several days
	>100	Large	Rapid	Slow	Desorption rate about same as on Ag; $E‡\approx$ 35 kcals/mole
	Ambient H_2O followed by O_2^{18}	....	....	Zero	H_2O^{18} formed, but no $O^{16}O^{18}$
	300	Large	Rapid	....	400 monolayers formed
	300, cooled to ambient	None	Zero	Zero	No chemisorption on PdO
	500	....	....	....	PdO formed
PdO.........	Ambient	Small	....	Slow........	Weak chemisorption on the oxide. H_2O vapor prevented the chemisorption
Pt..........	Ambient to 150	None	....	Zero	No dissociative adsorption
	250	Small	....	Very slow	
	300	Large	....	Slow, increasing with time	$O^{16}O^{18}$ off, $E‡$ 10 to 18 kcals/mole

$E‡$ is activation energy of desorption.

current-voltage curves depended on time of immersion.

The effect of adsorption of oxygen on the conductivity of nickel oxide was investigated (General Atomics, 233, August 1961 to March 1962). Frequency-dependent conductivity was determined on a packed bed of NiO prepared by decomposition of $NiCO_3$ in air at 2012" F (1100" C). The frequency dependence of conductivity usually showed no agreement with theoretical expectations. The surface was reduced by admitting a short pulse of hydrogen, which stripped off adsorbed oxygen and gave reproducible conductivity. On admitting a pulse of O_2 (mostly at 752" F (400° C)), the conductivity immediately rose tenfold and then slowly decreased, with a nonexponential decay, when the oxygen pulse had traveled through the bed. Similar results were obtained with measurements on single crystals. The initial increase of conductivity was ascribed to the formation of O^- and a positive hole. However, most of the oxygen was probably adsorbed as a transient, unstable, neutral species, which could either ionize or decay to a stable, neutral species (not desorbed or incorporated into the lattice). The O^- ions trapped positive holes (the charge carriers), re-formed the unstable neutral species and, hence, were gradually removed by formation of the stable neutral species.

The results could probably be explained by a number of different mechanisms. For example, if surface states exhibit band structure, there is no need to assume that an electron is localized on a specific oxygen atom to give O^-. There was no frequency region where the conductivity could be unambiguously assigned to surface conductivity; therefore, the results could not be treated quantitatively with any degree of certainty. The relevance of the work to electrocatalysis is not readily apparent.

17.3 CATALYSIS: HYDROGEN ELECTRODE

An excellent review of the present state of knowledge of hydrogen-electrode reactions has been given by Frumkin (ref. 17.8). The review shows that the fundamental kinetics are complex and although many hundreds of investigations have been made on hydrogen electrodes, a detailed description of the mechanisms, rate constants, effects of electrode material and electrolyte, etc., has not been developed. It is not surprising, therefore, that most development of fuel-cell catalysts has been carried out by trial-and-error procedures. Practical fuel-cell hydrogen electrodes nearly all use high-area platinum, palladium, or nickel as the catalysts. Some more basic approaches have been attempted under Government sponsorship and they are discussed here.

Two approaches can be used. First, if results are to be meaningful for the development of theories of catalysis, the experiments must be carried out under rigorously controlled conditions. This means that reactants, electrodes, and electrolytes must be ultrapure and the systems studied should be as simple as possible. Second, if the results are to be directly applied to fuel-cell work, a more empirical approach is adopted in which ordinary high-grade chemicals are used without ultrapure procedures. Results may be widely different depending on which approach is used; therefore, I have indicated those investigations which were conducted under ultrapure conditions.

Although not performed specifically for fuel-cell application, a study of hydrogen evolution at single-crystal metal electrodes was made under a Federal contract (Politecnico di Milano, 347 through 362, July 1959 to July 1961). Since hydrogen evolution and hydrogen ionization are obviously closely related, the results are of interest. The experiments were done with ultrapure techniques, using electropolished single crystals. The potentials were measured versus reference electrodes calibrated against a standard H_2(Pt) electrode in the same electrolyte as the test electrode. Anodic-cathodic preelectrolysis at auxiliary electrodes was used, with hydrogen bubbling to prevent oxygen buildup in the system. Electrolytes were sulfuric acid and perchloric acid, at 77° F (25" C). The major results are shown in figure 17.1. As the authors themselves conclude, they generated considerable empirical data with no theoretical interpretation. Different crystal faces of the same metal some-

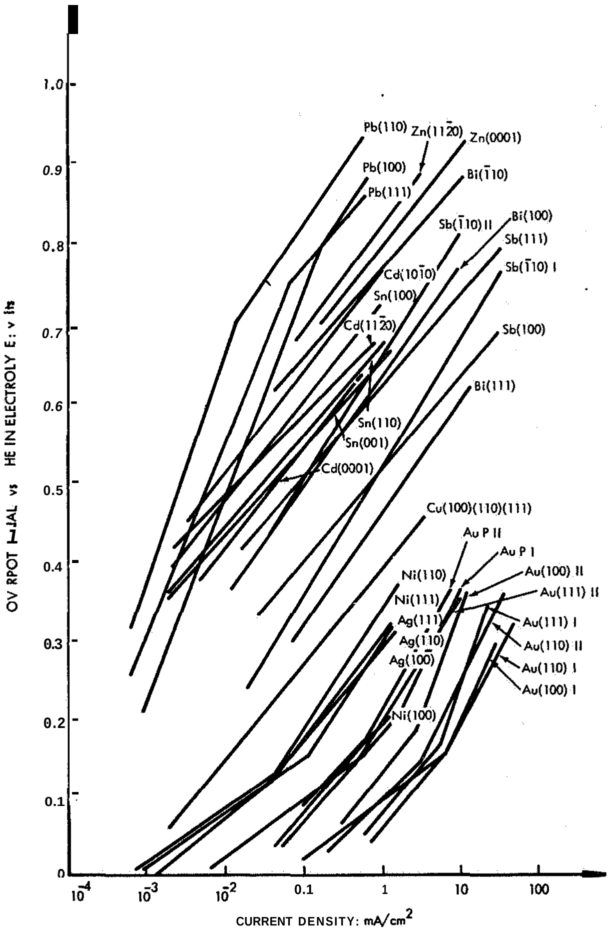

FIGURE 17.1.—Current-potential relations for hydrogen evolution in acid solutions at single-crystal faces of various metals (362).

times gave considerably different results. (An investigation (739) of hydrogen ionization on the 100, 101, and 111 planes of platinum showed no significant difference in Tafel parameters. Grain size of polycrystalline platinum also had no effect.) The position of gold is surprising, since it has not proved a useful catalytic material in fuel-cell work. The addition of 10^{-4} mole per liter of arsenic or antimony to the electrolyte gave considerable increase in the overpotential of hydrogen evolution on copper, demonstrating the poisoning effect of these substances.

Young and Rozelle (Alfred University, 19, September 1958 to September 1961) studied hydrogen ionization at porous carbon caps used as diffusion electrodes. The caps were vacuum impregnated with catalyst salt and reduced in hydrogen at 752" F (400° C) in the cell fixture. They were lowered into the electrolyte immediately after cooling and hydrogen passed into the cap. Table 17.4 gives the open-circuit potentials of the catalyzed anodes. The potentials are sometimes less than theoretical and this was ascribed to the slow rate of chemisorption of hydrogen on a poor catalyst. It is possible for an initially fast chemisorption to slow down to negligible rate as the surface is covered (see sec. 17.2). The electrode would then have a potential corresponding to the free energy of the chemisorbed gas, which might be far less than the theoretical equilibrium value. However, they obtained the same OCV from both the anodic and cathodic sides, which suggests that hydrogen can be generated at 1 atmosphere at potentials less than theoretical, which violates the first law of thermodynamics. It seems more likely that impurities in the system caused the anomalies. The method of using OCV as a guide to activity is crude and therefore the results must be considered with caution, especially since there was considerable variability between duplicates, but it is useful as a first comparison of different materials. Figure 17.2 shows the results of preparing alloys within the pores of carbon caps. The loss of activity was ascribed to the removal of d-band vacancies in the palladium as it was alloyed with silver, with the conclusion that d-band vacancies are necessary for chemisorption and activity.

TABLE 17.4.—*Anode* OCV (Millivolts) for Hydrogen-Gas Electrode at Ambient Temperatures (19): Versus *Normal* Hydrogen Electrode

Metal catalyst	15 percent aqueous sodium hydroxide electrolyte	10 percent aqueous potassiun carbonate electrolyte	CO	C_2H_4	C_2H_2
Tungsten	−801	...	−462	−390	−450
Osmium	−860	−737	−500	−338	−412
Iridium	−850	−737	−490	−329	−456
Platinum	−845	−750	−532	−352	−463
Gold	−305 to −800	−212	−157	−60	−199
Ruthenium	−870	−750	−460	−238	−416
Rhodium	−850	−750	−542	−341	−465
Palladium	−836	−730	−570	−265	−465
Silver	−382 to −712	−127	−227	−82	−282
Iron	−575	−700	...	−765	−784
Cobalt	−745	−700	−439	−667	−690
Nickel	−830	−737	−484	−428	−593
Copper	−385	−272	−180	−320	−462
Carbon	−200	...	...	...	...

Rhodium was a good catalyst on current drain, giving no polarization at 30 A/sq ft and 147"F (64"C). Potassium carbonate electrolytes gave a loss of about 0.15 volt compared to potassium hydroxide at appreciable currents. As can be seen from table 17.4, the potentials with acetylene or ethylene were low. Propane potentials were also low, but were much im-

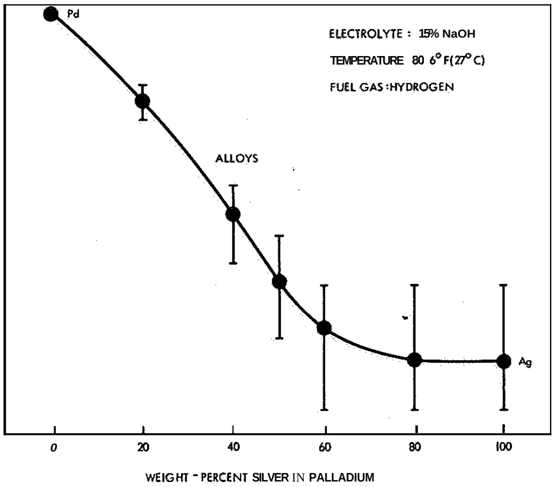

The alloys were formed in porous carbon-diffusion electrodes by reduction and annealing of salts impregnated into the carbon.

FIGURE 17.2.—Decrease in catalytic activity for hydrogen ionization when palladium is alloyed with silver (19).

proved by temperature, with temperature dependence characteristic of activation polarization.

Following the suggestions of Young, an attempt was made (Tyco Laboratories, ***647*** through ***650,*** April 1962) to correlate electrode behavior with the electronic properties (especially the number of vacant d-orbitals) of electrode materials. Nickel, nickel sulfide, nickel antimonide, nickel arsenide, nickel silicide, nickel oxide, and lithium-doped zinc oxide were used in 1 *M* $HClO_4$, 6 *M* KOH, and some buffered electrolytes. Immersed solid electrodes were used with bubbled gas, which led to mass-transfer limitations; in addition, corrosion and dissolution reactions were present. No useful results were obtained. A second contract (Tyco, ***626*** through ***639,*** April 1962 to 1964) appeared to have the same general purpose. Although the work is of high quality, very little is relevant to fuel cells. The overpotential of hydrogen evolution on mercury containing 0.028 atom-percent platinum or 0.006 percent palladium was shown to be the same as on pure mercury ***(632).*** It was claimed, therefore, that the effects of the two materials were not additive and that a synergistic effect was present. (Mercury is known to be a strong poison for platinum, so it is not surprising that small traces of platinum in mercury gave no catalytic effect.) Table 17.5 gives Tafel parameters for hydrogen evolution on various compounds.

TABLE 17.5.—Tafel Parameters *for* Hydrogen Evolution on Various *Surfaces* ***(627*** and ***637)***

	b(mV)	$-\log i_0$ (A/cm²)		
Ni	125	5.3		
Ni+As_2O_3	120	8.0		
NiAs	56	7.3	155	6.1
Si	No Tafel region		168	7.5
NiSi	113	5.4	145	5.4
Sb	170	5.7	260	5.3
NiSb	108	7.6	245	5.0
Te	48	11.0		
$NiTe_2$	55	8.0		
Ni /H_2S	80	9.4		
NiS	62	7.2	100	
In (solid)	120	11.0		

Hydrogen ionization at solid, bright platinum electrodes in 0.5 *N* hydrochloric acid was studied with a translating electrode (Leland Stanford Junior University, ***392,*** 1963). In this technique the metal electrode was mounted in the face of a vertical Lucite cylinder which was rotated around the electrolyte container at the end of a horizontal arm centered at the axis of the container. At low polarization (potential was held constant with a Wenking potentiostat) the reaction was mass transfer controlled and the diffusion coefficient of dissolved hydrogen was determined to be $(3.18)(10^{-5})$ cm²/sec, using a solubility at 77° F (25° C) of $(7.6)(10^{-7})$ g-moles/cm³. Higher current densities were obtained by increasing the rate of rotation and at about 0.2 volt versus SHE, the current density reached a limiting value of about 1 mA/cm² which was independent of the rotation rate and further polarization. This was ascribed to saturation of the active sites for chemisorption

$$H_2+2Pt\rightarrow 2Pt[H]$$
$$Pt[H]\rightarrow Pt+H^++e^-.$$

(Saturation of active sites, i.e., fractional coverage by chemisorbed [H] tending to 1, $\theta\rightarrow 1$, would not produce a kinetic-limiting current, since the rate of ionization of [H] is increased by more polarization. The kinetic-limiting current could be a limiting rate of chemisorption at θ tending to zero.) Beyond 0.4 volt, further current increase was observed which was ascribed to

$$Pt+H_2O\rightleftharpoons Pt[OH]+H^++e^-.$$

(This reaction cannot maintain steady current, nor does it increase the number of active sites, unless it is assumed that the new reaction is

$$2Pt[OH]+H_2\rightarrow 2Pt[OH]\,[H]$$
$$Pt[OH]\,[H]\rightarrow Pt[OH]+H^++e^-$$

with rates faster than the previous mechanism.) At potentials above 0.6 volt, the current density became lower, indicating poisoning of the electrode by

$$Pt[OH]\rightarrow Pt[O]+H^++e^-,$$

Pt[O] being a poor reaction surface. On decreasing voltage, the current density increased and maintained a fairly steady value until near-zero volt. This was attributed to formation of Pt[OH] on the reverse scan.

The principal argument appears to be that anodization followed by cathodic current increases the activity of the electrode to hydrogen ionization by forming Pt[OH] on the surface. This assumes that Pt[OH] is stable at near-zero volts, and that it is not stripped by hydrogen evolution

$$Pt[OH]+H^++e^-\rightarrow Pt+H_2O.$$

Anodization to oxygen-film formation poisons electrodes and hydrogen is usually evolved vigorously on the surface to activate it after anodization. Most fuel-cell electrodes have hydrogen electrodes which reach theoretical OCV and which do not show initial kinetic-limiting currents. From the theory proposed, this would be expected only if Pt[OH] were stable at zero volts. Alternatively, the kinetic-limiting current was possibly due to adsorbed impurity which was removed at more anodic potentials, opening up more active sites for hydrogen ionization. Table **17.6** gives some catalyst results taken from a number of contract reports.

17.4 CATALYSIS: OXYGEN ELECTRODE

17.4.1 Introduction

The oxygen electrode is the more polarized electrode in nearly all hydrogen-oxygen fuel cells. It performs especially poorly, in comparison to hydrogen electrodes, with acid or neutral electrolytes. This led to a number of investigations of the oxygen electrode, aimed at determining rate-limiting factors and improving current density.

The reaction sometimes proceeds reversibly to peroxide, and decomposition of the peroxide is slow until it builds up in concentration, (Note that a buildup of free peroxide implies also a buildup of surface peroxide.) If the peroxide concentration has to increase to, for example, 0.1 molar before it is further reduced at a satisfactory rate, then the oxygen electrode has a potential nearer to that of $O_2+H_2O+2e^-\rightleftharpoons HO_2^-+OH^-$ than to that of $O_2+2H_2O+4e^-\rightleftharpoons 4OH^-$. The standard-state cell potential (versus hydrogen) of the first reaction is 0.4 volt less than that of the second, which represents a considerable loss of efficiency. Provided the peroxide formation is reversible, an effective catalyst must increase the rate of further reduction or decomposition ($HO_2^-\rightarrow OH^-+\frac{1}{2}O_2$, with the O_2 being used at the electrode). When the formation of peroxide (either free or as surface complex) is irreversible, this step must also be catalyzed.

17.4.2 Western Reserve University, the Oxygen Electrode, 1951 to Present

Some of the best work on oxygen ionization has been carried out under the direction of Professor Seager. Berl (ref. **17.9**) had shown that

TABLE 17.6.—*Catalysis of Hydrogen Electrodes*

Reference	Electrolyte	Temperature	Pressure	Catalyst	Remarks
Electro-Optical Systems, *182* (July 1963)	35% KOH	Ambient	75 psig	Pt or Pd plated into porous nickel (Clevite)	Pd better than Pt
				Pt+Pd as above, 5 mg of each per cm^2 of geometric electrode area	50 Pt : 50 Pd wt-% better than either alone, or 75:25, 25:75 mixtures
				As above. Carbonate ion present	Poisons electrode
Alfred University, *28* (June 1964)	30% KOH	158° F (70° C)	1 atmosphere	Clevite No. 3 porous nickel, codeposit of Pt-Pd	Codeposit better than Pt or Pd alone. Has much absorbed hydrogen
General Electric, *310* (June 1964)	$6\ NH_2SO_4$	77° F (25° C)	1 atmosphere	General Electric Teflon-bonded Pt-black; 45 mg/cm^2	20 millivolts polarization at 400 mA/cm^2
				General Electric Teflon-bonded, platinum on B_4C; 0.16 mg Pt/cm^2	60 millivolts polarization at 400 mA/cm^2
General Electric, *255* (February 1961)	KOH-membrane	Ambient	1 atmosphere	General Electric Teflon-bonded. 10 percent catalyst on activated carbon	Pt>Co>Ni>Fe>Mn>Cr
256 (May 1961).......	....	....	....	High-area blacks in paste on screen	Pt, Pd>Rh, Au, Ag, Co
California Research, *140* (August 1963)	H_2SO_4	Ambient	1 atmosphere	Impregnated porous carbon (Pure Carbon FC–14)	Pt>Ru>Pd>Rh>Ir · 90 Pt 10:Ir mole percent same as Pt
Engelhard Industries, *200* (July 1962)	H_2SO_4	Ambient	1 atmosphere	5 weight-percent Pd on active carbon	Good activity but excessive dissolution of Pd
Alfred University, *23* (October 1962)	KOH	Up to 158° F (70° C)	1 atmosphere	Porous carbon immersed in chloroplatinic acid, dried, heated in H_2, 842° F (450° C) 13 hours	X-ray diffraction showed that H_2 reduction was necessary to give Pt metal
American Cyanamid, *86* (January 1964)	30% KOH	Ambient	1 atmosphere	Teflon-bonded American Cyanamid electrodes. Catalyst deposited on Stackpole C–2H carbon flour.	0.5 mg Rh/0.5 mg Pt/19 mgC per cm^2 gave same performance as 9 mg Pt $black/cm^2$. But 20 to 40 mg Pt/cm^2 gave slightly better performance
[a].....................	KOH	176° F (80° C)	1 atmosphere	Allis-Chalmers H_2-O_2 cell with porous Ni plaque	Nickel boride powder, alone or deposited in Ni plaque, was a good H_2 electrode catalyst
[b].....................	KOH	158° F (70° C)	1 atmosphere	Porous Ni, free electrolyte	Nickel boride, 30 m^2/g, deposited in nickel was good H_2 electrode catalyst. Boride reacts with KOH, leaving active Ni structure

---

[a] Jasinski, R. J., Fuel Cell Systems, Advances in Chemistry Series No. 47, American Chemical Society, p. 95 (1965).

[b] Lindholm, I., paper presented at Journées Internationales d'Ètude des Piles ò Combustibles, Brussels, June 1965.

the OCV of the oxygen-carbon electrode in alkali was determined by the reaction

$$O_2+H_2O+2e^- \rightleftharpoons O_2H^-+OH^-. \tag{17.2}$$

Yeager used a porous carbon electrode contained in a glass tube, with one face exposed to the electrolyte and the other fed with oxygen through the tube *(762,* March 1953). To prevent electrolyte from flooding the electrode, a suspension of active carbon with polyethylene was sprayed on the exposed carbon face to give a layer about 1 millimeter thick. This was heated to soften the plastic, giving a nonwetting layer in which the plastic also acted as binder for the active carbon. Since the natural equilibrium concentration of peroxide ion in potassium hydroxide is minute, a known concentration (0.2 *M*) of peroxide was added to give definite conditions. The reaction steps were postulated as

$$O_2 \rightarrow [2O] \underset{H_2O}{\overset{2e}{\rightleftharpoons}} O_2H^-+OH^- \tag{17.3}$$

where the brackets indicate chemisorbed oxygen atoms. The O_2H^- ion can diffuse and migrate away from the electrode, or decompose to oxygen and hydroxyl ions. Polarization was ascribed to the buildup of peroxide ion at the electrode (concentration polarization) and at currents less than 50 mA/cm², the decay of polarization on current interruption was slow (no decay in 200 microseconds), indicating mass-transfer effects rather than activation polarization. With pure oxygen, no limiting currents were observed out to 500 mA/cm², but they were observed with air. This was ascribed to diffusion limitations of oxygen in the air contained in the pores of the carbon. A later report *(764,* October 1954) gave a review of the oxygen electrode in alkali and concluded that the reaction steps were

$$\begin{gathered} O_2(g) \rightleftharpoons [O_2] \\ [O_2]+H_2O+2e^- \rightleftharpoons HO_2^-+OH^-. \end{gathered} \tag{17.4}$$

The reaction was reversible to over 100 mA/cm², with concentration polarization of HO_2^- and O_2 as the only polarization. Polarization could be decreased by greater partial pressure of oxygen and by using peroxide decomposition catalysts on the electrode. This mechanism was proved by an elegant work using oxygen 16 and 18 isotopes *(765,* August 1956). The electrode was fed with O_2^{16} enriched with O_2^{18}. After passing cathodic current, the electrolyte chamber was pumped out to remove dissolved oxygen. The electrolyte was then run into a lower cell portion which contained frozen ceric sulfate-sulfuric acid solution. On thawing and mixing, the electrochemically generated peroxide decomposed, giving a mixture of O_2^{16} and O_2^{18}. The ratios were those expected from the gas feed, showing that oxygen from the gas did not combine with oxygen from the water; therefore, the oxygen in the peroxide ion was from feed oxygen without breaking of the oxygen-oxygen bond on chemisorption.

A number of different activated carbons were used, with the spray method, to form active layers on a base carbon *(771,* November 1959). The pore-size distribution of the carbons was measured by gas adsorption. The sizes were classified into: macropores, 1- to 0.40-micron diameter; transition pores, 80- to 400-angstrom diameter; micropores, a few angstroms (10 000 angstroms = 1 micron). The nitrogen BET areas of the materials were usually about 1000 m²/g, but double-layer capacity measurements gave about 8 square centimeters per square centimeter of geometric area, indicating that the electrolyte penetration was small and that small pores were not filled with electrolyte. The performance of the different carbons indicated that the presence of transition pores was necessary; these acted as gas feeders to the electrolyte, while the smaller pores had slow diffusion rates and the larger pores flooded with electrolyte. Table 17.7 is a summary of the results *(772,* August 1960).

The study revealed that porous, baked-carbon electrodes must be thick to give long life, since electrolyte slowly crept into the electrode *(774,* December 1960). Thick electrodes suffered from concentration polarization with air because of the slow diffusion of oxygen to electrochemically active areas. Catalyzed electrodes were made by dispersing active carbon powder in ammoniacal silver nitrate, and adding sodium hydrosulfite with rapid stirring to deposit silver on the carbon. The material was filtered, washed, and heated to about 10 percent weight loss. This powder was again dispersed in benzene, and polystyrene, gum rubber, or polyethylene was added to form a spraying solution. An electrode containing 15 weight-percent Ag, 10 percent rubber, and 75

TABLE 17.7.—*Cathodic and Anodic Polarization Data (for* O_2*) and Surface Area for Electrodes Prepared From Various Types of Active Carbon (772)*

	Carbon	Polarization at 100 mA/cm^2 in volts[a]		Surface area in m^2/g for active carbon	
		Anodic	Cathodic	Before	In electrode
1	Atlas 61108–G–60	0.034	0.029	1265	687
2	Atlas 61109–S–51	.056	.032	634	296
3	Darco G–60 (C and B)	.030	.020	537	331
4	Barnebey-Cheney 1596	.036	.051	862	371
5	Barnebey-Cheney 1598	.53	.49	1047	560
6	Norit A No. 1	.079	.058	1230	524
7	Norit A No. 2	.054	.035	1062	482
8	Norit A No. 3	.043	.041	....	506
9	Mallinckrodt NF IX	.037	.021	660	441
10	Nuchar C–115	.090	.048	985	266
11	Nuchar C–115A No. 2	.058	.040	965	255
12	Nuchar C–115N No. 2	.064	.045	1063	248
13	Nuchar C–190A	.043	.038	990	546
14	Nuchar C–190N No. 3	.060	.055	1050	643
15	Nuchar C–190N No. 1	.061	.067	1040	472
16	Nuchar W	.081	.060	874	411
17	Nuchar C–1000 N	.150	.088	....	752
18	Aqua Nuchar A	.066	....	....	223
19	Nuchar (C and B)	.106	.110	....	441
20	Nuchar C–B	....	.039	1313	800
21	20 XVRX	.107	.072	671	54
22	DR–1	.099	−.003	1225	923

[a] Electrolyte: 5 M KOH+0.88 M H_2O_2; $T=77°$ F (25" C).

percent Nuchar C (West Virginia Pulp & Paper Co.) was tested in comparison with a noncatalyzed electrode. In 5 M sodium hydroxide plus 0.01 M H_2O_2, the interrupted (IR-free) polarization was about *0.12* volt at *400* mA/cm^2 for the catalyzed material, polarization being measured from an OCV of *0.003* volt versus SHE. Polarization was greater with the noncatalyzed carbon, and the difference was ascribed to the decomposition of peroxide by the catalyst. It was concluded that the silver would not decompose 0.01M peroxide very rapidly; therefore, the potential at low currents was still determined by reaction *(17.4)*. However, when the peroxide concentration at the electrode built up at higher cathodic current, it started to decompose at the catalyzed electrode, giving the observed improved performance. Polarization increased with increased current density even after the initial buildup of peroxide; this was believed to be due to IR polarization in the electrolyte in the pores of the carbon, which was not eliminated by the rapid current interruption technique (2 millisecond on, 100 microsecond interrupt).

The results discussed above could not be expressed in exact mathematical form for two reasons (776, July *1963).* First, use of porous carbons led to distributed effects in the pores (see sec. *18.7);* and, second, mass transfer of peroxide in the electrolyte could not be rigorously controlled. Therefore, electrodes were made from porous carbon, filled with paraffin wax and polished smooth. The electrodes were mounted in a rotating-disk assembly (see app. C) and oxygen dissolved in the electrolyte at various pressures. Pyrolitic graphite electrodes were also used. (Pyrolitic graphite is nonporous and has considerable crystalline order'.) The OCV obeyed the Nernst equation from 1 to 30 atmospheres of oxygen and over a wide range of peroxide concentration. Mass-transfer-limiting cathodic currents were found (in *4* M OH^-+0.016 M HO_2^-) which were dependent on the oxygen pressure. The slope of η versus log $[i/(i_L-i)]$ was 0.11

volt per decade. (It would be **0.03** for pure mass-transfer polarization without activation polarization.) The apparent exchange current was 0.17 mA/cm^2 for pyrolitic graphite and of the same order for various wax-filled electrodes. The slopes showed activation polarization to be present on these low-area electrodes, and a reaction path was proposed:

$$O_2+e^-\rightarrow[O_2^-]$$
$$H_2O+[O_2^-]+e^-\rightleftarrows HO_2^-+OH^-. \qquad (17.5)$$

When the first step was slow and when the surface coverage of adsorbed oxygen, e, tended to zero, a Tafel slope of about 0.12 would be expected and the limiting cathodic current would be proportional to the concentration of dissolved oxygen. The rate equations are

$$i=i_0[(O_2)_s/(O_2)_b]\ \exp\ (\alpha F\eta/RT)$$
$$i=k[(O_2)_b-(O_2)_s]$$
$$i_L=k(O_2)_b$$

and, therefore

$$i=i_0(1-i/i_L)\ \exp\ (\alpha F\eta/RT) \qquad (17.6)$$

$(O_2)_s$ is the concentration of dissolved oxygen at the electrode surface, $(O_2)_b$ that in the bulk of the electrolyte, and k the mass-transfer factor. The reaction scheme proposed would give the required cathodic rate equation only if the formation of the adsorbed O_2^- ion required transfer of an electron from the electrode through the double layer to an adsorbed ion at the electrolyte side of the double layer. Another mechanism which would give the same result but allow adsorbed species to be within the double layer is

$$O_2\rightleftarrows[O_2]$$
$$[O_2]+H_2O+e^-\rightarrow[HO_2]+OH^-$$
$$[HO_2]+e^-\rightleftarrows HO_2^- \qquad (17.7)$$

For θ tending to zero, this would give the same rate form as equation (17.6). Further reduction of peroxide might occur and the principal effect would be to change the value of i_0 by a factor of 2. **A** variation of i_0 of 2 over the potential range involved would appear as a slight change in Tafel slope.

Limiting currents were also obtained for oxygen evolution from various concentrations of peroxide, but they were much too low to be mass-transport-limited currents and were kinetic-limiting currents. Similar results were obtained with the rotating-disk electrode, with limiting currents being independent of speed of rotation and hydroxyl concentration. The slope of η versus log $[i/(i_L-i)]$ was 0.12 volt, which indicated activation polarization. These results were not explained. The oxygen-peroxide reaction in alkaline solutions was also studied at lithiated nickel oxide electrodes (777, January 1965). The lithiated oxide formed on nickel wires was resistant to dissolution in alkali and strong acids. In alkaline solutions the tentative conclusions were: *(a)* the O_2 to HO_2^- reaction is irreversible unless nickel (which becomes passivated) is heated in oxygen at high temperatures; *(b)* O_2 goes only to HO_2^- if no lithium is present, but a slow reduction of peroxide is obtained with lithiated NiO; *(c)* the reaction is more irreversible at nickel oxide prepared above 1382° F (750" C); *(d)* the reaction has kinetic-limiting currents; *(e)* HO_2^- to O_2 is more reversible on both NiO and lithiated NiO; *(f)* NiO(Li) is relatively stable in 1 *M* NaOH but has a low activity at 77" F (25" C).

The OCV of the oxygen reaction at pure solid nickel (Johnson-Mathey) obeyed the Nernst equation for O_2-HO_2^-, but impure nickel decomposed the ,peroxide. The cathodic oxygen reaction at platinum electrodes in sodium hydroxide was also studied and the amount of HO_2^- produced was determined. The results are shown in figure 17.3. The influence of surface pretreatment (anodization or cathodization) was quite considerable and divalent cations inhibited the formation of peroxide. In acid solutions, chloride ion poisoned the oxygen electrode but gave greater percentage conversion to peroxide.

17.4.3 Engelhard Industries, Inc., Fuel-Cell Catalysts, July 1960 to June 1962 and July 1962 to June 1963

Most of the work on this contract was concerned with catalysts for hydrocarbon fuels in acid electrolytes, but some work on oxygen catalysts was reported *(193)*. Since Berl and Yeager (see sec. 17.4.2) had shown that in alkaline solution the slow step was the reduction or decomposition of peroxide ion, a comparative test of peroxide (5 weight-percent) decomposition rate was performed with various noble-metal catalysts. Decomposition activity was lower for the

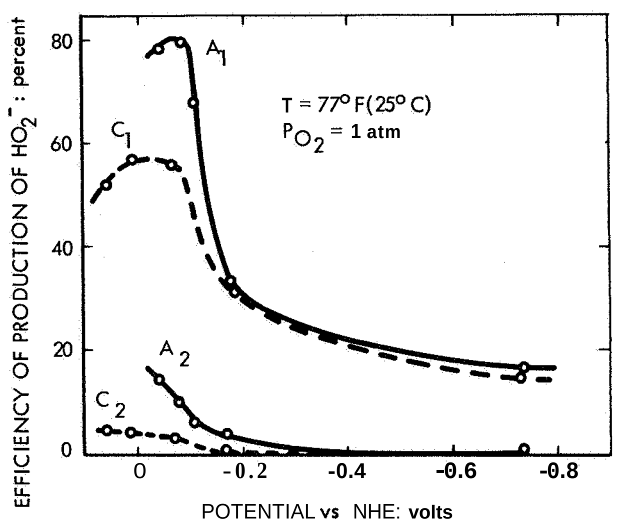

A, at an anodized electrode **in** 1 *M* NaOH; **A,** at an anodized electrode **in** 1 *M* NaOH+10^{-2} *M* $Ba(OH)_2$; *C,* at a cathodized electrode in 1 *M* NaOH; C_2 at a cathodized electrode in 1 *M* NaOH+10^{-2} *M* $Ba(OH)_2$. Barium ion inhibits the formation **of** peroxide.

FIGURE 17.3.—Faradaic efficiency for peroxide formation in the oxygen reduction process at platinum electrodes of various potentials in 1 *M* NaOH (777).

more acid electrolytes. Ruthenium on carbon was a good decomposition catalyst; palladium and platinum were good in alkaline solution but much poorer for strong acids. However, admixture of ruthenium black into a platinum electrode did not improve performance (see table *17.8).* Catalytic powders were tested by pasting a mixture in 5 *N* sulfuric acid onto one side of Fiberfrax paper (aluminum silicate paper) and constructing a cell: paste-paper-IEM-paper-paste. The paper was soaked with sulfuric acid and inert screens were pressed against the paste to act as current collectors. The comparative results are summarized in table *17.8,* with the same hydrogen electrode used for all tests. Platinum impregnated on active carbon to *10* weight-percent gave results almost as good as those for platinum black; the respective nitrogen BET areas were *1000* m^2/g and *25* m^2/g ***(194).*** Stronger acid gave better performance, as would be predicted from the mechanism

$$O_2+M \rightleftharpoons M[O_2]$$
$$M[O_2]+H^++e^- \rightarrow M[HO_2]$$
$$M[HO_2]+H^++e^- \rightarrow H_2O_2+M.$$

When methanol was used as fuel, carbon dioxide appeared at the oxygen electrode ***(195)*** and poisoned the platinum-carbon electrode; CO_2 added to the oxygen feed had the same effect. This poisoning effect was mitigated by hydrogen in the oxygen stream and by lead in the catalyst ***(196).*** Platinum sulfide catalyst also suffered the same poisoning. The CO_2 effect was almost eliminated at 180° F *(82"* C).

The diffusion of methanol from the fuel electrode to the oxygen electrode ***(197)*** greatly reduced the Performance of the oxygen electrode, (This is to be expected, since platinum is a good catalyst for methanol oxidation.) The addition of *10* weight-percent of gold to the platinum reduced this effect, as did the addition of lead. This was due to the inhibition of methanol oxidation ***(Z00).***

TABLE 17.8.—*Summary of Results* ***on*** *Oxygen Electrode Catalysts (ZOO), Sulfuric Acid Electrolyte, Ambient Temperature*

Electrode	Material	Result
H_2	5 wt-% Pd on carbon	Rapid steady state, active (but excessive Pd dissolution, 1*N* H_2SO_4)
O_2	Noble metals on carbon or as blacks	Pt best>Pd >Ir>Ru >Os >Au
	Pt on carbon	Increasing Pt better up to 10 wt-%. Almost equivalent to Pt black
	Ag on carbon	Good initially, falling with time
	Cooncarbon	High initial OCV, disappeared irrecoverably on load
	Pt-Ru mixtures	Poorer than Pt alone; therefore, no peroxide decomposition effect
	PtO_2 **(Adam's** catalyst)	Sluggish, improved with time under load

In a later contract (*213*), oxygen diffusion electrodes were made from platinum black-Teflon (see ch. 3) pressed into a current collector of platinum screen. Half-cell tests were performed using a counterelectrode and a reference electrode with a Luggin capillary. The system was built in a stainless-steel case which was pressurized with nitrogen to allow high-cell temperatures to be used (see app. C). Open-circuit voltage to ambient temperature was 1.04 to 1.07 volts (versus SHE in the same solution) and was 0.1 volt higher at 257" F (125° C). Even at 302" F (150" C), the performance under load with 2 *M* KHCO, and 2 *M* $Na_2H_2PO_4$ electrolytes was much poorer than with sulfuric acid (2 *N*). At 122" F (50° C) and 50 mA/cm², increasing oxygen pressure gave only slight increase in voltage; air was poorer until 5 atmospheres, which gave the same performance as 1 atmosphere of oxygen. Then further pressure increase gave little effect.

Methanol in the electrolyte (less than 1 weight-percent) gave reduced performance, as expected. At higher temperatures, smaller quantities of methanol could be tolerated, indicating that the increase in methanol oxidation rate with temperature was greater than the increase in oxygen reduction. However, as the oxygen pressure was increased, the tolerance to methanol increased, and at 13 atmospheres, 1 percent of methanol gave increased performance over lower or higher concentrations.

17.4.4 Esso Research & Engineering *Co.*, Soluble Carbonaceous Fuel-Air Fuel Cell, January 1962 to December 1963

A number of coprecipitates of platinum black-metal black, prepared as described in appendix C, were tested as cathode catalysts (*217*). Diffusion electrodes were made by pressing a paste of catalyst black and Teflon at 200 psi to give a thin sheet electrode. A layer of the paste was applied to the gas side of this electrode, without pressing. (The reports give no more detail on the method of electrode preparation.) The electrodes were pressed against an ion-exchange membrane saturated with 30 weight-percent H_2SO_4, since they flooded if used with free electrolyte, 140" F (60" C). Coprecipitates of Pt, with Pb, Sn, Ca, Se, Hg, Ag, or Sb gave poor activity. Platinum with Mo, Zn, Cd, Al, Ba, Hf, Mg, Sr, Y, Nd, Ir, Cu, Mn, U, Ni, or Cr gave lower performance than Pt alone. Pt with V, Pd, or small fractions of Au, Fe, or Rh performed about the same as platinum alone. Rh with Ir, Au, Fe, or Cu were poorer than platinum alone. Reproducibility of the voltage-current relations was poor, and for the second group of catalysts some results were better than the worst Pt results but poorer than the best Pt results.

Physical mixtures of platinum black mixed with oxide powders were tested as oxygen electrodes at 140" F (60" C) in 3.7 *M* H_2SO_4. Within the limit of reproducibility the electrodes generally performed similarly to platinum black alone, but were less active for high fractions of oxide. Compounds tested were $FeSO_4$, Pr_6O_{11}, Nd_2O_3, Sm_2O_3, Eu_2O_3, Gd_2O_3, Tb_2O_3, Dy_2O_3, Ho_2O_3, Er_2O_3, Tm_2O_3, V_2O_5, CuO, ZnO, Y_2O_3, Al_2O_3, CeO_2, BaO, Fe_2O_3, H_2WO_4, MnO_2, PbO, Pb_3O_4, SnO_2, and ZrO. Ternary codeposits of Pt-Fe-Co were tested over wide ranges of composition. Results were similar to platinum alone.

Platinum black treated for 150 hours in concentrated nitric acid showed no improvement over normal black.

17.4.5 Tyco Laboratories, Inc., Oxygen Electrode Studies, October 1961 to February 1963

This work was a basic study of the oxygen reaction on platinum and gold in sulfuric acid solutions (*625*). Ultrapurification techniques and half cells were used and the electrodes were of solid, bright platinum or gold completely immersed in electrolyte bubbled with oxygen or nitrogen. The low-area electrodes gave activation polarizations before the mass-transfer limits of dissolved oxygen were reached; current densities were usually below 1 mA/cm². Three overall reactions are possible

E,. volts

$$O_2+4H^++4e^-\rightleftharpoons 2H_2O \qquad 1.23 \qquad (17.8)$$

$$O_2+2H^++2e^-\rightleftharpoons H_2O_2 \qquad 0.68 \qquad (17.9)$$

$$H_2O_2+2H^++2e^-\rightleftharpoons 2H_2O \qquad 1.77 \qquad (17.10)$$

Cathodic polarization favors these reactions from left to right. Without any bubbled oxygen in the electrolyte and with added H_2O_2, the cathodic current on platinum was low until high polarization (electrode potential about 0.8 volt versus SHE), As peroxide concentration was decreased, the rate again became much slower. Therefore reaction (17.10) is slow from left to right and the reverse reaction would be expected only at potentials greater than 1.77 volts. The reaction can therefore be considered as irreversible for the experimental conditions; i.e., $H_2O_2+2H^++2e^-\rightarrow 2H_2O$. Oxygen evolution cannot occur via a free (dissolved in solution) peroxide intermediate, since reaction (17.9) is favored from right to left and peroxide has, therefore, to be produced from reaction (17.10) which is irreversible at the potentials used. Oxygen evolution must occur from water via reaction (17.8). Oxygen ionization via this reaction is also probable, without free peroxide as a necessary intermediate.

Oxygen ionization via reaction (17.9) can occur from left to right at potentials between 0.68 and 1.33 volts, provided that the H_2O_2 concentration at the electrode is kept low. Reaction (17.10) did not maintain H_2O_2 concentrations low, since it was too slow at low concentrations and at these potentials. Therefore, peroxide built up at the electrode and diffused away into the electrolyte. The reaction $H_2O_2\rightarrow O_2+2H^++2e^-$ was slow near 0.7 volt (unlike the alkaline systems reported by Yeager in sec. 17.4.2); the reverse reaction was also slow, since cathodic current-voltage curves (run at relatively short times before peroxide could build up in solution) at low concentrations of peroxide showed activation polarization. Direct ionization of oxygen according to the overall reaction $O_2+4H^++4e^-\rightarrow 2H_2O$ was slow and the potential must fall toward 0.68 volt to produce appreciable current. At steady state, the rate-limiting factor was thought to be the electrochemical decomposition of peroxide, $H_2O_2+2H^++2e^-\rightarrow 2H_2O$, although the rate of $O_2+2H^++2e^-\rightarrow H_2O_2$ was also slow at useful potentials.

Oxygen evolution caused the platinum to be coated with a thin film of oxide, which became thicker with more prolonged oxygen evolution. A heavily anodized surface gave a lower rate of oxygen evolution and a lower rate of oxygen ionization ($i_0 \sim 10^{-8}$ A/cm^2) than a freshly cathodized surface. Below about 0.7 volt, the surface behaved as a freshly cathodized surface, with no fall in voltage with time, at a given current. Without oxygen gas present, the oxygen coverage of the surface can be stripped as cathodic current, starting at about 0.8 volt.

The anodic and cathodic reactions of peroxide on gold surfaces were found to be first order (see fig. 17.4) with respect to peroxide concentration (0.1 to 10 N H_2SO_4; 10^{-3} to 1 M H_2O_2). Thus the mixed reactions

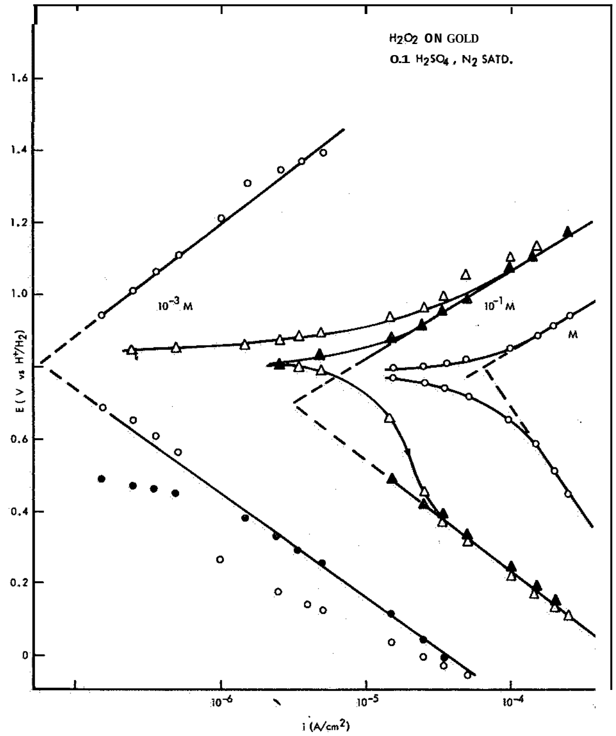

FIGURE 17.4.—Cathodic and anodic current densities for H_2O_2-H_2SO_4 solutions and a gold electrode *(625).*

$$\begin{aligned} &H_2O_2\rightarrow O_2+2H^++2e^- \\ &H_2O_2+2H^++2e^-\rightarrow 2H_2O \end{aligned} \qquad \textbf{(17.11)}$$

gave a resting potential of the electrode independent of peroxide concentration. The first-order relation implied that the surface intermediates of the reactions did not cover the surface to any great extent. A layer of chemisorbed oxygen formed on the gold at 1.4 volts, which grew into an oxide film at higher potentials; oxygen evolution from peroxide on this film was about 25 times slower than on bare gold. Unlike platinum, the monolayer and the film were not stable below 1.25 volts. As with platinum, the rate of oxygen evolution was 100 to 1000 times higher on the reduced surface than on the oxided. Oxygen ionization at gold did not give large buildup of peroxide in the electrolyte, but the polarization was about 0.4 volt higher than for platinum at a given current density. The slow step was presumed to be

$$M[H_2O_2]+H^++e^-\rightarrow M[OH]+H_2O.$$

The explanation of the constant rest potentials for gold in peroxide solution was extended to platinum in peroxide solutions bubbled with nitrogen. The experimental results on platinum, however, did not show a clear first-order reaction. When oxygen was present, the results were more complicated, since the rest potential after anodizing was lower than that after oxygen ionization. The primary reason for the rest potential of about 0.8 volt (dependent on pH and prehistory) was ascribed to the balance of the peroxide reactions (17.11).

The rate of discharge of oxide film from gold was investigated as part of another contract *(631)*. Gold was oxidized at potentials between 1.2 and 1.8 volts (versus an SHE in the same electrolyte), in perchloric or perchlorate solutions of pH 0.4 to 2.1. The amount of oxide formed was dependent on the potential and, when the oxide was discharged galvanostatically, the total amount that came off depended on the current density of discharge. Tafel lines were obtained by plotting the potential of discharge (approximately constant over the middle region of time) as a function of log current density. The exchange current was proportional to $(1/pH)^2$. A mechanism was proposed as follows:

$$\tfrac{1}{2}Au_2O_3H_2\cdot O\rightleftharpoons AuOOH$$

$$AuOOH+H^++e^-\rightleftharpoons AuO+H_2O$$

$$AuO+H^++e^-\xrightarrow{\text{slow}}AuOH$$

$$AuOH+H^++e^-\xrightarrow{\text{fast}}Au+H_2O.$$

Assuming a transfer coefficient $\alpha=\tfrac{1}{2}$, this mechanism gives a rate equation

$$i=K(\text{AuOOH})(H^+)^2\exp\left[(1+\alpha)F\eta/RT\right]. \qquad (17.12)$$

This has a Tafel slope at room temperature of 39 millivolts and gives the observed pH relation, When a thick layer of Au_2O_3 is present, the removal of surface oxide leaves porous gold which exposes underlying oxide film to electrolyte, and hence gives further discharge. The process continues until all the film has been stripped, when the surface concentration term (AuOOH) becomes zero and polarization increases rapidly (transition time).

If the reaction $4Au+3O_2+2H_2O\rightarrow 4AuOOH$ were rapid, the rate mechanism for the ionization of oxygen might be the same as that given above. However, the thick film of oxide does not appear to be formed by dissolved oxygen, but only by electrochemical discharge of oxygen. The properties of a monolayer of chemisorbed oxygen are possibly widely different from those of electrochemically formed oxygen. The previous work showed that current density of oxygen ionization was much higher for a surface which did not have the thick film. The relevance of this type of study to fuel cells is, therefore, open to question.

17.4.6 University of Pennsylvania, Reversible Oxygen Electrodes, November 1961 to Present

The first part of the program was an investigation of the oxygen-platinum electrode in sulfuric acid, under high-purity conditions (727). Electrodes were of bright platinum foil, anodized at about 20 mA/cm². After anodization, a few drops of hydrogen peroxide were added and the solution was heated until a negative result was obtained when tested for peroxide. The **OCV** in the presence of bubbled oxygen was 1.23±0.05 volt versus SHE, showing that an ideal, reversible rest potential could be obtained if peroxide were not present. At low cathodic currents the results were not reproducible, but between 10^{-2} and 1 mA/cm², a Tafel line with a slope of 0.12-volt-per-current decade and an exchange current of $(5)(10^{-7})$ mA/cm² was found. The rest potential **(OCV)** after oxygen ionization runs was 0.84 to 0.9 volt and hydrogen peroxide was present in solution. Adding a few drops of peroxide without heating produced an **OCV** of 0.84 volt.

Oxygen evolution produced films of oxide on the surface (728) and the **OCV** drifted to lower potentials on standing:

	E_0, *volts*
$PtO_3+2H^++2e^-\rightleftharpoons PtO_2+H_2O$	**1.5**
$PtO_2+2H^++2e^-\rightleftharpoons PtO+H_2O$	1.1
$PtO+2H^++2e^-\rightleftharpoons Pt+H_2O$	**0.98**

It was not explained where the electrons came from to reduce the higher platinum oxides and charge the double layer to lower potentials. Presumably oxygen slowly diffused away from the electrode, so that $H_2O \rightarrow H^+ + e^- + \frac{1}{2}O_2$, in the absence of added oxygen. When oxygen was added, the potential drifted to 1.23 volts after oxygen evolution. After oxygen ionization at voltages which stripped oxygen from the surface, the rest potential drifted to higher potentials, but not to 1.23 volts. The rest potential appeared to be a function of the partial pressure of oxygen, being 0.98 volt at 1 atmosphere and lower for lower pressures **(730)**.

The amount of oxygen adsorbed on the platinum surface was determined by stripping the oxygen with a constant cathodic current. Diffusion of dissolved oxygen to the surface was negligible at current densities greater than 10 mA/cm², although replenishment of surface oxygen was fast if a rapid stream of oxygen bubbles impinged on the electrode. The amount adsorbed, Q, was related to the partial pressure of oxygen, p, by a linear plot of $p^{1/2}/Q$ versus $p^{1/2}$. This form is predicted from a Langmuir isotherm assuming dissociative adsorption as oxygen atom. The slope of the line gave a maximum surface coverage of 350 μC/cm²; a perfectly smooth platinum surface would have about 230 μC/cm², assuming 1 oxygen atom per platinum atom. The double-layer capacity of the electrode was 27 μF/cm²; therefore, assuming a capacity of 17 μF/cm² of smooth area, the surface roughness was 1.6. The ratio of maximum oxygen adsorption to 230 μC/cm² is 1.5, which is almost the same; therefore, probably 1 oxygen atom adsorbs per surface platinum atom. The equilibrium was written

$$O_2(g) \rightleftharpoons O_2(s)$$
$$O_2(s) + 2Pt[H_2O] \rightleftharpoons 2Pt[O]2H_2O$$

with

$$\frac{Pt[O]}{[O_2(g)]^{1/2}Pt[H_2O]} = \sqrt{K}, \qquad (17.13$$

K being the overall equilibrium constant. By applying the Clapeyron-Clausius equation to isotherms between 32" and 176"F (0° and 80"C), values of enthalpy of adsorption were obtained and found to vary with surface coverage. (The linear plot of $p^{1/2}/Q$ as a function of $p^{1/2}$ is only expected for a Langmuir isotherm; i.e., for equilibrium constant not varying with coverage. Therefore, the results contradict one another.)

The value of rest potential did not follow a Nernst equation relation with respect to the partial pressure of oxygen. It was argued that no electrochemical reaction was occurring with the adsorption of oxygen, and the electrode behaved as an ideal polarizable electrode. The change in potential with oxygen chemisorption was due to the dipole moment of the adsorbed atoms and, therefore, the potential was proportional to the amount adsorbed. Note that the potential of an ideal polarizable electrode is not defined unless an external potential is applied, in which case electrons will flow from the external potential to charge or discharge the double layer until the electrode reaches the applied potential. If faradaic current is present, the electron transfer of the faradaic current will charge the double layer, even though the electrode is at open circuit $[i_c + i_f = 0]$, until *(a)* the OCV reaches a value at which the faradaic current is zero, in which case the Nernst equation should apply; or *(b)* if more than one faradaic process is occurring, the net faradaic current becomes zero and a mixed potential is obtained. If the chemisorption of oxygen produces a dipole moment, the same effect as a simple faradaic process is obtained, but the potential at a given amount of adsorption, Q, is dependent on Q and the dipole moment per adsorption.

The reactions leading to equation (17.13) are not charge transfer reactions, but the OCV of the electrode at a given partial pressure of O_2 was much lower than the theoretical value. Thus the electrode behaved as inert to O_2 ionization. It is difficult to see why the electrode at a given potential will pass faradaic current due to oxygen ionization when the electrode is tested in the normal way, while under the same conditions and potential it will behave as a nonionizing electrode when the external circuit is not connected. Possibly the double-layer potential under normal conditions is due to electrons on the metal and cations in the electrolyte, which give a potential acting across the transition state of ionization, while for open-circuit chemisorption conditions, the potential is due to dipole moments and does not act across the ionization transition state. Even if this were so, however, the change of potential on chemisorption would oppose further chemisorption and the chemisorption would not follow a Langmuir isotherm. Also, the electrode potential would not be defined, since chemisorption of molecules which have a dipole moment produces changes of potential; i.e., ΔV proportional to Q. The results quoted above imply that a precise V is obtained for a given Q; the theory predicts this only if the arbitrary starting electrode potential is the same for all experiments.

The results were not readily reproducible and continued oxygen evolution at a platinum electrode gave higher amounts of adsorbed oxygen. The amount of surface oxygen (placed on and stripped off) decreased after several cathodic cycles. A new technique was developed *(731)* in which the electrode was anodized for 5 seconds at 10^{-3} A/cm^2 and cathodized for 1 second at 50 A/cm^2. Reproducible results were obtained after five cycles; presumably this purified the surface from adsorbed contaminants but did not give a growth of oxide film on the platinum. In the absence of oxygen, the electrode behaved as an ideal polarizable electrode between 0.3 and 0.8 volt (versus hydrogen), giving a constant double layer capacity with no pseudocapacity due to $Pt[H] \rightleftharpoons H^+ + e^-$, $H_2O \rightarrow Pt[O] + 2H^+ + 2e^-$, or $H_2O \rightarrow Pt[OH] + H^+ + e^-$.

The amount of oxygen adsorbed on the surface as a function of oxygen pressure was obtained for palladium (not readily reproducible due to hydrogen adsorption), rhodium, iridium, ruthenium, gold, and platinum-rhodium alloys, using Wires of 1-square-centimeter area *(732)*. Langmuir isotherms were again obtained and the saturation coverage calculated. The results are shown in table 17.9. Assuming that the number of surface atoms which can act as bonding atoms is proportional to the number of d-band vacancies per atom, there was reasonable agreement between actual and predicted saturation coverage. Contrary to previous results, the saturation coverage of platinum was found to be 0.2 monolayer. The rate of rise of potential when an electrode, held at 0.3 volt at a given pressure of oxygen, was switched to open circuit, varied with the oxygen pressure, taking 100 seconds to reach steady OCV at 0.005 atmosphere. Growth of oxide film (more than a monolayer) was found only when the oxygen pressure was high enough to bring the electrode potential to 1 volt. Similarly, if the electrode was charged from 0.3 volt by external current, the current was capacitive until 1.0 volt, when oxygen

TABLE 17.9—Oxygen Adsorption on Metals and Alloys at 77° F (25° C) in 1N H_2SO_4 *(732)*

Metal	Saturation coverage observed, $\mu C/cm^{-2}$	Calculated monolayer coverage, $\mu C/cm^{-2}$	Fraction of total surface covered by O_2 at saturation coverage	Number of unpaired d-electrons per atom
Pd	[a]110	510	[a]0.22	0.55
Pt	[a]110	500	[a].22	0.55–0.6
Pt	135	500	.27	0.55–0.6
Rh	480	530	.90	[b]1.4
Ir	440	525	.84	[b]1.7
Ru	[a]500	530	.95	[b]2.2
Au	< 15	....	< .03	0

Alloy	Saturation coverage observed, in $\mu C/cm^{-2}$	Number of unpaired d-electrons per atom	Calculated saturation coverage on *d*-electron sharing
Pt-Rh	180	0.77	195
Pt-Rh	217	.91	230

[a] Observed coverage at 1 atm of oxygen.

[b] Number of unpaired d-electrons of the corresponding group number in the first long period.

started to deposit on the electrode ($Pt+H_2O\rightarrow Pt[O]+2H^++2e^-$).

Whether oxygen ionizes to water via a path which includes peroxide as intermediate or whether it can ionize without peroxide intermediate was investigated (737) using the rotating disk-and-ring electrode (ref. 17.10). This technique uses a normal rotating-disk electrode which is surrounded by, and electrically separated from, a ring which also rotates. The potential of the ring was set high enough for the reaction $H_2O_2\rightarrow O_2+2H^++e^-$ to be rapid, so that any peroxide reaching the ring was quickly destroyed. The potential of the central disk was set at a potential sufficient for the cathodic reactions to occur:

$$\begin{array}{lll} O_2\xrightarrow{i_1}H_2O & & \\ & & H_2O \\ & i_3 & \\ O_2\xrightarrow{i_2}H_2O_2 & i_2-i_3 & \\ & & \text{diffuse away.} \end{array}$$

The relation between disk current, ring current, and speed of rotation depends on i_1, i_2, and i_3. The variation of the relation with disk potential depends on change of the ratio of i_1 to i_2 with potential and also on how i_3 is affected by potential. For disk potentials between 0.6 and 0.8 volt (versus hydrogen in the same electrolyte), the following conclusions were drawn. In potassium hydroxide, i_1 was negligible and i_3 was not strongly dependent on potential. In sulfuric acid, i_1 and i_2 were both significant, but there was no i_3. The ratio of i_1 to i_2 decreased at more cathodic potentials.

Steady-state current-voltage relations for a number of solid, polished electrodes are summarized in table 17.10. These electrodes were prepared using ultrapure techniques which avoided coating the electrode with a surface oxide film. Voltage-log i curves showed that in all cases OCV was maintained to about 10^{-5} to 10^{-4} mA/cm^2, and approximate Tafel lines were then found, although values could not be taken beyond 10^{-1} mA/cm^2 because of mass-transfer limitations. Distinct changes of Tafel slope were found in some cases.

17.4.7 Tracor, Inc., Study of the Oxygen Electrode Mechanism, January 1962 to December 1963

The purpose of the contract was to test the postulate that adsorbed oxygen transports along

TABLE 17.10.—*Summary of Results on Oxygen Electrode Catalysts (727 through 734); Ambient Temperature*

Material; polished solid	Electrolyte	OCV	Voltage (vs. NHE in SE) at 10^{-1} mA/cm^2	Remarks
Pt	0.1 N NaOH	1.1	0.88	Pd>Pt>Ru∼Au>Ir>Ag>Cu, Rh, Ni, Fe, and Re
Pd		1.0	.9	
Rh		.94	.68	
Ir		.91	.79	
Au				
75-Au: 25-CU atom-percent		.92	.83	
Ru.		1.0	.82	
Ag..		.92	.72	
cu		.77	.72	
Ni		.81	.56	
Fe		.77	.56	
Re.		.66	.56	
Alloys:				
Pt-Rh		....	....	Between Pt and Rh
Pt-Ni		....	....	Between Pt and Ni
Pt	0.1 N $HClO_4$	**1.0**	.82	
Rh..		.91	.69	
Pt-Rh		....	....	**Near** Rh

electrode surfaces covered by electrolyte *(613).* The technique proposed was the measurement of double-layer capacity as a function of time after admission of oxygen. High-purity conditions were used and the test electrode was a small disk (0.117 cm^2) of platinum mounted in a Kel-F cylinder. Double-layer capacity was determined using square-wave alternating current, with an amplitude of **4** milliamperes and a pulse width of 10 microseconds. The high frequency was used to eliminate pseudocapacity effects, since the contribution of faradaic current to the pulse is small if the reactions are too slow to follow the rapid changes in current. Similar results were obtained using an impedance bridge and 1000-cycle alternating current. The electrode was held for long periods at a given starting potential using a potentiostat and the double-layer capacity measured at this potential immediately after disconnecting the potentiostat.

An electrode which had been reduced by prolonged hydrogen evolution gave almost constant capacities between 0.44 and 0.8 volt (versus SHE) in sulfuric acid. Values were about 20 $\mu F/cm^2$, but rose (up to 40 $\mu F/cm^2$) nearer hydrogen evolution (zero to **0.3** volt) or oxygen evolution (0.9 to 1.2 volts). The capacities were independent of the presence or absence of oxygen. When the surface was preoxidized, a capacity peak at about 0.64 volt was found when oxygen was present. A highly preoxidized surface, held between 0.4 and 0.8 volt, lost surface oxide over periods of hours, and double-layer capacity decreased in minutes. In alkaline solution, a capacity peak of nearly 70 $\mu F/cm^2$ was found between about 0.04 and –0.36 volt (versus SHE), which did not depend on the presence of dissolved oxygen. This was ascribed to adsorption of hydroxyl ion, which could not adsorb at more positive potentials due to the presence of oxide films. As the potential was lowered, the oxygen was removed so that OH– adsorbed, but lower potentials thermodynamically oppose the adsorption, leading to disappearance of the capacity peak. On either side of the capacity **peak,** the capacities were roughly **30** $\mu F/cm^2$.

Pseudocapacities were measured using the galvanostatic technique to discharge surface ***oxy*-**gen. Hydrogen had to be evolved briefly, the electrode brought to and held at the required oxygen potential, and the surface oxygen then measured by discharge. If this procedure was not followed, the pseudocapacities fell over some hours, and the surface oxygen could not be discharged with one pulse of current. This was ascribed to the slow adsorption of impurities on the electrode. Steady-state polarization measurements gave kinetic-limiting currents, with higher current values for those preoxidized electrodes which gave double-layer-capacity peaks.

No clear relation between amount of oxygen adsorbed and high-frequency double-layer capacity could be obtained, so the objective of the research could not be met. Double-layer capacity and pseudocapacity varied with thickness of oxide film produced on the platinum electrode by long periods of rest near oxygen evolution potentials. A relation between capacity and the presence of dissolved oxygen was found only at freshly preoxidized electrodes in acid solution. Presumably, this capacity was due to rapid adsorption-desorption of dissolved oxygen at a small number of very active sites, which were either poisoned with time or annealed out with time, since the capacity fell in a few minutes. The capacities of this peak or of that ascribed to hydroxyl adsorption in alkali were much too low to be due to adsorbed monolayers, which would give pseudocapacities at least an order of magnitude greater than those observed. Apart from this abnormal surface, double-layer capacities were independent of the presence of dissolved oxygen.

17.4.8 General Electric Co., Research on Low-Temperature Fuel Cells, February 1960 to November 1961

With the Teflon-bonded black electrodes used in the General Electric IEM cell, the theoretical cathode potential was obtained with anionic membranes soaked in strong KOH *(254).* With strong acid, the OCV was 1.05 to 1.07 volts (versus NHE in SE). After correcting for IR effects, the polarization at current densities from zero to 15 mA/cm^2 followed a Tafel Law, with about 0.35-volt polarization from theoretical at 15 mA/cm^2.

A confused mass of data from the work of General Electric and others is presented in a later report (257). The reactions involved are

$$H_2+\frac{1}{2}O_2+H_2O=2H^+(\text{anode})+2OH^-(\text{cathode})$$
$$H^++OH^-\rightarrow H_2O$$

The conclusion is reached that the "energy" of the fist reaction is the only one available. This concept is incorrect. The second reaction is a fast reaction chemically, both forward and backward, and is essentially at equilibrium at true zero-current conditions. If a reaction is at equilibrium, the free-energy change is zero and the ideal voltage of the cell must correspond to the free-energy change between the initial reactants and the final products. The concentration of OH– and H^+ will only affect the open-circuit potential when concentration gradients are present in the electrolyte which is, of course, covered by concentration polarization theory.

17.4.9 Conclusions From Oxygen Electrode Studies

The preceding sections show that the oxygen electrode reaction is not well understood and that contradictory data exist. Examination of the open literature (for example, the brief review by Breiter, ref. 17.11) confirms this impression. What is known and what is not known can be summarized as follows. Studies made on smooth metals indicate that platinum and palladium are the best oxygen catalysts in the low-temperature range. The performance of high-area diffusion electrodes cannot validly be compared with electrodes of lower area; active electrodes can be made from high-area carbons (carbon alone or silver catalyzed), but carbon or silver in solid form is not so good as platinum or palladium. The catalytic metals can be oxidized by external oxidation or by prolonged oxygen evolution. For platinum, the amount of oxygen which can be stripped from the surface by cathodic discharge depends on the oxidation potential and time, being up to 10 monolayers thick at potentials of 1.5 volts and about 1 monolayer at 1 volt (733). The question is in what state of oxidation is the surface of an oxygen-fuel-cell electrode. The active surface sites which are adsorbing reacting oxygen could be Pt, PtO, or PtO_n, the latter representing an oxidation layer several molecules thick. In all cases it should be remembered that H_2O is probably associated with the surface, and that reactions occur with solvation sheaths on all species, including the surface and surface transition states. The thick oxide layers will probably slowly lose oxygen with time, unless the potential is held above 1.2 volts; and some of the oxygen probably ionizes when cathodic current is drawn. The thick oxide film is a poor catalyst for oxygen adsorption and ionization (see sec. 17.4.5 and table 17.8). If the electrode is stripped free of oxygen by hydrogen evolution or by holding below 0.7 volt, the rate of ionization of oxygen is improved, although the electrode will not return to an OCV of 1.23 volts, which seems contradictory.

However, it has not been conclusively proved that a cathodic pulse to hydrogen evolution will remove all of the surface oxygen. In fact (sec. 17.3), at potentials near hydrogen evolution it has been suggested that the surface is covered with PtOH and is catalytic for hydrogen ionization (see sec. 17.3) according to $2PtOH+H_2\rightarrow 2PtOH+2H^++2e^-$. The evidence for this is that prior anodization increases the activity to hydrogen ionization considerably, although this could be due to the removal of adsorbed impurities, or due to roughening and production of active crystal-defect structures on anodization-cathodization. One point is clear: short-time, transient-state investigations on a surface which has just been heavily anodized probably measure rates at an abnormal surface, and the results cannot be extrapolated to long-term fuel-cell operation.

Irrespective of what surface is present during oxygen ionization, the reaction can be written, nonspecifically, as

$$O_2(g)\rightleftharpoons O_2(aq)$$
$$Pt^*+O_2(aq)\rightleftharpoons Pt[O]^*$$
$$Pt[O]^*+H^++e^-\rightleftharpoons \frac{1}{2}H_2O.$$

Pt* represents some undetermined state of the platinum surface, which may be oxidized, and Pt[O]* some undetermined chemisorbed surface complex of oxygen which is free to react. The theoretical OCV of the reaction is 1.23 volts at room temperature, irrespective of the steps or surfaces involved. It has been argued (ref. 17.12) that the actual potential is 0.98 because this is the potential of the reaction

$$PtO+2H^++2e^-\rightleftharpoons Pt+H_2O \qquad (17.14)$$

The argument is correct only for a deep oxide film entirely of PtO with the constant reaction enthalpy corresponding to bulk oxide, and even then it is implicit that ionization of dissolved oxygen, $O_2(aq)$, is so slow that a mixed potential weighted toward reaction (17.14) is obtained. As a thick layer of oxide builds up, the OCV would be expected to drift from 0.98 volt to higher values, since it is known that thicker layers have higher equilibrium potentials. The results discussed in section 17.4.5 showed that oxygen evolution rates at a given potential were much higher at a surface freshly cleaned by evolving hydrogen than at one which had time for the oxygen film to develop. Thus the oxide film is not the chemisorbed layer which acts as intermediate in the evolution-ionization reaction, since intermediate would be rapidly formed to a steady coverage at a given current density. The slowness of oxygen evolution on the oxided surface also indicates that the ionization of oxygen might almost cease as the film develops.

Oxygen electrodes usually need several tenths of a volt polarization to deliver useful cathodic current. One possible explanation is that the thick oxide film is unstable at the lower potentials, giving a relatively bare surface with a high rate of ionization. The process can be described by two alternative viewpoints:

$$
\begin{array}{llc}
(a) & Pt+\tfrac{1}{2}O_2 \rightleftharpoons PtO & E_0 \\
 & PtO+2H^+ +2e^- \rightleftharpoons Pt+H_2O & 0.98 \\
\hline
 & \tfrac{1}{2}O_2+2H^+ +2e^- \quad H_2O & 1.23 \\
(b) & PtO+2H^+ +2e^- \rightleftharpoons Pt+H_2O & 0.98 \\
 & \left.\begin{array}{r} Pt+\tfrac{1}{2}O_2 \rightleftharpoons Pt[O]^* \\ Pt[O.]^* +2H^+ +2e^- \rightleftharpoons Pt+H_2O \end{array}\right\} & 1.23
\end{array}
$$

Mechanism ***(a)*** states that oxide will build up until 0.98 volt is obtained and that further adsorption and ionization of oxygen is then so slow that 1.23 volts is not obtained. Appreciable cathodic current is not obtained until the potential is reduced below 0.98 volt, when adsorption of oxygen becomes fast enough to maintain the film of PtO. This mechanism can be called the oxide mechanism, since it considers the electrode to behave in the same way as, for example, a silver oxide battery electrode. In mechanism *(b)* the formation of PtO affects oxygen ionization by removing active platinum sites; the intermediate in oxygen ionization is $Pt[O]^*$ and not PtO.

The disadvantage of mechanism ***(a)*** is that it is implied that chemisorption of oxygen suddenly stops at 0.98 volt, whereas, thermodynamically, the potential should be able to reach 1.23 volts. If PtO is treated as a chemisorbed layer with Langmuir-type rate relations, then the ideal potential is 1.23 volts and the current density at a given polarization depends on the surface roughness, the activation energy for ionization, and the standard-state free energy of adsorption. The value of 0.98 volt then loses meaning. On the other hand, for mechanism *(b)* the rate equations for ionization are applied to the $Pt[O]^*$ intermediate, with the formation of PtO or PtO_n being a superimposed disturbing factor. The rate of formation of PtO_n could be slow, slower than oxygen ionization, but at potentials between 0.98 and 1.23 volts it might proceed to a steady state, giving reduced cathodic current due to the relative inertness to oxygen ionization of the film. A pronounced change in polarization characteristics would then be expected at near 0.98 volt, for any degree of surface roughness. An OCV of 0.98 volt might be a mixed potential of the reactions, with oxygen ionization matching the formation of PtO. From this line of reasoning, gold might be a catalytic electrode, since it loses its surface film at potentials nearer to 1.23 volts. However, the ionization rate on bare gold is so much lower than on platinum that the benefit of the absence of surface film is negated. Mechanism *(b)* seems more in accord with the available evidence.

Another question which has received much discussion is whether hydrogen peroxide is a necessary intermediate in the ionization of oxygen. The work of Yeager (sec. 17.4.2) and Bockris (sec. 17.4.6) indicates that H_2O_2 is a required intermediate in alkaline solutions. Their results also show that the further breakdown of peroxide at the electrode surface to give an overall four-electron process is not strongly (exponentially) voltage dependent, but depends mainly on catalytic decomposition. The formation of peroxide can be slow and activated at low-area electrodes, but for high-area electrodes it is fast, so that the controlling factor is the rate of decomposition of peroxide. When the concentration of dissolved peroxide at the surface has to build up to give sufficient activity for catalytic breakdown, an electrode inevitably suffers a sharp initial polarization. The activity can be very small, e.g., 10^{-9} mole per liter at 1.0 volt versus hydrogen in the same electrolyte, so that loss of peroxide by mass transfer away from the electrode at steady-state conditions is a small fraction of the total current passing. Thus, the process behaves as a four-electron transfer, but with considerable polarization.

Lingane (ref. 17.12) found that a freshly anodized-cathodized surface gave a four-electron process on galvanostatic discharge of dissolved oxygen at platinum, in alkaline solutions. This appears to be in direct contradiction to the previous results, since formation of high concentrations of free peroxide would have been observed as a lower transition time. The electrodes were, however, low-area electrodes, and the formation of peroxide was not reversible at the electrodes. Thus, it is not valid to calculate the HO_2^- concentration from the potential using the Nernst equation, as the polarization was undoubtedly activation polarization. It appears that the buildup of peroxide at the electrode, followed by catalytic decomposition, was not great enough to give observable mass transfer of peroxide away from the electrode over the transition time. The large activation polarization for the formation of peroxide placed the electrode at a potential at which peroxide was also reacted. The results shown in figure 17.3, obtained under similar conditions but using steady-state cathodic current, show significant percentage conversion to peroxide, unless the electrode is poisoned. The conversion is smaller at more cathodic potentials, so possibly the galvanostatic technique used by Lingane was not sufficiently sensitive to measure the relatively small amount of peroxide produced over the entire voltage trace. Alternatively, the heavy anodization used by Lingane may have left the surface in an abnormal condition even after brief periods of hydrogen elolution.

The reaction can be written as

$$M[O_2]^* + H_2O + e^- \rightleftharpoons M[HO_2]^* + OH^-$$

$$\begin{tikzcd}
M[HO_2]^* + e^- \arrow[r, shift left, "i_1"] \arrow[d, shift right, "i_2"'] & M + HO_2^-(aq) \arrow[l, shift left] \arrow[r, "\text{diffuse}", "\text{away}"'] \arrow[d, shift left] & {} \\
M[O]^* + OH^- \arrow[u, shift right] \arrow[r, shift left, "i_3"] & M[HO_2]^{**} + e^- \arrow[l, shift left] \arrow[u, shift left] &
\end{tikzcd}$$

where the asterisk denotes surface complexes of undetermined form (although Yeager showed that oxygen was not dissociately adsorbed on carbon). Whether the intermediate in the electrochemical formation of peroxide is the same as that for the decomposition of free peroxide has not been determined, so they have been represented as two distinct species. A four-electron (per oxygen molecule) reduction is obtained via i_2 or i_3, although when the intermediate is the same for both paths, they reduce to one common path and i_3 is zero.

An electrode may have the Nernst potential corresponding to reaction i_1 in equilibrium, but i_2 and/or i_3 can be fast enough to convert most of the peroxide formed to a four-electron reduction. This is what appears to happen for high-area active electrodes. At low-area electrodes, reaction i_1 is not at equilibrium at high current densities and activation polarization is present. In this case the concentrations of free peroxide can be small even at high polarization and a two-electron process is observed if further reduction of peroxide is by path i_3 only; that is, i_2 is not present (on carbon, for example). If i_2 is present, the surface complex $M[HO_2]^*$ can build up to high Concentrations and give four-electron reduction by i_2 even if the free-peroxide concentration is low. A method for deciding whether path i_3 exists at catalytic electrodes would be to pass cathodic current at irreversible polarizations and add different concentrations of peroxide. If i_3 did not exist, the efficiency of production of peroxide would be unaffected; if i_3 did exist, the efficiency of production of peroxide would be lower at higher peroxide concentrations and might even be negative.

In acid solution, the equilibrium potential of peroxide formation is near 0.8 volt versus SHE. Clearly the production of HO_2^- and OH^- is not favored by the positive potential and a change of mechanism will result. The corresponding mechanism using hydrogen ion is

$$M[O_2]^* + H^+ + e^- \rightleftharpoons M[HO_2]^*$$

$$M[HO_2]^* + H^+ + e^- \rightleftharpoons M + H_2O_2.$$

However, if oxygen adsorbs dissociatively, a surface peroxide complex would not be expected and the mechanism would be

$$M[O]^*+H^++e^-\rightleftharpoons M[OH]^*$$
$$M[OH]^*+H^++e^-\rightleftharpoons H_2O.$$

The evidence from section 17.4.6 supports this mechanism, although free peroxide was also produced. Tyco Laboratories, Inc., concluded in its study of oxygen electrodes (sec. 17.4.5) that the reaction occurred via a peroxide intermediate, but this conclusion was based mainly on the fact that current density was low until potentials were reached at which free peroxide was reduced. Active fuel-cell electrodes give a four-electron process, with very little production of peroxide in acid solution. This does not rule out a peroxide intermediate, since it implies only that the further reduction of peroxide is rapid enough to maintain very low concentrations of free peroxide or surface peroxide; however, catalytic decomposition of peroxide is not favored in strongly acid solutions (see sec. 17.4.3).

The oxygen electrode in acid does not follow the Nernst potential with respect to H_2O_2 concentration; therefore, if surface peroxide is a necessary intermediate, it appears to undergo further reduction much more rapidly than it desorbs to free peroxide. Existing information does not reveal whether a surface-peroxide intermediate is necessary or not. The slower breakdown of peroxide in acid solution indicates that the surface-peroxide complex may break down slowly, but does not prove this, since the effect may be due to slow rates of peroxide adsorption. If this is so, then the current has to be supported by the other mechanism. At present, researchers cannot predict from ***apriori*** information why the formation of $M[HO_2]^*$ should be slow or its stability high in acid solution, compared to alkali solution; there is little reason to expect that a material will dissociatively adsorb oxygen in acid but adsorb molecular oxygen in alkali. Probably both types of adsorption occur and M[O] is relatively stable to reduction. When oxygen ionization via molecular oxygen and surface peroxide is slow, M[O] is reduced, but at slower rates than those for ionization in alkali solutions.

In neutral solution, the reversible potential is not sufficiently negative to ionize water and oxygen to peroxide and hydroxyl ions at high rates. It is sufficiently negative to drive hydrogen ion plus oxygen to water, but the concentration of hydrogen ion is low, again **giving** low rates. Therefore, neutral solutions will probably not perform so satisfactorily as strong acids or bases.

With respect to open-circuit potential of the oxygen electrode, the proposal that the potential is due to the reaction $MO+2H^++2e^-\rightleftharpoons M+H_2O$, or the reaction $MO+H_2O+2e^-\rightleftharpoons M+2OH^-$, has already been discussed. For carbon electrodes in alkali, the OCV has been conclusively proved to correspond to the equilibrium $O_2+H_2O+2e^-\rightleftharpoons HO_2^-+OH^-$. In section 17.4.6 it is claimed that the OCV in acid is due to the dipole moment of adsorbed oxygen, while in section 17.4.5 it is ascribed to a mixed potential of $H_2O_2\rightarrow O_2+2H^++2e^-$, and $H_2O_2+2H^++2e^-\rightarrow 2H_2O$. The arguments are somewhat academic, since they all reduce to the fact that the ionization of oxygen is not sufficiently rapid to give 1.23 volts OCV when side reactions are present, unless the surface contains excess electrochemically evolved oxygen, which is an abnormal and unsteady condition for fuel-cell operation.

There is also disagreement on whether the fractional coverage of active sites with adsorbed oxygen is near 1 or much less than 1. This is complicated by the growth of oxide layers which are probably not the active sites, since the thicker the layers, the less active is the electrode for dissolved oxygen ionization. Little work has been done on the rate of adsorption of oxygen from solution, although this does not seem to be a primary rate-limiting factor. The energies of adsorption of oxygen on electrodes are not well known and they are always determined by application of the Clapeyron-Clausius equation to adsorption isotherms at various temperatures. Two major objections can be made to this technique. First, results must be compared at the same value of *8*, the fractional surface coverage. When the adsorbed oxygen contains adsorbed molecules of different energies, the ratio of the different types of molecule will change with temperature, so that the enthalpy deduced will be an empirical mean for different combinations of adsorptions. Second, the enthalpy of reaction is usually determined at various surface coverages, without determining the corresponding entropy. Surface reactions almost invariably show a compensation effect in which the variation of heat of reaction is almost balanced by variation in the entropy term, to give nearly constant standard-state free energies. Until this phenomenon is understood, no meaningful conclusions can be drawn from enthalpies of adsorption alone. Similarly, the mechanisms of reaction probably cannot be deduced from Tafel slopes alone. In many cases the slopes are not well defined and vary with changes in surface treatment, electrolyte, and time; frequently several reaction paths give similar Tafel slopes, and more direct evidence than steady-stage voltage-current relations must be obtained before a specific mechanism can be considered as proved.

17.5 CONCLUSIONS

Little useful information has been yielded by the foregoing experiments. Practical electrodes are developed by trial and error, using the general concepts that an electrode must have *(a)* high catalytic area, *(b)* good mass-transfer properties, and *(c)* low ohmic resistance. Experience shows that platinum and platinum-palladium alloys are the best catalysts for hydrogen; nickel is suitable in alkali at higher temperatures. Similarly, platinum is best for oxygen electrodes, with silver and nickel oxide suitable in alkali at higher temperatures.

Oxygen ionization is basically a much slower reaction than hydrogen ionization. Thus, a hydrogen-oxygen fuel cell with anode and cathode of comparable activity will experience more activation polarization at the cathode. A platinum cathode in contact with oxygen probably tries to reach **1.23** volts, but at potentials greater than about 0.8 volt, oxide layers start to form on the electrode. At about **1.0** volt the oxide film, formed over a long time, is thick enough to slow the rate of oxygen ionization considerably, compared to that of bare platinum, and the rate becomes so slow that secondary reactions interfere to give an OCV of about **1.0** to **1.1** volts. Gold does not form **a** low reactivity film until about **1.25** volts, but the rate of oxygen ionization on gold is much slower than on platinum.

In acid solution, hydrogen probably ionizes in the following steps, which may each consist of several steps:

$$H_2(aq) + 2Pt[H_2O] \rightarrow 2Pt[H] + 2H_2O$$

or

$$H_2(aq) + Pt[H_2O] + Pt[H] + H^+ . H_2O + e^-$$

and

$$Pt[H] + 2H_2O \rightarrow Pt[H_2O] + H^+ . H_2O + e^-.$$

In alkaline solution

$$H_2(aq) + 2Pt[H_2O] \rightarrow 2Pt[H] + 2H_2O$$

or

$$H_2(aq) + Pt[H_2O] + OH- + Pt[H] + 2H_2O + e^-$$

and

$$Pt[H] + OH^- + H_2O \rightarrow Pt[H_2O] + H_2O + e^-$$

All surface complexes have some bonding with further water molecules.

Oxygen ionizes, in alkaline solution, by the steps

$$O_2(aq) + Pt[H_2O] \rightarrow Pt[O_2 \cdot H_2O]$$
$$Pt[O_2 \cdot H_2O] + e^- \rightarrow Pt[HO_2] + OH^-$$
$$Pt[HO_2] + H_2O + e^- \rightarrow Pt[H_2O] + HO_2^-$$

and

$$Pt[HO_2] + 2H_2O + 2e^- \rightarrow Pt[H_2O] + 2OH^-.$$

The mechanism in acid solution is not understood, but may involve dissociative adsorption of oxygen.

17.6 REFERENCES

17.1. PARSONS, R.: Trans. Faraday Soc., London, vol. 54, p. 1053, 1958.

17.2. AUSTIN, L. G.: Proc. Inst. Elec. and Electron. Engrs., vol. 51, pp. 820-837, 1963.

17.3. BOND, G. C.: Catalysis By Metals, Academic Press, London, 1962.

17.4. EISCHENS, R. P.; AND PLISKIN, W. A.: Advances in Catalysis, vol. X, 1958.

17.5. TERENIN, A.; AND ROW, L.: Infrared Spectra of Nitric Oxide Absorbed on Transition Metals, Their Salts and Oxides. Spectrochim. Acta, vol. 11, 1959, pp. 946–957.

17.6. SANDLER, Y. L.; AND GAZITH, M.: Surface Properties of Germanium. J. Phys. Chem., vol. 63, 1959, pp. 1095–1102.

17.7. FARKAS, A.: Orthohydrogen, Parahydrogen and Heavy Hydrogen. Cambridge University Press, 1935.

17.8. FRUMKIN, A. N.: Advances in Electrochemistry and Electrochemical Engineering. Interscience Pub., New York, vol. 1, 1961, p. 71; vol. 111, 1963, pp. 287–391.

17.9. BERL, W. G.: Trans. Electrochem. Soc., vol. 83, 253, 1943.

17.10. LEVICH, V. G.: Physico-Chemical Hydrodynamics. Prentice-Hall, 1962, pp. 327–336.

17.11. BREITER, M.: Advances in Electrochemistry and Electrochemical Engineering. Vol. I, P. Delahay, ed., Interscience Pub., 1961, p. 123.

17.12. LINGANE, J. J.: Chronopotentiometric Study of Oxygen Reduction at a Platinum-Wire Cathode. J. Electroanal. Chem., vol. 2, 1961, pp. 296–309.

CHAPTER 18

Theories of Porous Electrodes

18.1 INTRODUCTION

After much speculation about gas-diffusion electrodes, there is still no definite answer to the question of their mode of operation. Most descriptions of the process in the reports reviewed in this book take the following form: "Reactant gas diffuses through the pores of the electrode and reacts electrochemically at the gas-electrolyte-electrode interface." Nonspecific descriptions of this kind are of little use in determining how an electrode can be improved by changes in structure. However, considerable progress has been made over the last few years in developing more precise and useful descriptions of the principles of gas-diffusion electrodes. A major difficulty is that practical electrodes have complex structures, and theories based on simple geometries will probably not entirely explain electrode performance. Solutions of the combined equations of mass transfer, kinetics, and electronic and ionic conduction are algebraically complex and must often be computed with several adjustable unknown parameters. Under these circumstances it is possible to fit limited experimental data by choosing appropriate values for the unknown parameters, but this is not satisfactory proof of the validity of the models chosen. Direct experimental evidence for the validity of a model is usually difficult to obtain, especially for electrodes with very small pores.

Three distinct systems will be discussed in this chapter: gas-diffusion electrodes, flooded-diffusion electrodes, and flowthrough electrodes. A flooded-diffusion electrode is defined as a two-phase (liquid-solid) porous-diffusion electrode. A porous electrode immersed in electrolyte containing dissolved reactant is a flooded electrode when the fuel electrolyte diffuses into, and reacts within, the interior of the electrode. A flowthrough electrode is also two-phase, but the electrolyte containing dissolved reactant is forced through the electrode, eliminating diffusion as the major mass-transfer factor.

18.2 GAS-DIFFUSION ELECTRODES: THIN-FILM MODEL

This model is attributed to **C.** Wagner, although his discussion was not published. The work of Sama (*447*), while extremely crude experimentally, indicated that when a copper cathode was pulled out of KOH into an atmosphere of oxygen it gave higher currents as more plate was exposed. Plate which was not covered with electrolyte tarnished. A thin film of electrolyte was estimated to extend up the plate about one-eighth inch beyond the visible meniscus. The first scientific investigation of the model was given by F. G. Will (ref. 18.1), who used partially submerged platinum wires as anodes in sulfuric acid, with an atmosphere of hydrogen around the exposed portion of the wire. A thin film of electrolyte was observed to creep up the wire. Hydrogen dissolved and diffused through this thin film and reacted at the platinum surface covered by the film. Figure 18.1(*a*) illustrates the thin film on the wire and the mode of operation. Figure 18.1*(b)* shows an idealized geometry for the thin film within a porous electrode. The current-voltage curves for the wire (assuming a long film about 1 micron thick) agreed with those predicted from a mathematical treatment of the model.

Some insight into the formation of thin films in porous electrodes was obtained as follows (Pennsylvania State University, *487).* When an ordinary fine-fritted-glass-filter disk was placed in a shallow layer of densely colored solution, the

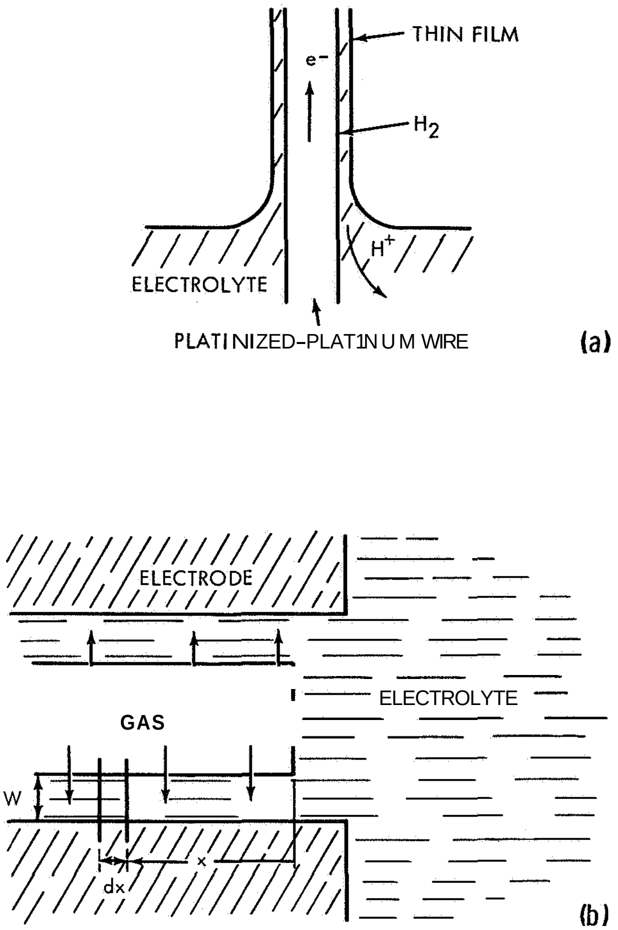

(*a*) Will (ref. 18.1) observed that a thin film of electrolyte (1 micron) was retained on the surface of a platinized-platinum wire when it was withdrawn from sulfuric acid electrolyte. Hydrogen dissolved in and diffused through the film and reacted at the electrode surface.

(*b*) The comparable idealized picture for a cylindrical pore in a vertical electrode.

FIGURE 18.1.—Thin-film models for gas-diffusion electrodes (not to scale).

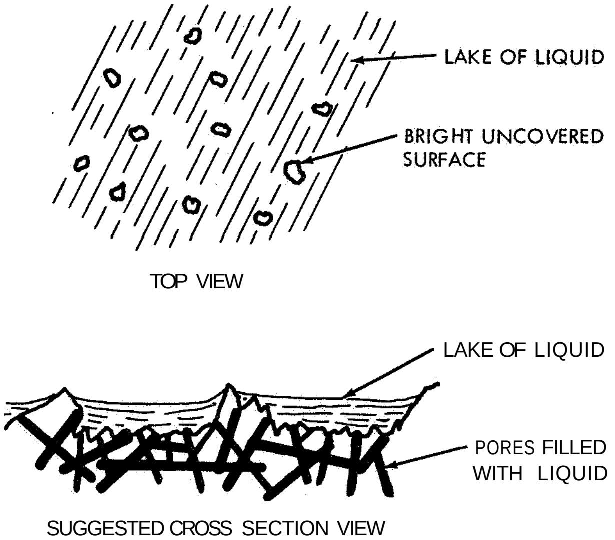

FIGURE 18.2.—Illustration of surface of porous material filled with liquid by capillary action.

liquid rapidly filled the frit by capillary action. Microscopic observation of the surface revealed a lake of fluid with a few islands of bright glass. This is illustrated in figure 18.2 (top view); a possible cross-sectional representation is also given (lower view). Although the surface is not completely covered by fluid, the total length of the boundaries of solid-liquid gas is considerably less than would be expected if the fluid rose only to the top of each pore. An ordinary plastic household sponge was also used as a simulation of a porous electrode. The sponge appeared to the naked eye very much like porous-electrode materials (especially carbon) when viewed under a microscope. A wide range of hole sizes was exhibited. Examination of a large hole revealed that its surface contained many smaller holes. The sponge was placed in the solution, and, although the larger surface holes were not filled, capillary action again filled the sponge with fluid to the surface. Microscopic examination of the inside surface of one of the empty holes showed a picture similar to that in figure 18.2. The surface was almost completely covered, with only a few bits and threads of uncovered material projecting from the fluid.

Although the above experiments were performed on relatively macroscopic systems, it seems reasonable that the fine-pore systems of fuel-cell electrodes will behave in a similar fashion, since surface tension effects become stronger as pore size decreases. Figure 18.3 may be a more realistic representation of the thin-film model. Differential gas pressure would be required to keep the coarser pores from filling with fluid. The mechanism of operation would then be: *(a)* reactant gas diffuses along a pore, through an atmosphere of inert impurities, reaction products (if any), water vapor, and the reactant gas itself; ***(b)*** reactant dissolves in the surface of the thin film of electrolyte at a rapid rate, yielding concentrations of dissolved gas in the surface layer almost equal to equilibrium concentrations; **(c)** dissolved reactant gas diffuses

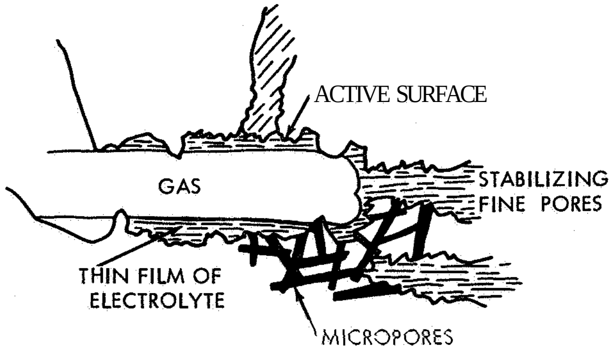

FIGURE 18.3.—Illustration of thin-film model applied to practical pore systems.

across the thin film and to the active surface area (area of both surface roughness and internal microporosity) and reacts; and *(d)* the ionic current flows through electrolyte which extends through the coarser pore layer without filling the coarse pores. The effective resistivity of this electrolyte based on the total electrode cross-sectional area is not known.

Considering a single pore, as shown in figure 18.1(*b*), it may be objected that the film observed by Will is not relevant, since a pore of small diameter penetrated by electrolyte will be rapidly and completely filled by capillary action. However, many practical electrodes have double-layer structures in which the bulk electrolyte meniscus is stabilized at the junction between a fine-pore layer and a coarser-pore layer. Examples of these are the Bacon electrode, the Justi "double skeleton katalyst" (D.S.K.) electrode, electrodes pressed against an ion-exchange membrane, and electrodes of powdered metal pressed against a microporous electrolyte matrix. Differential gas pressure is maintained between the gas side of the electrode and the electrolyte side; the coarser pores are kept from filling completely with fluid, while the fine pores, with stronger capillary forces, are kept full. When a microporous matrix is used, the amount of electrolyte is controlled to fill the electrolyte matrix without filling the electrode pores.

This model predicts that the reaction occurs at the surface of the coarse-pore layer. **A** catalyst, then, is necessary in this layer. It also predicts that the coarse-pore layer must be sufficiently thick to give an extended thin film. Otherwise a low mass-transfer-limited current will be obtained (see eq. (18.5)) because of insufficient area for diffusion of dissolved gas. Both of these requirements are found in results reported by Dittman, Justi, and Winsel (ref. 18.2). They found that for an electrode consisting of a coarser pore layer not flooded with electrolyte next to a finer pore layer which was flooded, then *(a)* catalyst was not required in the fine-pore layer, which behaved as an inert stabilizer, and *(b)* a minimum thickness of 0.5 millimeter of coarser pore layer was required to give the maximum current at any voltage.

A study of the formation of thin films on vertical wires is quoted in 675. It was found that the fluid on the surface of a wire drawn out of an electrolyte drained to a stable state over a period of about 12 hours. The stable thin film extended to over 3 centimeters above the bulk meniscus and was about 1 micron thick near the meniscus, decreasing to 0.2 micron at 3 centimeters. The physical reason for the presence of the stable thin film was not known.

Mathematical treatments of the thin-film model have varied in complexity. It is usually assumed that the film is long (l) compared to its thickness (W), so that diffusion of dissolved gas is linear across the film, while transfer of ionic species is linear along the film. For a vertical plane (normal to the x-axis) at X in figure 18.1(*b*), the steady mass transfer of an ionic species through the plane, along the x-axis, is

$$\text{Rate per unit area} = D(dR/dx) + RZu(dV/dx) + R\nu. \quad (18.1)$$

D is the effective diffusion coefficient of species R, R is the concentration of the species, Z is its charge, u its electrical mobility per unit valence charge, dV/dx is the potential gradient at X, and ν is the velocity of bulk flow along the x-axis. Similar equations have to be written for every component present in the electrolyte. Clearly, the algebraic treatment of several simultaneous equations of this kind is difficult and it is often assumed that (ref. 18.3)

$$\text{Rate per unit area} = \bar{D}dR/dx$$

or

$$i = nF\bar{D}dR/dx \quad (18.2)$$

where $\bar{D}$ is a mean effective diffusion coefficient which includes the effect of migration (the dV/dx term), of the same order of magnitude as the true diffusion coefficient. Similarly, application of Ohm's law at the plane gives

$$i=(1/\rho)dV/dx \tag{18.3}$$

where ρ is the effective specific resistance of the electrolyte in the thin film. In general, ρ will change along the film (and should, therefore, be within the differential) when the composition of the electrolyte changes along the film as current is drawn.

Considering element dx at plane x, the rate of transfer of dissolved gas to the submerged electrode surface is

Rate per unit cross section

$$=(DA/W)(H_b-H_s)dx$$

or

$$di=(DA/W)(H_b-H_s)dx \tag{18.4}$$

D is the diffusion coefficient of dissolved gas; A is the surface area, exposed to gas, of the thin film within unit volume of electrode; therefore, Adx is that within volume dx; W is the mean thickness of the film; H_b is the concentration of dissolved gas at the film surface; and H_s is that at the submerged electrode surface. When the electrode is l thick, i.e., the length of the thin film along the x-axis is t, the limiting current density of the electrode due to mass transfer of reacting gas through the film is

$$i_L=(nFDAt/W)H_b. \tag{18.5}$$

A and W are unknown and difficult to measure directly. The equilibrium solubility of gas, H_b, may vary along the film as electrolyte composition varies.

Finally, the rate of the electrochemical reaction at the surface can be expressed as

$$di=F(i_0, H_s, \text{pH}, \eta, P_s, \text{etc.})Sdx. \tag{18.6}$$

$F(i_0, H_s, \text{pH}, \eta, P_s, \text{etc.})$ is a function which gives the relation between electrochemical rate and concentration of reactant, pH, polarization η, concentration of product, etc. S is the reactive electrode surface area per unit volume; it is not necessarily equal to A, since the macropore surface may have microroughness or may contain micropores of high area.

The combined mass transfer, ohmic, and electrokinetic equations given above are solved with appropriate boundary conditions for specific systems. Analytical solutions can be obtained only by using restrictive assumptions, which depend on the system. For example, the reaction of hydrogen in strong acid electrolytes at a highly reactive electrode could be assumed to be reversible, the values of H_b and ρ to be invariant along the film, and the concentration of the product of reaction, H^+, not to change much along the film. Table 18.1 gives a list of treatments of the thin-film model, indicating some of the assumptions made. Where analytical solutions are obtained, they are usually based on equation (18.6) in the form

$$i=i_0\{(R/R_b)^r \exp(\alpha\eta/b) - (P/P_b)^p \exp[-(1-\alpha)\eta/b]\}, \tag{18.7}$$

where i is the current density at some differential element of area in the electrode; i_0 is the exchange current density on the same basis; R is the reactant concentration; R_b is the bulk or equilibrium reactant concentration for which i_0 is determined; P and P_b are the corresponding values for product concentration; r and p are the orders of reaction with respect to R and P; α is the transfer coefficient (often assumed equal to $\frac{1}{2}$); η is polarization in volts; and b/α is the natural logarithm Tafel coefficient in volts ($=RT/F\alpha=0.06/2.3\alpha$ volts at room temperature).

The general picture which emerges from these treatments is as follows. For long films (large t), the ohmic drop in the film accelerates the electrochemical rate so that reaction is concentrated at the electrolyte end of the pores. Since all the ions to support current have to pass through the pore mouth at this end while only a few reach the other end of the pore, the ohmic effect is highest at the electrolyte end. The high rate at this end reduces the concentration of hydrogen at the metal surface to zero, so that mass transfer of hydrogen across this section of the thin film is limiting. The situation is illustrated in figure 18.4. No analytical solution has been given to express current as a function of voltage over a complete range of current densities. The following approximation (487, or ref. 18.8) serves to illustrate the important features

$$i=[(2nFDH_bA/W\rho)(\eta_s-\eta_0)]^{\frac{1}{2}}, \tag{18.8}$$

TABLE 18.1.—*Treatments* of *Thin-Film* *Model*

Author	References and reports	System and assumptions	Results
Will, F. *G*.	18.1	Vertical Pt wire, H_2, H_2SO_4. Reversible electrochemical reaction, dissolved H_2 mass transfer and ohmic effects.	Analytical solution for long (semi-infinite) film. Experimental verification.
Austin, L. *G*.	*483*	Porous electrode, H_2, acid. Reversible reaction, H_2 mass transfer and ohmic effects.	Analytical solution for finite film length, low polarization. Analytical for long film, similar to Will's result.
		Porous electrode, H_2, acid. Irreversible reaction; uniform H_2 mass transfer, ohmic effect.	Analytical.
		Porous electrode, H_2, alkali. Reversible and irreversible, uniform H_2 mass transfer, OH^- mass transfer and ohmic effects.	Analytical.
Iczkowski, R. P.. . . .	18.4	Single-pore 5-micron radius, H_2 on nickel, NaOH. Reversible, irreversible. H_2, OH– mass transfer and ohmic effects. Allowance for concentration dependence of H_2 solubility, but not diffusion coefficient.	Analytical for low polarization. Computed for complete polarization range.
Rockett, J. A...	18.5	Bacon-type electrode, O_2, KOH. All effects considered.	Computed, matched to experimental results by selecting parameters to give best fit (only abstract available).
Bennion, D. N..	*674*	Vertical Ag or Ni wire, O_2, KOH. All effects considered.	Computed results. Some experimental verification.
Katan, T., et al.. . .	18.6	Parallel tubular pores, O_2, KOH. Irreversible. Constant solubilities and diffusion coefficient.	Analog computer solutions.
Austin, L. G., et al.	*487* (also, 18.7)	Porous electrodes. Irreversible. Mass transfer and ohmic effects, assuming constant diffusion coefficients and conductivity.	Approximate analytical solutions for long films.

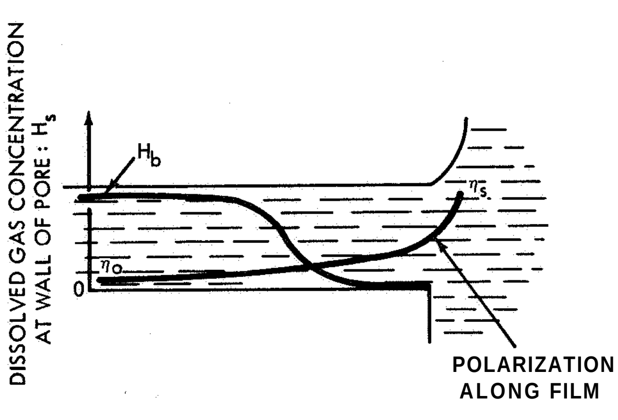

FIGURE 18.4.—Dissolved gas concentrations at pore wall, for a thick electrode.

where i is current density; η_0 is polarization at the gas entry face and is activation polarization; η_s is the total polarization; and $\eta_s-\eta_0$ is the extra polarization produced by mass transfer and ohmic effects through the thin film (see fig. 18.4). The equation only applies when the current density is not near the limiting current density given by equation (18.5). It can be seen that a high value of i at a given η_s is obtained when activation polarization is low (small η_0), when the diffusion coefficient of dissolved gas is high (large D), when the equilibrium concentration of dissolved gas is high (large H_b), when the specific area of the thin film is high (large A), when the mean thickness of the film is low (small W), and when the overall electrolyte resistivity of the thin film is low (small ρ). The amount of film electrolyte in unit volume of electrode is AW and the effective resistivity is

$$\rho=\rho' q/AW \qquad (18.9)$$

where ρ' is the electrolyte resistivity and q is a tortuosity factor greater than 1. In addition, the thickness of the electrode must be great enough to give a large limiting current (large t).

For short, thin films the concentration gradient of hydrogen at the wall of the pore (solid-liquid interface) is not so pronounced (ref. 18.4). The situation is as shown in figure 18.5. In this case, it can be assumed as a rough approximation that a mean value can be used for the gas concentration at the wall of the pore. The combined equation for ohmic and kinetic effects is then

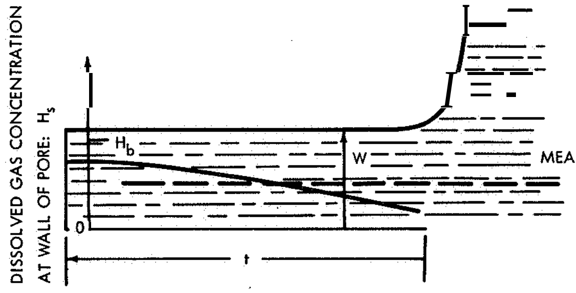

FIGURE 18.5.—Dissolved gas concentration at pore wall, for a thin electrode.

$$d^2\eta/dx^2=\rho S i_0\{(H_s/H_b)^h \exp(\alpha\eta/b) - \exp[-(1-\alpha)\eta/b]\}. \qquad (18.10)$$

For an irreversible reaction and constant ρ, assuming H_s to be constant along the pore, the solution leads to *(483)*

$$i=(H_s/H_b)^h(i_0 St)\exp(\alpha\eta/b) \qquad (18.11)$$

at low current density; at higher current density

$$i=[(2i_0 Sb/\alpha\rho)(H_s/H_b)^h]^{1/2}\exp(\alpha\eta/2b). \qquad (18.12)$$

Since H_s was assumed constant

$$i=(nFD\,At/W)(H_b-H_s), \qquad (18.13)$$

and from equation (18.5)

$$\eta=(2.3b/\alpha)\log[i/(1-i/i_L)^h]-(2.3b/\alpha)\log[i_0 St] \qquad (18.14)$$

or

$$\eta=(2.3b/\alpha)\log[i^2/(1-i/i_L)^h]-(2.3b/\alpha)\log[2i_0\,Sb/\alpha\rho], \qquad (18.15)$$

whichever gives the greater polarization, where

$$i_L=nFDAtH_b/W.$$

Note that $2.3b/\alpha$ is the normal Tafel coefficient of the electrochemical reaction.

The shape of the voltage-current curve predicted from equations (18.14) and (18.15), and the magnitude of the limiting currents, can be discussed by selecting some typical values. An electrode constructed of particles about **30** microns in diameter would have a thin-film specific area, A, of about 10^3 cm²/cm³. For concentrated electrolyte the solubility of reactant gas, H_b, is about 10^{-7} g-moles/cm³ at 1 atmosphere. For hydrogen, which has an unusually high diffusion coefficient, D can be taken as 10^{-5} cm²/sec in concentrated electrolytes. The electrode thickness, t, can be taken as 0.1 centimeter. The principal uncertainty is the value of W (the mean film thickness), but experimental evidence suggests it is of the order of 0.2 to 1 micron, and a value of 0.5 micron can be used. The limiting current density is then 400 mA/cm². A thin-film 0.5 micron thick and 1000 square centimeters in area is 0.05 cubic centimeter of electrolyte volume. In a porous electrode, the actual volume of electrolyte may be several times this, but the conductivity along the x-axis is reduced by tortuosity effects; therefore, the effective resistivity can be taken as about 1/20 of the normal electrolyte resistivity, giving a value of ρ of about 100 ohm-cm. The value of $i_0 S$ depends on the electrochemical reaction, the development of active microarea on the electrode particles, and the film area. For illustration, the Tafel coefficient can be taken as 0.12 volt, i_0 as 1 mA/cm², and S as 10^4 cm²/cm³. Figure 18.6 shows the result (taking the order of reaction with respect to dissolved gas as one, $h=1$), and also shows higher activation polarization when $i_0 S$ is tenfold lower.

If an ion is required for the reaction (e.g., $[H]+OH^- \rightarrow H_2O+e^-$, or $[O]+2H^+ \rightarrow H_2O+2e^-$), then a concentration gradient of the ion exists along the thin film, with the highest concentration at the pore mouth opening to the elec-

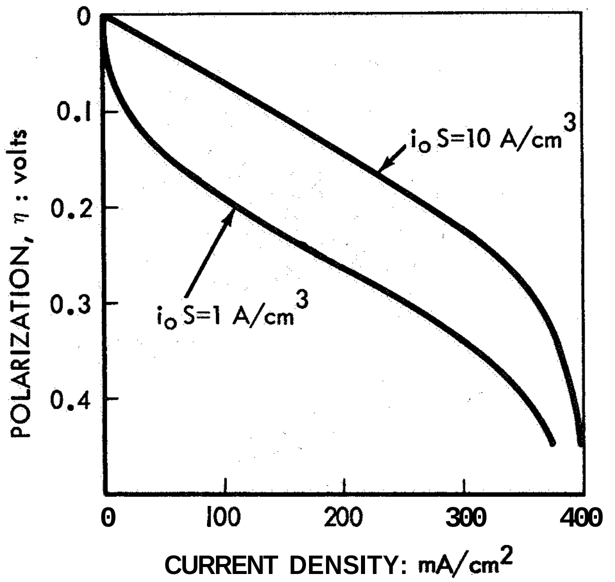

FIGURE 18.6.—Current-voltage relation for equation (18.15).

trolyte. Assuming, as before, that H_s is almost constant along the pore, it can be shown *(483)* that the combined equation for ion mass transfer and kinetic effects leads, for irreversible reaction, to

$$i = [i_0 SnFD_c C_b (H_s/H_b)^h]^{\frac{1}{2}} \exp(\alpha\eta/2b), \qquad \textbf{(18.16)}$$

where D_c is the effective diffusion coefficient of the ion along the thin film (based on unit cross section of electrode and allowing for migration effect),and C_b is the concentration of the ion at the pore mouth. This is used in place of equation *(18.12)* and the development as before gives an equation similar to equation *(18.15)*:

$$\eta = (2.3b/\alpha)\log[i^2/(1-i/i_L)^h] - (2.3b/\alpha)\log [i_0 SnFD_c C_b]. \qquad (18.17)$$

The shape of the current-voltage curve is identical to that shown in figure *18.6.* Whether equation *(18.15)* or equation *(18.17)* applies depends on the ratio

$$\phi = \rho nFD_c C\alpha/b. \qquad (18.18)$$

If ϕ is greater than *5,* equation *(18.15)* applies; if ϕ is less than *0.5,* equation *(18.17)* applies; and if ϕ is near *2,* the equations give identical results (ref. *18.8).* The effective resistivity of the thin film is higher than that of unit volume of electrolyte (because a much smaller volume of electrolyte is present in unit volume of electrode and because of tortuosity effects), but D_c is lower than normal diffusion coefficients by the same factor; therefore, ρD_c can be replaced by $(\rho D_c)_{\text{normal}}$. For example, assuming $\rho = 5$ ohm-cm, $D_c = 10^{-5}$ cm^2/sec, $n = 2$, $C = 5$ *M* (5×10^{-3} g-mole/cm^3), and $b/\alpha = 0.12/2.3$, then ϕ is *2.3.* In this case, both ohmic and ion mass-transfer effects are operative with the kinetic effect. Under these conditions the two equations give the same result and it is immaterial which is used.

18.3 GAS-DIFFUSION ELECTRODES: SIMPLE-PORE MODEL

The simplest mode of operation which can be envisaged for a gas diffusion electrode is illustrated in figure *18.7.* Gas dissolves in the electrolyte and diffuses along the pore, reacting at the pore walls. Assuming linear diffusion along the pore axis, it is readily shown *(483)* that

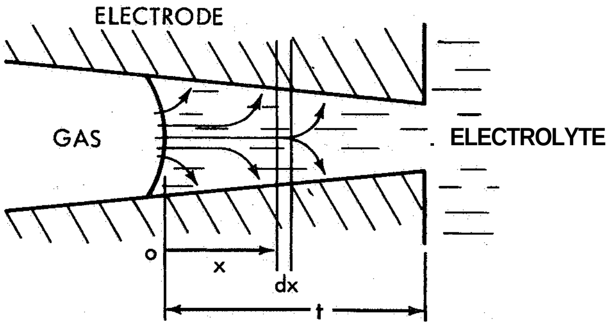

Gas dissolves in the electrolyte and diffuses to the pore walls. The mean diffusion path is smaller for small-pore radius, giving higher current densities per unit area of pore cross section.

FIGURE 18.7.—The "simple pore" model.

$$\eta_t - \eta_0 = i\rho t - \rho nFD(H_0 - H_t). \qquad \textbf{(18.19)}$$

H_0 is the concentration of dissolved gas at $x=0$, H_t that at $x=t$. As before, i is current density based on unit cross section of the electrode, and ρ and D are effective values on this basis. The second term on the right-hand side of equation *(18.19)* is easily estimated, since ρD can be replaced by $(\rho D)_{\text{normal}}$. For $\rho = 5$ ohm-cm, $D = 10^{-5}$ cm^2/sec, $n = 2$, and $H_0 = 10^{-7}$ g-moles/cm^3, the maximum value of the term (when $H_t = 0$) is 10^{-6} volt. Clearly this term is negligible even when the dissolved gas concentration is much higher. The physical meaning is that the polarization along the pore is small in the region in which the concentration of dissolved gas decreases to zero. Hence, polarization along the pore is appreciable only when the gas reacts in a thin layer near the pore mouth; the ionic current flows the whole length of the pore, giving ohmic polarization of ipt.

In general, at a plane at X in the pore, linear mass transfer and ohmic relations are $i = nFDdH/dx$ and $i = (1/\rho)d\eta/dx$; therefore

$$\Delta\eta = \rho nFD\Delta H. \qquad (18.20)$$

Thus the potential change, $\Delta\eta$, which occurs as reactant concentration changes, can be calculated. Substitution of values for ρ, D, and H_0 again shows that $\Delta\eta$ is very small over the region in which the gas is utilized. Since polarization is constant along the pore in the region in which gas is reacted, the analysis given in section 18.5 can be used. The penetration of dissolved gas along the pore is

$$p = 3nFDH_0/i. \qquad \mathbf{(18.21)}$$

For $n=2$, $D=10^{-5}$ cm^2/sec, $H_0=10^{-7}$ g-moles/cm^3, and $i=0.1$ A/cm^2, p is less than 0.1 micron. Appreciable currents, therefore, will cause reaction to occur near $x=0$ (see fig. 18.7).

When reaction is complete close to the electrolyte meniscus, a mass-transfer limitation arises due to gas dissolving in the electrolyte and diffusing to the pore walls. At this limit, diffusion is not linear along the axis, and a two-dimensional analysis must be applied. This was first done by Walker et al. (*679*), who calculated the limiting mass transfer of dissolved gas to the walls of the pore as a function of the radius of the pore. A more succinct treatment (487, ref. 18.8) shows that the limiting-current density is given approximately by

$$i_L = 12nFDH_0/r. \qquad (18.22)$$

Current density, A/cm^2, is based on unit area of pore mouths of radius r. For normal values of D and H_0, r must be less than 1 micron to support significant current densities. Figure 18.8 gives a representation of a possible physical model for a nonwetted electrode containing macro- and micropores.

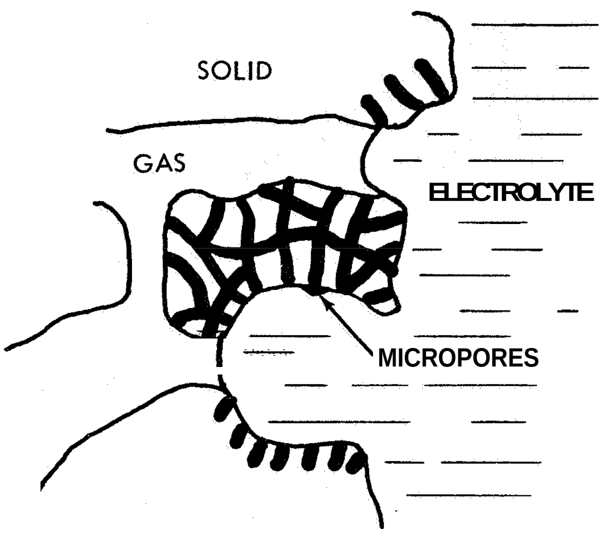

The macropores act as gas feeders to micropores near the electrode-electrolyte interface. Although the bulk of the electrode is nonwetting due to waterproofing, the catalytic micropores can wet and fill with electrolyte. Gas diffuses into the micropores and reacts at the high area available, with short diffusion paths in the electrolyte due to the small size of the pores.

FIGURE 18.8.—Representation of nonwetted electrode.

A similar model was proposed by Reti (*434*), who assumed that the micropores were filled with electrolyte and the macropores were filled with gas. Linear diffusion along the axis of the micropores was assumed, and the current density for micropores 30 angstroms in diameter and 4 microns long was calculated by numerical approximation for the case of O_2 in KOH. It was assumed that the wall of the pore would react oxygen at a rate of $(3)(10^{-4})$ A/cm^2. The current per square centimeter of pore mouth was calculated to be about 0.1 ampere. This is obviously less than the limiting current predicted by equation (18.22) for such small-pore diameters, and is therefore feasible. Equation (18.21) also shows that oxygen will be almost completely reacted within the pore at a current density of $i=3nFDH_0/p$, where p is 4 microns. Using $n=4$, $D=10^{-5}$, and $H_0=10^{-7}$, i is 3 mA/cm^2 of pore mouth. Because the pore is long compared to its diameter, linear diffusion will still apply for higher current densities, again showing that 0.1 A/cm^2 of pore mouth is a reasonable value.

The experimental evidence given in section 18.2 suggests that if micropores fill with electrolyte, the electrolyte will extend beyond the mouths of the pores and flood the internal surface of the electrode, covering the macropore surface with a thin film. This is presumably prevented by wetproofing the electrode, as used for porous-carbon electrodes and electrodes of platinum black mixed with small Teflon particles (less than 1 micron). It is difficult to envisage the formation of the thin films discussed in section 18.2 in nonwetted electrodes, and it is reasonable to suppose that the simple-pore model applies in the nonwetted case. Referring to figure 18.8, the nonwetted macropores act as gas diffusers to a layer of micropores in the electrode surface next to the electrolyte. Wetproofing prevents the electrolyte from penetrating the electrode to any depth. When a thin film forms within the electrode, it is possible to weigh the rather large pickup of electrolyte; but nonwetted electrodes show negligible increase in weight. The surface micropores and macropores are penetrated by electrolyte for some distance and form simple pores of the form shown in figure 18.7. Wetproofing by admixture of Teflon particles may allow wetting of platinum black at the electrode-electrolyte interface, but prevent penetration beyond this layer. Wetproofing by depositing wax within the macropores is beneficial, providing it is not so extensive as to wetproof the micropores and thus prevent the formation of contact between electrolyte and catalytic micropore area.

If this model for the mode of operation of nonwetted electrodes is correct, equation (18.22) predicts that the micropores must have small radii to give large limiting currents. When this stipulation is satisfied and the penetrated length of surface micropores is long compared to their radius, the current density under conditions where gas is utilized completely and irreversibly within the pores is (see sec. 18.5)

$$i = (i_0 SnFDH_b)^{1/2} (H_0/H_b)^{(h+1)/2} \exp\ (\alpha\eta/2b) \tag{18.23}$$

The term $(H_0/H_b)^{(h+1)/2}$ allows for reduction in the partial pressure of gas along the macropore; H_b is the equilibrium concentration of dissolved gas at the bulk pressure of reactant gas, p_b, and H_0 is the pressure of reactant gas at the electrolyte boundary, p_0; H_0/H_b can be replaced by p_0/p_b. S is the specific surface area of the reacting micropores and is greater for smaller pore diameter and greater microporosity. If ϵ_1 is the microporosity and r the pore diameter, cylindrical pores give

$$S = 2\epsilon_1/r, \quad \text{unit area per unit volume.} \tag{18.24}$$

For example, a microporosity of 10 percent and a mean micropore radius of 50 angstroms gives a specific surface area of 40 m^2/cm^3. Measurement of BET area of electrodes gives values of S, while measurement of double-layer capacity in electrolyte gives values of wetted area. A comparison of BET area with double-layer capacity would give information on the depth of penetration of electrolyte into the electrode.

18.4 GAS-DIFFUSION ELECTRODES: SURFACE-DIFFUSION MODEL

Justi et al. (ref. 18.9) proposed that the mode of operation of a gas-diffusion electrode was as follows. A three-phase boundary of gas-solid electrolyte is formed within the electrode. Under a differential gas pressure, the electrode does not fill with electrolyte because large pores are kept free by a balance of gas pressure against capillary forces. Gas adsorbs on bare electrode metal and moves along the metal by surface diffusion, passing through the three-phase boundary at reactive sites covered by electrolyte.

There are three main objections to this model. First, since gases (especially hydrogen) adsorb very rapidly on bare metal surfaces, only a small amount of nonsubmerged metal should be required. The experiments of Sama (*447*), Will (ref. 18.1), and Buvet (ref. 18.10) do not support this view, because for thin-wire electrodes they found that a minimum of several millimeters of exposed length was necessary to give a maximum limiting current. Second, experimental evidence suggests that a wetted electrode has a thin film of electrolyte covering the walls of the pores, even though the center of the pores are open for gas diffusion. Third, it is likely that submerged electrode surface has a strong bonding between surface atoms and water. The diffusing molecule might have to displace water in the process of surface diffusion, and it is not likely that the diffusion is rapid under such circumstances. Obviously, it is not correct to use rates of surface diffusion of gas on bare metal to predict the rates of diffusion on water-covered metal.

A theoretical examination of surface diffusion was given in 687. The process proved to be too slow to support large currents. This work, however, contains several physical and algebraic errors which tend to invalidate the results. Iczkowsi (ref. 18.4) also concluded, from a theoretical study, that the surface diffusion model could not support the currents observed in practice. An attempt to measure surface transport of oxygen on electrodes was not successful because of certain experimental difficulties *(616).*

Recent work by Boudart (ref. 18.11) indirectly offers support to the surface diffusion model. The work showed that tungsten trioxide is reduced at room temperature by atomic hydrogen but not by hydrogen molecule. When a mechanical mixture of platinum black and powdered WO_3 was exposed to dry H_2 at room temperature, rapid adsorption of H_2 occurred on the platinum to give PtH, but no adsorption was observed on WO_3 nor was WO_3 reduced. In the presence of sufficient water to form a monolayer on the particles, hydrogen rapidly reduced the surface of WO_3 in the mixture. The mechanism was explained as follows: adsorbed H on platinum is readily mobile at room temperature, but cannot transfer over the surface of dry WO_3 particles. In the presence of a monolayer of water, H transfers from Pt to WO_3, diffuses over the surface, and reduces it. The nature of the surface complexes formed is not known, but probably the compound $M\text{-}H_2O\text{-}H$ diffuses H over the surface at rapid rates (M stands for surface atoms). Thus the third objection to the surface diffusion model is removed, since adsorbed water on the surface aids diffusion rate, rather than retards it.

No mathematical treatment exists for the diffusion-limited currents expected from such a mechanism. The diffusion of adsorbed hydrogen atom along submerged surface can be treated in the same way as volume diffusion (see sec. 18.5) and gives an equation similar to equation (18.23)

$$i_0=(i_0SnFD_sSC_{so})^{1/2}(p_0/p_b)^{(h+1)/2} \exp(\alpha\eta/2b). \qquad (18.25)$$

D_s is the surface diffusion coefficient, and C_{so} is the surface concentration (g-mole/cm^2, for example). S occurs twice because it is the area for electrochemical reaction and the area for surface diffusion.

This model is likely to apply only to readily adsorbed gases which form mobile surface complexes. Hydrogen on platinum, palladium, and possibly nickel may behave in this way. It is unlikely that adsorbed hydrocarbons can diffuse rapidly over surfaces at low temperatures.

18.5 FLOODED ELECTRODES

Compared to gas-diffusion electrodes, the operation of a porous electrode which is submerged in an electrolyte containing dissolved reactant is relatively easy to describe. For an idealized plane geometry, as shown in figure 18.9, the mode of operation can be described in the following steps. Dissolved reactant diffuses to the surface of the electrode and then into the pores, and reacts on the internal area. When the current is low, the reaction can occur uniformly throughout the electrode and the current-voltage curve is the same as a solid-plane electrode of area equivalent to the internal area of the porous electrode. As current density increases, however, two effects occur. The rate of diffusion into the electrode may not be sufficient to maintain uniform reaction and a concentration gradient

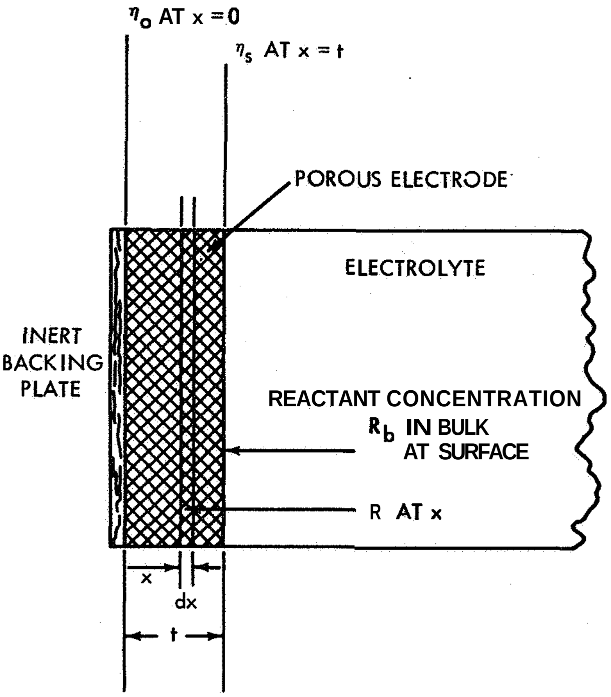

FIGURE 18.9.—Flooded porous electrode with one face exposed to electrolyte.

is established, with higher concentration at the outside and lower toward the back of the electrode. In addition, the ionic current density is greatest at the external face and zero at the back. Therefore, a potential gradient is established due to IR polarization in electrolyte in the pores of the electrode, and higher polarization at the external face accelerates reaction at this face. Thus, both internal effects, mass transfer and ohmic polarization, tend to give lower rates of reaction in the interior and higher toward the exterior. **A** porous electrode may have high internal area and, therefore, give high electrochemical rates per unit plane area of electrode, but this internal area cannot, in general, be completely utilized at high current densities.

Fuel-cell electrodes (with current collectors) have high conductivities compared to electrolytes; therefore, IR effects due to electron transfer in the metal can be ignored across the thickness of the electrode. For a small electrode, current density based on the plane area can be assumed constant over the cross section of the electrode. The conductivity of the electrolyte can be taken as reasonably constant for a strongly supported electrolyte, very concentrated electrolyte, or for nonionic reactants and products. Let ρ be the effective specific resistance of the electrolyte in the pores based on unit plane area of the electrode. Then, considering a system as shown in figure **18.9,** with linear mass transport and current, it is clear that the current produced in the electrode between 0 and x has to be supported by *(a)* the ionic current flowing through the plane at X, and *(b)* the mass transfer of reactant through the plane at X. Considering unit cross-sectional area of the plane, Ohm's law gives $i=(1/\rho)d\eta/dx$, and the mass transfer is given by $i=nFDdR/dx$, D being an effective diffusion coefficient. Therefore

$$(1/\rho)d\eta = NFDdR$$

and

$$\eta_s-\eta=\rho nFD(R_s-R). \qquad \textbf{(18.26)}$$

$\eta_s-\eta$ is the difference between the polarization at the external face and at X, while $R, -R$ is the corresponding difference in reactant concentration. When R is zero, this represents a depletion of reactant to zero within the electrode, and when R goes to zero near the external face, only a very small part of the electrode is being utilized. Clearly, mass transport effects are then extreme. Under these conditions $\eta_s-\eta$ is a maximum, given by $\rho nFDR_s$. If the porosity-tortuosity terms are the same for mass transfer and ionic conduction, then they cancel out in the product ρD, and normal ρ and D values can be used. Taking **1** N reactant concentration, $Rn=10^{-3}$ g-moles/cm^3, and assuming $p=5$ ohm-cm and $D=10^{-5}$ cm^2/sec, then $\eta_s-\eta=5.0$ millivolts. Such a small change in voltage will produce little effect compared to the corresponding depletion of reactant in the interior of the electrode. As current density is increased, the penetration into the electrode, at which R becomes nearly zero, becomes smaller. Due to this mass transport effect, the reaction is concentrated in the region towards the right-hand face of the electrode. The mean path through which ions have to travel becomes less. As i becomes greater, $d\eta/dx$ becomes greater, but this is accomplished by x being smaller and not by η becoming greater; $\eta_s-\eta$ remains the same. There will, therefore, be some cases in which the mass-transport effect will outweigh the ohmic effect.

It will be assumed that electrolytic current and mass transfer occur through one plane face, with negligible edge effects and negligible nonuniformity of current density in the electrolyte. For electrodes of reasonable thickness and pore size, the macropore size will be at least two orders of magnitude less than the thickness (**10** microns and **1** mm, for example). We can assume that mass-transfer effects across the radius of a pore are negligible compared to mass-transport effects along the axis of the pore.

Considering a differential element dx as shown in figure **18.9,** of unit cross-sectional area, the reacting area is Sdx and the current density, di, from the element is

$$di=i_0\{(R/R_b)\exp(\alpha\eta/b)-(P/P_b)\exp[-(1-\alpha)\eta/b]\}Sdx.$$

The amount of reactant diffused out of the element at the plane x is Ddr/dx. In the usual way, therefore, at steady state, $di=nFD(d^2R/dx^2)dx$ and

$$d^2R/dx^2=(i_0S/nFD)\{(R/R_b)\exp(\alpha\eta/b)-(P/P_b)\exp[-(1-\alpha)\eta/b]\}.$$

If ohmic effects are neglected, η is constant through the electrode. Little error is introduced by letting the diffusion coefficient of R and P be equal. Then, for equimolar countercurrent diffusion, $R+P=R_b+P_b$ and

$$d^2R/dx^2=(i_0S/nFD)\{[\exp(\alpha\eta/b)/R_b]+\{\exp[-(1-\alpha)\eta/b]/P_b\}\}R \\ -(i_0S/nFD)(R_b+P_b)(\exp[-(1-\alpha)\eta/b]/P_b\}=K_1R-K_2.$$

The boundary conditions are $dR/dx=0$ at $x=0$, since no mass transport occurs beyond the left-hand face, and $R=R_s$ at $x=t$, R_s being the concentration at the right-hand face. The solution for these boundary conditions is

$$(K_1R-K_2)/(K_1R_s-K_2)=[\exp(x\sqrt{K_1})+\exp(-x\sqrt{K_1})]/[\exp(t\sqrt{K_1})+\exp(-t\sqrt{K_1})]. \qquad (18.27)$$

The total steady-state current density from reaction in the interior of the electrode is $i=nFD(dR/dx)_{x=t}$; therefore,

$$i=(i_0St)\{(R_s/R_b)\exp(\alpha\eta/b)-(P_s/P_b)\exp[-(1-\alpha)\eta/b]\}(1/t\sqrt{K_1})\tanh(t\sqrt{K_1}). \qquad (18.28)$$

This is the usual form of rate equation, but modified by a factor $(1/t\sqrt{K_1})\tanh(t\sqrt{K_1})$. This i is that of reaction in the interior. The total i is given by this value plus current originating from the exterior of the electrode. The contribution of the exterior will be small for a reasonably thick electrode with highly developed internal area.

Several limiting cases can be described:

(a) Low exchange current, low to moderate polarization.

$$K_1=(i_0S/nFD)\{[\exp(\alpha\eta/b)/R_b]+\{\exp[-(1-\alpha)\eta/b]/P_b\}\}$$

If i_0S is low and polarization not too high, $t\sqrt{K_1}$ is small. Then $(1/t\sqrt{K_1})\tanh(t\sqrt{K_1})$ is near **1**, and

$$i=(i_0St)\{(R_s/R_b)\exp(\alpha\eta/b)-(P_sP_b)\exp[-(1-\alpha)\eta/b]\}. \qquad (18.29)$$

Thus, if there is negligible concentration drop from the bulk electrolyte to the electrode surface (as would be expected at low currents), then $R_s=R_b$ and $P_s=P_b$, and we obtain the usual form for a low-exchange-current reaction with the whole of the interior surface area (St) of the electrode being utilized. If i_0St is so small that $t\sqrt{K_1}$ is small for polarization above 50 to 100 millivolts, then equation **(18.29)** reduces to the normal Tafel form, with a slope of $2.3RT/\alpha nF$.

(b) Low or moderate exchange current, high polarization.

As η goes up (or as i_0S is higher), $t\sqrt{K_1}$ goes up. Eventually, the situation is reached where $t\sqrt{K_1}>2$. Then tanh $(t\sqrt{K_1})$ is equal to 1 and

$$i=\frac{i_0S\{(R_s/R_b)\exp(\alpha\eta/b)-(P_s/P_b)\exp[-(1-\alpha)\eta/b]\}}{\sqrt{(i_0S/nFD)\{[\exp(\alpha\eta/b)/R_b]-\{\exp[-(1-\alpha)\eta/b]/P_b\}\}}} \qquad (18.30)$$

The thickness of the electrode disappears from the equation, since the concentration of reactant in the interior reaches zero at some penetration less than the thickness. When η is great enough for $\exp[-(1-\alpha)\eta/b]$ to be negligible

$$i=(i_0SnFDR_b)^{1/2}(R_s/R_b)\exp(\alpha\eta/2b). \qquad (18.31)$$

For negligible concentration gradient outside of the electrode, $R_s/R_b=1$ and equation **(18.31)** is a Tafel form equation with a slope ***twice*** the expected normal value. The apparent exchange current density is i_0SnFDR_b.

(c) Assuming a simple stagnant film concept to be sufficiently accurate, the effect of mass transport outside of the electrode can be expressed by $R_s/R_b=1-i/i_L$. When the reaction is irreversible and when the concentration of the reactant in the interior of the electrode becomes small, then terms in $\exp[-(1-\alpha)\eta/b]$ can be neglected, the tanh term is **1**, and

$$\eta=(2b/\alpha)(2.3)\log[(ii_L)/(i_L-i)]-(b/\alpha)(2.3)\log(nFDR_bSi_0). \qquad (18.32)$$

The slope of η versus log $[(ii_L)/(i_L - i)]$ is ***double*** the normal Tafel slope and the intercept leads to the value of i_0S. Physically this equation represents the combined effects of electrochemical rate, internal diffusion, and external mass transport. This equation was experimentally verified (***486***), using a redox reaction of known kinetic form and porous carbon electrodes.

For an irreversible reaction at high current densities, the concentration of dissolved reactant tends to zero at the back of the electrode, and from equation (18.27)

$$R/R_s = \exp\,[-(K_1)^{1/2}(t - x)]$$

where

$$K_1 = (i_0S/nFDR_b)\ \exp\,(\alpha\eta/b).$$

The penetration of reaction into the electrode can be defined by the point at which R/R_s is 1/20, at which point virtually all of the reactant has been consumed. Denoting this point by a distance p from the electrode-electrolyte face

$$1/20 = \exp\,[(K_1)^{1/2}p]$$

and from equation (18.31)

$$p \cong 3nFDR_s/i. \qquad (18.33)$$

Clearly, an electrode which is thicker than p will not give improved performance at current densities of i, since the extra thickness of electrode is not utilized. Alternatively, if p is set equal to the thickness of the electrode, equation (18.33) shows that the current at which all the interior of the electrode is being utilized is greater for larger values of D and R,.

The above analysis can be repeated assuming that the concentration of reactant through the electrode is constant and ohmic polarization in the pores is large (***483*** and refs. 18.3 and 18.9). The equivalent result to equation (18.32) is then

$$\eta = (b/\alpha)\,(2.3)\log\,[(i^2i_L)/(i_L - i)] - (b/\alpha)\,(2.3)\log\,(2i_0Sb/\alpha\rho). \qquad (18.34)$$

Which system applies depends on the value of ϕ (see eq. (18.8) and its discussion).

The major drawback to the equations developed in this section is that they assume a simple, first-order rate equation of the form of equation (18.7). Many of the fuel-cell reactions of interest have more complex rate equations, and in most cases the form of the rate equation is not known with any degree of certainty. However, the general conclusions derived from a study of equations (18.32) and (18.34) are applicable to any system. Performance of porous, flooded electrodes is improved by large values of active surface area S, by high concentrations and diffusivities of reactant, and by low electrolyte resistance. The electrode must have an open-pore structure and a high porosity, so that the effective diffusion coefficients and conductivities through the electrode, based on unit area of the electrode, are not excessively reduced from normal values. The relation is

$$D_{\text{effective}} = D_{\text{normal}}(\epsilon/q) = D_{\text{normal}}/\lambda \qquad (18.35)$$

where ϵ is the porosity of the electrode and q is a tortuosity factor. The labyrinth factor, A, is greater than 1. Similarly

$$\rho_{\text{effective}} = \rho_{\text{normal}}\ \gamma. \qquad (18.36)$$

Labyrinth factors should be as close to 1 as possible (see ch. 3).

A summary of mathematical treatments of flooded electrodes is given in ***486*** (refs. 18.12 through 18.20).

18.6 FLOWTHROUGH ELECTRODES

Two limiting cases of flowthrough electrodes are possible. If the electrode consists of metal screen, through which electrolyte containing dissolving reactant is passed at high velocities, then the screen behaves much as would a solid electrode. The screen area is not very different from an equivalent solid, plane electrode. However, the diffusion layer through which mass-transfer limitations occur is smaller for the screen, and is illustrated in figure 18.10. The thickness of the boundary layer is less at high flow velocity. This type of electrode is suitable for a highly active reactant which has little activation polarization even on the low areas involved. A reasonable concentration of dissolved reactant is necessary to assure good mass transfer to the electrode, otherwise flow velocities will be unreasonably high. (For example, a limiting current of about 20 A/sq ft was obtained with O_2 in KOH at flow rates of 120 liters/min ft^2 (***434***).) It is obviously difficult to consume all of the reactant in one pass through the screen.

The other case is that of a high-area porous electrode with pores which are small in diameter compared to electrode thickness. Mass transfer to the walls of the pores is rapid due to the small distances involved (a few microns). It is, therefore, theoretically possible to consume all of the reactant in one pass through the electrode. This type of electrode is more suitable for activated reactions which require high catalytic area; to avoid excessive pressure drop (and hence pumping energy), the flow rates are low.

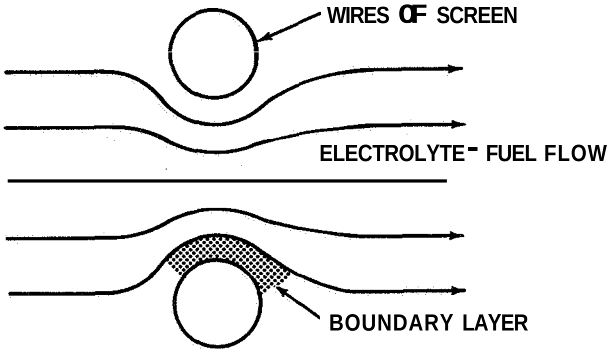

The limiting current at high flow rates depends on the mass transfer of fuel (or oxidant) dissolved in the flowing electrolyte through the boundary layer to the electrode surface.

FIGURE 18.10.—Boundary **layer at flowthrough electrode of screen.**

The theory of this type of electrode and experimental results on various systems are given in ***482, 484,*** and ***485.*** It is easily shown that the limiting current density of the electrode is

$$i_L = nFR_b v \tag{18.37}$$

Where R_b is the inlet concentration of reactant and v is the flow velocity (based on unit cross section of electrode). For example, hydrazine at $1M$ concentration (10^{-3} g-moles/cm^3) gives a limiting current of 0.6 A/cm^2 at a flow rate of 0.1 cm/min. The physical picture which emerges from solution (by computer) of the mathematical equations describing the electrode is as follows (ref. 18.21). The flowing electrolyte with a high concentration of fuel enters at one face, and when there is a suitable polarization, reacts. Ionic transfer through the electrolyte, which maintains charge balance, gives rise to an ohmic voltage gradient. This ohmic effect increases the polarization at further penetration into the electrode, and the reaction rate is increased. Therefore, as the fuel flows through the electrode, it is consumed more and more rapidly. This increases the cumulative ion transfer, causing increased ohmic effect, increased rate of consumption, and so on. For a large ohmic effect the reaction is concentrated toward the exit face of the electrode.

The system can be characterized in terms of the theoretical limiting current of equation (18.37), the exchange-current density of the electrode for uniform reaction through the electrode, i_0St, and the effective resistivity of the electrolyte in the pores of the electrode. The type of result obtained is shown in figure 16.5. Polarization becomes excessive if the electrode is run too near the limiting current, and it is possible to use only about 80 percent of the reactant in one pass through the electrode, even for active fuels and electrodes. Polarization at a current density not near the limiting current is less for higher values of i_0St and lower values of $i\rho t$. For a given current density, therefore, there is an optimum electrode thickness. If the electrode is too thin, activation polarization is high, but if it is too thick, the ohmic polarization within the pores of the electrode becomes too high and the interior of the electrode is only partially used.

Experimental investigations of flowthrough electrodes are described in reports ***482, 484, 485, 439, 436, 333, 404, 408,*** and ***456.***

18.7 UNSTEADY-STATE MEASUREMENTS ON POROUS ELECTRODES

Several unsteady-state methods are useful for investigating electrochemical parameters. For example, it is sometimes possible to get the current-voltage relation of an electrode reaction, without interference from mass-transfer effects, by passing a known current (from initial conditions of zero current) and measuring the change of voltage with time with an oscilloscope or fast recorder. If the double-layer capacity of the electrode is low, the activation polarization will be established so rapidly that the concentration of reactant will not have time to vary. Unsteady-state techniques are difficult to apply to fuel-cell electrodes for several reasons. First, the low solubility of dissolved gases makes it difficult to establish activation polarization before mass-transfer effects start to occur. Second, fuel-cell electrodes usually have large active areas, which give high double-layer capacities (and sometimes pseudocapacities due to gas adsorbed on the surface). Thus, to change the potential of the electrode rapidly may require a large current ($i = C dV/dt$, where C is total effective capacity) which is beyond the range of interest. If lower current is used, the electrode charges so slowly that mass-transfer effects come into play. Third, porous electrodes have distributed effects on sudden changes. The pore mouths opening into the electrolyte are charged or take part in reaction first, and the interior of the electrode is not used.

Distributed capacity effects are particularly noticeable at thick electrodes when ac techniques are used. De Levie (ref. 18.22) has described methods of investigating porous electrodes and demonstrated that only a thin layer near the exterior of the electrode may be used, which leads to false double-layer-capacity values and kinetic parameters unless allowance is made for this fact. For example, double-layer capacity is often measured with a high-frequency ac impedance bridge; high frequency is used because faradaic components of the impedance disappear at high frequency if the electrochemical reactions are not very fast. However, high frequency leads to distributed capacity effects, as discussed below.

The amount of interior electrode surface which is covered by electrolyte is of considerable interest for diffusion electrodes, since catalytic and mass-transfer behavior probably depend on the wetted area. If pseudocapacity effects are absent, the double-layer capacity of a smooth mercury surface in aqueous electrolytes is about 20 μF/cm^2 (ref. 18.23). Thus, an estimate of the wetted surface area of electrodes in square centimeters can be made by determining double-layer capacity and dividing by 20 μF. Double-layer capacity can be determined by several techniques, but for fuel-cell purposes it is best measured with an inert gas in the electrode (for gas electrodes) and a neutral electrolyte such as sodium sulfate. This avoids faradaic current and pseudocapacity. Alternatively, capacity should be measured at potentials between 0.4 and 0.6 volt (versus reversible hydrogen electrode in the same electrolyte), since neither hydrogen nor oxygen pseudocapacity (from the reactions $[H] \rightleftharpoons H^+ + e^-$, $[H] + OH^- \rightleftharpoons H_2O + e^-$, $H_2O \rightarrow 2H^+ + [O] + 2e^-$, and $2OH^- \rightarrow H_2O + [O] + 2e^-$) are pronounced in this voltage range in strong acids or bases. A method of estimating the correct time duration (or frequency) for a measurement is given below.

Consider a differential element of electrode as shown in figure 18.9, where L is the thickness of the wetted portion of the electrode. Let V_1 be the potential between electrolyte and electrode (versus a reference electrode) at zero time, with no current flowing. Let V be the change in potential from V_1 at time t, distance X. Let ρ be the specific resistance of the electrolyte in the pores of the electrode (ohm-cm) based on unit plane area of electrode. Consider a constant current density of i applied to the electrode (A/cm^2). Ohm's law is $i = -(1/\rho)(\partial V/\partial x)$. Double-layer capacity will charge with time according to

$$q = C(dx/L)(\partial V/\partial t)$$

where q is the rate of charge into the double layer in the element of volume dx, and C is the double-layer capacity per unit plane area of electrode. A current balance on the element gives, in the absence of faradaic current

$$q = (\partial i/\partial x)dx.$$

Therefore,

$$\partial V/\partial t = (L/\rho C)(\partial^2 V/\partial x^2). \qquad \textbf{(18.38)}$$

At $t > 0$, let a current i be passed; then

$$i = (1/\rho)(\partial V/\partial x)_{x=L}. \qquad \textbf{(18.39)}$$

The solution of equations (18.38) and (18.39) for appropriate boundary conditions gives potential as a function of time. For a constant charging current (galvanostatic technique), the boundary conditions are: i=constant at $t>0$; $V=0$ at $t=0$; and $(\partial V/\partial x)_{x=0}=0$, that is, no current flows through the plane at $x=0$. The solution for these boundary conditions is (ref. 18.24):

$$V=\frac{it}{C}+iL\rho\left\{\frac{3x^2-L^2}{6L^2}-\frac{2}{\pi^2}\sum_{n=1}^{\infty}\frac{(-1)^n}{n^2}\exp\left[-(n^2\pi^2t)/(\rho CL)\right]\cos\frac{(n\pi x)}{L}\right\} \qquad (18.40)$$

The measured potential difference is at the face where $x=L$ and values of V at this face, V_L, can be obtained from computed results of equation (18.40) given in Carslaw and Jaeger. Letting ϕ be defined by

$$V_L=iL\rho\phi+it/C, \qquad (18.41)$$

then

$t/\rho CL$ ……	0.005	0.01	0.02	0.03	0.04	0.06	0.08	0.1	0.15	0.2	0.3	∞
ϕ ………	.076	.102	.14	.162	.185	.215	.24	.255	.285	.306	.322	0.33

The apparent double-layer capacity, C', is $C'=it/V_L$; therefore

$$C'/C=1/[1+(CL\rho\phi/t)]. \qquad (18.42)$$

Thus, the correct result is obtained when $CL\rho\phi/t$ is much less than 1. Otherwise, the apparent capacity is less than the true capacity. For example, if $L=0.1$ cm, $C=10^4$ μF/cm^2, $\rho=10$ ohm-cm, then at $t=0.1$ second, $t/\rho CL=10$. Therefore, $\phi=0.33$ and $C'/C=1/1.03$. Times of greater than 0.1 second are necessary to get the correct double-layer capacity. Figure 18.11 shows the voltage-time curve for the galvanostatic charging. Values obtained by taking the initial slope of the voltage-time curve are incorrect. The desired time period for a particular range of potential over which double-layer capacity is to be measured is obtained by using a suitable current density. If the necessary current is small, it is often difficult to avoid secondary faradaic reactions of comparable magnitude, which interfere with the capacity measurement.

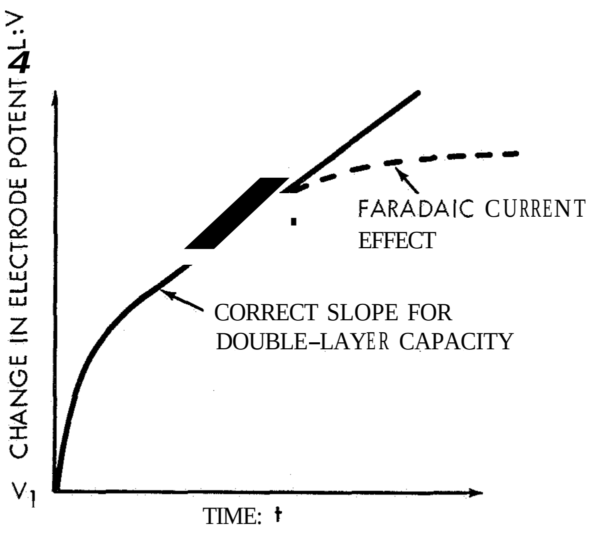

The initial slope of the voltage-time plot does not give the correct double-layer capacity, due to distributed capacity effects (see text).

FIGURE 18.11.—Variation of potential with time on galvanostatic charging of the double layer of a porous electrode.

The same line of reasoning applies to a repetitive square pulse of ac current. Only the exterior of the electrode will partake in charging, since before the interior is charged, the current will be reversed and the exterior discharged. This will give a curve of V as a function of t, which might appear linear over a short time. The capacity, however, would be much too low. Similarly, the capacity measured by an ac impedance bridge will be in error unless the frequency is low (less than 10 cps for the example given).

Results of investigations of electrode area are given in chapter 3.

18.8 EFFECT OF PULSATION ON GAS ELECTRODES

The discussions of the mode of operation of gas-diffusion electrodes given above assumed that mass transfer of dissolved gases and ions was accomplished by diffusion and migration. If mass-transfer factors are limiting performance of an electrode, then improvement of mass transfer by forced flow will be advantageous. It is necessary to have forced flow without destroying stability of the electrode-electrolyte contact. It has been proposed that this be done by pulsation of the electrolyte to impose a movement of the three-phase contact backward and forward along the pores. For example, withdrawal of electrolyte toward the pore mouth opening into electrolyte would leave bare surface (for nonwetted electrodes) or a thin film of electrolyte covering the pore walls. Gas diffusion and adsorption on the walls occur. When the electrolyte is forced back over the walls on the return stroke, the gas is available for reaction.

Effects of sound waves on several electrode reactions were investigated by Yeager (781). Lower polarization during deposition of Cu, Ag, Ni, and Cr was found, especially when low concentrations of ions were used. The effect was brought about by microagitation due to cavitation bubbles. These increased mass transfer across the boundary layer at the electrode-electrolyte interface. The effect is also explained by cavitation erosion of the surface (refs. 18.25, 18.26, and 18.27). Lower polarization (by a few millivolts) during hydrogen, oxygen, and chlorine evolution was also due to lower concentration polarization. The formation of chemical species and temperature rise due to increased pressure were calculated to be very small at 300 kcps and 1 W/cm^2. At a constant current, small cyclic fluctuations in voltage were observed when an electrode was placed at the node of a standing sound wave.

A cam-driven pulse pump was used to apply pressure pulses to the electrolyte of a fuel cell (Purdue University, 540). The cell consisted of a horizontal air cathode of micrometallic porous nickel, one-eighth inch thick, which rested on the top surface of the electrolyte, and a horizontal anode of 150-mesh platinized-nickel screen submerged in the electrolyte. The electrolyte and fuel consisted of 5 weight-percent methanol dissolved in 28 percent KOH. No effect of pulsation was observed, but the potentials and current densities were so low that the results were virtually meaningless. The methanol in contact with the cathode probably reacted to such an extent that the electrode could not behave as a satisfactory cathode.

Electrolyte was pulsed in a simple hydrogen-oxygen or hydrogen-air cell using Union Carbide carbon electrodes and concentrated KOH electrolyte (Union Carbide, 667 through 670). Amplitudes up to 14 psig and frequencies in the subsonic region gave no effect on performance of the cell or individual electrode performance (using a zinc wire as reference electrode). Mechanical vibration of electrodes gave no effect. Sixty-cps interruption of direct current gave the same potentials as the mean current applied continuously. Direct current with superimposed ac of frequency 20 to 20 000 cps gave no change from direct current alone. Electrolyte pulsing using sonic frequencies produced no effect.

A heavy discharge current of 2-second duration was applied every minute. The current was great enough to drive the cell potential beyond zero to about −0.5 volt. On returning the current to a normal working level, the cell potential was immediately improved, but fell by over 0.1 volt during the minute to the next pulse. The mean potential between pulses was better than if no pulse were used. The effect was ascribed to activation of electrode catalysts.

Results were obtained using current pulsing on a hydrogen-oxygen fuel cell with Clevite No. 3 porous-nickel electrodes (Alfred University, 34). The anode was catalyzed by electroplating with platinum and palladium and the cathode was catalyzed by platinum. Electrolyte was 30 weight-percent KOH retained in an asbestos matrix, and cell temperature was 140"F (60"C). Using an external power supply, a large current was passed through the cell for a short period of time and the cell allowed to rest until the next pulse; the duty time was 1 to 4 percent, and the rest time 99 to 96 percent. Frequencies of 500 to 2000 cps were used and the mean current and potential were compared with those of steady, direct-current operation. At a given cell potential the mean current density for pulsed operation was somewhat greater than for steady current. The steady limiting current was about 20 A/sq ft.

This system does not fully demonstrate improved power'output of the cell, since during the time the cell is supplying power an external power supply is also in operation. The mean cell current, i, is the total charge passed during the cycle divided by the cycle time, but the mean cell potential is not necessarily the potential available to do work. For example, energy produced by the cell during the duty part of the cycle, t_1 seconds, is $\int_0^{t_1} iVdt$; therefore, the mean power produced over a total cycle time of t_2 seconds is $\int_0^{t_1} iVdt/t_2$. If V is constant, then power $= V\int_0^{t_1} idt/t_2 = Vi$, but there is no proof that V is constant over the cycle. Since the current over the duty part of the cycle was up to 1 A/cm^2, V would be constant only if the system had a high capacitance. The circuit given did not contain external capacitance, so the double-layer capacitance of the cell electrodes would have to be high. It is more logical to avoid the use of an external power supply and simply interrupt the current. The system is then similar to the Kordesch-Marko interrupter circuit (see app. C), which also requires that the capacitance be great enough for V to remain constant during the on-off cycle. Investigations with the interrupter circuit show that the current-voltage curves (including IR effects) of fuel cells are the same using interrupted conditions as for steady-state operation. Contrary to the results quoted above, no improvement of power density is observed. The difference between these results and those given in the Union Carbide work is that the latter showed considerable voltage change due to an imposed high current pulse and the cell produced higher energy for the rest of the cycle. The energy produced was calculated using the sum of iV over the cycle. This second technique can be called a voltage-pulse technique, since it is probable that it is the extent of potential change which is significant.

In summary, electrolyte pulsation and on-off current pulsing have not produced significant changes in current density. Voltage pulsing may be effective by driving electrodes to potentials where catalysts are activated, presumably by stripping off adsorbed impurities (or byproducts of reaction) which poison the electrodes. Sufficiently positive electrode potentials produce oxide layers on metal surfaces. When the oxide is reduced at more negative potentials, the surface is more active. The process may produce a disordered, highly active, catalyst surface. Normally this activity disappears with time due to repoisoning or recrystallization, but repetitive pulsing will reactivate the surface.

18.9 CONCLUSIONS

It is readily demonstrated that the solubilities of hydrogen and oxygen are too low to give high rates of mass transfer through thick layers of electrolyte. Three theories have been proposed to explain how gas-diffusion electrodes can support high current densities without mass-transfer limitations of dissolved gas. The thin-film theory proposes that the macropores of a wetting electrode are covered with a thin film of electrolyte, giving a large area of electrolyte in which gases can dissolve and diffuse. Experimental and theoretical evidence indicates the films are about 1 micron thick. This model predicts that electrodes must be thick enough to supply sufficient thin-film area for dissolved gas diffusion. A very thin electrode would have a low limiting current. The simple-pore model proposes that gas dissolves rapidly in electrolyte and is reacted at pore walls very close to the point of solution. Analysis shows that the pore diameter must be small (certainly less than 1 micron) to give a small mean diffusional path length. This model may apply to electrodes which contain microporosity and which have bulk nonwetting properties. For example, an electrode of platinum black and Teflon particles resists wetting and penetration of electrolyte, but much of the platinum black may be in contact with electrolyte. The third theory proposes that gas adsorbs on bare electrode surface and transports by surface diffusion to surface sites covered by electrolyte.

It is possible that practical electrodes function by a combination of the above models. For example, calculations and experiments on partially submerged thin wires (674) show that the current is supported by diffusion through a thin electrolyte film and by diffusion to electrode surface submerged beneath the liquid level. The theoretical effects of pressure are difficult to verify experimentally because the amount of pore surface covered by electrolyte changes as pressure is increased if the pressure forces electrolyte out of large pores.

Mathematical models are fairly well developed for the current-voltage relations of porous, flooded electrodes in which reactant is dissolved in electrolyte. The major weakness of the treatments is that simple electrokinetic equations are used which are not likely to apply over wide potential ranges for the reactants of interest. In particular, when the potential of a platinum electrode is more positive than about 0.7 volt (versus reversible hydrogen electrode in the same solution), oxygen films start to build up on the surface. These films usually retard anodic rates of reaction. As potential becomes more positive, the retardation may almost match acceleration of the anodic reaction, leading to a pseudolimiting current. This limiting current, which is not usually well defined, will change with cell temperature and is usually considerably increased. A mass-transfer limited current does not change rapidly with increased temperature.

The application of conventional unsteady-state techniques to porous electrodes is not straightforward because of distributed capacity and ohmic effects.

Electrolyte pulsation and on-off current pulsing have not increased power outputs to any significant extent. Voltage pulsing has in some cases improved performance, possibly by cleaning and activation of the catalyst surface.

18.10 REFERENCES

18.1. WILL, FRITZ G.: Electrochemical Oxidation of Hydrogen on Partially Immersed Platinum Electrodes. I. Experiments and Interpretations. J. Electrochem. Soc., vol. 110, no. 2, 1963, pp. 145–151.

18.2. DITTMAN, H. M.; JUSTI, E. W.; AND WINSEL, A. W.: Symposium on Recent Advances in Fuel Cells. Am. Chem. Soc., Divisions of Fuel Chemistry and Petroleum Chemistry, vol. 6, no. 4–B, 1961, p. 139; vol. II, G. J. Young, ed., Reinhold Pub. Corp., 1962.

18.3. AUSTIN, L. G.; AND LERNER, H.: The Mode of Operation of Porous Diffusion Electrodes. I. Simple Redox Systems. Electrochim. Acta, vol. 9, no. 11, 1964, pp. 1469–1481.

18.4. ICZKOWSI, RAYMOND P.: Mechanisms of the Hydrogen Gas Diffusion Electrode. J. Electrochem. Soc., vol. 111, no. 9, 1964, pp. 1078–1086.

18.5. ROCKETT, J. A.: Extended Abstracts of Battery Division. J. Electrochem. Soc., vol. 8, 1963.

18.6. KATAN, T.; GRENS, E. A.; AND TURNER, R. M.: Symposium on Fuel Cell Systems. Am. Chem. Soc., Division of Fuel Chemistry, vol. 7, no. 4, Sept. 1963.

18.7. AUSTIN, L. G.; ARIET, M.; WALKER, R. D.; WOOD, G. B.; AND COMYN, R. H.: IEC Fundamentals. vol. 4, 1965, p. 321.

18.8. AUSTIN, L. G.: Tafel Slopes for Flooded Electrodes. Trans. Faraday Soc., vol. 60, no. 499, 1964, pp. 1319-1324.

18.9. JUSTI, I. E.; PILKUHN, M.; SCHEIBE, W.; AND WINSEL, A.: High Drain Hydrogen Diffusion Electrodes. Academie der Wissenschafter, Mainz. Steiner, 1959.

18.10. BUVET, R.; GUILLON, M.; AND WARSZAWSKI, B.: Electrochim. Acta, vol. 6, 1962, p. 113.

18.11. BOUDART, M.: Journal of Catalysis. (To be published in 1966).

18.12. KSENZHEK, O. S.; AND STENDER, V. V.: Dokl. Akad. Nauk S.S.S.R., vol. 106, 1956, p. 487; vol. 107, 1956, p. 280.

18.13. EULER, J.; AND NONNENMACHER, W.: Electrochim. Acta, vol. 2, 1960, p. 268.

18.14. NEWMAN, JOHN S.; AND TOBIAS, CHARLES W.: Theoretical Analysis of Current Distribution in Porous Electrodes. J. Electrochem. Soc., vol. 109, no. 12, 1962, pp. 1183–1191.

18.15. American Chemical Society: Advances in Chemistry Series, no. 47, 1965, p. 73.

18.16. AUSTIN, L. G.: Fuel Cells. Vol. 11, ch. 8. G. J. Young, ed., Reinhold Pub. Corp., New York, 1962.

18.17 KSENZHEK, O. S.: Russ. J. Phys. Chem., vol. 36, 1962, p. 121.

18.18. GRENS, E. A.; AND TOBIAS, W.: Extended Abstracts of Battery Division. Fall Meeting of the Electrochemical Society, vol. 8, 1963, p. 82.

18.19. KSENZHEK, O. S.; AND STENDER, V. V.: Zh. Prikl. Khim., vol. 32, 1959, p. 110.

18.20. MILNER, P. C.: Extended Abstracts of Battery Division. Fall Meeting of the Electrochemical Society, vol. 8, 1963, p. 37.

18.21. AUSTIN, L. G.; PALASI, P.; AND KLIMPEL, R. R.: Polarization at Porous Flow-Through Electrodes. Am. Chem. Soc. Advan. Chem. Ser., no. 47, 1965, pp. 35–60.

18.22. DE LEVIE, R.: Electrochim. Acta, vol. 8, 1963, p. 751; vol. 9, 1964, p. 1231.

18.23. RAMALEY, L.; AND ENKE, C. G.: The Double Layer Capacitance of Silver in Perchlorate Solution. J. Electrochem. Soc., vol. 112, no. 9, 1965, pp. 947–950.

18.24. CARSLAW, H. S.; AND JAEGER, J. C.: Conduction of Heat in Solids, Second ed., Clarendon Press, 1959, p. 112.

18.25. NYBORG, W.: J. Acoust. Soc. Am., vol. 30, 1958, p. 329.

18.26. KOLB, J.; AND NYBORG, W.: J. Acoust. Soc. Am., vol. 28, 1956, p. 1237.

18.27. EDER, S.: J. Acoust. Soc. Am., vol. 31, 1959, p. 54.

APPENDIX A

Fuel-Cell Glossary From Report 752

1. DEFINITIONS OF TERMS—GENERAL DEFINITIONS

Fuel Cell: A fuel cell is an electrochemical device in which part of the energy derived from a chemical reaction maintained by the continuous supply of chemical reactants is converted into electrical energy. The device itself remains basically unaltered in the process.

Primary Fuel Cell: A primary fuel cell is a continuously fed galvanic cell in which a primary fuel or a derivative of such a fuel is oxidized electrochemically with an oxidant, thereby releasing the main part of the free energy of the reaction in the form of electrical energy.

Primary Fuel-Cell Battery: A primary fuel-cell battery consists of one or more fuel cells, reactants with storage, and all auxiliary equipment required to deliver the electrical energy as required. [Called "stack" instead of "battery" in this monograph.]*

Ideal Efficiency: The ideal efficiency of a primary fuel cell is the ratio, expressed in percent, of the free energy of reaction to the heat of reaction when the reaction is isothermal and reversible at constant pressure.

Voltage Efficiency: The voltage efficiency of a primary fuel cell is the ratio, expressed in percent, of the terminal voltage to the reversible emf under given conditions.

Fuel-Utilization Eficiency: The fuel-utilization efficiency of a primary fuel cell is the ratio, expressed in percent, of the ampere-hours through the external terminals to the calculated ampere-hours, as determined by the rate of consumption of the reactants for the stated operating condition. [Also referred to as the ***faradaic efficiency.]***

Energy Efficiency: The energy efficiency of a primary fuel cell is the ratio, expressed in percent, of the usable electrical energy at the external terminals to the maximum available energy.

Overall Efficiency: The overall efficiency of a primary fuel cell is that fraction, expressed in percent, of the heat of combustion of the fuel which is converted into electrical energy under stated operational conditions.

Current Density: The current density is the current passing through the unit area of geometric electrode area. (Amperes per square foot or milliamperes per square centimeter.)

Power Per Unit Weight (Volume): The power per unit weight (volume) of a primary fuel-cell battery is the ratio of the electrical power obtainable to the weight (volume) of the fuel-cell battery. (Watts per pound or watts per cubic foot.) [Also called ***power density.]***

Energy Per Unit Weight (Volume): The energy per unit weight (volume) of a primary fuel cell battery is the ratio of the total electrical energy delivered for the stated operating conditions to the weight (volume) of the fuel cell battery. (Watt-hours per pound or watt-hours per cubic foot.) [Also called ***energy density.]***

Polarization: Polarization, overvoltage, or overpotential can be defined as the deviation from the reversible emf caused by current flow at the electrode-electrolyte interface (volts). ***[Overvoltage*** and ***overpotential*** are terms inherited from early studies of gas evolution and their use is not recommended.]

Activation Polarization: Activation polarization is that part of the deviation from the reversible emf which is created by energy losses encountered in activating the reactant so that it may participate in the reactions occurring at the electrode-electrolyte interface at a definite rate.

---

*Comments in brackets are additions to the original.

PRECEDING PAGE BLANK NOT FILMED.

Concentration Polarization: Concentration polarization is that part of the deviation from the reversible emf caused by a change in the activities of reactants at the electrode-electrolyte interface and in the activities of the electrolyte solution and of the reaction products due to current polarization.

Ohmic Polarization: Ohmic polarization is that part of the deviation from the reversible emf caused by the ohmic resistance of the electrochemical system to current flow.

Exchange Current Density: When an electrode is operated reversibly, the current density for the forward reaction is equal to that of the reverse reaction and is defined to be the exchange current density. In this condition of the electrode, the sum of the overvoltages is zero. This value can be used to predict electrode polarization at high current densities.

Limiting Current: Assuming that the electrode processes are not adsorption or activation limited, which is the case with active catalysts, gas-diffusion and ion-diffusion-limited currents can be observed.

Regenerative Galvanic Cell: A galvanic cell (g.c.) in which the fuel and the oxidant are regenerated from the reaction product of the electrochemical reaction by energy from outside.

Four types may be distinguished:

(a) Electrically regenerative g.c.
(b) Thermally regenerative g.c.
(c) Photochemically regenerative g.c. (photogalvanic cell)
(d) Radiochemically regenerative g.c.

Regenerative Galvanic System: One or more regenerative galvanic cells with devices to regenerate the reactants from the electrochemical reaction product, plus any storage or auxiliary equipment required to deliver the electrical energy as required.

Definitions Referring to Electrolytically Regenerative Galvanic Cells

Voltage Eficiency: The voltage efficiency of an electrolytically regenerative galvanic cell is the ratio, expressed in percent, of the electrical energy delivered during discharges to the electrical energy required during the charge.

Overall Eficiency: The overall efficiency of an electrolytically regenerative galvanic cell is the ratio, expressed in percent, of the energy delivered during discharge to the total energy required for regeneration.

Definitions Referring to Photochemically Regenerative Galvanic Cells and Photogalvanic Cells

Photochemical Process: One in which light energy causes dissociation or activation of molecules or atoms in a gaseous, liquid, or solid phase.

Photochemically Regenerative Galvanic Cell: A continuously fed galvanic cell whose reactants are the products of a photochemical process.

Photogalvanic Process (Effect): One in which light energy causes dissociation or activation of molecules or atoms in an electrolyte adjacent to an solid electrode or at an electrode itself giving rise to a change in the potential of that electrode.

Photogalvanic Cell: One in which a photogalvanic effect is utilized to produce electrical energy.

Quantum Eficiency: The total number of molecules dissociated, reacted, or activated per photon.

Definition Referring to Radiochemically Regenerative Galvanic Cells

"g" Value: The total number of molecules dissociated per 100 electron volts.

2. CONVENTIONS FOR REPORTING DATA, INCLUDING GRAPHIC PRESENTATION

Convention for Reporting Electrode Potentials: Use the Stockholm convention for reporting electrode potentials, or at least state clearly what sign convention is being followed. [In this convention, the potential of a standard, 1 atmosphere, 77° F (25° C), reversible-hydrogen electrode is zero in a unit activity acid electrolyte. This is the standard hydrogen electrode (SHE). In unit activity hydroxyl electrolyte, the normal reversible-hydrogen electrode (NHE or RHE), is −0.83 volt versus SHE, and the standard reversible-oxygen electrode is +0.4 volt versus SHE. In fuel-cell work, it is often convenient to express electrode voltage versus a standard hydrogen electrode in the same electrolyte (NHE in SE), since this automatically corrects for different pH values. Reversible hydrogen is 0 versus NHE in SE and oxygen is 1.23 volts versus NHE in SE. Best fuel-cell performance is obtained when the anode (fuel) voltage is more negative and the cathode (oxidant) more positive.]

Conditions** for **Measurement** of **Current-Potential Characteristics** of **Fuel-Cell Electrodes: Current-potential data should be accompanied by several statements qualifying the measured data: *(a)* were steady-state values obtained; *(b)* under what conditions; *(c)* how long could steady-state values be maintained; *(d)* specify operating conditions (temperature, pressures, concentrations); *(e)* specify electrolyte; (f) describe geometrical dimensions of experimental arrangement; (*g*) describe electrodes and catalysts; *(h)* describe observed scaleup effects; *(i)* describe effects due to change in configuration (change of current path, gas flow, electrolyte flow, etc.); (*j*) describe effects of pressure gradients; and (*k*) describe changes of current-potential characteristics under defined operating conditions with time.

Graphical Reporting: In data reporting of current-potential curves, important parameters such as temperature, rate of flow of gases and electrolyte, and geometrical design should be included.

3. DEFINITIONS OF PROPERTIES OF MATERIALS

a. Membrane and Matrix Electrolytes

Ion Exchange Membrane Electrolytes: This is a solid electrolyte usually in the form of an organic gel or film with fixed ionized groups. These membranes function as an ionic-transporting medium and not as a physical barrier for fuel-cell reactants. Anion- and cation-exchange membranes are being distinguished. The anion-exchange membranes have fixed positive charged groups and transport negatively charged ions. The cation-exchange membranes have fixed negative charged groups and transport positive charged ions.

Matrix Electrolyte: A solid porous matrix in which liquid electrolyte is absorbed.

Homogeneous Membrane Electrolytes: These are described as ion-exchange membranes polymerized from a homogeneous solution or formed by treating a film cast from a homogeneous solution or melt. They do not have discrete particles embedded in a matrix, but appear smooth and quite continuous under a microscope.

Heterogeneous Membrane Electrolytes: Ion-exchange membranes consisting of ion-exchange particles embedded in a nonconducting matrix. The membranes are readily identified by an examination with the naked eye or with a microscope.

Exchange Capacity** of **Ion-Exchange Membrane: This is defined as the equivalent of exchangeable counter-ions present in **1** square centimeter of membrane area. The exchange capacity of a membrane is determined by placing it into **a** given standard exchange state, followed by elution with neutral salt and direct titration.

b. Electrodes

Electrode: The physical component of a cell immersed in or adjacent to the electrolyte that serves in combination with that electrolyte as an electrochemical reaction zone and as the terminal for the external flow of current.

Solid Electrode: Any nonporous metal or mixtures of metals or oxides, etc., promoting electrochemical oxidation of fuel or electrochemical reduction of oxidants. Fuel or oxidant supply to the electrode surface by diffusion or convection.

Porous Electrode: Any porous metallic or nonmetallic body or mixtures thereof promoting fuel or oxidant supply to the active electrode zone by diffusion, flow, or convection (e.g., sintered nickel, porous carbon, etc.).

Powdered Electrode: The class of electrode structures involving finely divided physically separable particles or granules.

Electrode Carriers: The physical component of an electrode that acts as a support for the catalyst and as a conductive medium to the external circuit.

Hydrophobic Electrode: Water or aqueous electrolyte repelling.

Hydrophilic Electrode: Water or aqueous electrolyte attracting.

Heteroporous Electrode: Electrode with several different groups of pore sizes and volumes.

Homoporous Electrode: Electrode with practically the same pore radius over entire pore-size distribution.

Contact Angle: **A** definite angle of contact observed when a liquid is placed in contact with a solid. The angle is 180”for complete nonwetting, whereas an angle of zero degrees represents complete wetting.

Electrode "Drowning": Flooding of the pores, by the electrolyte, through which gas transportation to the reaction zone of a gas electrode occurs.

Three-phase Zone: The area of contact between three phases: solid, liquid, and gaseous.

Micropores: The pore groups with pore diameters less than 0.01 micron or the pores in which capillary condensation takes place.

Macropores: The pore groups with pore diameters greater than 0.01 micron.

Apparent, Geometric, or Projected Area: The area outlined by the macroscopic physical configuration of the electrode.

Effective Area: The area actually available for the electrochemical reaction under consideration.

APPENDIX B

Tabulated Data

The data contained here by no means represent a complete compilation of all the data useful in fuel-cell development. They are based on data reported only in the contract reports and were either determined experimentally in the contract work or obtained through extensive literature searching or calculation from known data. Data which are generally available from standard sources are not given. unless of particular reference to the understanding of fuel cells.

TABLE B.1.—*Maximum Performance of Various Fuel-Cell Reactants (583)*

Reaction	AF^0, kcal/mole	E^0 (volts). 25" C	W-hr/lb, reactants
$\frac{1}{2}H_2(g)+\frac{1}{2}F_2(g)\rightarrow HF(aq)$	66.1	2.87	1740
$O_3(g)+H_2(g)\rightarrow O_2(g)+H_2O(l)$	95.8	2.07	1010
$ClO_2(g)+\frac{1}{2}H_2(g)+OH^-(aq)\rightarrow H_2O(l)+ClO_2^-(aq)$	45.9	1.99	282
$H_2O_2(l)+H_2(g)\rightarrow 2H_2O(l)$	85.2	1.85	1240
$ClO_3^-(aq)+H_2(g)\rightarrow Cl^-(aq)+H_2O(l)$	79.1	1.72	780
$HClO_2(aq)+H_2(g)\rightarrow HClO(aq)+H_2O(l)$	75.9	1.64	473
$HBrO(aq)+\frac{1}{2}H_2(g)\rightarrow \frac{1}{2}Br_2(aq)+H_2O(l)$	35.8	1.55	193
$BrO^-_3(aq)+3H_2(g)\rightarrow Br^-(aq)+3H_2O(l)$	199.7	1.44	784
$\frac{1}{2}H_2(g)+\frac{1}{2}Cl_2(aq)\rightarrow HCl(aq)$	33.0	1.43	476
$CO(g)+\frac{1}{2}O_2(g)\rightarrow CO_2(aq)$	59.5	1.29	712
$H_2(g)+\frac{1}{2}O_2(g)\rightarrow H_2O(l)$	56.7	1.23	1660
$HClO_3(aq)+H_2(g)\rightarrow HClO_2(aq)+H_2O(l)$	56.0	1.21	341
$HClO_4(aq)+H_2(g)\rightarrow HClO_3(aq)+H_2O(l)$	54.8	1.19	282
$Ag(s)+\frac{1}{2}Cl_2(g)\rightarrow AgCl(s)$	26.2	1.13	96.1
$\frac{1}{2}H_2(g)+\frac{1}{2}Br_2(aq)\rightarrow HBr(aq)$	25.6	1.11	168
$CH_4(g)+2O_2(g)\rightarrow CO_2(g)+2H_2O(l)$	195.5	1.06	1280
$N_2O_4(g)+H_2(g)\rightarrow 2HNO_2(aq)$	49.1	1.06	275
$H_2SO_3(aq)+\frac{1}{2}O_2(g)\rightarrow H_2SO_4(aq)$	48.8	1.05	262
$Ag(s)+\frac{1}{2}Br_2(aq)\rightarrow AgBr(s)$	23.4	1.01	65.6
$Ag(s)+HCl(aq)+\frac{1}{4}O_2(g)\rightarrow AgCl(s)+\frac{1}{2}H_2O(l)$	23.2	1.00	89.1
$Fe^{3+}(aq)+\frac{1}{2}H_2(g)\rightarrow Fe^{2+}(aq)+H^+(aq)$	17.77	.77	164
$2Ag(s)+I_3^-(aq)\rightarrow 2AgI(s)+I^-(aq)$	31.7	.68	28.0
$H_2(g)+I_3^-(aq)\rightarrow 2HI(aq)+I^-(aq)$	24.7	.53	51.0
$CO(g)+Cl_2(g)\rightarrow COCl_2(g)$	17.5	.38	96.1
$2Fe^{3+}(aq)+3I^-(aq)\rightarrow 2Fe^{2+}(aq)+I_3^-(aq)$	10.8	.23	11.5
$NO(g)+\frac{1}{2}Cl_2(g)\rightarrow NOCl(g)$	4.86	.21	39.1

TABLE B.2.—*Energetics of Selected Fuel-Cell Systems* (*408*)

Fuel	Oxidant with or without peroxide mechanism[a]	E^0 (volts). (25° *C*)	W-hr/lb, fuel + oxidant
$NH_3(g)$	O_2	1.124	1000
	(HO_2^-)	.681	605
$NH_3(g)$	Air	1.124	2410
	(HO_2^-)	.681	1459
$N_2H_4(g)$	O_2	1.56	1185
	(HO_2^-)	1.12	805
$N_2H_4(g)$	Air	1.56	2370
	(HO_2^-)	1.12	1705
$H_2(g)$	O_2	1.23	1661
	(HO_2^-)	.787	1065
$H_2(g)$	Air	1.23	14 950
	(HO_2^-)	.787	9570
$CH_3OH(g)$	O_2	1.19	1086
	(HO_2^-)	.747	682
$CH_3OH(g)$	Air	1.19	2710
	(HO_2^-)	.747	1700
$CH_3OH(l)$	O_2	1.185	1080
	(HO_2^-)	.742	675
$CH_3OH(g)$	Air	1.185	2700
	(HO_2^-)	.742	1685
$CH_3OH(g)$	O_2	1.234	1130
$CH_3OH(g)$	Air	1.234	2820
$C_4H_{10}(g)$	O_2	1.12	1335
$C_4H_{10}(g)$	Air	1.12	6120

[a] Peroxide mechanism values are based on the production of standard state of $HO_2^-(aq)$ at the cathode.

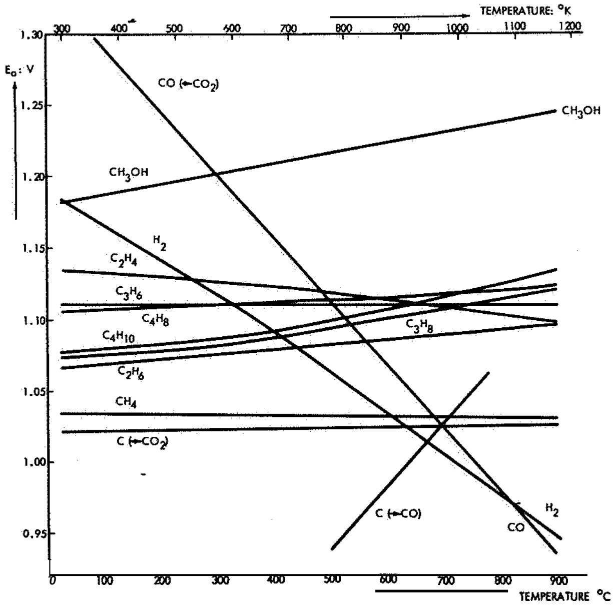

Standard state is 1 atmosphere of each reactant (gaseous state) and product (also gaseous state).

FIGURE B.1.—Standard cell emf for different fuels reacting with oxygen (*147*)

TABLE B.3.—*Thermodynamic Values for* H_2, O_2, N_2H_4, *and Some Common Hydrocarbon Fuels (397)*

Reactant (half-cell reaction or complete-cell reaction)	ΔF^0_f, kcal/mole	ΔF^0_r, kcal/mole	E^0, volts	ΔH^0_f, kcal/mole	ΔH^0_r, kcal/mole	$\Delta F^0_r/\Delta H^0_r$, ideal eff., %	M.W., g/g-mole	Theoretical energy density, kW-hr/lb fuel
Hydrogen	0			0			2.016	
$H_2 \rightleftharpoons 2H^+ + 2e^-$		0	0					
$H_2 + \frac{1}{2}O_2 \rightleftharpoons H_2O$		—56.69	1.229		—68.317	83.0		14.83
Oxygen	0			0			32.0	
$\frac{1}{2}O_2 + 2H^+ + 2e^- \rightleftharpoons H_2O$		—56.69	1.229					1.868 (per lb. of O_2)
Methane	—12.14			—17.889			16.04	
$CH_4 + 2H_2O \rightleftharpoons CO_2 + 8H^+ + 8e^-$		31.2	.169					
$CH_4 + 2O_2 \rightleftharpoons CO_2 + 2H_2O$		—195.5	1.060		—212.80	91.9		6.43
$CH_4 + H_2O \rightleftharpoons CH_3OH(aq) + 2H^+ + 2e^-$		27.1	.586					
$CH_4 + \frac{1}{2}O_2 \rightleftharpoons CH_3OH(aq)$		—29.56	.643		—46.65	63.4		.971
Methanol(*aq*)	—41.70			—58.79			32.04	
$CH_3OH(aq) + H_2O \rightleftharpoons CO_2 + 6H^+ + 6e^-$		4.13	.030					
$CH_3OH(aq) + 1\frac{1}{2}O_2 \rightleftharpoons CO_2 + 2H_2O$		—166.96	1.199		—171.90	97.1		2.75
$CH_3OH(aq) \rightleftharpoons HCHO(aq) + 2H^+ + 2e^-$		8.75	.189					
$CH_3OH(aq) + \frac{1}{2}O_2 \rightleftharpoons HCHO(aq) + H_2O$		—46.0	1.040		(—64)	(72)		.760
Formaldehyde(*aq*)	—31.0			(—38)			30.03	
$HCHO(aq) + H_2O \rightleftharpoons CO_2 + 4H^+ + 4e^-$		—6.6	—.072					
$HCHO(aq) + O_2 \rightleftharpoons CO_2 + H_2O$		—120.0	1.301		(—124)	(97)		2.11
$HCHO(aq) + H_2O \rightleftharpoons HCOOH(aq) + 2H^+ + 2e^-$		2.6	.056					
$HCHO(aq) + \frac{1}{2}O_2 \rightleftharpoons HCOOH(aq)$		—54.1	1.173		(—60)	(90)		.950
Formic acid(*aq*)	—85.1			—98.0			46.03	
$HCOOH(aq) \rightleftharpoons CO_2 + 2H^+ + 2e^-$		—9.05	—.196					
$HCOOH(aq) + \frac{1}{2}O_2 \rightleftharpoons CO_2 + H_2O$		—55.85	1.425		—64.37	86.8		.638
$HCOOH(aq) \rightleftharpoons CO + H_2O$		—4.398						
Carbon monoxide	—32.81			—26.42			28.0	
$CO + H_2O \rightleftharpoons CO_2 + 2H^+ + 2e^-$		—4.76	—.103					
$CO + \frac{1}{2}O_2 \rightleftharpoons CO_2$		—61.45	1.332		—67.63	90.9		1.16
Ethane	—7.86			—20.24			30.07	
$C_2H_6 + 4H_2O \rightleftharpoons 2CO_2 + 14H^+ + 14e^-$		46.5	.144					
$C_2H_6 + 3\frac{1}{2}O_2 \rightleftharpoons 2CO_2 + 3H_2O$		—350.7	1.085		—372.82	94.1		6.15
$C_2H_6 + H_2O \rightleftharpoons C_2H_5OH(aq) + 2H^+ + 2e^-$		21.2	.460					
$C_2H_6 + \frac{1}{2}O_2 \rightleftharpoons C_2H_5OH(aq)$		—34.5	.769		—48.61	71.0		.607
Ethanol(*aq*)	—42.4			—68.85			46.07	
$C_2H_5OH(aq) + 3H_2O \rightleftharpoons 2CO_2 + 12H^+ + 12e^-$		24.0	.087					
$C_2H_5OH(aq) + 3O_2 \rightleftharpoons 2CO_2 + 3H_2O$		—316.2	1.142		—324.21	97.5		3.62
$C_2H_5OH(aq) \rightleftharpoons CH_3CHO(aq) + 2H^+ + 2e^-$		8.86	.192					
$C_2H_5OH(aq) + \frac{1}{2}O_2 \rightleftharpoons CH_3CHO(aq) + H_2O$		—47.9	1.037		—49.35	97.1		.549
Acetaldehyde(*aq*)	—33.6			—49.88			44.05	
$CH_3CHO(aq) + 3H_2O \rightleftharpoons 2CO_2 + 10H^+ + 10e^-$		15.2	.066					
$CH_3CHO(aq) + 2\frac{1}{2}O_2 \rightleftharpoons 2CO_2 + 2H_2O$		—268.3	1.163		—274.86	97.6		3.21
$CH_3CHO(aq) + H_2O \rightleftharpoons CH_3COOH(aq) + 2H^+ + 2e^-$		—5.45	—.118					
$CH_3CHO(aq) + \frac{1}{2}O_2 \rightleftharpoons CH_3COOH(aq)$		—61.9	1.347		—66.86	92.6		.747

TABLE B.3.—*Thermodynamic Values for* H_2, O_2, N_2H_4, *and Some Common Hydrocarbon Fuels (397)*—Continued

Reactant (half-cell reaction or complete-cell reaction)	ΔF^0_f, kcal/mole	ΔF^0_r, kcal/mole	E^0, volts	ΔH^0_f, kcal/mole	ΔH^0_r, kcal/mole	$\Delta F^0_r/\Delta H^0_r$, ideal eff., %	M.W., g/g-mole	Theoretical energy density, kW-hr/lb fuel
Acetic acid(*aq*)	—95.51			—11[illegible]74			60.05	
$CH_3COOH(aq)+2H_2O \rightleftharpoons 2CO_2+8H^++8e^-$		20.37	0.110					
$CH_3COOH(aq)+2O_2 \rightleftharpoons 2CO_2+2H_2O$		—206.4	1.119		—208.00	99.2		1.82
$CH_3COOH(aq)+2H_2O \rightleftharpoons H_2C_2O_4(aq)+6H^++6e^-$		42.9	.310					
$CH_3COOH(aq)+1\frac{1}{2}O_2 \rightleftharpoons H_2C_2O_4(aq)+H_2O$		—128.0	.919		—147.15	87.0		1.12
Oxalic acid(*aq*)	—166.8			—195.57			90.03	
$H_2C_2O_4(aq) \rightleftharpoons 2CO_2+2H^++2e^-$		—22.6	—.490					
$H_2C_2O_4(aq)+\frac{1}{2}O_2 \rightleftharpoons 2CO_2+H_2O$		—78.4	1.719		—60.85	130		.46
Ethylene	16.28			12[illegible]0			28.05	
$C_2H_4+4H_2O \rightleftharpoons 2CO_2+12H^++12e^-$		22.0	.079					
$C_2H_4+3O_2 \rightleftharpoons 2CO_2+2H_2O$		—318.1	1.150		—337.24	94.3		5 8
Acetylene	5.00			54.19			26.04	
$C_2H_2+4H_2O \rightleftharpoons 2CO_2+10H^++1$[illegible]		—11.8	—.051					
$C_2H_2+2\frac{1}{2}O_2 \rightleftharpoons 2CO_2+H_2O$		—295.2	1.280		—310.61	95.0		5.98
Propane	—5.61			—24.82			44.09	
$C_3H_8+6H_2O \rightleftharpoons 3CO_2+20H^++20e^-$		62.97	.136					
$C_3H_8+5O_2 \rightleftharpoons 3CO_2+$ [illegible]H_2O		—503.93	1.095		—530.60	95.0		6.03
Propylene	14.99			4.88			42.08	
$C_3H_6+6H_2O \rightleftharpoons 3CO_2+18H^++18e^-$		42.37	.102					
$C_3H_6+4\frac{1}{2}O_2 \rightleftharpoons 3CO_2+3H_2O$		—467.84	1.127		—491.98	95.1		5.8 7
n-Butane	—3.75			—29.81			58.12	
[illegible]$H_{10}+8H_2O \rightleftharpoons 4C$[illegible]$+26H^++26e^-$		80.23	.134					
[illegible]$H_{10}+6\frac{1}{2}O_2 \rightleftharpoons 4C$[illegible]$_2+5H_2O$		—656.74	1.095		—687.98	95.5		5.96
Isobutane	—4.30			—31.45			58.12	
$C_4H_{10}+8H_2O \rightleftharpoons 4CO_2+26H^++26e^-$		80.78	.135					
$C_4H_{10}+6\frac{1}{2}O_2 \rightleftharpoons 4CO_2+5H_2O$		—656.19	1.095		—686.34	95.6		59 6
1-Butene	17.22			.280			56.10	
$C_4H_8+8H_2O \rightleftharpoons 4CO_2+24H^++24e^-$		59.26	.107					
$C_4H_8+6O_2 \rightleftharpoons 4CO_2+4H_2O$		—621.02	1.122		—649.75	95.6		5.84
Isobutene	14.58			—3.34			56.10	
[illegible]$H_8+8H_2O \rightleftharpoons 4CO_2+24H^++24e^-$		61.90	.112					
[illegible]$H_8+6O_2 \rightleftharpoons 4CO_2+$[illegible]$_2O$		—618.38	1.117		—646.13	95.7		5.81
cis-2-Butene	16.05			—1.36			56.10	
$C_4H_8+8H_2O \rightleftharpoons 4CO_2+24H^++24e^-$		60.43	.109					
$C_4H_8+6O_2 \rightleftharpoons 4CO_2+4H_2O$		—619.85	1.120		—684.11	95.6		5.83
trans-2-Butene	15.32			—2.41			56.10	
$C_4H_8+8H_2O \rightleftharpoons 4CO_2+24H^++2$[illegible]		60.43	.109					
$C_4H_8+6O_2 \rightleftharpoons 4CO_2+4H_2O$		—619.12	1.119		—647.06	95.7		5.82
n-Pentane	—1.96			—35.00			72.15	
$C_5H_{12}+10H_2O \rightleftharpoons 5CO_2+32H^++32e^-$		97.56	.132					
$C_5H_{12}+8O_2 \rightleftharpoons 5CO_2+6H_2O$		—809.48	1.097		—845.15	95.8		5.92
Neopentane	—3.64			—39.67			72.15	
$C_5H_{12}+10H_2O \rightleftharpoons 5CO_2+32H^++32e^-$		99.24	.135					
$C_5H_{12}+8O_2 \rightleftharpoons 5CO_2+6H\ O$		—807.80	1.095		—840.48	96.1		5.91

n-Hexane	.05			−39.96			86.17	
$C_6H_{14}+12H_2O \rightleftharpoons 6CO_2+38H^+ +38e^-$		114.67	.131					
$C_6H_{14}+9\frac{1}{2}O_2 \rightleftharpoons 6CO_2+7H_2O$		−962.44	1.098		−1002.56	96.0		5.89
Cyclohexane	7.59			−29.43			84.16	
$C_6H_{12}+12H_2O \rightleftharpoons 6CO_2+36H^+ +36e^-$		107.13	.129					
$C_6H_{12}+9O_2 \rightleftharpoons 6CO_2+6H_2O$		−913.29	1.100		−944.77	96.7		5.72
Benzene	30.99			19.82			78.11	
$C_6H_6+12H_2O \rightleftharpoons 6CO_2+30H^+ +30e^-$		83.73	.121					
$C_6H_6+7\frac{1}{2}O_2 \rightleftharpoons 6CO_2+3H_2O$		−766.62	1.108		−789.07	97.2		5.18
n-Heptane	2.09			−44.89			100.20	
$C_7H_{16}+14H_2O \rightleftharpoons 7CO_2+44H^+ +44e^-$		131.75	.130					
$C_7H_{16}+11O_2 \rightleftharpoons 7CO_2+8H_2O$		−1115.43	1.099		−1160.0	96.2		5.87
Toluene	29.23			11.95			92.13	
$C_7H_8+14H_2O \rightleftharpoons 7CO_2+36H^+ +36e^-$		104.61	.126					
$C_7H_8+9O_2 \rightleftharpoons 7CO_2+4H_2O$		−915.81	1.103		−943.57	97.1		5.24
n-Octane	4.14			−49.82			−114.23	
$C_8H_{18}+16H_2O \rightleftharpoons 8CO_2+50H^+ +50e^-$		148.82	.129					
$C_8H_{18}+12\frac{1}{2}O_2 \rightleftharpoons 8CO_2+9H_2O$		−1268.43	1.100		−1317.43	96.3		5.86
2,2,4-Trimethyl pentane	3.13			−53.57			114.23	
$C_8H_{18}+16H_2O \rightleftharpoons 8CO_2+50H^+ +50e^-$		149.83	.130					
$C_8H_{18}+12\frac{1}{2}O_2 \rightleftharpoons 8CO_2+9H_2O$		−1267.42	1.09[illegible]		−1313.68	96.6		5.86
n-Nonane	6.18			−54.74			128.25	
$C_9H_{20}+18H_2O \rightleftharpoons 9CO_2+56H^+ +56e^-$		165.90	.129					
$C_9H_{20}+14O_2 \rightleftharpoons 9CO_2+10H_2O$		−1421.42	1.101		−1474.88	96.4		5.85
n-Decane	8.23			−59.67			142.28	
$C_{10}H_{22}+20H_2O \rightleftharpoons 10CO_2+62H^+ +62e^-$		182.97	.129					
$C_{10}H_{22}+15\frac{1}{2}O_2 \rightleftharpoons 10CO_2+11H_2O$		−1574.42	1.101		−1632.32	96.5		5.84
n-Hexadecane	20.52			−89.23			226.44	
$C_{16}H_{34}+32H_2O \rightleftharpoons 16CO_2+98H^+ +98e^-$		285.40	.126					
$C_{16}H_{34}+24\frac{1}{2}O_2 \rightleftharpoons 16CO_2+17H_2O$		−2492.41	1.103		−2576.96	96.7		5.8[illegible]
Hydrazine(*aq*)	30.56			8.16			32.05	
$N_2H_4(aq)+4OH^- \rightleftharpoons N_2+4H_2O+4e^-$		−106.9	−1.158					
$N_2H_4(aq)+O_2 \rightleftharpoons N_2+2H_2O$		−143.9	1.559		−144.8	99.4		2.36

Unless otherwise indicated, a particular molecular or ionic species is in its standard state at 77° F (25° C). The symbol (*aq*) indicates a solution in water, with an activity of 1; H_2O refers to liquid water in all cases. Where there is some doubt about the thermodynamic value, it is given in parentheses. The European sign convention has been used for half-cell voltages. Half-cell voltages in standard acid (values given) can be converted to values in standard alkali by adding −0.823 volt. Half-cell voltages for the formation of standard-state $CO_3^{=}$ instead of $CO_2(g)$ are 0.4 volt more negative and the total cell potential is increased by 0.4 v t. The theoretical energy densities are per pound of fuel (not fuel plus oxygen).

The symbols used in table B.3 are:

ΔF_f^0 = Standard-state free energy of formation at 77° F (25° C)
ΔF_r^0 = Standard-state free energy of reaction at 77° F (25° C)
E^0 = Standard-state reversible voltage at 77° F (25° C)
ΔH_f^0 = Standard-state heat of formation at 77° F (25° C)
ΔH_r^0 = Standard-state heat of reaction at 77° F (25° C)
M.W. = Molecular weight of reactant

REFERENCES

1. Latimer, W. M.: The Oxidation States of the Elements and Their Potentials in Aqueous Solutions. Prentice-Hall, Inc., Englewood Cliffs, N.J., 1952.
2. Rossini, F. E.; et al.: Selected Values of Properties of Hydrocarbons, NBS Circular C461. U.S. Government Printing Office, Washington, 1947.
3. Handbook of Chemistry and Physics. Thirty-first ed. Chemical Rubber Pub. Co., Cleveland, 1948.

TABLE B.4.—*Thermal Dissociation of* C_nH_{2n+2} *into* C_nH_{2n} *and* H_2 *as a Function of the Temperature at 1 Atmosphere (147)*

Temperature, "K	Temperature, "C	Percent dissociation		
		C_2H_6	C_3H_8	n-C_4H_{10}
300	27	1.7×10^{-7}	3.2×10^{-6}	2.4×10^{-6}
400	127	1.7×10^{-4}	1.8×10^{-3}	1.4×10^{-3}
500	227	1.1×10^{-2}	8×10^{-2}	7×10^{-2}
600	327	0.17	1.04	0.89
700	427	1.45	6.61	5.8
800	527	6.73	25.7	23.2
900	627	21.9	61.8	58.3
1000	727	50.6	88.1	88.6
1100	827	79.1	96.7	963
1200	927	92.8	98.9	98.8

Electrolyte	Solubility, millimoles/liter				
	10" C	20" C	40" C	60" C	80" C
H_2O	7.29	5.18	3.36	2.64	2.36
1.09 *M* H_2SO_4	5.81	3.84	2.40	2.00	1.80
2.33*M* H_2SO_4	4.24	2.72	1.76	1.40	1.36
5.31*M* H_2SO_4	2.28	1.36	.76	.64	.56

TABLE B.6.—*Solubility of Ethane in Aqueous* H_2SO_4 *and* H_3PO_4 *(144)*

[Total pressure = 1 atmosphere]

Electrolyte	Solubility, millimoles/liter			
	10" C	30" C	50" C	70" C
H_2O	2.61	1.87	1.29	0.90
2 *N* H_2SO_4	1.92	1.43	1.05	.75
4 *N* H_2SO_4	1.43	1.10	.82	.60
2 *N* H_3PO_4	2.10	1.55	1.14	.82
4 *N* H_3PO_4	1.73	1.32	1.00	.72

Electrolyte	Solubility, millimoles/liter-atmosphere[a]				
	20" C	30" C	50" C	70" C	90" C
H_2O	1.42	1.15	0.75	0.46	0.33
2 *N* H_2SO_4	1.10	.91	.60	.41	.31
4 *N* H_2SO_4	.86	.71	.50	.37	.29
2 N H_3PO_4	1.22	1.00	.67	.45	.31
4 N H_3PO_4	1.06	0.87	.61	.43	.30

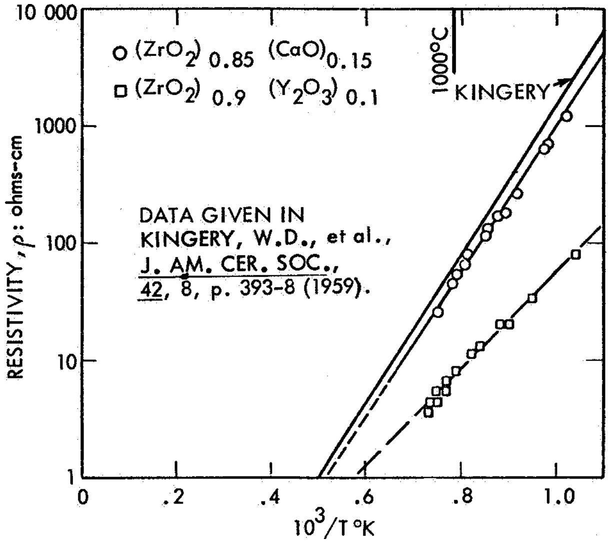

FIGURE B.2.—Resistivity of solid electrolytes *(792)*.

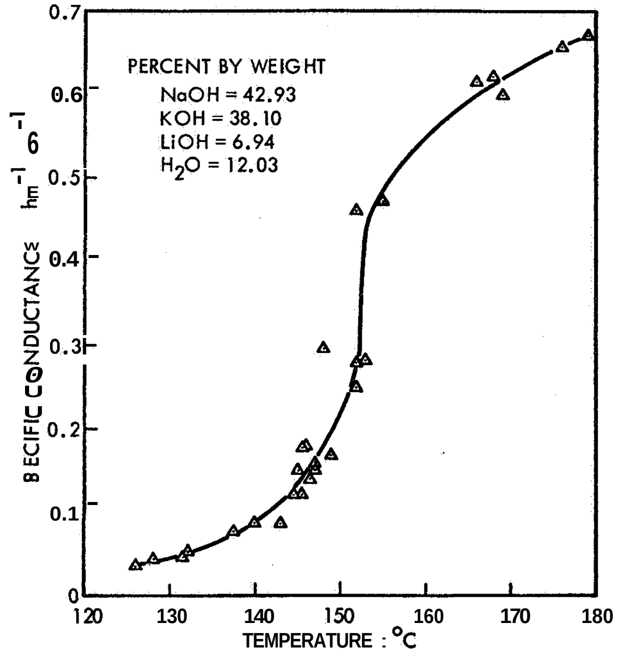

FIGURE B.3.—Specific conductance of NaOH-KOH-LiOH melt (408).

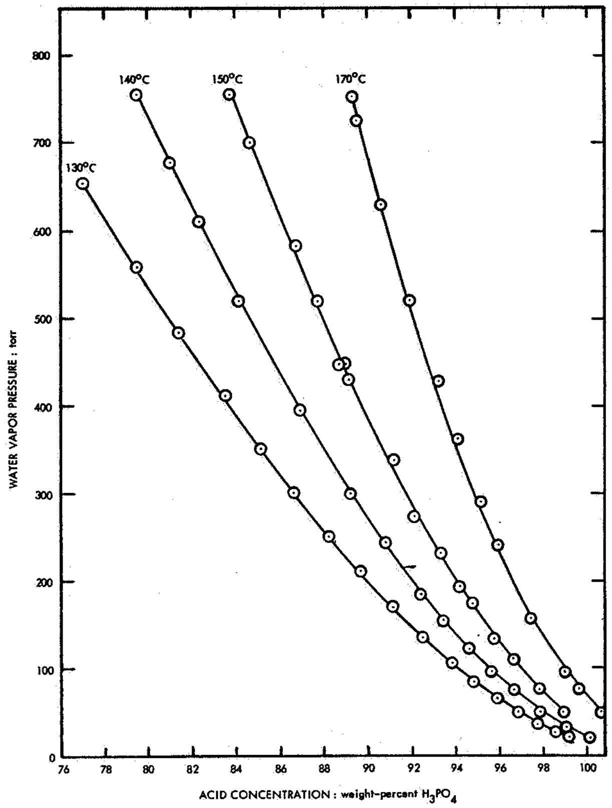

FIGURE B.4.—Vapor pressure of phosphoric acid solutions *(309)*.

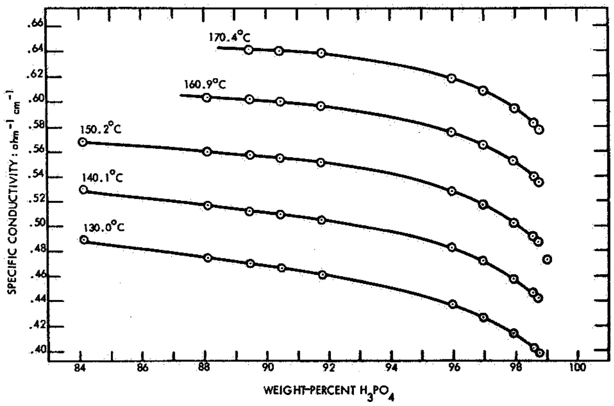

See also: Van Wazer, J. R.: Phosphorus and Its Compounds. Vol. I. Interscience Pub., Inc., New York. 1958.

FIGURE B.5.—Ionic conductivity of phosphoric acid solutions *(309)*.

TABLE B.8.—*Solubility of Propane in* H_3PO_4[a] *(310)*

Wt-% H_3PO_4	Temperature. °C	Partial pressure propane. mm Hg	Solubility, m/Mliter
85.0	100	127	0.039
85.0	100	328	.070
85.0	100	585	.172
93.0	100	100	.025
93.0	100	285	.068
93.0	100	435	.105
93.0	100	627	.161
93.0	100	754	.153
93.0	100	840	.205
85.0	120	97	.059
85.0	120	288	.073
85.0	120	316	.077
85.0	120	385	.092
85.0	120	414	.102
85.0	120	480	.114
85.0	120	567	.125

[a] The solubility of propane in concentrated Cs_2CO_3 solution was at least 10^3 less than in H_3P(

TABLE *B.9.—Solubility of* O_2 *in Various Electrolytes; 1 Atmosphere* O_2, *25° C (698. 699. 700)*

Normality of H_2SO_4	Solubility. mM/liter	Normality of KOH	Solubility. mM/liter	Normality of H_3PO_4	Solubility. mM/liter
0	1.263	1.08	0.759	0.995.	1.236
0.200.	1.229	2.35.	.444	1.23.	1.231
0.600.	1.183	3.96.	.270	2.04.	1.151
2.00.	1.014	5.15.	.159	3.58.	1.065
4.00.	.824	7.07.	.0803	5.44.	1.024
6.00.	.721	10.3	.0295	6.01.	.976
8.00.	.657	12.55.	.0290	12.47.	.769
12.00.	.601	14.0.	.0311	25.25.	.513
16.00.	.550			29.9.	.426
20.00.	.489			43.0.	.276
25.00.	.451				
27.4.	.452				
30.0.	.492				
31.3.	.568				
33.9	.860				
35.3.	1.105				

O_2 in 6.9 *M* KOH at 25° C. 1 atmosphere given as 0.194 in moles per liter (*408*).

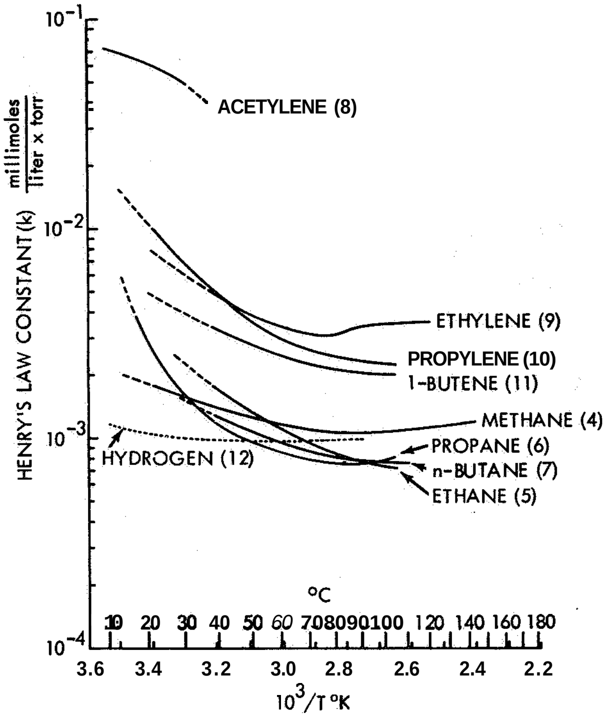

FIGURE B.6.—Solubilities of hydrocarbons and hydrogen in water.

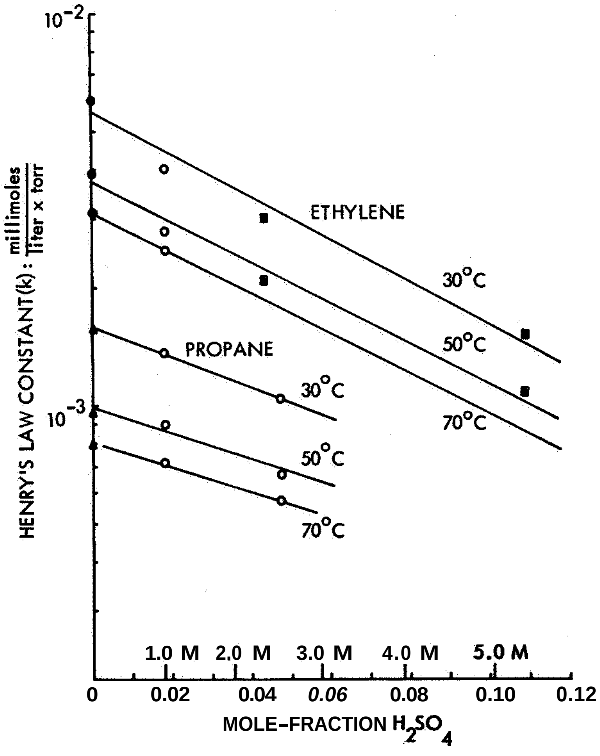

FIGURE B.7.—Solubilities of propane and ethylene in aqueous sulfuric acid (*139*).

TABLE B.10.—*Solubility of Li in LiCl and LiCl in Li (112)*

Temperature, °F	1130 (609° C)	1202 (650° C)	1322 (727° C)	1418 (770° C)	1832 (1000° C)
Atom-% Li in LiCl	1.3	0.5	3.1	2.6	2.0
Mole-% LiCl in Li	8.5	....	9.6	8.8	....

TABLE B.11.—*Solubility of Li_3Bi in LiCl-LiF Eutectic Salt Mixture (114)*

Temperature, °K	*Mole-percent* Li_3Bi *in* LiCl-LiF
873	0.056
973	.17
1073	.42
1173	.92
1273	1.8

TABLE B.12.—*Solubility of NH_3 in 30 Weight-Percent KOH Solution (404)*

Temperature, °F	*Grams* NH_3 *per liter of solution*
86 (30° C)	72
104 (40° C)	50
122 (50° C)	38
140 (60° C)	28
158 (70° C)	20
176 (80° C)	13

Temperature, °F	Solubility, moles/liter	
	3 *M* K_2CO_3	4 *M* K_2CO_3
77 (25° C)	1.07	0.5
131 (55° C)	1.67	1.26
176 (80° C)	2.72	2.18
212 (100° C)	....	2.44

TABLE B.14.—*Miscellaneous Data*

Report	*Results*
234	Heat transfer from Al to Al varied from 16 to 123 Btu/ft^2-hr-°F, depending on vacuum, smoothness of contact and contact pressure. In air, the value was 333. A layer of silicone grease between the surfaces gave 158.
408	Solubility of hydrazine in H_2SO_4. Sonner, F., and Weise, K., Z. Anorg. u. Allgem. Chem., vol. 94, pp. 51–91 (1916). Diffusion coefficient of N_2H_4 in 6.9 *M* KOH solution at 77° F (25° C) = $(1.94)(10^{-5})$ cm^2/sec.
456	Toxic levels: N_2H_4: 1 ppm for inhalation B_5H_9: 0.01 ppm
126	O_3: 0.1 ppm in submarines.

Element	Metal		Bromide		E^0	Iodide		E^0
	mp	bp	mp	bp		mp	bp	
Bi(+3)	271	1450	218	453	0.69	439	500	0.29
Ga(+3)	30	1700	122	279	1.17	212	345	.71
In(+3)	155	1450	436	subl.	1.22	210	500	.84
Li(+1)	186	1340	547	1265	3.42	446	1190	2.80
Pb(+2)	327	1620	373	918	1.22	402	954	.84
Sn(+2)	232	2260	216	620	1.15	320	720	.80
T1(+1)	303	1650	460	815	1.59	440	824	1.24

TABLE B.16.—*Thermodynamic Functions of Molten Salts* (*191*)

Group	Product	mp (M)°K	mp (MX)°K	ΔH_{fus} (M) kcal/mole	ΔH_{fus} (MX) kcal/mole	ΔF^0_{298} kcal/mole	ΔH^0_{298} kcal/mole	ΔS^0_{298} cal/deg mole	$\Delta F^0/\Delta H^0$ at 298° K	ΔF^0_{700} kcal/mole	ΔH^0_{700} kcal/mole	$\Delta F^0/\Delta H^0$ at 700° K
I A	LiH	459	957	1.6	7.0	−16.7	−21.3	−15.5	0.78	−10.0	−15.9	0.63
III A	$AlBr_3$	932	371	2.6	2.7	−124	−138	−46	.86	−108.3	−137.9	.79
IV A	$TiCl_2$	2000	950	4.6	6.0	−96	−114	−35	.84	−90.5	−113.6	.80
VI A	WCl_6	3650	548	8.4	5.7	−74	−96.9	−93	.76	−33.3	−99.6	.33
VIII	CoI_2	1766	790	3.7	6.0	−26	−36	−32	.72	−13.6	−33.7	.40
II B	$ZnCl_2$	693	556	1.6	5.5	−88.3	−99.4	−37.4	.83	−74.8	−95.7	.78
	CdI_2	594	660	1.5	3.6	−53.3	−63.3	−35.1	.84	−38.6	−61.2	.63
III B	GaI_3	303	485	1.3	3.9	−58	−73	−49	.80	−38.3	−70.5	.54
IV B	$SnCl_2$	505	520	1.7	3.0	−72.2	−83.6	−32	.86	−59.2	−79.8	.74
V B	$BiCl_3$	544	505	2.6	2.6	−76.3	−90.6	−47.8	.84	−57.4	−90.6	.63
	AsI_3	1087	415	6.6	2.2	−21.9	−35.9	−47	.61	−4.5	−40.3	.11
VI B	$TeCl_4$	723	497	4.3	4.5	−58.3	−77.4	−64	.75	−64	−77.2	.45

TABLE B.17.—*Calculated Permeability of Metals to Hydrogen at 1020° F and 760-mm Pressure* (*591*)

Metal	Hydrogen solubility, atom percent	Solubility, cc/cc	D_H, cm²/sec	Permeability, cm²/sec
Rhenium	nil	nil	....	....
Beryllium	10^{-3}	1.8×10^{-2}	....	....
Niobium (Columbium)	27	278	7×10^{-5}	20×10^{-3}
Tantalum	29	297	9×10^{-7}	0.27×10^{-3}
Vanadium	36	506	9×10^{-8}	0.05×10^{-3}
Titanium [a]	7.9	84	9×10^{-6}	0.76×10^{-3}
Titanium [a]	49.0	522	2.75×10^{-5}	14×10^{-3}
Zirconium	6.0	47	9×10^{-6}	0.42×10^{-3}
Zirconium hydride	65.0	555	1.05×10^{-6}	0.58×10^{-3}
Iron	....	7×10^{-2}	3.75×10^{-4}	0.026×10^{-3}
Thorium [a]	....	....	....	....

[a] Brittle, stable hydrides.

TABLE B.18.—*Biological Systems Which Produce Electroactive Products*

A. REPORT *417*

Source material	Biological system	Product
starch	*Bacillus* sp.	H_2
Glucose	*Clostridium butyricum*	
Malic acid	*Rhodospirillum* sp.	
Lactic acid	Lactic dehydrogenase	
Formic acid	Formic dehydrogenase	
Alanine	*Clostridium propionicum*	NH_3
Uric acid	*Clostridium acidiurici*	
Glycine	*Diplococcus glycinophilus*	
Urea	Urease	
Serine	Serine dehydrogenase	
L-amino acids	L-amino acid oxidase	

B. REPORT *448*

Source material	Biological system	Product
Glucose	1–20 21 22 23 25 27 28 29 30 32 33 34 37	H_2
Galactose	1 2 4 5 6 9 10 11 13 14 17 18 19 22 23 33 34	
Fructose	1 2 4 5 6 9 11 13 14 17 19 22 23 27 33 34	
Mannose	1 2 4 5 11 19 33 34	
Maltose	1 2 4 5 6 7 9 11 13 14 16 17 18 19 22 27 33 34	
Sucrose	1 2 5 8 16 17 18 20 21 22 27 29 33 34	
Mannitol	1 2 4 5 9 10 11 13 14 16 17 18 19 27 28 29 30 34	
Glycerol	1 2 5 8 11 13 18	
Starch	1 2 4 5 13 27 28 29 30 33 34	
Adonitol	2	
Arabinose	2 4 9 11 13 14 19 28 33 34	
Dextrin	2 13 14 33 34	
Inositol	2 13 34	
Lactose	2 9 10 1 13 14 16 17 18 19 20 21 23 27 28 29 30 33 34	
Rhaminose	2 9 11 19 28 29	
Sialicin	2 4 10 13 14 17 19 30 33 34	
Sorbitol	2 1 13 14 19 28 29 34	
Xylose	2 9 11 14 17 19 23 28 29 30 33 34	
Glycogen	4 33 34	
Esculin	4 13 30 33 34	
Trehalose	11 14 19 23 33 34	
Cellobiose	13 14 19	
Melibiose	19	
Sodium	20 21 24 36 37	
Formate		
Milk	25 26 32 34	
Pyruvate	26 31 37	
Tartrate	26	
Ethanol	35	
Threonine	38 39 40	NH_3, H_2
Serine	38 39 40	
Purines	38 39 40 41	
Pyrimidines	41	
Amino acids	41 42	

TABLE B.18.—*Biological Systems Which Produce Electronic Products—Continued*

Source material	Biological system	Product
Malate	43 44	H_2, organic acids
Glutamate	43	
Lactate	44	
Pyruvate	44	
Oxalacetate	44	
Fumarate	44	
Tartrate	44	
Succinate	44	

ORGANISMS AND REFERENCES CORRESPONDING TO TABLE B.18

1. *Aeromonas liquefaciens,* J. Gen. Microbiol., vol. 5, 299 (1951).
2. *Aeromonas insolita,* Bergey's Manual, 7th ed.
3. *Aeromonas punctata,* Bergey's Manual, 7th ed.
4. *Aeromonas salnionicida,* Bergey's Manual, 7th ed.
5. *Aeromonas hydrophila,* J. Bacteriol. vol. 46,213 (1946).
6. *Photobacterium phosphoreum,* Bergey's Manual, 7th ed.
7. *Photobacterium pierantonii,* Bergey's Manual, 7th ed.
8. *Xanthomonas nemmiana,* Bergey's Manual, 7th ed.
9. *Escherichia* ***coli,*** Bacteriol. Rev., vol. 18, 32 (1954).
10. *Escherichia aurescens,* J. Bacteriol., vol. 70, 498 (1955).
11. *Escherichia freundii,* Bergey's Manual, 7th ed.
12. *Escherichia intermedia,* J. Bacteriol., vol. 44,498 (1942).
13. *Aerobacter aerogenes,* Bacteriol. Rev., vol. 18, 43 (1954).
14. *Aerobacter cloacae,* Bacteriol. Rev., vol. 18, 43 (1954).
15. *Klebsiella pneumoniae,* Bergey's Manual, 7th ed.
16. *Klebsiella ozaenae,* Bergey's Manual, 7th ed.
17. *Erwinia carnegieana,* Phytopath, vol. 32, 310 (1942).
18. *Erwinia dissolvens,* Bergey's Manual, 7th ed.
19. *Erwinia nimipressuralis,* Bergey's Manual, 7th ed.
20. ***Serratia*** *plymuthica,* Bergey's Manual, 7th ed.
21. *Serratia kiliensis,* Bergey's Manual, 7th ed.
22. *Proteus vulgaris,* Bacteriol. Rev., vol. 18, 43 (1954).
23. *Proteus mirabilis,* Bergey's Manual, 7th ed.
24. *Methanococcus vannielii,* J. Bacteriol., vol. 62, 269 (1951).
25. *Veillonella parvula,* Bergey's Manual, 7th ***ed.***
26. *Veillonella gasogenes,* J. Gen. Microbiol., vol. 5, 317 (1951); J. Bacteriol., vol. 58, 25 (1948).
27. *Eubacterium tortusium,* Bergey's Manual, 7th ed.
28. *Bacillus polymyxa,* Bergey's Manual, 7th ed.
29. *Bacillus macerans,* Bergey's Manual, 7th ed.
30. *Clostridium butyricum,* Bergey's Manual, 7th ed.
31. *Clostridium butylicum,* J. Biol. Chem., vol. 145, 379 (1946).
32. *Clostridium multifermentans,* Bergey's Manual, 7th ed.
33. *Clostridium* ***amylosaccharobutylpropylicum,*** Bergey's Manual, 7th ed.
84. *Clostridium madisonii,* Bergey's Manual, 7th ed. (many other *Clostridium* species).
35. *Bacillus acetoethylicus,* Mikrobiologiya, vol. *27,* 302 (1958).
36. *Methanobacterium formicum,* J. Bacteriol., vol. 62, 269 (1951).
37. *Pseudomonas* (strain G4A), J. Biol. Chem., vol. 236, 2520 (1961).
38. *Peptococcus prevoti,* J. Bacteriol., vol. 56, 25 (1948).
39. *Peptococcus activies,* J. Bacteriol., vol. 56, 25 (1948).
40. *Peptococcus aerogenes,* J. Bacteriol., vol. 56, 25 (1948).
41. *Micrococcus aerogenes,* J. Bacteriol., vol. 63, 163 (1952).
42. *Clostridia,* Enzymologia, vol. 2, 175 (1937).
43. *Rhodospirillum rubrum,* Bacteriol. Rev., vol. 26, 51 (1962).
44. *Veillonella gasogenes,* J. Gen. Microbiol., vol. 5, 317, 326 (1951).

REFERENCES TO INFORMATION ON THE SOLUBILITY OF HYDROCARBONS *(138* AND *139)*

1. KERDIVARENKO, M. A.; ET AL.: J. Appl. Chem. USSR (English Translation), vol. 28, 44, 1955.
2. MORRISON, T. J.: J. Chem. Soc., 3814, 1952; MORRISON, T. J.; AND BILLET, F.: J. Chem. Soc., 3819, 1952; MORRISON, T. J.; AND JOHNSTONE, N. B. B.: J. Chem. Soc., 3655, 1955.
3. CLAUSSEN, W. F.; AND POLGLASE, M. F.: J. Am. Chem. Soc., vol. 74, 4817, 1952.
4. CULBERTSON, O. L.; AND MCKETTA, J. J.: Trans. AIME, Petrol. Div., vol. 192, 223, 1951, table II.
5. CULBERTSON, O. L.; HORN, A. B.; AND MCKETTA, J. J.: Trans. AIME, vol. 189, 1, 1950, fig. 4.
6. AZARNOOSH, A.; AND MCKETTA, J. J.: Petroleum Refiner, vol. 37, 275, 1958, table 2.
7. REAMER, H. H.; SAGE, B. H.; AND LACEY, W. N.: Ind. Eng. Chem., vol. 44, 609, 1952, table I.
8. HIROAKA, H.: Rev. Phys. Chem., Japan, vol. 24, 13, 1954.
9. DAVIS, J. E.; AND MCKETTA, J. J.: J. Chem. Eng. Data, vol. 5, 374, 1960, table 11.
10. AZARNOOSH, A.; AND MCKETTA, J. J.: J. Chem. Eng. Data, vol. 4, 211, 1959, table 11.
11. BROOKS, W. B.; AND MCKETTA, J. J.: Petroleum Refiner, vol. 34, 143, 1955, table 2.
12. Handbook of Chemistry and Physics, 40th ed., Chemical Rubber Pub. Co.

Hydrocarbon solubility *(139)* cannot be measured accurately by bubbling hydrocarbon into electrolyte and then stripping with inert gas to a chromatograph, because the electrolyte supersaturates with hydrocarbon. Approach to equilibrium is slow with stirring.

REFERENCES TO DISSOCIATIVE OR MOLECULAR ADSORPTION OF O_2 (789)

1. SMELTZER, TOFFELSON; AND CAMBRON: Can. J. Chem., vol. 34, 1046, 1956.
2. TWIGG, G. H.: Proc. Roy. Soc. (London), vol. 188A, 92, 105, 123, 1946.
3. MEISENHEIMER; RITCHIE; SCHISSLER; STEVENSON; VOGE; AND WILSON: Second Intl. Congress on Surface Activity. Butterworth & Co., 1957, p. 299.
4. ROSENBERG, A. J.: J. Am. Chem. Soc., vol. 78, 2929, 1956.
5. BRUNAUER; EMMETT; AND TELLER: J.A.C.S., vol. 60, 309, 1938.
6. KUMMER, J. T.: J. Am. Chem. Soc., vol. 63, 460, 1959.
7. DEBOER, J. H.: Advances in Catalysis, vol. 8, p. 76.
8. DAVIES; CLARK; YEAGER; AND HOVORKA: J. Electrochem. Soc., vol. 106, 56, 1959.

APPENDIX *C*

Techniques

Only those techniques considered to be either of general usefulness or novel are described below. Techniques already well known, even if slightly modified, and those limited in interest to work on a particular cell are not discussed here; it would not be feasible to describe each one here. The reader should refer to the original contract reports for information on those techniques not covered below.

C.1 FUEL-CELL TESTING

Several reports describe cell-testing installations for recording for the performance of a number of cells over hundreds of hours of life. A typical example is given in Report ***310*** (General Electric). The usual technique for determining steady-cell performance is to vary the external resistive load and wait for steady state to be obtained at a given setting. Cell current and potential are measured and the process repeated at a new setting; in this way an overall current-voltage curve is obtained for the cell or stack of cells. More detailed information is usually obtained only on smaller, single cells because *(a)* small cells can easily be constructed with reference electrodes, and ***(b)*** current interruption techniques can be applied to the low currents obtained from small cells. By measuring the potential of an electrode versus a reference electrode in the cell electrolyte, the voltage-current curve of the electrode can be obtained. This is done for both electrodes, and consequently the total cell polarization is split into anode and cathode polarization, and IR drop in the electrolyte between them. IR polarization is also measured by current interruption-establishment techniques, which use the principle that ohmic polarization disappears or appears very rapidly (10^{-12} seconds) when the circuit is opened or closed.

There are three major interruption-establishment techniques: the Kordesch-Marko bridge, simple interruption, and galvanostatic establishment. A circuit diagram for the Kordesch-Marko bridge is shown in figure C.l; the bridge is described in reference C.l.

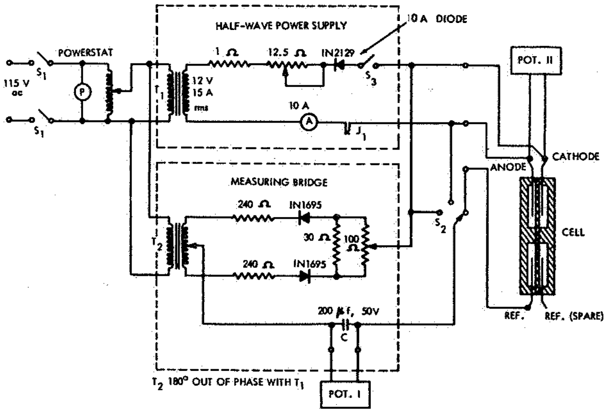

FIGURE C.1.—Circuit diagram of Kordesch-Marko bridge for currents up **to** 10 amperes ***(259)*.**

The principle is that transformer $\mathbf{T_1}$ produces a cyclic voltage which is greater than the cell voltage and, therefore, produces an ac current. However, the diode allows current passage only in the normal fuel-cell direction, electrons from anode to cathode. The current is maintained at each electrode by faradaic and capacitive processes, and current flow through the electrolyte via ions produces IR polarization. In the second half of the ac cycle, no current is flowing through the cell. The capacity of the fuel-cell electrodes seems to be sufficient to damp the system so that potentiometer II gives a mean cell potential identical to that obtained from a constant faradaic current of the same value as the mean current read on the ammeter. The potential of the cell with negligible current flowing is read from potentiometer I, which comes into operation when the main circuit is not passing current. The second transformer, T_2, operates the diodes in the secondary low-current circuit, thus switching-in potentiometer I, which, of course, is a high-impedance instrument. The potentiometer tap is to the center of the transformer and the circuit is symmetrical, so that without the test cell in the bridge circuit potentiometer I can be brought readily to zero by a small adjustment in the tap to the 100-ohm resistance. The reading of potentiometer I is the IR-free cell potential at the mean current of the main circuit, provided that other forms of polarization do not change during the off period (damped system). This is tested by varying the ac frequency, since higher frequency gives less time for decay of activation and concentration polarization. It was found *(248)* that variation of frequency from 60 to 240 cps produced no change in results and that values from the bridge agreed with values by other methods (263).

The Kordesch-Marko bridge can handle large current densities and is easy to use. If reference electrodes are used in the cell, IR polarization from electrode and contact resistance at each electrode can be determined, as well as total cell IR polarization. The major disadvantage is that for scientific studies on small half cells there may be doubt whether the bridge has effectively separated only IR polarization and whether the effect of half-wave ac current gives the same polarization as a steady value of current. In addition, it is often desirable to follow the buildup or decay of polarization with time, and this cannot be done with the bridge.

A circuit for the simple interruption technique is shown in figure C.2 (Texas Instruments, *607*). The fuel cell is run at a steady current and the potential is obtained in the usual way. The current is then switched off, using a wetted-mercury relay, and the potential is followed with an oscilloscope. The break of the mercury in the relay occurs very rapidly and switching transients are less than a few microseconds. The oscilloscope trace immediately jumps to the IR-free polarization and then changes slowly to a less polarized potential. Even if appreciable change of non-IR polarization occurs in a few milliseconds, the oscilloscope sweep rate can be increased until only the disappearance of IR polarization is obtained, and a horizontal trace is obtained after switching. Once again, use of reference electrodes enables IR polarization to be measured for each electrode and the cell electrolyte. IR effects are thus measured directly on a cell which is in normal running conditions before switchoff.

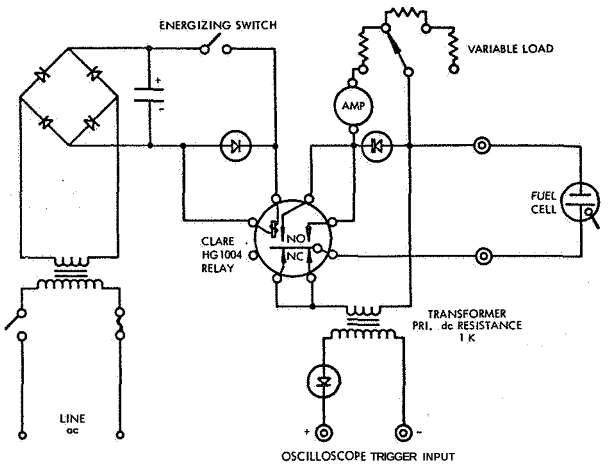
ENERGIZING SWITCH
VARIABLE LOAD
AMP
FUEL CELL
CLARE HG1004 RELAY
NO
NC
TRANSFORMER PRI. dc RESISTANCE 1 K
LINE ac
+
-
OSCILLOSCOPE TRIGGER INPUT

FIGURE C.2.—Interrupter circuit (607).

A circuit for rapid establishment of a constant current (galvanostatic technique) through **a** cell is shown in figure C.3 (Pennsylvania State University, ***486,*** refs. C.2, C.3). This circuit is capable of providing a square wave-current pulse with

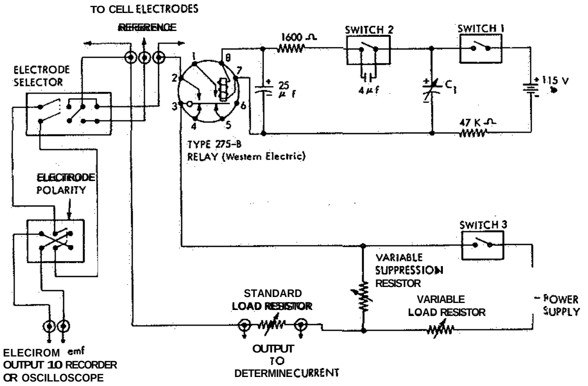
TO CELL ELECTRODES
REFERENCE
ELECTRODE SELECTOR
1600 Ω
SWITCH 2
SWITCH 1
1
2
3
4
5
6
7
8
25 μf
4 μf
C_1
115 V
47 K Ω
TYPE 275-B RELAY (Western Electric)
ELECTRODE POLARITY
SWITCH 3
VARIABLE SUPPRESSION RESISTOR
STANDARD LOAD RESISTOR
VARIABLE LOAD RESISTOR
POWER SUPPLY
ELECIROM emf OUTPUT 10 RECORDER CR OSCILLOSCOPE
OUTPUT TO DETERMINE CURRENT

FIGURE C.3.—Circuit for rapid galvanostatic measurement ***(486).***

a rise time of less than 5 microseconds, and virtually eliminates the switching transients normally associated with the opening and closing of relays. In addition, by means of the variable capacitor (C_1), it provides a simple means of automatically controlling the duration of the current pulse (e.g., for $C_1 = 0.2\ \mu F$, the relay is closed for about 2 milliseconds). This can be a distinct advantage where it is desirable to shut off the current rapidly at the end of a measurement. A constant current is obtained from a constant voltage power supply in series with a relatively large resistor. This resistor, the variable load resistor, is at least 100 times the maximum calculated resistance of the electrolytic cell. The value of the current can be determined by measuring the voltage drop across the standard load resistor in series with the cell.

The procedure for performing the galvanostatic measurements was as follows. The scale markings on the oscilloscope were illuminated and photographed, after which they were turned off so that they would not interfere with the recording of the voltage-time trace. Switches 1 and 3 (fig. C.3) were then closed and the shutter of the Polaroid camera was opened. The closing of the switches resulted in the charging of C_1 and a flow of current through the suppression resistor (the value of which was the same as the variable load resistor) but not through the cell. The function of this suppression resistor was to reduce the switching transients. The 4 μF and 25 μF capacitors in the relay circuits had a similar function. After some time, when C_1 had become fully charged, switch 2 was closed so that C_1 would discharge through the mercury-wetted relay. This gave rise to a pulse of current through the cell (the 47 KΩ resistor prevented the 115-volt battery from energizing the relay once the capacitor had been discharged), which, in turn, generated the voltage-time trace on the oscilloscope. The oscilloscope had been set to "internal trigger," so that the voltage change being recorded would set the time base into operation. The shutter of the camera was then closed and switch 2 was opened to allow C_1 to recharge for the next test. As before, IR polarizations are rapidly established and can be determined unambiguously at small times after switching on; they can be measured for anode, cathode, and total cell. Circuits of this type are also used for galvanostatic half-cell studies of small electrodes.

In some of the early work on fuel cells, the performances of cells were measured but reference electrodes were not used. It was, therefore, difficult to tell whether the anode, the cathode, or both were giving polarization. It is obviously desirable to use a reference electrode to give this information. With some types of cells a thin glass or metal capillary (hypodermic needle, for example, Monsanto, 460) can be run into the electrolyte between anode and cathode, joining the electrolyte-filled capillary to a standard reference electrode. Since negligible current is passed between a working electrode and the reference electrode, a high-impedance potentiometer connecting the reference to the working electrode measures the potential (difference) between the electrode and the electrolyte at the tip of the capillary, plus the reference electrode potential. If the reference potential is known, including any liquid junction potentials, the electrode to electrolyte potential can be calculated. The sum of anode-electrolyte potential plus cathode-electrolyte potential equals the total cell potential if the working electrodes have uniform current, temperature, and concentration conditions at all points. If IR polarization is measured using the techniques described above, the sum of IR polarization between anode-electrolyte and cathode-electrolyte equals the total cell IR polarization.

A disadvantage of this technique is that IR polarization cannot readily be split into anode, cathode, and electrolyte polarization. This can be overcome if two capillaries are used, one in electrolyte very near the anode, and the other in electrolyte near the cathode. Other disadvantages are that it is sometimes experimentally difficult to station the capillaries between the electrodes, or suitable capillary materials cannot be found, or reference electrodes cannot be found which are compatible with fuel-cell electrolyte. A common technique to overcome these problems avoids the use of capillaries by using a patch from a fuel-cell electrode as a reference. A patch is cut out of the electrode and remounted in its former position, but not in electrical contact with the main electrode. A separate current lead is taken from this patch and a high-impedance potentiometer is connected between the working electrode and the reference patch. The technique is best suited for electrodes mounted against an electrolyte matrix. The small patch is under identical conditions to the working electrode, except that it is not passing current. Therefore, the difference in potential between the two, as current density is increased, is the increase in polarization. The absolute polarization is not obtained unless the patch gives the ideal reversible potential expected of the gas-electrolyte system. This is normally true for H_2 in concentrated electrolytes with a platinum electrode. Therefore, an anode reference patch is frequently used in H_2-O_2 cells. Measurement of IR polarization between anode-anode patch gives anode IR, and between cathode-anode patch gives cathode+electrolyte IR. Electrolyte IR can again only be clearly separated if a cathode patch reference is also used.

The mounting of the reference patch shown in figure 6.4 is not recommended, although it may be experimentally necessary to use this method. As discussed by Broers *(147)* and General Electric (*182, 263*), appreciable errors can arise with this placement of the reference patch. The extension of electrolyte beyond the facing areas of anode and cathode provides an extra path for ionic current between anode and cathode. The reduced resistance of the mean path at the edge leads to higher current density than at the rest of the electrode and, hence, more activation or concentration polarization and less IR polarization. When IR effects between electrodes and reference are measured by interruption techniques, less IR is obtained than actually exists between the main anode and cathode. The sum of resistances measured with the reference is less than that measured directly on the whole cell.

It is usual in fuel cells to insure that the electrode or electrode-current collector assembly has sufficient conductivity to give low IR drop along the electrode. In addition, thick connectors and leads are used to reduce electronic IR effects. However, current may be passed between conductors which are in press contact only, giving contact resistance. Contact resistance is usually measured out of the cell, and the materials and assembly pressures that will reduce it to small values are determined. If the materials in contact have negligible resistance themselves, contact resistance is easily measured. If they have appreciable resistance, more elaborate techniques are required. The contact resistance of metal screen cast in IEM was determined by measuring the resistance, using ac technique, between two parallel strips of screen, separated by a fixed distance, cast into a membrane (General Electric, *248,* 1961). This was repeated with different membrane thicknesses, keeping the other geometry of the system identical in each case. The resistance-thickness curve was extrapolated to zero thickness to give contact resistance.

The contact resistance of a current collector pressed against an electrode on an IEM was measured as shown in figure C.4 (General Electric, *248,* 1961). A small direct current was passed, and conditions were allowed to stabilize for 10 minutes. The contact resistance and resistance of the electrode between contacts were measured from the readings of potentiometers P_1 and P_2, respectively, and the known current. The IEM resistance was relatively high and conduction in the membrane could be neglected. The resistance of thin-metal films fused onto solid electrolytes was measured by Westinghouse *(791)* using probe techniques (refs. **C.4** and C.5).

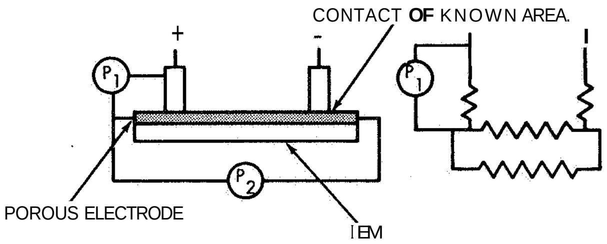

FIGURE C.4.—Technique for measuring contact resistance and electrode resistance *(248).*

Another resistance measurement of importance is the effective resistivity of a porous matrix filled with electrolyte. The relation between resistance of an equivalent shape of free electrolyte and the matrix-electrolyte resistance is

$$\begin{aligned}\rho_{\text{effective}} &= \rho_{\text{free}}\, q/\theta \\ &= \rho_{\text{free}}\, \lambda \qquad \text{(C.1)}\end{aligned}$$

e is the porosity of the matrix and is, therefore, the fraction of volume filled with electrolyte; *4* is an empirical tortuosity factor (for well-interlinked pore systems without constrictions *q* is about $\sqrt{2}$ to 2, but for highly consolidated pore systems it may be as high as 20 or 30); and λ is the labyrinth or formation factor. It is clearly desirable to have λ as close to 1 as possible to give the best conductance through the matrix-electrolyte. Labyrinth factors of porous ceramic disks were measured by using a disk filled with standard KCI solution as electrolyte and Hg at each face as electrodes (Allison, ***68***). This eliminated contact resistances. Resistance was measured with 10 kcps ac. Measurement with molten-salt electrolyte used gold-plated nickel electrodes pressed against the disk, with gold leaf between electrode and disk. The electrode-disk-electrode assembly was clamped together in a furnace.

The potential established across a membrane, which separates electrolytes of different concentration, is a function of the transport of ions in the electrolyte. For example, a cationic membrane separating two acid solutions tends to pass H^+ from the side of higher concentration to the lower. If the anion cannot also pass through the membrane, the passage of H^+ produces excess positive ions on the weak side and excess negative ions on the strong side, setting up an electrical double layer across the membrane. The potential gradient of the double layer opposes further H^+ movement and an equilibrium membrane potential is established. The selectivity of a membrane can be determined by the magnitude of the membrane potential. The transport numbers H^+ and Cl^- in an IEM were measured from the potential difference between two silver-silver chloride electrodes placed in dilute HCl solution of different concentration separated by the IEM (General Electric, *263*). Transport number was determined from

$$E=\left(\frac{\tau^+-\tau^-}{\tau^++\tau^-}\right)\left(\frac{2RT}{F}\right)\ln\,(\alpha_{H_1^+}/\alpha_{H_2^+}) \qquad (C.2)$$

where E is the potential difference, τ the transport number and $\alpha_{H_1^+}$, $\alpha_{H_2^+}$ the activities of H^+, assuming the transport number of Cl to be small in the denominator. Since $\tau^++\tau^-=1$, the values of τ could be determined; τ^+ was found to be 0.997. The effective diffusion coefficient of Cl^- through the membrane was estimated to be $(1.3)(10^{-6})$ cm²/sec. See also Reports ***316*** through ***327***.

A quantitative method of determining the adhesion of an electrode to an IEM was used by General Electric ***(289)***. The method involved scratching by a vertical point at varying pressures, and is based on the following references: Heavens, O. S.: J. Phys. Rad., vol. 11, 355, 1950; Benjamin. P.; and Weaver, C.: Proc. Royal Soc. (London), vol. A254, 163, 1960; Tabor, D.: Proc. Royal Soc. (London), vol. A251, 378, 1953; Bowden, F. P.; and Tabor, O.: Friction and Lubrication of Solids. Clarendon Press, 1958, ch. 5.

C.2 HALF-CELL TESTING

It is often more convenient to test an electrode in a half-cell arrangement instead of in a complete cell assembly. The test electrode is placed in electrolyte with a counterelectrode and a reference capillary (Luggin capillary), and current passed through the test electrodes and counterelectrodes from an external voltage supply. For example, an H_2 anode can be studied with a counterelectrode of platinum screen at which H_2 will be evolved when current is passed. The theory of electrode reactions shows that the current which can be passed through an electrode depends on the potential difference between the electrode and the electrolyte, measured using the reference capillary, and it is immaterial whether the potential is generated by a fuel cell or applied from an external source. Thus, the current-voltage relations of an anode and a cathode can be determined separately and the complete fuel-cell performance predicted from the results.

The prediction is not necessarily accurate for several reasons. First, the anode-electrolyte-cathode geometry may be different in a complete cell, leading to effects (concentration polarization of ions in the electrolyte, temperature change, etc.) which did not occur in half-cell tests. Second, in a complete cell there may be appreciable diffusion of one reactant to the opposite electrode, giving poorer performance than obtained in half-cell studies. Third, since the potential applied to the electrode can be externally controlled, it is possible to take an H_2 electrode anodic to the point of O_2 evolution, and vice versa. This can lead to electrode poisoning, which could not occur in a fuel-cell system. However, if major influences of this kind are not present, half-cell studies will give results which can be directly converted to complete cell performance.

The half-cell technique is also used in the more basic investigations of catalysis and reaction mechanism at solid, nonporous electrodes. The three current interruption techniques discussed in section C.1 can be used with solid electrodes, but there are a number of other techniques which are also used to get different kinds of information:

(1) *Galvanostatic (also known as chronopotentiometry or voltammetry).*—A constant current is passed through the electrode, and electrode potential versus reference followed as a function of time. If the current is less than the limiting current of the electrode under the conditions used, the potential-time relation has three general regions. First, IR polarization is immediately established and can be measured as a jump on the oscilloscope. Second, activation polarization is more slowly established and the potential levels off with time. Third, concentration polarization is yet more slowly established and develops a drift of potential to more polarized values. It is sometimes possible to distinguish clearly between region 2 and region 3 and thus estimate the activation polarization at the current used, usually by extrapolation to zero time. When the current is greater than the steady-state limiting current, the electrode cannot reach a steady state of potential and the polarization in region 3 increases suddenly as the rate-controlling concentration falls to zero. The time at which this occurs is called the transition time, τ. For simple redox reactions and unsteady-state linear diffusion, $i\tau^{1/2}$ is a constant, provided i is considerably greater than the steady-state limiting current (ref. C.6). If a slow preceding chemical reaction (adsorption, for example) is influencing the overall rate, $i\tau^{1/2}$ goes down as i is increased (refs. C.6 and C.7). If rapid gas adsorption-desorption equilibrium changes during the test, $i\tau^{1/2}$ increases with i (ref. C.8).

(2) *Potentiostatic.*—The potential between electrode and reference is rapidly brought to a constant value and the current followed as a function of time. At lower currents it may be possible to estimate the pseudo-steady current corresponding to the activation polarization in a manner similar to that of the galvanostatic technique. If current decreases with time, due to simple transient-state diffusion effects, $it^{1/2}$ is a constant.

(3) *Linear voltage sweep (also known as triangular voltage sweep or cyclic voltammetry).*—The potential between electrode and reference is changed linearly with time ($dV/dt = K$, sweep rate) to a preset polarization, and then brought back linearly to the original potential. Current is measured as a function of time, which is also a function of voltage. At low sweep rates, the current-voltage curve is the same as the steady-state curve. At high sweep rates, unsteady-state, mass-transfer relations apply, and the current passes through a peak and then falls at longer time. The mathematical relations for this system have only been developed for simple reactions (refs. C.6 and C.9). For complex reactions involving adsorbed species, it is possible to obtain several peaks or shoulders in the curve.

(4) AC *or faradaic impedance techniques (ref. C.10)*.—The effective impedance of the electrode is measured with an ac bridge. The electrode has an equivalent circuit consisting of its double-layer capacity in parallel with its faradaic impedance. The faradaic impedance in general is made up of two resistances in series, the charge-transfer resistance and the mass-transfer resistance, and a mass-transfer capacity also in series. Electrodes can only behave as simple resistances and capacitances when the cyclic potential amplitude is restricted to a few millivolts; also, the effective resistances and capacitances change with frequency. Double-layer capacity dominates over faradaic effects at high frequency and it is sometimes possible to determine double-layer capacity from the high-frequency impedance.

In general, the results from galvanostatic or potentiostatic techniques are easier to interpret for complex reactions involving adsorbed reactants than ac impedance results. Solid electrodes are usually tested in the form of small electrodes of 1 cm² area or less, and consequently currents are small. There are many circuits described in the literature for various tests on small electrodes, but it is becoming common practice to use commercial equipment. The Wenking potentiostat with a function (signal) generator, an oscilloscope and camera, a recorder, and a mercury-wetted relay switching circuit gives a versatile system which can be used for most of the available techniques. The components of the system are shown in figure C.5. The potentiostat operates by varying the electrode current to make the potential between reference and test follow the

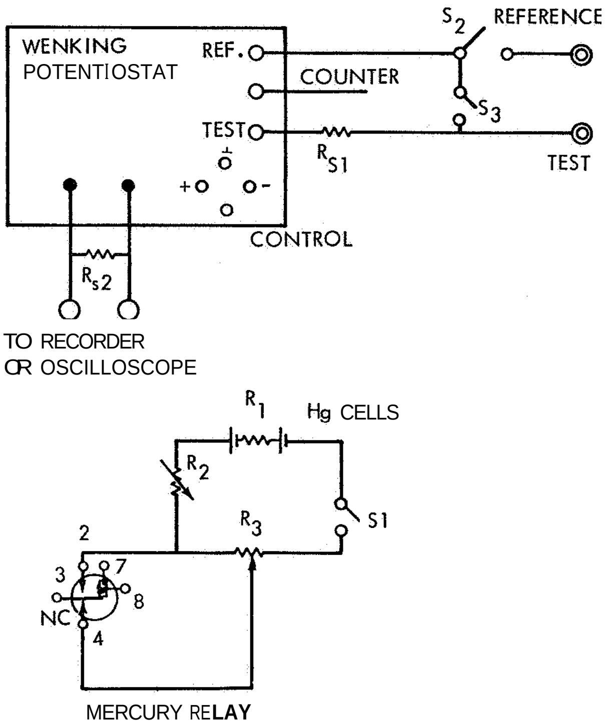

FIGURE C.5. — Potentiostat and auxiliary switching circuit.

potential fed to the control circuit (+ and *control* terminals). A potential function of any desired form (triangular voltage, for example), obtained from the function generator, is fed into the control circuit, and the electrode current as a function of time determined by the potential drop over standard resistor R_{s2} (S_2 closed, S_3 open, R_{s1} not in). Current functions of desired form, such as square wave pulses, are obtained by feeding a corresponding voltage function into the control circuit, with S_2 open, S_3 shut and standard resistor R_{s1} in series with the electrode as shown in the figure ($R_{s2} \cong 0$). The potentiostat forces potential across R_{s1} to follow the applied potential, and thus generates the required current form through R_{s1} and the electrode; for example, a square potential applied to R_{s1} through the control circuit produces a square-wave current. The potential of test electrode to reference is followed by an oscilloscope or recorder connected between them in the normal way. For galvanostatic tests with very fast rise time, the auxiliary switching circuit shown is more satisfactory than direct use of the signal generator. Connections are 3 to Wenking +, 4 to Wenking *control,* signal generator output to 7 and 8. The signal from the generator activates the relay (S_1 closed), and the desired potential from the mercury cells and resistances R_1, R_2, and R_3 is fed to the control circuit, and is hence reproduced across R_{s1}. The rise time of this system was less than the response time of the oscilloscope used, that is, less than 2 μsec.

The potentiostat can also be used with a set potential having a superimposed, small-amplitude cyclic potential. Differential electrode capacities can then be measured at varying electrode potentials or current densities. In addition, it can be readily used with single pulses. As discussed in chapter 15, repetitive-pulse techniques can be misleading if surface-adsorbed material is being reacted during the pulse and only partially replaced before the next pulse. Also, distributed capacity effects are obtained with porous electrodes, and the mathematical relations developed for transient-state measurements on solid electrodes cannot, in general, be used for porous electrodes (see ch. 18).

An advantage of half-cell studies on small 'electrodes is that it is relatively easy to insure that current density is uniform and IR loss in the electrode is small. Another advantage is that the electrolyte can be stirred to see whether variations of mass transfer in the electrolyte affect performance. For solid electrodes, effects of mass transfer can be most precisely investigated using spinning electrodes. Levich (ref. C.11) showed that the current density across a spinning, horizontal, disk electrode was constant and that the mass transfer could be rigorously described. The current density and boundary-layer thickness is also constant along the cylindrical surface of a spinning, vertical-wire electrode. For many fuel-cell reactions, the kinetics are too complex to apply simple rate equations and simple mass-transfer relations. However, when spinning electrodes are spun at high rotation speeds, mass-transfer effects decrease due to thinning of the boundary layer. A stage is reached where performance is not changed by higher spinning rate and mass-transfer effects have been eliminated. Another interesting application is that if desorbable intermediates are formed in the reaction, high spinning rates aid their mass transfer away from the electrode and increased spinning rate can then decrease the current density.

The spinning disk-and-ring technique discussed in section 17.4.5 also has considerable value for determining reaction paths. An assembly for testing nonporous carbon electrodes is described in Report 776 (Western Reserve University). It consisted of a hollow steel shaft covered with a Teflon sleeve. The carbon was mounted in a Teflon holder fitted into the end of the shaft. The back of the carbon was cemented with conductive cement to the bottom of a steel cup, which fitted higher in the shaft. The cup contained a spring-loaded contact to a nonrotating rod in the shaft' center; the rod formed the electrical connection.

Many types of cell assembly are used for half-cell testing, both for porous and solid electrodes. The test electrodes and counterelectrodes are often contained in different compartments connected by an arm (H cell) to prevent contamination of the test electrode due to diffusion of products from the counterelectrode. The best method is to use a wide-bore arm, containing a porous-glass frit to prevent electrolyte circulation since a narrow-bore arm can give inconveniently high ohmic resistance across the cell. Aqueous electrolytes can be tested only at temperatures well below the electrolyte boiling point at atmospheric pressure, unless the cell is pressurized. Leaktight cells are hard to build and control and an alternative method is to enclose a simple cell in a pressure atmosphere (Engelhard, *213*) as shown in figure C.6. The cell was pressurized with CO_2 or N_2, in a stainless-steel case. The reactant gas pressure at the inlet valve A (near the top of the figure) was brought to a pressure slightly greater than that in the cell. The valve was then cracked and gas allowed to flow into the cell. The differential pressure between the reactant gas and the case pressure was set by the few inches of electrolyte in the bubbles, thus preventing flooding of the electrode by electrolyte.

C.3 PROPERTIES OF ELECTRODES

In addition to the obvious properties of electrodes such as dimensions, porosity, and weight, surface area and pore size are considered important. The total surface area of high-area electrodes is measured using conventional BET

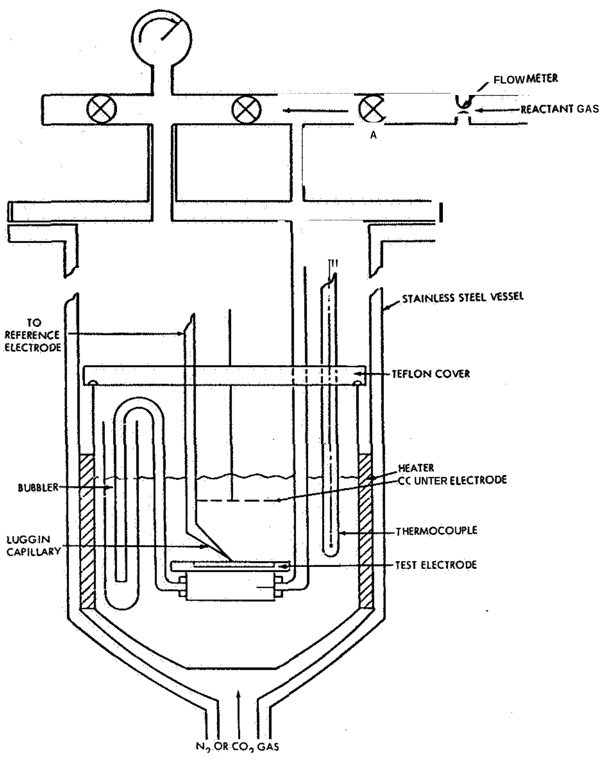

FIGURE C.6.—High-pressure test cell (Engelhard, *213*).

techniques; krypton adsorption rather than nitrogen adsorption is preferred for low areas. The area of Clevite No. **3** porous nickel was 0.2 m^2/g (28). The area of commercial platinum blacks is about 15 to **30** m^2g. Another method for measuring the area of porous solids is to measure the permeability of laminar flow of gas or liquid through the material. The permeability coefficient is obtained from

$$p_1u_1=B_0(\bar{p}/\eta)(\Delta p/L)+K_0\bar{C}(\Delta p/L) \qquad \text{(C.3)}$$

where u_1 is the linear velocity of flow at pressure p_1, η the viscosity,? the arithmetic mean pressure over length ***L***, ***Ap*** the pressure difference across length ***L***, and $\bar{C}$ the mean molecular velocity. In many cases the last term is negligible for gas flow and it can be neglected for liquid flow. For η in centipoises, p in atmospheres, M in cm

$$B_0=(\epsilon/q^2)(M^2/2)(10^8)\text{ darcies,} \qquad \text{(C.4)}$$

where E is the material porosity, q a tortuosity factor lying between $\sqrt{2}$ and 2, and M is the effective mean hydraulic radius of the pores of the material. The mean hydraulic radius can be related to the surface area of the macropores through which most of the flow occurs by

$$S_0=\epsilon/(1-\epsilon)M. \qquad \text{(C.5)}$$

S_0 is the surface area in cm^2/cm^3 of solid and S_0/ρ is the area per gram. Area can be estimated from equations (C.4) and (C.5). This area does not include micropores and microsurface roughness, and is usually considerably less than the BET area.

Both of the above methods have the disadvantage that they do not necessarily give the actual area taking part in the electrode reaction. A closer approach to this value would presumably be the area wetted by the electrolyte under cell conditions. Double-layer capacity and H_2 or O_2 coverage have been used to determine the wetted area. In the double-layer-capacity technique, it is assumed that true capacity is about 20 $\mu F/cm^2$ of smooth area, based on the value for Hg, and the measured capacity divided by this value gives an approximation to the wetted area. Double-layer capacity can be measured by "fast" techniques involving high-frequency, low-amplitude alternating current or single pulses at short times. For example, repetitive square current pulses ($\pm i$) applied to an electrode produce triangular voltage changes of electrode-reference potential when the amplitude of the current is small and the frequency high, because $dV/dt=i/C$. If faradaic impedance is present, the triangular shape becomes sawtoothed. Similarly, a single galvanostatic pulse can be used and the relation $dV/dt=i/C$ applied to very short times, before faradaic impedance comes into effect.

Another fast method is the current interruption technique: the rate of fall of potential immediately after cutting off a steady current is used in the equation, since it is assumed that the steady faradaic current charges the double layer at constant rate when the change of potential, excluding IR change, is small as $t\rightarrow 0$. These methods are not directly applicable at a platinum electrode between 0 and 0.4 volt versus NHE in SE because the reaction $[H]\rightleftharpoons H^+ + e^-$ is fast enough to give pseudocapacity.

Another galvanostatic method is to make the electrode, without H_2 or O_2 present, pass between 0.4 and 0.7 volt, since pseudocapacity is not present in this region, A linear variation of V with t is obtained and again $C=idt/dV$. This method will be referred to as the "slow" galvanostatic method, since it does not rely on potential measurements at times tending to zero or on high frequencies. In principle, the current can be made very low so that the rate of change of voltage is very slow. Distributed capacity effects are then a minimum. If currents are very low, it may be necessary to correct for slow faradaic processes occurring between 0.4 and 0.7 volt. If the current is switched off in this region, faradaic processes will continue to charge or discharge the double layer and

$$i=C[(dV/dt)_1v-(dV/dt)_2v], \qquad \text{(C.6)}$$

where i is the galvanostatic current, $(dV/d^2)_1v$ is the rate of change of potential, at V, when the current is on, and $(dV/dt)_2v$ is the rate of change of potential, again at V, when the current is off.

The hydrogen-coverage technique is based on the fact that platinum at zero volts is almost completely covered with adsorbed H from the reactions

$$[H]\rightleftharpoons H^+ + e^- \quad \text{or} \quad [H]+OH^-\rightleftharpoons H_2O+e^-.$$

[H] can be anodically stripped off the surface by taking the electrode rapidly to about 0.4 volt, and the charge passed is a measure of the amount of [H]; correction for double-layer capacity is usually small. Galvanostatic or voltage-sweep methods are used. It is then assumed that the charge capacity of [H] is 0.23 millicoulomb/cm^2 of true area. The O_2 area method is similar: the electrode is taken rapidly from 0.4 volt to about 1.2 volts, before O_2 evolution, and immediately cathodically discharged to about 0.6 volt. The quantity of charge passed in the stripping is used to calculate true area. The charge-discharge cycle is rapid to assure that neither H_2 nor O_2 desorb and diffuse away during the sweep, or that [O] does not form to a thickness of several monolayers by incorporation into the platinum. These methods work well on smooth or lightly roughened solid electrodes, especially if various corrections are made, but distributed effects occur on porous electrodes which, theoretically, lead to values of area which are too small.

The double-layer capacities of Th/Hg liquid mixtures were determined in 0.1 M $HClO_4$ at 77° F (25° C) (Tyco, *643).* At –1.2 volts versus standard H_2, the values were 18, 20, and 21 μF/cm² at 10, 30, and 40 percent Th. At –0.7 volt, values were 26, 30, and 30 μF/cm²; at –0.5 volt, 40 and 50 μF/cm². This last potential was near the zero charge point, and the increase in capacity was attributed to diffuseness of the double layer at this point.

It was concluded (General Electric, *292)* that the double-layer capacity of smooth Pt in *N* $HClO_4$, 572° F (300° C), rose from 33 μF/cm² true area at 0.4 volt to a maximum of 170 μF/cm² at 1.1 volts versus reversible H_2. The change was attributed to change in the structure of the double layer. Surface oxidation or adsorption of neutral molecules produced a decrease in capacity. A comparison (ref. C.14) of double-layer and PtO area for smooth, lightly platinized and heavily platinized electrodes is given in table C.1.

TABLE C.1.—*Comparison of Double-Layer and* PtO *Area for Smooth, Lightly Platinized and Heavily Platinized Electrodes*

[Ref. C.14]

Form	Apparent area, cm²	Double-layer capacitance, μF	PtO formed at 1.52 V, mCb	True area from double-layer capacity, cm²	True area from PtO formation, cm²
Wire	0.32	18	0.40	0.75	0.57
Wire	.32	1 000	22	54	31
Square	2.0	240 000	3200	10 000	4600

A slow galvanostatic technique gave double-layer capacities of Pt in H_2SO_4 of 850 μF/cm² for bright electrodes and 50 000 μF/cm² for platinized electrodes (Esso, *214)*. Later work using 40-cps alternating current superimposed on a steady direct current gave 40 μF/cm² and 960 μF/cm².

A number of different methods were used to get the double-layer capacity of electrodes of platinum black bonded on to phenolsulfonic acid-formaldehyde ion-exchange membranes (General Electric, *263)*. Measurements were performed with the electrode in the potential range 0.4 to 0.9 volt versus NHE in SE. Slow galvanostatic tests gave 14 to 44 μF/cm² true area. (True area was about 10³ cm²/cm² plane area.) A high-frequency bridge technique at 1000, 2000, and 3000 cps gave about 6 μF/cm². Capacity by current interruption was 14 μF/cm². It was concluded that true values of capacity could not be obtained due to the heterogeneous nature of the surface.

A thin sheet of powder platinum black, pressed between a platinum backing plate and a 2 *N* H_2SO_4 equilibrated membrane, was charged and discharged from O_2 evolution to H_2 evolution and back with a constant current density (General Electric, *254)*. Assuming no diffusion of surface chemisorbed gas, the surface coverage with H_2 was calculated to be about 1×10^{15} atoms/cm² of true area. (The true area was measured by krypton adsorption.) The initial oxygen coverage was also about 1×10^{15} atoms/cm². Double-layer capacity was 85 to 105 μF/cm² krypton area. At a current of 30 mA, times of hundreds of seconds were involved. Clevite No. 3 porous nickel, 30 mil thick, was impregnated with chloroplatinic acid solution with ultrasonic stirring for 5 minutes, and plated at 45 mA/cm² for 1 minute (Alfred University, *30*). Anodic [H] stripping of the electrode saturated with alkaline electrolyte gave $(2)(10^{18})$ atoms of H per cm² of plane area of electrode. Assuming one H per surface Pt atom and $(7.6)(10^{-16})$ cm²/Pt, the total area was 1500 cm² per cm² of plane area. Uncatalyzed electrode had a BET nitrogen adsorption area of 200 cm²/cm² and a double-layer capacity (slow galvanostatic) of 0.025 F/cm². Assuming a double-layer capacity of 30 μF/cm² for nickel; the area was about 800 cm²/cm². The hydrogen area was about 200 cm²/cm². The double-layer capacity of the platinized electrode was 0.5 F/cm². Either the true value of double-layer capacity for Ni is more than 30 μF/cm², or the measured capacity of the electrode was too high. Similarly, if a value of 20 μF/cm² is assumed for Pt, the area of the platinized electrode predicted from 0.5 F/cm^2 is 25 000 cm^2/cm^2, which is over 10 times the hydrogen area.

The interruption method gave a value of 8 cm^2 of wetted area per cm^2 of plane area for an activated carbon electrode (Western Reserve University, *771*), and it was concluded that penetration of electrolyte into the electrode did not fill the micropores. However, theory predicts that fast methods applied to porous electrodes penetrated by electrolyte give values which are too low.

In summary, measurements of the wetted area of porous electrodes give contradictory results. Fast methods sometimes give too low results, but the slow galvanostatic method has given absurdly high double-layer capacities in some cases and reasonable results in others.

The pore-size distribution of strong porous electrodes has been measured by mercury porosimeter techniques. Most of the pore volume of Clevite No. 3 was between 2 and 12 μ (Alfred University, *28*). The technique does not work with plastic-bonded electrodes because of deformation under the high pressures used in the porosimeter. The mean hydraulic radius of equation (C.3) can be converted to an equivalent mean pore diameter, $D=4M$. The pore size of Darco Carbon G 6 0 (Engelhard) was determined by measuring the hydrostatic head required to produce bubbles from water-wetted carbon (General Electric, *263*). This was 50 cm H_2O pressure, and using $p = 2\sigma \cos\theta/r$, where T is the surface tension, θ the contact angle, and r the pore radius, 7 was calculated to be **7** μ. Gas permeability gave a value of 1 μ. **A** porosimeter curve showed a wide range of pore size, from 0.1 μ to 40 μ.

C.4 PREPARATION OF CATALYSTS

A method of preparing small solid electrodes which gives a well-defined surface for fundamental studies is as follows (University of Pennsylvania, *736*). To avoid any uncontrolled influence of temperature, which could affect the catalytic activity, especially of alloys, the wire electrodes were sealed in glass with the aid of a chuck; while the electrode was sealed into a glass tube, the outer part of the electrode was placed in the chuck with a hole whose dimension was close to the electrode diameter. The metal block of the chuck took away the excessive heat during the sealing of the electrode. Pretreatment of the electrode consisted of degreasing with organic solvents, washing with sulfuric acid, and thoroughly washing with conductivity water. Such electrodes were then thermally treated by heating in a stream of purified hydrogen for 2 to 5 minutes, and then for about 10 minutes in highly purified nitrogen. The temperature was about 662" F (350" C) for noble metals and their alloys, and about 1112" F (600" C) for nonnoble metals (Fe, Cu, and Ni). The fornace was mounted on the test cell so that the electrodes were lowered into the cell and used without exposure to the atmosphere. (The ruthenium electrode was a thin metal block, thickness—1 mm, total area 2 cm^2, which was spot welded to a thin platinum wire. To obtain an oxide-free surface, the ruthenium electrode was treated with dilute HF. The electrode was subsequently carefully washed by flowing freshly redistilled (deoxygenated) conductivity water for about 10 minutes, and then finally it was washed inside the cell with conductivity water and NaOH solution. The thermal treatment had not been applied. Instead, a few short (~1 sec) cathodic pulses were applied by means of a potentiostat at 0.3 volt.)

Codeposition of metals on a solid-platinum electrode was performed by electroplating from a 1.5 weight-percent solution of $H_2PtCl_6 : 6H_2O$ plus dissolved metal chloride (Esso, ***214***). Platinum started to deposit below 0 volt versus NHE in SE, went to a limiting deposition current as the potential was made more negative, and platinum and metal were codeposited at a more negative potential. The metals codeposited were Fe, Rh, Rh-Fe, Ni, Co, Cu, Au, Pd, and Pb from the nitrate. Sn and Mo precipitated, and Ir, Ru, and W could not be plated. Cr prevented the deposition of platinum black. X-ray examination showed the Pt-Fe codeposit to be a true alloy and the Fe was not removed in 30 weight-percent H_2SO_4 at 140" F (60" C). **A** standard method of platinization is given in reference C.13.

Methods of impregnating solid electrodes with catalyst have been described in chapter 3, as has the preparation of electrodes of plastic-bonded metal blacks. Methods of preparing the blacks are as follows. **A** half milliliter of 0.5 M Na_2PtCl_2 was added, drop by drop, to 45 milliliters of 2 weight-percent aqueous $NaBH_4$ (Esso, *214*). This was allowed to stand until H_2 had completely diffused off, then filtered and washed. Pt, Ru, Ir, Ni, Pt-Fe, Pt-Co, Pt-Ni, and Pt-Mo were prepared in this way. Pt, Pt-Au, and Pt-Fe prepared in methanol gave the same performance as the preparation in water ***(215).*** Hypophosphorous acid and N_2H_4 were not as effective reducing agents as KBH_4. Zn and Mn precipitated as hydroxides; W and Cr precipitated slowly; and Mo and W precipitated as mixed oxides. Coprecipitates were true alloys (X-ray studies). $NaBH_4$ and $LiBH_4$ in various organic solvents produced similar blacks. The temperature of precipitation and stirring or bubbling with O_2 or A produced little effect.

For use as anode catalysts, the blacks were best stored in 0.01 *M* HCHO; otherwise, O_2 that had adsorbed on the black reacted when fuel was admitted, causing heating and deactivation. Alternatively, they could be dried in N_2 and be used dry, provided hydrogen was evolved on the anode before use ***(217)*** Platinum black that was comparable to available commercial black was prepared by $NaBH_4$ reduction in solution sparged with H_2, followed by drying in hydrogen at 176" F (80° C). Treatment of the black with concentrated HNO_3 for 150 hours did not improve the black as a cathode catalyst. Metals were dissolved in molten lithium under dry argon at 662" F (350" C), cooled under argon, and leached with water (General Electric, ***256).*** The technique was successfully used with Pt, Pd, Rh, Au, Ag, and Co. Thermal decomposition of ammonium chloroplatinate gave a black of 1.5 m^2/g BET area ***(263).***

Platinum blacks prepared by $NaBH_4$ reduction of chloroplatinic acid or by reduction of chloroplatinic acid with a silane in ethanol at 167" F (75" ***C)*** were no better than a standard Engelhard black when made into Teflon-bonded electrodes (American Cyanamid, ***86).*** These high-area blacks had to be stored in N_2 after preparation and adjusted slowly to air, or they would heat and sinter. Sintering and loss of area also occurred during electrode preparation; this loss of area explained why the blacks were not better than commercial blacks. Sintering of blacks was also observed by **Lockheed *(404);*** sintering for 1 hour at 392" F (200" ***C)*** produced an area decrease from 8–14 m^2/g to **4** m^2/g; at 806° F (430" C) area was 1.8 m^2/g, and at 1112" F (600" C), area was 0.6 m^2/g.

C.5 MISCELLANEOUS

Attempts have been made to study the infrared adsorption spectra of molecules adsorbed on electrodes. Multiple internal reflection in germanium wafers was found to be unsatisfactory (American Oil, ***93*** through ***101).*** The principle of multiple internal reflection was also applied in a light pipe cell (Atomics International, ***122*** and ***123).*** The cell consisted of two concentric tubes of quartz, bent into a single coil. Liquid was placed in the annulus between the tubes, and monochromatic light passed into the center tube. The light from the outlet of the center tube was analyzed for infrared adsorption spectra in the usual way. The resulting spectra included that of quartz, but also showed characteristic spectra for the liquid. The log of intensity of a given band was inversely proportional to the concentration of the absorbing component in the liquid (Beer-Lambert law). At high concentrations, an intercept in log *I* versus ***C*** was obtained due to material adsorbed on the outer wall of the inner tube. **A** thin film (175 angstroms) of palladium on the wall reduced the intensity of the liquid absorption peak to one-tenth, but did not eliminate it. It was suggested that such a film could be used as an electrode and the infrared spectra of adsorbed molecules thus studied.

Vacuum-evaporated films were deposited on various substrates using a Veeco 400 evaporator and pumping station (Atomics International, ***122*** and ***123).*** Three 20-mil W wires were wound with a platinum wire at 212" F (100° C), using a drill to twist the wires into a filament. This filament had a high evaporating area of platinum but a low radiation area, *so* that platinum could be readily evaporated.

In a study on sorption of radio-labeled fuels (American Oil, ***90*** through *101*)**,** a thin layer of platinum spattered onto a thin mica film formed the electrode. Radioactive hydrocarbon, in solution in electrolyte, adsorbed on the platinum and a Geiger counter placed near the mica window measured the adsorption. Peeling away of platinum from the mica was a major problem. A similar technique used a 20 000-angstrom gold foil as electrode, platinized on the side in contact with the electrolyte (University of Pennsylvania, *737* through *739)*. A Geiger counter placed near the gold window measured adsorption of radioactive hydrocarbons on the electrode. EPR was used to detect unpaired electrons on electrodes (California Research, *139)*. It was concluded that the steady-state concentrations on the electrode surface may be below sensitivity of the instrument and the absence of EPR effects does not mean that free radicals do not exist on the surface. ESR was used to detect free radicals in solution (General Electric, *291–293*) ; none were found.

Analysis for formic acid by spectrophotometer at 205 millimicrons was carried out (Baylor University, *9)*. Analysis for formaldehyde used the technique of Thompsett and Smith (*Analyst,* vol. 78, no. 209 (1953)). For formic acid in the presence of formaldehyde and H_2SO_4 (California Research, *133*), most of the formaldehyde was converted to nonvolatile phenylhydrazone and the formic acid vacuum distilled out. Correction was required for formaldehyde which is not converted. Formaldehyde in 2 *N* H_2SO_4 was analyzed using chromotropic acid (Engelhard, *213)* as in Feigel, F., ***Spot Tests in Organic Analysis,*** Elsevier Pub. *Corp.*, 1960. Formic acid is reduced to HCHO with magnesium and HCHO redetermined. Magna *Corp.* *(423)* used the method of W. **M.** Grant (***Anal. Chem.,*** vol. 20, no. 267, 1948); colorimetric at 570 mμ.

A technique for electroplating Plexiglas 55 or Lucite (Electro-optical Systems, *191)* was as follows. Sandblast, clean, apply stannous chloride solution. Deposit Ag on surface by immersing in formaldehyde-ammonia silver solution. Electroplate with Ni from sulfanate bath. A better technique *(185)* was to blast, wash with detergent, and rinse with water. Apply 0.1 *N* stannous chloride plus 2 milliliters/liter of Dupenol wetting agent and rinse with water. Spray with mirror silver (L. H. Butcher **Co.)**. Plate from acid copper sulfate (**32** ounces per gallon, pH 0.35, 158" F (70" C) at 40 A/sq ft, for 2 hours) to 3 mils of Cu. Rinse, put into 40 percent H_2SO_4 and rinse. Plate from nickel sulfanate (10 ounces per gallon, pH 5.2, 100° F (38" C), 30 A/sq ft, for 2 hours) to 3 mils Ni.

C.6 GENERAL REFERENCES FOR THE PREPARATION OF METAL CHELATES *(466)*

Chelate type	*Ref.*
1. Hexafluoroacetylacetonates	1
2. Acetylacetonates	2
3. *bis*-acetylacetoneethylenediamines	3
4. 8-Hydroxyquinolines	4
5. *bis*-salicylaldehydeethylenediamine	5, 6
6. Tetraphenylporphines	7, 8
7. Phthalocyanines	9

1. Belford et al., J. Inorg. and Nucl. Chem., vol. 2, 11, 1956.
2. Charles et al., J. Phys. Chem., vol. 62, 440, 1958.
3. Welcher, F. J., Organic Analytical Reagents, vol. I, D. Van Nostrand Co., Inc., New York, 1955, p. 266.
4. McCarthy et al., J. Am. Chem. Soc., vol. 77, 5820, 1955.
5. Pfeiffer et al., J. Prakt. Chem., vol. 145, 243, 1936.
6. Bailes and Calvin, J. Am. Chem. Soc., vol. 69, 1886, 1947.
7. Thomas and Martell, Arch. Biochem. Biophys., vol. 76, 286, 1958.
8. Sharp, U.S. Patent 2 950 237, Aug. 1963, **C.A.,** 3289, 1962.
9. Barret et al., J. Chem. Soc., 1719–1736, 1936.

REFERENCES

C.1. KORDESCH, K. V.; AND MARKO, A.: J. Electrochem. Soc., vol. 107, 480, 1960.

C.2. ANSON, F. C.: Anal. Chem., vol. 33, 939, 1961.

C.3. MATTSON, E.; AND BOCKRIS, J. O'M.: Trans. Faraday Soc. (London), vol. 55, 1586, 1959.

C.4. VAN DER PAUW, L. G.: A Method of Measuring Specific Resistivity and Hall Effect on Discs of Arbitrary Shape. Phillips Research Reports, vol. 13, Feb. 1958, pp. 1–9.

C.5. LOGAN, A. M.: An A.C. Bridge for Semiconductor Resistivity Measurements Using a 4 Point Probe. Bell System Technical Journal, vol. 40, No. 3, May 1961, pp. 885–919.

C.6. DELAHAY, P.: New Instrumental Methods in Electrochemistry. Interscience Pub., New York, 1954.

C.7. GIERST, L. E.: Zeit Elektrochem., vol. 59, 784, 1955.

C.8. MUNSON, R. A.: J. Phys. Chem., vol. 727, 1962.

C.9. NICHOLSON, R. S.; AND SHAIN, I.: Anal. Chem., vol. 36, 706, 1964.

C.10. DELAHAY, **P.;** AND *C.* TOBIAS, eds.: Advances in

Electrochemistry and Electrochemical Engineering. Vol. I. Interscience Pub., New York, 1961, pp. 233–318.

C.11. **Levich, V.** *G.:* Physicochemical Hydrodynamics. Prentice-Hall, 1962.

C.12. **Gottlieb,** M. H.: **J.** Electrochem. **Soc., vol. 111,** 465, 1964.

C.13. **Atkinson, R. H.:** Electrodeposition of Pt for Chloroplatinic Acid. Inst. Metal Finishing Trans., **vol.** 36, 7, 1958.

APPENDIX D

Materials

Surveys of materials were carried out in several contracts to determine those materials most suitable for certain conditions. The materials chosen for cell construction have already been given in the descriptions of the cells, but it may also be useful to know the results of tests on materials which were not chosen. In this appendix, therefore, the results of material surveys are briefly summarized in tabular form. The tables are intended to be only an approximate guide to the contents of the original source, which should be consulted for details.

TABLE D.1.—*Halogens*

Report	System	Results
155........	Cl_2, 1562° F (850° C).............	Tungsten carbide, W, Mo, 304 stainless steel, Ni, some alloys, not alright; Au, Pt alright.
583........	NOCl (liquid)+$AlCl_3$, Cl_2, ambient temperature 30–100 days	Tantalum showed no weight change. Udimet, Ni, Monel, Inconel, Pb, Mo, Ag, Co, Au, less than 1 percent weight change. 20 percent Ir 80 percent Pt, Hastelloy D, large weight loss. Pt, Haynes Stellite N–25, Hastelloy B, C, F, X, 430, 316 stainless steel, Nispan, Ti; completely reacted.
		Kel-F film, Teflon: alright. Polyethylene, Silastic LS–53, Kel-F elastomers, Viton **A,** Hypalon, Stillman Rubber Co. No. TH1030 (silicone), Scotchcast 808, sealing wax, Vinylloyd No. 4003: not alright.
249........	Bromine, bromide in 6.0 *N* HCl.....	Ti, Ta, silicon-carbide bonded graphite, silicon carbide, platinum-clad Ta, alloy of Ti+0.1 percent Pd, graphite: alright.
	5.4 *N* HCl, Ti^{3+}, Ti^{4+}, Br^-.........	Ta, Au, Pd, Mo, Zircalloy 2, 3, Pt coated Ta, Hastelloy B, Pt coated (0.02 mil) Ti: alright.

TABLE D.2.—*Molten Salts*

Report	System	Results
68	K amalgam and molten $KOH+KBr$ $=KI$	Low C steels, 400 stainless, W, Mo, Cr, alright. 300 stainless steel attacked by Na, K; Magnesia, spinel, thoria, alright; Alumina, silica, zirconia, B_3N, calcia, not alright. Au alright, Pt not.
102-114	Molten KCl-LiCl	Pt, Pd-Ag corroded rapidly, pure Fe alright. Beryllium oxide crucible disintegrated.
	Molten Li/Bi, Cd, Pb, Zn, Sn, Te	Tantalum alright for all except Te.
155	Molten Li	Alumina attacked, beryllium oxide not attacked.
403	Molten LiI_2, PbI_2, CdI_2	Stainless steel 316, **quartz:** alright, but some corrosion of stainless steel by I_2·Mo: not alright.
156	Molten KOH-NaOH in paste with MgO	Oxidized Ni, and Au alright; ceramics not alright.
495	Molten Na_2CO_3 in refractory	Alundum (Norton Co.), Harbison-Walker Periklase, forsterite, mullite, Kaosil. Only periklase showed low weight loss.
496		Remmey 50-D, Remmey CMP-21-A, Stupakoff Stupalith: rapid reaction, not alright. Norton Magnorite, Remmey CZ61-P (zirconia), Remmey 99AV-29 (alumina): moderate reaction High purity MgO: little reaction, alright.

TABLE D.3.—*Sulfuric Acid* (605)

(a) 6 *N* H_2SO_4 at 60° C

Material	Test duration, hours	Percentage weight, loss or gain	Observations
Titanium	550	−100	Specimen disintegrated
Platinized titanium	550	−11.0	Platinum coating loosened
Gold-plated titanium (200 microinches)	140	−100	Titanium completely dissolved
Gold-plated titanium (400 microinches)	650	−2.1	No change
Monel alloy 400	530	−1.5	Surface became copper colored
Ionics 61–AZG membrane	550	−12.7	Turned reddish brown
Buna-N on nylon	550	−5.5	Solution yellowish; specimen warped
Epoxy fiber glass	550	+8.4	No change
Teflon	550	−.8	No change
Halon TVS 300	580	.0	No change
Kel-F	580	.0	No change
Trilok 6001–1–1	550	−.3	Loss of springiness

(b) Corrosion of Metals and Alloys in 6 *N* H_2SO_4 at 95" C

Material	Specific gravity	Thickness of sheet, mils	Approximat electrical resistivity, microhm-cm room temp.	Test duration, hours	Corrosion rate, mils/year
Ta	16.6	32	15.	350	0
Ta+Pt				350	0
Nb	8.4	40-mil wire	20	350	5.0
Nb+Pt				350	5.4
Zr	6.5	30	41	350	1.26
Zr+Pt				350	1.28
Ampco No. 8 (1.5 Fe:Al 7:Cu 91.5)	7.78	123	10	137	9.6
Ampco No. 8+Pt				137	18
Ampco No. 775 (10 Ni: 1.25 Fe: 88.4 Cu:0.4 Mo)	8.50	45		137	43
Ampco No. 755+Pt				137	38
Ampco No. 702 (30 Ni:0.5 Fe: 68.9 Cu:0.6 Ma)	8.40	48	37	137	47
Ampco No. 702+Pt				137	51
Monel CG–S (Ni:Cu)	8.90	60	48	98	67
Monel CG–S+Pt				98	58
Carpenter 20–3 (29 Ni:46 Fe:3 Cu:1 Ma:20 Cr:1 C)	8.00	57	130	306	21
Carpenter 20–3+Pt				306	22
Hastelloy B–1 (Ni:Cr)	9.24	190	135	297	9
Hastelloy B–1+Pt				297	12
Cu	8.94	5	2	22	55
Ti (commercial)		12	3	24	>1000
Ti (0.27 percent Pd) alloy		3		24	>1000

TABLE D.3.—*Sulfuric Acid* (*605*)—Continued

(c) Description of Nonmetallic Materials

Material	Composition	Color and shape
Ion-exchange membranes:		
Ionics, 61-AZG	Sulfonated Polystyrene	Tan rectangle
AMF, C–313	Sulfonated polystyrene	Clear, rectangular sheet
AMF, C–60	Sulfonated polystyrene	Brown, rectangular sheet
Gelman Acropor	PVC-acrylonitrile	White, rectangular sheet
Gasketing:		
Red silicone	Silicone rubber	Red, rectangular sheet
Gray silicone	Silicone rubber	Gray, rectangular sheet
Buna-N	Butadiene and acrylonitrile copolymer	Black, rectangular sheet
Butyl rubber	Butyl rubber	Black, triangular sheet
Viton-A	Fluorinated hydrocarbon	Black, rectangular sheet
Compartment frame:		
Teflon	Fluorocarbon resin	White, rectangle
Kel-F	Copolymer of chlorotrifluoroethylene and vinylidene fluoride	Clear, rectangular sheet
Penton	Chlorinated polyether	Green, square
Halon TVS	Fluorohalocarbon resin	White, rectangle
Epoxy fiber glass	Epoxy fiber glass	Green, rectangles: 100-125 mil thick
Polyester fiber glass	Isophthalic polyester	Green, rectangles: 100–125 mil thick
ADM Aropol 7250	Chemically resistant polyester	Yellow, rectangles: 100–125 mil thick
DAP	Dapon-35 in diallylphthalate monomer	Tan, rectangles: 100-125 mil thick
Hetron 92	Polyester	Yellow, rectangles: 100–125 mil thick
Buton	Hydrocarbon resin	Clear, rectangles: 100-125 mil thick
Laminac 4173	Chemically resistant polyester	Yellow, rectangles: 100–125 mil thick
Stypol 2012	Flexible polyester resin	Yellow, rectangles: 100–125 mil thick
Nypol 4050	Acrylic modified chemically resistant polyester	Yellow, rectangles: 100–125 mil thick
Atlac 382	Chemically resistant polyester	Yellow, rectangles: 100–125 mil thick
Laminac W/G/255	Laminac with glass reinforcement	Gray, rectangles: 100–125 mil thick
Spacer mesh: Trilok 6001–1–1	36 percent polyethylene and 64 percent Saran mesh	Black, square

(d) Nonmetallic Materials in 6 *N* H_2SO_4 at 95° C

Material	Test duration, hours	Percent weight, loss or gain	Observations
Ion-exchange membranes:			
Ionics, 61–AZG	308	−15.2	No change
AMF, C–313	353	2.35	Slight darkening, shriveled
AMF, C–60	353	17.4	Extreme darkening
Gelman Acropor	48		Fell apart
Gasketing:			
Red silicone	281	−19.0	Cracked, disintegrated
Gray silicone	611	−11.65	Flaky
Buna-N	114	18.9	Disintegrated
Butyl rubber	285	.07	Slight disintegration
Viton-A	285	1.73	No change
Compartment frame:			
Teflon	611	.0	No change
Kel-F	611	.53	Curled
Penton	447	−.37	No change

TABLE D.3.—*Sulfuric Acid* (*605*)—Continued

(d) Nonmetallic Materials in 6 N H_2SO_4 at 95" C—Continued

Material	Test duration, hours	Percent weight, loss or gain	Observations
Compartment frame—Continued			
Halon TVS	308	0.03	No change
Epoxy fiber glass	611	37.2	Extreme darkening, brittle
Polyester fiber glass	611	22.3	Yellow, brittle, swollen
ADM Aropol 7250	471	.17	No change
DAP	471	–1.34	Charred
Hetron 92	471	.28	Very slight darkening
Buton	471	–.94	Considerable darkening
Laminac 4173	471	.32	Slight darkening
Stypol 2012	471	–35.5	Darkened, cracked, brittle
Nypol 4050	471	–.88	No change
Atlac 382	471	–.74	No change
Lamiiac W/G/255	471	.0	Considerable darkening
Spacer mesh: Trilok 6001–1–1	611	–2.70	No change

TABLE D.4.—*Acid and Alkaline Cells*

Report	System	Remarks
126	H_3PO_4-H_2O	Paper, cotton, asbestos, rayon, nylon: not alright. Dacron, Dynel, Vinyon: alright.
214	30 percent H_2SO_4	Viton, Hypalon, and AMF-C313 IEM had to be pretreated with strong acid to prevent poisoning of electrodes.
216	....	Penton (chlorinated polyether, Hercules Powder), polypropylene alright. Lustron, Viton, epoxy resin showed weight gains. Lustron poisoned Pt electrodes.
217	....	Viton-A, Kynar (partially fluorinated hydrocarbon, Pennsylvania Fluorocarbon Co.), Vix-Syn (propylene-ethylene copolymer, Houghton Co.): alright. Polyethylene: not alright. Permutit C–20, Ionics CR-61, Nafilm D–30: alright. Asahi CA–1: not alright, even after repeated washing with H_2SO_4.
185	KOH/asbestos/O_2 100 psig/ 257" F (125" C)/24 hours	Ni alright. Stainless steel 302, 304, 321, 410, 430, brass, heavy surface oxidation. Stainless 301, Monel, moderate; 347, 316, light surface oxidation. Buna rubber went powdery. Nylon dissolved. RTV rubber (General Electric) reacted on surface. Vitron, Plexiglas 55, Sierracin 880, became pliable.
	O_2/257° F (125" C)/60 hours/ 50 psi	Silicone, RTV, Neoprene, buna: alright.
	O_2/257° F (125" C)/60 hours/ 400 psi	Silicone, RTV, Neoprene, buna: not alright.
	O_2/300 psi in fuel cell	Buna-*N* O-rings burned.
124	O_2/KOH/392° F (200" C)	Teflon charred at 482" F (250" C).
54	Allis-Chalmers O_2-KOH-H_2 cell	Epoxy enamel satisfactory for external surfaces of cell.
478	KOH-H_2O, 500" F (260" C)	Teflon gaskets failed. Klingerite (rubber base asbestos) alright.
466	Cs_2CO_3 solution, 302" F (150" C)	Viton A not alright.

TABLE D.5.—*Catalyst Stability in Cesium Carbonate, Hydrogen Fluoride and Phosphoric Acid Solutions (309)*

Report	System	Results
309......	92 wt-%, Cs_2CO_3 solution, 338° F (170"C) *air*, 1 week	Pt, Ru, Co, Ir, Au: excellent. Rh, Pd, Ta, Hf, Zr, Fe, MnO_2, Fe_2O_3, TaN: good. B_4C, TiC, $B_{13}P_2$, Re: fair.
	Aqueous CsF-HF, 338" F (170" C) *air*	Pt, Pd, Ir, Au, Rh: alright.
	90 wt-% H_3PO_4, 302° F (150° C)	Au, Pt, Ta, Pd-Ni or Pd-Cr with high Pd, Ta-W, W-Ir, Mo-Tit-Zr, TiC, Ta-Zr-carbides: alright ($< 10 \mu g/in.^2$ hour).
	Plus 1-volt potential (versus SHE)	Only Au, Pt, Ta, Au-Ag-Pd, alright. Evidence of Pt dissolution from Niedrach-Alford electrode.
	Above plus JP4. ....,.......	Teflon and glass-filled Teflon (TFE Du Pont). Kel-F-81 (MMM) were alright. Other plastics attacked.
185......	Plastic plated with Ag/Cu/Ni plate (see A.3) temperature sterilized	Plate lifted from Sierracin 880 (acetal), Delrin (polycarbonate), Lexon (phenolic Nema Grade C). Melamine (Nema Grade G 5) alright.
286......	General Electric-IEM H_2-O_2 cell	Silicone rubber deteriorated in 2000 hours. Aclar, Mylar used instead.
538......	KOH-H_2O, 500° F (260° C). ...	Asbestos, stainless steel 316: not alright. Stainless steel 321, 347, nickel: alright.
462......	....	Stainless-steel sheet with 14-mil holes. Perforated Products, Inc.

TABLE D.6.—*Some Sources of Metal Powders for Fuel Cell Electrodes*

Company	Product
1. International Nickel Co., Inc., 67 Wall St. New York 5, N.Y.	Carbonyl Ni powders: Grade **A 4 7** μ; Grade B—3–4 μ; Grade **D—7–9** μ; The particles are compact and granular, not spherical.
2. Linde Co., Crystal Products Dept., division of Union Carbide *Corp.*, 270 Park Ave., New York 17, N.Y.	Spherical metal particles of copper, aluminum, nickel, tungsten, nichrome alloy and type 316 stainless steel; particle size from less than 20 μ to 150 μ.
3. Federal-Mogul Division, 2355 West Stadium Blvd., Ann Arbor, Mich.	Spherical metal powders of type 316 stainless steel, iron, silver, copper, cobalt-chromium alloy and others on specification. Particle sue from below 30 microns and up.
4. Vanadium-Alloys Steel Co., Latrobe, Pa.	Spherical metal powders of various stainless steels; particle size of below 37 microns and up.
5. Bendix Filter Division, 434 West 12 Mile Rd., Madison Heights, Wis.	Poromesh and micromesh sintered wire cloth with pore ratings of 2 to 1000 microns (made of stainless steel).
6. National Carbon Co., division of Union Carbide Corp., 270 Park Ave., New York 17, N.Y.	3 grades of graphite cloth, 99.9+ percent carbon.
7. Micro Metallic Division, Pall *Corp.*, Glen Cove, N.Y.	Rigimesh, a woven sintered wire mesh with pore openings 2 microns and up. Also make various parts from metal powders to specification.
8. Metals & Chemical, 420 Lexington Ave., New York, N.Y.	Metal powders.
9. Clevite Corp., Mechanical Research Division, Cleveland, Ohio	Standard and custom-built porous metal sheet; Ni, Ti, and others.
10. Exmet Corp., 355 Hanover St., Bridgeport, Conn.	Fine expanded metal screen.

TABLE D.7.—*Survey of High Temperature Electrode Materials (790)*

(a) Silicides

Material	O_2 or fuel	Melting point, °C	Resistivity ohm-cm	Temperature range	Remarks
Chromium silicide	Fuel or O_2	**1500-1570**	....	....	Metals of groups IVA, VA and VIA.
Molybdenum disilicide	Fuel or O_2	**2030**	28.3×10^{-6}	Room	Not attacked by air or O_2 at red heat.
Tungsten disilicide	Fuel or O_2	**2180**	33.4×10^{-6}	Room	Oxidation resistance inferior to $MoSi_2$.
Titanium disilicide coatings 70	Fuel or O_2	....	123×10^{-6}	Room	Slowly oxidizes in bunsen burner flame.
Zirconium silicide	Fuel or O_2	....	161×10^{-6}	Room	Similar properties to $TiSi_2$.
Vanadium silicide	Fuel or O_2	....	9.5×10^{-6}	Room	Not attacked by O_2 at elevated temperatures.
Niobium disilicide	Fuel or O_2	2000	6.3×10^{-6}	Room	
Tantalum disilicide	Fuel or O_2	2200	8.5×10^{-6}	Room	Oxidation resistant to 1500° C. Tested—failed by decomposition below 1000° C in *air.*

*(General Carbon additions have been used to increase melting points.)

TABLE D.7.—*Survey of High-Temperature Electrode Materials* (*790*)—Continued

(b) Borides

Material	O_2 or fuel	**Formula**	Melting point, °C (approximate)	Resistivity, ohm-cm	Temperature range	Remarks
Zirconium boride. . .	O_2 fuel.	ZrB_2	3000	72×10^{-6}	1235.	Fairly oxidation resistant to 1300" or 1400" *C.* Oxide film was porous.
Titanium boride. . . .	O_2 fuel.	TiB_2	2600	15 to 50 $\times10^{-6}$	Room.	Fairly oxidation resistant to 1400" or 1500" C. Thick oxide film was formed.
Molybdenum boride	Fuel. . .	MoB_2	2100	40 to 50 $\times10^{-6}$	Room.	
Niobium boride. . . .	Fuel. . .	NbB_2	2000	28 to 65 $\times10^{-6}$	Room.	Fairly stable, reducing conditions.
Cerium boride.	Fuel. . .	. . . .	. . . .	. . . .	. . . .	
Tantalum boride. . .	Fuel. . .	2000	. . . .	68–100 $\times10^{-6}$	Room.	Fairly stable. reducing conditions.
Chromium boride. . .	. . . .	. . . .	. . . .	. . . .	. . . .	
Hafnium boride. . . .	. . . .	. . . .	. . . .	. . . .	. . . .	

(c) Oxides

Material	O_2 or fuel	Melting point, "C	Resistivity, ohm-cm	Temperature range	Remarks
Chromic oxide.	O_2.	2265	23	1200" C	Easily reduced. Volatilizes rapidly above 2000° C.
			4.5×10^{-3}	1100" C	Defect semiconductor. Little used alone.
Manganese oxide.	Fuel.	1780	1×10^{8}	20" C	Easily oxidized. Not a commercial product. Defect semiconductor.
Niobium oxide.	Fuel.	1772	8.6×10^{-2}	20" C	Easily oxidized. Classes as metallic conductor. Not a commercial product.
Tantalum oxide.	. . . .	1890	1x 105	. . . .	Excess semiconductor. Commercial product costly.
Vanadium trioxide.	Fuel.	1977	5.5×10^{-3} 1.75×10^{-3}	20 1967	Easily oxidized. Classed as metallic conductor.
Zinc oxide..	O_2.	. . . .	6.75x 103	800	Easily reduced. Volatilizes above 1700" C.
			5	1350	Excess semiconductor.
Ferric oxide (hematite)					
Forsterite					
Copper oxide					
Aluminum oxide	}	. . . .	30	1500" *C*	
Chromium oxide	. . . .	. . . .	200	600° C	
Aluminum oxide.	. . . .	. . . .	4	1500" C	
Chromium oxide 1percen Mg	. . . .	. . . .	20	600" C	

TABLE D.7.—*Survey* d *High-Temperature Electrode Materials* (790)—Continued

(d) Carbides

Material	O_2 or fuel	Formula	Melting point, °C	Resistivity ohm-cm	Temperature range	Remarks
Silicon carbide	Fuel	SiC	...	107–200	20" C	Carborundum. Stable in air below 1000° C and above 1140" C. Forms volatile halides above 800" C.
Titanium carbide	Fuel	TiC	...	1×10^{-4}	...	Stable to 2500" C in N_2, oxidizes in O_2, N_2O and slowly in COZ.
Tungsten carbide	Fuel	WC	...	1.2×10^{-5}	...	
Boron carbide	Fuel	B_4C	...	3 to 8	20" C	Oxidizes rapidly above 1000° C.
Silicon carbide	Fuel	SiC	...	...	...	Niafrax.
Silicon nitride	Fuel	SiN	...	...	...	
Tantalum carbide	Fuel	Ta_2C	...	2×10^{-5}	...	Attacked by O_2 at high temperatures.
Chromium carbide	Fuel	Cr_2C_3	...	...	...	
Hafnium carbide	Fuel	HfC	...	...	...	
Niobium carbide	Fuel	NbC	3500	7.4×10^{-5}	...	Stable to 2500" C in N_2, decarburizes slightly in air.
Uranium carbide	Fuel	U_2C_3	...	...	...	Stable; 196" to 1800" C.
Vanadium carbide	Fuel	VC	...	1.5×10^{-4}	...	Burns in O_2; stable in N_2 to 2500" C.
Zirconium carbide	Fuel	...	...	6.3×10^{-5}	...	Oxidizes readily at high temperatures.
Molybdenum carbide	Fuel	...	...	...	...	Less stable than others.

TABLE D.8.—*Materials Used for Ion-Exchange-Membrane Manufacture by Gregor (316–327)*

Code	Polyelectrolytes
MPVI (anionic)	Poly-N-methyl vinyl imidazolium iodide; soluble H_2O, DMF, DMSO, cresol, Eth CO_3.
BPVI (anionic)	Poly-N-vinyl-n-butyl imidazolium iodide; soluble above plus methanol.
GAF (cationic)	Maleic anhydride methyl vinyl ether (General Aniline & Film *Corp.)* (carboxylate ion).
PSA–5, PSA-6 (cationic)	Polystyrene sulfonic acid (sulfonate ion) prepared from Lustrex X–710 (Monsanto) base resin. Water soluble. **Also** Dowex 50X8 (Dow Chemical).
	Epoxy *Resins* **and** Crosslinking Agents
Epon 828 plus TET	Epon 828, low-molecular-weight epoxy resin, epoxide equivalent of 185–205 (the term “epoxide equivalent” refers to grams of resin containing 1 gram-equivalent of epoxide). **In** Epon resins the only chain linkage other than carbon to carbon is an ether linkage. The chemical resistance of this bond in contrast with an ester linkage is extremely good. The reactive hydroxyl and epoxide groups are widely spaced along the chain so that the curing agents which crosslink the resin and make it thermosetting are sufficiently far apart to give rise to flexibility in the cured resin. Pourable liquid at room temperature. Soluble in ketones (acetone, methylethylketone, etc.), ether alcohols (“cellosolves,” “carbitols”), esters (ethyl acetate, n-butyl acetate, etc.). DMSO, DMF, PCO_3 and several mixed solvent (aromatic hydrocarbons plus ketones or ether-alcohols) systems. Epon resins **can** be effectively cured with polyfunctional amines (diethyleneamine, triethylenetetramine) as well as organic acids and anhydrides. Manufactured by Shell Chemical Corp. TET; Triethylenetetramine, room temperature curing agent for Epon 828. It is manufactured by the Fisher Scientific Co.
ERL plus ZZL	ERL; Bakelite ERL–2774, epoxy resin of standard bisphenol-A type, as is Epon 828. High chemical resistance, being particularly resistant to hydroxide solutions, excellent strength and toughness. The epoxide equivalent ranges from 185–195 (Union Carbide Plastics Co.). ZZL; Bakelite ZZL–0814 is the liquid hardener associated with ERL–2774. It should be used in approximately a 4: 1 ratio of resin to hardener.
BRL–1100	Phenol formaldehyde resins, 65 percent solids in toluene (Union Carbide).
Epon 1009	**Bisphenol-epichlorohydrin** condensate (Shell Chemical Co.). Crosslinks through alcohol groups.
	Solvents
DMF	Dimethyl formamide.
DMSO	Dimethyl sulfoxide.
PCO_3	Propylene carbonate (Jefferson Chemical **Co.)**.
Eth CO_3	Ethyl carbonate.
ACE	Acetone.
CPA	Cyclopentanone.
NME	Nitromethane.
	Matrix Polymers
Kynar	High-molecular-weight crystalline thermoplastic polymer of vinylidene fluoride, containing 59 percent fluorine. Resistant to attack or penetration by most corrosive chemicals and organic compounds, including acids, alkali, strong oxidizers and halogens. Unchanged when exposed to 50 percent sodium hydroxide as well as 50:50 mixture of sulfuric and hydrochloric acids. Thermally stable (no significant dehydrofluorination or chain scission) for periods greater than 2 years at 300° F (149” C). Pennsalt Chemicals Corp. (Box 4388, Philadelphia, Pa.), supplied in pellet form, powder, or dimethylacetamide solution.
Dynel	1:1 vinyl chloride-acrylonitrite copolymer (Bakelite Division, Union Carbide). Resistant to acids and alkalis.

TABLE D.9.—*Characteristics* of *IEM Reinforcing Materials* (*248*)

Code or designation	Thickness, in.	wt, g/in.²	Description
DN	0.005	0.031	Dacron filament fabric.
234	.024	.055	Dynel mat fabric.
424	.006	.055	Dynel mat—compressed.
429	.005	.030	Dynel mat-compressed.
Wool rayon	.037	.41	50 percent wool–50 percent rayon mat (National Felt Co.).
Waumbec	.015	.092	70 percent Dacron–30 percent wool woven.
Dacron felt	.250	.19	Dacron mat (National Felt Co.).
Polypropylene felt	.250	.30	Polypropylene mat (National Felt Co.).
Porous polyethylene	.016	.053	80 percent void volume, 100-micron porous polyethylene (F. S. Reeves Co.).
Rubber separator	.045	.39	60 percent volume, natural rubber battery separator (U.S. Rubber Co.).
Tissue glass No. 1	.009	.019	Nonwoven glass mat (American Machine & Foundry Co.).
Tissue glass No. 2	.026	.067	Nonwoven glass mat (American Machine & Foundry Co.).

Cell construction	Thickness, in.	Membrane resistance, ohm-cm²	Burst strength, psig	40 percent R.H. dryout, minutes
DN/234/DN	0.029	2.64	280	50
4241234	.030	6.08	110	55
½234/424/½234 [a]	.021	4.44	140	90
234/DN/234	.032	3.60	285	55–150
DN/ 1½234/DN [a]	.029	3.26	340	50
DN/1½234/DN [a]	.022	3.50	340	45
1½234 [a]	.019	2.11	80	30
DN/234/DN	.025	2.42	300	20
424/234/424	.030	6.90	265	200
1½234/1½234 [a]	.032	4.25	250	200
2341234	.033	2.74	130	45
DN/polyethylene/DN	.025	18.13	275	(b)
Dacron felt	,030	5.46	350	60
Polypropylene felt	.030	5.67	450	120
Rubber separator	.055	12.36	20	10
Wool-rayon	.025	17.10	0	(c)
DN/tissue glass/DN	.025	wuld not be handled		
DN/tissue glass/DN	.025	Could not be handled		
234/Waumbec/234	.027	6.18	350	790
429/Waumbec/429	.025	6.30	270	60

[a] Reference is made to such compositions as 1½234, ½234. This material is the same type as 234, but 1½ or ½ times as thick as the normal 234 material.

[b] No failure.

[c] Too brittle to handle.

TABLE D.10.—*Physical Data of Tape Materials (Monsanto, 462)*

Product designation	Name or type of material	Thickness, mils	Weight, g/in.^{2}	Electrolyte retention 30 percent KOH g/in.^{2}	Manufacturer	Remarks
Tapes:						
N561	Nonwoven nylon	3–4	0.034	0.135	Pellon Corp.	
2505K	Nonwoven nylon	5–6	.038	.115	Pellon Corp.	
2505	Nonwoven nylon	8–10	.038	.33	Pellon Corp.	
2505B	Nonwoven nylon	10–12	.038	.35	Pellon Corp.	
N524	Nonwoven nylon	6	.032	.80	Pellon Corp.	
EM403	Nonwoven Dynel	0.8	.012	.04	Kendall Co.	
EM436	Nonwoven Dynel	5–9	.027	....	Kendall Co.	
EM476	Nonwoven polypropylene	2.7	.023	.04	Kendall Co.	
EM4858	Nonwoven cellulosic	5	.031	.10	Kendall Co.	
M1410	Nonwoven Dynel	3.7	.029	.05	Kendall Co.	
OH 1.5	Porous polyethylene	6–7	.027	.03	Millipore Filter	1.5-micron holes
OS10	Porous polyethylene	9–10	.034	.19	Millipore Filter	10-micron holes
GWA	Ion-exchange membrane[b]	5	.038	....	Gelman Instrument	Nylon-reinforced weak acid type, 5-micron holes (dry)
GPVA	Semipermeable membrane	5	.038	[a]	Gelman Instrument.	Nylon-reinforced polyvinyl alcohol 5-micron holes (dry)
Binders:						
Gelvatol R 20–30	Polyvinyl alcohol	....	....	....	Shawinigan Resins	Slow to wet with strong KOH
Methocel R 65HG	Hydroxypropylmethyl cellulose	....	....	....	Dow Chemical	Very slow to wet with strong KOH
PVP K–30	Polyvinyl pyrrolidone	....	....	....	Antara Chemicals	Slow to wet with strong KOH
CMC 7 HCP	Cellulose gum	....	....	....	Hercules Powder	Produced brittle coatings, slow to wet
Acrysol	Polyacrylic acid		.....		Rohm & Haas	Produced brittle coatings, slow to wet

TABLE *D.ll.-Low- Temperature Cements*

Report	*Results*
234	Plastilock No. **604,** B. F. Goodrich, bonds to stainless steel. Bostick B. and B. Chemical, cement plastic frame to above.
384	Ag-Ag bond to resist KOH at **150**" F **(65.6**" C). Handy-Harman Brazing alloys; TEC **(95** percent **Cd, 5** percent Ag), Easy-flo **(45** percent Cd), attacked. Handy-Harman Silflake **855** (silver powder paste), fired 1000° F **(538**" C), **20** minutes, absence **of** O_2, good conductor but not strong. Impregnated with Epoxolite **807** to make strong.
583	Teflon pretreated with Na in liquid NH_3. Surface will then bond to Scotchcast No. **808** epoxy potting resin.
584	Viton **PR1730** putty (Products Research **Gorp.,** Los Angeles), insulating glass-to-metal seal.
767	Duco cement all right in concentrated KOH; not attacked by Cl_2.
774	Pliciene cement (Fisher Scientific) good in concentrated NaOH.

TABLE D.12.—*Seals Between Refractories at 1832° F (1000° C)*

Report	*Results*	
791	Pt paint-Pt gasket-Pt paint, fire **4** hours, **1832**" F (1000" C). Strong but not gastight. Vitreous enamel, SiO_2 67-B_2O_3 18-Na_2O **8** wt-%, rest K_2O, Al_2O_3, CaOl-BaO (O. Hommel ***Co.,*** Pittsburgh). Good seal, resistant to oxidation and crazing.	
792	Enamel used as seal from lava to Pt gasket to electrode. Not entirely gastight.	
793	Best seal: Pt paint, electroplate with **Pt** to **3** mils, electroplate with Au to **0.7** mils. Insert brazing shim **18** wt-% Ni **82** percent Au between each surface treated as above. Heat **2089**" F (1125° C) 20 minutes, in H_2.	
4	Ag paint (Microcircuit Co.):	Formed good seal Ni to lava, **1472**" F **(800**" C) in air. Impermeable coat on porous ceramic, **1472**" F (800° C).
	Astrocerams (Astroceram Co.):	Unsatisfactory.
	Rokide "A" (alumina base) (Metallizing *Corp.* of America):	Unsatisfactory.
	Pyrochrome H.T. paint (Preferred Utilities Mfg. Corp.):	Unsatisfactory.
	Sauereisen cements **7, 8, 29, 31, 32:**	No. **7** best when glazed with sodium silicate.
155	Paste of sugar in H_2O formed good bond between C and W on firing at **2192**" F **(1200**" C).	

REFERENCES TO ORGANIC BINDERS (F. HUMMEL, PENNSYLVANIA STATE UNIVERSITY)

1. FISHER AND POTTER: Factors Affecting the Physical Structure **of** Dry Pressed Steatite. Bull. Amer. Cer. Soc., vol. **34,** no. **6,** June **1955,** p. **177.**

   Requirements:

   1. Freedom from sticking.
   2. Sufficient plasticity.
   3. High mechanical strength at low forming pressures.
   4. Plastic dry strength.
   5. Tough granules.
   6. Proper softness.
   7. Easy removal of air.
   8. Disintegration on firing.
   9. Dispersion characteristics.
   10. Nontoxic.
   11. Efficiency in low concentration.
   12. Storage stability.

   Superloid: Kelco **Co.,** New York **5,** N.Y.
   Methocel: Dow Chemical, Midland, Mich.
   Carbowax: Carbide & Carbon Chemical Co., New York **17,** N.Y.
   Halowax: Halowax Products Division, New York **17,** N.Y.
   Alwax: Emulsions—American Cyanamid Co., New York **20,** N.Y.
   Hyform: Emulsions—American Cyanamid Co., New York **20,** N.Y.
   Emulsion **4–119:** Wilmington, Del.
   Polyvinyl alcohol: E. I. du Pont de Nemours & Co.

2. KNAPP, **THOMAS:** Glaze Binders. Bull. Amer. Cer. Soc., vol. **33,** no. **1,** Jan. **1954,** p. **11.**
3. WILD, ALFRED: Review of Organic Binders for Use in Structural Clay Products. Bull. Amer. Cer. Soc., vol. **33,** no. **12,** Dec. **1954,** p. **368.**
   1. Flours and starches.
   2. Gums
   3. Alginates
   4. Alcohols and celluloses.
   5. Wood extracts
   6. Miscellaneous
4. WHITTEMORE, JOHN W.: Industrial Use of Plasticizers, Binders **and** Other Auxiliary Agents. Bull. Amer. Cer. Soc., vol. **23,** no. **11,** Nov. **1944.**

APPENDIX E

Hydrogen Generation and Gas Storage

Hydrogen-oxygen or hydrogen-air fuel cells have much better performance than other economically feasible fuel cells. There is great interest, therefore, in producing hydrogen from fuels which are cheap and which can be easily handled. A fuel cell-hydrogen generator system has to compete with utilization of the fuels directly in a fuel cell and with other methods of power generation. It is known that a number of firms are actively developing plants for converting liquid hydrocarbons to hydrogen for use in their fuel cells, but no details are available. The work in the contracts under discussion here has been principally concerned with hydrogen generation for specialized military application, although some of the material is of more general interest.

Small generators for portable power packs were investigated in two contracts. Reactions between CaH_2 and excess H_2O gave 95 percent H_2 yield at 100° C; that between $NaOH$-H_2O-$NaBH_4$, catalyzed by cobalt sulfate, foamed badly; $NaBH_4$ plus twice the stoichiometric amount of H_2SO_4 gave 100 percent H_2 yield without foam (General Electric, ***248***). A small system using this last reaction was developed *(274)*. It was necessary to provide surge volume to prevent acid and sodium borohydride blowing out of the reactor in the H_2 stream; and only 50 to 60 percent of the theoretical H_2 capacity was obtained. The system was no better in energy storage density than high-pressure bottled H_2. Reactions between $NaBH_4$, NaH-CaH_2 and H_2O or KOH-H_2O were not satisfactory with stoichiometric amounts of water (Union Carbide, ***653***). NaH formed hydrates and physically adsorbed water. 100 S cu ft of H_2, 0.5 pound, was stored in a 15-inch i.d. sphere at about 3000 psi, with a total weight of 14 pounds.

Designs for mobile H_2 generators were given by the Kellogg Co. ***(386)***. Naphtha was assumed to be the highest hydrocarbon to be used without carbon formation and the process selected was steam re-forming followed by water gas shift. The molal steam-carbon ratio used was 5.0. For 50 S cu ft/hr of H_2, the hydrogen was recovered from the process stream with a Pd-Ag membrane diffuser operating at 700" F and 150 psi. The unit designed weighed 1500 pounds and could be mounted on a 4- x 4- x 5-foot skid. Predicted thermal efficiency was 49 percent, with 4 hours' startup time and 24 hours' continuous operation. A 2000 S cu ft/hr unit design -had: weight, 29000 pounds; dimensions, 8- x 8- x 20 feet; efficiency, 52 percent; startup time, 4 hours; continuous operation, 150 hours. Two thousand S cu ft/hr is approximately 150 kilowatts of fuel-cell output. The process stream was stripped of CO_2 by absorption in monethylamine; desulfurization was to be accomplished by passing gas over a Co-Mo catalyst ($S+H_2 \rightarrow H_2S$) followed by H_2S removal with pelleted iron oxide ($FeO+H_2S \rightarrow FeS+H_2O$). Predicted thermal efficiencies for a partial oxidation process were somewhat higher, but the process was considered to be unfavorable compared to steam re-forming due to requirements of: larger shift converter, larger CO_2 absorbers, more cooling water, and larger power requirement for O_2 compression.

Five design studies for a hydrogen generator suitable for 'use in a submarine were sponsored by the Bureau of Ships. The required rating was: continuous 20 lb/hr of H_2; maximum 70 lb/hr of H_2 for 2-hour periods (20 pounds H_2/hr would correspond to about 200 kW). The M. W. Kellogg Co. prepared a preliminary design based on catalytic steam re-forming of methanol at

PRECEDING PAGE BLANK NOT FILMED.

500° F, followed by conversion of CO to C02 and removal of CO_2. Table E.1 gives estimated weights and volumes of the system. Power density was thus approximately 40 lb/kW, 25 W/lb, and ½ kW/cu ft. Startup time was estimated as 30 minutes, with a 1½-minute time to go from 5 pounds H_2/hr to 70 lb H_2/hr. Several processes for decomposition of NH_3 were considered by American Cyanamid (86 through *89*), including thermal decomposition by electrical heat at 35 psig, higher pressure decomposition, and high-pressure partial combustion. Power density was about ½ kW/cu ft, but 1.35 gallons of NH_3 were required per pound H_2 compared to 0.5 for partial oxidation of naphtha or 0.9 for methanol, because of the low-energy density of ammonia. The Lumus Co. also considered ammonia decomposition. Efficiency of H_2 production of 70 percent was predicted, but the volume of components, including storage, was 2500 cubic feet, giving a power density of ½ kW/ft. Estimated startup time was 12 hours; response time, 3 minutes. The Girdler *Corp.* considered steam re-forming and partial oxidation of methanol, with purification by palladium diffusion. Efficiency of H_2 production was predicted to be 76.6 percent, but no total weights or volumes were given. **A** mixed steam re-forming-partial oxidation of JP–4 was proposed by the Chemical Construction Co.

Equipment No.	Description	Weight, pounds	Volume, cubic feet
B–1	Combustion chamber	1230	9.62
C–1	Primary feed heater	195	1.01
C-2	Secondary feed heater	92	.23
C–3	LOX vaporizer	92	.23
C–4	Oxygen heater	92	.23
D–1	Reactor (including insulation)	1150	14.20
J–1	Methanol feed pump	200	.94
J–2	Water feed pump	200	.94
J–3	LOX pump	400	16.00
J–4	Recycle gas circulator	150	3.20
L	Purification Unit	1650	34.40
	Catalyst in reactor	312	
	Instrumentation	1800	[a] 24.00
	Piping, valves, fittings, etc.	800	
Total		8363	105.00

A short comparison of the designs was prepared by the General Electric Co. (E–1). No volumes or weights of generator and purification systems were quoted, although it was pointed out that the high power density of the Kellogg unit was dependent on a 1-to-1 steam-carbon ratio in re-forming, which might not be obtainable in practice. It was concluded that the systems were feasible within the volume specifications required, but that many development problems would have to be overcome.

The Engelhard Industries is developing a portable generator using NH_3 or hydrocarbons and Pd-Ag diffusers (*208* and *209*). The specifications were 0.25 pound H_2/12 hours (approximately 4 S cu ft/hr and 200 watts) with weight less than 15 pounds and volume less than 2 cubic feet. Units of 17 pounds weight operative at 70 percent efficiency with NH_3 were delivered (207). These were self-contained and came up to full capacity in 30 minutes. Units are being developed for steam re-forming of JP4. The principle is shown in figure E.1; larger units are being constructed with the specifications given in table E.2. Auxiliary power consumption is 775 watts for pumps, blowers, solenoids, etc.

TABLE E.2.—*Engelhard* Hydrogen *Generator Specifications* (*209*)

(1) Fuel	JP-4 (< 50 ppm S)
(2) H_2O/C	3/1
(3) H_2 produced	160 S cu ft/hr
(4) Fuel consumption	3.36 lb/140 S cu ft/hr of H_2 after startup
(5) H_2O consumption	13.0 lb/140 S cu ft/hr of H_2 after startup
(6) Startup time	About 30 min
(7) Response time	4–8 min
(8) Heat losses	3800 Btu/hr
(9) Re-form temperature	1500" F
(10) Flue gas temperature	600° F
(11) H_2 delivery temperature	160° F
(12) Weight of unit	615 lb
(13) Volume of unit	18 ft^3
(14) H_2 pressure	3 psig and 60 psig

$$(15)\ \frac{\text{GHV of } H_2 \text{ produced at full rate}}{\text{GHV of JP-4 consumed at full rate}} = 0.67$$

(GHV=gross heating value)

Net power, assuming a fuel-cell efficiency of 60 percent, would be approximately 8 kW, and power density of the generator is, therefore, approximately 75 lb/kW or 13 watts/lb.

Texas Instruments has developed a partial oxidation unit specifically for providing hot, impure H_2 for high-temperature cells from liquid hydrocarbons *(608,* 609). Pressurized fuel is sprayed through a jet and partially burnt with preheated air in a tube, and the products mixed with steam to prevent carbon deposition. The gases pass through a catalytic shift converter to produce more H_2. Efficiencies of 60 to 70 percent were obtained in a crude prototype producing about 10 S cu ft/hr. It is planned to integrate this re-former with the fuel-cell system to reduce heat losses.

Liquid-phase re-forming of liquid hydrocarbons was proposed by Allis-Chalmers as a means of reducing re-former volume *(58).* Production of hydrogen from n-octane and electrolyte, heated up to 300° C in the presence of noble-metal catalysts, was negligible or very slow. Electroforming was investigated; in theory, reaction of fuel at an electrode would enable H_2 to be evolved at the other electrode with only a small expenditure of energy. Of course, if hydrocarbon electrode reactions were fast, they could be used directly in a fuel cell and it is not surprising that hydrogen was evolved only at potentials near those of water electrolysis.

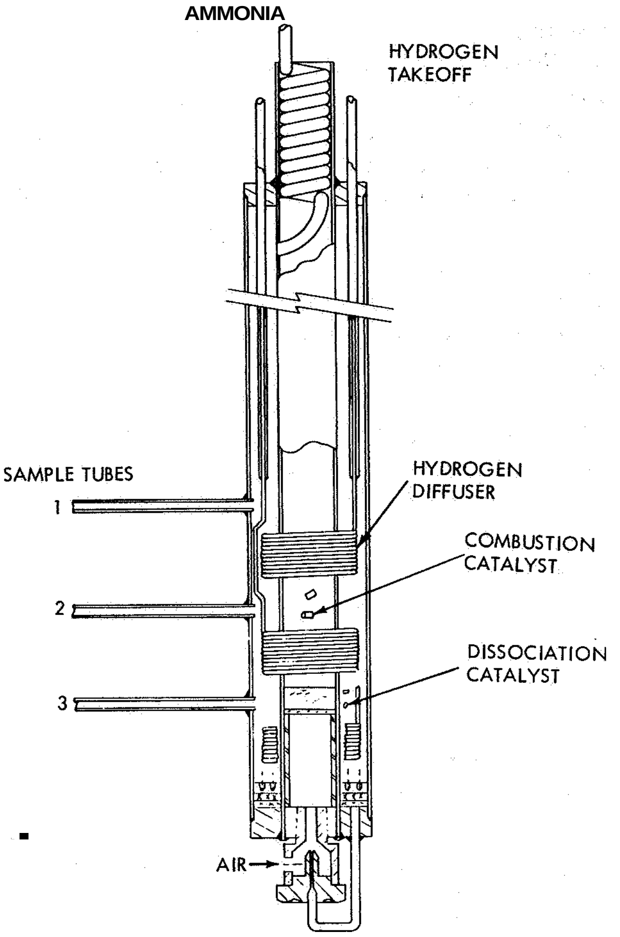

Ammonia is preheated in the top coil and passed to the annulus, which is packed with decomposition catalyst. It flows down the annulus, decomposes to N_2 and H_2 at a pressure of 35 psig, and hydrogen diffuses into the coils of Pd-Ag tubes shown (75 percent Pd–25 percent Ag will diffuse H_2 but no other gas). These coils are of 1/16-inch diameter with a wall thickness of 3 mils and a total diffusion area of 32 square inches. Hydrogen inside the coils is removed for fuel cell use; N_2 plus undiffused H_2 in the annulus passes to the burner jet and is catalytically burnt with air to provide the reactor heat. Catalysts are proprietary, noble-metal catalysts.

FIGURE E.1.—Engelhard generator (*206*).

Brief reviews of hydrogen generation and storage *(332)* and oxygen generation and storage *(330)* were prepared at Harry Diamond Laboratories. Packaged hydrogen generators were rated at 36 W/lb inclusive of fuel and water.

A detailed and valuable discussion of the prospects of fuel cell-re-former units for vehicle propulsion has been given in reports by California Research Corp. ***(137*** and ***144).*** A computer program was given which could optimize an integrated system. It was concluded that a high-temperature fuel cell integrated with a liquid hydrocarbon re-former would be capable of 50 percent overall efficiency, taking a net fuel-cell efficiency of 60 percent. The power density would be half of present engine-power densities, even if the fuel cell had no volume. A re-former used with a low-temperature fuel cell could give an overall efficiency of about 40 percent, since heat for re-forming could not be used in the fuel cell. Power densities were about one-fifth of engine power densities for no fuel-cell volume, due to the bulky re-former furnace. Purification of hydrogen would reduce efficiency and power density even further. These estimates were based on current practice, but optimistic conditions were generally used, and they should probably be considered as the limit of current practice.

Studies of cryogenic oxygen or hydrogen storage are outside the scope of this book, since the technology has been developed for other purposes and is borrowed for fuel-cell applications. Application of cryogenic techniques, and others, to storage of H_2 and O_2 were discussed in a report which is frequently quoted (Beechcraft Research & Development, Inc., ***129).*** It was concluded that cryogenic storage could give storage densities of up to 4000 W-hr/lb for H_2 and 1000 W-hr/lb for oxygen. Cryogenic techniques for H_2 are much more difficult to develop than for O_2 because of the low boiling point of H_2; cryogenic technology for O_2 is well advanced.

REFERENCES

E–1. Hensel, S. L.: Hydrogen Generation for JP–5, Methanol and Ammonia. G.E. Technical Information Service Rept. 63DE17, General Electric, West Lynn, Mass., Sept. 12, 1963.

Also, the Society of Automotive Engineers has complete copies of the four papers presented Oct. 19–23, 1965, on "Gas Generation for Fuel Cells." The symposium was part of the National Transportation, Powerplant and Fuels and Lubricants Meeting, Baltimore. Order by paper number:

9354 Meek, J.; Baker, B. S.; Eckert, C. H.; and Todesca, F.: Hydrogen from Liquid Hydrocarbons for Fuel Cells. Institute of Gas Technology, Chicago 16, Ill.

935B Pfefferle, W. C.: Ultra-Pure Hydrogen for Fuel Cells. Engelhard Industries, Newark, N.J.

935C Rothfleisch, J. E.: Hydrogen From Methanol for Fuel Cells. Development Dept., Union Carbide Corp., Cleveland, Ohio.

9350 Allen, Duane: Low Temperature Formation of Hydrogen from $CO+H_2O$. Chemetron Corp., Louisville, Ky.

APPENDIX F

List of Contract Reports

[All sources for fuel-cell information were covered, including Power Information Center, Defense Documentation Center, and NASA Scientific and Technical Information Division]

[* = Multiple authorship involved. ** = Information not available. Dates given refer to dates of reports issued by contractor. *** = Subcontracted from North American Aviation, Downey, Calif.]

Report reference No. in fuel-cell compendium	Report	Contractor	Contract scope	Contract No. and dates
1..	1st Quarterly Rept. (7/1/61–9/30/61) "Investigation of an Energy Conversion Device," Fogle, R. F.* (All reports are titled the same)	Aerojet-General Corp., Azusa, Calif.	Study of energy conversion devices	DA-36-039-SC-87229, USAERDL/NJ 7/61–9/62
2..........	2d Quarterly Rept. (10/1/61–12/31/61) *AD* 278480			
3..........	3d Quarterly Rept. (1/1/62–3/31/62) *AD* 278426			
4..........	Final Rept. (No. 4) (7/1/61–6/30/62) *AD* 285667			
5..	Rept. No. 575, Annual (11/15/50–11/14/51) *AD* 209055, "Research on Electrochemical Fuel Cells," Davis, E. P. (All reports are titled the same)		Research on electrochemical cells	NOnr-46207, ONR/DC 1/53–1/57
6..........	Rept. No. 665, Annual (11/15/51–11/14/52) *ATI* 205535, Davis, E. P.			
7..........	Final Rept. No. 1233 (11/51–8/56) *AD* 133949, Cramer, M. J.			
8..........	Interim Rept. No. 2807–24 (2/1/56–3/31/56) *AD* 99998, Cramer, M.J.			
9..........	Semiannual Tech. Rept. (7/1/61–12/31/61) *AD* 276281, "Energy Conversion Research Program," Hess, F. D.*	Aerospace Corp., El Segundo, Calif.	Energy conversion research program	AFO4(647)–930, USAF-DCAS 61–62**
10..	Rept. No. TDR–930(2240–55) TN–1 (5/17/62) *AD* 282283, "Equivalent Circuits and Efficiencies of Fuel Cells," Slaughter, J. I.			
11..	Rept. No. TDR–930(2240–55) TN–2 (5/17/62) *AD* 408917, "Economic Limits of a Fuel Cell Technology," Slaughter, J. I.			
12..	Rept. No. TDR–930(2701–01) TN–1, Part 1, No. 4 (10/61) *AD* 278130, "Applied Research Management Abstract Bulletin" (All reports are titled the same)			
13..........	Rept. No. TDR–930(2701–01) TN–1, Part 1, No. 5 (11/61) *AD* 273677			
14..........	Rept. No. TDR–930(2701–01) TN–1, Part 1, No. 6 (12/61) *AD* 273678			
15..........	Rept. No. TDR–930(2701–01) TN–1, Part 1, No. 7 (1/62) *AD* 273679			
16.	Rept. No. TDR–69(2220–30) TN–1 (6/18/62) *AD* 282902, "Chronopotentiometric Measurements of Electrode Kinetics for Chlorides of W, Sb, P and Group IV A," Mayer, S. W.*		Energy conversion research program	AFO4(695)–69, USAF/DCAS 62**
17.	Semiannual Tech. Rept. TDR–69(2220–30) TR–2 (1/1/62–6/30/62) *AD* 285084, "Energy Conversion Research Program," Hess, F. D.*			

List of Contract Reports (Cont.)

Report reference No. in fuel-cell compendium	Report			Contract No. and dates
18	Semiannual Tech. Rept. (1/1/61–6/30/61) *AD* 266441, "Fuel Cell Research Program—Chlorine-PCl_3 Fuel Cell Investigations," Hess, F. D.*		Fuel-cell research program Cl_2-PCl_3 fuel-cell investigations	AFO4(647)–594, USAF/DCAS 6/61**
19	Final Rept. (8/61), "Fuel Cell Electrode Processes," Young, G. J.*	Alfred University, College of Ceramics, Alfred, N.Y.	Electrode catalysts in fuel-cell operation	NOnr1503(03), ONR/DC 7/58–6/61
20.	Quarterly Tech. Prog. Rept. No. 1 (3/15/62) *AD* 274614, "H_2-O_2 Electrode Study in Hydrox Fuel Cells," Gray, T. J.		H_2-O_2 fuel-cell study	AF33(657)–7564, USAF/WP 12/61–6/64
21.	"Fuel Cell Bibliography" (6/15/62) *AD* 277350			
22.	Qtr. Tech. Prog. Rept. No. 2 (6/15/62) *AD* 288952 (All reports are titled the same)			
23.	Qtr. Tech. Prog. Rept. No. 3 (9/15/62) *AD* 284522			
24.	Qtr. Tech. Prog. Rept. No. 4 (12/15/62)			
25.	Qtr. Tech. Prog. Rept. No. 5 (3/15/63)			
26.	Qtr. Tech. Prog. Rept. No. 6 (6/15/63) *AD* 414696			
27.	Qtr. Tech. Prog. Rept. No. 7 (9/15/63) *AD* 417359			
28.	Qtr. Tech. Prog. Rept. No. 8 (12/15/63)			
29.	Qtr. Tech. Prog. Rept. No. 9 (3/15/64) *AD* 432973			
30.	Tech. Doc. Rept. No. APL TDR 64–88			
31.	Tech. Rept. No. 1 (11/59) *AD* 232641, "1. Catalysis and Chemisorption," Young, G. J.*		Fuel-cell electrode processes	NOnr 65619, ONR/DC 11/59**
32.	Semiannual Status Rept. No. 1 (6/63–12/63), "Fuel Cell Research," Gray, T. J.*		Investigation of fuel-cell performance	NsG–384, NSAS/Lewis 6/63—Act.
33.	2d Semiannual Rept. (12/63–5/64) (Title same as above)			
34.	3d Semiannual Rept. (6/1/64–12/31/64), "Fuel Cell Research—An Investigation of Non-Steady-State Operation," Gray, T. J.*			
35	Phase I Rept. (12/11/61–6/30/62) *AD* 282294, "Engineering Research Study of Fuel Cell Power Pack" (All reports are titled the same)	Allis-Chalmers Manufacturing Co., Milwaukee 1, Wis.	Operational characteristics of a fuel-cell power pack	DA–49–186–502–ORD–1057, HDL 12/61–8/64
36	Phase II Rept. (7/1/62–1/31/63) *AD* 401163			

37.	1st Quart. Rept. (5/14/62–9/30/62), "R&D of an Open Cycle Fuel Cell System" (All reports are titled the same)	Open-cycle fuel-cell system	NAS8-2696, NASA/Marshall 5/62—Act.
38.	2d Quart. Rept. (10/1/62–12/31/62)		
39.	3d Quart. Rept. (1/1/63–3/31/63)		
40.	4th Quart. Rept. (4/1/63–6/30/63)		
41.	5th Quart. Rept. (7/1/63–9/30/63)		
42.	6th Quart. Rept. (10/1/63–12/31/63)		
43.	7th Quart. Rept. (1/1/64–3/31/64)		
44.	8th Quart. Rept. (4/1/64–6/30/64)		
45.	Summary Report (1/1/64–8/31/64)		
46.	1st Quart. Prog. Rept. (10/30/64), "R&D on Fuel Cell Systems," Hess, P. D.*		
47.	1st Quart. Rept., Revised (1/20/65) (Title same as above)		
48.	3d Quart. Rept. (1/1/65–3/31/65)		
49.	1st Quart. Tech. Prog. Rept. (8/15/62) *AD* 282178, "Design of 400 Watt H_2-O_2 Capillary Type Fuel Cell" (All reports are titled the same)	Capillary fuel cells	AF33(657)–8970, USAF/WP 3/62–3/64
50.	2d Quart. Tech. Prog. Rept. (11/15/62) *AD* 288645		
51.	3d Quart. Tech. Prog. Rept. (2/15/63)		
52.	4th Quart. Tech. Prog. Rept. (5/15/63) *AD* 404661		
53.	5th Quart. Tech. Prog. Rept. (8/15/63) *AD* 413916		
54.	6th Quart. Tech. Prog. Rept. (8/1/63–10/31/63) *AD* 423722		
55.	Final Rept. No. APL–TDR–64–54 *AD* 600658		
56.	4th Quart. Tech. Prog. Rept. (8/1/64–10/31/64) *AD* 608239, "Design of H_2-O_2 Capillary Type Fuel Cell"	Design of H_2-O_2 fuel cells	AF33(615)–1185, USAF/WP 11/63–1/65
57.	Final Rept. (11/1/63–1/31/65) *AD* 610722 (Title same as above)		
58.	Final Technical Rept. (6/64), "Liquid Phase Reforming of Liquid Hydrocarbons"	Liquid phase re-forming of hydrocarbons to produce H_2 for fuel cells	DA–44–009–AMC–180T, USAERDL/Va. 6/63–7/64
59.	1st Quart. Rept. (5/1/63–7/31/63), "Study of Energy Conversion Systems," Marshall, G. C.	Study of energy conversion systems	NAS8–5392, NASA/Marshall 6/63—Act.
60.	Summary Rept. (5/8/63–6/15/64) (Title same as above)		
61.	1st Quart. Prog. Rept. (11/15/64), "R&D of Open Cycle Fuel Cells"		
62.	Semiannual Tech. Rept. (6/11/63–2/1/64), "5-KW Hydrocarbon-Air Fuel Cell System," Cade, G.*	5-KVA re-former—fuel-cell power	DA–44–009–AMC–240(T),

List of Contract Reports (Cont.)

Report reference No. in fuel-cell compendium	Re	Contractor	Contract scope	Contract No. and dates
				USAERDL/Va. 6/63—Act.
63.	Semiannual Tech. Sum. Rept. (2/1/64–6/11/64) *AD* 451438 (Title same as above)			
64.	Tech. Sum. Rept. (6/11/63–3/15/65) *AD* 614717, "5 KVA Hydrocarbon-Air Fuel Cell System," Engle, M. L.			
65.	1st Quart. Rept. (1/1/62–3/31/62) *AD* 274197, "Design and Development of a Liquid Metal Cell," Agruss, B. (All reports are titled the same)	Allison Division, General Motors Corp., 4700 West 10th St., Indianapolis 6, Ind.	uid metal hermally reg tive fuel cell	AF33(657)–7847, USAF/WP 12/61–3/64
66.	2d Quart. Prog. Rept. (7/13/62) *AD* 277707			
67.	3d Quart. Prog. Rept. (10/12/62) *AD* 285948			
68.	Final Rept. No. ASD–TDR–62–1045 (12/62) *AD* 296861			
69.	1st Quart. Tech. Prog. Rept. (12/12/62–3/12/63), "Development and Testing of Electrolyte Matrix Combinations for Hg-K Fuel Cell" (All reports titled the same)		ectrolyte matrix combinations for Hg-K fuel cell	NaSw–476, NASA/Lewis 12/62–11/63
70	3d Monthly Prog. Rept. (2/12/63–3/12/63)			
71	4th Monthly Prog. Rept. (3/12/63–4/12/63)			
72	5th Monthly Prog. Rept. (4/2/63–5/12/63)			
73	6th Monthly Prog. Rept. (6/26/63)			
74	2d Quart. Tech. Prog. Rept. (3/13/63–6/12/63)			
75	7th Monthly Prog. Rept. (6/12/63–7/12/63)			
76	8th Monthly Prog. Rept. (7/12/63–8/12/63)			
77	9th Monthly Prog. Rept. (8/12/63–9/12/63)			
78	3d Quart. Tech. Prog. Rept. (6/12/63–9/12/63)			
79	10th Monthly Prog. Rept. (9/12/63–10/12/63)			
80	11th Monthly Prog. Rept. (10/12/63–11/12/63)			
81	Final Rept. (1/64)			
82	1st Quart. Prog. Rept. (5/28/63) *AD* 405481, "Research and Development of an Advanced Laboratory Liquid Metal Regenerative Fuel Cell," Karas, H. R.*		esearch and development regenerative cell	AF33(657)–11032, USAF/WP 3/63–12/63**
83.	2d Quart. Prog. Rept. (9/9/63) *AD* 418027 (Title same as above)			
84.	3d Quart. Prog. Rept. (9/1/63–11/30/63) *AD* 425422, "Research and Development of an Advanced Laboratory Liquid Metal Regenerative Fuel Cell," Mangus, J. D.			
85	Final Rept. No. APL–TDR–64–41 (4/64)			

	(Title same as above)			
86.	1st Quart. Rept. (11/1/63–1/31/64), "Research and Development of High Performance Light-Weight Fuel Cell Electrodes," Barber, W. A.*	American Cyanamid Co., Central Research Division, 1937 West Main St., Stamford, Conn.	High-performance lightweight electrode system for H_2-O_2 fuel cells	NAS3–2786, NASA/Lewis 10/63—Act.
87.	2d Quart. Rept. (2/1/64–4/30/64) (Title same as above)			
88.	3d Quart. Rept. (5/1/64–7/31/64), "Research and Development of High Performance Light-Weight Fuel Cell Electrodes," Haldeman, R. G.			
89.	"Generation of H_2 for Fuel Cells in Submarine Propulsion," (Oct. 1962) *AD* 292246		Generation of H_2 for fuel cells in submarine propulsion	NObs–86745, USN/BuShips 10/62**
90.	1st Quart. Rept. (9/13/61–12/13/61) *AD* 458303, "Basic Study of Sorption of Organic Fuels During Oxidation at Electrodes," Flannery, R. J.* (All reports are titled the same)	American Oil Co., 910 South Michigan Ave., Argonne, Ill.	Physicochemical study of electrode fuel reactions	DA–11–022–ORD–4023, ARO/Durham 9/61–11/64
91.	2d Quart. Rept. (12/11/61–3/10/62) *AD* 458304			
92.	3d Quart. Rept. (3/11/62–6/10/62) *AD* 458305			
93.	4th Quart. Rept. (6/11/62–9/24/62)			
94.	5th Quart. Rept. (9/25/62–12/31/62)			
95.	6th Quart. Rept. (1/1/63–3/31/63) *AD* 402821			
96.	7th Quart. Rept. (4/1/63–6/30/63)			
97.	8th Quart. Rept. (7/1/63–9/30/63)			
98.	9th Quart. Rept. (8/1/63–12/31/63)			
99.	10th Quart. Rept. (1/1/64–3/31/64)			
100.	11th Quart. Rept. (4/1/64–6/30/64)			
101.	Final Rept. (9/13/61–10/21/64) *AD* 454676			
102.	C.E. Div. Summary Rept. No. ANL–6379 (4/61–6/61)	Argonne National Laboratory, 9700 South Cass Ave., Argonne, Ill., 60440	Thermally regenerative fuel cells	W–31–109–ENG–38, USAEC 4/62–4/64**
103.	C.E. Div. Summary Rept. No. ANL–6413 (7/61–9/61)			
104.	C.E. Div. Summary Rept. No. ANL–6477 (10/61–12/61)			
105.	C.E. Div. Summary Rept. No. ANL–6543 (1/62–3/62)			
106.	Special Report for C.E. Div. Review Committee (5/1/62)			
107.	C.E. Div. Summary Rept. No. ANL–6569 (4/62–6/62)			
108.	C.E. Div. Summary Rept. No. ANL–6596 (7/62–9/62)			
109.	C.E. Div. Summary Rept. No. ANL–6648 (8/62–12/62)			
110.	C.E. Div. Summary Rept. No. ANL–6687 (1/63–3/63)			
111.	C.E. Div. Research Highlights No. ANL–6766 (5/62–4/63)			
112.	C.E. Div. Summary Rept. No. ANL–6725 (4/63–6/63)			
113.	C.E. Div. Semiannual Rept. No. ANL–6800 (7/63–12/63)			
114.	C.E. Div. Research Highlights No. ANL–6875 (5/63–4/64)			

List of Contract Reports (Cont.)

Report reference No. in fuel-cell compendium	Report	Contractor		
115	Semiannual Progress Rept. (9/18/61–3/18/62) *AD* 276601, "Fuel Cell Cathode Structures and Reactions," Recht, H. L.*	Astropower, Inc., 2968 Randolph Ave., Costa Mesa, Calif.	Metallic O_2 electrodes	DA–49–186–ORD–1036 HDL 9/61–9/62
116	Final Rept. (9/62) *AD* 286698 (Title same as above)			
117	Quart. Prog. Rept. 108–Q1 (9/18/62), "Investigation of Zeolite Membrane Electrolytes for Fuel Cells," Kelmers, A. D.		Investigation of zeolite membranes for fuel cells	NAS–7–150, NASA/Lewis 6/62—Act.
118	Quart. Prog. Rept. 108–Q2 (12/18/62) (Title same as above), Levy-Pascal, A. E.			
119	Quart. Prog. Rept. 108–Q3 (3/18/63) (Title same as above), Levy-Pascal, A. E.			
120	Monthly Prog. Rept. 108–M3 (9/7/63) (Title same as above), Kelmers, A. D.			
121	Final Rept. 108F (3/64) (Title same as above), Berger, C.			
122	Tech. Summ. Rept. No. A1–7082 (9/7/61–12/31/61), "Infrared Reflectance Study of Gas-Solid Interaction," Hansen, W. N. (All reports are titled the same)	Atomics International, Division of North American, P.O. Box 309, Canoga Park, Calif.	An infrared study of hydrocarbon electrodes	DA–44–009–ENG–4835, USAERDL Va. 9/61–11/63
123	Final Summ. Rept. (10/62)			
124	Tech. Rept. No. AMRL–TDR–62–94 (8/62) *AD* 289024, "Research on the Electrolysis of H_2O With a H_2-Diffusion Cathode To Be Used in a Rotating Cell," Clifford, J.*	Battelle Memorial Institute, Columbus, Ohio	Equipment for life support in aerospace	AF33(616)–8431, USAF/WP 6/61–5/62
125	Tech, Doc. Rept. No. MRL–TDR–62–44, "Research on the Electrolysis of H_2O Under Weightless Conditions," Clifford, J.*		Equipment for life support in aerospace	AF33(616)–7351, USAF/WP 6/60–11/61**
126	Tech. Doc. Rept. No. AMRL–TDR–63–95 (10/63) *AD* 423680, "Research on Solid P_2O_5 Electrolytes in Electrolysis Cell for Production of Breathing O_2," Beach, J. G.*		Equipment for life support in aerospace	AF33(657)–9355, USAF/WP 6/62–6/63**
127	Scientific Rept. No. 2 (8/62) *AD* 286472, "The Mechanism of Oxidation of Low Molecular Weight Organic Compounds at Pt Electrodes in Aqueous Solutions," Franklin, T. C.*	Baylor University, Waco, Tex.	The mechanism of oxidation of low molecular weight organic compounds	AF19(604)–8414, USAF/Mass. 8/62**
128	Scientific Rept. No. 3 (4/63) *AD* 410477, "Catalytic Processes on			

	Platinized Pt Electrodes," Franklin, T. C.		at platinum electrodes in aqueous solutions	
129	WADC Tech. Rept. 58–542, Final (10/58) *AD* 203521, "H_2-O_2 Fuel Electrolytic Battery Container Study," DeHaan, J. R.*	Beechcraft Research & Developments, Inc., Boulder, Colo.	H_2-O_2 fuel electrolytic battery container study	AF33(616)–5833, USAF/WP 10/58**
130	Quart. Rept. No. 1 (7/25/60), "Investigative Study Relating to Fuel Cells" (All reports are titled the same)	California Research Corp., 200 Bush St., San Francisco 20, Calif.	Hydrocarbon fuel-cell research	DA–49–186–502–ORD–929, HDL 4/60–8/64
131	Quart. Rept. No. 2 (7/25/60–10/25/60) *AD* 249123			
132	Quart. Rept. No. 3 (10/26/60–1/25/61) *AD* 254312			
133	Quart. Rept. No. 4 (1/26/61–4/25/61)			
134	Prog. Rept. No. 5 (4/26/61–8/25/61) *AD* 267073			
135	Prog. Rept. No. 6 (8/26/61–12/31/61) *AD* 273427			
136	Prog. Rept. No. 7 (1/1/62–4/30/62) *AD* 277063			
137	Prog. Rept. No. 8 (5/1/62–8/31/62) *AD* 291173			
138	Prog. Rept. No. 9 (9/1/62–12/31/62) *AD* 400917			
139	Prog. Rept. No. 10 (1/1/63–4/30/63) *AD* 416370			
140	Prog. Rept. No. 11 (5/1/63–8/31/63)			
141	Special Rept. No. 1 (9/6/63), "Appraisal of State of Development of Low Temperature Hydrocarbon-Oxygen (Air) Fuel Cells," Schlatter, M. J.*			
142	Prog. Rept. No. 12 (9/1/63–12/31/63), "Investigative Study Relating to Fuel Cells"			
143	Special Rept. No. 3 (12/27/63), "History of Fuel Cell Contract Work at Cal. Research Corp.," Macdonald, R. T.*			
144	Prog. Rept. No. 13 (1/1/64–6/30/64) *AD* 450963, "Investigative Study Relating to Fuel Cells"			
145	Special Rept. No. 2, Part 1 of 2 parts (2/1/65), "An Evaluation of Fuel Cell Systems for Military Vehicle Propulsion and Portable Electric Power Generation," Schlatter, M. J.			
146	Special Rept. No. 2, Part 2 of 2 parts (2/1/65) (Title same as above)			
147	Final Rept. (1/1/59–12/31/59), "High Temperature Galvanic Fuel Cells," Broers, G. H. J.*	Central Technical Institute, TNO, 5 Konigskade, The Hague, Netherlands, P.O. Box 614	High-temperature galvanic fuel cells	DA–91–591–EUC–1023, USDA/ERO 1/59–12/59**
148	Final Rept. (11/1/60–1/31/61) *AD* 256337, "High Temperature Galvanic Fuel Cells," Schenke, M.*		High-temperature galvanic fuel cells	DA–91–591–EUC–1398, USDA/ERO 11/60–1/61**

List of Contract Reports (Cont.)

Report reference No. in fuel-cell compendium	Report	Contractor	Contract scope	Contract No. and dates
149.	1st Quart. Rept. (2/1/61–4/30/61), "High Temperature Galvanic Fuel Cells," Schenke, M.* (All reports are titled the same)		High-temperature galvanic fuel cells	DA–91–591–EUC–1701, USDA/ERO 2/61–1/62**
150.	2d Quart. Rept. (5/1/61–7/31/61)			
151.	Final Rept. (11/1/61–1/31/62)			
152.	Rept. No. CWR 700–23, Final Report on Fuel Cells	Curtiss-Wright Corp., Quehanna, Pa.	High-temperature fuel cells	DA–44–009–ENG–3457
			High-temperature fuel cells	DA–44–009–ENG–3957 6/59–6/60
153.	"Power Generation" (6/63) *AD* 405957	Defense Documentation Center, Arlington Hall Station, Arlington 12, Va.	Power generation	DDC 6/63**
154.	Final Rept. (3/30/63) *AD* 403290, "Feasibility Studies of the Electrothermally Regenerative Transducer," Weaver, R. D.	Delco-Remy Division, General Motors Corp., Electrochemical Research Department, Anderson, Ind.	The electrothermally regenerative transducer	DA–33–008–ORD–2335(T), HQ/USATAC 5/62–2/65
155.	Final Rept. Part II (6/30/64) *AD* 607293 (Title same as above)			
156.	1st Quart. Rept. (7/1/63–10/1/63) *AD* 428052, "Direct NH_3-Air Fuel Cell," Kuppinger, R. E. (All reports are titled the same)	Electrochimica Corp., Research and Development Laboratory, Menlo Park, Calif.	Direct NH_3-air fuel cell	DA–36–039–AMC–03245(E), USAERDL/NJ 7/63—Act.
157.	Rept. No. 2 (10/1/63–1/1/64) *AD* 601268			
158.	3d Quart. Rept. (1/1/64–4/1/64) *AD* 445865			
159.	Final Rept. (7/1/63–8/31/64) *AD* 454420			
160.	Interim Eng. Rept. 1584–IR–1 (9/21/60–3/3/61), "Evaluation of Regenerative Fuel Cell," Ludwig, F. A. (All reports are titled the same)	Electro-Optical Systems, Inc., 125 North Vinedo Ave., Pasadena, Calif.	Evaluation of electrolytically regenerative H_2-O_2 fuel cell	NAS7–7, NASA/DC 9/60–8/62
161.	Monthly Prog. Rept. for Apr. 1961, No. 1584–M–1 (5/19/61), Frank, H. A.			
162.	Monthly Prog. Rept. for May 1961, No. 1584–M–2 (6/23/61)			
163.	Monthly Prog. Rept. for July 1961, No. 1584–M–4 (8/18/61)			

164	Interim Report No. 1584–IR–2 (3/8/61–9/8/61)			
165	Monthly Prog. Rept. for Dec. 1961, No. 1584–M–9 (1/20/62)			
166	Monthly Prog. Rept. for Jan. 1962, No. 1584–M–10 (2/20/62)			
167	Final Rept. No. 1584—Final (9/21/60–3/9/62)			
168	Addendum Rept. No. 1584—Addendum (5/2/62)			
169	ARL Tech. Note 60–135 (8/60) *AD* 247197, "Research on Chemical Reactions Capable of Converting Solar Energy Into Forms Which Can Be Used as Power Sources," Rowlette, J. J.		Chemical reactions capable of converting solar energy into forms for use as power sources	AF33(616)–6546, USAF/WP 4/60–4/61
170	Rept. No. ARL 60 (5/15/59–4/1/61) *AD* 269508, "Chemical Reactions to Convert Solar Energy Into Power Sources," Rowlette, J. J.			
171	Final Rept. No. ASD–TDR–62–89 (6/62) *AD* 282849, "Energy Conversion Study of Semiconductor Electrodes," Tannenbaum, I. R.		Semiconductor electrodes for fuel cells	AF36(616)–7939, USAF/WP 1/61–5/62
172	First Semiannual Rept. (3/15/61–6/30/61), "Investigation of New Solar Regenerative Fuel Cell Systems," Rowlette, J. J. (All reports are titled the same)		Study of fuel-cell systems	DA–36–039–SC–87425, USAERDL/NJ 3/61–3/62
173	2d Semiannual Rept. (7/1/61–12/31/61)			
174	Final Rept. No. 1720 (3/15/61–3/14/62) *AD* 275646			
175	Interim Tech. Rept. No. 3310–Q–1 (6/25/62–9/25/62), "Evaluation of Regenerative Fuel Cell," Rowlette, J. J. (All reports are titled the same)		Regenerative fuel cell	NAS7–181, NASA/Lewis 6/62–7/63
17.	Prog. Rept. No. 3310–ML–1 (8/14/62)			
17.	Prog. Rept. No. 3310–ML–2 (9/7/62)			
17.	Prog. Rept. for Nov. 1962			
17.	Prog. Rept. No. 3310–ML–3 (10/62)			
18.	Interim Tech. Rept. No. 3310–Q–2 (9/25/62–12/25/62)			
18.	Prog. Rept. for Jan. 1963			
18.	Final Rept. No. 3310—Final (6/25/62–2/25/63)			
183	1st Quart. Rept. (4/10/62–7/10/62), "Fuel Cell Assemblies," Frank, H. (All reports are titled the same)		Fuel-cell assemblies	NAS7–100, JPL 4/62–10/63
184	2d Quart. Rept. (7/10/62–10/10/62)			
185	Final Rept. No. 3070—Final (1/63–3/63)			
186	EOS Rept. 4110–QL–1 (10/18/63), "H_2-O_2 Electrolytic Regenerative Fuel Cells," Rowlette, J. J.		H_2-O_2 electrolytic regenerative fuel cells	NAS3–2781, NASA/Lewis 7/63—Act.
187	EOS Rept. 4110–QL–2 (1/18/64), "Hydrogen-O_2 Electrolytic Regenerative Fuel Cells," Frank, H.			
188	EOS Rept. 4110–QL–3 (4/15/64), "H_2-O_2 Electrolytic Regenerative Fuel Cells," Klein, M.			

List of Contract Reports (Cont.)

Report reference No. in fuel-cell compendium	Report	Contractor	Contract scope	Contract No. and dates
189	1st Semiannual Tech. Sum. Rept. (11/30/59–11/30/60) *AD* 233236, "Investigation of New Solar Regenerative Fuel Cell Systems," Ludwig, F. (All reports are titled the same)		Solar regenerative fuel-cell systems	DA-36-039-SC-85270, USAERDL/NJ 11/59–11/60
190	2d Semiannual Tech. Sum. Rept. (1/1/60–6/30/60) *AD* 255462			
191	Final Rept. (11/30/59–11/30/60) *AD* 255463			
192	WADD Tech. Rept. 60-699, Vol. VI (9/60) *AD* 257358, "Energy Conversion Systems Reference Handbook—Vol. VI," Menetrey, W. R.		Energy conversion reference handbook	AF33(616)-6791, USAF/WP 9/60**
193	1st Quart. Rept. (7/1/60–9/30/60) *AD* 254010, "Fuel Cell Catalysts," Hauel, A. P. (All reports are titled the same)	Engelhard Industries, Inc., Newark, N.J.	Fuel-cell catalysts	DA-36-039-SC-85043, USAERDL/NJ 6/60–6/62
194	2d Quart. Rept. (10/1/60–12/31/60) *AD* 254011			
195	3d Quart. Rept. (1/1/61–3/31/61)			
196	4th Quart. Rept. (4/1/61–6/30/61)			
197	5th Quart. Rept. (7/1/61–9/30/61) *AD* 269217			
198	6th Quart. Rept. (10/1/61–12/31/61) *AD* 275645, "Fuel Cell Catalysts," Adlhart, O. J.			
199	7th Quart. Rept. (1/1/62–3/31/62) *AD* 276109			
200	Final Rept. (No. 8) (7/1/60–6/30/62) *AD* 284167			
201	1st Quart. Rept. (5/1/62–7/31/62), "H_2 Generation for Fuel Cells," Emerson, E. J.* (All reports are titled the same)		H_2 generation for fuel cells	DA-36-039-SC-89077, USAERDL/NJ 4/62—Act.
202	2d Quart. Rept. (8/1/62–10/31/62)			
203	3d Quart. Rept. (11/1/62–1/31/63) *AD* 404582			
204	4th Quart. Rept. (2/1/63–4/30/63) *AD* 414542			
205	5th Quart. Rept. (5/1/63–7/31/63) *AD* 424671			
206	6th Quart. Rept. (8/1/63–10/31/63) *AD* 433276			
207	7th Quart. Rept. (11/1/63–1/31/64) *AD* 438850			
208	Final Rept. (5/1/62–9/30/64) *AD* 462470			
209	Semiannual Progress Rept. (6/21/63–1/21/64), "H_2 Generator Program," Kurpit, S. S.		H_2 generator for 5-kW fuel-cell power source	DA-44-009-AMC-242(T), USAERDL NJ 6/63—Act.

210.	1st Quart. Rept. (7/1/62–9/30/62) *AD* 292631, "Fuel Cell Catalysts," Adlhart, O. J. (All reports are titled the same)		Fuel-cell catalysts	DA-36-039-SC-90691, USAERDL/NJ 6/62–4/63
211.	2d Quart. Rept. (10/1/62–12/31/62) *AD* 403389			
212.	3d Quart. Rept. (1/1/63–3/31/63) *AD* 409751			
213.	Final Rept. No. 4 (7/1/62–6/30/63) *AD* 419912			
214.	1st Semiannual Rept. (1/1/62–6/30/62) *AD* 282297, "Soluble Carbonaceous Fuel-Air Fuel Cell," Heath, C. E.	Esso Research & Engineering Co., P.O. Box 172, Linden, N.J.	Soluble carbonaceous fuel-air fuel cell	DA-36-039-SC-89156, USAERDL/NJ 1/62–12/62
215.	Final Rept. (No. 2) (1/1/62–12/31/62) (Title same as above), Tarmy, B. L.			
216.	1st Semiannual Rept. (1/1/63–6/30/63) *AD* 418092 (Title same as above)		Soluble carbonaceous fuel-air fuel cell	DA-36-039-AMC-00134(E), USAERDL/NJ 1/63—Act.
217.	Final Rept. (No. 4) (1/1/63–12/31/63) *AD* 432865 (Title same as above)			
218.	Quart. Eng. Prog. Rept. (3/19/63–6/19/63), "Study of Basic Bio-Electrochemistry," Boyer, M. H.* (All reports are titled the same)	Ford-Aeronutronic, Ford Road, Newport Beach, Calif.	Fundamental bio-electrochemistry	NASw-655, NASA/Lewis 3/63–6/64 773
219.	Quart. Eng. Prog. Rept. No. U-2332 (6/20/63–9/19/63)			
220.	Quart. Eng. Prog. Rept. No. U-2479 (9/20/63–12/19/63)			
221.	Final Tech. Rept. (3/63–3/64), "Study of the Fundamental Principles of Bio-Electrochemistry," Bean, R. C.			
222.	Tech. Rept. No. ASD-TDR-62-162 (6/62) *AD* 283336, "SO_2-SO_3 Regenerative Fuel Cell Research," Kumm, E. L.	Garrett Corp., AiResearch Mfg. Co., 402 South 36th St., Phoenix, Ariz.	SO_2-SO_3 regenerative fuel cell	AF33(616)-7975, USAF/WP 3/61–4/62
223.	4th Quart. Rept. (4/1/62–6/30/62), "Gas-Solid Interactions at Electrode Surfaces," Saltsburg, H. (All reports are titled the same)	General Atomic Division of General Dynamics, P.O. Box 608, San Diego, Calif.	Gas-solid interactions at electrode surfaces	DA-44-009-ENG-4832, USAERDL/Va. 8/61–3/64
224.	Tech. Sum. Rept. (8/30/61–8/30/62)			
225.	5th Quart. Rept. (9/1/62–12/31/62)			
226.	Tech. Sum. Rept. (9/1/62–3/31/63) *AD* 403373			
227.	6th Quart. Rept. (4/1/63–6/30/63)			
228.	Tech. Sum. Rept. (4/1/63–9/30/63)			
229.	Rept. No. GA-4494, Reprint from J. Phys. & Chem. of Solids (10/17/63), "The Frequency-Dependent Electrical Conductivity of Powders: NiO," Snowden, D. P.*			
230.	7th Quart. Rept. (10/1/63–12/31/63)			
231.	Report No. GA-4969; Publ. in J. Phys. Chem. (2/12/64), "O_2 Adsorption on ZnO," Saltsburg, H.*			

List of Contract Reports (Cont.)

Report reference No. in fuel-cell compendium	Report	Contractor	Contract scope	Contract No. and dates
32	Report No. GA-4979; Publ. in J. Phys. Chem. (3/4/64), "Transient Ionic Species Resulting From Gas-Solid Interactions: O_2 Adsorption on NiO," Saltsburg, H.*			
233	Final Rept. (8/30/61–3/20/64)			
234	Final Rept.—Phase I (4/61–6/62) *AD* 291621, "HOPE Fuel Cell Program"	General Electric Co. (M.S.V.D.), P.O. Box 8555, Philadelphia 1, Pa.	H_2-O_2 primary extraterrestrial (HOPE) fuel cell	AF33(616)8159, USAF/WP 4/61–7/62
235	Final Rept.—Phase I, Appendices (4/61–6/62) (Title same as above)			
36	Quart. Prog. Rept. (5/1/62–8/1/62) *AD* 282423, "HOPE Fuel Cell Program, Phase IA," Barchett, R. J.		H_2-O_2 primary extraterrestrial (HOPE) fuel cell	AF33(657)8960, USAF/WP 4/61–10/62
37	Final Rept. (6/62–10/62) *AD* 410532 (Title same as above)			
8	Tech. Documentary Rept. No. ASD–TDR–62–19 (3/62) *AD* 276272		Flight analysis of ion-exchange membrane fuel cells	AF33(616)–7579 SA/1, USAF/WP 10/60–2/62
239	Semiannual Rept. (1/29/60–6/30/60) *AD* 242465, "Ion Exchange Regenerative Fuel Cell R&D Program," Niedrach, L. W.*		Ion-exchange regenerative fuel cell	DA–36–039–SC–85277, USAERDL/NJ 1/60–12/60
240	Final Rept. (1/29/60–9/29/60) *AD* 248480 (Title same as above)			
41	Quart. Rept. No. 1 (10/62–12/62), "Research Study of Bio-Electrogenesis as an Approach to Waste Management," Reynolds, L. V.		Bioelectrogenic system	NASw–511, NASA/? 9/62**
242	"Electrical Energy From Biological Systems," Konikoff, J. J.,* No. N63–15799			
243	"A Preliminary Report on Two Bio-Electrogenic Systems," Reynolds, L. W., No. N63–12826			
244	Prog. Rept. No. 2 (9/30/60–11/30/60), "Research on Compact Fuel Cell Power Supplies" (All reports are titled the same)	General Electric Co., 950 Western Ave., West Lynn 3, Mass.	Research of electrochemical energy conversion system	DA–19–129–QM–1705, QREC/Mass. 9/60–9/61
245	Prog. Rept. No. 3 (11/30/60–1/30/61)			
246	Prog. Rept. No. 4 (1/30/61–3/30/61)			
247	Prog. Rept. No. 6 (5/30/61–7/30/61)			

248.	Summary Rept. (No. 7) ([illegible]/3[illegible]/2[illegible])			
249.	Summary Rept. No. 9 (10/15/58–4/15/60) *AD* 247300, "Research on Redox and Related Fuel Cell Systems"		Auxiliary power devices	DA–19–129–QM–1730, QREC/Mass. 12/60–11/62
250.	Progress Rept. No. 10 (2/15/60–4/15/60) *AD* 243474, "Research on Low Temperature Fuel Cell Systems" (All reports are titled the same)		Research on low-temperature fuel cells	DA–44–009–ENG–3771, USAERDL/Va. 11/60–4/62
251.	Prog. Rept. No. 11 (4/15/60–6/15/60) *AD* 246736			
252.	Prog. Rept. No. 12 (6/15/60–8/15/60) *AD* 250488			
253.	Prog. Rept. No. 13 (8/15/60–10/15/60)			
254.	Prog. Rept. No. 14 (10/15/60–12/12/60) *AD* 256939			
255.	Prog. Rept. No. 15 (12/15/60–2/15/61) *AD* 260739			
256.	Prog. Rept. No. 16 (2/15/61–5/15/61) *AD* 264309			
257.	Prog. Rept. No. 17 (5/15/61–8/15/61)			
258.	Special Prog. Rept. No. 18 (6/1/61–9/30/61) *AD* 268235			
259.	Summary Rept. Sec. I—Rept. No. 19 (11/1/59–11/30/61) *AD* 269227			
260.	Summary Rept. Sec. II—Rept. No. 19 (11/1/59–11/30/61) *AD* 273971			
261.	Report No. 1 (10/1/61–12/31/61) *AD* 273107, "Ion-Exchange Fuel Cell," Oster, E. A. (All reports are titled the same)		Ion-exchange fuel cell	DA–36–039–SC–89140, USAERDL/NJ 11/61–10/62
262.	Report No. 2 (1/1/62–6/30/62)			
263.	Final Tech. Summary Rept. (No. 3) (10/1[illegible]1–9/30/62) *AD* 295615, Maget, H. J. R.			
264.	Quart. Prog. Rept. No. 1 (6/30/60–9/30/60) *AD* 246735, "Voltage Regulation and Power Stability in Unconventional Electrical Generator Systems" (All reports are titled the same)		Voltage regulation and power stability in unconventional electrical generator systems	NOW60–0824–C, USN/BuNWep 6/60–12/61
265.	Quart. Prog. Rept. No. 2 (9/30/60–12/31/60) *AD* 254324			
266.	Quart. Prog. Rept. No. 3 (12/31/60–3/31/61) *AD* 282718			
267.	Quart. Prog. Rept. No. 4 (3/31/61–6/30/61) *AD* 265158			
268.	Quart. Prog. Rept. No. 5 (6/30/61–9/30/61) *AD* 266028			
269.	Quart. Prog. Rept. No. 6 (9/30/61–12/31/61) *AD* 273869			
270.	Prog. Rept. No. 2 (9/30/59–12/30/59), "200 Watt Fuel Cell Power Pack Development Program" (All reports are titled the same)		200-watt fuel-cell power-pack program	NOBsr–77620, USN/BuShips 5/59–6/61
271.	Prog. Rept. No. 3 (12/30/59–5/30/60)			
272.	Prog. Rept. No. 4 (5/30/60–9/30/60)			
273.	Prog. Rept. No. 5 (9/30/60–12/31/60)			

List of Contract Reports (Cont.)

Report reference No. in fuel-cell compendium	Report	Contractor	Contract scope	Contract No. and dates
274	Prog. Rept. No. 6 (Final) (1/1/61–5/31/61)		Research and design on redox and/or related fuel-cell system	DA-8-18-16-420, USAERDL/Va. 9/59–?
275	Final Rept. (11/22/60), "Solar Regenerated Fuel Cell," Foley, R. T.		Solar regenerated fuel cell	DA-30-069-ORD-2782, USABMA/NY 6/59–11/60**
276	Quart. Repts. 1 and 2 (1/1/62–6/30/62) *AD* 296193, "Voltage Regulation and Conversion in Unconventional, Electrical Generator Systems"		Voltage regulation and conversion in unconventional electrical generator systems	NOw62-0984-d, USN/BuNWep 1/62–7/63
277	Prog. Rept. No. 3 (7/1/62–9/30/62) *AD* 294578, "Voltage Regulation and Conversion in Unconventional Electrical Systems"			
278	Quart. Rept. No. 4 (10/1/62–12/31/62) *AD* 407435, "Voltage Regulation and Conversion"			
279	Quart. Prog. Rept. No. 5 (1/1/63–3/31/63) *AD* 432929, "Voltage Regulation and Conversion in Unconventional Electrical Generator Systems," Christianson, C. C.			
280	Final Rept., Vol. 1 of 2 (1/1/62–8/31/63) *AD* 433159 (Title same as above)			
281	Final Rept., Vol. 2 of 2 (1/1/62–8/31/63) *AD* 432679, "Voltage Regulation and Conversion"			
282	A Report on Contract Programs at G.E., NOw60-0824c, NOw62-0984d (7/18/63) *AD* 432896, "Power Transformation and Voltage Regulation"			
283	Quart. Prog. Rept. No. 1 (11/1/61–1/31/62), "Ion-Exchange Membrane Fuel Cell for Submarine Propulsion" (All reports are titled the same)		Ion-exchange membrane fuel cell for submarine propulsion	NObs-86380, USN/BuShips 11/61–9/63
284	Quart. Prog. Rept. No. 2 (2/1/62–4/30/62)			
285	Quart. Prog. Rept. No. 3 (5/1/62–7/31/62)			
286	Quart. Prog. Rept. No. 4 (8/1/62–10/11/62), "Naval Propulsion"			
287	Final Rept., "Naval Propulsion"			
288	1st Semiannual Tech. Rept. (10/1/62–12/31/62) *AD* 400919, "Ion Exchange Fuel Cell," Maget, H. J. R.*		Ion-exchange fuel cell	DA-36-039-AMC-00095(E), USAERDL/Va. 10/62–11/64
289	2d Semiannual Tech. Rept. (1/1/63–6/30/63) *AD* 415681			

90.	Final Rept. (10/1/62–9/30/63) *AD* 423285, "Ion-Exchange Membrane Fuel Cell," Maget, H. J. R.			
291.	Interim Rept. No. 1 (1/24/62) *AD* 274931, "Hydrocarbon Fuel Cell Research," Gilman, S.	General Electric Co., Research Labs., Schenectady, N.Y.	Electrochemistry of ambient temperature hydrocarbon fuel cells	DA-44-009-ENG-4853, USAERDL/Va. 1/61–11/62
292.	Final Tech. Summary Rept., Sec. I (12/1/61–12/31/62), "Saturated Hydrocarbon Fuel Cell Program"			
293	Final Tech. Summary Rept., Sec. II (12/1/61–12/31/62) *AD* 400366L (Title same as above)			
294	Interim Rept. No. 1 (3/15/62) *AD* 274734L, "On the Reactions of Propane at the Surface of a Working Fuel Cell Anode," Grubb, W. T.		Saturated hydrocarbon fuel-cell program	DA-44-009-ENG-4909, USAERDL/Va. 1/62—Act.
295	Interim Rept. No. 4 (6/30/63) *AD* 412594L, "Mechanism of Electrochemical Oxidation of CO and CH_3OH on Pt," Gilman, S.			
296	Interim Rept. No. 5 (6/30/63) *AD* 412595L, " 'Reactant Pair' Mechanism for Electrochemical Oxidation of CO and CH_3OH," Gilman, S.			
297	Interim Rept. No. 6 (12/31/63), "Studies of Anion Adsorption on Pt by MPP," Gilman, S.			
298	Interim Rept. No. 7 (12/31/63) (Title same as above)			
299	Interim Rept. No. 8 (12/31/63), "Measurement of H_2 Adsorption by MPP," Gilman, S.			
300.	Interim Rept. No. 9 (12/31/63), "Catalytic Activity of Noble Metal Alloys," McKee, D. W.*			
301.	Interim Rept. No. 10 (12/10/63), "A Review of the Literature on Materials Resistant to Hot Concentrated H_3PO_4 for Fuel Cell Applications," Popat, P. V.*			
302	Tech. Summary Rept. No. 1 (12/1/61–6/30/62) *AD* 282851L, "Saturated Hydrocarbon Fuel Cell Program" (All reports are titled the same)			
303.	Tech. Summary Rept. No. 2, Sec. I (7/1/62–12/31/62) *AD* 400367L			
304.	Tech. Summary Rept. No. 2, Sec. II (12/1/61–12/31/62) *AD* 299195L			
305.	Tech. Summary Rept. No. 3, Part I—Task I and Task II (1/1/63–6/30/63) *AD* 412596L			
306.	Tech. Summary Rept. No. 3, Part I—Task III (1/1/63–6/30/63)			
307.	Tech. Summary Rept. No. 3, Part I—Task IV (1/1/63–6/30/63)			
308.	Tech. Summary Rept. No. 3, Part II—All Tasks (1/1/63–6/30/63)			
309.	Tech. Summary Rept. No. 4, Parts 1 and 2—All Tasks (7/1/63–12/31/63)			
310.	Semiannual Tech. Summary Rept. No. 5 (1/1/64–6/30/64) *AD* 446629, "Hydrocarbon-Air Fuel Cells"			

List of Contract Reports (Cont.)

Report reference No. in fuel-cell compendium	Report	Contractor	Contract scope	Contract No. and dates
311.	Semiannual Tech. Summary Rept. No. 6 (7/1/64–12/31/64) *AD* 612766 (Title same as above)			
312.	Tech. Doc. Rept. No. AMRL–TDR–63–62 (3/63) *AD* 407000, "Research of Electrolysis Cell-Fuel Cell Method of Recovering Potable Water From Urine," Rudek, F. P.	General Electric Co., Valley Forge Space Technology Center, King of Prussia, Pa.	Fuel-cell method of recovering potable water from urine	AF33(657)–7667, ?
313.	Report No. ASD–TR–61–475 (3/62) *AD* 277211, "Research on H_2 Evolution and Dissolution," Breiter, M.*	Germany, Physical and Electrochemical Institute of Technology, Munich, Germany	H_2 evolution and dissolution	AF61(052)–305, USAF/WP 10/59–9/60*
314.	Tech. Doc. Rept. No. ASD–TDR–62–1067 (3/63) *AD* 403343, "Studies of H_2 and O_2 Evolution and the Influence of Adsorbed Substances," Kandler, L.			
315	"Design Study on the Generation of H_2 from CH_3OH for Fuel Cell Systems on Board Submarines," Bennet, H. A., Jr.* (10/12/62) *AD* 292273	Girdler Corp., Louisville, Ky.	Design study on the generation of H_2 from CH_3OH for fuel-cell systems on board submarines	NObs–86743, USN/BuShips 10/62*
316.	Rept. No. 1 (9/1/60–11/30/60), "Fuel Cell Materials," Gregor, H. P. (All reports are titled the same)	Gregor H. P., Ph. D. (Polytechnic Institute of Brooklyn), 150 Lakeview Ave., Leonia, N.J.	Fuel-cell materials	DA–36–039–SC–85384, USAERDL/NJ 9/60–2/62
317.	Rept. No. 2 (12/1/60–2/28/61) *AD* 262528			
318.	Rept. No. 3 (3/1/61–5/31/61) *AD* 272863			
319.	Rept. No. 4 (6/1/61–8/31/61) *AD* 272864			
320.	Rept. No. 5 (9/1/61–11/30/61) *AD* 272865			
321.	Rept. No. 6 (12/1/61–2/28/62) *AD* 283651			
322.	Rept. No. 1 (3/1/62–5/31/62) *AD* 289082, "Ion Exchange Membrane Electrolytes," Gregor, H. P. (All reports are titled the same)		Ion-exchange membrane electrolytes	DA–36–039–SC–89197, USAERDL/NJ 2/62–11/64
323.	Rept. No. 2 (6/1/62–8/31/62) *AD* 418243			
324.	Rept. No. 3 (9/1/62–11/30/62) *AD* 418244			
325.	Rept. No. 4 (12/1/62–2/28/63) *AD* 418245			

326	Rept. No. 5 (3/1/63–5/31/63) *AD* 418246			
327	Rept. No. 6 Final (3/1/62–8/31/63) *AD* 434245			
328	Rept. No. TR–891 (10/24/60), "Status of DOFL Fuel Cell Program on 10/1/60," Gibson, H. F.	Harry Diamond Laboratory, Washington 25, D.C.	Fuel-cell research	DA–5B51–02–004, HDL Proj 96094 10/60–9/64
329	Rept. No. TR–923 (4/24/61) *AD* 255944, "Characteristics of O_2 Electrodes for Low Temperature Fuel Cells," Denison, I. A.			
330	Rept. No. TR–1128 (4/25/63), "O_2 Sources for Fuel Cells," Forziati, A. F.*		O_2 sources for fuel cells	DA–1P010501A002, HDL 4/63**
331	Rept. No. TR–1163 (10/4/63) *AD* 424580, "Flow-Through Porous Electrodes for Redox Couples," Singman, D.		Porous electrodes	DA–1P022001A002, HDL Proj 96000 10/63**
332	Rept. No. TR–1168 (11/1/63), "H_2 Sources for Fuel Cells," Singman, D.*		H_2 sources for fuel cells	DA–1P022001A002, HDL Proj 96094 11/63**
333	Rept. No. TR–835 (4/15/60), "Electrode Kinetics of Oxidation Reduction Couples," Bond, A. P.*		Electrode kinetics of oxidation reduction couples	DA–5N06–01–010 4/60**
334	Final Rept.—Parts A and B (12/7/59) *AD* 248428, "Survey of State-of-the-Art Fuel Cell Development," Smatko, J. S.*	Hoffman Electronics Corp., 3740 South Grand Ave., Los Angeles, Calif.	Survey of state-of-the-art fuel-cell development	AF30(635)–12857, USAF 12/59**
335	Final Rept. (4/15/56–7/15/57) *AD* 158048, "Continuous Feed Battery," Bauman, H. F.*	Illinois Institute of Technology, Armour Research Foundation, Technology Center, Chicago 16, Ill.	Continuous feed battery	NObs–72131, USN/BuShips 9/57**
336	Tech. Rept. 61–4/U (5/16/60) *AD* 257806, "R&D on Power Sources and Energy Conversion in the Dept. of Defense, AED and NASA," Snyder, N. W.	Institute for Defense Analysis, Washington, D.C.	Research and development on power sources and energy conversion	SD–50, OFMO/? 5/60**
337	Rept. R–103 (6/63) *AD* 429058, "Dept. of Defense R&D on Power Sources," Hamilton, R. C.*			
338	Interim Rept. (12/30/60) *AD* 252024, "Study of Ion Exchange Membrane Fuel Cell Components," Lurie, R. M.* (All reports are titled the same)	Ionics, Inc., 152 6th St., Cambridge 42, Mass.	Study of ion-exchange membrane fuel components	DA44–009–ENG–4554, USAERDL/Va. 6/60–4/62

List of Contract Reports (Cont.)

Report reference No. in fuel-cell compendium	Report	Contractor	Contract scope	Contract No. and dates
339	Monthly Rept. for Jan. 1961 (2/7/61) *AD* 252025			
340	Mar. 1961 Progress Rept.			
341	Apr. 1961 Progress Rept.			
342	Final Rept. (10/30/61) *AD* 266036			
343	Unidentifiable Rept. (No date or author)			
344	Unidentifiable Rept.			
345	"Study of a Graphite-O_2 High Temperature Fuel Cell," Duke, F. R., and Copeland, J. L.	Iowa State University of Science and Technology, Ames, Iowa		W-7405-ENG-82, USAEC 8/63**
346	Ph. D. Dissertation (1963) *AD* 416424, "Electrochemical Processes in Fused Salts," King, L. A.			
347	Tech. Sci. Note No. 1 (9/59), "Researches on Hydrogen Overvoltage on Metallic Single Crystals: Ag and Pb," Bicelli, L. P.*	Italy, Laboratori di Elettrochimica Chimica Fisica e Metallurgia del Politecnico di Milano, Milan, Italy	Researches on hydrogen overvoltage on metallic single crystals	AF61(052)-144. USAF/WP 2/61-5/62*
348	Tech. Sci. Note No. 2 (12/59), "Researches on Hydrogen Overvoltage on Metallic Single Crystals: Sn," Bicelli, L. P.*			
349	Tech. Sci. Note No. 3 (5/60), "Researches on Hydrogen Overvoltage on Metallic Single Crystals: Ni," Bicelli, L. P.*			
350	Tech. Sci. Note No. 4 (6/60), "Researches on Hydrogen Overvoltage on Metallic Single Crystals: Cd," Bicelli, L. P.*			
351	Annual Rept. (7/60), "Research on H_2 Overvoltage on Metallic Single Crystals," Piontelli, R.*			
352	Tech. Sci. Note No. 6 (2/61), "Research on H_2 Overvoltage on Metallic Single Crystals: Zn," Piontelli, R.*			
353	WADD Tech. Rept. 60-769 (2/61) *AD* 407725, "Research on H_2 Overvoltage on Metallic Single Crystals," Piontelli, R.*			
354	Tech. Sci. Note No. 7 (6/61), "Research on H_2 Overvoltage on Metallic Single Crystals: Sb," Piontelli, R.*			
355	Annual Rept. (7/61)			
356	WADD Tech. Rept. 61-33 (9/61) *AD* 269067, "Research on H_2 Overvoltage on Metallic Single Crystals: Bismuth," Bicelli, L. P.			
357	Tech. Note No. 8 (9/61), "Researches on the Influence of Some Minor Constituents of the Solution on H_2 Overvoltage of Cu Single Crystals," Rivolta, B.*			
358	Tech. Doc. Rept. No. ASD-TN-61-73 (2/62) *AD* 276193, "Research on H_2 Overvoltage on Metallic Single Crystals: Zinc," Bicelli, L. P.			
359	Tech. Doc. Rept. No. ASD-TN-61-157 (3/62) *AD* 275899, "Research			

	on H_2 Overvoltage on Metallic Single Crystals: Antimony," Bicelli, L. P.			
360..	Tech. Doc. Rept. No. ASD-TN-61-158 (3/62) *AD* 277018, "Research on H_2 Overvoltage on Metallic Single Crystals," Piontelli, R.*			
361..	Tech. Doc. Rept. No. ASD-TDR-62-229 (3/62) *AD* 276870, "Researches on the Influence of Some Minor Constituents of the Solution on H_2 Overvoltage of Cu Single Crystals," Rivolta, B.*			
362..	Tech. Doc. Rept. No. ASD-TDR-62-357 (5/62) *AD* 281805 (Title same as above), Piontelli, R.*			
363..	Tech. Note No. 1 (5/60) *AD* 242313, "Electrochemical Behavior of O_2 and H_2O_2 on Ag Electrodes," Bianchi, G.*	Italy, University of Milano, Milan, Italy	Electrochemical behavior of O_2 and H_2O_2 on metal electrodes	AF61(052)-260, USAF/OSR/Eur 4/59-3/62
364..	Tech. Note No. 2 (AFOSR TN 60/859), "Electrochemical Behavior of O_2 and H_2O_2 on Titanium Electrodes," Bianchi, G.*			
365..	Tech. Note No. 3 (10/60), "Electrochemical Behavior of O_2 and H_2O_2 on Magnetite Electrodes," Bianchi, G.*			
366..	Tech. Note No. 4 (12/60), "Electrochemical Behavior of O_2 and H_2O_2 on Al, Ta, and Zr Electrodes," Bianchi, G*.			
367..	Tech. Note No. 5 (12/61) *AD* 276134, "O_2 and H_2O_2 Electrochemical Behavior on Au Electrodes," Bianchi, G.*			
368..	Tech. Note No. 6 (12/61) *AD* 277394, "Cathodic Reduction of O_2 and H_2O_2 on Pt, Pd and Ir Smooth Electrodes," Bianchi, G.*			
369..	Tech. Note No. 7 (1/62), "O_2 and H_2O_2 Electrochemical Behavior on Cu Electrodes," Bianchi, G.			
370..	Tech. Note No. 8 (2/62), "O_2 and H_2O_2 Electrochemical Behavior on Cr, Ni, Co and Stainless Steel Electrodes," Bianchi, G.*			
371..	Tech. Final Rept. (3/62) *AD* 283522, "Basic Researches in Metal Corrosion: Electrochemical Behavior of O_2 and H_2O_2," Bianchi, G.			
372..	Tech. (Scientific) Note No. 1 (4/30/59) *AD* 219364, "Influence of Surface Preparation of Pt Electrodes on Cathodic Processes of H_2O_2," Bianchi, G.*			AF61(052)-85, USAF/OSR/Eur 4/58-3/59
373..	Tech. (Scientific) Note No. 2 (4/30/59) *AD* 232054, "The Electrochemical Behavior of H_2 and O_2 Mixtures on Pt Electrodes," Bianchi, G.*			
374..	Tech. Note No. 3 (4/30/59) *AD* 219263, "Electrochemical Behavior of Graphite Electrodes in Solutions of Various pH Containing O_2 and H_2O_2," Bianchi, G.*			
375..	Tech. (Scientific) Note No. 4 (4/30/59) *AD* 226591, "Anodic Behavior of H_2O_2 on Pt Electrodes," Bianchi, G.*			
376..	Final Report (4/30/59) *AD* 218388, "Basic Researches in Metal Corrosion," Bianchi, G.			
377..	Tech. Release No. 34-38 (4/10/60) *AD* 235688, "Spacecraft	Jet Propulsion Labo-	Gravitational effects	JPL

List of Contract Reports (Cont.)

Report reference No. in fuel-cell compendium	Report	Contractor	Contract scope	Contract No. and dates
	Secondary Power Requirements During the Sixties," Hamilton, R. C.*	ratory, California Institute of Technology, 48 Oak Grove Dr., Pasadena, Calif.	on electrode behavior	6/62—Act.
378	Tech. Rept. No. 32–105 (5/25/61) *AD* 259854, "Efficiency of Fission Electric Cells," Heindl, C. J.		Efficiency and comparison of geometry of fission electric cells	NASw-6, NASA/? 4/60–9/61**
379	Prog. Rept. No. 4 (RL–61–886) (6/30/61), "15-Cell Continuous Feed Primary Battery"	Kellogg, M. W., Co., 711 3d Ave., New York, N.Y.	Sodium amalgam-oxygen fuel cell	NObs-78461, USN/BuShips 12/58–6/63
380	Prog. Rept. No. 5 (RL–61–901) (9/20/61) (Title same as above)			
381	Rept. No. RD–61–904 (10/2/61), "Na Amalgam-O_2 Primary Batteries for Submarine Propulsion," Miller, K. D., Jr.			
382	Prog. Rept. No. 6 (RD–62–917) (1/11/62), "5-Cell Continuous Feed Primary Battery"			
383	Prog. Rept. No. 8 (RD–62–944) (7/12/62) (Title same as above)			
384	Final Rept. RD–62–960—Vol. I (11/9/62) (Title same as above)			
385	Rept. No. RD–63–1009 (12/16/63), "Na Amalgam-O_2 Fuel Cell Power Plant for Submarine Application," Gilbert, N.			
386	Report No. CE–61–211 (3/20/61) *AD* 256709, "Preliminary Process Studies on the Generation of H_2 for Small Fuel Cell Systems," Ozkardes, H.*		Preliminary process studies on the generation and use of H_2 for a fuel-cell system	DA–44–009–ENG–4578, USAERDL/NJ 3/61**
			H_2 fuel sources and storage	NObs-77021, USN/BuShips
387	Rept. No. RD–62–953 (9/30/62) *AD* 292134, "Design Study of a H_2-Generating Plant for Submarine Use Based on the Steam Reforming of CH_3OH," Veueka, H.		Design study of a H_2 generating plant for submarine use based on the steam re-forming of CH_3OH	NObs-86744, USN/BuShips 9/62**

388.	Quart. Prog. Rept. (4/1/62–7/1/62) *AD* 291153, "Direct Energy Conversion Systems," Eustis, R. H.	Leland Stanford Junior University, Stanford, Calif.	Direct energy conversion systems	AF49(638)–1123, ARPA 11/61—Act.
389.	Semiannual Tech. Summary Rept. (4/1/62–10/1/62) *AD* 291154, (Title same as above), Kruger, C. P.			
390.	Semiannual Tech. Summary Rept. No. 3 (10/1/62–4/1/63) *AD* 406355 (Title same as above), Eustis, R. H.			
391.	Semiannual Tech. Summary Rept. (4/1/63–10/1/63) *AD* 423164 (Title same as above), Eustis, R. H.			
392.	Semiannual Tech. Summary Rept., Suppl. No. 2 (4/1/63–10/1/63), "Electrode Kinetics and Diffusion Using a Translating Electrode," Eustis, R. H.			
393.	Quart. Tech. Summ. Rept. (10/1/63–11/30/63) *AD* 430023, "Direct Energy Conversion Systems," Eustis, R. H.			
394.	Quart. Tech. Summary Rept. (3/1/64–5/31/64), "The Anodic Oxidation of CH_3OH on Single Crystal and Polycrystalline Pt," Eustis, R. H.			
395.	Supplement to Quart. Tech. Summary Rept. (3/1/64–5/31/64) *AD* 460947 (Title same as above), Smart, W. and Mason, D. M.			
396.	Quart. Tech. Summary Rept. (6/1/64–8/31/64) *AD* 609415, "Direct Energy Conversion Systems," Eustis, R. H.			
397.	Final Rept. (7/65), "A Review of Low Temperature Hydrocarbon Fuel Cells," Lerner, H.	Lerner, H., Ph.D. (Pennsylvania State University), 224 Bradley Ave., State College, Pa.	A review of low temperature hydrocarbon fuel cells	61533–1731–65, MEL 2/65–7/65
398.	Rept. No. 1 (9/4/59–12/31/59) *AD* 233858, "Solar Regenerative Chemical Systems," Silverman, H. P.	Lockheed Aircraft Corp., Missiles & Space Division, Sunnyvale, Calif.	Solar regenerative chemical system	DA–36–039–SC–85245, USAERDL/NJ 9/59–7/62
399.	Rept. No. 2 (1/1/60–6/30/60) *AD* 242591 (Title same as above), Silverman, H. P.			
400.	Rept. No. 3 (7/1/60–12/30/60) *AD* 254841 (Title same as above)			
401.	Rept. No. 4 (1/1/61–6/30/61) *AD* 268401 (Title same as above), Silverman, H. P.			
402.	Rept. No. 5 (7/61–12/61) (Title same as above) Gandel, M. G.			
403.	Rept. No. 7 (Final) (9/4/59–9/30/62) *AD* 289294			
404.	Final Rept. (11/61) *AD* 273049, "Basic Research in Fuel Cells: NH_3, Ethylene Glycol and Urea Systems"		Fuel-cell research	DA–44–177–TC–634, USATREC/Va. 6/60–11/61

List of Contract Reports (Cont.)

Report reference No. in fuel-cell compendium	Report	Contractor	Contract topic	Contract No. and notes
405.	1st Quart. Rept. (5/19/61–8/15/61) *AD* 298768, "Basic Studies on Fuel Cell Systems" (All reports are titled the same)		Basic study on fuel-cell research	NOw 60–0738–d, USN/BuNWeps 5/61–7/63
406.	3d Quart. Rept. (11/3/61–2/12/62) *AD* 273702			
407.	Quart. Rept. No. 4 (2/12/62–5/14/62) *AD* 278353			
408.	Final Rept. (5/19/61–7/19/63) *AD* 420170			
409	Tech. Rept. LSMD–480464 (10/14/59) *AD* 232126, "Gravity Field Effects on Zn Anode Discharge in Alkaline Media," Eisenberg, M.		Gravity field effects on zinc anode discharge in alkaline media	NOrd 17017, 10/59**
410	Tech. Doc. Rept. No. ASD–TDR–62–1 (4/62) *AD* 277171, "New Cathode-Anode Couples Using Nonaqueous Electrolytes" (All reports are titled the same)		New cathode-anode couples using nonaqueous electrolytes	AF33(616)7957, USAF/WP 3/61–7/63**
411.	Annual Tech. Rept. No. ASD–TDR–62–837 (9/62) *AD* 286889			
412.	Quart. Tech. Prog. Rept. No. 1 (12/15/62) *AD* 294308, Bauman, H. F.*			
413.	Quart. Tech. Prog. Rept. No. 2 (4/15/63) *AD* 401846, Bauman, H. F.			
414.	Quart. Tech. Prog. Rept. No. 3 (7/15/63) *AD* 411314			
415.	2d Annual Rept. No. RTD–TDR–63–4083 (10/63) *AD* 425876			
416.	Final Rept. (9/30/62) *AD* 292139, "Design Study for a H_2 Generation Plant for Submarine Fuel Cells"	Lummus Co., New York, N.Y.	Design study for a H_2 generation plant for submarine fuel cells	NObs–86746, USN/BuShips 9/62
417.	Rept. No. 1 (7/1/62–9/30/62) *AD* 296802, "Biochemical Fuel Cells," Silverman, H. P. (All reports are titled the same)	Magna Corp., 1001 South East St., Anaheim, Calif.	Biochemical fuel cell	DA–36–039–SC–90866, USAERDL/NJ 7/62—Act.
418.	Rept. No. 2 (10/1/62–12/31/62) *AD* 403822, Brake, J. M.*			
419.	Rept. No. 3 (1/1/63–3/31/63) *AD* 419298, Brake, J. M.*			
420.	Rept. No. 4 (4/1/63–6/30/63), Brake, J. M.*			
421.	Rept. No. 5 (7/1/63–9/30/63), Brake, J. M.			
422.	Rept. No. 6 (10/1/63–12/31/63), Brake, J. M.			
423.	Rept. No. 7 (1/1/64–3/31/64), Silverman, H. P.			
424.	Rept. No. 8 (4/1/64–6/30/64) *AD* 450037, Cavallo, J. J.			
425.	Rept. No. 9 (7/1/64–9/30/64) *AD* 454777, Brake, J. M.			

426.	Rept. No. 10 (10/1/64–12/31/64) *AD* 460795, Brake, J. M.			
427.	Final Rept. (3/14/63–3/13/64), NASA CR-54077, "Research on Applied Bioelectrochemistry," Canfield, J. H.		Applied bioelectrochemistry	NASw–623, NASA/Lewis 3/63–6/64
428.	Rept. No. 1 (3/22/63–7/31/63), "Biochemical Fuel Cells," Ellis, G. E.* (All reports are titled the same)	Marquardt Corp., 16555 Saticoy St., Van Nuys, Calif.	Bioelectrochemical development	NASw–654, NASA/Lewis 3/63—Act.
429.	Rept. No. 2 (9/1/63–11/31/63)			
430.	Rept. No. 3 (11/1/63–1/31/64)			
431.	Final Rept. (3/19/63–9/19/64)			
432.	Semiannual Tech. Sum. Rept. No. 1 *AD* 267028, "Research on Materials, Processes, and Devices Related to Energy Conversion"	Massachusetts Institute of Technology, Electrical Engineering Department, Cambridge 39, Mass.	Research on energy conversion	NOnr 1841(78), ONR/DC 6/61–1/64
433.	Semiannual Tech. Sum. Rept. No. 2 (3/30/62) *AD* 275610 (Title same as above)			
434.	Scientific Rept. No. 3 (4/62) *AD* 286959, "Rate Limiting Steps on Fuel Cell Electrodes," Reti, A. R.			
435.	Scientific Rept. No. 5 (1/63) *AD* 401932, Ph. D. thesis—"Electrochemical Oxidation of HCOOH," Slott, R.			
436.	Semiannual Summary Rept. No. 6 (12/31/62) *AD* 407856, "Research on Materials, Processes, and Devices Related to Energy Conversion"			
437.	Final Summary Rept. (No. 8) (5/31/63) *AD* 416132 (Title same as above)			
438.	"Studies of Molten Salt Thermocells," Ulrich, G. D.—Ph. D. thesis (2/64)			
439.	"Fuel Cells Using Flooded Flow Electrodes, Appendix II–B," Meissner, H. P.			
440.	Tech. Prog. Rept. No. 3 (5/31/61) *AD* 262354, "Magnetohydrodynamics and Energy Conversion"		Research on energy conversion	AF33(616)7624, USAF/WP 9/60–8/63
441.	Tech. Prog. Rept. No. 5 (12/15/61) *AD* 272657 (Title same as above)			
442.	Tech. Doc. Rept. ASD–TDR–63–118 (1/63) *AD* 408205, "Rate Limiting Steps on Fuel Cell Electrodes," Reti, A. R.			
443.	Final Rept. (5/15/62) *AD* 289270, "Properties and Reactions of H_2O_2," Satterfield, C. N.		H_2O_2 studies	NOnr–1841(11), ONR/DC 47
444.	WADC Tech. Note 59–20 (8/58) *AD* 208544, "Study of Electrical Energy Conversion Systems for Future Aircraft," White, D. C.*		Metal oxide-O_2 electrodes and fuel cells	AF33(616)–3984, USAF/WP 5/60**
445.	WADD Tech. Rept. 59–116, Part 1 (2/1/57–3/1/59) *AD* 227320, "Summary Rept.: Study of Electrical Energy Conversion			

List of Contract Reports (Cont.)

Report reference No. in fuel-cell compendium	Report	Contractor	Contract scope	Contract No. and dates
	Systems for Future Aircraft" White, D. C.			
446	WADD Tech. Rept. 60–148 (2/1/59–1/31/60) *AD* 243592 (Title same as above), Woodson, H. H.*			
447	WADD Tech. Rept. 60–166 (5/60) *AD* 240793, "Metal Oxide-Oxygen Electrodes and Fuel Cells," Sama, D. A.			
448	1st Quart. Prog. Rept. (7/1/62–9/30/62) *AD* 292694, "Biochemical Fuel Cell," Foley, R. T.* (All reports are titled the same)	Melpar, Inc., 3000 Arlington Blvd., Falls Church, Va.	Biochemical fuel cell	DA-36-039-SC-90878, USAERDL/NJ 7/62—Act.
449	Rept. No. 2 (10/1/62–12/31/62) *AD* 403880			
450	Rept. No. 3 (1/1/63–3/31/63) *AD* 409750			
451	4th Quart. Prog. Rept. (4/1/63–6/30/63) *AD* 421906			
452	5th Quart. Prog. Rept. (7/1/63–9/30/63) *AD* 428050			
453	6th Quart. Prog. Rept. (10/1/63–12/31/63) *AD* 436338			
454	7th Quart. Prog. Rept. (1/1/64–3/31/64) *AD* 602089			
455	Rept. No. 8 (4/1/64–6/30/64) *AD* 450452, Blanchard, G. C.*			
456	Final Rept. No. ASD-TDR-62-42 (6/62) *AD* 282862, "Compact-Power Fuel Cell"	Monsanto Chemical Co., Special Projects Department, Everett Station, Boston 49, Mass.	Compact-power fuel cell	AF33(616)-7735, USAF/WP 11/60–5/62
457	Final Rept. (9/29/60–9/28/61) *AD* 289274, "Electrochemical Energy Conversion Systems Research," Smith, J. O.*		Electrochemical energy conversion systems research	DA-19-129-QM-1698, QREC/Mass. 9/60–9/61
458	Rept. No. 1, Final (1/15/62–10/17/62) *AD* 408974, "Investigation of Organic Fuels for Electrochemical Use," Gentile, R. G.*		Investigation of organic fuels	DA-36-039-SC-88945, USAERDL/NJ 1/62–10/62
459	Quart. Rept. No. 1 (6/28/63–9/28/63), "Study of Fuel Cells Using Storable Rocket Propellant," Smith, J. O.*		Study of fuel cells using storable rocket propellants	NAS3-2791, NASA/Lewis 6/63—Act.
460	Final Rept. (6/28/63–1/27/64) (Title same as above)			

461.	Quart. Rept. No. 1 (6/14/63–9/30/63), "Development and Feasibility Proof of the Dry Tape Battery Concept," Gruber, A.*		Development and feasibility proof of the dry tape battery concept	NAS3–2777, NASA/Lewis 6/63–4/64
462.	Rept. No. MRB 5001F (6/14/63–1/23/64) (Title same as above), Borsany, A. S.*			
463.	1st Quart. Prog. Rept. (9/10/63), "Research to Improve Electrochemical Catalysts" (All reports are titled the same), Smith, J. O.*		Research to improve electrochemical catalysts	DA–44–009–AMC–202(T), USAERDL/Va. 5/63–5/64
464.	Semiannual Tech. Sum. Rept. (5/15/63–11/15/63), *AD* 434194, Smith, J. O.*			
465.	3d Quart. Prog. Rept. (11/15/63–2/15/64), Orth, J. C.*			
466.	Final Tech. Rept. (5/15/63–5/15/64) *AD* 447152			
467.	2d Quart. Prog. Rept. (1/1/60–3/31/60) *AD* 244775, "Fuel Cells" (All reports are titled the same)		Fuel cells	DA–44–009–ENG–4154, USAERDL/Va. 10/59–12/60
468.	3d Quart. Prog. Rept. (7/15/60) *AD* 244776, Leitz, Jr.			
469.	Final Rept. (10/1/59–12/1/60) *AD* 272352, Gentile, R. G.			
470.	Rept. No. 1 (7/1/59–9/30/59) *AD* 230503, "Study of Energy Conversion Devices," Shearer, R. E. (All reports are titled the same)	M.S.A. Research Corp., Mine Safety Appliance Co., Callery, Pa.	Regenerative continuous feed galvanic systems	DA–36–039–SC–78955, USAERDL/NJ 7/59–5/61
471.	Rept. No. 2 (10/1/59–12/31/59) *AD* 234482			
472.	Rept. No. 3 (4/29/60) *AD* 238235			
473.	Rept. No. 4 (4/1/60–6/30/60) *AD* 250695			
474.	Final Rept. No. 7 (7/59–5/61)			
475.	Tech. Prog. Rept. (1/64) *AD* 427999, "Chronopotentiometric Study of Anionic Diffusion in the K-Liquid NH_3 System," Gordon, R. P.	New York University, New York, N.Y.	Electrode processes in molten salts	NOnr 285(37), ONR/DC 6/58—Act.
476.	"Transport Processes in Fused Salts—Part I," Sundheim, B. R., *AD* 296566			
477.	Tech. Doc. Rept. No. ASD–TDR–62–377 (12/1/60–12/31/61) *AD* 284881, "Study of Bioelectric Energy Sources," VanWinkle, Q.	Ohio State University, Columbus 1, Ohio	Study of organic (bioelectric) fuel cell	AF33(616)–7693, USAF/WP 11/60–3/62
478.	Tech. Rept. No. WADC TR–57–605, Part II (4/62) *AD* 276524, "Continuous Feed Fuel Cell Systems"	Patterson-Moos Research, division of Leesona Corp., Jamaica, N.Y.	Continuous feed fuel-cell systems	AF33(600)–34709, USAF/WP 2/57–2/62**
			H_2-O_2 fuel cells	NOAS 58–414C, USN/BuNWeps 5/58–12/59

List of Contract Reports (Cont.)

Report reference No. in fuel-cell compendium	Report	Contractor	Contrat ope	Contract No. and dates
[illegible]	ARL Tech. Rept. 60–325 (10/60) *AD* 249381, "The Photochemical Decomposition of H_2O," West, R. E.	P.E.C. Corp., Boulder, Colo.	Research on liquid-phase photolysis of water	AF33(616)6529. USAF/WP 10/60*
480	Final Rept. (8/62), "Redox Fuel Cells: The Fuel Regenerator," Austin, L. G.	Pennsylvania State University, Department of Fuel Technology, University Park, Pa.	Fuel cells	DA–49–186–ORD–917, HDL 3/60–4/64
481	Tech. Rept. No. 1 (6/62), "A Discussion of Some Aspects of Electrode Kinetics Relevant to Fuel Cell Studies," Austin, L. G.			
482	Tech. Rept. No. 2 (9/62, "Polarization at Porous Flow-Through Electrodes," Austin, L. G., and Klimpel, R. R.			
483	Tech. Rept. No. 3 (11/62), "The Mode of Operation of Porous Diffusion Electrodes," Austin, L. G.			
484	Tech. Rept. No. 4 (5/63), "Preliminary Investigations of Porous Flow-Through Electrodes of Pt Black," Palasi, P., and Austin, L. G.			
485	Tech. Rept. No. 5 (11/63), "Further Investigations of Porous Flow-Through Electrodes of Pt Black," Palasi, P., and Austin, L. G.			
866	Tech. Rept. No. 6 (5/64), "Kinetics of a Redox Reaction at Solid and Porous Electrodes," Lerner, H., and Austin, L. G.			
47.	Tech. Rept. No. 7 (5/64), "Simple-Pore and Thin-Film Models of Porous Gas Diffusion Electrodes," Austin, L. G.			
888	Tech. Rept. No. 8 (1/65), "Bibliography of Fuel Cell Contracts," Lerner, H., and Austin, L. G.			
89	Rept. No. 1 (5/1/54–7/31/54), "Conversion of Carbonaceous Fuels to Electrical Energy," Gorin and Recht (All reports are titled the same)	Pittsburgh Consolidation Coal Co., Research and Development Division Library, Pa.	Conversion of carbonaceous fuels to electrical energy	DA–36–039–63090, USAERDL/NJ 5/54–4/57
490	Rept. No. 2 (8/1/54–10/31/54)			
491	3d Quart. Rept. (11/1/54–1/31/55)			
492	4th Quart. Rept. (2/1/55–4/30/55)			
493	5th Quart. Rept. (5/1/55–7/31/55)			
494	6th Quart. Rept. (8/1/55–10/31/55)			
495	7th Quart. Rept. (11/1/55–1/31/56)			
496	Rept. No. 8 (2/1/56–4/30/56)			
497	Rept. No. 9 (5/1/56–7/31/56)			
498	Rept. No. 10 (8/1/56–10/31/56)			
499	Rept. No. 11 (11/1/56–1/31/57)			
500	Rept. No. 12 (2/1/57–4/30/57)			
501	Final Rept. (12) (5/1/57–4/30/57)			

502.	Rept. No. 13 (5/1/57–8/14/57), "Conversion of Carbonaceous Fuels to Electrical Energy," Gorin and Recht (All reports are titled the same)		Conversion of carbonaceous fuels to electrical energy	DA–36–039–SC–74941, USAERDL/NJ 5/57–8/58
503.	Rept. No. 14 (8/15/57–11/30/57)			
504.	Rept. No. 15 (12/1/57–2/28/58)			
505.	Rept. No. 16 (3/1/58–5/31/58)			
506.	Rept. No. 17, Final Rept. (6/1/58–8/14/58)			
507.	Tech. Note No. E–2TN098–332 (9/3/58) *AD* 202224, "Bibliography—Fundamental Investigation of Electrical Power Sources for Electric Thrust Devices," Fife, H.	Plasmadyne Corp., Santa Ana, Calif.	Fundamental investigations of electrical power sources	AF49(638)–332, USAF/OSR/DC 8/58–4/59**
508.	Vol. VII, Bibliographies, AFOSR TR 59–104 (4/24/59) *AD* 227934, "Fundamental Investigation of Power Sources," Fife, H.			
509.	Bimonthly Prog. Rept. (7/16/60–9/15/60) *AD* 252101, "Correlation Between Magnetic Susceptibility and Catalytic Activity of Electrode," Chu, J. C.* (The following 5 reports are titled the same)	Polytechnic Institute of Brooklyn, 333 Jay St., Brooklyn, N.Y.	Fuel cell and its related technology	DA–44–009–ENG 4586, USAERDL/Va. 6/60–4/62
510.	Bimonthly Prog. Rept. (9/16/60–11/15/60) *AD* 252102			
511.	Bimonthly Prog. Rept. (11/16/60–1/15/61) *AD* 252103			
512.	Bimonthly Prog. Rept. (1/16/61–3/15/61) *AD* 255732			
513.	Bimonthly Prog. Rept. (3/16/61–5/15/61) *AD* 270000			
514.	Final Rept. (7/16/60–7/15/61) *AD* 269999			
515.	Bimonthly Prog. Rept. (7/16/60–9/15/60) *AD* 252104, "Correlation Between IR Spectrum and Catalytic Activity of Electrode," Chu, J. C. (The following 5 reports are titled the same)			
516.	Bimonthly Prog. Rept. (9/16/60–11/15/60) *AD* 252105			
517.	Bimonthly Prog. Rept. (12/16/60–1/15/61) *AD* 252106			
518.	Bimonthly Prog. Rept. (1/16/61–3/15/61) *AD* 255733			
519.	Bimonthly Prog. Rept. (3/16/61–5/15/61) *AD* 270001			
520.	Final Rept. (7/16/60–7/15/61) *AD* 269998			
521.	Bimonthly Prog. Rept. (7/16/60–9/15/60) *AD* 252107, "Correlation Between Surface Conductivity and Catlytic Activity of the Electrode," Chu, J. C. (The following 4 reports are titled the same)			
522.	Bimonthly Prog. Rept. (9/16/60–11/15/60) *AD* 252108			
523.	Bimonthly Prog. Rept. (11/16/60–1/15/61) *AD* 252109			
524.	Bimonthly Prog. Rept. (1/15/61–3/15/61) *AD* 255734			
525.	Bimonthly Prog. Rept. (3/16/61–5/15/61) *AD* 270002			
526.	Tech. Rept. No. 1 (9/1/58) *AD* 210686, "On the Theory of Electrochemical and Chemical Electron Transfer Processes," Marcus, R. A.		Fundamental study of electrode processes	NOnr 839(22), ONR/DC 3/61**
527.	Tech. Rept. No. 2 (7/1/59) *AD* 218735, "A Theory of Electron			

List of Contract Reports (Cont.)

Report reference No. in fuel-cell compendium	Report	Contractor	Contract scope	Contract No. and dates
	Transfer Processes at Electrodes," Marcus, R. A.			
528	Tech. Rept. No. 3 (6/15/60) *AD* 239108, "A Theory of Solvent Effects on Electronic Transition," Ooshika, Y.			
529	Tech. Rept. No. 4, Final (3/15/61) *AD* 253491, "Fundamental Study of Electrode Processes and Related Problems," Marcus, R. A.			
530	Proceedings of the Biochemical Fuel Cell Session (9/28/62) *AD* 292163	Power Information Center, University of Pennsylvania Philadelphia, Pa.	Proceedings of Biochemical Fuel Cell Session IAPG, 9/26/62, held at the Rand Corp., Santa Monica, Calif.	DA-36-039-SC-90831, IAPG 9/62
531	Final Rept. (9/1/61-12/31/61) *AD* 283789, "System Analysis of a Regenerative H_2-O_2 Fuel Cell Power Plant," Ching, A. C.	Pratt & Whitney Aircraft 400 Main St., East Hartford, Conn.	Regenerative 500-watt H_2-O_2 fuel cell	DA-36-039-SC-88903, USAERDL/NJ 2/61-1/63
532	1st Quart. Rept. (7/1/61-9/30/61), "Design and Development of H_2-O_2 Fuel Cell Powerplant," Edward, A. E.		Design and development of the 250-watt H_2-O_2 fuel cell	NAS3-1724, NASA/Lewis 6/61-6/62
533	2d Quart. Rept. (1/20/62) (Title same as above), Edwards, A. E.			
534	3d Quart. Rept. (4/20/62) (Title same as above)			
535	Final Rept. (6/15/62) (Title same as above), Latimer, H. J.			
	No reports available.		H_2-O_2 fuel cell for Apollo command module primary electrical power	NAS9-150,*** NASA/Houston 11/61—Act.
536	1st Semiannual Rept. (10/15/59-12/31/59) *AD* 234095, "Research on a 500 Watt Solar Regenerative H_2-O_2 Fuel Cell Power Supply System," Lee, J. M. (All reports are titled the same)		500-watt solar regenerative H_2-O_2 fuel-cell power supply system	DA-36-039-SC-85259, USAERDL/NJ 10/59-10/60
537	2d Semiannual Rept. (1/1/60-6/30/60) *AD* 241839			
538	Final Rept. (10/15/59-10/15/60)			

539........	Final Rept. (10/7/60–10/31/62) *AD* 416507, "Electrochemistry of Films," Enke, C. G.	Princeton University, Department of Chemistry, Princeton, N.J.	Electrochemistry of films	AF–49(638)–973, USAF/OSR/DC 10/60–10/62
			Electrochemistry of films	AF–AFOSR–151–63, USAF/OSR/DC 10/62–?
540........	M.S. thesis in Chem. Eng. (8/62) *AD* 288784, "The Effect of Pulsation on Fuel Cell Performance," Klang, D. R.	Purdue University, Department of Chemical Engineering, Lafayette, Ind.	The effect of pulsation on fuel-cell performance (M.S. thesis)	USAF 10/62
541........	Tech. Rept. No. 1 (9/58) *AD* 208648, "Bibliography and Lit. Review for Li, Na, and K Carbonates," Lorenz, M. R.	Rensselaer Polytechnic Institute, Troy, N.Y.	Electrochemistry of fused carbonates	NOnr 591(10), ONR/DC 11/57—Act.
542........	Tech. Rept. No. 2 (10/58) *AD* 206282, "Thermogravimetric and Corrosion Studies and Phase Equilibria for Li, Na, and K Carbonates," Lorenz, M. R.			
543........	Tech. Rept. No. 3 (8/59) *AD* 226420, "Precise Measurement of Density and Surface Tension at Temperatures up to 1000° C in One Apparatus," Lorenz, M. R.			
544........	Tech. Rept. No. 4 (9/59) *AD* 226419, "O_2 Overpotential in Molten Carbonates," Janz, G. J.			
545........	Tech. Rept. No. 5 (4/60) *AD* 236206, "Solid-Liquid Phase Equilibria for Mixtures of Li, Na, and K Carbonates," Janz, G. J.			
546........	Tech. Rept. No. 6 (8/60) *AD* 244946, "A Dynamic Method for the Dissociation Pressures of Carbonates," Janz, G. J.			
547........	Tech. Rept. No. 7 (8/60) *AD* 245346, "A Capillary Type Conductance Cell for Molten Fluorides, Oxides and Carbonates," Janz, G. J.			
548........	Tech. Rept. No. 8 (8/60) *AD* 245100, "Molten Carbonates, Part IV—Surface Tensions for Li_2Co_3, Na_2Co_3, K_2CO_3 and Na, K/CO_3 Mixtures," Janz, G. J.			
549........	Tech. Rept. No. 9 (8/60) *AD* 245691, "Molten Carbonates, Part V. Densities and Molar Volumes for Li_2CO_3, Na_2CO_3, K_2CO_3 and Na_2CO_3-K_2CO_3 Mixtures," Janz, G. J.			
550........	Tech. Rept. No. 10 (8/60) *AD* 245823, "Molten Carbonates, Part VI. Electrical Conductances of Li_2CO_3, Na_2CO_3, and K_2CO_3," Janz, G. J.			
551........	Tech. Rept. No. 11 (10/60) *AD* 246625, "Molten Carbonates, Part VII. Mechanisms of O_2 Producing Reactions in Molten Carbonate Electrolytes," Janz, G. J.			
552........	Tech. Rept. No. 12 (3/61) *AD* 256280, "Molten Carbonate Electrolytes: Physical Properties, Structures and Mechanism of Electrical Conductance," Janz, G. J.			

List of Contract Reports (Cont.)

Report reference No. in fuel-cell compendium	Report	Contractor	Contract scope	Contract No. and dates
553. . .	Tech. Rept. No. 13 (9/61) *AD* 263953, "The O_2 Electrode in Fused Electrolytes," Janz, G. J.			
554. . .	Tech. Rept. No. 14 (9/62) *AD* 285190, "Molten Carbonates in Electrolytes: Viscosity and Transport Properties," Janz, G. J.			
555. . .	Tech. Rept. No. 15 (9/62) *AD* 285649, "High Temperature Heat Content and Related Properties for Li_2CO_3, Na_2CO_3, K_2CO_3 and the Ternary Eutectic Mixtures," Janz, G. J.			
556.	Tech. Rept. No. 16 (10/62) *AD* 289005, "Corrosion Studies in Molten Alkali Carbonates: Part I. Silver Metal," Janz, G. J.			
557. . .	Scientific Rept. No. 1 (7/18/62) *AD* 284809, "Theoretical Analysis of Electrochem. Energy Conversion Systems," Greene, S. B.			AF19(604)–8377, USAF/Mass. 6/62–9/62
558. . .	Scientific Rept. No. 2 (9/25/62), "Electrochemical Behavior of a Pd H_2 Diff. Electrode," Lederer, L.			
559.	Scientific Rept. No. 4 (12/15/64) *AD* 608839, "Electrochemical Energy Conversion in a Palladium Hydrogen Diffusion Electrode," Cleary, H. J.*			
560.	Final Rept. (12/15/64) *AD* 609718, "Investigation of the Fundamental Electrochemical Parameters Influencing Fuel Cell Performance," Greene, N. D.			
561.	WADC Tech. Rept. 59–780 (11/60), "Organic Fuel Cell System," Baum, G. A.	Resin Research Laboratories, Inc., Newark, N.J.	An organic fuel cell	AF33(616)–6399, USAF/WP 6/59–6/60
562.	"Novel Power Sources for Shelters," Lauck, F. W.	Smith, A. O., Corp., Long Range Research Lab., Milwaukee, Wis.	Novel power sources for shelters	OCD–OS–62–243, OCD/DC 7/63–3/64
563. . .	"Theory of Electrochemical Cell Reactions, Part II, Vol. II, Irreversible Processes," Crispino, P. A. P., *AD* 62402	Snell, Foster D., Inc., 29 West 15th St., New York 11, N.Y.	Theory of electrochemical cell reactions	DA–36–039–SC–15545, USAERDL/NJ 4/54–4/55*
564. . .	"Theory of Electrochemical Cell Reactions, Part III, Alkaline Electrolytes," Crispino, P. A. P., *AD* 84398			
565. . .	"Electrochemical Cells with Alkaline Electrolytes (cont.), Part IV," Crispino, P. A. P., *AD* 124271		Theory of electrochemical cell reactions	DA–36–039–SC– USAERDL/NJ 4/56*
566. . .	"Theory of Electrochemical Cell Reactions, Vol. V, Part III, Alkaline Electrolytes," Crispino, P. A. P., *AD* 147110			

567.	"Theory of Electrochemical Cell Reactions, Part III, Vol. VI, Alkaline Electrolytes," Crispino, P. A. P.		Theory of electrochemical cell reactions	DA-36-039-SC-73137, USAERDL/NJ 4/58*
568.	Final Rept. (1/1/63–9/30/63), "Study of the General Properties of Some Mineral Ion Exchange Membranes as Well as Their Possible Use in Low Temperature Fuel Cells"	Societe d'Etudes de Recherches et d'Applications Pour l'Industrie, Brussels, Belgium	Study of the general properties of some mineral ion exchange membranes as well as their possible use in low-temperature fuel cells	DA-91-591-EUC-2773, USDA/ERO 10/63*
569.	Rept. No. 1 (7/1/60–9/30/60) *AD* 250821, "Development of Electrode Materials for Fuel Cells" (All reports are titled the same)	Speer Carbon Co., Inc., Research Laboratory, Niagara Falls, N.Y.	Electrode materials for fuel cells	DA-36-039-SC-85356, USAERDL/NJ 6/60–6/62
570.	Rept. No. 2 (10/1/60–12/31/60) *AD* 254459			
571.	Rept. No. 3 (1/1/61–3/31/61) *AD* 260120			
572.	Rept. No. 4 (4/1/61–6/30/61) *AD* 265346			
573.	Rept. No. 5, Final (6/30/60–9/30/61)			
574. .	Rept. No. 1 (3/1/62–5/31/62) *AD* 284521, "Fuel Cell Electrode Materials" (All reports are titled the same)		Electrode materials for fuel cells	DA-36-039-SC-88954, USAERDL/NJ 6/62–6/63
575.	Rept. No. 2 (6/1/62–8/31/62) *AD* 293490			
576.	Rept. No. 3 (9/1/62–11/30/62) *AD* 298246			
577.	Rept. No. 4, Final (3/1/62–2/28/63) *AD* 410993			
578. .	Final Rept. AFCRC TR-60-223 (4/1/58–12/31/59), "Photochemistry in the Solar Furnace," Marcus, R. J.*	Stanford Research Institute, Menlo Park, Calif.	Photochemistry in the solar furnace	AF19(604)3477, USAF/Mass. 4/58–12/59
579.	Scientific Rept. No. 1, AFCRL TN-60-639 (8/15/60) *AD* 242972, "Photochemical Systems for Solar Energy Conversion—Nitrosyl Chloride," Marcus, R. J.		Photochemical systems for solar energy conversion	AF19(604)7302, USAF/Mass. 3/60–6/62
580.	Scientific Rept. No. 2, AFCRL 254 (2/3/61) *AD* 254801, "Photochemistry in the Solar Furnace-Flow Systems and the Decomposition of Nitrosyl Chloride," Marcus, R. J.			
581.	Scientific Rept. No. 3, AFCRL 62-256 (2/7/62) *AD* 273662, "The Effect of Concentrated Light on Photochemical Energy Conversion by NOCl Solutions," Marcus, R. J.			
582.	Final Rept. AFCRL 62-687 (3/15/60–6/30/62) *AD* 282502, "Photochemical Flow Systems in the Solar Furnace," Marcus, R. J.			

List of Contract Reports (Cont.)

Report reference No. in fuel-cell compendium	Report	Contractor	Contract scope	Contract No. and dates
583	WADD Tech. Rept. 60–821, Part I (4/59–10/60) *AD* 257898, "A Nitrosyl Chloride Solar Regenerative Fuel Cell System," McKee, W. E.	Sundstrand Turbo Division, Sundstrand Machine Tool Co., Pacoima, Calif.	A solar regenerative fuel cell	AF33(616)–6585 USAF/WP 4/59–5/61
584	WADD Tech. Rept. 60–821, Part II (10/60–5/61) (Title same as above)			
585	Final Rept. (6/30/62) *AD* 285656L, "High Temperature Fuel Cell Systems"	Surface Processes Research & Development Corp., Country Club Road, Dallas, Pa.	Status of high-temperature fuel-cell research and development	DA–44–009–ENG–4944, USAERDL/Va. 2/62–6/63
586	Final Rept. (4/10/62), "Electrochemical Oxidation of Ethane, Propane and Isobutane in Low Temperature Fuel Cells"		Electrochemical oxidation of low molecular weight hydrocarbons	DA–44–009–ENG–4917, USAERDL/Va. 11/61–1/64
587	"The Electrochemical Oxidation of Liquid Hydrocarbons in Low Temperature Fuel Cells" (2/26/62)		Electrochemical oxidation of gasoline and liquid hydrocarbon components in a low-temperature fuel cell	DA–44–009–ENG–4864, USAERDL/Va. 10/61–4/62
588	Final Rept. (11/62) *AD* 298141, "Catalyst and Electrode Structure Development for Hydrocarbon Fuel Cells"		Catalyst and electrode structure development for hydrocarbon fuel cells	DA–44–009–ENG–5090, USAERDL/Va. 5/62–10/62
589	Quart. Letter Rept. (10/10/63)		Electrochemical oxidation of hydrocarbons in low-temperature fuel cells	DA–44–009–AMC–56(T), USAERDL/Va. 11/62–9/64
590	WADD Tech. Rept. 60–442 (5/60), "Regenerative Fuel Cell	TAPCO, division of	Nuclear regenerative	AF33(600)–39573,

	System Investigation," Fuscoe, J. M.*	Thompson Ramo Wooldridge, Inc., 7209 Platt Ave., Cleveland 4, Ohio	fuel cell	USAF/WP 6/59–3/62
591	Tech. Doc. Rept. No. ASD–TDR–62–18 (4/62) *AD* 277805 (Title same as above)			
592	Tech. Doc. Rept. No. ASD–TDR–62–240 (6/62) *AD* 284474, "Zero Gravity Separator Development for Regenerative Fuel Cell," Stromquist, A. J.		Electrode development program	AF33(600)–42449, USAF/WP 1/61–8/61
593	Tech. Doc. Rept. No. ASD–TDR–62–241 (6/62) *AD* 284434, "Electrode Development Program," Carlton, S. S.			
594	Monthly Prog. Rept. No. 1 (7/62), "Development of the Dual Membrane Fuel Cell" (All reports are titled the same)			
595	Monthly Prog. Rept. No. 2 (8/62)			
596	Monthly Prog. Rept. No. 3 (9/62)			
597	Monthly Prog. Rept. No. 4 (10/62)			
598	Monthly Prog. Rept. No. 5 (11/62)			
599	Monthly Prog. Rept. No. 6 (12/62)			
600	Monthly Prog. Rept. No. 7 (1/63)			
601	Monthly Prog. Rept. No. 8 (2/63)			
602	Monthly Prog. Rept. No. 9 (3/63)			
603	Monthly Prog. Rept. No. 10 (4/63)			
604	Monthly Prog. Rept. No. 11 (5/63)			
605	Final Rept. (6/30/62–12/15/63)			
606	Quart. Prog. Rept. (2/15/63–5/15/63) *AD* 405571, "Molten-Carbonate Fuel Battery Program" (All reports are titled the same)	Texas Instruments, Inc., 13500 North Central Exp., Dallas 22, Tex.	Study of molten carbonate hydrocarbon-air fuel cells and delivery of a 400-watt module	DA–44–009–AMC–54(T), USAERDL/Va. 2/63—Act.
607	Tech. Summary Rept. (2/15/63–8/15/63) *AD* 416422			
608	2d Quart. Prog. Rept. (8/16/63–11/15/63)			
609	Final Rept. (2/15/63–2/15/64) *AD* 450397, "Molten-Carbonate Fuel Battery Program, Task I"			
610	Tech. Sum. Rept. (7/1/64–10/23/64) *AD* 452636, "Extended Molten-Carbonate Fuel Cell System Program," Truitt, J. K.			
611	2d Quart. Prog. Rept. (10/24/64–1/1/65) *AD* 460354 (Title same as above)			
612	Final Tech. Rept. (7/1/64–2/15/65) *AD* 463008 (Title same as above), Tasks II, III, and IV			
613	1st Semiannual Rept. (1/10/62–7/10/62) *AD* 283653, "Study of the Oxygen Electrode Mechanism," Schmid, G. M.	Tracor, Inc., 1701 Guadalupe St., Austin, Tex.	Effect of mass transport parameters of O_2 electrodes	DA–36–039–SC–89159, USAERDL/NJ 1/62–5/64
614	Rept. No. 2 (7/10/62–1/9/63) *AD* 299063 (Title same as above), Hurd, R. M.*			
615	3d Semiannual Rept. (1/10/63–7/9/63) *AD* 415090			

List of Contract Reports (Cont.)

Report reference No. in fuel-cell compendium	Report	Contractor	Contract scope	Contract No. and [illegible]
	(Title same as above), Wrotenbery, P. T.*			
616	Rept. No. 4, Final (1/1/62–12/31/63) *AD* 437157 (Title same as above), Hurd, R. M.			
617	Quart. Rept. No. 1 (9/20/61–12/31/61) *AD* 270302, "Research Relating to Fuel Cells," Shamsul Huq, A. K. M.	Tyco Laboratories, Inc., Bear Hill, Waltham 54, Mass.	O_2 electrode studies	DA–49–186–ORD–982, HDL 9/61–8/64
618	Quart. Rept. No. 2 (1/1/62–3/30/62) *AD* 275416 (Title same as above)			
619	Final and Summary Rept. (10/1/62–6/30/64) (Title same as above), Makrides, A. C.			
620	Quart. Prog. Rept. No. 1 (1/63) *AD* 298119, "H_5 Diffusion Electrode," Makrides, A. C.			
621	Quart. Prog. Rept. No. 2 (1/1/63–3/31/63) *AD* 409320 (Title same as above)			
622	Quart. Prog. Rept. No. 3 (4/1/63–6/30/63) *AD* 285658 (Title same as above)			
623	Quart. Prog. Rept. No. 4 (7/1/63–9/30/63) *AD* 290803 (Title same as above)			
624	Quart. Prog. Rept. No. 5 (Title same as above)			
625	Final Rept. (10/1/61–2/28/63) *AD* 414800, "The O_2 Reaction on Pt and Au in Acid Solutions," Shamsul Huq, A. K. M.			
626	1st Semiannual Tech. Sum. Rept. (10/30/62) *AD* 287665, "Electrochemistry of Fuel Cell Electrodes," Makrides, A. C.		Electrochemistry of fuel-cell electrodes	NOnr 3765(00), ONR/DC 4/62—Act.
627	Tech. Memo. No. 1 (4/1/63) *AD* 411167, "Electrochemistry of Fuel Cell Electrodes: The H_2 Evolution Reaction of NiSi, NiAs, NiSb, NiS, $NiTe_2$ and Their Constituent Elements," Shamsul Huq, A. K. M.			
628	Tech. Memo. No. 2 (4/1/63) *AD* 411166, "Electrochemistry of Fuel Cell Electrodes: Kinetics of Redox Reactions on Passive Electrodes," Makrides, A. C.			
629	Tech. Memo. No. 3 (4/1/63) *AD* 411165, "Electrochemistry of Fuel Cell Electrodes—Electrochemistry Behavior of Ni Compounds—II. Anodic Dissolution and O_2 Reduction in Perchlorate Solutions," Shamsul Huq, A. K. M.*			
630	Tech. Memo. No. 4 (6/63) *AD* 411164, "Electrochemistry of Fuel Cell Electrodes: Kinetics of the Fe^{3+}/Fe^{2+} Reaction on Fe-Cr Alloys," Makrides, A. C.			

631..	Tech. Memo. No. 6 (10/63) *AD* 423991, "Electrochemistry of Fuel Cell Electrodes," Brummer, S. B.*			
632..	Tech. Memo. No. 7 (10/63) *AD* 423992, "Electrochemistry of Fuel Cell Electrodes—H_2 Evolution at Dilute Pt and Pd Amalgam Electrodes," Butler, J. N.*			
633..	Tech. Memo. No. 8 (11/63) *AD* 424479, "Adsorption and Oxidation of HCOOH on Smooth Pt Electrodes in $HClO_4$ Solutions," Brummer, S. B.*			
634..	Tech. Memo. No. 9 (1/64) *AD* 428228, "Electrochemistry of Fuel Cell Electrodes—Activity Coefficients of Liquid Indium Hg Amalgam at 25° C," Butler, J. N.			
635..	Tech. Memo. No. 10 (2/64) *AD* 433655, "H_2 Evolution at a Dropping Indium Amalgam Electrode," Butler, J. N.			
636..	Semiannual Tech. Summary Rept. (3/30/64) *AD* 438821, "Electrochemistry of Fuel Cell Electrodes," Makrides, A. C.			
637..	Tech. Memo. No. 11 (4/64) *AD* 440751, "Electrochemistry of Fuel Cell Electrodes—H_2 Evolution at a Solid Indium Electrode," Butler, J. N.*			
638..	Tech. Memo. No. 12 (5/64) *AD* 441919, "Electrochemistry of Fuel Cell Electrodes—Computer Programs for Calculations Relating to Dropping Amalgam Electrodes," Butler, J. N.			
639..	Tech. Memo. No. 13 (8/64) *AD* 445787, "The Use of Large Anodic Galvanostatic Transients to Evaluate the Maximum Adsorption on Pt from HCOOH Solutions," Brummer, S. B.			
640..	Tech. Memo. No. 14 (8/64) *AD* 446423, "Electrochemistry of Fuel Cell Electrodes—(a) Galvanostatic Studies on CO Adsorption on Pt Electrodes; (b) Comparison of Adsorbed Formic Acid and CO on Pt Electrodes," Brummer, S. B.			
641..	Tech. Memo. No. 15 (9/64) *AD* 448933, "Electrochemistry of Fuel Cell Electrodes—The Electrical Double Layer on Indium Amalgams in 0.1 *M* $HClO_4$ at 25° C," Butler, J. N.			
642..	Semiannual Tech. Sum. Rept. (9/30/64) *AD* 606347, "Electrochemistry of Fuel Cell Electrodes," Makrides, A. C.			
643..	Tech. Memo. No. 16 (10/64) *AD* 450685, "Electrochemistry of Fuel Cell Electrodes—The Electrical Double Layer on Thallium Amalgam Electrodes," Butler, J. N.			
644..	Semiannual Tech. Sum. Rept. (3/30/65) *AD* 461759, "Electrochemistry of Fuel Cell Electrodes," Makrides, A. C.			
645..	Tech. Memo. No. 18 (3/65) *AD* 461760, "Temperature Dependence of H_2 Overvoltage on Indium Amalgams," Butler, J. N.*			
646..	Tech. Memo. No. 19 (4/65) *AD* 462038, "Interfacial Tension of Indium Amalgams on 0.1 *M* $HClO_4$ at 25° C," Butler, J. N.			
647..	1st Quart. Letter Rept. (7/16/61) *AD* 265508, "Electrochemistry of Fuel Cell Electrodes" (All reports are titled the same)		Electrochemistry of fuel-cell reactions	NObs-84770, USN/BuShips 5/61–3/62

List of Contract Reports (Cont.)

Report reference No. in fuel-cell compendium	Report	Contractor	Contract scope	Contract No. and dates
48.	Semiannual Tech. Sum. Rept. (10/31/61) *AD* 278443, "Electrochemistry of Fuel Cell Electrodes," Rosenberg, A. J.			
49.	2d Quart. Letter Rept. (1/15/62) *AD* 278496			
50.	Final Tech. Sum. Rept. (4/27/62)			
51.	Report No. ASD-TDR-62-1044 (4/61-12/62) *AD* 271971 "Carbon Electrode Fuel Cell"	Union Carbide Corp., Parma Research Laboratory, Cleveland, Ohio	Carbon electrode fuel-cell	AF33(616)-7256 SA/5, USAF/WP 4/61-2/63
52.	Report No. ASD-TDR-61-342 (3/63) *AD* 403890 (Title same as above)			
53	Final Rept. (7/1/60-2/28/61) *AD* 413795, "Low Temperature Fuel Cell Battery," Schumacher, E. A.*		Low-temperature fuel-cell battery	DA-36-039-SC-78367, USAERDL/NJ 7/60-8/63
54	Quart. Rept. No. 7 (2/28/62), "H_2-O_2 Prototype Fuel Cell," Litz, L. M.* (All reports are titled the same)		H_2-O_2 fuel cell	NObs-78633, USN/BuShips 6/60-3/64
55.	Quart. Rept. No. 8 (6/1/62)			
56.	Quart. Rept. No. 9 (9/1/62)			
57.	Quart. Rept. No. 10 (12/1/62)			
58.	Quart. Rept. No. 11 (3/1/63)			
59.	Quart. Rept. No. 12 (6/1/63)			
60.	Quart. Rept. No. 13 (9/1/63)			
61.	Quart. Rept. No. 15 (3/1/64)			
62	Final Rept. (5/24/63) *AD* 422728, "Nuclear Regenerative Fuel Cell"		Nuclear regenerative fuel cell, 5 watts	NObs-78828, USN/BuShips 6/60-9/62
63	1st Quart. Rept. (6/1/63-9/1/63) *AD* 425031, "Thin Fuel Cell Electrodes," Kordesch, K. V. (All reports are titled the same)		Fuel-cell electrode materials	DA-36-039-AMC-02314(E), USAERDL/NJ 5/63—Act.
64	2d Quart. Rept. (9/1/63-12/1/63) *AD* 430802			
65	3d Quart. Rept. (12/1/63-3/1/64) *AD* 600951			
66	Final Rept. (6/1/63-5/31/64) *AD* 615160			
67	1st Quart. Rept. (7/1/63-9/30/63), "Study Program to Improve Fuel Cell Performance by Pulsing Techniques," Kronenberg, M. L.		Study program to improve fuel-cell	NAS3-2752, NASA/Lewis

	(All reports are titled the same)		performance by pulsing technique	
668.	2d Quart. Rept. (10/1/63–12/31/63)			
669.	3d Quart. Rept. (1/2/64–3/31/64)			
670.	Final Rept. (6/28/64), Kronenberg, M. L., and Kordesch, K. V.			
671.	Final Rept. (1/15/59–10/10/60), "Magnesium Anode as a Power and H_2 Source in Sea Water," Zimmerman, H. M.		Magnesium anode as a power and hydrogen source in sea water	NObs-77055, USN/BuShips 1/59–10/60
672.	Rept. No. RADC-TR-60-251 (10/25/60) *AD* 248204, "Fuel Cell Investigation," Vinal, A. F.*		Fuel-cell investigation	AF-30(602)-2199, USAF/Griffiss 10/60**
673.	Tech. Rept. No. 1 (5/15/63) *AD* 423570, "Transport Processes in Electrode Systems—Investigations of Ionic Diffusion and Migration by a Rotating Disk Electrode," Gordon, S. L.	University of California, Dept. of Chemistry and Chemical Engineering, Berkeley 4, Calif.	Physical aspects of electrode phenomena	DA-36-039-SC-89153, USAERDL/NJ 3/62—Act.
674.	Tech. Rept. No. 2 (12/1/63) *AD* 426444, "Transport Processes in Electrode Systems—The Effect of Buoyancy Forces on Forced Convection Ionic Mass Transfer at Horizontal Planar Electrodes," Hickman, R. G.			
675.	Tech. Rept. No. 3 (6/1/64) *AD* 602701, "Transport Processes in Electrode Systems," Bennion, D. N.			
676.	Semiannual Status Rept. (9/1/63–2/29/64), "Dynamic Behavior of Porous Electrode Systems," Tobias, C. W.*		Research on the dynamic behavior of porous electrode systems	NSG-150-61, NASA/DC 7/61–7/64
677.	Ph. D. thesis, Edward A. Grens II, "Dynamic Analysis of a One-Dimensional Porous Electrode Model" (9/63)			
678.	Quart. Prog. Rept. (1/1/60–3/31/60), "Fuel Cells"	University of Florida, P.O. Box 3027, University Station, Gainesville, Fla.	Fuel-cell research	DAI-49-186-502-ORD(P)-860, HDL 2/60–8/64
679.	Special Report No. 1 (3/18/60), "Fuel Cells—Hydrocarbon Regeneration of the Anolyte in a Redox Fuel Cell"			
680.	Special Rept. No. 2 (6/15/60), "Fuel Cells—Preliminary Calculations of the Regeneration and Recovery Requirements for a Bromide-Bromine Electrode for a Redox Fuel Cell"			
681.	Quart. Prog. Rept. (4/1/60–6/30/60), "Fuel Cells"			
682.	Summ. Rept. No. 3 (4/26/62) *AD* 275013, "Hydrocarbon Regeneration of the Anolyte in a Redox Fuel Cell System: *n*-Hexane, *n*-Hexanol," Mailen, J. C.			
683.	Summ. Rept. No. 4 (1/31/62), "Fuel Cells—Feasibility Study of Redox Fuel Cell Without Separator"			
684.	Quart. Prog. Rept. (4/1/62–6/30/62), "Fuel Cells"			
685.	Quart. Prog. Rept. (7/1/62–9/30/62), "Fuel Cells"			
686.	Summ. Rept. No. 5 (10/1/62) *AD* 287055, "Fuel Cells—A Feasibility Study of Pd as a H_2 Diffusion Electrode Material for Fuel Cells"			

List of Contract Reports (Cont.)

Report reference No. in fuel-cell compendium	Report	Contractor	Contract scope	Contract No. and dates
687.	Summ. Rept. No. 6 (12/15/62) *AD* 293849, "Fuel Cells—A Study of the Contribution of Surface Flow to Mass Transport in Porous Gas Diffusion Electrodes"			
688.	Quart. Prog. Rept. (10/1/62–12/31/62), "Fuel Cells"			
689.	Summ. Rept. No. 7 (2/8/63), "Fuel Cells—The Current Density Supportable by Mass Transport at Submerged Electrodes"			
690.	Summ. Rept. No. 8 (3/15/63) *AD* 411266, "Fuel Cells—I. Mass Transfer Through a Single Cylindrical Pore to a Semi-Infinite Reactive Annulus"			
691.	Summ. Rept. No. 9 (3/15/63) *AD* 410332, "Fuel Cells—Section II"			
692.	M.S. thesis, Reneke, W. E., "Air Regeneration of Bromine-Bromide Fuel Cell Catholyte"			
693.	Summ. Rept. No. 10 (5/24/63), "Fuel Cells—Section III"		Fuel-cell research	DA–49–186–AMC–45(X), HDL 5/63–6/64*
694.	Quart. Prog. Rept. (4/1/63–6/30/63), "Fuel Cells"			
695.	Summ. Rept. No. 11 (7/26/63) *AD* 434196, "Fuel Cells—A Review of Fuel Cell Construction," Gubbins, K. E.			
696.	Quart. Prog. Rept. (7/1/63–9/30/63), "Fuel Cells," Walker, R. D., Jr. (All reports are titled the same)			
697.	Quart. Prog. Rept. (10/1/63–12/31/63) *AD* 446698			
698.	Quart. Prog. Rept. (1/1/64–3/31/64)			
699.	Quart. Prog. Rept. (4/1/64–6/30/64) *AD* 453304			
700.	Quart. Prog. Rept. (7/1/64–9/20/64) *AD* 453305			
701.	Prog. Rept. No. 1 (10/1/61–3/31/62), "Electrochemistry of Fused Salts," Laitinen, H. A.*	University of Illinois, Chemistry Department, Urbana, Ill.	Electrochemistry of fused salts	DA–ARO(D)–31–124–G204, ARO/Durham 10/61–10/62
702.	Prog. Rept. No. 2 (4/1/62–9/30/62) (Title same as above)			
703.	Prog. Rept. No. 3 (10/1/62–3/31/63), "Electrochemistry of Fused Salts," Laitinen, H. A. (All reports are titled the same)		Electrochemistry of fused salts	DA–31–124–ARO(D)–55, ARO/Durham 10/62—Act.
704.	Prog. Rept. No. 4 (4/1/63–9/30/63)			
705.	Prog. Rept. No. 5 (10/1/63–3/31/64)			
706.	Status Rept. No. 1 (10/1/55–1/1/56), "Electrochemistry of Fused Salts," Laitinen, H. A.* (All reports are titled the same)		Electrochemistry of fused salts	DA–11–022–ORD–1987, ? 10/55–9/61

707.	Status Rept. No. 2 (1/1/56–4/1/56)			
708.	Status Rept. No. 5 (10/1/56–12/31/56)			
709.	Status Rept. No. 8 (7/1/57–9/30/57)			
710.	Status Rept. No. 9 (10/1/57–12/31/57)			
711.	Status Rept. No. 10 (1/1/58–3/31/58)			
712.	Status Rept. No. 12 (7/1/58–9/30/58)			
713.	Status Rept. No. 13 (10/1/58–12/31/58)			
714.	Status Rept. No. 14 (1/1/59–3/31/59)			
715.	Status Rept. No. 15 (4/1/59–6/30/59)			
716.	Status Rept. No. 16 (7/1/59–9/30/59)			
717.	Status Rept. No. 17 (10/1/59–12/31/59)			
718.	Status Rept. No. 18 (1/1/60–3/31/60)			
719.	Status Rept. No. 19 (4/1/60–6/30/60)			
720.	Status Rept. No. 20 (7/1/60–9/30/60)			
721.	Status Rept. No. 21 (10/1/60–12/31/60)			
722.	Status Rept. No. 22 (1/1/61–3/31/61)			
723.	Status Rept. No. 23 (4/1/61–6/30/61)			
724.	Final Rept. (10/1/55–9/30/61)			
725.	No. AEDC–TDR–62–18 (1/62) *AD* 270480, "Energies of Interaction Between Gases and Various Surfaces," Huang, [illegible] B.		Energies of interaction between gases and various surfaces	AF40(600)–909, USAF/AEDC 1/62**
726	"Survey and Evaluation of Power Sources Systems, Part V—Chemical Components (Batteries)" (9/15/53–12/1/55) *AD* [illegible]133[illegible]	University of Minnesota, Minneapolis, Minn.	Survey and evaluation of power source systems	DA–36–039–SC–56649, USAERDL/NJ 9/53–6/55
727.	Rept. No. 1 (11/1/61–1/31/62) *AD* 275811, "Reversible O_2 Electrode" (All reports are titled the same)	University of Pennsylvania, The Electrochemistry Laboratory, Philadelphia 4, Pa.	Reversible O_2 electrode	DA–36–039–SC–88921, USAERDL/NJ 11/61—Act.
728.	Rept. No. 2 (2/1/62–4/30/62) *AD* 282922, Devanathan, M. A. V.			
729.	Rept. No. 3 (5/1/62–7/31/62) *AD* 291763			
730.	Rept. No. 4 (8/1/62–10/31/62) *AD* 405675, Damjanovic, A.*			
731.	Rept. No. 5 (1/1/63–3/31/63) *AD* 417857			
732.	Rept. No. 6 (4/1/63–6/30/63) *AD* 423021			
733.	Rept. No. 7 (7/1/63–9/30/63) *AD* 431148			
734.	Rept. No. 8 (10/1/63–12/31/63) *AD* 438512			
735.	Rept. No. 9 (1/1/64–3/31/64) *AD* 603411			
736.	11th Quart. Rept. (7/1/64–9/30/64) *AD* 459568			
737.	1st Semiannual Progress Rept. (10/1/62–3/31/63), "Studies of the Fundamental Chemistry, Properties and Behavior of Fuel Cells," Bockris, J. O'M. (All reports are titled the same)		Chemistry of fuel-cell reactions	NsG–325, NASA/DC 10/62—Act.

List of Contract Reports (Cont.)

Report reference No. in fuel-cell compendium	Report	Contractor	Contract scope	Contract No. and dates
738	2d Semiannual Progress Rept. (4/1/63–9/30/63)			
739	Semiannual Progress Rept. (3/1/64–9/30/64)			
740	Prog. Rept. No. 1 (11/15/62)	University of Pennsylvania, Towne Building, Philadelphia 4, Pa.	Research in the conversion of various forms of energy by unconventional techniques	NsG316, NASA/DC 7/62—Act.
741	Status Rept. as of Oct. 1963, Inst. for Direct Energy Conversion			
742	Status Rept. as of Jan. 1964, Inst. for Direct Energy Conversion			
743	Status Rept. INDEC-SR-5 (1/4/65)			
744	Final Tech. Rept. FTR-2 (1/1/59–1/31/60) *AD* 238708	University of Rome, Rome, Italy	Chemisorption and catalysis studies on metal oxides	DA-91-591-EUC-1057, USDA/ERO?
745	Tech. Note, RADC-TN-60-118 (7/60) *AD* 241034, "Fuel Cell Systems," McCormick, J. E.	U.S. Air Force, Rome Air Development Center, Air Research and Development Command, Griffiss Air Force Base, N.Y.	Fuel-cell systems	USAF/Griffiss 7/60*
746	Eng. Rept. No. E-1163 (1/1/56) *AD* 95841, "Galvanic Fuel Cells," Kornfeil, F.	U.S. Army Electronics, Research and Development Laboratory, Fort Monmouth, N.J.	Fuel-cell systems	?USAERDL/NJ ?—Act.
747	USASRDL Tech. Rept. 2001 (12/15/58) *AD* 219732, "Investigation of the H_2-O_2 Fuel Cell," Hunger, H.			
748	LTIS Bibliography No. 1 (11/59) *AD* 231326, "Bibliography on Unconventional Sources of Electrical Power," Forlini, J. B.	U.S. Army Engineers, Research and Development Laboratories, Fort Belvoir, Va.	Bibliography on unconventional sources of electrical power	USAERDL/Va. 11/59–1/61*
749	LTIS Bibliography No. 5 (1/61) *AD* 248615, "Supplement to LTIS Bibliography No. 1," Forlini, J. B.			
750	ARO Rept. No. 1 (6/59), "Status Report on Fuel Cells," Stein, B. R.	U.S. Army Research Office,	Fuel-cell status reports	ARO/DC and USAERDL/NJ
751	2d Status Rept. on Fuel Cells (12/60), ARO Rept. No. 2, Stein, B. R.			

752	3d Status Rept. on Fuel Cells (6/1/62), Hunger, H.	Washington, D.C., and USAERDL/NJ		6/59-12/60*
753	4th Status Report on Fuel Cells, Frank, F. R. (by USAERDL)			
754	NRL Rept. 5561 (11/3/60) *AD* 247708, "The Ag-AgO Electrode, Part I—Anodic Oxidation in Alkaline Solutions," Wales, C. P.	U.S. Naval Research Laboratory, Code 6160, Washington 25, D.C.	Fuel cells—electrode processes	PO-1-0001, USN/BuShips 7/60—Act.
755	NRL Rept. 5596 (3/21/61) *AD* 254667, "H_2 Overpotential, Part I—Characteristic Functions and Parameters in the Theory of H_2 Overpotential," Castellan, G. W.			
756	NRL Rept. 5597 (3/21/61) *AD* 254668, "H_2 Overpotential, Part II—Interpretation of Some Measurements of H_2 Overpotential on Pd," Castellan, G. W.			
757	NRL Rept. 5999 (9/30/63), "The Pd/O_2 Electrode in Sulfuric Acid Solution," Schuldiner, S.*			
758	NRL Rept. 6136 (9/4/64), "Investigations of the Kinetics of H_2 and O_2 Reactions on a Pt Electrode in Acid Solution Using Pulse and Decay Techniques," Schuldiner, S., and Warner, T. B.			
759	NRL Rept. 5998 (10/4/63), "Experiments With a Mg Seawater Cell Incorporating a Bacterial Colonized Cathode," Wilson, B. J.	U.S. Naval Research Laboratory Code 5230, Washington 25, D.C.	Mg seawater battery with bacterial assisted cathode	SF 013-06-29, USN/BuShips 7/61-2/64
760	M.S. thesis (1963) *AD* 417216, "The Measurement of Short Transients in a Fused Salt Electrolytic Reaction," Veaga, R. A. de la	Washington State University, Pullman, Wash.	Measurement of short transients in a fused salt electrolytic reaction	?, USAF/? 63*
761	Tech. Rept. No. 1 (12/15/51), "The Study of the Kinetics of the H_2, O_2 and Related Electrodes," Yeager, E.*	Western Reserve University, Department of Chemistry, Cleveland, Ohio	The O_2 electrode	NOnr 581(00), ONR/DC 3/53-10/54*
762	Tech. Rept. No. 2 (3/15/53) *AD* 7654, "The Cathodic Polarization Associated with the Oxygen Electrode," Yeager, E.*			
763	Tech. Rept. No. 3 (4/1/53) *AD* 7512, "The Electrochemical Properties of Dilute Sodium Amalgams," Dietrick, H.			
764	Tech. Rept. No. 4 (8/1/54), "The O_2 Electrode," Witherspoon, R. R. *			
765	Tech. Rept. No. 6 (8/1/56) *AD* 104135, "The Study of the O_2 Electrode With Isotopic Techniques," Davies, M. O.			
766	Tech. Rept. No. 7 (6/1/57) *AD* 138849, "The Physical and Chemical Properties of Dilute Alkali Metal Amalgams—Part I. Physical Properties," Davies, M. O.*			
767	Tech. Rept. No. 8 (2/1/58) *AD* 159561, "The Anodic and Cathodic Properties and the Chlorine Electrode," Aylward, J.			
768	Tech. Rept. No. 9 (4/15/58) *AD* 203573, "The Electrochemistry of Ni: I. Codeposition of Ni and H_2 From Simple Aqueous Solutions," Yeager, E.*			

List of Contract Reports (Cont.)

Report reference No. in fuel-cell compendium	Report	Contractor	Contract scope	Contract No. and dates
769	"The Kinetics of the O_2 Electrode on Active Carbon," Davies, M. O. *AD* 74373			
770	Tech. Rept. No. 10 (12/1/58) *AD* 209152, "A Review of the State of the Art and Future Trends in Fuel Cell Systems, Yeager, E.		Kinetics of electrode processes	NOnr 2391(00), ONR/DC 8/51—Act.
771	Tech. Rept. No. 11 (11/15/59), "The O_2 Electrode on Carbon Surfaces," Davies, M. O.*			
772	Tech. Rept. No. 12 (8/1/60) *AD* 240883, "The O_2 Electrode in Aqueous Fuel Cells," Yeager, E.			
773	Tech. Rept. No. 13 (9/1/60) *AD* 246363, "The Measurement of Polarization," Yeager E.			
774	Tech. Rept. No. 14 (11/60) *AD* 248803, "The Sodium Amalgam-Oxygen Continuous Feed Cell," Yeager, E.			
775	Tech. Rept. No. 15 (8/15/62) *AD* 289213, "The Electrochemistry of Ni, II. Anodic Polarization of Ni," Kronenberg, M. L.*			
776	Tech. Rept. No. 16 (6/15/63) *AD* 409121, "The Kinetics of the O_2-Peroxide Couple on Carbon," Yeager, E.			
777	Tech. Rept. No. 17 (1/15/64) *AD* 429248, "Kinetic Factors in the Fuel Cell System: The O_2 Electrode," Yeager, E.			
778	Tech. Rept. No. 20 (7/15/63) *AD* 609294, "The Physical and Chemical Properties of Dilute Alkali Metal Amalgams—A Review—Part II. Chemical Properties and Structures," Davies, M. O.*			
779	Tech. Rept. No. 20 (12/1/58) *AD* 207675, "Quantitative Studies of Colloidal Vibration Potentials," Dereska, J.*		Fundamental and processing applications for sound waves in chemistry	NOnr 1439(04), ONR/DC 7/61**
780	Tech. Rept. No. 21 (12/1/58) *AD* 229511, "A.C. Streaming Potentials," Galperin, I.			
781	Tech. Rept. No. 22 (4/1/59) *AD* 219279, "Acousto-Electrochemical Effects in Electrode Systems," Yeager, E.			
782	Tech. Rept. No. 23 (12/1/60) *AD* 256870, "Colloidal Vibration Potentials in Silica Suspensions"			
783	Tech. Rept. No. 24 (7/1/61) *AD* 261641, "Fundamental and Processing Applications for Sound Waves in Chemistry," Yeager, E.			
784	Tech. Rept. No. 25 (7/1/62) *AD* 282814, "Ultrasonic Relaxation in Electrolytic Solutions: I. A Review"			
785	Tech. Rept. No. 26 (9/1/62) *AD* 285432, "Ultrasonic Relaxation in Electrolytic Solutions: II. The Hydrolysis of KCN"			

786.	Tech. Rept. No. 27 (6/15/64) *AD* 604113, "Studies of Relaxation Effects in Electrolytic Solutions With the Pressure-Step Method," Hoffmann, H.			
		Westinghouse Electric Corp., Pittsburgh, Pa.	Anion conducting, solid oxide fuel cell	NOnr 3800(00), ONR/DC 4/62—Act.
787.	Rept. No. 1 (7/15/61–11/15/62) *AD* 274764, "A Study of the Adsorption Mechanisms on O_2 Electrodes," Sandler, Y. L.		Study of adsorption mechanism on O_2 electrodes	DA-36-039-SC-89138, USAERDL/Va. 7/61–7/62
788.	Rept. No. 2 (1/15/62–7/15/62) *AD* 285425 (Title same as above)			
789.	Rept. No. 3 (7/15/61–7/15/62) *AD* 289503			
790.	1st Quart. Tech. Prog. Rept. *AD* 277224, "An Investigation of Solid Electrolyte Fuel Cells," Archer, D. H.* (All reports are titled the same)		Chemistry of fuel-cell reactions	AF33(657)-8251, USAF/WP 2/62–3/63
791.	2d Quart. Tech. Prog. Rept. *AD* 283434			
792.	3d Quart. Tech. Prog. Rept. *AD* 291882			
793.	Final Rept. No. ADS-TDR-63-448 (7/63) *AD* 412789			
794.	Rept. No. 1 (9/6/62–12/31/62) *AD* 406235, "A Study of the Adsorption Mechanisms on O_2 Electrodes," Sandler, Y. L. (All reports are titled the same)		Study of adsorption mechanisms on oxygen electrodes	DA-36-039-AMC-00136(E), USAERDL/NJ 1/63–3/64
795.	Rept. No. 2 (1/1/63–5/31/63) *AD* 415348			
796.	Rept. No. 3—Semiannual Rept. (6/1/63–12/31/63) *AD* 438942			
797.	Rept. No. 4—Final Rept. (9/6/62–3/5/64)			
798.	MEWD Rept. No. 1129 (5/62) *AD* 282389, "Lightweight, Extremely High-Power Electrical Sources," DeMoulin, D. A.*	White Sands Missile Range, New Mexico	Lightweight, extremely high-power electrical sources	?, USASMS/New Mex. 5/62**

Subject Index

A

Absolute potential, 33
Acetaldehydes, 257
Acetals, 227
Acetic acid, 214, 257, 269
Acetronitrile, 176
Acetylacetone, 236
Acetylacetoneethylenediimines, 236
Acetylene, 249, 282
Acetylene black, 75, 236
Acid and alkaline cells, survey, 360
Acid electrolytes, **7-8**, 21, 44, 198, 266, 275, 288, 299, 301
Adsorption, 3
    adsorbed oxygen, transport, 296
    adsorption in aqueous electrolytes, 276
    chemisorption, 276–281
    dissociative, 340
    energies of, 300
    enthalpies of, 300
    molecular, 340
    rates of, methanol, 255, 258
Aerobacter aerogenes, 216
Aerobacter cloacae, 216
Aeromonas formicans, 214–215
Aeromonas hydrophila, 216
Aerospace use, 56, 204
Air electrodes, 3, 16
Air pollutants, 7
Aldehydes, 225
Alkaline electrolytes, 1–2, 8–9, 21, 44-45, 266, 271, 275, 286, 288, 292, 298, 301, 359
Alkyl halides, 227
Aluminum, 72, 180,204, 219
Aluminum chloride, 191
Aluminum oxide, 114
Amalgam fuel cells, 6–7, 16, 47, 55, 134–138, 173–175
    cell and stack construction, 134-138
    mercury amalgamator, 16
    potassium-amalgam cell, Allison Div., **GM**, 52,173–175
    sodium-amalgam, Kellogg, 135-138
    sodium-amalgam, Yeager, 134–135
    submarine applications, 135
Amides, 226
Amines, 226
Ammonia, 5, 14, 20–21, 44, 52, 55, 80, 96, 213–214, 217, 235,261–263,270-274
Ammonia fuel cells, 20-21, 52
    Electrochimica Corp., 270–272
    Lockheed Aircraft, 262–263
Ammonium carbonate, 214,218
Anodes, 2, 7, 10, 14, 20
    cobalt tin, 47
    hydrogen-alkaline, **7**
    iron, 47
    nickel, 14
    stainless-steel plate, 47
    zinc, 20
Antimony, 239,282
Apollo program, 4, 51, 100, 116
Applications of fuel cells,
    commercial, 5, 223
        adapting electric equipment, 152
        automobile headlights, 6
        automobile power, motor, 7
        control systems, unattended operation. 5
        electric automobile, market, 7
        electric drive, potential, 7
        electric razors, 6
        5-kW unit, 6
        generator, for house trailer, 6
        golf carts, 6
        home generators, natural gas, 6
        large-scale electricity production, 6, 56
        power supplies, portable, 4
        secondary fuel-cell system, 153
        small powerplants, future, 5
        tractors, 6
    military, 223
        aerospace, 56, 204
        electric motors, compared with gasoline, 5, 53–55
        electricity generation, biochemical fuel cells, 22
        fuel cell-hydrogen generator, 6
        generators, 51–52
        Mark 46 torpedo, 5
        military vehicle, 5, 52–55
        power supplies, portable and semiportable, 4, 51
        submarine propulsion, 5, 16, 55, 95–97, 101–102, 135, 203
        torpedo propulsion, 5, 55
    space,
        adaptation, hydrogen-axygen cell, 105–109
        capsule electrical power sources, 51
        dark interval, direct fuel cell system, 156–157
        ecological cycle, biochemical fuel cell, 22, 209
        electrolytically regenerative cells, 153–165
        ideal space system, 13
        orbital applications, 153, 159, 165
        satellites, 4, 153, 165

PRECEDING PAGE BLANK NOT FILMED.

- Applications of fuel cells—Continued
    - space—Continued
        - solar regenerative cell, 500-W, 157–159
        - space power system, 310-W, 27, 173–174
        - space travel (see also Space travel), 2–4, 12, 22
        - space vehicle, power **source,** 116
        - spacecraft, secondary-power, 51
- "Appreciable current," 254
- Aqueous electrolytes, 9, 10, 14, 43, 61, 65, 80–83, 131, 161, 194, 204, 240, 276
- Argon, 279
- Arsenic, 239, 282
- Asbestos, 10, 11, 44, 48, 76, 81, 86, 103, 107, 120–121
- Automatic control systems, 13
- Automobile, motor powered, 7

B

- *Bacillus pasteurii,* 218
- Bacon cell, 10, 45, 113
- Bacterial agents, 213
- ***Bacterium pasteurella,*** 212–213
- Baked carbon electrodes, 7–8
- Batteries (see also Primary cells), 1, 3–5, 9
    - battery-solar cell system, 47, 154–157
    - cadmium silver oxide battery, 48
    - comparison with fuel cell, 4, 154–157
    - 50-W dual-purpose unit, battery comparison, 160
    - fuel-cell-electrolyzer battery, comparison with conventional batteries, 154
    - H-O fuel cell system as battery, 47, 153–154
    - high-capacity batteries, 4, 5, 47, 155–157
    - silver-cadmium cells, 156–157
    - zinc-silver oxide battery, 48, 51, 154–155
- Benzene, 286
- Benzene sulfonic acid, 265
- Benzoquinone, 224
- Biochemical fuel cells, 22–23, 209–221
    - bacterial strains, selective breeding, 220
    - bioagents, formic acid without hydrogen, 214
    - biochemical production of chemicals, 220
    - biochemical reactions, study, 215
    - bioelectric energy sources, 210–211
    - bioelectricity, phenomena, 220
    - chemical production, rate, 23
    - current production by concentration differences, 212
    - desirable condition, 209
    - direct biocatalysis by enzymes, 214, 216, 220
    - discardable electrolyte, 209
    - electric eel, 221
    - electric organs and membrane potentials, 210
    - electricity from vegetable products, 212
    - electrochemical energy from bacterial reaction, 209
    - electrode performance, 23, 220
    - electroplaque, mode of operation, 210–211
    - enzyme-substrate mixtures at bright platinum anode, results, 218
    - General Electric, yeast-glucose cell, 217
    - growth medium system, bacteria, 210
    - growth rate and hydrogen production, 212
    - human urine and feces as fuel, space travel, 217–219
- Biochemical fuel cells—Continued
    - hydrogen generation by micro-organisms, 216
    - hydrolyzed **urea,** reaction, 213
    - ideal system, 22, 209
    - indirect bioanode, 212, 214, 220
    - induction period, 216
    - low current densities, 220
    - Magna *Corp.,* ***A. formicam,*** 214–215
    - major uses, 22, 209
    - Marquardt Corp., three-legged cell, 219
    - Melpar, Inc., biochemical systems, 216–217
    - modes of operation, 22, 209, 212
    - nonbiological anodic reaction of dissolved hydrogen, 214
    - permeable membrane, separator, 22
    - potentialities of, 215
    - power density, 210
    - results summary, Magna *Corp.,* 213
    - steady resting concentration system, bacteria, 210
    - sugar composition, grains and grasses, 217
    - University of Pennsylvania, formic acid cell, 215-216
    - voltage-current curve, biochemical cell, Magna Corp., 215
- Biological systems, electroactive products, 336-337
- Bismuth, 185–187, 239
- Bismuth iodide, 18, 181–182
- Boron carbide, 7, 73, 77
- Borosilicate glass, 187
- Bottled gas (LGP re-formed), 6, 13
- Brass, 219
- ***Brevibacterium ammoniagenes,*** 218
- Bromine, 19, 180, 199–200
- Butane, 15, 46, 228, 246, 258, 277
    - i-Butane, 228
    - *i*-Butanol, 224
- Butene, 246
- Butyl rubber, 219

C

- Cadmium, 136, 172–173, 183, 185
- Cadmium iodide, 172–173, 181, 183
- Cadmium-silver oxide, 48
- Calcia, 128
- Carbon, 7–8, 13, 18–19, 25, 43, 60, 63, 65, 76–77, 81, 94–95, 132, 134, 172, 187–188, 191, 203, 206, 213, 223, 236–237, 239, 246, 248, 266–267, 269, 279, 282, 286–287, 289, 319
- Carbon cube experiments, 237
- Carbon dioxide, 9, 14, 16, 25, 44–46, 62, 70, 78, 82, 118–121, 123–126, 131, 151–152, 223–224, 232, 237–238, 240, 242–243, 246, 251–256, 258, 279, 289
- Carbon electrodes, 10, 18, 60, 62, 300
- Carbon monoxide, 15, 25, 46–47, 67, 118, 122, 125, 132, 151, 199, 223, 228, 245-246, 251-252, 254, 276, 279
- Carbon tetrachloride, 191
- Carboxylic acids, 226
- Catalysis, 9, 24, 36, 100–101, 281–301
    - hydrogen electrode, 281–285
        - electrodes, practical, 281
        - evolution,
            - single-crystal metal electrodes, 281–282
            - Tafel parameters, 283

- Catalysis—Continued
  - hydrogen electrode—Continued
    - ionization,
      - acid solutions, 301
      - alkaline solution, 301
      - solid platinum electrodes, 283
    - kinetic limiting current, 284
    - open-circuit potentials, catalyzed anodes, 282
    - reactions, review, 281
  - oxygen electrode, 284–301
    - activated carbons, polarization and surface area, 286–287
    - adsorbed oxygen transport, electrode surfaces, 296
    - best catalysts, various conditions, 301
    - carbon electrodes in alkali and in acid, 300
    - cathode catalysts, tested, Esso, 290
    - diffusion electrodes, carbon, 290
    - energies of adsorption of oxygen, electrodes, 300
    - enthalpies of adsorption, 300
    - evolution rate, gold, 292
    - **GE** IEM cell, reactions, 300–301
    - ionization,
      - acid solution, 301
      - alkaline solution, 301
      - nonspecific reaction, 297
      - rate, compared with hydrogen, 301
      - steady state, rate limiting factor, 291
    - mechanisms of reaction, from Tafel slopes, 300
    - oxide film discharge rate, gold, 292
    - oxygen-carbon electrode, reaction mechanisms, 286
    - oxygen peroxide reaction, 288
    - oxygen platinum electrode, 292–295
    - peroxide,
      - buildup, 284
      - decomposition rate, test, 288–289
      - equilibrium potential, in acid, 299
      - on gold surfaces, 291
    - polarization need, 297–298
    - potential reactions, 300
    - practical electrode properties, 301
    - pyrolytic graphite electrodes, 287–288
    - reaction, platinum and gold, 290–292
    - studies, summarized, 296-300
    - surface-peroxide intermediate, in acid, 299
- catalysts,
  - catalytic activity, metals and alloys, 228, 231–233
    - anodic oxidation of hydrocarbons, 231
    - metal and alloy catalytic activity, 232
    - platinum black catalytic activity, comparison, 231
    - rate of CH_4 formation, platinum black, 233
  - catalytic film, 3, 8
  - catalytic materials, 228–240, 258, 350–353, 356–365
  - depositing of, 59
  - effective area, 8, 9
  - empirical testing of, future, 27–28
  - extenders, 7.9
  - future needs, 27
- Catalysis—Continued
  - hydrogen electrodes, catalysts, 9, 24
  - material-reactant adsorption, 275
  - most acceptable, 275
  - ratings, 24–25, 59
  - stability study, various solutions, 361
  - structure study, 25
  - summary, 9
  - testing,
    - cell performance, 238
    - chelates, 235–236
    - electrolyte performance, 237–238
- Cathodes, 10, 14, 16–17, 20, 24–25
  - air, 49
  - chlorine diffusion, 18
  - current collectors, 102–105
  - hydrogen diffusion rates, membrane, 161
  - improvement of, **IEM** fuel cell contract, 102
  - molten silver, 47
  - niobium-foil, 17, 171
  - platinum. 25
  - porous sintered silver, 47
  - redox, 20
  - self-breathing, 103–104
  - silver, 14, 16
  - tape, 20
  - Union Carbide, 40
- Cellulose acetate, 219
- Cerisin wax, 63
- Cerium, 19, 190, 199
- Cesium, 198
- Cesium carbonate, 25, 82.88, 228, 236–237, 240
- Cesium fluoride, 9, 15, 238
- Cesium fluoride-hydrogen fluoride, 82, 228, 238, 258
- Chemisorption, gas-phase, 276–281
  - adsorbed gases, various metals, 276–278
  - electrochemical catalysis, 276
  - electrochemical reaction, rates of, 276
  - free energies of, 276
  - gas-phase catalysis, 276
  - heats of, gases on solids, 276
  - oxygen adsorption, pure metals, 280
  - oxygen adsorption, various materials, 278
  - potential energy curves, 276
  - release equation, rate of, 279
  - surface reactions, 276
- Chlorides, various, 176
  - chloride ions, platinum reaction to, 9
  - reduction of, 176
- Chlorine, 6, 9, 18–19, 48, 153, 180, 187, 191, 194, 203, 211, 319
- Chlorine trifluoride, 267, 269
- Chloroplatinic acid, 162, 232
- Chromium, 191, 199, 204
- Chromium oxide, 267
- Circulation,
  - electrolyte circulation, 11, 36, 60, 142, 149
  - hydrogen circulation, 12, 140–141, 145–151
- ***Clostridium butyricum,*** 212–214, 216
- ***Clostridium welchii,*** 216–217

Coal, 13, 129–130
Cobalt, 191, 198
Cobalt phosphide, 235
Cobalt-tin, 47
Coconut juice, 214
Components of fuel cells,
    condenser and separator assembly, 147
    conductive carriers, 9
    current collector, 10
    diffusers, 6, 7
    electrode holder, bipolar, 10
    electrodes (*see* also Electrodes), 8
    frames, 10
    gas circulation pumps, 147
    inert, 8
    lattice, 15
    membranes, 10
    mounting methods, components, 93
    permeable packing, 93
    separators, 10
    wicks, water absorbent, 10
Computer control, 13, 29, 151
Concentrations (see also particular fuel cell), 2, 9–10, 13, 15, 39, 61, 81
Conductivity, 2, 61
Contact resistance, 10
Continuous rated capacity, 5
Contract reports, 373–415
Control systems (see also Systems and control), 5–6, 139–152
    automatic, 11
    computer, 13, 29, 151
    flow regulators, 13
    malfunction correction, 13
    pressure controllers, 13
    semiautomatic, 11
    temperature controllers, 13
Copper, 77, 120, 135–136, 204, 219, 228, 236, 239, 275, 279, 282
Copper iodide, 181
Copper oxide, 119
Cryogenic storage, 4–5, 55, 153
Current collectors, 10, 59
Current densities, 3, 7, 34–35, 37–38, 61, 228–229
Current-voltage curves, 121
Cyano compounds, 227
Cyclohexane, 228
Cyclopentane, 228
Cyclopropane, 245

D

Deuterium, 232, 276, 278
Diesel, 4, 14, 52–55
Diffusers, 6–7
Diffusion, hydrogen through palladium, 79
Digital computer, 13, 29
Dimethyl sulfoxide, 176
Dimethylformamide, 176, 236
Dissociative or molecular adsorption, 340
Double layer electrodes, 8, 10, 14, 349–350
Double layer of charge, 33, 35
Double membrane, sulfuric acid cell, 12, 109–111
Dry-tape fuel cells, 20
    dry-tape materials, data, 367
    Monsanto dry-tape battery, 204–206

E

Economics of fuel cells,
    competitive cost, 7, 56
    cost factors, 6
    cost limits, amalgam cell, 55
    economics of application, 6
    fuel cell power cost, 7
    hydrogen-oxygen cell, costs, 7
    nuclear regenerative cell, high cost, 198
    re-forming cost estimate, hydrogen, 14
    regeneration of reactants, economics, 201
    standard production costs, fuel cell, 7
Efficiency measures, terms,
    activation polarization, 2, 3, 9, 14, 15, 16, 19, 24, 25, 34
    amperes per square foot, 3
    Carnot-type relation, 1, 176, 182–184
    concentration polarization, 2, 15, 34
    continuous rated capacity, gasoline and electric, 5
    current densities, 3, 7, 34, 35, 37–38, 228–229
    double layer voltage, change (mass transfer effect), 35
    electrical (coulombic) efficiency, 2, 19, 25, 36
    energy loss, resistance to mass transfer, 35
    energy storage density, 3
    fuel efficiency, 5, 7, 13
    Gibbs free energy of reaction, 1, 2, 17, 34
    high-power density, kW/lb, 153
    IR loss (polarization), 2, 7, 9, 34–35, 42, 98–99, 126
    kilowatts per cubic foot, 35
    large capacity, A-hr/lb, 153
    "limiting current density," 39
    mathematical optimization, 4, 7
    ohmic effects, electrolyte, 35
    ohmic resistance, 2, 7, 9, 34–35
    polarization or voltage loss, 2, 7, 9, 34–35, 42, 98–99, 126
    power densities, 12, 13, 35, 36
    power density per square foot, 35
    rated capacity, military engine, 5
    specific energy, 5
    thermal efficiencies, 1, 2
    thermodynamic voltage, 2
    total electrically available energy, 2
    voltage efficiency (see also Gibbs free energy of reaction), 2, 34
    watt-hours per pound, 2, 139
    watts per pound, 35
    watts per square foot, 3, 34
    working voltage, 2, 36
Electric motors, 5–7
Electricity production,
    batteries (see also Primary cells), 1–5, 47–48, 50, 154–157
    biochemical fuel cells, 22–23, 209–211

Electricity production—Continued
  fuel cell, 1, 2, 4–5, 9
  fuel cell-electric motor, ignition engines, compared, 53–54
  generators, compared, 4-6, 51–52
  low-voltage, high-amperage, direct-current output, 7, 152
  nuclear energy systems, 4, 56, 198
  power supplies, portable, 4, 51
  primary cells (see also Primary cells and Batteries), 1–5, 47–48, 51, 154–157
  small plant efficiency, 5
  solar cell-battery systems, 4, 12–13, 47, 156
Electrochemical reaction, 3
Electrochemical theory, 31, 57
Electrode-electrolyte interface, 2–3
Electrode interspace, 10
  asbestos membrane, 10, 149
  ionexchange membranes, 9–13, 15, 19, 21, 27, 82–87, 100–101, 109–111
  palladium membrane, 7–8
  permeable membrane, 22
  plastic mesh, 10
  polystyrene cationic membrane, 10, 100–101
  resistance between electrodes, 2
  silver-plated metal mesh, 10
  vapor-permeable membrane, 13
Electrodes (see also appendixes *C* and **D** and particular type),
  absolute potential of, 33
  air, 3, 16
  anodes, 2, 7, 10, 14, 20, 47
  carbon, 10, 18, 60, 62, 300
  cathodes, 10, 14, 16–18, 20, 24, 25
  construction, different catalysts, 224
  double layer, 8, 10, 14, 349–350
  double layer of charge, 33, 35
  flooded, 312, 315
  flooding. (See Flooding and Flooded electrodes.)
  flowthrough, 315
  gas diffusion (see also Gas diffusion electrodes), 303–312
  high conductivity, 2, 7, 8
  hydrogen chemisorption, 164, 281–283
  impregnated, 60
  ionization, function, 3, 33–35
  life, 8–9
  nitric acid-oxygen, 200
  nonwetting, 8, 63-65
  oxide film effect, 248
  oxygen (*see* also Oxygen electrodes), 3, 7, 9, 10, 292–300
  Palladium membranes, 7-8
  plastic-bonded, 8, 10, 12–13, 60
  platinum, 9
  poisoning, 62
  pore sizes, 59
  porous, behavior testing, 28, 37
  practical properties, 301
  preparation of, 8
  pressure gradient across, 39
  properties, 23
  recent advance, causes, 7-8
  redox, 200
  sintered metal, 60
  smooth, solid surface, 32
  temperature, 7
  vanadium solid state, 172
Electrokinetics (see also Kinetics), 2, 36, 57
Electrolysis of water, weightless conditions, 160–162
Electrolyte selection, 9, 62, 152
  buffered electrolytes, 61
  change of volume, 15
  limited choice of, 61
Electrolytes (see also particular electrolyte),
  absolute potential, 33
  acid, 7–8, 21, **44**, 198, 266, 275, 288, 299, 301
  alkaline, 1–2, 8–9, 21, 44–45, 266, 271, 275, 286, 288, 291, 298, 301, 360
  aqueous, 9–10, 14, 43, 61, 65, 80–83, 132, 161, 194, 204, 240, 276
  carbon dioxide removal, 62
  circulation of, 11, 36, 60, 142, 149
  comparisons, general, 152
  concentrated electrolytes, performance, inorganic fuels, 274
  concentration gradients, 147
  concentration of, 2, 9–10, 13, 15, 39, 61, 81
  conductivity, 2, 61
  film, 7
  impurities in, 8
  ion-exchange membrane use as electrolyte, 9
  mechanism studies of electrolytes, perchloric acid, 62
  molten-salt electrolyte, 167
  nonaqueous, 270
  ohmic effects, 35
  performance, 237–238
  pressurized, 140–141
  selection, 9, 15, 61-62, 152
  stabilization, 8
  standard state concentrations, 33
  storage of water in, 154
  uniform concentration, 60
  voltage gradient, 35
  waste, heat, removal, 11
Electrolytically regenerative cells, 13
  alkali amalgam-halogen cell, 153
  Battelle electrolyzer, 161
    electrolysis cell, 162
    initial design, 161
    oxygen vortex cell, 161
  Electro-optical Systems, hydrogen-oxygen cell, 13, 162–165
    EOS cell compared with Battelle electrolyzer, 163
    nine-cell unit, EOS, 164
    75-W unit, EOS, 164
    38-cell unit, EOS, 164
  fuel-cell-electrolysis cycle, orbital, 153
  fuel cell electrolyzer battery, compared, 154

- Electrolytically regenerative cells—Continued
  - General Electric dual-purpose unit, 50-W, 160
  - General Electric 500-W system, 159
  - Pratt & Whitney 500-W solar regenerative cell, 140-141, 149–150, 154, 157–159
  - regenerative cell stacks, EOS, 163
  - single battery, electrolytic regeneration, 153
  - sodium/molten salt/chlorine cells, hot and cold, 153
- Energy, 3, 55
- Epoxides, 224, 227
- Epoxy, 86, 100, 136, 191, 219
- Equations,
  - absolute potential difference, electrode-minus-electrolyte, 36
  - basic rate, as current density, 37
  - basic rate, reaction, 36–37
  - calculated limiting current densities, 40
  - cathodic rate, hydrogen ionization, 275
  - Clapeyron-Clausius, 293, 300
  - current rate law, oxidation, 255
  - decrease in density, 41
  - electrode dimensions and heat generated, 147
  - Elovitch rate law, 256
  - "exchange current density," 38
  - Fick's first law of diffusion, mass transfer, 38
  - Fick's simple law, correction, 40
  - fluid dynamics, 38
  - Frumkin's equation, 255
  - Gibbs free energy of reaction, 34
  - ion mass transfer and kinetic effects, combined, 309
  - Langmuir isotherms and kinetics, 241, 252, 293–294
  - mass transfer, 7, 39–40
    - limiting current form, 40
    - mass transport, steady state, 38
    - normal binary diffusion coefficient, use in equations, 40
  - Nernst equations and potentials, 34–35, 37–38, 119, 124, 127, 132, 196, 224, 241, 287–288, 298–299
  - net current density, 38
  - ohmic and kinetic effects, combined, 308
  - operating equations, hybrid cell, 203
  - photodecomposition, longest wavelength equation, 189
  - power density, calculation, required life, 36
  - rate equation, simple reaction, 37, 275
  - rate equations, complex reactions, 36, 38, 275
  - rate of adsorption, 255
  - standard-state enthalpy change, 37
  - standard-state free energy of activation, 36
  - standard-state free energy of reaction, 36
  - steady mass transfer, rate, 305
  - surface activity term, electrodes, 37
  - Tafel equations and slopes, 38, 233–234, 247–249, 253, 271, 288, 292, 295, 300–301, 308
  - Temkin isotherms, 255–256
  - transition-state theory, applied, 36
  - water-mass balance, 146
- Equilibrium potential, 266
- ***Escherichia coli*,** 212–213, 215–216
- Esters, 224, 226
- Ethane, 15, 228, 243–246, 248–249, 258
- Ethanol, 13, 214, 223–225, 229, 257
- Ethers, 225
- Ethyl alcohol, 217
- Ethylene, 15, 25, 228, 232, 234, 244–250, 258, 276–277, 282
- Ethylene fuel cell, 15
- Ethylene glycol, 262
- Ethylenethiourea, 228
- Existing fuel cells, types, 31, 42
- Experimental approaches, catalysts, 281
- Experimental fuel cells, 31
- Extenders, catalyst material, 7, 9
- External flow, current, 32

F

- Faradaic efficiency, 19, 25, 36, 41
- Feces, 217
- Fick's first law of diffusion, mass transfer, 38
- Fick's simple law, 40
- 5-kW unit, 6
- Flat cells, 10
- Flooded electrodes, 7, 59, 63, 312–315
  - flooded-diffusion electrode, 27, 303, 312–315
  - mathematical treatment, 313–315, 320
  - mode of operation, 312–313
- Flooding, 7, 59-63
  - aliphatic monohydroxy alcohols, 63
  - control, 59–62, 310–311
  - immunity to, 61
  - preventing, 62–63
  - resistant to, 60
- Flowthrough electrodes, 20, 27, 272, 315–316
  - anodic currents, 272
  - cathodic currents, 273
  - definition, 303
  - experimental investigations, 316
  - gas evolution in, 274
  - high area, characterized, 316
  - high area, limiting current density, 316
  - screen, high velocity electrolyte, 315
- Fluoboric acid, 265
- Forced flow, 39, 102
- Formaldehyde, 199, 240, 243, 254–256, 258
- Formamide, 224
- Formic acid, 22, 25, 212–216, 223, 236, 240, 245, 251–256, 258
- Frames, 10
- Free energy of activation, 37
- Fructose, 214
- "Fuel Battery" (see also Stack construction), 91
- Fuel cell (general),
  - cell and circuit design, 151
  - current supply, 1–2
  - description, 1, 31–32
  - ease of maintenance, 5
  - energy storage, variable weight, 3
  - fuel-cell batteries compared, 9
  - recharging, 2
- Fuel-cell electrolysis cycle, 153–154

- Fuel cell fuels (see also particular fuel name):
  - ammonia, 5, 14, 20-21, 44, 52, 55, 80, 96, **213–214,** 217, 235, 261–263, 270-274
  - bottled gas, LPG, re-formed, 6, 13
  - coal, 13, 131–132
  - diesel fuel, 4, 14, 52–53, 55
  - formic acid, 22, 25, 212–216, 223, 236. 240, 251–255
  - gasoline, 4–5, 15, 52–53, 54-55, 228
  - hydrazine, 5, 14, 20-21, 25, 29, 44, 55, 82, 84, 223, **235–236,** 261,263–269
  - hydrocarbon fuels *(see* also Hydrocarbon fuels and particular fuel name), 3, **5–6,** 13–16, 20, **25–26,** 54, 223–260
    - butane, 15, 46, 228, 246,258, 277
    - ethane, 15, 243–246,248–249, 258
    - ethanol, 13, 214, 223, 229, 255, 257
    - ethylene, 15, 25, 228, 232, 234, 244–250, 258. 276–277, 282
    - methane, 6, 14–16, 55, 122, 132, 223, 225, 232, 235, 243–246, 258–259
    - methanol, **5–6,** 13, 15–16, 25, 44, 46, 55, 152, 223, 229–230, 235, 238–240, 254–255, 257–258, 289–290, 319
    - propane, 15–16, 55, 223, **234–238, 243–246,** 248, 258-259, 282
  - hydrogen. (See Hydrogen.)
  - **JP–4,** 4, 5, 15, 51, 127
  - natural gas, 6, 13
  - pulverized or gasified coal, 13, 131–132
  - sodium, 5, 18, 47, 134–137, 153, 180, 187–188, 211
  - sodium amalgam, 6, 16, 47, 55, 66, 134–138
- Fuel cell stacks (see also Stack construction), 3, 6–7, 10, 91–137
  - cell modules, 7, 11
  - heat removal, 11
  - high temperature cells, 119–132
  - low temperature cells, 91–111
  - medium temperature cells, 113–117
  - regenerative cells, 163–164
  - sodium-amalgam-oxygen cells, 134–138
- Fuel cell systems, energetics, 328
- Fuel cell temperature,
  - cell temperature-performance, 2, 6, 10-13
  - high temperature cells, 6, 9, 12, 14, 15, 17–19, **45–46,** 119–132
  - low temperature cells, 6, 9–16, **42–45, 91–111**
  - medium temperature cells, **9,** 10–13, 45-46, 113–117
  - temperature of electrode, nonuniform, 7
  - variation of, Pratt & Whitney hydrogen-oxygen cell, 116
- Fuel cell testing, 341–345
- Fuel efficiency, 5, 7, 13
- Fuel, rates of flow, 16

G

- Gallium, 185
- Gas diffusion electrodes, 3, **7–8,** 13, 26–27, 39, 59-61, 303–312, 320
  - development of, general rules, 59-61
- Gas diffusion electrodes—Continued
  - principles of, 303, 320
  - simple-pore model, 309-311, 320
    - flooding control, wetproofing the electrode, 310-311
    - mathematical treatment, 309-311
      - current density, 311
      - dissolved gas, pore penetration, 310
      - limiting current density, approximate, 310
      - mass transfer and ohmic relations, 310
    - mode of operation, 309
    - nonwetted electrode, 310
    - pore system, mechanism of operation, 304–305
  - surface-diffusion model, 311–312, 320
    - adsorbed hydrogen diffusion, 312
    - mode of operation, 311
      - Boudart mode, 312
      - Justi mode, 311
  - thin-film model, 303–309, 320
    - dissolved gas concentration, thick electrode, 307
    - dissolved gas concentration, thin electrode, 308
    - double layer structures, electrodes, 305
    - mathematical treatment of model, 303,305–309
      - current as function of voltage, 306–307
      - equation choice, 309
      - film electrolyte in electrode, effective resistivity, 308
      - ion mass transfer and kinetic effects, combined equation, 309
      - limiting current density of the electrode, 306
      - ohmic and kinetic effects, combined equations, 308
      - Ohm's law, application of, 306
      - rate of reaction, surface, 306
      - rate of transfer, dissolved gas, 306
      - steady mass transfer, ionic species, rate, 305
    - thin film formation, vertical wires, 305–306
    - thin film on wire, mode of operation, 303–304
    - thin film within porous electrode, geometry, 303
- Gas pressure balance, 8, 13, 32
- Gas turbine-ac aircraft generator, 50
- Gasoline, 4–5, 15, 52–53, 54–55, 228
- Gemini program, 4, 51, 100
- Generators, **4–6**
  - gas turbine-ac generator, 51
  - home, natural gas, 6
  - house trailer, 6
  - power generators (self-contained), comparison, 52
  - power supplies, portable, 4
  - small power plants, future, 5
- Germanium, 87
- Gibbs free energy of reaction, 1, 2, 17, 34
- Glossary, 323–326
- Glucose, 212–215, 217
- Glycol, 262
- Glyoxal, 199
- Gold, 25, 82, 99, 129, 141, 187, 205, 214, 233, **266–267,** 269,271,275, 279, 282,291, 293, 294, 301
- Gold chloride, 181

Government. (See particular agency.)
Grains, 217
Graphite, 147, 187, 287–288
Grasses, 217
Gregor membranes, 85, 365
Gum rubber, 286

H

Half-cell testing, 264–270, 345–348
Halogens, survey report, 355
Helium, 148
Hexafluoroacetone, 236
High temperature cells, 12, 14–19, 45–46, 118–133
  General Electric, molten silver cell, 47
  Iowa State University, graphite-oxygen cell, 206
  molten carbonates, 12, 14–15, 45–46, 118–127, 131–133
  Pittsburgh Consolidation Coal, solid electrolyte cell, 118–121
  solid electrolyte cells, 15, 46, 118–119, 127–133
  Texas Instruments Co., molten carbonate cell, 123–127
  Westinghouse cell, solid electrolyte, 46, 127–128
High temperature electrode, materials, 362–364
Hybrid fuel cells, 49, 203–207
  Aerojet-General, submarine battery cell, 203–204
  Armour Research, IIT, continuous feed battery, 204
  Iowa State University, graphite-oxygen cell, 206
  Iowa State University, sodium tungstate-tungstic cell, 206–207
  Monsanto, dry tape battery, 204–206
  Resin Research Lab., organic fuel cell, 204
Hydrazides, 224
Hydrazine, 5, 14, 20–21, 25, 29, 44, 55, 82, 84, 223, 235–236, 261, 263–270, 273–274
Hydrazine fuel cells, 20–22, 261, 263–270, 273–274
Hydrocarbon electrodes, 16, 223, 229–251, 253–259
  carbon monoxide adsorbed, platinum in sulfuric acid, 251
  catalyst activity, chelates, Shawinigan, 236–237
  catalyst performance, best, 3, 258
  catalyst results, electrode preparation, Esso, 233–234
  catalyst results, electrode preparation, Monsanto, 233
  catalyst testing, chelates, Monsanto, 235–238
  catalytic activity, propane, 235
  catalytic activity, metals and alloys, 228, 231–233
  catalytic activity, noble metals, ethylene oxidation, 232–233
  electrode construction, different catalysts, 224
  ethanol at platinized platinum, 257
  formic acid, rate of adsorption, 252
  fuel current density vs. hydrogen electrode, 224, 228
  galvanostatic stripping technique, 251
  method of preparing catalyst, test, methane rate, 232
  molybdenum cocatalysts, 234
  oxidation of ethylene, rotating disk electrode, 247
  oxygen supply at the anode, 14
  stability factors, catalysts, 236
  steady current-voltage relations, platinized carbon electrode, 248
  voltage sweep methods, 246–248, 253, 258
Hydrocarbon fuel cells, 3–5, 7, 9, 13–16, 223–260
  California Research Corp., ethylene cell, 15, 246, 249–250
  General Electric, propane cell, low temperature, 245, 258
  long-term prospects of, 258
  main techniques for use of, 5, 14–16, 223
  major breakthrough, future, 259
  mass transfer limitations, 223
  medium temperature propane cell, GE, 15–16, 237–238
  methanol fuel cells, 238–240
    GE propane cell, using methanol vapor, 240
    methanol, 5-kW unit, Shell Research, England, ***6***
    methanol-air cells, Brown-&veri, 6
    methanol-air fuel cell, Esso Research Engineering, 239
    methanol fuel cell, England, 239–240
    performance, 258
  organic fuel cells, low temperature, compared with H-0,223–224
  polarization, pH independence, unsaturated hydrocarbon, 250
  semidirect fuel cells, 14
  stage of development, 258
Hydrocarbon fuels, 3, 5–6, 13–16, 20, 25–26, 223–260
  acetylene, rate determining step, postulated, 250
  anodic oxidation, formic acid, proposed mechanisms, 251–252
  anodic oxidation some hydrocarbons, results, 250
  butane, 15, 228, 246, 258
  carbon monoxide similarity to acetylene, anodic reaction, 251
  CH_3OH, HCOOH, and HCHO oxidation, 256–257
  chloride ion effect, methanol oxidation, 256
  common rate-controlling step, nonoxygenated hydrocarbons, 249
  complete reaction of ethylene and propane, 223, 237, 258
  double layer capacity method, rate of adsorption, methanol, 256
  electrochemical oxidation of hydrocarbons, 224
  electrolytes, effective, 258
  ethane, 15, 243–246,248–249,258
  ethane, ethylene, and acetylene, comparison, 249
  ethanol, 13, 223, 225, 229, 257
  ethylene, 15, 25, 234–250,258
  fuel utilization, 224
  gas-phase decomposition of propane, 244–245
  hydrocarbon derivatives, 223–224
  mechanisms and rate studies, 224, 240-245, 258
  methane, 6, 14–16, 55, 223, 225, 232, 235, 244–246, 258–259
  methanol, 5–6, 13, 15–16, 25, 55, 229–230, 238–240, 254–255, 258
  methanol adsorption, noble metals, 255
  organic fuels, power densities, study results, 224–228
  oxidation of methanol, anodic intermediates, 254
  oxidation of vapors, selected, 228
  oxygenated hydrocarbons and carbon monoxide, 251–258

- Hydrocarbon fuels—Continued
  - pH effects, 250, 254, 256
  - propane, 15–16, 55, 223, 235, 237–238, 243–246, 248, 258–259
  - rate control, steady current, 251, 254
  - rate of absorption, carbon monoxide, platinum in $HClO_4$, 251
  - reactivity, unsaturated hydrocarbons, **248–250**
  - repetitive voltage sweep methods, 256
  - saturated hydrocarbons, straight chain, relative reactivity, 228, 230
  - solubilities of hydrocarbons, 246
- Hydrochloric acid, 9, 62, 85, 88, 198, 256, 265
- Hydrogen, 1–7, 11, 13–15, 18–19, 22–24, 29, **31–33, 43–44,** 47–50, 52, 55, 61, 65, 68, 73–75, 78–82, 84, 91, 94, 97, 100, 102–109, 113, 116, 118–119, 125, 132–133, 137, 139–143, 147–151, 157, 160–162, 164, 216, 223, 232, **235–237, 241, 247, 251–252, 262–263, 265, 272, 274–276,** 281–284, 289, 296, 301,303, 312, 317, 319–320
  - circulation, 140–141
  - diffusion and reaction, 32
  - dissociation of, high temperature, **175–176**
  - electrodes (see also Electrodes), 3, 9, 16, 25, 281–283
  - generating plant, weight and volume, 370
  - generation and gas storage, 369-372
  - generator, Engelhard specifications, 371
  - generators, 6
  - hydrogen-oxygen electrolysis, 160–162
  - ionization, in acid, 24, 301
  - ionization, in alkali, 301
  - reactions in aqueous electrolyte, 61
  - re-forming from hydrocarbons, 7, 14
  - re-forming system for submarines, 5
- Hydrogen-air cell generator, 6
- Hydrogen air fuel cells, 6, 9–10
  - General Electric, hydrogen-air cell, 9–13, 43, 97–102, 142–145, 149–150
- Hydrogen fluoride, 9, 228, 238, 269
- Hydrogen-oxygen fuel cells, 3–5, 7, 9-13, 16
  - Allis-Chalmers, 4-6, 10-13, 43–44, 48, 62, 103-109, 145–151
  - electrolytes used, 9, **10,** 61-62
  - Electro-Optical Systems, 48
  - Engelhard, 288–289
  - General Electric Co., IEM, **10–13, 62, 97–102, 142–145,** 149–150
  - Ionics double membrane, **109–111**
  - Justi-Brown-Boveri, 44
  - Monsanto, half cell, **266–267**
  - performance, table, 11
  - Pratt & Whitney Aircraft, 140-141, 149-150
  - Tyco Laboratories, half cell, 290–292
  - Union Carbide, 7, 10-13, 43, 94-95, 141–142, 149
- Hydrogen peroxide, 11, 20-21, 25, 48, 77, 80-82, **84–85,** 87, 95, 105, 108, 141, 165, 197, 204, 261–262, 266–267, 272–274, 284, 287–288, 291–292, 295, 298, 300
- Hydrogen peroxide fuel cells, 11, 261–262, **272–274,** 300
- Hydrogen sulfide, 133, 199, 245
- Hydrogenlyase enzymes, 214, 216
- Hydroxy compounds, 225

I

- Imides, 226
- Impurities in electrolyte, 3, 6, 7, 8, 25
- Indium, 185
- Internal area of electrodes, 3, **8**
- Internal flow, 32
- Iodine, 179-181, 183
- Ion-exchange membrane, 9–13, 15, 19, 21, 29, 62; 82-88, 97–105, **109–111, 142–143,** 145, 149-150, 159, **365–366**
  - binder materials, 86, 368
  - cation exchange polymers, 83
  - double membrane, 109-111
  - effect of liquid organic fuels, 84
  - gas permeabilities of, 85
  - Gregor membranes, 85
  - inorganic membranes, zeolitic materials, 86-87
  - materials, **365–366**
    - borides, 363
    - carbides, 364
    - oxides, 363
    - silicides, 362
  - performance of, various systems, 84
  - polystyrene, sulfonated, **100–101**
  - properties of, 85
  - rates of electro-osmotic water flux, 86
  - resistance of anionic membranes, 85
- Ion-exchange membrane cells, 9-13, 84–85, 97–102, **109–111,** 142–145, 149–150, 159-160
  - flight analysis of, **99–100**
- Ionic conductivity, phosphoric acid, 339
- Ionization function, 3, 33, 35
- **IR** loss, polarization, 2, 7, 9, 34–35, 42, 98–99, 126
- Iridium, 25, 82, 230, 232–233, 238, 244, 250, 273, 294
- Iron, 19, 46-47, 67, 120, 180, 188, 191, 197–198, 239, 270
- Iron oxide, 68, 135
- Iso-butane, 46, 243–244
- Iso-octane, 228

J

- **JP–4,** 4, 5, 15, 52, 126
- "Junction potential," 266
- Justi-type electrode, 8

K

- Ketal, 227
- Ketene, 227
- Ketones, 225
- Kinetics,
  - adsorbed hydrogen, 25, 241–242
  - anodic oxidation, nonoxygenated hydrocarbons, **243–244**
  - best catalysts, 24
  - carbon monoxide oxidation, mechanisms, 251
  - chemical kinetic restriction, 36
  - chemisorption, gas phase, 276–281
  - electrochemical kinetics, 36, 57
  - electrode potentials, 240–241
  - equilibration time, effect, 244–245
  - hydrocarbon mechanism, 25

- Kinetics—Continued
  - hydrocarbon oxidations, 240
  - hydrogen,
    - catalysis, 281–284
    - ionization, in acid, 24
    - ionization, in alkali, 24–25
    - reaction, aqueous, 61
  - hydrogen-oxygen kinetic mechanisms, 23, 275–302
  - limiting current, 284
  - mechanisms and rate studies, 240-245
  - noble metal electrodes in aqueous electrolytes, 240
  - oxidation in acid electrolyte, theory, 242–243
  - oxygen catalysis, 284-301
  - oxygen ionization, in alkali (peroxide mechanism), 25
  - pH and reactant concentration, 243
  - rate-limiting factors, hydrocarbons, 242
  - rates of adsorption, fuels, 26
  - stagnant film concept, 38
  - standard-state, open circuit potential of the electrode reaction, 33
  - surface activity, 37, 296
  - surface conversions, ethylene, 245
  - surface oxygen, 241
  - surface reactions, electrodes, 24
  - theory of electrode reactions, 61
- Knudson diffusion, 40, 102
- Krypton, 278

L

- Lactic acid, 214
- Lead, 18, 48, 180, 183, 185, 219, 289
- Lead-acid, 155
- Lead bromide, 18, 180
- Lead iodide, 48, 172, 180, 183
- Lead oxide, 200
- Leucine, 212
- Lithium, 48, 132, 169–171, 180, 183, 186–187
- Lithium bismuth, 186–187
- Lithium carbonate (molten), 14, 88, 235
- Lithium chloride, 17, 167–169, 171, 184, 186–187
- Lithium fluoride, 17, 167–169, 186–187
- Lithium hydride, 17, 48, 167–171, 177
- Lithium hydroxide, 263
- Lithium iodide, 180, 183
- Lithium nitrate, 176
- Lithium oxide, 125
- Lithium, potassium hydrogen sulfates, 176
- Logistics, 5, 50–52
- Low temperature cells, 9–16, 42–45, 91–111
  - Allis-Chalmers, hydrogen-oxygen cell, 4-6, 10-13, 43-44, 48, 62, 103–109, 145–151
  - catalysis, importance of, 4243
  - cell and stack construction, 91–111
  - electrode structure, importance of, 4243
  - fuel cell battery, 95
  - General Electric, IEM, hydrogen-oxygen cell, 9-13, 43, 97–102, 142–145, 149–150
  - General Electric, propane cell, 245, 258
  - Ionics double membrane, sulfuric acid cell, 109–111
- Low temperature cells—Continued
  - modes of operation, 42–45
  - most advanced cell systems, 93, 97, 109
  - mounting methods, cell components, 93
  - Union Carbide Co., hydrogen-oxygen cell, 10–13, 43, 94–97, 141–142, 149
- Low temperature cements, 367
- Lucite, 194–283

M

- Magnesium, 103, 105, 108, 165, 204, 206
- Magnesium bromide, 204
- Magnesium hydroxide, 204
- Magnesium oxide, 14, 46, 66, 68-69. 75–76, 87, 119–123, 173. 272
- Magnesium perchlorate, 270
- Manganese. 180, 191, 239
- Mass transfer (transport), 35, 38, 60
  - diffusion through another (gas) component, 39
  - effects, voltage change, 35
  - electroendosmosis, 84
  - equations, 7, 38–40
  - forced flow, 39
  - hydrogen dissolved equals current, 35
  - in solid-state diffusion electrode, 60
  - limitation, 36, 42
  - mechanisms of, 39
  - oxygen, through a film of water, 101
  - reactant supply, speed of, 36
  - resistance to, 35
- Massive rearrangement, constituents, 9
- Materials (see also particular material and particular fuel cell),
  - acid and alkaline cells, 359
  - borides, 362
  - carbides, 363
  - cements, low temperature, 367
  - cesium carbonate, 360
  - halogens, 354
  - hydrogen fluoride, 360
  - ion-exchange membrane materials, Gregor, 364–365
  - metal powders, sources, 361
  - molten salts, 355
  - oxides, 362
  - phosphoric acid, 360
  - seals, high temperature, 367
  - silicides, 361
  - sulfuric acid, 355–358
  - tape materials, 366
- Mathematical models, electrodes, 7, 320
- Mathematical optimization, 4, 7, 14, 147, 149, 165, 303, 305, 315
  - system analysis, 500-W cell. 157–158
- Matrices, 82-88
  - ceramic, labyrinth factors, 174
  - electrolyte-filled, 62, 162
  - materials, 10, 14, 62, 87–88
  - molten-salt electrolytes, matrices for, 88

Matrices—Continued
  permeable electrolyte, 160
  porous. 3, 9-10, 12, 14, 46, **48, 65, 86**
  porous refractory, matrix of, 14
Medium temperature cells, 9-13, **45-46,** 113-117
  Allis-Chalmers, lab. cell, 46
  Allison Division, GM, 17
  Bacon, **F.** T., fuel cell, 10, 45, 113
  cell and stack construction, 113-117
  Electrochemical Corp., ammonia-molten alkali-hydroxide cell, 270-272
  General Electric, lab. cell, 46
  General Electric, propane cell, **15-16, 237-238, 258**
  Patterson, hydrox cell, 113-114
  Potassium hydroxide, in, 9
  Pratt & Whitney (Bacon modification), 10-12, 45, 113-117
  sulfuric acid, in, 9
Membrane electrodes, 10, 75, 78-80
Membranes,
  asbestos, 10, 149
  cationic, mechanism for, 43
  ion-exchange, 9, 10, 12, 15, 19, 21. 29, 62, 82-88, 97-105, **109-111,** 364-365
    anionic, 9, 300
    cationic, 9-10, 83, 239
    double, 109-111
    ion-exchange, performance, 274
    ion-exchange, sulfonated-polystyrene, 85, 100-101
  molybdenum-iron-alloy diaphragms, 171
  palladium, 7-8, 75, 78-80
  permeable, 22, 85
  polystyrene (cationic), 10, 83, 85, **100-101**
  study of ion-exchange membrane cell, **100-101**
  vapor-permeable, 13
Mercury, 6, 16, **17, 47, 66,** 134-137, 173-175, 185, 271, 283
  amalgamator, 16
  potassium amalgam, 52, 172-175
  sodium dissolved in (*see* also Sodium), 47
Mercury iodide, 181
Metadinitrobenzene, 206
Metal powders, sources, 361
Metals, various, 295
Methane, 6, **14-16,** 55, 122, 132, 199, 223, 225, **232-233, 235,** 243-246, 258-259
Methanol, 5-6, 11, 13, 15-16, 25, **44-46,** 55, 81-82, 84, 152, 200, 223-224, 229-230, 235, **238-240, 251-258,** 289-290, 319
Methylpentane, 228
Methylthiocyanate, 176
Micrococcus ureae, 218
Military engine, rated capacity, comparison, 5, 29, 53-55
Military uses (see also Applications of fuel cells, military)
Mission time, space, 4, 51
Molten carbonate, 9, 12, 14-15, *46,* 62, 118-121, 132
Molten carbonate cells, 12, 14-15, ***46,*** 118-127, 131-133
  Central Technical Institute, disk cell, 121-123
  Pittsburgh Consolidation Coal Co., sodium carbonate cell, 118-121
Molten carbonate cells—Continued
  technical problems **of,** 131-132
  Texas Instruments **Co.,** disk cell, 123-127, 131-132
Molten salts, 66, 133, 153, 167, 180, 355
Molybdenum, 140
Molybdenum cocatalysts, 234
Molybdenum-iron, 171
Molybdenum oxide, 206, 235
Monel, 213
Monomethyl hydrazine, 269

N

NASA, **50, 100**
Natural gas, fuel, 6, 13
Navy,
  amalgam cell **use,** 16, 55, 135-138
  buoyancy increase, 55
  buoyant submarines, 5
  hybrid fuel cell research, 203
  nuclear regenerative fuel cell, 197-198
  one-man submarine, 5
  submarine propulsion, 5, 16, 55, **95-97,** 101-102, 135, 203
  torpedo propulsion, 5
  two-man submarine, 138
Neoprene, **10, 95,** 137, 160, 205
Nernst equations and potentials, 34-35, 37-38, 119, 124, 127, 132, 196, 224, 241, 287-288, 298-299
Nickel, 8, 10-11, 14, 24, 44-46, 48, 59-60, **65-69,** 73-74, 76-77, **81, 87-88,** 103, 108, **113-115,** 120, 123, 131-132, 157, 160, 162-163, 188, 191, 204, 214, 234, 244, 262-264, **271-272,** 275, 281-283, 288, 301, 312, 319
Nickel anodes, 14
Nickel boride, 7, 9
Nickel cadmium, 155
Nickel chromium, 115
Nickel electrodes, porous, 13
Nickel iron. 155
Nickel oxide, **9, 24, 59, 68, 113,** 120, 132, 276, 280, 283, 301
Nickel phosphide, 235
Niobium, 17, 171, 362-363
Nitric acid, 21, 84, **200,** 238-239, 261, 263-266, 269, **273-**274, 290
Nitric oxide, 265, 274
Nitrobenzene, 204
Nitrogen, 20, 40-44, 102, 123, **140-141,** 162, 169, 263, 289
Nitrogen dioxide, 19, 21, 48, 191, 194, 200, 204
Nitrogen peroxide, 269
Nitromethane, 176
Nitroso compound, 227
Nitrosyl chloride, 19, 48, 191, 194
Nitrous oxide, 265
Nonaqueous electrolytes, 270
Nonwetting and wetproofing electrodes, **8, 63-65**
Nuclear energy systems, 4, **56,** 198

O

Octachlorophthalocyanine, 236

Ohmic resistance, **IR** (see also Polarization, **IR** loss), 2, 7, 9, 34–35
Organic binders, references, 367
Organic fuel, direct use, 6
Organisms and references, biological systems, 337
Ortho ester, 227
Osmium, 231
Oxalic acid, 199, 265
Oxides, various, 275, 290
Oxime, 227
Oxygen, 1–4, 9, 11, 15, 18–19, 23–25, 29, 31–33, 40, 43–44, 47, 61, 65, 73–75, 81–84, 91, 94, 100–109, 113, 116, 119, 127, 132–133, 136, 242–243, 245–247, 249–250, 262, 265, 276, 278–280, 284, 287–301, 310, 316–317, 319–320
  diffusion and reaction, 32
  evolution rate, gold, 292
  ionization,
    acid solution, 301
    alkaline solution, 301
    nonspecific reaction, 297
    rate, 301
    steady state, rate-limiting factor, 291
  reaction, platinum and gold, 290–292
Oxygen electrodes (see also Catalysis, oxygen electrode), 3, 7, 9–10
  oxygen-carbon, mechanisms, 286
  oxygen-carbon, various electrolytes, 290
  oxygen-platinum, sulfuric acid, 292–295
  polarization need, 297–298
  potential reactions, 300
  studies, 296–300
Oxygen-peroxide, reaction, 288

P

Palladium, 7–8, 10, 24–25, 61, 76, 78–80, 82, 161, 163, 214, 232–233, 240, 272, 279, 281–283, 294, 296, 312, 319
Palladium-acetylacetone, 236
Palladium black, 164, 214, 238
Palladium chloride, 181
Palladium oxide, 79
Palladium-platinum black, 97–99
Palladium-silver, 8, 61, 78, 80, 236, 272
Paraffin wax, 63, 213
Paste, electrolytes, 88, 122–123, 213, 263, 276, 289
Pentaborane, 265
Pentanes, 277
Perchloric acid, 19, 62, 80, 190, 238, 251–253, 255–256, 258, 281, 283, 292
Performance of fuel cells,
  current densities, 3, 7, 34–35, 228–229
  decay of, 8
  electrical, comparison, 3
  first indication, 35
  fuel efficiency, 5, 7, 13
  methanol cells, 15
  molten carbonate cell, 14
  power densities, 2, 4–5, 7, 12–13, 34–36, 41, 154–158, 225–228
  single fuel cell, 7, 12
Peroxide decomposition inhibitors, 267
Petroleum hydrocarbons (see also Hydrocarbon fuels), 13
Phenolformaldehyde, 159
Phenolics, 86
Phosphoric acid, 9, 15, 46, 62, 73, 75, 77, 82, 86–87, 162, 224, 228, 236–238, 245, 258, 265
Phosphorus pentachloride, 176
Photochemical decomposition, 189
Photochemically regenerative cells, 19, 48, 189–193
  compared with solar cells or solar boilers, 201
  complex ion reducing-agent systems, 195
  conversion of radiant energy to electrical energy, cell, 189
  double cell, stannous-stannic couple, 196
  direct reduction by hydrocarbons, 199
  dye-coated electrode systems, 195
  dye-plus reducing agent systems, 194
  economical regeneration of reactants, 201
  efficiency of conversion, absorbed to free energy, 189
  efficiency of conversion, spectral range of light, 190
  Electro-Optical Systems, solar regenerative systems, 196–197
  endothermic reaction, 189
  energy in spectral band, 190
  enthalpy, endothermic photochemical reaction, 190
  500-W flight design, future, 191
  hydrogen regeneration reaction, 190
  irradiated aqueous solutions, various, 194
  Lockheed Missiles & Space Div., solar regenerative cells, 194–196
  nitrosyl chloride solar-regenerative cell, Sundstrand Machine Tool, 191, 194
  other suitable reactions, 191
  oxygen regeneration from water with stannous ion, 190
  photo- or helio-chemical decomposition, water, 200–201
  photodecomposition, longest wavelength equation, 189
  photolysis, 191, 194, 196
  threshold wavelength, definition, 189
  ultraviolet endothermic reactions, 192
  Victoria blue, solid coat electrode, 196
Phthalocyanines, 236
Plastic (see also Materials), 8, 10, 60–61, 65, 70, 75–76, 81, 95, 135–136, 163
Platinic iodine, 179–180
Platinum (see also Materials), 7, 9–10, 15, 24–25, 46, 59, 65–66, 70, 73, 75–76, 81–82, 86, 108, 121, 127–129, 157, 159–161, 163, 179–181, 187, 194–195, 198–200, 204, 206, 213–214, 216, 218–219, 224, 229, 230–235, 237–238, 241–246, 249–254, 256–257, 262–267, 269, 271–274, 276, 278–279, 281–284, 289–293, 296–298, 301, 303–304, 312, 319–320
Platinum black, 3, 8–10, 15, 60, 65, 67, 72, 80–81, 87, 98, 109–110, 160, 213–214, 217, 229–230, 233, 238–239, 244, 254, 272, 289–290, 312
Platinum cocatalysts, 234
Platinum coprecipitates, 290
Platinum-palladium, 9, 24, 59, 65, 81, 103, 163–164, 199, 232, 301

- Platinum-ruthenium, 232, 238
- Platinum-ruthenium-tungsten, 240
- Poisoning, electrodes, 3, 6-8, 25
- Polarization (see also Principle of fuel cell, polarization), 2, 9, 34
  - activation polarization, 2-3, 9, 14-16, 19, 24-25, 34, 41
  - causes of, 42
  - concentration polarization, 2, 15, 34, 39, 301
  - current-voltage curve, use of, 41
  - decreasing polarization, 41
  - IR loss, 2, 7, 9, 34-35, 42, 98-99, 126
  - measurement techniques, 98-99, 341-345
  - uniform concentration, 60
- Polyethylene, 95, 136, 160, 219, 286
- Polyethylene oxide, 66
- Polypropylene, 95
- Polysaccharides, 217
- Polystyrene, 10, 85, 94, 100-101, 139, 265, 286
- Polyvinylchloride, 162, 205
- Polyvinyls, 219
- Porous electrodes, 7, 8, 10, 13, 18, 27, 32, 37
  - gas diffusion electrodes, mode of operation, 303-304, 309, 311, 320
- Potable water production, for space use, 12
- Potassium, 168, 174-175, 177, 180, 211
- Potassium amalgam, 17, 173, 175, 177
- Potassium bicarbonate, 82, 239, 240, 244, 290
- Potassium borohydride, 270
- Potassium bromide, 173
- Potassium carbonate, 14, 82, 262, 282
- Potassium chloride, 171, 184, 213
- Potassium dihydrogen phosphate, 238
- Potassium fluoride, 254
- Potassium hydride, 25, 168
- Potassium hydroxide, 3, 9-10, 16, 20, 39, 43, 45, 62-63, 65, 73-74, 76-78, 80-81, 85-86, 94, 103, 105-108, 110, 113, 115-116, 135, 146, 148-150, 160-162, 164, 173, 205, 223-224, 228, 236, 244, 252, 254, 256, 258, 262-267, 273. 279, 282-283, 286, 300, 310, 316
- Potassium iodide, 173, 181
- Potassium monohydrogen phosphate, 216
- Potassium-sodium hydroxides, 80, 271
- Potassium-sodium-lithium carbonates, 46, 87, 123, 263
- Potassium-sodium-lithium hydroxides, 77
- Potassium zinc oxide, 205
- Power density, 2, 12-13
  - best existing direct fuel cells, 154
  - conventional battery, subsystem, 154
  - conventional high capacity batteries, 154-157
  - energy storage density, 3
  - effective energy density, 4
  - fuel cell subsystem, 154
  - fuels tested, Monsanto, 225-228
  - increasing power density, 41
  - maximum, 36
  - per square foot, 35
  - relationship to current density, 35, 41
  - requirements, 5, 7

Power density—Continued
  - silver-cadmium cells, 156-157
  - solar cells, 158
  - solar cells plus nickel-cadmium batteries, 156
- Power plants, 5-6, 113, 116-117
  - fuel cell system, Pratt & Whitney, 113, 116-117
  - nuclear, XIII
  - 1000-MW plant, 6
  - operating and system problems, 151.
- Power ratings, fuel cells (see also Types of fuel cells),
  - Allis-Chalmers cell, 44
  - biochemical fuel cells, 50
  - cells for highly soluble fuels, 45
  - General Electric cell, 44
  - higher power (rating) fuels, 52
  - hydrogen and ammonia cells, 52
  - medium temperature cells, laboratory, 46
  - solar cells, 51
  - Union Carbide cell, 43
- Pressure gradients, 39
- Primary cells (see also Batteries),
  - cadmium silver oxide, 48
  - energy conversion, fixed weight, 3
  - high-energy primary cell, 2, 4-5, 47, 155-157
  - silver-cadmium cells, 156-157
  - zinc-silver oxide battery, 48, 51, 154-155
- Principle of the fuel cell,
  - basic theory, 31
  - catalysis (see also Catalysis), 9, 24, 36, 100-101, 281-301
  - effect of catalysis, rate of reaction, 37
  - efficiency (see also Efficiency measures), 201
    - determinants, 36
    - terms defined, 36, 323-326
    - voltage efficiency of cell, improvement, 34
  - electrochemical basis of fuel cell, 31
  - electrochemical-engineering problems, 24, 28-29, 59
  - electrochemical kinetics, 36-38
  - electron transfer, described, 36
  - fuel cell, definition of, 31-32
  - gas diffusion, function, 3, 7, 38
  - hydrocarbon reaction mechanisms, 23, 25, 223, 242-243, 245, 249-253, 255-257
  - hydrogen, ionization steps, 24
  - hydrogen, surface reaction, 241
  - hydrogen peroxide, kinetic mechanisms, 21, 23
  - kinetics, 36-38, 61
  - oxygen ionization, 25, 61
  - oxygen, surface reaction, 241-242
  - peroxide mechanism, 25
  - polarization (see also Polarization),
    - activation polarization, 2, 9, 35, 36
    - concentration polarization, 2, 35, 39
    - decreasing polarization, 41
    - mass transfer equations, 7, 38-40
    - mass transport (transfer), diffusional. approximated, 38
    - Ohm's law, applied, 35
    - ohmic (or IR), polarization, 2, 9, 34-35

- Principle of the fuel cell—Continued
  - polarization—Continued
    - ohmic resistance, defined, 35
    - ohmic voltage loss, calculated, 35
    - overvoltage or overpotential, 34
  - power density (see also Power density),
    - ideal open-circuit potential, fuel cell or electrode, estimate, 34
    - loss of reversible potential, 34
    - maximum, 36
    - most compact fuel cell configuration, 34
  - terms, defined, 23–26, 323–326
  - thermodynamics of fuel cell, 33–36
  - thermodynamics tables, 329–331
  - transition state, defined, 36
  - voltage gradient, electrolyte, 35
- Propane, 15–16, 46, 55, 223, 228, 233–238, 243–246, 248. 258–259, 282
- Propane cell, 15–16, 46,237–238, 258
- Properties of electrodes, 348–351
- Propylene, 228, 245–247
- ***Pseudomonas,*** 216
- ***Pseudomonas formicans,*** 214
- Pulsation effects, gas electrodes, 318–320
  - discharge current pulses, 319
  - effects of sound waves, 318–319
  - interrupter circuit, 319–321
  - mass transfer study by pulsation of electrolyte, 318
  - mechanical vibration, 319
  - pressure pulses, 319
  - voltage pulsing, 320–321
- Purging, 11, 39-41, 143, 151

Q

- Quality control, 8
  - current collector, contact loss, 8
  - dissolution of cell components, 8
  - electrode disintegration, 8
  - impurities in electrolyte, 8
  - loss of wetproofing, 8
  - pure materials, use, 8
  - recrystallization of catalyst, 8
- Quinone, 195

R

- Raney process, 8
- Rate of diffusion of hydrogen, palladium-silver alloy membrane, 80
- Rates of electro-osmotic water flux, ion-exchange membranes, 86
- Reactants (see also Fuel cell fuels),
  - catalytic processes, 32
  - continuous feed of, 32
  - high concentration, rates, 37
  - high concentration reactants, 37
  - maximum performance, 327
  - reactants of fuel cells, comparison, 32
  - redox reactant, 19
  - storage space requirements, 7
- Reactants—Continued
  - supply, speed, 36
- Recharging, 2, 48
- Redox fuel cells, 19–20, 198–201
  - activation polarization, avoidance of, 19
  - anode couples, 20, 199
  - aqueous redox couples, 19
  - cathode couples, 199
  - free energies of conversion to alcohol, calculations, 199
  - low temperature, acid electrolyte, redox cells, **GE,** 198–199
  - nitric acid-oxygen redox electrode, 200
  - redox cathode, 20
  - redox cell principle, 189
  - "redox couples," 48–49, 198–200
  - regeneration of redox couples, 199
  - regeneration of stannous ion, 198–199
  - regeneration of titanous ion, 199
  - standard state free energy of conversion, 49
- Resistance,
  - between electrodes, 2
  - formation factor, labyrinth, 62
  - IR loss (see also IR loss, polarization), 62
- Resistivity, solid electrolytes, 338
- Rhodium, 25, 82, 214, 219, 230, 232–233, 236, 238–239. 244, 250, 267, 273–274,294
- Rhodium-palladium, 232, 294
- Rubber, 162
- Rubidium, 180
- Rubidium chloride, 168
- Ruthenium, 230–232, 269, 289,294
- Ruthenium-rhodium, 25, 232

S

- Sarcina urea, 218
- Satellites, 4, 13
  - auxiliary power supply, 47
  - direct fuel cells for dark interval, 156–157
  - 500-W solar regenerative system, 157–159
  - fuel cell system for orbital use, 48, 154
  - hydrogen-oxygen fuel cells charged by solar cells, 153
  - secondary batteries, fuel cell, 153
- Saturated hydrocarbons, **26**
- Seals between refractories, 368
- Second-generation fuel cells, 12–13
- Selenium, 185
- Separators, 10
- ***Serratia kielensis,*** 216
- Silicon, 165
- Silicon oxide, 88
- Silicone rubber, 86, 219
- Silver, 10, 14, 16, 24, 46–47, 59, 66, 68–70, 76–77. 81-82, 88, 108, 122–123, 127, 132, 135–136, 161, 180, 205, 228–239, 271, 275, 278, 287. 301
- Silver cadmium, 155–157
- Silver chloride, 18, 180
- Silver iodide, 179-180
- Silver nitrate, 77, 286
- Silver oxide, 20, 124, 164, 205

Silver zinc, 51, 154–156
Silver-zinc oxide, 48, 50, 99
Smooth electrode surface, considered, 32
Sodium, 18, 47, 134–137, 153, 180, 187–188, 211
  activities in sodium amalgam, 134
  sodium-amalgam cell (see also Amalgam fuel cells), 6
  sodium borohydride, 8
Sodium amalgam, 6, 16, 47, 55, 66, 134–138
Sodium-amalgam-oxygen cell, 134–138
Sodium borohydride, 8, 98, 232, 234, 267
Sodium carbonate, 14, 88, 119–120
Sodium chloride, 18, 187–188
Sodium chloride-potassium chloride, 219
Sodium dihydrogen phosphate, 239
Sodium ferrite, 68
Sodium formate, 215, 232
Sodium hydroxide, 16, 47, 76, 134, 137, 230, 250-253, 263, 287
Sodium-lithium carbonate, 120–122, 125
Sodium molybdate, 206, 267
Sodium nitrate, 200, 265
Sodium phosphorate, 82, 215, 239
Sodium silicate, 88, 118
Sodium sulfate, 200, 214, 239, 250
Sodium tungstate, 206
Solar cells, 13, 47
  battery-solar cell system, 47
  nitrosyl chloride solar-regenerative cell, 191
  photochemically regenerative, Lockheed, 194–195
  silicon, 165
  solar cell-electrolysis-fuel cell, 13
  solar cell electrolyzer, 158
  solar cells plus nickel-cadmium batteries, power density, 156
  solar regenerative (see also Electrolytically regenerative cells, Thermally regenerative cells, Photochemically regenerative cells, and Thermogalvanic cells), 173, 175–176, 180, 182–184, 196–197
    EOS, 173, 175–176, 182, 196–197
    GE, 180
    Lockheed, 180, 183–184
Solid-electrolyte fuel cells,
  comparison with molten salt cell, 133
  Pittsburgh Consolidation Coal Co., solid electrolyte cell, 118–119
  Westinghouse solid-electrolyte fuel cell, 127–133
Solid rocket, torpedo, 5
Solvay process, 6
Space travel (see also Solar cells), 2, 3, 4, 12, 22
  adaptation of Allis-Chalmers hydrogen-oxygen cell to space, 105–109
  capsule electrical power sources, 51
  dark interval, 156–157
  ecological cycle, biochemical fuel cell, 22, 209
  electrolytically regenerative cell, 153–165
  ideal space system, characteristics, 13
  mission time, weight, 4
  orbital applications, 153, 159
  potassium amalgam cell, 174–175
Space travel—Continued
  satellites, 4, 153
  secondary power, spacecraft, 51
  solar cell-electrolysis-fuel cell, 13
  solar regenerative cell, 157–159
  solid electrolyte cell, 132–133
  space power system, 310-W, 23, 173–174
  space program, potential market, 27
  space vehicle power source, 116
Specific conductance, NaOH-KOH-LiOH melt, 338
Stack construction, fuel cells (see also Fuel cell stacks),
  amalgam, 134–138
  high temperature, 118–131
  low temperature, 91–111
  medium temperature, 113–117
  regenerative, EOS, 163–164
Stabilization of electrolyte, 8
Stainless steel, 68, 96, 100, 104, 120, 126, 141, 160, 169, 219, 265–266, 269
Standard-state concentrations, 33
Standard-state enthalpy change, 37
Standard-state, open circuit potential, electrode reaction, 33
Standard state of reactions, 61
State of the art, fuel cells, 5
Steady state measurements, 257–258
Stearic acid, 165
Steel, 126, 135, 137
Stoichiometric, 16
Submarine,
  amalgam cell use, 16, 55, 135–138
  buoyancy increase, 55
  hybrid fuel cell research, 203
  nuclear regenerative fuel cell, underwater applications, 197–198
  one man, 5
  propulsion, 5, 16, 55, 95–97, 101–102, 134, 203
  two man, 138
Sucrose, 214
Sulfur compounds, 227
Sulfur dioxide, 176
Sulfur trioxide, 176
Sulfuric acid, 9, 15, 62, 65, 73, 75–77, 80–82, 84, 87, 98, 101, 110, 160, 181, 197–198, 200, 228–230, 232–234, 238–239, 243, 245–246, 250–254, 256–257, 262–267, 269, 273, 281, 289-290, 292–294, 296
Survey of high temperature electrode materials, 361–363
Systems and control (see also Control systems), 5–6, 139–152
  condenser and separator assembly, 147
  digital computer control, 13, 29
  gas circulation pumps, 147
  mechanical automatic control, 151
  systems problems, future, 152

T

Tafel equations and slopes, 38, 233–234, 248–249, 253, 271, 288, 292, 295, 300-301, 308
Tantalum, 72–73, 186, 191, 269
Techniques, 341–353

- Teflon, 8–11, 26–27, 40, 46, 61, 66-67, 71–75, 77, 81–82. 86, 101, 113–115, 160-161, 165, 191, 204, 214, 228–229, 236–237, 239–240, 269, 290, 320
- Tellurium, 185
- Temperature control, 139–152
  - electrolyte circulation, 11, 36, 142, 149
  - heat removal, 144
  - heat removal, coolant flow, 145, 150
  - heat transfer, 139–140, 147–148
  - hydrogen circulation, 12, 140–142, 145–151
  - mean equilibrium temperatures, equation, 143
  - nonuniformity of temperature, 151
  - radiation heat loss, 149
  - space radiators, 151
  - thermal balance, 145–146
  - thermal conduction, 150
  - water evaporation, 144, 146
- Tetrachloroethane, 191
- Thallium, 180, 185
- Theory of transfer of hydride, 78–79
- Thermal dissociation, various, 332
- Thermally regenerative cells, 16–18, 167–177
  - Aerospace, regenerative cell, 176
  - Allison Division, GM, potassium amalgam cell, 17, 52, 173–175
  - Argonne National Laboratories, thermally regenerative cells, 171–172
  - complete thermal regeneration, 177
  - development prognosis, 18
  - efficiency, maximum theoretical, 167
  - efficiency, simple system, 173
  - Garrett Corp., regenerative cell, 176
  - iodine monobromide, **use,** 176
  - lithium hydride systems, 167–172
  - Lockheed Aircraft, solar regenerative cells, 172–173
  - Mine Safety Appliance Research, lithium hydride regenerative cell, 167–168
  - open circuit cell voltage, 167
  - potassium-amalgam cell, advantages of, 177
  - SO_2-SO_3 regenerative cell, 176
  - solar regenerative systems, EOS, 173, 175–176
  - system limits, 177
  - Tapco, division of TRW, lithium hydride regenerative cell, 168–171
  - various chloride reductions, 176
  - zero-gravity conditions, nuclear heat source, 169
- Thermodynamics, fuel cell,
  - absolute potential of the electrode, 33
  - absolute potential of the electrolyte, 33
  - current densities, 35
  - double layer, composition, 34
  - double layers, relationship between, 34
  - dynamic equilibrium, 33
  - electrochemical free energy, 33
  - free energy of hydrogen, frictional heat, 35
  - Gibbs chemical free energy, overall reaction, 34
  - half-cell potentials, reduction, 33
  - heat, frictional, 35
  - Nernst equations (see also Equations)
- Thermodynamics, fuel cell—Continued
  - plane of closest approach, ions, 34
  - potential relations of a complete cell, 33
  - resistance to mass transfer, heat, 35
  - standard reduction potential, 34
  - standard-state,
    - chemical free energy, 34
    - concentrations, 33
    - open circuit potential of the electrode reaction, 33
  - tables of standard potentials, 34, 327–336
- Thermogalvanic cells, 18–19, 48
  - Argonne National Laboratories, thermally regenerative cells, 184–187
  - Aerojet-General, thermogalvanic cell, 181–182
  - basic principle, thermodynamics, 18
  - definition, 179
  - Delco-Remy Division, GM, double thermogalvanic cells, 18, 187–188
  - double thermogalvanic cells, 179–180, 183–188
  - EOS solar regenerative cells, 182–183
  - General Electric, solar regenerative cell, 180
  - Lockheed Aircraft, solar regenerative cells, 180-181, 183–184
  - materials, 181, 355–368
  - OCV variation/temperature mole fraction, lithium, 186
  - polarization curves, lithium-metal cells, 185
  - potential reagents in molten electrolyte, 181
  - properties, lithium anodes, various cathodes, 185
  - ratio of maximum electrical output to thermal flux, 181
  - reaction equations, 179, 181–182
  - reliable single cell, future, 188
  - simple cells, 179–183
  - solar regenerative cells, 179–184
  - thermal concentration cells, 182–187
  - thermocells, molten salt electrolytes, OCV, 180
- Thioacetic acid, 228
- Thioglycolic acid, 228
- Thiourea, 228
- Tin, 49, 87, 185, 196, 199, 219
- Tin iodide, 172
- Titanium, 10, 19–29, 87, 97–99, 102, 198–199
- Titanium carbide, 99
- Titanium oxide, 19–20, 267
- Torpedo, 5, 55
- Tryptophan enzyme, 218
- Tungsten, 72, 187
- Tungsten carbide, 99
- Tungsten trioxide, 118, 312
- Types of electrode,
  - air, 3, 16
  - baked carbon, 7–8
  - double layer, 8, 10, 14, 60, 62
  - flooded, 7, 59, 63, 312–315
  - flowthrough, 20, 27
  - gas diffusion, 7-8, 13, 26–27, 39, 59–61, 303–312, 320
  - Justi type, 8
  - matrix, porous, 3, 9–10, 12, 14
  - membrane, 10.75, 78–80
  - plastic-bonded metal, 60

Types of electrode—Continued
  porous, 7, 8, 10, 13, 18, 27, 32, 37, 62
  solid-state diffusion, 60
Types of fuel cells,
  amalgam, 6–7, 16, 47, 55, 134, 137, 173–175
    Allison Division, GM, potassium amalgam, 17, 52, 173–175
    Yeager-Kellogg, sodium amalgam, 16, 47, 134–138
  ammonia, 20-21, 51
    Electrochemical Corp., ammonia air, 270–272
    Lockheed Aircraft, ammonia, 262–263
  Bacon, 10. 45, 113
  biochemical, 22–23, 50, 209–221
    General Electric, yeast-glucose, 217
    Magna Corp., **A. formicans,** 214–215
    Marquardt Corp., three-legged, 219
    Melpar, biochemical systems, 216–217
    University of Pennsylvania, formic acid, 215–216
  dry-tape, 20, 366
    Monsanto, dry-tape, 20, 204–206
  electrolytically regenerative, 13, 153–167
    alkali amalgam-halogen, 153
    Battelle electrolysis, 162
    Battelle electrolyzer, initial design, 161
    Battelle oxygen vortex, 161–162
    EOS nine-cell unit, 163
    EOS 38-cell unit, 164
    EOS 75-W unit, 164
    General Electric, 50-W unit, 160
    General Electric, 500-W system, 159
    Pratt & Whitney Aircraft, electrolytically regenerative, 140–141, 149–150, 154, 157–159
  existing types, classification, 31, 42
  high temperature (see also Thermally regenerative cells), 12, 14–19, 4546, 118–133
    General Electric, molten silver, 47
    Iowa State University, graphite-oxygen, 206
    molten carbonates; 12, 14–15, 45–46, 118–127, 131–133
    Pittsburgh Consolidation Coal, solid electrolyte, 118–121
    solid electrolyte, 15, *46,* 118–121, 128–132
    Texas Instruments Co., molten carbonate, 125–127
    Westinghouse cell, solid electrolyte, 46, 127–128
  hybrid, 49
    Aerojet-General, submarine battery, 203–204
    Armour Research, IIT continuous feed battery, 204
    Iowa State University, graphite-oxygen, 206
    Iowa State University, sodium tungstate-tungstic acid, 206–207
    Monsanto, dry-tape battery, 204–206
    Resin Research Lab., organic, 204
  hydrazine, 20-22
    Allis-Chalmers, 750-W unit, 5
    Lockheed Aircraft, hydrazine, 263–264
    Monsanto Chemical, hydrazine half cell, 264–266
  hydrocarbon, 3–5, 7, 9, 13–16, 223–260
    ethylene cell, California Research *Corp..* 15, 246,

Types of fuel cells—Continued
  hydrocarbon-continued
      249–250
    methanol, Engelhard, 239–240
    methanol, 5-kW unit, Shell Research, England, 6
    methanol-air, Brown-Boveri, 6
    methanol-air, Esso Research, 239
    propane, General Electric, 245, 258
  hydrogen-air, 6, 9-10
    General Electric, hydrogen-air, 9–13. 43, 97–102, 142–145, 149–150
  hydrogen-oxygen, 3–5, 7, 9–13, 16
    Allis-Chalmers, 4, 6, 10–13, 44, 48, 62, 103–109, 145–151
    Electro-optical Systems, electrolytically regenerative, 13, 162–164
    500-W solar regenerative, Pratt & Whitney Aircraft, 154, 157–159
    free electrolyte type, 62
    General Electric, ion-exchange membrane, 10–13, 62, 97–102, 142–145, 149–150
    Ionics double membrane, 109–111
    Justi-Brown-Boveri, 44
    matrix type, 62
    Pratt & Whitney Aircraft, 140-141, 149–150
    Union Carbide, 7, 10–13, 43, 94–95, 141–142, 149
  hydrogen peroxide, 11,261–262, 272–274,299
    Allis-Chalmers, capillary cell, 105–109
    Electro-optical Systems, 48
    Engelhard, 288–289
    Monsanto, half cell, 266–267
    Pratt & Whitney Aircraft, 140-141, 149–150
    Tyco Laboratories, half cells, 290–292
    Union Carbide Corp., 95–97, 141–142, 149
  low temperature, 9–16, 42-45, 91–111
    Allis-Chalmers, hydrogen-oxygen, 4-6, 10–13, 43–44, 48, 62, 103–109, 145–151
    cells for highly soluble fuels, 44
    General Electric, hydrogen-air cell, 9-13, 43, 97–102, 142–145, 149–150
    General Electric, propane cell, 245, 258
    Ionics double membrane, sulfuric acid cell, 12, 109–111
    Union Carbide, 10–13, 43, 94–97, 141–142, 149
  medium temperature, 10–13, 45-46, 113–117
    Allis-Chalmers, laboratory cell, 46
    Allison Division, GM, 17
    Bacon, F. T., fuel cell, 10, 45, 113
    Electrochemical Corp., ammonia molten KOH-NaOH cell, 270–272
    General Electric, laboratory cell, 46
    General Electric, propane cell, 15–16, 237–238, 258
    Patterson-Moos, hydrox cell, 113–114
    Pratt & Whitney Aircraft, 10-12, 45, 113–117
  miscellaneous,
    Monsanto, rocket propellant half cells, 267–270
    Nuclear regenerative cells, Union Carbide, 197–198
  photochemically regenerative, 19, 48, 189–194

T

Electro-Optical Systems, 196–197
Lockheed Missiles & Space Division, 194–196
Sunstrand Machine Tool, 191, 194
redox, 19–20, 49–49
General Electric, low temperature acid, 198–199
Esso Research, 200
sodium/molten salt/chlorine, hot and cold, 153
solar regenerative (see also Electrolytically regenerative cells, Thermally regenerative cells, Photochemically regenerative cells, and Thermogalvanic cells), 173, 175–176, 180, 182–184, 191–197
solid electrolyte (see also High temperature cells), 15, 46, 119–132
thermally regenerative, 16–18, 48, 167–177
Aerospace, 176
Allison Division, GM, potassium-amalgam, 17, 52, 173–175
Argonne National Laboratories, 171–172
Garrett Corp., 176
Lockheed Aircraft, solar, 172–173
Mine Safety Appliance Research, LiH, 167–168
Tapco, Division of TRW, LiH, 168–171
thermogalvanic, 18–19, 48
Aerojet-General, 181–182
Argonne National Laboratories, thermally regenerative, 184–187
Delco-Remy Division, GM, double thermogalvanic. 18, 187–188
double thermogalvanic, 179–180, 183–184, 187–188
EOS, solar regenerative, 182–183
General Electric, solar regenerative, 180
Lockheed Aircraft, solar regenerative, 180–181, 183–184
simplest cell, example, 179

U

Unsaturated hydrocarbons, 26
Unsteady-state measurements, porous electrodes, 316–318
apparent double-layer capacity, 318
correct double-layer capacity, 318
difficulty of application, fuel cells, 316–317, 320–321
methods of investigating, 317
methods of measurement, 318
potential as a function of time, 317
time duration (or frequency) for measurement, 317
Urea, 212–213. 226, 262
Urease, 212–213
Urine, 217–218
U.S. Government. (See particular agency.)
U.S. Signal Missile Support Agency, 51

V

Vanadium, 172, 191
Vanadium oxide, 235
Vapor pressure, phosphoric acid, **338**
Vehicle battery,
electrolytic regeneration, 153
two cells, different temperatures, 153
Vehicle propulsion, 5, 52–55
Voltage,
efficiency, 2
gradient, electrolyte, 35
sweep methods, 246–248, 253, 258
acetylene, wire electrode, 248
ethylene, rotating disk electrodes, 247
formic acid oxidation, 253
hydrocarbons, linear method, 246
peak currents, 246
thermodynamic, 2
working, 2

W

Waste heat, removal, 11, 13
heat absorption by a fuel cell, 267
Water control,
avoidance, design, 13
"dynamic water vapor pressure method," 106–107, 146–147, 150–151
electroendosmosis, 84
electrolysis cell, water removal, 162
electrolyte circulation, 142
hydrogen and oxygen circulation, 142
long-term water balance, 60
reactant gas, condenser system, 140
static water-vapor-control method, 10, 146
static water-vapor-pressure method, 107–109, 148–151
temperature-compensating electronic pressure controller, 148–149
transpiration through electrodes, 142
voltage sensing, method, 103–106, 146, 150–151
water-mass balance, equation, 146
water recovery, 13
water removal by wicks, 97–98, 142–144, 150
Wetproofed electrodes (see also Flooding), 8, 63

Y

Yeast, 216–217
Yttrium oxide, 88, 128

Z

Zeolite, 86
Zinc, 20, 88, 185, 203–204, 219
Zinc anodes, 20
Zinc chloride, 203
Zinc hydroxide, 205
Zinc iodide, 181
Zinc-silver oxide cell, primary, 2, 155
Zirconia-calcia, 15, 128
Zirconia-thoria, 15, 46
Zirconia-yttria, 129
Zirconium, 73
Zirconium oxide, 86–88, 128–129

Author—Corporate Source Index

A

Adams, D. R., 57
Advanced Station Vehicle Missions, 149
Aerojet-General Corp., 181, 203
Aerospace Corp., 176
Air Force, U.S., XIII, 51
Aircraft Porous Media, Inc., 144
Alamaula, B. **C.,** 52, 57
Alexander, N. E., 221
Alford, H. R., 89
Alfred University, 56, 282, 285, 319, 350–351
Allen, Duane, 372
Allied Chemical, 6
Allis-Chalmers, 4–6, 10–13, 43, 46, 48, 62, 65-66, 86, 103, 105–109, 145, 147–150, 162, 285, 360
Allison Division, GM, 17, 52, 174, 344
American Chemical Society, 29, 58, 224, 285, 321
American Cyanamid Co., 12, 73–74, 86, 239, 285, 352, 367, 370
American Hard Rubber, Amerace Corp., 86
American Institute of Biological Sciences, 221
American Machine & Foundry, Inc., 84, 100–101, 365
American Oil Co., 256, 352
Ames Chemical Co., 205
Andrus, D. E., 89
Anson, F. C., 353
Antara Chemicals, 366
Argonne National Laboratories, 80, 171. 184
Ariet, M., 321
Armour Research Foundation, 204
Astroceram Co., 367
Astropower, 86
Atkinson, **R.** H., 354
Atomics International, 276, 352
Austin, L. G., XIII, 56–58, 89, 177, 302, 321
Azarnoosh, A., 340

B

Bacon, F. T., 89
Bailey, R. V., 152
Bakelite Division, Union Carbide, 364
Baker, B. S., 372
Bartosh, S. J., 58
Battelle Memorial Institute, 29, 78, 160–161, 163, 171
Baur, E., 193
Baxter, W. P., 193
Baylor University, 256, 353
Beals, D. **L.,** 260
Beechcraft Research and Development, Inc., 372
Belford, et al., 353
Bendix Filter Division, 361
Benjamin, P., 245
Berl, W. **G.,** 284, 288, 302
Binder, **H.,** 259
Bockris, J. O'M.. 57, 58, 257, 259, 298, 353
Bogotsky, V. S, 260
Bond, C. **G.,** 302
Boos, D. L., 260
Boudart, M., 312, 321
Bowden, F. P., 345
Bowen, E. J., 193
Branson Ultrasonic, 233
Breiter, M. W., 203, 259, 260, 296, 302
British Electricity Authority, 56–57
Broers, G. **H.** J., 127, 132, 344
Brooks, W. B., 340
Brown, W. E., 89
Brown-Boveri Corp., **6.** 44, 152
Brummer, S. B., 259
Bruning, **H.,** 78
Buck, R. P., 259
Butcher Co., L. H., 353
Buvet, R., 311, 321

C

California Research Corp., 15, 54, 228, 234, 245–246, 249. 253–254, 353, 372
Calvert, J. G. (now Chevron Research), 193. 201
Carbide & Carbon Chemical Co., 367
Carslaw, H. S, 317, 321
Cather, H. D., 52
Central Technical Institute TNO (Holland), 121
Chemetron Corp., 372
Chemical Construction Co., 370
Chrisney, J. B., 57
Claussen, W. F., 340
Clevite Corp., 65-66, 285, 361
Cochran, N. P., 56–57
Cohn, Ernst M., XIII, 51, 54, 57, 58
Colichman, E. **L.,** 58
Comyn, **R.** H., 321
Cook. C. **C.,** 57
Crawford, I. P., 221
Culbertson, **O.** L., 340

D

Dahms, H., 259
Daniels, F., 193
Dartyan, **O.** K., 119–120, 132

D

Davis, J. E., 340
DDC (Defense Documentation Center}, 58
de Boer, cf. J. H., 340
de Levie, R., 317, 321
Del Duca, M. G., 221
Delahay, P.. 58, 353
Delco-Remy, 18. 187
Diamond Ordnance Fuze Laboratories (now Harry Diamond Laboratories), 199
Dickenson, R. G., 193
Dittman, H. M., 89, 305, 321
Dow Chemical Co., 86, 89, 205, 364, 367
Drazic, V., 259
du Pont de Nemours & Co., E. I.. 265, 367
Duffie, J. A., 193
Durrant, G. G., 193

E

Eckert, C. H., 372
Eder. S., 321
Eischen, R. P., 276, 302
Eisen, M. P., 140, 152
Electric Auto-Lite Co., 146
Electric Storage Battery Co., 16, 47, 66, 134–135
Electrochimica Corp., 80, 270
Electro-Optical Systems, 13, 48, 65, 86, 162–165, 173, 175, 182, 196, 285, 353
Engelhard Industries, Inc., 70, 213, 239, 279, 285, 288, 299, 348, 351, 353, 370-372
Enke, C. G., 321
Esso, 6, 20, 65, 75
Esso Research & Engineering Co., 200, 228, 233–234, 238–239, 290
Euler, J., 321
Evans, E. L., 177
Evans, G. E., 151, 152

F

Farkas, A., 302
Federal-Mogul Division, 361
Feigel, F., 353
Firewel Co., 146
Fisher, J. H., 51, 57, 367
Fisher Scientific, Morton Chemical Co., 87, 365, 367
Fleischman, C. W.. 259
Flinn, P. A., 194.201
Ford-Aeronutronic, 218
Fox, H. W., 56, 58
Francis, Howard T., 166
Franke, F. H., 58
Fricke, H., 201
Frumkin, A. N., 281, 302
Fuel Cell Corp., 29
Fuscoe, J. M.. 221

G

Galstaum, L. S., 78
Gambrill, W. R.. 188
Garner, R. V., 166
Garrett Corp., 176
Gazith, M., 302
Gelman Instrument, 367
General Aniline & Film Corp., 364
General Atomics, 280
General Electric Co., 9–13, 15–16, 43, 46–47, 62, 71, 73–74, 83–85, 97, 100–103, 142–143, 145, 149–150, 159, 180, 198, 217, 228, 232, 237–238, 240, 244–245, 258, 285, 300–301, 344, 350-352, 360, 369–370, 372
Gest, H., 216, 221
Gibb, T. R. P., Jr., 177
Gierst, L. E., 353
Gileadi, E., 259
Gillespi, L. J., 78
Gilman, S., 259, 260
Giner, J., 259
Girdler Corp., 370
Glickman, R., 228
Goodrich, B. F., 367
Gorin, E., 132
Gottleib, M. H., 259, 354
Gould National Batteries, 65, 76, 162
Grant, W. M., 353
Green, M., 259
Gregor, H. P., 85, 364
Grens, E. A., 321
Griffin, L. R., 259
Griffith, R. O., 193
Groth, W., 193
Guillon, M., 311, 321

H

Hagen, H., 78
Hall, F. P., 78
Halowax Products Division, 367
Hansen, M., 177, 188
Hart, A. B., 56–57
Hart, E., 201
Hartung, E. J., 193
Heavens, O. S.. 345
Heidt, L. J., 193
Hensel, S. L., 372
Hercules Powder, 366
Hilvety, N., 152
Hiraoka, H., 340
Hoffman Electronics Corp., 56–57
Holmquist, J. P., 193
Hommel Co., O., 367
Hooker Chemical Co., 203
Hopkins Marine Station, 214
Horn, A. B., 340
Houghton Co., 360
Howard, H. C., 56–57
Hunger, H. F., 52, 57–58, 65

I

Iczkowsi, R. P., 312, 321
Illinois Institute of Technology, 204
Institute of Physics (Bonn), 6
International Nickel Co., 361

Ionics, 12, 85, 109–111, 238
Iowa State University, 206

J

Jaeger, J. C., 317,321
Jasinski, R. J., 7, 29, 56, 58, 285
Jefferson Chemical Co., 364
Jet Propulsion Laboratory, 163
Johns-Manville, 86
Johnson, G. K., 259
Johnson, J. W., 259
Johnson-Mathey, 288
Juliard, A. L., 259
Justi, E. W., 56, 58, 66, 89, 305, 311,321

K

Katan, T., 321
Ke, B., 193
Kelco Co., 367
Kellogg Co.. M. W., 16, 47, 135–138, 369–370
Kendall Co., 366
Kerdivarenko, M. A., 340
Ketelaar, J. A. A., 132
Kirkland, T. G., 56, 58
Kistiakowsky, G. B., 193
Klimpel, R. R., 321
Knapp, T., 367
Kohling, A., 259
Kolb, J., 321
Kordesch, K. V., 58, 353
Kornfeld, G., 193
Kortum, G., 57, 58
Ksenzhek, O. S., 321
Kuhn, A. T., 259
Kummer, J. T., 340
Kurbaschewski, O., 177

L

Lacey, W. N., 340
Laidler, K. J., 193
Latimer, W. M., 331
Laudenkloe, H., 193
Leighton, P. A., 193
Leland Stanford Junior University, 256, 283
Lerner, H., 321
Levich, V. G., 302, 347, 354
Liebhafsky, H. A., 167, 177
Linde Co., 86, 276.361
Lindholm, I., 285
Lingane, J. J., 298,302
Lockheed Aircraft Corp., 56–57, 66, 75, 77, 172, 180, 183, 194, 228, 262, 264, 352
Logan, A. M., 353
Lumas Co., 370
Luther, R., 193

M

MacNevin, W. M.. 193
Maget, H. J. R., 111
Magna Corp., 212,215, 217,353
Mahefsky, E. T., 166
Makrides, A. C., 259
Markham, M. C., 193
Marko, A., 353
Markus, R. J., 201
Marotta Corp., 144
Marquardt Corp., 219
Massachusetts Institute of Technology, School of Engineering, 273
Mattson, E., 353
McCormick, J. E., 56–57
McDonagh, J. M., 58
McKeown, A., 193
McKetta, J. J., 340
Meek, J., 372
Melpar, Inc., 216
Menetrey, W. R., 15, 57
Messer, C. E., 177
Metallizing Corp. of America, 367
Metals & Chemicals, 362
Micro Metallic Division, Pall Corp., 361
Microcircuit Co., 367
Millipore Filter, 366
Milner, P. C., 321
Mine Safety Appliance Research Corp., 167
Mitchell, W., 56, 58
Monsanto Chemical Co., 20, 75, 80, 191, 204–205, 207, 233, 235–236, 264, 266–267, 343
Monsanto Research Corp., 224,228
Montgomery, C. W., 193
Moos, A. M.. 228
Morganite, Inc., 88, 173
Morill, C. C., 116
Morrison, T. J., 340
Munson, R. A., 259, 353

N

NASA, XIII, 51, 100,374
National Carbon, 172, 191, 265, 361
National Felt Co., 365
Neish, A. C., 221
Neuimin, H., 193
Neuweiler, C., 193
New York State University, 57
Newman, J. S., 321
Nicholson, R. S, 353
Niedrach, L. W., 89
Nonnenmacher, W., 321
Norris, L. F., 39
Norstrand Co., Inc., D. Van, 353
North American Aviation, 56–57
Norton Co., 86, 356
Noyes, W. A., Jr., 193
Nyborg, W. J., 321

O

Office of Coal Research, 70, 129
Ohio State University, 210
Oster, E. A., 111

P

Palasi, P., 321
Parsons, R., 302
Patterson-Moos Research, 113–114
Peattie, C. G., 58
P.E.C. Corp., 194
Pellon Corp., 366
Pennsalt Chemicals Corp., 364
Pennsylvania Fluorocarbon Co., 359
Pennsylvania State University, 199, 303
Perforated Products, Inc., 269, 360
Pfefferle, W. C., 372
Piersma, B. J., 259
Pittsburgh Consolidation Coal Co., 118, 122
Pivnick, H., 221
Plishin, W. A., 276, 302
Polglase, M. F., 340
Polytechnic Institute of Brooklyn, 278
Polytechnico di Milano, 281
Posner. A. M., 200
Poterill, R. H., 193
Potter, E. C., 57–58, 367
Potter, M. C., 209,221
Pratt & Whitney Aircraft Co., 10–12, 45, 67, 113, 115–117, 140–141, 149–150, 154, 157–158
Products Research Co., 191, 367
PSC Publication Committee, 58
Purdue University, 319
Pure Carbon Co., 224, 248

R

Rabinowitch, E., 193
Radiation Applications, Inc., 84
Rakin, G. T., 193
Ramaley, L., 321
Reamer, H. H.. 340
Rebmann, A., 193
Recht, H. L., 132
Reeves Co., F. S., 365
Reid, W. T., 7, 29
Rensselaer Polytechnic, 79
Resin Research Laboratories, Inc., 204
Reti, D. R., 310
Rhodes, D. R., 259
Rightmire, R. A., 260
Roberts, R., 56, 58
Rockette, J. A., 321
Rohm & Haas, 366
Rollefson, G. K., 193
Rosenberg, A. J., 340
Rosenwalt, A. J., 219, 221
Rossini, F. E., 331
Rothfleisch, J. E., 372
Row, L., 302
Rowland, R. L., 260
Rozelle, R. B., 282
Rubin, T. R., 193
Rusinko, F., Jr., 89

S

Sabina, L. R., 221
Sage, B. H., 340
Sama. D. A., 303,311
Sandler, V. L., 302
Sauber, W. J., 89
Schlatter, M. J., 15, 53, 54, 228, 259
Schuldiner, S., 259
SERAI, 87
Servionics Instruments, Inc., 146
Shain, I.. 353
Shalit, H., 259
Sharp, J. F., 193, 353
Shawinigan Resins, 205, 236, 366
Shell Chemical Corp., 364
Shell Research (England), 6
Shecke, M., 132
Shub, O. M., 193
Siemens-Schuckertwerke, 80
Sieverts, A., 78
Smatko, J. S., 57
Snell, Inc., Foster D., 57–58
Society of Automotive Engineers, 372
Sonner, F., 334
Stafford, G. B., 166
Stanford Research Institute, 190
Starkey, G. E., 51, 57
Steigelmann, E. F., 259
Stein, B. R., 56, 58
Steiner, A. B., 193
Stender, V. V., 321
Stephens, R. E., 193
Sterer *Corp.*, 144
Suess, H., 193
Sundstrand Machine Tool Co., 191
Surface Processes, 228, 243–244
Szego, G. C., 51, 54, 57

T

Tabor, D., 345
Tapco, division of TRW, Inc., 168
Taschek, W. G., 58, 65
Terenin, A., 193, 302
Texas Instruments, 12,6849, 123–126,342
Theurer, K., 193
Thielman, J. H., 166
Thompson & Co., John I., XIII
Thompson Fiber Glass Co., H. I., 86
Thompson-Ramo-Wooldridge, Inc., 75, 168
Tobias, C. W., 58, 321, 353
Todesca, F., 372
Tracor, Inc., 296
Trans-Sonics, Inc., 144
Trivich, D., 193, 201
Turner, R. M., 321
Twigg, G. H., 340
Tyco Laboratories, Inc., 78–79, 283, 290, 299

U

U.S. Army Signal R&D Lab., 58
U.S. Rubber Co., 111, 365
Union Carbide **Corp.,** 6–7, 10–13, 40, 43, 62–63, 74, 77, 94–96, 134, 141, 149, 181, 197–198, 319–320, 364, 369, 372
Union Carbide Plastics Co., 364
United Carbon, 181
United Water Softeners, Ltd., 84
University of Florida, 79, 199–200
University of Pennsylvania, 57, 215, 220, 232, 248, 292, 342, 351, 353
Uri, N. J., 193
Utilities Mfg. Corp., 367

V

Vail, C. B.. 193
Valcor, 144
Van der Pauw, **L.** G., 353
Van Wazer, **J.** R., 339
van Winkle, J., and Carlson, W. N., Jr., 140
Vanadium-Alloys Steel ***Co.,*** 361
Vasilyer, Y. B., 260
Vaughan, W. E., 193
Venture-Tech., Inc., 29, 89
Veseloushii, **I.,** 193
Vetter, **K.** J., 57–58
Vielstich. W., 29, 57, 58, 152
Villars, D. S. 193
Von Fredersdorff, C. ***G.,*** 29, 228
Von Stackelberg, M., 58

W

Wagner, C., 303
Walker, **O.** J., 193
Walker, R. D., 310, 321
Warburg, **E.,** 193
Warner, T. B., 259
Warszawski, **B.,** 311,321
Weatherhead Co., 146
Weaver, ***C.,*** 345
Weber, J., 259
Weigert, F., 193
Weise. K., 344
Weiss, **J.,** 193
Welcher, F. J., 353
West Virginia Pulp & Paper Co., 77, 134, 287
Western Reserve University, 16, 134–135, 284, 348, 351
Westinghouse Electric Corp., 7, 46, 87–88, 127–131, 278. 344
White, L., Jr., 193
Whittaker Controls and Guidance, 146
Whittemore, J. W., 367
Wild, **A.,** 367
Will, F. *G.*, 303, 305, 311, 321
Winsel, A. W., 58, 89, 305, 311, 321
Winters, C. E., 152
Wohlers, **H.** C., 201
Wood, ***G.*** B., 321
Wroblowa, **H.,** 259

Y

Yeager, E., 16, 47, 56–57, 134, 284, 286, 288, 291, 298–299, 318, 340
Young, ***G.*** J., 282–283

Z

Zapf, G., 78
Zurilla, R. W., 221

☆U.S. GOVERNMENT PRINTING OFFICE: 1967—O 230-752

> *"The aeronautical and space activities of the United States shall be conducted so as to contribute . . . to the expansion of human knowledge of phenomena in the atmosphere and space. The Administration shall provide for the widest practicable and appropriate dissemination of information concerning its activities and the results thereof."*
>
> —NATIONAL AERONAUTICS AND SPACE ACT OF 1958

NASA SCIENTIFIC AND TECHNICAL PUBLICATIONS

TECHNICAL REPORTS: Scientific and technical information considered important, complete, and a lasting contribution to existing knowledge.

TECHNICAL NOTES: Information less broad in scope but nevertheless of importance as a contribution to existing knowledge.

TECHNICAL MEMORANDUMS: Information receiving limited distribution because of preliminary data, security classification, or other reasons.

CONTRACTOR REPORTS: Technical information generated in connection with a NASA contract or grant and released under NASA auspices.

TECHNICAL TRANSLATIONS: Information published in a foreign language considered to merit NASA distribution in English.

SPECIAL PUBLICATIONS: Information derived from or of value to NASA activities. Publications include conference proceedings, monographs, data compilations, handbooks, sourcebooks, and special bibliographies.

TECHNOLOGY UTILIZATION PUBLICATIONS: Information on technology used by NASA that may be of particular interest in commercial and other nonaerospace applications. Publications include Tech Briefs; Technology Utilization Reports and Notes; and Technology Surveys.

Details on the availability of these publications may be obtained from:

SCIENTIFIC AND TECHNICAL INFORMATION DIVISION
NATIONAL AERONAUTICS AND SPACE ADMINISTRATION
Washington, D.C. 20546